

System Simulation in Buildings 2014

December 10 – 12, 2014

Proceedings of the Ninth International Conference

Organised by :
The Thermodynamics Laboratory
Aerospace & Mechanics Department
University of Liège

Campus du Sart-Tilman
Bâtiment B49 – Parking P33
B-4000 Liège, Belgium

2015

**System Simulation
in Buildings 2014**

Université de Liège - Atelier des Presses
Chemin des Amphithéâtres - Bât B7a
4000 Liège (Belgique)

© 2015

 Atelier des Presses

Tous droits de reproduction,
d'adaptation et de traduction
réservés pour tous pays.

Ouvrage mis en page par l'auteur
Imprimé en Belgique

D/2015/13.315/5
ISBN : 978-2-930772-10-3

Organised by :
**The Thermodynamics Laboratory
of the University of Liège**

**System Simulation
in Buildings 2014**

*Proceedings of the Ninth
International Conference*

SYSTEM SIMULATION IN BUILDINGS 2014

Proceedings of the Ninth International Conference

Organized by:

**The Thermodynamics Laboratory
Aerospace & Mechanics Department
University of Liège
Campus du Sart-Tilman
Bâtiment B49 – Parking P33**

December 10-12, 2014

2015

Organization Committee



Vincent Lemort
Conference Chairman
Thermodynamics Laboratory
Université of Liege
vincent.lemort@ulg.ac.be



Philippe André
Scientific Committee Chairman
BEMS - Arlon
Université of Liege
p.andre@ulg.ac.be



Francois Randaxhe
Conference Secretary
Thermodynamics Laboratory
Université of Liege
F.Randaxhe@ulg.ac.be

Scientific Committee

BERTAGNOLIO Stephane	Emerson Climate Technologies GmbH, Germany
BRAUN James	Purdue University, U.S.A.
CORGNATI Stefano	Politecnico di Torino, Italy
CUEVAS BARRAZA Cristian	Universidad de Concepcion, Chile
DEWALLEF Pierre	University of Liege - Thermodynamics Laboratory, Belgium
FISSORE Adelqui	Universidad de Concepcion, Chile
HEISELBERG Per	AAU - Aalborg University, Denmark
HELSEN Lieve	Leuven University (KUL), Belgium
JIANJUN Xia	Tsinghua University, P.R. China
KUMMERT Michael	Ecole Polytechnique de Montréal, Canada
LEBRUN Jean	University of Liege / JCJ Energetics / ATIC
MADJIDI Madjid	Ingenieurbüro Madjidi
MASY Gabrielle	HEPL – CECOTEPE
RASLAN Rokia	The Bartlett School of Graduate Studies – UCL
SAELENS Dirk	Leuven University (KUL), Belgium
STABAT Pascal	Ecole des Mines – ParisTech, Belgium
THOMAS Sébastien	SECOLUX, Luxembourg
VERHELST Clara	3E, Belgium
WOLFRAM Stephan	Technische Hochschule Nürnberg Georg Simon Ohm
XIAOHUA Liu	Tsinghua University, P.R. China

Table of Contents

FOREWORD

LIST OF PARTICIPANTS

FIRST SESSION – ADVANCED CONTROL OF SYSTEMS IN BUILDINGS

- ***P01: A convex approach to energy use minimization of buildings equipped with hybrid ground-coupled heat pumps***
Ercan Atam, Damien Picard, Lieve Helsen – Department of Mechanical Engineering, KU Leuven (Belgium)
- ***P02: Comparisons of model structure and identification methods for multiple-RTU coordination***
Donghun Kim, Jie Cai, James E. Braun – Ray W. Herrick Laboratories, School of Mechanical Engineering, Purdue University, (USA)
- ***P03: Extraction of heating control rules from the dynamic programming method for load shifting in energy-efficient buildings***
Maxime Robillart, Patrick Schalbart and Bruno Peuportier– MINES ParisTech, PSL - Research University, CES - Centre for energy efficiency of systems (France)
- ***P04: Assessing simplified and detailed models for predictive control of space heating in homes***
Kun Zhang, Narges Roofigari E., Humberto Quintana, Michaël Kummert– Polytechnique Montréal, Montréal (Canada)

SECOND SESSION – INTEGRATION OF RENEWABLE ENERGY SOURCES IN BUILDINGS

- ***P05: Impact of storage tank control and hydraulic configuration on solar heat pump system performance***
John Veeken, Jan Verheyen and Maarten Sourbron – KU Leuven (University of Leuven), Department of Mechanical Engineering, Technology Campus De Nayer, Sint-Katelijne-Waver (Belgium)

- ***P06: Simulation of a passive house coupled with a HP/ORC reversible unit***
Olivier Dumont¹, Carolina Carmo², François Randaxhe¹, Sylvain Quoilin¹, Vincent Lemort¹ – ⁽¹⁾Thermodynamics laboratory, University of Liege, Liege (Belgium), ⁽²⁾Department of Energy Technology, Aalborg University, Aalborg (Denmark)
- ***P07: Integration and Evaluation of Innovative and Renewable Energy Technologies in a Canadian Mid-rise***
Martin Kegel, Justin Tamasauskas and Roberto Sunye – Natural Resources Canada, Varennes (Canada)
- ***P08: A computational model for optimizing district heating systems using a slow responsive renewable heat source and thermal storage***
F.F.M. Soons^{1,2}, J. Ignacio Torrens¹, J.L.M. Hensen¹, R.A.M. De Schrevel² – ⁽¹⁾Dep. Building Physics and Services, Eindhoven University of Technology, (Netherlands), ⁽²⁾Dep. Business Development Energy, Cofely Netherlands NV., Maastricht (Netherlands)

THIRD SESSION – SIMULATION ASSISTED ANALYSIS AND EVALUATION OF BUILDING ENERGY USE

- ***P09: Office building HVAC system analysis through integrated dynamic simulation***
Wout Parys, Hugo Hens and Dirk Saelens – Building Physics Section, KU Leuven, Leuven (Belgium)
- ***P10: The influence of realistic schedules for the use of appliances on the total energy performances in dwellings***
Tiziana Buso, Simona D'Oca, Stefano Paolo Corgnati – TEBE Research Group, Energy Department, Politecnico di Torino, Corso Duca degli Abruzzi 24, 10129, Torino (Italy)
- ***P11: The Energy Performance Certification: A tool for smarter cities?***
Stephane Monfils, Jean-Marie Hauglustaine – University of Liege (Belgium)
- ***P12: The Mapping of Climate-Dependent Simplified Thermal Systems using State Space Models***
A.W.M. (Jos) van Schijndel – Eindhoven University of Technology, (Netherlands)

FOURTH SESSION – ADVANCES IN DESIGN AND OPTIMIZATION OF BUILDING COMPONENTS AND SYSTEMS

- ***P13: Application of users' light-switch stochastic models to dynamic energy simulation***
V. Camisassi, V. Fabi, RK. Andersen, SP. Corgnati – ⁽¹⁾TEBE Research Group, Department of Energetics, Politecnico di Torino, Corso Duca degli Abruzzi 24, 10129 Torino (Italy), ⁽²⁾ICIEE, Department of Civil Engineering, Technical University of Denmark, Nils Koppels Allé Building 402, 2800 Kgs. Lyngby (Denmark)
- ***P14: Low order model selection for optimised heating start-up in tertiary buildings: Review and comparison of different approaches through a case study***
Joachim Verhelst¹, Dirk Saelens², Geert Van Ham¹ and Lieve Helsen³ – ⁽¹⁾Knowledge Centre for Energy, KU Leuven Faculty of Engineering Technology, Geel (Belgium), ⁽²⁾Building Physics Section, KU Leuven, Leuven (Belgium), ⁽³⁾Mechanical Engineering Department, KU Leuven, Leuven (Belgium)
- ***P15: Design and Optimization of Geothermal Heat Pumps in Combination with TABS***
Arno Dentel¹, Thomas Dippel², Mario Franz¹, Wolfram Stephan¹ – ⁽¹⁾Technische Hochschule Nürnberg Georg Simon Ohm, Institute for Energy and Buildings, Energie Campus Nürnberg, Keßlerplatz 12, 90489 Nürnberg (Germany), ⁽²⁾TEB – Transferzentrum Energieeffizientes Bauen GmbH Kehlstraße 27/1, 71665 Vaihingen an der Enz, (Germany)
- ***P16: Modelling the impact of integrated electric vehicle charging and domestic heating strategies on future energy demands***
John Hand, Nick Kelly, Aizaz Samuel – Energy Systems Research Unit (ESRU), Department of Mechanical and Aerospace Engineering, University of Strathclyde Glasgow (Scotland)

FIFTH SESSION – EXPERIMENTAL STUDIES

- ***P17: ISABELE method: In-Situ Assessment of the Building Envelope Performances***
Pierre Boisson and Rémi Bouchié – Université Paris Est - Centre Scientifique et Technique du Bâtiment, Marne-la-Vallée (FRANCE)

- ***P18: Modeling of the Indoor Thermal Comfort in Passive Houses heated by Wood Stoves***
Laurent Georges¹, Øyvind Skreiberg² – ⁽¹⁾Department of Energy and Process Engineering, Norwegian University of Science and Technology (NTNU), Trondheim (Norway), ⁽²⁾Department of Thermal Energy, SINTEF Energy Research, Trondheim (Norway)
- ***P19: A TRNSYS-LabVIEW bi-directional connection for HVAC equipment testing using hardware-in-the-loop simulation***
Francesca Macdonald¹, Katherine D'Avignon¹, Michaël Kummert¹, and Ahmed Daoud² – ⁽¹⁾Polytechnique Montréal, Mechanical Engineering, Montréal (Canada), ⁽²⁾Institut de Recherche d'Hydro-Québec, Shawinigan, Canada
- ***P20: Experimental study on a new energy-efficient VRF system***
Xiaochen Mao, Jianjun Xia – Building Energy Research Centre, Tsinghua University, Beijing (China)

SIXTH SESSION – BUILDING MODEL VALIDATION

- ***P21: Calibrating whole house thermal models against a coheating test standard: solid wall case studies***
James Parker, David Farmer, Martin Fletcher – Leeds Beckett University, Leeds, (UK)
- ***P22: An adapted co-heating test and experimental infrastructure for thermal dynamic response and performance identification of residential building***
Guillaume Lethé, Paul Steskens, Gilles Flamant, Brieuc Meurisse – Belgian Building Research Institute, Brussels (Belgium)
- ***P23: Full scale empirical validation for building energy simulation programs***
Matthias Kersken¹, Ingo Heusler¹ and Paul Strachan² – ⁽¹⁾Fraunhofer Institute for Building Physics IBP, Holzkirchen (Germany), ⁽²⁾University of Strathclyde, ESRU, Dept. of Mechanical and Aerospace Eng. (UK)
- ***P24: Back from Holzkirchen full scale dynamic testing experiment***
Gabrielle Masy¹, Florent Delarbre¹, Jean Lebrun², Emeline Georges³, François Randaxhe³, Vincent Lemort³, Imane Rehab⁴ and Philippe André⁴ –

⁽¹⁾Master School of Province de Liège (Belgium) ⁽²⁾JCJ Energetics, Liège (Belgium) ⁽³⁾Labothap, University of Liège (Belgium), ⁽⁴⁾BEMS, University of Liège (Belgium)

SEVENTH SESSION – INTEGRATION OF BUILDINGS IN SMART ENERGY GRIDS

- ***P25: Impact of net metering programs on optimal load management in US residential housing – a case study***
Emeline Georges¹, Jim Braun², Eckhard Groll², Travis Horton² and Vincent Lemort¹ – ⁽¹⁾Thermodynamics Laboratory, University of Liège, Liège (Belgium), ⁽²⁾Ray W. Herrick Laboratories, Purdue University, West-Lafayette, Indiana (USA)
- ***P26: GIS supported city district energy system modeling***
Jan Schiefelbein¹, Amir Javadi¹, Michael Diekerhof¹, Dirk Müller¹, Antonello Monti² – RWTH Aachen University, E.ON Energy Research Center, ⁽¹⁾Institute for Energy Efficient Buildings and Indoor Climate ⁽²⁾Institute for Automation of Complex Power Systems, Aachen (Germany)
- ***P27: Strategies for an Optimal Chiller Operation (in a Smart Grid)***
Julian Buderus, Arno Dentel, Wolfram Stephan – Technische Hochschule Nürnberg Georg Simon, Institute for Energy and Building, Nuremberg, (Germany)
- ***P28: Residential buildings with heat pumps, a verified bottom-up model for demand side management studies***
Dieter Patteeuw, Lieve Helsen – Applied Mechanics and Energy Conversion, Department of Mechanical Engineering, KU Leuven (Belgium)

EIGHTH SESSION – ADVANCES IN COMPONENT MODELING

- ***P29: Finite cylinder-source model for pile/borehole heat exchangers: effects of temperature response to time varying thermal load***
Tatyana V. Bandos^{1,3}, Álvaro Campos-Celador², Luis M. López González³, José M. Sala Lizárraga^{1,2} – ⁽¹⁾Dpto. de Máquinas y Motores Térmicos, University of the Basque Country UPV/EHU, Bilbao (Spain), ⁽²⁾Grupo de Investigación ENEDI, Dpto. de Máquinas y Motores Térmicos, University of the Basque Country UPV/EHU (Spain), ⁽³⁾Grupo de Investigación GI-TENECO, Universidad de La Rioja (Spain).

- ***P30: Thermodynamic Modeling of a Membrane Dehumidification System***
John D. Bynum¹ and David E. Claridge² – ⁽¹⁾Eindhoven University of Technology, Eindhoven (The Netherlands), ⁽²⁾Texas A&M University & Energy Systems Laboratory, College Station, TX (USA)
- ***P31: Numerical analysis on the performance of two-stage desiccant wheel system***
Yuwei Zheng¹, Xiaohua Liu¹, Rang Tu² – ⁽¹⁾Department of Building Science, Tsinghua University, Beijing (China), ⁽²⁾School of mechanical engineering, University of Science and Technology Beijing, Beijing (China)
- ***P32: Model development and experimental parameter identification for biomass pellet boilers in buildings***
Jens Petzold, Daniel Büchner, Andreas Ortwein – Deutsches Biomasseforschungszentrum gemeinnützige GmbH (Germany)

NINTH SESSION – MODEL REDUCTION

- ***P33: Bottom-up modeling of the Belgian residential building stock: influence of model complexity***
Glenn Reynders^{1,2,3}, Jan Diriken^{1,3}, Dirk Saelens^{1,2} – ⁽¹⁾Energyville (Belgium), ⁽²⁾Building Physics Section, Civil Engineering Department, KU Leuven (Belgium), ⁽³⁾Unit Energy Technology, VITO (Belgium)
- ***P34: ISABELE: a Method for Performance Assessment at Acceptance Stage using Bayesian Calibration***
Pascal Schetelat and Remi Bouchie – Centre Scientifique et Technique du Bâtiment (France)
- ***P35: A practical and scalable inverse modeling approach for multi-zone buildings***
Jie Cai and James E. Braun – Ray W. Herrick Laboratory, Purdue University (USA)
- ***P36: Comparative analysis of model reduction methods applied to building simulation benchmarks***
Jordan Gauvrit, Guillaume Ansanay-Alex – Centre Scientifique et Technique du Bâtiment (France)

TENTH SESSION – SIMULATION ASSISTED ANALYSIS AND EVALUATION OF BUILDING ENERGY USE

- ***P37: Bottom-up modelling of the Belgian residential building stock: impact of building stock descriptions***
Christina Protopapadaki^{1,2}, Glenn Reynders^{1,2,3} and Dirk Saelens^{1,2} –
⁽¹⁾Building Physics section, KU Leuven (Belgium), ⁽²⁾Energyville (Belgium)
- ***P38: Dynamic exergy simulation coupled with thermoeconomic analysis to support retrofit decisions in non-domestic buildings***
Ivan Garcia Kerdan¹, Rokia Raslan² and Paul Ruyssevelt¹ – ⁽¹⁾Energy Institute, University College London, (UK), ⁽²⁾Institute for Environmental Design and Engineering, University College London, (UK)
- ***P39: The Potential of Air-Water Heat Pumps in a Belgian Residential Retrofit Context in relation to Future Electricity Prices***
Evelyn Heylen¹, Romain Jordens¹, Dieter Patteeuw², Lieve Helsen² –
⁽¹⁾Master Energy KU Leuven, Leuven (Belgium), ⁽²⁾Department of Mechanical Engineering, Division of Applied Mechanics and Energy Conversion (TME), Leuven, (Belgium)

CONCLUSIONS

Foreword

This 9th International Conference on System Simulation in Buildings has been the opportunity to gather researchers coming from 13 countries, sharing the last results of their research works. Some of the presented works were conducted in the frame of projects from the International Energy Agency's Energy in Buildings and Communities Programme (EBC).

In the name of the organizing committee, I would like to thank:

- The authors who wrote highly interesting papers reviewed afterwards by their peers.
- The members of the Scientific Committee who conducted an excellent reviewing of the papers, and contributed to maintain the high quality of the conference.
- The participants for the interesting and fruitful discussions they initiated during and after the presentations.
- The research and administrative team of the Thermodynamics Laboratory, and particularly François Randaxhe and Isabelle Cosyns, who made this event possible and successful.

I hope that the diffusion of the present proceedings will contribute, even to a small extent, to improving the energy performance of buildings by promoting the development of simulation tools and by sharing these tools among scientist and engineering offices.

I wish you a pleasant reading.

Vincent Lemort
Chairman of SSB 2014

Liège, March 31st 2015. Vincent Lemort

List of Participants

Aertgeerts	Arnout	KU Leuven	BEL
André	Philippe	Université de Liège	BEL
Ansanay	Guillaume	CSTB	FRA
Aparecida S.	Cleide	JCJ Energetics	BEL
Atam	Ercan	KU Leuven	BEL
Attia	Shady	Université de Liège	BEL
Bandos	Tatyana	Universidad del Pais Vasco	ESP
Bertagnolio	Stephane	Emerson Climate Technologies GmbH	BEL
Boisson	Pierre	CSTB	FRA
Bouche	Rémi	CSTB	FRA
Boydens	Wim	Studiebureau r. boydens nv	BEL
Buderus	Julian	T.H. Nürnberg Georg Simon Ohm	DEU
Buso	Tiziana	Politecnico di Torino	ITA
Braun	Jim	Purdue University	USA
D. Bynum	John	Eindhoven University of Technology	NED
Camisassi	Vittoria	Politecnico di Torino	ITA
Carmo	Carolina	Aalborg university	DNK
Carton	Julien	ICSEED	FRA
Corgnati	Stefano	Politecnico di Torino	ITA
Cuevas	Cristian	Universidad de Concepción	CHL
Daoud	Ahmed	Hydro-Québec (LTE)	CAN
Dechesne	Bertrand	Université de Liège (Labothap)	BEL
Dewallef	Pierre	Université de Liège	BEL
Dentel	Arno	T.H. Nürnberg Georg Simon Ohm	DEU
Dippel	Thomas	TEB GmbH	DEU
Dumont	Olivier	Université de Liège (Labothap)	BEL
Garcia Kerdan	Ivan	Energy Institute, University College London	GBR
Gendebien	Samuel	Université de Liège (Labothap)	BEL
Georges	Bernard	Université de Liège (Labothap)	BEL
Georges	Emeline	Université de Liège (Labothap)	BEL
Georges	Laurent	Norwegian University of Science and Technology	NOR
Hannay	Jules	JCJ Energetics	BEL

Helsen	Lieve	University of Leuven (Energyville - KU Leuven)	BEL
Heylen	Evelyn	KU Leuven	BEL
Jianjun	Xia	Tsinghua University	CHN
Johra	Hicham	Aalborg university	DNK
Jorissen	Filip	KU Leuven	BEL
Kegel	Martin	Canmet ENERGY/Natural Resources Canada	CAN
Kelly	Nick	University of Strathclyde	GBR
Kersken	Matthias	Fraunhofer Institute for Building Physics IBP	DEU
Lebrun	Jean	JCJ Energetics	BEL
Lemort	Vincent	Université de Liège (Labothap)	BEL
Lethe	Guillaume	CSTC – WTCB – BBRI	BEL
Madjidi	Madjid	Ingenieurbüro Madjidi	DEU
Masy	Gabrielle	Haute Ecole de la Province de Liège	BEL
Monfils	Stephane	University of Liege	BEL
Patteeuw	Dieter	KU Leuven	BEL
Parker	James	Leeds Metropolitan University	GBR
Parys	Wout	Building Physics Section, KU Leuven	FRA
Petzold	Jens	DBFZ gGmbH	DEU
Protopapadaki	Christina	KU Leuven	BEL
Randaxhe	Francois	Université de Liège (Labothap)	BEL
Ransy	Frederic	Université de Liège (Labothap)	BEL
Raslan	Rokia	The Bartlett School of Graduate Studies – UCL	GBR
Reynders	Glenn	Building Physics Section, KU Leuven	BEL
Robillart	Maxime	MINES ParisTech	FRA
Ruiz	Roberto	Université de Liège (Labothap)	BEL
Saelens	Dirk	Katholieke Universiteit Leuven	BEL
Schetelat	Pascal	CSTB	FRA
Schiefelbein	Jan	RWTH Aachen University, E.ON Energy	DEU
Heylen	Evelyn	KU Leuven	BEL
Soons	Frank	Eindhoven University of Technology	NED
Sourbron	Maarten	Campus De Nayer, KU Leuven	BEL
Stabat	Pascal	Ecole de Mines - ParisTech	FRA
Thomas	Sébastien	SECOLUX	BEL

Torrens Galdiz	Ignacio	Eindhoven University of Technology	NED
Van der Heijde	Bram	KU Leuven	BEL
Van Schijndel	Jos	Eindhoven University of Technology	NED
Veeken	John	Campus De Nayer, KU Leuven	BEL
Verhelst	Joachim	KU Leuven	BEL
Verhelst	Clara	3E	BEL
Wolfram	Stephan	T.H. Nürnberg Georg Simon Ohm	DEU
Xiaochen	Mao	Tsinghua University	CHN
Zhang	Kun	École Polytechnique de Montréal	CAN
Zheng	Yuwei	Tsinghua University	CHN
Ziviani	Davide	University of Gent	BEL

FIRST SESSION
**ADVANCED CONTROL OF
SYSTEMS IN BUILDINGS**

A Convex Approach to Energy Use Minimization of Buildings Equipped with Hybrid Ground-Coupled Heat Pump Systems

Ercan Atam, Damien Picard, Lieve Helsen

Department of Mechanical Engineering, KU Leuven, Celestijnelaan 300A, Leuven 3001, Belgium.

1. ABSTRACT

In this paper a convex approach through convexification is presented for non-convex optimal control and non-convex model predictive control based energy use minimization of buildings equipped with the hybrid ground-coupled heat pump systems. The original non-convex problems are convexified using a convex envelope approach. The results of convexified optimal control problem are compared with dynamic programming based optimal control, which is a global and closed-loop control approach. The comparison results show that the convex approximation of the optimal control problem gives almost global optimal results in terms of responses and cost criteria. The suggested method is especially useful for optimal/model predictive control or optimal design of energy-efficient buildings integrated with thermal systems, where the source and sink temperature dependent coefficient of performance of some thermal components introduces non-convexity into the system.

Keywords: Hybrid ground-coupled heat pumps, Convex optimization, Convex envelope, Optimal control, Nonlinear model predictive control.

2. NOMENCLATURE

Variables	Description
COP_{ch}	chiller coefficient of performance
COP_{hp}	heat pump coefficient of performance
COP_{pc}	passive cooler coefficient of performance
c_e	electricity price
c_g	gas price
J	total cost
t_c	control horizon
t_p	prediction horizon
t_s	sampling period
\dot{P}_{ch}	power used by chiller
\dot{P}_{gb}	power used by gas boiler power
\dot{P}_{hp}	power used by heat pump
\dot{P}_{pc}	power used by passive cooler
\dot{Q}_c	cooling load demand
\dot{Q}_{ch}	thermal energy extracted from the building through active cooling
\dot{Q}_{ext}	heat extracted from ground
\dot{Q}_{gb}	thermal energy supplied to the building by gas boiler
\dot{Q}_h	heating load demand
\dot{Q}_{hp}	thermal energy supplied to the building by the heat pump

\dot{Q}_{inj}	heat injected to ground
\dot{Q}_{net}	net heat injected to ground
\dot{Q}_{pc}	thermal energy extracted from the building through passive cooling
T_a	ambient air temperature
T_f	fluid mean temperature
η_{gb}	gas boiler efficiency

3. INTRODUCTION

In last decades, ground-coupled heat pumps (GCHP) and hybrid ground-coupled heat pumps (HybGCHP) combined with low-exergy heat emission systems received considerable attention (Chiasson, 2007)(Hackel et al., 2011)(Atam et al., 2013). This attention comes from having the potential to reduce the primary energy use related to space heating and cooling by 70% compared to conventional heating and cooling systems (DHC, 2014). For GCHP systems with vertical borehole heat exchangers (BHE), however, the large investment cost of the borefield represents a major bottleneck. This explains the trend towards compact, hybrid GCHP systems which combine smaller boreholes with supplementary heating or cooling devices such as gas-fired boilers and chillers. Although the design of a compact HybGCHP system is often driven by cost considerations to limit the drilling cost without compromising thermal comfort in the building, sometimes other reasons may also lead to HybGCHP systems, such as limited drilling area for boreholes, the specific ground characteristics, regulation or too high imbalance of the thermal load. Under normal conditions, the efficiency of the additional heating or cooling devices being lower, a long-term cost-optimal operation boils down to maximizing the use of the heat pump and passive cooling in covering the heating and cooling loads within certain temperature constraints for the heat carrier fluid. Although we have this kind of a qualitative nature of optimal control policy in our mind, determination of quantitative values of optimal load sharing between components requires an intelligent control strategy when multiple operational constraints such as maximum machine power and temperature bounds of the heat carrier fluid have to be taken into account.

A rule-based controller that uses the most efficient machine at each time step might be the simplest algorithm to use. This kind of controller is, however, not able to make full use of the temperature constraints of the heat carrier fluid. For example Cullin et al. (2010), proposed rule-based control strategies coupled with a set of parameters to optimize the system performance using a simulation based optimization method. Multiple simulations with different initial-boundary conditions and heating-cooling demand scenarios have been considered and the optimization parameters are optimized either manually or through a simulation-coupled optimization program such as GenOpt (Wetter, 2001) until satisfactory performance was observed in the simulations. The main drawbacks of these approaches are that firstly, they suffer from a mathematical model-based optimization/control and hence the suggested rule-based control methods may be very suboptimal strategies in general and secondly, the number of variables to be optimized in a rule-based control is restricted most of the time since few parameters are chosen to characterize the optimal control performance.

Ridder et al. (2011) and Verhelst (2012) used, in contrast to rule-based approaches, mathematical model-based control methods, which allow global optimization. However, they are based on some simplifications and/or some unrealistic assumptions introduced during the controller design. For example, Ridder et al. (2011) used dynamic programming. Dynamic programming is a powerful method since it is a closed-loop, global optimal control algorithm. However, the model used in Ridder et al. (2011) for dynamic programming is a very simple

first-order model for the ground mean temperature. The chosen sampling period for the system is one week, which is very long since typical control actions for buildings may require sampling times in order of minutes or hours. Moreover, the realization of the designed controller requires the measurement of the underground field temperature, for which measurement may be either difficult or non-accurate. As a result, the approach of Ridder et al. (2011) involves both some modeling simplifications and a hard-to-realize implementation. As to Verhelst (2012), a linear optimal control method is applied. The simplification made in that work is that the coefficients of performance (COP) for heat pump and chiller were taken to be constant, in contrast to being functions of source and sink temperatures. COP values were taken to be constant because otherwise the optimization problem is a nonlinear, non-convex problem, which cannot be solved over a couple of years especially when short sampling times are considered. Although a mathematical model-based optimal control was considered, the simplifications of taking the mentioned COPs as constant values without a formal justification restricts the validity of the work of Verhelst (2012). Moreover, the model used for control and emulator are the same, which eliminates the impact of model mismatch and therefore limits the generality of the approach followed by Verhelst (2012).

The optimal control of HybGCHP systems for total energy use minimization is a nonlinear, non-convex optimization problem due to the appearance of heat pump coefficient of performance in the cost function. This makes the optimization problem difficult for short sampling periods in the order of minutes or hours because short sampling periods increase the number of decision variables considerably. Current solvers have difficulty in solving a non-convex, nonlinear optimization problem with a large number of decision variables. Even in case of a solution, a global minimum cannot be guaranteed. An approximate solution to the above problem is the convex relaxation of the nonlinear, non-convex optimization problem through the use of a convex envelope approach. The convex envelope of a function is the largest convex function majorized by that function. Approximation of the non-convex terms by their convex envelopes will transform the optimization problem to an approximate problem which is convex and for which the global minimum can be found, if the problem is feasible. In convex optimization problems, a local minimum is a global minimum. Although the calculation of a convex envelope for a general multi-variable function is non-deterministic polynomial-time hard, there exist analytical formulas for a bilinear function or a rational function of two variables, the type of functions encountered in energy use minimization of HybGCHP systems. In this paper, the use of a convex relaxation method is given for non-convex optimal control and non-convex model predictive control of HybGCHP systems, by replacing the non-convex term with its convex envelope. The results of optimal control case are compared with dynamic programming control results (an approximate global optimal control algorithm) to assess the optimality of the convex envelope approach. The proposed approach gives promising results for optimal control of HybGCHP systems. The utilization of convex envelope approach for nonlinear, non-convex model predictive control formulation is also illustrated. Since model predictive control does not see the whole control period over which the system is controlled, it was not perfectly meaningful to compare with dynamic programming which sees the whole control period.

The rest of paper is structured as follows. In Section 2, the HybGCHP system is described with the associated operational constraints. Section 3 deals with the formulation of the non-convex optimal control problem for the total energy use minimization for HybGCHP systems. The convexification of the optimization problem starting from basic elements of convex optimization and the convex envelope concept is given in Section 4. The dynamic programming-based control formulation and solution of the problem is given in Section 5 where dynamic programming is used as the base reference for comparing the results. Section 6

discusses the applicability of the proposed method in the context of nonlinear, non-convex model predictive control. Finally, Section 7, concludes with the main findings of this study.

4. GCHP SYSTEM DESCRIPTION & OPERATIONAL CONSTRAINTS

The hybrid system is presented in Figure 1 and consists of a heat pump, a gas-fired boiler, a passive cooler and an air-cooled chiller. It is assumed that the heat demand (\dot{Q}_h) is provided by heat pump and boiler and the cold demand (\dot{Q}_c) is provided by passive cooler (using a heat exchanger instead of an active chiller) and chiller. The expressions for the efficiencies (η) and coefficient of performance (COP) of all components presented in Figure 1 are given by

$$COP_{hp} = \frac{\dot{Q}_{hp}}{P_{hp}}, \eta_{gb} = \frac{\dot{Q}_{gb}}{P_{gb}}, COP_{pc} = \frac{\dot{Q}_{pc}}{P_{pc}}, COP_{ch} = \frac{\dot{Q}_{ch}}{P_{ch}},$$

where P_{hp} denotes the electricity consumption of the heat pump compressor and the power consumed by circulation pumps from the borefield side, P_{gb} denotes the rate of primary energy use of the gas boiler, P_{pc} the electricity power used for the circulation pumps of the passive cooling installation and finally P_{ch} denotes the electricity power consumption of the chiller compressor and the circulation pumps of the cooling tower.

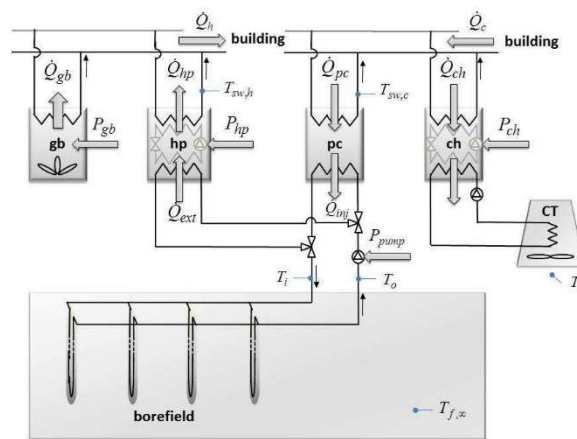


Figure 1: Schematic presentation of hybrid system: heat pump, gas-fired boiler, passive cooler and chiller.

The coefficients of performance given by the above expressions depend on the temperatures of the source and the emission system, as expressed by

$$COP_{hp} = f_{hp}(T_f, T_{sw,h}), COP_{pc} = f_{pc}(T_f, T_{sw,c}), COP_{ch} = f_{ch}(T_a, T_{sw,c}),$$

where $T_{sw,h}$, $T_{sw,c}$ represent the water supply temperature for heating and water supply temperature for cooling, respectively. T_a is the ambient temperature and T_f is the circulating fluid mean temperature. The gas boiler efficiency, η_{gb} , is given a constant value of unity. The electricity price $c_e(t)$ varies in the range [0.09, 0.15] euro/(kWh) and $c_g(t)$ is taken 0.06 euro/(kWh) (Verhelst, 2012). Here, COPs and efficiencies are fitted to TRNSYS data (TRNSYS, 1998):

$$COP_{hp}(t) = \alpha_0 + \alpha_1 T_f(t), COP_{ch}(t) = \beta_0 + \beta_1 T_a(t) + \beta_2 T^2(t), COP_{pc} = 12 \quad (1)$$

where COP_{hp} and COP_{ch} are fitted for a supply water temperature of $T_{ws,h} = 40^\circ\text{C}$ for heating and a supply water temperature of $T_{ws,c} = 18^\circ\text{C}$ for cooling. Using $c_e(t)$ and $c_g(t)$, the optimal

control problem to be solved to minimize the energy use cost function for HybGCHP system operation over a time period $[t_0, t_f]$ is

$$J \cong \sum_{k=0}^{N-1} t_s \left[c_e(k) \left(\frac{\dot{Q}_{hp}(k)}{COP_{hp}(k)} + \frac{\dot{Q}_{pc}(k)}{COP_{pc}(k)} + \frac{\dot{Q}_{ch}(k)}{COP_{ch}(k)} \right) + c_g(k) \frac{\dot{Q}_{gb}(k)}{\eta_{gb}} \right] \quad (2)$$

where t_s is the sampling period and “k” is the sampling instant. The cost function presented by Eq. (2) has to be minimized under operational temperature constraints, heat/cold demands, maximum net heat injected in the ground and power constraints. Next, we will discuss these constraints and present their expressions.

4.1 Heat & cold demand satisfaction and circulating fluid temperature bounds

The building loads should be satisfied with some acceptable violation margins:

$$\dot{Q}_h(t) - \varepsilon_{h-l}(t) \leq \dot{Q}_{hp}(t) + \dot{Q}_{gb}(t) \leq \dot{Q}_h(t) + \varepsilon_{h-u}(t) \quad (3a)$$

$$\dot{Q}_c(t) - \varepsilon_{c-l}(t) \leq \dot{Q}_{pc}(t) + \dot{Q}_{ch}(t) \leq \dot{Q}_c(t) + \varepsilon_{c-u}(t) \quad (3a)$$

where $\dot{Q}_h(t)$ and $\dot{Q}_c(t)$ are the building heat and cold demands, respectively, $\varepsilon_{h-l}(t)$, $\varepsilon_{h-u}(t)$ are time-dependent lower and upper violation margins for heating demand and $\varepsilon_{c-l}(t)$, $\varepsilon_{c-u}(t)$ the lower and upper violation margins for cooling demand. Note that \dot{Q}_h and \dot{Q}_c are assumed to be given. The cooling of a building requires heat injection to ground during summer. This increases the ground temperature towards winter, which, in turn, increases COP_{hp} . However, the ground temperature, which is represented indirectly by T_f , should be kept below the water supply temperature, $T_{ws,c}$, for passive cooling of the building. Similarly, heating of a building requires heat extraction from the ground. This decreases the ground temperature towards summer, which, in turn, increases COP_{pc} . However, again the ground temperature represented indirectly by T_f should not decrease to a value below freezing point to avoid frost problems. All these aspects require to put lower and upper bounds on T_f :

$$T_{f-min}(t) < T_f(t) < T_{f-max}(t) \quad (4)$$

4.2 Heat exchange with ground

Heat extraction/injection from/to the ground and the net heat transfer with the ground are given by the following equations

$$\dot{Q}_{ext}(t) = \frac{COP_{hp}(t) - 1}{COP_{hp}(t)} \dot{Q}_{ext}(t), \quad \dot{Q}_{inj}(t) = \frac{COP_{pc}(t) - 1}{COP_{pc}(t)} \dot{Q}_{pc}(t), \quad (5)$$

$$\dot{Q}_{net}(t) = \dot{Q}_{inj}(t) - \dot{Q}_{ext}(t).$$

To limit the degree of thermal build up or depletion in the ground, the following bound may be put on the net annual heat transfer with the ground

$$\left| \sum_{1year} \dot{Q}_{net} \right| < \dot{Q}_{max}. \quad (6)$$

4.3 Borehole Dynamics

In this section the borefield system shown in Figure 1 is modeled as a single equivalent borehole which is sized according to the specified building loads to be considered in the next sections.

This is an approximation neglecting the interaction between different boreholes in a borefield. In the equivalent diameter approach, the heat transfer from the U-tube is approximated by the heat transfer from a single pipe with a hypothetical diameter through which the heat exchanging fluid circulates. The objective is the determination of the circulating fluid mean temperature over the borehole length, $T_f(t)$, corresponding to a net (injected - extracted) heat profile per unit length, u_{net} . The one-dimensional radial conduction heat transfer equation is considered. Next, the grout and ground regions are divided into thermal nodes and an energy balance for the equivalent borehole is considered. Using the finite volume technique, the following large-scale dynamic model is obtained

$$x_e(k+1) = A_e(p)x_e(k) + B_e(p)u_{net}(k), \quad y(k) = T_f(k) = C_e x_e(k) \quad (7)$$

where $x_e = [T_f \ T_{g1} \ \dots \ T_{g_{n_g}} \ T_{s1} \ \dots \ T_{s_{n_s}}]^T$. Here, T_f is the circulating fluid mean temperature, $[T_{g1} \ \dots \ T_{g_{n_g}}]^T$ are grout nodal temperatures, $[T_{s1} \ \dots \ T_{s_{n_s}}]^T$ are soil (ground) nodal temperatures and p is the know parameters vector including thermal, physical and other parameters of the system (diffusivities α_g , α_s , conductivities k_g , k_s , different radii r_{fg} , r_{gs} , discretization step sizes, etc.) and u_{net} is the net heat injected to the ground. A full derivation of (7) can be found in Atam (2013).

The next step is obtaining a reduced-order model from the large-scale model given in Eq. (7) which has 506 states. As a model-order reduction technique, we use the Proper Orthogonal Decomposition (POD) method (Holmes et al., 1996)(Astrid, 2004).

The reduced-order model is given by

$$x_r(k+1) = A_r x_r(k) + B_r u_{net}(k), \quad y(k) = C_r x_r(k) \quad (8)$$

and details can be found in Atam (2013) The model order of the chosen reduced-order model is four. Figure 2 shows mean and maximum absolute mismatch error for T_f of reduced-order models with respect to that of large-scale model as a function of model order. The results are based on simulations of models with a multi- sine input signal consisting of 30 sines. From Figure 2 we get the maximum absolute mismatch error for T_f around 0.63°C and the mean absolute mismatch error around 0.14°C for a reduced-order model of fourth order.

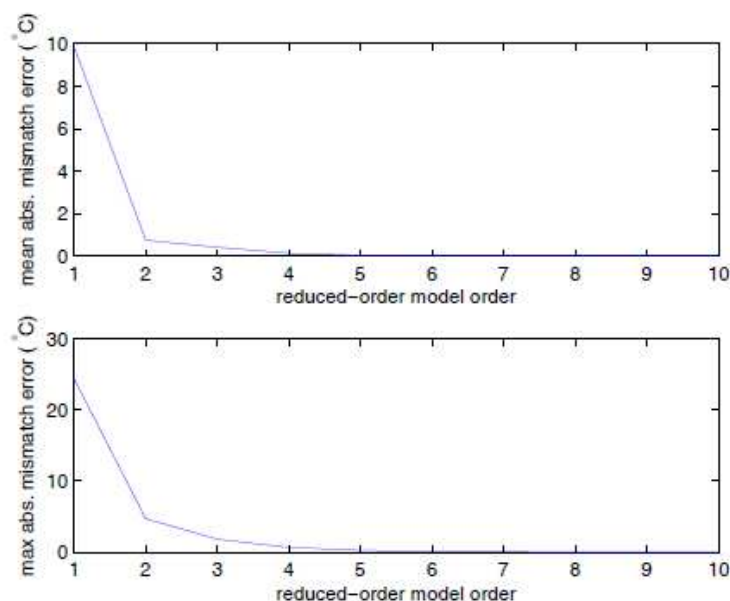


Figure 2: Reduced-order model T_f mismatch error as a function of model order.

5. NONLINEAR, NONCONVEX OPTIMAL CONTROL PROBLEM FOR TOTAL ENERGY USE MINIMIZATION

Letting $u_1 \triangleq \dot{Q}_{hp}$, $u_2 \triangleq \dot{Q}_{gb}$, $u_3 \triangleq \dot{Q}_{ch}$, $u_4 \triangleq \dot{Q}_{pc}$, $\tilde{u}_1 \triangleq \frac{\dot{Q}_{hp}}{COP_{hp}}$, $u_{net} \triangleq \dot{Q}_{net}$, $COP_{pc} = 12$,

$\eta_{gb} = 1$, we obtain the following optimization problem with the associated constraints from the related equations defined before in Section 4.

$$\text{mimimize } \sum_{k=0}^{N-1} t_s \left\{ c_e(k) \left(\tilde{u}_1(k) + \frac{u_4(k)}{12} + \frac{u_3(k)}{\beta_0 + \beta_1 T_a(k) + \beta_2 T_a^2(k)} \right) + c_g(k) u_2(k) \right\} \quad (9a)$$

subject to

$$\dot{Q}_h(k) - \varepsilon_{h-l}(k) \leq u_1(k) - u_2(k) \leq \dot{Q}_h(k) - \varepsilon_{h-u}(k), \text{ (heating demand satisfaction)} \quad (9b)$$

$$\dot{Q}_c(k) - \varepsilon_{c-l}(k) \leq u_3(k) - u_4(k) \leq \dot{Q}_c(k) - \varepsilon_{c-u}(k), \text{ (cooling demand satisfaction)} \quad (9c)$$

$$u_{net}(k) = \frac{13}{12} u_4(k) - u_1(k) + u_1(k), \text{ (expression for } u_{net}(k)) \quad (9d)$$

$$x_r(k+1) = A_r x_r(k) + B_r u_{net}(k), \text{ (borehole state-space dynamics)} \quad (9e)$$

$$T_f(k) = C_r x_r(k), \text{ (output equation)} \quad (9f)$$

$$T_{f-min} < T_f(k) = C_r x_r(k) < T_{f-max}, \text{ (circulating fluid temperature bounds)} \quad (9g)$$

$$\left| \sum_{k=0}^{N-1} u_{net}(k) \right| < \dot{Q}_{max}, \text{ (bounding the total net heat injected to the ground)} \quad (9h)$$

$$COP_{hp} = \alpha_0 + \alpha_1 C_r x_r(k), \text{ (heat pump coefficient of performance)} \quad (9i)$$

$$u_1(k) = COP_{hp}(k) \tilde{u}_1(k), \text{ (relation between } u_1, COP_{hp} \text{ and } \tilde{u}_1) \quad (9j)$$

With this formulation, the nonlinearity of the optimal control problem comes from Eq. (9j): a bilinear term. Note that the rational term including T_a in the cost function does not create any nonlinearity because T_a is not a decision variable or a function of decision variables. In the next subsection, Eq. (9j) will be replaced by its convex approximation.

6. CONVEXIFIED OPTIMIZATION PROBLEM

In this section, before formulating a convex approximation of the optimization problem presented in Eq. (9), we start with the definitions of basic ingredients of convex optimization problems.

6.1 Overview of convex optimization

In words, a convex optimization problem is simply a convex function to be minimized over a convex set.

Definition 4.1 (Convex Optimization Problem: less general form). Given a convex function f , convex functions g_i , affine functions h_i and the decision variable vector x , the associated less general convex optimization problem is defined as

$$\text{mimimize } f(x) \quad (10a)$$

subject to

$$g_i(x) \leq 0, i = 1, \dots, p. \quad (10b)$$

$$h_i(x) \leq 0, i = 1, \dots, r. \quad (10c)$$

6.2 Convex Envelope

Next, the concept of convex envelope is defined.

Definition 4.2 (Convex envelope). Given a continuous function $k(x)$, its convex envelope, denoted by $\text{conv } k(x)$, over a convex set S is defined as the pointwise supremum of all convex functions which are majorized by $k(x)$:

$$\text{conv } k(x) = \sup\{r(x) \mid r \text{ convex and } r(y) < k(y) \quad \forall y \in S\}.$$

In other words, $\text{conv } k$ is the largest convex function such that $\text{conv } k(x) \leq k(x)$ for $x \in S$.

A positive bilinear function $f(x_1, x_2) = x_1x_2$ has the convex envelope

$$\text{conv } f(x_1, x_2) = \max\{\underline{x}_1x_2 + \underline{x}_2x_1 - \underline{x}_1\underline{x}_2, \bar{x}_1x_2 + \bar{x}_2x_1 - \bar{x}_1\bar{x}_2\} \quad (11)$$

over the rectangular region $S = [\underline{x}_1, \bar{x}_1] \times [\underline{x}_2, \bar{x}_2]$, which is called McCormick envelope (McCormick, 1976). Similarly, the negative bilinear function $f(x_1, x_2) = -x_1x_2$ has the convex envelope (McCormick, 1976)

$$\text{conv } f(x_1, x_2) = \max\{-\bar{x}_1x_2 - \underline{x}_2x_1 + \bar{x}_1\underline{x}_2, -\underline{x}_1x_2 - \bar{x}_2x_1 + \underline{x}_1\bar{x}_2\} \quad (12)$$

over the rectangular region $S = [\underline{x}_1, \bar{x}_1] \times [\underline{x}_2, \bar{x}_2]$.

Using (11) and (12), the equality constraint $w = f(x_1, x_2) = x_1x_2$ is convexified by

$$\begin{aligned} w &\geq \underline{x}_1x_2 + \underline{x}_2x_1 - \underline{x}_1\underline{x}_2, & w &\geq \bar{x}_1x_2 + \bar{x}_2x_1 - \bar{x}_1\bar{x}_2 \\ w &\geq \bar{x}_1x_2 + \underline{x}_2x_1 - \bar{x}_1\underline{x}_2, & w &\geq \underline{x}_1x_2 + \bar{x}_2x_1 - \underline{x}_1\bar{x}_2 \end{aligned} \quad (13)$$

6.3 Convexified optimization problem

The convexified optimization problem is the same problem as in Eq. (9) except Eq. (9j) is replaced by (13) with

$$w = u_1(k), \quad x_1 = \text{COP}_{hp}, \quad x_2 = \tilde{u}_1(k)$$

Note that all other constraints are already/or can be easily put into the form given in Eq. (10). The lower bound for the coefficient of performance of heat pump, COP_{hp} , is set to 2 and the upper bound, $\overline{\text{COP}_{hp}}$, is set to 6. Similarly, the lower bound of $\tilde{u}_1 = \dot{Q}_{hp}/\text{COP}_{hp}$, $\underline{\tilde{u}_1}$, is set to 0W and the upper bound, \tilde{u}_1 , is set to 3000W, assuming a maximum heat pump power of 6000W.

6.4 Bilinear versus rational function

We formulated the optimization problem in Eq. (9) such that the resulting non-linearity was of type bilinear. It is possible to formulate the problem in such a way that the nonlinearity is a rational function $f(x_1, x_2) = \frac{x_1}{x_2}$ over a positive rectangle in the first quadrant $[a_1, a_2] \times [b_1, b_2]$. In this case, the analytical formula for the convex envelope is given as (Locatelli et al., 2013)

$$\text{conv } f(x_1, x_2) = \frac{b_1 - x_1}{b_1 - a_1} \frac{a_1}{\max\left\{a_2, \frac{b_2 - x_2}{b_1 - x_1} (a_1 - x_1) + x_2, \frac{x_2\sqrt{a_1}(b_1 - a_1)}{(b_1 - x_1)\sqrt{a_1} + (x_1 - a_1)\sqrt{b_1}}\right\}} \quad (14)$$

$$+ \frac{x_1 - a_1}{b_1 - a_1} \frac{b_1}{\min \left\{ \frac{x_2 - a_2}{x_1 - a_1} (b_1 - x_1) + x_2, b_2, \frac{x_2 \sqrt{b_1} (b_1 - a_1)}{(b_1 - x_1) \sqrt{a_1} + (x_1 - a_1) \sqrt{b_1}} \right\}}$$

6.5 Solution of the convexified problem

The optimization problem is coded using YALMIP (Lofberg, 2014) under MATLAB and calling CPLEX (IBM, 2014) as solver. Note that in convex optimization problems, any local minimum is also a global minimum. This nice property makes convex optimization formulations very attractive.

6.6 Results for convexified optimization problem

The results for the convexified optimization problem are shown in Figure 3. Simulations are run for a duration of one year and with a sampling period of 4 hours. Figure 3(a) shows the time evolution of the mean temperature of the circulating fluid (T_f), Figure 3(b) shows the heat pump power and heating demand (\dot{Q}_{hp} , \dot{Q}_h), Figure 3(c) shows the chiller power and cold demand (\dot{Q}_{ch} , \dot{Q}_c) and finally Figure 3(d) shows the evolution of accumulated cost (J). These results will be compared with dynamic programming results in Section 5.

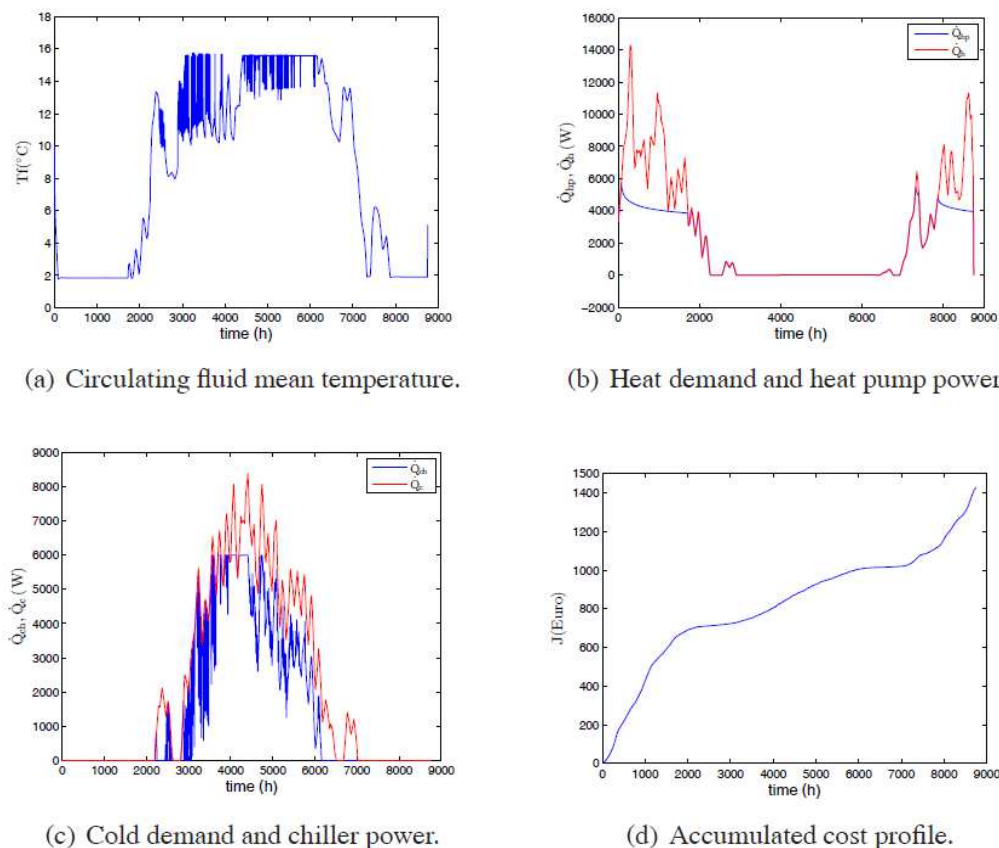


Figure 3: Controlled system variables for convexified optimization problem.

7. DYNAMIC PROGRAMMING-BASED OPTIMAL CONTROL

Dynamic programming is a closed-loop, global optimal control method (global optimal up to approximations due to state-input gridding and interpolations). It is based on the “principle of optimality” (Kirk, 1970) which simply says that in a multi-stage process whatever the previous states are, the remaining decisions must be optimal with regard to the state following from the

current state. This principle allows the optimal control problem of a K -stage process to be recursively formulated starting from the last stage. If g denotes the function inside the summation of the cost function J in (9a) and x, u, w states, inputs and measurable disturbances, respectively, then

$$J_{N-K,N}^*(x(N-K)) = \min_{u(N-K)} \{g(x(N-K), u(N-K), w(N-K))\} + J_{N-(K-1),N}^*(x(N-K), u(N-K), w(N-K)), \quad (15)$$

where $J_{N-K,N}^*$ is the optimal cost of the K -stage policy starting from stage $N-K$ to the final stage N and $J_{N-(K-1),N}^*$ is the optimal cost of the $K-1$ -stage policy. To start with the algorithm, we set $J_{N,N}^* = 0$, which is the cost stage number zero, $K = 0$. For dynamic programming-based control methods, the most important issue is to have an accurate model with minimum number of states and inputs due to the famous curse of dimensionality problem (Kirk, 1970)(Bertsekas, 2000). As a result, the optimization problem given by Eq. (9) will be equivalently reformulated with two inputs instead of four. (Kirk, 1970)(Bertsekas, 2000) can be referred for details on dynamic programming.

The requirement of heating and cooling load satisfaction gives (ignoring violation flexibilities)

$$\dot{Q}_{gb}(k) = \dot{Q}_h(k) - \dot{Q}_{hp}(k), \quad (16a)$$

$$\dot{Q}_{pc}(k) = \dot{Q}_c(k) - \dot{Q}_{ch}(k). \quad (16a)$$

Then, the expression inside the summation in the cost function (2) becomes

$$g(\dot{Q}_{hp}, \dot{Q}_{ch}, \dot{Q}_h, \dot{Q}_c, COP_{hp}, COP_{ch}, c_e, c_g) = t_s \left[\frac{c_e(k)}{COP_{hp}(k)} + \frac{c_g(k)}{\eta_{gb}} \right] \dot{Q}_{hp}(k) + t_s \left[\frac{c_e(k)}{COP_{ch}(k)} + \frac{c_e(k)}{COP_{pc}} \right] \dot{Q}_{cp}(k) + t_s \left[\frac{c_g(k)}{\eta_{gb}} \dot{Q}_h + \frac{c_e(k)}{COP_{pc}} \dot{Q}_c \right] \quad (17)$$

To put a constraint on $\dot{Q}_f = C_r x_r$, we prefer to transform the borehole state dynamics in reduced-states as $\tilde{x}_r = T x_r$, where

$$T = \begin{pmatrix} C_r \\ 0_{3 \times 1} & I_3 \end{pmatrix} \quad (18)$$

such that $\tilde{x}_{r1} = C_r x_r = y = T_f$. The reason for such transformation is the fact that this allows an easy use of an existing dynamic programming toolbox (ETH, 2014)

Then, the reduced-order transformed borehole state-space dynamics becomes

$$\tilde{x}_r(k+1) = \tilde{A}_r \tilde{x}_r(k) + \tilde{B}_r u_{net}(k), \quad y(k) = T_f(k) = \tilde{x}_{r1}(k), \quad (19)$$

so that the first state becomes output and hence the circulating fluid temperature bounds can be put on the first state. The optimization problem to be solved by dynamic programming is as follows:

$$\min \sum_{k=0}^{N-1} g(\dot{Q}_{hp}, \dot{Q}_{ch}, \dot{Q}_h, \dot{Q}_c, COP_{hp}, COP_{ch}, c_e, c_g) \quad (20a)$$

subject to

$$\tilde{x}_r(k+1) = \tilde{A}_r \tilde{x}_r(k) + \tilde{B}_r u_{net}(k), \text{ (borehole state-space dynamics)} \quad (20b)$$

$$T_{f-min} < T_f(k) = x_{r1}(k) < T_{f-max}, \text{ (circulating fluid temperature bounds)} \quad (20c)$$

$$|\sum_{k=0}^{N-1} u_{net}(k)| < \dot{Q}_{max}, \text{ (bounding the total net heat injected to the ground)} \quad (20d)$$

$$COP_{hp}(k) = \alpha_0 + \alpha_1 \tilde{x}_{r_1}(k), \text{ (heat pump coefficient of performance)} \quad (20e)$$

$$u_{net}(k) = \frac{13}{12} [\dot{Q}_c - \dot{Q}_{ch}] - \frac{COP_{hp}^{-1}}{COP_{hp}} \dot{Q}_{hp}, \text{ (expression for } u_{net}(k)) \quad (20f)$$

Note that for $g(x, u, w)$ in (17), we have $u = [\dot{Q}_{hp} \ \dot{Q}_{ch}]^T$ and $w = [\dot{Q}_h, \dot{Q}_c, COP_{ch}, c_e, c_g]^T$ and COP_{hp} depends on the state \tilde{x}_{r_1} .

Dynamic programming is applied to (20). Typically in dynamic programming, the feasible states and feasible inputs are gridded into quantized values and then at a given stage with a chosen feasible state value, all possible quantized inputs are tried until the minimum of (20a) is determined at that stage. This is done for all feasible gridded states. Hence, the dynamic programming control algorithm is a *closed-loop* and *global optimal* control algorithm (global optimal up to the approximations due to state-input gridding and interpolations). As mentioned before, for dynamic programming-based control methods, the most important issue is to have an accurate model with minimum number of states/inputs due to the curse of dimensionality problem. The nonlinearity of the model is not an issue for dynamic programming. Interpolation is required when the predicted states are not the gridded states.

In the optimal control problem, the control input range for both \dot{Q}_{hp} and \dot{Q}_{ch} is taken to be $[0, 6000]$ W and is gridded into 60 points. The range for output y is taken as $[0.5, 15.5]$ °C and it is gridded into 50 points. All other transformed states of the reduced-order model are also divided into 50 grid points. The control results are shown in the next subsection.

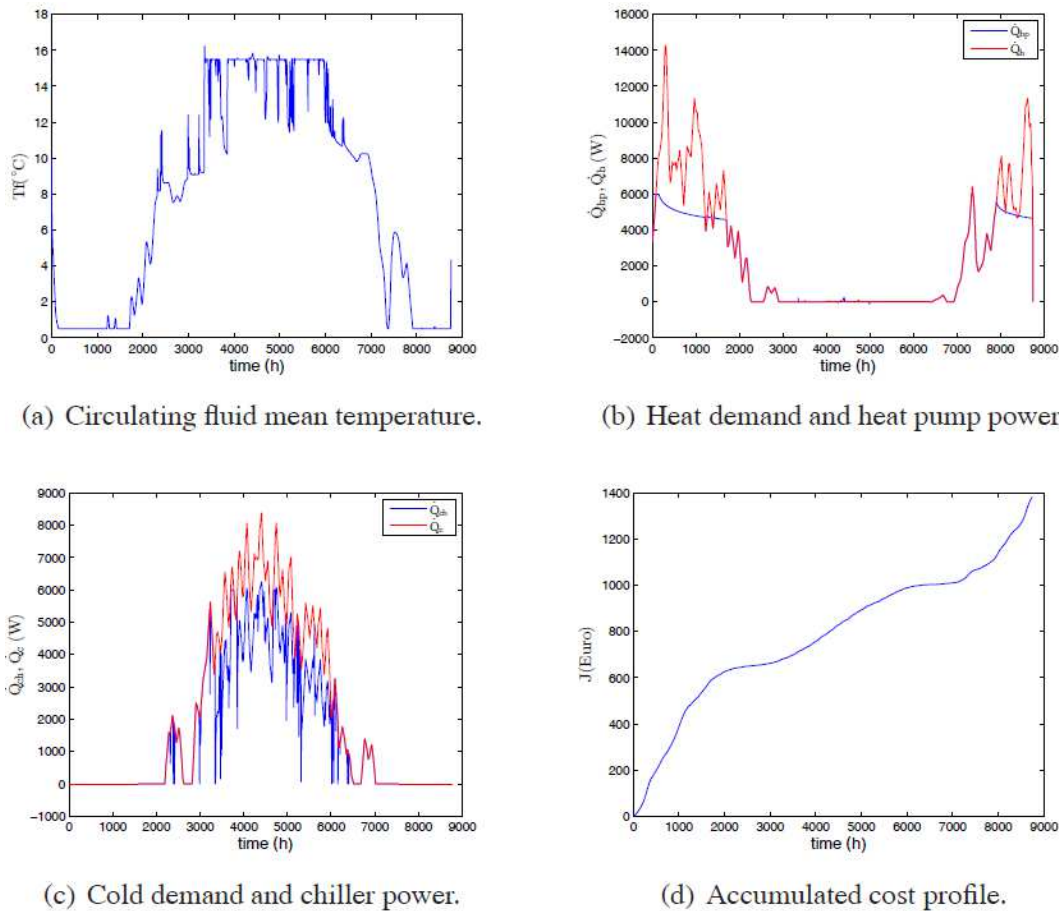


Figure 4: Controlled system variables for dynamic programming-based control.

7.1 Dynamic Programming Results

The results for dynamic programming are shown in Figure 4. When the results of the convexified solution in Figure 3 are compared to these of Figure 4, we see that they are close to each other, except that for the convexified problem the circulating fluid is more oscillatory around the upper temperature bound, which is due to the more oscillatory action of the chiller. This oscillatory behaviour of chiller is caused by the involved convex approximation. The cost profiles are almost the same.

8. APPLICATION OF THE PROPOSED METHOD IN NMPC

The nonlinear, non-convex model predictive control (NMPC) problem is shortly described as follows. Given the borehole dynamics

$$x_r(k+1) = A_r x_r(k) + B_r u_{net}(k), \quad y(k) = C_r x_r(k), \quad (21)$$

the objective of NMPC is the minimization of

$$\text{mimimize} \sum_{i=k}^{k+t_p} t_s \left\{ c_e(i) \left| \left(\hat{u}_1(i) + \frac{\hat{u}_4(k)}{12} + \frac{\hat{u}_3(i)}{\beta_0 + \beta_1 T_a(i) + \beta_2 T_a^2(i)} \right) + c_g(i) \hat{u}_2(i) \right\} \quad (22)$$

subject constraints

$$\dot{Q}_h(k) - \varepsilon_{h-l}(k) \leq \hat{u}_1(k) - \hat{u}_2(k) \leq \dot{Q}_h(k) - \varepsilon_{h-u}(k), \text{ (heating demand satisfaction)} \quad (23a)$$

$$\dot{Q}_c(k) - \varepsilon_{c-l}(k) \leq \hat{u}_3(k) - \hat{u}_4(k) \leq \dot{Q}_c(k) - \varepsilon_{c-u}(k), \text{ (cooling demand satisfaction)} \quad (23b)$$

$$\hat{u}_{net}(k) = \frac{13}{12} \hat{u}_4(k) - \hat{u}_1(k) + \hat{u}_1(k), \text{ (expression for } \hat{u}_{net}(k) \text{)} \quad (23c)$$

$$T_{f-min} < \hat{T}_f(k) = C_r \hat{x}_r(k) < T_{f-max}, \text{ (circulating fluid temperature bounds)} \quad (23d)$$

$$\left| \sum_{k=0}^{N-1} \hat{u}_{net}(k) \right| < \dot{Q}_{max}, \text{ (bounding the total net heat injected to the ground)} \quad (23e)$$

$$\widehat{COP}_{hp}(k) = \alpha_0 + \alpha_1 C_r \hat{x}_r(k), \text{ (heat pump coefficient of performance)} \quad (23f)$$

$$\hat{u}_1(k) = \widehat{COP}_{hp}(k) \hat{u}_1(k), \text{ (relation between } \hat{u}_1, \widehat{COP}_{hp} \text{ and } \hat{u}_1(k) \text{)} \quad (23g)$$

where

$$\hat{x}_r(k+1) = A_r \hat{x}_r(k) + B_r \hat{u}_{net}(k), \text{ with } \hat{x}_r(k) = x_r(k). \quad (23h)$$

and

$$\hat{u}_x(s) = \hat{u}_x(k+t_c), \quad k+t_c \leq s \leq k+t_p, \quad t_c \leq t_p, x = 1, \dots, 4, \quad (24a)$$

$$\hat{u}_{net}(s) = \hat{u}_{net}(k+t_c), \quad k+t_c \leq s \leq k+t_p, \quad t_c \leq t_p. \quad (24b)$$

Here t_p and t_c are called prediction and control horizons, respectively. The hat notation denotes the internal control variables (the calculated control inputs) and the resulting predicted states or variables which are functions of states and inputs over the given horizons. A distinction between the real system variables and the variables in the predictive controller design (denoted with a hat) is necessary because the calculated inputs and the predicted values may not be the same as the ones in the real time controlled system. The crossed out term (23e) means that this constraint cannot be applied in NMPC because NMPC does not see all the future. As we see, the NMPC problem is in a fact a kind of optimal control problem over a shorter horizon. As a result, for the application of the proposed convexification to NMPC, the convexification of

(23f) is done, after which the NMPC becomes convex model predictive control. Here, we do not present the results for convexified NMPC, rather we just wanted to show how the proposed idea can be used in the context of NMPC.

9. CONCLUSION

In this paper a convexification approach using convex envelopes for hard-to- solve nonlinear, non-convex optimization problems involving rational and/or bi- linear terms of decision variables is proposed for optimal/model predictive control- based total energy use minimization of buildings using hybrid ground-coupled heat pump systems. The results presented are for an idealized optimal control case: building interaction ignored, loads as input, constant COPs for everything except the heat pump and simplified borehole model. Rather than going a through detailed application, the objective was to show how the convexification ideas are used in the considered control frameworks.

The results of the convexified optimal control problem were compared to dynamic programming based control results. The results of the proposed method were close to (in terms of dynamic trends, global cost) these of dynamic programming, which verifies the effectiveness of the proposed method. To the authors' best knowledge, the proposed idea is the first in the field of optimization or control of energy efficient buildings equipped with thermal systems. The overall message of this paper is that given a nonlinear, non-convex optimization/control problem of thermal systems, the first step should be to analyse the given system in terms of the nonlinear, non-convex terms and then investigate whether convex envelopes for the associated terms exist or not. If they exist, then these terms should be replaced with their convex approximations, thus approximating the original non- linear, non-convex optimization/control problem by a convex one. Note, however, that analytical convex approximations exist only for a set of non-convex functions. Last but not least, in general convexified optimization results are better than linearized optimization results but are not as good as global optimal results. The accuracy degree of the approximation of the original non-convex optimization problem by a convex one is very case dependent.

ACKNOWLEDGEMENTS

The authors want to acknowledge the Agency for Innovation by Science and Technology in Flanders (IWT) and the Scientific and Technical Center for the Building Industry (WTCB) for supporting the post-doctoral research work of Ercan Atam within the VIS SMART GEOTHERM project.

REFERENCES

- A. Chiasson, Simulation and design of hybrid geothermal heat pump systems, Ph.D. thesis, University of Wyoming, USA (2007).
- S. Hackel, A. Pertzborn, Effective design and operation of hybrid ground-source heat pumps: Three case studies, *Energy and Buildings* 43 (12) (2011) 3497–3504.
- E. Atam, C. Verhelst, L. Helsen, Development of a control-oriented model for borehole dynamics for buildings equipped with ground-coupled heat pumps, in: BS 2013 Conference, District heating cooling - dhc, Online: <http://www.dhcplus.eu/wp-content/uploads/2012/05/120529-Vision-DHC-final.pdf> (2014).
- J. Cullin, J. Spitler, Comparison of simulation-based design procedures for hybrid ground source heat pump systems, in: Proceedings of the 8th International Conference on System Simulation in Buildings, Liege, Belgium, 2010.

- M. Wetter, Genopt, generic optimization program, in: Seventh International IBPSA Conference, Rio de Janeiro, Brazil, August 13-15, 2001.
- F. De Ridder, M. Diehl, G. Mulder, J. Desmedt, J. Van Bael, An optimal control algorithm for borehole thermal energy storage systems, *Energy and Buildings* 43 (2011) 2918–2925.
- C. Verhelst, Model predictive control of hybrid ground coupled heat pump systems in office building, Ph.D. thesis, Katholieke Universiteit Leuven, Belgium (2012).
- TRNSYS, A transient simulation program: Trnsys 16 reference manual (1998).
- P. Holmes, J. Lumley, B. G., Turbulence, Coherence Structure, Dynamical Systems and Symmetry, Cambridge University Press, Cambridge, 1996.
- P. Astrid, Reduction of process simulation models: a proper orthogonal decomposition approach, Ph.D. thesis, Technische Universiteit Eindhoven, Netherlands (2004).
- G. McCormick, Mathematical programming computability of global solutions to factorable nonconvex programs: Part i-convex underestimating problems, *Mathematical programming* 10 (1976) 147–175.
- M. Locatelli, F. Schoen, Global Optimization: Theory, Algorithms, and Application, Mos-Siam Series on Optimization, 2013.
- J. Lofberg, YALMIP: A toolbox for modeling and optimization in matlab, Online: <http://users.isy.liu.se/johanl/yalmip/> (2014).
- IBM, CPLEX Optimizer, Online: <http://www01.ibm.com/software/commerce/optimization/cplex-optimizer/> (2014).
- D. Kirk, Optimal Control Theory, An introduction, Englewood Cliffs, New Jersey, 1970.
- D. Bertsekas, Dynamic Programming and Optimal Control, 2nd ed. Athena Scientific, 2000.
- ETH, Institute for Dynamic Systems and Control, dpm-function, Online: <http://www.idsc.ethz.ch/Downloads/DownloadFiles/dpm> (2014).

COMPARISONS OF MODEL STRUCTURE AND IDENTIFICATION METHODS FOR MULTIPLE-RTU COORDINATION

Donghun Kim, Jie Cai, James E. Braun

Ray W. Herrick Laboratories, School of Mechanical Engineering, Purdue University, USA

1. ABSTRACT

Small and medium commercial buildings, such as retail stores, restaurants and factories, often utilize multiple roof top units (RTUs) to provide cooling and heating for open spaces. For these types of buildings, advanced control algorithms are not typically implemented due to practical difficulties such as lack of a building management system (BMS), high sensor costs, and high costs for controller design and programming. Our work is focused on development of a plug-and-play self-learning controller for coordinating RTUs in order to minimize energy usage and reduce short cycling while maintaining comfort. The approach relies on learning the relationships between thermostat responses and RTU on/off cycling. Needless to say, the crucial and difficult part for the RTU coordination is to choose a proper model structure and an identification algorithm to learn the underlying relationship between the multiple RTU actions and multiple thermostat temperatures. In this paper, we compare and evaluate prediction accuracies of several linear model structures, including multiple-input, multiple-output (MIMO) autoregressive models with exogenous inputs (ARX) and auto-regressive moving average models with exogenous inputs (ARMAX) using available site data for a typical small restaurant.

Keywords: RTU coordination, Recursive least square (RLS), ARX

2. INTRODUCTION

Buildings are responsible for about 40% of the total primary energy usage in the US. In the past three decades, various advanced control approaches have been studied to reduce energy consumption especially for large commercial buildings. One of the most popular and widely studied approaches is Model Predictive Control (MPC), in which an optimal control problem over a finite prediction horizon is solved at each sampling time using a system model. Many papers show the capability of MPC to reduce energy consumption (Privara et al., 2011; Ma et al., 2010) and demand cost (Braun, 1990). The controller communicates with the Building Management System (BMS) where real-time measured data are stored. The control algorithm relies on future predictions of disturbances such as outdoor air temperature, solar radiation and occupancy. The information are obtained through a weather forecast or using a model, such as an ARMA/ARIMA model, driven by sensor data.

Many small/medium commercial buildings, such as retail stores, restaurants and factories, utilize multiple roof top units (RTUs) to provide heating and cooling for open spaces. For this application it is difficult to apply an MPC algorithm because small commercial buildings typically do not have a BMS system and it would be expensive to add the required sensors. A conventional approach for this application relies on local feedback control, where each RTU is cycled on and off using its own thermostat that is located in the vicinity of its supply diffusers in the open space. This can lead to poor coordination among the RTUs where some units carry the majority of the load, some units cycle on and off very frequently, and others operate infrequently. Due to these practical difficulties, there have been very few advanced control algorithms developed for these buildings.

Our modelling approach relies only on thermostat signals, i.e. thermostat temperatures and RTU on/off stages, with no additional measurement requirements. Using the thermostat outputs, a system identification algorithm is applied to identify the underlying relationship between the multiple RTU actions and multiple thermostat temperatures. This leads to a lower cost and more practical solution for model-based RTU coordination in this type of building. However there are numbers of difficult questions to be answered; How to treat unmeasured disturbances such as internal gains and solar radiation? What is the limitation of disturbance modelling approaches? How to get or to choose persistently exciting data for these types of buildings? How to treat the correlation between disturbances and manipulated inputs, which will deteriorate model performance? These questions are fundamental issues in system identification and are out of the scope of this paper. Instead, we focus on how to choose a proper model structure and an identification algorithm for the RTU coordination control. Candidate identification algorithms are the recursive least square method (RLS) using the structure of multi-input and multi-output (MIMO) autoregressive exogenous (ARX) models and the recursive prediction error method (RPEM) for auto-regressive moving average models with exogenous inputs (ARMAX). The best model structure and identification algorithm may differ from system to system. However, it should be possible to automate the selection process and use measurement data for a system of interest to make site-specific choices.

In this paper, we want to find suitable model structures and corresponding identification algorithms to describe input-output relationships based on site data for a typical sit-down restaurant served by four RTUs.

3. SYSTEM DESCRIPTION/ DIFFICULTIES

Some major challenges in modelling small/medium size commercial buildings controlled by multiple RTUs are summarized as follows:

- 1) Unknown but possibly significant inter-zonal coupling, namely the state of one zone affecting the dynamics of neighbouring zones;
- 2) Unknown supply air duct systems that may be significantly different for each RTU and site, making modelling very site-specific;
- 3) Lack of sensors and BMS system, implying lack of information about measured buildings performance;
- 4) Time varying system behaviour due to time varying disturbances, performance degradation (e.g., RTUs), etc.;
- 5) Unmeasured but significant disturbances due to occupant schedules, solar radiation, etc.;
- 6) Relatively large number of controlled variables (e.g., zone thermostat set points) and manipulated variables (actions of RTUs).

Fig. 1 shows an example small commercial building served by multiple RTUs that is used as a case study in this paper. Because of difficulties 1) and 2), a data-driven modelling approach is chosen. RTUs are controlled by thermostats, which measure room air temperature and provide ON/OFF signals to compressors. In order to avoid the need for additional sensors, ON/OFF modes of the RTU compressors are selected as model inputs and the thermostat temperatures are chosen to be the model outputs. To handle difficulties 4) to 6), recursive algorithms are considered.

4. CHOICE OF MODELS AND IDENTIFICATION METHODS

For MIMO system identification, a polynomial model, e.g. ARX and ARMAX, and a state-space model are some standard choices for a black-box model (Ljung, 1999).

We chose to consider recursive identification algorithms instead of batch algorithms in order to capture the time varying system properties. For recursive algorithms, numerical stability is one of the most important issues since the failure of parameter convergence will show undesirable closed loop performance. RLS (recursive least squares) methods have several desired properties. The exponential convergence property is guaranteed as long as data is persistently exciting and is independent of the number of parameters. Therefore it can be applicable to buildings served by multiple RTUs. Furthermore the implementation of RLS for SISO can be easily extended to MIMO RLS. Therefore it is selected as a candidate identification method for RTU control modelling.

The MIMO ARX model has the following general form

$$\begin{aligned} A(z^{-1})y(k) &= B(z^{-1})u(k) + e(k) \\ A(z^{-1}) &= I + A_1z^{-1} + \dots + A_{n_a}z^{-n_a}, \\ B(z^{-1}) &= B_1z^{-1} + \dots + B_{n_b}z^{-n_b}. \end{aligned} \tag{1}$$

z^{-1} is the backward shift operator such that $z^{-1}x(k) = x(k-1)$. $y(k) \in \mathbb{R}^p$ and $u(k) \in \mathbb{R}^m$ are the outputs and inputs, respectively. $e(k) \in \mathbb{R}^p$ is a white noise process. The matrices of $A_j \in \mathbb{R}^{p \times p}$ for $j \in \{1, \dots, n_a\}$ and $B_j \in \mathbb{R}^{p \times m}$ for $j \in \{1, \dots, n_b\}$ are the parameters to be determined based on input/output (IO) data. (n_a, n_b) is the degree of matrix polynomials of $A(z^{-1}), B(z^{-1})$. We denote a ARX model with degree of (n_a, n_b) as $ARX(n_a, n_b)$.

The number of parameters to be estimated for $ARX(n_a, n_b)$ is $p \times (p \times n_a + m \times n_b)$ where p and m are the number of output and inputs. Even for a small building having 4 single-stage RTUs, at least 32 parameters need to be determined. Therefore a MIMO ARX structure has significant model complexity.

We want to find simpler model structures. One candidate form is as follows.

$$\begin{bmatrix} a_1(z^{-1}) & 0 & \dots & 0 \\ 0 & a_2(z^{-1}) & \dots & 0 \\ \vdots & \vdots & \ddots & \vdots \\ 0 & 0 & \dots & a_p(z^{-1}) \end{bmatrix} y(k) = B(z^{-1})u(k) + e(k) \tag{2}$$

It is called *diagonal from matrix fraction description*, Green et al. (2012). $a_i(z^{-1})$ is now a scalar polynomial instead of a matrix polynomial. It can be easily shown that the description is nothing but a parallel MISO ARX model that is

$$\begin{aligned} a_1(z^{-1})y_1(k) &= B_{11}(z^{-1})u_1(k) + \dots + B_{1m}(z^{-1})u_m(k) + e_1(k) \\ &\vdots \\ a_p(z^{-1})y_p(k) &= B_{p1}(z^{-1})u_1(k) + \dots + B_{pm}(z^{-1})u_m(k) + e_p(k) \end{aligned} \tag{3}$$

We denote this MIMO representation as “dARX” to emphasize that the $A(z^{-1})$ in Eqn. 2 is a diagonal polynomial matrix. Some advantages of dARX are:

- significantly fewer parameters need to be determined; For example, with 4 single-stage RTUs, ARX requires at least 32 parameters while dARX requires only 20.
- it is much easier to be interpret the model parameters; i.e. SISO ARX interpretation can be directly applied.
- a MISO identification algorithm for ARX can be applied.

Although the degrees of $a_i(z^{-1})$ differ in general, we assume all orders are the same ($=n_a$) for all $i \in [1, p]$ due to lack of *prior* order information. A similar assumption is applied for each element of $B(z^{-1})$. A more simplified structure for MIMO system representation may be possible. Consider the following transfer function: $G(z):U(z) \mapsto Y(z)$, where $H(z)$ is a matrix having rational polynomials for each entity and $z \in \square$ not the time shifting operator. Let denote the i, j component of the transfer function, $G_{i,j}(z) = n_{i,j}(z) / d_{i,j}(z)$ where $n_{i,j}(z), d_{i,j}(z)$ are numerator and denominator polynomials. Let $p(z)$ be a least common multiple for all the denominator polynomials, $d_{i,j}(z)$, for all i, j . We assume that $p(z)$ is a monic scalar polynomial such that the leading coefficient is unity. Then it can be shown that $p(z)Y(z) = H(z)U(z)$ where $H(z)$ is a polynomial matrix. Thus we are also interested in the following structure;

$$y(k) + a_1 y(k-1) + \dots + a_{n_a} y(k-n_a) = B_1 u(k-1) + \dots + B_{n_b} u(k-n_b) + \epsilon(k) \quad (4)$$

where a_j is a scalar $\forall j \in [1, n_a]$, while B_j is a matrix with the size of $p \times m$. We denote this model structure as “arX” to emphasize that the auto-regression terms, the coefficients of $a(z^{-1})$ are scalars. Stoica and Jansson (2000) compared prediction results for this model structure to those of a space-space form.

Besides ARX models, an ARMAX structure is also considered.

$$\begin{aligned} A(z^{-1})y(k) &= B(z^{-1})u(k) + C(z^{-1})e(k) \\ A(z^{-1}) &= I + A_1 z^{-1} + \dots + A_{n_a} z^{-n_a}, \\ B(z^{-1}) &= B_1 z^{-1} + \dots + B_{n_b} z^{-n_b}. \\ C(z^{-1}) &= I + C_1 z^{-1} + \dots + C_{n_c} z^{-n_c}. \end{aligned} \quad (5)$$

The only difference compared to the ARX form is the inclusion of $C(z^{-1})$. It acts as a filter for a white noise process and is called the moving average process. The ARMAX structure is much more complex than the ARX structure since it is nonlinear with respect to parameters and requires a non-linear recursive algorithm, called RPEM, that is more complex than RLS. The next section describes the RLS algorithm but not the REPM. For readers who are interested in the RPEM algorithm, refer to Ljung et al. (1983) and Goodwin and Sin (2013).

5. RECURSIVE LEAST SQUARE ALGORITHM AND PREDICTION

5.1 RLS formulation

Before we describe RLS, reformulation of the white noise process $e(k)$ is required.

Taking conditional expectation of Eqn. 1, i.e. $A(z^{-1})y(k) = B(z^{-1})u(k) + e(k)$, with respect to $\{y(k-1), y(k-2), \dots, u(k-1), u(k-2), \dots\}$ leads to

$$\hat{y}(k|k-1) = (I - A(z^{-1}))y(k) + B(z^{-1})u(k) = -A_1 y(k-1) \dots - A_{n_a} y(k-n_a) + B_1 u(k-1) + \dots + B_{n_b} u(k-n_b) \quad (6)$$

where $\hat{y}(k|k-1) = E(y(k) | y(k-1), y(k-2), \dots, u(k-1), u(k-2), \dots)$.

It is assumed that the current noise $e(k)$ is independent of past inputs and outputs and has zero mean. By taking the difference between Eqn. 1 and Eqn.6, one can get $e(k) = y(k) - \hat{y}(k|k-1)$, showing that the white noise process is the one-step ahead prediction error.

For a SISO system, the objective of least squares (LS) is to minimize $\frac{1}{2} \sum_{k=1}^n (y(k) - \phi(k-1)^T \theta)^2$,

where $\phi(k-1)^T = [y(k-1), y(k-2), \dots, u(k-1), u(k-2), \dots]$, $\theta^T = [a_1, \dots, a_{n_a}, b_1, \dots, b_{n_b}]$ and n is the size of data. Since $\phi(k-1)^T \theta = \hat{y}(k|k-1)$, the LS algorithm can be viewed as minimizing the sum of squares of the one step ahead prediction error. Let the optimal solution with data length n be $\hat{\theta}_n$. Recursive Least Square methods tend to find a transition $\hat{\theta}_n$ to $\hat{\theta}_{n+1}$ without resolving the optimization problem with data size of $n+1$.

The transition is;

$$\begin{aligned} \hat{\theta}(n) &= \hat{\theta}(n-1) + P(n-2)\phi(n-1)(1 + \phi(n-1)^T P(n-2)\phi(n-1))^{-1} (y(n) - \phi(n-1)^T \hat{\theta}(n-1)) \\ P(n-1) &= P(n-2) - P(n-2)\phi(n-1)(1 + \phi(n-1)^T P(n-2)\phi(n-1))^{-1} \phi(n-1)^T P(n-2) \end{aligned} \quad (7)$$

The derivation for Eqn. 7 is straightforward but is omitted. For MIMO RLS, Eqn. 6, i.e. $\hat{y}(k|k-1) = -A_1 y(k-1) \dots - A_{n_a} y(k-n_a) + B_1 u(k-1) + \dots + B_{n_b} u(k-n_b)$, can be expressed as follows.

$$\hat{y}(k|k-1) = [A_1, \dots, A_{n_a} | B_1, \dots, B_{n_b}] \begin{bmatrix} y(k-1) \\ \vdots \\ y(k-n_a) \\ u(k-1) \\ \vdots \\ u(k-n_b) \end{bmatrix} \quad (8)$$

By denoting $\Theta = [A_1, \dots, A_{n_a} | B_1, \dots, B_{n_b}]$ and

$\phi^T(k-1) = [y^T(k-1) \dots y^T(k-n_a) \quad u^T(k-1) \dots u^T(k-n_b)]$, Eqn. 8 becomes $\hat{y}(k|k-1) = \Theta \phi(k-1)$.

Then i^{th} element of $\hat{y}(k|k-1)$, denoted as $\hat{y}_i(k|k-1)$, can be expressed as

$\hat{y}_i(k|k-1) = \Theta_i \phi(k-1) = \phi(k-1)^T \Theta_i^T$, where Θ_i is the i^{th} row vector. Because the one-step ahead predictor form for each element of $\hat{y}(k|k-1)$ is the same for the MISO case, the MIMO RLS can be solved by p independent MISO identification.

5.2 Optimal d -step ahead prediction

For a model-based predictive control, we are interested in several step ahead predictions under candidate inputs. Suppose we are interested in the optimal output d -step ahead prediction of $y(k+d)$, given past historical data, $y(k), y(k-1), \dots, u(k-1), u(k-2), \dots$ and given candidate current and future inputs $u(k+d-1), u(k+d-2), \dots, u(k)$. Here ‘optimal’ means minimal variance. The one-step ahead prediction was derived in Eqn.4.

Since $y(k+2) = -A_1 y(k+1) - A_2 y(k) \dots - A_{n_a} y(k-n_a+2) + B_1 u(k+1) + B_2 u(k) + \dots + B_{n_b} u(k-n_b+2) + \epsilon(k+2)$, the optimal two-step ahead predictor form can be obtained by taking conditional expectation with respect to $y(k), y(k-1), \dots, u(k+1), u(k), \dots$ and is

$$\hat{y}(k+2|k) = -A_1 \hat{y}(k+1|k) - A_2 y(k) \dots - A_{n_a} y(k-n_a+2) + B_1 u(k+1) + B_2 u(k) + \dots + B_{n_b} u(k-n_b+2) \quad (9)$$

This can be generalized to d -step ahead prediction as follows.

$$\begin{aligned} \hat{y}(k+d|k) &= -A_1 \hat{y}(k+d-1|k) \dots - A_{d-1} \hat{y}(k+1|k) - A_d y(k) \dots - A_{n_a} y(k-n_a+d) \\ &\quad + B_1 u(k+d-1) + \dots + B_{n_b} u(k-n_b+d) \end{aligned} \quad (10)$$

6. CASE STUDY RESULTS AND DISCUSSION

6.1 Building description

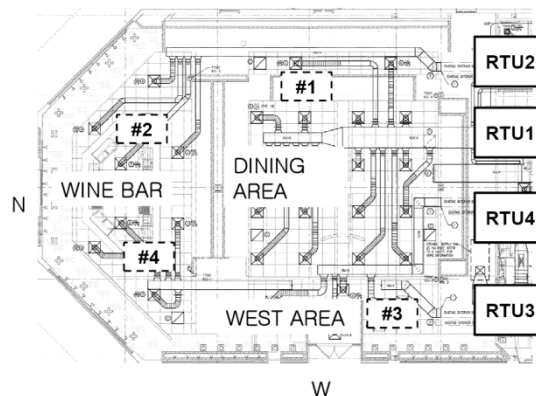


Figure 1: Locations of sensors and RTUs

A restaurant in suburban Philadelphia (see Fig 1) is a demonstration site for the Department of Energy Consortium for Building Energy Innovation. The indoor restaurant area is about 70ft long, 65ft wide and 11ft high. For this case study, the resolution of the existing thermostats was not sufficient for model construction. Therefore, additional wireless temperature sensors were located near the thermostats as shown in Fig.1.

The building has 4 RTUs and one of them, RTU1, has two stages of cooling and the others are single stage. We treated the two-stage unit as two different single-stage units. Therefore we have 4 outputs corresponding to the temperatures at the thermostats and 5 inputs that are the RTU stages. The temperatures and each RTU ON/OFF mode were recorded with one-minute sampling times where each mode was controlled by a thermostat (a conventional feedback controller). The data sets for model training were obtained using the conventional feedback closed-loop control system.

6.2 Results and discussion

The measured temperature and on/off mode data were recorded from August 15, 2013 to September 6, 2013. A sample IO data set is shown in Fig. 2. Based on the measured data, the described identification algorithms were implemented for different model structures. A sample result for the data of Fig. 2 with $d=60$ is shown in Fig.3 for the ARX(2,2) model. Since the sampling time is one minute, this is equivalent to a one-hour look ahead prediction. Each I/O variation had its sample mean subtracted such that ΔT in Fig.3 represents the shifted thermostat and predicted temperatures. The result shows the modelling approach can predict thermostat temperatures one hour in advance very accurately. In this case there were 72 parameters to be determined and all parameters were initialized with 1. Despite the large number of parameters, the RLS converged to reasonable values within about two days from the start.

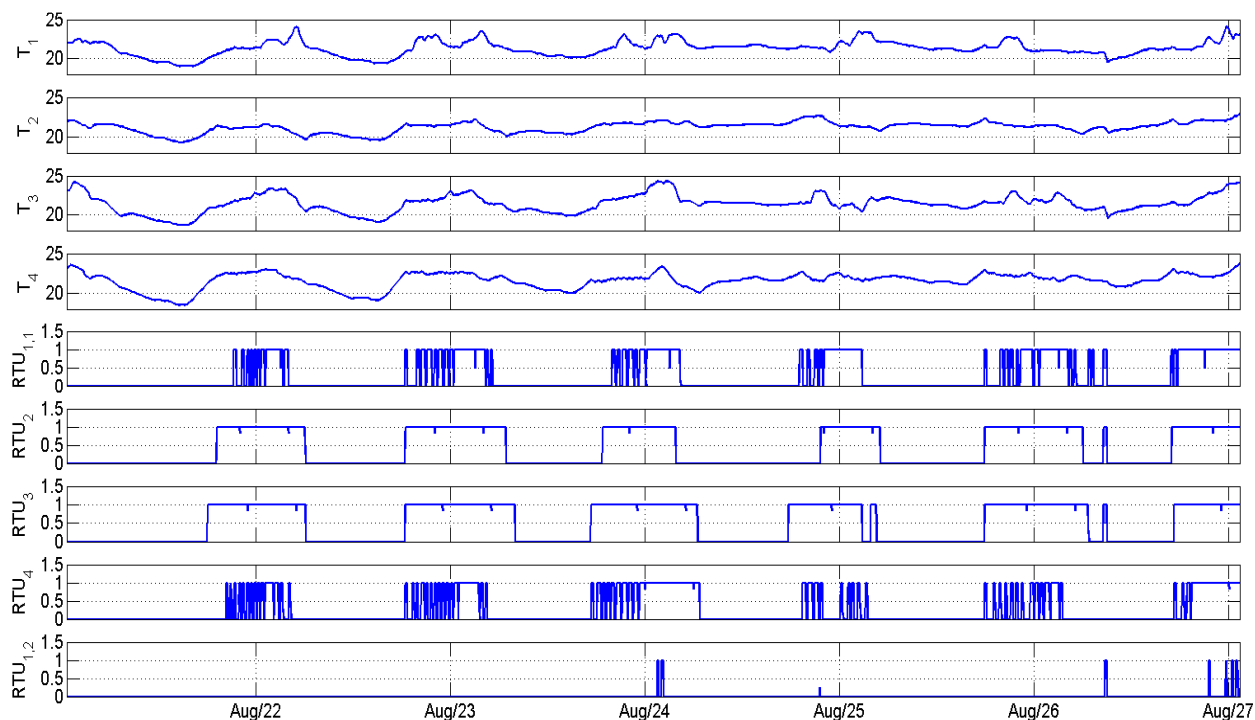


Figure 2: Example measured thermostat temperature and ON/OFF stages

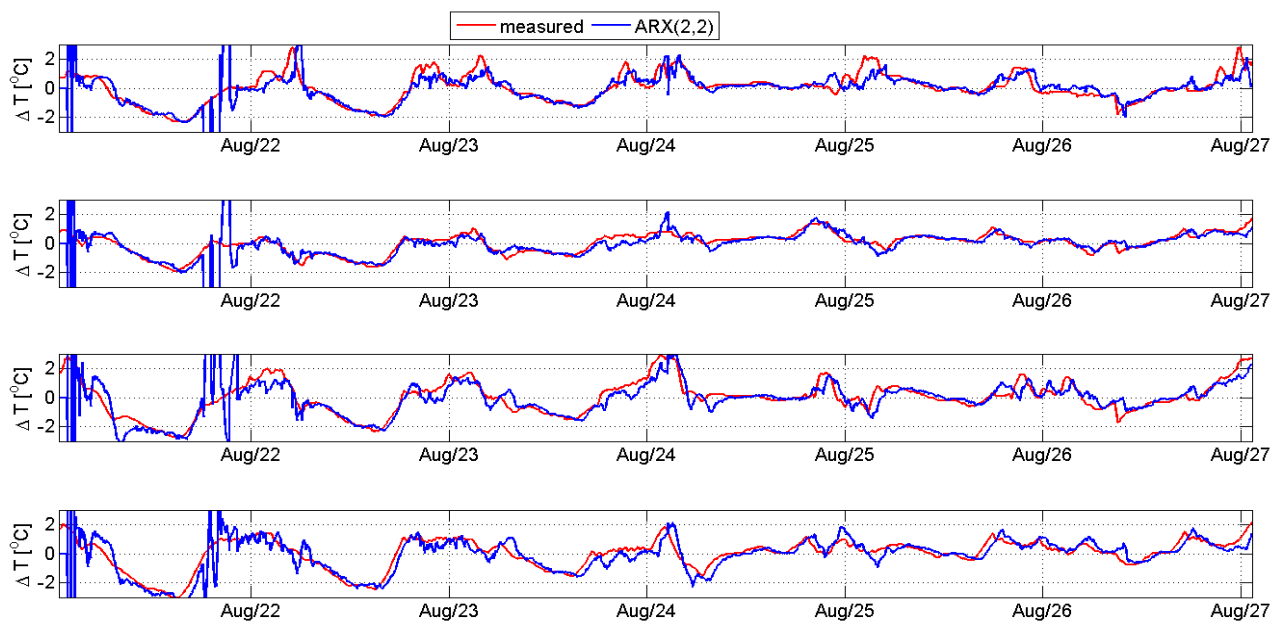


Figure 3: Example comparisons of measurement data and 1-hr predicted RLS with ARX(2,2)

In order to measure the prediction error (P.E.) we used the following metric;

$$\sigma = \frac{1}{4} \sum_{i=1}^4 \frac{1}{N} \sqrt{\sum_{k=0}^N (y_i(k+d) - \hat{y}_i(k+d|k))^2}. \quad (11)$$

where i is an index corresponding to each thermostat temperature, σ represents the average standard deviation of prediction errors for the four thermostat temperatures, and N represents the number of data points. In subsequent results, we used all the data from August 15 to September 6 to quantify σ , which depends on the prediction horizon, d , and the model structure and order.

Intuitively, as the prediction horizon, d , increases, the d -step prediction error has to increase. Fig. 4 shows how σ increases w.r.t. the horizon for different model structures and model orders (n_a). For these results, n_b was set to one for all the model structures and n_c was set to 2 for the ARMAX structure. The number of parameters to be learned depends on the model structures as summarized in Table. 1.

Table 1: the number of parameters depending on model structures in Fig. 4 and Fig. 5

	ARX($n_a,1$)	dARX($n_a,1$)	arX($n_a,1$)	ARMAX($n_a,1,1$)
# parameters	$16 \times n_a + 20 \times 1$	$4 \times n_a + 20 \times 1$	$n_a + 20 \times 1$	$16 \times n_a + 20 \times 1 + 16 \times 1$

For most prediction horizons and for various n_a , ARX and dARX provide better predictions (i.e., lower σ values). Even though the ARMAX structure includes ARX, the prediction performance for longer prediction horizon is worse than for the ARX for all n_a . Since the RLS/REPM algorithm minimizes the one-step ahead prediction, the ARMAX is slightly superior for shorter prediction horizons as shown in Fig. 4. However, this does not imply that it is superior for longer prediction horizons.

Fig.5 provides the same information as Fig. 4 but it more clearly shows how σ changes with n_a . Consider the case where $d=30$. The number of parameters for ARX(1,1) is 36 and the corresponding σ is about 0.30°C. On the other hand, the number of parameters for arX(15,1) is 35 and the corresponding σ is about 0.51°C. Although the numbers of parameters are similar, the arX structure shows worse prediction performance for this case study. Meanwhile, the dARX(4,1) has a σ value of 0.26°C. The dARX is superior among the model structures we investigated.

Before further discussions, it is important to mention how the fitness behaves as a model order increases. In general, σ decreases rapidly until a guessed model order meets the true order. This is the process to capture major dynamics contained in data. However even after a model order reaches its true order, σ keeps decreasing but slowly. This is the process called *overfitting*, where the additional parameters of a higher order model fit to noise process in the model. One of the goals of this paper is to find a point around which σ is insensitive.

It is interesting that σ is not sensitive to the selection of n_a even for $n_a = 1$, which is not true for SISO system identification. This may attributed to the MIMO structure. For example, for the ARX(1,1), the corresponding transfer function for each y_i will have four poles unless there is a zero-pole cancelation. Likewise, ARX(2,1) will have 8 poles. Therefore even with small n_a , it could have enough coefficients to describe the dynamics in the data.

However there is a concern about the models with $n_a = 1$. It turns out model structures with $n_a = 1$ likely have all poles close to $z = 1$ on the complex domain. This results in a trivial model structure $y_n \approx y_{n-1}$. The prediction performance of the model looks good since it just shifts the measurement data. However it is useless for any purpose. This clearly can be seen in Fig. 5: arX(1,1) is superior to any other higher order arX($n_a,1$). With this concern, we exclude model structures with $n_a = 1$ for the modelling of multiple-RTU coordination.

The dARX model structures with $n_a=2$ or $n_a=3$ provide reasonable prediction accuracy. By Eqn. 3, this implies about 2 or 3 poles per each zone could be suitable to describe dynamics of the building at least approximately. Although an ARX model also provides reasonable accuracy, a dARX model is preferred since excessive numbers of parameters will increase the parameters uncertainty (Gustavsson, I. et. al. 1977) and cause overfit.

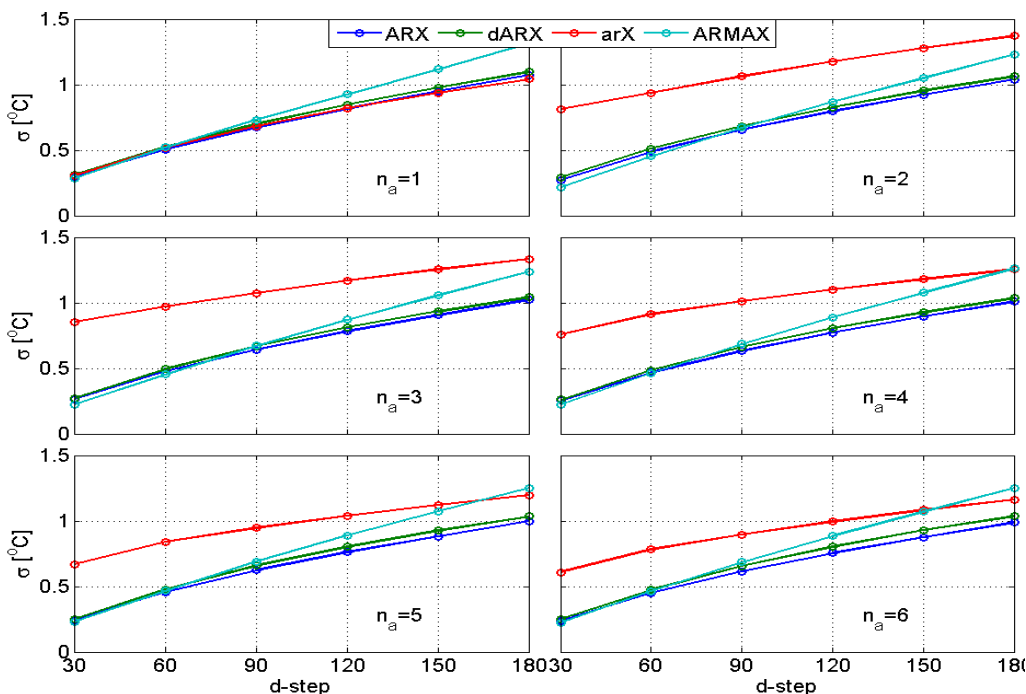


Figure 4: Standard deviation of prediction errors as a function of prediction horizon for different model structures and orders (sampling time =1 min)

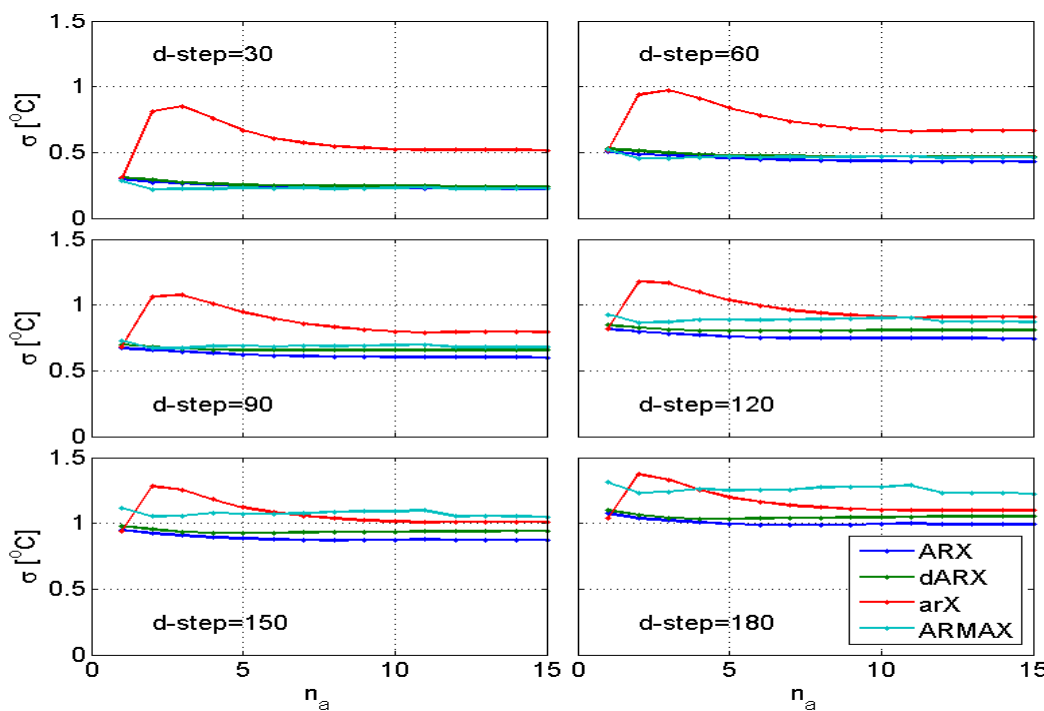


Figure 5: Standard deviation of prediction errors as a function of order of $A(z^{-1})$ polynomial (sampling time =1 min)

The sensitivity w.r.t. n_b is shown in Fig. 6. For the ARMAX structure, the effect of n_c on σ is shown in Fig. 7. These results show that the prediction error is relatively insensitive to the selection of n_b and n_c , even for $n_b = 1$ and $n_c = 1$. This implies the dynamics can be explained without any additional zeros; note that both n_b and n_c are related to zeros of the transfer functions.

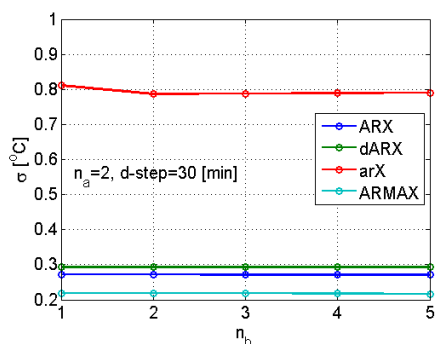


Figure 6: Standard deviation of prediction errors as a function of order of $B(z^{-1})$ polynomial (sampling time = 1 min)

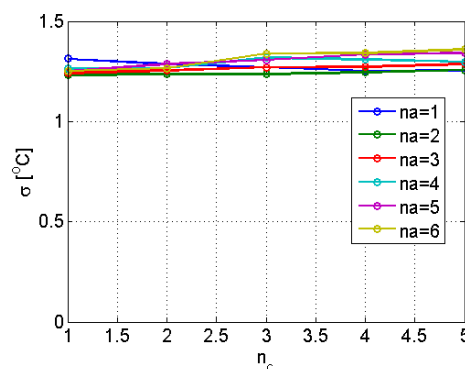


Figure 7: Standard deviation of prediction errors as a function of order of $C(z^{-1})$ polynomial for ARMAX model

7. CONCLUSION

This paper compares prediction accuracies of several linear model structures that describe the relationships between thermostat responses and RTU on/off cycling for a case study building served by several RTUs. The purpose of this comparison is to identify a suitable model structure and order for a RTU coordination control algorithm. RLS is used for ARX types of models and RPEM is used with ARMAX types as an identification algorithm. We also considered special forms of ARX, e.g. diagonal matrix fraction description, to find a simpler model structure. The linear models provided reasonable prediction errors, around 0.5°C s.t.d. for one-hour predictions. Parallel implementations of a MISO model structure, denoted as dARX structure with 2-3 for n_a and 1-2 for n_b in this paper, provided reasonable prediction accuracies while reducing model complexity. An arX with a low n_a was too simplified model to capture the MIMO relationship. A more complex model, ARMAX, showed better agreement with the measurements for a short prediction horizon but became poor as the prediction step increased.

ACKNOWLEDGMENTS

This work was supported by the Department of Energy through the Consortium for Building Energy Innovation.

REFERENCES

- Braun, J. 1990. *Reducing energy costs and peak electrical demand through optimal control of building thermal storage*. ASHRAE transactions, 96(2):876–888.
- Goodwin, G. C. and Sin, K. S. 2013. *Adaptive filtering prediction and control*. Courier Dover Publications.
- Gustavsson, I., Ljung, L. and Söderström, T. 1977. *Identification of processes in closed loop—identifiability and accuracy aspects*. Automatica, 13(1), 59-75.

- Ljung, L., 1999. *System Identification (2Nd Ed.): Theory for the User*. Prentice Hall PTR, Upper Saddle River, NJ, USA.
- Ljung, L. et al. 1983. *Theory and practice of recursive identification*, Cambridge, MA: M.I.T. Press, 1983
- Ma, Y., Borrelli, F., Hancey, B., Coffey, B., Bengea, S., and Haves, P. 2010. *Model predictive control for the operation of building cooling systems*. In American Control Conference (ACC), 2010, pages 5106–5111. IEEE.
- Prívará, S., Široký, J., Ferkl, L., and Cigler, J. 2011. *Model predictive control of a building heating system: The first experience*. Energy and Buildings, 43(2):564–572.
- Stoica, P. and Jansson, M. 2000. *MIMO system identification: state-space and subspace approximations versus transfer function and instrumental variables*. Signal Processing, IEEE Transactions on, 48(11):3087–3099.
- Zhu, Y. 2001. *Multivariable system identification for process control*. Elsevier.

Extraction of heating control rules from the dynamic programming method for load shifting in energy-efficient building

M. Robillart, P. Schalbart, B. Peuportier

MINES ParisTech, PSL - Research University, CES - Centre for energy efficiency of systems,

60 Bd St Michel 75006 Paris, France

*maxime.robillart@mines-paristech.fr

1. ABSTRACT

In France, 40 % of buildings are heated with electrical devices causing high peak load in winter. In this context, optimal strategies (under constraints related to comfort and maximum heating power) have been developed using the dynamic programming method in order to shift electricity consumption used for heating, taking advantage of the building thermal mass. However, this exact optimisation method is computationally intensive and can hardly be applied to real-time control. Complementary statistical techniques exist that allow for the extraction of logistic decision models from the optimal control simulation results. These rule extraction techniques model the relationship between explanatory variables and a response variable. In this study, a generalised linear model was used because it is able to mimic the general characteristics of the dynamic programming results with good precision and greatly reduced computational effort (150 times faster than the dynamic programming method).

Keywords: Rule extraction, optimal control, load shifting.

2. INTRODUCTION

2.1 Existing control schemes

In modern construction of buildings, the main objectives for the control systems are to save energy (Nygard Ferguson, 1990), to increase comfort (Mathews et al., 2000) and to reduce peak electricity demand (Greensfelder et al, 2011). To meet such objectives, control systems have to be able to anticipate the weather, the occupancy, and the solar and internal gains. Dounis and Caraiscos (2009) reviewed many advanced control systems meeting such objectives. For instance, during a summer period, control systems are used to maintain comfort using passive cooling (Braun et al, 2001), to reduce energy consumption of air conditioning (Chahwane, 2011), or to control solar protections (Nielsen et al, 2011). During a winter period, control systems are used to decrease the energy consumption of the heating system (Le, 2008) or to reduce peak demand (Malisani et al. 2011).

2.2 Load shifting

Recently, numerous efforts have been made to reduce electricity peak-demand. In Europe, these peaks mostly appear during winter periods and are due to heating systems. For example in France, the building sector represents 68 % of the final electricity consumption (ADEME, 2012). To guarantee the grid stability, some studies have been done on electrical load shifting.

Thanks to electricity demand-side response (DSR), the consumer demand for energy can be modified through various methods such as financial incentives or education. Many economical models are used by the demand side response programs. Two categories may be distinguished: time based programs and incentive based programs (Marwan et Kamel, 2011; Federal Energy

Regulatory Commission, 2006). Examples of application of time based programs are Time Of Use (with fixed electricity prices for off-peak and peak hours), or Real Time Pricing (with variable electricity tariffs). For incentive based programs, an example is the Direct Load Control, which allows to turn specific appliances on and off during peak demand periods.

At the level of the individual houses, the electricity peak reduction can be achieved thanks to a careful architectural design to efficiently manage solar gains (Nygard Ferguson, 1990). An advanced control system can also be used to reduce heating consumption. Such control can be based on power tariff (Hämäläinen et al., 2000; Pineau et Hämäläinen, 2000) or the use of the thermal mass of the building to shift part of electricity consumption (Wyse, 2011; Hong et al., 2011). For instance, Favre and Peuportier (2014) used the dynamic programming method to shift the building consumption. The proposed method consisted in over-heating the building in the hours before the peak based on weather forecast, and occupancy and internal gains schedules for the next 7 days. However, this exact optimisation method is time-consuming and can hardly be applied to real-time control.

2.3 Rule extraction

In developing an operational strategies framework, exact optimisation results can be used to extract simplified control rules that are implementable in real-time.

This approach was first applied in water resource management. The application was to develop simplified control rules for reservoir management based on the results of offline model predictive control (MPC) (Wei et Hsu, 2009). The approach has recently been used in the building context. For instance, May-Ostendorp et al. (2013) used many data mining techniques (generalised linear models, classification and regression trees and adaptive boosting) to extract rules from offline MPC results for a mixed mode building operated during the cooling season. To our knowledge, this approach was never applied to shift the heating consumption in building.

The present study is based on the results of Favre and Peuportier (2014) and its objective is to develop operational strategies to shift the heating load in building. A new methodology is proposed to extract decision models from dynamic programming results and then compare them.

3. MODELS

3.1 Thermal model of the building

The building is modelled considering spatial zones of homogenous temperature. For each zone, each wall is meshed according to the finite volume technique with a uniform temperature and thermal capacity. Another mesh is added for the zone's air and furniture. Energy conservation equations are written on each mesh within the building and form a system of equations:

$$C_i \frac{dT_i}{dt} = Gains - Losses \quad (1)$$

with

- C_i the thermal capacity of the node i ,
- T_i the temperature of the node i ,
- $Gains$ the solar and internal gains (due to heating, occupancy and other appliances),
- $Losses$ the heat losses by conduction, convection and radiation.

Repeating energy conservation equations for each mesh leads to a linear time-invariant system (Peuportier and Blanc-Sommereux, 1990), temporal variation terms being added in the simulation :

$$\begin{aligned} C\dot{T}(t) &= AT(t) + EU(t) \\ Y(t) &= JT(t) + GU(t) \end{aligned} \quad (2)$$

with

- T the node temperature vector,
- C the diagonal thermal capacity matrix,
- U the driving forces (climate parameters, heating, etc.),
- Y the output vector (indoor temperatures accounting for air and wall surfaces),
- A, E, J, G the state, input, output and feedforward matrices, respectively.

In order to perform simulation, it is important to know the occupancy of the building which defines the emission of heat by the inhabitants and appliances, and the thermostat setpoint influencing the heating equipment. Another important aspect is the weather model influencing heat losses and solar gains. The data regarding house occupancy and weather models were included in the driving forces vector U .

The high order linear model (2) needed to be reduced because its state dimension was too large to allow a fast convergence of the optimisation algorithm. A reduction method (modal reduction) was thus applied to lower the state dimension. In this work, the building energy simulation tool COMFIE was used because it presents a degree of accuracy equivalent to international benchmarks (Brun et al., 2009) and has a fast calculation time thanks to the modal reduction method (Peuportier and Blanc-Sommereux, 1990).

3.2 Optimisation algorithm

The dynamic programming method was developed by Bellman (1957). It is a sequential optimisation method which examines all possible ways to solve an optimisation problem and provides, given a discretisation, an optimal set of commands over a period.

To apply dynamic programming, a state variable describing the system is used and discretised temporally :

$$x(t) = x_t \in X_t, X_t \subset \mathbb{R}^{N_s} \quad (3)$$

where X_t is the set of possible states and N_s the dimension of X_t . The control vector u can be chosen in a set $U_t \subset \mathbb{R}^{N_c}$ (the set of possible controls) where N_c is the dimension of the control vector :

$$u(t) = u_t \in U_t, U_t \subset \mathbb{R}^{N_c} \quad (4)$$

One can act on the system state through the control variable u . The state space equation of the dynamical system $f(\cdot)$ is thus :

$$x(t) = x_t, \quad x(t+1) = f(x(t), u(t)) \quad (5)$$

A value function v_t is defined, which is the cost to go from $x(t)$ to $(t+1)$:

$$v_t(x_t, x_{t+1}) \quad (6)$$

Under these assumptions, a finite-horizon decision problem takes the following form :

$$V_0^t = \max\left[\sum_{j=0}^{t-1} v_j(x_j, x_{j+1})\right] \tag{7}$$

subject to the constraints (3) and (4) and the state space equation (5). V_0^t denotes the optimal value that can be obtained by maximising the objective function subject to the assumed constraints. The dynamic programming method is then applied to break this decision problem into smaller sub-problems. Bellman's principle is thus used: "An optimal policy has the property that whatever the initial state and initial decision are, the remaining decisions must constitute an optimal policy with regard to the state resulting from the first decision".

Equation (7) becomes :

$$V_0^t = \max[v_0(x_0, x_1) + \sum_{j=1}^{t-1} v_j(x_j, x_{j+1})] \tag{8}$$

Figure shows how the dynamic programming operates :

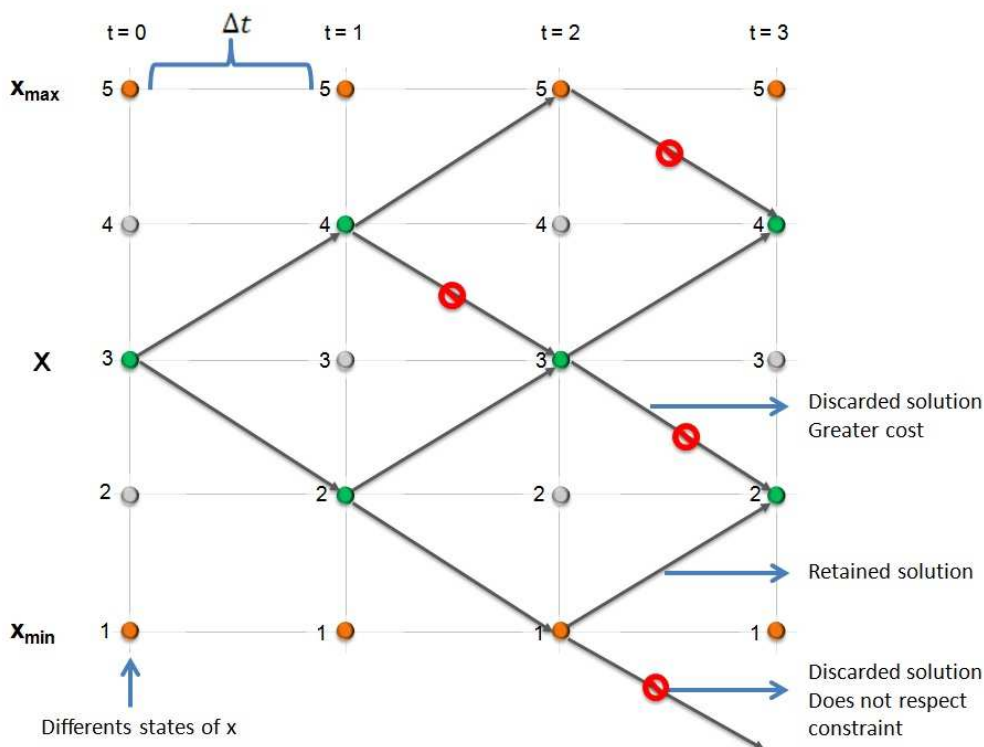


Figure 1: Dynamic programming description

In Figure , the state variable x is discretised in five states. Optimisation aims at minimising the state variable. In this example, thanks to Bellman's principle, four solutions can be discarded either because they trespass the constraints or because they reach the same states as solutions with lower costs.

For the application of dynamic programming in building context, the chosen state variable and the cost function are defined in § 5.2.1.

3.3 Rule extraction: Generalised linear model

The generalised linear model (GLM) framework was used to derive simplified decision models from the dynamic programming results allowing a small computational expense adapted to real

time control. GLM models the relationship between regressors x_j (explanatory variables) and response y . It consists of three elements:

- a random component (the response y is assumed to be generated from a particular probability distribution),
- a deterministic component (a linear combination of explanatory variables x_j),
- a link function (that provides the relationship between the linear combination of explanatory variables and the mean of the distribution function).

We have thus to estimate the following model:

$$f_l(E[y]) = \sum_j a_j x_j + b \quad (9)$$

with

- $f_l(\cdot)$ the link function,
- $E[y]$ the expected value of y .

The unknown parameters a_j and b are typically estimated with maximum likelihood (Gill, 2004).

4. METHODOLOGY

The following section describes techniques employed to extract decision models from dynamic programming results. Dynamic programming was used to generate training data and validation data to identify a GLM's parameters and to evaluate its performance, respectively. It was done in two stages.

As a first step, Test Reference Year-type (TRY) weather data were used to perform optimisation using dynamic programming and to elaborate an optimal strategy. This optimal strategy (training data) was then used to identify the GLM's parameters with the same weather data. This step corresponded to the model identification process (§ 4.1).

As a second step, the predictive capacity of the model was assessed with a more precisely recorded local weather data. We compared the GLM's results with the optimal strategy calculated by dynamic programming (validation data). This step corresponded to the model comparison process (§ 4.2).

4.1 Model identification

Model identification was done in a four-step process (Figure 2). First, all data used by dynamic programming were collected (Test Reference Year-type weather data, electricity tariff, occupancy). Secondly, the optimal strategy was elaborated using dynamic programming (training data). Thirdly, we identified the GLM's parameters thanks to optimal strategy. Fourthly, the resulting control models were implemented within the simulation platform (COMFIE).

4.2 Model comparison

Model comparison was done in a three-step process (Figure 3). Firstly, all data used by the optimisation method and the GLM were collected (local weather data, electricity tariff, occupancy). Secondly, we performed optimisation with dynamic programming and GLM to determine optimal strategy and operational strategies respectively. Finally, we compared performances of operational strategies against the optimal strategy.

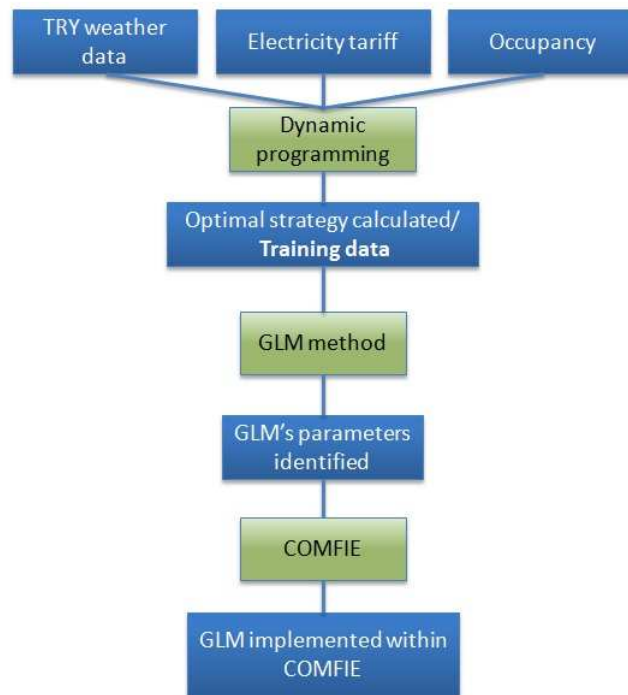


Figure 2: Model identification

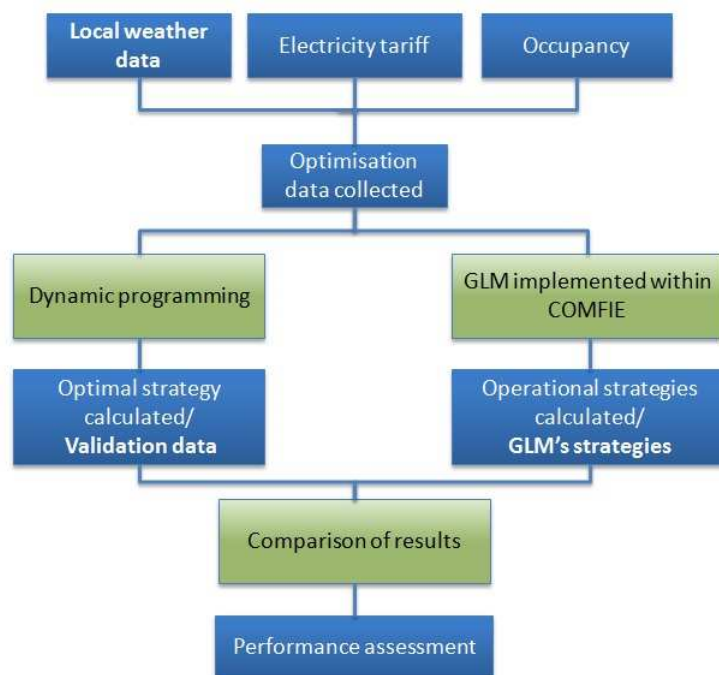


Figure 3: Model comparison

5. CASE STUDY

5.1 Building description

The building under study is a single-family house based on an actual experimental passive house being part of the INCAS platform built in Le Bourget du Lac, France, by the National Solar Energy Institute (INES). The studied house has two floors and a total living floor area of

89 m² (Figure 4). The North facade has only two small windows whereas 34 % of the South facade is glazed. The building's façades include double ($U_{gw} = 1.1 \text{ W} \cdot \text{m}^{-2} \cdot \text{K}^{-1}$, $SF = 0.6$) and triple on the North ($U_{gw} = 0.7 \text{ W} \cdot \text{m}^{-2} \cdot \text{K}^{-1}$, $SF = 0.45$) glazing windows of various dimension. The south façade also includes solar protection for the summer period. The house is highly insulated with a high thermal mass as shown in Table 1.

Table 1: Building description

	External wall	Ground	Intermediate floors	Ceiling	Interior partition
Composition	15 cm thick concrete 20 cm of extruded polystyrene	20 cm concrete slab 20 cm external insulation	16 cm concrete screeds and girders 12 cm concrete slab floor	40 cm of glass wool	4 cm of glass wool
U (W.m ⁻² .K ⁻¹)	0.15	0.15	2.2	0.09	0.96

The main thermal bridges as well as the building air tightness have been carefully designed and implemented. The house is heated by an electrical resistance integrated in an efficient heat recovery ventilation system. According to thermal simulation results using the thermal model described in § 3.1, the annual heating load is 14 kWh.m⁻².



Figure 4: view of the house (west and south façades)

5.2 Optimisation parameters

5.2.1 Dynamic programming parameters

The chosen state variable for dynamic programming is the total energy E_t stored in the building, calculated as follows (Favre et Peuportier, 2014) :

$$E_t = \sum_{i=0}^{N_{nodes}} C_i (T_i - T_{ref}) \quad (10)$$

with

- T_{ref} the reference temperature chosen at 0°C,
- N_{nodes} the number of nodes

An upper and lower bound of this state variable was defined according to its initial value. Then it was discretised in 800 nodes.

To ensure thermal comfort in the building, indoor temperature had to be maintained between 19°C (T_{min}) and 26°C (T_{max}). We considered a typical four people family occupancy: the building was non-occupied only during the working days from 8 a.m. to 5 p.m. Each occupant emitted 80 W due to their metabolism, and internal gains from appliances were also considered during occupied hours. The heating power was in the range of 0 W (P_{min}) to 5000 W (P_{max}).

The model of the building was mono-zonal and the optimisation was done over 34 days (which was the maximal decision problem's horizon solved by dynamic programming), with one hour time step, to generate training and validation data. The goal of dynamic programming was to minimise the heating cost of the building by determining a set of commands (heating power P) with constraints on thermal comfort and heating power. Thus, the finite-horizon decision problem took the following form:

$$\min_P \sum_{t=0}^{t=tf} C_{elec_t} P_t \quad (11)$$

with constraints

$$T_{min} \leq T(t) \leq T_{max} \quad (12)$$

$$P_{min} \leq P(t) \leq P_{max} \quad (13)$$

with

- P_t the heating power at time step t ,
- C_{elec_t} the electricity cost at time step t .
- tf the duration of the optimisation period

5.2.2 Electricity tariff

To shift electricity demand, a time-of-use pricing was considered (Table 2):

Table 2: Electricity prices

	Off-peak hours	Peak hours	High peak hours
Hours	12 a.m. to 9 a.m.	9 a.m. to 5 p.m. 10 p.m. to 12 a.m.	5 p.m. to 10 p.m.
Cost per kWh (€)	0.0864	0.1275	0.255

5.2.3 Weather data

Meteonorm data from Chambéry (to generate training data) and local weather conditions data (to generate validation data) measured at the Chambéry airport which is 300 meters away from the building, were used to perform simulations. Test Reference Year-type (TRY) were used to develop GLM (model identification process) because these weather data represent the typical long-term weather patterns. Thus, GLM's results were adjusted with the long-term average climatic conditions. Then, we used local weather conditions data (model comparison process) to assess GLM's behaviour in real conditions. This local weather data corresponded to measurements at the Chambéry airport (France) from January 15th to February 17th, 2012. Meteorological features are summarised in Table 3.

Table 3: Weather data

	Training data	Validation data
Minimum temperature (°C)	-9.10	-14
Average temperature (°C)	1.44	-0.22
Maximum temperature (°C)	11.50	11.33
Average global horizontal irradiance (W.m ⁻²)	58	60
Maximum global horizontal irradiance (W.m ⁻²)	486	569

5.3 Performance evaluation

Objective criteria for evaluating the predictive quality of the model were required. Therefore, the following indicators were used to assess its performance:

- the mean absolute error (MAE), between heating powers P calculated by dynamic programming and GLM,
- the average heat power,
- the cumulative cost,
- the percentage of high peak hours which are load shifted,
- the percentage of peak hours which are load shifted,
- the thermal discomfort rate TI_{min} representing the number of hours when the indoor temperature falls below 19°C (in %),
- the thermal discomfort rate TI_{max} representing the number of hours when the indoor temperature rises above 26°C (in %).

6. RESULT ANALYSIS

6.1 Explanatory variables

Explanatory variables that can be measured in building were used to develop GLM. Thus, to determine the heating power P at time step $t + \Delta t$, we used explanatory variables at time step $t + \Delta t$: outdoor temperature T_{out} , global horizontal irradiance I_{gh} and electricity tariff (C_{elec}). Explanatory variables at time step t were also considered: indoor temperature T_{in} , and heating power.

6.2 Models developed

To apply generalised linear model (GLM), we had to define the link function. That is why we changed the response variable as a proportion of maximum heating power (5000 W). For example, a heating power at time step $t + \Delta t$ of 2500 W, corresponds to a predicted variable by GLM of 50 %. The statistical model used by GLM is thus a multiple logistic regression and the link function is the logit function $f_l(x) = \ln\left(\frac{x}{1-x}\right)$. This model was used to relate the proportion of maximum heating power to predictor variables x_j through the logistic link function :

$$\ln\left(\frac{E(P)}{1-E(P)}\right) = \sum_j a_j x_j + b \quad (14)$$

Five models were developed, each one using all or some of the training data (Table 4). Training data were divided into three groups: off-peak hours training data (TD_{OPH}), peak hours training data (TD_{PH}) and high peak hours training data (TD_{HPH}).

In the implementation, the heating power at time step $t + \Delta t$ was set at 0 W in the following cases :

- during high peak hours for GLM_2, GLM_3, GLM_4 and GLM_5 models,
- during peak hours for GLM_3 and GLM_5 models.

These choices were done in order to ensure load shifting during peak and high peak hours.

Table 4: Training data

	Off-peak hours	Peak hours	High peak hours
GLM_1	TD _{OPH}	TD _{PH}	TD _{HPH}
GLM_2	TD _{OPH}	TD _{PH}	-
GLM_3	TD _{OPH}	-	-
GLM_4	TD _{OPH}	TD _{PH}	TD _{HPH}
GLM_5	TD _{OPH}	TD _{PH}	TD _{HPH}

As a more specific example, GLM_3 and GLM_5 models were different because they did not have the same training data. Indeed, GLM_3 was trained only on off-peak hours training data (TD_{OPH}) whereas GLM_5 was trained on complete training data (TD_{OPH}, TD_{PH}, TD_{HPH}). However, in the implementation, the heating power at time step $t + \Delta t$ was set at 0 W during high peak hours et peak hours for both models. The same logic was applied for GLM_2 and GLM_4 models.

6.3 Results

Each GLM model was implemented in the building energy simulation tool COMFIE. Table 5 summarises GLM models' results obtained on validation data. The dynamic programming reference results are described in the DP column.

The resulting model predictions of GLM_1 and GLM_2 and the original optimised sequence are presented in Figure 5. We can clearly observe that GLM_1 and GLM_2 did not follow the dynamic programming's behaviour. For example, we can see that the GLM_2 model performed significantly worse than dynamic programming, with a very high thermal discomfort rate TI_{max} (93 %) and an indoor temperature exceeding 30°C (30.6°C). GLM_1 had a similar behaviour with a significant cumulative cost (137 €) and a high mean absolute error (111 %).

Figure 6 shows that predictions of GLM_4 and GLM_5 are also different from the optimised results. For instance, we can see that GLM_4 and GLM_5 had a significant cumulative cost (105 € and 92 € respectively) and a high average power (1347 W and 1309 W respectively). Moreover, GLM_4 and GLM_5 had a relatively large mean absolute error (88 % and 71 % respectively).

However, Figure 7 illustrates the interesting behaviour of GLM_3. Firstly, due to its design, no electricity was consumed during high peak hours and peak hours. Secondly, it had a cumulative cost and an average heat power close to dynamic programming (72 € and 1023 W compared to 68 € and 936 W for DP). Thirdly, its mean absolute error (40 %) and mean relative error (9 %) were reasonable. Finally, GLM_3's computational time was 150 times smaller than the dynamic programming method, using a desktop computer.

Table 5: GLM models' results

	GLM_1		GLM_2	GLM_3	GLM_4	GLM_5	DP
Average heat power (W)	1353		1811	1023	1347	1309	936
Cumulative cost (€)	137		158	72	105	92	68
High peak hours load shifted (%)	0		100	100	100	100	99
Peak hours load shifted (%)	0		0	100	0	100	88
TI_{min} (%)	0		0	8	0	0	0
TI_{max} (%)	3		93	0	2	0	0
T_{min} / T_{max}	21.2 / 26.15		21.4 / 30.6	18.4 / 23.8	20.7 / 26.1	19.6 / 26	19 / 23.4
MAE (%)	111		153	40	88	71	-

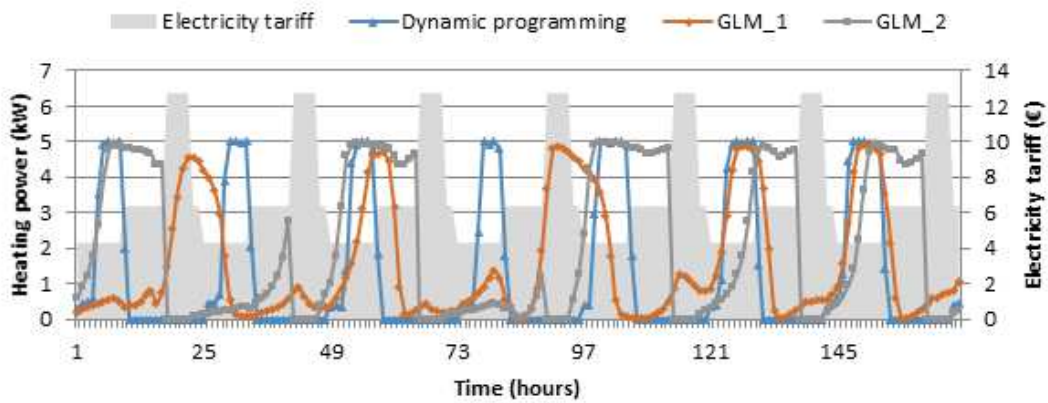


Figure 5: Heating power calculated by dynamic programming, GLM_1 and GLM_2 (Third week)

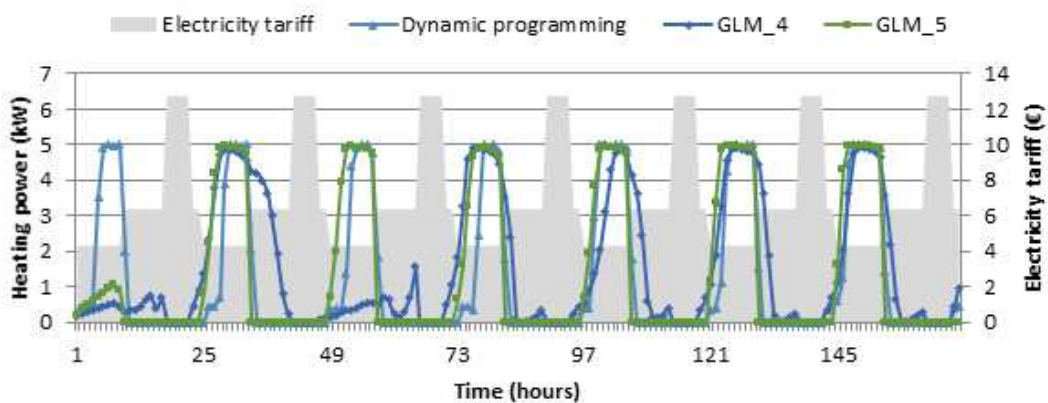


Figure 6: Heating power calculated by dynamic programming, GLM_4 and GLM_5 (Third week)

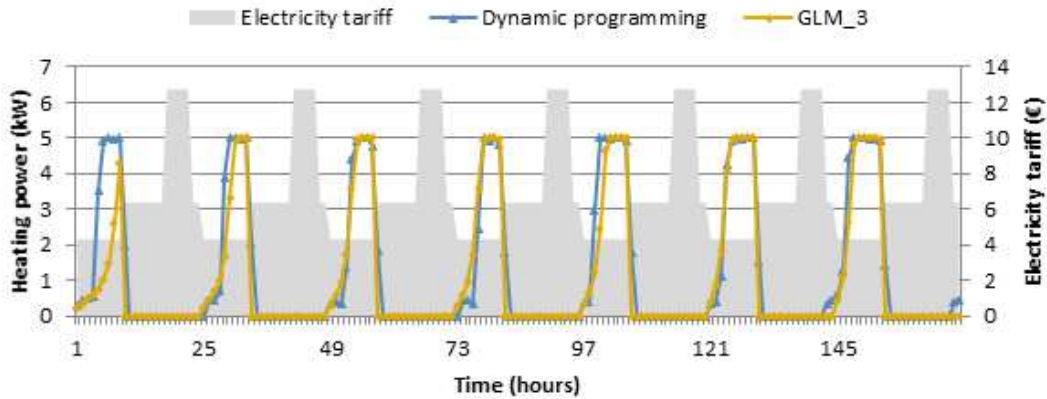


Figure 7: Heating power calculated by dynamic programming and GLM_3 (Third week)

The GLM_3 model presented a satisfactory behaviour and seemed a possible candidate to be used as simplified control system. However, on some occasions, it did not respect the thermal comfort constraints. Therefore, an improved controller was considered that switched heating on as soon as the indoor temperature was below 19°C.

6.4 Application controller

An ideal on-off controller was considered. It was applied during peak and high peak hours as GLM_3 did not work during these periods. Its control law switched between the minimum heating power (0 W) and the maximum heating power (5000 W). The ideal on-off controller was switched on when the indoor temperature fell below 19°C - ε and was switched off when the indoor temperature rose above 19°C + ε (in order to respect the 19°C set point temperature). Assuming that ε tended toward 0, the deadband of the on-off controller ($\pm\varepsilon$) tended toward 0. The use of this ideal on-off controller aimed at assessing maximum performance of GLM_3 + controller.

The control law was the following :

- During off peak hours

$$P(t + \Delta t) = \begin{cases} \text{GLM}_3 & T_{\text{in}}(t) \leq T_{\text{max}} \\ 0 & T_{\text{in}}(t) > T_{\text{max}} \end{cases} \quad (15)$$

- During peak and high peak hours

$$P(t + \Delta t) = \begin{cases} \text{Controller on} & T_{\text{in}}(t) < 19^\circ\text{C} - \varepsilon \\ \text{Controller off} & T_{\text{in}}(t) \geq 19^\circ\text{C} + \varepsilon \end{cases} \quad \varepsilon \rightarrow 0 \quad (16)$$

The obtained results are shown in *Table 6*. We can notice the interesting behaviour of GLM_3 + controller. Firstly, thanks to the on-off controller, GLM_3 + controller respected temperature constraints (the lowest temperature reached was 19°C). Then, we can see a slight deterioration of peak hours and high peak hours shifted. For example, GLM_3 + controller had 92 % of high peak hours which were load shifted in comparison with the 100% of GLM_3 (and the 99 % of dynamic programming). Similarly, GLM_3 + controller had 95 % of peak hours which were load shifted. It was less efficiency than GLM_3 (100 %) but it was better than dynamic programming (88 %). Finally, GLM_3 + controller had a cumulative cost (72.9 €) and an average heat power (1029 W) close to GLM_3 and dynamic programming.

Table 6: GLM_3 + controller results

	GLM_3	GLM_3 + Controller	DP
Average heat power (W)	1023	1029	936
Cumulative cost (€)	72.2	72.9	68
High peak hours load shifted (%)	100	92	99
Peak hours load shifted (%)	100	95	88
TI_{\min} (%)	8	0	0
TI_{\max} (%)	0	0	0
T_{\min} / T_{\max}	18.4 / 23.8	19 / 23.8	19 / 23.4
MAE (%)	40	41	-

Consequently, adding an on-off controller with GLM_3 enabled to improve the GLM_3's behaviour and to respect temperature constraints. Figure 8 shows the GLM_3's behaviour both with and without the on-off controller. To plot GLM_3+controller's graph, the heating power was averaged over one hour time periods.

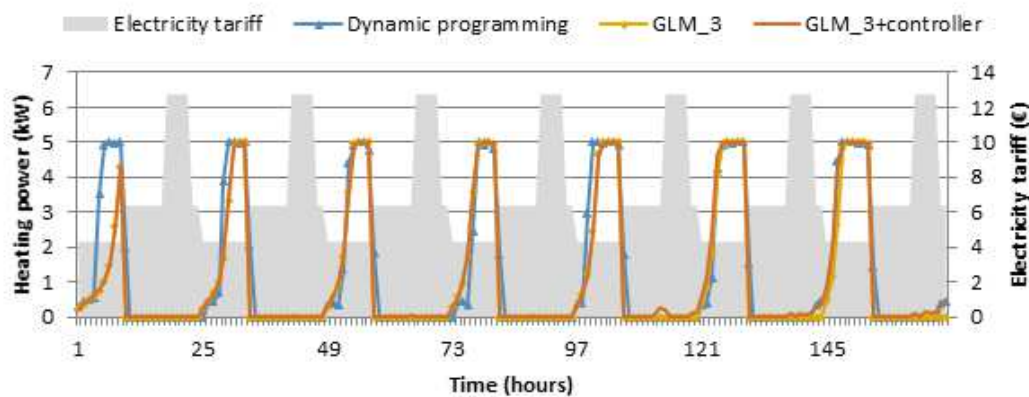


Figure 8: Heating power calculated by dynamic programming, GLM_3 and GLM_3 + controller (Third week)

7. CONCLUSION

Dynamic programming method has been used to study load shifting of heating systems in an energy-efficient building. Due to its computational expense, a statistical technique (generalised linear model) has been introduced that allows for the extraction of logistic decision models from the dynamic programming results. This method models the relationship between explanatory variables and a response variable. The results showed that generalised linear models were able to imitate the general characteristics of the dynamic programming results, with a much smaller computational expense and limited overshooting of the setpoint. To improve the GLM's behaviour, an on-off controller was added that switched heating on as soon as the indoor

temperature did not respect temperature constraints. The results showed that the GLM+on-off controller respected temperature constraints and that there were a slight deterioration of peak hours and high peak hours shifted. Therefore, rule extraction (generalised linear model) is a promising technique for developing operational control strategies. Given their simple mathematical formulation, generalised linear models could be implemented in real-time building systems control. Amongst possible perspectives, the method could be extended for multi-zone building model but this would require to take into account interaction between the several zones of the building and consequently to define a specific explanatory variable.

NOMENCLATURE

Latin			
A	state matrix	P	heating power [W]
a_j	regression parameters	P_{max}	maximum heating power [W]
b	regression parameter	P_{min}	minimum heating power [W]
C	diagonal thermal capacity matrix [J.K ⁻¹]	P_t	heating power at time t [W]
$C_{elec,t}$	electricity price at time t [€]	T	node temperature vector [°C]
C_i	thermal capacity of node i [J.K ⁻¹]	T_i	temperature at node i [°C]
$E[.]$	expected value (first moment)	T_{in}	indoor temperature [°C]
E	input matrix	T_{max}	maximal temperature [°C]
E_t	total energy stored in the building [J]	T_{min}	minimal temperature [°C]
$f(.)$	dynamical system	T_{out}	outdoor temperature [°C]
$f_i(.)$	link function	T_{ref}	reference temperature [°C]
G	feedforward matrix	TI_{max}	high thermal discomfort rate [%]
$Gains$	solar and internal gains [W]	TI_{min}	low thermal discomfort rate [%]
I_{gh}	global horizontal radiation [W.m ⁻²]	u	control vector
J	output matrix	U	driving forces [°C] / [W]
$Losses$	heat losses by conduction, convection, and radiation [W]	U_{gw}	window overall heat transfer coefficient [W.m ⁻² .K ⁻¹]
N_c	dimension of U_t	U_t	set of possible controls at time t
N_{nodes}	number of nodes	v_t	value function at time t
N_S	dimension of X_t	V_0^t	finite-horizon decision problem
SF	Solar Factor (glazing transmittance) [-]	x	state variable describing the system
		x_j	explanatory variables

X_t	set of possible states at time t
y	output variable
Y	outputs vector [°C]

Greek

Δt	time step
$\pm \varepsilon$	controller's dead band [°C]

Abbreviations

DP	Dynamic Programming
GLM	Generalised Linear Model
MAE	Mean Absolute Error
TD_{HPH}	High peak hours training data
TD_{OPH}	Off-peak hours training data
TD_{PH}	Peak hours training data
TRY	Test Reference Year

ACKNOWLEDGEMENT

This work has been supported by the French Research National Agency (ANR) through the "Villes et Bâtiments Durables (VDB) 2012" program (project ANR-12-VBDU-0006).

REFERENCES

- ADEME. 2012. « Chiffres clés du bâtiment ».
- Bellman, Richard. 1957. « E. 1957. Dynamic Programming ». *Princeton University Press. Bellman Dynamic programming 1957.*
- Braun, James E., Kent W. Montgomery, et Nitin Chaturvedi. 2001. « Evaluating the Performance of Building Thermal Mass Control Strategies ». *HVAC&R Research* 7 (4): 403-428. doi:10.1080/10789669.2001.10391283.
- Brun, A., Spitz, C., et Wurtz, E.. 2009. « Analyse du comportement de différents codes de calcul dans le cas de bâtiments à haute efficacité énergétique ». *IXeme colloque interuniversitaire Franco-québécois sur la thermique des systèmes.*
- Chahwane, Layal. 2011. « Valorisation de l'inertie thermique pour la performance énergétique des bâtiments ». Université de Grenoble.
- Dounis, A.I., et C. Caraiscos. 2009. « Advanced control systems engineering for energy and comfort management in a building environment—A review ». *Renewable and Sustainable Energy Reviews* 13 (6–7): 1246-1261. doi:10.1016/j.rser.2008.09.015.
- Favre, Bérenger, et Bruno Peuportier. 2014. « Application of dynamic programming to study load shifting in buildings ». *Energy and Buildings*. doi:10.1016/j.enbuild.2014.07.018.
- Federal Energy Regulatory Commission. 2006. *Assesment of demand response and advanced metering*. Washington DC: Department of Energy.
- Gill, Jeff. 2004. « Generalized Linear Models ». *Encyclopedia of Social Science Research Methods*. Sage. doi:doi: http://dx.doi.org/10.4135/9781412950589.n371.
- Greensfelder, Erik M., Gregor P. Henze, et Clemens Felsmann. 2011. « An investigation of optimal control of passive building thermal storage with real time pricing ». *Journal of Building Performance Simulation* 4 (2): 91-104. doi:10.1080/19401493.2010.494735.

- Hämäläinen, Raimo P, Juha Mäntysaari, Jukka Ruusunen, et Pierre-Olivier Pineau. 2000. « Cooperative consumers in a deregulated electricity market — dynamic consumption strategies and price coordination ». *Energy* 25 (9): 857-875. doi:10.1016/S0360-5442(00)00024-4.
- Hong, J., N. J. Kelly, I. Richardson, et M. Thomson. 2011. « The influence of thermal storage on microgeneration flexibility ». *Microgen II*.
- Le, Ky. 2008. « Gestion optimale des consommations d'énergie dans les bâtiments ». Institut National Polytechnique de Grenoble - INPG.
- Malisani, Paul, B. Favre, S. Thiers, B. Peuportier, Francois Chaplais, et N. Petit. 2011. « Investigating the ability of various buildings in handling load shiftings ». In *2011 IEEE Power Engineering and Automation Conference (PEAM)*, 2:393-397. doi:10.1109/PEAM.2011.6134968.
- Marwan, M., et F. Kamel. 2011. « Demand Side Response to Mitigate Electrical Peak Demand in Eastern and Southern Australia ». *Energy Procedia* 12: 133-142. doi:10.1016/j.egypro.2011.10.019.
- Mathews, E. H, D. C Arndt, C. B Piani, et E van Heerden. 2000. « Developing cost efficient control strategies to ensure optimal energy use and sufficient indoor comfort ». *Applied Energy* 66 (2): 135-159. doi:10.1016/S0306-2619(99)00035-5.
- May-Ostendorp, Peter T., Gregor P. Henze, Balaji Rajagopalan, et Charles D. Corbin. 2013. « Extraction of supervisory building control rules from model predictive control of windows in a mixed mode building ». *Journal of Building Performance Simulation* 6 (3): 199-219. doi:10.1080/19401493.2012.665481.
- Nielsen, Martin Vraa, Svend Svendsen, et Lotte Bjerregaard Jensen. 2011. « Quantifying the potential of automated dynamic solar shading in office buildings through integrated simulations of energy and daylight ». *Solar Energy* 85 (5): 757-768. doi:10.1016/j.solener.2011.01.010.
- Nygaard Ferguson. 1990. « Predictive thermal control of building systems ». Lausanne.
- Peuportier, Bruno, et Isabelle Blanc Sommereux. 1990. « Simulation tool with its expert interface for the thermal design of multizone buildings ». *International Journal of Sustainable Energy* 8 (2): 109-120. doi:10.1080/01425919008909714.
- Pineau, Pierre-Olivier, et Raimo P. Hämäläinen. 2000. « A perspective on the restructuring of the Finnish electricity market ». *Energy Policy* 28 (3): 181-92.
- Wei, Chih-Chiang, et Nien-Sheng Hsu. 2009. « Optimal tree-based release rules for real-time flood control operations on a multipurpose multireservoir system ». *Journal of Hydrology* 365 (3-4): 213-224. doi:10.1016/j.jhydrol.2008.11.038.
- Wyse, Bryan. 2011. « Investigation into the Time-Shifting of Domestic Heat Loads ». Glasgow, Scotland: University of Strathclyde.

Assessing simplified and detailed models for predictive control of space heating in homes

Kun Zhang¹, Narges Roofigari E.¹, Humberto Quintana¹, Michaël Kummert¹

⁽¹⁾ Polytechnique Montréal, Montréal, Canada

1. ABSTRACT

A model of a real system is required for predictive control to determine the best control sequence when disturbance forecasts and future system status are considered over a defined time horizon. The selected model should strike a balance between its accuracy and simplicity. This paper presents a comparison between different modeling approaches for predictive control of space heating. The case study is electric baseboard heating in homes within cold climate regions with the objective of reducing peak electricity demand (and saving costs if tariffs include a peak power charge). Detailed TRNSYS models of the selected house are developed and predictive control is implemented by using GenOpt as the optimization tool. This approach is compared with optimal predictive control algorithms based on simpler models. These models are obtained by parameter identification using data generated from the detailed TRNSYS models. Both approaches use perfect forecasts for the occupancy and the weather data in order to focus the analysis on model differences. Results show that MPC can deliver a significant reduction in power demand during on-peak periods with both modelling approaches (55% with detailed model, 33% with simplified model). The detailed model delivers significantly better savings but implies a calculation time that is more than 2 orders of magnitude higher. The potential of both approaches is discussed in the context of residential heating control to support a smart grid.

Keywords: simplified model, model predictive control, TRNSYS, GenOpt

2. INTRODUCTION

In cold climates, the peak power demand on the electrical grid is generally reached during the coldest day(s) of winter, due to the significant contribution of space heating to the peak load. In the Canadian province of Québec, the most recent historical peak was reached on January 22nd, 2014 at 7h26 AM, while the temperature was below -25 °C across most of the province (Hydro-Québec, 2014). It is estimated that residential electric heating accounts for 30 % of the grid peak electrical demand, with a market share of 70 % (Kummert, Leduc , & Moreau , 2011). Critical peak events typically represent some 50 h per year, generally occurring during a morning peak (approximately 6 AM to 9 AM) and an afternoon/evening peak (approximately 4 PM to 8 PM). Utility companies place a high value on kWh used during these critical peak events, and this paper looks at the potential of reducing the peak power demand of residential heating in a typical house during these two daily peak periods. The analysis focuses on the coldest day of the year, which is January 12th for the typical weather file used in the study.

Model predictive control has shown potential for load shifting and energy and costs savings by taking into account predictions of process states in the decision making. (Oldewurtel F. , Parisio, Jones, & Morari, 2010) and (Oldewurtel F. , et al., 2012) compared the current practice, Rule Based Control (RBC), with prediction-based approaches and confirmed additional energy savings by using a Stochastic Model Predictive Control (SMPC) as well as a predictive non-stochastic controller, so called Certainty Equivalence (CE).

MPC has been practically applied and theoretically investigated in chemical engineering since 1960s (Morari & Lee, 1999) and lately it has drawn increasing interest for supervisory control in building engineering field (Coffey, 2013). The idea of MPC proposed for building supervisory control can be dated back as early as in 1988 (Kelly, 1988) but it does not witness a steady growing research until the last decade (Prívarva, et al., 2013).

The MPC research on buildings has seen a wide variety of systems including ice and building thermal mass storage (Henze, Felsmann, & Knabe, 2004) and (Henze, Le, Florita, & Felsmann, 2006), window operation for mixed natural and mechanical ventilation in an office building (May-Ostendorp P. , Henze, Corbin, Rajagopalan, & Felsmann, 2011) and (May-Ostendorp P. , Henze, Rajagopalan, & Corbin, 2013), VAV control (Wang & Jin, 2000) and (Nassif, Kajl, & Sabourin, Simplified model-based optimal control of VAV air conditioning system, 2005a), (Nassif, Stainslaw , & Sabourin, 2005b) and other systems proposed in the Model Predictive Control in Buildings workshop in Canada (IBPSA-Canada, 2011) such as thermally activated building system with ground coupled heat pump (Verhelst, Sourbron, Antonov, & Helsen , 2011), chiller and cooling tower system (Ma & Borrelli, 2011), and so on.

Among the research issues in MPC on buildings, the foremost is the choice of building models, which determines the effectiveness and efficiency of control strategies. The main building models utilized by researchers can be divided into three categories: physical models built by building energy software programs (e.g. EnergyPlus, TRNSYS), grey box (e.g. RC network) and data-driven black box models. Because of the complexity and high-computation requirement of the physical models, they are mostly used with other optimization tools (e.g. GenOpt) for offline predictive control (Coffey, 2013) and control rules extraction (May-Ostendorp P. , Henze, Rajagopalan, & Corbin, 2013). Simpler models can be used for real-time online MPC due to their better suitability for online parameter identification and their lower computational requirements.

A simplified model for the transient heat transfer through a multilayer structure can be developed based on simulating the heat transfer by the concept of lumped resistance and capacitances. There exist two general approaches for obtaining proper values for this network of lumped resistance and capacitances. One approach is based on physical characteristics of building elements. This approach requires knowledge about details of building elements including zones specifications, constructions and materials. Sturzenegger et al. in (Sturzenegger, Gyalistras, Semeraro, Morari, & Smith, 2014) developed a Toolbox for generation of bi-linear resistance-capacitance models based on this approach. Lehmann et al. in (Lehmann, Gyalistras, Gwerder, Wirth, & Carl, 2013) also proposed an intermediate-complexity (12th order) bilinear model for a single room. The other approach is based on parameter identification. This approach requires sufficient excitation conditions that yield determining a precise model. This approach can be performed in time or frequency domain. Also there exist different mechanisms for identifying the parameters. Time domain input/output data-based techniques include extended Kalman filters (Huchuk, A. Cruickshank, O'Brien, & Gunay, 2014), maximum likelihood, prediction error minimization and subspace system identification (Candanedo, Dehkordi, & Lopez, 2014). This approximation results in a simplified model which in general is not adaptable to parameter variations. The model may or may not describe long-term dynamics depending on the number of time constants of the corresponding RC network. Madson and Holst in (Madson & Holst, 1995) suggested using a two time constant model for a single-story building. They utilized maximum likelihood method for identifying the model parameters. (Wang & Xu, 2006) combined physics law approximation with parameter identification based on operation data to obtain a simplified model of a thermal zone in a building yielding a multiple time constant model that takes into

account internal mass and multilayer external wall/roof thermal dynamics. They used a genetic algorithm to identify the parameters corresponding to the internal mass.

3. OBJECTIVE AND METHODOLOGY

The objective of this work is to contrast two modeling approaches in assessing the potential of MPC to reduce the power demand associated with space heating during critical grid peak event. The first method uses a detailed (physical) building model implemented in TRNSYS and a generic optimization tool (GenOpt) to perform control optimization. The second approach uses a simple RC network to model the same building, together with a parameter identification method and an optimization process implemented in Matlab. Both methods are compared using a simulation environment based on TRNSYS and combining GenOpt to TRNSYS (detailed model) or Matlab to TRNSYS (RC model).

3.1 Methodology

The following steps are the common path for the implementation of the two approaches. More details can be found in the corresponding sub-sections.

- Define the main assumptions (optimization problem) for this study
- Implement a TRNSYS model of the selected building to act as a reference that will be used to assess the different control strategies
- Define a cost function that includes on-peak/off-peak electricity cost and penalties for constraints violation
- Implement the MPC approach with both models
 - Couple GenOpt and TRNSYS and compare different optimization strategies based on the detailed TRNSYS model
 - Develop a simplified RC model in Matlab, perform parameter identification, couple Matlab to TRNSYS and implement the optimal MPC strategy in Matlab.
- Assess both control strategies using the detailed TRNSYS model – this means that the first control strategy will have no modeling error, as the same model is used both to develop the control strategy and to assess its performance

3.1.1 Main assumptions – optimization problem

The considered problem is to reduce the electrical demand for heating in a typical house during the two periods representing critical conditions for the electrical grid. For the sake of this study, the critical period is defined as 5:30 AM to 9:30 AM and 4:30 PM to 8:30 PM. Electricity is not considered to be free outside of these on-peak periods but its value is significantly reduced – the context is to assess the potential of peak savings for a utility, not to optimize a customer's electrical bill with a realistic on-peak / off-peak tariff.

The control system is allowed to modify the setpoints in the basement and the living area of the house, but not in the bedrooms (which are also electrically heated). It is assumed that the thermostat setpoint can be adjusted between 20 °C and 23 °C when the rooms are occupied; between 18 °C and 23 °C when they are not occupied. Occupancy in the living area and basement is assumed to be the same, during a morning period (6:30 AM to 8:00 AM after the occupant wake up and before they leave the house) and an evening period (4:30 PM to 10 PM after the occupants return from school/work and before they go to their bedrooms).

Figure shows the on-peak periods as yellow areas and the occupancy periods as blue rectangles. The allowable range for the thermostat setpoints is also shown by dotted lines.

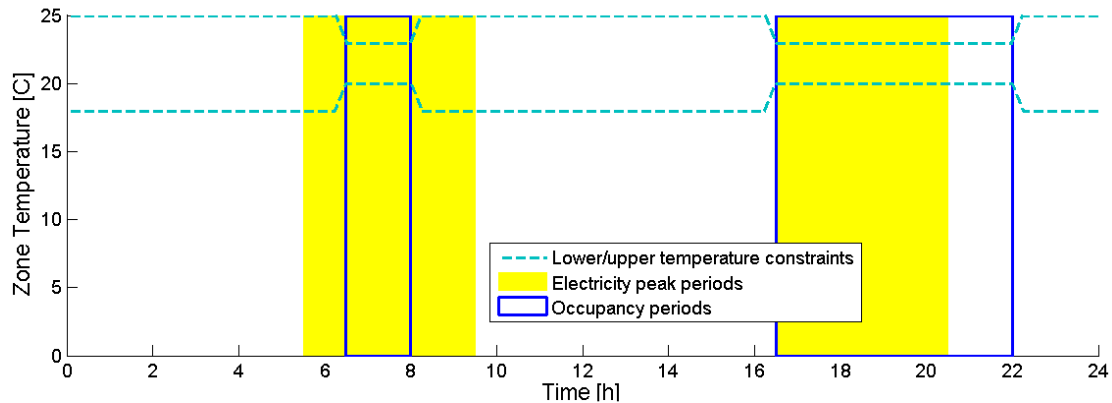


Figure 1: Occupancy, on-peak periods and allowable range for thermostat setpoint

Only one day is considered in the optimization study, January 12th. That day is the coldest day in the typical weather year (CWEC) for Ottawa. The simulation is run from January 1st to January 12th to allow for building pre-conditioning, as the multizone building model in TRNSYS (Type 56) is initialized with unrealistic temperature profiles (uniform temperature across zones and building envelope).

Uncontrolled disturbances such as weather variables (temperature, solar radiation, etc.) and internal gains (from occupants, lighting and appliances) are considered to be known to the optimization process (perfect forecasts). This will provide a higher bound for the performance of both MPC algorithms and isolate the differences attributable to different models from other influences.

3.1.2 Selected house

In 1998, the Canadian Centre of Housing Technology (CCHT) built twin houses for research purposes according to the R-2000 standard (increased energy performance and air tightness). The houses (Figure 2) are typical North-American wood-frame buildings with brick facing, and have five main zones (basement, two floors, garage and attic) and the liveable area is approximately 210 m². Home automation systems simulate occupancy by activating appliances, lights, water valves and incandescent bulbs (for internal gains due to humans). Measures are collected by 23 meters and more than 250 sensors providing 12000 readings every 24 hours (Swinton, et al., 2001).

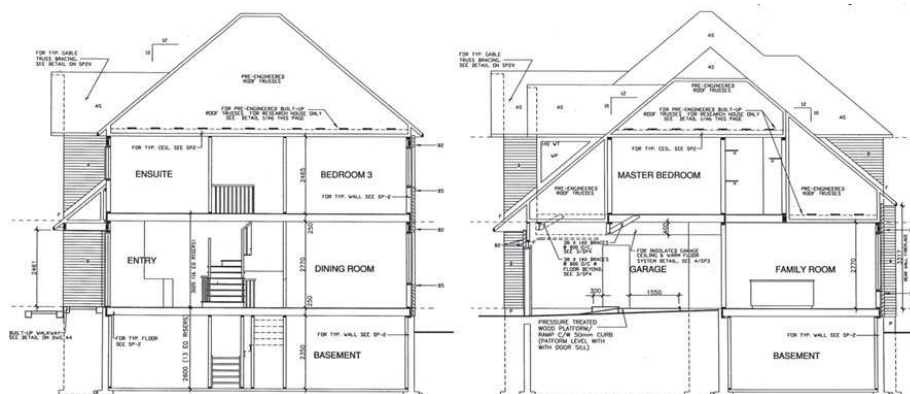


Figure 2: CCHT house drawings

3.1.3 TRNSYS model

The TRNSYS model of the CCHT house has five thermal zones (first floor, second floor, basement, garage, and attic) and schedules for thermal internal gains (people, appliances and lighting). The basement and first floor are assumed to be living spaces, while the second floor is a sleeping space with a different occupancy profile. Other zones are not occupied. No detailed HVAC system is modeled and the idealized convective heating available in the TRNSYS multizone building model (Type 56) is used, as it is a reasonably accurate representation of electric baseboard heating commonly used in Québec. The maximum heating power in living room, sleeping room and basement is set to 7.5kW, 5kw and 5kW to represent the capacity of installed electric baseboards.

Type 56, the multizone building model in TRNSYS, is the main element of the system model. This component (TRNSYS “Type”) has all the details about house’s geometry and materials, and optional inputs for external heating/cooling and internal gains. Other elements of the TRNSYS model define the shading and the *basement-ground coupling model* (Type 1244). Infiltration is set to a constant value of 0.075 ACH.

3.1.4 Cost function

The cost function J , in equation (1), represents a measure of the power demand for the on-peak and off-peak hours but not the real cost of electricity or power.

$$J = \sum_{i=1}^{96} \{R_i U_i + \mu \{ \max(0, T_i - T_{u_i}) + \max(0, T_i - T_i) \} \} \quad (1)$$

In this cost function the first term represents the heat power demand costs, where U_i denotes the heat power at time i . R_i denotes the heat power price. As the optimization objective is to minimize power demand during peak hours, a relatively larger weighting factor is assigned for the on-peak power by setting the price to be 100 times of that in off-peak periods.

The second term in this cost function is a penalty function that guarantees the desired temperature comfort levels. i.e., $T_{l_i} \leq T_i \leq T_{u_i}$, where T_i denotes the temperature and T_{l_i} and T_{u_i} represent the lower and upper bounds at time i respectively. μ denotes the weighting factor for this penalty function. Its value is selected to be 10000 by trial and error to implement a soft constraint on the room temperature without compromising numerical stability. The penalty function is evaluated as zero when the room temperature is between the defined intervals but is much larger when the temperature does not obey the comfort limits.

The actual cost function implemented in the two MPC approaches is slightly different (see details in the corresponding sections below), but the performance presented in the Results section is always assessed using the cost function described here above.

4. IMPLEMENTATION

4.1 Optimization with GenOpt

GenOpt is a generic program developed mainly for building system optimization with an extended library of optimization algorithms. It can be used with any text-based simulation program (Wetter, 2001).

As illustrated above, TRNSYS is used for the building simulation. Before launching the optimization in GenOpt, templates of input and output files have been created in TRNSYS. In each optimization, GenOpt updates the variables, i.e. set points in this case, in the templates.

GenOpt then searches for the minimal cost function value among all the optimization results. In this study, the ‘‘Hybrid Generalized Pattern Search Algorithm with Particle Swarm Optimization’’ Algorithm is employed (Wetter, 2011).

The cost function is calculated inside of TRNSYS, as well as penalty function and all other constraints, so that GenOpt only needs to read the designated parameters in corresponding files.

4.2 Optimization with Matlab

In this section, the procedure for developing an online MPC-based heating control is presented. The following subsection derives the simplified model that is required for this control approach.

4.2.1 Simplified model and parameter identification

The concept of thermal zone can be utilized to describe the heat flux in a building. Once a thermal zone is specified, a lumped RC network can describe the zone temperature at each time. The model may or may not describe long-term dynamics depending on the number of time constants of the corresponding RC network. In this work we use a network consisting of six resistances and three capacitances as shown in Figure 3. In this figure, ϕ_s , ϕ_l and ϕ_b denote the overall heat that is being injected in the zones. This heat includes the (controlled) heating power, internal heat gains and solar radiation.

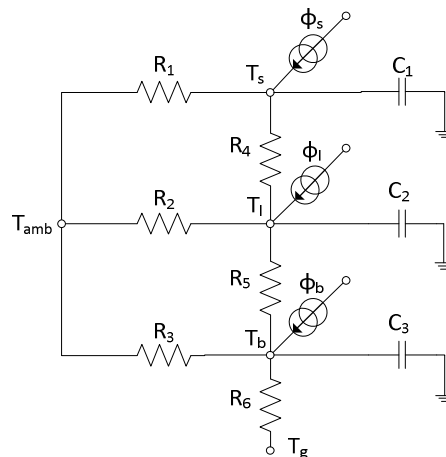


Figure 3: RC model schematic

Therefore, the following model describes thermal dynamics in the model.

$$\dot{x} = A_c x + B_c U + E_c W \quad (2)$$

Where the vector $x = [T_s \ T_l \ T_b]^T$ denotes the matrix of system states consisting the sleeping room, living room and basement temperatures. $U = [U_s \ U_l \ U_b]^T$ denotes the control inputs which are heat addition rates (heating power) to each zone, and $W = [\phi_{IG_s} \ \phi_{IG_l} \ \phi_{IG_b} \ \phi_{sol} \ T_{amb} \ T_g]$ represents the disturbance inputs where ϕ_{IG_s} , ϕ_{IG_l} and ϕ_{IG_b} denote the internal heat gains corresponding to each zone, ϕ_{sol} denotes the solar radiation incident on the South façade (used as a proxy for the total solar gains), T_{amb} denotes the ambient temperature and T_g denotes the ground temperature. The triple (A_c, B_c, E_c) is obtained as follows and consists of parameters that will be identified.

$$A_c = \begin{bmatrix} -\left(\frac{1}{R_4 C_1} + \frac{1}{R_1 C_1}\right) & \frac{1}{R_4 C_1} & 0 \\ \frac{1}{R_4 C_2} & -\left(\frac{1}{R_4 C_2} + \frac{1}{R_2 C_2} + \frac{1}{R_5 C_2}\right) & \frac{1}{R_5 C_2} \\ 0 & \frac{1}{R_5 C_3} & -\left(\frac{1}{R_3 C_3} + \frac{1}{R_5 C_3} + \frac{1}{R_6 C_3}\right) \end{bmatrix}, B_c = \begin{bmatrix} \frac{1}{C_1} & 0 & 0 \\ 0 & \frac{1}{C_2} & 0 \\ 0 & 0 & \frac{1}{C_3} \end{bmatrix}, E_c = \begin{bmatrix} \frac{1}{C_1} & 0 & 0 & \frac{\alpha_1}{C_1} & \frac{1}{R_1 C_1} & 0 \\ 0 & \frac{1}{C_2} & 0 & \frac{\alpha_2}{C_2} & \frac{1}{R_2 C_2} & 0 \\ 0 & 0 & \frac{1}{C_3} & \frac{\alpha_3}{C_3} & \frac{1}{R_3 C_3} & \frac{1}{R_6 C_3} \end{bmatrix} \quad (3)$$

Where α_1 , α_2 and α_3 denote multiplication coefficients applied to the solar radiation for each thermal zone.

We used prediction error minimization for the purpose of identifying the twelve parameters. As such, we consider the discrete time form of the equation (2) as follows:

$$x(k+1) = Ax(k) + BU(k) + EW(k) \quad (4)$$

Where the triple $(A, B, E) \in \mathfrak{R}^{3 \times 3 \times 6}$ denotes the discretized form of (A_c, B_c, E_c) by using zero-order hold method.

We assume the availability of the information about the state vector, control inputs and the disturbance inputs and estimate the parameter values that result in the minimal error between the predictions and true states by solving the following problem for the parameter identification of the three-zone building:

Given $x(k)$, $U(k)$ and $W(k)$ for $k = 0, 1, \dots, N$, find the matrices A , B and E that minimize the error function E :

$$E = \sum_{k=0}^{N-1} (\hat{x}(k+1) - x(k+1))^T (\hat{x}(k+1) - x(k+1)) \quad (5)$$

Where $\hat{x}(k)$ denotes the model state at time k and depends on the 12 parameters, namely R_1 , R_2 , R_3 , R_4 , R_5 , R_6 , C_1 , C_2 , C_3 , α_1 , α_2 , α_3 , as follows:

$$\hat{x}(k+1) = Ax(k) + BU(k) + EW(k) \quad \text{for } k = 0, 1, \dots, N-1 \quad (6)$$

In this identification problem, N denotes the number of training samples and therefore the period of time selected for training will be $N \times \frac{1}{f_s}$ hours where f_s denotes the sampling frequency ($\lfloor \frac{1}{hour} \rfloor$). In the next section, we use the identified building thermal model for the purpose of centralized control of zone temperature setpoints.

The identification and validation algorithms can be summarized by the following steps:

- Identification

- [Training Step]: The optimal control input (Power heat) $U(k) = [U_s(k) \ U_i(k) \ U_b(k)]^T$ corresponding to the obtained temperature setpoints from the GenOpt optimization are considered as the control input during the first 12 days of January. This choice ensures that the generated input/output training data provides enough excitation. The corresponding outputs, i.e., the zone temperatures $T_s(k)$, $T_i(k)$ and $T_b(k)$ for $k = 0, 1, \dots, 12 \times 24 \times f_s - 1$ are “measured” (received from the TRNSYS simulation) and the disturbance inputs $W(k)$ for $k = 0, 1, \dots, 12 \times 24 \times f_s - 1$ are collected. Note that due to the modelling structure, all

of the states of the system are measurable and therefore there is no need to observe the states.

- b) The one-step ahead predicted outputs, i.e., $\hat{x}(k+1) = [\hat{T}_s(k+1) \ \hat{T}_l(k+1) \ \hat{T}_b(k+1)]^T$ for $k = 0, 1, \dots, 12 \times 24 \times f_s - 1$ are formulated based on current system states $x(k) = [T_s(k) \ T_l(k) \ T_b(k)]^T$, current control input $U(k) = [U_s(k) \ U_l(k) \ U_b(k)]^T$, current disturbance input $W(k)$ for $k = 0, 1, \dots, 12 \times 24 \times f_s - 1$, and the unknown model, i.e., (A, B, E) and by using equation (6).
- c) The prediction error minimization problem is solved by using interior point algorithm, yielding (A, B, E) .
- d) Finally, the parameters are identified as follows:
- The diagonal values of the matrix B give the capacitance values (C_1, C_2, C_3) .
- Once the capacitance values are determined,
- The 4th column of the matrix E gives the solar radiation coefficient values $(\alpha_1, \alpha_2, \alpha_3)$.
 - The 5th and the 6th columns of the matrix E give R_1, R_2, R_3, R_6 values.
 - $A_{1,2}$ and $A_{2,3}$ give R_4 and R_5 .

- Validation

- a) The optimal control input (Power heat) $U(k) = [U_s(k) \ U_l(k) \ U_b(k)]^T$ corresponding to the obtained temperature set-points from the GenOpt optimization are considered as the control input during 12th day of January. The corresponding outputs, i.e., the zone temperatures $x(k+1) = [T_s(k+1) \ T_l(k+1) \ T_b(k+1)]^T$ for $k = 11 \times 24 \times f_s, \dots, 12 \times 24 \times f_s - 1$ are “measured” (received from the TRNSYS simulation) and the disturbance input $W(k)$ for $k = 11 \times 24 \times f_s, \dots, 12 \times 24 \times f_s - 1$ are collected. As mentioned previously, all of the states of the system are measurable and therefore there is no need to observe the states.
- b) The one-step ahead predicted outputs, i.e., $\hat{x}(k+1) = [\hat{T}_s(k+1) \ \hat{T}_l(k+1) \ \hat{T}_b(k+1)]^T$ for $k = 11 \times 24 \times f_s, \dots, 12 \times 24 \times f_s - 1$ are calculated based on current system states $x(k) = [T_s(k) \ T_l(k) \ T_b(k)]^T$, current control input $U(k) = [U_s(k) \ U_l(k) \ U_b(k)]^T$, current disturbance input $W(k)$ for $k = 11 \times 24 \times f_s, \dots, 12 \times 24 \times f_s - 1$, and the previously determined model, i.e., (A, B, E) and by using equation (6).
- c) The root mean square deviation (RMSD) between the measured outputs and the one-step ahead predicted outputs corresponding to all three zone temperatures during 12th day of January are calculated and obtained as 0.07, 0.4 and 0.5 °C for sleeping room, living room and basement respectively and the corresponding RMSD for the 24 hours-step ahead predictions are obtained as 0.7, 1.15 and 2.05 °C for sleeping room, living room and basement respectively.

4.2.2 MPC Approach

This section presents the optimal set-point solution to the MPC problem for the building. In this structure the following dynamic thermal equations that were developed in Section 4.2.1, govern the control design through performing the predictions based on the control input information.

$$x(k+1) = Ax(k) + BU(k) + EW(k) \quad (7)$$

We are now in position to state our MPC problem.

At any time t_k , $k \in \{0, 1, 2, \dots\}$, given $x(k)$ and $\{W(k), W(k+1), \dots, W(k+P-1)\}$, find the input sequence $\{U(k|k), U(k+1|k), \dots, U(k+P-1|k)\} \in \mathfrak{R}^3$, that minimizes the cost function $J(k)$:

$$J(k) = \sum_{i=0}^{P-1} U^T(k+i|k)R(k+i)U(k+i|k) \quad (8)$$

Where the prediction equations are as follows

$$x(k+i+1|k) = Ax(k+i|k) + BU(k+i|k) + EW(k+i|k) \quad \text{for } i = 0, 1, \dots, P-1 \quad (9)$$

and $x(k|k) = x(k)$

Moreover, the constraints of the problem are given by

$$S(k+i)U(k+i|k) \leq s(k+i) \quad \text{for } i = 0, 1, \dots, P-1 \quad (10)$$

$$G(k+i)x(k+i+1|k) \leq g(k+i) \quad \text{for } i = 0, 1, \dots, P-1 \quad (11)$$

$$G_{eq}(k+i)x(k+i+1|k) = g_{eq}(k+i) \quad \text{for } i = 0, 1, \dots, P-1 \quad (12)$$

In equation (8), the prediction horizon is represented by P and $\{U(k|k), U(k+1|k), \dots, U(k+P-1|k)\}$ denotes the set of designed control inputs that minimize the objective function. $R(k+i) \in \mathfrak{R}^{3 \times 3}$ denotes a positive definite matrix representing the input penalty matrix corresponding to the time instant $k+i$ for $i = 0, 1, \dots, P-1$. In equation (9) (A, B, E) represents the linear state space model as previously given in equation (7). Equation (10) represents the constraints on inputs. Equation (11) represents the set of state constraints at each time instant $k+i+1$ for $i = 0, 1, \dots, P-1$. These constraints represent the lower and upper limits of temperature, i.e., the temperature comfort zone. Finally, equation (12) represents a set of equality constraints on zones temperatures, namely, the zones that are assigned to have equal temperatures and the zones that are assigned to have a certain temperature value. The constraints stated in equation (10) (11) and (12) can be translated to constraints on control input by using equation (9) and represented in the form of linear constraints as follows

$$\begin{cases} S(k+i)U(k+i|k) \leq s(k+i) \\ G(k+i)(Ax(k+i|k) + BU(k+i|k) + EW(k+i|k)) \leq g(k+i) \\ G_{eq}(k+i)(Ax(k+i|k) + BU(k+i|k) + EW(k+i|k)) = g_{eq}(k+i) \end{cases} \quad \text{for } i = 0, 1, \dots, P-1 \quad (13)$$

The optimization algorithm can be summarized by the following steps:

- At any time t_k , $k \in \{0, 1, 2, \dots\}$:
 - a) $T_s(k)$, $T_l(k)$ and $T_b(k)$ are “measured” (received from the TRNSYS simulation).
 - b) The MPC optimization problem is solved by using active set algorithm, yielding $U^*(k+i|k)$, for $i = 0, 1, \dots, P-1$.

- c) The zone temperatures $T_s^*(k)$, $T_l^*(k)$ and $T_b^*(k)$ corresponding to the optimal control signals are obtained from the internal model provided in equation (9).
- d) $T^*(k) = [T_s^*(k) \ T_l^*(k) \ T_b^*(k)]$ are sent to the TRNSYS model to be used as thermostat set-points ($T_s^*(k)$ is actually ignored in this study)
- e) Only the first control signal, i.e., the heating power, is applied and the optimization process is started again at the next time step (receding horizon).

5. RESULTS

All the results presented in this section are for January 12, as an example of a very cold day that would cause a critical peak event on the electrical grid. From the utility's point of view the objective is to reduce the peak power demand of a large set of houses where demand-shifting strategies would be implemented. The main criterion used to assess the performance of different control strategies has therefore been selected as the average power used during the on-peak period, rather than the absolute peak power for one particular house. The maximum power during the on-peak period is also reported in the results.

5.1 Base cases

Two base cases are considered for comparison with MPC results: constant setpoint and night setback cases, as shown in Figure 4 and Figure 5. The heating power in the sleeping zone is reported only for reference, because it will not be affected by predictive control strategies.

The constant setpoint profile in Figure 4 results in a significant electrical demand during the on-peak periods; while the demand is actually lower during most of the day (January 12th is a sunny day, which is often the case for extremely cold days in Québec). The average power demand during on-peak periods is 6 kW.

The night setback setpoint profile shown in Figure 5 leads to a large increase of the heating power at the end of the 2 setback periods, which were set between 7:45 and 16:00, and between 21:30 and 6:00 (the setback periods are chosen by trial and error so that the temperature can reach the thermal comfort requirement just when the living room is occupied). This results in a higher power demand at the beginning of the morning on-peak period but since the setback period starts within the on-peak period, the overall performance (indicated by the average electrical power demand during the on-peak periods) is marginally worse than for the constant setpoint scenario, at 6.6 kW.

In both Figure 4 and Figure 5, we can see that the heating power drops suddenly at around 19 h because dishwasher (1.7 kW) and dryer (8.1 kW) are turned on at this moment. Other drops are due to one or more zones overheating due to internal gains or solar gains.

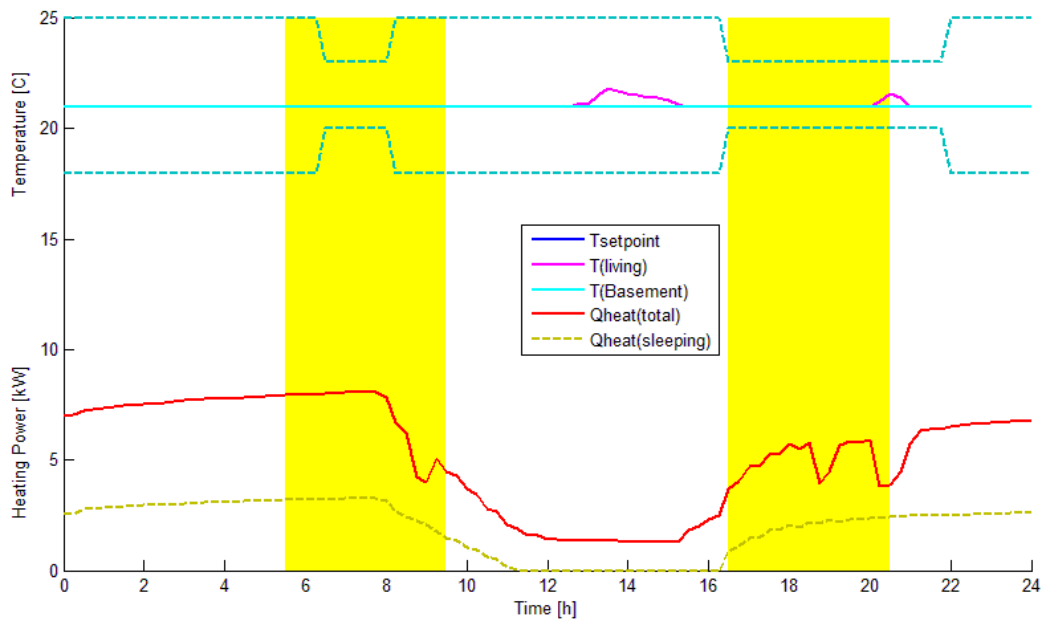


Figure 4: Constant Setpoint

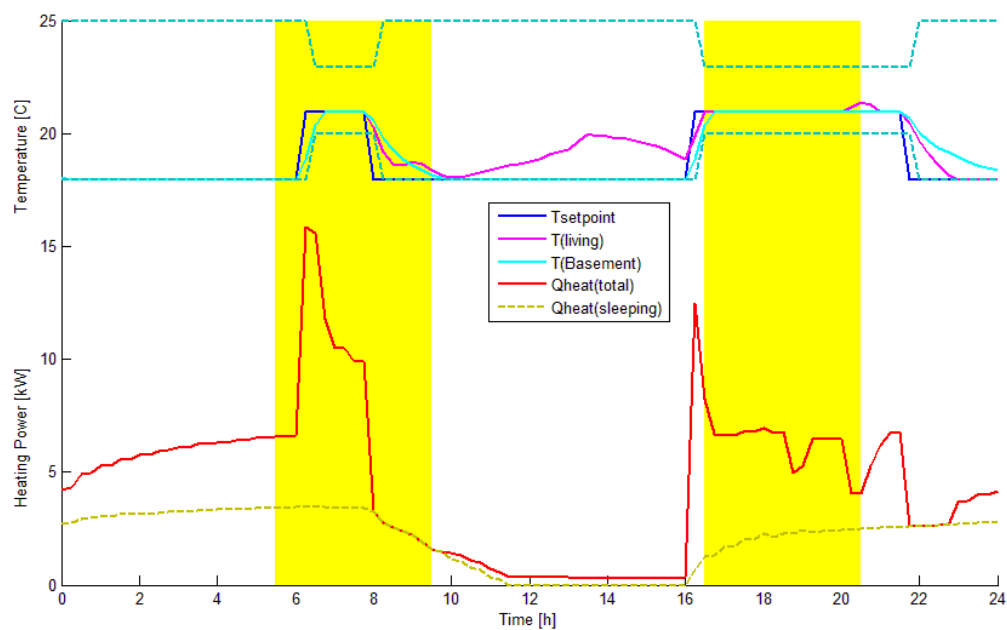


Figure 5: Night Setback

5.2 GenOpt + TRNSYS MPC

The setpoint profile obtained by MPC with GenOpt is shown in Figure 6. The optimal control strategy reduces the heating setpoint during unoccupied periods (even though the “cost” associated with electricity within these periods is very low), and ramps up the setpoint to the maximum allowed value approximately 3 h before the on-peak periods so that the building is preheated (the preheating is shorter in the afternoon). The building is then left free-floating until it cools down to the lower setpoint limit.

While the general shape of the setpoint profile corresponds to what was expected, the jagged profile is somewhat surprising. The sudden changes in the setpoint can be attributed to two phenomena. First, there is a lack of feedback to the optimization process in case of a sudden drop: once the setpoint drops faster than the rate at which the building cools down naturally,

there is no difference in the cost function until the setpoint reaches some constraints. Second, GenOpt algorithms are sensitive to numerical noise in the cost function and building simulation programs often results in noisy numerical results. The optimization process was also found to be sensitive to initial values, as will be shown below in Section 5.4.

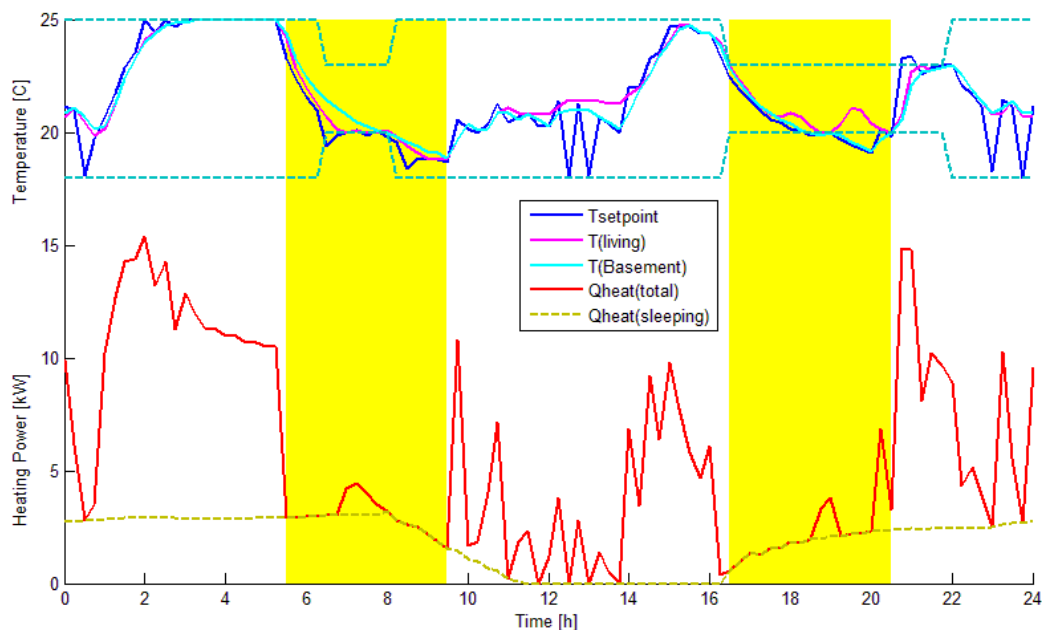


Figure 6: MPC with GenOpt

The average power demand during on-peak periods is 2.6 kW, which is a significant reduction (over 50 %) compared to the base cases. The computing time is very significant, with a 12-day simulation (with a 1-day optimization) taking more than 16 h of computing time on an i7-4770 CPU (3.5 GHz) – the same simulation with a constant setpoint or night setback profile takes about 20 seconds.

5.3 Matlab (RC-model) MPC

The internal model required by the online MPC approach was obtained using first 12 days of January as the training samples. For the purpose of online control with MPC, the optimization problem was solved by using FMINCON function in MATLAB. The prediction horizon is set to 24 hours as in the case of the GenOpt optimization. However, other tests have shown that similar results are obtained for any prediction horizon longer than 4 hours. A receding horizon is applied and the process is repeated at every time step. It can be clearly observed from Figure 7 that the online controller decides to preheat the living room around 1:15 AM, a long time before the peak period starts. The strategy then differs from the GenOpt-TRNSYS results in that some heating is applied during the first on-peak period. This results in a lower cooling down rate that seems to miss the minimum allowable value at the end of the morning occupancy period. Preheating is then used again before the second on-peak period, although not using the maximum available power. Again, the profile is sometimes jagged, which can be partly attributed to the same reasons as for the GenOpt-TRNSYS results. In addition, the model used internally by the optimization algorithm is not 100 % accurate (as shown by RMSD values in section 4.2.1), which leads to corrections at each time step given the receding horizon method. The MPC results are also sensitive to initial values and to cost function parameters, as discussed below.

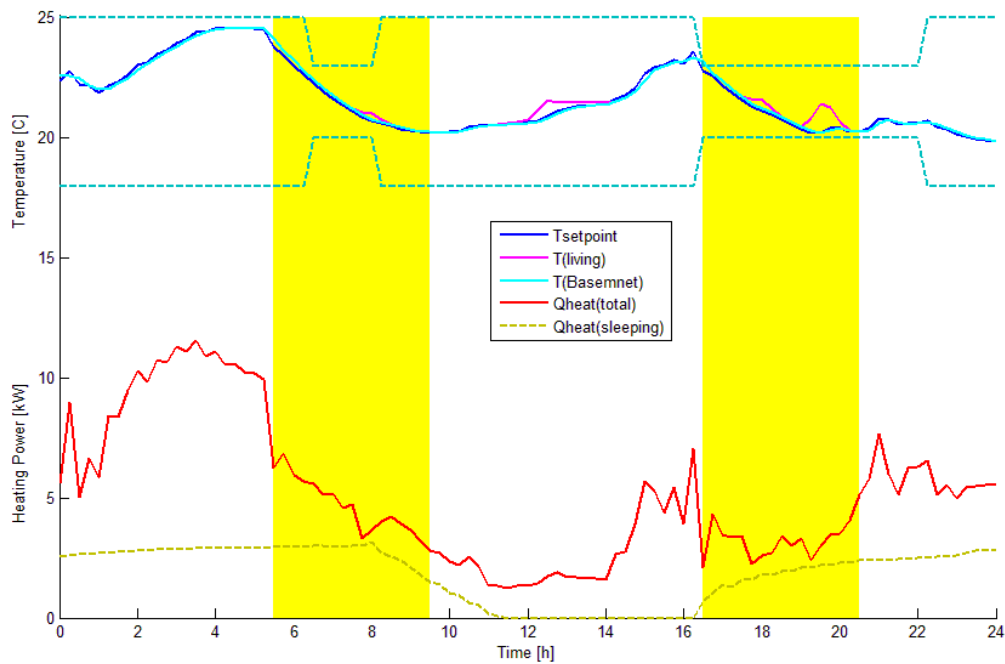


Figure 7: MPC with MATLAB

The average power demand during on-peak periods is about 4 kW, which is not as impressive as the GenOpt-TRNSYS results but is still a significant reduction (33 %) compared to the base cases. The computing time is very acceptable, with the 12-day simulation taking about 4 minutes (12 times longer than the constant profile, but about 250 times faster than TRNSYS-GenOpt).

5.4 Sensitivity of the optimization processes

During the development of the optimization methodology, several different initial conditions were tested. The results presented above for the GenOpt-TRNSYS optimization rely on initial values that are based on a previous study (Kummert et al, 2011).

If initial values are set to 21 °C for the whole day, the optimization process reaches a very different solution with large oscillations shown in Figure 8. Even though the difference in cost function (power used during the on-peak periods) is only marginally affected, the solution is clearly less desirable than the one obtained with “informed” initial values. The computational time is also affected (more than doubled).

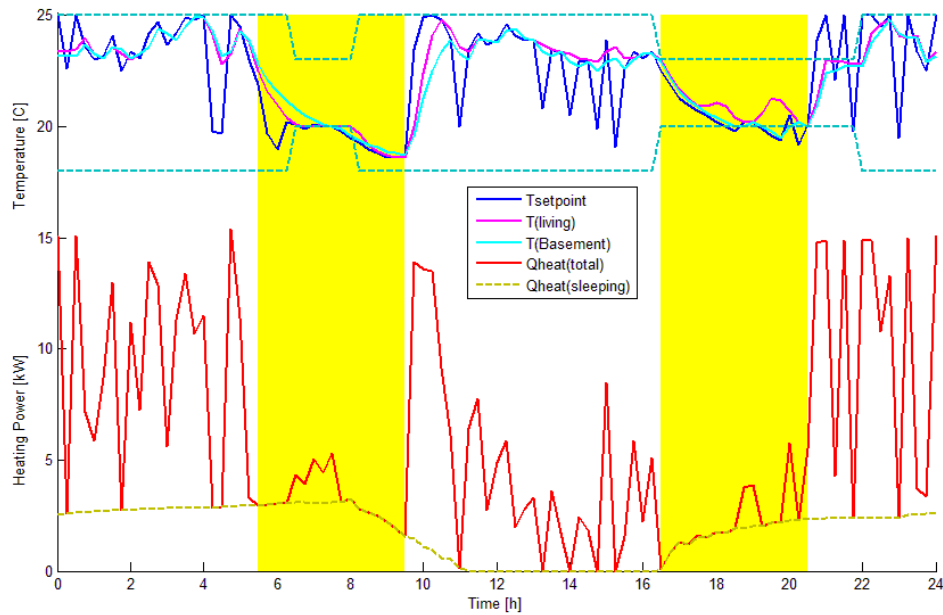


Figure 8: GenOpt-TRNSYS MPC with poor initial values

Very large oscillations can be observed on setpoint temperatures and heating power. This can be partly explained by the fact that the exact value of the setpoint has no impact on the building behavior once it is above the temperature that could be reached with full power or once it is below the temperature that would be reached in free-floating, without heating. So there is no impact on the cost function when GenOpt tries very different values of the setpoint. To illustrate this, consider the situation at 11 AM. GenOpt reduces the setpoint drastically, which results in no heating power being required. The building reaches a temperature close to 23.5 °C in free-floating, while the setpoint is at 20 °C. For that particular time step, the results and the cost function would be exactly the same for any setpoint below 22.5 °C. So the value of 20 °C is somewhat arbitrary and affected by numerical artifacts. One possible workaround to avoid such behavior would be to impose an additional penalty on rapid changes in the setpoint.

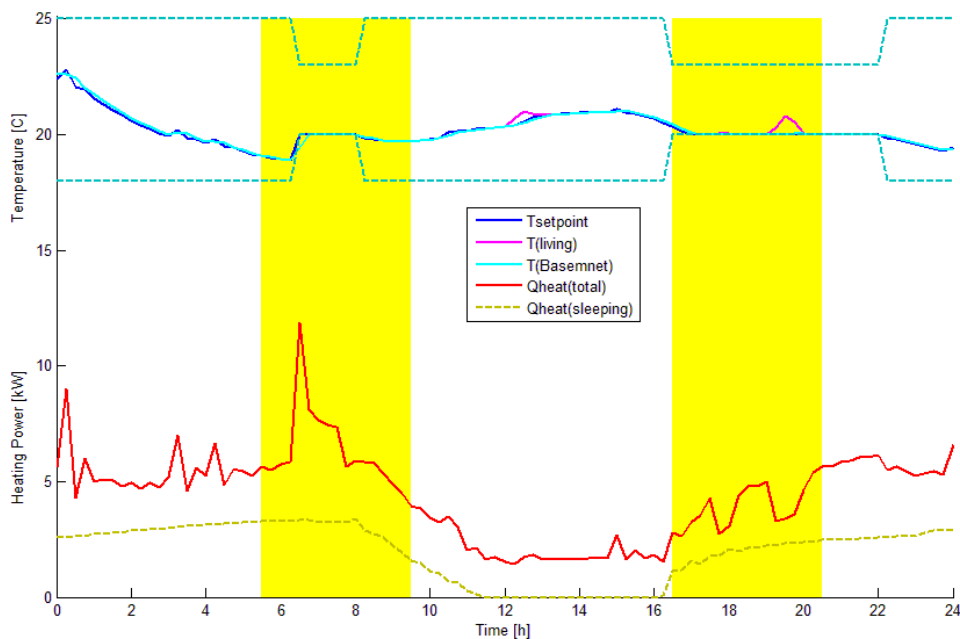


Figure 9: MPC with MATLAB Sensitivity with off-peak cost of 0.1

The Matlab (RC-model) MPC is also sensitive to optimization parameters. The result obtained by assigning different values for the heating power matrix, i.e., the off-peak cost of 0.1 instead of 0.01 is depicted in Figure 9. It can be concluded that if we consider higher cost for the heat power during the off-peak period, no preheating is applied in the morning, nor in the afternoon. While it can be expected that preheating will become less interesting as the cost of off-peak power rises, the ratio of 0.1 is still sufficiently high that some level of preheating would be expected to lower the overall cost.

5.5 Adding heuristics to the GenOpt-TRNSYS optimization

Simplified setpoint profiles were shown to decrease the computational requirements of complex optimization processes while delivering almost the same cost savings, e.g. in (Braun, 2006). Figure 10 illustrates the “Jump and Trim” profile, where 5 setpoint values are optimized (versus 96 for a daily optimization problem with a 15-min time step). This method delivers almost the same savings (48.6% as shown in Table 1) as the GenOpt-TRNSYS optimization, with a much reduced computational time (20 minutes vs. 16 hours).

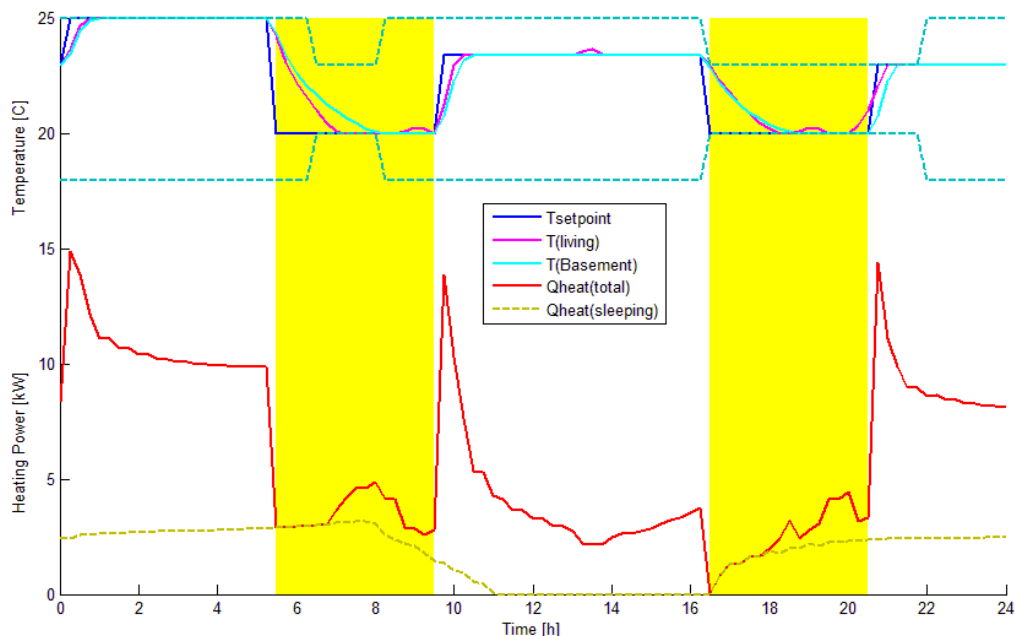


Figure 10: Jump and Trim profile

The “Linear Setpoint” profile differs from Jump and trim in that the temperature drops linearly during each 4h stretch instead of one time step as shown in Figure 11; while “Exponential Setpoint Profile” lets the setpoint decrease exponentially, with two different time constants during the two on-peak periods. The exponential profile delivers 49.4% savings while the linear profile 37.9%; but both methods show about the same reduction in computational time (down to 20 minutes).

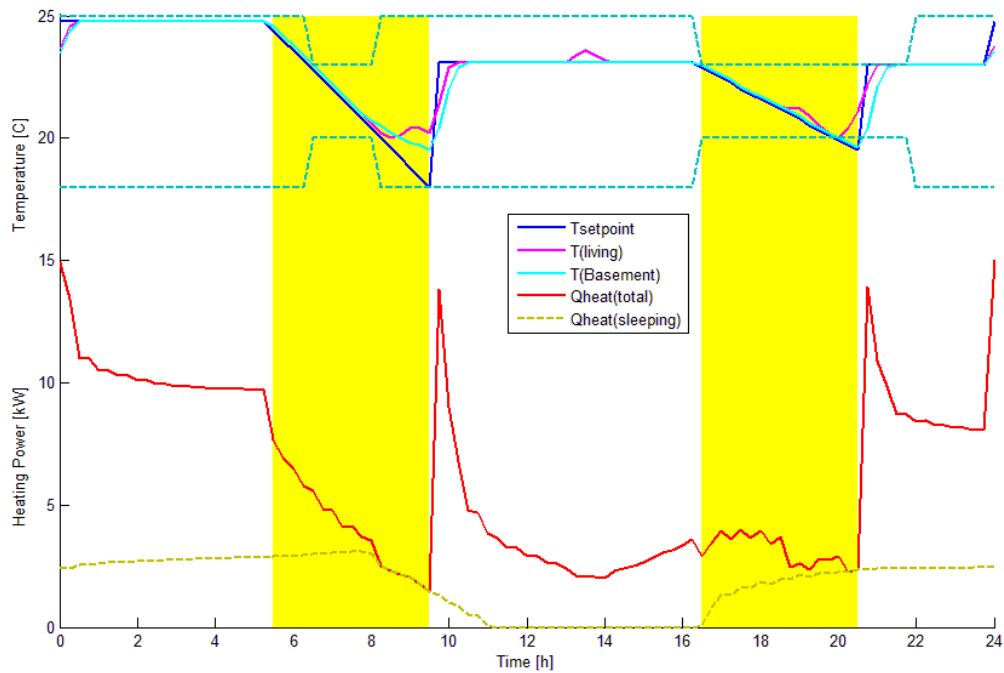


Figure 11: Linear Setpoint Profile

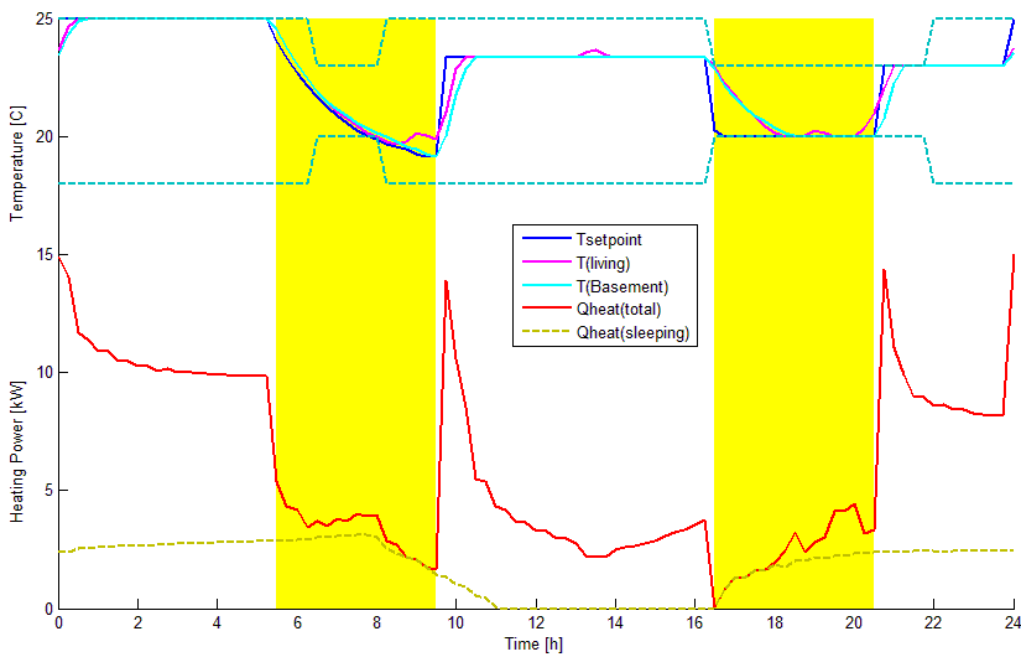


Figure 12: Exponential Setpoint Profile

Finally, the last heuristic method considered is to find the lowest power demand during the peak time, which might be interesting in the perspective of a utility company allowing a given power usage to selected customers during critical peak events. Figure 13 illustrates the results of this approach. The average power usage during on-peak periods is slightly higher than for the other optimization results, but the maximum power requested at any 15-min time step by the house is the lowest of all, at 4 kW (vs. 5 to 8 kW for the other results).

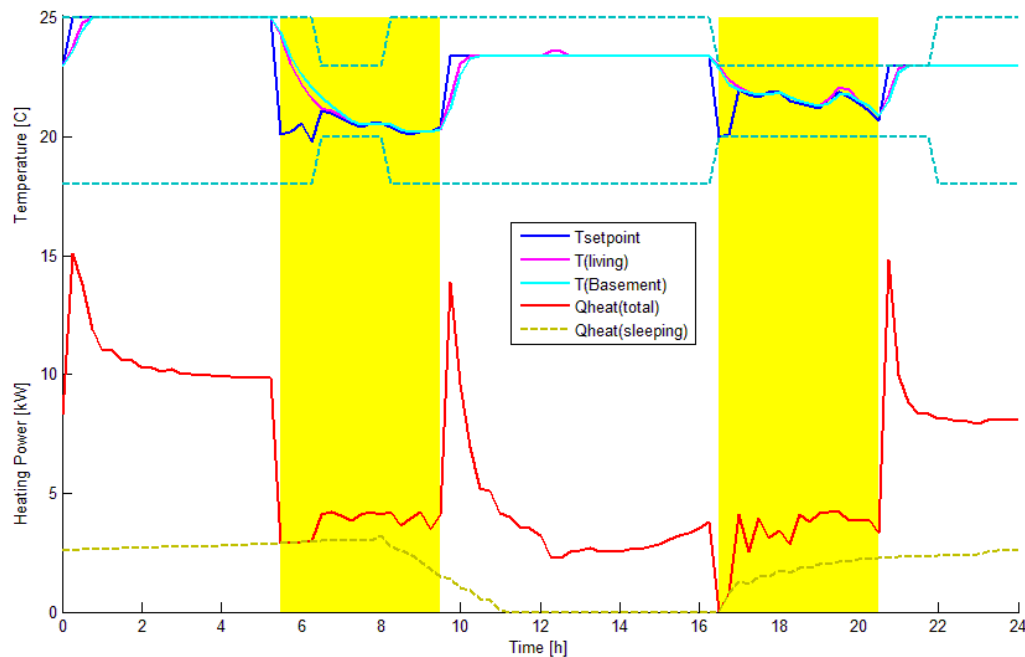


Figure 13: Minimum Power Demand at Peak Time

6. DISCUSSION

Table 1 summarizes all the approaches mentioned above. Power cost means the final value of cost function in each optimization and the reduction percentage is based on the “constant set point” case. Average and maximum power demand indicate the mean and maximum values of the heating power during the on-peak periods.

The GenOpt-TRNSYS MPC results in the lowest cost. Significant cost savings are obtained from the online Matlab (RC-model) MPC. The latter implies considerably lower computational efforts compared to the GenOpt-TRNSYS approach, as depicted by the Indicative CPU Time. The Exponential profile shows near-optimal results while its computational time is much less than the “full” GenOpt-TRNSYS MPC. Jump and trim results in savings very close to the exponential profile. The GenOpt-TRNSYS MPC has the minimum electricity cost while the Min Power Demand method has the lowest power demand, which is just over 4kW.

Table 1: Summary of Results

	Power Cost [-]	Power Cost Reduction [%]	Average Power Demand (peak) [kW]	Max Power Demand (peak) [kW]	Indicative CPU Time[-]*
Constant	51.4	0.0%	6.0	8.1	16 sec
Night Setback	56.3	-9.5%	6.6	15.9	19 sec
MPC with GenOpt	23.2	54.9%	2.6	5.6	16.3 h
MPC with Matlab	34.5	32.8%	3.9	6.8	4 min
Jump and trim	26.4	48.6%	3.0	4.9	18 min
Linear	31.9	37.9%	3.6	7.7	25 min
Exponential	26.0	49.4%	2.9	5.4	21 min
Min Power Demand	31.2	39.3%	3.5	4.2	6.7 h

* Indicative CPU Time is the time taken to run a 12-day TRNSYS simulation including the GenOpt or Matlab optimization process (only one day is optimized). The figures above show that the heating power profile during off-peak is affected by the different strategies, with large peaks at the beginning of

preheating periods. These large peaks would also be present with more conventional setbacks strategies, but not with a constant setpoint. The impact on overall system efficiency, capital or maintenance cost is probably negligible for electric baseboard heating, as considered in this study. However, this impact needs to be taken into account if other heating system types were considered (e.g. hydraulic heating with boiler or heat pump).

6.1 Limitations of the present study

This study considers the performance of different control strategies for the coldest day of the simulated period, and measures that performance by the average power use during on-peak periods. This is in line with the paper objective, which is to compare different model structures and to adopt the point of view of a utility trying to assess potential strategies to be implemented in a large number of individual houses. It could be used to deal with critical peak demand events that typically occur a few times per year. Different contexts would obviously require a different cost function and might require a performance comparison on a longer period.

The selected house is a relatively lightweight building, and results would be different for very light or heavy buildings.

Two main simplifications were made in this study in developing predictive control strategies. First, perfect forecasting was assumed for internal gains, occupancy and weather. Second, the model used to assess the results is the same model as the one used internally by the GenOpt-TRNSYS approach. The Matlab (RC-model) approach on the other hand used a simplified model internally but was assessed with the detailed TRNSYS model, which can be seen as more realistic, as all models will likely have errors compared to a real building. Results need to be confirmed using realistic forecasts and even more detailed models for the assessment or experimental validation.

The obtained profiles are sensitive to optimization parameters (cost function and initial values) and to numerical noise. The unintuitive shape of some results, such as the lack of pre-heating before the afternoon on-peak period in some of them, seems to indicate that the optimization results may still be quite far from the actual optimum. With this in perspective, the simplified (heuristics-based) GenOpt-TRNSYS methods definitely seem to be more interesting than the “brute force” approach.

Further work will address these points, first by investigating the sensitivity of optimization methods and alternative implementations, then by implementing the developed algorithms in real buildings.

7. CONCLUSIONS

Two different approaches were compared to optimize the power usage of electric heating during critical peak events in a typical Canadian house. Perfect forecasts were assumed in both cases. Both methods were tested in TRNSYS using a detailed building model. One method (GenOpt-TRNSYS) used the same model internally to perform the optimization, while the second method relied on a much simpler (RC) model implemented in Matlab.

Both methods deliver a significant reduction in power usage during the on-peak periods. The GenOpt-TRNSYS method delivers the largest savings (more than 50 %) at the cost of a very high computational effort (simulation time increased by a factor of over 3000 compared to the base case). The RC-model approach delivers less impressive savings (33 %) but at a much more reasonable computational cost (simulation time increased by a factor 12 compared to the base case). Heuristic methods restricting the possible setpoint profiles to predefined shapes were

shown to deliver near-optimal savings with significantly reduced computational power (simulation time increased by a factor of 60 to 80 compared to the base case).

Both methods are sensitive to optimization parameters and results need to be confirmed on a wider set of test cases to assess the optimality of obtained results and their robustness. Realistic forecasts should also be introduced prior to implementation into real buildings in order to validate the proposed methodology.

ACKNOWLEDGEMENT

The authors gratefully acknowledge Martin Kegel (CanmetENERGY, Natural Resources Canada) for providing the original TRNSYS model of the CCHT house.

REFERENCES

- Braun, J. E.-H. (2006). Assessment of demand limiting using building thermal mass in small commercial buildings. *ASHRAE Transactions*, 112 PART 1, 547-558.
- Candanedo, J., Dehkordi, V., & Lopez, P. (2014). A multi-level architecture to facilitate MPC implementation in commercial buildings: basic principles and case study. *Proceedings of eSim 2014 conference*.
- Coffey, E. B. (2013). Approximating model predictive control with existing building simulation tools and offline optimization. *Journal of Building Performance Simulation*, 6(3), 220-235.
- CSTB. (2012). *Règlementation Thermique 2012 - Règles d'application Th-Bât*. CSTB Edition.
- Henze, G., Felsmann, C., & Knabe, G. (2004). Evaluation of optimal control for active and passive building thermal storage. *International Journal of Thermal Sciences*, 43(2), 173-183.
- Henze, G., Le, T., Florita, A., & Felsmann, C. (2006). Sensitivity Analysis of Optimal Building Thermal Mass Control. *Journal of Solar Energy Engineering*, 129(4), 473-485.
- Huchuk, B., A. Cruickshank, C., O'Brien, W., & Gunay, H. (2014). Recursive thermal building model training using Ensemble. *Proceedings of eSim 2014 conference*.
- Hydro-Québec. (2014, 01 22). *Hydro-Québec demande à ses clients de poursuivre leurs efforts de réduction de la consommation d'électricité en période de pointe et les remercie de leur collaboration*. Retrieved August 01, 2014, from <http://cnw.ca/ONjV5>
- IBPSA-Canada. (2011). *Model predictive control in buildings workshop*. Retrieved September 10, 2014, from <http://www.ibpsa.us/conferences>
- ISO-1. (2008). ISO 10211:2008 - Thermal bridges in building construction - Heat flows and surface temperatures - Detailed calculations.
- ISO-2. (2008, June). ISO 10456: 2008 - Building materials and products - Hygrothermal properties - Tabulated design values and procedures for determining declared and design thermal values.
- ISO-3. (2008, April). ISO 13370: 2008 - Thermal performance of buildings - Heat transfer via the ground - Calculation methods.
- ISO-4. (2013). ISO 13790: 2013 - Energy performance of buildings - Calculation of energy use for space heating and cooling. *Energy performance of buildings - Calculation of energy use for space heating and cooling*.

- ISO-5. (2008). ISO 6946:2008 - Building components and building elements - Thermal resistance and thermal transmittance - Calculation method.
- Kelly, G. (1988). Control system simulation in North America. *Energy and Buildings*, 10(3), 193–202.
- Kummert, M., Leduc, M.-A., & Moreau, A. (2011). Using MPC to reduce the peak demand associated with electric heating. *Model Predictive Control in Buildings Workshop*. Montréal.
- Lehmann, B., Gyalistras, D., Gwerder, M., Wirth, K., & Carl, S. (2013). Intermediate complexity model for Model Predictive Control of Integrated Room. *Energy and Buildings*(58), 250–262.
- Ma, Y., & Borrelli, F. (2011). Hierarchical Predictive Control Energy Efficient Buildings. *Model Predictive Control in Buildings Workshop*. Montreal.
- Madson, H., & Holst, J. (1995). Estimation of continuous-time models for the heat dynamics. *Energy and Buildings*, 67-79.
- May-Ostendorp, P., Henze, G., Corbin, C., Rajagopalan, B., & Felsmann, C. (2011). Model-predictive control of mixed-mode buildings with rule extraction. *Building and Environment*, 46(2), 428–437.
- May-Ostendorp, P., Henze, G., Rajagopalan, B., & Corbin, C. (2013). Extraction of supervisory building control rules from model predictive control of windows in a mixed mode building. *Journal of Building Performance Simulation*, 6(3), 199-219.
- Morari, M., & Lee, J. (1999). Model predictive control: past, present and future. *Computers & Chemical Engineering*, 667–682.
- Nassif, N., Kajl, S., & Sabourin, R. (2005a). Simplified model-based optimal control of VAV air conditioning system. Montreal: Proceedings of the 9th international building performance simulation association (IBPSA) conference.
- Nassif, N., Stainslaw, K., & Sabourin, R. (2005b). Optimization of HVAC control system strategy using two-objective genetic algorithm. *International Journal of HVAC&R Research*, 11(3), 459-486.
- Oldewurtel, F., Parisio, A., Jones, C., & Morari, M. (2010). Energy efficient building climate control using Stochastic Model Predictive Control and weather predictions. *American Control Conference (ACC)*, (pp. 5100 - 5105). Baltimore, MD .
- Oldewurtel, F., Parisio, A., Jones, C. N., Gyalistras, D., Gwerder, M., Stauche, V., . . . Moraria, M. (2012). Use of model predictive control and weather forecasts for energy efficient building climate control. *Energy and Buildings* (45), 15–27.
- Prívará, S., Cigler, J., Váňa, Z., Oldewurtel, F., Sagerschnig, C., & Žáčková, E. (2013). Building modeling as a crucial part for building predictive control. *Energy and Buildings*, 56, 8–22.
- Sturzenegger, D., Gyalistras, D., Semeraro, V., Morari, M., & Smith, R. S. (2014). BRCM Matlab Toolbox: Model Generation for Model Predictive Building Control. *American Control Conference*.
- Swinton, M. C., Moussa, H., & Marchand, R. J. (2001). Commissioning Twin Houses for Assessing the Performance of Energy-Conserving Technologies. Thermal Performance of the Exterior Envelopes of Whole Buildings VIII.

- Verhelst, C., Sourbron, M., Antonov, S., & Helsen, L. (2011). Towards MPC for office buildings with TABS connected to a GCHP system controller model. *Model Predictive Control in Buildings Workshop*. Montreal.
- Wang, S., & Xu, X. (2006). Simplified building model for transient thermal performance estimation. *International Journal of Thermal Sciences*(45), 419–432.
- Wang, S., & Jin, X. (2000). Model-based optimal control of VAV air-conditioning system using genetic algorithm. *Building and Environment*, 35(6), 471–487.
- Wetter, M. (2001). GenOpt® -- A Generic Optimization Program. Proceedings of the 7th IBPSA Conference. Retrieved from <http://gundog.lbl.gov/GO/>
- Wetter, M. (2011). *GenOpt, Generic Optimization Program, User Manual Version 3.1.0*. Retrieved July 01, 2014, from <http://gundog.lbl.gov/GO/>
- Wystrcil, e. a. (2013). Model-based optimization of control strategies for low-exergy space heating systems using an environmental heat source. *13th Conference of International Building Performance Simulation Association*. Chambéry: BS2013.

SECOND SESSION
**INTEGRATION OF
RENEWABLE ENERGY
SOURCES IN BUILDINGS**

Impact of storage tank control and hydraulic configuration on solar heat pump performance

J. Veeken, J. Verheyen, M. Sourbron

KU Leuven (University of Leuven), Department of Mechanical Engineering, Technology Campus De Nayer, Sint-Katelijne-Waver, Belgium

1. ABSTRACT

For a solar heat pump system, combining solar thermal collectors and a heat pump, with a combined storage tank, the system performance is evaluated for different hydraulic configurations and controls of the storage tank. The results show the importance of an adequate hydraulic configuration and control of the storage tank to support the process of combined heat production by the heat pump and solar thermal collectors and heat distribution to space heating and domestic hot water. Adapting demand side temperature levels and correctly inserting the produced heat from heat pump and solar thermal collectors in the storage tank increases the system efficiency substantially. The Seasonal Performance Factor (SPF) changed from 3.72 to 5.56 by changing storage tank sensor positions and set points of the heat pump control, correctly addressing the produced heat to storage tank levels and changing the positions from where the stored heat is extracted from storage. The SPF increase is caused by an augmented share of solar energy in the overall system balance, an increased heat pump efficiency and a reduced storage thermal losses. This work concludes that the storage tank is a crucial factor in these system types with two collaborating heat sources.

Keywords: solar thermal, heat pump, hydraulics, control

2. INTRODUCTION

This research is conducted in the framework of IEA Solar Heating and Cooling (SHC) Programme task44, investigating space heating and domestic hot water systems that have an increased renewable energy share, lower electricity demand than competitive solutions, lower primary energy demand, and lower CO₂ emission depending on the electricity mix feeding the heat pump. IEA Solar Heating and Cooling (SHC) Programme task44 operated from 2010-2013 to contribute to better understanding of S+HP (Solar and Heat Pump) systems (task44.iea-shc.org/).

Both heat pumps and solar thermal collectors have gained considerable popularity in the European and Belgian market. The similarity of these trends is striking, though unfortunately, it remains unknown to what extent these components are installed in combined systems. Combinations of heat pump and solar thermal systems applied for residential heating and domestic hot water production are considered potentially interesting to contribute to the targets as set by the EPBD (energy performance of buildings directive) and RESD (directive on the promotion of energy from renewable sources). These systems are able to improve the energy performance of buildings and augment the share of energy from renewable energy sources. The potential of these combined systems is gradually confirmed and elimination of pitfalls for long-term successful commercialization is aimed at.

The combined solar heat pump installation has to supply heat at the required conditions (Figure): (1) the correct quantity, (2) the required temperature and (3) at the right moment in time. Domestic hot water is characterised by a peaked demand, which implies a high thermal power and at a relatively high temperature of 45-60°C. Space heating has a more flat demand

throughout the day, at a lower temperature of 25-45°C. Because of the increasing insulation levels, the yearly heat demand for space heating is becoming equal to the yearly heat demand for domestic hot water.

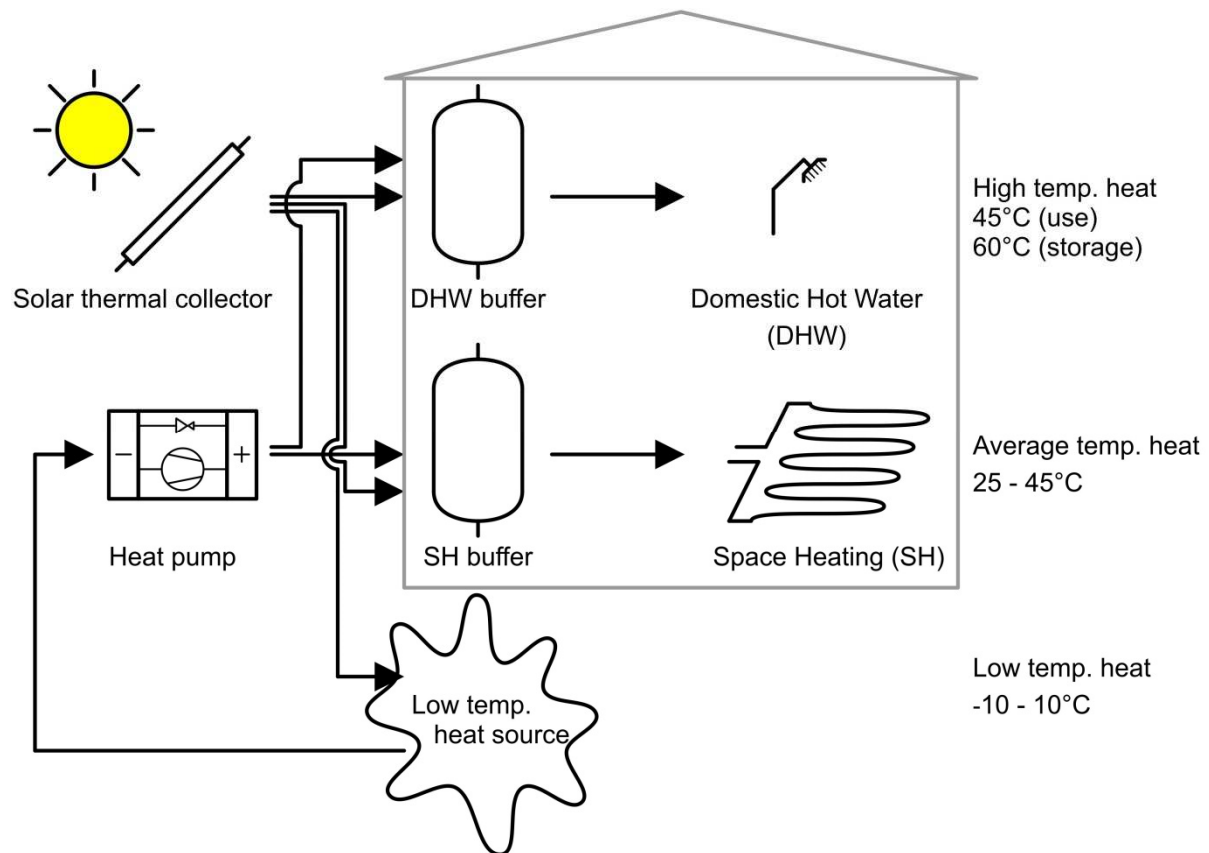


Figure 1: Two heat suppliers (solar thermal collectors and heat pumps) deliver heat at two temperature levels for Space Heating and Domestic Hot Water.

Solar thermal collectors and the heat pump produce the required heat by using either the sun or a low temperature heat source such as the ground or the outside air. Compared to a boiler using fossil fuels, these renewable energy sources are, from the point of view of the installation that is, (1) limited in heat quantity, (2) limited in heat power and (3), in the case of solar energy, not always available. These properties have an important repercussion on the design and the control of solar heat pump systems.

Heat for space heating and domestic hot water has to be produced and delivered by either the heat pump or the solar thermal collectors. Heat pumps can deliver heat at a performance factor (supplied heat versus required electricity use) in the range of 2.5 to 5, while solar thermal collectors do that at a performance factor of roughly 40-100, although factors above 250 are also measured (Goovaerts et al., 2014). Therefore, the solar heat pump system should be designed and controlled to give priority to the solar thermal collectors.

The typically peaked domestic hot water demand and the limited availability in time and thermal power of solar energy, imposes the use of thermal buffering in the solar heat pump system. The typical system configurations depicted as concepts of various combinations of components within SHP systems in the publication by Henning et al. (2008) are used in the task44-project as reference combinations (Figure 2).

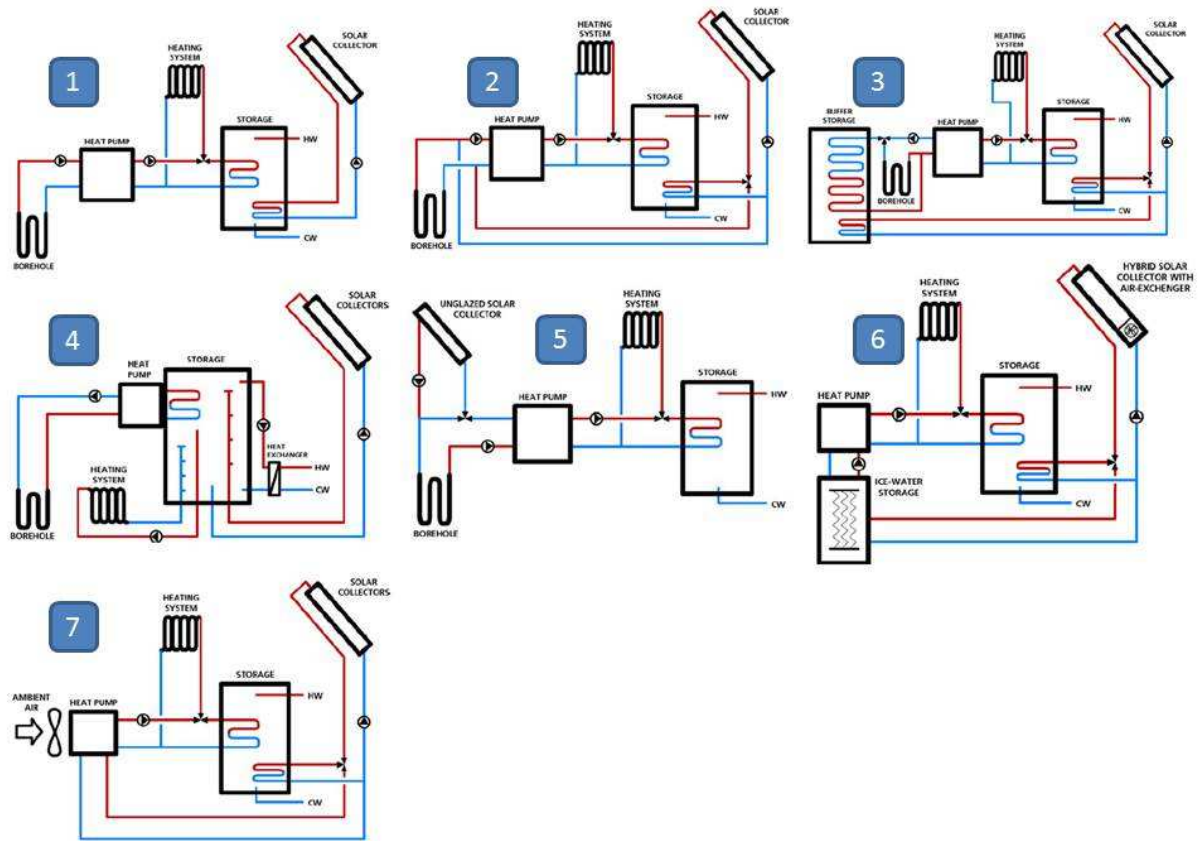


Figure 2: Overview of existing SHP system configurations; numbering according to original publication [Henning et al.; 2008].

This paper focusses on a variation of solar heat pump system nr. 4, with a combi-storage tank storing heat for both space heating and domestic hot water production. A version of the system was installed as a test-setup and a simulation model of this system was made in the Polysun software, as shown in Figure 3.

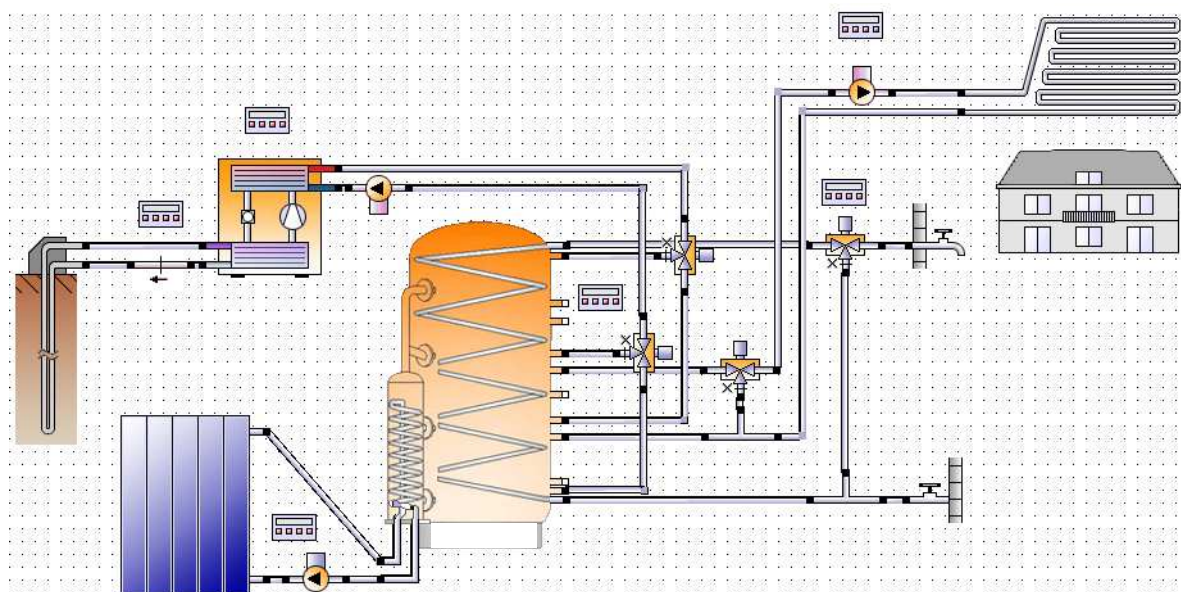


Figure 3: Solar heat pump system configuration with combi-storage tank as implemented in the Polysun software.

The simulation analysis in this paper focusses on the impact of the hydraulic configuration and control settings on the overall performance of the solar heat pump systems. Starting from the reference system as it was installed in the test-setup, the position of hydraulic connections are varied, and therefore the reserved storage volume for either domestic hot water, space heating or the heat exchanger of the solar thermal collectors. Furthermore, control strategy is varied by adapting dead band parameters and applying adapted control strategies to have a better control to heat the different sections in the combi-storage tank.

3. SIMULATION MODEL

The parameters of the reference system are presented in Table .

Table 1: Parameters of the reference system.

System component	Parameter value
Building	
Heated area (m ²)	140
Specific heating energy demand (kWh/m ² /year)	15.6
Domestic hot water use (l/day)	140
Domestic hot water draw-off temperature (°C)	45 (55, see Table 2)
Ground coupled heat pump	
Heat pump heating power (0/35) (kW)	5
Single U ground loop length (m)	86
Solar collector	
Flat plat solar collector area (m ²)	8.6
Combi-storage tank	
Volume (liter)	512

3.1 Building and domestic hot water

Further details on the building, of which a view is presented in Figure 4, can be found in Dott et al. (2013). The IEA SHC Task44 DHW draw-off profile is used in this paper which is based on the EU mandate M/324 tapping cycle M (CEN/TC113N380, 2003) and (FprEN 16147 2010) and is expressed as a medium tapping profile (Haller et al., 2013). This can be considered as valid for a family with an average household size.

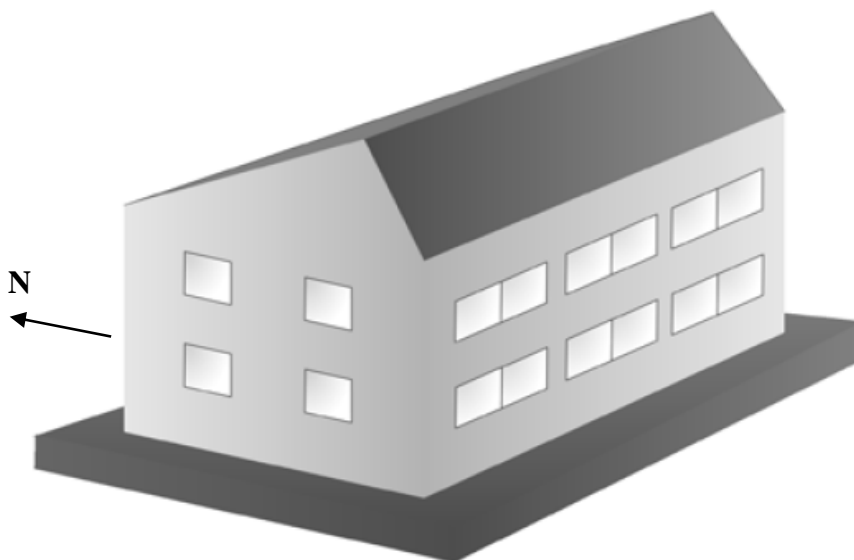


Figure 4: View of the buildings showing South and West facades [Dott et al., 2013].

Table 2: Domestic hot water profile as adopted in the simulation model (Haller et al., 2013)

Legend: S=Small; Sh=Shower; FC=Floor cleaning; DW= Dish washing; HC=Household cleaning; Ba=Bath tub; Sunday only: bath tub replaces evening shower

Nr.	Start time (h:min)	Energy Q_{DHW} (kWh)	Type	Flow Rate (Litres/h)	Min. Temp. $T_{DHW,set}$ (°C)
1	07:00	0.100	S	240	45
2	07:15	1.315	Sh	600	45
3	07:30	0.100	S	240	45
4	08:00	0.100	S	240	45
5	08:15	0.100	S	240	45
6	08:30	0.100	S	240	45
7	08:45	0.100	S	240	45
8	09:00	0.100	S	240	45
9	09:30	0.100	S	240	45
10	10:30	0.100	FC	240	45
11	11:30	0.100	S	240	45
12	11:45	0.100	S	240	45
13	12:45	0.300	DW	240	55
14	14:30	0.100	S	240	45
15	15:30	0.100	S	240	45
16	16:30	0.100	S	240	45
17	18:00	0.100	S	240	45
18	18:15	0.100	HC	240	45
19	18:30	0.100	HC	240	45
20	19:00	0.100	S	240	45
21	20:30	0.700	DW	240	55
22	21:15	0.100	S	240	45
23	21:30	1.315	Sh	600	45
Total		5.530			
Sunday only					
23	21:30	3.520	Ba	600	45

The climatic conditions used for the simulations are taken from the Polysun database for Brussels, Belgium.

3.2 Ground properties

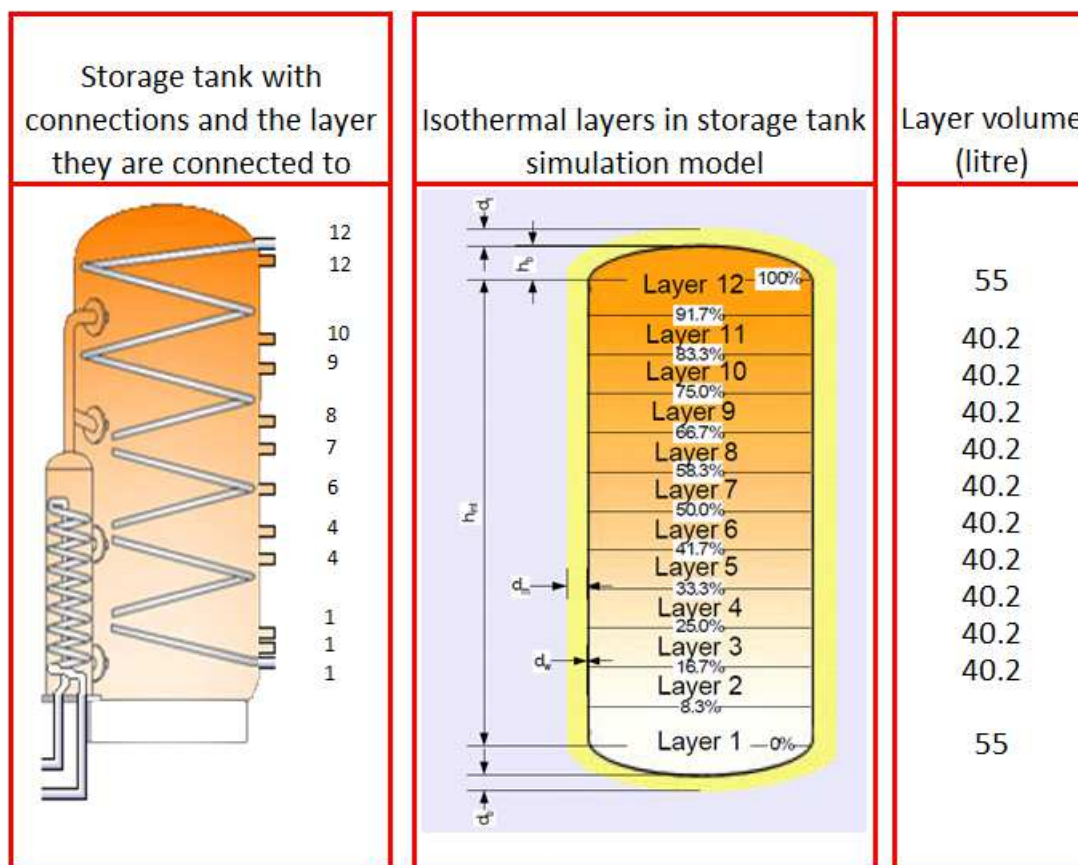
The characteristics of the ground, considered representative for the Belgian context and used as boundary condition for the simulations of SHP systems are adopted from T44 [Haller et al., 2013] and Geotrainet [McCorry et al., 2011].

- Soil warming (average difference between the earth surface temperature and the air temperature): 0.8°C

- Axial temperature gradient: 0.03 K/m
- number of earth layers: 1
- density of earth layer material: 2500 kg/m³
- specific heat capacity of earth layer material: 800 J/(kgK)
- thermal conductivity of earth layer material: 2 W/(mK)
- thickness of earth layer 1: 400 m

3.3 Combi-storage tank

The combi-storage tank volume of 512l is divided in 12 isothermal layers in the reference simulation model. Layers 1 and 12 contain the volume of the other layer added with the volume of the bulge (Figure 5). The upper part (layers 8-12) is reserved for domestic hot water production, while the lower part (layers 1-7) for space heating. The solar collector heat exchanger is located on the side of the combi-storage tank with 4 inlets so heat enters the storage volume at layers with the corresponding temperature (Figure). In the reference system, no separate cold volume at the bottom of the tank is foreseen for the solar collector heat exchanger. The domestic hot water is heated by an internal coiled stainless steel heat exchanger of 25m and a surface area of 6.45m².



Figure

Figure 5: Combi-storage tank layout in the simulation model

3.4 Reference system control parameters

In the reference system the domestic hot water production is controlled by a temperature sensor located in the upper tank layer (top layer 12), working with a set point of 55°C and a dead-band

of +1°C/+5°C. This means that the heat pump starts whenever the upper layer temperature is lower than 56°C and stops at a temperature of 60°C.

The space heating control is equal to the domestic hot water control, with a temperature sensor located in layer 7, a set point of 35°C and a dead-band of +1°C/+5°C.

The domestic hot water always has priority to space heating. In these simulations no clock is installed in the controller to limit domestic hot water operation to certain hours. Both space heating and domestic hot water controllers are always activated.

3.5 Evaluation criteria

The system performance is evaluated by comparing the seasonal performance factor, taking into account all electrical users in the system (heat pump compressor, solar collector pump, heat pump circulation pump and ground loop circulation pump):

$$SPF = \frac{Q_{SH} + Q_{DHW} (kWh_{therm})}{P_{compr} + P_{circulators} (kWh_{elec})} \quad (1)$$

Additionally, a parameter ‘Availability’ checks the time the system can provide domestic hot water at the required temperature level, as an indicator for user comfort. Space heating demand is always met in the different simulation runs, which means that thermal comfort is always supplied. Therefore, this criterion is not evaluated further on.

Table 3: Hydraulic connection and control parameters adaptations towards improved system performance

Adap- tation	Lay-out of combi-storage tank					
	Heat pump to DHW-layer		Heat pump to SH-layer		Tank to SH	
	Layer in – Layer out	Volume (l)	Layer in – Layer out	Volume (l)	Layer in – Layer out	Volume (l)
Ref.	12-8	216	4-1	176	7-4	161
1.	12-8	216	4-1	176	7-4	161
2.	12-8	216	7-4	161	6-4	121
3.	93%-59% 12-8	216	52%-30% 7-4	161	43%-25% 6-4	121
4.	93%-59% 12-8	216	52%-30% 7-4	161	43%-25% 6-4	121
5.	93%-71% 12-9	176	52%-30% 7-4	161	43%-25% 6-4	121
6.	93%-78% 12-10	135	52%-30% 7-4	161	43%-25% 6-4	121

3.6 Hydraulic connection, control and simulation parameters

In different steps the system performance is increased by adapting hydraulic connections and control parameters.

1. Correcting a control error where the heat pump was set ON with an OR-function on SH and DHW requirements but was set OFF with an AND function on SH and DHW set point. The layer control was adapted from one-layer dead-band control to two-layer set point control
2. Creating a cold zone at the bottom of the storage tank by reducing and moving the space heating volume to layers 7-4 (161 l instead of 296 l)
3. Space heating storage with heating curve control instead of a fixed setpoint
4. Lowering domestic hot water set point from 55°C to 50°C
5. Reducing the domestic hot water volume to layers 9-12 (176l instead of 216l)
6. Reducing the domestic hot water volume to layers 10-12 (135l instead of 216l)

Table 3 shows these steps with their impact on the buffer volumes.

4. DISCUSSION AND RESULT ANALYSIS

4.1 General overview

In a general overview, the different adaptations clearly show an important increase in system seasonal performance (Figure 5). The SPF of the system increases from 3.72 to 5.56, while no changes are made to the size of the major system components, such as the solar thermal collector area or the storage volume. Only hydraulic connections and control parameters are changed.

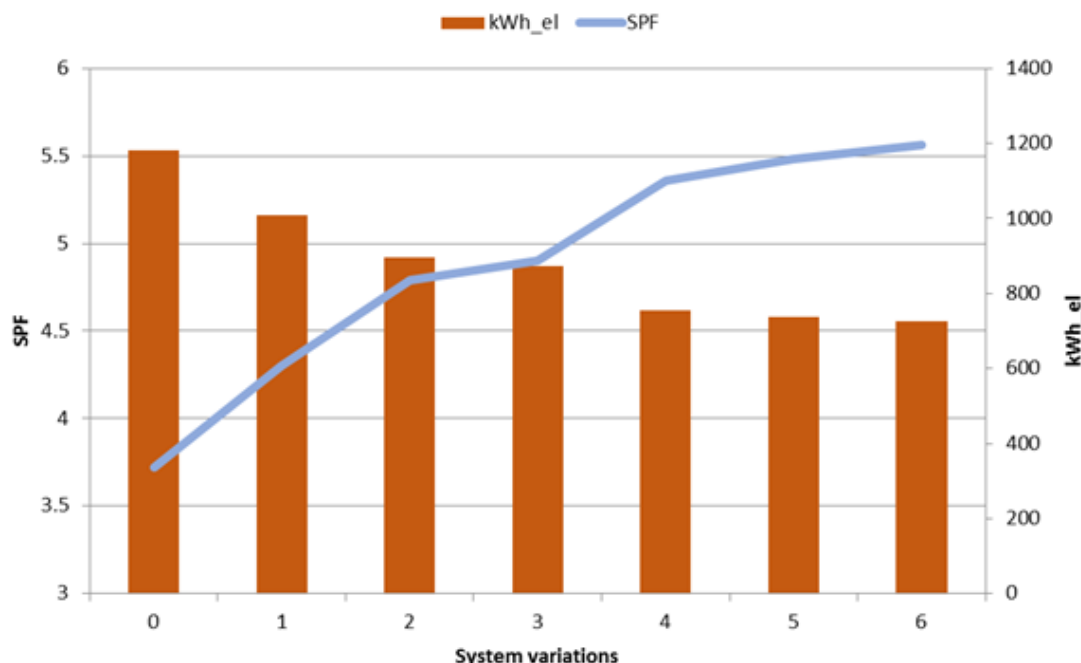


Figure 5: General overview of the simulation results, showing SPF and systems electrical energy use

It is interesting to go through the different steps to explain the cause of the changes in system behaviour.

4.2 Step 1: fixing erroneous control

In the reference system, the control logic had an important logical error where SH or DHW operation from the heat pump was switched on when the one of the set point values was trespassed (OR-function). However, the heat pump operation was only switched off when both SH and DHW set point values were satisfied. This means that the storage volume was always heated to DHW set point value (DWH switches off at 60°C in layer 12) even if SH operation was switched on: SH is required when layer 4 drops below 36°C and should switch off when layer 4 reaches 40°C, but due to the logical error in the control, the heat pump only switches off when layer 12 reaches 60°C. This means the the whole storage volume is heated because in SH-operation the heat pump injects in layer 4 and ejects from layer 1.

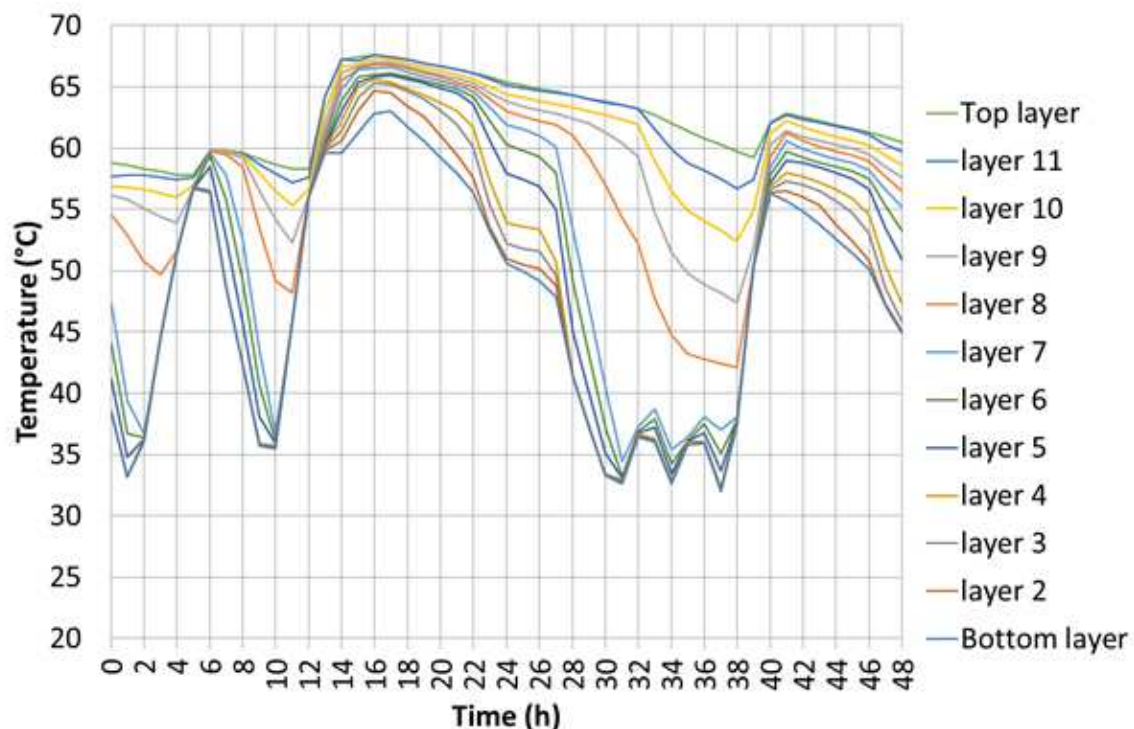


Figure 6: Storage tank temperature levels with wrong control logic in the reference system

Figure 6 shows that at hour 1 the SH set point is trespassed (layer 4 drops below 36°C), while the DHW set point criterion was satisfied (layer 12 is above 56°C) and that the whole storage tank is heated up afterwards until layer 12 reaches 60°C at hour 6. Together with this adaptation, in this first adaptation the heating control of either DHW- and SH-layers is changed. Where in the reference system the one-layer dead-band control was applied, now the two-layer set point control is installed. This means that two temperature sensors are installed, one in the upper layer of the specific tank volume and one in the lower layer (respectively layers 12 and 8 for DHW and layers 4 and 1 for space heating). If the upper temperature sensor reading drops below the set point, the heatpump starts heating that part of the tank volume, until the lower temperature sensor reading is higher than the lower set point temperature. This ensures that the whole reserved storage volume is heated up by the heat pump, while in the reference system the implemented dead-band was not always able to do this in all circumstances. It does however imposes the use of two temperature sensors per heat pump operation mode (SH or DHW).

These measures show the importance of correct control implementation: the system SPF increases from 3.72 to 4.30, while the systems electrical consumption drops with 14.7% from 1182 kWh to 1008 kWh.

4.3 Step 2: Reducing SH volume and ensuring cold storage volume for solar heat exchanger

In the reference system, the upper part is heated for domestic hot water (DHW), while the lower part of the tank is kept warm by the heat pump-to-space heating (SH) connection which is located at the bottom of the tank. Therefore, the heat exchanger (HX) of the solar thermal collectors always 'sees' warm water, hampering solar heat to be stored in the storage tank.

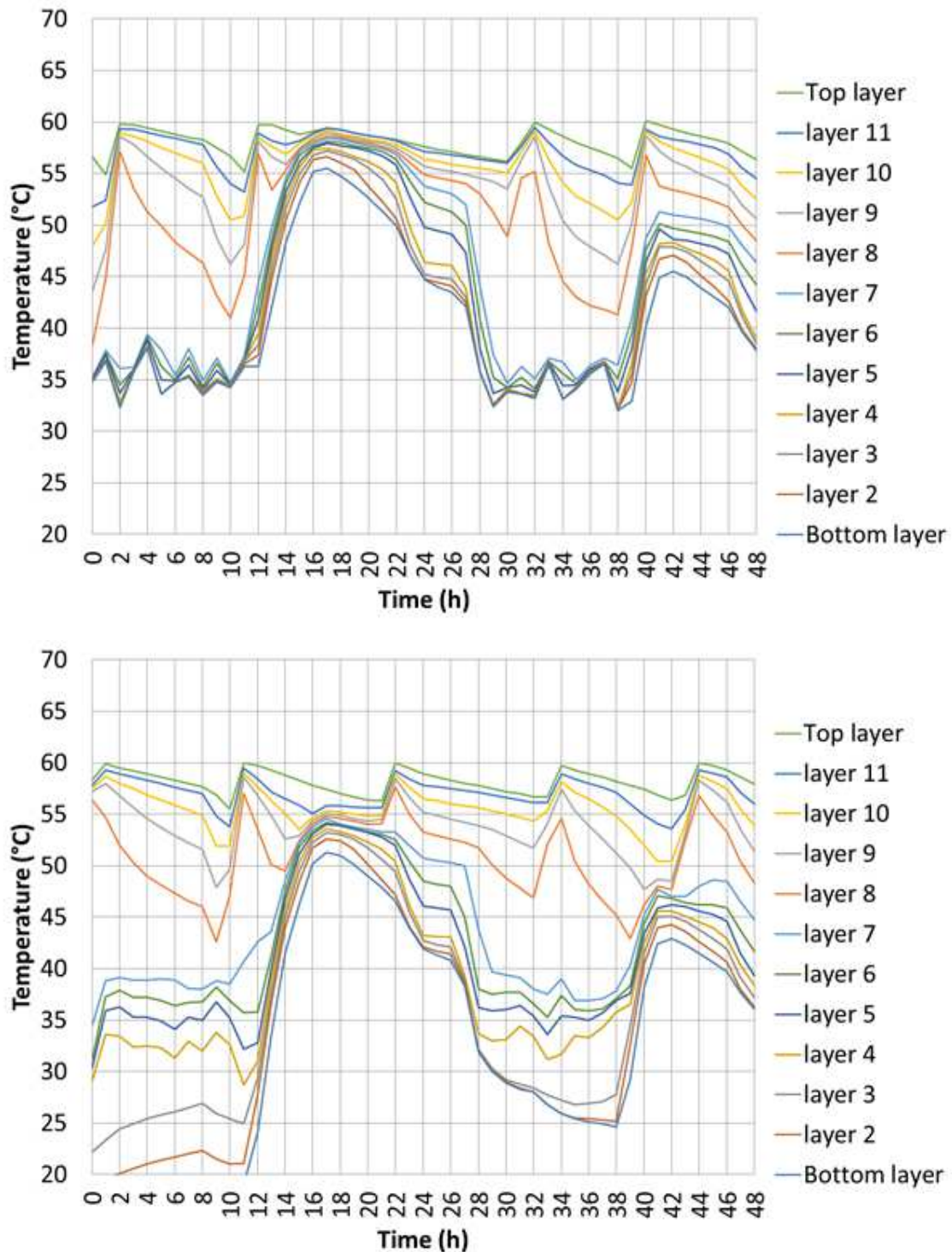


Figure 7: The effect of reserving cold storage for the solar heat exchanger on the temperature profile in combi-storage tank on February 5-6 (Top figure-without cold volume; bottom figure-with cold volume)

This is solved in the second adaptation (first hydraulic adaptation), where the lower part of the tank (layers 1 to 3, 135 litre or 26% of the storage volume) is kept cold for the solar collector heat exchanger.

The amount of reserved storage volume for space heating is reduced from the volume in layer 7 to 1 to the volume in layers 7 to 4 (296 l to 161 l).

Figure 7 shows the effect adaptation step 2 has on the temperature profile in the combi-storage tank on two typical winter days, where both days have an important amount of solar radiation. The upper part of Figure 7 shows the result for the system 1, while the lower part for the adapted hydraulic lay-out. The average tank temperature lowers, while more solar heat has been stored: 17.0 kWh instead of 15.4 kWh, or an increase of 10%. On an annual base, the solar fraction (this is the share of solar heat in the whole heat demand) increases from 45.2% to 45.7%. Although the annual impact is rather limited, the example of Figure shows the impact on colder days with limited solar radiation. On these days, the system is able to capture more solar heat, which reflects in an SPF increase from 4.30 to 4.79, with a corresponding decrease in electrical energy consumption of 11%. Note that the increase in SPF is not only caused by an increased share of solar heat, but also by a decrease of storage losses with 2% and mostly by a more efficient heat pump operation due to the lower overall storage temperatures: the SPF(only heat pump) increases from 3.5 to 3.9.

This measure does not influence the availability of domestic hot water, nor the heat supply for space heating.

4.4 Step 3: Heating curve control

In the 3rd adaptation, the temperature control for the space heating layer is adapted from fixed temperature control (at 35°C) to heating curve control. This further reduces the average temperature of the storage tank and increases the SPF to 4.90. The storage tank losses reduce with another 4% and the SPF(heat pump only) increases to from 3.9 to 4.3.

4.5 Step 4-6: Domestic hot water temperature and volume

In the last three steps, the parameters of the domestic hot water part are adapted. First, the temperature set point is reduced from 55°C to 50°C. This increases the SPF to 5.36. By reducing the storage volume for domestic hot water in the last two steps, the system-SPF eventually ends up to be 5.56. For this last system, the SPF(heat pump only) eventually is increased up to 4.7, the solar fraction becomes 48.7% and the storage heat losses are 6% lower than after the second adaptation, where the cold volume for the solar collectors was introduced.

Two remarks should be made for this last adaptation. The temperature setting of 55°C was originally chosen in the project, to prevent the growth of legionella bacteria, although this is not specifically requested by law for residential applications (in Belgium). Reducing the set point temperature to 50°C increases the risk of bacteria growth.

Furthermore, by reducing the storage volume for domestic hot water, the availability of DHW decreases to a small extent, certainly in winter months with a low solar irradiation (Figure 8).

Therefore, this measure of reducing the domestic hot water storage volume should be introduced with care, because the comfort is also decreasing. The system performance results should not be evaluated without also evaluating the delivered comfort.

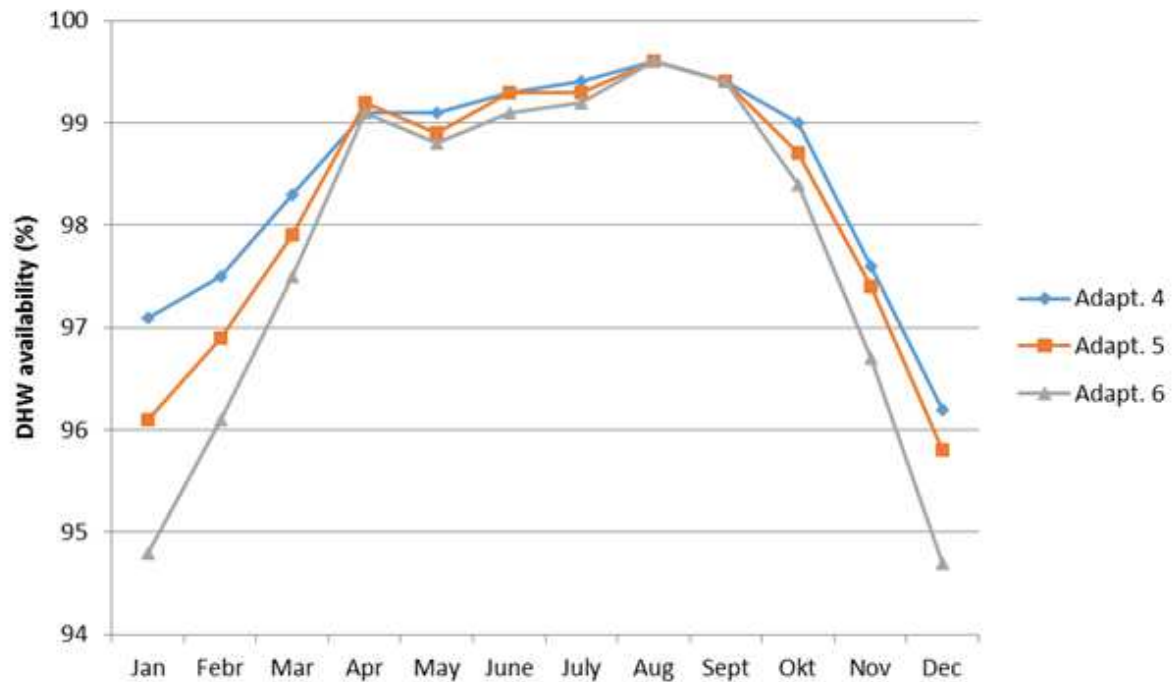


Figure 8: Availability reduction by reducing the domestic hot water storage volume

5. CONCLUSION

Where typical simulation studies focus on parameter analysis and optimal design or control issues, this paper demonstrates that a huge gain is to be found in a correct control and design of the storage tank and its hydraulic connections. The simulation study clearly shows the important impact the storage tank has on the overall system performance. With equal system design parameters such as heat pump power, solar thermal collector area and storage volume, the seasonal system performance factor is increased from 3.72 in the reference system to 5.56 in the best tuned system. This is achieved merely by changing the hydraulic connections of the storage tank, by adapting the reserved storage volumes for the solar heat exchanger, for space heating and for domestic hot water and by changing the controller settings and adapting the temperature control.

The design and installation guidelines that arise from these results are the importance to have a cold volume in the storage tank in order to optimally benefit from the solar thermal collectors (which have a substantially higher performance factor than the heat pump), to avoid mixing of the different storage layers at different temperatures and to reduce the high temperature storage volume as much as possible. This last measure should be implemented with care in order to avoid a decrease in delivered comfort and to avoid the growth of bacteria due to lower storage temperatures.

From these results, it must be concluded that high quality and high performance of a solar heat pump system not only depends on system parameters such as the installed solar collector square metres, the COP of the heat pump or the volume of the storage tank, but also on installation related aspects, such as the hydraulic connections and controls of the storage tank. This is an important conclusion for integrated system suppliers, but even so for quality label schemes which have the ambition of increasing confidence in the performance of these kind of systems.

REFERENCES

- Dott R., Haller M.Y., Ruschenburg J., Ochs F., Bony J.; 2013; The Reference Framework for System Simulations of the IEA SHC Task 44 / HPP Annex 38 - Part B: Buildings and Space Heat Load - A technical Report of Subtask C - Report C1 part B; Institut Energie am Bau - Fachhochschule Nordwestschweiz, IEBau - FHNW, Muttenz, Switzerland; September 6, 2013
- Goovaerts L., Verheyen J., Van Aken D., Veeken J. and Sourbron M., 2014, Thermische zonnecollectoren en warmtepompen werken samen?, Power Pro Magazine, September 2014
- Haller M., Haberl R., Mojic I. and Reber A., 2013, IEA SHC Task 44/HPP Annex 38, Hydraulic Integration of Heat Pumps with Combistores, International Symposium, Combined solar thermal and heat pump systems, for residential applications, April 8 2013
- Henning H.-M., Miara M.; 2008; Systems using solar thermal energy in combination with heat pumps – 1st concept paper; 64th ExCo meeting; Winterthur, Switzerland; November 19-21
- McCorry M., Jones G.LI. (eds), 2011, Geotrained Training Manual for Designers of Shallow Geothermal Systems, Geotrained, European Federation of Geologists, Brussels.

ACKNOWLEDGEMENTS

This research is conducted in the framework of the IWT-TETRA project 'SolarHeat'. The authors greatly acknowledge the financial support of IWT, the Flemish government agency for Innovation by Science and Technology, and of the collaborating companies of this research project (list is available at <http://zon-warm.lessius.eu>).

Simulation of a passive house coupled with a heat pump/organic Rankine cycle reversible unit

Olivier Dumont¹, Carolina Carmo², François randaxhe¹, Sylvain Quoilin¹,
Vincent Lemort¹

⁽¹⁾ Thermodynamics laboratory, University of Liege, Liege, Belgium

⁽²⁾ Department of Energy Technology, Aalborg University, Aalborg, Denmark

1. ABSTRACT

This paper presents a dynamic model of a passive house located in Denmark with a solar absorber, a horizontal ground heat exchanger coupled with a HP/ORC unit. The HP/ORC reversible unit is a module able to work as an Organic Rankine Cycle (ORC) or as a heat pump (HP). There are 3 possible modes that need to be chosen optimally depending on the weather conditions, the heat demand and the temperature level of the storage. The ORC mode is activated, as long as the heat demand of the house is covered by the storage, to produce electricity based upon the heat generated by the solar roof. The direct (free) heating is used when the storage cannot cover the heat demand of the house. Finally, when direct heating is not sufficient to cover the heat demand because of poor weather conditions, the HP mode is activated.

Dynamic simulations of the whole system are presented for different typical days of the year in Modelica language. A peak of 3.28 kW of power is reached in ORC mode with a heat input of 59.5 kW from the solar roof (23.9 kWh are produced during a typical summer day). In a representative winter day, 5.81 kWh are consumed by the heat pump with a daily average COP of 4.3. Conclusions regarding control strategies and enhancement of the global system are drawn. A control strategy with a low storage temperature set-point (50°C) allows reducing electrical consumption from 20% up to 60% when compared to higher set-point (60°C). The system performance to produce power could also be optimized if an extra tank is included to store heat uniquely to produce electricity with the ORC during the peak electricity consumption. Finally, the paper points that this technology is a promising way to achieve Plus Energy Building at low price and higher efficiency compared to competitive systems, as photovoltaic-thermal solar heat pump.

Keywords: Net Zero Energy Building, Reversible Heat Pump/Organic Rankine Cycle, Solar energy.

2. INTRODUCTION

According to the European commission directive (European commission, 2011), all new buildings in Europe should be Net Zero Energy Building from 2019 (Jagemar et al, 2010; Kurnitski et al, 2014). In this context, heat pumps should play a major role (Bettgenhäuser et al, 2013; Hepbasli and Yalinci, 2009). This paper investigates a heat pump which presents the ability to operate as an organic Rankine cycle without increasing the costs significantly (Dumont, 2014(a)). This reversible HP/ORC unit is coupled to a passive house (Figure) with a large solar absorber and a horizontal ground source heat exchanger (Innogie, 2013).

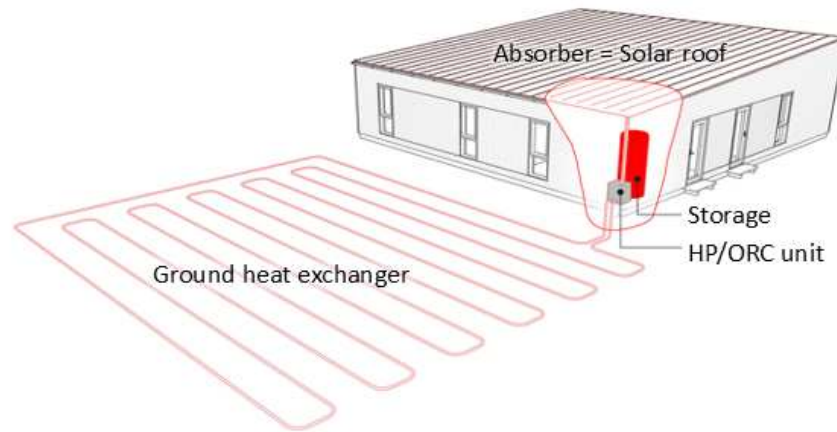


Figure 1: The reversible HP/ORC unit integrated in the house (Dumont, 2014)

The paper is organized into 4 parts. Firstly, the reversible HP/ORC unit is introduced. Then, the models of the components are presented. Thereafter, results from simulation on typical days are described and discussed. Finally, prospects and conclusions are discussed.

A simplified scheme of the system, operating in ORC mode, is presented in Figure 2.

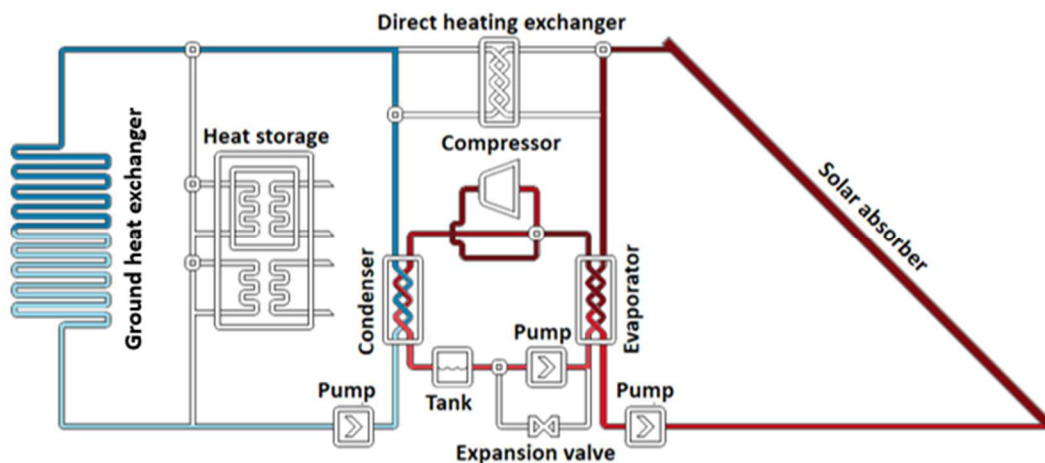


Figure 2: Simplified scheme of the unit (ORC mode) (Dumont, 2014(a))

Dynamic modelling of the whole system including the solar roof, the ground source heat exchanger, the storage tank, the reversible HP/ORC unit and the house is necessary to simulate the performance of the system. These simulations help to evaluate the performance with different climates, house envelope, storage size and control strategies.

3. MODELING

3.1 Introduction

In this chapter, the model of each sub-system is described. The control strategy is also introduced.

In the law of conservation of energy, if the mass and volume (or time constant) are negligible, then the equation becomes independent of time. Thus, it is important to evaluate the inertia of each component, fast transients should not be taken into account because their influence is negligible. Furthermore, the system composed of sub-systems having very different time

constant requires very long simulation time. Time constant (τ) are evaluated experimentally or estimated with Eq. 14 and compared in Table 1.

$$\tau = \frac{0.63 \cdot M \cdot \Delta T}{\dot{m}} \quad (14)$$

In this equation, M is the mass of the system, \dot{m} is the typical flow and ΔT is taken equal to 10°C. This results from an energy balance assuming that flow and specific heat are constant. The time constant is reached when the increase in temperature has reached 63% of its final value.

Table 1: Time constant of the different sub-systems

Sub-system	Method	Time constant [min]
Reversible HP/ORC unit	Experimentation	5
Solar roof	Eq. 14	18
Storage	Eq. 14	87
House	Simulation	3133 (50h)
Ground source heat exchanger	Experimentation (see section 3.6)	

The inertia of the unit is, therefore, neglected because of its very low time constant. Solar roof, house and storage dynamics are of course modeled. The ground source heat exchanger inertia is discussed in section 3.6.

3.2 Reversible HP/ORC unit

The unit has been tested in a wide range of conditions experimentally (Dumont, 2014(a)). Following that, semi-empirical models have been calibrated to fit the measurements. In heat pump mode, the sub-cooling is imposed at 2 K and the over-heating at 6 K. In ORC mode, the sub-cooling is imposed by the NPSH (net positive suction head) of the pump and the over-heating is optimized (by adjusting the pump speed) to maximize the electrical power production. As shown in Dumont (2014(b)) the polynomials used to evaluate the outputs of the reversible unit.

3.3 Storage

The water tank storage system is described by partial differential equations which consist of derivatives with respect to time and space for an incompressible fluid. The spatial equations are discretized according to the finite volume method. Dymola/Modelica solves the dynamic part of those equations using DASSL solver.

Figure 3 shows the structure of the tank model. The water tank model can be divided into three subsystems: tank subsystem, one parallel internal heat exchanger subsystem and one counter flow internal exchanger subsystem.

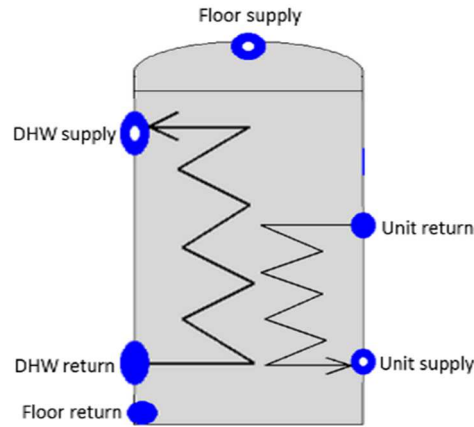


Figure 3: Water storage unit with internal coils diagram.

The tank subsystem comprises the water tank, a top outlet and the bottom inlet that are part of the floor heating circuit. The tank is discretized using a modified version of the incompressible Cell1Dim model adding an additional heat port, which represent a model of a stratified tank and ambient losses (Quoilin et al, 2014). This subsystem is discretized into 20 cells, where the energy and mass conservation equations are applied. The momentum balance is neglected and the pressure is assumed to be constant in the whole tank. Each layer is described by one temperature variable. Each control volume takes into account water inflows, water outflows and conductive heat transfers with neighboring layers and with the environment.

The heat exchangers are modelled using the Flow1Dim component (Quoilin et al, 2014) and a wall component. The bottom heat exchanger - part of the reversible unit circuit and responsible for supply heat in DH and HP modes - is modelled using an original Flow1Dim component and a wall component. The top heat exchanger - the domestic hot water coil - is discretized using a modified version of Flow1Dim with a Countcurr component (Quoilin et al, 2014).

The fluid properties for the selected medium, StandardWater, are computed using the ThermoCycle library (Thermocycle, 2014). The dimensions and thermal constant of the tank model are summarized in Table 2.

Table 2: Water tank with two heat exchangers model parameters

Parameter	Value	Parameter	Value
Tank total height [m]	1.44	Top Heat exchanger area (one side) [m ²]	2.5
Height bottom HX inlet [m]	0.54	Tank capacity [m ³]	0.5
Height bottom HX outlet [m]	0.09	Internal volume bottom HX [m ³]	0.011
Height top HX inlet [m]	0.09	Internal volume top HX [m ³]	0.025
Height top HX outlet [m]	1.225	U-value between inside of tank and ambient[W/m ² K]	2.7
Total heat exchange area of tank with ambient [m ²]	3.27	U-value of the heat exchanger[W/m ² K]	4000
Bottom Heat exchanger area [m ²]	1.8		

3.4 Solar roof

Since the recently patented roof (Innogie ApS, 2013) is being tested for the first time, no performance data is available and the solar roof is modeled with the classical correlation (Eq. 15) based on the ambient temperature (T_{amb}) and on the mean temperature of the heat transfer fluid (T_m) with the area ($A = 138.8 \text{ m}^2$) of the roof and the solar irradiance absorbed by a

collector per unit area of absorber (I). U is evaluated through the model of Klein (Klein, 1975). Finally the energy balance (Eq. 16) allows to evaluate the exhaust roof temperature with the mass M (104.6 kg), the specific heat (C_p), and the mass flow rate of the working fluid, in this case 30% glycol based water solution (\dot{m}).

$$\dot{Q}_{col} = A(I - U(T_m - T_{amb})) \quad (15)$$

$$M \cdot C_p \cdot dT_m = \dot{Q}_{col} - \dot{m} \cdot C_p \cdot (T_{w,roof,ex} - T_{w,roof,su}) \quad (16)$$

3.5 House model

The present simulation model relies on a simplified multi-zone building model. The building is divided into 5 zones based on the house layout and the use of the spaces. The main characteristics of the building are presented by zone in Table 3.

Table 3: House main characteristics

	Unit	Zone 1	Zone 2	Zone 3	Zone 4	Zone 5
Floor area	m ²	41.8	18.2	7.8	19.1	45.7
Volume	m ³	117.2	45.5	19.5	47.8	114.3
Slab U-Value	W/m ² .K	0.08	0.08	0.08	0.08	0.08
Roof U-Value	W/m ² .K	0.09	0.09	0.09	0.09	0.09
External wall area	m ²	none	20.4	4.5	24.8	41.5
External wall U-value	W/m ² .K	none	0.15	0.15	0.15	0.15
Window area (orientation)	m ²	14.7(S)	2.4(S)	0.84(W)	0.84(W) 0.84(N)	6.7(E) 2.4(S)
Window U-value	W/m ² .K	0.63	0.68	0.8	0.8	0.8
Window solar factor	-	0.5	0.5	0.5	0.5	0.5
Infiltration rate	ACH	0.3	0.3	0.3	0.3	0.3
Space activity	-	Kitchen Dining	Main Bedroom	Bathroom	Hall Others	Living Bedroom
Lighting nominal power	W/m ²	5	5	3	3	5
Appliances nominal power	W/m ²	3	3	3	3	3
Air temperature Setpoint	°C	20	Only imposed in zone 1	Only imposed in zone 1	Only imposed in zone 1	Only imposed in zone 1

The Modelica model diagram of the house is presented in Figure 4. It is composed of models developed based on the Modelica Standard Library model (version 3.2) and also use the “*MixingVolume*” and “*RadiantSlabs.SingleCircuitSlab*” models developed in the Modelica library “*Buildings*” (Wetter et al, 2013). Hourly schedules are associated to the occupancy, the domestic hot water use, the lighting and appliances in each zone (Bertagnolio, et. al., 2013). The weather data used for the external temperature and the solar irradiance are provided by the DMI - Danmarks Meteorologiske Institut - (Wang et al, 2010).

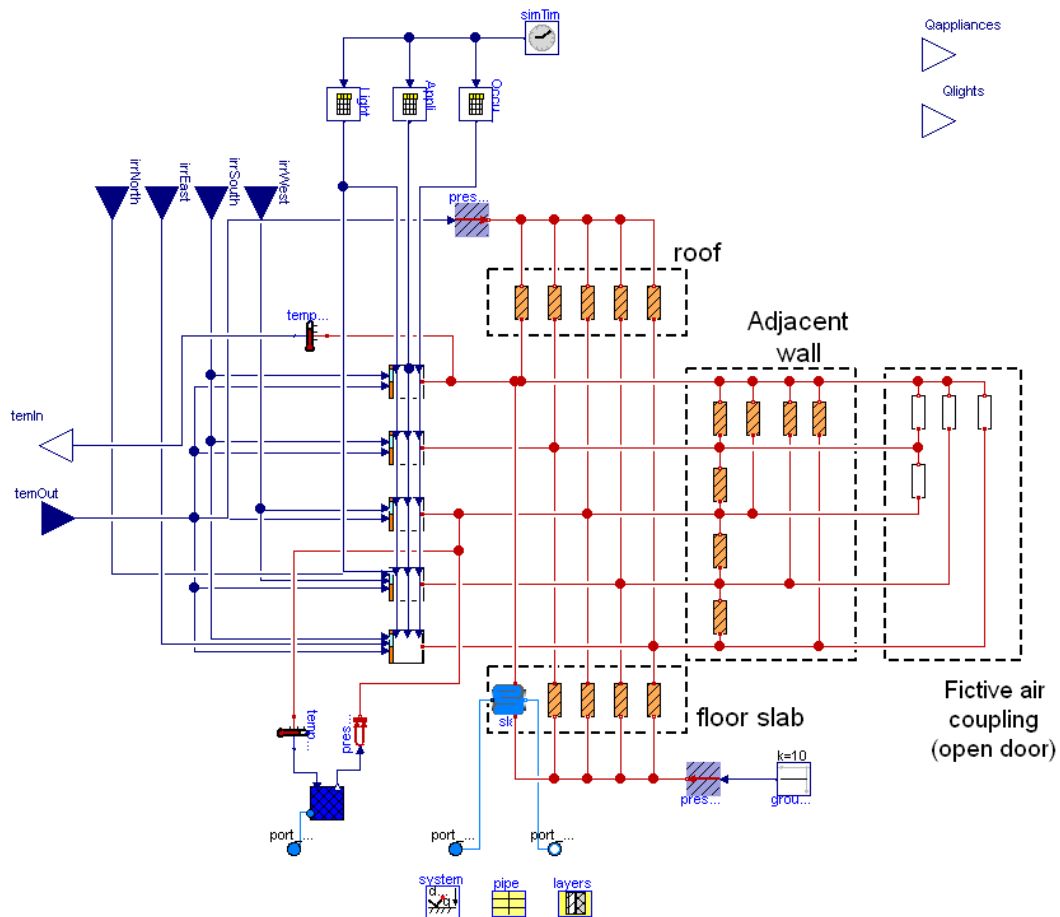


Figure 4: House model diagram in Dymola/Modelica

Each zone model is based on an equivalent R-C network including 5 thermal masses (Masy, 2006), corresponding to one occupancy zone, surrounded by external glazed and opaque walls (Figure 5).

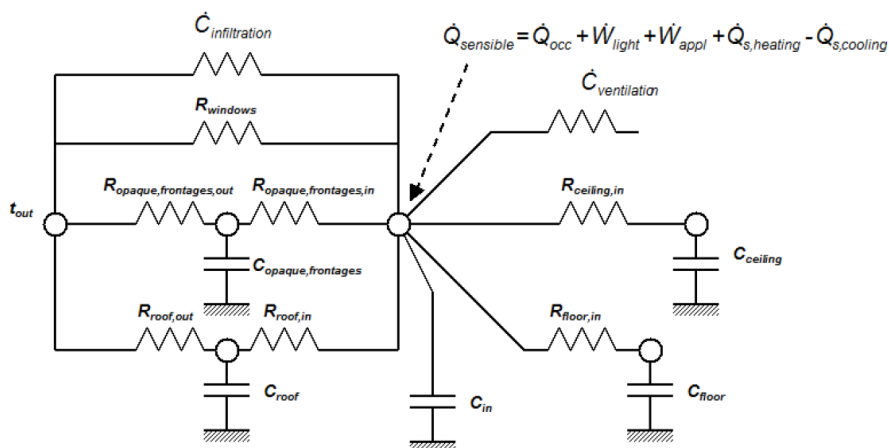


Figure 5: Zone Model – Equivalent R-C Network Model

Massive walls are simulated using first order R-C “two-port networks”. A 2RC module is associated to each massive wall (Figure 6). The parameter of each “two-port network” are adjusted in order to produce wall admittance transmittance for a 24 hour period (Masy, 2006).

The wall stationary U-value equals the invert of the whole two-port resistance. Ventilation system were not considered by means of computational simulation at this stage. To control indoor temperature rise a louver system is included.

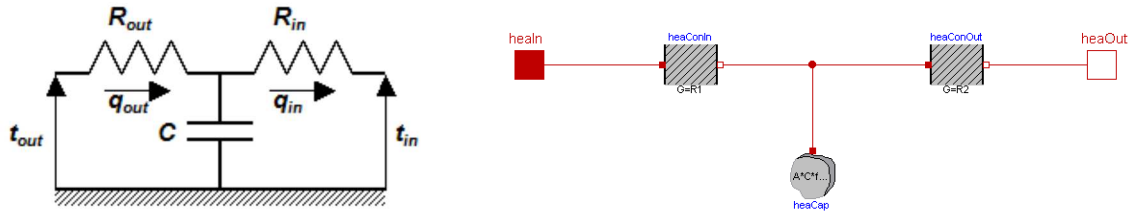


Figure 6 - Capacitive wall and equivalent Dymola/Modelica model diagram

A PID controller controls the floor heating flow to regulate the ambient temperature (zone 1) inside the house close to the set point which is chosen equal to 20°C.

3.6 Ground heat exchanger

The ground heat exchanger is composed of a 300 meters long circuit disposed one meter deep in the ground. 36 thermocouples are disposed over the whole system (on third is 0.5 meter depth, the second third at 1 meter depth and the last one at 1.5 meter depth). Measurements in a second basis on the horizontal ground source heat exchanger showed that the ground temperature is very stable whatever the heat input/output. This temperature varies from 7°C in winter to 12°C in summer (day 182) with fall and spring temperatures of 10°C. For the moment, the temperature of the ground exchanger is therefore imposed following the measurements.

3.7 Global model

Figure 7 presents the flowchart of the global model combining the storage, building, roof, reversible unit and ground. The external inputs are meteorological data (ambient temperature and Direct Normal Radiation on hourly basis– Wang et al, 2010) and occupant behavior in the house (detailed in house model sub-section). The time step is fixed at 900 s. The consumption of auxiliary pumps is neglected, they represent less than 10% of the system consumption.

Some parameters have to be fixed: Roof water flow, ground water flow, storage water flow and temperature set points of the storage. Practically, the following values are used for the flow based on real values measured in the house:

- Roof water flow = 0.6 kg/s,
- Ground water flow = 1.5 kg/s,
- Storage water flow = 0.6 kg/s
- Floor water flow = 0.4 kg/s.

These flows should be optimized in future investigations to increase the energy efficiency of the system (Wystrcil, 2013). The influence of the set points values of the storage is investigated later (section 4.4).

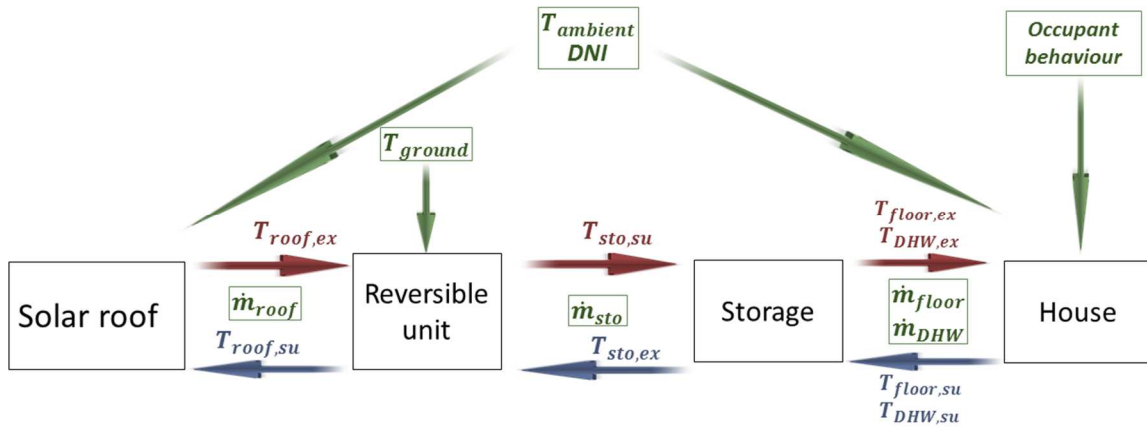


Figure 7: Flowchart of the global model

3.8 Control strategy

The control strategy is based on the following idea: Ensure the heat demand is covered while maximizing the net electricity production (Figure 8). That is the reason why the first control variable which is used is the storage temperature.

If the storage control temperature (T_{sto}) is below a fixed low temperature threshold ($T_{sto,low}$), the heat pump mode is activated to guarantee the space heating (SH) and the domestic hot water (DHW). The heat pump cold source is the ground heat exchanger or the solar roof depending on which one is the warmest. If the storage control temperature is above the high temperature threshold ($T_{sto,high}$), the ORC mode is activated if the roof temperature is above the minimum temperature to get a net electrical production ($T_{ORC,min}$). If the storage control temperature lies between the high and low threshold, the former mode is kept to avoid excessive chattering between modes reducing performance and reliability in practice. Finally, the by-pass mode is used if the storage temperature cannot be increased and if the ORC mode is not able to produce a positive net electricity production. In the by-pass mode, only the roof pump is running to homogenize the roof temperature. This control strategy is relatively simple and should be improved in future works.

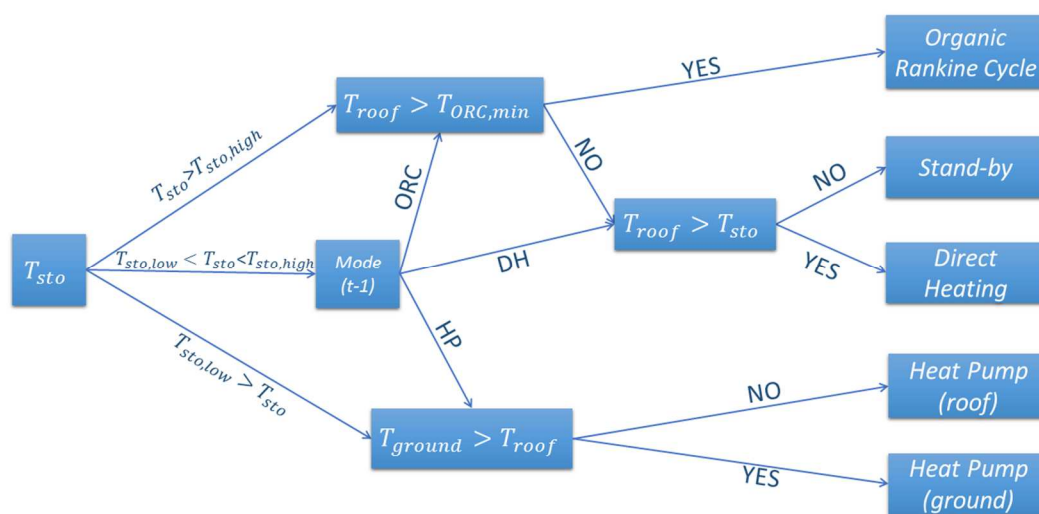


Figure 8: Control strategy of the global model

4. RESULTS FROM SIMULATIONS

Three typical days are simulated to evaluate the behaviour of the system with different inputs: a winter day (day 1), a spring day (day 62) and a summer day (day 182). To ensure steady-state conditions and for initialization each simulation is started 3h before the day considered. The two set points of the storage ($T_{sto,low}$ and $T_{sto,high}$) are 40°C and 50°C in this section. For each simulation, the following variables are plotted:

- Storage temperature from 10th cell ($T_{sto,ctrl}$),
- Outdoor temperature (T_{out}),
- House ambient temperature – zone 1 (T_{house}),
- Exhaust roof temperature ($T_{roof,ex}$),
- Heat flow for floor heating (\dot{Q}_{floor}),
- Heat flow for domestic hot water (\dot{Q}_{DHW}),
- Heat flow from unit (\dot{Q}_{unit}),
- Electrical unit power consumption(-)/production(+) (\dot{W}_{el}),

The mode in operation is detected by looking at the power and heating variables. If electrical unit power consumption is negative (resp. positive), it means that HP (resp. ORC) mode is activated. If heat flow coming from unit is positive and there is no electrical consumption, then DH mode is operating. Finally, in all the other cases, the bypass mode is enabled.

4.1 Winter - Day 1

Figure 9 shows the regulation mechanism during the first day of the year. When the storage temperature decreases down to the low threshold value (40°C) because of SH and/or DHW demand, the heat pump is activated to heat the storage to the high temperature threshold (50°C). This control leads to 3 starts of the HP using the ground heat exchanger as heat source. The total electrical consumption of the heat pump is 5.81 kWh, leading to a daily average COP of 4.34 (Eq. 4).

$$COP_{unit} = \frac{\int (\dot{Q}_{hp} + \dot{Q}_{ah}) dt}{\int \dot{W}_{el} dt} \quad (17)$$

The ambient temperature in the house is fairly well regulated around the set point (20°C) thanks to the regulation of the floor heating flow.

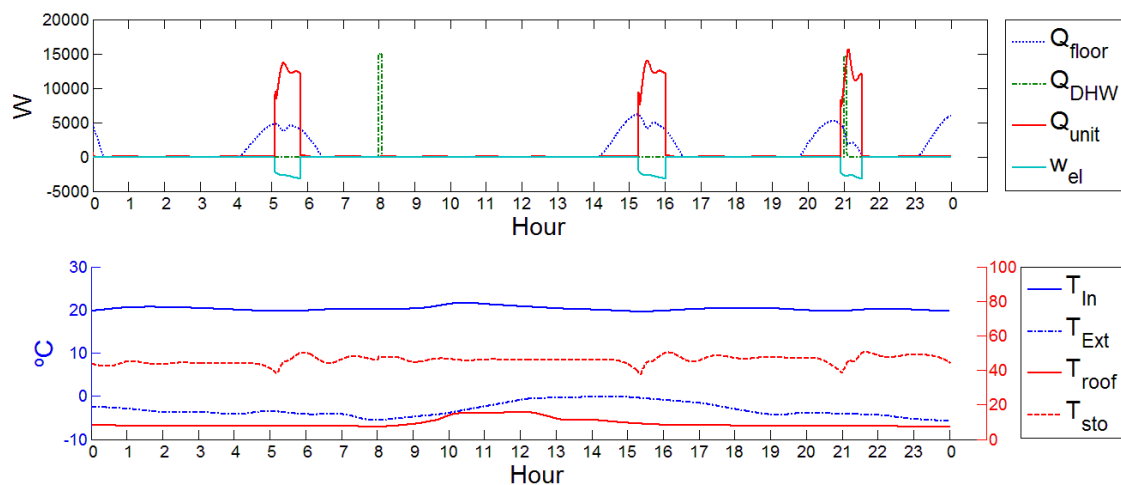


Figure 9: Dynamic simulation of the reversible unit coupled to a passive house for the 1st day of the year

4.2 Spring - Day 62

Figure 10 shows the main inputs and outputs for a typical spring day. In the morning, the HP is needed to keep the storage temperature higher than the low threshold temperature (40°C). From 10 AM to 12 PM, the direct heating increase the storage temperature until the storage temperature reaches the roof temperature (60°C). This heat coming from the roof allows to avoid the starting of the HP before next day. The electrical consumption of the HP is 1.68 kWh, leading to a daily COP_{unit} of 10.48 (Eq. 3).

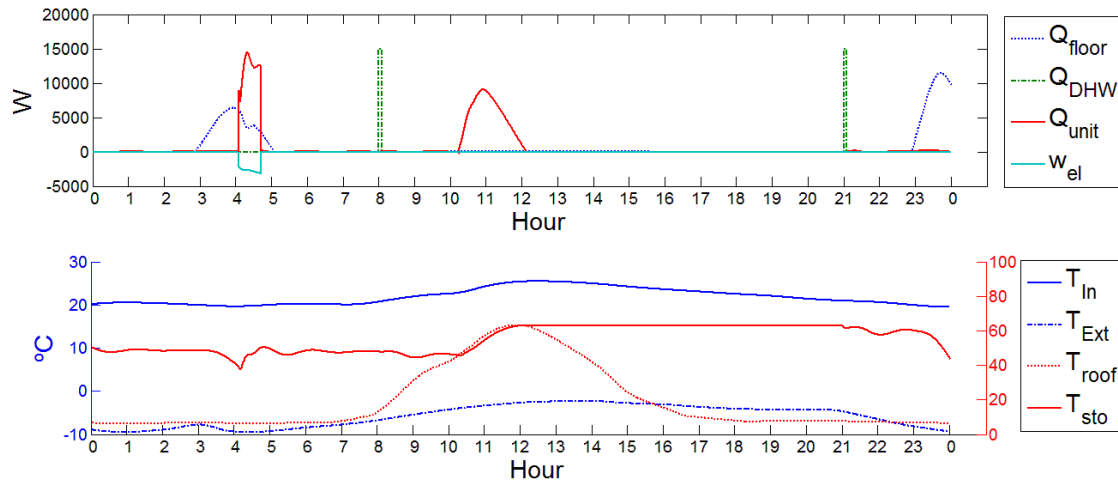


Figure 10: Dynamic simulation of the reversible unit coupled to a passive house for the 62nd day of the year

4.3 Summer – Day 182

Figure 11 shows the main variables for a typical summer day (182nd day). Different inferences can be drawn. Firstly, the only heat demand affecting the storage is the DHW (at 8h and 21h) because the house temperature is always above the temperature set point (20°C). It leads to the use of only two modes (ORC and bypass). Direct heating is used only a few decades of minutes to heat the storage when the temperature is below the low threshold value (not necessary all the days, see Figure 11). The ORC mode is activated as soon as the roof temperature reaches 70°C (i.e. the minimum value to start the ORC). The electrical production of the ORC reaches a maximum of 3.28 kW with a heat input on the roof of 59 kW (23.9 kWh are produced by the ORC during day 182). This leads to an efficiency of 5.5% to be compared with the theoretical one (7.5%). The main reason is that the model used for the ORC is based on the performance of the unit tested experimentally. Several factors like low expander efficiency, high sub-cooling and no thermal insulation explain this difference (see Dumont et al 2014(a)).

4.4 Control strategies

A lot of parameters have to be optimized in this model. The two main parameters of the control flowchart (Figure 8) are the high and low set-points of the storage. Two different control strategies are therefore investigated for the winter day and spring day. The first strategy control uses $T_{sto,low} = 40^{\circ}\text{C}$ and $T_{sto,high} = 50^{\circ}\text{C}$ and the second strategy respectively 40°C and 60°C .

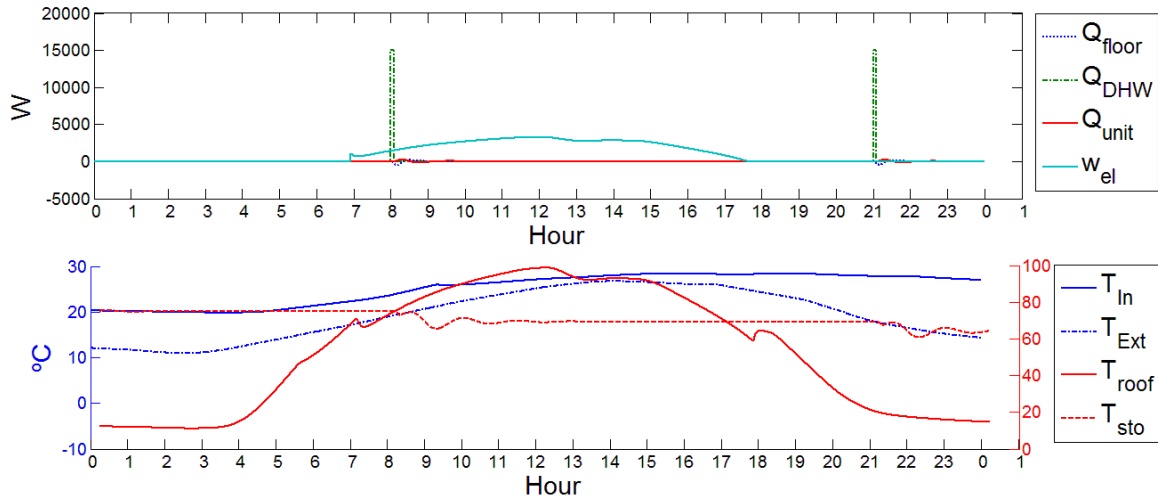


Figure 11: Dynamic simulation of the reversible unit coupled to a passive house for the 182nd day of the year

Looking at the summer day results (Figure 11), the control strategy is not influencing the results since storage temperature is always higher than $T_{sto,high}$. Table 4 presents a comparison in terms of minimum DHW temperature (T_{DHW}), electrical energy production (+) /consumption (-) of the unit (W_{el}), number of times the mode changes, the daily COP (Eq. 17) and house temperature (T_{house}). For day 182, the daily ORC efficiency is evaluated with Eq. 18.

$$\eta = \frac{\int \dot{W}_{el} dt}{\int \dot{Q}_{roof} dt} \quad (18)$$

Several conclusions can be drawn from this comparison. Firstly, the temperature of the domestic hot water, which always needs to be at 40°C at least, is always guaranteed. But, if for some reason the DHW consumption happens at a different time, the storage temperature in the top should be sufficient at any time in the day. In this case, the second control strategy offers more security in terms of temperature level. Also, it is observed that the first strategy needs more mode changes compared to the first one. This could be an issue in terms of control and reliability. Nevertheless, the electrical consumption is 20% lower with the first strategy on D1 and 2.45 times lower for D62. This lower consumption for strategy one results from less energy in the storage (lower average temperature over time), highest COP due to lower condensation temperature and more heat coming from direct heating (because the lower storage temperature). To complete, further investigations should be performed to evaluate the decrease in efficiency due to start and stop of the unit. Finally, the house ambient temperature is very slightly affected by the control. In conclusion, a strategy with a colder storage leads to a significant reduction of the electrical consumption but, on the other hand, leads to the possibility of slightly low DHW temperature and more mode changes.

Table 4: Comparison of different control strategies

Day	D1 – Winter		D62 - Spring		D182 -Summer
Strategy	1	2	1	2	1/2
T_{DHW} [°C]	46.1	53.6	47.6	44.7	70
W_{el} [kWh]	-5.81	-7.33	-1.68	-4.12	23.9
Mode changes [-]	6	4	4	3	2
T_{house} [°C]	[19.6:21.6]	[19.7:21.7]	[19.5:25.5]	[19.5:25.6]	[19:28]
COP_{unit}/η [-]	4.34	3.54	10.48	2.91	0.06

5. CONCLUSION

A dynamic model of a reversible HP/ORC unit integrated in a passive house was developed. The electrical production in summer reaches 23.9 kWh while the consumption of the HP in a typical winter day reaches 5.81 kWh. Based on these first results, the electrical production of the house is estimated to be the double of the energy consumption. This indicates that this technology is a promising way to achieve Plus Energy Building at low price.

Three main conclusions can be drawn. First, an optimized control strategy with a low temperature set-point on the storage allows higher COP and energy savings up to 20% in a typical winter day.

Also the production of electricity during the sunniest days does not match with the demand. A possible improvement would be to store the heat produced during the day to shift the electricity production of the ORC in time to match the electricity demand of the house. A second, large, thermal storage is therefore necessary to store sufficient heat for the ORC production shifting.

Finally, the simulations show that the solar roof produces huge amount of heat. This heat is unused if the storage has reached the roof temperature and if the roof is too cold to start the ORC. A solution to avoid this loss of heat at low temperature could be the valorisation of the surplus heat in an external district heat network.

More simulations need to be performed to evaluate the system annual performance and to compare it with competitive products. An estimation of the price of this system compared to competitive products (heat pump combined with PVT for example) can be drawn. First, the reversible unit presents almost the same components (Dumont, 2014(c)) as a classical heat pump (meaning the same costs if produced in large series). Also, the solar absorber presents a cost close to PV panels (Abdul-Zahra et al, 2014). This shows that the price of the described system is close to competitive products. Further investigations will present a detailed analysis of the investment and running costs (or benefits). In conclusion, this technology is a promising way to achieve Plus Energy Building at low price and higher efficiency compared to competitive systems as photovoltaic-thermal solar heat pump which performance is half of the HP/ORC system (Fang, et al., 2010).

NOMENCLATURE

Variables

$A [m^2]$	Area	$\eta [-]$	ORC daily efficiency
$C_p [J/(kg.K)]$	Specific heat	$\dot{Q} [W]$	Heat rate
DNI	Direct normal irradiation	$\tau [s]$	Time constant
Δ	Difference	$T [^{\circ}C]$	Temperature
$I [W/m^2]$	Solar irradiance	$U [W/(m^2.K)]$	Heat loss coefficient
$M [kg]$	Mass	$\dot{W} [W]$	Power
$\dot{m} [kg/s]$	Mass flow	$W [J]$	Energy

Subscripts

amb	Ambient	ex	Exhaust
app	Appliances	Out	outdoor

<i>cd</i>	Condenser	<i>ORC</i>	Organic Rankine Cycle
<i>ctrl</i>	Control	<i>sc</i>	Sub-cooling
<i>DH</i>	Direct heating	<i>su</i>	Supply
<i>DHW</i>	Domestic hot water	<i>Sto</i>	Storage
<i>el</i>	Electrical	<i>Roof</i>	Solar roof
<i>ev</i>	Evaporator		

REFERENCES

- Abdul-Zahra, A., Fasßnacht, T., Wagner, A., 2014. Evaluation of the combination of hybrid photovoltaic solar thermal collectors with air to water heat pumps, proceeding of the conference eurosun 2014.
- Bertagnolio, S., Georges, E., Gendebien, S. and Lemort, V., 2013. Modeling and simulation of the domestic energy use in Belgium following a bottom-up approach, Proceedings of the CLIMA 2013 11th REHVA World Congress & 8th International Conference on IAQVEC, <http://hdl.handle.net/2268/147390>
- Bettgenhäuser K., Offermann M., Boermans T., Bosquet M., Grözinger J., von Manteuffel B. and Surmeli N., 2013. Heat Pump Implementation Scenarios until 2030: An analysis of the technology's potential in the building sector of Austria, Belgium, Germany, Spain, France, Italy, Sweden and the United Kingdom, ECOFYS Report, Project number: BUIDE12080.
- Dumont, O., Quoilin, S., Lemort, V., 2014 (a). Design, modelling and experimentation of a reversible HP/ORC prototype, Proceedings of the 11th International Energy Agency Heat Pump Conference.
- Dumont, O., 2014 (b). Annexes of the paper “simulation of a passive house coupled with a Heat Pump/Organic Rankine Cycle reversible unit”, <http://orbi.ulg.ac.be/handle/2268/171470>.
- Dumont, O., Quoilin, S., Lemort, V., 2014 (c). Design, modelling and experimentation of a reversible HP/ORC prototype, Proceedings of the turbine technical conference and exposition ASME TURBO EXPO 2014.
- Fang, G., Hu, H. and Liu, X., 2010. Experimental investigation on the photovoltaic-thermal solar air-conditioning system on water-heating mode, 2010, Experimental Thermal and Fluid Science, pp. 736-743, doi:10.1016/j.expthermflusci.2010.01.002
- Hepbasli, A., Yalinci, Y., 2009. A review of heat pump water systems, IRESR, 13, 1211-1229.
- Innogie ApS, 2013. Thermal solar absorber system generating heat and electricity, United States Patent Application Publication, US 2013/025778 A1.
- Jagemar, L., Schmidt, M., Allard, F., Heiselberg, P., et Kurnitski, J., 2011. Towards NZEB – Some example of national requirements and roadmaps, REHVA Journal, May 2011, 14-17.
- Klein, S. A., 1975. Calculation of flat-plate loss coefficient, Soar Energy, 17, 79.
- Kurnitski, J., Corgnati, S., Tiziana, B., Derjanecz, A., Litiu, A., 2014. NZEB definitions in Europe, REHVA Journal, March 2014, 6-9.
- Masy, G., 2006. Dynamic Simulation on Simplified Building Models and Interaction with Heating Systems. Proceedings of the 7th International Conference on System Simulation in Buildings, Liège, Belgium.

Quoilin, S., Desideri, A., Wronski, J., Bell, I., Lemort, V., 2014. ThermoCycle: A Modelica library for the simulation of thermodynamic systems, Proceedings of the 10th International Modelica Conference, Modelica Association., 10.3384/ECP14096683.

Thermocycle library, 2014. <http://www.thermocycle.net/>, consulted the 20th of June 2014.

Wang, P.G., Scharling, M., Nielsen, K. P., Kern-Hansen, C., 2010. Technical Report 13-19: 2001 – 2010 Danish Design Reference Year, Climate Dataset for Technical Dimensioning in Building, Construction and other Sectors, <http://www.dmi.dk/fileadmin/Rapporter/TR/tr13-19.pdf>

Wetter, M., Zou W., Nouidui T.S., Pang X., 2012. Modelica Buildings library, Journal of Building Performance Simulation, March 2013.

Wystreil, E. A., 2013. Model-based optimization of control strategies for low-exergy space heating systems using an environmental heat source. *13th Conference of International Building Performance Simulation Association*. Chambéry: BS2013

Integration and Evaluation of Innovative and Renewable Energy Technologies in a Canadian Mid-rise Apartment

M. Kegel, J. Tamasauskas, R. Sunye

Natural Resources Canada, Varennes, Canada

1. ABSTRACT

This paper presents an analysis of the impact of various energy efficiency measures towards achieving net zero energy in comparison to using photovoltaics to offset the energy consumption. Using TRNSYS, an energy model of a typical newly constructed four storey mid-rise apartment was developed complying with the current energy code for the Montreal region in Canada. Standard energy efficiency improvements such as reduction of base electrical loads, high efficiency fans, building insulation improvement and heat recovery were evaluated as well as several high efficient systems such as air to air heat pumps, ground source heat pumps and solar assisted ground source heat pumps. The results indicated that air to air heat pumps are a more cost effective approach to reducing the building energy consumption in comparison to using photovoltaics as well as the reduction of base electrical loads and recovering heat from the building exhaust. Little benefit was found improving the building insulation level beyond the minimum levels. When taking the additional land value required by a photovoltaic system into account, the higher capital costs of the ground source heat pump systems become cost competitive.

Keywords: Net zero energy, air to air heat pump, ground source heat pump, solar thermal, photovoltaics

2. INTRODUCTION

The residential sector accounts for 16% of Canada's secondary energy consumption and 15% of the greenhouse gas (GHG) emissions (Natural Resources Canada, 2009). Although energy efficiency standards have improved over the years, there has still been a steady increase in the residential sector annual energy consumption as new houses are continuously built, while the existing housing stock remains. With the American Society of Heating, Refrigeration and Air Conditioning Engineer's (ASHRAE) vision of market viable net zero energy buildings by 2025 (ASHRAE, 2008) research must be conducted to develop a design guide for building owners and building designers. Furthermore, with half of the existing building stock constructed today being still in existence by 2050, it is important that building energy efficiency strategies are well suited to future net zero energy targets.

To achieve net zero energy two standard approaches can be taken:

- Adoption of a high efficient building envelope with the use of passive gains and meeting the remaining loads through renewable energy sources.
- A combination of a reasonably good building envelope with a high efficient heating and cooling system and a high share of renewable energy.

The question still remains however at which point it no longer becomes cost effective to reduce the building loads and meet the remaining load with renewable energy sources. The Canadian Green Building Council (CAGBC) recommends a building energy intensity of 100 kWh/m² (CAGBC, 2014), while Natural Resources Canada has recommended to reduce the housing

energy consumption by 50% (Parekh, 2010). By meeting these targets the building or house is considered to be net zero ready, where it economically makes sense to add renewable energy sources to make the building net zero.

This paper examines and evaluates several energy efficiency pathways to make a 4-storey mid-rise apartment located in Montreal, Canada become net zero. The analysis is conducted on a newly constructed mid-rise apartment designed to meet the current National Energy Code of Canada for Buildings (NECB) (NRC, 2011) and energy efficiency improvements made in regards to building insulation, reduction of electrical loads, heat recovery and the use of heat pump systems. An economic analysis for each combination of systems is performed to make the mid-rise apartment net zero through the use of photovoltaics. Net zero in this paper considers that the photovoltaic system generates as much electricity as the building consumes on an annual basis. Excess electricity is sold back to the grid at the same rate electricity is purchased.

3. METHODOLOGY AND SIMULATION

To perform the analysis an energy model of a typical mid-rise apartment was developed using the TRNSYS simulation tool (Klein et al., 2010). The shape and dimensions of the mid-rise apartment were taken from the Department of Energy (DOE) benchmark models (DOE, 2013). The mid-rise apartment is four floors, with each floor comprised of 8 equally sized apartment units. Each apartment unit has a floor area of 88 m² and includes a kitchen, two bedrooms, living room and a bathroom. The total heated floor area of the building is 3,135 m² with a footprint area of 784 m². The building has a 15% fenestration to wall ratio. The 3D model and floor plan is shown in figure 1. The 2nd and 3rd floor was grouped into one zone to reduce the number of thermal zones in the model. The apartment suites are maintained between 21°C and 23°C and relative humidity above 30%. Lighting, occupancy and receptacle schedules were assumed to follow those outlined in the NECB. Each apartment unit has its own 110 L domestic hot water (DHW) heater, with a hot water draw profile assumed to follow that of the IEA Annex 42 DHW Load profile (Knight et al., 2007) for Canada (approximately 184 L of hot water per day per apartment unit). The energy models were run using the Montreal TMY2 weather file and 5 minute timestep. It is also estimated that the roof area can have a 172 m² PV array facing south at a 45° tilt angle such that there is no shading of the panels on one another.

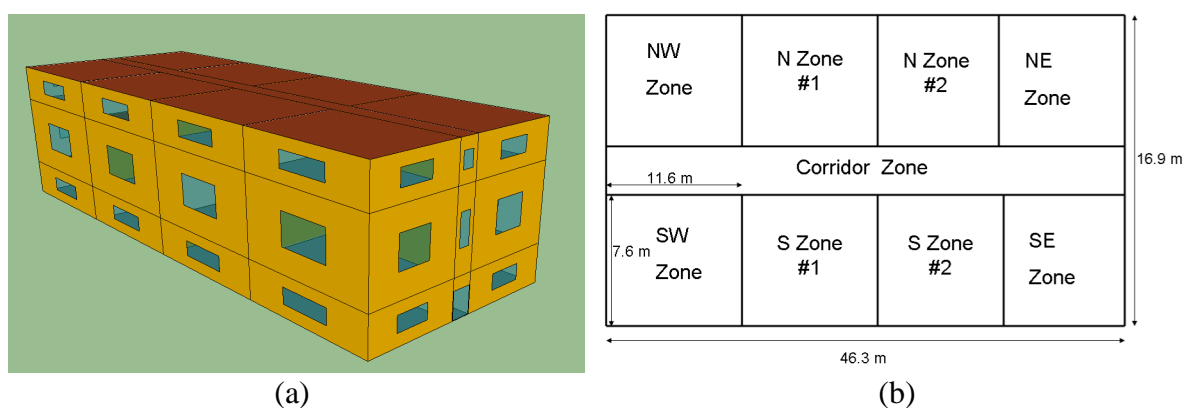


Figure 1: (a) 3D model (b) Floor plan of mid-rise apartment

3.1 Base Case

The reference mid-rise apartment characteristics were set from the NECB minimum efficiency requirements for the Montreal region (Zone 6). The key characteristics of the reference building are summarized in table 1.

Table 1: Mid-rise apartment characteristics

Characteristic	Description
Roof Insulation Level	0.181 W/m ² °C
Wall Insulation Level	0.248 W/m ² °C
Windows	1.98 W/m ² °C Double Glazed
Heat Recovery Ventilator	None
Heating and Cooling	Packaged Terminal Air Conditioning (PTAC) with electric resistance heater
Fans	Permanent Split Capacitance (PSC) (1 W/L/s)
Domestic Hot Water	Electric
Humidification	Electric

Standard TRNSYS components were used to model the building HVAC systems and operating schedules. Although the simulation was run with a 5 minute time step, the heating and cooling capacity of the HVAC system was modulated constantly to maintain the desired room temperature setpoints. As the standard TRNSYS air conditioning components do not model part load performance, each apartment suite cooling system was modeled with the Type 42a (conditioning equipment, 3 independent variables) component relating the total cooling capacity, sensible cooling capacity and compressor power draw to the outdoor temperature and indoor dry bulb and wet bulb temperature. The cooling capacity was then modulated with a PID controller (Type 23) to the desired room temperature and the capacity was transferred to the air stream using the Type 693 (flowstream loads, air) component. The part load performance was then calculated using curves determined by the DOE (Henderson et al., 1999). The annual energy end use breakdown is shown in figure 2.

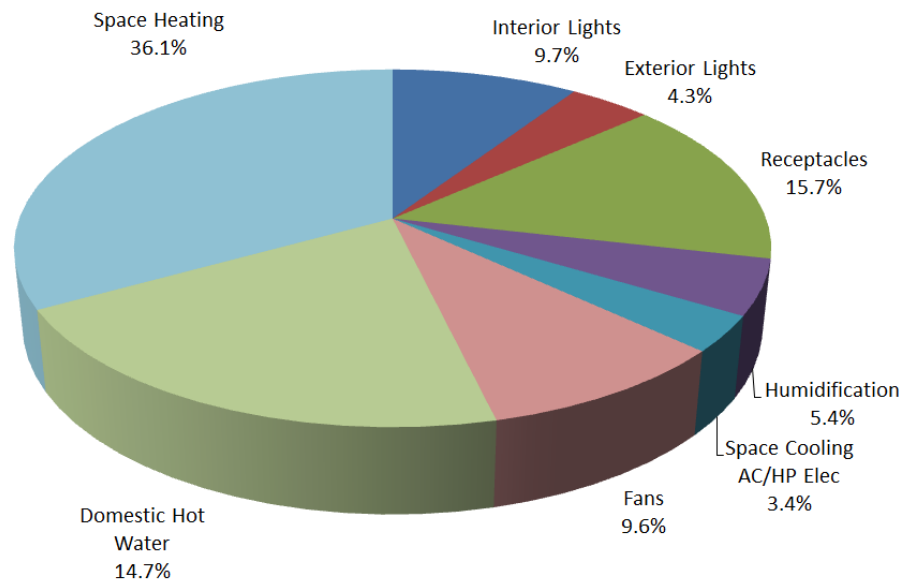


Figure 2: Baseline energy end use breakdown

The annual energy consumption, utility cost and energy intensity is summarized in Table 2. The utility cost was estimated using the most recent electricity rates from Hydro Quebec (2014) of approximately \$0.07/kWh.

Table 2: Baseline annual energy consumption, utility cost and energy intensity

Characteristic	Value
Annual energy consumption	595,982 kWh
Annual utility cost	\$43,461 CDN
Annual energy intensity	190.1 kWh/m ²

3.2 Photovoltaics

To achieve net zero, the use of photovoltaics (PV) will be investigated to determine at which point it becomes economically feasible to install a PV system to offset electricity consumption compared to conventional energy efficiency measures. Using TRNSYS and the manufacturer published characteristics of a monocrystalline PV panel (Grape Solar, 2014), it was estimated that a PV system could produce 285 kWh annually per square meter of array area facing south and at a 45° angle (manufacturer rated performance is 155 W/m²). Thus to make the baseline mid-rise apartment net zero, a PV array area of approximately 2,100 m² would be required. The average of the estimated installed PV cost of \$3.90/W reported by Luukkonen et al., (2013) was used for the analysis, which also assumes there is sufficient land space to install the PV system, which may not be the case. Table 3 summarizes the anticipated PV cost and array area to make the baseline building net zero.

Table 3: Baseline PV requirements to achieve net zero

Characteristic	Value
PV Array Size	2,100 m ²
PV Array Cost	\$1,269,000 CDN

3.3 Standard Energy Efficiency Improvements

To quantify the benefit to reducing the annual energy consumption of the mid-rise apartment compared to simply adding PV to make it net zero, several energy efficiency measures are investigated. From the energy end use graph (figure 2), space heating, lighting and receptacle loads, fans and domestic hot water heating make up just over 85% of the energy end use. Thus energy efficiency measures addressing these end uses are selected to reduce the energy consumption. These measures include:

- Reduction in base electrical loads through energy efficient lighting and appliances
- Reduction of fan power using electronically commutated motors (ECM)
- Reduction in the space heating load through a high efficient building envelope
- Reduction in the space heating load through the heat recovery from exhaust air

To perform the economic analysis the incremental costs of implementing the energy efficiency measures are estimated from RSMMeans (RSMMeans, 2013) as well as contractor surveys.

3.3.1 Reduction of base electrical loads

The base electrical loads were modelled based on the recommended appliance and lighting loads. Energy Star® packages are often offered and can have substantial energy savings compared to standard equipment in new housing developments. A 60% reduction in lighting power and a 25% reduction in appliance electrical consumption were assumed for this case (Energy Star®, 2014). The estimated incremental costs for the efficient base electrical loads are \$25,000 CDN.

3.3.2 High efficient fan motors

Each apartment unit has a central heating and cooling system with a two speed indoor blower assumed to draw 1 W per L/s of airflow. ECM motors are variable speed and can have significant savings compared to PSC motors. For the analysis, the ECM motors are assumed to be two speed and conservatively draw 0.5 W per L/s of airflow (Gusdorf et al., 2002). The estimated incremental cost for the ECM motors is \$7,000 CDN total.

3.3.3 High efficient building envelope

The building envelope insulation levels were set to the minimum levels outlined by the NECB for the Montreal region. This efficiency measure evaluates whether there is a benefit to heavily insulating the building using realistic construction practices to further reduce the space heating loads. The estimated incremental cost to improve the insulation level of the building envelope is \$145,000 CDN. Table 4 summarizes the proposed changes.

Table 4: Proposed building envelope insulation improvement

Characteristic	Baseline	Proposed
Roof u-value	0.181 W/m ² °C	0.125 W/m ² °C
Wall u-value	0.248 W/m ² °C	0.188 W/m ² °C
Window u-value	1.98 W/m ² °C Double Glazed	1.31 W/m ² °C Triple Glazed

3.3.4 Heat Recovery

Due to the improved air tightness of the building, fresh air must be brought in to each apartment unit. Heat recovery ventilators are only required however in colder Canadian regions (Region 7A and higher) (NRC, 2011). This measure evaluates the benefit of adding in suite heat recovery ventilators to recover the exhaust heat. Approximately 33 L/s of fresh air is brought into each apartment unit. The anticipated total cost to install heat recovery ventilators in all apartment suites is \$84,000 CDN.

3.4 Energy Efficient Systems

Building upon the above four energy efficiency measures, four efficient heating systems for each scenario are compared to evaluate the impact of selecting high efficient heating systems to meet a net zero energy target. The systems are:

- Conventional air source heat pumps (ASHP)
- Cold climate air source heat pumps (CC ASHP)
- Ground source heat pumps (GSHP)
- Solar assisted ground source heat pumps (SA GSHP)

In each case the packaged terminal air conditioning system with an electric heating is replaced by a reversible air source or water source heat pump system.

3.4.1 Heat Pump System Modeling

As the cyclic on-off operation of a heat pump can have a significant impact on the energy consumption of the system, it is important to take this into account in the energy models. As the standard TRNSYS models of the air to air heat pump systems are not well adapted to taking into account the part load performance, the air to air heat pumps were modelled using the TRNSYS Type 42 components relating the heating (Type 42b) or cooling capacities (Type 42a) to outdoor and indoor ambient temperatures and applying the estimated loads to the air stream using the Type 693 component. The capacity of the air to air heat pump is modulated with a

PID controller and the compressor power draw calculated according to the estimated percent heating/cooling demand. A schematic of the modelling strategy is provided in figure 3. The part load performance curves for the conventional air to air heat pumps were estimated from DOE (Henderson et al., 1999) and the cold climate inverter driven heat pump performance curves were derived from the performance measured by the Swedish Energy Agency (Filliard et al., 2009).

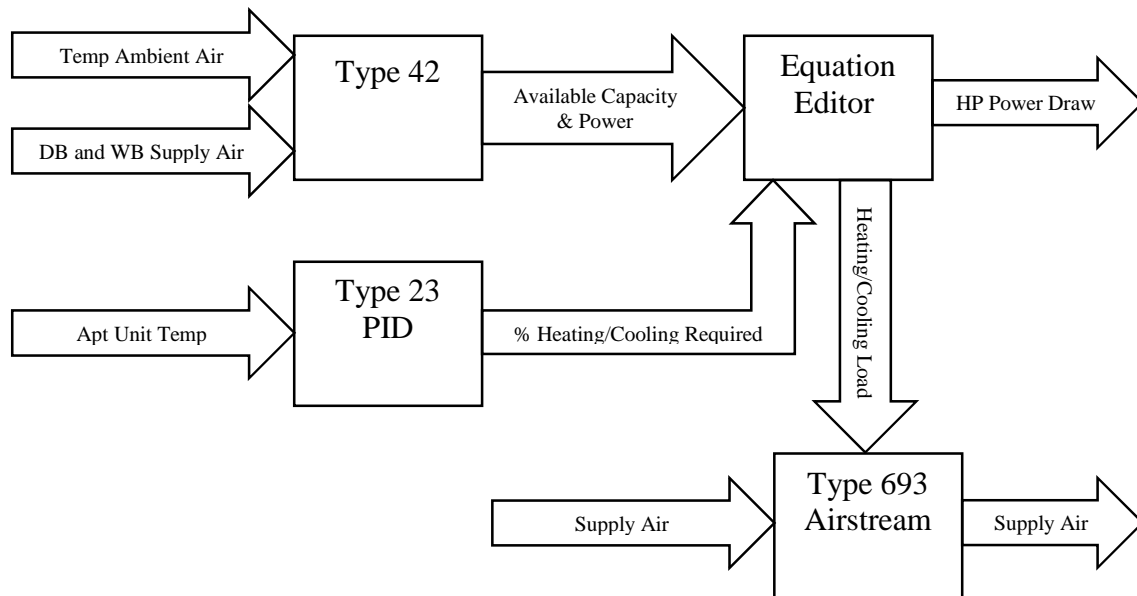


Figure 3: Air to Air Heat Pump System Model

For the apartment unit water source heat pumps, TRNSYS Type 919 was used. Unlike the air to air heat pumps, the Type 919 component can take a control signal and modulate the heating/cooling capacity of the heat pump. The part load performance curves of the water source heat pumps were estimated from DOE (Henderson et al., 1999).

3.4.2 Conventional air source heat pump system

This efficiency measure evaluates replacing each apartment suite packaged terminal air conditioning system with electric heating with an air to air heat pump system. The benefit of air source heat pumps (ASHP) are that the space heating loads are met by upgrading the available energy in the colder outside ambient air. In moderate climates the ASHPs operate very efficiently delivering between two to three times the energy consumed. As ambient temperatures decrease, the heating capacity and efficiency of the heat pump drastically decrease not always making them suitable in a Canadian climate. To avoid space temperatures falling below the desired setpoint each apartment unit heating system is also equipped with a full sized back-up electric heating coil. Thus if the heat pump is unable to meet the space heating load, the electric back-up heating coil provides supplemental heating.

As a preliminary analysis two standard air source heat pump sizes are evaluated – the smallest market available size of 1.5 tons (5.3 kW heating capacity) and a 2.0 ton (7.0 kW heating capacity). The heat pumps have an ARI rated coefficient of performance of 3.3 in heating mode and 3.1 in cooling mode (Carrier, 2008). A fully sized back-up electric resistance heater supplements the heating capacity of the heat pumps capable of operating efficiently down to - 20°C according to the manufacturer performance curves.

A comparative energy analysis between the 2.0 ton and the 1.5 ton system is first performed to determine the optimum air source heat pump size for the mid-rise apartment units. While the 2.0 ton system has a higher fan power and will operate at a lower part load, the increase in available heating capacity at lower temperatures may outweigh the benefits of the smaller 1.5 ton system. Table 5 summarizes the results of the two air source heat pump sizes implemented into the baseline apartment building, highlighting the 1.5 ton system as being a better choice. While this analysis focuses on evaluating existing systems, future work will look at the optimum air to air heat pump size for this type of building.

Table 5: Optimum air to air heat pump size analysis

Characteristic	1.5 ton ASHP	2.0 ton ASHP
Annual energy consumption	487,526 kWh	508,434 kWh
Annual utility cost	\$35,021 CDN	\$36,308 CDN
Annual energy intensity	155.5 kWh/m ²	162.2 kWh/m ²

3.4.3 Cold climate air source heat pump system

With the degradation of performance and heating capacity of conventional air source heat pumps at lower ambient temperatures, these systems are often not a suitable choice for the Canadian climate as the potentially inefficient back-up heating system must operate more frequently. Relatively new to the market and gaining interest in Canada are cold climate air to air heat pumps, which maintain their capacity and coefficient of performance much better at lower temperatures through the use of variable capacity compressors. Furthermore, with the variable capacity compressors, the cold climate air to air heat pump can modulate to reduce the on-off cycling often seen in conventional air source heat pumps.

The cold climate air source heat pump (CC ASHP) selected for the analysis has a rated heating capacity of 11.1 kW with a rated heating COP of 3.0 and a rated cooling capacity of 10.0 kW and cooling COP of 3.5 (Mitsubishi Electric, 2011). While the rated heating and cooling capacities exceed the building heating and cooling demand requirements, the variable capacity compressor of the heat pump permits modulation down to 40% of the rated capacities to meet the heating or cooling loads without having to cycle on and off. Performance curves of the cold climate air source heat pump were estimated from the inverter compressor type heat pump performance published by the Swedish Energy Agency (Filliard et al., 2009).

For this scenario, the CC ASHP replaces the packaged terminal air conditioning system with electric heat. The cold climate air source heat pump is equipped with a small back-up electric heater in the event ambient temperatures fall and there is insufficient heating capacity to meet the space heating requirements. While the analysis in this paper uses existing technology, future work will evaluate the optimum cold climate air to air heat pump size for this type of building.

3.4.4 Ground source heat pumps

Instead of using the ambient air as an energy source to meet the space heating load, ground source heat pumps (GSHP) use the thermal energy stored in the ground. The ground remains at a fairly stable temperature and if sized correctly provides a renewable energy source for space heating and cooling. The borefield was sized following the Kavanaugh and Rafferty equation (1997) taking into account the annual ground imbalance, peak monthly ground load and peak hourly ground load. For the mid-rise apartment building, a required borefield of 30 boreholes (6 x 5 configuration) at 100 m length spaced 6.1 m apart was calculated to meet the thermal loads of the building. The design fluid temperatures for space heating and cooling were set to 0°C and 35°C, respectively. The apartment unit GSHPs were sized to meet the space heating load resulting in unit sizes rated between 1.5 and 3 tons of cooling (5.3 kW and 10.6 kW). A

separate GSHP for each apartment unit was decided upon in the event that there could be simultaneous heating and cooling loads. Future work will look into using one unique heat pump for the entire building as it could be a more cost effective approach. The borefield was sized, such that neither a back up boiler was required to meet the space heating demand, nor a back-up cooling tower to meet the space cooling load. The boreholes were also sized to ensure the borefield energy would not become depleted due to an imbalance in the heating and cooling ground loads. A schematic of the proposed system is shown in figure 4 below.

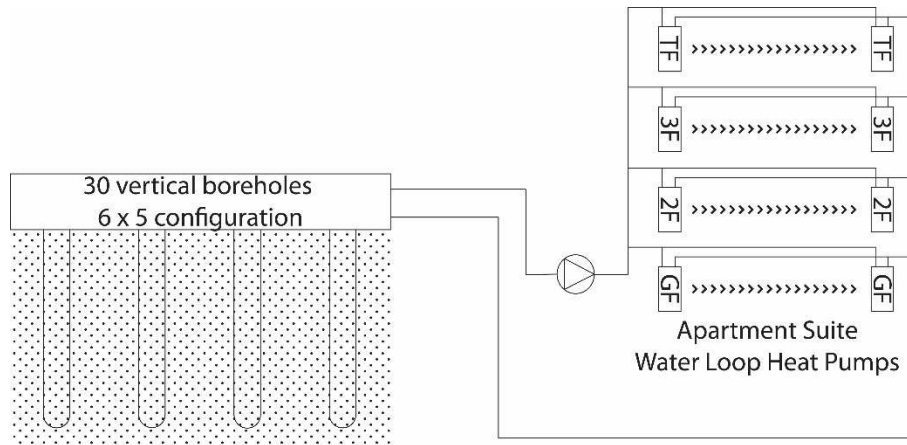


Figure 4: Ground source heat pump schematic

The benefit of the GSHP system is that the system utilizes the renewable energy of the ground providing a uniform, constant source temperature for the heat pumps. At design conditions, the GSHPs have a heating COP of 4.6, essentially gaining 4.6 units of energy for every 1 unit of energy input into the system. The downfall, is the high associated cost with the borefield. For this analysis, borefield drilling costs of \$80/m is assumed – the midpoint of the range of borefield drilling costs reported by Kummert and Bernier (2008).

3.4.5 Solar assisted ground source heat pump system

Close to 15% of the mid-rise apartment energy end use is for domestic hot water heating. Thus with the space heating demand efficiently being met by a heat pump system, addressing the domestic hot water energy consumption will become important as it may represent the highest energy end use. This section evaluates the potential use of solar thermal collectors in conjunction with a ground source heat pump system to meet the space heating and cooling loads in addition to the domestic hot water demand.

A south facing evacuated tube solar thermal array mounted on the roof of the apartment is proposed angled at 45° - the latitude of Montreal. Evacuated tube collectors (Vitosol 300 SP3) were selected with the performance characteristics taken from the Directory of SRCC Certified Solar Collector Ratings (2006). Ensuring the solar collectors do not shade one another, a total of 40 collectors are proposed to be installed on the mid-rise apartment roof for a total collector area of 172 m². Thermal energy is stored in a 10,000 L storage tank.

As a preliminary analysis, the borefield was sized assuming the solar energy injected into the ground would help offset the peak monthly ground load and annual ground imbalance. The solar thermal system would inject heat into the ground loop when the supply fluid temperature falls below 0°C. Through the use of solar energy, a 35% reduction in the borehole depth was estimated (30 boreholes, 6 x 5 configuration, 65 m deep). To make more use of the solar energy, the domestic hot water is also supplemented by the solar thermal system. Figure 5 provides a schematic of the proposed system.

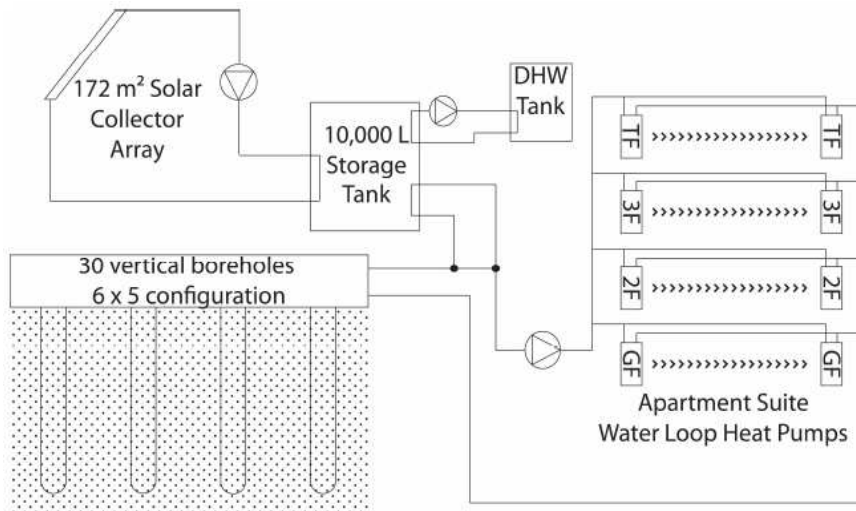


Figure 5: Solar assisted ground source heat pump system schematic

4. RESULTS AND DISCUSSION

4.1 Standard Energy Efficiency Results

Energy models of the following energy efficiency measure combinations were developed to evaluate the energy saving potential versus cost over a PV system to achieve net zero energy.

- Measure 1: Reduction of base electrical loads
- Measure 2: Reduction of base electrical loads and use of ECM fan motors
- Measure 3: Reduction of base electrical loads, use of ECM fan motors and building insulation improvement
- Measure 4: Reduction of base electrical loads, use of ECM fan motors and heat recovery on the apartment unit exhaust air
- Measure 5: Reduction of base electrical loads, use of ECM fan motors, heat recovery on exhaust air and building insulation improvement

From RSMMeans (2013) and contractor surveys the estimated energy efficiency measure cost was estimated and summarized in table 6.

Table 6: Estimated incremental costs for standard efficiency measure combinations

Energy Efficiency Measure	Estimated cost
Measure 1	\$25,000 CDN
Measure 2	\$32,000 CDN
Measure 3	\$177,000 CDN
Measure 4	\$115,000 CDN
Measure 5	\$260,000 CDN

Figure 6 presents the results of the standard energy efficiency measure impact. Figure 6a summarizes the final energy consumption intensity for each measure, figure 6b presents the annual utility costs with no PV system, figure 6c compares the PV array cost difference to achieve net zero energy (NZE) over the baseline energy consumption and figure 6d presents the cost comparison between using a PV array and the efficiency measure to achieve the same level of energy savings. A negative cost indicates that it is economically more beneficial to install a larger PV system than implement the proposed energy efficiency measure. A positive cost indicates that it is more beneficial to implement the energy efficiency measure to save energy rather than using a PV array.

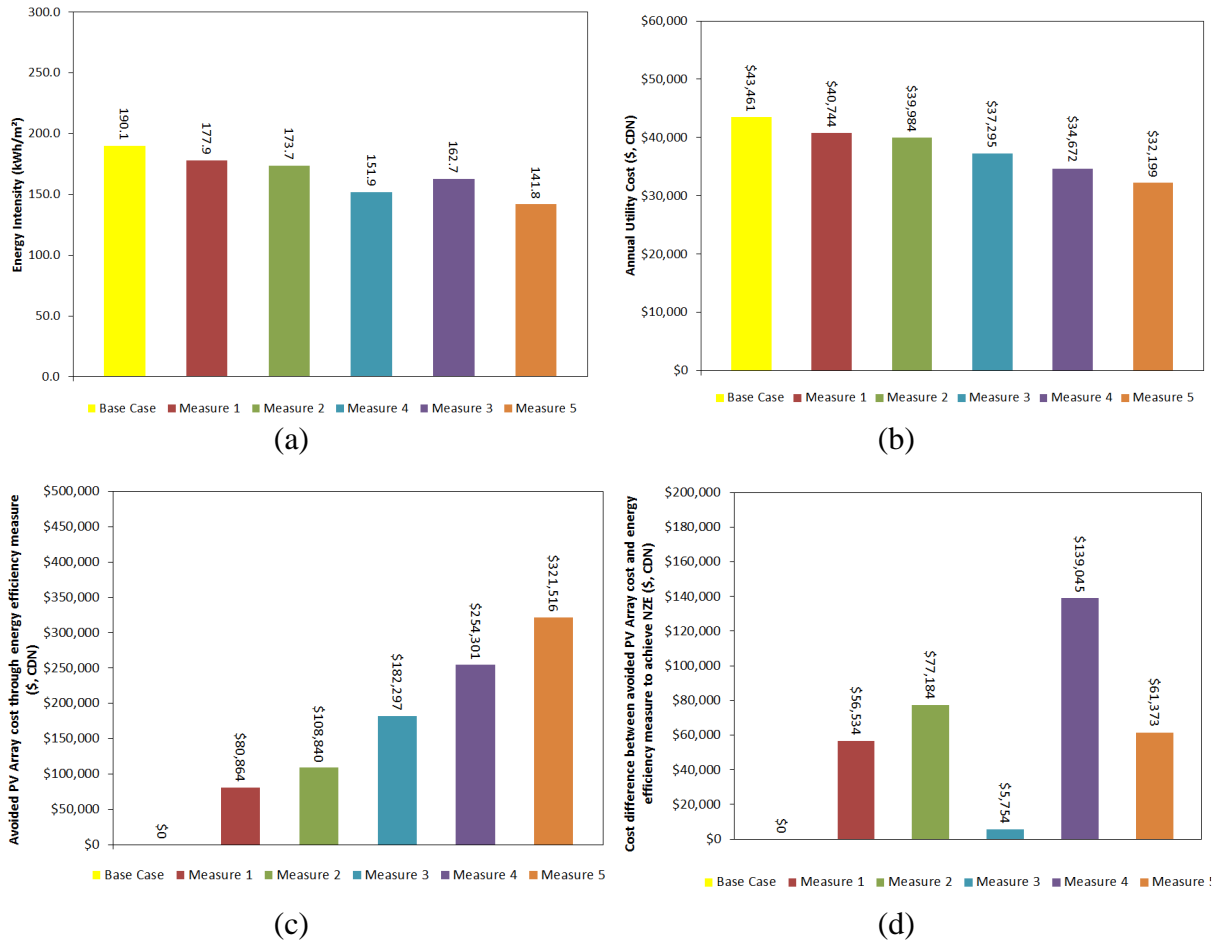


Figure 6: Comparison of the base case and energy efficiency measure (a) annual energy intensity (b) annual utility cost (c) PV array cost to achieve NZE and (d) cost difference between the efficiency measure and using PV to achieve the same energy savings

As can be seen in figure 6d, all energy efficiency measures are beneficial in comparison to using photovoltaics to offset the same amount of energy. However, comparing the energy efficiency measures among one another, it is seen that the addition of building insulation is not beneficial as the cost difference between the energy efficiency measure and PV array to achieve the same energy savings significantly decreases (Measure 3 and Measure 5). This is further highlighted in figure 7, where the cost difference between the avoided PV array cost and the energy efficiency measure cost for Measures 3, 4 and 5 in comparison to the Measure 2 is shown. A negative cost difference highlights that a PV array is a more suitable economic choice than the energy efficiency measure. Due to the already decent building envelope, it becomes difficult to economically justify further improving the building insulation. The building owner is better off in this case to use a PV system to offset the building energy consumption. There is a benefit however to installing heat recovery ventilators as opposed to using a PV array. Future work will investigate the breakeven point of adding insulation versus the incremental PV array cost.

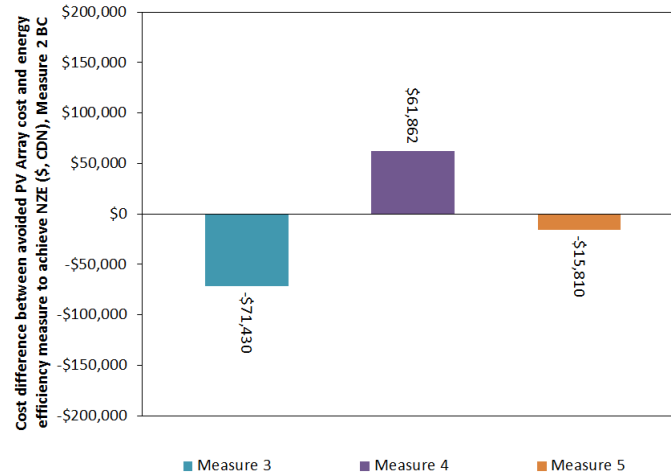


Figure 7: Cost difference between the efficiency measure and using PV to achieve the same energy savings in comparison to energy efficiency measure 2

4.2 Energy efficient system results

To evaluate how the energy efficient systems compare in achieving energy savings with a PV system, each heat pump system was evaluated in the base case and five standard energy efficiency measures combinations identified in section 4.1. From RSMeans (2013) and contractor surveys, table 7 summarizes the estimated incremental costs for each heat pump system compared to the defined base case heating and cooling system (packaged terminal air conditioner with electric back-up heating).

Table 7: Estimated incremental costs for proposed heat pump systems

Heat pump system	Estimated incremental cost
1.5 ton ASHP	\$102,500 CDN
CC ASHP	\$166,250 CDN
GSHP	\$396,500 CDN
Solar assisted GSHP	\$414,250 CDN

For the GSHP and the solar assisted GSHP systems, the borefields were resized for energy Measures 3, 4 and 5 as the building heating and cooling loads changed. The borefield size and estimated incremental cost in comparison to the base case with the same energy efficiency measure is summarized in table 8.

Table 8: Estimated borefield size and incremental cost for the GSHP heat pump systems

Heat pump system	Borefield	Estimated incremental cost
Measure 3 GSHP	5 x 5, 95 m	\$343,250 CDN
Measure 4 GSHP	5 x 4, 93 m	\$300,500 CDN
Measure 5 GSHP	4 x 4, 85 m	\$259,000 CDN
Measure 3 Solar Assisted GSHP	4 x 4, 98 m	\$382,250 CDN
Measure 4 Solar Assisted GSHP	4 x 4, 76 m	\$352,000 CDN
Measure 5 Solar Assisted GSHP	4 x 3, 80 m	\$331,000 CDN

4.2.1 Conventional air source heat pump system

Figure 8 presents the results of the conventional air source heat pump evaluated in each of the standard energy efficiency models outlined in section 4.1. Figure 8a compares the annual energy intensity for each case, figure 8b compares the annual utility cost with no PV system, figure 8c compares the PV array cost difference to achieve NZE over the baseline energy consumption and figure 8d presents the cost comparison between using a PV array and the efficiency measure to achieve the same level of energy savings. A comparison to the base case with no energy efficiency measures is also provided.

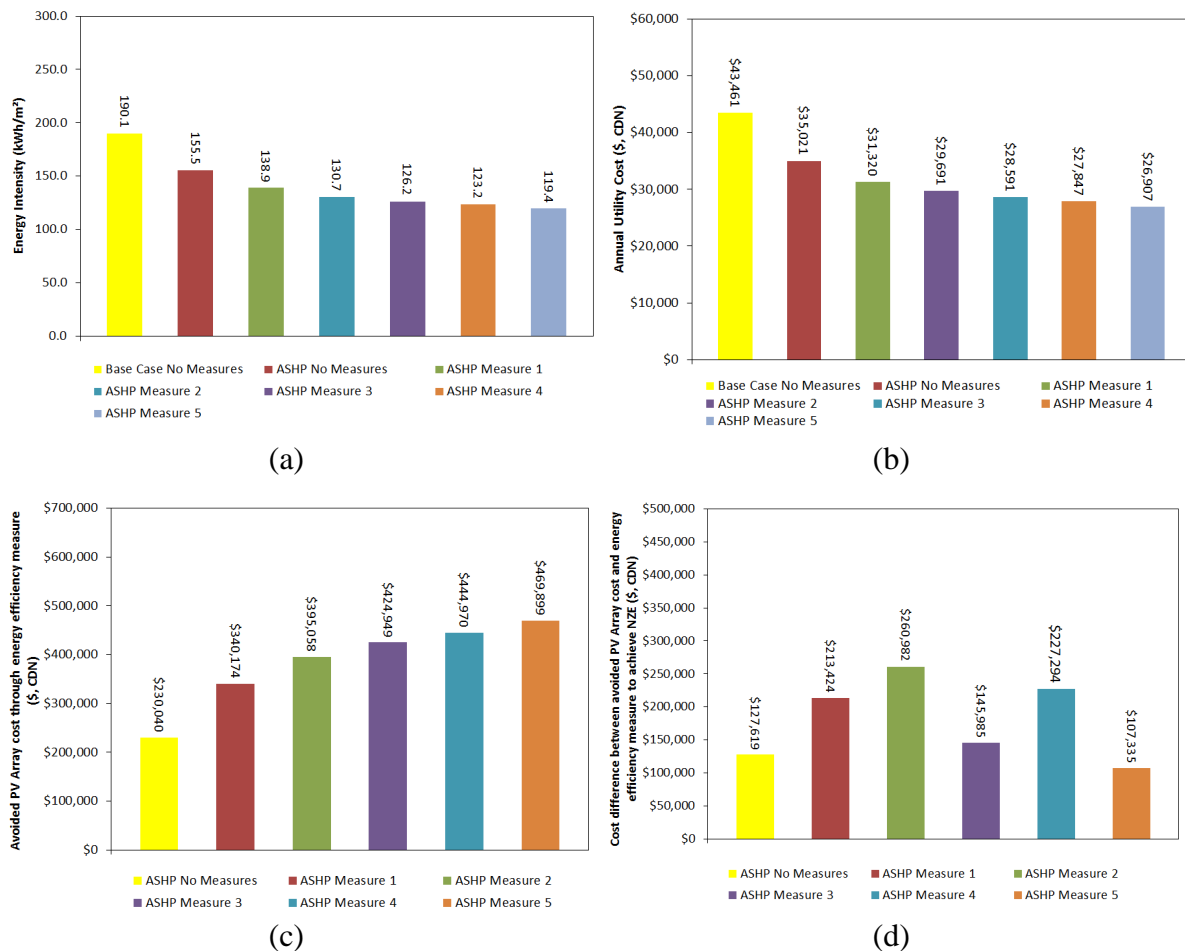


Figure 8: Comparison of the air source heat pump (a) annual energy intensity (b) annual utility cost (c) PV array cost to achieve NZE and (d) cost difference between the efficiency measure and using PV to achieve the same energy savings

From the results it can be seen that the use of an air source heat pump is profitable with an increased heating load on the building. By reducing the internal gains through Energy Star® lighting, appliances and the ECM fan motors, the heating load increases and the air source heat pump has a larger beneficial impact compared to using PV to offset the energy consumption. Similar to the base case, all efficiency measures are beneficial over using a PV array to achieve the same energy savings. However, when comparing the results of Measure 3 with Measure 2, it can be seen that the benefit of adding insulation to reduce the space heating load is still difficult to economically justify compared to a PV array. While the energy efficiency measure as a whole is economically beneficial in comparison to using a PV array, the incremental benefit of improving the building envelope has no advantage as the cost difference decreases. A similar

conclusion can be drawn with the use of heat recovery ventilators (Measure 4) and the combination of improved building envelope and use of heat recovery ventilators (Measure 5).

4.2.2 Cold climate air source heat pump system

Figure 9 presents the results of the CC ASHP evaluated in each of the standard energy efficiency models outlined in section 4.1. Figure 9a compares the annual energy intensity for each case, figure 9b compares the annual utility cost with no PV system, figure 9c compares the PV array cost difference to achieve net zero energy over the baseline energy consumption and figure 9d presents the cost comparison between using a PV array and the efficiency measure to achieve the same level of energy savings. A comparison to the base case with no energy efficiency measure is also provided. It should also be noted that the CC ASHPs already have ECM fan motors and thus there is no difference between energy Measure 1 and Measure 2.

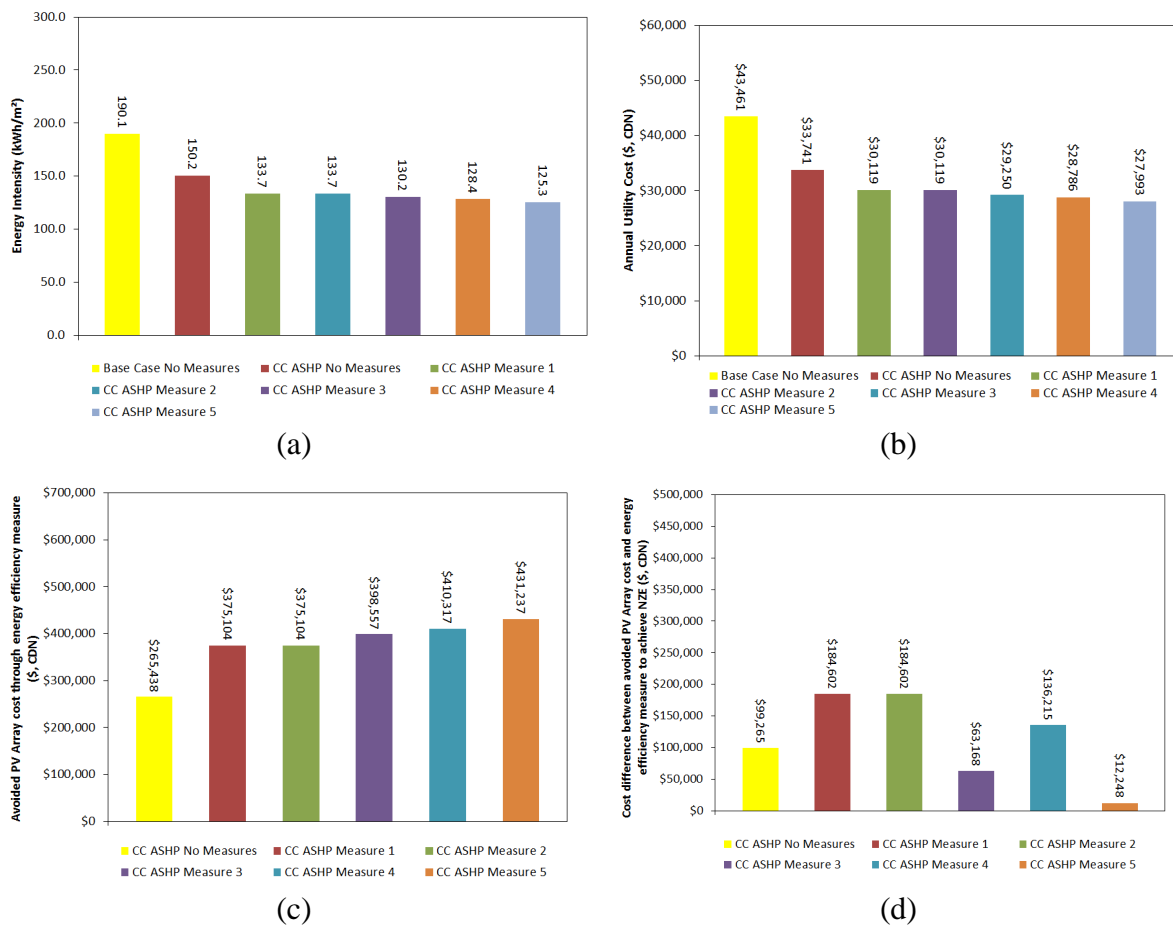


Figure 9: Comparison of the air source heat pump (a) annual energy intensity (b) annual utility cost (c) PV array cost to achieve NZE and (d) cost difference between the efficiency measure and using PV to achieve the same energy savings

A similar trend to the conventional ASHP system is seen with the CC ASHP. A cost benefit is seen for all efficiency measures, especially at higher heating loads, where there is a benefit towards implementing the CC ASHP system to reduce the annual energy consumption compared to using a PV system. However, similar to the conventional ASHP, as the building heating load is reduced through building insulation or heat recovery, the energy saving benefit of the CC ASHP is unable to overcome the cost of the incremental PV system required.

Comparing the cold climate ASHP results to the conventional ASHP, it can be seen that the conventional ASHP system has a lower annual energy intensity for Measures 2 through 5.

Although the cold climate ASHP has improved performance at lower ambient temperatures and a variable capacity compressor, the system is still significantly oversized for the requirements of each apartment unit and thus operates at low part loads (below 40%). Future work will investigate the optimum size for a cold climate ASHP.

4.2.3 Ground source heat pump system

Figure 10 presents the results of the GSHP evaluated in each of the standard energy efficiency models outlined in section 4.1. Figure 10a compares the annual energy intensity for each case, figure 10b compares the annual utility cost with no PV system, figure 10c compares the PV array cost difference to achieve net zero energy over the baseline energy consumption and figure 10d presents the cost comparison between using a PV array and the efficiency measure to achieve the same level of energy savings. A negative cost difference indicates the PV array is more cost beneficial than the efficiency measure, while a positive cost indicates the efficiency measure is worthwhile implementing to offset the energy consumption to achieve net zero energy. A comparison to the base case with no energy efficiency measures is also provided.

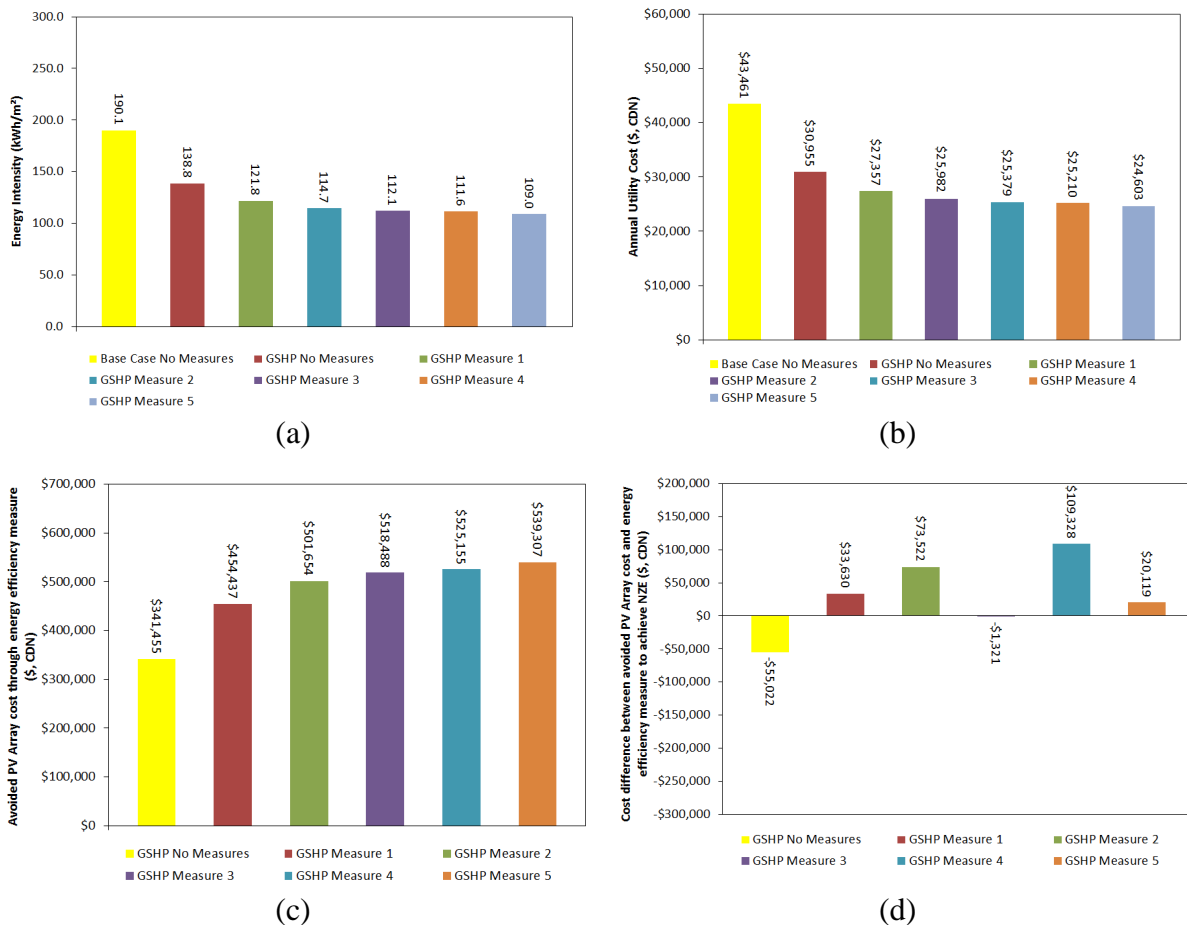


Figure 10: Comparison of the air source heat pump (a) annual energy intensity (b) annual utility cost (c) PV array cost to achieve NZE and (d) cost difference between the efficiency measure and using PV to achieve the same energy savings

In this scenario, the GSHP alone did not demonstrate a benefit over using a PV array system to meet the same energy saving target. This is attributed to the cost associated with a larger borefield requirement to meet the space heating load. As the space heating load increases through a reduction of interior gains, the GSHP system becomes more cost competitive. Similar to the air to air heat pump systems evaluated the benefit of adding insulation to reduce the

building heating load is not advantageous in comparison to using a PV array - even with a reduction in the borefield size. However, contrary to the air to air heat pump systems, the use of heat recovery ventilators is beneficial as the lower cost of the energy efficiency measure combined with a reduction in the borefield size, ultimately makes the GSHP system cost beneficial over using a PV array.

4.2.4 Solar assisted ground source heat pump system

Figure 11 presents the results of the SA GSHP evaluated in each of the standard energy efficiency models outlined in section 4.1. Figure 11a compares the annual energy intensity for each case, figure 11b compares the annual utility cost with no PV system, figure 11c compares the PV array cost difference to achieve net zero energy over the baseline energy consumption and Figure 11d presents the cost comparison between using a PV array and the efficiency measure to achieve the same level of energy savings. A comparison to the base case with no energy efficiency measures is also provided.

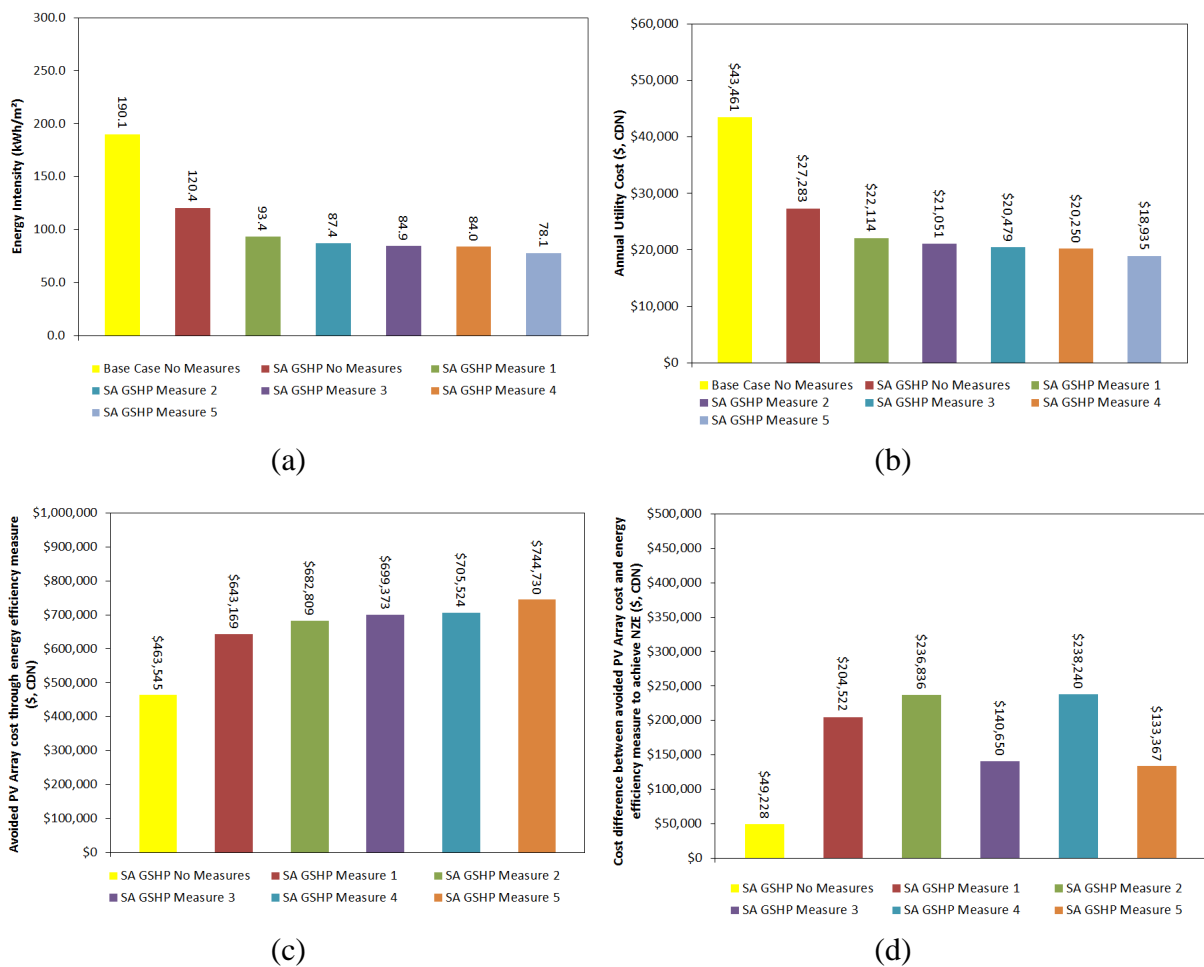


Figure 11: Comparison of the air source heat pump (a) annual energy intensity (b) annual utility cost (c) PV array cost to achieve NZE and (d) cost difference between the efficiency measure and using PV to achieve the same energy savings

The use of solar energy to reduce the borefield size and meet a portion of the domestic hot water load is beneficial in all cases in comparison to using a PV system to meet the same electricity savings. Similar to the GSHP system, by reducing the borefield size through the use of heat recovery ventilators to meet a portion of the heating load, the greatest cost difference savings

is achieved. The high cost of improving the building envelope insulation is unable to compete with the reduced cost of the borefield and use of PV.

Comparing the results of the GSHP system only to the SA GSHP system, it is interesting to see that the use of solar thermal energy has a benefit. By reducing the borefield size and meeting a portion of the domestic hot water load, the incremental cost of the solar thermal system is able to outweigh the cost of a PV array.

4.3 Heat pump system comparison analysis

Comparing the heat pump systems analyzed, it is seen that the conventional ASHP system and the SA GSHP system are the most favourable selections as both systems had similar cost differences between the efficiency measure and the avoided PV array cost. The conventional ASHP system was found to be the most suitable for Measures 1 through 3, with the SA GSHP being the most suitable selection for Measures 4 and 5. This is highlighted in Figure 12, comparing the estimated simple payback period of the heat pump systems without a PV array and figure 13 with a PV Array. Without the PV array, the conventional ASHP system has the lowest simple payback period for all Measures ranging between 10 and 22 years. With the PV array to achieve net zero energy, the simple payback period significantly increases due to the current low utility rates in Montreal. Here, the conventional ASHP has the lowest simple payback period for all Measures with the exception of 4 and 5, where the SA GSHP system is better. Simple payback periods range between 23 and 30 years for all systems.

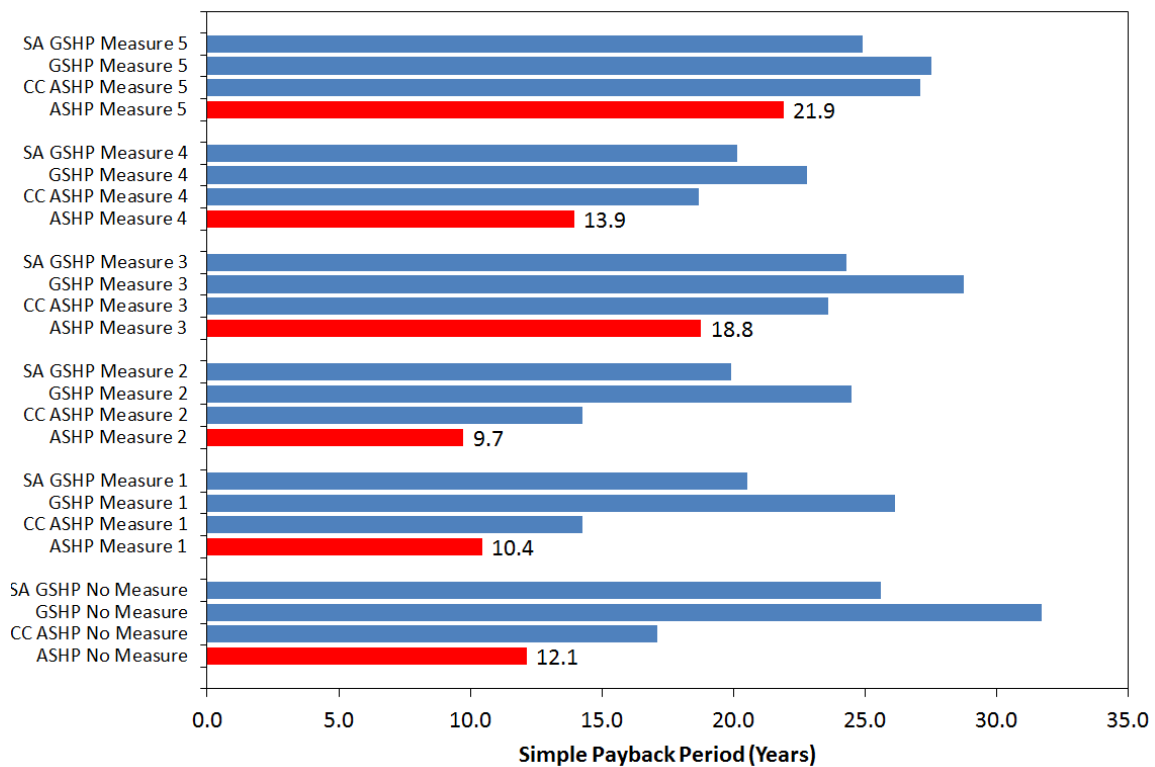


Figure 12: Simple payback period for the heat pumps systems without a PV Array in comparison with the base case with no efficiency measures

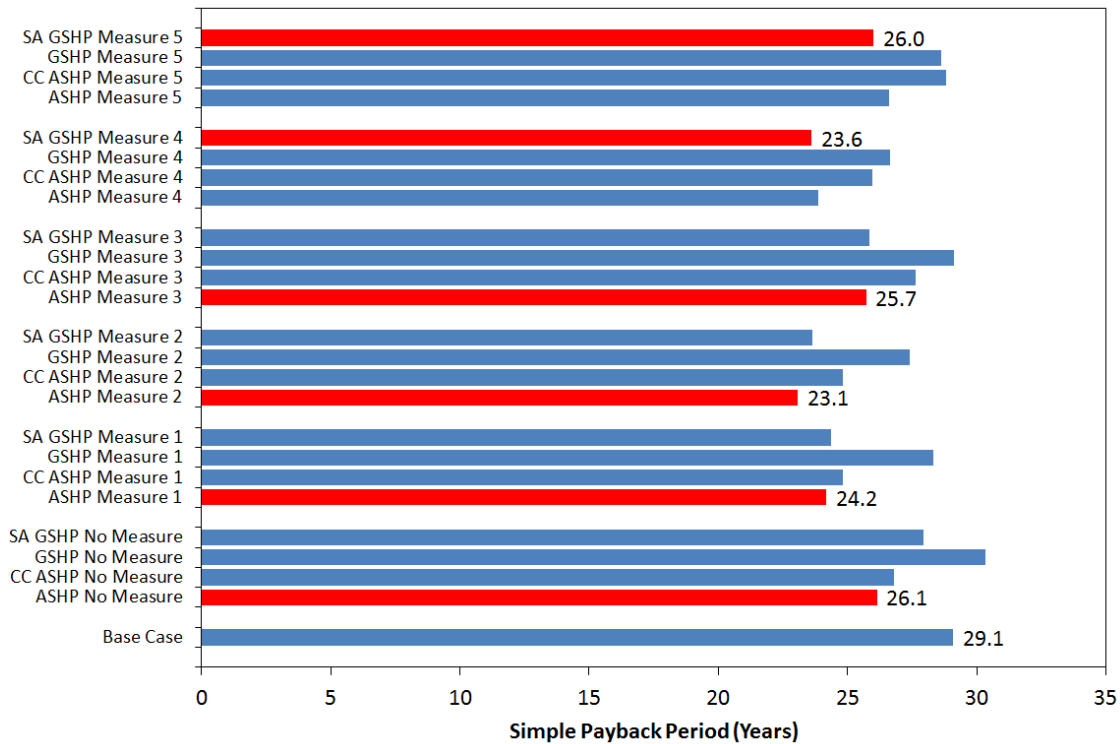


Figure 13: Simple payback period for the heat pumps systems with a PV Array to achieve Net Zero Energy in comparison to the base case with no efficiency measures

Plotting the energy efficiency measure to PV array cost difference to achieve the same energy savings (figure 14a), it can be seen that the conventional ASHP generates the highest cost difference. Thus implementing any efficiency measures evaluated in this paper beyond this is not as beneficial as using a PV array. To evaluate the impact of borefield drilling costs on the most suitable system selection, the energy efficiency measure to PV cost array difference is plotted for a \$50/m borefield cost (figure 14b). The results here highlight that the solar assisted GSHP system is the most suitable achieving the highest cost difference.

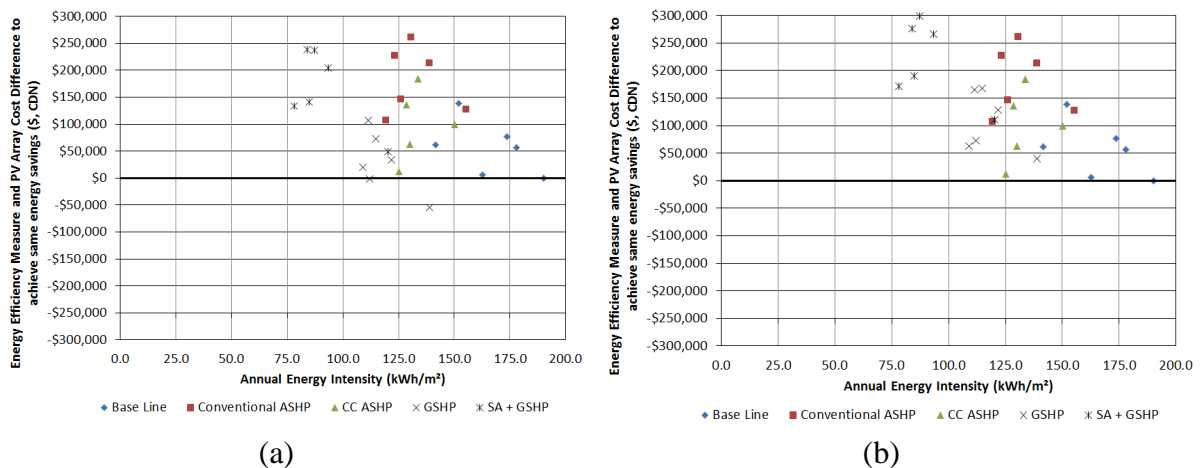


Figure 14: Energy efficiency impact cost comparison (a) \$80/m borefield drilling cost and (b) \$50/m borefield drilling cost

In all measures, it was assumed that there is sufficient land space to install a PV array. In the event there is a land cost associated with installing a PV array, it can be seen that achieving energy efficiency through more efficient heating systems becomes beneficial (Figure 15) –

especially when the value of land approaches \$100/m². Currently in Montreal, the cost of land is approaching \$2000/m² (Évaluation Foncière, 2014).

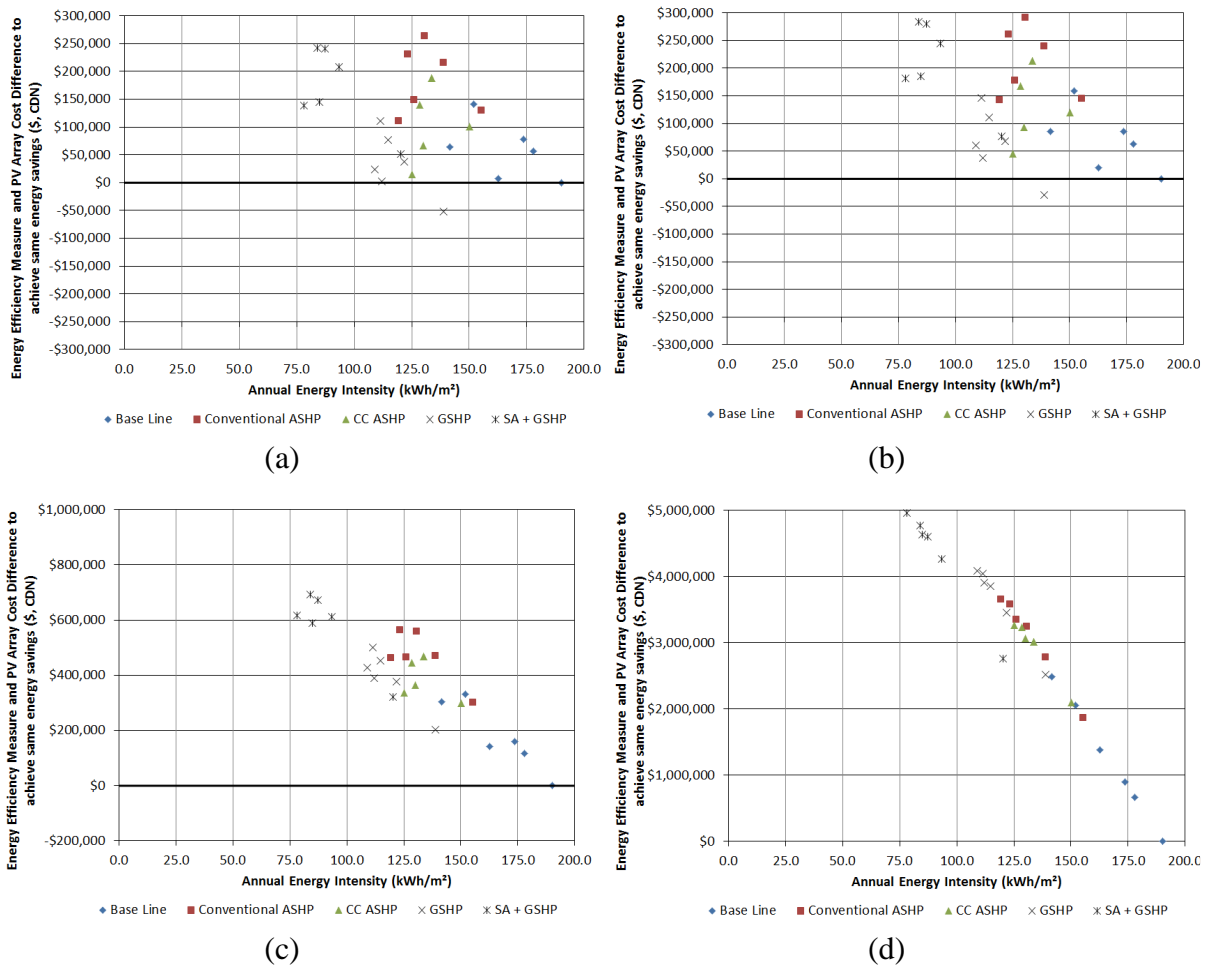


Figure 15: Energy efficiency impact cost comparison for (a) \$1/m² (b) \$10/m² (c) \$100/m² (d) \$1000/m² land value

Thus when taking the land value into account, it can be seen that it becomes beneficial to reduce the annual energy consumption as much as possible if net zero energy is the end target. The land cost breakeven point is estimated to be around \$15/m² where it becomes beneficial to implement a solar assisted ground source heat pump system.

5. CONCLUSION AND FUTURE WORK

An analysis was presented on several energy efficiency strategies to achieve net zero energy in comparison to simply offsetting the annual energy consumption through an onsite photovoltaic array. The analysis was performed on a newly constructed, four storey mid-rise apartment located in Montreal, Canada meeting the minimum energy efficiency requirements of the National Energy Code of Canada for Buildings. Standard energy efficiency measures were evaluated including reducing the base electrical loads, replacing PSC fan motors with ECM fan motors, improving the building insulation levels and adding heat recovery on the exhaust. The results indicated that reducing the base electrical loads through EnergyStar® lighting and appliances, use of ECM fan motors and recovering heat from the exhaust were more economical energy efficiency measures to reduce the building energy consumption in comparison to using photovoltaics. Meeting the minimum energy efficiency requirements, the building envelope is

already well insulated and thus energy efficiency improvements in this area demonstrated little benefit in comparison to other energy efficiency measures evaluated.

To evaluate alternate strategies to achieve net zero energy using energy efficient heating systems and a reasonably good building envelope, several heat pump systems were evaluated for each of the standard energy efficiency measures. In all standard energy efficiency cases it was found that the conventional air to air heat pump system and solar assisted ground source heat pump system were beneficial in reducing the building energy consumption compared to using a PV array. The cold climate air to air heat pump was found to be only beneficial when the building heating load was greater as the nominal capacity of these systems are significantly higher than the required heating load of the apartment unit. The use of a PV array over a ground source heat pump system was proven to be a better selection as the high associated costs of the borefield are difficult to overcome. Comparing all heat pump systems, the air to air heat pump system with a reduction in base electrical loads and efficient fans was found to have the lowest simple payback period both with and without a PV array. Performing a sensitivity analysis on the borefield drilling costs indicated that with a 37.5% reduction (\$80/m to \$50/m reduction), the solar assisted GSHP system is a more suitable system to offset the PV array costs to achieve net zero energy.

An analysis was also conducted on the impact of land costs associated with the PV array, where it was shown that it becomes quickly beneficial to reduce the building energy consumption as much as possible making the solar assisted ground source heat pump to the best choice.

With the cost of photovoltaic systems on the decline, there is the ongoing question when it is beneficial to install the system. Future work will evaluate the 20 year life cycle cost of the systems evaluated and determine which system is most suitable for planned future photovoltaic installations.

The solar assisted ground source heat pump system demonstrated some promising results having the lowest energy intensity of all system evaluated. Future work will look into further optimizing the system, such as evaluating different solar panel types and areas, thermal storage capacity and borefield size.

REFERENCES

- ASHRAE, 2008. *ASHRAE Vision 2020 – Producing Net Zero Energy Buildings*. American Society of Heating, Refrigeration and Air Conditioning Engineers, Atlanta, USA.
- CAGBC, 2014. *How to get a “Net Zero Ready” Building*, <<http://www.cagbc.org/AM/Template.cfm?Section=How_to_get_a_Net_Zero_Ready_building>> Last Accessed: August 2014.
- Carrier, 2008. *25HBB3 – Base 13 Heat Pump with Puron® Refrigerant*, Carrier Corporation, Indiana, USA.
- Energy Star®, 2014. *Efficient Lighting and Appliances*. <<http://www.energystar.gov/ia/partners/bldrs_lenders_raters/downloads/Lighting_Appliances_Factsheet.pdf?a2e3-352d>> Last Accessed: August 2014.
- Évaluation Foncière, 2014. *Rôle d'évaluation foncière*, <<http://ville.montreal.qc.ca/portal/page?_pageid=3077,3528875&_dad=portal&_schema=PORTAL>> Last Accessed: August 2014.
- Filliard, B., Guiavarch, A., Peuportier, B., 2009. *Performance Evaluation of an Air to Air Heat Pump Coupled with Temperature Air-Sources Integrated into a Dwelling*, International Building Performance Simulation Conference, Glasgow, Scotland, p. 2266 to 2273.

- Grape Solar®, 2014. *High Efficiency Mono-crystalline photovoltaic module*, <<http://www.grapesolar.com/files/3113/3789/6931/GS-S-250-Fab5_Rev-2.pdf>> Last Accessed: August 2014, Grape Solar, Eugene, Oregon, USA.
- Gusdorf, J., Swinton, M., Entchev, E., Simpson, C., Castellan, B. 2002. *The Impact of ECM Furnace Motors on Natural Gas Use and Overall Energy Use During the Heating Season of CCHT Research Facility*, Canadian Centre for Housing Technology, Ottawa.
- Hydro Quebec, 2014, *Residential Rate D*, <<<http://www.hydroquebec.com>>> Last Accessed: February 2014, Hydro Quebec, Montreal.
- Kavanaugh, S.P., Rafferty, K., 1997. *Ground-Source Heat Pumps: Design of Geothermal Systems for Commercial and Institutional Buildings*, ASHRAE, Atlanta, 167 p.
- Klein S. A., et al., 2010. *TRNSYS 17 – A TRaNsient SYstem Simulation program, user manual*, University of Wisconsin-Madison, Solar Energy Laboratory, Madison, USA.
- Knight, I., Kreutzer, N., Manning, M., Swinton, M., Ribberink, H., 2007. *European and Canadian non-HVAC Electric and DHW Load Profiles for Use in Simulating the Performance of Residential Cogeneration Systems*, Annex 42 of the International Energy Agency Energy Conservation in Buildings and Community Systems Programme, 84 p.
- Luukkonen, P., Bateman, P., Hiscock, J., Poissant, Y., Howard, D., Dignard-Bailey, L., 2013. *National Survey Report of PV Power Applications in Canada 2012*, Canadian Solar Industries Association, Ottawa, Ontario, Canada.
- Mitsubishi Electric 2011. *Zuba Electric Sales Inc. Air Conditioning and Heating*, <<<http://mitsubishielectric.ca/en/hvac/zuba-central/index.html> >> Last Accessed: August 2014.
- National Research Council, 2011. *National Energy Code of Canada for Buildings (NECB)*, National Research Council of Canada, Ottawa, Canada.
- Natural Resources Canada, 2009. *Energy Efficiency Trends in Canada 1990 – 2007*. Natural Resources Canada, Ottawa, Canada.
- Parekh, A. 2010. *Path to Net Zero Energy Homes*, <<<http://www.mb-ec.ca>>> Last Accessed: Dec 15, 2011.
- RSMeans, 2013, *Cost Data Handbooks*, RSMeans a division of Reed Construction Data, USA.
- Solar Rating and Certification Corporation, 2006. *Directory of SRCC Certified Solar Collector Ratings 2006*, Solar Rating and Certification Corporation, Florida, USA.
- U.S Department of Energy (DOE), 2013. *Commercial Reference Buildings*, <<http://www1.eere.energy.gov/buildings/commercial/ref_buildings.html>> Last Accessed: August 2014.

A Modelica based computational model for evaluating a renewable district heating system

F.F.M. Soons^{1,2*}, J. Ignacio Torrens¹, J.L.M. Hensen¹, R.A.M. De Schrevel²

⁽¹⁾ Dep. Building Physics and Services, Eindhoven University of Technology, The Netherlands

⁽²⁾ Dep. Business Development Energy, Cofely Netherlands NV., Maastricht, The Netherlands

1. ABSTRACT

District heating (DH) systems are considered a viable method for mitigating long-term climate change effects, through reduction of CO₂ emissions, their high conversion efficiencies and their ability to be integrated with renewable energy sources (RES). The current evolution towards sustainable DH, e.g. integration of RES, results in increased complexity and diversity during the early-design phase.

In the early-design phase of DH systems a feasibility study is conducted to assess if the economic and environmental factors of the project meet the given requirements. This assessment is generally conducted with traditional district heating computational models (DHCM), utilizing a simulation language which limits the evaluation of sustainable DH systems in terms of flexibility and comprehensibility. The need for an alternative language capable of effectively modeling DH systems with integrated RES led to the use of Modelica, which offers improved flexibility, reusability as well as hierarchical and multi-domain modeling. This paper presents a case study, for the evaluation of a new DHCM analyzing its modeling capabilities and system performance, of an educational campus formed by eight institutional buildings connected to a centralized power plant, holding among others a biomass gasifier and a gas boiler. For an optimum utilization of the biomass gasifier, two power plant configurations are assessed: a biomass gasifier system with and without thermal energy storage (TES).

The system performance evaluation indicates a significant increase in the utilization of the biomass gasifier with 8.2% (353 hours) compared to results obtained from the traditional DHCM. This deviation is due to a more accurate consideration of the DH thermal capacity and the space heating demand. Furthermore, the models in this DHCM enable assessments of the impact of building retrofits or climate change scenarios. Thus, the increased modeling capabilities and system performance demonstrate that this new DHCM is suitable and beneficial for early-design feasibility studies of innovative RES integrated DH systems.

Keywords: Renewable Energy, District Heating Systems, Simulation Modelica & Dymola

2. INTRODUCTION

The building sector is responsible for approximately 34% of global primary energy demand, of which 75% is used for thermal purposes (IIASA, 2012). DH systems currently provide 12% of the building thermal demand in the European Union alone. Integrated with power plants, combined heat and power units or industrial waste-heat sources, these DH systems have proved in the last decades to be capable of reducing the use of primary energy (European Commission, 2012; IIASA, 2012).

Through the first three DH generations, the techniques evolved towards lower distribution temperatures, material lean components and prefabricated equipment. The latest or 4th generation of DH systems, which is currently under research, is able to further decrease grid

losses, supply renewable DH and be an integrated part of smart grid systems (e.g. supply and demand controlled systems) (Lund et al., 2014). Energy services companies, like Cofely Netherlands, aim to introduce these 4th generation DH systems applying sustainable energy sources and/or smart grid features.

At the early-design phase of DH systems, the feasibility of multiple system configurations are evaluated both economically and technically. The assessment of these system configurations is generally performed with a DHCM developed for traditional DH systems. This traditional DHCM restricts the assessment of new developments (e.g. integration of RES) due to the lack of flexibility and inability to resolve the complexity of such systems. These restrictions make feasibility studies, using a traditional DHCM, a challenging and labor intensive task, with an unreliable output.

This paper presents and discusses the development and evaluation of a DHCM. The use of Modelica as simulation language provides a modeling environment with a natural representation, increases the reusability of models and components, grants higher flexibility in system configuration as well as facilitates hierarchic and multi-domain modeling, enabling assessments of combined thermal, electrical and control related problems. These aspects are key for early-design phase assessments of multiple DH configurations, contributing to a more reliable and detailed final design.

The suitability of this new DHCM for early-design phase feasibility studies is analyzed through the re-evaluation of a renewable DH system for an educational campus. This case-study considers a DH system connecting 8 institutional buildings to a state of the art biomass gasifier, enabling the generation of renewable heat and electricity from locally collected residue of wood cuttings. Two configurations are considered for the case study, respectively a power plant with or without a stratified thermal storage system in an attempt to increase the gasifier utilization.

3. METHODOLOGY

The methodology for the development and evaluation of the new DHCM is presented in this section. In subsection 3.1, *Building performance simulation*, the motivation for using building performance simulation is emphasized and the choice for Modelica as a modeling and simulation language will be discussed. In subsection 3.2, *Case study*, the technical aspect of the case study will be described since the subsequent section is presented according to the case study specifics. In subsection 3.3, *Computational model*, the approach taken for the development of the DHCM is presented following the components: heat generation, heat distribution, heat consumers and thermal energy storage.

3.1 Building performance simulation

Computational building performance simulation aims to provide an approximate solution of a realistic model in the real world (Hensen & Lamberts, 2012). The development towards the integration of RES in DH systems, with their intermittent behavior, or smart grid features, adds increased complexity to the current computational models. These models typically lack, among other things, modularity, multi-domain capabilities, realistic control behavior and flexibility for the users (Wetter, 2011). These shortcomings do not benefit users who seek a way to quickly assess, among others, innovative system designs or operation strategies.

To determine the platform for the development of a new DHCM a functional comparison is conducted (Table 1, Table 2) between, Dymola (Modelica), TRNSYS and Matlab Simulink. The comparison indicates that Dymola (Modelica) performs better in terms of modularity, multi-domain modeling, realistic control behavior and flexibility. Modelica is a freely-

available, equation-based object-oriented language that is designed for component-oriented multi-domain modeling of dynamic systems. The equation-based feature permits acausal modeling, thus without considering computational order (Musić & Zupančič, 2006), which makes the reuse of classes easier and reduces faults compared to assignment-based modeling (e.g. TRNSYS, Matlab Simulink). Object-oriented modeling facilitates encapsulation which allows both reuse of components and evolution of models (e.g. referring to existing scripts). Multi-domain modeling enables modeling of combined disciplines such as electrical, thermodynamics, fluid dynamics and controls systems.

Furthermore, reusability makes it easy to use models and components, for example, from the Buildings library used in this study and developed by the Lawrence Berkeley National Laboratory (Wetter, 2010). The LBNL Buildings library is a freely available, open-source library with currently over 200 components and systems models for modeling building energy and control systems (Wetter, Zuo, Nouidui, & Pang, 2013). These features and available libraries make Modelica suitable for computational applications with high complexity requiring high performance simulation (Fritzson, 2010).

Table 1: Functional comparison simulation environments, part I

<i>Functional comparison simulation environments</i>				
	Properties	Dymola	Simulink (Matlab)	TRNSYS
General	Programming language	Modelica	M-code	Fortran
	Developer	Dassault Systemes	Mathworks	University of Wisconsin
	Software costs Academic	+	++	+
	Software costs Commercial	0	++	+
	Simulation time	0	+	+
Development time	++	0	+	
Handling	Scripting editor	+	++	+
	Graphical editor	++	0	+
	Symbolic manipulation	++	0	0
	Hierarchic modeling	++	+	0
	Reusability of models	++	0	+
	Post processing capabilities	0	++	0
	Model documentation	++	+	+
	Software documentation	+	++	++
Natural representation	++	0	0	
Library	Ease of use	++	+	+
	Open and editable libraries	++	+	0
	Validated libraries	+	++	++

Table 2: Functional comparison simulation environments, part II

<i>Functional comparison simulation environments</i>				
	Properties	Dymola	Simulink (Matlab)	TRNSYS
Library domains	Mechanics	++	+	-
	Controls	+	++	++
	Thermodynamics	+	+	++
	Hydraulics	++	+	++
	Electronics	+	++	+
	Buildings	+	0	++
Simulation	Continuous time systems	++	++	++
	Discrete time systems	++	++	++
	Debugging facilities	+	+	++
	Diagn. and sim. event logging	+	+	+
	Coupling features (FMI)	++	++	++
	Errors Description	+	0	++
Specific	Model calibration	+	++	+
	Design optimization	+	++	+
	Model management	++	+	++
	Code and Model export	++	++	0

3.2 Case study

In 2013, Cofely conducted a feasibility study during a tender for the transformation of an existing educational campus into a renewable educational campus. The tender required a proposal that would be able to reduce energy related CO₂ by 80% and provide long term cost reduction as well as added value for education. To satisfy these requirements Cofely designed and evaluated a combination of RES (e.g. solar PV and wind energy) and a DH system connecting the 8 institutional buildings with a centralized power plant (Figure 1). The power plant would use locally harvested biomass in a state of the art gasifier to convert it to syngas. The production of this syngas enables, by means of a combined heat and power unit, generation of renewable heat as well as electricity.

Two power plant configurations were considered during the evaluation: with and without a TES system. The development and integration of the biomass gasifier and the TES, as part of the traditional DHCM, was a time consuming and complicated process which led to uncertainties in the system performance and restricted optimization of the DH design. In the end, none of these configurations achieved the performance requirements that would ensure the economic viability of the design. A new DHCM with increased modeling capabilities will result in a more efficient system design and performance evaluation. Thus, the DH system and the two configurations will be re-evaluated with a new developed DHCM and compared with results obtained from the traditional DHCM.



Figure 1: Artist impression renewable campus

3.3 Computational model

The methodology for the development of the four essential DH aspects is presented and described in this section. Firstly, *heat generation*, which contains the biomass gasifier, peak installation and an emergency chiller integrated in the power plant model. Secondly, *heat distribution*, supply and return pipelines that circulate the heat carrying fluid (i.e. hot water) and enable the consumer to extract heat to satisfy its space heating demand. Thirdly, *heat demand*, where each of the 8 institutional buildings and their characteristic space heating demands are represented by a thermal energy model. And fourthly, *thermal energy storage*, a hot water stratified TES system to store or use heat originated from the biomass gasifier to increase its utilization factor. The four components combined form the DHCM (Figure 2) according to the specifics of the case study. The four components and their underlying models are designed to be able to be reused for other types of DH system configurations.

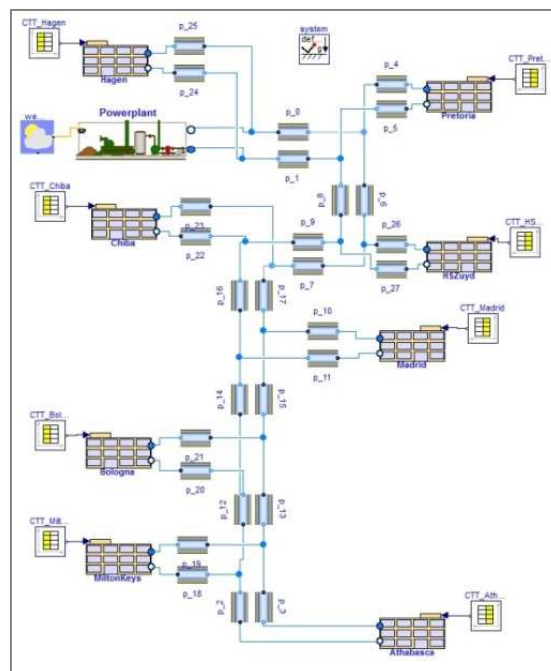


Figure 2: Top level of DH

3.3.1 Heat generation

The heat generation side (Figure 3) is represented by two closed loops, each of them connected by a heat exchanger to the distribution network. Both loops consist of a thermal energy source, respectively a gas boiler and a biomass gasifier, based on an existing boiler model.

The top loop containing the model of the gas boiler ensures the right supply temperature in the distribution systems (i.e. during peak demand) and operates as backup in case the biomass gasifier is shut down. The bottom loop contains the model of the biomass gasifier and its controller which is modeled to resemble the operation of a real gasifier. Furthermore an emergency chiller is connected to the gasifier loop to prevent the system from overheating since the gasifier has a slow response time to demand fluctuations.

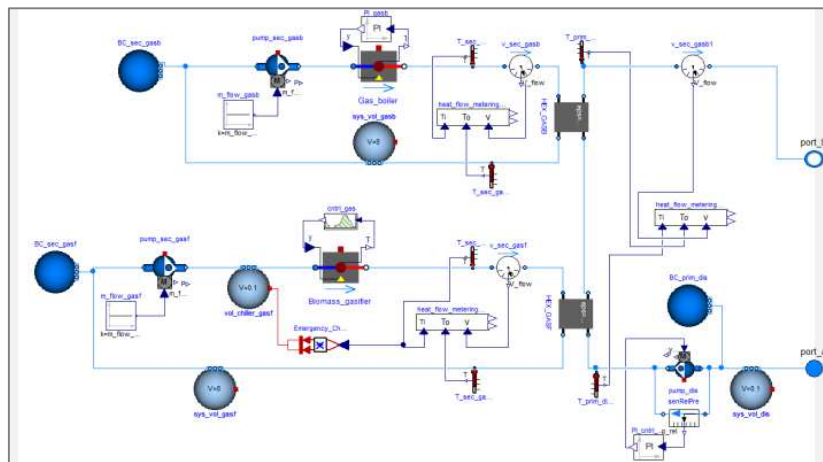


Figure 3: Model view, power plant without TES

The control strategy is designed to prioritize RES based heat generation, i.e. biomass gasifier over the gas boiler. The controllable models (e.g. heat sources and pumps) are connected to controllers specifically designed and tuned for the intended behavior of the models. The gas boiler is controlled by a standard PID, while the gasifier is controlled by multiple conditional statements, loops and timers since the operational behavior of the biomass gasifier is very distinctive compared to conventional heating sources. To illustrate this behavior, Table 3 indicates the specifications and a figure illustrating the slow reactivity of the gasifier to a random heat demand profile.

Table 3: Operation specification biomass gasifier (left) and its illustrating figure (right)

Operation specifications gasifier	
Maximum thermal output	720 kW _{th}
Minimum thermal output	180 kW _{th}
Thermal power rate	180 kW _{th} / hr.
Shutdown delay period	8 hours
Shutdown period	12 hours
Start-up period	8 hours

Furthermore, for the pumps two types of controllers are present: a constant flow controller for the heat source loops and a differential pressure controller for the distribution loop. For the latter the actual flow control is provided by the adjustable valves present at the institutional buildings (Frederiksen & Werner, 2013).

3.3.2 Heat distribution

The distribution network is modeled as a two-way, supply and return, buried piping system enabling the transport of the heat carrying fluid. The distance covered by this network is about 560 meters with various pipe diameters according to the capacity required by the end-users. The piping network is modeled by connecting piping models (Figure 4), each of them accounting for friction and thermal losses, for uninterrupted sections of the network.

The friction losses, due to the fluid interaction with the piping inner wall, will result in a pressure drop that is accounted for by the distribution pump. The electrical energy required by the distribution pump will be dissipated as heat to the heat carrying fluid. The thermal losses, from the heat carrying fluid, through the insulated piping wall, to the ambient environment, can require a large share of the total heat production for a DH system (Elci, Narmsara, Kagerer, & Herkel, 2013). To increase the accuracy, the thermal losses are calculated as a function of the soil temperature using the Kusuda model (Kusuda & Achenbach, 1965). This model calculates the soil temperature at the desired depth, time and soil properties. The influence of various depths over soil temperature is illustrated in Figure 5. A constant depth of 1 meter for the piping network is considered for this case study.

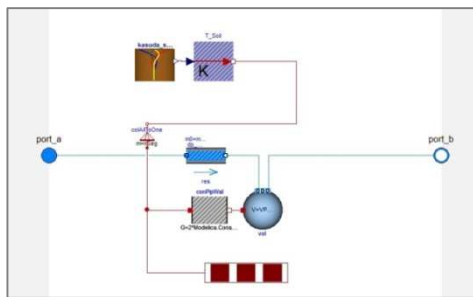


Figure 4: Modified pipe model

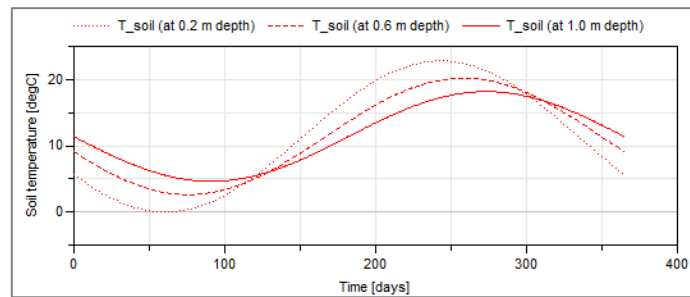


Figure 5: Temperature soil at various depths

3.3.3 Heat demand

This section presents the development, validation and calibration of a thermal building model accounting for the space heating demand of the institutional buildings. The demand caused by domestic hot water use is, in this case study, negligible and is therefore not considered.

3.3.3.1 Structure of the building model

The building model, extracting heat from the distribution network to satisfy the space heating demand, consists of a building and a distribution loop (Figure 6). The building loop (right), connected to the distribution loop (left) by means of a heat exchanger, is designed to resemble the operational behavior of a radiator heating system consisting of thermostatic radiator valves. This is achieved by using a distribution pump, which flow is regulated by a PID controller to deliver a fluid return temperature according to a set point. Furthermore, a heat metering device is implemented to be able to monitor the space heating demand by considering the flow temperatures and volume flow. The distribution loop, a direct extension of the distribution network, has a controllable valve on the supply line, which controls the fluid flow to satisfy the supply temperature in the building loop and enables a minimal flow to keep a minimum supply temperature at the distribution side to reduce the startup delay.

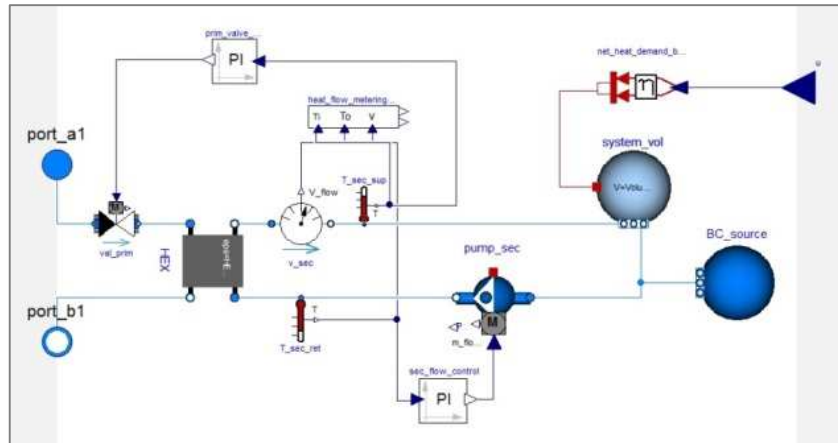


Figure 6: Model view, building model

Thermal energy is extracted from the building loop according to a space heating demand profile, with an hourly time step, that is connected to the model. The demand profiles for each building are computed using a thermal network model, as opposed to scaling demand profiles of buildings nearly identical to the institutional buildings, the method used by the traditional DHCM. Some benefits gained from using a thermal network model are that differences in building characteristics and the impact of climate change or retrofitting of the space heating demand can now be considered. The impact of climate change and retrofitting is not taken into account in this research, but it would be advisable for feasibility studies, since long term agreements are typical and retrofitting can have a large impact on the economics of a DH system (Elci et al., 2013).

The computation of the space heating demand profiles is performed with a thermal network model. This is an efficient way to keep the simulation time within a practical limit. Therefore, thermal network models are used widely for DH computational studies (Fuchs, Dixius, et al., 2013; Elci et al., 2013; Fuchs, Teichmann, Streblow, & Müller, 2013). The ISO 13790 simplified hourly model (ISO, 2005) calculates the space heating demand of the institutional buildings in this case study. This ISO model has been adopted for research (Van Dijk, Spiekman, & De Wilde, 2005; Kokogiannakis, 2007) and has been shown to yield satisfactory results when compared to similar second order thermal network models such as VDI 6007 (Lauster, Teichmann, Fuchs, Streblow, & Mueller, 2014).

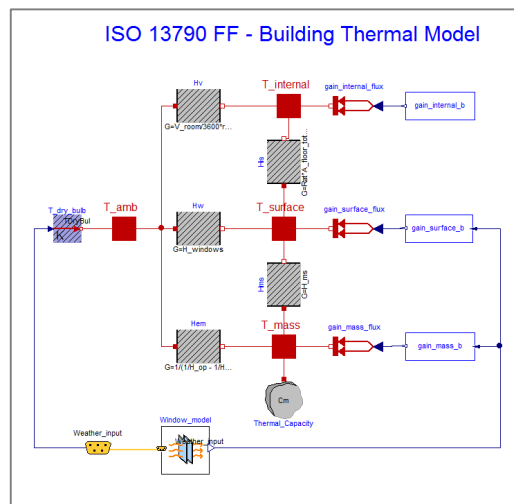


Figure 7: ISO 13790 FF thermal network

The ISO thermal network model is based on a 5 resistances and 1 capacitance electrical circuit model (Figure 7). Each of the resistances compute a heat flow from a building component (e.g. external wall, window, ventilation) while the capacitance accounts for the thermal inertia of the buildings thermal mass (i.e. walls, floors, ceilings). Furthermore, gains by solar radiation (diffuse and direct radiation) and internal heat sources (e.g. lighting, ICT) are considered by adding heat flows on the correct nodes, which can represent the surface, mass, ambient or internal air temperature.

3.3.3.2 Validation and calibration of thermal network model

The first validation of the thermal network model, conducted by simulating the BESTEST 600 case (Neymark & Judkoff, 1995), benchmarks the annual and peak demands for heating and cooling with those originated from a series of other building performance tools. The validation indicates annual and peak heating demands within the range of the benchmark. The results for the annual cooling peak and demand are off target, respectively -20.4% and -14.9%, compared to the benchmark minimums. Since cooling is not considered in this work, this deviation will have no influence on the accuracy of the case study conducted with this DHCM.

The second validation, is conducted by simulating the space heating demand of a large office building and comparing it with measured gas consumption data (Figure 8, left graph). The results of the comparison are evaluated by calculating the CV-RMSE (Coefficient of Variation - Root Mean Square Error) and the MBE (Mean Bias Error) for an hourly and monthly time step and comparing them with the ASHRAE guidelines (ASHRAE, 2002). The CV-RMSE value indicates the overall magnitude of the errors and the amount of scatter normalized to the mean of the observed values, while the MBE indicates the overall deviation between the simulated and measured data. Furthermore, the MBE indicates how much error would be introduced into annual energy consumption estimates, therefore minimizing MBE has priority for this case study in which the annual performance of the DH system is evaluated.

The resulting CV-RMSE and MBE values are unacceptable for both time steps (Table 4). To reduce the errors value the model is calibrated using the calibration signature method (Wei, G., Liu, M., and Claridge, 1998). The calibration is able to decrease the MBE value for both hourly and monthly time steps and the CV-RMSE for its monthly time step to well within the calibration guideline specifications (Table 4). However, the CV-RMSE value, at an hourly time step, indicates 122%. After analysis, this significant share is caused by operational schedules for the HVAC that where changed randomly at daily basis and during weekend operation. The simulated results are filtered excluding weekends and outliers in the CV-RMSE calculation. This resulted in a decreased CV-RMSE, for an hourly time step, from 122% to 55% which is still outside the guideline specification, however in better agreement (Figure 8, right graph).

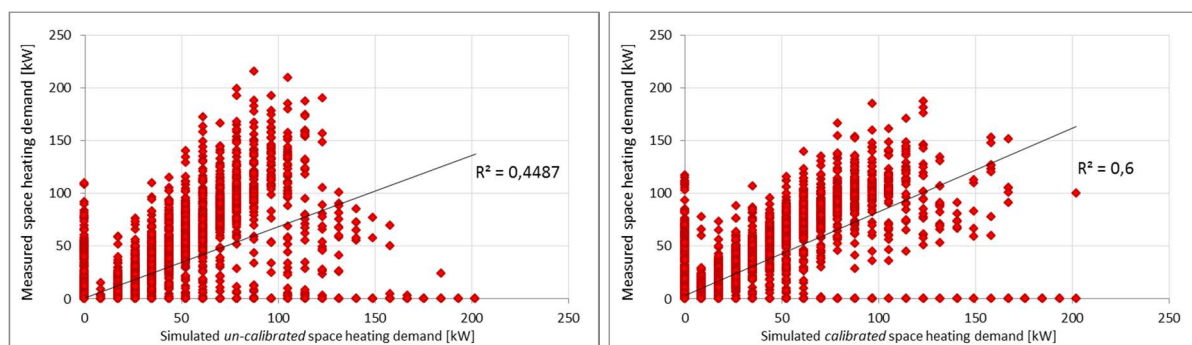


Figure 8: Space heating demand: measured versus simulated un-calibrated (left) and calibrated (right)

To summarize, the hourly CV-RMSE value (Table 4) of the calibration does not satisfy the guideline specifications, the residual CV-RMSE can be attributed to the following uncertainties: Firstly, specification uncertainties in the assumed input parameters that are introduced due to incomplete documentation of building characteristics and noticeable human-introduced changes in HVAC set-points during the year. Secondly, modelling uncertainty related to the ISO model implemented in Dymola and assumptions made (e.g. a one zone model is used and untraceable values in the ISO specifications). Thirdly, numerical uncertainty introduced by Dymola in the discretization of the model. And fourthly, scenario uncertainty introduced by the climate file obtained from a climate observatory located 15 km away from the actual building site.

Table 4: Results of the ISO calibration

Measure	Guideline		Un-calibrated		Calibrated & Filtered	
	Hourly	Monthly	Hourly	Monthly	Hourly	Monthly
MBE	< 10%	< 5%	-26%	-26%	-0.4%	-0.6%
CV-RMSE	< 30%	< 15%	149%	30%	55%	11%

3.3.4 Thermal energy storage

The buildings connected to this DH system have a fluctuating space heating demand at a daily and seasonal level. Implementing a TES will flatten the short and high demand peaks (Basciotti & Judex, 2011) occurring during the early morning on the generation side. The flattening of the peaks could increase the utilization of the biomass gasifier which has a limited maximum thermal output and reacts slowly to the changes in demand. Thus, limiting the use of the fossil fueled gas boiler which will decrease operational expenditures and CO₂ emissions.

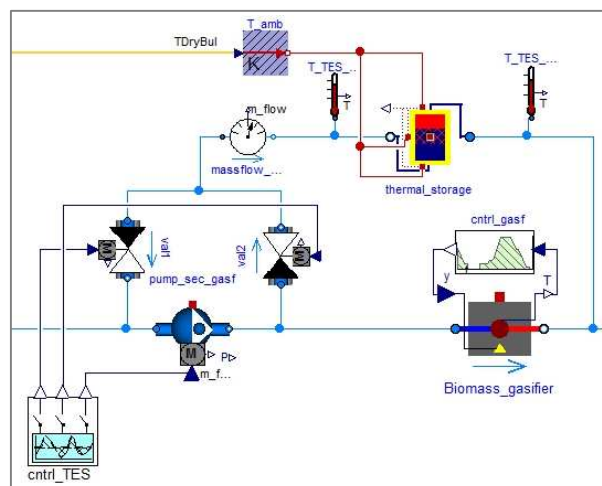


Figure 9: Model view, TES system integrated in power plant

A model of a 100 m³ stratified hot water storage device is integrated. The stratification, layering of water temperatures inside the storage vessel, occurs by injecting water into a temperature corresponding layer, increasing the energy density that can be stored. Heat loss of the TES is computed by considering the temperatures of the various volumes as a function of the ambient temperature.

The stratified storage system is controlled by two 2-way valves (Figure 9) which enable loading or un-loading (Frederiksen & Werner, 2013). When valve 1 (val1) is opened, cold water is extracted from the bottom and used as supply for the gasifier. Whereas valve 2 (val2) is opened,

hot water is extracted from the top and delivered to the distribution system resulting in additional peak power. The control algorithm is designed as a reactive algorithm by continuously monitoring the conditions and adjusting the valves and fluid flow correspondingly. During the nights and weekends, loading can commence if the heating demand is below the maximum thermal output of the biomass gasifier. During the day, unloading can begin if the heating demand exceeds the maximum thermal output of the gasifier. The latter will not only result in valve control, but also in increased fluid flow, so that the fluid originated from the TES can be considered as additional peak flow.

4. RESULTS AND DISCUSSION

The simulation results obtained from the DHCM are presented and discussed for two DH designs, with and without TES.

4.1 DH case without TES

The energy performance of this DH system is evaluated based on an energy balance, with a focus on the distribution losses, space heating demand by the consumers and the utilization of the biomass gasifier. The energy flows across the system are expressed using the first law of thermodynamics (Incropera & DeWitt, 2007), which states that the total energy of an isolated system is constant, and is reflected on this system (eq.1).

$$Q_{consumers} + Q_{gasifier} + Q_{peak\ boiler} + Q_{emergency\ chiller} + Q_{losses} + Q_{auxiliaries} = 0 \quad (eq.1)$$

The thermal distribution losses (Figure 10) consist of two patterns, namely the annual cosine shaped temperature fluctuation which depends on the ambient temperature. And, the distribution temperature related pattern which fluctuates hourly and depends on the heating demand. During the year the thermal losses for this specific DH system vary from 30 kW_{th} to 41 kW_{th}, and in total, they account for an annual thermal loss about 1,077 GJ (Table 5). Approximately 6.9% of the total annual space heating demand.

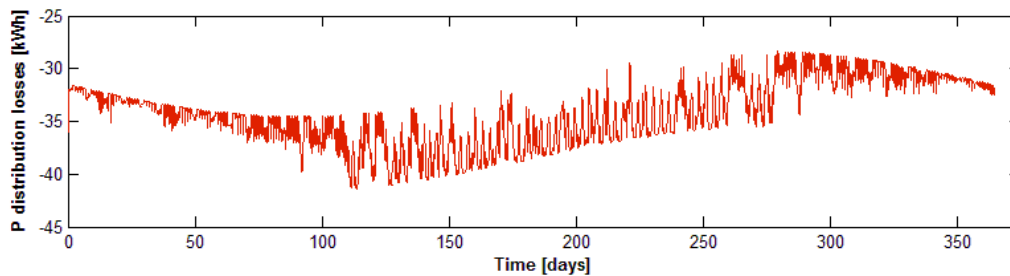


Figure 10: Thermal distribution losses

The space heating demand of the 8 institutional buildings is measured in the model at each building and the total demand is displayed in Figure 11. The analysis of this graph indicates a fluctuating heating demand with peaks exceeding 3 MW_{th} during the colder seasons and very low space heating demand required in the warm seasons. The total space heating demand by consumers (Table 5) is about 15,523 GJ per year, matching nicely with the 15,250 GJ per year obtained from the traditional DHCM. However, in this new DHCM the building characteristics could be changed (e.g. better insulation or a heat recovery ventilation system) to evaluate the effect of a changing space heating demand on the system performance.

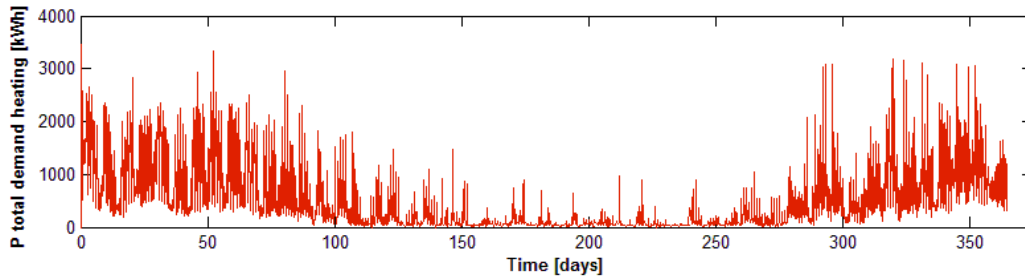


Figure 11: Total demand for space heating by the consumers

The utilization of the biomass gasifier (Figure 12, top graph) is evaluated by computing the effective utilization. This is the heat originated from the biomass gasifier effectively used for system operation, thus excluding heat extracted from the system by the emergency chiller (434 GJ per year) or, if applicable, losses from the TES. This indicates about 4,371 hours of effective utilization of the biomass gasifier (Table 5). This is 418 hours or 9.6 % higher than computed with the traditional DHCM (about 3,953 hours), and even higher than its results with TES, indicating a utilization of about 4,311 hours. The reason is likely due to the thermal capacity of the DH system itself that acts as a thermal buffer, flattening the demand peaks at the generation side, which has a positive effect on the utilization of the biomass gasifier.

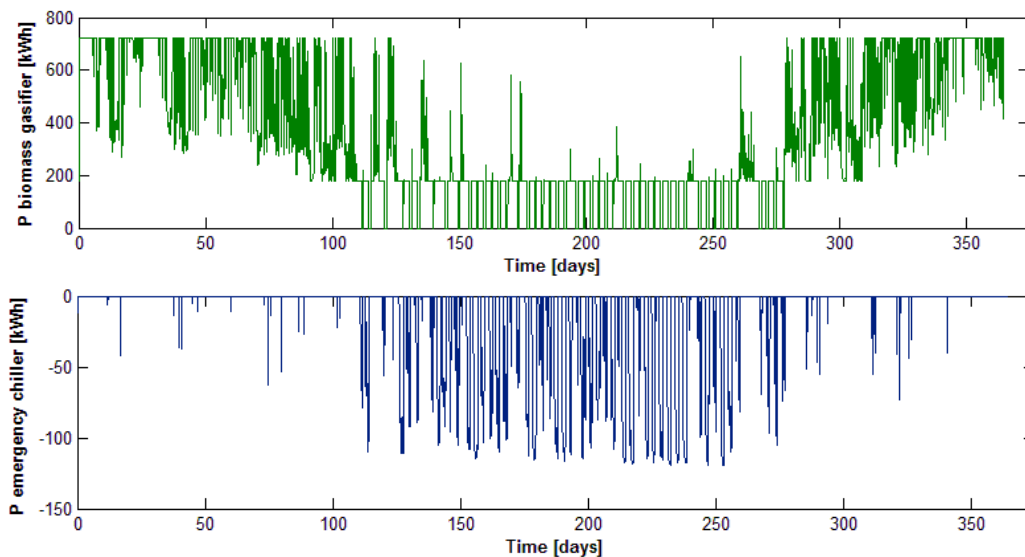


Figure 12: Generated heat by gasifier (top) and extracted heat by emergency chiller (bottom)

The space heating demand exceeding the maximum thermal output of the biomass gasifier is generated with the peak boiler (Figure 13). In this case almost 78.8 % of the maximum peak is delivered by the peak boiler and accounts for 33% of the total energy demand.

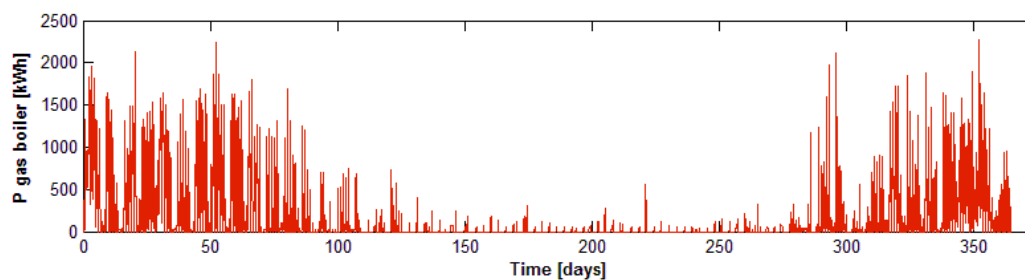


Figure 13: Generated heat by peak boiler

4.2 DH case with TES

For the second case the power plant configuration with TES is used. During the analysis of the first results new insights led to additional modifications that resulted in better operation and performance of the system. These modifications were related to controls (e.g. timing settings and statement adjustments) and components (e.g. increased buffer size from 100 m³ to 150 m³). Figure 14 (top graph) shows that the thermal output of the biomass gasifier is at its maximum (720 kW_{th}) between the peaks of the total heat delivered by both the heat generation loops. This is due to the TES being loaded at that time (bottom graph). When the total heat delivered peaks the heat delivered by the gasifier loop (middle graph) rises up to about 2000 kW_{th}. This is due to the unloading of the TES at that moment (bottom graph), which delivers additional peak power to the gasifier loop. Furthermore it can be seen that during the weekends (starting at 35th and 42th day) the TES is able to be loaded to nearly 98% of its capacity, which is set to be the maximum. During the first day after the weekend (37th and 44th day) the fully loaded TES enables delivery of heat for a longer period compared to other weekdays. During the nights of the weekdays there is not enough overcapacity of the biomass gasifier to effectively fill the TES and therefore it is not always loaded up to 98% of its capacity. This all indicates that the TES is effectively controlled and that the storage capacity is efficiently being used.

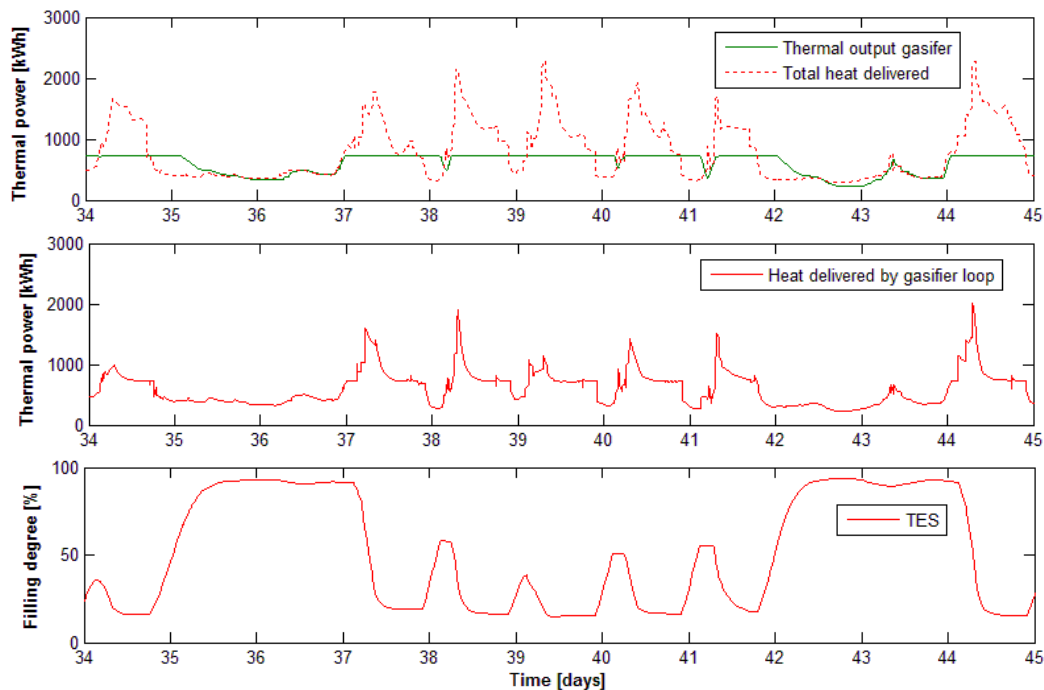


Figure 14: Total heat delivered by loops (Top), Heat delivered by gasifier loop (middle), Filling degree TES (bottom)

The full annual simulation with the TES system shows an increase of the utilization of the gasifier to 4,664 hours, 293 hours or 6.7%, compared to the DH case without TES (Table 5). In absolute as well as relative terms this is less than adding TES in the traditional DHCM. Even while the new DHCM is considering a 150 m³ TES system and the traditional DHCM is considering a 100 m³ TES system. The lower gained utilization could be due to the earlier gained utilization in the case without TES, which limits the potential improvement of the gasifier utilization by integrating a TES.

Table 5: Overview of system performance indicators

Computational Model (CM) + Scenario	Energy demand			Gasifier	
	Consumers [GJ/a]	Losses Distr. [GJ/a]	Losses TES + Chiller [GJ/a]	Ratio over peak boiler [/]	Eff. utilization [hr.]
Traditional CM	15250	1300	190	0.61	3953
Traditional CM + TES	15250	1300	310	0.66	4311
New CM	15523	1077	434	0.67	4371
New CM + TES	15523	1077	545	0.71	4664

Nonetheless, computing the DH case with TES, using the new DHCM, shows an overall increase of 353 hours or 8.2% in utilization of the biomass gasifier compared to the traditional DHCM. This is a substantial increase of the utilization that, during a feasibility study, would contribute to the economic and the environment impact of this case study.

5. CONCLUSION

This paper describes the development process of a DHCM, considering heat generation, heat distribution, heat demand and TES. The use of the object-oriented modeling language Modelica has proven to be suitable and beneficial for increasing the modeling capabilities during early-design phase feasibility analysis of projects.

The evaluation of a DH case study with TES using the new DHCM shows an 8.2% (353 hours) higher utilization of the biomass gasifier then when compared to a traditional DHCM. Differences in utilization of components of this magnitude can substantially influence the economic feasibility and environmental impact of a project. Since, the biomass gasifier can deliver an additional 353 hours of renewable combined heat and power.

The realistic behavior and natural representation of the systems modeled in Modelica contribute to the understanding of the thermodynamic and control related systems. This can be an advantage for educational purposes for students or academics and even for engineering professionals. Furthermore, for commercial purposes, where deadlines constrain the effort, the quick development capability that Modelica offers as a simulation language, could be a great advantage.

Efficient use of Modelica based models and systems will require additional development and possible customization per company (e.g. own control strategies, system designs). The development of blocks, models and control strategies will require collaboration in multi-disciplinary fields and inter-organizational levels. The development of more elaborate application-oriented guidelines (e.g. designing controls) could further improve the new-users experience.

The DHCM described in this paper is likely to contribute to future early-design phase projects for Cofely, delivering and evaluating system configurations for renewable DH systems. The improved accuracy and level of detail, compared to the traditional DHCM, could make a difference for considering the feasibility of a particular DH project. Thus, this new DHCM can result in additional renewable energy projects being delivered, that otherwise would be labeled as unfeasible, and indirectly contribute to the global challenges concerning climate change mitigation.

ACKNOWLEDGEMENTS

This paper is based on a graduation report for the master program Sustainable Energy Technology. I want to thank Jan Hensen for his advice, and providing me during the process with interesting literature and tips. Furthermore, I want to thank Ignacio Torrens for his dedication and enthusiasm in evaluating and guiding this research. Then, I want to thank Raymond De Schrevel as mentor from Cofely Netherlands for his trust, enthusiasm and support. A big thanks to all the members of the department Buildings Physics and Services, in special John, Jad, Roel and Mohammed, who were very helpful when advice or collaboration was needed.

REFERENCES

- ASHRAE. (2002). ASHRAE Guideline 14 -2002: Measurement of Energy and Demand Savings. *American Society of Heating, Ventilating, and Air Conditioning*.
- Basciotti, D., & Judex, F. (2011). Sensible heat storage in district heating networks: a novel control strategy using the network as storage. *Energy Storage*.
- Elci, M., Narmsara, S., Kagerer, F., & Herkel, S. (2013). Simulation of energy conservation measures and its implication on a combined heat and power district heating system: A case study. *Building Simulation*, 104–111.
- European Commission. (2012). *Energy Roadmap 2050*. Luxembourg. doi:10.2833/10759
- Frederiksen, S., & Werner, S. (2013). *District Heating and Cooling* (First edit., p. 586). Lund, Sweden: Studentlitteratur AB, Lund.
- Fritzson, P. (2010). *Principles of object-oriented modeling and simulation with Modelica 2.1* (p. 939). Wiley-IEEE Press.
- Fuchs, M., Dixius, T., Teichmann, J., Lauster, M., Streblow, R., & Müller, D. (2013). Evaluation of interactions between buildings and district heating networks. *Building Simulation*, (2013), 96–103.
- Fuchs, M., Teichmann, J., Streblow, R., & Müller, D. (2013). Energy simulation of a research campus with typical building setups. *Building Simulation*, 769–775.
- Hensen, J., & Lamberts, R. (2012). *Building performance simulation for design and operation*.
- IIASA. (2012). *Global Energy Assessment (GEA)*. (T. B. Johansson, N. Nakicenovic, A. Patwardhan, & L. Gomez-Echeverri, Eds.). Cambridge: Cambridge University Press. doi:10.1017/CBO9780511793677
- Incropera, F. P., & DeWitt, D. P. (2007). *Fundamentals of Heat and Mass Transfer*. Water (Vol. 3, p. 997).
- ISO. (2005). *Thermal performance of buildings — Calculation of energy use for space heating and cooling - ISO 13790:2005*.
- Kokogiannakis, G. (2007). Impact of using different models in practice-a case study with the simplified methods of ISO 13790 standard and detailed modelling programs. *BPSA Conference*.
- Kusuda, T., & Achenbach, P. (1965). Earth temperature and thermal diffusivity at selected stations in the United States.

- Lauster, M., Teichmann, J., Fuchs, M., Streblow, R., & Mueller, D. (2014). Low order thermal network models for dynamic simulations of buildings on city district scale. *Building and Environment*, 73, 223–231. doi:10.1016/j.buildenv.2013.12.016
- Lund, H., Werner, S., Wiltshire, R., Svendsen, S., Thorsen, J. E., Hvelplund, F., & Mathiesen, B. V. (2014). 4th Generation District Heating (4GDH). *Energy*, 68, 1–11. doi:10.1016/j.energy.2014.02.089
- Musić, J., & Zupančič, B. (2006). Modeling, Simulation and Control of Inverted Pendulum on a Chart Using Object Oriented Approach with Modelica. *Electrotechnical and Computer Science Conference ERK 2006*.
- Neymark, J., & Judkoff, R. (1995). International energy agency building energy simulation test (BESTEST) and diagnostic method. *National Renewable Energy Laboratory*.
- Van Dijk, D., Spiekman, M., & De Wilde, P. (2005). A monthly method for calculating energy performance in the context of European building regulations. *Building Simulation*, (pp. 255–262).
- Wei, G., Liu, M., and Claridge, D. E. (1998). Signatures of Heating and Cooling Energy Consumption for Typical AHUs. In *Fort Worth, TX: Proceedings of the Eleventh Symposium on Improving Building Systems in Hot and Humid Climates*.
- Wetter, M. (2010). A Modelica-based model library for building energy and control systems. *Lawrence Berkeley National Laboratory*.
- Wetter, M. (2011). A view on future building system modeling and simulation. *Building Performance Simulation for Design and Operation*, 1–28.
- Wetter, M., Zuo, W., Nouidui, T. S., & Pang, X. (2013). Modelica Buildings library. *Journal of Building Performance Simulation*, (October), 1–18. doi:10.1080/19401493.2013.765506

THIRD SESSION
SIMULATION ASSISTED
ANALYSIS AND EVALUATION
OF BUILDING ENERGY USE

Impact of refined HVAC systems efficiency determination on EPR energy calculations

Wout Parys^{1*}, Hugo Hens¹, Dirk Saelens^{1,2}

⁽¹⁾Building Physics Section, KU Leuven, Leuven

⁽²⁾Energyville, Waterschei

1. ABSTRACT

In this paper, integrated yearly dynamic simulations of a thermal system coupled to 6 variants of a medium-sized office building are performed and discussed. A traditional hydronic heating system is considered, consisting of a modulating condensing gas boiler and radiators in every heated zone. No active cooling is provided, though only building variants able to provide summer comfort through passive cooling only are selected. Hygienic ventilation is provided by a mechanical extraction system.

From the integrated simulations, monthly efficiencies for the generation, distribution and emission subsystems are deduced. The latter are expressed depending on the monthly heat-balance ratio, which equals the ratio of heat gains over heat losses on the building level. The heat-balance ratio thus represents the part load ratio, but can be calculated without taking the system into account. This variable is used in order to generalize the results and at the same time use them in an Energy Performance Regulation (EPR) context, which requires relatively simple calculations where the system cannot be taken into account in detail.

The resulting subsystem curves correlate quite well with the monthly heat-balance ratio (R^2 -values of 0.84 or higher). These curves show the heating subsystem efficiency drops in months with higher heat-balance ratios (and thus lower heating demands). These refined efficiencies are subsequently used in an EPR-type calculation, in which the monthly net heating demand is divided by the subsystem efficiencies to estimate the monthly final energy use. The results of this calculation are compared to similar calculations using annually averaged efficiencies deduced from the integrated simulations and using the default fixed EPR values for the subsystem efficiencies. It is shown that using the refined efficiencies yields better results in intermediate months, when the heating demand is lower. However, when looking at the total annual final energy use, the impact of using the refined efficiencies is modest.

Keywords: Integrated simulation, HVAC system analysis, efficiency, building energy use

2. INTRODUCTION

In the current context of global efforts towards a less energy-intensive society, accurately estimating the energy use of building designs becomes increasingly pertinent. In the framework of the European Energy Performance of Buildings Directive (EPBD), a series of standards was developed, of which the most elaborate is EN13790 (ISO/FDIS, 2007), offering procedures to estimate the characteristic total final energy use of buildings. All are based on the same principle of dividing the net energy demand, quite straightforward to calculate, by the efficiencies of the subsystems, i.e. emission, distribution, generation, storage and control. The current Energy Performance Regulations (EPR) calculation procedure of Flanders, the northern part of Belgium (Flemish Government, 2005), contains standard tabulated values for those subsystem efficiencies, constant throughout the year. More refined approaches exist, taking several influences into account, for example in EN15316 (CEN, 2007b). However, all methods to

calculate the subsystem efficiencies are defined at that very subsystem level, ignoring the complex interaction of the building, the occupants and the system. As argued by Zhang et al. (2006) and Van Der Veken and Hens (2008), an integrated approach is therefore better suited, where a dynamic simulation is set up that includes both the building and the system (denoted as level D calculations in EN15316). Though holistic studies on HVAC system performance characterisation are rather rare (Shahrestani et al., 2013), this approach has been successfully adopted in a few studies, illustrating the influence of the building and the building use on the HVAC system efficiency.

Korolija et al. (2011) compared the energy use of a very well insulated office building equipped with either an all-air VAV system or fan coil units combined with a dedicated outdoor air system. The system efficiency was assessed for different levels of internal heat gains. Its value for the same secondary HVAC system was found to vary for different building loads, though no formal correlation is deduced. An analogue observation was made in ref. (Korolija et al., 2009), where the energy use of an office building with different secondary HVAC systems, namely CAV and VAV, was compared. The system efficiency varies not only with different control settings, but also with the insulation level of the building.

The CAV, VAV and fan coil systems plus the combination of chilled ceilings and radiator heating were further analyzed by Korolija (2011). A large amount of office buildings varying in orientation, insulation, glazing-to-wall ratio, glazing type, structural shading and daylighting coupled to the 4 secondary systems were simulated for several weather data files using an integrated approach. The results indicated clearly that the annual heating and cooling system efficiency and the annual auxiliary energy use for the different systems are not constant, but depend instead on the building variations.

Peeters et al. (2008) performed an analysis of residential heating energy use for several combinations of boiler type, boiler control and emitter control through integrated dynamic simulation of building and systems. A rather strong relationship between the monthly total efficiency and the heat-balance ratio of the building, the ratio of heat gains over heat losses, was found. This effect was attributed to component efficiencies decreasing for lower part load ratios and overheating due to imperfect control occurring mainly when heating demand is low.

Bauer (1999) established correlations between the heating emission and control efficiency and a parameter characterising the building for different combinations of emitter and control systems. His findings are integrated in the German standard DIN 4701-10 (DIN, 2003).

In this paper, the integrated approach is used to assess the performance of a relatively simple heating system commonly found in office buildings in Flanders, including their auxiliary energy use. In extension to the research carried out by Korolija et al. (2013), both the primary and secondary HVAC system are modelled. Radiator heating, coupled to a condensing gas boiler is considered. The aim of this paper is to analyze the monthly subsystem efficiencies calculated with this integrated approach and to express them depending on the monthly building's heat-balance ratio, in analogy with the work of Peeters et al. (2008) for residential buildings, to acknowledge the influence of the building and building use on the HVAC system performance. These newly defined subsystem efficiencies will subsequently be compared to the current standard EPR values and their influence on the EPR calculation of characteristic energy use assessed.

3. TERMINOLOGY

The conceptual framework for the evaluation of heating systems in buildings as laid out in the European standard EN 15316 (CEN, 2007b), serves as the basis for this study, both for heating

and cooling system analysis. The performance of the system is analyzed at four sublevels: emission, distribution, storage and generation. The generation and storage together form the primary HVAC system, while the emission and distribution form the secondary HVAC system. Figure 1 offers a graphical overview of this framework.

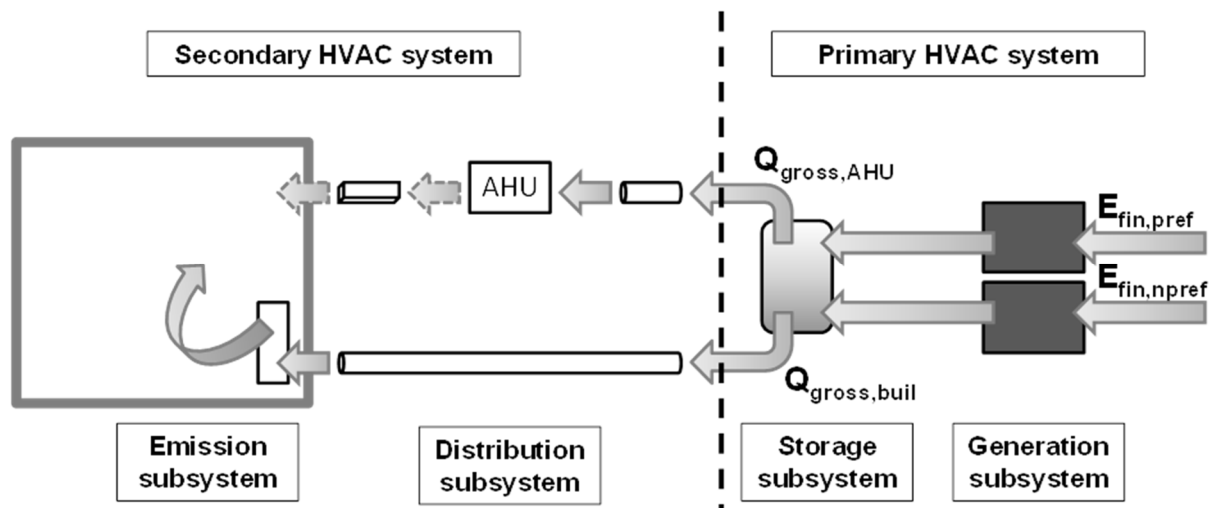


Figure 1: Conceptual scheme of subsystems and energy flows in an HVAC system (air thermal flows are indicated by dotted arrows, all other thermal flows are hydronic).

Emission and distribution are divided into building zone level, denoted with index *buil*, and air handling unit level, denoted with index *AHU*, in analogy with the German standard DIN V 4701-10 (DIN, 2003). The distribution on air handling unit level is partly hydronic (between the primary HVAC system and the AHU) and partly by air transport (between the AHU and the building zone).

The control of heat and cold emission in the zones is not regarded as a separate sublevel, as is sometimes done, but instead integrated in the emission efficiency (η_{em}), by defining the latter as the ratio between the net energy demand and the energy delivered to the emission device. In addition to imperfect control, emission efficiency losses can occur due to temperature stratification, shielding of the emission device or through ‘short-circuiting’ by locally heating the building envelope, increasing the heat losses (or vice versa for cooling).

Distribution efficiency (η_{dis}) losses are due entirely to energy losses - in case of heating - or gains - in case of cooling - through the walls of the hydronic pipes and air ducts to unconditioned spaces. The thermal insulation of the pipes and ducts obviously plays a key role, but also the temperature difference between the fluid and the environment and the total length of the distribution network. In addition, strongly intermittent operation of the system will lower the distribution efficiency, since the fluid content will cool down in between heating periods (or vice versa for cooling).

The storage efficiency (η_{stor}) is, quite straightforwardly, equal to the ratio of net energy output to the distribution subsystem over the energy input from the generation subsystem. Energy transfer through the wall of the storage tank is the only source of efficiency loss. Energy storage is however not included in the HVAC system typologies considered here (see 4.2).

The generation efficiency (η_{gen}) equals the ratio between the thermal energy output of the generation subsystem and the energy input by the respective energy carrier, limited to electricity or natural gas in this research. The source of efficiency losses depends highly on the type of generation device.

The definitions and symbols of the main quantities discussed in this section are summarized in Table 1.

Table 1: List of symbols and definitions of the terms used to describe HVAC system performance.

Term	Symbol	Definition
Net energy demand	Q_{net}	The energy that needs to be delivered in a building zone during a certain time to maintain the desired temperature.
Gross energy demand	Q_{gross}	The energy that needs to be delivered during a certain time to the secondary HVAC system.
Final energy use	E_{fin}	The energy used during a certain time by the generation systems.
Auxiliary energy use	W_{aux}	The energy used during a certain time by those components of the HVAC system that do not generate heat or cold (pumps, fans, humidifier, ...)
Primary energy use	E_p	The energy use converted to energy source level; default conversion factors (f_p) of 1 for fossil fuels and 2.5 for electricity are used (Flemish Government, 2005).
Emission efficiency	η_{em}	The ratio between the net energy demand and the energy delivered to the emission subsystem.
Distribution efficiency	η_{dis}	The ratio between the energy delivered to the emission subsystem and the energy delivered to the distribution subsystem.
System efficiency	η_{sys}	The ratio between the net energy demand and the gross energy demand.
Storage efficiency	η_{stor}	The ratio between the energy delivered to the distribution subsystem and the energy delivered to the storage subsystem by the generation subsystem.
Generation efficiency	η_{gen}	The ratio between the final energy use and the energy delivered to the storage subsystem (or directly to the distribution subsystem, if no storage tank is placed) by the generation subsystem.
Total efficiency	η_{tot}	The ratio between the net energy demand and the primary energy use.

4. METHODOLOGY

4.1 General

The analyses of the subsystem efficiencies are carried out on a monthly time base, which is also used in the context of the EPR. In order to generate enough data points for the analysis, the HVAC system is sized for and implemented in several building design variants of a reference office building (section 4.2). A detailed discussion of the selected HVAC system is given in section 4.3.

Integrated dynamic simulation models are set up for every combination of building design variant and HVAC system (section 4.4). Apart from the integrated simulation, a building simulation to calculate the net energy demand needs to be performed. The time step of the latter is typically 1 hour.

In order to be able to compare the performance of the different systems fairly, the resulting thermal comfort in the building needs to be similar in all cases. The thermal comfort is evaluated

according to the degree hours criterion of the European standard EN15251 (CEN, 2007a), with the difference between the occurring temperature and the limit temperature as weighting factor. Deviations during 5% of the occupied time on a yearly and monthly basis are accepted, which means about 100 h per year and about 10 h per month. In addition to thermal comfort, the indoor air quality (IAQ) in terms of amount of fresh air per person is equalized for all considered systems. An air flow rate of 36 m³/h per person for the design occupancy (IDA2 class, (CEN, 2004)) is supplied in each case.

The monthly subsystem efficiencies will be expressed as a function of the monthly heat-balance ratio of the building γ , as defined in EN13790 (ISO/FDIS, 2007). This variable represents the part load ratio (Olesen, 2001), but can be calculated without knowledge of the HVAC system nominal properties. In the framework of the EPR, this is a prerequisite. It incorporates the climate, building characteristics, internal gains and occupant behaviour. Equation 1 defines the heat-balance ratio depending on the building's solar heat gains (Q_{sol}), internal heat gains (Q_{int}), transmission heat losses (Q_{tr}), ventilation heat losses (Q_{vent}) and infiltration heat losses (Q_{inf}). The heat-balance ratio is closely related to the net energy demand. As shown in ref. (Van Der Veken & Hens, 2008), it has a strong correlation with the overall heating system efficiency in dwellings.

$$\gamma = \frac{Q_{gains}}{Q_{losses}} = \frac{Q_{sol} + Q_{int}}{Q_{tr} + Q_{vent} + Q_{inf}} \quad [-] \quad (1)$$

As mentioned before, the current EPR calculation of the characteristic primary energy use consists of two steps, identical for cooling and heating energy use. The net energy demand for each month ($Q_{net,m}$) is calculated in a first step, which is then divided by the subsystem efficiencies (and primary energy conversion factor) to obtain the primary energy use. Currently, those subsystem efficiencies are constant throughout the year.

$$E_p = \sum_{m=1}^{12} \frac{Q_{net,m}}{\eta_{sys}\eta_{gen}f_p} \quad (2)$$

The refined approach studied in this paper consists of defining monthly subsystem efficiencies depending on the monthly heat-balance ratio γ .

$$E_p = \sum_{m=1}^{12} \frac{Q_{net,m}}{\eta_{sys,m}\eta_{gen,m}f_p} \quad (3)$$

4.2 Building description

A generic reference office building with cellular office spaces is assembled for this research, based on statistical data (BBRI, 2001). The reference building is a detached office building with 4 floors of 500 m² each, the floor plan of which can be found in Figure 2. The main axis of the building lies in east-west direction (the office zones façades facing south and north). The floor-to-floor height is 3.5 m, hence the building's total height is 14 m. This results in a protected volume of 7000 m³, 2680 m² loss surface and a compactness of 2.6 m. The internal walls bounding the offices and the conference room are lightweight gypsum board walls. All other internal walls are heavy brick walls.

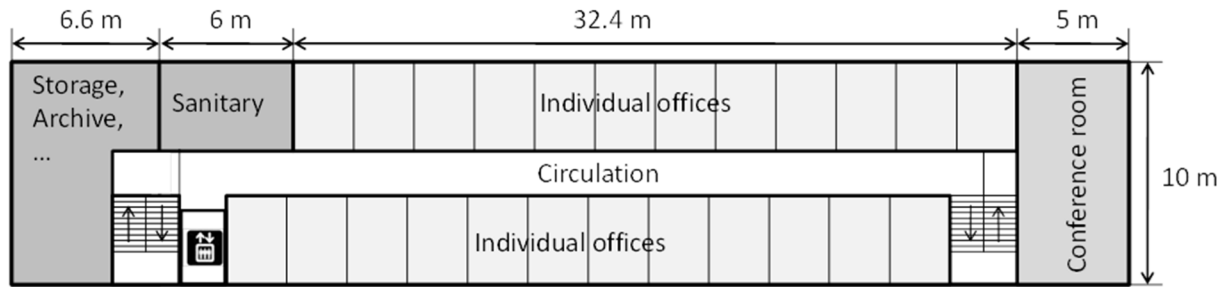


Figure 2: Floor plan of the medium-sized office building model.

As explained in section 4.1, the HVAC system is coupled to the different building design variants, in order to assess the influence of the interaction of the building and the system. A selection of 6 variants of the reference building is made. Table 2 offers a concise overview of the combinations of the building variables' values that form the building design variants. The imposed internal boundary conditions are described in Table 3. A typical weather data set for Uccle (Belgium) is used. The selection of building design variants is made to represent a wide range in annual net heating demand (NHD) (Table 4), while still allowing for passive cooling (Parys et al., 2012).

Table 2: Selected building design variants.

Nr.	U_{wall}	U_{roof}	U_{glazing}	g-value glazing	Glass to wall ratio	Shading device	n_{50}
	[W/m ² K]	[W/m ² K]	[W/m ² K]	[-]	[%]		[ACH]
1	0.20	0.20	0.6	0.48	71	yes	1
2	0.40	0.30	1.1	0.59	21	no	2.5
3	0.20	0.20	1.1	0.26	31	no	1
4	0.40	0.30	1.1	0.44	21	yes	2.5
5	0.40	0.30	1.1	0.26	71	yes	2.5
6	0.60	0.40	1.1	0.29	31	yes	2.5

Table 3: Internal boundary conditions.

	Offices	Meeting	Sanitary	Storage	Circulation
Installed lighting power ⁽¹⁾	11 W/m ²	11 W/m ²	4.5 W/m ²	3.5 W/m ²	3.5 W/m ²
Occupancy ⁽²⁾	9 am-6 pm (70% of nominal)	3 rd floor: 10 am - 11 am and 2 pm - 3.30 pm (15 persons) 4 th floor: 9 am - 10.30 am (15 persons)	8 am-6 pm	-	8 am-6 pm
Ventilation rate ⁽³⁾	36 m ³ /hpers supply	36 m ³ /hpers supply (3.6 m ³ /hm ² non-occupied)	15 m ³ /hm ² extraction	3 m ³ /hm ² extraction	extraction
Int. gains occupied ⁽⁴⁾	8.7 W/m ²	15 W/m ²	-	-	8 W/m ²
Int. gains unoccupied ⁽⁴⁾	2 W/m ²	-	-	-	1 W/m ²
Heating set points ⁽⁵⁾	21.5°C	21.5°C	16°C	16°C	-

- (1) The lights are assumed to be switched on whenever the zone is occupied. The internal heat gains are 50% convective and 50% radiative.
- (2) The sensible heat gain of 1 person is 75 W, 60% of which is convective. The latent heat gain of 1 person is 55 W or 0.081 kg/h (ASHRAE, 2009).
- (3) Ventilation starts at 7 am and ends at 6 pm. 95% of the supplied fresh air is assumed to be extracted.
- (4) Internal gains due to appliances based on ref. (Wilkins & Hosni, 2000). The split between convective and radiative gains is 50/50.
- (5) Set point for operative temperature during occupancy. These are optimal operative temperatures for a metabolic rate of 1.2 met clothing values of 1 and 0.5 respectively, according to ISO7730 (ISO, 2005).

Table 4: Annual net heating demand for the selected building design variants.

Nr.	NHD [kWh/m ² a]
1	14.8
2	22.6
3	20.1
4	26.5
5	33.7
6	37.0

4.3 HVAC system

The system consists of a traditional hydronic heating system with a modulating condensing gas boiler and radiators in every heated zone (offices, meeting rooms, sanitary, storage, see section 3.2). No active cooling is provided. The heating system (Figure 3) is switched between 7 am and 6 pm during the heating season, i.e. from October 1st to June 1st. When there is no heating demand in the building, the boiler and the boiler circulation pump are switched off. The control of the system can be considered as good practice: thermostatic radiator valves (TRVs), supply temperature varying between 60°C and 45°C depending on the outside temperature (average of the previous 6 hours), variable speed pumps in distribution circuits with variable flow rate. The open header in the boiler circuit ensures a constant water flow rate. Since this is achieved by

mixing return water from the secondary system with boiler outlet water, this will result in a higher inlet water temperature for the boiler and a reduced condensing effect.

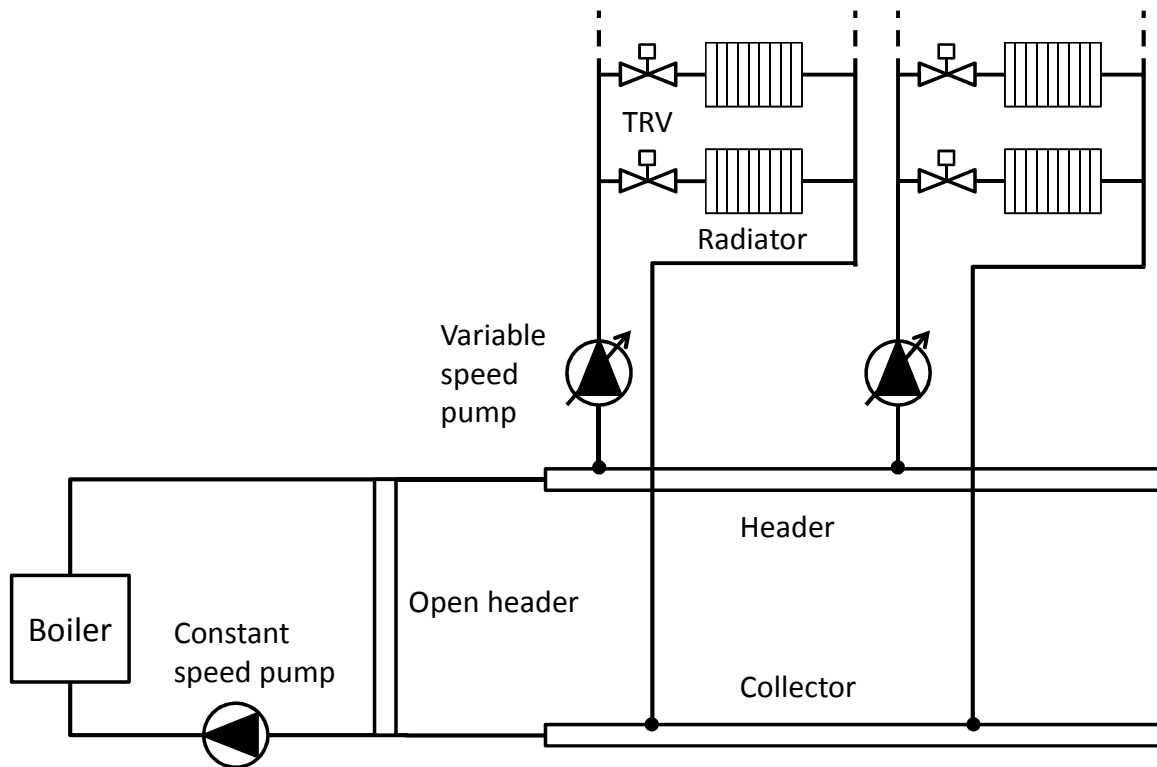


Figure 3: Schematic overview of radiator heating system (HVAC system 1) ¹.

The boiler is assumed to be located in an unheated basement, as is the horizontal main piping circuit, from which vertical piping leaves to supply the radiators. The vertical pipes thus run through the heated zones. Two parallel circuits are implemented, one for the south zone (offices and meeting rooms) and one for the north zone (offices, storage and sanitary).

Hygienic ventilation is provided with an extraction system consisting of window grilles for supply and constant speed fans for the extraction in the offices, the meeting room and the sanitary. This does imply however that the relative humidity in the zones cannot be controlled.

Since no active cooling is provided, this HVAC system typology cannot be applied in every office building design (see 4.2).

4.4 Integrated simulation model

The integrated building and systems model is set up in TRNSYS17 (Klein et al., 2010), a dynamic simulation tool well suited for HVAC system studies (Crawley et al., 2008). The time step is set at 1.5 minutes for these integrated models.

Only the 3rd and 4th floor of the building are modelled in the simulations, implying their energy demands to be representative for the entire building. This simplification can be justified by the good thermal insulation values of both roof and floor, while it drastically reduces the computational time. A multi-zone model with 14 thermal zones is defined: the 1-person offices are thus modelled as one single zone per floor and orientation (Figure 2).

¹ The system scheme shown is simplified to show only those components that influence the thermal calculations and are integrated in the simulation models. Indispensable hydraulic components such as balancing valves are not printed.

The HVAC system component models and their main characteristics are summarized in Table 5. The selected and implemented component models are all able to describe part load performance and the influence of non-rated conditions. Transient effects are included as much as possible, as the thermal inertia of the heaviest elements (boiler, radiator) and most of the water or air content of the system (pipes, ducts, boiler, radiator) are modelled. The system thermal losses both during and in between periods of operation are thus mostly accounted for in the simulations.

Each thermal zone is represented by a single node in the TRNSYS building model (TRANSSOLAR, 2011). Hence, except for the control aspect, the emission efficiency cannot be calculated in this simulation set-up due to inherent limitations and is therefore a constant input. The generation and distribution efficiencies are calculated, though neglecting start-up phenomena for the former and valve inertia and inaccuracy for the latter.

No hydraulic calculations are included in the simulations, implying a perfectly balanced system is assumed. As a consequence, the auxiliary energy use for pumps and fans can only be calculated indirectly. For the pumps, this is done based on the model of (Bernier & Lemire, 1999), with which non-dimensional power curves as a function of non-dimensional volumetric flow rates are derived. The fan energy use is calculated as a function of the volumetric flow rate, using the polynomials proposed in AIVC technical note 65 (Schild & Mysen, 2009).

Table 5: Overview of the main HVAC system component simulation models.

Component	Model	Performance under non-rated conditions?	Part Load performance ?	Device thermal inertia?	Fluid content thermal inertia?
Gas boiler	(Haller et al., 2009)	Yes	Yes	Yes	Yes
Radiator	(Holst, 1996)	Yes	Yes	Yes	Yes
Pipes/ducts	Plug-flow	Yes	N.A.	No	Yes

5. RESULTS

Firstly, the integrated simulation is assessed in terms of simulation quality (5.1) and in terms of system sizing and implementation by evaluating the obtained thermal comfort (5.2). In section 5.3, the performance of the HVAC system is analyzed, focusing on monthly subsystem efficiencies, expressed depending on the heat-balance ratio and primary energy use. Subsequently, the results of this integrated approach are used to derive refined monthly subsystem efficiencies which are assessed and compared with the standard values of the subsystem efficiencies of the Flemish EPR calculation method in section 5.4.

5.1 Integrated simulation quality

The integrated model is computation-heavy, given the multitude of modelled components, the large differences in their time constants and the small calculation time step. A straightforward indicator to assess the convergence and correct execution of the simulation is to compare the difference in input and output of energy flows in the thermal system with the calculated energy losses. When this is calculated on a monthly basis, the error - denoted here as ΔQ_{sim} - thus found should be close to 0, though not necessarily equal to 0, as slight differences in internal energy between the beginning and end state are possible. The monthly simulation error, defined as the relative difference between the system energy input (heat produced by the boiler, $Q_{\text{boiler,out}}$) and output (heat emitted in the building zones, Q_{emit}), and the system's thermal losses (Q_{loss}).

$$\Delta Q_{sim} = \frac{(Q_{boiler,out} - Q_{emit}) - \sum Q_{loss}}{(Q_{boiler,out} - Q_{emit})} \quad (4)$$

The monthly simulation error is found to be on average 3.5%, with a maximum of 12.5%. This is deemed acceptable.

5.2 HVAC system performance

In all cases, the desired room temperatures are met, indicating that all systems components are properly sized for every respective building design variant and the control works well. Figure 4 illustrates this for building design variant 3 (Table 2) by showing the operative temperature in the north facing office zone on a random winter day.

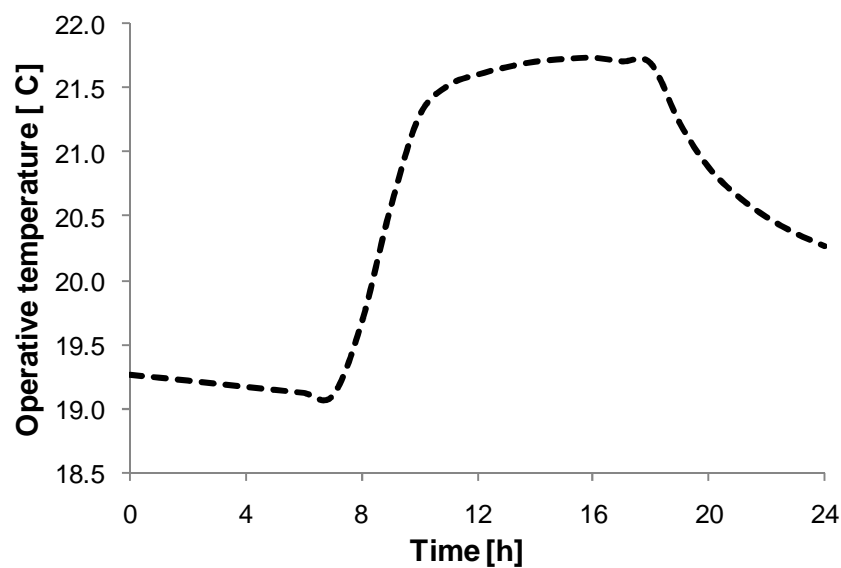


Figure 4: The daily operative temperature profile in north-facing offices between HVAC systems on a random winter day.

5.3 HVAC system performance analysis

5.3.1 Primary system efficiency

Figure 5a shows the monthly heat generation efficiency of the gas boiler as a function of the heat-balance ratio for the 6 selected building design variants. The efficiency drops significantly during months with higher heat-balance ratios - and thus lower part load ratios. When looking in detail to the boiler thermal losses proportional to the total heat production (Figure 5b), a decrease in latent flue gas losses is found for higher heat-balance ratios, due to the external temperature dependent heating curve resulting in lower water return temperature and thus more condensation. This small efficiency enhancement is however countered by a much greater increase in thermal losses to the surroundings. Lower part load ratios lead to intermittent boiler use and higher relative environment losses through cooling down between operational periods.

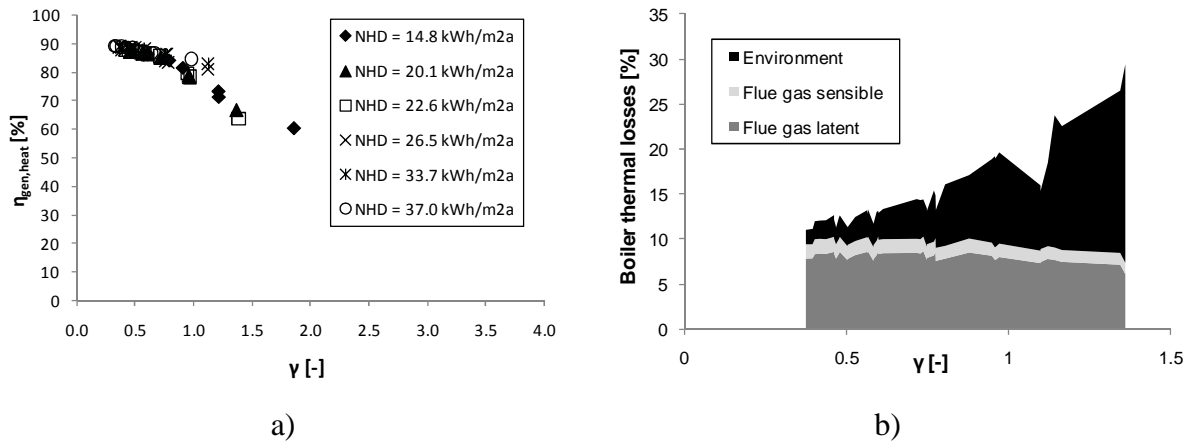


Figure 5: a) Monthly heat generation efficiency; b) Boiler thermal losses.

5.3.2 Secondary system efficiency

Figure 6a shows the emission efficiency, calculated as the ratio of the net heating demand over the net energy delivered to the radiators. The emission efficiency consists of a factor including losses on component level, which is fixed at 95% (3.4), and a factor accounting for the control efficiency, shown in Figure 6a. The latter is thus about 1 at heat-balance ratios below 0.5, indicating the heat demand is met, but drops significantly for higher heat-balance ratios. This is due to overheating at times with very low heat demands due to imperfect control. A few outliers are found on the curve, but these represent months with negligible net heat demands (Figure 6b).

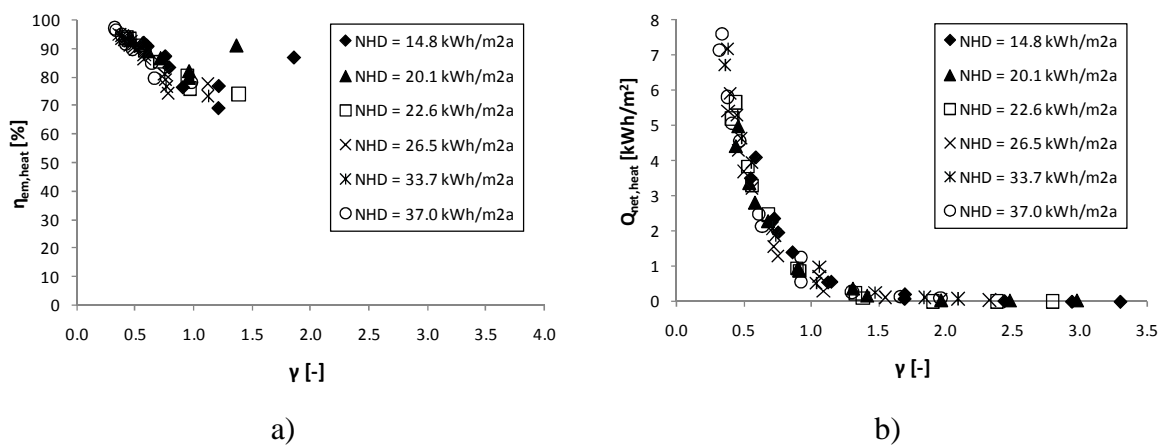


Figure 6: a) Monthly heat emission control efficiency; b) Monthly net heat demand.

The distribution efficiency, defined as the ratio of the energy delivered to the radiators over the gross energy demand, is shown in Figure 7. A clear decreasing trend towards higher monthly heat-balance ratios is visible. This is due to the cooling down of the water in the system pipes in between heating periods gaining importance when the part load ratio drops.

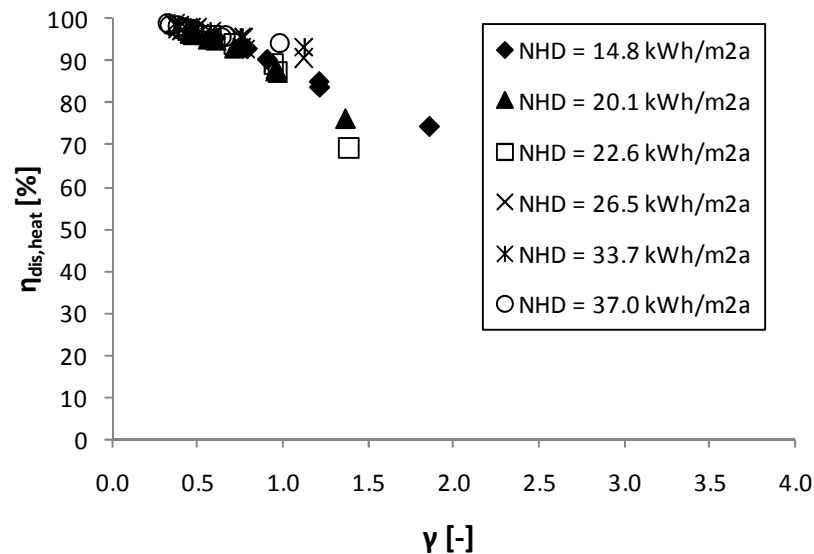


Figure 7: Monthly heat distribution efficiency.

5.3.3 Primary energy use

Table 6 summarizes the results of all integrated simulations in terms of total annual primary energy use of the HVAC systems in the selected building variants of Table 2.

The auxiliary energy use comprises the pumps, the fans and the boiler electrical energy use. The latter is negligible with values between 6 kWh and 10 kWh per month. The fan electrical energy use equals about 2200 kWh or 1.1 kWh/m² per year. The pump energy use depends on the heat demand. When looking at the total primary energy use per building for heating and ventilating (Figure 8), the boiler gas consumption is by far the largest fraction, while the pump energy use constitutes only between 1% and 2%. Figure 8 clearly indicates the relatively increasing share of the auxiliary energy use for buildings with lower net heat demands in the total primary energy use, which will function as a mitigating secondary effect on potential energy savings.

Table 6: Total annual primary energy use of the HVAC system for the selected building design variants.

Nr.	Total annual primary energy use [kWh/m ²]
2	21.2
3	30.9
4	27.5
5	35.9
6	43.2
7	47.8

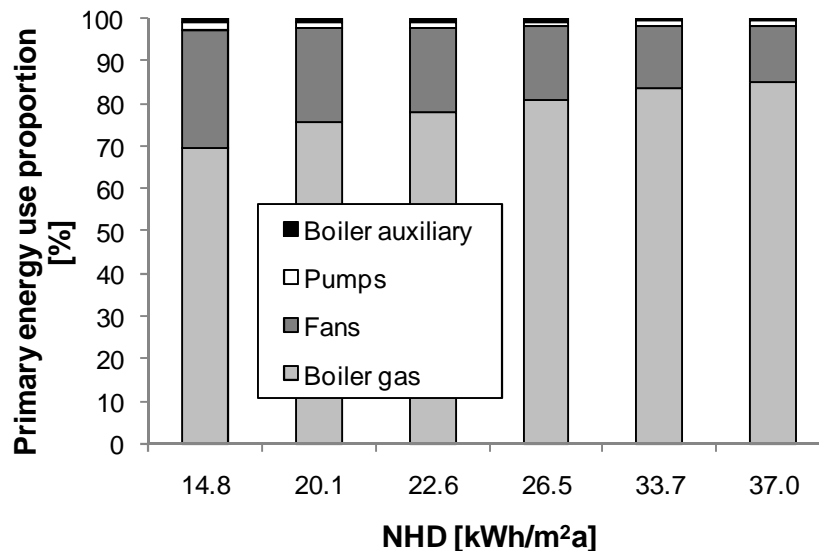


Figure 8: Breakdown of annual total primary energy use.

5.4 Calculation with refined monthly subsystem efficiencies

In a first section (5.4.1), correlations of the subsystem efficiencies as a function of the monthly heat-balance ratio are deduced based on the results of the integrated simulations. In the following section (5.4.2) the refined subsystem efficiencies are implemented in the EPR to evaluate their impact.

5.4.1 Subsystem efficiency regression models

Based on Figure 5 to Figure 7, correlations can be fitted expressing the monthly subsystem efficiencies depending on the heat-balance ratio γ_m , which can then be used in energy calculations of other buildings with similar thermal systems. The correlations are established as follows:

$$\eta_m = a \gamma_m^2 + b \gamma_m + c \quad (5)$$

Table 7: Regression coefficients and R2-values for the subsystem efficiency correlations

subsystem	a	b	c	R ²
Emission	0	-25.728	103.440	0.84
Distribution	-4.509	-9.417	102.690	0.84
Generation	-8.183	-3.888	91.688	0.90

5.4.2 Impact of EPR calculation with refined subsystem efficiencies

In this section, the impact of using the refined subsystem efficiencies depending on the monthly heat-balance ratio, as defined in Table 7, in EPR calculations of the monthly energy use is assessed by comparing the results with the default fixed values for subsystem efficiencies as defined in the Flemish EPR calculation software (see 3.1). In addition, the calculation with the refined subsystem efficiencies is compared to a calculation using annual average efficiencies deduced from the integrated simulations, to assess the influence of the dependency on the monthly heat-balance ratio.

The default value Flemish EPR value for a condensing gas boiler, based on the manufacturer's data for 30% part load ratio and corrected for the design return water temperature, equals 89.4%.

This is quite comparable to the annual average efficiency of 87.1% that is found in the integrated simulations across all building variants. A default value of the system efficiency for hydronic secondary heating systems in buildings without a cooling system as defined in the Flemish EPR equals 85.5%. From the integrated simulations, average annual values of 96.4% for the distribution efficiency and of 91.2% for the emission efficiency are found. Combined, this yields a system efficiency of 87.9%, which is again close to the default EPR value. It can thus already be concluded that the EPR values are well chosen.

In Figure 9, the mean bias error (MBE) over the building variants, defined here for absolute values of the error, is shown for the 3 aforementioned EPR-type calculation methods for the monthly final energy use - dividing the monthly net heat demand by the monthly subsystem efficiency values - compared to the final energy use as calculated in the integrated simulations, which is thus regarded as the reference.

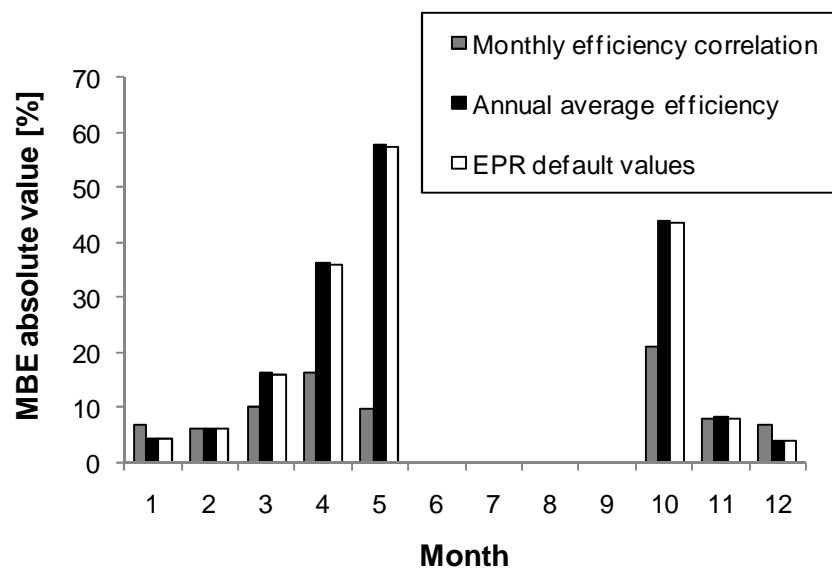


Figure 9: Comparison of the MBE (for absolute values of the error) of the 3 EPR type calculation methods for the monthly final energy use compared to the results of the integrated simulations.

As can be seen in Figure 9, the MBE is small and comparable for all 3 calculation methods in the winter months, when the heating demand is high. However, when going to the intermediate seasons, with lower demands and higher heat-balance ratios, the calculation with the refined subsystem efficiencies yields remarkable better results in terms of MBE. Thus, taking into account the dependency of the heat-balance ratio, integrating the subsystem efficiencies drop in months with higher heat-balance ratios, is shown to significantly improve the calculation results in months with lower demands.

However, the impact on the calculated annual final energy use for heating is quite modest. Where the calculation with the default EPR values yields a MBE of 7.2% compared to the results of the integrated simulation and the calculation with average annual efficiencies a MBE of 5.0%, the calculation with the refined subsystem efficiencies depending on the monthly heat-balance ratio yields an MBE of 3.9%.

6. DISCUSSION AND CONCLUSION

In this paper, integrated dynamic simulations of a thermal system coupled to 6 variants of a medium-sized office building are performed and discussed. A traditional hydronic heating system is considered, consisting of a modulating condensing gas boiler and radiators in every

heated zone. No active cooling is provided, though only building variants able to provide summer comfort through passive cooling only are selected. Hygienic ventilation is provided by a mechanical extraction system.

From the integrated simulations, monthly efficiencies for the generation, distribution and emission subsystems are deduced. The latter are expressed depending on the monthly heat-balance ratio, which equals the ratio of heat gains over heat losses on the building level. The heat-balance ratio thus represents the part load ratio, but can be calculated without taking the system into account. This variable is used in order to generalize the results and at the same time use them in an EPR context, which requires relatively simple calculations where the system cannot be taken into account in detail.

The integrated simulations contain some model necessary model simplifications. The thermal inertia and water content of the most important is modelled, though not of all components. Moreover, the heat emission in the building zones is not modelled, as the latter are represented by a single thermal node. Finally, no hydraulic calculations are included, implying the assumption of a perfectly balanced system.

The resulting subsystem curves correlate quite well with the monthly heat-balance ratio (R^2 -values of 0.84 or higher). These curves show the heating subsystem efficiency drops in months with higher heat-balance ratios (and thus lower heating demands). These refined efficiencies are subsequently used in an EPR-type calculation, in which the monthly net heating demand is divided by the subsystem efficiencies to estimate the monthly final energy use. The results of this calculation are compared to similar calculations using annually averaged efficiencies deduced from the integrated simulations and using the default fixed EPR values for the subsystem efficiencies. It is shown that using the refined efficiencies yields better results in intermediate months, when the heating demand is lower. However, when looking at the total annual final energy use, the impact of using the refined efficiencies is modest.

The subsystem efficiency curves depending on the monthly heat-balance ratio deduced in this paper are only valid for similar heating systems. In future work however, these curves will also be established for a selection of thermal systems (including active cooling) common in Belgium.

ACKNOWLEDGEMENTS

This research was funded by the Institute for the Promotion of Innovation through Science and Technology in Flanders (IWT-Vlaanderen). This support is gratefully acknowledged.

In addition, we would like to express our gratitude to Dr. Stéphane Bertagnolio for his help in implementing thermal system component models.

REFERENCES

ASHRAE. (2009). *Fundamentals*.

Bauer, M. (1999). *Methode zur berechnung und bewertung des energieaufwandes fur die nutzenubergabe bei warmwasserheizanlagen*. Universitat Stuttgart.

BBRI. (2001). *Kantoor2000 - Study of energy use and indoor climate of offices (in Dutch)*. Centrum (p. 202).

Bernier, M. A., & Lemire, N. (1999). Non-dimensional pumping power curves for water loop heat pump systems. *ASHRAE Transactions*, 105(2), 1–7.

- CEN. (2004). *EN 13779 Ventilation for non-residential buildings - Performance requirements for ventilation and roomconditioning systems*. Brussels.
- CEN. (2007a). *EN 15251 Indoor environmental input parameters for design and assessment of energy performance of buildings addressing air quality, thermal environment, lighting and acoustics* (p. 52). Brussels.
- CEN. (2007b). *EN 15316 Heating systems in buildings - Method for calculation of system energy requirements and system efficiencies - Part 2-1: Space heating emission systems* (p. 41). Brussels.
- Crawley, D. B., Hand, J. W., Kummert, M., & Griffith, B. T. (2008). Contrasting the capabilities of building energy performance simulation programs. *Building and Environment*, 43(4), 661–673. doi:10.1016/j.buildenv.2006.10.027
- DIN. (2003). *DIN V 4701-10 Energy efficiency of heating and ventilation systems in buildings - Part 10: Heating, domestic hot water, ventilation* (p. 156). Berlin.
- Flemish Government. Decision of the Flemish Government regarding the definition of the requirements for energy performance and indoor climate of buildings (in Dutch) (2005). Brussels.
- Haller, M., Konersmann, L., Haberl, R., Dröscher, A., & Frank, E. (2009). Comparison of different approaches for the simulation of boilers using oil, gas, pellets or wood chips. In *Building Simulation 2009* (pp. 732–739). Glasgow, Scotland, 27-30 July.
- Holst, S. (1996). *TRNSYS-Models for Radiator Heating Systems*. Munich.
- ISO. (2005). *ISO 7730 Ergonomics of the thermal environment - Analytical determination and interpretation of thermal comfort using calculation of the PMV and PPD indices and local thermal comfort criteria*. Geneva. doi:10.1016/j.soildyn.2004.11.005
- ISO/FDIS. (2007). *EN 13790 Energy performance of buildings - Calculation of energy use for space heating and cooling*. Geneva.
- Klein, S. A., Beckman, W. A., Mitchell, J. W., Duffie, J. A., Duffie, N. A., Freeman, T. L., ... Kummert, M. (2010). TRNSYS 17 a transient system simulation program. Solar Energy Laboratory, University of Wisconsin-Madison.
- Korolija, I. (2011). *Heating, Ventilating and Air-conditioning System Energy Demand Coupling with Building Loads for Office Buildings*. De Monfort University, Leicester.
- Korolija, I., Marjanovic-Halburd, L., Zhang, Y., & Hanby, V. I. (2011). Influence of building parameters and HVAC systems coupling on building energy performance. *Energy and Buildings*, 43(6), 1247–1253. doi:10.1016/j.enbuild.2011.01.003
- Korolija, I., Zhang, Y., Marjanovic-halburd, L., & Hanby, V. I. (2009). Selecting HVAC Systems for Typical UK Office Buildings. In *ISHVAC09* (pp. 388–396). Nanjing, China, 6-9 Nov.
- Korolija, I., Zhang, Y., Marjanovic-Halburd, L., & Hanby, V. I. (2013). Regression models for predicting UK office building energy consumption from heating and cooling demands. *Energy and Buildings*, 59, 214–227. doi:10.1016/j.enbuild.2012.12.005
- Olesen, B. W. (2001). Control of floor heating and cooling systems. In *CLIMA 2000* (pp. 1–15). Napoli, Italy, 15-18 Sept.

- Parys, W., Breesch, H., Hens, H., & Saelens, D. (2012). Feasibility assessment of passive cooling for office buildings in a temperate climate through uncertainty analysis. *Building and Environment*, 56, 95–107. doi:10.1016/j.buildenv.2012.02.018
- Peeters, L., Van Der Veken, J., Hens, H., Helsens, L., & Dhaeseleer, W. (2008). Control of heating systems in residential buildings: Current practice. *Energy and Buildings*, 40(8), 1446–1455. doi:10.1016/j.enbuild.2008.02.016
- Schild, P. G., & Mysen, M. (2009). *Technical Note AIVC 65 - Recommendations on specific fan power and fan system efficiency. Management* (p. 32).
- Shahrestani, M., Yao, R., & Cook, G. K. (2013). Characterising the energy performance of centralised HVAC&R systems in the UK. *Energy and Buildings*, 62, 239–247. doi:10.1016/j.enbuild.2013.03.016
- TRANSSOLAR. (2011). Trnsys 17 Multizone Building Modeling with Type56 and TRNBUILD.
- Van Der Veken, J., & Hens, H. (2008). Determination of the heating efficiency at building level. In *Building Physics Symposium* (pp. 101–104). Leuven, Belgium, 29-31 Oct.
- Wilkins, C., & Hosni, M. H. (2000). Heat gain from office equipment. *ASHRAE Journal*, 42(6), 33–39. doi:10.1016/0140-7007(84)90067-7
- Zhang, Y., Wright, J. A., & Hanby, V. I. (2006). Energy Aspects of HVAC System Configurations — Problem Definition and Test Cases. *HVAC&R Research*, 12(3c), 871–888.

The influence of realistic schedules for the use of appliances on the total energy performances in dwellings

Tiziana Buso¹, Simona D'Oca¹, Stefano Paolo Corgnati¹

⁽¹⁾TEBE Research Group, Energy Department, Politecnico di Torino, Corso Duca degli Abruzzi 24, 10129, Torino, Italy

1. ABSTRACT

The use of lighting and appliances influences buildings energy performance by affecting electricity and thermal loads. Nevertheless, their use is often predicted by arbitrary assumptions during the design phase. The paper focuses on the realistic description of domestic equipment use and its impact on the prediction of energy consumption in homes. A method for creating schedules of domestic appliances use, based on dwelling field monitoring is proposed. The method is validated by calibrating the simulated electric consumption with the monitored one. A baseline simulation model is developed in IDA Ice, in which the developed schedules (named Calibrated Realistic Schedules) are implemented. Then, the same model is used to implement the schedules for domestic appliance use proposed by the Italian reference standard for energy calculation UNI/TS 11300. The simulated energy performances are finally compared. Results shows that values for usage times and power from UNI/TS 11300 are appropriate references for predicting the equipment energy use at the design stage. However, standardized schedules do not take into account the lower use of equipment in summer, leading to higher predicted internal gains and consequently to oversizing the cooling system. The paper demonstrates the need for more realistic descriptions of appliances use to be included in simulation software, particularly in high performing buildings. Moreover, it gives evidence of the impact that actual occupant behaviour has on building energy performance.

Keywords: Building Energy Performance, Energy Simulation, Domestic Equipment, Occupant Behaviour, Calibrated Schedules.

2. INTRODUCTION

The 2009 update of the EU energy trends to 2030 reports an average 2% increase in the electricity consumption in the EU-25 households during the last 10 years and projects by 2030 a final net electricity demand in the residential sector grown by 3600 TWh/year. This 2009 baseline scenario improves the 2007 projection, which envisaged growth by 3800 TWh/year by 2030, but points out that, regarding appliances and lighting in dwellings, the changes in the 2009 baseline from the 2007 baseline are rather small. Current policies for buildings accelerate progress of energy efficiency in houses implying larger effects in terms of energy savings for heating and cooling uses (8% in 2020 and 14% in 2030 compared to 2007 Baseline), while energy efficiency improvements from eco-design measures are somewhat masked by stronger increase of use of appliances and plugs.

Some of the reasons for such increase in the residential sector electricity consumption are associated with a higher degree of basic comfort and level of amenities (particularly in the

new EU member countries) and also with the widespread utilization of relatively new types of loads whose penetration and use have experienced a very significant growth in recent years.

Moreover, despite the introduction of energy labels, implemented with EU Directives in the last 10 years, has produced a positive trend in the sales of more energy efficient appliances, white goods and appliances have now reached an asymptote in enhancement of energy efficiency with the current technologies.

In view of these facts, the relevance of energy uses for lighting and appliances in dwellings' energy balance is increasing. Two main reasons can be identified:

- 1) they affect the electricity needs of the building and drastically raise the primary energy use (because of the conversion factor for electricity). Since the nZEB target imposed by the EPBD recast is based on primary energy consumption, managing the energy uses related to highest share of the total building energy balance becomes crucial;
- 2) in the thermal energy balance of buildings, appliances, plug loads and lighting are internal gains that need to be managed during the heating and cooling seasons, in order to properly size the systems and to ensure occupants' comfort.

2.1 Building energy simulations, occupants' behavior and use of appliances

A building energy simulation is a theoretical representation of the status and operation of a building, with the ideal goal of predicting accurately the real dynamics which govern building energy uses. This prediction is dampened by the lack of knowledge about the real functioning of a building: final realization of construction and technical installations and the utilization of the building systems can lead to a significant mismatching between predicted and actual energy use. Indeed these aspects are affected in the real world by many unpredictable and accidental factors, which are usually implemented in simulation software by using arbitrary assumptions. Among them, users' actions in buildings emerged to be the crucial aspect to be investigated for achieving realistic energy predictions (IEA Annex 53 Final Report, 2013).

With the raising awareness of the key role played by occupants in affecting buildings' actual energy consumption, new methodologies and technique able to comprehend, describe and reproduce the leverage of occupant behaviour on building operation have been the object of various studies in the current years. Realistic descriptions of occupants' behaviour to be embedded in simulation tools have been proposed by many researchers (Bourgeois et al. 2006, Rijal et al. 2007).

In contrast with the static description of occupant behaviour, based on assumptions made in literature, the new approach to occupant behaviour simulation, proposed among the firsts by Nicol (2001) and Raja et al. (2001), takes into account that users do not always make logical choices and they act stochastically, not deterministically.

As stated by Papakostas and Sotiropoulos (1997), occupants' behaviour in buildings includes two main categories of actions: (1) operations aiming at controlling the indoor environment and (2) operations associated with the use of appliances.

At the present stage, mathematical models describing users' interaction with the building control systems (1) were developed. The implementation of these probabilistic behavioural models in building simulation software is possible because they occur as a response to indoor environmental conditions, which are outputs provided by the simulation tools.

The same method cannot be used when occupants' operations are associated with the use of domestic appliances (2): no significant statistical correlations can be found between indoor conditions and use of equipment. Indeed the use of appliances is mainly driven by the occupant's practical needs, for instance willing to cook food or operate the clothes- or dish-washing machine. With the increasing role of electric loads in buildings' energy balances, a realistic prediction of the use of appliances and plug loads is crucial nowadays.

2.2 Overview

In this paper, an approach for the definition of a realistic model of occupants' use of appliances and plug loads is proposed. Since the probabilistic models predicting the use of appliances cannot fit with the currently available simulation tools, a deterministic approach is presented for the implementation. Daily profiles for the use of equipment, composed of 24 hourly values, and corresponding to a fraction of a given peak load, are loaded in the tool as fixed schedules.

However, "deterministic" does not necessarily means "not realistic". The study proposes a method to create deterministic schedules, here named Calibrated Realistic Schedules (CRS), based on field monitoring of actual occupants' use of appliances. The CRS predict the occupants' behaviour related to the use of appliances and plugs for a given situation and incorporate this behaviour in the modelling of building energy performance. In particular, the focus is on the use of electric appliances in dwellings, where the component of electricity consumption is for the majority unpredictable (Wood and Newborough 2003). The method is validated by implementing the learned Calibrated Realistic Schedules in IDA Ice, reproducing the monitored building features and comparing monitored and simulated electric consumption.

The data used as basis for this study were gathered in the context of an on-going Italian initiative among private companies dealing with white goods and communication technologies: the project aims at enhancing the energy efficiency of the entire house system by providing users with information on household consumption directly on the point of use.

Final purpose of this paper was to highlight the role of a realistic description of the use of appliances in influencing the predicted energy performance of a building. With this goal, simulations in IDA Ice were run and results were compared. Energy consumptions of the baseline model with Calibrated Realistic Schedules were compared to the energy consumption of the same model running schedules proposed by the Italian standard UNI/TS 11300. The schedules (hourly values as fractions of the peak load) were first applied to the actual installed power of the monitored appliances, then to the average installed power given by the same Italian standard.

Results of the simulations showed a gap in the simulated electric consumption between the model running realistic and standard schedules referring to the actual installed power. Compared to a standard schedule simulation model, the electricity use doubled when simulating the Calibrated Realistic Schedules.

3. SIMULATION

The present study investigated the role of realistic description of the use of appliances and plug loads, pursuing two subsequent goals:

- 1) proposing a method for developing realistic schedules for occupants' use of domestic appliances, to be implemented in simulation software, by using recorded electrical energy consumption. The predictive power of the learned schedules, named Calibrated

Realistic Schedules (CRS), was tested by comparing monitored and simulated electric consumptions;

- 2) testing the suitability of the standard assumption, proposed by the Italian standard UNI/TS 11300, for predicting electricity uses and internal gains in a dwelling, by comparing results obtained in simulations running the realistic schedules previously developed and the schedules given in the standard.

3.1 Calibrated Realistic Schedules

3.1.1 Data collection and elaboration

Recorded data of electrical energy consumption were used to develop realistic schedules related to occupants' use of domestic appliances.

Data collection was performed in the framework of an Italian initiative among private companies dealing with communication technologies and white goods, among whom Telecom Italia was a key actor. This collaborative project aims at improving energy efficiency in dwellings by providing users with information on their household consumption directly on the display of the appliance itself, on the smart phone or on their computer by means graphical user/friendly interfaces. With this purpose, smart devices involved in the residential energy management were developed and installed in trial dwellings around Italy: the electronic meter, which is responsible for providing certified metering data; smart appliances, able to collect their own metering data and to adjust their power consumption by modifying their behaviour; smart plugs, able to collect metering data and to implement a simple on/off control on the plugged energy loads other than smart appliances; the home gateway, which acts as the central coordinator of the entire home; and the customer interfaces, i.e. all the devices used by customers to monitor and configure their energy behaviour. In the on-going testing phase of the project, started in December 2011, the number of installed kits increased step by step, reaching the total of 23 only in January 2013.

For the purpose of the present study, electricity consumption data, recorded with a 2 minutes time-step by the electronic meter, smart appliance and smart plugs, were collected and analysed in one trial user (coded as trial A), for which 1 year of monitored data and detailed information about the household characteristics and the dwelling features were available. The chosen time step for data elaboration was hourly, in order to compare and combine the realistic schedules deriving from data analysis with the schedules proposed by Italian standards.

In trial A disaggregated data were available from 1st January 2012 to 31st December 2012 for: electronic meter, smart plug, refrigerator, TV, washing machine and dish washer. The contribution of the unconnected single elements, here named unconnected, among whom a key role is played by lighting, was not possible through recordings. For each set of yearly monitored data (each smart appliance, smart plug and the unconnected load) a logistic regression was inferred in order to understand if and which parameters could influence the data variation and the result was that the season of the year, the day of the week and the hour of the day were the most influencing factors in the use of these domestic appliances. Following these remarks, detailed disaggregated hourly electric consumption data from the smart appliances – dish washer, washing machine, refrigerator, TV –, the smart plug and the unconnected elements were divided by season and in each season the different weekly energy consumption profiles were compared. This method of clustering information takes into account

the differences in occupants' interaction with home amenities in different hours of the day, days of the week and seasons of the year.

For each smart appliance and the unconnected appliances, the weekly energy consumption profiles for winter (from 21-12-2012 to 31-12-2012 and from 01-01-2012 to 20-03-2012), spring (from 21-03-2012 to 20-06-2012), summer (from 21-06-2012 to 20-09-2012) and fall (from 21-09-2012 to 20-12-2012) were plotted.

These data organization was the basis for the creation of the Calibrated Realistic Schedules.

3.1.2 Calibrated Realistic Schedules

The first step toward the development of realistic schedules was the observation of the monitored weekly electric consumption profiles. Depending on the considered appliance, different usage trends were noticed and taken into account for the creation of CRSs.

Similar trends were found in the use of washing machine dish washer and smart plug, on-off white goods not used with a daily frequency. In this case the schedule creation method consisted of:

- 1) calculation of average daily usage times (i.e. twice per day);
- 2) calculation of the average weekly use (i.e. twice per week);
- 3) calculation of the average use duration (i.e. 2 hours per time);
- 4) detection of the weekdays having the highest use frequency (i.e. Monday and Thursday);
- 5) detection of the hours having the highest use frequency (i.e. from 8 p.m. to 10 p.m.)
- 6) calculation of the average energy consumption when in use (i.e. 850 Wh).

Dealing with the use of TV, the data analysis revealed an almost continuous use, all day long and during the whole week. Therefore, even if dealing with a classical on-off appliance, the schedule creation steps were slightly different from the ones described above:

- 1) calculation of the amount of usage hours typical of every weekday;
- 2) detection of the most frequent switching-on hour;
- 3) calculation of the average hourly energy consumption for each week day.

A different approach was followed for the refrigerator, the only continuous use appliance in the house. From the analysis of the seasonal weekly schedules it came out that in trial 7 the refrigerator energy consumption was not constant all day long, but presented periodical significant peaks. Therefore the schedules took into account:

- 1) the average number of peaks per day and per week;
- 2) the average duration of each peak;
- 3) the average energy consumption during peaks;
- 4) the average consumption out of peaks.

Finally, the unconnected appliances' electric consumption was analysed. Since their nature is unknown - apart from the fact that lighting is included - the method followed to create the calibrated schedules only relies on the monitored values available; no average times of use or peaks presence were considered and the schedules was simply derived from the calculation of

the average hourly energy consumption for every day of the week and, subsequently, by regularizing the obtained average profile.

Summing it up, methods for the creation of schedules are related to the single appliances' monitored use. However a common approach among the different procedures presented comes out clearly: the seasonal weekly profiles are all based on the calculation of average values for both the energy consumption and the usage time. The obtained seasonal appliances' weekly use profiles can be implemented in simulation software as schedules for the use for the equipment.

3.1.3 Implementation in IDA Ice

In order to verify the suitability of the proposed empirical methods for developing realistic schedules, they were implemented in the building energy dynamic simulation software IDA Ice: the schedules were applied to a virtual model reproducing the monitored dwelling features and then the simulated electric consumption results were compared to the monitored ones.

Purpose of the simulation model was twofold: on one side to verify the ability of CRSs to reproduce the actual electricity consumption, on the other to assess the percentage relevance that electricity consumption had on the total energy consumption of the flat. Since only electricity consumption was monitored in the trial, the thermal energy needs were simulated in IDA Ice by implementing in the virtual model the physical and thermal features of the monitored house. No monitored data for heating and domestic hot water were available for comparison.

The simulated dwelling is a 2-levels flat, at the top floor of a residential building in Turin suburbs, built in the 90's. The internal layout is shown in Figure 1. Living-room, kitchen, the 2 bedrooms and the 2 bathrooms were the thermal zones taken into account in the simulation software. Envelope properties were derived by the Italian Typology Brochure, final outcome of the European project Tabula, whose aim was to provide national average data for buildings properties regarding the residential sector.

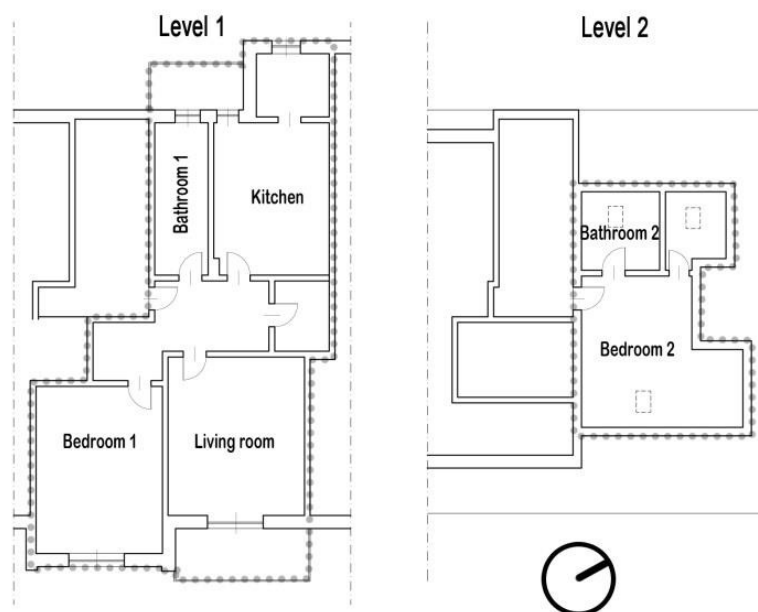


Figure 1. Internal layout of trial A.

The flat is heated by water radiators with centralized heat production (fuel: natural gas) and temperature control and by an additional electrical fan coil (for heating and cooling) installed in the attic. Plants' operation hours were described by standard schedules for the heating and cooling season and the chosen temperature set points were 20°C for heating and 26°C for cooling, as suggested by the II comfort category presented in EN15251.

Information about the household's characteristics and the occupancy rate were obtained by interviewing the occupants; the monitored family is composed by a married couple, a working man out of home from 8 a.m. to 7 p.m. and a housewife, with a 3-years-old children and a 10-month's baby.

Once the model was built, the developed Calibrated Realistic Schedules were implemented coherently with the requirements of the simulation software: IDA Ice deals with the electric load of the zones by generically dividing them into "equipment" and "lighting", while profiles describing the use of single appliances were obtained from the analysis of the monitored data. Therefore, in order to implement the obtained realistic schedules in each thermal zone of the model, the single profiles were gathered according the appliances location in the flat. For each zone the "comprehensive" Calibrated Realistic Schedule became the schedule for the equipment. The kitchen CRS for equipment included refrigerator, dishwasher and smart plug CRSs; living room CRS was coincident with TV CRS; Bathroom 1 CRS corresponded to washing machine CRS. Unconnected use profiles, which include lighting, were implemented in the software as "lighting" schedules, with loads shared among zones, adapting the figures proposed by the Italian project MICENE to the house object of our study: 40% of "unconnected" electricity uses in the living room, 20% in the kitchen, 11% in bedroom 1, 15% in bedroom 2 (it includes a studio), 7% in each bathroom. With all the calibrated deterministic schedules implemented, a yearly simulation, from 1st January to 31 December 2012, was run for this model, here named "real schedule-real power" model. In Figure 2 the implemented weekly schedules for autumn season are displayed as an example.

The dwelling's yearly delivered energy simulation results were converted in primary energy, in order to assess the weight of use of lighting and equipment on the total energy balance. As defined by the AEEG, the Italian Authority for Gas, Electricity and Water, the considered primary conversion factor was 1 for natural gas and 2,18 for electricity

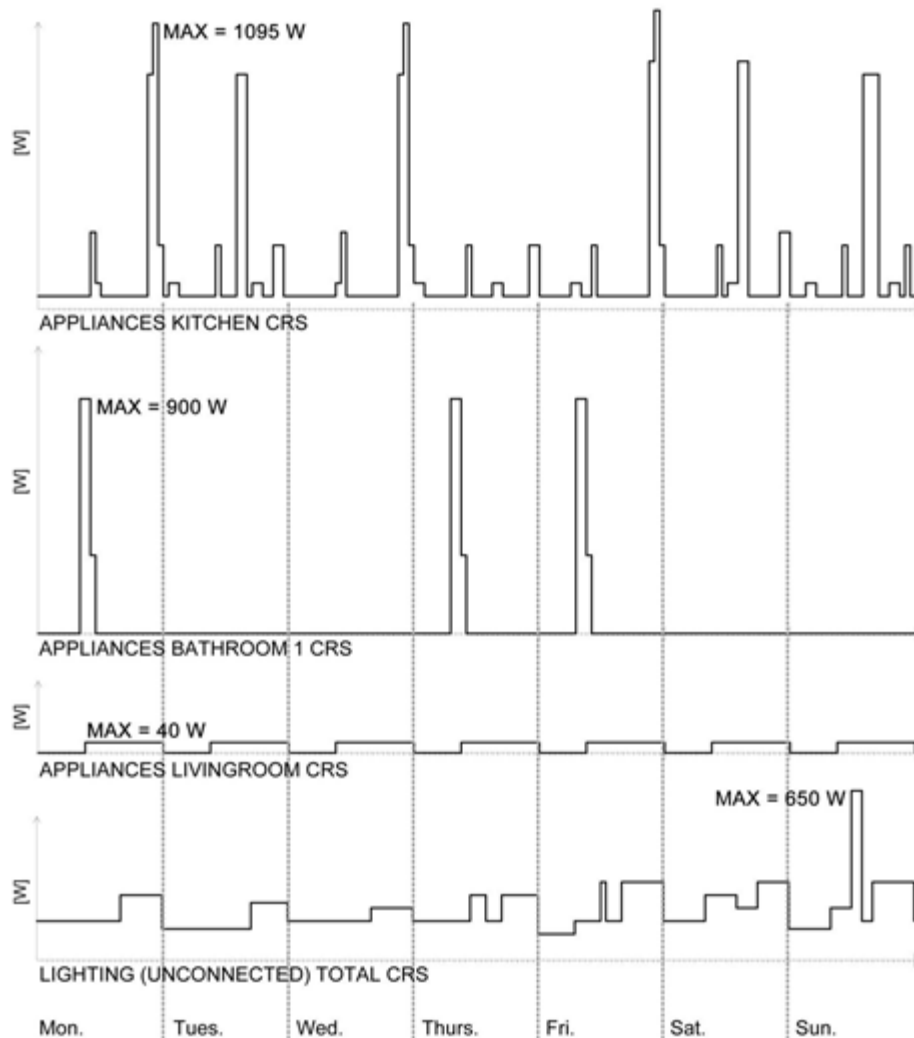


Figure 2: Weekly Calibrated Realistic Schedules for the use of smart and unconnected appliances in autumn.

3.2 Implementation of standard schedules from UNI/TS 11300

This section of the study aimed at verifying whether the schedules proposed by standards are appropriate for describing the actual energy consumptions related to the use of appliances and their effects on the building energy needs.

The Italian Standard UNI/TS 11300 was used as reference. This standard defines a common calculation methodology for assessing buildings energy performances and it is divided in 4 sections, each dealing with different aspects of the calculation process. Schedules for electric loads are given in UNI/TS 11300 Part 1, section 13 “Internal heat gains”. In residential buildings, internal gains from equipment (including lighting) and occupancy are defined as a single heat contribution normalized for the floor area (W/m^2), whose intensity varies according to the day of the week, the hour of the day and the room considered. Table 1 reports the standard schedule. Two levels of application of these schedules were tested in the building model of trial A.

First, just the schedules, intended as hourly variations of the fraction of a peak load, were applied to the actual peak loads monitored in each thermal zone of the flat and implemented

in IDA Ice. In Figure 3 the implemented schedules are displayed. Occupancy schedules were modified coherently and, with these inputs, a yearly simulation was run. This built model was named “standard schedule-real power”.

Then, both standard schedules and loads were implemented as schedules for equipment and occupancy in the model. To properly share the internal gains between occupancy and equipment, as required in IDA Ice, the heat produced by the occupants in each thermal zone was calculated (converting MET to W/m^2 and multiplying this value for $1,8 m^2$, the average human body area) and deducted from the total internal gains. The obtained internal gains are shown in Table 2. With these schedules implemented, shown in Figure 4, a yearly simulation for this model, named “standard schedule-standard power”, was run.

For each simulated model, the annual delivered energy was converted into primary energy by applying to the different energy carriers the Italian conversion factors defined by AEEG.

Table 1. Schedule for internal gains in residential buildings proposed by UNI/TS 11300.

Days	Hours	Kitchen, living room ($\Phi_{occ.} + \Phi_{equip}$)/ A_f [W/m^2]	Other rooms ($\Phi_{occ.} + \Phi_{equip}$)/ A_f [W/m^2]
Working days	7:00-17:00	8	1
	17:00-23:00	20	1
	23:00-7:00	2	6
Weekend	7:00-17:00	8	2
	17:00-23:00	20	4
	23:00-7:00	2	6

Φ_{occ} = internal gains produced by occupants

Φ_{equip} = internal gains produced by the equipment
 A_f = floor area

Table 2. Internal gains from equipment obtained referring the UNI/TS 11300

Days	Hours	kitchen	livingroom	bedroom 1	bathroom 1	bedroom 2	bathroom 2
		[W]	[W]	[W]	[W]	[W]	[W]
Weekdays	7:00-17:00	125	128	15	5	21	2
	17:00-23:00	313	319	15	5	21	2
	23:00-7:00	31	32	88	28	128	14
Weekend	7:00-17:00	125	128	29	9	43	5
	17:00-23:00	313	319	59	19	85	9
	23:00-7:00	31	32	88	28	128	14

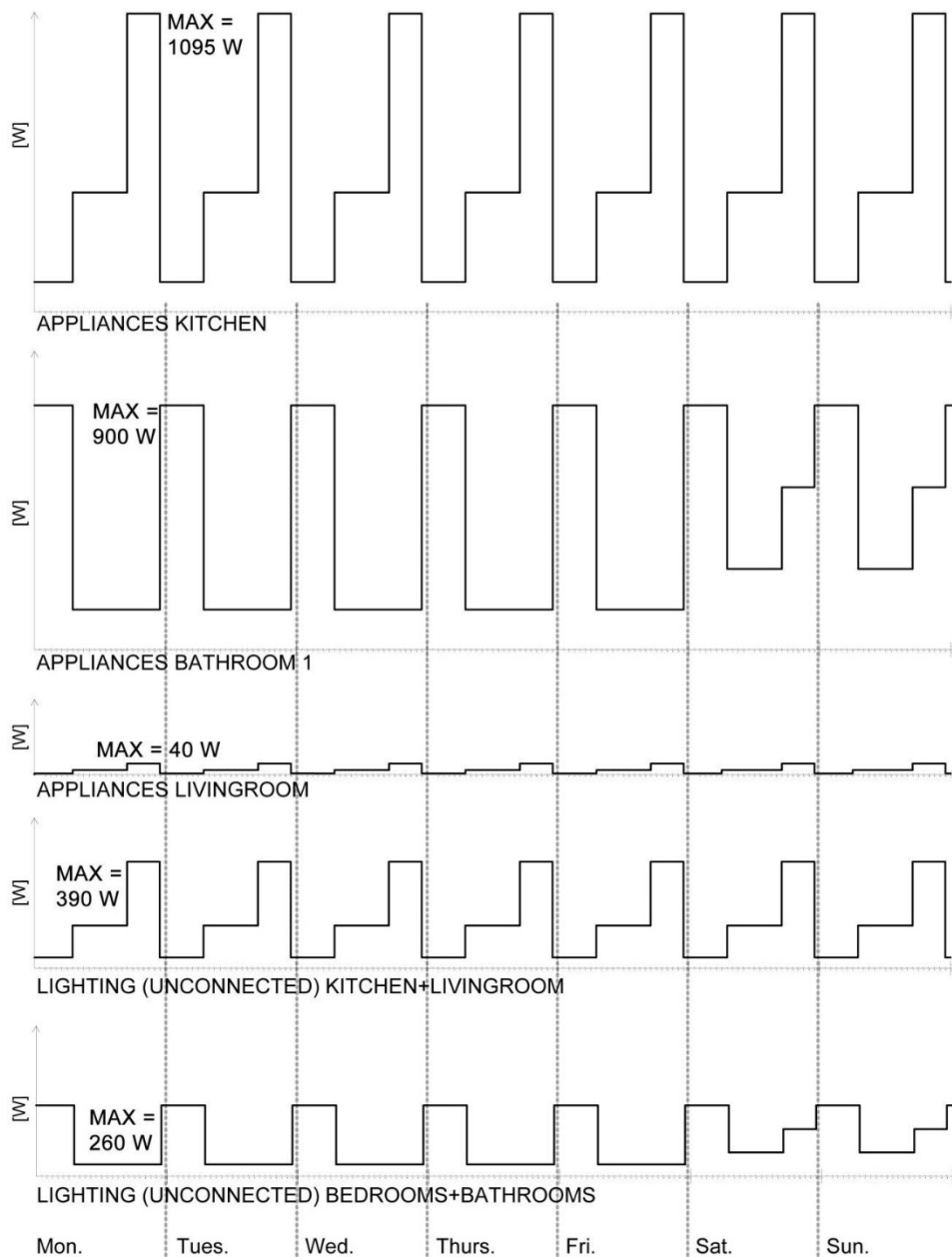


Figure 3. Weekly schedules for the use of appliances and lighting in the “standard schedule-real power” simulation model.

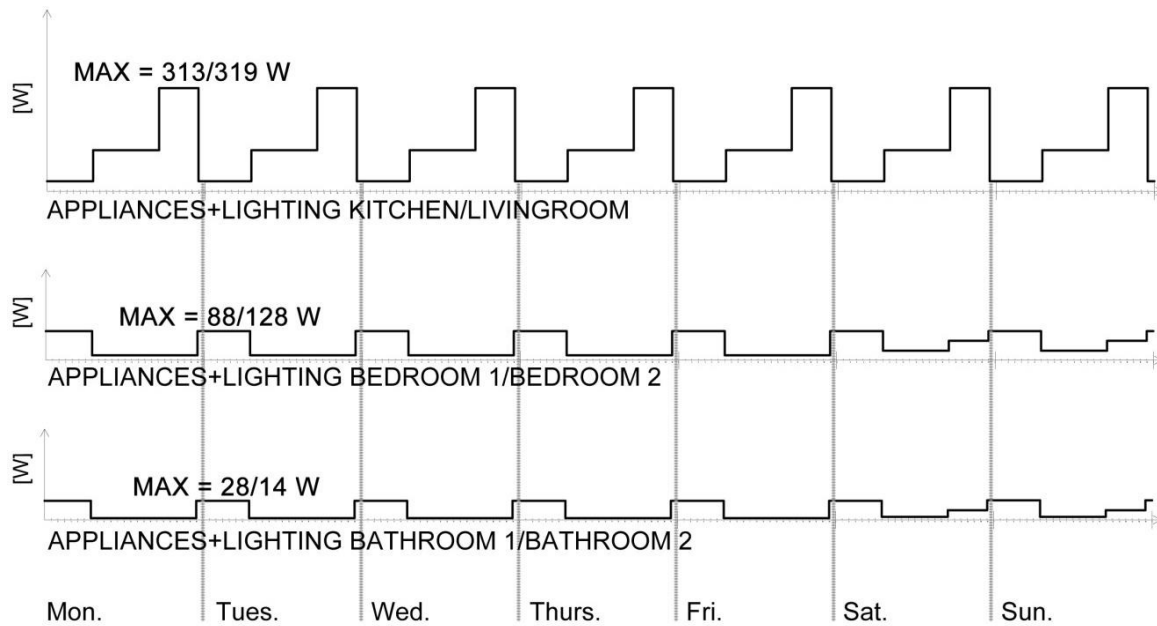


Figure 4. Weekly schedules for the use of appliances and lighting in the “standard schedule-standard power” simulation model.

4. RESULTS AND DISCUSSION

In this section, results of the two phases of the research are presented:

- 1) the results of the simulation model running the CRSs are compared to the monitored data and the relevance of electricity use on the total energy needs is shown;
- 2) the energy needs of the virtual model running CRSs (model “real schedule-real power”) are compared to the energy needs of the model using standard schedules (model “standard schedule-real power”) and standard schedules and power (model “standard schedule-standard power”).

4.1 Calibrated Realistic Schedules

Results concerning electric consumption coming out from the simulation run are indicator of the predictive power of the implemented CRSs; the closer they are to the monitored values, the higher the predictive power. Beside the gap between real and simulated electric consumption, the presence of recorded data and their reliability was object of analysis for the electronic meter.

On a yearly basis, 84% of the recorded data was considered valid (5% missing, 11% not reliable). The monthly percentage of invalid data is shown in Figure 7, in relation to the monthly monitored and simulated electric consumption. A connection between the percentages of unreliable data and the differences between predicted and monitored electric consumption comes out clearly.

Once the amount of valid data is defined, a more informed comparison between simulated and monitored electric consumption is possible. Simulated and monitored yearly electric consumption are compared; the discrepancies between the actual and the predicted values are highlighted in terms of total electric consumption in Figure 5 and divided in electric consumption for each thermal zones’ equipment and for all the unconnected appliances (here defined as “lighting”) of the whole flat in Figure 6.

The relevance of the electricity needs on the total energy needs of the house is shown in terms of primary energy in Figure 8: lighting and equipment cover 37% of the building primary energy demand.

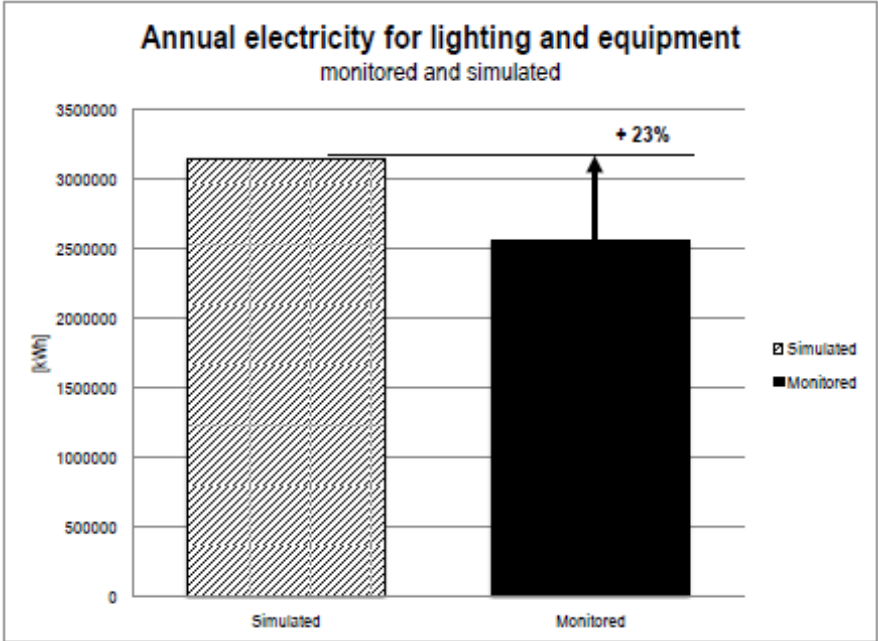


Figure 5. Total monitored and simulated annual electricity use for lighting and equipment in trial A.

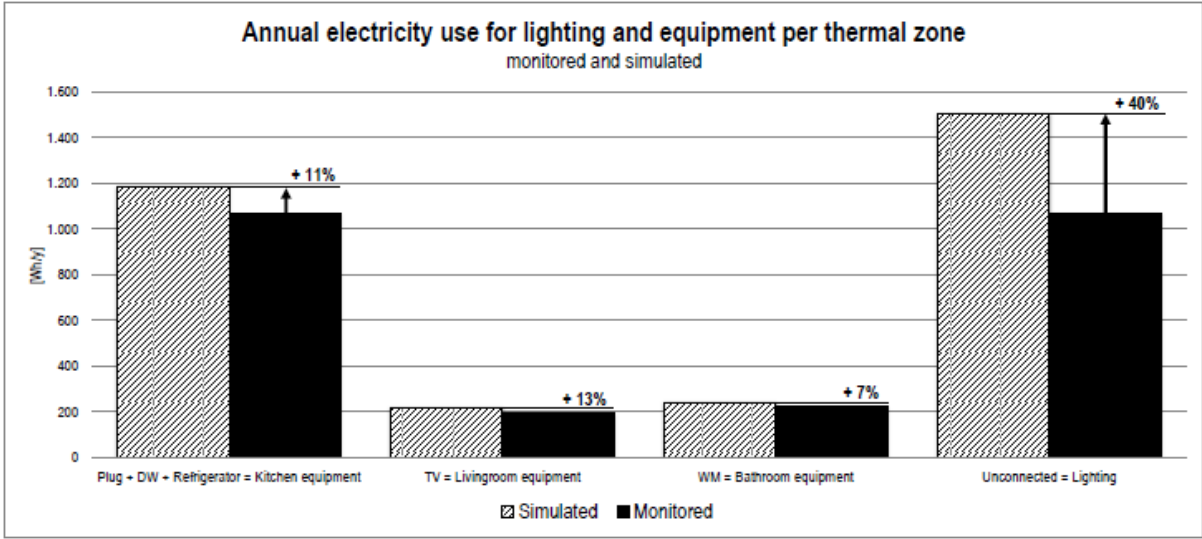


Figure 6. Monitored and simulated annual electricity use for lighting and equipment in each considered thermal zone of trial A.

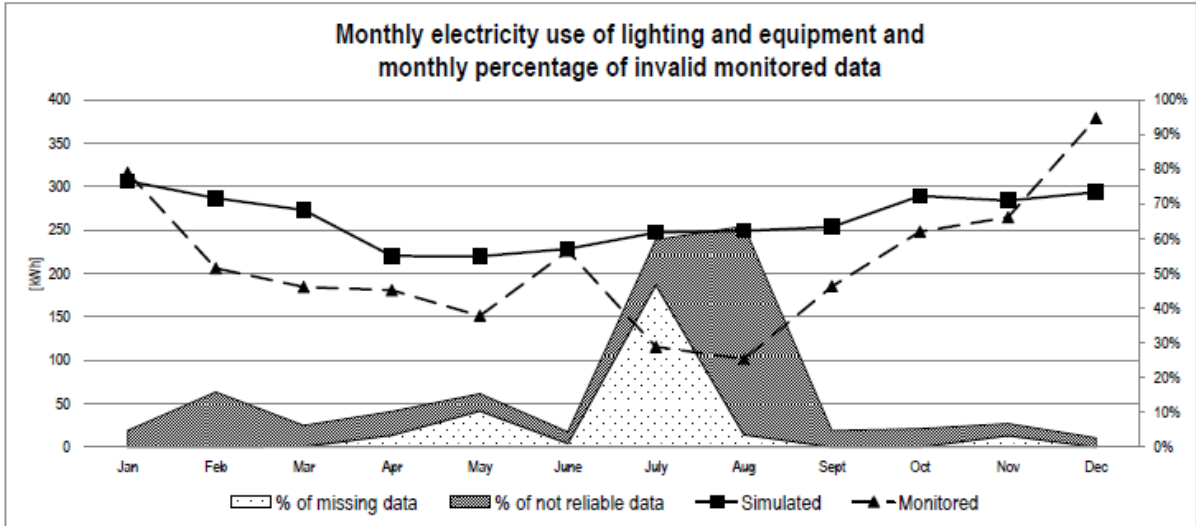


Figure 7. Monitored and simulated monthly electricity use for lighting and equipment of trial A, in relation to the amount of invalid data recorded.

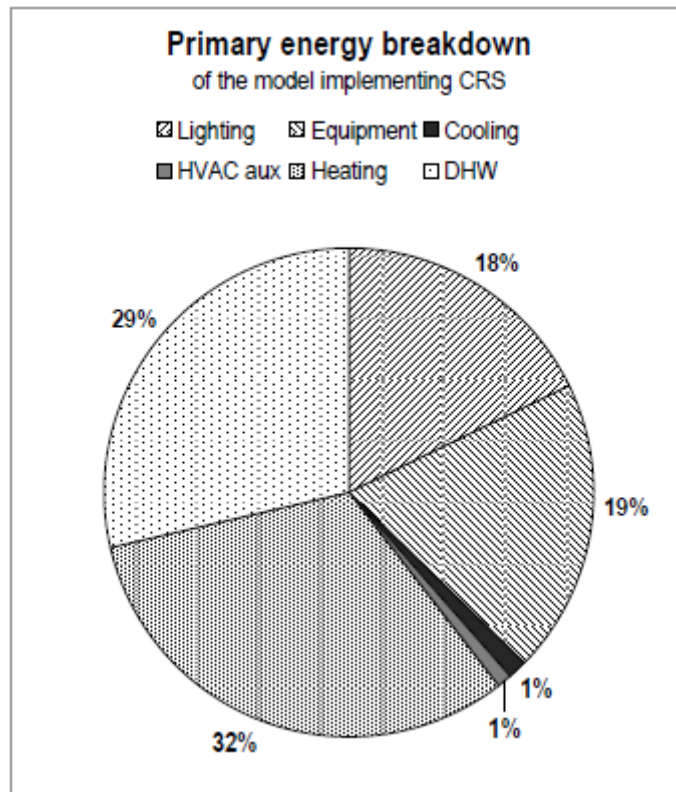


Figure 8. Primary energy breakdown on the “real schedule-real power” model.

4.1.1 Discussion

Observing Figure 5, the first general remark is that simulated electric consumption is higher than the monitored one. However, this evaluation method implies monitored data to be reliable and continuous. Nonetheless, during the monitoring campaign many tests on the installed

kit were performed and some unexpected problems were faced during the monitored period. Therefore observations about simulated VS. monitored electricity were coupled with information about the quality of the monitored data. This comparison allowed understanding that the mismatching was an expected outcome: while the simulated energy consumption covered the whole year, the monitored one missed some recordings.

Regarding the data availability, several but short holes in recordings, common to all the components of the kit, were detected. Dealing with data reliability, the only certain knowledge about the recorded data is that the electronic meter electric recorded values should always be higher than or equal to the sum of the electric loads of the smart appliances and plugs. This is the reason why detecting the amount of invalid data – missing or not realistic - coming from the monitoring campaign was possible only for the electronic meter.

Figure 7 shows the widest gap between simulated and monitored data when the percentage of missing and invalid monitored data is the highest (July and August). In July the difference of 132 kWh between simulated and real energy consumption is coupled with a total percentage of missing and invalid data of 60%; in August a difference in predicted and real electricity use of 148 kWh show up with a share of not consistent data of 64%. Excluding the electricity consumption for July and August, the simulated results over-estimate the actual energy consumption of a monthly average percentage of 24%.

As shown in Figure 6, in thermal zones where the CRSs were coincident with smart appliances – single or sum of them – schedules (TV=living room, washing machine=bathroom, dish washer+plug+refrigerator=kitchen), the CRSs' predictive power was high. On the opposite, the simulated yearly electricity consumption for unconnected appliances shows a significant discrepancy (+40%) with respect to the monitored data. Reasons for this gap have to be found both in the quality of the monitored data and in the method applied to create CRSs. Since the nature of the unconnected appliances is unknown, the schedules were based only on the calculation of average hourly values: results have proved that this method does not provide realistic prediction.

Figure 8, showing that 37% of primary energy needs of the simulated building are for lighting (18%) and equipment (19%), confirms the importance of taking into account these loads during the very first design stages, when a design energy rating is required. Moreover, it must be noted the presented energy breakdown refers to a dwelling with poor thermal properties, typical of the building type and year of construction (e.g. $U_{\text{external walls}}=0,59 \text{ W/m}^2\text{K}$). In new or renovated buildings, complying with stricter energy performance requirements, the percentage relevance of electric loads grows further.

4.2 Implementation of standard schedules from UNI/TS 11300

In order to investigate how realistic and standard schedules influence the simulated energy consumption of the same building, results of 3 simulation models – “real schedule-real power”, “standard schedule-real power”, “standard schedule-standard power” – were compared. The only differences among models were the implemented schedules for occupancy, lighting and equipment.

In Figure 9 the differences in yearly internal gains among the models are shown. The graph presents the different shares of internal gains due to equipment (appliances and lighting) and to occupants, in order to highlight the prevailing role of appliances and lighting. The biggest gap in prediction is shown in the “standard schedule-real power” model, where they are about 3 times higher than the “real schedule-real power” one. On the opposite, using standard

schedule and power provide quite similar electricity uses. The monthly equipment electricity consumption for each model is shown in Figure 10.

Additionally, aiming at verifying the influence of different schedules for the use of appliances and lighting on a building energy use, for the simulated models the total primary energy need and the percentage relevance of each energy use were calculated, as presented in Figure 11.

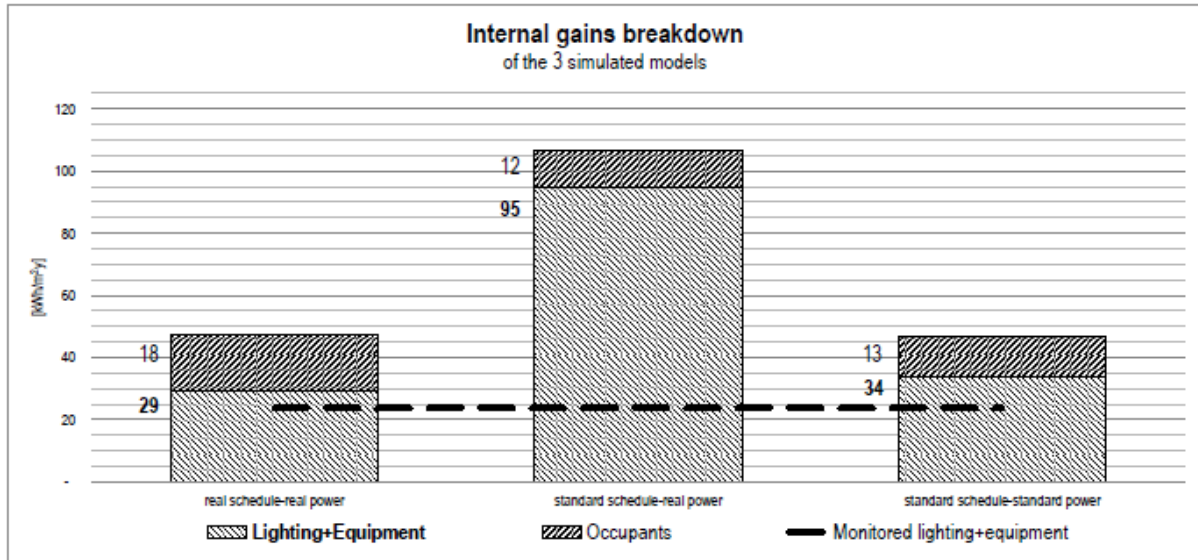


Figure 9. Internal gains from occupants, equipment and lighting for the 3 models “real schedule-real power”, “standard schedule-real power”, “standard schedule-standard power”.

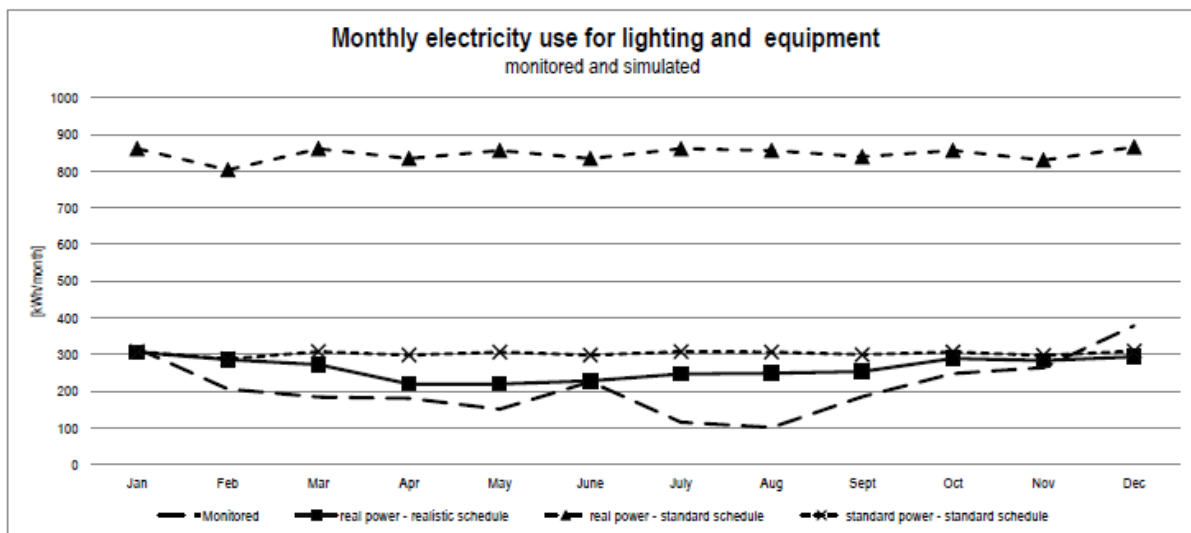


Figure 10. Monitored and simulated (3 models) monthly electricity consumption for lighting and equipment.

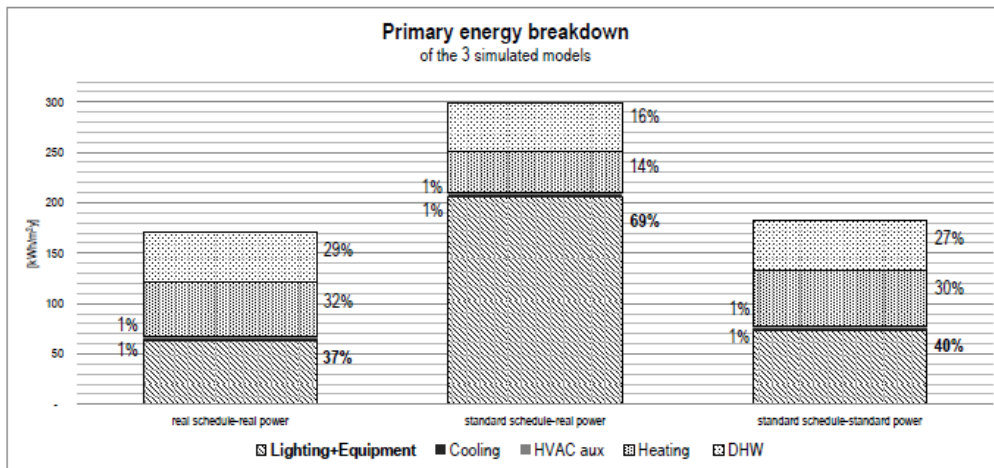


Figure 11. Annual primary energy breakdown and percentage relevance of each contribution to the total for the 3 models

4.2.1 Discussion

Results shown in Figure 9 suggest two different suitable strategies to follow for including equipment loads in the design stage: either standard values and standard power, or realistic schedules and real power should be implemented in simulation software to have realistic electricity prediction. Indeed, in the “standard schedule-standard power” model, used in the design stage energy rating, electricity consumption for equipment is 16% higher than the “real schedule-real power” one, which is an acceptable approximation. On the contrary, applying standard schedules to the actual installed power significantly overestimate the electricity energy uses (+223% with respect to the “real-real” model). Therefore, when detailed information about the house equipment are available, CRSs are more appropriate to estimate the actual energy consumption.

Accordingly, the total primary energy needs of the 3 simulated models, displayed in Figure 11, are slightly different between the “real-real” and the “standard-standard” models’ primary energy (+ 6%), and show a wider gap between the “real-real” and the “standard-real” ones (+ 75%). Besides the obvious variations in primary energy due to the use of the equipment - + 223% in “real-standard” and + 16% in “standard-standard” - the energy uses for heating and cooling are also varying because of the different internal gains.

Heating needs are almost unvaried in the “standard-standard” model (+1%) and are 25% lower in the “standard-real” one. Cooling needs increase respectively of 27% and 24% in the “standard-real” and the “standard-standard” model. It must be noted that the very similar cooling energy uses between these 2 models, having very different equipment internal loads, are due to the limited cooling capacity of the installed fan coil. In this naturally ventilated dwelling, the extra internal gains in the “standard-real” model are balanced with a 67% increase in the heat losses through infiltrations and openings.

Additionally, Figure 10, showing the monthly values of internal gains, highlights the reason for the increasing cooling needs in the models using standard schedule, which do not consider seasonal variation. Indeed, the schedule proposed by UNI/TS 11300 overestimates the equipment electricity consumption in spring and summer, leading to increased cooling needs. In the simulated buildings, the difference in cooling load from model “real schedule-real power” to the ones using standard schedules is about 25%, but in buildings with mechanical ventilation systems a more significant increasing can be assumed.

5. CONCLUSION

This study investigated a methodology to realistically predict the electricity uses for appliances in dwellings by means the implementation of Calibrated Deterministic Schedules (CDSs) in a simulation tool.

First, a method for creating deterministic schedules able to provide realistic prediction of a household's future energy related behaviour based on the household past behaviour, suitable for implementation in simulation software, was presented. The Calibrated Realistic Schedules, developed from the analyses of one year of monitored data in a dwelling, were tested through simulations and the simulations results gave a positive feedback to the method: even if the simulated total annual electric energy consumption differs from the annual monitored value of for 23%, this gap was caused mainly by the lack of consistent data and by the uncertainties in dealing with the monitored data for unconnected appliances. When data were available and the nature of the white good was known, the accuracy of the prediction was high, as proved by the very similar electric consumption for the simulated and the real use of the washing machine (simulated energy use 13% higher than monitored) and the TV (simulated energy use 7% higher than monitored).

From the authors' standpoint, this section of the study, creating specific behavioural patterns for a single family, is just an intermediate step toward the creation of energy use profiles typical of homogenous groups of users. Starting from the assumption that households with similar characteristics (family and house type) are likely to show similar energy consumption patterns (Guerra Santin 2011), the analysis of similar users' energy profiles will lead to the creation of normalized profiles related to the users' group.

The second step of the present study was to assess, once the CRSs were developed, the influence of different schedules for the use of appliances on a baseline simulation model. Delivered and primary energy of 3 models, using CRS and real loads, UNI/TS 11300 schedules and real loads and UNI/TS 11300 schedules and loads were compared. Results showed similar equipment electricity use (difference of 5 kWh/m²/year) and primary energy (difference of 11 kWh/m²/year) for the "realistic schedule-real power" and the "standard schedule-standard power" models. On the opposite, applying standard schedules to real installed power entailed more than doubled predicted electricity uses for the equipment. As a conclusion, values for usage times and power from UNI/TS 11300 are appropriate references for predicting the equipment energy uses at the design stage.

Beside the similar results obtained in models "real schedule-real power" and "standard schedule-standard power", this study pointed out the risk of oversizing the cooling system when using standard schedules and loads: these schedules do not take into account the lower use of equipment in summer, leading to higher predicted internal gains and consequent cooling needs.

On the authors' view, these findings open possibilities for further investigations on the topic, such as studying the influence of implementing these different schedules for use of equipment in a high performing building with mechanical ventilation, where internal gains plays an important role. Moreover, this study only proves the reliability of standard schedules in replicating the energy behaviour of a specific household type. It would be interesting to investigate whether the same results are obtained when analysing different household compositions (e.g. singles, old couples).

ACKNOWLEDGEMENTS

This work of Politecnico di Torino was partly supported by a grant of Telecom Italia in the context of the Italian initiative Energy@home. Authors wish to thank Telecom Italia for making available the description of the system, the monitored data and for fruitful discussions on the subject of this research.

REFERENCES

- Bourgeois D., Reinhart C., Macdonald I., Adding advanced behavioural model in whole building energy simulation: A study on the total energy impact of manual and automated lighting control, *Energy and Buildings* 38 (2006) 814-823.
- Corrado V., Ballarini I., Corgnati S. P., Talà N., Building Typology Brochure – Italy, TEBE Research Group, Energy Department, Polytechnic of Turin (December 2011).
- EN 15251:2007. Indoor environmental input parameters for design and assessment of energy performance of buildings- addressing indoor air quality, thermal environment, lighting and acoustics. CEN, Brussels.
- European Commission “EU energy trends to 2030” (2009) Publications Office of the European Union, Luxembourg. ISBN 978-92-79-16191-9.
- Guerra Santin O., Behavioural Patterns and User Profiles related to energy consumption for heating, *Energy and Buildings* 43 (2011) 2662-2672.
- <http://www.autorita.energia.it/it/index.htm>
- IDA ICE 4.6, Manual version 4.6 EQUA Simulation AB (2013).
- IEA Annex 53 Task Force. Final Report (2012), Total energy use in buildings- the modelling and simulation of occupant behaviour.
- Misure dei consumi di energia elettrica nel settore domestico. Risultati delle campagne di rilevamento dei consumi elettrici presso 110 abitazioni in Italia, Energy Department, Polytechnic of Milan (2004).
- Nicol J.F., Characterizing occupant behaviour in buildings: toward a stochastic model of occupant use of windows, lights, blind heaters and fans, Proceedings of the 7th International IBPSA Conference, August 13-15, 2001, Rio de Janeiro, Brazil.
- Papakostas K. T., Sotiropoulos B.A., Occupational and energy behaviour patterns in Greek residences, *Energy and Buildings* 26 (1997) 207-213.
- Raja I.A., Nicol J.F., McCartney K.J., Humphreys M.A., Thermal comfort: use of controls in naturally ventilated buildings, *Energy and Buildings* 33 (2001) 235-244.
- Rijal H.B., Tuohy P., Humphreys M.A., Nicol J.F., Samuel A., Clarke J., Using results from field surveys to predict the effect of opening windows on thermal comfort and energy use in buildings, *Energy and Buildings* 39 (2007) 823-836.
- UNI/TS 11300 – 1:2008. Prestazioni energetiche degli edifici. Determinazione del fabbisogno di energia termica dell’edificio per la climatizzazione estiva ed invernale. CTI, Rome.
- Wood G., Newborough M., Dynamic energy-consumption indicators for domestic appliances: environment, behaviour and design, *Energy and Buildings* 35 (2003) 821-841.

The Energy Performance Certification: A tool for smarter cities?

S. MONFILS¹, J.-M. HAUGLUSTAINE¹

⁽¹⁾University of Liege, Belgium

1. ABSTRACT

One of the existing tools that could help creating *smart cities* is the Energy Performance Certification (EPC) of residential buildings, by introducing energy efficiency as a comparative criterion for real-estate purchase choices, influencing real-estate market value, stimulating energy saving investments, moving the housing market towards greater energy efficiency and creating comprehensive databases which are fundamental for shaping smart strategies on urban, regional and national levels. The impact on potential buyers or tenants is crucial in order to reach these goals but EPC's results, in their actual form, do not help raise people awareness: often distant from reality, overestimating consumption, they usually result in a general misunderstanding and misuse of the document.

This study aims at verifying that the actual calculation method used in certification could approach real building consumption, by using additional data on occupant behaviour and household characteristics. It first presents the concepts behind smart cities, then an overview of the uncertainties that weight on the Belgian certification calculation method parameters. It also presents variations that could be applied to the EPC calculation method in order to add behavioural parameters... inspired from case studies of buildings.

Keywords: energy performance certification, behavioural patterns, smart city.

2. INTRODUCTION

A new strategic concept recently appeared on the European energy efficiency landscape: smart cities, defined as “cities well performing in governance, economy, environment, mobility, people and living, built on the ‘smart’ combination of endowments and activities of self-decisive, independent and aware citizens” (Giffinger, et.al, 2007).

In order to reach energy efficiency at any level, human factor is crucial: on one hand, efficient solutions (regarding transport, building energy consumptions, water and waste management...) have to be implemented by an intelligent decision-making authority who understands the complexity of the urban context and its impacts on environment. On the other hand, smart cities authorities need smart citizens, who are aware of their environmental impact, to use smart solutions to their full potential. In the field of residential use of energy, people are therefore a crucial parameter of both the problem and its solution.

“Against the background of economic and technological changes caused by the globalisation and the integration process, cities in Europe face the challenge of combining competitiveness and sustainable urban development simultaneously. Very evidently, this challenge is likely to have an impact on issues of Urban Quality such as housing, economy, culture, social and environmental conditions.”¹

European Union's strategy for a sustainable growth makes the building sector energy consumption reduction a central objective for meeting the commitments taken under the Kyoto protocol on climate change. At a worldwide scale, this sector is thus regarded as one of the most

¹ <http://www.smart-cities.eu>

cost-effective options for saving CO₂ emissions (IPCC, 2007). Newly built housing can obviously enter the “smart cities” frame more easily than the existing building sector, but a tool has been developed to target this potential: the European Union introduced (through the 2002/91/CE European Directive) Energy Performance Certificates (EPC), which should provide clear information about the energy performance of a building when it is sold or rented, including an assessment of the building energy performance and reference values, allowing performance comparisons between buildings. The EPC also includes recommendations for technically possible improvements. It is believed that the clear information given by the certificate should increase investments in energy efficiency, move the housing market towards greater energy efficiency, influence real-estate market value and help built up comprehensive benchmarking databases, which are fundamental for shaping smart strategies on a local (‘smart cities’), regional (‘smart regions’) and national levels.

The impact on potential buyers or tenants is therefore crucial in order to reach these goals. Two different families, living in two identical homes, would receive identical EPCs, but their real consumption would vary from one to three or four (CPDT, 2005), depending on occupants’ behaviour and household characteristics. The actual calculation method does not provide realistic results, and this is confirmed by energy bills; as a consequence, crossing several studies that have been led in Belgium (Vanparys et al., 2012), the UK (Laine, 2011; O’Sullivan, 2007) or in Germany (Amecke, 2012) allows us to draw general conclusions: the EPC is often considered unhelpful, unrealistic (and therefore mistrust), distant from reality, overestimating consumption, too long and technical, confusing...

This proves that, in order to achieve its goals, the EPC needs to be improved, by closing the gap between theoretical and real consumptions; this way, it can be understood, trusted and used by its owner.

3. UNCERTAINTY PARAMETERS OF THE EPC

The first step is to identify in the regulatory calculation method those uncertainty parameters that create a gap between calculated and measured consumptions and put the software precision into perspective. The idea here is not to question every parameter or to blame the calculation method, as it often results from a difficult balance between necessary parameters, precision possibilities and the time and cost required to make a full calculation. Any parameter could be pointed out as uncertain, as it is often the reflection of an average or a disadvantageous default value that secures best results when more precise information is available. The calculation method has been designed to compare buildings, not their users; this paper will focus on those general shortcuts that have been decided in order to withdraw human factor from equations.

First to be pointed out is the fundamental choice² that led to the use of a standardised consumption calculation method instead of a measured-data based method. Measured certification normalizes real consumption data in order to reach standardized energy consumption, using calculation parameters such as climate, building size and type, behavioural habits and pattern of use (EPBD, 2011³). Besides the need to divide the measured energy into its different uses, adjustments to standardised energy use can be a huge problem, as real consumption data are obviously greatly influenced by the behaviour of the occupants. In contrast, the calculated energy rating evaluates the performance using building characteristics

² The 2002/91/Ce and 2010/31/UE European Directives imposed domains of energy consumption that had to be considered, but left the choice of the calculation method and its details to the member states (or regions).

³ This source states that, in 2010, Sweden, Finland, Germany and Luxemburg used measured data. Every other country used calculated consumption to assess a building’s performance.

(as close to reality as possible), default values (when no accepted proof of a more accurate value is available) and standardized parameters (which cannot be replaced by more accurate values, even if they are known).

The Belgian regulatory calculation method uses, for outside climate, the average monthly temperature in Uccle (Brussels) for the last 50 years, preventing “unnecessary” geographical differentiation in such a small country. But variations do exist: there is a 3°C variation gap in the annual average temperatures of the main Belgian climatic station⁴; one can easily argue that the lower the outside temperature, the higher the energy consumption in order to reach the same indoor climate.

In order to “certify the building, not its users”, occupants’ behaviour, comfort and building occupation have been standardized: the whole dwelling is considered used at all times, and heated at a constant temperature of 18°C; though permanent occupation increases internal loads, it also extends heating periods and, therefore, energy consumption. Reality displays a complete range of behaviours, set temperatures and heating habits that are bound to influence greatly the final energy consumption. Examples of previous studies on behaviour – related residential energy consumption are given by P. O. Fanger (1977), J.-M. Hauglustaine (1979), L. Lutzenheiser (1993), H. Wilhite et al. (1996, 1998 and 2000), A.-L. Linden et al. (2005), G. Wallenborn (2006), De Groot et al. (2008) or, more recently, O. Guerra-Santin (2010) and B. Allibe (2012). These studies pointed metabolism, activity, gender and clothing amongst important comfort factors, provided insight into behavioural patterns (describing the inside climate as a rather energy-intensive heating habit) or showed variations in household behaviours, equipment rates and energy consumption.

The building being ideally empty of any occupancy, other ways of estimating behaviour-related consumptions have been imagined, such as domestic hot water (DHW, which should be based on the number of inhabitants and personal hygiene habits), ventilation rates (normally depending on household composition and windows opening habits) or internal gains (with no consideration for the level of equipment or human presence). Those consumptions are, indeed, evaluated on the basis of the protected volume only.

We will, in this paper, focus on the behavioural variables that could be added to the calculation method in order to close the gap between real and estimated consumptions.

4. SIMULATION

The study concentrates on three dwellings, each representing a widely spread building typology in Belgium. We created for these three dwellings an EPC with precision and respect to the regulation. Then we created “alternative” certificates by entering the calculation method and establishing different values for standardized parameters, in order to compare results.

4.1 Dwellings and households description

4.1.1 Apartment

The first dwelling is a two bedrooms apartment, located in a 1920’s building in Liege:

- Total heated floor surface (A_{ch}): 95 m² (walls included);
- Total heated volume (V_p): 330 m³ (walls, floor and ceiling included);
- Its envelope is composed of brick walls, concrete floors and ceilings and recent (2011)

⁴ www.meteobelgique.be

double glazed windows. The average envelope U-value (according to regulatory calculation method) is 2.2 W/m²K;

- There is no ventilation system; the owner, however, opens his windows quite often, even during winter (at nights). An extractor hood in the kitchen exhausts vapour when preparing meals;
- The system producing heat and domestic hot water is an old (1985) shared (between ten flats) oil-fired boiler (the EPC considered a 68% efficiency for heat production, 40% for hot water production); a non insulated hot water loop with a very low efficiency (30%) worsens the global efficiency. There is no thermostat in the dwelling, so that the owner heats up the place with only reference to his comfort, and shuts down the system at night (or when opening windows).
- It is occupied by a single person, who works full-time outside of his apartment (only heating in the evenings during the winter weeks), but is often present in the week-ends. He is aware of his environmental impact and tries to limit his consumption. The heating is usually completely shut down from May to October.
- He owns a relatively high number of electrical equipment, but he tries to completely shut some of them down when possible.

The results of the regulatory calculation indicate a total primary energy consumption of a 148,933 MJ per year (which represents a specific primary energy consumption of 433.4 kWh/m²

- labelled F on the EPC scale - or an equivalent fuel consumption of 3,835 litres per year).

The real average consumption however (which data could only be collected for the three previous years), is approximately five times lower (around 800 litres of fuel per year).

4.1.2 Detached house

The second dwelling analysed in this study is a more recent (1985) detached house, in the suburbs, quite representative of the post-WWII extra-urban development, representing about 15% of the Walloon housing (Monfils and Hauglustaine, 2013). It has:

- A total heated floor surface (A_{ch}) of 205 m² (walls included);
- A total heated volume (V_p) of 517 m³ (walls, floor and ceiling included);
- An envelope composed of cavity walls (with unknown presence of insulation – the default value considers them to be slightly insulated, due to the building date), concrete floor (insulated with 4 cm of expanded polystyrene), well insulated roofs and ceilings (20 to 24 cm of mineral wool witnessed by the certifier) and double glazed windows (from different manufacture dates). Its calculated global average U-value is 1 W/m²K.
- An incomplete ventilation system (only natural extraction from both bathrooms).
- A rather recent (yet high temperature) oil-fired boiler producing heat and domestic hot water heating system (global efficiency: 66.4% for heat production, distribution, emission and storage, 65% for hot water); a thermostat, placed in the living room, monitors the temperature and insures a constant 21°C in winter days, 16°C in winter nights. There is also a wood-supplied fireplace, which the owners like to use in winters and mid-seasons.

In this house lives a family of four (father, mother and 2 children). The father works out of home, the children go to school (away from home from 8 AM to 4 PM in average, even on Wednesdays, when they go to sport activities) and the mother works outside of home also, but is present when her children are. They consider their house well insulated and heat for comfort.

They usually use the boiler for heating from October to May (included), and use the fireplace as extra, also in mid-season periods if needed. But they would not give specific periods of non-heating, for “it depends too much on Belgian weather”.

The regulatory certification would present an annual theoretical consumption of 299.4 kWh/m² (221,727 MJ or 5,703 litres of fuel-equivalent), which classes this building at the D level of the certificate scale.

The real consumption data, relating to the last ten years, reveals a real consumption around 2,500 litres a year (around 25,000 kWh). The regular use of wood in the fireplace (around 1 ton a year) adds another 3,500 kWh⁵ to the total (28,500 kWh or 140 kWh/m².yr).

4.1.3 Row house

The third dwelling, which also represents around 15% of Walloon dwellings, is a three bedrooms row house, built in the early 1970's:

- It has a total heated floor surface (A_{ch}) of 225 m², for a total heated volume (V_p) of 612 m³. These unusually high values (for this kind of typology) translate the inclusion of basement rooms, indirectly heated through the open staircase;
- This building has been slightly renovated on several occasions. As a result, (relatively thin) layers of insulation here and there improve the overall thermal efficiency (the average envelope U-value is 1.6 W/m²K).
- The only ventilation system is a mechanical extractor in the bathroom. Attention is paid to close windows when the heating is on.
- The heating (and hot water producing) system is a rather new condensation boiler (global heat system efficiency: 80%; global hot water system efficiency: 75%); a thermostat is set to keep the temperature at 16°C during cold nights and 21°C during cold days; an external probe measures outside temperature and communicates with the boiler. A wood fireplace is present in the living room, as an extra heating source.

It is occupied by a family of four people as well, with grown-up children (one of which leaves the house for the whole week, but was present for the period covered by the real consumption data). Both parents work full-time, the mother being there for her children after school. They are environment-conscious and careful about their consumption.

Its calculated annual consumption rises to 3,609 litres of fuel-equivalent (or 152,229 MJ), whereas the real consumption reaches 2,000 m³ of natural gas and around 1 ton of wood per year. The announced specific consumption, 188.5 kWh/m², would credit the building with a C label on the official scale.

4.2 Tool

This study uses the regulatory EPC calculation method (Wallonia, 2013) provided by the Walloon public administration in charge of the certification, for the simulations. The only official tool implementing it, however, does not allow any modification: we therefore used an Excel sheet. This tool was initially developed, before EPBD implementation, to help voluntary architects to undertake an early evaluation of their clients' house performances, in exchange for advice and subsidies in the “Building with Energy... Naturally” action frame, set up since 2004 by Wallonia in order to introduce the building sector with the EPB regulations). The sheet has been modified to stick to the certification calculation method, and is used in parallel with the

⁵ Considering 1kg of wood supplies 3,5kWh (<http://www.apere.org/index/node/41>)

been modified to stick to the certification calculation method, and is used in parallel with the official certification software (for U-values or system efficiency default values, for example). For each of the following parameter variation, the modifications proposed to the equations will be explained.

4.3 Modification of the calculation method

In this next part, we will develop the method used to introduce new parameters in the calculation method, such as the “real” inside set temperature and outside climate, the equipment rate (influencing internal gains and electricity consumption) or the occupation rate of the building, which influences heating periods and internal gains calculation.

4.3.1 Climate and location

Climate can (even in small Belgium) be dependant on the location, and it obviously influences heating habits and real annual consumptions. It seems therefore important to assess the variation gap brought by the “single climate zone” hypothesis, using more realistic climates from cities closer to the actual location of the studied dwellings: Spa for the row house, Liege (Bierset) for the others. The data, given by the official Belgian weather forecast website⁶, correspond to the years for which we possess real consumption data.

In the official calculation method (Wallonie, 2013), the targeted parameter is $\theta_{e,m}$, the average monthly outside temperature. The table hereunder shows the official values (1st line) and the average (between 2003 and 2013) temperatures in Spa and Liege. In the following graphs, monthly temperature of each year have been used in calculations, in order to compare with real consumption data.

Table 1: Average monthly temperature comparison

Average monthly temperature $\theta_{e,m}$ [°C]	Jan	Feb	Mar	Apr	May	Jun	Jul	Aug	Sep	Oct	Nov	Dec
Uccle (official)	3.2	3.9	5.9	9.2	13.3	16.2	17.6	17.6	15.2	11.2	6.3	3.5
Spa (average 2010 to 2012)	0.2	-0.1	5.4	8.7	11.6	14.6	16.2	16.2	13.1	9.3	5.5	0.7
Liege (average 2010 to 2012)	2	1.6	6.9	10.2	13.1	16.4	18.2	17.9	14.7	10.9	6.9	2.4

4.3.2 Internal gains

It is widely acknowledged that inhabitants (their number, habits and equipment) influence the consumption (EPBD, 2011; Hauglustaine, 1979; Hauglustaine, 2002; Guerra Santin, 2010) by increasing heating and Domestic Hot Water (DHW) demand, as well as internal loads; these last are composed of metabolic loads (depending in reality on the occupation rate, clothing, activities...) and equipment loads (mainly depending on the equipment level and devices efficiencies).

In the official calculation method, internal gains vary linearly with the protected (heated) volume; the monthly internal loads (from both metabolisms and equipment) are evaluated as follows:

$$Q_{i,seci,m} = (0,67 * VPER + 220) * t_m * V_{sec,i}/VPER \quad (1)$$

⁶ www.meteobelgique.be

With:

- $Q_{i,seci,m}$: the monthly internal gains for the energy sector 'i' [MJ];
- V_{PER} : the protected volume of the dwelling [m³];
- $V_{sec,i}$: the protected volume of the energy sector (part of the unit heated and cooled by the same systems) [m³];
- t_m : the length of the month [Ms].

The proposition in this study consists in taking a more realistic approach on the evaluation of internal loads, considering electrical equipment, lighting and dwelling occupation. For each of the houses, a small questionnaire to the occupants allowed to set up the list of actual equipment that are used in the dwelling, as well as all other parameters that will be discussed below (number of inhabitants, heating patterns...).

Equipment

Only main appliances were considered here: fridges, freezers, electric hobs, ovens, dishwashers, microwaves ovens and extractor hoods in the kitchen; washing and drying machines, irons and vacuum cleaners in the laundry; televisions, computers and others entertainment devices in the living room. Their annual consumption has been evaluated (see table 2) according to literature (Hauglustaine, 1979; Sidler, 1998), technical product specifications from commercial websites, average power values and use patterns⁷. In order to consider the consumption due to other small appliances, occasional uses and sleep modes, a consumption of 100 kWh/year + 25 kWh/person.year is added to the total. By hypothesis, we considered that the whole installed power takes part in the internal loads. The complete list can be seen in the table below.

Some appliances are used all year round, others on very occasional times. For most of them however, the size of the chosen device or use pattern can depend on the number of inhabitants, the area of the dwelling (influencing the use of the vacuum cleaner for example) or the tendency to adopt environment-friendly behaviours (which can be obtained from the questionnaire). These parameters were taken into account for the consumption evaluation.

For each case study, the sum of every appliances consumptions is therefore made considering the questionnaire each household filled, then the corresponding daily internal loads are evaluated as follows:

$$Q_{E,d} = (C_A * t_d * 1000)/N_h \quad (2)$$

With:

- $Q_{E,d}$: the daily internal loads due to the equipment [J];
- C_A : Sum of every appliances consumptions [kWh/year];
- t_d : the length of the day: 86400 seconds.
- N_h : the length of the year: 8760 hours

⁷ www.energuide.be; www.curbain.be;
<http://documentation.bruxellesenvironnement.be>; www.lesnumeriques.com;
<http://energie-developpement.blogspot.be>;

Table 2: Calculation of the equipment-related internal loads

EQUIPMENT	Average power [W]	Considered use pattern		Consumption			Case studies consumptions [kWh/yr]			
		Fixed	Variable	Per cycle [kWh/cycle]	Annual		Apartment	Detached house	Row house	
					[kWh/yr]	[kWh/pers.yr]				
Fridge A+++ (with freezer)		continuous				117	9			
Fridge A++ (with freezer)		continuous				169	14			
Fridge A+ (with freezer)		continuous				212	19		288	288
Other fridges		continuous				277	25	302		
Electrical hobs	1500	15 min/day	5 min/pers.day			130	45		310	310
Separate freezer A+++		continuous				74	14			
Separate freezer A++		continuous				165	16		229	
Separate freezer A+		continuous				205	18			
Other freezers		continuous				300	20			380
Dishwasher A+++			1 cycle/pers.week	0.83			42			
Dishwasher A++			1 cycle/pers.week	0.92			46		184	
Dishwasher A+ ou A			1 cycle/pers.week	1			50			
Other dishwashers			1 cycle/pers.week	1.2			60	60		240
Microwaves ovens	900	30 min/week	10 min/pers.week			22	8	30	54	54
Oven	2500	30 min/week	10 min/pers.week			60	20	80	140	140
Extractor hood	120	15 min/day	5 min/pers.day			11	4	25	37	37
Washing machine A+++		1 cycle/week	1 cycle/pers.week	0.85		43	43		215	
Washing machine A++/A+		1 cycle/week	1 cycle/pers.week	1		50	50	100		250
other washing machine		1 cycle/week	1 cycle/pers.week	1.2			120			
Dryer A+++	32 weeks/yr		1 cycle/pers.week	1.43			45.8			
	50 weeks/yr		1 cycle/pers.week					71.5		
Dryer A++	32 weeks/yr		1 cycle/pers.week	1.75			56			
	50 weeks/yr		1 cycle/pers.week					87.5		
Dryer A+	32 weeks/yr		1 cycle/pers.week	2.25			72		288	
	50 weeks/yr		1 cycle/pers.week					112.5		
Dryer A	32 weeks/yr		1 cycle/pers.week	3.7			118.4			
	50 weeks/yr		1 cycle/pers.week					185		
Other dryers	32 weeks/yr		1 cycle/pers.week	4			128			512
	50 weeks/yr		1 cycle/pers.week					200		
Iron	2400	1 hr/week	30 min/pers.week			120	60	180	360	360
Vaccum cleaner	1820		1 min/m ² .week			1,52 *		115.5	250.2	272.8
Television (new, flat)	50	20 h/week				50		50	50	50
Television 2 (old, flat)	100	20 h/week				100				
Television (cathod screen)	150	20 h/week				150				
Flat screen computer	130	20 h/week				130				
Cathod screen computer	150	20 h/week				150				
Laptop	25	20 h/week				25		25	25	100
(TVD/ADSL) decoder	25	20 h/week				25		25	25	25
Wi-Fi/TV/Telephone router	20	continuous				175.2		175.2	175.2	175.2
OTHERS (small appliances, occasional uses and sleep modes)						100	25	125	200	200
* : kWh/m ² .yr						TOTAL	[kWh/yr]	1292.7	2830.4	3394
							[W/m ²]	1.55	1.57	1.73

Occupation pattern

The occupation pattern influences heating and lighting periods (see below) as well as internal gains. 4 different patterns of use have been proposed to the users, and internal loads have been evaluated in accordance:

- Pattern 1: someone is present the whole day, which is then split between 8 hours of sleep, 1 hour of family morning presence, 10 hours of “light work” during the day and 5 hours of family evening presence.
- Pattern 2: someone is present half the day, which is split between 8 hours of sleep, 1 hour of family morning presence, 4 hours of “light work” at home, 6 hours of absence and 5 hours of family evening presence.

- Pattern 3: the household is present 8 hours a night (sleep), 1 hour in the mornings and 5 hours in the evenings; the house is empty of occupants for 10 hours a day.
- Pattern 4: the house is considered unoccupied for 14 hours a day, the household being there 1 hour in the mornings, 1 hour in the evening, and 8 hours at nights.

Users were asked, in the questionnaire, to describe an average week using these four patterns; the number of days a week corresponding to each pattern is then used to calibrate monthly loads. For each period (sleep, morning presence, day presence, absence and evening presence) of each pattern, internal loads are evaluated as follows:

$$Q_{O,i,j} = P_{O,i,j} * N_{O,i,j} * t_{O,i,j} \quad (3)$$

With

- $Q_{O,i,j}$: the internal gains due to occupation patterns, during the period 'i' of the pattern 'j' [J];
- $P_{O,i,j}$: the load due to the metabolism of the person present during the period 'i' of the pattern 'j' (ISO 7730: 2005):
 - o $P_{O,i,j} = 80$ W/person at night;
 - o $P_{O,i,j} = 100$ W/person during mornings and evenings;
 - o $P_{O,i,j} = 120$ W/person during daytime;
- $N_{O,i,j}$: the number of occupants present during the period 'i' of the pattern 'j' [-];
- $t_{O,i,j}$: the length of the period 'i' of the pattern 'j' [s].

Then, adding periods of a pattern 'j':

$$Q_{O,T,j} = \sum_i Q_{O,i,j} \quad (4)$$

With $Q_{O,T,j}$: the daily total internal gains due to the pattern 'j' of occupation [J]. Finally, using the number of days a week corresponding to each pattern:

$$Q_{O,T,a} = \sum_j Q_{O,T,j} * N_{d,j}/7 \quad (5)$$

With :

- $Q_{O,T,a}$: the daily average internal gains due to occupation [J];
- $N_{d,j}$: the number of days a week corresponding to the pattern 'j' [-].

Lighting

Lighting is not usually evaluated in residential EPB calculation, believed to be rather insignificant with regards to other energy uses. It is, however, part of electricity bills; in order to ease comparisons between measured and calculated consumptions, it has been decided to include it in the calculated results. The default installed power, used in non residential calculations, is 20 W/m², which is considered far above real installations. A more realistic approach has been inspired by (CSTC, 2011) and (SPW, 2013), considering several installations efficiencies and average rooms areas. Some rooms are obviously better provided with natural light, some need more artificial installations; these first results rely more on statistical average: very efficient, minimal installations have an average 3 W/m² artificial lighting power, whereas less efficient installations see their power rise to 8 W/m².

The importance of natural light also influences the number of hours during which artificial lighting is needed. In Liege, the year is shared between 4474 hours and 15 minutes of daylight,

and 4285 hours and 45 minutes of night⁸. Considering 3 annual weeks of absence (2 in the summer, 1 in the winter) and sleep hours (8 hours a night for the remaining 344 days), this leads to 1307 hours and 30 minutes of darkness a year that has to be artificially illuminated. Calculation to obtain an equivalent fixed power value for the whole year is as follows:

$$P_L = P_r * N_{h,l}/N_h \quad (6)$$

With:

- P_L : the equivalent fixed lighting power, considered used the whole year [W/m^2];
- P_r : the realistic installed power, according to installation efficiency [W/m^2];
- $N_{h,l}$: the number of hours during which artificial lighting is needed: 1,307.5 hours/year.
- N_h : the length of the year: 8,760 hours.

This gives, for the three case studies, an equivalent fixed power value of 0.6 W/m^2 for the apartment, 0.75 W/m^2 for the row house and 0.9 W/m^2 for the detached house. The corresponding internal gains are evaluated as follow:

$$Q_L = P_L * A_{ch} * t_d \quad (7)$$

With:

- Q_L : the daily internal gains due to artificial lighting [J];
- A_{ch} : the heated floor area, as defined in the regulatory calculation method (Wallonie, 2013) [m^2];
- t_d : the length of a day: 86,400 s.

Internal gains

These three components are added as follows, to represent the average internal gains corresponding to the occupation pattern distribution, equipment and lighting:

$$Q_{I,a,d} = Q_E + Q_{O,T,a} + Q_L \quad (8)$$

With $Q_{I,a,d}$: the average total daily internal gains due to equipment, occupation and lighting [J]. The value for each month is obtained thus:

$$Q_{I,a,m} = Q_{I,a,d} * N_{d,m} * 10^{-6} \quad (9)$$

With:

- $Q_{I,a,m}$: the monthly internal gains due to occupation patterns, electric equipment and lighting habits [MJ].
- $N_{d,m}$: the number of days in the month (taking winter and summer vacations into account).

Here are the final results for $Q_{i,seci,m}$ and $Q_{I,a,m}$:

Apartment:

- Official loads: $Q_{i,seci,m} \in [1,066 \text{ MJ}, 1,180 \text{ MJ}]$
- Calculated loads: $Q_{I,a,m} \in [548 \text{ MJ}, 686 \text{ MJ}]$

Detached house:

- Official loads: $Q_{i,seci,m} \in [1,369 \text{ MJ}, 1,516 \text{ MJ}]$

⁸ www.ephemeride.com

- Calculated loads: $Q_{I,a,m} \in [1,024 \text{ MJ}, 1,323 \text{ MJ}]$

Row house:

- Official loads: $Q_{i,seci,m} \in [1,524 \text{ MJ}, 1,687 \text{ MJ}]$
- Calculated loads: $Q_{I,a,m} \in [1,002 \text{ MJ}, 1,295 \text{ MJ}]$

The lower calculated values can be explained by a single occupant in the apartment and out-working occupation patterns.

Table 3: calculation of the internal loads for the row house

Total internal heat gains - row house								
Patterns of use	$N_{d,j}$	Description	$t_{o,i,j}$	$N_{O,i,j}$	$P_{O,i,j}$	P_L	P_E	$Q_{I,a,d,j}$
	[-]		[s]	[-]	[W]	[W/m ²]	[W/m ²]	[J]
Pattern 1	1	8h sleep	28,800	4	320	0.75	1.73	16,033,421
		1h morning presence	3,600	4	400	0.75	1.73	2,292,178
		10h day presence	36,000	4	480	0.75	1.73	25,801,776
		5h evening presence	18,000	4	400	0.75	1.73	11,460,888
		Daily total	86,400					55,588,263
Pattern 2	1	8h sleep	28,800	4	320	0.75	1.73	16,033,421
		1h morning presence	3,600	4	400	0.75	1.73	2,292,178
		4h day presence	14,400	4	480	0.75	1.73	10,320,710
		6h absence	21,600	0	0	0.75	1.73	5,113,066
		5h evening presence	18,000	4	400	0.75	1.73	11,460,888
Daily total	86,400					45,220,263		
Pattern 3	5	8h sleep	28,800	4	320	0.75	1.73	16,033,421
		1h morning presence	3,600	4	400	0.75	1.73	2,292,178
		10h absence	36,000	0	0	0.75	1.73	8,521,776
		5h evening presence	18,000	4	400	0.75	1.73	11,460,888
		Daily total	86,400					38,308,263
Pattern 4	0	8h sleep	28,800	4	320	0.75	1.73	16,033,421
		1h morning presence	3,600	4	400	0.75	1.73	2,292,178
		14h absence	50,400	0	0	0.75	1.73	11,930,486
		1h evening presence	3,600	4	400	0.75	1.73	2,292,178
		Daily total	86,400					32,548,263
Presence/absence ratio [s]		403200	201,600				$Q_{I,a,d} = 41,764,263$	

In the official calculation method, these loads (added to solar gains), are tamed by a reduction factor, $\eta_{util,heat,seci,m}$, the monthly heat gains application rate. It depends on the heat losses (through thermal envelop and ventilation) and heat gains ratio, and applies the following principle: when losses diminish and gains increase (in summer), the internal loads will be less used than in cold weather conditions: occupants use windows openings to regulate their indoor thermal comfort under overheating, so that the air renewal is larger than the fixed constant value used in the calculation. It has been decided to keep that part of the calculation method, taking the new internal gains into account to calculate that factor.

4.3.3 Heating habits

Heating period

In order to adapt the calculation method to a more realistic, behaviour based approach, the next step is, obviously, to consider the heating patterns of the users. In the official approach, the heat is turned on when needed, in order to obtain an inside temperature of 18°C, day or night, which

can even lead to a heating consumption during the summer. In reality, dwellings are obviously not heated all day, let alone all year round. In the Belgian temperate climate, heating systems are often shut out from May to September included (depending, of course, on the climate, the building characteristics and the occupants' comfort). This hypothesis will be considered here, since this particular enquiry was missing from the "beta version" questionnaire filled by the owners. Knowing the occupation patterns, it is however easy to extrapolate daily heating patterns and average number of heating hours per day. This last data is obtained using the presence/absence ratio, as visible in the table 3 above. The number of seconds in a month (t_m in the official calculation method, see above Eq. 1) can be split between three terms:

$$t_m = t_{m,h} + t_{m,lh} + t_{m,nh} \quad (10)$$

With:

- $t_{m,h}$: the number of seconds during which the heat is on [Ms];
- $t_{m,lh}$: the number of seconds during which the set temperature is lowered [Ms];
- $t_{m,nh}$: the number of seconds during which the heat is shut out [Ms].

Set temperature

Some people tend to heat less because of low income, environment-friendly behaviour or low-temperature comfort standard (Guerra-Santin, 2010); others tend to heat more (for obvious and opposite reasons). Some people heat the whole house; others only specific rooms (living room, bathroom...). Some need a strict and define comfort temperature; others tolerate a wider range of them. The definition of a comfort temperature is quite hard, as it depends on many parameters, among which the air temperature and average walls temperature, activity, clothing (Fanger, 1977), gender or even the time elapsed since the occupant last ate... When no thermostat allows precise temperature control, people are often not able to tell whether they heat to reach 18 or 22°C. They just seek sensible comfort, which could therefore fluctuate.

All those parameters of comfort are difficult to apprehend in a questionnaire. Thus, this calculation method will use simple data:

- Both houses owners announced the use of a thermostat, set to 21°C when inhabitants are present, and 16°C otherwise. Both set temperatures have to be integrated in the calculation method; they will referred below as " $T_{set,max}$ " et " $T_{set,min}$ ".
- The apartment owner does not have a thermostat, and is therefore heating his home with deemed comfort for only parameter. The widely accepted average comfort temperature of 20°C will be adopted for this dwelling.

Equations

The set temperatures being integrated early (from the heat losses calculation) in the calculation method, the modifications have to be made in consequences.

The heat losses through envelope are evaluated as follows in the official method:

$$Q_{T,heat,seci,m} = H_{T,heat,seci} * (18 - \theta_{e,m}) * t_m \quad (11)$$

With:

- $Q_{T,heat,seci,m}$: the monthly heat losses through the envelope [MJ];
- $H_{T,heat,seci}$: the transmission heat losses coefficient [W/K];
- $\theta_{e,m}$: the monthly average exterior temperature [°C];
- t_m : the length of the month [Ms].

The modification is proposed as follows, for envelope heat losses:

$$Q_{T,heat,seci,m} = H_{T,heat,seci} * [(T_{set,max} - \theta_{e,m}) * t_{m,h} + (T_{set,min} - \theta_{e,m}) * t_{m,lh}] \quad (12)$$

The same modification have to be implemented in the ventilation heat losses evaluation:

$$Q_{V,heat,seci,m} = H_{V,heat,seci} * [(T_{set,max} - \theta_{e,m}) * t_{m,h} + (T_{set,min} - \theta_{e,m}) * t_{m,lh}] \quad (13)$$

These manipulations have two consequences: first, when $t_{m,h} = t_{m,lh} = 0$ (see Eq. 10), the heat losses will also equal zero. Second, by using other set temperatures and other climatic data, it happens that these equations result in negative figures, meaning heat gains instead of heat losses. No heating is therefore needed, and the related periods of time will not be taken into account in the heating consumptions ($Q_{T,heat,seci,m} = 0$). The same happens with the $\eta_{util,heat,seci,m}$ (monthly heat gains application rate, see above) calculation, which has to be annulled when heat gains exceed heat losses. These adaptations insure that the net heating demand is null (not negative), and so will be the consumptions.

4.3.4 Domestic Hot Water

The other consumption evaluation which depends on the number of inhabitants is the domestic hot water (DHW) production. In the official method, the demand is calculated with the building's protected volume as only parameter:

$$Q_{water,bathi,net,m} = f_{bathi} * \max [64, 64 + 0,22 * (V_{PER} - 192)] * t_m \quad (14)$$

$$Q_{water,sinki,net,m} = f_{sinki} * \max [16, 16 + 0,055 * (V_{PER} - 192)] * t_m \quad (15)$$

With:

- $Q_{water,bathi,net,m}$, $Q_{water,sinki,net,m}$: the net energy demand for a bath or a kitchen sink DHW consumption [MJ];
- f_{bathi} , f_{sinki} : the part of the bath or kitchen sink in the total DHW net energy demand [-];
- V_{PER} : the protected (heated) volume of the EPB unit, as defined in the regulatory calculation method (Wallonie, 2013) [m³];
- t_m : the length of the month [Ms].

In this study, we adopted as first approach the hypothesis of 45l of water to be heated, everyday, for each occupant, to a minimal temperature of 60°C (Hauglustaine, 1979). The water supplied everywhere in Belgium comes out of the network at an average temperature of 10°C. The net energy demand for DHW consumption becomes:

$$Q_{water,net,m} = [N_{lt} * N_{d,m} * 4,1855 * (\theta_{water,out} - \theta_{water,in})]/1000 \quad (16)$$

With:

- $Q_{water,net,m}$: the net energy demand for domestic hot water production [MJ];
- N_{lt} : the number of litres to be heated [l];
- $N_{d,m}$: the number of days in the month (see above Eq. 9) [-];
- 4,1855: the energy needed to raise of 1°C the temperature of 1 cm³ of water [J];
- $\theta_{water,out}$: the temperature of the heated water = 60°C;
- $\theta_{water,in}$: the temperature of the supplied water = 10°C.

Here are the final results variations for $Q_{water,net,m}$:

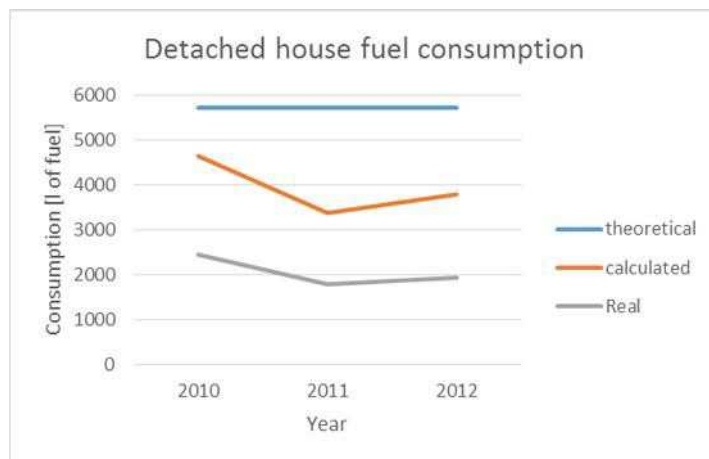
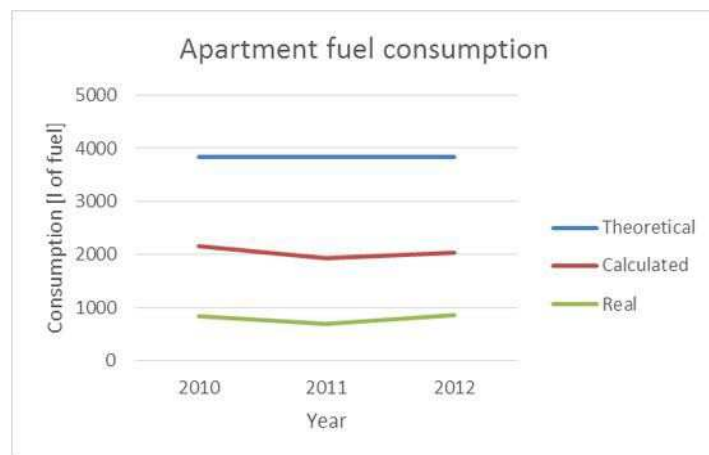
- Apartment:
 - o Official demand: $Q_{water,seci,net,m} \in [285 \text{ MJ}, 315 \text{ MJ}]$;
 - o Calculated demand: $Q_{I,a,m} \in [226 \text{ MJ}, 292 \text{ MJ}]$;
- Detached house:

- Official demand: $Q_{i,seci,m} \in [409 \text{ MJ}, 453 \text{ MJ}]$;
- Calculated demand: $Q_{I,a,m} \in [904 \text{ MJ}, 1168 \text{ MJ}]$;
- Row house:
 - Official demand: $Q_{i,seci,m} \in [473 \text{ MJ}, 524 \text{ MJ}]$;
 - Calculated demand: $Q_{I,a,m} \in [904 \text{ MJ}, 1,168 \text{ MJ}]$.

5. RESULTS

Here are graphs that show three different consumptions for each dwelling:

- The theoretical consumption: the result of the official Energy Performance Certificate, calculated with strict respect to the only regulatory method and procedure.
- The calculated consumption: the result of all the modifications proposed here above: change of climate, adaptation to real occupancy, heating patterns and more realistic internal loads...
- The real consumption, as announced by the dwellings owners.



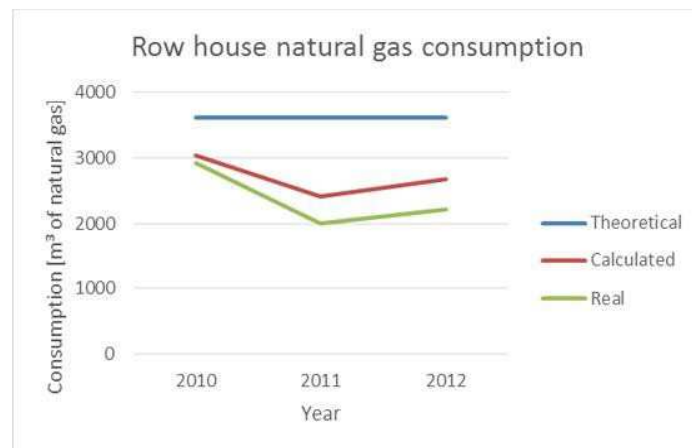


Figure 1: Comparison of the theoretical (official) consumption, calculated (proposal) consumption and real consumption in the cases of the apartment (a), detached house (b) and row house (c).

In the case of the apartment, the official standardised consumption was 4.46 to 5.49 times the real consumption on these 3 years (4.79 on average). The calculated consumption that integrates behaviour parameters is now 2.37 to 2.75 times the average real consumption (2.5 on average). The average consumption was thus decreased by 44 to 50% (47% on average).

In the case of the detached house, the official standardised consumption was 2.33 to 3.19 times the real consumption on these 3 years (2.77 on average). The calculated consumption that integrates behaviour parameters is now 1.89 to 1.95 times the average real consumption (1.91 on average). The average consumption was thus decreased by 19 to 41% (31% on average).

In the case of the row house, the official standardised consumption was 1.24 to 1.81 times the real consumption on these 3 years (1.52 on average). The calculated consumption that integrates behaviour parameters is now 1.04 to 1.21 times the average real consumption (1.15 on average). The average consumption was thus decreased by 16 to 33% (25% on average).

6. DISCUSSION AND CONCLUSION

As foreseen, the calculated results are closer to real results, without entirely closing the gap. This is normal: the uncertainties of the Energy Performance Certificate approach are not all behaviour-related, but also stand in other specificities of the protocol. One examples stands in the default values that are attributed to heating and DHW systems efficiencies, according to their type and age, and induce obvious reservations towards consumption results.

In the row house, better insulated and equipped with new systems characterised by “real” (acknowledged) efficiency rates, the gap is narrower, thanks to the increased data precision. This can also be seen in the case of the apartment, where the DHW system was given (by default) a (very) bad efficiency, due to an old boiler and a non insulated hot water loop. Having decreased the heating consumption, the part of DHW in the overall balance increases, inversely proportional to the accuracy of the data. As a general rule, the better known the heating and hot water producing systems efficiencies, the lower the influence of the number of inhabitants on the certification result. One idea could be to use another requirement of the 200/91/CE European Directive, the annual inspection of heating production systems, to get more accurate efficiency rates.

The influence of the climate data is clear however: using real climatic data is surely an important factor to compare calculated results with real consumption data.

It seems that, with a small amount of additional data (on the number of inhabitants, the set temperatures, the heating schedules), the certification calculation method is strong enough to approach real consumption data. These results are encouraging but other parameters ought to be studied as well, like the presence of a thermostat which allows to better knowing the set temperature and heating periods, the actual heated volume as opposed to the indirectly heated volume... Literature (Allibe, 2012; De Groot et al., 2008; Wallenborn et al., 2006) brings also out several factors that influence the energy consumption of a dwelling:

- Socio-demographic variables: skills and knowledge, income, occupation, type of housing, age of the head of the household, size of the family, rights on the dwelling (owner / tenant)...
- Attitudes and representations: motivation to save energy, attitudes towards energy saving, comfort representation, perceived behaviour efficiency, social standards, identification to others, image of the dwelling, costs and benefits evaluation, representation of the available technology...
- Behaviour variables: temperature in the main room, global temperature management, proportion of house not heated, number of days spent outside home, habits of ventilation, shower and bath frequency, use of available devices...

The Energy Performance Certification is a great opportunity for monitoring and trying to improve the housing stock, in every country that wishes to reduce its energy consumption, but that potential remains underexploited. In order for the scheme to reach its goals, it is essential to find a way to make it understandable by anybody. Though acknowledging the necessity of presenting a “legal” result as a comparison base, based on the approved standardized calculation method, it is believed that other results could be displayed, based on building characteristics and a minimum of behavioural inputs, creating a closer bond between future renters/owners and the results displayed in the EPC. Also, a highlight of the financial implications is now evidently necessary: the certificate could be used to foresee a rough monthly bill (taking energy and rent or loan repayment into account). The expected outcomes would be the creation of a complementary “custom-made” certification that would help raise energy consumers’ awareness of their environmental impact. Also, data collection and actuation of the existing buildings stock energy consumption would be possible, with the creation of comprehensive benchmarking databases, fundamental for shaping smart strategies on urban / regional / national levels.

Then, and only then, the EPC will be able to reach its goal and so become a tool for smarter cities.

ACKNOWLEDGEMENTS

Special thanks have to be given to the owners of the three analysed houses, for their help and understanding when being interviewed.

REFERENCES

2010/31/UE, 2010, *European Parliament and Council Recast Energy Performance of Buildings Directive*, Moniteur, official journal of the European Union, L153/13 to L153/35.

Allibe, B., 2012, *Modélisation des consommations d’énergie du secteur résidentiel français à long terme, amélioration du réalisme comportemental et scénarios volontaristes*, PhD thesis, Ecole des Hautes Etudes en Sciences Sociales, France, 361 p.

Amecke, H., 2012, The Impact of Energy Performance Certificate: A Survey of German Home Owners, Elsevier – Energy Policy 46, pp. 4 – 14.

CSTC (Centre Scientifique et Technique de la Construction - Belgian Building Research Institute), 2011, Practical and Technical Guide to Residential Lighting, ECLOS Research Program, Brussels, 62 p.

De Groot, E., Spiekman, M., Opstelten, I., PLEA 2008, *Dutch research into user behavior in relation to energy use of residence*, 25th Conference on Passive and Low Energy Architecture, Dublin, 22 to 24th October 2008.

Descamps, M., 2008, *Approche d'un gisement d'économie d'énergie par la rénovation du secteur résidentiel wallon*, DEA thesis, University of Liege.

Econotec, *Consommations de chauffage du secteur résidentiel*, in Institut wallon de développement économique et social et d'aménagement du territoire, *À la rencontre de l'énergie – Le secteur résidentiel*, Éditeur: J. DARAS, Ministre wallon de l'Énergie et des Transports, 8 p., 2000.

EPBD – Concerted Action, 2011, Implementing the Energy Performance of Buildings Directive (EPBD), Featuring country reports, EU Publications Office.

Fanger, P. O., 1977, *Human comfort and energy consumption in residential buildings*, Energy use management proceedings of the international conference, Tucson, Arizona.

Giffinger, R., Fertner, C., Kramar, H., Meijers, E., Pichler-Milanović, N., 2007, *Ranking of European medium-sized cities*, Final Report, Vienna.

Guerra Santin, O., 2010, Actual energy consumption in dwellings, the effect of energy performance regulations and occupant behaviour, Sustainable Areas Series, TUDelft, Delft, The Netherlands, 242 pp.

Hauglustaine, J.-M., 1979, Incidences du comportement humain sur la consommation d'énergie dans les habitations sociales, Master thesis, University of Liege.

IPCC, 2007: Climate Change 2007: Synthesis Report. Contribution of Working Groups I, II and III to the Fourth Assessment Report of the Intergovernmental Panel on Climate Change [Core Writing Team, Pachauri, R.K and Reisinger, A. (eds.)]. IPCC, Geneva, Switzerland, 104 pp.

ISO 7730:2005, Ergonomie des ambiances thermiques - Détermination analytique et interprétation du confort thermique par le calcul des indices PMV et PPD et par des critères de confort thermique local, International Standardisation Organisation, Switzerland, 52 p.

Laine, L., 2011, As easy as EPC? Consumer views on the content and format of the energy performance certificate, Consumer Focus, United Kingdom.

Linden, A.-L. et al., 2005, Efficient and inefficient aspects of residential energy behaviour: what are the policy instruments for change?, Energy Policy 34 (2006) 1918-1927.

Lutzenheiser, L., 1993, *Social and behavioral aspects of energy use*, Washington State University, Pullman, Washington, Annu. Rev. Energy Environ., 18 :247-89.

Monfils, S., Hauglustaine, J.-M., 2009, Etude énergétique et typologique du parc résidentiel wallon en vue d'en dégager des pistes de rénovation prioritaires, Reno2020 Research project scientific interim report, University of Liege.

O'Sullivan, A., 2007, *Urban Economics*, Boston, Massachusetts, McGraw-Hill, London. SPW (Service Public de Wallonie), 2013, *L'éclairage efficace des logements, Guide pratique à destination du particulier*, Programme de Recherche ECLOS, Namur, 36 p.

Vanparys, R., Niclaes, E., Lesage, O., 2012, *Certificat énergie, la base d'un véritable audit ?*, Test-Achats n°562, pp. 10 to 16.

Wallenborn, G, et al., 2006, *PADDII : Détermination de profils de ménages pour une utilisation plus rationnelle de l'énergie, Partie 1 : Modes de production et de consommation durables*, Politique d'Appui scientifique à une politique de Développement Durable, Politique Scientifique Fédérale, Bruxelles, 106 p.

Wallonie, 2013, *Arrêté du Gouvernement Wallon du 12 Décembre 2013, Annexe 1, Méthode de détermination du niveau de consommation d'énergie primaire des bâtiments résidentiels* [trad.: Walloon Government Decree of the 12/12/2013, Annex 1, Method to determine the primary energy consumption level of residential buildings], Namur, 133 p.

Wilhite, H., et al., 1996: *A cross-cultural analysis of household energy-use behaviour in Japan and Norway*. Energy Policy 24(9): pp.795-803.

Wilhite, H. and Lutzenhiser, L., 1998: *Social loading and sustainable consumption*. Advances in Consumer Research 26: pp. 281-287.

Wilhite, H. et al., 2000, *The Legacy of Twenty Years of Energy Demand Management: we know more about Individual Behaviour but next to Nothing about Demand*, E. Jochem et al. (eds.), *Society, Behaviour, and Climate Change Mitigation*, 109–126

The Mapping of Climate-Dependent Simplified Thermal Systems using State Space Models

A.W.M. (Jos) van Schijndel

Eindhoven University of Technology, Netherlands

1. ABSTRACT

Performances of thermal systems are most of the time dependent on the external climate conditions. This means a high performance of a specific innovation in a certain part of Europe, does not imply the same performances in other regions. The mapping of simulated building performances at the EU scale could prevent the waste of potential good ideas by identifying the best region for a specific system. This paper presents a methodology for obtaining maps of performances of simplified thermal systems that are virtually spread over whole Europe using state space models. It is concluded that these maps are useful for finding regions at the EU where systems have the highest expected performances.

Keywords: mapping, modeling, building, performance, state space

2. INTRODUCTION

Due to energy efficiency, there exist a lot of studies on thermal buildings systems. The performances of these systems for example, plate & tube collectors, air heat collectors, PV panels, etc., are mostly dependent on the external climate conditions. This also means that a high performance of a specific system in a certain part of Europe, does not imply the same performances in other regions. Similar, systems that did not perform very well due to local climate conditions, and therefore not commercialised, could still perform quite well in other climates. The latter can be seen as 'wasted' innovations. The mapping of simulated building systems performances at the EU scale could prevent this wasting of potential good ideas by identifying the best region for a specific system. This paper presents a methodology for obtaining maps of performances of thermal building systems that are virtually spread over whole Europe using state space models. This work presents a new and important step towards mapping of building systems performances and is based on two recent publications of van Schijndel and Schellen (2013) and Kramer et al. (2012). These two publications are summarized below as background information. A comprehensive literature study with references is already presented in both mentioned publications and therefore marginally included in this paper.

2.1 Related work on maps by Schijndel and Schellen (2013)

Due to the climate change debate, a lot of research and maps of external climate parameters are available. However, maps of indoor climate performance parameters are still lacking. Van Schijndel and Schellen (2013) present a methodology for obtaining maps of performances of similar buildings that are virtually spread over whole Europe. The produced maps are useful for analyzing regional climate influence on building performance indicators such as energy use and indoor climate. This is shown using the Bestest building as a reference benchmark. An important application of the mapping tool is the visualization of potential building measures over the EU. Also the performances of single building components can be simulated and mapped. It is concluded that the presented method is efficient as it takes less than 15 minutes

to simulate and produce the maps on a 2.6GHz/4GB computer. Moreover, the approach is applicable for any type of building.

2.2 Related work on state space modeling by Kramer et al. (2012)

Kramer et al. (2012) provide a systematic literature review on simplified building models. Questions are answered like: what kind of modeling approaches are applied? What are their (dis)advantages? What are important modeling aspects? The review showed that simplified building models can be classified into neural network models (black-box), linear parametric models (black box or grey-box) and lumped capacitance models (white box). Research has mainly dealt with network topology, but more research is needed on the influence of input parameters. The review showed that particularly the modeling of the influence of sun irradiation and thermal capacitance is not performed consistently amongst researchers. Furthermore, a model with physical meaning, dealing with both temperature and relative humidity, is still lacking. Inverse modeling has been widely applied to determine models parameters. Different optimization algorithms have been used, but mainly the conventional Gaus-Newton and the newer Genetic Algorithms. However, the combination of algorithms to combine their strengths has not been researched. Despite all the attention for state of the art building performance simulation tools, simplified building models should not be forgotten since they have many useful applications.

2.3 Goal and Outline

The goal of this work is to present a methodology for producing performance maps of external climate related building systems by combining the above mentioned publications on mapping and state space modeling. Section 3 presents the mentioned methodology to produce maps of simplified thermal systems using state-space models based on a commercial case study. In Section 4, the conclusions and future research are provided.

3. CREATING MAPS OF SYSTEMS INNOVATIONS USING STATE-SPACE (SS)

A commercial case study is presented in this Section. Due to the patent protection of the industrial partner, some specific information is omitted without loss of generality. The innovation consists of a novel heat exchanger built inside a construction acting as a solar collector. Figure 1 shows the principle construction of the solar collector (in reality this is much more complicated). The solar collector will be used for the heating of water that directly can be used or stored for later use. Due to insulation, the heat exchange with the internal environment is negligible.

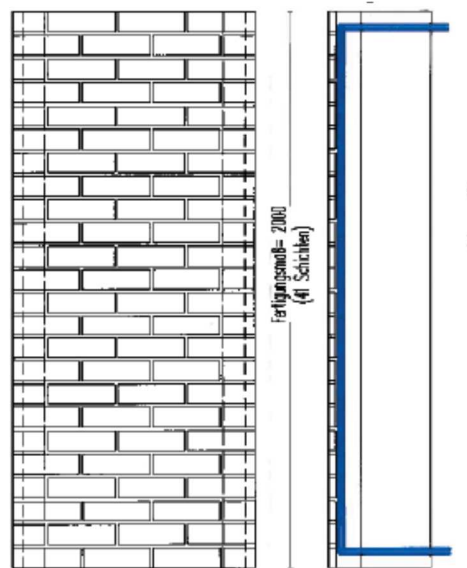


Figure 1: Construction of the solar collector

3.1 Modeling

A 3-State (3S) model was developed:

$$C_1 \frac{dT_1}{dt} = h A (T_{amb}(t) - T_1) - \frac{(T_1 - T_2)}{R_1} + a_1 A I(t) \quad (1)$$

$$C_2 \frac{dT_2}{dt} = \dot{m} c (T_{sup}(t) - T_2) + \frac{(T_1 - T_2)}{R_1} - \frac{(T_2 - T_3)}{R_2} \quad (2)$$

$$C_3 \frac{dT_3}{dt} = \frac{(T_2 - T_3)}{R_2} \quad (3)$$

Where

$T_{amb}(t)$ ambient (external) air temperature [$^{\circ}\text{C}$]

$T_{sup}(t)$ water supply temperature [$^{\circ}\text{C}$]

$I(t)$ external solar irradiance [W/m^2]

T_1 external surface temperature [$^{\circ}\text{C}$]

T_2 water return temperature [$^{\circ}\text{C}$]

T_3 internal wall temperature [$^{\circ}\text{C}$]

Parameters:

\dot{m} water mass flow [kg/s]

c heat capacity of water [J/kgK]

a_1 solar absorption factor [-]

h heat transfer surface coefficient [$\text{W}/\text{m}^2\text{C}$]

A surface [m^2]

d_1 distance pipe to surface [m]

d_2	distance pipe to insulation [m]
k	heat conductivity of concrete [W/mK]
R_1	heat resistance [K/W] = $d_1/(kA)$
R_2	heat resistance [K/W] = $d_2/(kA)$
C_i	heat capacity [J/ K]

The model was implemented using standard state-space modeling facilities of MatLab HAMLab (2014). The next Section shows the simulation and validations results.

3.2 Validation

Laboratory experiments were used to validate the models. We refer to the appendix for the details on the testing conditions. All experiments were simulated using the proper parameters and boundary conditions. The results were compared in order to evaluate the predictability of the model. In Figure 2 the results for a typical experiment A is shown.

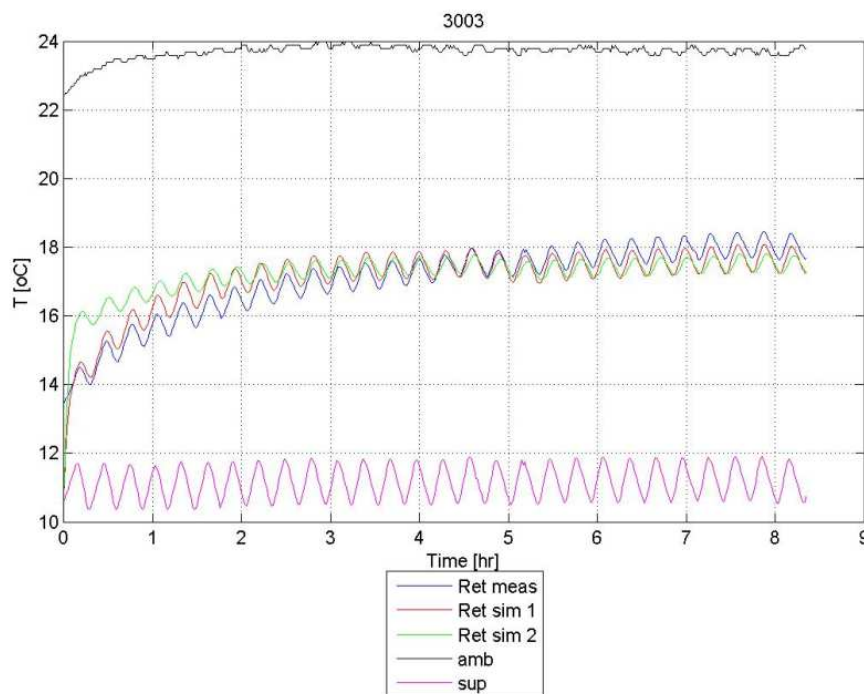


Figure 2: The simulation of experiment A: Temperatures vs time of the measured supply water(sup), the measured ambient air (amb), the simulated return water (Ret sim 1 & 2) and the measured return water (Ret).

From Figure 2 we observed that the predictability of model was satisfactory. All other tested configurations provided similar good results. Therefore we conclude that the model is quite usable for further use.

3.3 Simulation using a typical Dutch climate

The model configuration A was simulated using a reference standard Dutch climate of deBilt. Figure 3 presents the result.

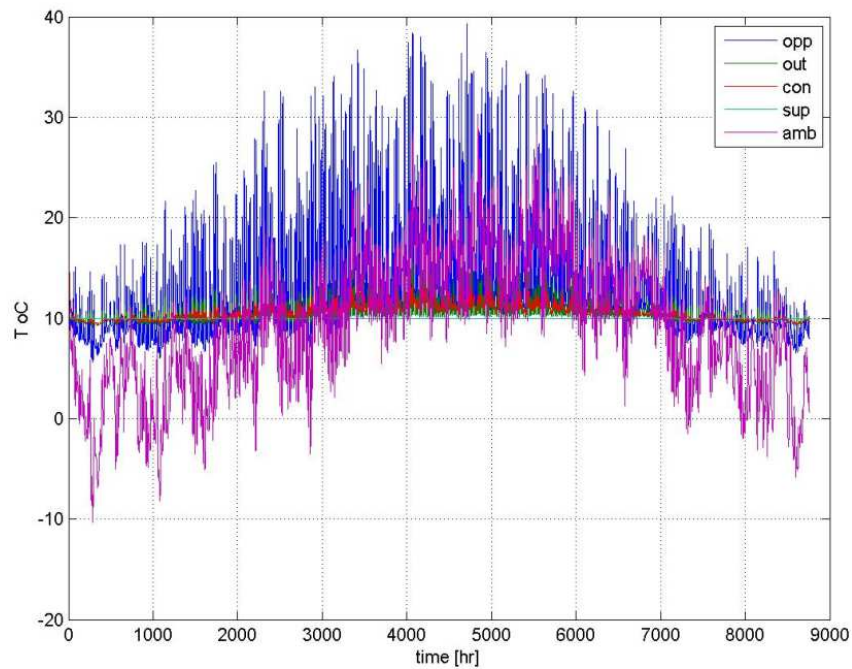


Figure 3: Simulation of model configuration A using a reference standard Dutch climate of deBilt. Temperatures versus time of the external wall surface (opp), the water return (out), the mid wall (con), the water supply (sup) and ambient air (amb).

The water supply temperature was constant held at 10 °C. The other two input signals: Ambient air temperature and solar irradiation were taken from the climate file. The main output signal is the return temperature (out). With this signal the output power can be calculated. This is shown in the next Section.

3.4 Performance evaluation

Figure 4 shows details of the model A configuration performance results.

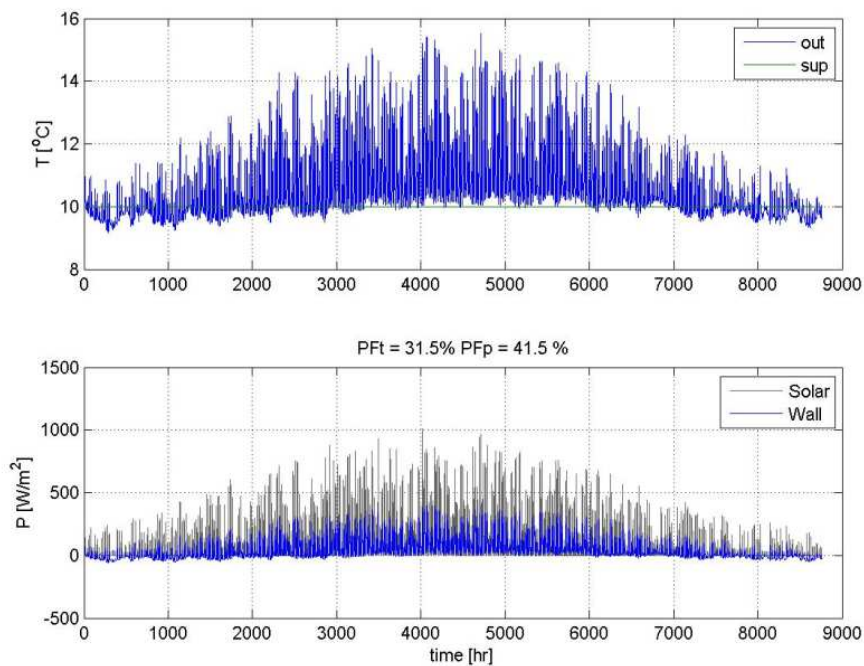


Figure 4: Performance evaluation. Top: The simulated supply and return water temperatures versus time. Bottom: The heat flux [W/m^2] of the incoming solar irradiation (Solar) and simulated output flux of the wall. 31.5 % of the year the wall system can be operated (PFt) The yearly mean efficiency is 41.5 % (PFp).

The output flux P_{out} is calculated by:

$$P_{out}(t) = (\dot{m}) \cdot c \cdot (T_{ret}(t) - T_{sup}(t)) / A \quad (4)$$

The overall performance is evaluated as follows: Firstly, $P_{50}(t)$ is defined as $P_{out}(t)$ with a threshold of 50 W/m^2 . Below 50 W/m^2 , the water return temperature drops below 10.7 °C and the wall system is too inefficient. For these values $P_{50}(t) = 0$. Secondly, two performance (PF) indicators are defined as follows:

$$P F_t = \text{Percentage of time of } P_{out}(t) \text{ above threshold of } 50 \text{ W} \quad (5)$$

i.e. percentage of time of possible operation [%].

$$P F_p = 100 \cdot \sum(P_{50}(t)) / \sum(I(t)) \quad (6)$$

i.e. the yearly mean efficiency [%]

From Figure 4 it follows for configuration A, $P F_t = 31.5\%$ and $P F_p = 41.5\%$. The main parameter that affects the simulated performances is the mass flow of the water. Figure 5 provides the simulated performances $P F_t$ and $P F_p$ as functions of the mass flow.

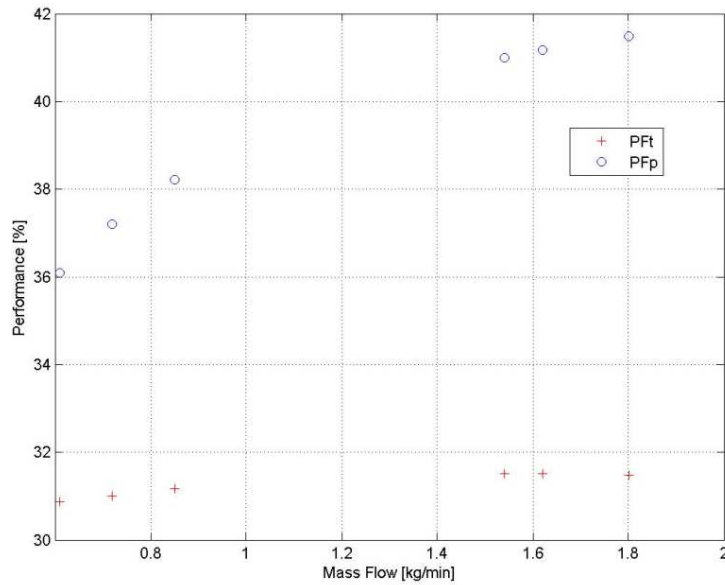


Figure 5: The simulated performances versus the mass flow.

Figure 6 presents the influence of the pump energy and surface heat transfer coefficient.

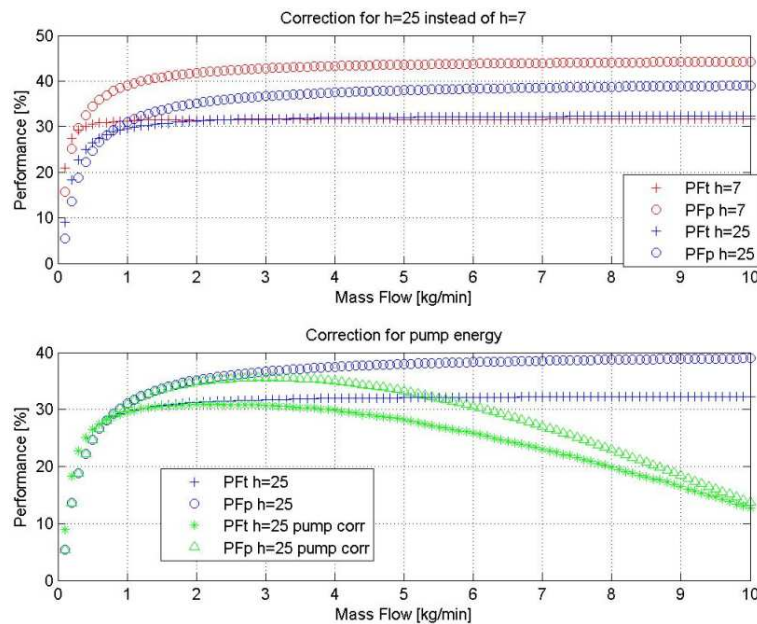


Figure 6: Influence of the pump energy and surface heat transfer coefficient. Top: The influence of a change in heat transfer surface coefficient. Bottom: Correction of the performances using pump energy.

For further simulations a more realistic surface heat transfer coefficient of 25 W/m²K is used instead of 7 W/m²K from the indoor experiment. The latter (i.e. h=7 W/m²K) was used for the validation of the experiments. Furthermore, for the water mass flow, values between 0.2 and 2 l/min are used.

3.5 Parameter study

During the project, the manufacturer of the solar collector wanted to know how the collector performed by changing the distance from the pipe to the surface and by changing the mass flow. Therefore the following parameters were varied for the parameter simulation study:

- * The distance from the pipe to the surface (default 35 mm) was varied: 20, 35 and 50 mm.
- * The mass flow (default 1 kg/min) was varied: 0.5, 1 and 2 kg/min.

The results of the nine simulations are shown in Table I and II.

Table 1: Efficiency Performance

Simulated yearly mean efficiency PFp [%]			
	d=20 mm	d=35 mm	d=50 mm
MF=0.5 kg/min	30.6	24.7	20.2
MF= 1 kg/min	39.0	30.9	25.2
MF= 2 kg/min	44.3	34.8	28.0

Table 2: Operation Time Performance

Simulated Operation time PFt [%]			
	d=20 mm	d=35 mm	d=50 mm
MF=0.5 kg/min	29.8	26.5	23.7
MF= 1 kg/min	33.1	29.5	26.5
MF= 2 kg/min	34.5	30.9	27.7

The increase of the efficiency performance by moving the pipe more towards the surface and the increase in mass flow is of course quite obvious. The efficiency performance for a Dutch climate is 44.3% with the accompanying mass flow of 2 kg/min and pipe depth of 20 mm. This is a significant increase compared with 30.9% (flow of 1 kg/min and pipe depth of 35 mm). However there is a limitation on the smallest distance because due to constructive reasons the depth can not be smaller as 20 mm. Therefore a pipe depth of 20 mm is optimal. From figure 6, it can be seen that a mass flow of 2 kg/min is also optimal, taking the pump energy into account.

3.6 EU Mapping of the standard configuration

By replacing the Dutch climate with the climates of weather stations presented in van Schijndel and Schellen (2013), it is quite easy to simulate the response of the system to each external climate using Meteororm (2014). From the responses the performance indicators can be calculated (See previous Section). The results of the standard wall performances are shown in Figures 7 and 8. These results are still based on the standard wall configuration A.

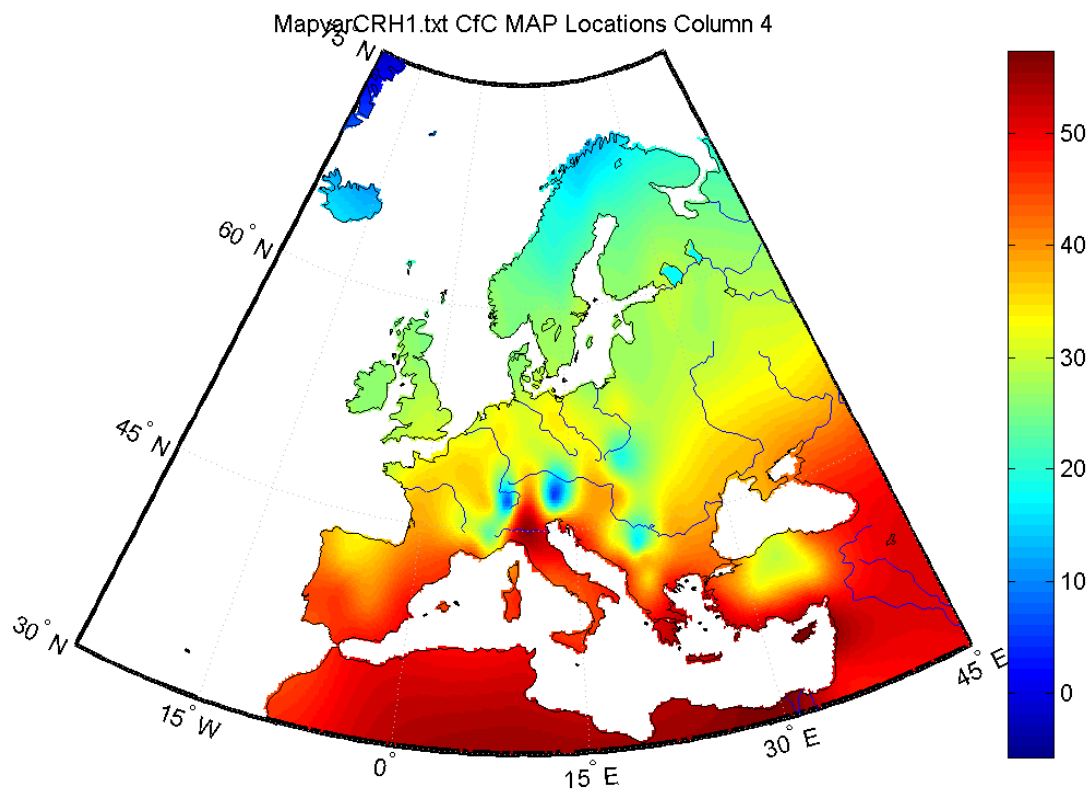


Figure 7: Efficiency (PFp) of the standard wall configuration.

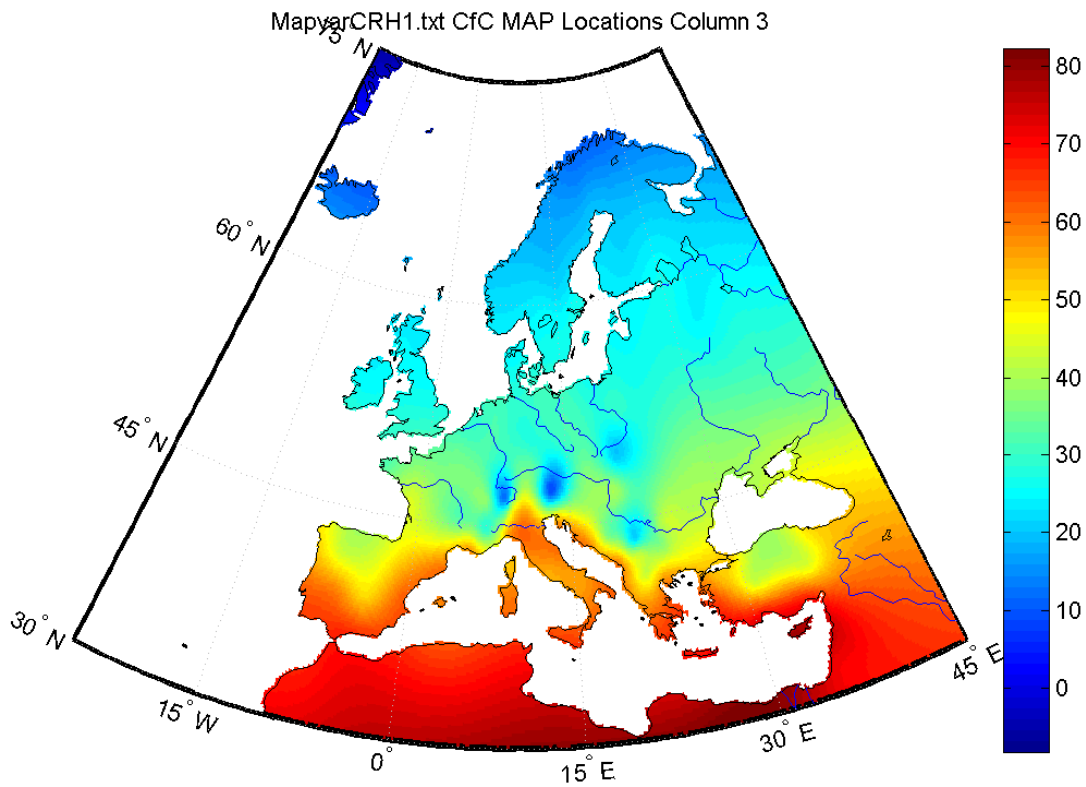


Figure 8: Percentage of time operation (PFt) of the standard wall configuration.

3.7 Simulation of optimized wall configurations

All nine configurations of the parameter study (see Table I and II) were also simulated on the EU scale. For each weather station the best configuration out of nine was selected. These optimized wall configuration performances are presented in Figures 9 and 10.

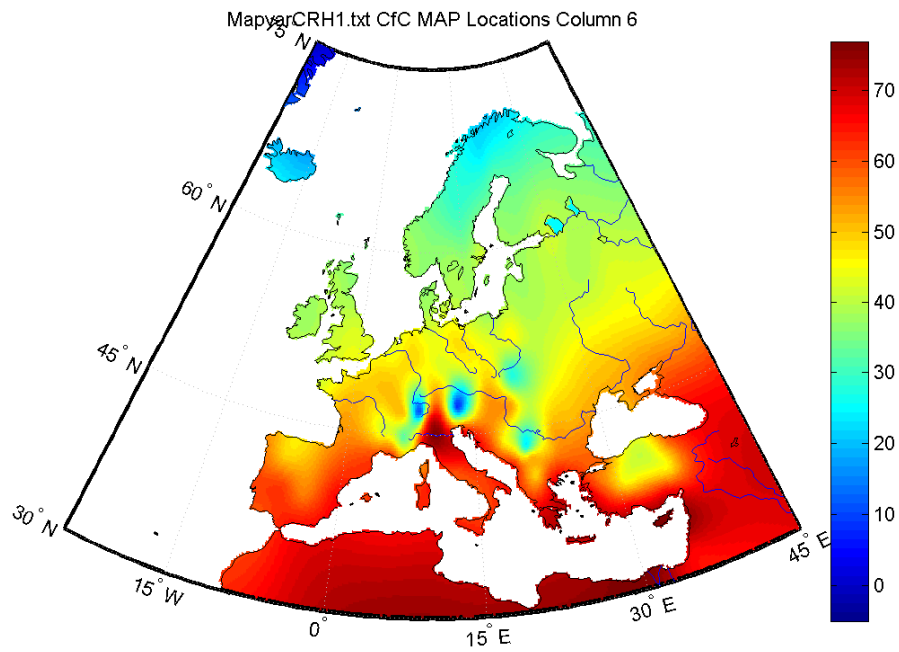


Figure 9: Optimized wall configuration Efficiency (PFp).

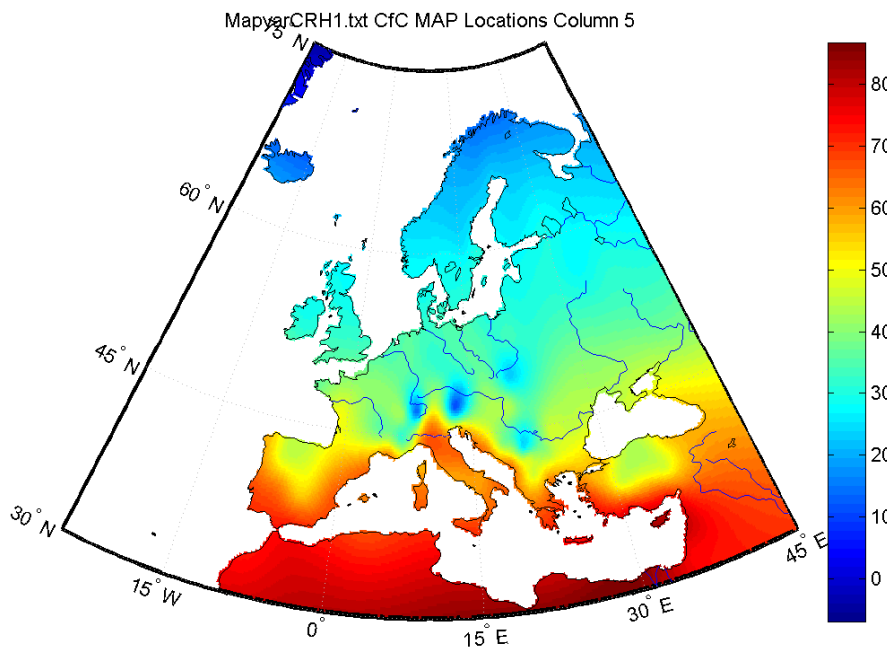


Figure 10: Optimized wall configuration Percentage of time operation (PFt).

From figure 10 it can be seen that large parts of Europe have efficiencies of at least 45%. From figure 10 it can be seen that the areas near the Mediterranean have percentages of time of operation above 60%. The latter means that the wall collector is also operational during parts of the night.

4. DISCUSSION AND CONCLUSIONS

In this paper a methodology was presented, for producing maps of external climate dependent simplified thermal systems, based on state-space models. The approach was successfully applied for a commercial case where, the main objective was to simulate and optimize the thermal performance of solar wall collector under different EU climate conditions using state space modeling:

- (1) The solar collector was successfully modelled;
- (2) The validation of this model using existing measurements was satisfactory;
- (3) The solar collector model was successfully simulation using 130 EU weather stations;
- (4) Estimation of minimal and maximal performance was done by a parameter study;
- (5) EU Maps of the performance were created.

Large parts of Europe have solar collector efficiencies of at least 45%, the exact details are provided in Figure 9. Furthermore, areas near the Mediterranean have percentages of time of operation above 60% (exact details are shown in Figure 10). The latter means that the solar collector is even operational during parts of the night. It is concluded that this study shows that the solar collector could be applicable in large parts of Europe.

Limitations.

However, the reader should notice that the solar collector simulation results in this study are based on two assumptions: The supply water temperature is constant at 10 °C and all heat produced by the wall collector is usable at any time. Under most circumstances this is not very realistic. Therefore it is recommended to include buildings, systems and controllers details into the modeling for more realistic performance simulations and design of promising integrated configurations.

Benefits.

Currently we are working on a more general state space mapping tool in MatLab. This tool will become public available. With this tool the performances of any state-space can be mapped.

REFERENCES

- HAMLab (2014), <http://archbps1.campus.tue.nl/bpswiki/index.php/Hamlab>
- Kramer, R.P., Schijndel, A.W.M. van & Schellen, H.L. (2012). Simplified thermal and hygric building models : a literature review. *Frontiers of Architectural Research*, 1(4), 318-325.
- Meteonorm (2014).<http://meteonorm.com/>
- Schijndel, A.W.M. van & Schellen, H.L. (2013). The simulation and mapping of building performance indicators based on European weather stations. *Frontiers of Architectural Research*, 2, 121-133.

APPENDIX Testing Conditions

To reach the main objective of providing a first estimate of the efficiency numerous experimental measurements are executed. A test setup was build at the laboratory consisting of an array of infrared lamps, a cold water machine, pump with flow adjustment valves, temperature sensor in the ingoing flow and outgoing flow, four temperature sensors inside the solar collector, an air temperature sensor, pyrano meter and a balance for measurement of the flow quantity . Photo 1, 2 and 3 give an impression of the test setup. Each configuration has been measured for at least 5 hours to ensure that a stationary state was reached.



Photo 1: Array with IR lamps



Photo 2: Front side of collector



Photo 3: Back site of collector with cool water unit, circulation pump and temperature sensors

The settings for a typical experiment in the stationary part (between 350 and 525 minutes) were:

- Radiation average 964 W/m^2
- Flow average state $1,80 \text{ kg/min}$
- Average water temperature supply $11,2 \text{ }^\circ\text{C}$
- Average air temperature $23.7 \text{ }^\circ\text{c}$

The results of the experiment in the stationary part (between 350 and 525 minutes) were:

- Average temperature return $18,0 \text{ }^\circ\text{c}$
- Average power out. 491 W/m^2
- Average efficiency $51,0\%$

FOURTH SESSION
ADVANCES IN DESIGN AND
OPTIMIZATION OF BUILDING
COMPONENTS AND SYSTEMS

Application of users' light-switch stochastic models to dynamic energy simulation

V. Camisassi¹, V. Fabi¹, RK. Andersen², SP. Corgnati¹

⁽¹⁾TEBE Research Group, Department of Energetics, Politecnico di Torino, Corso Duca degli Abruzzi 24, 10129 Torino, Italy

⁽²⁾ICIEE, Department of Civil Engineering, Technical University of Denmark, Nils Koppels Allé Building 402, 2800 Kgs. Lyngby, Denmark.

1. ABSTRACT

The design of an innovative building should include building overall energy flows estimation. They are principally related to main six influencing factors (IEA-ECB Annex 53): climate, building envelope and equipment, operation and maintenance, occupant behaviour and indoor environment conditions. Consequently, energy-related occupant behaviour should be taken into account by energy simulation software. Previous researches (Bourgeois et al. 2006, Buso 2012, Fabi 2012) already revealed the differences in terms of energy loads between considering occupants' behaviour as stochastic processes rather than deterministic inputs, due to the uncertain nature of human behaviour. In this paper, new stochastic models of users' interaction with artificial lighting systems are developed and implemented in the energy simulation software IDA ICE. They were developed from field measurements in an office building in Prague. The aim is to evaluate the impact of a user's switching action over whole building energy consumption. Indeed, it is interesting not only to see the variance related to electric energy consumption, but the overall effect on a building's energy load.

Keywords: Lightswitching behaviour, stochastic models, energy simulation

2. INTRODUCTION

To predict better building energy consumption, as well as, occupant necessity in term of comfort, human interaction with building and its systems needs further investigations. Several experts from branches of study that vary from philosophy, social studies to more technical and scientific areas, tackle the uncertainty and differences of human behaviour. Building science undertook this effort observing reality. Researchers try to reproduce, as well as, forecast behaviours developing stochastic model, through statistical and random processes, based on environmental conditions. Different models and observations were carried out on how people interact with buildings adjusting blinds, opening or closing windows, changing temperature set point, switching on and off the light (Parys, 2011). These studies were undertaken through the implementation in energy simulation software of several occupant behaviour models. Fabi (2012) implemented, on the simulation software IDA ICE, stochastic models for window controls in residential buildings. Buso (2012) considered human uncertain interaction with shading devices and window operation in office buildings. Bourgeois et al. (2006) assessed the total energy impact of occupant behaviour in relation to lighting systems using Reinhart's light-switch 2002 model (Reinhart, 2004) inside the sub-hourly occupancy control enabled on ESP-r. In fact, the most well-known and utilized stochastic model of occupant behaviour over artificial lighting system was developed by Reinhart in 2002. This study takes into account findings from different studies and it was firstly implemented in the lighting analysis software DAYSIM and online software light-switch Wizard. Here, occupants' behaviour toward manual

lighting operational system in office buildings is modelled in order to expand the knowledge on which indoor and outdoor environmental conditions influence peoples' behaviour as well as to predict their impact on electric energy usage in buildings. In fact, the development of this work is to implement part of the models built in energy simulation software in order to achieve predictions of possible energy consumptions, which take into consideration the uncertainty of user actions. The models were built over field measurements recorded from an office building in Prague.

In this paper, firstly the light-switch 2002 developed by Reinhart is displayed, since it represents the principal reference in literature, then the method of implementation is illustrated along with its differences with the previous one.

2.1 People actions upon artificial lighting in simulation software

Even if ESP-r includes Hunt's stochastic algorithm for manual light-switch, the most known and used algorithm for artificial lighting is the one developed by Reinhart (2004). This study was first implemented in the daylight simulation program DAYSIM and the online tool light-switch Wizard. Then, other researchers incorporated this algorithm into whole-building energy simulation programs: Bourgeois (2006) included this algorithm into his Sub-Hourly Occupancy Control (SHOCC) enabled on ESP-r; Daum and Morel (2009) used it on IDA ICE in order to assess the total energy impact of manual and optimized blind controls with different lighting schedules.

Reinhart proposed a manual stochastic lighting and deterministic blind control algorithm based on a recent review, made by himself and Voss (2003), on a section of studies made in Canada, Japan, Germany, the UK and the United States. The figure below illustrates in detail how the Lightswitch-2002 algorithm processes every 5-min: illuminance and occupancy are the input data. The occupancy is simulated with an adapted version of Newsham's stochastic model (Reinhart, 2001). At each time-step the electric lighting and blind status are set according to the outcome of the loop illustrated. The coloured parts of the graph represent the stochastic model used to infer the switching probability: the red part represents switch on at arrival and it is employed twice; the green part represents the switch on during the presence; the blue part represents switch off at departure.

In processing the model, it is possible to choose between 4 types of occupants (Fig. 2), depending on their attitude towards operating blinds and windows. Two users are distinguished for lighting in this model:

- Users who paid more attention to the indoor lighting conditions and used the artificial lighting system in relation to daylight availability on the work plan. In particular, in this case, he included the probability inferred by Hunt (1979) concerning the switch on action on arrival, and the one inferred by Pigg et al. (1996) for the switch off, and, eventually, his own study for the intermediate switch on probability.
- Users who do not care about daylight and continually use artificial lighting.

The stochastic models for the first user type ran through random processes while the latter is represented as deterministic factor.

For the blinds instead, he inserted one automated and two manual blind control strategies. An automated blind control if blinds are completely lowered when incoming direct solar irradiance reaches more than $50\text{W}/\text{m}^2$ over the work plan while the blinds are fully opened otherwise. A dynamic manual blind control if blinds are completely lowered when incoming direct solar irradiance above $50\text{W}/\text{m}^2$ superscripts the work plan and fully re-opened just once a day in the

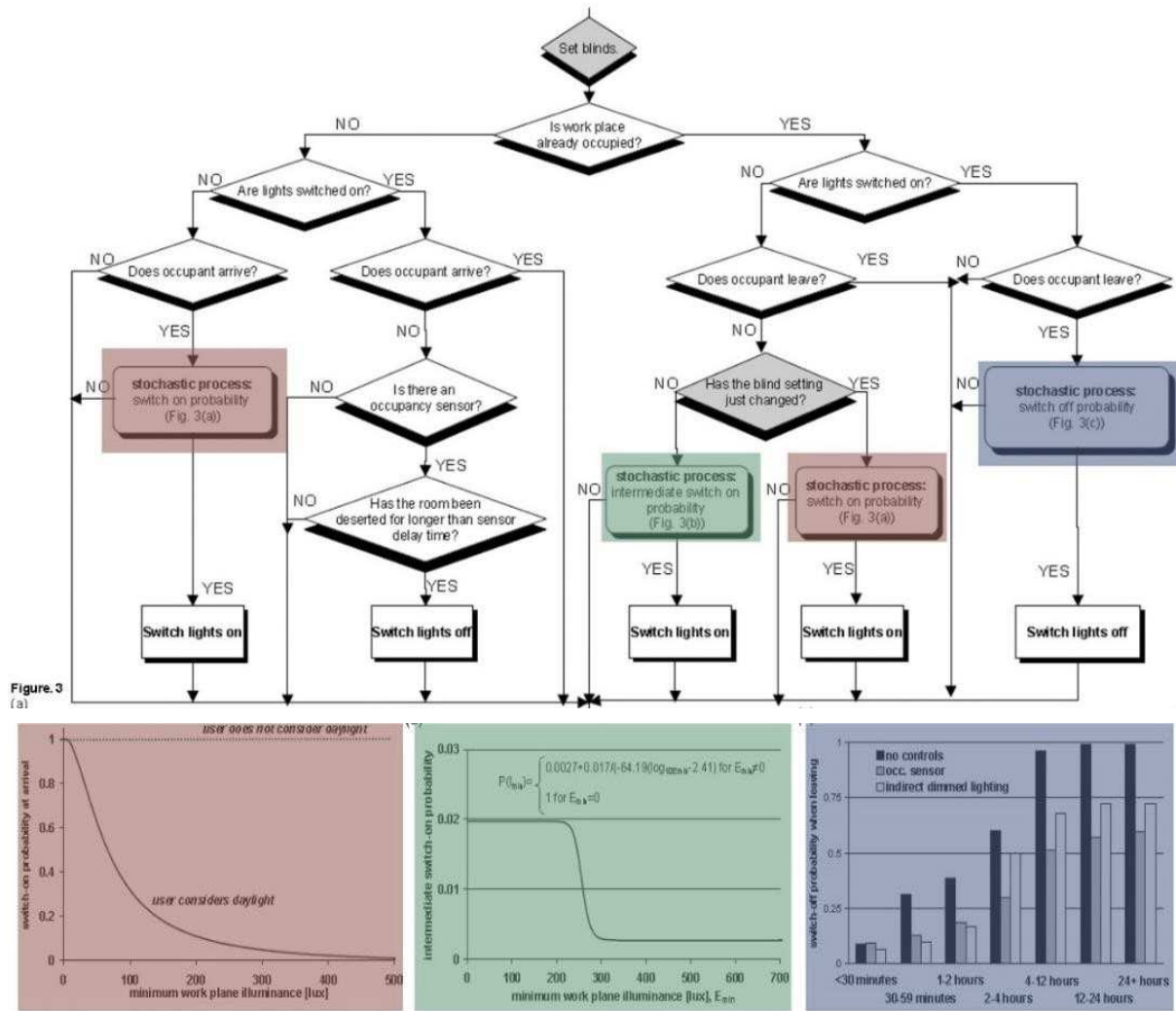


Figure 1: Light-switch 2002 algorithm

morning upon arrival. Moreover a static manual blind control is taken into account if blinds are always entirely lowered.

As we can see from the algorithm represented in Fig.1, the lighting system is directly interrelated with the blinds' setting. However, the blinds' position is deterministically treated, even if it is based on assumptions made after a review of field observations.

user $DdBd^x$	The user controls the lighting system with sensitivity to ambient daylight conditions and uses the blinds on a daily basis
user $DiBd$	The user controls the lighting system independent of ambient daylight conditions and uses the blinds on a daily basis
user $DdBs$	The user controls the lighting system with sensitivity to ambient daylight conditions and keeps the blinds permanently lowered with a slat angle of 75° .
user $DiBs$	The user controls the lighting system independent of ambient daylight conditions and keeps the blinds permanently lowered with a slat angle of 75° .

^x)Dd: Daylight dependant lighting use; Di: Daylight independent lighting use; Bs: Blinds static; Bd: Blinds dynamic.

Figure 2: User types described by Light-switch 2002.

3. CASE STUDY

Data on how people interact with artificial lighting in real life are needed in order to develop a stochastic model on how light switch's operations are carried out by occupants. In this study the data are collected within the framework of the European project "Clear-up".

Its aim is the development of new technological solutions, based on the integration of new building technologies along with control strategies, in order to optimize the energy efficiency and indoor quality of existing buildings, while also stressing the importance of their affordability and user-handiness. To achieve results, several tests on real building have been carried out. The data, used to model occupant behaviour, were measured at the Czech Technical University (CTU) Civil Engineering Faculty Building in Prague. It is a typical example of 1970's architecture, a sixteen-storey building, which has a centralized heating and ventilation system but it is characterized by poor thermal insulation and no air conditioning and no building management system (It has actually just been refurbished in July 2013.)



Figure 3: Building's localization and views.

The Clear-up team instrumented for measurements eight almost identical offices, located on the second floor, and provided them with an “active” management system. They are 5 m x 3 m in size with a floor to ceiling height of 3.3 m. There is just one insulated external wall, facing South-West, with two windows 1.5 m x 1.6 m, while the others walls separate each room from the others and the corridor.

The following variables were organized together with a common time step of 5 minutes. Indoor environment:

- Air temperature [°C]
- Relative Humidity [%]
- VOC concentration [ppm]
- Illuminance in the middle of the room(depth) [lux]
- Illuminance on the desk [lux]
- Illuminance at the window [lux]
- Illuminance ratio depth/window [-]
- Illuminance ration depth/desk [-]
- Blind position [%]
- Operating state of ceiling luminaire [0/1]
- Operating state of standing lamp [0/1]
- Door contact [0/1]
- Window contact [0/1]
- Ceiling luminaire switch [0/1]
- Standing lamp switch [0/1]
- Moment of presence [arrival/intermediate/departure]

Outdoor environment:

- Air temperature [°C]
- Relative Humidity [%]

- Vertical illuminance on the façade [lux]
- Horizontal illuminance [lux]
- Wind velocity [m/s]
- CO2 concentration [ppm]
- VOC concentration [ppm]
- Sun elevation [°]
- Azimut [°]
- Rain detector [0/1]

3.1 Models development

Multivariate logistic regression with interactions between selected variables was used to infer the probability of a light switching on and off event. The method relies on the probability function described on equation 1. The models predict the probability of an action (switching on or switching off) using equation 1, where p is the probability of switching on/off the light, a and b_n are the coefficients in the tables presented in figure 4 and x_n are the associated variables (temperature, CO2 concentration etc.). Moreover, this equation takes into account the interactions between variables by adding interaction terms to the model.

$$\log\left(\frac{p}{1-p}\right) = a + b_1 \cdot x_1 + b_2 \cdot x_2 + \dots + b_n \cdot x_n + c_{12} \cdot x_1 \cdot x_2 + c_{13} \cdot x_1 \cdot x_3 + \dots \quad (1)$$

The models are described in the following figure (Figure 4).

SWITCH ON MODEL for IDA ICE				IDA ICE SWITCH OFF MODEL			
UNITED DATABASE	Variables	Moment of presence	Estimates	ACTIVE		Estimate	
		Intercept - Active user	Arrival		4.3337	Intercept	-0.5068
			Departure		0.6414	illuminance_Depth	-0.0053
	Intermediate		2.7841	Azimut	0.0053		
	Intercept - Passive user	Arrival	1.4181	PASSIVE	Intercept (arrival)	-13.3400	
		Departure	-2.2742		Departure	0.7955	
		Intermediate	-0.1315		Intermediate	-0.9821	
	illuminance_window [log +1]		illuminance_window [log]		-0.3234		
	illuminance_Depth		Room temperature		0.6324		
	Room temperature		illuminance_Depth		-0.0011		
Elevation							

Figure 4: Stochastic model, based on logistic regression, to implement on IDA ICE

For example, the probability of switch on actions during occupants' periods of arrival could be inferred using the following logistic regression function:

$$\log\frac{p}{1-p} = 1.42 - 0.22 \log(E_{v,w} + 1) + 1.8 * 10^{-3} E_{mr} - 0.26 T_r - 4.2 * 10^{-2} Elevation \quad (2)$$

Where $E_{v,w}$ represents the variable illuminance at the window, E_{mr} the illuminance in the middle of the room and T_r the room temperature.

It is possible to see that, in order to formulate the equation, type of user as well as the moment of the presence were specified since the intercept values depend upon these factors as figure 4 describes. It is evident that the equation does not present interactions among variables and its simplicity is useful for its final implementation in simulation software.

The switch-off models were inferred from active and passive databases. The probability of turning off the light for active users does not display the moment of presence as a factor and always results higher than the one inferred from passive occupants.

4. SOFTWARE IMPLEMENTATION

The stochastic models inferred from field measurement in the office building of the Czech Technical University (CTU), Civil Engineering Faculty in Prague (paper II) were implemented in the simulation software IDA ICE.

IDA ICE is a whole-building simulation software for thermal indoor climate and energy consumption, developed by EQUA. The first version, made in 1998, was originally elaborated at the Royal Institute of Technology in Stockholm (KTH) and at the Helsinki University of Technology.

Its strength lies in the fact that it is an equation based modelling tool which uses the formal languages Modelica or Neutral Model Formal. For this reason it is user friendly and, with its expert interface (Fig. 4), allows quick expansion with the addition of new mathematical equation. Fabi (2013), D'Oca (2012) and Buso (2012) already implemented different stochastic models in IDA ICE to predict occupant actions over several building system in both residential and office buildings. In this work the expert edition of the latest version 4.5.1 was used.

It was decided to use as a reference building the construction where the measures were recorded. This choice was taken in order to not disregard the overall applicability of the illustrative model in the general context of office building, but it is necessary to assess it firstly on its original context in order to evaluate the differences between the deterministic approach and the stochastic one in building energy simulation. Specifically, an office of the Micro-environmental and Building Services Engineering Department of the CTU university in Prague was modelled on IDA ICE.

In particular the location, orientation and building envelope characteristics were set in accordance to the real construction. The office, 5 m x 3 m, is at the second floor of the sixteen-storey building, the floor to ceiling height is 3.3 m and it was provide with two south-west facing windows of 1.4m x 1.6 m.

Since it is a typical example of 1970's architecture, it could be assumed that it was predominantly made by concrete with poor insulation level and thermal bridge prevention. However, the model was implemented with the Vacuum Insulated Panel that were added to the external wall from the inside in order to carry out other experiments connected to the European Clear-up project, that aim to the development of new technological solutions in order to optimize the energy efficiency and indoor quality of existing buildings. The thermal transmittances adopted are described in the following figure (Figure 5).

Construction	U [W/m ² .K]	Construction	U [W/m ² .K]
Insulated perimeter wall	0.15	Interior wall	2.55
Window	4.10	Partition wall	2.00
Floor	0.85	Door	3.50
Ceiling	0.85		

Figure 5: Stochastic model, based on logistic regression, to implement on IDA ICE.

During the measurement period, the building was provided with diverse control strategies for the heating as well as for mechanical ventilation systems. In this modelling, the air change flow rate was fixed to 30 m³/h, which represents the basic operational state of the system. The thermal zone was equipped with 2 waterborne radiators with constant heating set-point of 21°C,

in accordance to the comfort category I for cellular offices described in Standard EN 15251:2006.

The office was provided with an additional standard cooling device, having set-point of 25.5°C (Standard EN 15251:2006), in order to evaluate also how cooling and heating loads varies in relation to the stochastic and deterministic approach for simulating artificial lighting use. Indeed, it was already proved how, in general, the use of artificial lighting effects not only the electrical energy consumption but also the heating and cooling demands. The boiler operational schedule was set always on while chiller's operational time was adopted almost to users' occupancy from 9.00 to 18.00 during working days. Specifically, the occupancy schedule was set from 9.00 to 12.00 in the morning and 13.00 to 18.00 in the afternoon in the attempt to better replicate the occupancy resulted from measurements. The artificial lighting system was composed by six sources with an emitted power for unit of 35 W, a luminous efficacy of 80 lm/W and it was scheduled as the occupant presence. The emitted heat for the equipment was set 15 W/m² following the setting described by TEBE research group for the office reference building (Buso, 2012). Only internal blinds were considered in the model and they were included with a deterministic control strategy based on sun and occupant's schedule. In particular blinds were disposed to be fully lowered when incoming direct solar irradiance is above 50W/m².

5. RESULTS

The energy loads obtained from deterministic simulation are displayed first. In particular, two outputs characterized by different controls of lighting are stressed:

1. Lights are always set on during occupancy presence (Figure 6)
2. Ideally controlled lighting use: lights are turned on if the daylight level at the work plan is lower than 100 lux, while they are automatically switched off when it is higher than 500 lux (Figure 7)

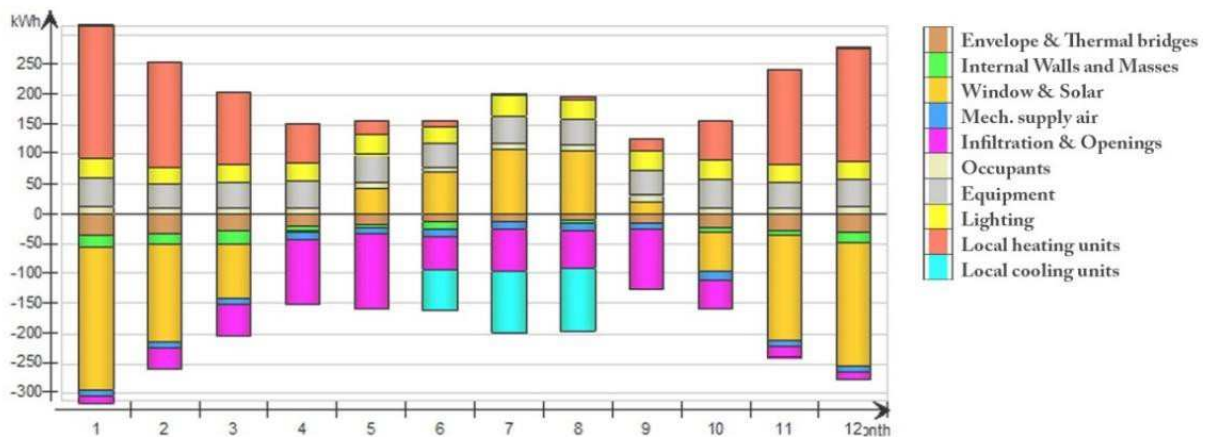


Figure 6: Output graph of IDA ICE describing energy balance on yearly base with a constant use of lighting during occupancy

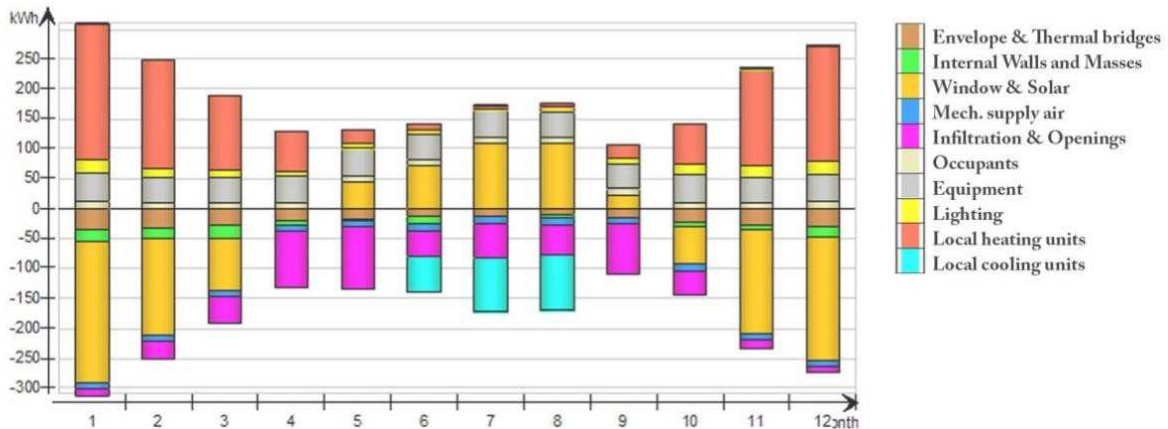


Figure 7: Output graph of IDA ICE describing energy balance on yearly base with a lighting use dependent on daylight level.

This setting, even if it considers two values highlighted by Reinhart (2001) and Hunt (1979) has turning points for people actions, still represents a deterministic input and of course it is strictly related by the blinds position. It reproduces the operation of an automatic controller. From these two settings it emerges already the range between what it is supposed to be an ideal control and a pessimistic option. However it does not depict a high difference between heating and cooling loads.

5.1 Stochastic algorithm implementation

The models described in the previous tables (figure 4) were implemented on IDA ICE following a similar algorithm used by Valentina Fabi (2013).

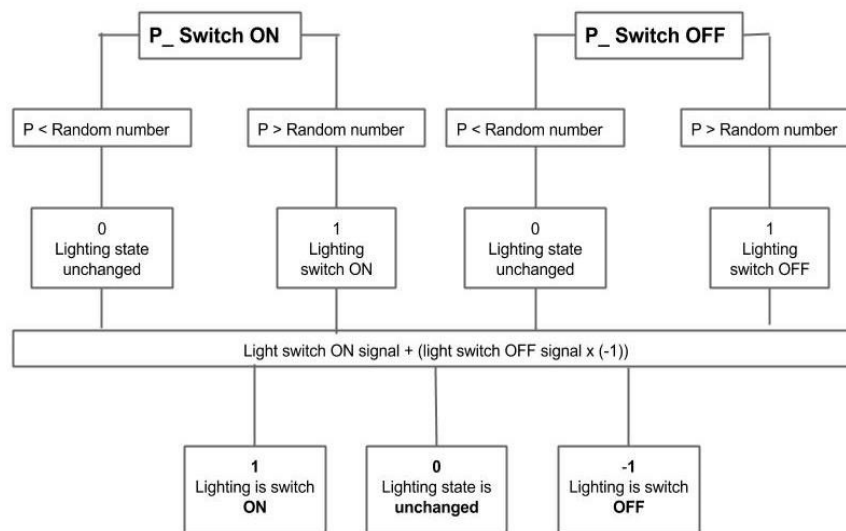


Figure 8: Algorithm for the implementation in IDA ICE

The logistic regression model for switching on and off the lights could be directly inserted in IDA ICE thanks to its equation-based modelling system. All the variables needed were connected to those corresponding in the simulation program, for example the room temperature was directly inserted as a continuous input for the logistic function. In order to distinguish among arrival, intermediate and departure period a schedule was introduced.

Given the probability outcome, it is compared to a random number in order to get the deterministic signal, for example a P value higher than the random number will give as output 1 (switch on). Then the signals are checked through a simple equation in order to make sure that a switch-on signal is not given at the same time of a switch-off one. Finally the control is given. The algorithm loop for every time step and since there are two types of users the algorithm was applied twice.

6. DISCUSSION AND CONCLUSION

From the implementation carried on so far, general limitations could be outlined in order to suggest improvements in its implementation for further researches on energy consumption related to artificial lighting. Moreover, a general comparison with the light-switch 2002 model along with its results' review is undertaken in order to emphasize the importance of how a stochastic models of occupants' behaviour related to artificial lighting could affect energy consumption.

Actually, two main limitations of the implementation can be recorded. Firstly, the occupancy has been scheduled deterministically and even if the switching actions will take place randomly according to the logistic function, the fixed schedule influenced the probability since the moment of presence is introduced as drivers: in the first 15 minutes of presence there is a higher probability that the light will be turned on and in this case, the 15 minutes are fixed from 6:00 to 6:15 in the morning. Furthermore, all the variables presented in the statistical results were related to their correspondence in the simulations software, but for some of them approximations were made. The lux levels measured in the middle of the room were included as illuminance at the desk. For what concern the illuminance values recorded at the window, the software's corresponding variable took into account the blinds since the lux level is evaluated behind the shading; consequently, within this implementation, the simulation can be run only without considering blinds. Another loop in order to solve this situation should be added with the perspective to combine this model with a stochastic model for shading control.

Reinhart's model and the stochastic model presented in this paper differ even if they got the same long-term aim to develop a more reliable users' action control strategy in energy simulation.

First of all, Reinhart developed a model with a higher level of applicability. It is already implemented in several simulation software and used by designers. It is based on a review of field studies and only considered the main drivers gathered: moment of users' presence; duration of absence time; daylight illuminance at the work plan.

Its use already highlights how actual electric lighting energy demand in an office is closely associated with the occupant's user type (Reinhart, 2004): it varies between 10 and 39 kWh/m²/year depending if active or passive users is considered. Bourgeois et al. (2006) showed a similar discrepancy and furthermore, they also evaluated how much impact there is on heating and cooling energy loads.

The results support the general knowledge that reduction in lighting use will create, not with a linear proportion, a reduction in cooling loads while increase heating needs. On the other hand, they also underlined how the presence of a switch off sensor could imply a reduction in energy consumption of 20 % since the probability to turn off the lights spontaneously is very low. Nevertheless, despite its recognised relevance, in this model the majority of users' profiles are still fixed. Only one light switch profile is based on the stochastic approach and its definition is strictly related to the blinds' positions that are set deterministically. As Reinhart stressed the underlying behavioural patterns still represent a "preliminary" option.

The data collected in Prague inferred models that do not highlight interrelation between blind state and user interaction with the lighting system. Consequently, simulation does not integrate lighting and shading system patterns.

It could be assumed that the use of these models will determine even lower energy consumption than the one evaluated by light-switch 2002 since the probability of switching the light on is so infrequent. However, probably also in this case the addition of an occupancy-sensing switching OFF system could produce lower energy consumption.

Nevertheless, undoubtedly the two new models do not reflect all possible users' behaviour in relation to lighting system and its uncertainties. They are based upon the observation of only few users and, even if they have been called active and passive, in general, they could be seen as different hints of a single user type: people not so used to operate actions over the light system.

The differences between all the models highlights how interaction between users and artificial lighting is strictly related to the users themselves and probably to some circumstantial aspects that the models do not consider in their implementation for example seating orientation and controls' location. In particular, the new models' accuracy is decrease by the presence of a floor standing lamp.

For all the above-mentioned aspects, it becomes even more relevant the stochastic approach proposed by Fabi (2013) and Corgnati et al. (2006). It implies a probabilistic approach for the evaluation of both input and output parameters, due to the variability and unpredictability related to the whole building operation. The result of the design process should not be a single value, but the probability to fulfil a certain performance. Concerning human behaviour, the probabilistic output could be evaluated considering several user types, defined by different stochastic processes, for each interaction between occupants and building systems.

REFERENCES

J. Bartoňová, M.Kabrhel, K. Kabele, simulation of the impact of pcm plasters on thermal comfort and indoor environmental quality in offices

<http://www.clear-up.eu/>

Bourgeois D., Reinhart C., Macdonald I.A., (2006), Adding advanced behavioural models in whole building energy simulation: A study on the total energy impact of manual and automated lighting control. *Energy and Buildings* 38: 814–823

Buso T., Robustness of building design with respect to occupant behaviour, [master thesis] Torino: Politecnico of Torino, 2012

Corgnati S.P., Filippi M., Perino M., (2006), A new approach for the IEQ (Indoor Environmental Quality) assessment, *Research in Building Physics and Building Engineering. Proceeding of 3rd International Conference on Research in Building Physics IBPC 2006*, Montreal.

Daum D., Morel N., (2010) Assessing the total energy impact of manual and optimized blind control in combination with different lighting schedules in a building simulation environment. *Journal of Building Performance Simulation*, 3(1): 1-16

D'Oca S., Influence of occupants' behaviour on heating energy consumption and thermal comfort in residential buildings, [master thesis] Torino: Politecnico of Torino, 2012

Fabi V., Influence of Occupant's behaviour on indoor Environmental Quality and Energy Consumption, [Doctoral Dissertation] Torino: Politecnico of Turin, 2013.

Hunt D.R.G., (1979), The Use of Artificial Lighting in Relation to Daylight Levels and Occupancy. *Building and Environment*, 14: 21-33.

Reinhart C.F., (2004) Lightswitch-2002: a model for manual and automated control of electric lighting and blinds. *Solar Energy*, 77 (1):15-28

Reinhart C.F., Daylight availability and manual lighting control in office buildings – Simulation studies and analysis of measurements [Doctoral Dissertation] Dusseldorf: University of Karlsruhe, 2001.

Reinhart C.F., Voss K., (2003), Monitoring manual control of electric lighting and blinds. *Lighting Research and Technology*, 35: 243-260

Low order model selection for optimised heating start-up in tertiary buildings: Review and comparison of different approaches through a case study

J. Verhelst^{1,3,5}, D. Saelens^{2,5}, G. Van Ham^{1,4}, L. Helsen^{3,5}

⁽¹⁾ Knowledge Centre for Energy, KU Leuven Faculty of Engineering Technology, Geel

⁽²⁾ Building Physics Section, KU Leuven, Leuven

⁽³⁾ Mechanical Engineering Department, KU Leuven, Leuven

⁽⁴⁾ Electrical Engineering Department, KU Leuven, Leuven

⁽⁵⁾ Energyville, Waterschei

1. ABSTRACT

The energy use saving potential by improving the operation of building control is estimated to range from 10 to 30% of total HVAC energy use, in addition to savings from major retrofits performed in the same buildings. Often, inefficient operation is caused by control flaws, equipment flaws or changes in the building use. Continuous Commissioning (CC) is the set of actions taken to optimize the operational efficiency of the HVAC system.

Recent advances in the framework of system identification can help to realize and automate part of this CC process, by using low order predictive models as controller models. However, a crucial aspect for model based CC is the selection of a suitable simplified model.

To demonstrate this point, one specific CC task has been chosen: Optimized heating start-up (OS). For this task, a case-specific comparison is made between several model based algorithms: a first order bi-linear, second order non-linear and high-order black box model, using a detailed multi-zone white box model as an emulator.

The prediction accuracy, simulation performance and control performance in this CC-task are investigated for each of these low order models, taking into account the required information, the model development time and the simulation time. This comparison sheds light on the (dis)advantages of each simplified model structure for the chosen CC-application.

Keywords: HVAC start-up, simulation based performance evaluation, model selection, low order modelling

2. INTRODUCTION

Most tertiary buildings are occupied only during fixed, scheduled periods, mainly coinciding with weekdays. The primary purpose of a heating, ventilation, and air conditioning system (HVAC-system) is to maintain indoor conditions (a.o. temperature) at an acceptable comfort level during these occupied periods. Thermal comfort is mostly controlled by keeping the operative temperature within a fixed temperature band, determined by one or more set points and/or a dead band. A secondary target is to obtain this comfort level in an energy-efficient way.

During the unoccupied off-hours this tight zone temperature control is mostly not required, and is therefore often loosened to a much wider temperature band to save energy. The latter control strategy, called night or weekend setback (NSB), has received substantial academic and industrial attention since the energy crisis in the 70's, due to the relatively high potential for energy savings (12-34% according to Yang I.H. (2003)), its simple implementation and minimal

impact on thermal comfort during occupancy, compared to other energy saving control strategies.

It is widely accepted and illustrated (Bloomfield et al, 1977, Fraisse et al 1997) both by simulations and real-life demonstrations, that NSB-control strategy is especially valuable in buildings with lower insulation levels and low thermal mass, in cold climates with a mild mid-season. Energy savings up to 34% were realised, compared to a fixed set point control, while ensuring thermal comfort during scheduled occupancy (Yang et al, 2003). In buildings with higher thermal mass, savings up to 15% were reported (Moretza M. et al,1995), but for some combinations of building usage and HVAC-specifications in buildings with high thermal mass, a NSB strategy can even be less efficient than maintaining constant zone temperatures during unoccupied periods². The savings potential of NSB is positively correlated with the diurnal temperature difference, and negatively with the outdoor night temperature, duration of occupancy and switching frequency of occupancy. The magnitude of night setback is also a decisive factor, with typical optimal values between 2 and 12°C, highly dependent on the climate, HVAC capacity and building thermal capacity. In this paper, a night and weekend setback of 5°C has been selected, based on the research of Guo W. et al (2010), who investigated optimal NSB values for double-corridor classroom buildings in several climate zones.

To ensure that the thermal conditions are restored to a tight thermal comfort band before the building is occupied, the HVAC-system (including plant, distribution system and emitters) should be re-activated at a suitable time, early enough to guarantee thermal comfort, but late enough to increase energy savings to a maximal extent.

For heating mode, the required time with continuous full capacity heating, to reach the comfort set point just before scheduled occupancy, is called the “warm-up time” (WT) or “ramp time”. Its magnitude depends on many factors, a.o. the ambient conditions, building/ HVAC sizing, building/ HVAC states, timing and magnitude of external (e.g. irradiation) and internal gains (e.g. occupancy, equipment, lighting) and HVAC control settings. Especially buildings with higher thermal mass (Moretza.et all, 1995) have potentially large benefits from an optimised HVAC start-up strategy. But, also light-weight buildings in harsh climates, where (mid-season) ambient conditions can substantially deviate from the design conditions may benefit from improved start-up control (Bloomfield et al, 1977).

A similar start-up control strategy might be applied to cooling mode or ventilation. However, in most office buildings, the main occupation period starts after the coldest diurnal period of the day (the night), which typically has lower internal and external heat gains. Therefore, cooling (start-up) is rarely required in the morning. Optimised night (purge) ventilation timing or optimised cooling stop timing might have a slight energetic and comfort impact, but since the considered case is in a heating-dominated climate, it is not taken into account in this paper. It could however be evaluated in a similar way as heating start-up control.

2.1 Optimised start-up (OS) timing: State of the art

Optimised start-up (OS)³ timing is an operational strategy in HVAC-automation, which “automatically” determines the appropriate time to start HVAC systems to ensure the facility

² For example, when limited reheating capability is available (small pre-heating ratio), or when HVAC full-load efficiency is (substantially) lower than part load efficiency.

³ A plethora of methods and names are used to describe these algorithms,, both in industry and academia: the algorithms have been labelled with “Optimum”, “Optimal”, “Optimised”, “Adaptive” or “Intelligent”-tags, or are referred to with brand specific terminology. In this paper, the family of algorithms used for these purposes, is consistently named “Optimised Start-up (OS) timing”.

is comfortably conditioned for occupants during a scheduled time (Johnson Controls, 2011). These strategies can result in important energy savings and reduced HVAC operating hours, compared to a fixed start-up timing during the year, determined based on the worst case design conditions (coldest or warmest morning in the year). The maximum savings attainable using OS, are negatively correlated with the unoccupied period (%) and the steady state heat losses (W/m^2); and positively with the dominant time constant(s) (h^{-1}), occupation frequency (Hz) and the installed HVAC capacity (W/m^2) (Bloomfield, 1977).

The modelling and implementation for a stop (pre-emptive shutdown) of the HVAC system before the occupancy period is over (optimised stop timing) is very similar to the methodologies used for OS, but for a heating and cooling system in commercial buildings, the savings related to optimised stop at the end of the (scheduled) occupation period are negligible compared to the heating savings potential for optimised start-up (Bloomfield et al, 1977). Therefore, this paper focusses on heating OS only.

Theoretically, optimal start-up timing of an existing HVAC plant in a building, is attainable using the optimal control theory (Pontryagin, 1964) applied through emulations (Zaheer-uddin, 1993, House et al., 1994). However, this would require access to (near-)perfect thermal models of the building and HVAC system, a means to accurately estimate the current states of this building and HVAC system, together with (near-)perfect forecasts of the occupancy and disturbances. Despite the high penetration of distributed sensor networks and centralised building energy management systems (BEMS) in tertiary buildings, acquiring such detailed models, predictions and state information is still not economically feasible for “a typical” HVAC control application in “a typical” tertiary building.

The response of a zone temperature to the start-up of an HVAC-system (on/off) can typically be modelled by a multiple input, single output (MISO) system, with a dominating time constant for each set of thermal capacitances in the room (Trčka 2010). The most important thermal capacitances in HVAC in buildings (especially heavy-weight buildings) are the activated thermal capacity in building components (e.g. walls and floors), and the thermal capacity in zone areas (air/furniture) (Sourbron et al, 2011). As an OS control strategy is often embedded in a fast feedback loop, information about model and plant mismatch can be used to improve model parameters (manually or adaptively), or can be fed back to the process through a (local) PID loop. These two factors contribute to the fact that low order models can be used successfully in OS algorithms, which might be slightly sub-optimal (Bloomfield, 1977), but less burdensome to implement in practice.

Although the first thermostats incorporating NSB were developed more than 100 years ago (1904), the first OS-algorithms were developed and patented much later, around the start of the energy crisis in 1973 (Bloomfield et al, 1977). The interest in NSB, OS and other energy saving algorithms has increased again since the beginning of the 21st century, both due to the more stringent energy regulations in Europe (EPBD recast, 2010) and due to vastly modified building practices in Western Europe. The steady state losses and heat production capacity in modern tertiary buildings are significantly reduced, compared to older buildings (due to the increased building envelope insulation and modern HVAC technologies, e.g. heat pumps) (BPIE, 2010).

On the other hand, due to large glazing percentage and intense building use and consumer electronics, the influence of internal and solar gains is increasing in modern buildings. Under these conditions, the transient heat gains (solar and internal gains) become more dominant compared to the steady state heat losses (Kummert M. et al, 2001, Van Der Veken J., 2011, Ardehali et al, 1997). This results in large variations of the “heat gains to heat losses”-ratio over the year, leading to reduced energetic efficiencies for conventional, control strategies such as weather compensated control (WCC) (Verhelst, 2010) and fixed start-up timing after NSB.

For these building types, a more dynamic HVAC start-up strategy can lead to additional savings.

2.2 OS algorithms

Despite the prevalence of OS algorithms in both ancient thermostats and modern BEMS, very few BEMS manufacturers openly document the model structure and algorithms used in their products; and only a limited amount of standardisation around this topic exists in Europe. Two European standards (EN 12098-2:2003 and EN 12098-1: 2013) describe the minimal theoretical requirements⁴ and test conditions for “optimal start-up algorithms”, but no further enforcements are made.

Nevertheless, an overview of the evolution of OS-algorithms can be made, based on the existing literature and patents. Table 1 provides a (non-exhaustive) overview of commercial OS algorithms, whereas table 2 gives a summary of academic OS algorithms. For each algorithm, the algorithm name, author, model structure and type, meaning of parameters and level of implementation are mentioned.

All patented OS algorithms listed in table 1, use a single control (output) variable y , namely the time of HVAC start-up t_{start} . Two input variables are used in each OS-algorithm, namely the start time of occupancy $t_{\text{occ,start}}$ and the desired set point temperature at the start of the occupied period $T_{\text{zone, set point}}$. Frequently, additional input variables are: the outdoor air temperature T_{ex} , current or historic internal zone air temperatures T_{zone} , current temperatures of adjacent zones T_{adj} , occupation schedules, HVAC schedules, and historic measurements of temperatures, states, occupancy and performance. Some algorithms are trained only once during commissioning, with fixed model parameters per zone or per plant, others algorithms are self-learning, which means that tuning parameters are adjusted online, based on (short or long-term) historical performance. More recent patents also include OS algorithms which take into account utility time of day pricing information (e.g. Patent US 8204628 B2).

The listed academic OS-algorithms (see table 2), range from applying a “simple” adjustable start-up time per zone (0th order model), a fixed schedule based on outdoor temperature value or difference between indoor temperature and set point (linear, 1st order models), over exponential models (nonlinear), to “more complex” algorithms with multiple input parameters (MISO, piecewise linear or non-linear, n^{th} order models).

⁴ Using a simple building and HVAC emulation model, the BEMS OS-performance is judged at two ambient conditions (-5 °C and +5 °C), by the timely realization of zone set point temperature (allowed offset: 15 minutes) and a limited zone temperature overshoot (allowed offset: 0.5 °C).

Table 1: (non-exhaustive) Summary of Optimised HVAC start-up (OS)-algorithms found in patents

Brand, product & algorithm name	Model type and structure	Meaning of model Parameters	Level of implementation and notes
Johnson controls Metasys (DX9100), Optimal start/stop (Johnson Controls, 2010)	Type: bi-linear Structure: $\Delta t_z = a \Delta T_{ex} + b \Delta T_t + c$	a: insulation and HVAC capacity dependence b: thermal capacity dependence c: lag time dependence	Plant level
Siemens, visonik BPS, Optimum start-stop program (OSTP) (Siemens, 2000)	Type: Dynamic, adaptive bi-linear Structure: $\Delta t_z = a \Delta T_{ex} + b \Delta T_t$	a: insulation and HVAC capacity dependence b: thermal capacity dependence	Zone level
Honeywell, Adaptive Intelligent Recovery (AIR) (Honywell, 2012)	Type: Non-linear, transient model, Structure: $\Delta T_z = \Delta T_t + (1 - e^{\Delta T_{ex}/a}) * (b - \Delta T_t)$	a: dominant time constant = τ , b: Steady state heat rise ΔT_{ss} .	Zone level Adaptive recalculation
Computrols CBAS, Adaptive Optimal Start and Internal Set points (Computrols 2005)	Type: bi-linear model Structure: $\Delta T_z = a \Delta T_{ex} + b \Delta T_t + c$	a: insulation and HVAC capacity dependence b: thermal capacity dependence c: lag time dependence	Zone level Adaptive recalculation (<16days history)
Nest, Night time temperature economiser (Nest 2012)	Type: non-linear (Exponential) model Structure: $\Delta T_z = a / (1 - e^{b * \Delta T_{ex} - a}) - a^{-1.95}$	N/A	Zone level, adaptive tuning
Sauter EQJW145 heating controller	Type: Linear model Structure: $\Delta T_z = a * \Delta T_t$	a: insulation and HVAC capacity dependence	Plant level

Table 2: (non-exhaustive) Summary of Optimised HVAC start-up (OS)-algorithms found in the literature

Researcher(s), Publication Year and algorithm name	Model type and structure	Model Parameters	Level of implementation and notes
Bloomfield et al, 1977 , Optimum start control	Type: Linear model, (states assumed known) Structure: $\Delta T_z = a \Delta T_{ex} + b \Delta T_t + c$	a,b and c can be identified uniquely, for a perfect 1R2C building and no disturbances, using building and HVAC properties.	Plant level (emulated RC network) Linear RC model with two thermal capacities. Control model equals emulator model.
Zaheer-Uddin,1993, Modified Lag compensation	Type: Polynomial (linear) model with feedback. Structure: $\Delta T_z = a_i * [T_{ex}, T_t, T_{adj}] + b_i * (e_i)$	a _i : plant response parameters b _i : loop gain sensitivity	Plant level
Fraisse et al, 1996, Optimising heating-restart time	Type: Fuzzy Logic model using PI, PD and PID Structure: $\Delta T_z = PID(a T_{start} + b e_i)$	P, I, D parameters empirically defined as a function of T _{start} , based on historic data.	Plant level Adaptive, using “Activation degree (alfa)”, forgetting factor k
Yang in-Ho (2003) , Applications of Artificial neural networks	Type: ANN Structure: 8 nodes in hidden layer	Each node has a weighting factor for the inputs T _z , T _{ex} , ΔT _z and ΔT _{ex}	Zone level (on emulated RC network)
Suykens et al (2002), Li, (2009), Wang W. (2008); Support vector machine SVM	Type: Least squares support vector machines Structure: $\Delta T_z = a_{(1/e)} * T_i * T_i + (b_{(1/e)} * T_h)_c * T_i$	a _n and b _n are defined using penalty parameter, c: the radius; e, number of support vectors	Implemented at Zone level in FP7 Tibucon project [Van Der Veken J., 2011]. To our knowledge, no other or previous OSS applications used SVM.

2.3 Objectives

The variation and differences present in OS algorithms (tables 1 and 2) illustrate that in the past, a wide range of parameter models have been investigated and implemented for OS control already. However, in existing literature, it is not illustrated nor assumed that the predictive performance of a model is correlated with the task performance of an implemented OS controller. In other words, the following question arises: Is a more complex or a more accurate model always better at reaching the desired temperature in time (in a realistic setting)? The first goal of this paper, is to address this question.

The second goal is to evaluate the economic performance of the different control models in their execution of the OS-task. Each of the models requires input data, identification of parameter values, implementation time, and maintenance, and delivers a certain task (OS) performance. These aspects all have an economic impact.

3. METHODOLOGY

To evaluate the economic impact, a comparison framework is set up. Three existing predictive models (listed in the previous section) are implemented in an OS controller, operating on an emulator of a case study. To evaluate the performance of these algorithms, following key performance indicators (KPIs) are used:

- The yearly energy use $J_{e,tot}$ (kWh/m²/y), scaled by building surface
- An averaged and worst yearly discomfort $J_{d,aver}$ and $J_{d,max}$, expressed in (K²h/y),
- The tuning process difficulty, evaluated qualitatively [simple, medium, complex], based on average parameter identification time t_{ident} (s),
- The algorithm implementation difficulty [easy, moderate, hard], based on required time for implementation t_{work} (h)
- Required measurement data quantity and quality [high/medium/low], based on required number of input variables.
- The algorithm emulation time $t_{simulation}$ (minutes / year)
- The one-step and one-hour-ahead prediction accuracy, using several statistical metrics, e.g. Mean bias error (MBE) and *covariance*(RMSE) (dimensionless)

Due to the broad scope of this (CC) domain, and many existing models for OS, it is not feasible to model, identify and evaluate all existing commercial OS algorithms (table 1) and academic OS algorithms (table 2) simultaneously. But, thanks to the increase in computational speed, it is now feasible to evaluate multiple controllers over long periods of time, against detailed emulator models. Therefore, a subset of three models is retained for comparison amongst each-other, and against a reference controller (fixed time start-up). Apart from the model structures, also the number of inputs (1-7), and the model order (0-4th order) were limited per scenario. Following control models are selected, implemented on a case study and compared to a reference (no OS control) in this paper:

- **Reference controller:** Fixed start-up timing, thus no OS.
- **First order black box (BB) model:** Reference controller settings, with OS timing based on a bi-linear armax model of temperature response to heating, as a function of current zone and ambient temperature. This model is based on the model proposed by Bloomfield (1977).
- **Second order, non-linear BB:** Reference controller settings, but with OS timing based on an exponentially decaying temperature model of the zone temperature to heating energy input. This controller uses the model structure proposed by Honeywell (1991).
- **High order BB:** Reference controller settings, with OS timing based on a support vector machine (SVM) model as a function of current outdoor temperature, zone temperature,

occupancy & adjacent zone temperatures. This model uses the least-squares (ls-SVM) methodology and toolboxes, based on the frameworks developed by Suykens et al (2002)

The control performance of each of the evaluated algorithms is quantified by emulation of each control strategy, executed on a detailed white box model of a tertiary (office) building, using identical assumptions and boundary conditions. The white box model, assumptions and boundary conditions, as well as the structure and identification of the evaluated OS algorithms are described in the case study section (section 4).

In the end, choices should be made using one single evaluation criterion, based on appropriate weighting factors. In this paper, the final evaluation criterion is the summed monetary cost of investments, direct and indirect costs without VAT (Net present value), evaluated over a 5-year depreciation period (life cycle) of the OS control process. A 5-year depreciation period has been chosen for the OS evaluation, despite the fact that the expected total lifetime of a BEMS system is higher (around 20y), to allow for model and HVAC-updates if more effective techniques or methodologies appear.

For this purpose, a monetary weighting factor is defined for each of the relevant KPIs in the comparison. The process to estimate these weighting factors, the reoccurrence frequency of the costs and their proposed values are described below and summarized in table 3. In addition to these weighting factors, several assumptions about the economic environment have to be made. In this paper, the economic influences such as inflation, indexation of wages and energy cost increase are assigned fixed values (inflation: 3%/y; wage indexation: 3%/y, energy cost increase (before inflation): 4%/y). In future research, the sensitivity to these parameters can be investigated.

Table 3: Overview of applied monetary weighting parameters to calculate the NPV of the OS controller.

Influential parameter	Monetary weighting factor	Occurrence frequency over the lifetime of the BEMS
Energy use	0.00938 € / kWh _{heat}	Yearly
Discomfort cost	5 € / K ² _{average} / m ²	Yearly
Implementation	50 € / h _{work}	Once
Parameter tuning (based on qualitative ease of tuning)	[simple-medium-complex] 25 € -50 € -100 € / model	Yearly

In following paragraph, the methodology for determining each of the monetary conversion factors and KPIs is described. Some of the costs are assumed to reoccur yearly (e.g. energy cost, discomfort cost and supervised tuning) while others occur only once (e.g implementation).

The energy use (kWh/y/m²) is the heating energy use, as injected in the hydronic heating system by the heat generation plant. Heat used for ventilation preheating is not included, only the energy supplied to the distribution system (connected to the radiators). As the equivalent surface, the available zone surface on the fourth floor was used, which equals 760 m². The amount of lettable space on this floor is 330 m², when omitting the hallways, stairs, elevator shafts, sanitary and kitchen areas. The average temperature in the zones (°C) is the average thermostat temperature, evaluated over the whole year (both summer, mid-season and winter periods, workdays, weekend and nights). This value is defined as a weighted sum of radiative (star) temperature and air temperature. The monetary value of energy use (€/kWh) was determined based on an energy cost of 0.075 €/kWh_{gas} and a system efficiency (excluding the

efficiency of heating-up control) of $0.80 \text{ kWh}_{\text{heat}} / \text{kWh}_{\text{gas}}$. This results in an energy cost of $0.0938 \text{ €/kWh}_{\text{heat}}$

The underheating discomfort (K^2h_{aver}/y) is calculated for each zone separately, as the number of hours that the zones were underheated, weighted per time step by the squared magnitude of underheating degrees (K^2). K^2h was used as KPI, since it has correspondents better to productivity decrease (figure 1) and PPD (Sourbron et al, 2011), than other discomfort metrics such as underheating hours (h) or weighted underheating hours (Kh). As KPIs, both the averaged underheating discomfort [K^2h_{aver}/y] and the maximal underheating discomfort [K^2h_{max}/y] were defined by respectively averaging the discomfort over all heated zones, and finding the maximum discomfort [K^2h_{max}/y] attained in any of the heated zones. The underheating (dis)comfort was only evaluated during the heating season and during (emulated) occupancy.

The monetary value of discomfort ($\text{€/K}^2h_{\text{average}}/\text{m}^2$) is calculated, based on an estimated productivity reduction of 1% among office employees, when faced with a constant zone temperature of 19 °C during heating season (Seppänen et al, 2006). When using an assumed occupancy use of $10\text{m}^2/\text{employee}$ and $1850 \text{ working hours } h_{\text{work}}$ during the year, this corresponds to $185 \text{ K}^2h/y$ for our case study, which translates to a cost of $925 \text{ €/m}^2/\text{year}$, when using $50 \text{ €/h}_{\text{work}}$. By dividing these factors, the estimated monetary discomfort cost of $0.5 \text{ (€/m}^2/\text{K}^2h_{\text{average}})$ is attained.

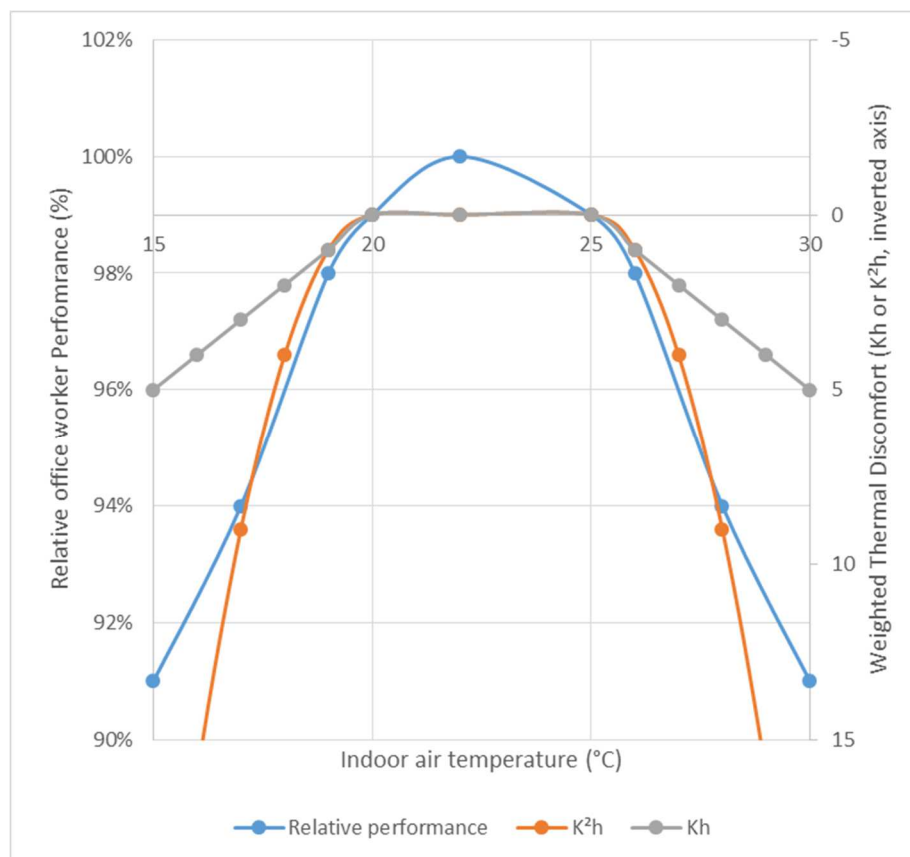


Figure 1: Relative office worker performance (left axis) as a function of indoor air temperature. Figure based on graph from Seppänen et al (2006). On the same graph, two thermal discomfort weighting methods are given as, a function of indoor temperature: Kh method and K^2h method (right axis), with a dead band between 20 and 25 °C . Note that the K^2h method has good correlation with the relative performance, especially in the regions with ambient temperatures 17 - 20 °C and 25 - 28 °C .

The implementation time is based on the estimated number of hours (h) required by the primary author of this paper, to develop and implement the control strategy on the emulator model. Despite the fact that the absolute values of this implementation time are highly dependent on the knowledge and skill level of the author, relative ratios between implementation times of different algorithms are meaningful weighting parameters. The monetary weighting factor linked to this estimation, is fixed at 50 €/h_{work}, with a multiplication factor of 10, to take into account practical difficulties for implementing it in a real case study.

The parameter tuning difficulty is a qualitative value [simple-medium-complex], based on the measured number of seconds required by the simulation program, to determine the parameters based on the emulator model. A low tuning time (< 10 seconds) corresponds to a simple tuning process, while a high value (>3600 seconds) qualifies as a complex tuning process. It is assumed that this tuning is executed unsupervised (either once or recurring for adaptive parameter control), but that it is supervised once a year during the process life cycle. This yearly supervising time of the tuning process is weighted based on the ease of tuning (qualitatively defined), with 0.5 h_{work} for re-assessment of a simple tuning process, 1h for medium and 2 h for complex tuning process, using a cost of 50 €/h_{work}.

The one-step-ahead (1TS) and one-hour-ahead (1HR) prediction accuracy are evaluated using the covariance of the root mean square error (CV(RMSE)) and the mean bias error (MBE), evaluated every simulation time step (150 s) when the OS algorithm is active (between 3 and 8 AM, on weekdays during the heating season), with a prediction horizon of resp. 150 s and 3600 s (1 h). No monetary weight has been defined for this parameter, since it is not taken into account directly for the control performance evaluation, only a-posteriori, to evaluate the relation between predictive performance and control performance.

The algorithm emulation time is a quantitative value based on the measured time for emulation of a reference year, using a white box TRNSYS 17 (for the emulator model) and Matlab 2010a (for the OS control), on a Desktop PC with following specifications: Dual core, 3 GHz CPU with 4 GB of RAM memory, with Win7 Enterprise OS. No monetary weight has been defined for this parameter, since it is not taken into account directly for the control performance evaluation, only a-posteriori, to evaluate the relation between predictive performance and control performance.

4. CASE STUDY AND OS ALGORITHM DESCRIPTION

In this section, the case study (emulator model) used for the comparison of different model-based optimised start-up algorithms is described, together with the evaluated control models.

“The typical building” does not exist as such. Especially in the tertiary building sector, there is a wide diversity in typology and building use. Therefore, it is difficult to select one relevant case study to evaluate the control performance of OS algorithms in general. The report made by BPIE (Buildings Performance Institute Europe, 2011) gives a good framework to situate the building types in the European tertiary building stock. The report states that 23% of the European non-residential building stock (in m³) consists of offices, and that around 19% of this portfolio is built between 1991 and 2010. About 50% of the tertiary buildings have a building ground surface between 200 and 1000 m². Average specific energy use for this sector is around 280 kWh/m²/y, and 26% of European energy use in buildings per year, can be allotted to office buildings.

In this paper, a white box model of a recently built office building is used as a reference for the emulations. The selected building is a representative sample of the building stock, as described above. This white box model is based on a real 4-story building, located in Warsaw, Poland.

The building was constructed in 2002 and measures 34.4 m by 22.1m (length & width). Figure 2 (a) presents the building and a schematic view of the building and the (b) distribution of internal walls. U-values for the building are listed in table 4. Each floor contains a central core, and a landscape office space around it. It can be randomly subdivided by the occupants, by erecting thin walls. For the simulations, the modelled (top) floor contains a central core, 4 meeting rooms, 2 kitchens, 4 individual offices and 2 landscape offices.

One floor (top floor) and its HVAC system are modelled in detail in Trnsys 17, using a multi-zone white box model with 16 thermal zones. The large landscape offices were split in three virtual zones, with large convective airflow exchanges, to take solar irradiation effects and temperature differences into account (see figure 2 b). As ambient conditions, a meteorological weather file for Warsaw (TMY2) is used. The occupancy schedules, and internal gains are modelled based on simulated yearly datasets from the EL²EP project (Parys W. et al, 2011).

Table 4: Building envelope material properties assumed for the simulations

	U-Value [W/m ² K]
Roof	0.26 (max 0.3)
Ground slab	0.58 (max 0.6)
Internal wall (around central core)	0.39 (max 0.55)
Internal wall	1
External wall	0.39 (max 0.55)
Windows (frames + glass)	Frame: 1.5 Glass: 1.1

Hot water for space heating is generated by two non-condensing boilers (2x130 kW) in the technical room. The heat is distributed to each radiator on the considered floor, located under each window, through a common collector and a distribution network in Tichelmann-configuration per floor. Each radiator is equipped with an electronically controlled on-off valve for flow control. The heating supply water temperature is controlled using outdoor temperature compensation (Weather compensated control (WCC)). Using On/off control instead of the more typical proportional control (e.g. thermostatic control) is not inefficient in this case, since the control time step (150 s) used is much higher (faster) than the dominant time constants (2-5 h). Furthermore, with a linear (heating) cost function, optimal control with perfect knowledge, always boils down to bang-bang control (on/off control) (Bloomfield, 1977).

Ventilation air is pre-conditioned in a central AHU, and supplied to fresh air supply grilles in each zone. Extraction is mainly performed in the central core but also through gratings in the recessed ceiling at several locations on each floor. The air is supplied at constant volume (CAV) during office hours at a rate of 0.8 air-changes per hour (2.4 m³/hr /m²), and at reduced rate (20% of nominal flow rate) during night and weekend hours.

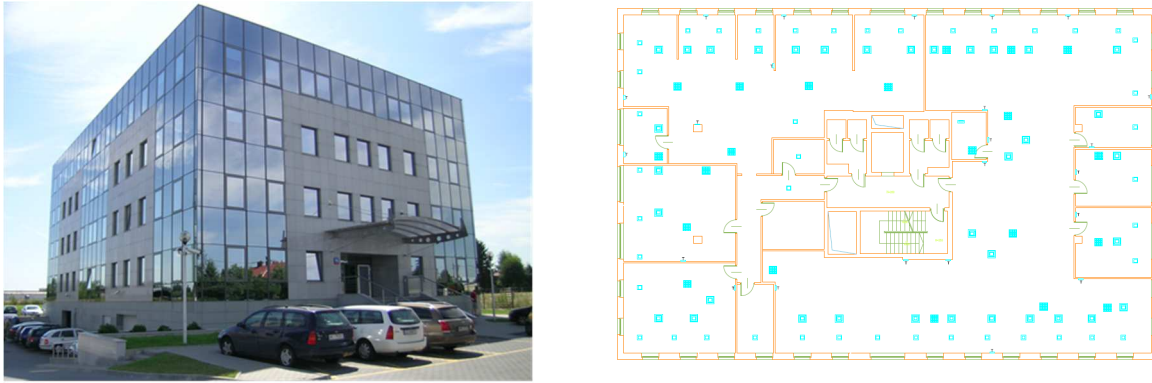


Figure 2: (a) Overview of emulated building, and (b) top view of the emulated (top) floor, with internal wall divisions as chosen by the occupants.

To evaluate (verify) the simulation accuracy of the emulator model in relation to the real building, 20 simultaneous measurements of temperature, relative humidity and occupancy were performed throughout the reference floor during winter, mid-season and summer conditions, using the “Reference” (A) and “high order BB” (D) control strategies (see Research Methodology). Each of the measurement datasets was split into two subsets: one subset of data was used as a training set, to fine-tune some of the unknown parameters (ventilation rate, heat transfer convection coefficient between virtual zones, heating curve parameters) of the emulator model. The other subset was used for cross-validation of the emulator prediction accuracy for the inside zone temperature (in an open loop simulation). The CV(RMSE) and MBE errors of these comparisons, are all in the acceptable range as prescribed by ASHRAE guideline 14 (Van Der Veken J., 2011).

Following four controller models were defined for the OS algorithms, identified and compared in yearly simulations (using Trnsys17 & Matlab 2010a):

- **Reference controller:** 5°C NSB, with fixed start-up timing ($t_{\text{start}} = -180$ min), thus no OS.
- **First order BB:** Reference controller settings with bi-linear OS having following structure:

$$y = a * \Delta T_t + b * \Delta T_{ex} \quad (1)$$
- **Second order, non-linear BB:** OS timing based on an exponentially decaying temperature response to heating:

$$y = a * e^{b/\Delta T_t} \quad (2)$$
- **High order BB:** OS timing based on a support vector machine (SVM) model, with inputs $T_z, \Delta T_t, \Delta T_{ex}, T_{ex}, T_{adj}, Irr$

For each of these model structures (besides the reference controller (A)) three variants were developed, to estimate (predict) following parameters:

- **Variante 1: Warm-up time length prediction (WT):** the time of continuous heating required to reach the zone temperature set point, given initial conditions.
- **Variante 2: One-step-ahead-prediction (1TS):** the temperature difference over one time step of heating (150 s).
- **Variante 3: One-hour-ahead-prediction (1HR):** the temperature difference over one hour of heating (60 minutes).

The predictive performance of each model is verified through auto-correlation with the training-set and cross-validation with the validation set. Also the prediction accuracy to estimate the one-hour-ahead temperature during implementation in control models (cross-validation 2) is determined.

5. VIRTUAL EXPERIMENT

This section discusses the training (tuning) methodology and performance evaluation methodology of the different model-based OS algorithms. Also, some typical temperature profiles encountered in the simulation runs are shown.

All (low order) models used, require parameter identification using a training data set, and ideally also a cross-validation data set. For this purpose, data was extracted from a yearly simulation with the emulator, without OS controller (case A1). The initial conditions (inputs to the models), heating periods and final conditions (zone temperatures) for all available periods of continuous heating are extracted from this data. The resulting dataset is split into a training dataset (1000 samples per zone) and cross-validation dataset (rest of data). The deterministic models are identified in Matlab, with respectively the Matlab ident-toolbox for the linear model (B), the Matlab surface fitting toolbox (sftool) for the exponential models (C) and ls-SVM toolbox for the SVM models (Suykens et al, 2002).

This training dataset and these predefined model structures are used to identify suitable parameters for each model variant. A posteriori, the validity of the model parameters is verified by evaluation of the prediction accuracy using the cross-validation dataset, against emulation with the white box model. A graphical representation of the training dataset and exponential WT model prediction is shown in figure 3, for one landscape zone (K). The prediction accuracy results of all models are presented in tabulated format (tables 8 and 9) and discussed in the results section.

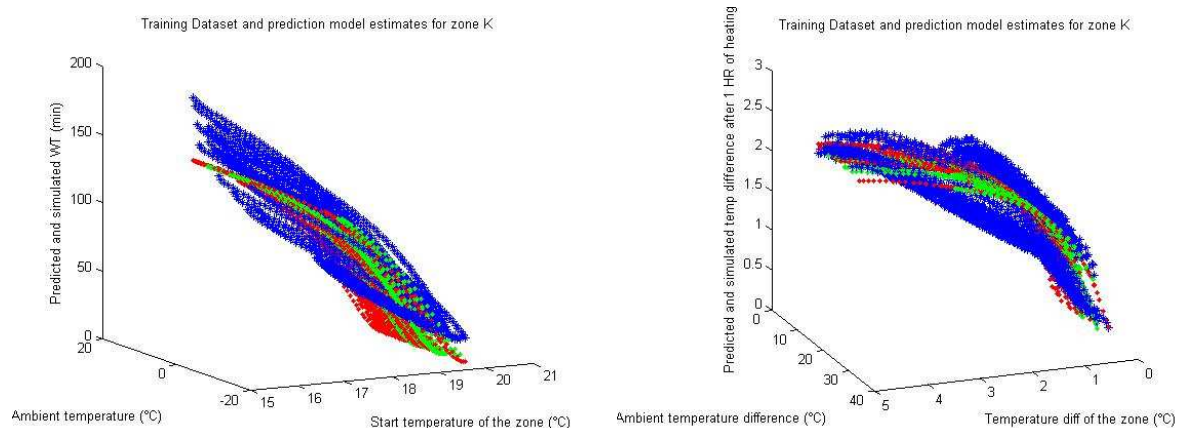


Figure 3 (a) Warm-up-length (blue dots, left figure) and (b) Temperature increase after 1HR of heating (blue dots, right figure) as a function of outdoor temperature T_{ex} and initial zone temperature T_z . The auto-correlation predictions (green dots) of exponential WT model (left) and exponential 1HR model (right) are given, together with their cross-validation predictions (red dots). Note the curved shape of the graph, especially in the dimension of the initial zone temperature.

Table 5: Ease of implementation of reduced models

Implementation KPI	Ease of parameter tuning (parameter identification time (s))	Algorithm implementation time t_{impl} (h)	Emulation time with OS-control (minutes)	Required data quantity and quality (qualitative: high – medium – low)	The ease of implementation (qualitative: easy – moderate – hard)
A: Reference controller (no OS)	0 s	0 h	63 min	None	Easy
B: Linear OS model	1 s	1 h	73 min	Low	Easy
C: Exponential OS model	30 s	3 h	78 min	Medium	Easy
D: High order OS (lsSVM)	1800 s	6 h	390 min	High	Medium

These four control algorithms (and three variants) were used in the OS controller, and emulated over a reference year. In the emulator, these models predict the WT time required per zone, at every time step. When the estimated WT is lower than (or equal to) the available time before occupation is scheduled, the heating is turned on. The quantitative output of the simulations, and several statistical indices, related to the predictive capability of the reduced order models, can be found in the results section.

Also the implementation time and difficulty was recorded (table 5). Several conclusions can be made here. The more simple models (linear, exponential) were processed quite fast by Matlab, both in parameter tuning and during emulation. This results in a relatively small emulation time (73-78 minutes). However, with more complex models (e.g. ls-SVM) using more parameters, both the simulation time and parameter tuning time increased substantially.

Typical simulated daily heating profiles with each of the OS controllers are shown in figures 3 and 4, both at the beginning of the week (Monday) and mid-week (Thursday). Only one variant (WT) is shown, for brevity. Figure 4 shows a cold winter period, whereas Figure 5 visualises typical temperature profiles on milder (mid-season) days. A fixed dead band of 0.5°C above the comfort setpoint (20°C) was applied for all controllers.

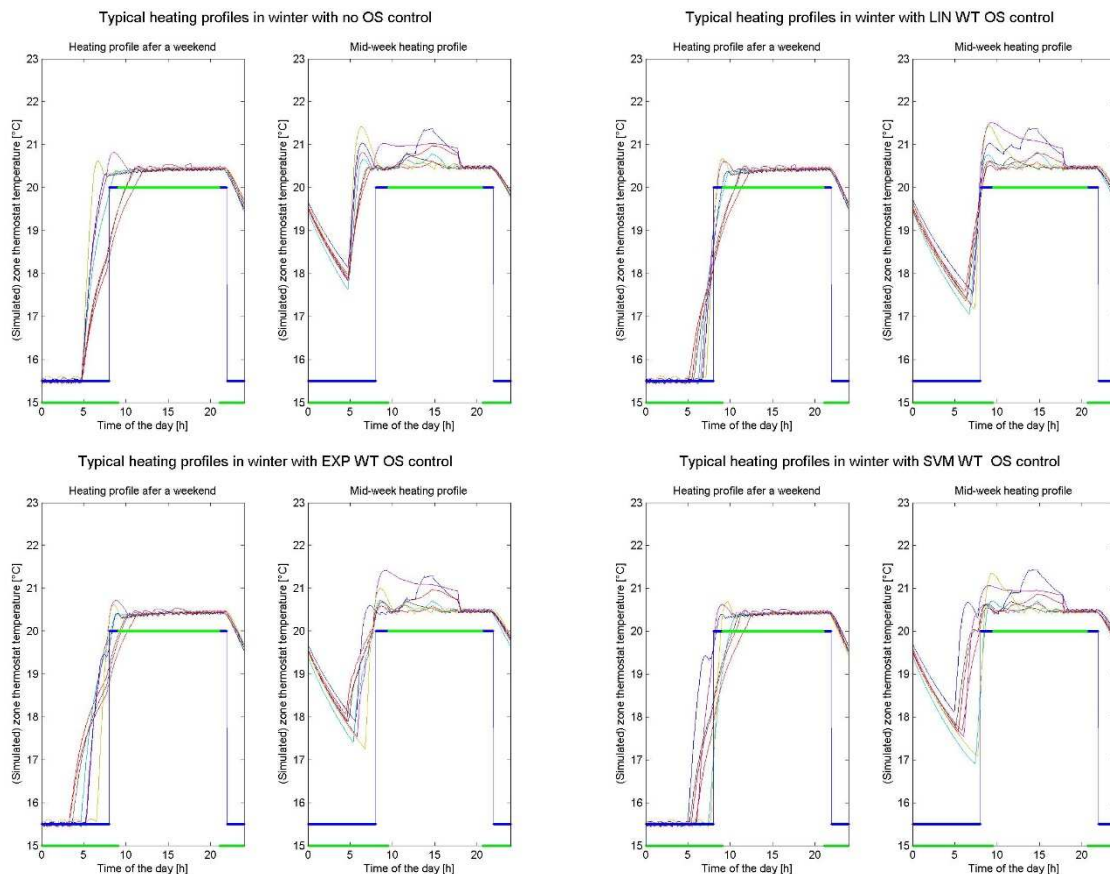


Figure 4: Simulated zone temperatures against time of the day during a cold week, on Monday (left pane) and Thursday (right pane), for 4 OS control models: (a) reference, (b) linear OS, (c) exponential OS and (d) SVM OS, each using the WT-prediction model. Graph contains office zone temperatures (thin colored lines), the heating set point (comfort) temperature (blue dashed line), and simulated office occupancy (green line). Note that in this cold week, the disturbance of solar gains and internal gains to zone temperature increase are limited.

From Figure 4, it can be concluded that during cold winter days, the reference controller always starts heating at 5 AM, which is not necessary for most zones. Especially in mid-week conditions, this results in a larger span of comfort temperature conditions, at an increased energy cost. In comparison, almost all of the other OS controllers are capable to act at the right moment, to heat up the zones at the ideal time, as to reach the set point just in time. Also, it can be noted that in some zones, none of the controllers (also not the reference controller) is able to reach the set point after a weekend, resulting in slight discomfort in some of the zones. Applying OS itself will not alleviate this problem, but the OS period might be expanded slightly (e.g. -2 hours) compared to reference control, leading to improved comfort in these zones as well, without drastically increasing energy cost.

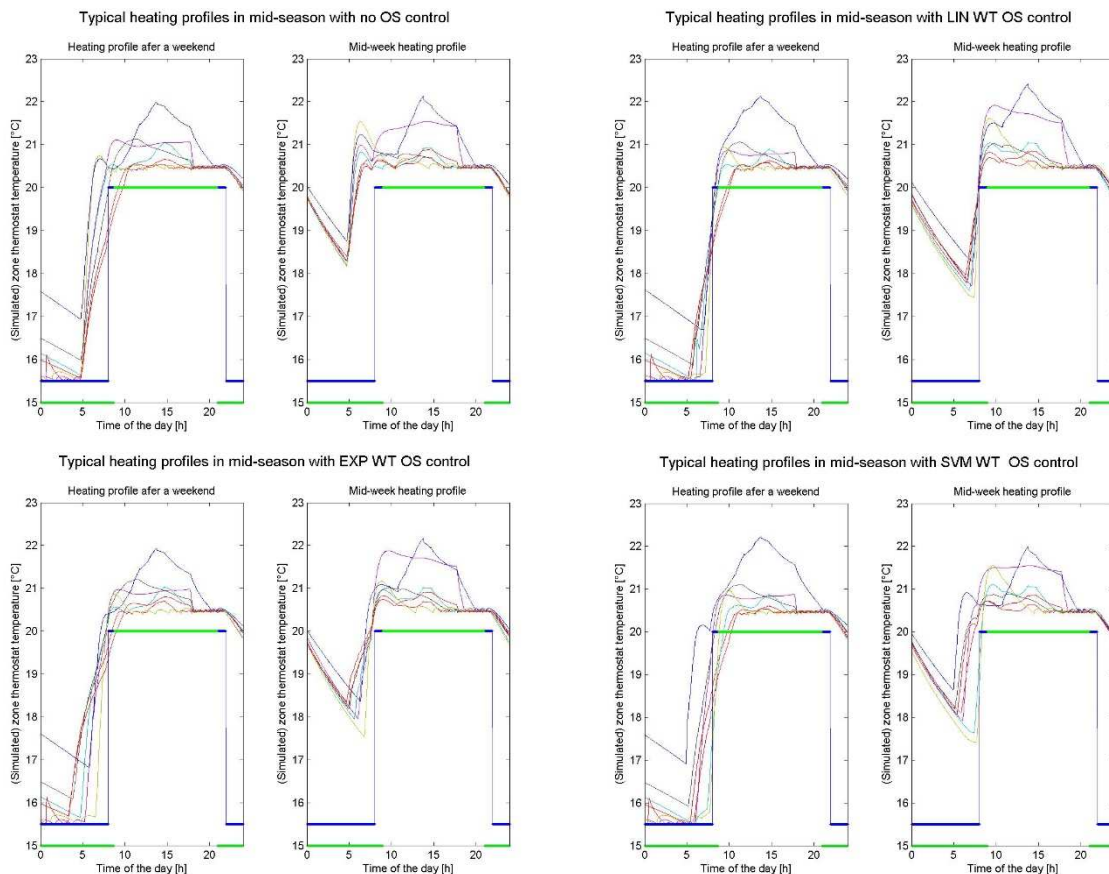


Figure 5: Simulated zone temperatures against time of the day during a mid-season, on Monday (left pane) and Thursday (right pane), for 4 OS control models: (a) reference, (b) linear OS, (c) exponential OS and (d) SVM OS, each using the WT-prediction model. Graph contains office zone temperatures (thin colored lines), the heating set point (comfort) temperature (blue dashed line), and simulated office occupancy (green line). Note that the contribution of solar and internal gains to zone temperature increase is significant in this season.

Figure 5 compares similar zone temperature profiles, but during a warmer period in the year (mid-season). Notice that with OS, the heating can start up at a later time during the morning (or sometimes not at all) in this period with fluctuating outdoor temperature. This results in reduced heating energy costs, while at the same time reducing afternoon overheating (or cooling energy cost). It can be noted that some models (e.g. linear) have a slight difficulty to estimate the heating behaviour for all zones correctly. It is assumed that the variation of outdoor conditions during WT and interaction between different zones are the main reasons for this mismatch. It is possible that these variations are insufficiently captured in the used training data. If so, adaptive parameter adjustment based on historic data (online model training) may lead to improved OS performance.

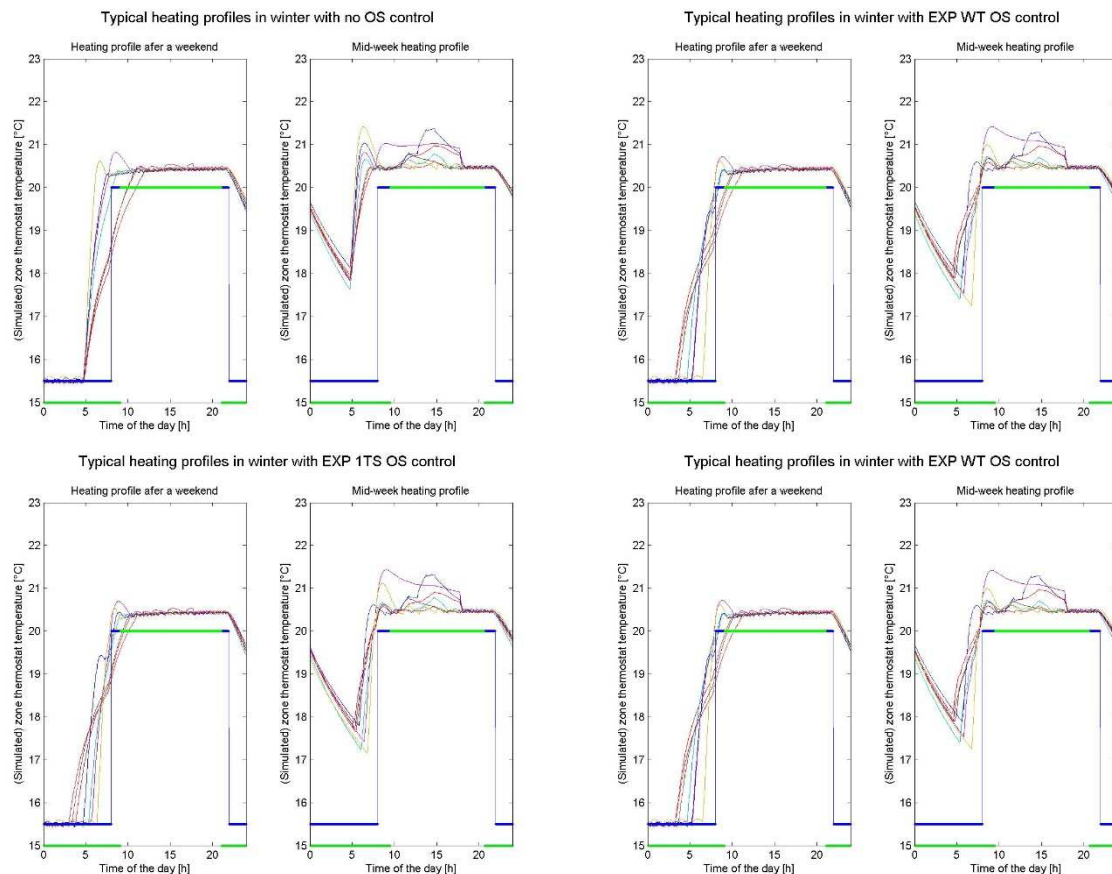


Figure 6: Simulated winter zone temperature against time of the day, on Monday (left pane) and Thursday (right pane), for reference control and 3 variants (WT, 1TS and 1HR) of one OS control model (exponential). Graph contains office zone temperatures (thin colored lines), the heating set point (comfort) temperature (blue dashed line), and simulated office occupancy (green line).

Figure 6 visualises the difference in warm-up profile (in winter) between the three variants (1TS: one-time step ahead, 1HR: one hour ahead prediction and WT: warm-up time prediction), for one of the models (exponential model). These figures show that all temperature profiles are quite similar, but that the WT prediction gives slightly more impulsive estimates than the 1TS prediction, whereas the 1HR prediction has a more aggressive behaviour (on/off cycling) during cold periods. During mid-season periods (figure not shown), their performance is very comparable.

6. SIMULATION RESULTS

As described in the Experiment section, emulations were performed, and the prediction performance of the models was evaluated a-posteriori. Tables 6 and 7 give the auto validation and cross validation statistics, as average values over the 10 evaluated zones. Note that the WT variant should not be compared directly to the 1TS and 1HR variant, since the units and scale of the prediction parameter is very different (minutes vs. °C), with average around 100 minutes for WT and 19°C for temperatures. However, the results can be compared among each other and other references.

Table 6: Auto-validation performance of linear and exponential predictive models, using training- dataset generated by simulation with reference controller

	Linear			Exponential			ls-SVM		
	WT	1TS	1HR	WT	1TS	1HR	WT	1TS	1HR
ae	1.73E+01	1.85E-02	2.65E-01	2.10E+01	1.85E-02	2.03E-01	1.70E+01	6.30E-03	2.20E-03
ape	2.16E-01	2.65E-01	2.06E-01	2.63E-01	2.65E-01	1.58E-01	2.36E-01	1.03E-01	1.60E-03
maxae	7.49E-01	2.73E+00	2.67E+00	9.70E-01	2.73E+00	7.15E-01	1.05E+00	6.80E-01	5.52E-02
mbe	2.04E+00	1.20E-03	1.48E-02	4.08E+00	1.20E-03	2.50E-03	1.70E+01	0.00E+00	0.00E+00
mae	1.73E-02	0.00E+00	3.00E-04	2.10E-02	0.00E+00	2.00E-04	1.70E-02	0.00E+00	0.00E+00
rmse	2.14E+01	2.23E-02	3.05E-01	2.44E+01	2.23E-02	2.47E-01	1.70E+01	7.30E-03	3.20E-03
cvmrse	2.64E-01	3.18E-01	2.38E-01	3.08E-01	3.18E-01	1.93E-01	2.36E-01	1.19E-01	2.50E-03
Mape	2.00E-04	3.00E-04	2.00E-04	3.00E-04	3.00E-04	2.00E-04	2.00E-04	1.00E-04	0.00E+00
stdAE	5.47E-01	6.00E-04	8.40E-03	6.64E-01	6.00E-04	6.40E-03	5.36E-01	2.00E-04	1.00E-04
sdAPE	6.80E-03	8.40E-03	6.50E-03	8.30E-03	8.40E-03	5.00E-03	7.40E-03	3.30E-03	1.00E-04
Cross covarian ce	96%	75%	88%	94%	106%	93%	90%	96%	71%
Covariance	96%	66%	87%	94%	68%	92%	90%	95%	71%

Table 7: Cross-validation performance of linear and exponential predictive models, using cross-validation dataset generated by simulation with reference controller

	Linear			Exponential			ls-SVM		
	WT	1TS	1HR	WT	1TS	1HR	WT	1TS	1HR
ae	1.51E+01	1.67E-02	2.40E-01	1.87E+01	1.67E-02	1.89E-01	4.82E+01	1.13E+00	3.18E-01
ape	1.92E-01	2.61E-01	2.05E-01	2.39E-01	2.61E-01	1.59E-01	6.47E-01	1.61E+01	2.67E-01
maxae	7.90E-01	3.45E+00	2.91E+00	9.52E-01	3.45E+00	6.97E-01	1.21E+01	3.80E+02	3.03E+00
mbe	6.98E-01	6.80E-03	9.45E-02	4.25E+00	6.80E-03	6.10E-03	1.34E+01	-2.57E-01	3.50E-02
mae	5.80E-03	0.00E+00	1.00E-04	7.40E-03	0.00E+00	1.00E-04	2.09E-02	6.00E-04	2.00E-04
rmse	1.92E+01	2.02E-02	2.85E-01	2.24E+01	2.02E-02	2.32E-01	7.46E+01	2.08E+00	4.77E-01
cvmrse	2.43E-01	3.24E-01	2.47E-01	2.87E-01	3.24E-01	1.97E-01	9.71E-01	2.94E+01	3.98E-01
Mape	1.00E-04	1.00E-04	1.00E-04	1.00E-04	1.00E-04	1.00E-04	3.00E-04	7.30E-03	1.00E-04
stdAE	2.81E-01	4.00E-04	5.30E-03	3.52E-01	4.00E-04	4.20E-03	9.50E-01	2.51E-02	6.80E-03
sdAPE	3.90E-03	5.20E-03	4.00E-03	5.00E-03	5.20E-03	3.10E-03	1.41E-02	3.35E-01	5.20E-03
Cross covarian ce	87%	65%	76%	86%	103%	81%	91%	2196%	65%
Covariance	86%	60%	76%	86%	60%	80%	78%	53%	50%

From the autocorrelation statistics (table 6), the temperature prediction models (1TS and 1HR) stand out as being very capable at predicting based on the training dataset, with a low average error (ae < 0.25K), and a low mean error (MBE < 10⁻³ K). Also, the standard deviation of the absolute error is low (below 10⁻³ K) for the temperature models. Note that the covariance of the RMSE shown in tables 6 and 7, is the covariance with the temperature difference prediction, (ΔT_z), not with direct temperature prediction (T_z). The average and variance of the original time series is thus very low (near 0°K), resulting in relatively high covariance of RMSE. These results are confirmed when evaluating the models against a cross validation dataset (table 7). The cross-correlation statistics (table 7) also show that the WT models (except for the ls-SVM model) are able to estimate the WT with an acceptable average error (ae) below 19 minutes.

The resulting covariance between simplified model prediction and detailed model emulation (prediction of cross-validation output based on model made on training-set data) is 50% to 86%. Especially the ls-SVM models seem to have trouble predicting the validation set correctly. This may be caused by over fitting, or cross-correlation between input parameters. But, overall, in a time window of 0-5 hours, reasonably good predictions are attainable with a low order models (1-7 parameters) to approximate a complex HVAC and building process as emulated by the white box model. Therefore, these models are deemed sufficiently accurate for OS control in a closed loop setting.

The in-simulation prediction performance during application of these models in a closed loop OS controller on the emulator is shown in table 8. For this 1HR ahead prediction, the average error is 0.7 to 2°C, which corresponds to 5 to 10% of the total estimate (ape). The covariance of RMSE of predictions against emulated temperatures, is below 11% for all models, which indicates that acceptable predictions were made by all variants (WT, 1TS, and 1HR) of the 3 model types. This is confirmed by the high covariance of predictions versus emulation (68-97%).

Table 8: One-hour-ahead temperature prediction performance for the predictive models during emulation using model based OS control. Since no temperature predictions are made for the WT-variant emulations, some columns in this table are unavailable (N/A). Columns marked in bold show the controllers with the best NPV performance.

	Linear			Exponential			ls-SVM		
	WT	1TS	1HR	WT	1TS	1HR	WT	1TS	1HR
ae	N/A	8.82E-01	1.05E+00	N/A	9.96E-01	7.33E-01	N/A	1.61E+00	1.09E+00
ape		4.51E-02	5.33E-02		5.09E-02	3.65E-02		8.27E-02	5.40E-02
maxae		8.29E-02	9.07E-02		6.99E-02	6.52E-02		2.22E-01	1.16E-01
mbe		8.08E-01	9.87E-01		9.22E-01	6.14E-01		-1.05E+00	4.13E-01
mae		1.90E-03	9.60E-03		4.20E-03	2.83E-01		1.70E-03	1.40E-02
rmse		9.35E-01	1.10E+00		1.04E+00	8.10E-01		1.95E+00	1.21E+00
cvmse		4.78E-02	5.59E-02		5.33E-02	4.04E-02		1.00E-01	5.99E-02
Mape		1.00E-04	5.00E-04		2.00E-04	1.37E-02		1.00E-04	7.00E-04
stdAE		3.58E-02	6.68E-02		5.58E-02	N/A		4.48E-02	8.82E-02
sdAPE		1.80E-03	3.40E-03		2.80E-03	N/A		2.30E-03	4.30E-03
Cross covariance		86%	107%		87%	N/A		92%	114%
Covariance		82%	97%		85%	84%		72%	68%

To evaluate the task performance of each of the OS algorithms, several KPIs are obtained, among which the Energy use per year (kWh/y/m²) and average/worse thermal discomfort (K²h/y). The simulation results are listed in table 9. The meta-simulation results, about the ease of generating and tuning the models, are given in table 5.

The simulation results (Table 10) show that the OS models result in a mediocre energy saving between 1 and 2.6 kWh/m²/y compared to the reference controller (which in our case study, corresponds to 0.5 to 2.62% compared to case A). This saving is generated, with a simultaneous decrease of thermal discomfort with -1.04 to -1.4 K²h/y or a 34% to 63% reduction compared to the reference). The preferred OS model highly depends on the costs and penalties given to each term, as shown in the economic analysis.

Table 9: Simulation output related to OS control performance. Columns marked in bold are the best variant (lowest NPV) within one model type

OS control performance Control algorithm: Model type & variant	Heating energy savings relative to reference (kWh/m ² /y)	Average Under-heating Discomfort in heated zones (K ² h/y)	Worse Under-heating Discomfort in heated zones (K ² h/y)	Average number of under-heating hours in heated zones (h/y)
A: Reference controller (no OS)	0 (ref:90.18)	3.80	17.6	9.2
B: Linear model, variant WT (B1)	-1.28	7.25	23.7	15.4
B: Linear model, variant 1TS (B2)	-1.27	2.56	5.07	5.5
B: Linear model, variant 1HR (B3)	-0.76	1.76	3.55	6.9
C: Exponential model, variant WT (C1)	-1.24	2.95	6.75	9.7
C: Exponential model, variant 1TS (C2)	-1.08	2.51	5.03	9.1
C: Exponential model, variant 1HR (C3)	-0.98	2.53	5.46	9.1
D: lsSVM, variant WT (D1)	-0.98	5.25	14.8	3.9
D: lsSVM, variant 1TS (D2)	-1.53	1.40	3.27	5.54
D: lsSVM, variant 1HR (D3)	+1.04	2.52	10.5	7.4

7. DISCUSSION AND RESULT ANALYSIS

When evaluating the model prediction efficiency on a one-hour-ahead prediction during heating phase, tables 7, 8 and 9 show that the exponential model with 2 inputs provides, on average, the most accurate estimations. Lower order models, such as the linear model, with 2 input variables (ΔT_i and ΔT_{ex}) also capture slow building dynamics reasonably well during the heating period, resulting in high prediction accuracy on the 1HR models (cross-correlation covariance around 85%), but lower prediction accuracy on the 1TS variants. The more complex models, e.g. ls-SVM variant 1HR have a slight tendency of over-fitting to the training data, as visualised by the substantial reduction of the covariance from auto-validation (67%) to cross-validation (41%).

Based on the results of the experiments, using the KPIs summarized in tables 3 and 5, the effectiveness of the evaluated algorithms can be investigated. The simulation results described in tables 9 are used as inputs for the economic NPV calculation and comparison (table 10). The NPV is calculated based on initial and yearly recurring cost, all recalculated to monetary value in the base year (year 0), taking into account monetary inflation (equation 3). By summing the three related costs over 5 years, the OS-control related NPV for the different controllers are obtained. The best (lowest) NPV for each of the controller type is given in table 10, together with three averaged yearly costs, in order to evaluate their relative importance in this comparison: Energy cost, Comfort cost and other costs (implementation and parameter tuning). The highest NPV (closest to 0) corresponds to the most beneficial control algorithm.

$$NPV_{ref=y_0} = \sum_{y=0}^n \frac{-C_y}{(1+i)^y} \quad (3)$$

Table 10: Economic comparison of the relative OS performance on Energy usage, Comfort and other related indirect costs for the case study, evaluated over a period of 5 years, and recalculated to the base year. Right side of the table gives the simple yearly cost of each KPI. Averaged values includes economic effects such as inflation, energy cost increase and indexation. The NPV (left column) is the sum of all related costs over 5 years.

Economic metrics	OS-control related NPV (€/m ² /5y)	Average Energy cost, (€/m ² /y)	Average comfort cost, (€/m ² /y)	Average other indirect costs (€/m ² /y)	Yearly Energy cost (€/m ²)	Yearly Discomfort cost (€/K ² h _{ve} /m ²)	Initial implementation cost (€/m ²)	Yearly Parameter tuning cost (€/m ²)
Control algorithm								
A: Reference: Fixed starting time	-53.83	8.62	2.15	0.00	8.45	1.90	0.00	0.00
B3: Linear OS, 1HR variant	-49.26	8.55	0.99	0.31	8.38	0.88	1.52	0.01
C2: Exponential OS, 1TS variant	-51.26	8.52	1.42	0.32	8.35	1.26	1.52	0.02
D2: ls-SVM OS, 1TS variant	-56.78	8.72	0.79	1.85	8.55	0.70	9.09	0.03

From the economic performance of the best control model variants (table 10), it can be seen that globally, the Linear 1HR OS has the best NPV of all other compared controllers, with both a decrease in discomfort cost (-54%) and a small decrease in energy use cost (-1.4%) compared to the reference. The fixed start (reference control A) results in quite low thermal discomfort (2.15 €/m²/y), which can be increased slightly by preponing the start-time, but at the cost of increased energy usage. Compared to this reference control, both the linear OS and exponential OS models result in small energy usage reduction (-0.8 to -1.4%), and moderate discomfort reduction (-34 to -54%). The ls-SVM model is capable of reducing discomfort cost even more (-63%), but does so at a slight increase of energy use (+1.2%), and along with a very significant parameter tuning and implementation cost (above 1.8 €/m²/y). Since the spread (standard deviation) of the discomfort cost between different OS-models is quite large compared to the spread on energy costs, the models can be differentiated mainly on this axis. In this economic evaluation, the largest cost (also with large spread) is the indirect parameter tuning and model implementation cost, which is detrimental to the NPV of the ls-SVM model.

When comparing the covariance on cross-validation of the best performing (lowest NPV) models for each type, none of the variants with the best cross-validation performance, has the highest modelling accuracy. For example, the 1TS variant of the exponential and ls-SVM models outperformed their 1HR or 1WT variants on KPI performance during emulation, despite their relatively lower modelling accuracy. However, the prediction performance during control operation (table 10), is correlated with the performance on energy and comfort cost, both between types and between variants of one model type.

Thus, based on the comparison of the model task performance and model accuracy on this case study, it cannot be concluded that the more complex models integrally outperform the lower order models, when taking into account the total NPV including energy, discomfort and parameter tuning costs.

Also, when evaluating OS-control performance in detail, e.g. evaluating only energy performance, thermal discomfort performance or the other related costs (implementation and tuning cost), no single linear relation could be found between the task performance and simplified model prediction accuracy on the auto validation or cross-validation dataset or for this case study.

8. CONCLUSION

No single significant positive correlation could be detected between the prediction accuracy of the training or cross-validation data on the one hand, and either the energy use, thermal discomfort or other related costs on the other hand. However, several trade-offs can be found in the range of evaluated algorithms. For more complex predictive models, an important increase in modelling and tuning difficulty is observed. This is accompanied by an improved cross-validation prediction accuracy on emulation data, and reduction in thermal discomfort.

If all costs (NPV) are taken into account, the low order models seem to excel at OS. However, both low (linear) and very high order (SVM) models show good KPI performance, when the importance given to parameter tuning cost and initial implementation cost is lowered.

Due to large variations in KPI performance, the selection of the most suitable OS model analysis very much depends on the actual monetary weighting put on the KPIs (evaluation criteria), that can be very case-specific. In this case study, discomfort and parameter tuning were heavily penalised. The high parameter tuning cost causes a distortion towards models with lower parameter tuning cost. Increasing the monetary cost linked to thermal discomfort, would e.g. tilt the comparison towards the more complex models (e.g. ls-SVM), with better thermal comfort performance.

9. FUTURE WORK

The sensitivity of these conclusions to variations in controller- and building parameters, which were assumed to have fixed values in this paper, such as length of OS window, level of night setback, insulation level, ventilation rate, etc. could be investigated further. The control strategies discussed in this paper, can be tuned further (or even be tuned specifically/adaptively) for other trade-off ratios between energy use and thermal discomfort, and for different scenarios (e.g. Monday v.s. the rest of the week). A-symmetrical mismatch penalty factors during identification might be a useful tool to identify a good control model directly. Last but not least, the identification of grey box models based on physical relations between HVAC energy flows and based on simulation data, can be valid alternatives to reduce implementation time.

REFERENCES

- Bloomfield D.P., and Fisk D.J., 1977. *Optimisation of intermittent heating*. Building and Environment, vol:12, i:1, p: 43-55
- Moretza M., and al., 1995. *Evaluation of HVAC system operational strategies for commercial buildings*. Energy Conversion and Management, vol:38, i:3, p:225-236
- Kummert M., André P., and Nicolas J., 2001. *Optimal heating control in passive solar commercial building*, Proceedings of ISES-Europe Solar Congress, vol:69, i:1-6, p:103-116
- Guo W., and Nutter D.W., 2010. *Setback and setup temperature analysis for a classic double-corridor classroom building*. Energy and Buildings vol: 42, i: 2, p189–197

- Van der Veken J., Verhelst J., and Croonenborghs T., 2011. *Building thermal simulation and control models to support "Self Powered Wireless Sensor Network for HVAC System Energy Improvement"*. Available online at: <http://www.tibucon.eu/docs/newsletter-2-INDD->
- Sourbron, M., and Helsen, L., 2011. Evaluation of adaptive thermal comfort models in moderate climates and their application to office buildings equipped with Thermally Active Building Systems (TABS). *Energy & Buildings*, vol:43, i:2,p:423-432
- House J. M., and Smith T. F. 1994. *A General Purpose Simulation Code for Optimal Control for Building and HVAC Systems*. Technical Report, ME-TFS-94-008. Department of Mechanical Engineering. The University of Iowa, Iowa City.
- Aldehali, 1997. *Evaluation of HVAC system operational strategies for commercial buildings*. *Energy conversion and management (0196-8904)* vol:38 nr:3 p:225 -236
- Zaheer-uddin M., 1993. *Intelligent control strategies for HVAC processes in buildings*. *Energy* vol:19, i:1, p:67-79
- Zaheer-Uddin M., 1993. *Energy start-stop and fluid flow regulated control of multizone hvac systems*. *Energy* vol: 18, i:3, p:289-302
- Moon J.W., Sung K.J., Kim Y., and Han S.H., 2011. *Comparative study of artificial intelligence-based building thermal control methods – Application of fuzzy, adaptive neuro-fuzzy inference system, and artificial neural network*. *Applied Thermal Engineering*, vol:31, i:14–15,p:2422-2429
- Hensen J.L.M., and Yahiaoui A., 2006. *Model based optimal control for integrated building systems*, Proc. of 6th int. postgraduate research conf in the built and human environment
- Lu X., Clements-Croome D.J., and Viljanen M., 2009. *Past, present and future mathematical models for buildings (ii)*. *Intelligent Buildings International Journal*, vol: 1 i: 2, p:131-141.
- Trčka M., Hensen, J. L.M., 2010. Overview of HVAC system simulation. *Automation in Construction*, vol:19,i:2,p.93-99
- BPIE report, 2011. ISBN: 9789491143014 Available online at <http://europeanclimate.org/documents/>
- Yang I.H., 2003, *Application of artificial neural network to predict the optimal start time for heating system in building*. *Energy Conversion and Management*, vol:44, i:17, p:2791–2809
- Yun J., and Kwang-Ho W., 2003, *Building Environment Analysis based on Temperature and Humidity for Smart Energy Systems* Sensors (Basel). vol:12, i:10,p:13458–13470.
- Wang W., 2008. *Online prediction model based on support vector machine*. *Neurocomputing*, vol:71, i:4–6, p:550–558
- Parys W., Saelens D., and Hens H., 2011, *Coupling of dynamic building simulation with stochastic modelling of occupant behaviour in offices – a review-based integrated methodology*. *Journal of building performance simulation*, vol:4 i:4 p: 339 -358
- Suykens J.A.K., Van Gestel T., De Brabanter J., De Moor B., and Vandewalle J., *Least Squares Support Vector Machines*. Publisher: World Scientific, Singapore, 2002 (ISBN 981-238-151-1). ls-SVM Toolbox available online at <http://www.esat.kuleuven.be/sista/lssvmlab/>
- De Coninck R., Magnusson F., Akesson J., and Helsen L., 2014. *Grey-Box Building Models for Model Order Reduction and Control*. Proceedings of Modelica conference, Lund
- Seppänen, P., and Wargocki O., 2006. *REHVA Guidebook No. 6*. Publisher: REHVA , Brussels, www.rehva.eu

- Johnson controls, 2010. *Metasys data sheet*. Available online at http://cgproducts.johnsoncontrols.com/MET_PDF/1201527.PDF, accessed on 15/06/2014
- Siemens, 2000. *Function sheet CM2N8892en / 02.2000 Siemens VISONIK® Optimum Start/Stop Program BPS*. Available online from www.siemens.com, accessed on 26/6/2014
- Honeywell, 1991-2012. *Patent US 4660759, 1884, US5192020 and US502598*. Available online at <http://patents.google.com/>, accessed on 26/6/2014
- Computrols, 2005. *Computrols website*. Available online at <http://www.computrols.com/> , accessed on 26/6/2014
- Nest L., 2012. *Patent US8554376 (Nest Labs)*. Available online at <http://www.google.com/patents/>, accessed on 26/6/2014
- Matlab, 2010. *Matlab system identification toolbox*. Available online at <http://www.mathworks.nl/products/sysid/>
- Fraisse, G., Virgone, J. and Brau J., 1997. *An Analysis of the Performance of Different Intermittent Heating Controllers and an Evaluation of Comfort and Energy Consumption*. HVAC&R Research, 1997, vol:3, i:4, p.369-386

Design and Optimization of Geothermal Heat Pumps in Combination with TABS

Arno Dentel^{1*}, Thomas Dippel², Mario Franz¹, Wolfram Stephan¹

⁽¹⁾ Technische Hochschule Nürnberg Georg Simon Ohm, Institute for Energy and Buildings, Energie Campus Nürnberg, Keßlerplatz 12, 90489 Nürnberg, Germany

⁽²⁾ TEB – Transferzentrum Energieeffizientes Bauen GmbH Kehlstraße 27/1, 71665 Vaihingen an der Enz, Germany

1. ABSTRACT

For the design and optimization of ground-coupled heat-pump systems (GCHP) in combination with thermally activated building systems (TABS), several methods were investigated and presented. At first an optimization of the hydraulic system of the GCHP is done. One alternative, in comparison with a best practice example, is splitting up the ground heat exchanger (GHX) into two bore fields to optimize the operation between passive and active cooling. Furthermore, the brine in the system is replaced by water, from this, it follows that the amount of heat exchangers and circulation pumps are reduced. In addition, a second hydraulic concept based on the previous one was defined and evaluated. This time, only water is used as medium at the condenser side of the heat pump, through the ground heat exchanger and at the evaporator side, a glycol-water mixture is used. This concept optimizes only the cooling site of the system. For each hydraulic concept, different mass flow rates were studied. The results show that the system with an optimized hydraulic concept has a 15% higher seasonal coefficient of performance (SCOP) than a built best practice system. For the simulations, a complex simulation model of an office building with TABS, a heat pump, ground heat exchanger, and system control was built in TRNSYS 17 (Klein, S.A. et al., 2012). As a second method, a parametric study was carried out for the design parameters, like storage volume and number of boreholes. For the optimization studies, the software GenOpt (Wetter, 2009) was used, a co-simulation with TRNSYS.

Keywords: simulation, hydraulic, optimization, TABS, heat pumps

2. INTRODUCTION

Modern office buildings are characterized by high-comfort features at the one hand and minimum energy consumption on the other hand. This can be realized with enhanced ecological innovative building and system concepts. A possible combination to achieve this goal is a ground-coupled heat-pump system (GCHP) in combination with thermally activated building systems (TABS), that allow both low temperature heating and high temperature cooling, which are very interesting from an energetic and exergetic point of view. The design of GCHP and TABS is completely different from quick-reacting heating and cooling systems. An efficient and high quality control of these systems is needed due to the inert performance. In addition, a careful design is a requirement for an energy-efficient building and system operation. These facts are taken up in the research project GEOTABS (Hoogmartens & Helsen, 2012). The aim of the project is to use monitoring and simulation data as feedback to improve the design of office buildings. This paper represents outcomes concerning improved hydraulic concepts for a GCHP and TABS systems.

2.1 Hydraulic Layout of the Reference System

The reference system is also modeled and shown in Figure 1. For the reference case, an installation of an existing building is chosen. The name of the building is “Hollandsch Huys” and it is analyzed in a case study in the context of the GEOTABS project. The office building has approximately 4000 m² floor area; more details about the case study “Hollandsch Huys” can be found in Lemort (2012).

The installed hydraulic of the geothermal heat-pump system of the Hollandsch Huys consists of the following components:

- Ground heat exchanger with 22 single non-interacting double-U-type probes, tube diameter 32 mm
- Length of a single probe: 75 m
- Linear arrangement of the probes, separated into two fields
- Operating point of the ground heat exchanger: turbulent flow conditions
- Heat transfer medium of the ground heat exchanger: glycol-water mixture
- Storage for hot and cold water, each with a volume of 1 m³
- Heat pump with three power levels: 45 kW, 45 kW, and 55 kW
- One cold and one hot water collector
- Seven circulation pumps

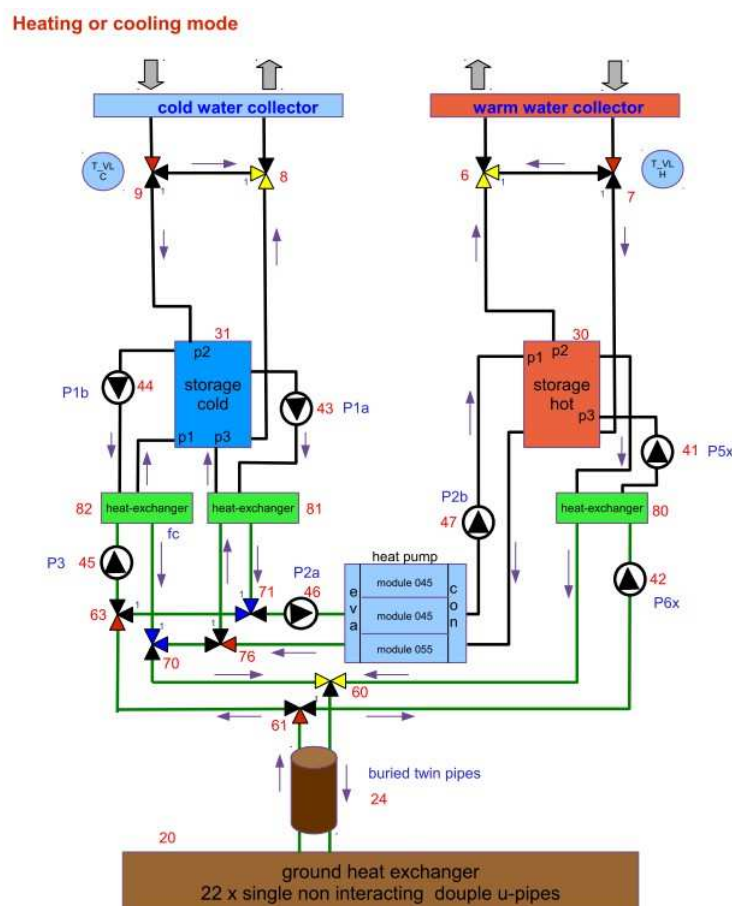


Figure 1: Hydraulic scheme of the reference case

In heating mode, only the pumps 2a and 2b are running; in active cooling mode, the pumps 1a, 2a, 2b, 5x, and 6x are operative; and in passive cooling mode, just the pumps 1b and 3 are

running. At this, the pumps are always running with a constant mass flow rate with turbulent flow conditions for all operating modes.

Apart from the reference case, two alternative hydraulic schemes were investigated, using the example of the case study:

- New hydraulic system layout 1: Divided GHX with complete water loop GHX
- New hydraulic system layout 2: Divided GHX with water loop only on the condenser site of the heat pump

2.2 New Hydraulic System Layout 1

Figure 2 shows an overview of the first modified hydraulic concept. The main change in the hydraulic configuration is the division of the GHX into two separate fields to optimize the passive cooling opportunity. The basic idea of the two fields is that the first field is mainly for the use of passive cooling. The second field has, in the active cooling mode, the function of a cooling tower and discharges the warm storage tank during active cooling operation. This can be done without heating up GHX 1. Thus, the first GHX still has potential for passive cooling after a phase of active cooling.

To increase the capacity in the GHX, loop water is used as heat-transfer medium in the ground heat exchanger. This is done for many reasons: water is more cost-effective compared with brine, easy to handle, and can comply with environmental regulations. The advantage of a higher thermal conductivity of water, as the glycol-water mixture, is accompanied by a temperature range in the GHX above freezing point.

With the reduction to one-water loop, three heat exchangers can be eliminated. This results to a cost benefit and there is no temperature loss due to the heat exchangers. A reduction in the number of circulation pumps comes along with HX reduction. The result is a reduction in electrical energy consumption aside from other cost benefits.

In case of layout 1, an operational advantage is the central integration of the heat pump between the two storage tanks. The heat pump can be operated hydraulically and independently when switching over to the probes. Only the two storage tanks are connected to the ground heat exchanger. Variable mass flow rates of the brine pump are possible without affecting the safety function of the heat pump. The circulation pumps of the heat pump are power-controlled, due to different HP power levels. Through this hydraulic scheme, a simultaneous heating and cooling operation becomes possible.

Depending on the operation mode, the following pumps are on:

- heating mode: pumps c_1, h_2, and b_4,
- active cooling mode: all three pumps are active and
- passive cooling mode: b_4 is running.

The control strategy used here for switching between the first and second GHX field is:

- activating the passive cooling mode: using GHX field 1
- ongoing passive cooling mode, but temperature exceeds threshold: using GHX field 1+2
- activating the active cooling mode: using GHX field 2
- ongoing active cooling mode, but temperature exceeds threshold: using GHX field 2+1
- activating the heating mode: using GHX field 1+2
- minimum time for connection: 30 minutes

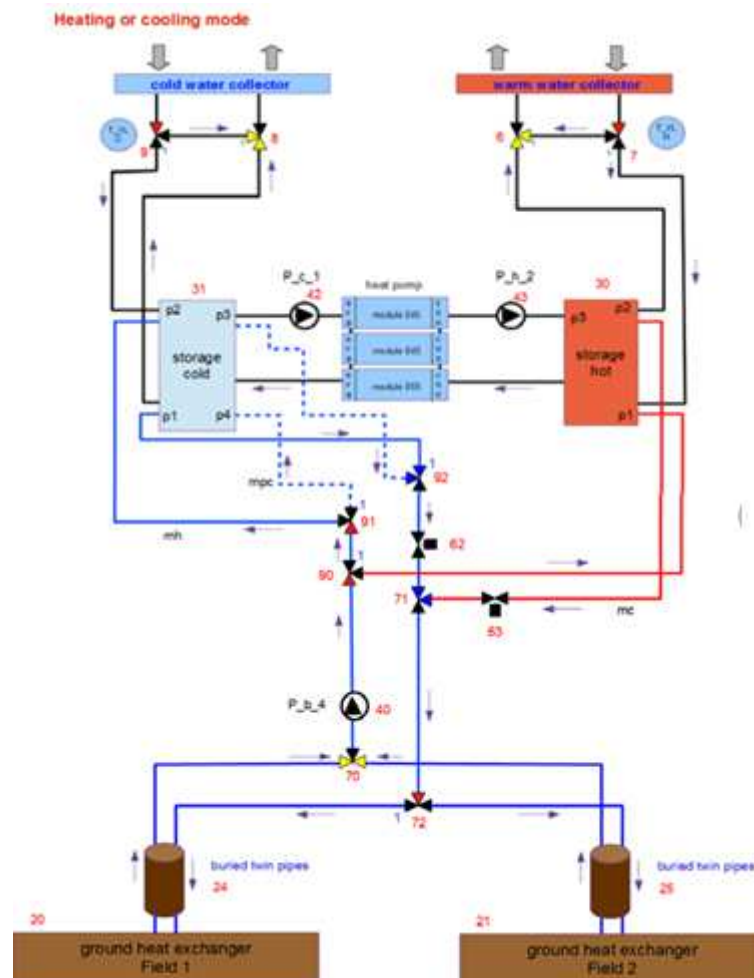


Figure 2: Hydraulic scheme of the new system layout 1

2.3 New Hydraulic System Layout 2

A second hydraulic concept based on the previous system is illustrated in Figure 3. This time, only water is used as medium at the condenser side of the heat pump, through the ground heat exchanger and at the evaporator side, a glycol-water mixture is used. Therefore, compared with the previous version, this variant contains two additional fluid-to-fluid heat exchangers and five pumps with variable mass flow rates.

Depending on the operation mode, the following pumps are on:

- heating mode: pumps c_1, h_2, and c_4,
- active cooling mode: all five pumps are active and
- passive cooling mode: b_4 and c_5 are running.

The brine pump still operates with variable flow rates, 1,600 kg/h per borehole when operating with turbulent flow conditions and 750 kg/h when operating with laminar flow conditions.

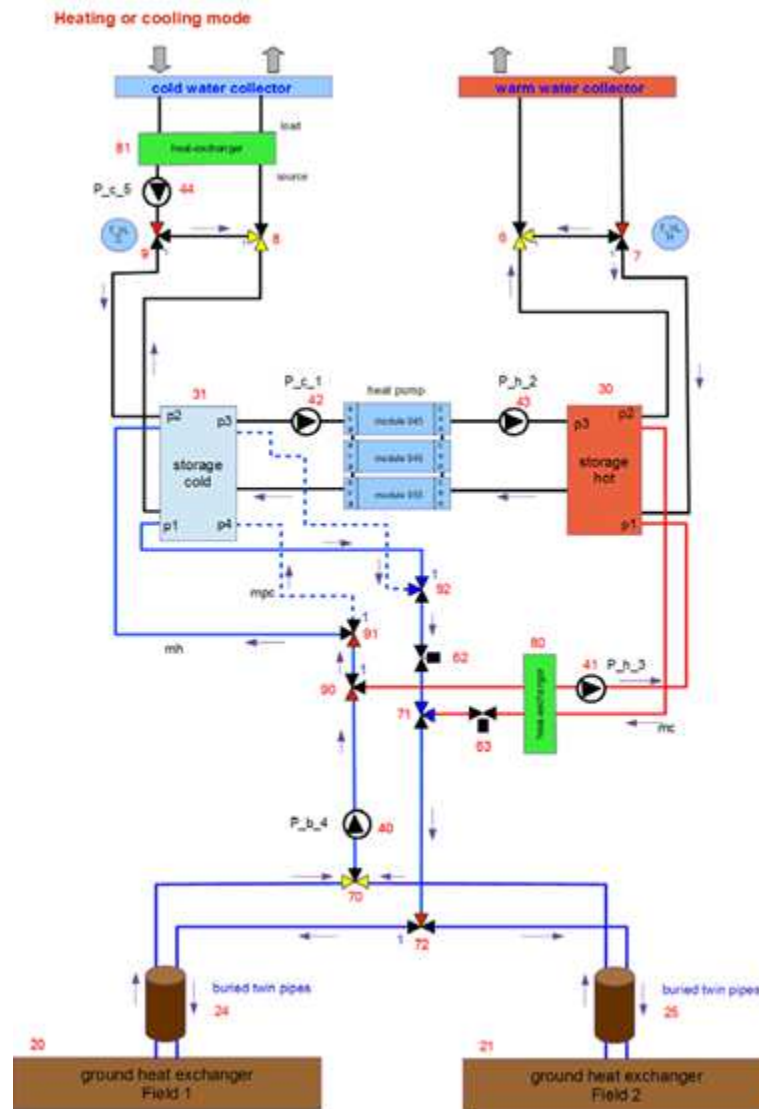


Figure 3: Hydraulic scheme of the new system layout 2

2.4 Definition of the Seasonal Coefficients of Performance and Defining the System Boundaries

In this chapter, the seasonal coefficients of performance (SCOP) for the different operating modes and system boundaries are defined.

Figure 4 shows the several system boundaries used to reflect the different seasonal coefficients of performance (SCOP).

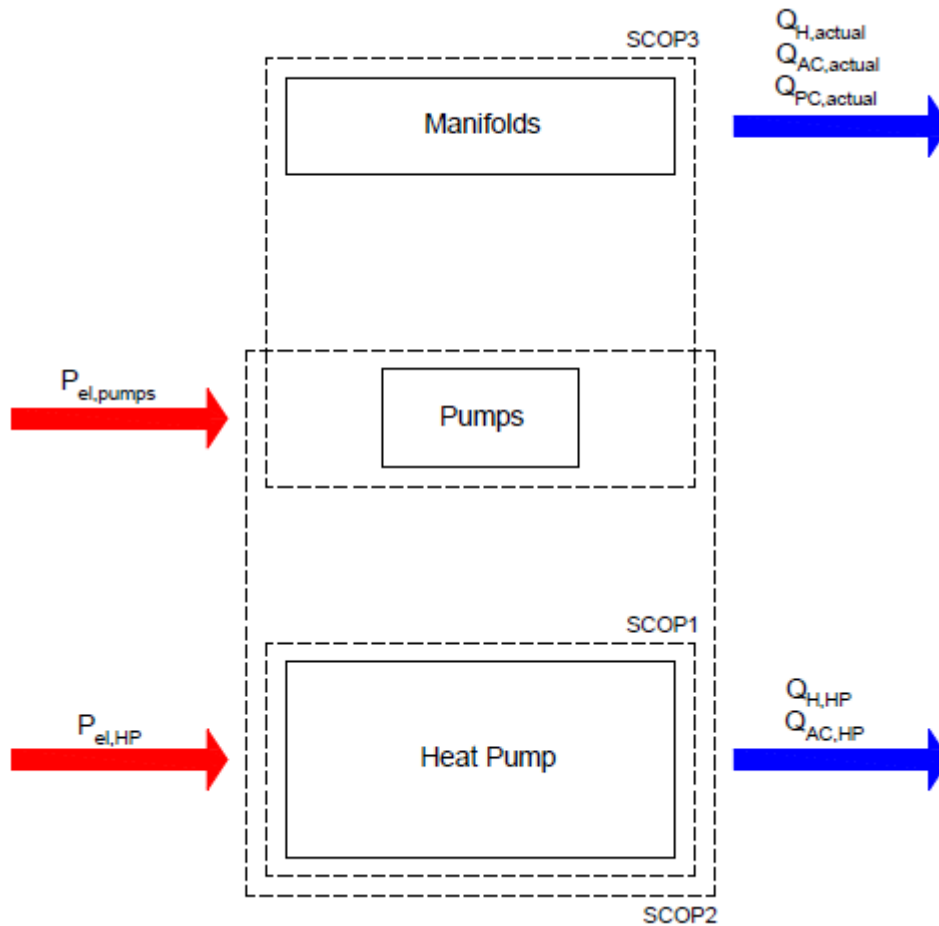


Figure 4: System boundaries for the calculation of the different SCOP

Abbreviations used in Figure 4:

$Q_{H,HP}$:	Thermal energy output of the heat pump in heating mode [kWh]
$Q_{AC,HP}$:	Thermal energy output of the heat pump in active cooling mode [kWh]
$Q_{H,actual}$:	Thermal energy available at the hot water collector in heating mode [kWh]
$Q_{C,actual}$:	Thermal energy available at the cold water collector in active cooling mode [kWh]
$Q_{PC,actual}$:	Thermal energy available at the cold water collector in passive cooling mode [kWh]
$P_{el,H,HP}$:	Electrical input to the heat pump in heating mode [kWh]
$P_{el,AC,HP}$:	Electrical input to the heat pump in active cooling mode [kWh]
$P_{el,H,pumps}$:	Electrical auxiliary energy to operate the heat pump in heating mode [kWh]
$P_{el,AC,pumps}$:	Electrical auxiliary energy to operate the heat pump in active cooling mode [kWh]
$P_{el,PC,pumps}$:	Electrical auxiliary energy in passive cooling mode [kWh]

2.4.1 Seasonal Coefficients of Performance in Heating Mode Operation

The overall seasonal coefficient of performance (SCOP) of the heat pump in heating mode only is defined as:

$$SCOP_{1,H} = \frac{Q_{H,HP}}{P_{el,H,HP}} \quad (1)$$

The overall seasonal coefficient of performance of the heat pump in heating mode, taking into account energy consumption of the pumps is defined by:

$$SCOP_{2,H} = \frac{Q_{H,HP}}{(P_{el,H,HP} + P_{el,H,pumps})} \quad (2)$$

The overall seasonal coefficient of performance regarding the thermal energy available at the hot water collector in heating mode is defined as follows:

$$SCOP_{3,H} = \frac{Q_{H,actual}}{(P_{el,H,HP} + P_{el,H,pumps})} \quad (3)$$

2.4.2 Seasonal Coefficients of Performance in Active Cooling Mode Operation

The overall seasonal coefficient of performance of the heat pump in active cooling mode only is described by:

$$SCOP_{1,AC} = \frac{Q_{AC,HP}}{P_{el,AC,HP}} \quad (4)$$

The overall seasonal coefficient of performance of the heat pump in active cooling mode, including the energy consumption of the pumps is defined by:

$$SCOP_{2,AC} = \frac{Q_{AC,HP}}{(P_{el,AC,HP} + P_{el,AC,pumps})} \quad (5)$$

The overall seasonal coefficient of performance regarding the thermal energy available at the cold water collector in active cooling mode is defined as follows:

$$SCOP_{3,AC} = \frac{Q_{AC,actual}}{(P_{el,AC,HP} + P_{el,AC,pumps})} \quad (6)$$

2.4.3 Seasonal Coefficients of Performance in Passive Cooling Mode Operation

The overall seasonal coefficient of performance regarding the thermal energy available at the cold water collector in passive cooling mode is described as follows:

$$SCOP_{3,PC} = \frac{Q_{PC,actual}}{P_{el,PC,pumps}} \quad (7)$$

2.4.4 Seasonal Coefficients of Performance in Total Cooling Mode Operation

The overall total cooling seasonal coefficient of performance of the heat pump only is given by:

$$SCOP_{1,TC} = \frac{Q_{AC,HP}}{P_{el,AC,HP}} \quad (8)$$

The overall total cooling seasonal coefficient of performance of the heat pump, taking into account the energy consumption of the pumps is described as:

$$SCOP_{2,TC} = \frac{Q_{AC,HP}}{(P_{el,AC,HP} + P_{el,AC,pumps})} \quad (9)$$

The overall seasonal coefficient of performance regarding the total cooling energy available at the cold water collector is defined as follows:

$$SCOP_{3,TC} = \frac{(Q_{AC,HP} + Q_{PC,actual})}{(P_{el,AC,HP} + P_{el,AC,pumps} + P_{el,PC,pumps})} \quad (10)$$

2.4.5 Overall Seasonal Coefficients of Performance

The overall total seasonal coefficient of performance of the heat pump only is defined as:

$$SCOP_{1,TOT} = \frac{(Q_{H,HP} + Q_{AC,HP})}{(P_{el,H,HP} + P_{el,AC,HP})} \quad (11)$$

The overall total seasonal coefficient of performance of the heat pump including the energy consumption of the pumps is described as:

$$SCOP_{2,TOT} = \frac{(Q_{H,HP} + Q_{AC,HP})}{(P_{el,H,HP} + P_{el,H,pumps} + P_{el,AC,HP} + P_{el,AC,pumps})} \quad (12)$$

The overall seasonal coefficient of performance regarding the total energy available at both water manifolds is defined as follows:

$$SCOP_{3,TOT} = \frac{(Q_{H,HP} + Q_{AC,HP} + Q_{PC,actual})}{(P_{el,H,HP} + P_{el,H,pumps} + P_{el,AC,HP} + P_{el,AC,pumps} + P_{el,PC,pumps})} \quad (13)$$

3. SIMULATION

For the evaluation of the three hydraulic layouts, a simulation study was conducted. A complex simulation model of an office building with TABS, a heat pump, ground heat exchanger, and system control was built in TRNSYS 17 (Klein, S.A. et al., 2012). On the basis of the three models, several design parameters were studied:

- Turbulent and laminar flow conditions through the ground heat exchanger
- Number of boreholes
- Storage size
- Supply temperature

In addition to these parameter studies, the method of numerical optimization for the design process was tested within this model. For the optimization studies, the software GenOpt (Wetter, 2009) was used in a co-simulation with TRNSYS.

In the following subchapters, the simulation results of each parameter study are presented.

3.1 Boundary Conditions and Reference Model Description

For simulating the reference case, a TRNSYS model according to the hydraulic scheme as shown in Figure 1 was used. The building itself was modeled with TRNBuild (Type 56 multi-zone building) and represented through 26 thermal zones on three floors.

The weather data for the simulation were generated with MeteoNorm (Version 4) for Hasseltin Belgium. Figure 5 provides an overview of the climate data used in the simulation.

The windows have triple glazing ($U = 0.66 \text{ W/m}^2\text{K}$, $g = 0.41$). Most of the windows have a height of 2.76 m and a width of 0.93 m. The windows are not on the surface of the façade, but are retreated for 40 cm. This was modeled in TRNSYS through Type 34, overhang and wing-wall shading. All these windows, on each façade orientation, have external movable shading devices. The shading factor of this system is 30% (70% solar radiation is blocked). The shading devices are controlled by the solar radiation (threshold $180 \text{ W/m}^2 / 100 \text{ W/m}^2$) on each façade.

The built-in ‘active layer’ algorithm of Type 56 is used for TABS modeling. The pipe spacing is 0.3 m, outside diameter of 0.0266 m, wall thickness of 0.002 m, and wall λ -value of 1.44 kJ/hmK . The mass flow for the modeled TABS system is equal to the mass flow of the double layer TABS system, as built in the Hollandsch Huys. The external TABS floor and TABS roof constructions have an additional insulation layer (material: polyurethane, 0.15m; λ -value, 0.30 W/mK). The U-value of this construction is 0.19 $\text{W/m}^2\text{K}$. For the roof, without TABS, the U-value is 0.24 $\text{W/m}^2\text{K}$. The exterior wall with the brick cladding is modeled with an interior insulation layer. The U-value for the wall is 0.14 $\text{W/m}^2\text{K}$. The internal walls between zones are modeled as a light wall with gypsum wallboards and an insulation material between (material: insulation wool, 0.10 m; λ -value, 0.40 W/mK).

Each zone has artificial lighting. The total heat gain for each zone is 13 W/m^2 (40% convective, 60% radiative). It is assumed that the light is controlled semi-manually through the users of the building with dependence to the horizontal radiation.

The occupancy load is modeled with 10 m^2 per person. The total heat gain of each person is 115 Watts (70-Watt sensible and 45-Watt latent). The occupancy time is from 8.00 am to 6.00 pm (Monday till Friday).

The heat gain of electrical equipment (computer, switches, printer, etc.) is 200-Watt per person in most of the zones. Modeled convective gain is 60% and radiative gain is 40%. The time schedule is directly coupled with the occupancy of the persons in the building.

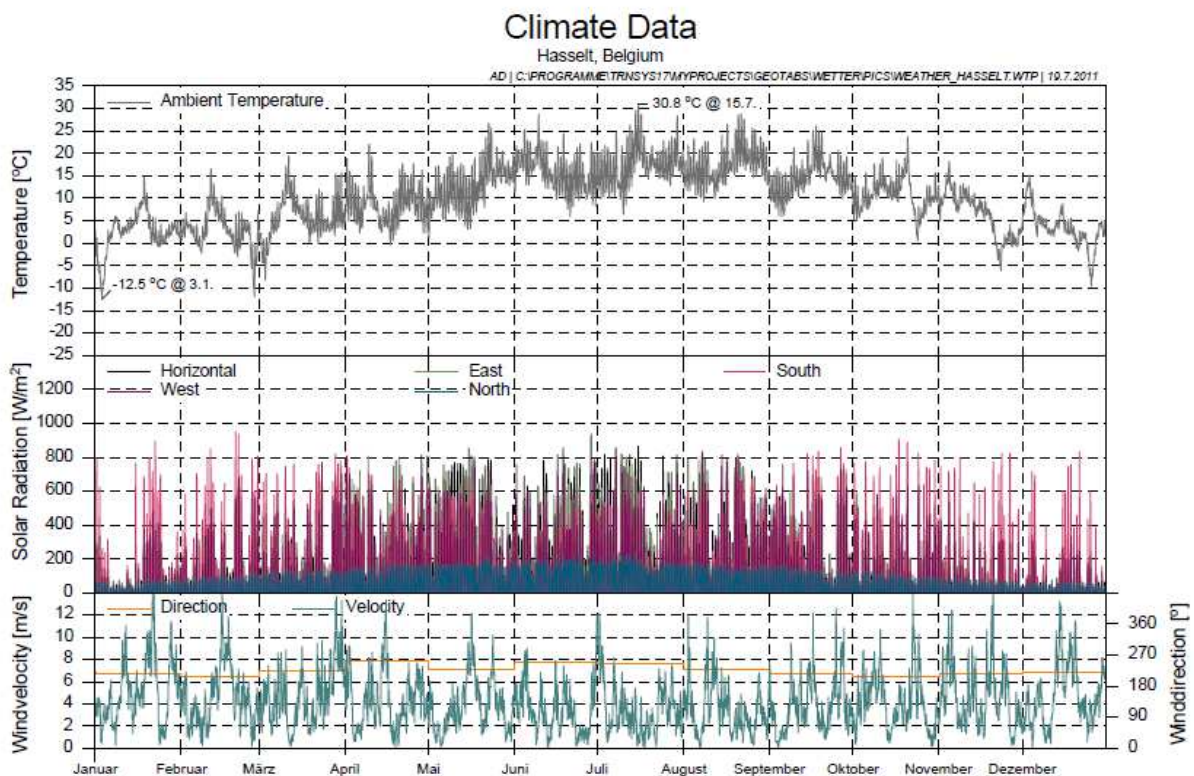


Figure 5: Climate data for Hasselt, Belgium

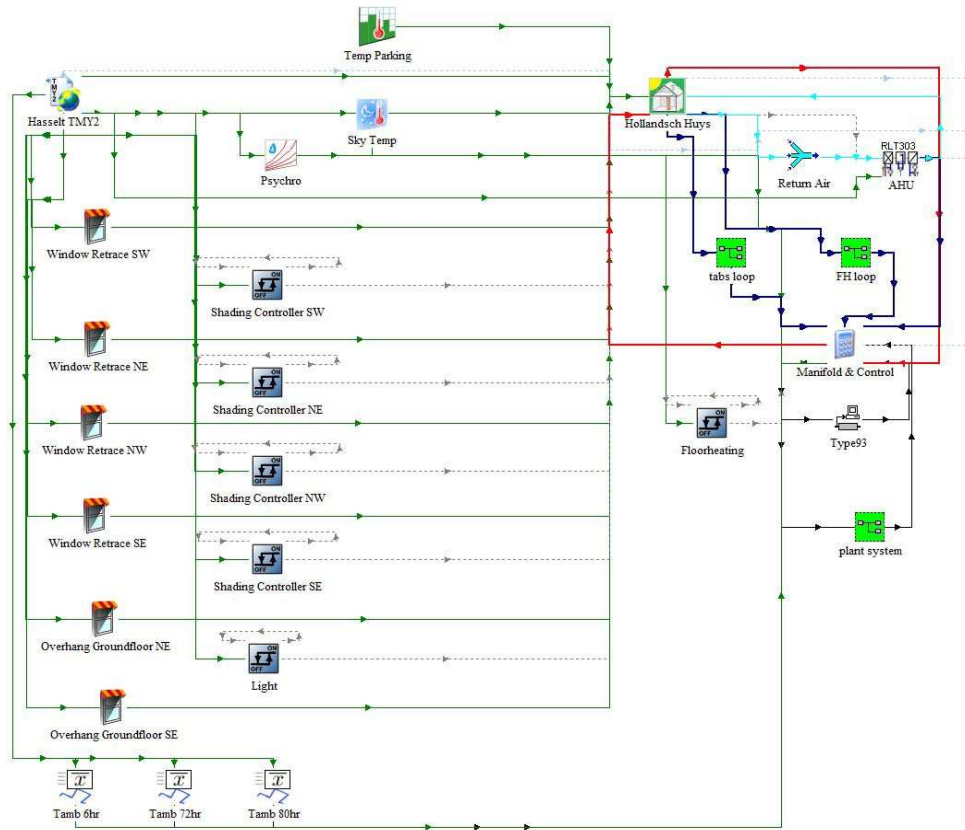


Figure 6: TRNSYS overall simulation model

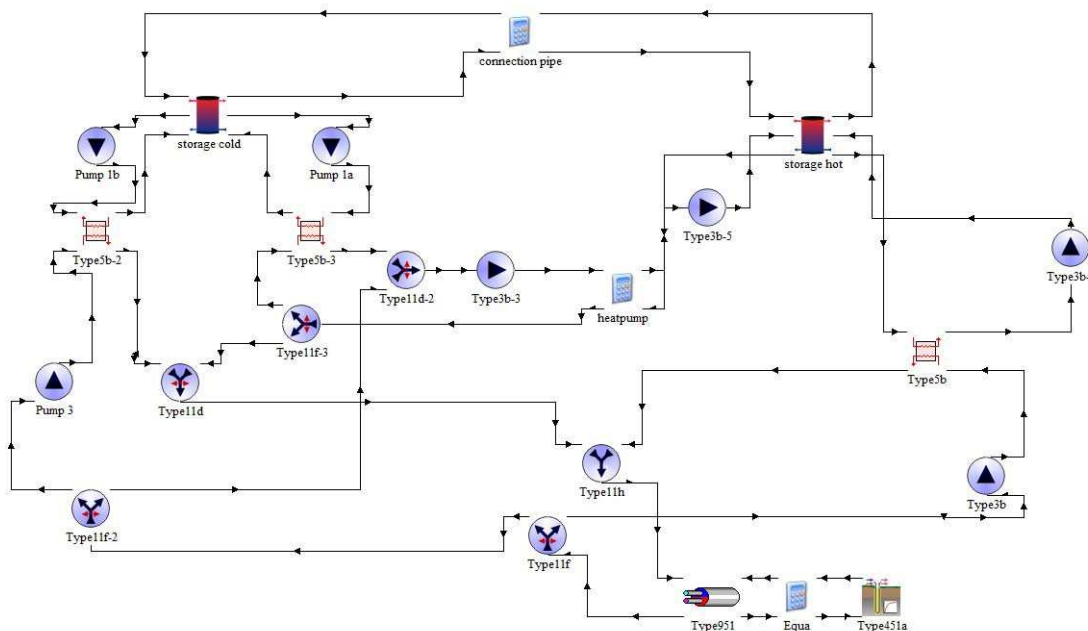


Figure 7: TRNSYS macro plant system: HP model

The air-handling unit (AHU) is modeled as an idealized air-treatment process (Mollier h, x-diagram) with TRNSYS Type 303 (Stephan & Dentel, 2006). The set point (supply air

temperature) is always achieved; therefore, a possible deficit demand is calculated and observed in the model.

The supply temperature of the tabs is controlled by a heating/cooling curve, which is based on the 6 hour mean value of the ambient temperature. The tabs subcollectors are controlled intermediately by opening the valve every hour for 10 minutes, to measure the temperature difference. The valve is open until the temperature difference is greater than 2 K.

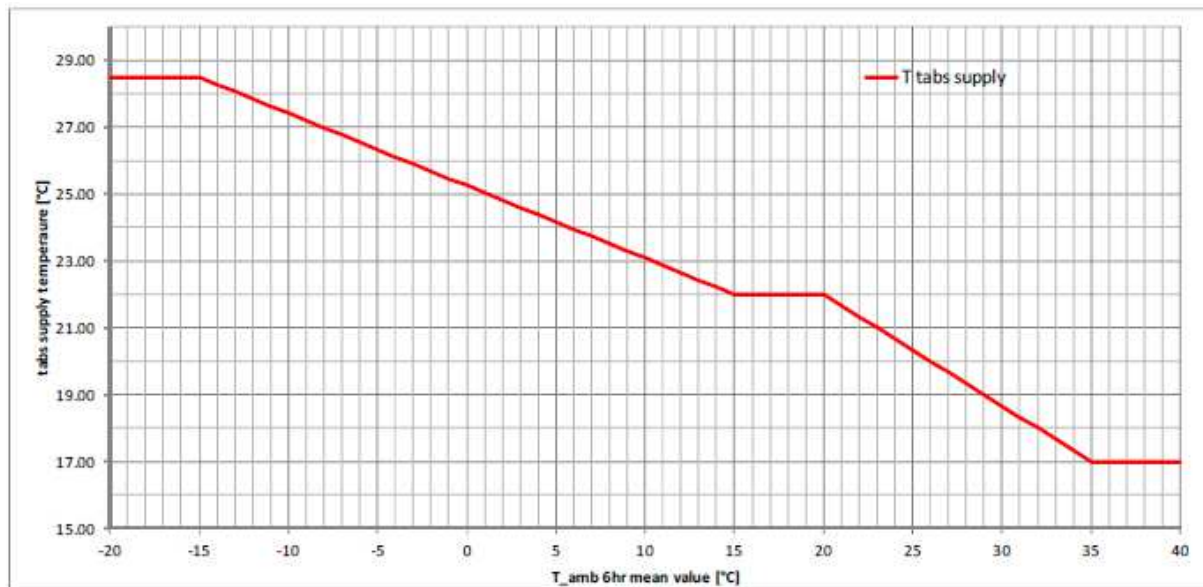


Figure 8: TABS supply temperature: heating mode $T_{amb_6hr_mean} < 15^{\circ}\text{C}$; neutral mode $T_{amb_6hr_mean} \geq 15^{\circ}\text{C}$ and $\leq 20^{\circ}\text{C}$; cooling mode $T_{amb_6hr_mean} > 20^{\circ}\text{C}$

As a special feature in the TRNSYS simulation of the plant model, consecutive time-critical decisions are implemented in terms of a trigger-induced time-dependent operation. In other words, one system state releases an action, which starts after a given time or which lasts for a given time. Thus, a control structure can be simulated which is more common in the field of process and control techniques.

The heat-pump model consists of three individual modules. The heat pump was modeled using a characteristic curve and loads depending on the necessary supply temperatures of the building by the assigned storage tanks. The heat pump can modulate in three power stages:

1. Modus_S1_hp (45 kW)
2. Modus_S2_hp (45 kW)
3. Modus_S3_hp (55 kW)

The stages of the heat pump are operated in the following sequence:

stage 1(45 kW) $\leftarrow \rightarrow$ stage 1 + stage 2 (90 kW) $\leftarrow \rightarrow$ stage 1 + stage 2 + stage 3 (145 kW)
 When the set point of the corresponding storage in heating or active cooling mode is not reached in a given time ($Zeit_Sp_T$), the next power stage is activated. When the set point is reached, the power stages of the heat pump are consequently shut down with a given time delay.

A minimum operating time of the heat pump is controlled to avoid damage on the machine. Before the next start of the machine is enabled, a minimum non-operating time has to be observed.

For the cold and hot storage, the TESS Type 534 was used. Each tank has a volume of 1 m³ and three double ports. The ports are connected to the GHX, building manifold, and the heat pump.

The layout of the ground heat exchanger of the reference building is divided into two GHX fields, drilled in a line. One GHX field is located in the east of the building and consists of eight double U boreholes, and the second GHX field is located across the building, on the west side. The second field consists of 14 boreholes. The total amount of boreholes is 22 with an individual length of 75 m.

From the layout discussion, the TRNSYS Type 451 vertical borehole heat exchanger, EWS Model (Wetter & Huber, 1997) was chosen. Type 451 models a single double U-tube borehole with no interaction between its neighbors. An alternative Type to model the GHX is the DST model ("Type 557: Vertical U - Tube or Tube in Tube Ground Heat Exchanger," 2005), that models a concentric borehole field with the total number of boreholes. Both types do not represent the GHX of the reference building, but the used Type 451 is a slightly closer to the built design.

3.2 Simulation Results of the Reference Case

Due to the possibility of running the heat pump in active cooling mode (reversible heat pump) and to use this waste heat during the heating period, the three cases were calculated with active cooling mode.

This subchapter features the results for the standard case with active cooling mode to compare it with the following variants. Table 1 details the respective monthly total energy demand for generation (primary, end, and useful energy consumption in absolute and specific values). In Table 2 and Table 3, the total energy demands for distribution and emission regarding the building alone are provided. In Table 4, the total ground energy budget is presented, giving an overview of how much energy is provided by the ground heat exchanger per month.

Table 1: Total energy demand for generation - plant

	Generation (HP, GHX)												
	jan	feb	mar	apr	may	jun	jul	aug	sep	oct	nov	dec	sum
primary energy consumption [kWh/(m ² a)]	4.30	3.67	3.09	2.48	1.65	0.89	1.57	1.85	0.78	1.47	2.88	3.79	28.42
primary energy consumption [kWh/a]	17283	14759	12423	9969	6616	3592	6315	7430	3132	5900	11581	15240	114239
end energy consumption [kWh/(m ² a)]	1.59	1.36	1.14	0.92	0.61	0.33	0.58	0.68	0.29	0.54	1.07	1.40	10.53
end energy consumption [kWh/a]	6401	5466	4601	3692	2450	1330	2339	2752	1160	2185	4289	5644	42311
useful energy consumption - electrical [kWh/(m ² a)]	1.59	1.36	1.14	0.92	0.61	0.33	0.58	0.68	0.29	0.54	1.07	1.40	10.53
useful energy consumption - electrical [kWh/a]	6401	5466	4601	3692	2450	1330	2339	2752	1160	2185	4289	5644	42311
useful energy consumption - heating & cooling [kWh/(m ² a)]	6.06	5.10	4.35	3.56	2.36	1.10	2.06	2.03	1.07	2.24	2.24	5.30	39.37
useful energy consumption - heating & cooling [kWh/a]	24352	20503	17472	14328	9500	4439	8263	8177	4316	9025	9025	21288	158282
useful energy consumption - heating [kWh/(m ² a)]	6.06	5.10	4.35	3.56	1.89	0.13	0.00	0.00	0.57	2.21	4.13	5.30	33.29
useful energy consumption - heating [kWh/a]	24352	20503	17472	14328	7596	513	0	0	2280	8883	16620	21288	133834
useful energy consumption - cooling [kWh/(m ² a)]	0.00	0.00	0.00	0.00	0.47	0.98	2.06	2.03	0.51	0.04	0.00	0.00	6.08
useful energy consumption - cooling [kWh/a]	0	0	0	0	1904	3926	8263	8177	2037	142	0	0	24448

A = 4,020 m², primary energy factor: 2.7

Table 2: Total energy demand for distribution - building

	Distribution (ventilation fan, pumps)												
	jan	feb	mar	apr	may	jun	jul	aug	sep	oct	nov	dec	sum
primary energy consumption [kWh/(m ² a)]	4.40	3.83	4.21	4.02	4.39	3.92	4.15	4.36	3.70	4.35	4.18	4.02	49.52
primary energy consumption [kWh/a]	17702	15393	16932	16161	17634	15746	16664	17526	14871	17472	16812	16162	199073
end energy consumption [kWh/(m ² a)]	1.63	1.42	1.56	1.49	1.62	1.45	1.54	1.61	1.37	1.61	1.55	1.49	18.34
end energy consumption [kWh/a]	6556	5701	6271	5986	6531	5832	6172	6491	5508	6471	6227	5986	73731
useful energy consumption - electrical [kWh/(m ² a)]	1.63	1.42	1.56	1.49	1.62	1.45	1.54	1.61	1.37	1.61	1.55	1.49	18.34
useful energy consumption - electrical [kWh/a]	6556	5701	6271	5986	6531	5832	6172	6491	5508	6471	6227	5986	73731

A = 4,020 m², primary energy factor: 2.7

Table 3: Total energy demand for emission - building

	Emission (TABS circulation pumps and other pumps)												
	jan	feb	mar	apr	may	jun	jul	aug	sep	oct	nov	dec	sum
primary energy consumption [kWh/(m ² a)]	2.27	2.05	2.24	2.14	2.17	2.04	2.10	2.10	2.05	2.19	2.16	2.26	25.77
primary energy consumption [kWh/a]	9144	8246	9000	8598	8707	8193	8437	8437	8260	8803	8700	9073	103598
end energy consumption [kWh/(m ² a)]	0.84	0.76	0.83	0.79	0.80	0.75	0.78	0.78	0.76	0.81	0.80	0.84	9.54
end energy consumption [kWh/a]	3387	3054	3333	3185	3225	3034	3125	3125	3059	3260	3222	3360	38370
useful energy consumption - electrical [kWh/(m ² a)]	0.84	0.76	0.83	0.79	0.80	0.75	0.78	0.78	0.76	0.81	0.80	0.84	9.54
useful energy consumption - electrical [kWh/a]	3387	3054	3333	3185	3225	3034	3125	3125	3059	3260	3222	3360	38370

A = 4,020 m², primary energy factor: 2.7

Table 4: Total ground energy budget [kWh]

	jan	feb	mar	apr	may	jun	jul	aug	sep	oct	nov	dec
ground year energy budget [kWh]	17959	15388	13544	11226	4289	-3016	-7627	-7868	-344	6105	11707	15227

Table 5 gives an overview of the yearly seasonal coefficients of performance for the different operating modes and the total system. Due to the passive cooling mode there is a certain memory effect concerning the pre-conditioning of the cold storage. During the passive cooling mode the cold storage is loaded with cooling energy (2,979 kWh/a), whereas only 1,060 kWh/a are withdrawn from the cold storage. This difference leads to an increased cooling down of the cold storage and has therefore a positive effect during active cooling mode on the SCOP3, despite the fact that the cooling energy offered from the heat pump is smaller than the amount withdrawn from the cold storage.

In Table 6, the runtime of the heat pump for the different operating modes and the pump P3 (for passive cooling mode) are shown, whereas in Table 7, the amount of time in which energy is withdrawn from the cold and hot storages, respectively, to guarantee the energy demand of the building, is featured.

Table 5: Annual seasonal coefficient of performance - SCOP [-]

	SCOP1 (HP)	SCOP2 (HP)	SCOP3 (Manifold)
Heating	4.49	3.85	3.85
Active Cooling	4.37	2.65	2.93
Passive Cooling	-	-	15.72
Total Cooling	4.37	2.65	3.04
Total	4.48	3.64	3.71

Table 6: Runtime - heat pump, pump P3 (passive cooling mode) [h]

Heating [h]	2,152
Active Cooling [h]	301
Passive Cooling [h]	31
Total Cooling [h]	332

Table 7: Runtime - energy withdrawal from storage [h]

Heating [h]	4,557
Active Cooling [h]	1,096
Passive Cooling [h]	31
Total Cooling [h]	1,128

Table 8: Total energy budget for the reference case.

	Input (kwh/a)	Output (kWh/a)
Heating	133,880	133,834
Active Cooling – Hot Storage	24,285	24,263
Active Cooling – Cold Storage	21,472	21,470
Passive Cooling	2,979	1,060

The total energy budget for the reference case is presented in Table 8. Figure 9 describes the annual temperatures in the ground heat exchanger (supply and return temperatures) and the supply temperatures from the hot and cold storage tanks, respectively, supplying the different building systems.

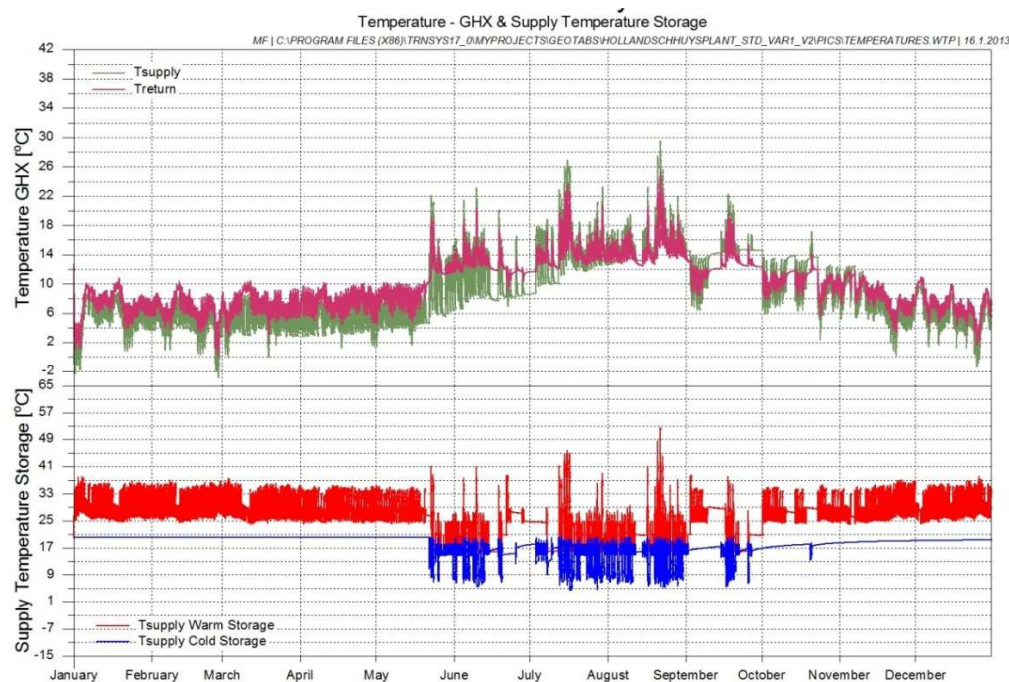


Figure 9: Temperatures in the GHX and in the storage tanks (reference case)

3.3 Simulation Results of the New Hydraulic Layout 1

For the evaluation of efficiency of the new hydraulic layout 1, two different flow rates were investigated:

- Turbulent flow conditions through the ground heat exchanger: 1,600 kg/h per borehole
- Laminar flow conditions through the ground heat exchanger: 750 kg/h per borehole

3.3.1 Simulation Results: Layout 1 for Turbulent Flow Conditions

The first variant of this new hydraulic system considers turbulent flow conditions through the borehole heat exchanger system. Table 9 provides the annual seasonal coefficients of performance for the different operating modes and the total for the new hydraulic system with turbulent flow conditions.

Figure 10 displays the annual temperatures through the ground heat exchanger (supply and return temperatures) and the supply temperatures from the hot and cold storages, respectively, supplying the different building systems.

Table 9: Annual seasonal coefficient of performance for layout 1 turbulent flow conditions - SCOP [-]

	SCOP1 (HP)	SCOP2 (HP)	SCOP3 (Manifold)
Heating	4.42	4.02	4.01
Active Cooling	4.83	4.66	4.65
Passive Cooling	-	-	145.80
Total Cooling	4.83	4.66	5.49
Total	4.47	4.09	4.18

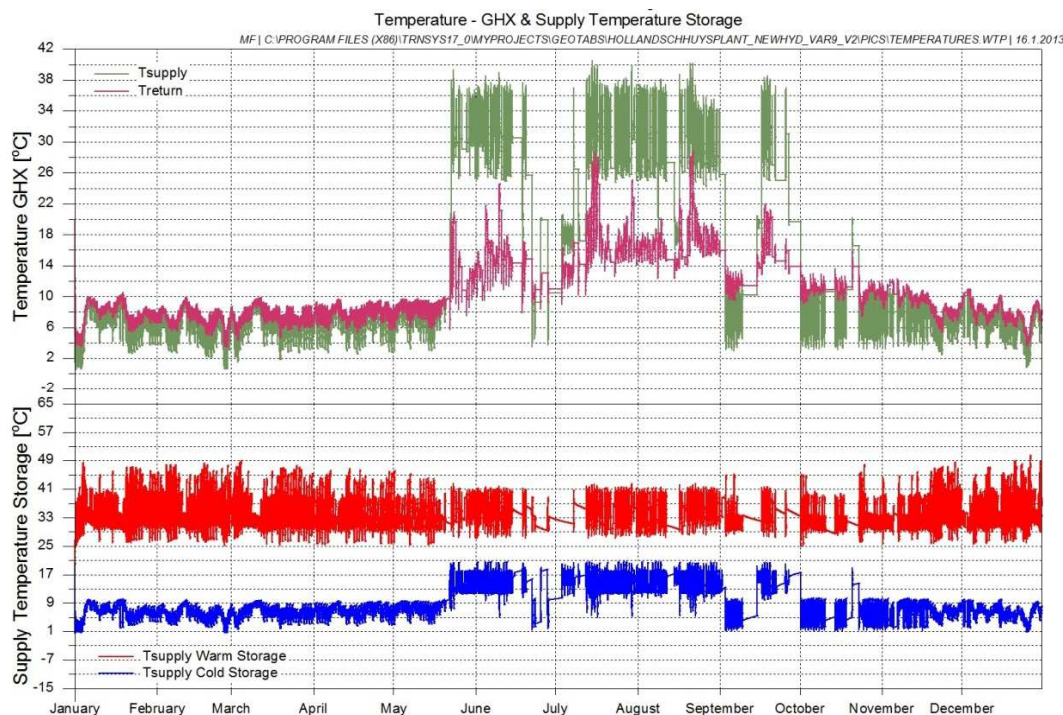


Figure 10: Temperatures in the GHX and in the storage tanks (layout 1, turbulent flow)

3.3.2 Simulation Results: Layout 2 for Laminar Flow Conditions

The second variant of this new hydraulic system considers laminar flow conditions through the borehole heat exchanger system. Table 10 shows the annual seasonal coefficients of performance for the different operating modes and the total for the new hydraulic system with laminar flow conditions. The temperatures of the GHX are shown in Figure 11.

Table 10: Annual seasonal coefficient of performance for layout 1 laminar flow conditions - SCOP [-]

	SCOP1 (HP)	SCOP2 (HP)	SCOP3 (Manifold)
Heating	4.59	4.45	4.44
Active Cooling	4.85	4.71	4.70
Passive Cooling	-	-	1,081.33
Total Cooling	4.85	4.71	5.45
Total	4.62	4.48	4.57

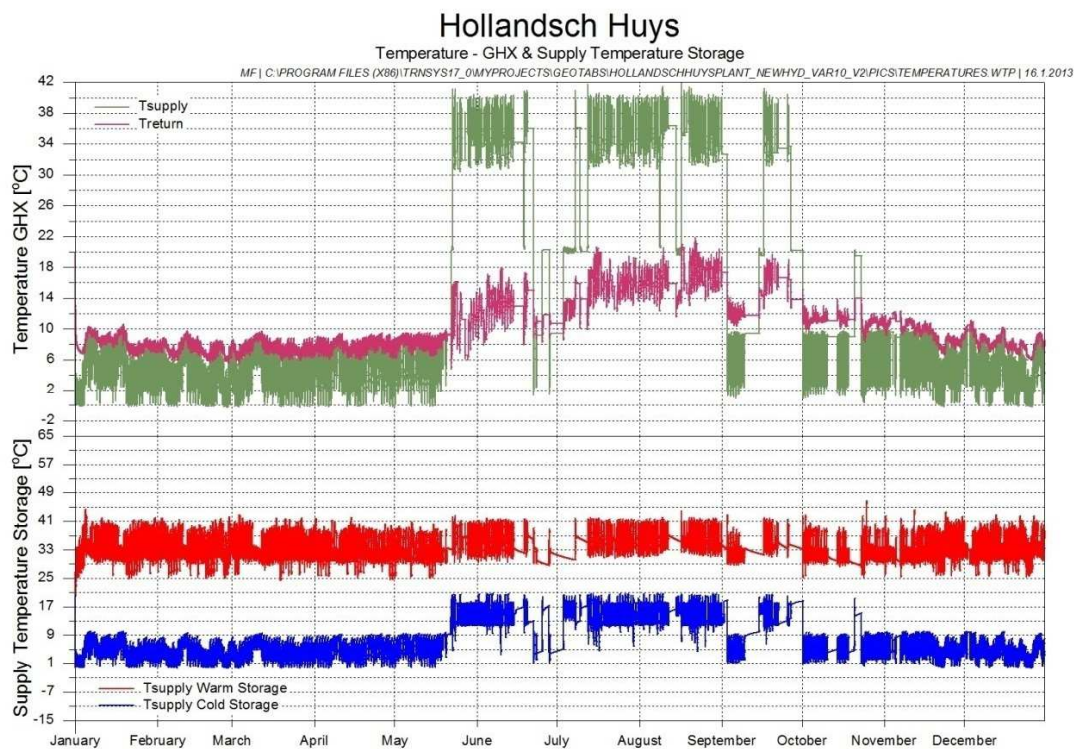


Figure 11: Temperatures in the GHX and in the storage tanks (layout 1, laminar flow)

3.4 Simulation Results of the New Hydraulic Layout 2

Figure 3 displays the second hydraulic brine pump that still operates with variable flow rates, 1,600 kg/h when operating with turbulent flow conditions and 750 kg/h when operating with laminar flow conditions.

3.4.1 Simulation Results: Layout 2 for Turbulent Flow Conditions

The first variant of this second hydraulic system considers turbulent flow conditions through the ground heat exchanger. Table 11 presents the results concerning the SCOP, and Figure 12 displays the temperatures of the storage tanks and the GHX temperatures.

Table 11: Annual seasonal coefficient of performance for layout 2 turbulent flow conditions - SCOP [-]

	SCOP1 (HP)	SCOP2 (HP)	SCOP3 (Manifold)
Heating	4.44	3.22	3.22
Active Cooling	3.86	3.38	3.29
Passive Cooling	-	-	34.30
Total Cooling	3.86	3.38	3.46
Total	4.35	3.24	3.25

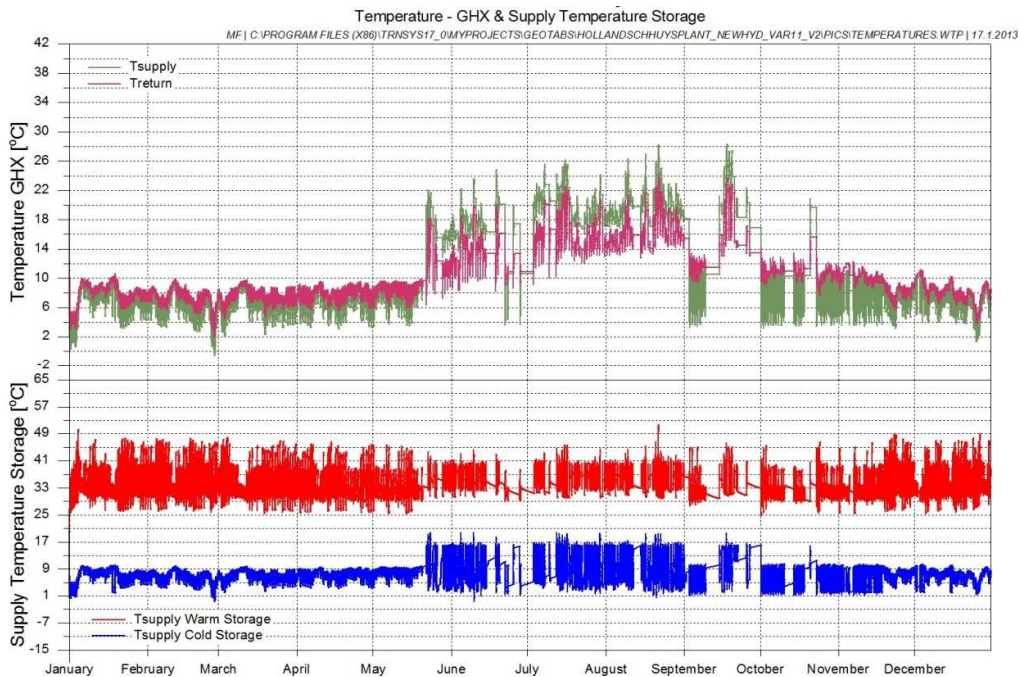


Figure 12: Temperatures in the GHX and in the storage tanks (layout 2, turbulent flow)

3.4.2 Simulation Results: Layout 2 for Laminar Flow Conditions

This variant of the second hydraulic system includes the results for laminar flow conditions through the ground heat exchanger. Table 12 presents the results concerning the SCOP and figure 12 displays the temperatures of the storage tanks and the GHX temperatures.

Table 12: Annual seasonal coefficient of performance for layout 2 laminar flow conditions - SCOP [-]

	SCOP1 (HP)	SCOP2 (HP)	SCOP3 (Manifold)
Heating	4.44	4.15	4.15
Active Cooling	3.75	3.50	3.41
Passive Cooling	-	-	87.38
Total Cooling	3.75	3.50	3.64
Total	4.32	4.04	4.06

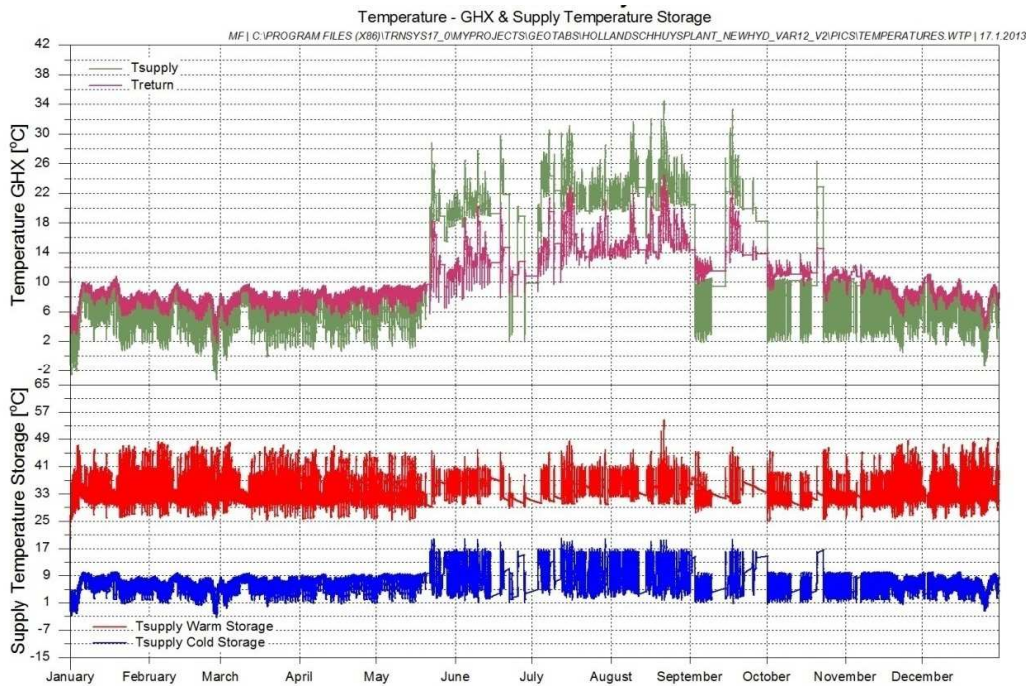


Figure 13: Temperatures in the GHX and in the storage tanks (layout 2, laminar flow)

3.5 Parametric Studies of Design Parameters

The second method in optimizing the design of a GCHP system is a variation of the following parameters:

- storage volume
- number of boreholes

For the optimization of the storage volume, the software GenOpt (Wetter, 2009) was used, in a co-simulation with TRNSYS. For the calculation concerning the number of boreholes, a simple parametric study was done.

3.5.1 Optimizing the Storage Volume

For the optimization study, a cost function was defined. The overall aim was to minimize the total primary energy consumption by fulfilling the temperature set points in the system. The used cost function is defined as:

$$\min \sum_{k=0}^{H_p} (\alpha_1 \cdot Q_{P,total} + \alpha_2 \cdot \Delta T_{set,supply}) \quad (14)$$

The cost function has equal weights for primary energy demand and set the point difference. An observation of the thermal comfort and a penalty, whenever necessary, for the discomfort are not considered in the cost function.

The simulations were done on the basis of the reference case.

The constraints for the optimization were a minimum storage volume of 1 m³ and a maximum storage volume of 20 m³. Two different cases were investigated:

- case 1: identical sizes for heat and cold storage tanks
- case 2: independent sizes for heat and cold storage tanks

The optimum for case 1 results to a storage volume of 8 m³. A reduction of 27% of the primary energy demand can be reached through this configuration.

For case 2, different storage sizes are efficient. The results show that a small heat storage (2 m³) and a big cold storage (17 m³) are the optimum configuration. The primary energy demand can be reduced by 7% compared with the system with identical storage tanks.

3.5.2 Parametric Study of the Number of Boreholes

On the basis of the hydraulic layout 1, a parametric study for 10 different borehole configurations was carried out. Table 13 gives an overview of the studied cases. The result of the parametric study is that a design with approximately 50% more boreholes in field 1 than in field 2 has the best system performance (configuration 4 and 5). The primary energy demand can be reduced, according the base case (configuration 7), by 13% with this configuration. The reason for this reduction is the increased possibility for passive cooling, due to the additional 9 or rather 11 boreholes. Another simulation case for the hydraulic layout 1 with only one common GHX showed that primary energy demand for that configuration is only 1% less than the layout 1 with two separate GHX fields.

Table 13: Configurations for the parametric study for the variation of number of boreholes

Configuration	Number of boreholes in	
	Field 1	Field 2
1	14	8
2	16	9
3	18	10
4	20	11
5	22	12
6	16	6
7	11	11
8	13	13
9	15	15
10	17	17

4. DISCUSSION AND ANALYSIS OF RESULTS

This chapter gives an overview of the main results for the different simulated variants, whereas only the versions with active cooling mode are compared with each other. Table 14 reflects the overall seasonal coefficients of performance (SCOP) for the different operating modes for all researched versions. The SCOP is shown in this table for all system boundaries (ct. Figure 4). The results for the SCOP3 are similar to the results for the SCOP2, due to the similar amounts of the energy provided by the heat pump, the energy which is actually delivered to the building. The values range from a SCOP of 3.25 (new hydraulic layout 2, turbulent flow conditions, “C2-turb”) to 4.57 (new hydraulic layout 1, laminar flow conditions, “C1-lam”). The individual SCOP at each system boundary for each case is given in Table 14. The main benefit of the most efficient system “new hydraulic layout 1, laminar flow conditions, “C1-lam” is the smallest amount of the auxiliary energy demand. The reduction of the energy demand is due to the reduction of the amount of circulation pumps.

The SCOP1 of the active cooling in C1-lam is larger than that in C1-turb, because operating in stage two respectively stage three leads to a higher energy consumption of the heat pump (worse COP) and therefore to a worse SCOP1 for turbulent flow conditions. Further reasons for the slightly higher SCOP1 in active cooling mode with laminar flow than in turbulent conditions are the switching conditions of the heat pump (i.e. minimum running and shutting down time of the heat pump).

Compared with the case with two separate ground heat exchanger fields, the results for the one single ground heat exchanger field (“C1-lam-1BH”) are almost the same. The difference concerning the SCOP for the passive cooling mode is due to the different operating times, the version with one GHX features less operating hours in passive cooling mode and more hours operating in active cooling mode. These results show that there is hardly any difference when using one single or two separate ground heat exchanger fields. The difference in the SCOP can be neglected: 4.57 with 2 GHX fields vs. 4.55 with 1 GHX field. The technical effort and costs for the control are also not justified for this technical feature. Due to this state of knowledge, the division or layout of the two different GHX fields can be neglected in design.

An enlargement of the number of boreholes up to 50 % results in a reduction of 13% of the primary energy demand.

In Table 15, the annual primary energy demand is listed for all investigated cases. The hydraulic optimization of the GCHP system has a saving potential of approximately 18%. The absolute primary energy demand decreases from 114,239 to 94,079 kWh/a.

The result of the optimization tends to cause a smaller storage volume for the hot water tank as for the cold water tank. This is based on the increasing heat losses with an increasing volume for the hot water buffer storage. Due to an optimization of the passive cooling, a big cold water storage volume should be aspired. The primary energy demand can be reduced through this optimization by up to 30%.

The abbreviations of the researched variants are as follows:

- SC1: reference case with active cooling
- C1-turb: new hydraulic layout 1 with turbulent flow conditions through the GHX
- C1-lam: new hydraulic layout 1 with laminar flow conditions through the GHX
- C2-turb: new hydraulic layout 2 with turbulent flow conditions through GHX
- C2-lam: new hydraulic layout 2 with laminar flow conditions through the GHX

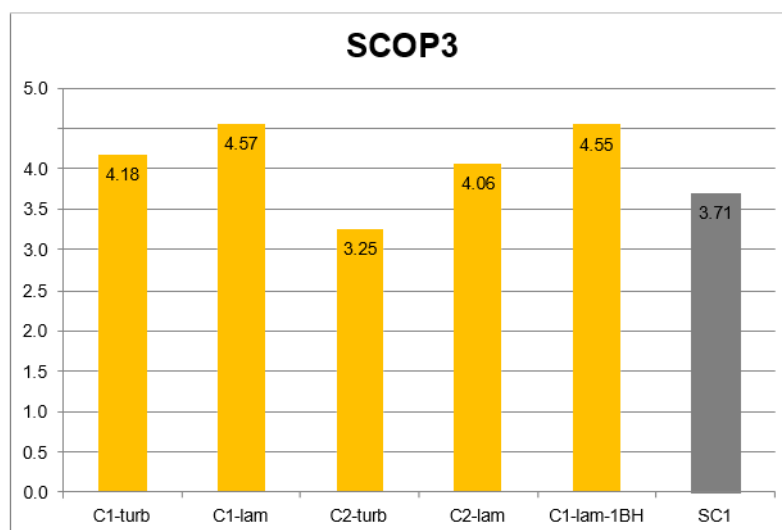


Figure 14: Seasonal coefficient of performance for system boundary 3 – comparison of all studied cases

Table 14: Annual seasonal coefficient of performance - SCOP [-]

SCOP	C1-turb	C1-lam	C2-turb	C2-lam	C1-lam-1BH	SC1
H1	4.42	4.59	4.44	4.44	4.58	4.49
H2	4.02	4.45	3.22	4.15	4.44	3.85
H3	4.01	4.44	3.22	4.15	4.43	3.85
AC1	4.83	4.85	3.86	3.75	4.84	4.37
AC2	4.66	4.71	3.38	3.50	4.71	2.65
AC3	4.65	4.70	3.29	3.41	4.69	2.93
PC3	145.80	1,081.33	34.30	87.38	980.96	15.72
TC3	5.49	5.45	3.46	3.64	5.40	3.04
TOT1	4.47	4.62	4.35	4.32	4.61	4.48
TOT2	4.09	4.48	3.24	4.04	4.47	3.64
TOT3	4.18	4.57	3.25	4.06	4.55	3.71

Table 15: Annual primary energy demand [kWh/a]

Primary energy demand [kWh/a]	C1-turb	C1-lam	C2-turb	C2-lam	C1-lam-1BH	SC1
Heating	94,074.5	82,306.9	118,110.5	91,687.4	82,100.7	94,172.5
Active cooling	11,653.9	11,764.4	19,122.2	18,222.8	11,877.1	19,883.9
Passive cooling	69.6	8.2	104.4	50.1	8.6	182.1
Total cooling	11,723.5	11,772.5	19,226.6	18,272.9	11,885.7	20,066.0
Total	105,798.0	94,079.4	137,337.1	109,960.3	93,986.4	114,238.5

The different values for the SCOP3 during passive cooling mode are due to the different amounts of electrical power consumptions for the brine pumps in use and the different operating times. Table 16 shows the maximum design values for the electrical power consumption of the pumps operating during passive cooling mode for the single researched variants and the operating time during passive cooling mode.

Table 16

	C1-turb	C1-lam	C2-turb	C2-lam	SC1
Maximum design electrical power consumption of the pumps during passive cooling mode [W]	1,010 (P_b_4)	65 (P_b_4)	2,460 (P_b_4)	303 (P_b_4)	1,305 (P3)
			546 (P_c_5)	546 (P_c_5)	851 (P1b)
Run-Time operating mode "passive cooling" [h/a]	165	160	47	59	31

5. CONCLUSION

The example results show that an optimized hydraulic layout can increase the SCOP and decrease the primary energy demand of the system, for these four different hydraulic layouts compared with a reference case in practice. An intermodal comparison showed that not all new hydraulic layouts have a better performance than the reference case. A variation of the mass flow rate in the GHX has a big influence on the SCOP and the primary energy demand. This is

based on the auxiliary energy demand of the circulation pumps. The most efficient hydraulic layout is a system with less pumps and heat exchangers. One disadvantage, in the case of system security, is that the system is operated with pure water. In operation, the temperatures in GHX should be very carefully observed. Beware of temperatures near the freezing point in the GHX loop and on the evaporator site of the heat pump.

Dividing the GHX into two fields should be avoided. The benefit on energy savings is lower than the economical benefit. The assumption in design of reserving on the GHX field only for passive cooling and the second one for active cooling is not efficient in practice. The reason for this is that the changeover to active cooling in the example is already after one hour. Parametric studies, with a switching time up to 6 hours, have shown that there is no real advantage in the case of primary energy reduction by splitting up the GHX in two separate fields.

In the case of sizing the storage volume, the optimization study tends to cause a smaller storage volume for the hot water tank as for the cold water tank. This is based on the increasing heat losses with an increasing volume for the hot water buffer storage.

Finally, it should be remarked that the studies on the design parameters are all done with the same load profile. A variation of different loads or building types is not done in the frame of this project.

REFERENCES

Hoogmartens, J. & Helsen, L. (2012). GEOTABS - Towards optimal design and control of geothermal heat pumps combined with thermally activated building systems in offices: Final Report. Retrieved from http://www.geotabs.eu/Publication/final/at_download/file

Klein, S.A. et al. (2012). TRNSYS 17: A Transient System Simulation Program. Madison, USA: Solar Energy Laboratory, University of Wisconsin. Retrieved from <http://sel.me.wisc.edu/trnsys>

Lemort, V. (2012). GEOTABS - Towards optimal design and control of geothermal heat pumps combined with thermally activated building systems in offices: Deliverable 4.1: Report of energy performance and control strategy evaluation for each detailed case.

Retrieved from http://www.geotabs.eu/Publication/wp4/D4_1/at_download/file (2014). ModeFrontier: Esteco. Retrieved from <http://www.esteco.com/>

Stephan, W. & Dentel, A. (2006). Simulation of Air Conditioning Systems with different Tools - Minimum Requirements for different Applications. 7th International Conference on System Simulation in Buildings, Liège, Belgium.

(2005). Type 557: Vertical U - Tube or Tube in Tube Ground Heat Exchanger. Madison, USA: Thermal Energy Systems Specialists.

Wetter, M. & Huber, A. (1997). TRNSYS TYPE 451 - Vertical Borehole Heat Exchanger - EWS Model, Transsolar GmbH.

Wetter, M. (2009). Generic Optimization Program - GenOpt. Berkeley: Wetter, Michael.

ACKNOWLEDGEMENT

The GEOTABS project was supported in part by the EraSME FPR 7 program. The German contribution was supported by the Federal Ministry of Economic Affairs and Energy (BMWI/ZIM, FKZ: KF2188202TL0). We are grateful for the financial support and for the collaboration of all the project partners.

Modelling the impact of integrated electric vehicle charging and domestic heating strategies on future energy demands

John Hand, Nick Kelly*, Aizaz Samuel

Energy Systems Research Unit (ESRU), Department of Mechanical and Aerospace Engineering, University of Strathclyde Glasgow

1. ABSTRACT

The next 30 years could see dramatic changes in domestic energy use, with increasingly stringent building regulations, the uptake of building-integrated microgeneration, the possible electrification of heating (e.g. heat pumps) and the use of electric vehicles (EV). In this paper, the ESP-r building simulation tool was used to model the consequences of both the electrification of heat and EV charging on the electrical demand characteristics of a future, net-zero-energy dwelling. The paper describes the adaptation of ESP-r so that domestic electrical power flows could be simulated at a temporal resolution high enough to calculate realistic peak demand. An algorithm for EV charging is also presented, along with the different charging options. Strategies by which EV charging and electrified heating could be controlled in order to minimise peak household electrical demand were assessed. The simulation results indicate that uncontrolled vehicle charging and the use of electrified heating could more than double peak household power demand. By contrast, a more intelligent, load-sensitive heating and charging strategy could limit the peak demand rise to around 40% of a base case with no vehicle or electrified heating. However, overall household electrical energy use was still more than doubled.

Keywords: EV, zero energy dwelling, electrical demand, simulation

2. INTRODUCTION

The next 30 years are likely to herald a substantial change in the demand characteristics of new and refurbished dwellings, brought about by a combination of improved thermal performance, increased integration of microgeneration technologies such as PV, the possible electrification of heat through the use of heat pumps and the widespread adoption of plug-in hybrid electric vehicles (PHEV) and all-electric vehicles (EV). Together, these changes would result in household demand characteristics radically different from those seen today.

Improved thermal performance in both newbuild and retrofitted housing will reduce the primacy of domestic space heating demands and place more of a focus on electrical demands and hot water use. For example, in a typical UK house, space heating accounts for around 65% of its overall energy demand (Palmer and Cooper, 2012), whilst in Passive House designs, heating can account for as little as 40% of the household's overall energy demand (Feist, 2006). This reduction in heating demand is becoming evident now, with total UK household space heating demand declining by 21% since 2004. Conversely, total household energy demand associated with electrical appliance use has increased by approximately 15% over the same period (Palmer and Cooper, 2012).

In parallel with changes in fabric performance, the supply of energy to UK dwellings is also undergoing a transformation, through the provision of thermal and electrical energy from local, low-carbon sources. For example, more than 2GW of microgeneration capacity has been installed in the UK since the introduction of a feed-in-tariff (FIT) in 2010 (OFGEM, 2013); this

provides small scale producers (i.e. householders) with a guaranteed payment for each kWh of electricity produced by a household renewable source such as photovoltaic panels (PV).

If the UK is to achieve its ambitious targets for an 80% carbon emissions reduction by 2050, then the use of fossil fuels for space heating will need to be virtually eliminated (DECC, 2008) and replaced with zero carbon sources such as biomass (which realistically could only supply a fraction of heat demand [Castillo and Panoutsou, 2011]), and renewable electricity. The latter source requires the widespread uptake of heat pumps, shifting the demand for space and water heating from the gas grid to the electricity network. Given that the vast majority of UK dwellings likely to be extant in 2050 are already constructed (Hinnels et al, 2007) a widespread heat pump retrofit programme would be required. Air source heat pumps (ASHPs) have the potential to act as a replacement for the fossil-fuelled boilers commonly found in UK housing. Additionally, their relatively low cost of installation and the lack of a requirement for ground works makes ASHPs a more feasible mass retrofit option than ground source heat pumps (GSHP). However, Wilson et al (2013) indicate that a shift of only 30% of domestic heating to heat pumps could result in an increase in the total UK electrical demand of some 25%.

The final development likely to have a significant impact on the characteristics of domestic demand is the growth in the use of electric vehicles (EVs). In the UK, the number of electric vehicles is still small as a percentage of the total fleet: some 0.1% of the total passenger cars licenced on UK roads. However, their number is increasing exponentially (DfT, 2014). EVs shift the energy used for transportation from refined fossil fuels to the electricity network. In the UK, the domestic sector accounts for around 29% of UK final energy consumption, whilst the transport sector accounts for another 36% of demand (DECC, 2014). The deployment of EVs at an increasing rate and the widespread electrification of domestic heating could lead to a massive rise in the demand for electricity and necessitate the upgrading of the UK's electricity distribution infrastructure. In this paper, the potential increase in electricity demand at the individual dwelling level is examined along with an investigation into the strategies that could be employed to mitigate the worst effects of this increase.

2.1 Previous Work on EV Integration with Buildings

There are large bodies of literature looking at the thermal performance of future buildings (e.g. Attia et al, 2013), microgeneration and the electrification of heat, and the potential impact of EVs on the electrical network (e.g. Pudjianto et al, 2013). However, there is a paucity of material looking specifically at the combinatorial effects of heat pumps and EVs on domestic energy demands, and strategies to mitigate their impact. Typically, studies treat the two topics separately. There are some examples in the literature that look at the integrated control of EV charging within a domestic context in order to mitigate demand peaks, but the majority of work focuses on the charging of vehicles at the larger scale. Robinson et al (2013) analysed the results from a large UK field trial of electric vehicles, where the charging times of vehicles were unconstrained and vehicles could be charged at home or when parked away from home. Their results indicated a significant amount of peak-time charging. Razeghi et al (2014) used real domestic electricity demand data coupled with stochastic vehicle charging profiles to look at the potential impact of EV charging on distribution transformers. The authors concluded that only in the case of uncontrolled fast charging of vehicles would there be the risk of transformer overloading. In a study using economic optimisation, Hedegaard et al (2012) looked at the possible impact of EV charging, indicating that coordinated charging of EV's can boost investment in wind power and reduce future investment requirements for thermal power plants. However, the study did not look at the implications for the transmission and generation infrastructure.

Of the studies looking at both the dwelling and EV, Asare-Bediako et al (2014) looked at the potential effect of heat electrification, micro-CHP and electric vehicles on domestic load profiles in the Netherlands using a bottom-up modelling approach. The authors concluded that the electrical load profile characteristics changed dramatically with reduced electrical peak demand in summer and increased demand in winter. The authors did not investigate the possibility of co-operation between the house and vehicle to limit peak demand, nor did they address the issue of heat pumps. Munkhammar et al (2013) used a stochastic, high-resolution model to examine the impact of EVs on domestic load and the self-consumption of PV-generated power. Their paper highlighted the increase in domestic power consumption with the introduction of EVs and also noted that in many cases the use of EVs decreased the amount of load covered by the PV. This was due to the temporal mismatch between when PV power was available and when the EV charged (typically early morning or evening). Haines et al (2009) looked at the so-called vehicle-to-home concept (V2H), using the vehicle battery to co-operatively limit the peak demand of a household. The authors concluded that EVs could be used to limit peak demand and improve domestic load factors, other than in cases where the EV was used for a sizable commute. However, the study did not consider electrification of heating, nor of the impact of microgeneration such as PV.

3. SCOPE OF THE PAPER

There is a gap in the literature in that the impact of wholesale domestic electrification (extending to heating and transportation) is rarely considered, and by extension, most mitigation strategies focus on only one aspect of demand. Consequently, this paper explores a range of integrated strategies aimed at limiting the impact of both heat pumps and EVs on the electrical demand of future dwellings. The paper examines the peak electrical demand and the increase in household electrical energy use as both will have an impact on electrical infrastructure. Increased electrical energy use will lead to higher temperatures in electrical equipment and ultimately a shortening of its lifespan. However, a radical increase in peak demand could have the most acute impact, necessitating the wholesale replacement of electrical infrastructure such as cabling and electrical transformers.

A simulation model of a hypothetical future zero-energy dwelling (described in detail later) was used to calculate the total electrical demand at high resolution, accounting for electrified space heating, hot water demand, appliance and vehicle charging loads. The specific demand-limiting strategies to be investigated using the model were as follows.

- Time shifting of heating: where the operation of a heat pump is moved to periods of off-peak electrical demand. This required that the heat pump was coupled to the heating system of the dwelling via a buffer tank.
- Fast and slow battery charging rates, at 3.3 and 6.6 kW, respectively.
- Time shifting of battery charging: battery charging was restricted to periods of off-peak electrical demand.
- Co-operative battery charging: the battery was only charged when the load of the dwelling fell below a user specified threshold of 7.5 kW¹.

¹ IEA EBC Annex 42 measured data (IEA, 2014) was reviewed to determine a typical dwelling maximum electrical demand limit for many of the scenarios above; this data shows maximum demand in UK-housing varying between 3.5 and 7.5 kW. In order to mitigate the effects of vehicle charging and electric heating on the existing electrical infrastructure it would be necessary to keep overall demand below these peaks. Consequently, the upper demand value of 7.5kW was used in this paper in the control of heating and vehicle charging. However, the impact of varying the demand limit merits further investigation.

Later, these individual strategies were combined into a set of modelled scenarios, which explored increasing levels of demand intervention in both vehicle charging and heating use.

4. MODELLING TOOL AND ADAPTATIONS

Hawkes and Leach (2005) and Knight and Ribberink (2007) argue that to properly capture the electrical demand characteristics and the exchange of electrical power between a dwelling and the grid, simulation time steps of less than 10 minutes are required. Consequently, to fully assess the impact of vehicle charging and the electrification of heating, the version of ESP-r (ESRU, 2014) used for this paper has been upgraded to enable it to work at high resolution and simulate vehicle charging loads. Further, a hypothetical zero-energy dwelling simulation model has been developed (Hand et al, 2014), complete with an EV.

ESP-r, allows the energy and environmental performance of the building and its energy systems to be determined over a user defined time interval (e.g a day, week, year). The tool explicitly calculates all of the energy and mass transfer processes underpinning building performance. These include conduction and thermal storage in building materials, all convective and radiant heat exchanges (including solar processes and long wave exchange with the sky), air flows, interaction with plant and control systems. To achieve this, a physical description of the building (materials constructions, geometry, etc.) is decomposed into thousands of “control volumes”. In this context, a control volume is an arbitrary region of space to which conservation equations for continuity, energy (thermal and electrical) and species can be applied and one or more characteristic equations formed. A typical building model will contain thousands of such volumes, with sets of equations extracted and grouped according to energy system. The solution of these equations sets with real, time-series climate data, coupled with control and occupancy-related boundary conditions yields the dynamic evolution of temperatures, energy exchanges (heat and electrical) and fluid flows within the building and its supporting systems.

4.1 Adaptations to ESP-r

The ESP-r software has been extended from the standard release to enable its electrical systems model to use stochastic, electrical appliance demand data as a boundary condition. This data was generated at a 1-minute time resolution using a customised version of a domestic appliance demand profile tool (Richardson et al, 2010), which also produced matching thermal gains profiles. Additionally, a new algorithm was developed, based on the work of Jordan and Vagen (2005), which enabled stochastic, sub-hourly resolution domestic hot water draws to be generated during a simulation. Finally, using the work of McCracken (2011), 1-minute solar data was generated, based-on the existing hourly solar data found in ESP-r’s climate data files. This allowed the electrical output from PV to reflect the variability observed in solar radiation levels for a maritime climate like the UK’s. This variability is lost when using the hourly-averaged climate data typically used by building simulation tools. These adaptations to ESP-r are described in more detail by Hand et al (2014). Figure 1 shows typical high-temporal-resolution simulation output including appliance electrical demand and demand associated with the operation of a heat pump.

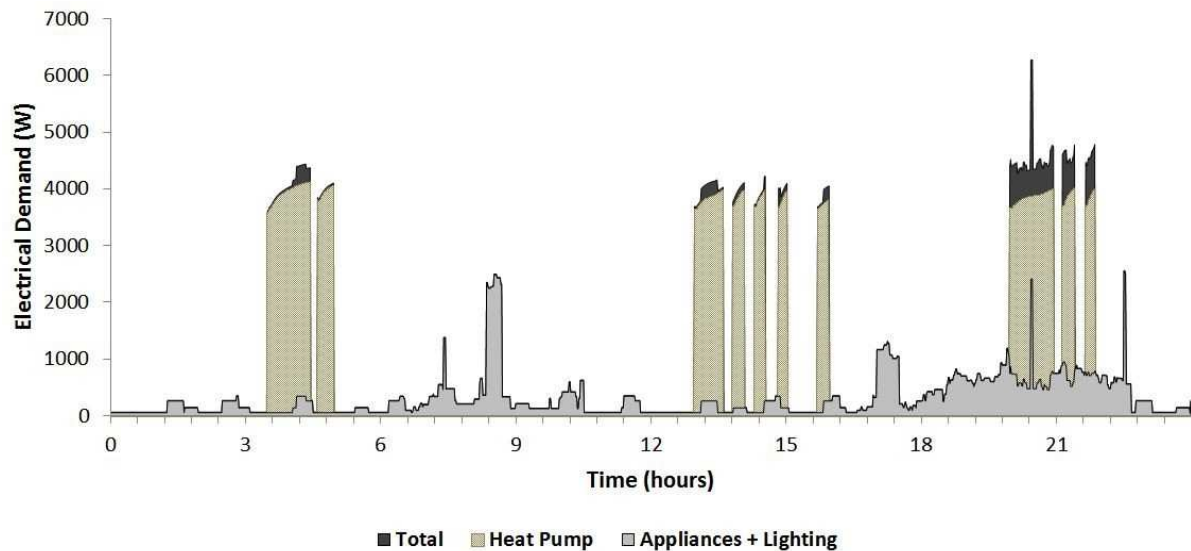


Figure 1: simulation output at 1-min time resolution.

4.2 Vehicle and Battery Algorithm

In addition to the modifications outlined in the previous paragraphs, a stochastic, electric vehicle (EV) algorithm has been developed. The primary role of this algorithm is to mimic the effect of electric vehicle charging on the dwelling's overall electrical demand. The model has several functions, these are: 1) determine when a vehicle leaves and then returns from a trip; 2) calculate the trip distance and subsequent depletion of the battery; and 3) re-charge the battery according to a user-selected control strategy.

The EV model can take three basic states: 'idle' – the vehicle is present and not charging; 'absent' – the vehicle is on a trip and 'charging' – the vehicle is present and charging, depending on the battery control strategy. Also, there is an explicit assumption made in the algorithm that all trips have 1 outward and 1 return leg and that the distance travelled in the return leg is the same as the outbound trip.

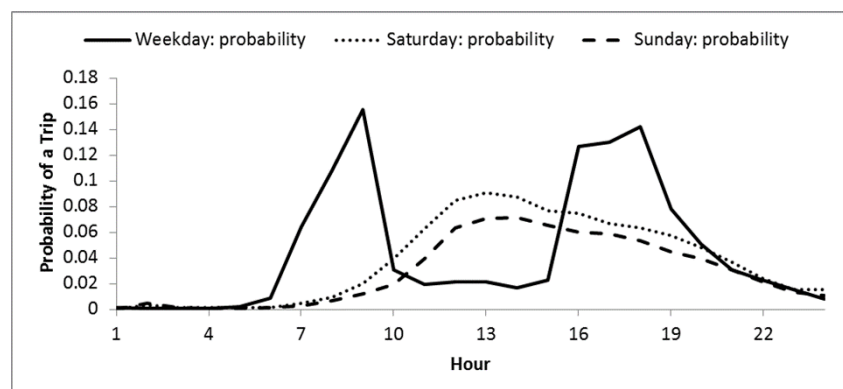


Figure 2: hourly probabilities of a trip leg being taken over a 24-hour period (Huang and Infield, 2010).

To determine if a trip leg is made, the algorithm generates a random number, x , at each simulation time step and this is tested against a time-dependent trip probability $p(t)$ (see

Table 1) to determine:

- whether the EV will depart on a trip (if the vehicle is present); or
- when it returns home from a trip (when the vehicle is absent).

The time-varying hourly probabilities for one leg of a trip for weekdays, Saturdays and Sundays are shown in Figure 2; these were taken from the 2013 UK travel survey (DFT, 2014) and Huang and Infield (2010). The probabilities needed to be modified as follows to account for sub-hourly time steps and the assumption that each vehicle trip comprises two legs.

$$p(t) = p_h(t) \cdot \left(\frac{\Delta t}{3600}\right) \cdot n \quad (1)$$

Here, $p_h(t)$ is the probability that a trip leg will be made in a particular hour, Δt is the simulation time step and n is the assumed number of legs per trip.

Table 1: vehicle status changes.

Test result	Vehicle status	Vehicle Status changes to
$x \geq p(t)$	Home	Absent
	Absent	Home
$x < p(t)$	Absent	Absent
	Home	Home

The model also includes an allowance for ‘range anxiety’. It is assumed that if the state of charge (SOC) is below 35% (i.e. enough charge for an average trip) then the vehicle will continue to charge and a trip will not be made. If the vehicle has returned from a trip (status has changed from ‘absent’ to ‘home’), the model calculates a feasible distance travelled and then the state of charge of the battery. The probability of particular trip distance being travelled could be best characterised using a Weibull distribution with a λ value of 22.4 and a k value of 0.8.

$$F = 1 - e^{-\left(\frac{d}{\lambda}\right)^k} \quad (2)$$

To calculate the total distance travelled (over the two legs) a random number, y , is generated, with a value between 0 and 1 and the distance, d , is calculated using Equation 3.

$$d = \lambda(-\ln(1 - y))^k \quad (3)$$

This distance is checked against the time the vehicle has been absent (Δt) and the maximum speed that the vehicle can legally travel, v_{max} , giving a maximum permissible distance travelled $d_{max} = v_{max} \Delta t$: if the distance travelled exceeds this, then d is set to d_{max} .

The SOC of the battery on returning from a trip is calculated using Equation 4, where D is the nominal discharge rate of the battery in kWh/km and L represents any user-defined parasitic losses for the battery when the car is moving (e.g. any draws on the battery from the heating or cooling system not accounted for in D).

$$SOC(t + \Delta t) = SOC(t) - (D + L)v \quad (4)$$

Finally, the model encompasses a range of charging strategies, as outlined in Table 2. Depending on the strategy chosen for the model, the vehicle state will change from ‘idle’ to ‘charging’ on return.

Note that the random number generator in both the hot water draw algorithm, mentioned previously and the vehicle algorithm employs a seed, which generates a unique pseudo-random series. Additionally, the high resolution solar data and electrical demand use pre-simulated profiles. Consequently, the simulations described later are repeatable, provided that the same seeds are used in the random number generator.

Table 2: vehicle battery charging strategy summary.

Strategy	Comments	Criteria
Fast charge	Vehicle will charge at the maximum allowable rate $P_{V\text{FAST}}$ until the battery is fully charged	$SOC < SOC_{MAX}$
Slow charge	Vehicle charges at a reduced rate P_{SLOW}	$SOC < SOC_{MAX}$
Off peak fast or slow charge	Vehicle charged at $P_{V\text{SLOW/FAST}}$ if within the off peak period 11pm-7am	$SOC < SOC_{MAX}$; $t_{OP-START} < t < t_{OP-END}$
Load sensitive fast or slow charging	Vehicle charged at $P_{V\text{SLOW/FAST}}$ only if the house demand is below a user defined maximum. Otherwise the charging is stopped or the charging rate is modulated.	$SOC < SOC_{MAX}$; $t_{OP-START} < t < t_{OP-END}$; $P_H < P_{H\text{MAX}}$.

4.3 ESP-r Model

The ESP-r model of the zero-energy dwelling is shown in Figure 3. The model is divided into three main thermal zones: a loft zone and two composite zones describing (respectively) the areas of the dwelling hosting active occupancy such as the living room and kitchen and those areas that have low occupancy rates or that are occupied at night such as bathrooms and bedrooms, respectively. The geometric characteristics are summarised in Table 3; this geometrically aggregated form of the model captures the pertinent thermodynamic characteristics of the building's performance and has been deployed successfully in other studies, e.g. (Clarke et al, 2008).

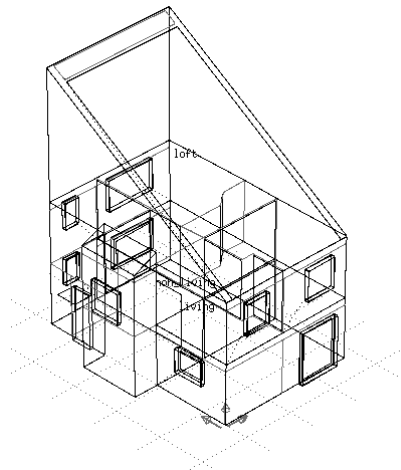


Figure 3: Wireframe view of the zero-energy dwelling model.

The model features a mono pitch roof to accommodate the 45m² (8 kWp) of PV panels used to offset the regulated electrical demands and appliance energy demands. Note that the PV does not offset the electrical demand of the EV. The building has a wooden frame construction, is super-insulated with triple-glazed windows, has high airtightness, mechanical ventilation heat recovery (MVHR) and meets passive house standards. The characteristics of the key fabric elements are as shown in Table 4.

Table 3: summary of dwelling geometric characteristics.

Floor area (m ²)	82.7
External surface area (m ²)	151
Heated Volume (m ³)	230
Glazed Area (m ²)	21.45
'Day' zone floor area (m ²)	34.8
'Night' zone floor area (m ²)	47.9

Table 4: characteristics of constructions used in the dwelling model.

Construction	Details	U-value (W/m ² K)
External walls	Weatherboard air SIP panel with 300mm insulation service void plasterboard 484mm	0.104
Floor	200mm insulation under concrete slab with void and carpet over plywood	0.151
Ceiling	Plasterboard with 400mm glass wool 420mm	0.098
Roofing	Slate roof over battens (cold roof)	3.636
Glazing	Triple glazing argon filled low-e coatings 42mm	0.89

The heating ventilation and air conditioning (HVAC) system used with the dwelling is shown in Figure 4. This is modelled using a network, which comprises a linked collection of plant components. Each component (e.g. duct, heat exchanger, pipe, etc.) is modelled explicitly using a dynamic plant component algorithm.

The primary heat source is an air source heat pump (ASHP) with a 6kW capacity and nominal coefficient of performance (COP) of 3. In the model, both COP and the heating capacity of the ASHP vary with the ambient temperature and the 500L buffer tank temperature. The buffer allows the heat pump to be operated flexibly in time: the heat pump charges the thermal buffer, which then supplies the heat for space heating and hot water at a later time. The primary means of heat distribution in the system of Figure 4 is convective, via the MVHR.

The system also includes a dedicated 500 L solar domestic hot water (DHW) tank and 3m² of roof-mounted solar thermal collectors. Another feature of the model is a 200 L grey-water-heat-recovery-system (GWHR): this collects wastewater from the baths, showers, etc., which pre-heats the incoming cold-feed to the DHW tank via a heat exchanger.

The EV model used in the simulations is based on a Nissan Leaf (Nissan, 2014) and the key model parameters are shown in Table 5.

Finally, in order to capture all of the electrical power exchanges within the building and between the building, vehicle and the grid, an electrical systems network was developed. This features explicit representations of the cabling and electrical infrastructure coupling the local micro-generation and power consuming devices (fans, pumps, heat pump, appliances, etc.). The network also features a coupling point to the local grid. The electrical network was solved to predict the main electrical real power flows associated with the dwelling model, particularly supply and demand, import and export with the grid and losses, including inverter and cable losses.

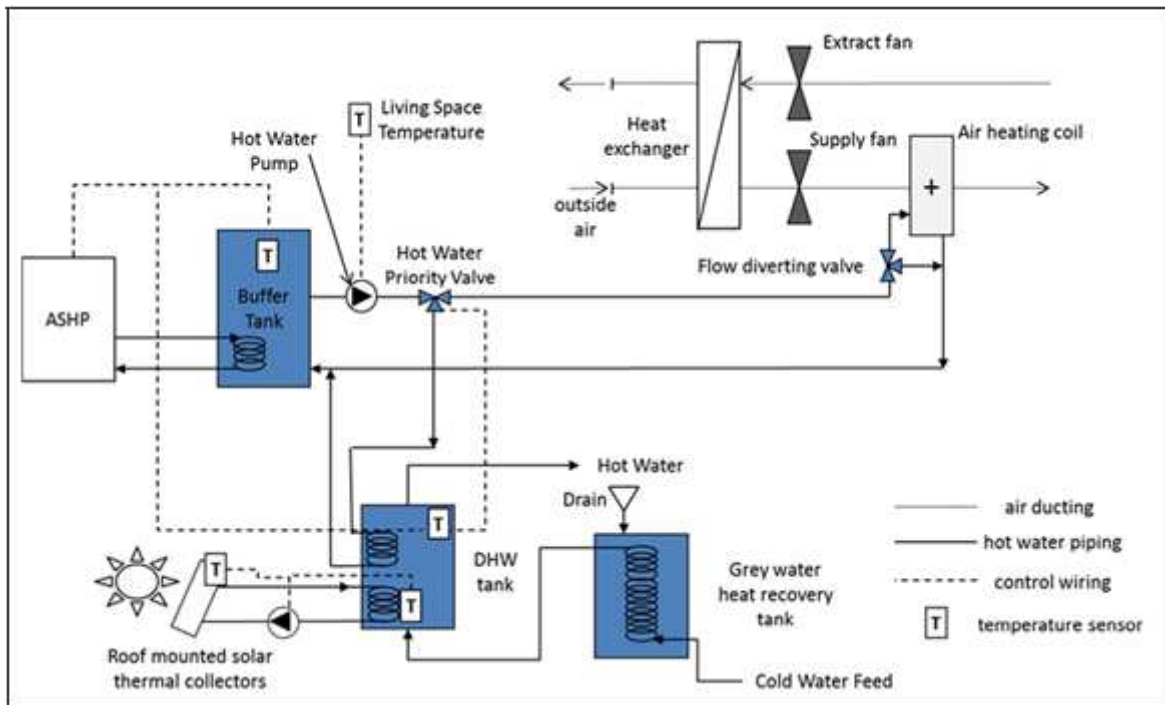


Figure 4: systems model for the dwelling

Table 5: key EV model characteristics (Nissan, 2014; DFT, 2014).

Battery capacity (kWh)	24
Fast charging power (kW)	6.6
Slow charging power (kW)	3.0
Minimum (SOC %)	20
Range anxiety (SOC %)	35
Charge/discharge efficiency (%)	90
Discharge rate (kWh/km)	0.15
Nominal annual distance travelled (km)	13,600
Nominal trip distance (km)	22.1
Distance equation 'λ' (-)	22.4
Distance equation 'k' (-)	0.8

5. SIMULATIONS

A scenario-based approach was adopted in this paper in order to assess the impact of different combinations of heating and EV charging strategies. These are summarised in Table 6.

All of the scenarios were simulated at 1-minute time resolution over the winter months of January and February using a southern UK climate data set. A winter period such as this constitutes a 'worst case' scenario for electrical demand, as the dwelling heating demand will be at its highest and consequently this provides a useful test bed for the demand mitigation scenarios.

Table 6: scenarios modelled.

Base Case – no EV, no Heat Pump	The house is assumed to be heated using biomass and there is no EV.
Case 1 – unrestricted slow charging	Both heating system operation and vehicle charging are uncontrolled. The vehicle is slow charged (3.3kW – up to 6.5 hrs) when it returns from trips and heat is supplied when required.
Case 2 – Unrestricted fast charging	Both heating system operation and vehicle charging are uncontrolled. The vehicle is fast charged (6.6kW – up to 3hrs) when it returns from trips and heat is supplied when required.
Case 3 – load sensitive vehicle battery slow-charging	The vehicle battery is only slow charged at full power if the dwelling and vehicle demand would be less than 7.5 kW.
Case 4 – load sensitive vehicle battery fast-charging	The vehicle battery is only fast charged at full power when the overall dwelling and vehicle demand would be less than 7.5 kW.
Case 5 – off-peak heating and unrestricted slow charging	The heating buffer tank (figure 4) is charged during off peak periods (11 pm – 7am), slow vehicle charging is unrestricted.
Case 6 – off peak heating and unrestricted fast charging	The heating buffer tank (figure 4) is charged during off peak periods (11 pm – 7am), fast vehicle charging is unrestricted.
Case 7 – off peak slow charging and heat load shifting	Both slow vehicle charging and heating system buffer tank charging are shifted to off peak periods (11 pm – 7am).
Case 8 – off-peak fast battery charging and heat load shifting	Both fast vehicle charging and heating system buffer tank charging are shifted to off peak periods (11 pm – 7am).

6. RESULTS AND DISCUSSION

Three key areas were analysed using the results from the scenarios listed in Table 6, these were: 1) the combined electrical demand of the dwelling and vehicle, specifically looking at the peak demand and overall electrical energy use; 2) the performance of the EV over the simulated period, looking at the number of trips and charge times; and 3) the energy performance of the heating system under load-shifted and normal operating conditions. The simulation results are summarised in Tables 7a – 7c.

Comparing the results from scenarios 1 and 2 shown in Table 7a (unrestricted slow and fast vehicle charging, respectively, and unrestricted heating operation) to the base case indicates that the addition of the EV and shift to heat-pump-based-heating more than doubles the overall electrical demand. For the two winter months simulated, demand increases from approximately 390 kWh in the base case to over 1000 kWh in all other scenarios. The peak electrical demand in the base case is 5.1 kW, which occurs around 7pm. The peak demand increases to 10.1 kW with unrestricted heating operation and unrestricted slow charging, or

12.2 kW with unrestricted heating and fast charging: these peak demands occur in the morning period (7am-9am). Figures 5a and 5b show the resulting electrical demand profiles. Table 7b shows maximum charge times, these were 328 minutes with slow charging, and 172 minutes

Table 7a Electrical demand data from the base case and Scenarios 1-8.

Scenario	1	2	3	4	5	6	7	8
Base Case								
Elec. demand (kWh)	1106.1	1136.9	1081.2	1074.6	1137.6	1133.3	1124.1	1144.2
EV demand (kWh)	395.8	426.4	379.8	365.0	443.4	426.4	408.8	425.9
Appl. demand (kWh)	463.7	463.7	463.7	463.7	463.7	463.7	463.7	463.7
ASHP demand (kWh)	-	273.9	273.9	271.6	269.7	269.7	269.1	269.1
PV output (kWh)	223.7	223.7	223.7	223.7	223.7	223.7	223.7	223.7
Elec. export (kWh)	139.3	112.9	110.1	118.5	106.3	116.3	128.2	128.2
Self-consumption (kWh)	84.4	110.8	113.6	105.2	117.4	107.4	95.5	95.5
BOP and losses kWh	160.4	144.0	149.9	131.0	156.6	133.9	113.1	110.1
Max P demand W	5116.52 @7d19h41m	10083.6 @4d7h46m	12222.1 @7d9h11m	8251.56 @4d8h11m	7960.59 @4d1h6m	11327.5 @4d1h6m	9088.01 @12d1h1m	11571.9 @16d1h16m
Max P export W	2287.16 @45d11h51m	2239.83 @45d11h51m	2239.83 @45d11h51m	2239.83 @45d11h51m	2239.83 @45d11h51m	2239.83 @45d11h51m	2239.83 @45d11h51m	2239.83 @45d11h51m

** @44d1h6m - indicates occurrence on day 44 at 1:06am

Table 7b EV performance data from the base case and Scenarios 1-8.

Scenario	Base Cas	1	2	3	4	5	6	7	8
EV demand (kWh)	-	395.8	426.4	379.8	365.0	443.4	426.4	408.8	425.9
Distance travelled (km)	-	2388.4	2588.7	2292.4	2219.6	2673.5	2588.7	2547.2	2620.3
Return trips (-)	-	107.0	112.0	111.0	109.0	112.0	112.0	103.0	105.0
Maximum charge time (mins)	-	328.0	172.0	368.0	190.0	348.0	172.0	1156.0	998.0
Mean SOC (%)	-	97.1	98.3	96.8	99.0	96.0	98.3	74.1	78.2

Table 7c: Heating performance data from the base case and Scenarios 1-8.

Scenario	Base	1	2	3	4	5	6	7	8
ASHP demand (kWh)	-	279.8	273.9	273.9	271.6	269.7	269.7	269.1	269.1
ASHP heat output (kWhrs)	-	858.5	841.3	839.3	832.1	833.8	833.8	832.3	832.3
Mean air temp. occupied	21.4	21.3	21.4	21.3	21.3	21.2	21.2	21.2	21.2
% of time air temp < 18°C	0.17	0.	0.	0.	0.2	3.9	3.	4.	4.
Mean hot water temp. hours	53.8	53.8	54.0	54.1	54.1	53.3	53.3	53.3	53.3

with fast charging. With slow charging, the vehicle was used for 107 trips and 112 with fast charging. The distance travelled with fast charging was 2588 km compared to 2388 km with slow charging, indicating slightly reduced availability of the vehicle with slow charging in this instance. In both the fast and slow charging cases, the self-consumption of PV-generated electricity (Table 7a) was increased at the expense of electricity exported to the network. In the base case, for the two months simulated, self-consumption was 84.4 kWh, whilst 139 kWh of electricity was exported. With the addition of the EV and heat pump, self-consumption in the slow and fast charging cases rose to 111 and 108 kWh, respectively. Conversely, electrical exports dropped to 113 and 116 kWh, respectively, over the same period. The same trend was evident in all of the other 6 scenarios simulated.

In scenarios 3 and 4, charging of the battery was subject to a demand limit of 7.5 kW, with charging being modulated or stopped if the household demand (including the heat pump) exceeded this limit. Table 7a shows the maximum demand of the house occurring in this scenario: this was approximately 8.0 kW in the slow charging case and 8.3 kW with fast charging. Overall, electrical demand still exceeded 1000kWh. The maximum battery charge time (Table 7b) increased slightly for slow charging from 328 to 368 minutes and for fast charging from 172 to 190 minutes, indicating some modulation of both the and slow fast charge due to the 7.5kW constraint. The modulation of full-power charging is clearly shown in Figure 5d. The number of trips taken was unaffected.

In scenarios 5 and 6, fast and slow vehicle charging was unrestricted. However, the operation of the heat pump was re-scheduled to off-peak periods between midnight and 7am as shown in Figures 5e and 5f, with the heat pump charging the buffer tank during this time. Table 7a shows that the peak electrical demands in these scenarios were 8.0 and 11.3 kW for fast and slow charging, respectively. Both peaks occurred around 1am in the morning. Focusing on the heat pump results, its energy use reduced from approximately 280 kWh to 270 kWh. However, this was not a genuine energy saving as it resulted from the restricted operational hours. Further, the shift to off-peak heating increased the occurrence of low air temperatures (<18oC) in the dwelling to approximately 4% of occupied hours, as shown in Table 7c.

In scenarios 7 and 8, both the charging of the vehicle and the operation of the heat pumps were restricted to off peak periods; this resulted in peak demand of 9.1 and 11.6 kW for slow and fast charging, respectively (Table 7a). Both peaks occurred around 1am in the morning as shown in figures 5g and 5h. The results for these scenarios, shown in Table 7b indicate that there was a slight reduction in the number of trips taken: down from approximately 110 and over in the other scenarios to 103 and 105 for slow and fast charging scenarios, respectively; this indicated that the SOC of the battery was occasionally below the range anxiety limit of 35% when a trip was required. The performance of the heating systems was the very similar to scenarios 5 and 6, with Table 7c showing that air temperatures drop below 18oC for approximately 4% of occupied hours.

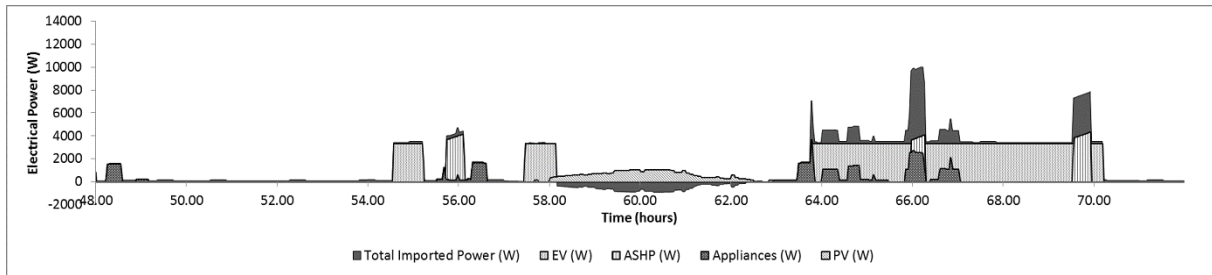


Figure 5a: typical daily profile of electrical supply and demand for unrestricted slow vehicle charging and heat pump operation.

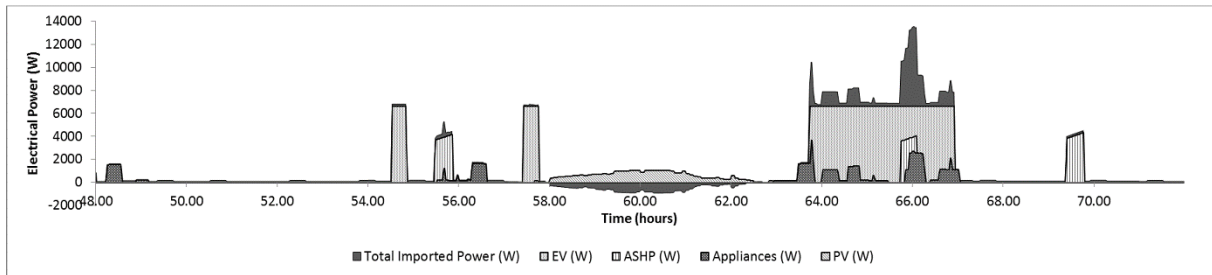


Figure 5b: typical daily profile of electrical supply and demand for unrestricted fast vehicle charging and heat pump operation.

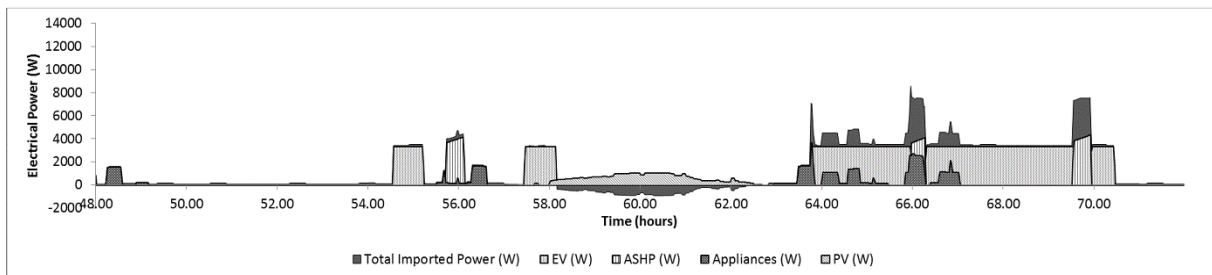


Figure 5c: typical daily profile of electrical supply and demand for load restricted slow vehicle charging and unrestricted heat pump operation.

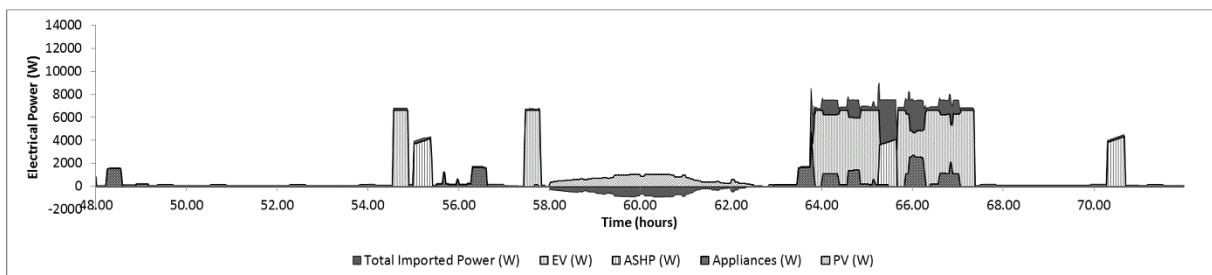


Figure 5d: typical daily profile of electrical supply and demand for load restricted fast vehicle charging and unrestricted heat pump operation.

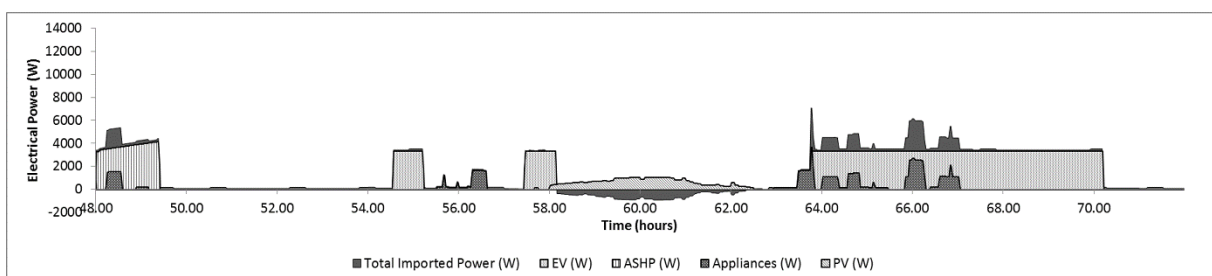


Figure 5e: typical daily profile of electrical supply and demand for unrestricted slow vehicle charging and off-peak heat pump operation.

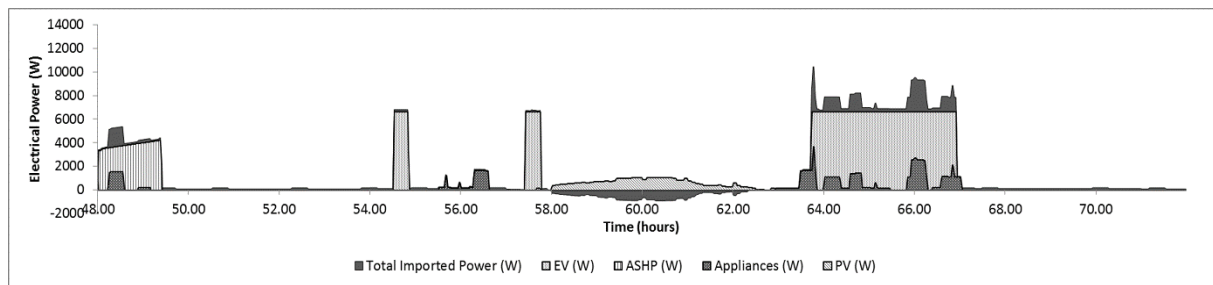


Figure 5f: typical daily profile of electrical supply and demand for unrestricted fast vehicle charging and off-peak heat pump operation.

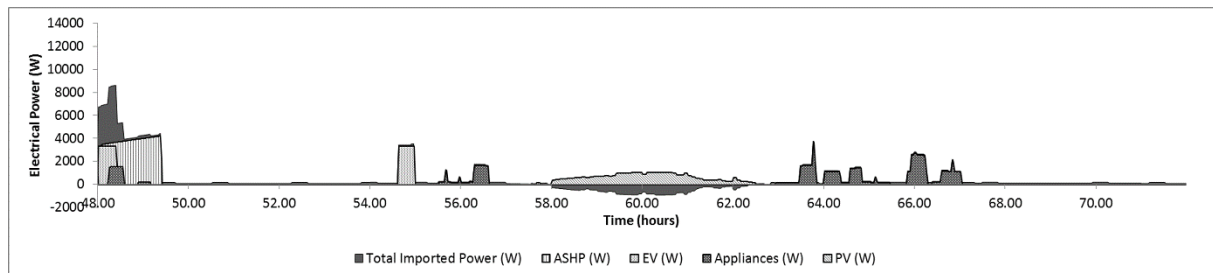


Figure 5g: typical daily profile of electrical supply and demand for off-peak slow vehicle charging and off-peak heat pump operation.

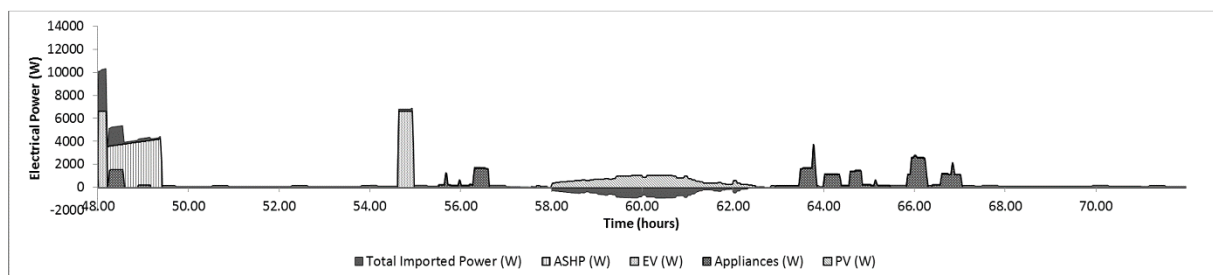


Figure 5h: typical daily profile of electrical supply and demand for off-peak fast vehicle charging and off-peak heat pump operation.

7. CONCLUSIONS

The simulations of this hypothetical, zero-carbon building indicated that the use of an electric vehicle and the electrification of domestic heating more than doubled the electrical consumption of the dwelling in all of the cases simulated bar the base case, which featured biomass heating and no EV. The use of the EV and heat pump also increased the self-consumption of PV generated electricity and decreased the amount of power exported to the grid.

In the worst case of unrestricted vehicle charging and heat pump operation (Scenarios 1 and 2), the peak demand was increased 96% to 10kW for slow vehicle charging and increased 155% to 13 kW for fast charging. As the electrical distribution network is sized for peak demand, this would result in the possible need for network reinforcement to accommodate EVs and heat pumps, if replicated on a large scale.

Several approaches to limiting the increase in peak demand were assessed, including limiting vehicle charging based on the household demand, shifting heat pump demand to UK off-peak periods (midnight-7am) and shifting both heat pump and vehicle operation to off-peak periods.

Shifting the heat pump to off-peak periods between midnight and 7am resulted in peak night time demands of 8.0 and 11.3 kW with slow and fast vehicle charging, respectively: increases of 57 and 121% on the base case peak. Peak demand was moved to 1am. Shifting of the heat

pump operation also resulted in the some occurrences of low indoor air temperatures (<18oC) during occupied hours in the dwelling.

Shifting both heat pump operation and vehicle charging to off-peak periods resulted in a night-time peak demand of 9.1 and 11.6 kW for fast and slow charging; increases of 78 and 127%, respectively on the base case peak. However, this means of reducing demand was at the expense of a 5% reduction in the availability of the vehicle and a reduction in the performance of the heating system.

The most effective means of limiting the peak demand (for both fast and slow charging) was control of EV charging with a demand limit. If the limit was set such that vehicle charging was modulated or stopped when household demand rose above 7.5 kW, then the peak demands were limited to 8.0 and 8.3 kW in the slow and fast charging cases, respectively (increases of 57% and 63% of the base case peak demand). In these cases, there was no deterioration of the heating system performance and vehicle availability was little affected. Charging times however increased slightly through modulation or interruption of the charge when the demand limit was reached.

8. FURTHER WORK

This paper looks only at the impact of wholesale electrification and demand limiting measures on a single dwelling. Work is underway to extend the detailed modelling work described here to populations of dwellings in order to assess aggregate network impacts.

ACKNOWLEDGEMENTS

The simulation work described in this article was done with the support of the Top and Tail Grand Challenge in Energy Networks research consortiums and the authors gratefully acknowledge the funding and support provided by the UK Research Council's Energy Programme under grant EP/I031707/1.

REFERENCES

- Asare-Bediako B., Kling W.L., Ribeiro P.F., 2014. Future residential load profiles: Scenario-based analysis of high penetration of heavy loads and distributed generation, *Energy and Buildings*, Volume 75, Pages 228-238.
- Attia S, Hamdy M, O'Brien W, Carlucci S, 2013. Assessing gaps and needs for integrating building performance optimization tools in net zero energy buildings design, *Energy and Buildings*, Volume 60, Pages 110-124.
- Clarke J A, Johnstone C M, Kim J M and Tuohy P G, 2008. Energy, Carbon and Cost Performance of Building Stocks: Upgrade Analysis, Energy Labelling and National Policy Development. *Advances in Building Energy Research*. 3, Earthscan, London. Pages 1-20.
- DECC, Department for Energy and Climate Change 2008. The UK Low Carbon Transition Plan. The Stationary Office, London, UK.
- DECC, Department for Energy and Climate Change, 2013. Energy Consumption in the United Kingdom: 2012, DECC Factsheet URN 13D/154, London, UK.
- DFT, UK Department for Transport 2014. On-line Vehicle Registration Statistics: <https://www.gov.uk/government/collections/vehicles-statistics> Accessed: 10/06/14. ESRU, 2014. www.esru.strath.ac.uk/Programs/ESP-r.htm Accessed: 17/1/2014.

- Feist W, 2006. 15th Anniversary of the Darmstadt - Kranichstein Passive House. Available at: http://www.passivhaustagung.de/Kran/First_Passive_House_Kranichstein_en.html Accessed 05 January 2014.
- Haines G, McGordon A, Jennings P, Butcher N, 2009 The Simulation of Vehicle-to-Home Systems – Using Electric Vehicle Battery Storage to Smooth Domestic Electricity Demand. Proc. Ecologic Vehicles/Renewable Energies - EVRE, Monaco. Pages 1-9.
- Hand J, Kelly N J, Samuel A, 2014. High Resolution Modelling for Performance Assessment of Future Dwellings, Proc. BSO' 14 Building Simulation and Optimisation, University College London, UK, Pages 1-8.
- Hawkes, A, Leach, M., 2005. Impacts of temporal precision in optimisation modelling of micro-Combined Heat and Power. Energy 30, Pages 1759–1779.
- Hedegaard K, Ravn H, Juul N, Meibom P, 2012. Effects of electric vehicles on power systems in Northern Europe, Energy, Volume 48, Issue 1, Pages 356-368.
- Hinnells M, Boardman B, Darby S, Killip G, Layberry R. 2007. Transforming UK homes: achieving a 60% cut in carbon emissions by 2050 Proc. ecee 2007 Summer Study, La Colle sur Loup, France. Pages 1105-1109.
- Huang S, Infield, D 2010. The impact of domestic Plug-in Hybrid Electric Vehicles on power distribution system loads, 2010 International Conference on Power System Technology (POWERCON), Hanzhou, China, pp.1-7.
- IEA, 2014. International Energy Agency, Energy Conservation in Buildings and Community Systems Annex 42, www.ecbcs.org/annexes/annex42.htm Accessed 11/05/14
- Jordan U and Vajen K, 2005. DHWCALC: Program to Generate Domestic Hot Water Draws with Statistical Means for User Defined Conditions, Proc. ISES Solar World Congress, Orlando, USA. Pages 1-8.
- Knight I and Ribberink H, 2007. European and Canadian non-HVAC Electric and DHW Load Profiles for Use in Simulating the Performance of Residential Cogeneration Systems, IEA ECBCS Annex 42 Report, HMQR, Ottawa, Canada, ISBN 978-0-662-46221-7.
- McCracken D, 2011. Synthetic High Resolution Solar Data, MSc Thesis, University of Strathclyde, Glasgow, UK.
- Munkhammar J, Grahn P, Widén J, 2013. Quantifying self-consumption of on-site photovoltaic power generation in households with electric vehicle home charging, Solar Energy, Volume 97, Pages 208-216.
- Nissan UK, 2014. Nissan Leaf Data Sheet: <http://www.nissan.co.uk/content/dam/services/gb/brochure/LEAF%20Tech%20Spec.pdf> Accessed 11/06/14
- OFGEM, 2013. Feed in Tariff Update 14. Available at: <https://www.ofgem.gov.uk/publications-and-updates/feed-tariff-update-quarterly-report-issue-14>. Accessed on 12 December 2013.
- Palmer J, Cooper I (eds.). 2011. Great Britain's Housing Energy Fact File. Department for Energy and Climate Change Publication, London, UK. URN 11D/866.
- Panoutsou C, Castillo A, 2011. Outlook on Market Segments for Biomass Uptake by 2020 in the UK, Intelligent Energy Europe Report, Imperial College, Available at: http://www.biomassfutures.eu/public_docs/final_deliverables/WP2/D2.3%20Outlook%20on

%20Market%20Segments%20for%20Biomass%20Uptake%20by%202020%20in%20the%20UK.pdf Accessed on 10/06/2014.

Pudjianto D, Djapic P, Aunedi M, Gan CK, Strbac G, Huang S, Infield D, 2013. Smart control for minimizing distribution network reinforcement cost due to electrification, *Energy Policy*, Volume 52, Pages 76-84.

Razeghi G, Zhang L, Brown T, Samuelsen S, 2014. Impacts of plug-in hybrid electric vehicles on a residential transformer using stochastic and empirical analysis, *Journal of Power Sources*, Volume 252, Pages 277-285.

Richardson I, Thompson M, Infield D, Clifford C 2010. Domestic electricity use: A high-resolution energy demand model. *Energy and Buildings* 42(10) Pages 1878-1887.

Robinson A P, Blythe P T, Bell M C, Hübner Y, Hill G A, 2013. Analysis of electric vehicle driver recharging demand profiles and subsequent impacts on the carbon content of electric vehicle trips, *Energy Policy*, Volume 61, Pages 337-348.

Wilson I A G, Rennie A J R, Ding Y, Eames P C, Hall P, Kelly N J 2013. Historical daily gas and electrical energy flows through Great Britain's transmission networks and the decarbonisation of domestic heat. *Energy Policy*, 61, Pages 301-305.

FIFTH SESSION
EXPERIMENTAL STUDIES

ISABELE method: In-Situ Assessment of the Building Envelope performances

P. Boisson^{1*}, R. Bouchié¹

⁽¹⁾ Université Paris Est – Centre Scientifique et Technique du Bâtiment (CSTB), 84 avenue Jean Jaurès – Champs-sur-Marne 77447 Marne-la-Vallée, FRANCE

1. ABSTRACT

The development of high energy performance buildings requires specific tools in order to assess their actual thermal performances, regardless of building use and climatic conditions.

The scope of this work is to assess “intrinsic” energy performance of a building by developing a measurement methodology applicable at the acceptance step during the construction process of a new building or after deep refurbishment works on an existing building. This methodology must be short enough and is only applicable in buildings without occupant inside. The general principle is to inject a controlled heating power inside the tested building and to measure its thermal reaction in order to deduce the thermal properties of the envelope.

To achieve that, an identification method has been developed, based on the thermal model used in the international standard ISO 13790. The aim is to identify the heat loss coefficient by transmission through the building envelope H_{tr} , and thermal inertia parameters. A comparison between this identification method and numerical experiments based on more detailed modeling tools (SIMBAD) has validated the principle for several parameters (thermal inertia, insulation level...).

The final aim is to detect gaps between the design and as-built thermal performances of the envelope, especially for heat losses.

Keywords: performance assessment, building envelope, in-situ measure protocol, identification, heat loss coefficient, numerical experiments

2. INTRODUCTION

The scarcity of natural energy resources and the climate change issue have led all building industry actors to reduce energy consumption by constructing new efficient buildings and by improving existing buildings by refurbishments. Mostly, requirements and labeling of the building energy performances are based on theoretical calculations of energy use in the design phase. However several studies showed that the actual energy performance after the construction phase may deviate significantly from the theoretical designed calculations (Sutton, et al., 2012).

ISABELE method is a short method to characterize the thermal properties of the envelope of a building at the acceptance stage in controlled test conditions. It has been developed in order to be able to compare design and real building envelope performance.

It is important to notice that even if occupant behavior and energy system management are key points to achieve this goal, the real intrinsic thermal performance of the envelope is crucial. Performance gaps have been identified due to bad conception or workmanship: air circulations around insulation products can increase the U-value of a cavity wall by more than 300% (Hens, et al., 2007), and it has been shown that the overall heat loss through the envelope of houses, measured by co-heating tests, can be up to 200 % of its designed value (Sutton, et al., 2012).

ISABELE method is intended to help to reduce gap between design and real energy performance and then promote the energy performance guarantee approach.

3. STATE OF ART

Methods developed to deduce intrinsic thermal performance of the building envelope from data measurements on the field have been studied both in the PERFORMER project (PERFORMER Project, 2014) and in the IEA EBC Annex 58 project on “reliable building energy performance characterization based on full scale dynamic measurements” (Roels, 2014).

These methods, consisting in deducing from data measurements (i.e. energy consumption, internal and external solicitations...) the thermal behavior of the building envelope, can be split in two parts:

- Methods applicable when the building is in use, so with occupancy
- Methods only applicable when the building is empty for a certain time, so with no occupancy

Methods with occupancy need as much data as possible in cold period: several cold seasons are recommended. The first concept is based on energy signature and consists in performing a simple energy balance, plotting for example energy consumption as a function of temperature difference between inside and outside environments and deducing a heat loss coefficient for this analysis. This concept, described for example in the PRISM method (Fels, 1986), can measure the efficiency of a deep refurbishment but it may be difficult to deduce from the global gain (including energy system efficiency, hot water consumption, user behavior...) the contribution of the envelope alone. Other methods of parameter identification based on dynamic measurements have been used to identify suitable models to describe the thermal characteristics of a building including its energy systems, by using lumped parameter RC-models (Bacher & Madsen, 2011). This approach may be useful to predict the dynamic behavior of buildings for optimizing energy grids for building communities, but it may be difficult to link RC-models used in this approach with physical quantities as U-value for example. Other methods (Berger, et al., 2010) are based on a physical thermal modeling and consist in calibrating the envelope performance described in this model by injecting both measurements and occupant behavior information based on inquiries.

All these methods, aiming to deduce intrinsic properties of the building envelope, and applicable when the building is in use, have to deal with the impact of the occupancy which is rather unpredictable and difficult to measure. This effect, together with other aspects such as how deducing air ventilation rate, solar radiation and how taking strong thermal inertia into account, may probably decrease their accuracy.

Thus, other ways to deduce intrinsic thermal performances of a building envelope have then been applied with no occupant inside the building in order to avoid the uncertainty on intrinsic performances linked with the building usage. The most studied method with no occupancy is the co-heating test, originally applied to determine the efficiency of duct heating and cooling systems (Sonderegger, et al., 1979). The global principle, similar to energy signature methods, is to identify the Heat Loss Coefficient (HLC, in W/K) of the tested building by plotting daily heat consumption as a function of daily averaged temperature difference between inside and outside environments. An improvement of this method was to include solar gains by applying a linear regression identifying the HLC and an equivalent solar aperture (Everett, 1985).

A recent review on co-heating test recommended analyzing the test data by a multi-linear regression in order to properly identify both the HLC coefficient and the solar aperture coefficient (Bauwens & Roels, 2014). In this review, all assumptions lumped into the simplified

heat balance used for co-heating test were described: the HLC coefficient is a global heat loss coefficient including air infiltration rate, and the equivalent solar aperture has lost its physical relevance by including both short and long wave radiation effects. It is also recommended in this review to average data for at least several days, depending on the thermal inertia of the tested building, in order to avoid thermal lag effects.

Therefore, the co-heating test can provide a quite accurate indication on the global heat loss coefficient HLC of the test envelope. Two co-heating tests, using the same methodology, and applied on the same dwelling by two different teams on two different periods have shown a very small difference on the identified HLC coefficient ($< 1\%$), and the co-heating test has demonstrated its capability to detect the impact of retrofitting (Gorse, et al., 2014).

Nevertheless, a co-heating test can be quite difficult to apply in practice mainly because:

- The best accuracy is obtained in cold season, that make co-heating test difficult to run during summer for example,
- Co-heating test needs a certain amount of daily averaged data, so at least several weeks of test is necessary.

This last point is critical regarding to the aim of testing real buildings in which the time with no occupant inside is very limited: a new (or new retrofitted) building may be empty for several days during the acceptance stage, some occupied buildings as school or office may be partially empty for holidays for example, but it is clearly impossible to have an empty building for about one month in order to test the intrinsic thermal performance of its envelope.

This is the main reason for developing and testing different methods based on short measurements (under a week) as ISABELE.

Another method called QUB (Quick U-value of Buildings) has been developed by Saint-Gobain (Mangematin, et al., 2012) to assess the heat loss coefficient of a building in a short period of time. The feasibility of this measurement has been demonstrated experimentally (Pandraud, et al., 2013), validated numerically (Alzetto, et al., 2014) and validated experimentally in the Energy House of the University of Salford (Pandraud & Fitton, 2013).

As part of PERFORMER project an implementation and a comparison of results of both ISABELE and QUB methods have been satisfactorily realized on a real test house (Bouchié, Alzetto, Brun, Boisson & Thebault, 2014)

4. DESCRIPTION OF THE DEVELOPPED METHOD

4.1 Test protocol

The purpose of this paper is to present a new building performance assessment method called ISABELE, which stands for “In-Situ Assessment of the Building Envelope performancEs”. This method has been developed in order to characterize the thermal properties of the envelope of a building at the acceptance stage after the construction process of a new building or after deep refurbishment works on an existing building. Therefore it must be short enough (2 weeks maximum) and is only applicable in buildings with no occupant inside. The general principle is to inject a controlled heating power inside the tested building and to measure its thermal reaction in order to deduce the thermal properties of the envelope.

The thermal properties we want to assess are the heat loss coefficient by transmission through the building envelope H_{tr} and linked thermal inertia. Performances are obtained by identification using a thermal model based on the French Thermal Regulation RT2012 (Th-BCE, 2012) which is derived from the international ISO standard 13790:2013 (ISO-1, 2013). The identification process consists in fitting the thermal model to the measured dynamic

internal temperature using least squares minimization. It runs using hourly average data.

The experimental test protocol includes three steps, as shown in Figure 1:

- **Step 1:** No heating power injected. The aim at this stage is to assess initial thermal energy stored in the thermal mass of the building. If the building is in a quasi-permanent state before starting the test (internal temperature maintained to a quasi-constant value for several weeks), this step is not required.
- **Step 2:** Heating power injected to lead internal temperature to a fixed setpoint. The temperature setpoint is deduced from internal average temperature measured in step 1 in order to increase it by about 10 K.
- **Step 3:** Heating power is turned off to observe a free-decrease of the internal temperature.

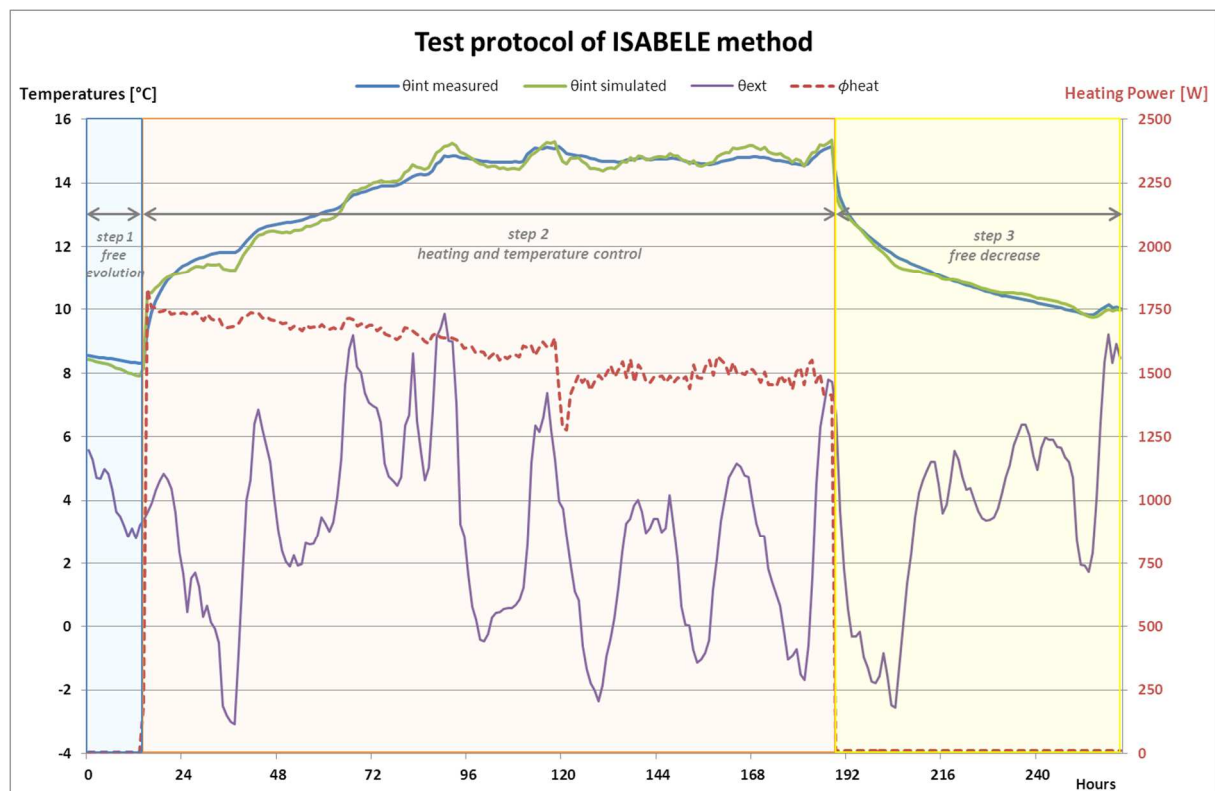


Figure 1: Principle and experimental steps for ISABELE method

At all steps, internal temperature, heat power injected, air infiltration rate and external climatic conditions (outside temperature, solar radiation, long-wave radiation, wind speed), are measured (or estimated) and then inputted in the model to identify H_{tr} and inertia parameters. Time step of several minutes are required for data measurements.

The identification process is based on the global heating power, so one of the difficulties is to reduce thermal impact of other parameters such as air infiltration and solar gain. To achieve this, all window shading devices must be shut down, ventilation must be turned off and the air intakes and outlets must be blocked during the entire test. It is also possible to measure thermal impact of air infiltration rate (by a gas tracer dilution method) or estimate it by calculation using airtightness and wind speed data.

For light inertia buildings a sequence of 2 or 3 days can be considered as sufficient. For higher inertia buildings this could lead to a reduced accuracy of results. Works are in progress to find the best balance between the results accuracy and the aim to have a short period for the experiment.

4.2 Thermal model used

The identification procedure is based on the building thermal model used in French Thermal Regulation RT 2012 (Th-BCE, 2012). This model runs with an hourly time step and includes five thermal resistances and one thermal capacity (Figure 2).

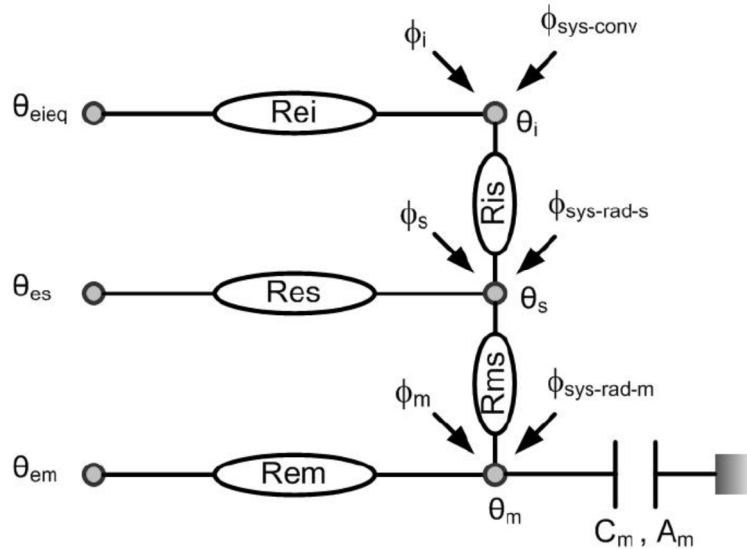


Figure 2: 5RIC thermal model used for the identification procedure (from (Th-BCE, 2012))

θ_{eieq} , θ_{es} and θ_{em} are equivalent external temperatures, respectively for the air incoming in the building by ventilation and infiltration, for glazing components (windows, curtain walls...) and opaque walls.

θ_i and θ_s are indoor air temperature and a temperature mixing indoor air temperature with mean indoor radiant temperature. θ_s results from a conversion of a delta network in a star network.

R_{ei} and R_{es} are thermal resistances, in K/W, due to air renewal (by ventilation and by infiltration through to envelope) and thermal transmission through glazing components.

R_{is} is the thermal resistance due to internal thermal exchanges by convection and radiation.

Glazing components are supposed not to have a significant thermal mass that is why an equivalent external temperature θ_{es} variation is immediately visible on temperature node θ_s .

Thermal resistance of all opaque walls and thermal bridges R_{th} is splitted in two parts: an equivalent thermal resistance of the thermal mass R_{ms} due to internal exchanges between the thermal mass of heavy components and indoor environment, and the complementary resistance R_{em} (with $R_{th} = R_{em} + R_{ms}$). Between these two thermal resistances, the temperature node θ_m , corresponding to equivalent temperature of the thermal mass of the building, is plugged on the thermal capacity C_m .

Thermal flows injected on different internal nodes are divided between solar and internal free gains (Φ_i , Φ_s and Φ_m) and another part due to energy production of thermal emitters ($\Phi_{sys-conv}$, $\Phi_{sys-rad-s}$, $\Phi_{sys-rad-m}$). Thermal flows partition between these three temperature nodes depends on the type of emitted flows and standardized hypothesis (for example on partition between convective and radiant parts and on partition of direct solar gains (short longwaves) transmitted through windows on the air temperature θ_i and the other nodes θ_s and θ_m).

This thermal model is very close to that described in the International standard ISO 13790: 2013 (ISO-1, 2013) (simple hourly method, clause 7.2.2). General principles and intrinsic properties of the envelope are the same:

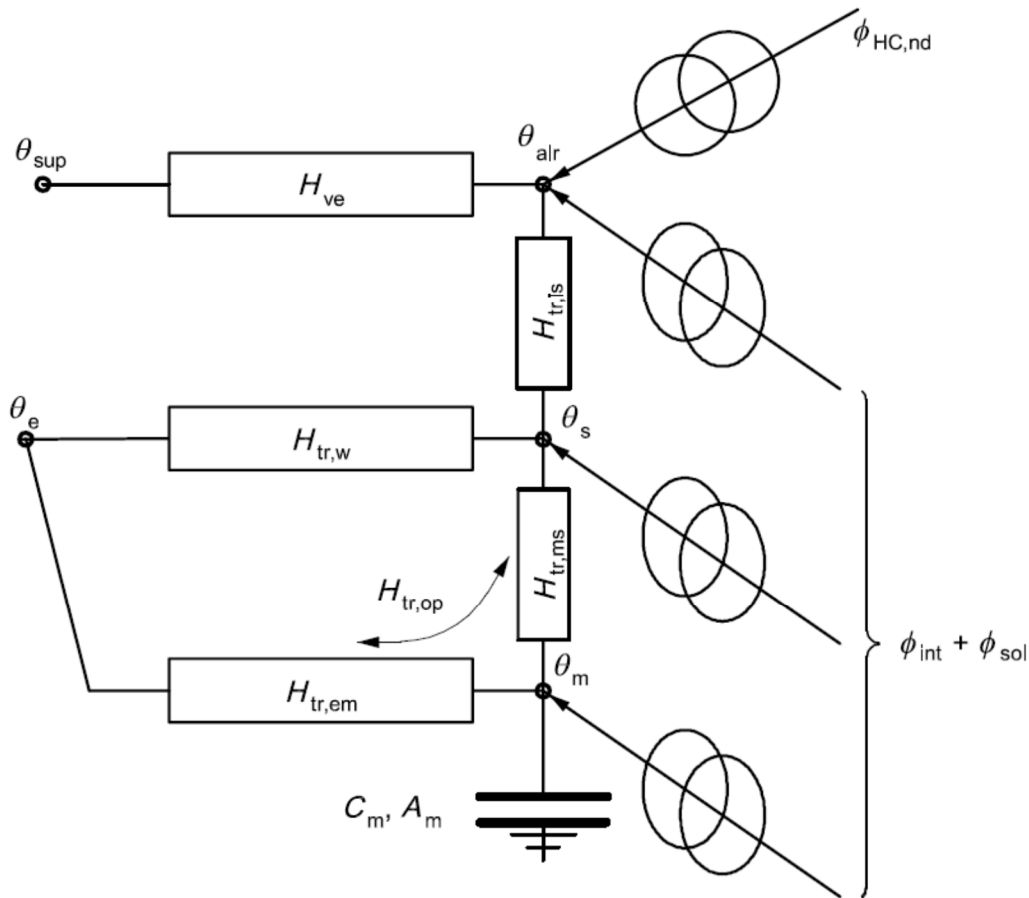


Figure 3: 5R1C model described in the international standard ISO 13790:2013

Concerning the envelope thermal behavior, the main difference is based on how free gains (in particular solar gains) are considered. Considering the case where no other free gain than solar gains are presents, and where direct solar gain are negligible (if tested building have shading devices on windows):

- Solar gains injected on internal temperature nodes in the RT 2012 model are then negligible ($\Phi_i = \Phi_s = \Phi_m = 0$). Both solar radiation absorbed by external opaque walls and longwave radiation with the sky are included in the calculated equivalent external temperatures θ_{em} and θ_{es} .
- In the international standard model, external solicitations are grouped in a single node corresponding to external air temperature θ_e . Both solar radiation absorbed by external opaque walls and longwave radiation with the sky are included in a thermal flow Φ_{sol} conventionally splitted between internal temperature nodes.

In the case where neither glazing components nor structural thermal bridges are present, global thermal flow Φ_{sol} calculated according to ISO 13790:2013 is linked with equivalent external temperature θ_{em} calculated according to RT 2012 model by the formula:

$$\Phi_{sol} = \left(\sum_k A_{p,k} \times U_{p,k} \right) \times (\theta_{em} - \theta_e) \quad (1)$$

With:

$$\theta_{em} = \frac{\sum_k A_{p,k} \times U_{p,k} \times \theta_{em,k}}{\sum_k A_{p,k} \times U_{p,k}} \quad (2)$$

And:

$A_{p,k}$ Surface of the opaque component k, in m²

$U_{p,k}$ Thermal transmission coefficient of the opaque component k, included the effect of integrated thermal bridges, in W/(m.K)

θ_e External air temperature, in °C

θ_{em} Mean equivalent external temperature of the building, in °C

$\theta_{em,k}$ Equivalent external temperature of the opaque component k, in °C

Global calculated solar gains are the same between these two models, only their conventional partition between internal temperature nodes is different.

A sensor has been especially designed and validated to measure external thermal radiation effects on the envelope (solar absorption and long-wave radiation), i.e. to measure the equivalent external temperatures per façade (Bouchié, Abele, Derouineau & Millet, 2014).

The conditions of the test protocol (no internal gain due to occupancy, all shutters closed) imply that:

$$\Phi_i = \Phi_s = \Phi_m = 0 \quad (3)$$

Concerning the heat production during the test protocol, the thermal flows due to emitters are considered only convective. Indeed the heat is provided by electric heaters that are accompanied with fans in order to homogenize the air temperature in the entire heated volume:

$$\Phi_{\text{sys-rad-s}} = \Phi_{\text{sys-rad-m}} = 0 \quad (4)$$

4.3 Modeling of inertia

The thermal inertia used in the model of the RT2012 is the daily inertia that characterizes the damping of the daily temperature wave and the recovery rate of heat gains in winter (over 24 hours).

Th-I Rules (Règles Th-I, 2012) define daily thermal inertia of a building zone with two parameters:

- The heat capacity for a wave of 24 hours (C_m , in kJ/K);
- The equivalent exchange surface of heavy walls with the indoor environment (A_m , in m²).

These two parameters are calculated as follows:

$$C_m = \sum_k A_k \times \chi_{d,k} \quad (5)$$

$$A_m = (\sum_k A_k \times \chi_{d,k})^2 / (\sum_k A_k \times \chi_{d,k}^2) \quad (6)$$

With:

A_k Surface of the wall k, in m²

$\chi_{d,k}$ Surface heat capacity of the wall k for a period of 24 hours (index d for daily period), in kJ/(m².K), calculated according to standard ISO 13786: 2008 “Thermal performance

of building components — Dynamic thermal characteristics — Calculation methods” (ISO-2, 2008), without taking into account the surface resistance.

In Equation 3, C_m is calculated without the inertia of furniture, which is normally considered on a fixed basis in Th-I Rules.

In the 5R1C model, the equivalent exchange surface A_m is used to calculate the thermal resistance R_{ms} with the following formula:

$$R_{ms} = 1/h_{is} \times A_m \quad (7)$$

With:

h_{is} sum of convective and radiant heat exchange coefficients

The first experiments of ISABELE method showed that for tests over one week and for buildings with heavy inertia, the daily inertia is not sufficient to reproduce the dynamic behavior of the building. Thus, it has been decided to slightly modify the model by adding a longer-term inertia, called “sequential inertia” (in Th-I Rules) and characterized by a wave of a period of 12 days.

Similarly as for the daily inertia, sequential inertia is defined by the parameters C_{ms} et A_{ms} :

$$C_{ms} = \sum_k A_k \times \chi_{s,k} \quad (8)$$

$$A_{ms} = (\sum_k A_k \times \chi_{s,k})^2 / (\sum_k A_k \times \chi_{s,k}^2) \quad (9)$$

With:

$\chi_{s,k}$ Surface heat capacity of the wall k for a period of 12 days, in kJ/(m².K)

The impacts of inertia are dealt by the principle of superposition of states: sequential effects using the RC network on a time step of one day can be superimposed on the daily effects treated in terms of deviation from the sequential values. Therefore an additional flow resulting from the resolution of a differential equation using the sliding 24h - mean value of θ_m and the sequential capacitance C_{ms} is injected in the temperature node θ_m in the 5R1C model.

Figure 4 illustrates the complementary RC network taking into account the sequential effects.

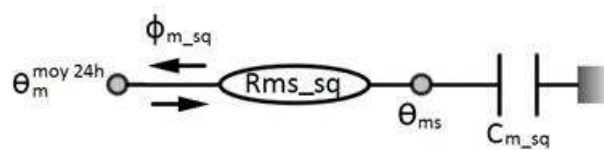


Figure 4: Secondary RC network for sequential inertia calculations

The resolution of the differential equation is performed using the sliding 24h - mean value of θ_m and the following parameters:

$$C_{msq} = C_{ms} - C_m \quad (10)$$

$$R_{ms_sq} = R_{ms_s} - R_{ms} \quad (11)$$

Where:

$$R_{ms_s} = 1/h_{is} \times A_{ms} \quad (12)$$

4.4 Identification with the least squares minimization

It aims to identify the coefficient H_{tr} and A_m , C_m , A_{ms} and C_{ms} . H_{tr} is defined from the resistances of the model as follows:

$$H_{tr} = H_{tr,op} + H_{tr,w} = 1/(R_{em} + R_{ms}) + 1/R_{es} \quad (13)$$

With:

$H_{tr,op}$ Heat loss coefficient by transmission through the opaque walls, in W/K

$H_{tr,w}$ Heat loss coefficient by transmission through the windows, in W/K

In the minimization algorithm to converge faster and avoid getting away from the most likely solution, we choose to start from the theoretical solution, which corresponds to the design calculated values. We define the theoretical values of the desired parameters: $H_{tr,th}$, $H_{tr,op,th}$, $H_{tr,w,th}$, $A_{m,th}$, $C_{m,th}$, $A_{ms,th}$ and $C_{ms,th}$.

To limit the number of parameters to be identified, we choose to identify only one parameter for daily inertia (and similarly for sequential inertia). Indeed, A_m and C_m are relatively linked according to their formula, which suggests that they vary in the same direction and almost proportionally.

Thus we define the following ratios:

$$Cid_{Htr} = H_{tr}/H_{tr,th} \quad (14)$$

$$Cid_{Cm} = C_m/C_{m,th} = A_m/A_{m,th} \quad (15)$$

$$Cid_{Cms} = C_{ms}/C_{ms,th} = A_{ms}/A_{ms,th} \quad (16)$$

In this way, the three parameters that are identified are: Cid_{Htr} , Cid_{Cm} et Cid_{Cms} , and initial values are 1.

The RC network takes as inputs the following variables from the measurements:

- Rate of air infiltration, which is used to calculate R_{ei} .
- External temperature θ_e ($\theta_{e,ieq}$ is equal to θ_e because we consider only air infiltration from outside)
- Solar radiation and longwave radiation with the sky which are used to calculate the equivalent external temperatures θ_{em} and θ_{es}
- Heating power $\Phi_{sys-conv}$

The identification method minimizes the mean square error between simulated and the measured indoor temperature θ_i and uses “fminsearch” Matlab function, in which the algorithm is a Nelder-Mead simplex search method (Lagarias, et al., 1998).

5. SIMULATION

5.1 Simulations with SIMBAD

A first validation step was to apply the method on controlled cases not from field measurements. For this we decided to use numerical experiments to generate the variables normally resulting from actual measurements on site. These numerical experiments were performed with a detailed simulation tool to finely represent the dynamic thermal behavior of a building. The tool is SIMBAD which is a library of building modeling components developed at CSTB in Matlab / Simulink. (Husaunndee, et al., 1997)

At first, very simple cases of buildings have been modeled in order to verify the feasibility of the method. Following was to perform a parametric study to test the sensitivity of certain parameters on the resolution of the identification.

The comparison between this identification method using a simplified model and numerical experiments based on more detailed modeling tool has validated the principle for several parameters (thermal inertia, insulation level...) and allowed to appreciate the accuracy of the simplified thermal model used for identification.

5.2 Building models

Four basic buildings were modeled, corresponding to mono-zone rooms composed of six strictly identical walls without glazing. The differences between the four buildings relate to their level of insulation (50 or 200 mm) and inertia (outer or inner position of the insulation). The combination of these characteristics forms these four virtual reference buildings.

These reference buildings are $5 * 5 = 25\text{m}^2$ with a ceiling height of 2.5 m. Their six walls are in contact with the outside air (no contact with the ground or other boundary condition)

The theoretical design values of the thermal characteristics of the four building envelopes are described in Table 1.

Table 1: Theoretical design values of thermal characteristics of the four virtual reference buildings

Building name	Insulation	Inertia	H_{tr} [W/K]	A_m [m ²]	C_m [kJ/K]	A_{ms} [m ²]	C_{ms} [kJ/K]
if_50	low	light	62.89	100	1694	100	2316
if_200	high	light	18.39	100	1298	100	1594
IFO_50	low	heavy	62.89	100	16956	100	30635
IFO_200	high	heavy	18.39	100	17035	100	32195

Inertial parameters are calculated using the detailed method of the International Standard ISO 13786: 2008.

From these four reference buildings, derivatives were constructed to diversify thermal envelope characteristics in terms of size, shape, heterogeneity of walls:

- Size: floor area of 9m², 25m², 64m², 144m²
- Shape: square, rectangular, oriented N-S, rectangular oriented W-E
- Heterogeneity of walls: Fixed inertia and different insulation (half walls, according to orientations), fixed insulation and different inertia, inertia and fixed intermediate insulation, insulation and fixed intermediate inertia.

For heterogeneity, for example, three ranges of inertia were established (light / medium / heavy), with for the medium inertia range, various combinations mixing heavy and light walls but having overall the same inertia (same value of C_m).

In total, with combinations of the four reference buildings, the sample is made up by 40 buildings.

5.3 Numerical parametric study

Each building was simulated in different conditions:

- Climate Zone: French zones H1A (Trappes) or H3 (Nice)
- Period of the year (~ season): January / April / July / October

A parametric study was conducted to test the sensitivity of several parameters on the resolution of identification. The parameters studied are:

- Taking (or not) into account of sequential inertia in the thermal model
- Insulation and inertia levels (heterogeneous buildings included)
- Climate and season

5.4 Results

Figure 5 illustrates the result of the identification for the building case “if_50” for a test of 15 days in January. The building has a light inertia and therefore reacts quickly to the heating solicitation (of $\Delta\theta = 20^\circ\text{C}$).

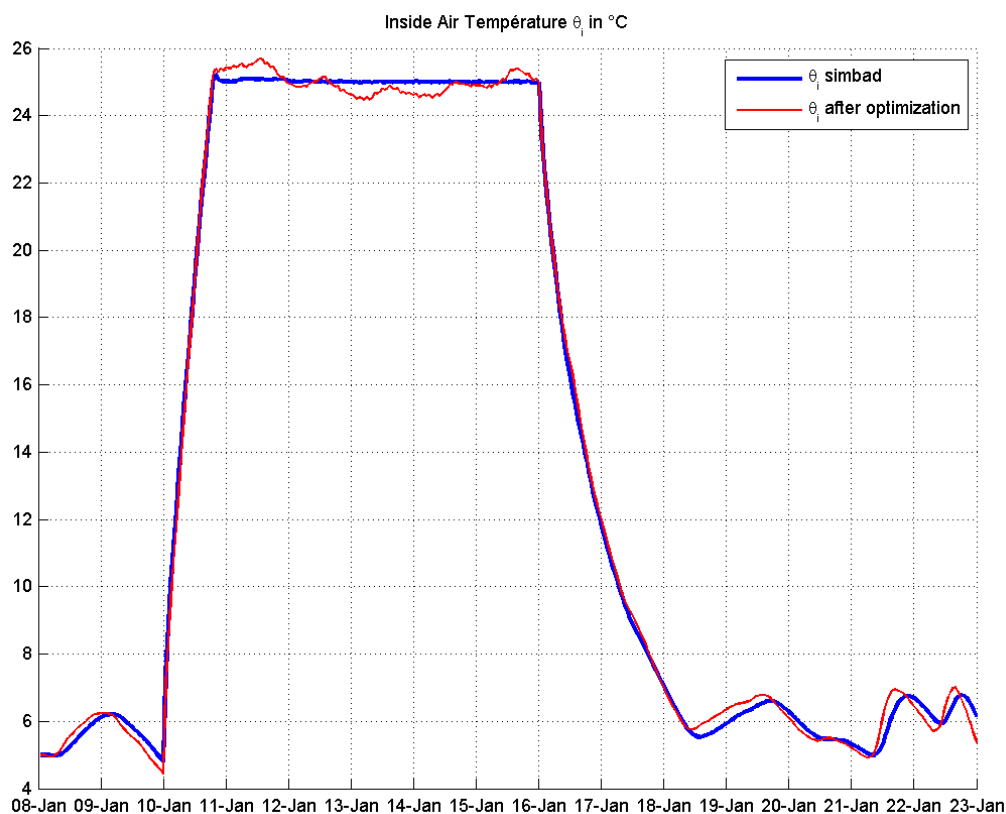


Figure 5: Fitted and simulated indoor temperature for the building case “if_50”

We can see that the optimized curve θ_i is very close to the simulation curve with SIMBAD.

Some oscillations remain in the stabilization phase and a short phase difference appears in the free evolution phases. It can be explain by using a simplified thermal model with only one capacitance in the walls. Indeed, the external variations (solar radiation and outdoor temperature) are directly impacted on the internal mass node θ_m , which is not actually the case.

For heavy inertia buildings we have observed a worse optimization due to the modeling of inertia. Given that the test lasts 15 days in the simulations, the daily inertia is not sufficient

because we load a longer capacitance. So we decided to modify the model adding a sequential inertia which is characterized by a period of 12 days, as explained in section 4.3.

The Figure 6 shows improved results of the identification, taking into account sequential inertia in the model for the building “IFO_200” (heavy inertia, high insulation). We can notice that the residuals are controlled in the case with sequential inertia. The root-mean-square errors (RMSE) are 0.71°C and 0.22°C for the cases respectively without and with sequential inertia.

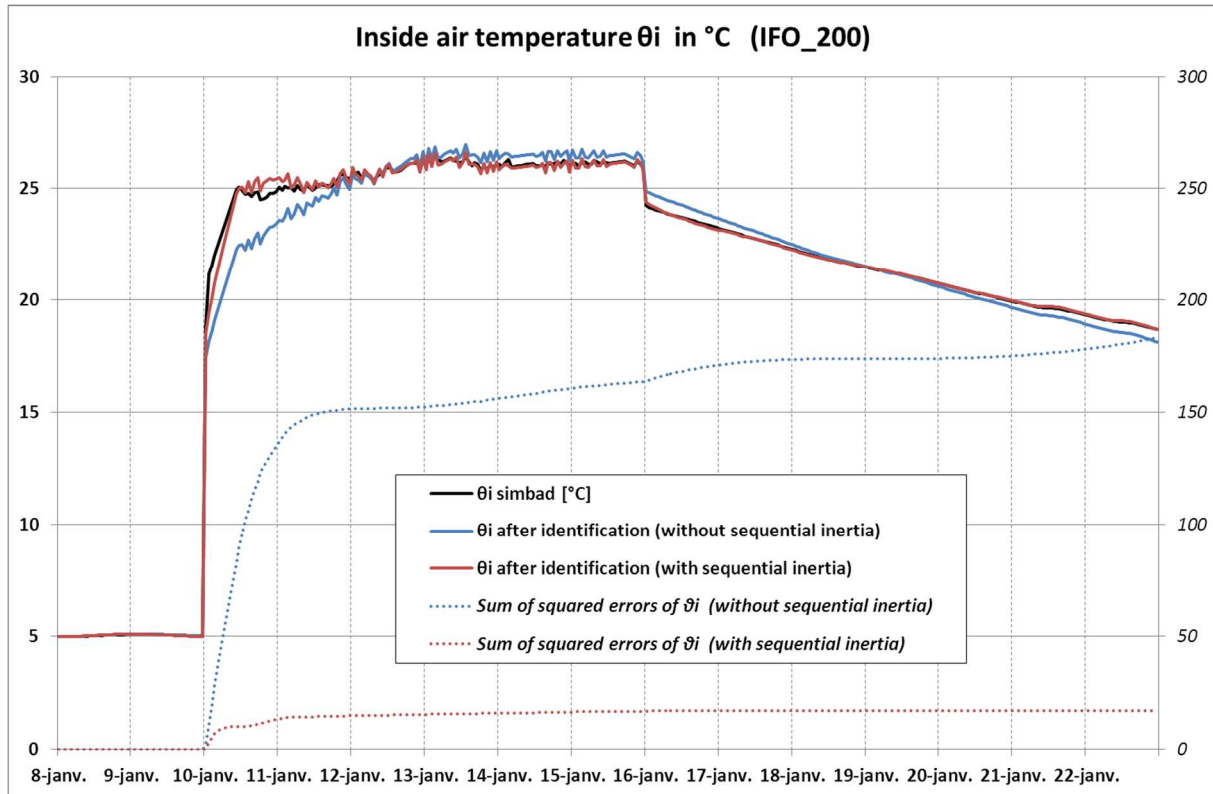


Figure 6: Fitted and simulated indoor temperature for the building case “IFO_200”

For the four reference buildings, Figure 7 presents the graphs of the identified absolute values of H_{tr} and C_m and their identification coefficients $C_{id_{H_{tr}}}$ and $C_{id_{C_m}}$. The histograms show the values without sequential inertia (first series in blue), with sequential inertia (second series in red) and the desing theoretical value (third series in green).

The identification of H_{tr} is quite better with the sequential inertia (deviations $< 3\%$). Identification of inertia parameters is also better even if the deviations can appear not negligible (until $+30\%$ with sequential inertia or $+80\%$ without sequential inertia, for heavy building IFO_200). But if we see the fourth chart, the identified values of C_m have the right ordre of magnitude. Furthermore, the importance of C_m on the building energy performance calculation (energy consumption) is lower than for H_{tr} , as evidenced by the definition of inertia class in the RT2012 and Th-I Rules, which give standard values of A_m and C_m depending on the class.

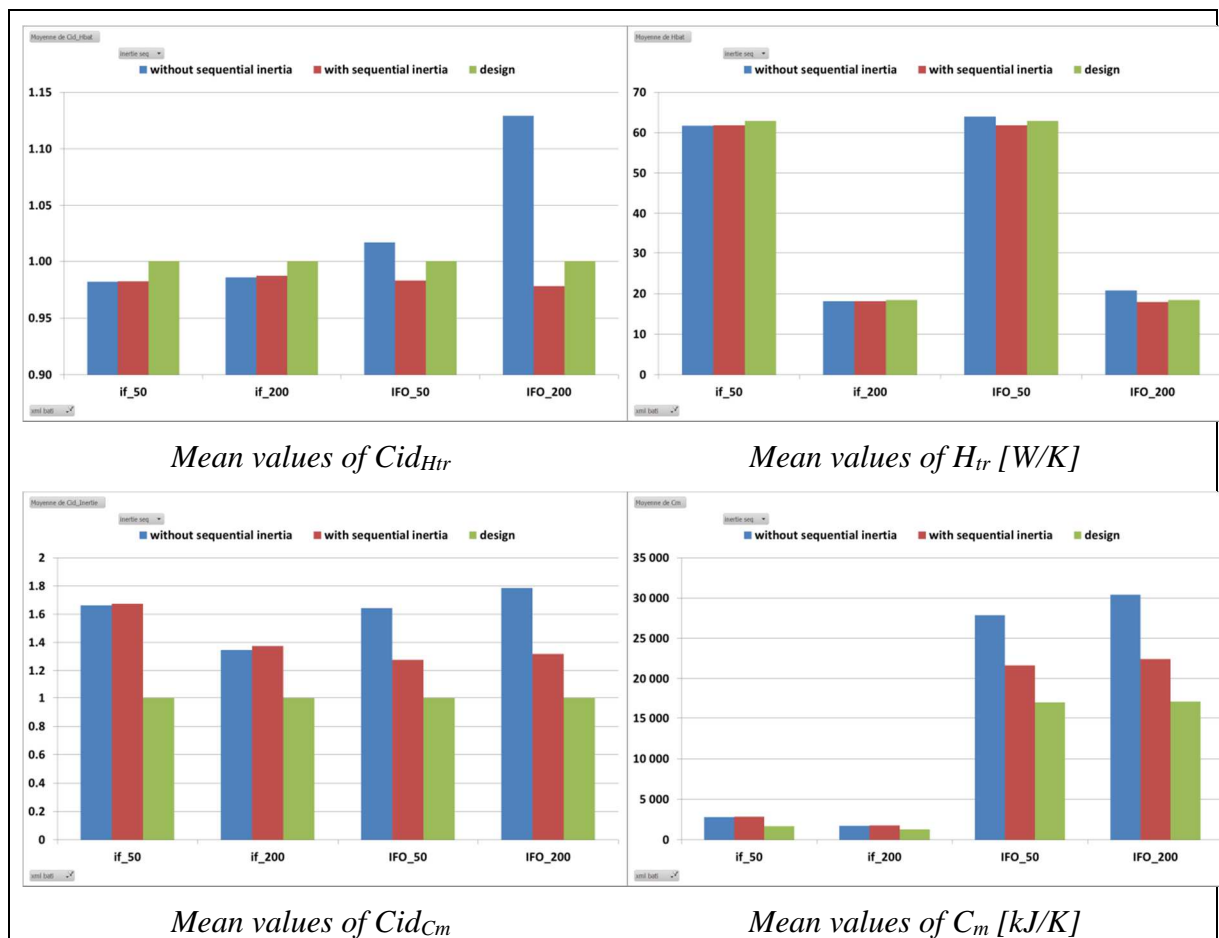


Figure 7: Differences of identifications with or without sequential inertia, compared with design

Table 2 gives the final values of the identified parameters of the four reference buildings (with the sequential inertia model).

Table 2: Identified values of H_{tr} with sequential inertia

Building name	theoretical / identified	H_{tr} [W/K]	A_m [m ²]	C_m [kJ/K]	A_{ms} [m ²]	C_{ms} [kJ/K]
if_50	<i>theoretical</i>	62.89	100	1694	100	2316
	identified	61.78	167	2835	125	2889
if_200	<i>theoretical</i>	18.40	100	1298	100	1594
	identified	18.16	138	1785	109	1730
IFO_50	<i>theoretical</i>	62.89	100	16 956	100	30 635
	identified	61.82	128	21 661	96	29 485
IFO_200	<i>theoretical</i>	18.40	100	17 035	100	32 195
	identified	17.99	132	22 464	100	32 242

The deviations of identified H_{tr} can be illustrated for the 40 buildings and their multiple simulations. The chart in Figure 8 shows the repartition of coefficient $Cid_{H_{tr}}$ for the identifications with or without taking into account of sequential inertia in the thermal model. Without sequential inertia some heavy and large buildings present bad identifications of H_{tr} (until +72%), whereas with the sequential inertia model H_{tr} is identified with a deviation inferior to 10% and to 5% in 95% of cases).

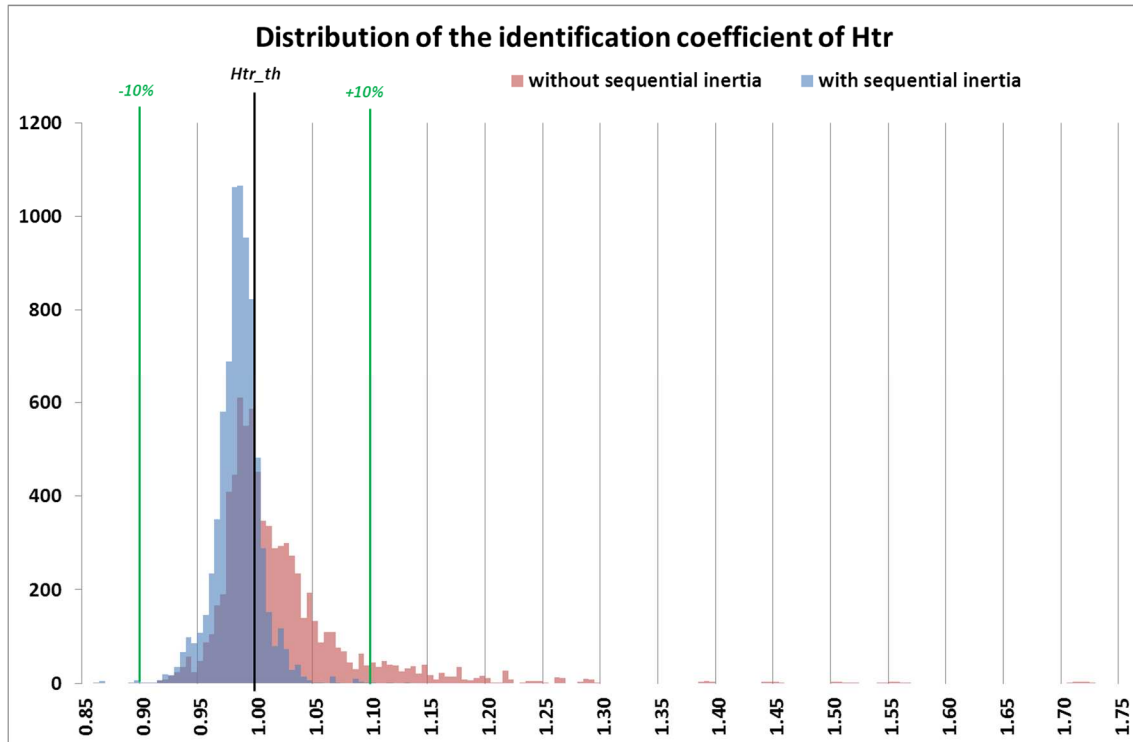


Figure 8: Distribution of the identification coefficient $Cid_{H_{tr}}$ with and without sequential inertia

Residuals analysis in Figure 9 shows a decrease of RMSEs for heavy inertia buildings when we put the sequential inertia. For low inertia buildings, the RMSEs sometimes exceed 0.4°C , which may be due to remaining oscillations on θ_i as we can see in Figure 5. But overall residuals are low (under 0.8°C) and are indicators of correctly fitted temperatures.

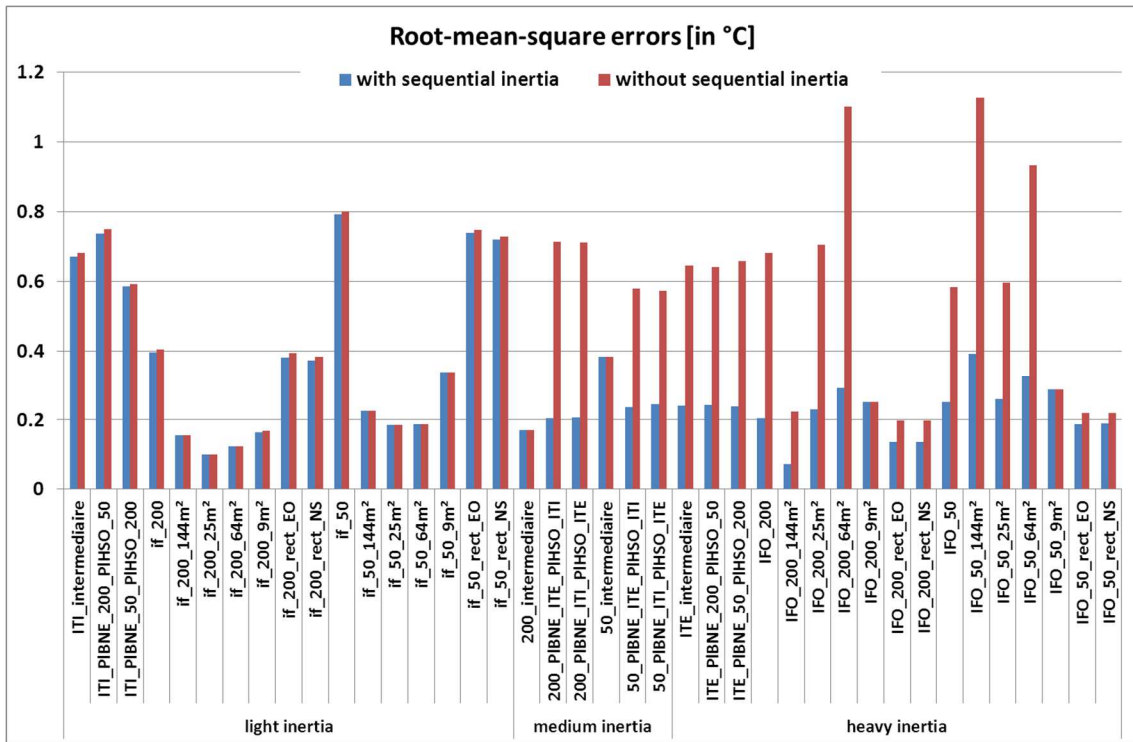


Figure 9: Root mean square errors

Using the thermal model with sequential inertia we can study the influence of inertia and insulation level on the identification. In Figure 10 are shown the identified values of H_{tr} for 12 buildings having different insulation level and inertia.

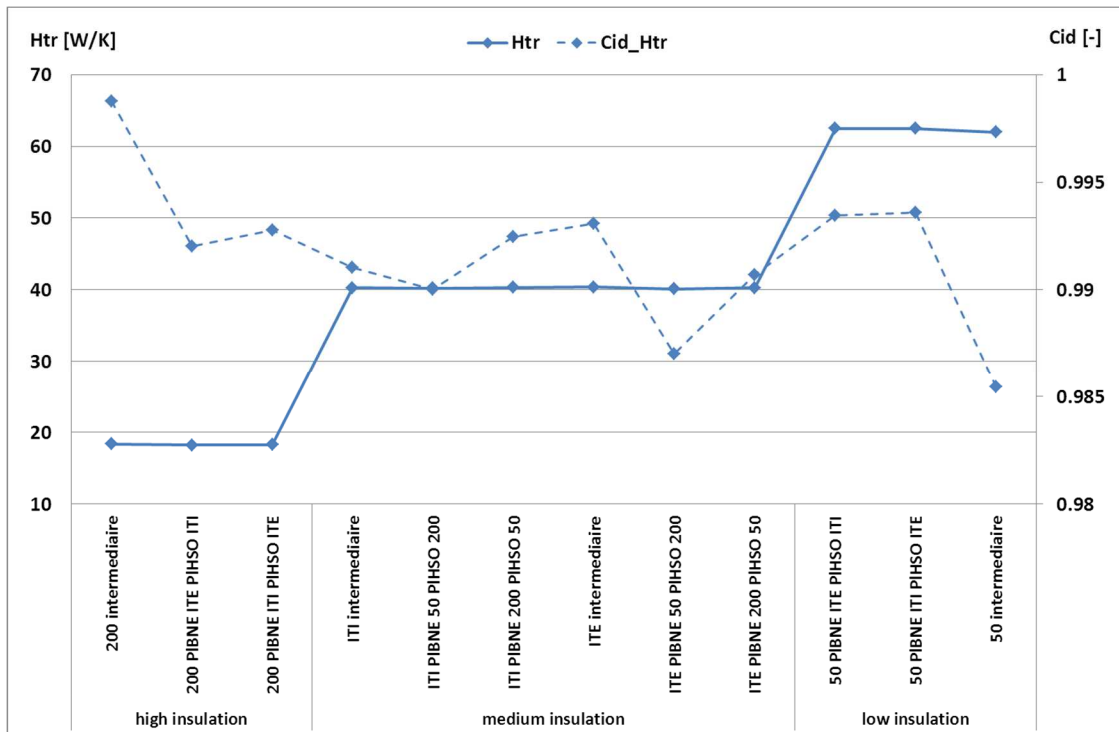


Figure 10: Identification of H_{tr} values for buildings having different insulation level and inertia

Medium inertia and insulation can be either a mix of heavy and light walls (or high and low insulated walls) or an intermediate inertia (or insulation) equally on all walls, but in both cases they present the same value of inertia (or insulation).

We observe a same identification of H_{tr} for the 3 distinct insulation levels with deviations between -0.1% and -1.5% of the theoretical value.

The other parameters of the study did not show a greater sensitivity on the results of identification, as for example the sensitivity to testing conditions, namely the period of the year when the test is performed and the climatic influence. Figure 11 illustrates the results of identification of the parameters H_{tr} and C_m (and their identification coefficient) on the four virtual reference buildings. The combination of the two climatic zones (North (Trappes) and South (Nice) in France) and four months of the year (January, April, July, October) generates 8 situations for each building.

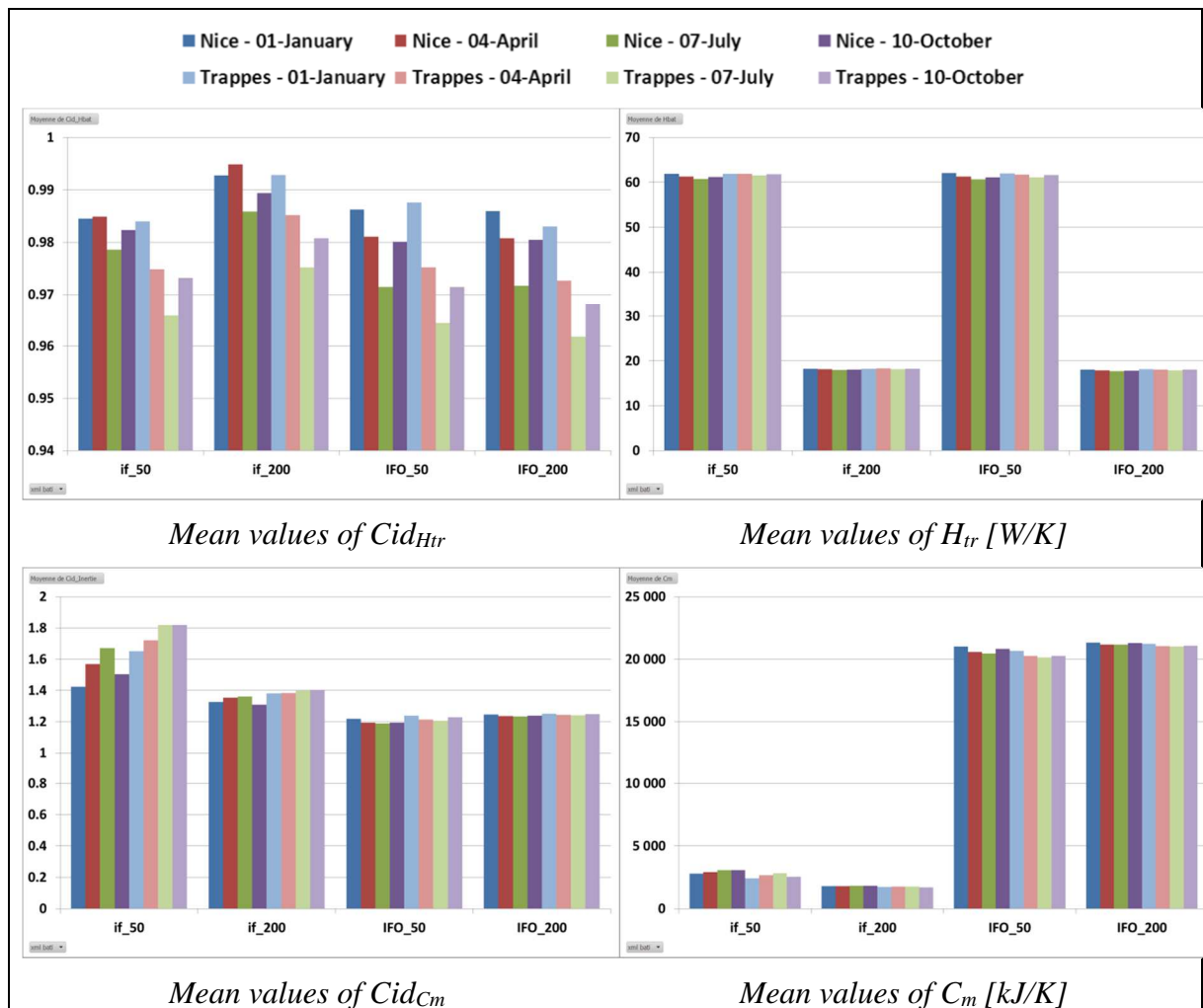


Figure 11: Differences of identifications between climatic zones and periods of year

The results show a low disparity in obtained values. The two upper histograms show the identification of comparable values of H_{tr} : differences with theoretical values for all situations are between -4% and -0.5%. The two histograms below show the identification of comparable values of C_m : large deviations for the building with light inertia and low insulation (+40% to +80%) but reasonable for the other 3 buildings (between +25% and +30% or around 20%).

6. DISCUSSION

All the results have highlighted the need to use a model with sequential inertia for test durations higher than a week and for buildings with high inertia. Identification of heat loss coefficient by transmission through the building envelope H_{tr} is greatly improved, with a deviation of less than 10% and even 5% in most cases. This identification gap is to be attributed to the accuracy of the thermal model, which is simplified, but has the advantage of being used in the RT2012 (so all new buildings in France are modeled and simulated with the regulation tool). Thus we are able to compare the identified thermal parameters with the design values calculated for the same model.

For buildings with low inertia, the method works very well. Given the speed of their response, it may be possible to reduce the test duration without degrading the result, and in this way to reduce the cost of the protocol to the future.

For a same building simulated in different climates and at different times of the year, the identification results are almost identical, allowing for reassurance about the reproducibility of the method. Indeed, one of the searched benefits of ISABELE method is that it is intended to apply at any time of the year (thus at the acceptance stage of a building regardless of its date) and without preconditions on the thermal state of the building. The history of the building behavior (impacted by climatic solicitations and heating loads) in the days preceding the test does not need to be known.

The identification of inertia parameters is less precise, even if it has a lesser interest compared to H_{tr} . The daily capacity C_m can be identified with bias of about 50%. However, the design calculation of theoretical C_m is delicate and often done by engineering consultants using standard values. Indeed, the precise value of C_m is not so important because its impact is limited in the calculation of energy consumption. The main objective is to be able to identify the inertia class (very light to very heavy), so the order of magnitude, which is properly done with ISABELE method given the range of values of C_m between inertia classes.

The impact of air renewal has not been studied in this paper, but has nevertheless a strong interest. Indeed, ISABELE method has been established to uniquely identify the heat loss coefficient by transmission, that is to say that the heat loss coefficient due to air renewal. In the test run, the ventilation system is turned off and the air renewal is reduced to infiltration through the envelope. For new buildings with low permeability, the impact of infiltration on the identification of H_{tr} should be lower, but it would be necessary to study the sensitivity. In addition, as part of the test protocol, the question of the need to estimate the rate of air infiltration using measurement or calculation based on wind speeds is important.

Finally the parametric study seems to presage good results on in-situ testing of real buildings. Initial tests have also been carried out satisfactorily on a wood experimental cell (Schetelat & Bouchié, 2014) and on a new house (Bouchié, Alzetto, Brun, Boisson & Thebault, 2014).

The method should nevertheless still be validated in particular on buildings of larger sizes and multi-zone (e.g. apartment buildings or non-residential buildings). An important issue is the uncertainty of the parameters identified taking into account the measurement uncertainties and their propagation. This uncertainty must also be compared to the uncertainty of the theoretical design calculations, which is not at all negligible (Schetelat & Bouchié, 2014).

7. CONCLUSION

In this paper we presented a new in-situ evaluation method of the intrinsic performance of a building at the acceptance stage. This method called ISABELE consists in subjecting the unoccupied building to a controlled heating power for a few days in order to identify properties of the thermal envelope and in particular the heat loss coefficient by transmission H_{tr} . The measurement protocol and the thermal model on which the method is based have been described. The method was tested in the early stages of its development, using numerical experiments, instead of future measurements on real site. Detailed simulations with SIMBAD tool have shown that taking into account the inertia in the identification model was not optimal. This has led to modify the model by incorporating the sequential inertia, which greatly improved the results of the identification of the heat loss coefficient H_{tr} . A large number of simulations were performed on basic buildings to test the limits of the method. A parametric study allowed observing the low sensitivity of certain parameters on the identification, such as insulation level, inertia or the season and climate. Initial results are encouraging for the future because the coefficient H_{tr} is correctly identified: in the range of +/-5% in most cases. The parameters of inertia are identified less accurately but satisfactorily.

Studies are still being conducted on a broader spectrum, both in simulation and experimental tests to confirm the validity of the method and its feasibility.

REFERENCES

- Alzetto, F., Gossard, D. & Pandraud, G., 2014. *Mesure rapide de la perte thermique des bâtiments*. Proceedings in EcoBat 2014, Paris.
- Bacher, P. & Madsen, H., 2011. Identifying suitable models for the heat dynamics of buildings. *Energy and Buildings*, 43(7), pp. 1511-1522.
- Bauwens, G. & Roels, S., 2014. *Co-heating test: a state-of-the-art*. International Energy Agency / EBC / Annex 58 6th Expert meeting – April 14-16, 2014, Gent, Belgium.
- Berger, J., Tasca-Guernouti, S. & Humbert, M., 2010. Experimental method to determine the energy envelope performance of buildings.
- Bouchié, R., Abele, C., Derouineau, S. & Millet, J.-R., 2014. *Conception et validation d'un capteur de mesure de la température extérieure équivalente d'une paroi opaque d'un bâtiment*. In IBPSA France. Arras.
- Bouchié, R., Alzetto, F., Brun, A., Boisson, P., Thebault, S., 2014. *Short methodologies for in-situ assessment of the intrinsic thermal performance of the building envelope*, In Sustainable Places 2014, Nice (to be published).
- Everett, R., 1985. *Rapid thermal calibration of houses*, s.l.: Milton Keynes UK.
- Fels, M., 1986. PRISM: an introduction. *Energy and Buildings*, Issue 9, pp. 5-18.
- Gorse, C. et al., 2014. *The gap between calculated and real performance: experiences from the field and the measures to address the difference*. Gent, Belgium, s.n.
- Hens, H. et al., 2007. Brick cavity walls: a performance analysis based on measurements and simulations. *Journal of Building Physics*, 31(2), pp. 95-124.
- Husaunndee, A., Lahrech, R., Vaezi-Nejad, H., & Visier, J.-C. (1997). SIMBAD: A simulation toolbox for the design and test of HVAC control systems. In *Proceedings of the 5th IBPSA Conference* (pp. 269–276).

- ISO-1, 2013. *ISO 13790: 2013 - Energy performance of buildings - Calculation of energy use for space heating and cooling*. s.l.:s.n.
- ISO-2, 2008. *ISO 13786: 2008 - Thermal performance of building components - Dynamic thermal characteristics - Calculation methods*. s.l.:s.n.
- Lagarias, J.C., Reeds, J. A., Wright, M. H., & Wright, P. E., 1998. "Convergence Properties of the Nelder-Mead Simplex Method in Low Dimensions", *SIAM Journal of Optimization*, Vol. 9 Number 1, pp. 112-147, 1998.
- Mangematin, E., Pandraud, G. & Roux, D., 2012. Quick measurements of energy efficiency of buildings. *Comptes Rendus Physique*, 13(4), pp. 383-390.
- Pandraud, G. & Fitton, R., 2013. *QUB: Validation of a rapid energy diagnosis method for buildings*. International Energy Agency / EBC / Annex 58 4th Expert meeting – April 8-10, 2013, Holzkirchen, Germany.
- Pandraud, Mangematin, Roux & Quentin, 2013. *QUB: a new rapid building energy diagnosis method*. Proceedings in Clima 2013.
- PERFORMER Project, 2014. *Portable, Exhaustive, Reliable, Flexible and Optimized approach to Monitoring and Evaluation of building energy performance*. [online]
Available at: <http://performer-project.eu/> [Accessed 1st July 2014].
- Règles Th-I, 2012. Caractérisation de l'inertie thermique des bâtiments. Règles Th-Bât Réglementation Thermique 2012, CSTB Marne-la-Vallée, France.
- Roels, S., 2014. *The IEA EBC Annex 58 - project on 'reliable building energy performance characterisation based on full scale dynamic measurements'*. International Energy Agency / EBC / Annex 58 6th Expert meeting – April 14-16, 2014, Gent, Belgium.
- Schetelat, P. & Bouchié, R., 2014. *ISABELE: a Method for Performance Assessment at Reception Stage using Bayesian Calibration*. Liège, Belgium, (to be published).
- Sonderegger, R., Modera, M. & March, M., 1979. *Electric Co-heating: A method for Evaluating Seasonal Heating Efficiencies and Heat Loss rates in Dwellings*. s.l., Lawrence Berkely National Laboratory.
- Sutton, R., Stafford, A. & Gorse, C., 2012. *The coheating test: the value of a number*. Bilbao, s.n.
- Th-BCE, 2012. Arrêté du 30 avril 2013 portant approbation de la méthode de calcul Th-BCE 2012 prévue aux articles 4, 5 et 6 de l'arrêté du 26 octobre 2010 relatif aux caractéristiques thermiques et aux exigences de performance énergétique des bâtiments nouveaux. *Journal Officiel n°0106*, p. 7782.

Modeling of the Indoor Thermal Comfort in Passive Houses heated by Wood Stoves

Laurent Georges^{1*}, Øyvind Skreiberg²

⁽¹⁾ Department of Energy and Process Engineering, Norwegian University of Science and Technology (NTNU), Trondheim, Norway

⁽²⁾ Department of Thermal Energy, SINTEF Energy Research, Trondheim, Norway

1. ABSTRACT

Space-heating using wood stove is a popular solution in many European countries. Nevertheless, nominal powers of state-of-the-art stoves are oversized compared to the needs of highly-insulated building envelopes, such as passive houses. In this respect, a simplified wood stove model has been developed in order to investigate the thermal comfort using detailed dynamic simulations (e.g. TRNSYS) at an acceptable computational cost. A specific experimental setup has been developed to validate this modelling procedure, especially as regards the interaction between the stove and the building. The largest source of error appears to be the thermal stratification in the room where the stove is placed. This can simultaneously affect the conductive heat transfer between rooms, the thermal comfort sensation in the room as well as the convective heat exchange by flows through doorways. Nonetheless, the present work proposes a correction to circumvent this last effect. Finally, thermal comfort measurements during the experimental campaign confirm the conclusions of previous simulation results (Georges, Skreiberg, & Novakovic, 2014), supporting their proposed guidelines for the integration of wood stoves in passive houses.

Keywords: space-heating, wood stove, passive house, thermal comfort

2. INTRODUCTION

On the one hand, space-heating (SH) using wood stoves is a widespread strategy in many countries such as Norway. In Norway, wood stoves provide about 20% of the SH needs of the residential building stock and accounts for about half of the bioenergy use. In parallel, Norway has decided to double its use of bioenergy within 2020 (Norwegian Ministry of Petroleum and Energy, 2008). In total, wood stoves also represent the second largest installed power after hydroelectricity in Norway.

On the other hand, energy consumption of buildings in developed countries comprises 20-40% of the total energy use (Pérez-Lombard, Ortiz, & Pout, 2008) so that its reduction has become a major concern, as illustrated by the European Performance of Building Directive (European Parliament, 2010). A common strategy is to reduce the SH needs by a better insulation of the building envelope. Among building concepts that has emerged, the passive house (PH) is based on a super-insulated building envelope (Feist, Schnieders, Dorer, & Haas, 2005). Let us also mention that Norway has developed its own national definition of the PH standard, the NS 3700 (Standard Norge, 2010). Furthermore, the concept of Zero Energy Buildings (ZEB) has also been increasingly popular (e.g. net and nearly ZEB). In many research developments, the PH standard is often considered as a minimal performance requirement for ZEB envelopes.

The SH of highly insulated buildings using wood stoves is thus a strategic area. Furthermore, state-of-the-art stoves present acceptable energy conversion efficiency (e.g. 85%).

Nevertheless, the integration of wood stoves in PH is currently seen as problematic. In practice, it faces two major challenges:

- (a) Firstly, a good indoor air quality (IAQ) and good combustion must be reached in an airtight building envelope equipped with balanced mechanical ventilation.
- (b) Secondly, the minimal combustion power of wood stoves currently available on the market (typically 6-8 kW) is well above the SH power of PH (roughly < 3 kW). This power oversizing may lead to overheating in the room where the stove is placed.

The PH definition is also closely related to the potential to simplify the SH distribution system. It was typically proposed using the air-heating concept (Feist, et al., 2005; Georges, Berner, & Mathisen, 2014). Therefore, it is also worth investigating how a wood stove can contribute to this simplification and how it distributes heat throughout the entire building envelope. The present research aims at answering these challenges dedicated to indoor thermal environment (i.e. IAQ is not part of the work).

A large set of detailed dynamic thermal simulations have already been performed, here using TRNSYS (TRANSSOLAR, 2009), in order to determine in which conditions a stove can be properly integrated in a PH. Both a single-family detached house typology for the temperate climate of Belgium (Georges, Skreiberg, & Novakovic, 2013) and Nordic conditions (Georges, Skreiberg, et al., 2014) have been investigated. These conditions for good integration are linked to the stove thermal properties (e.g. nominal power, power modulation range, stove thermal mass) but also to the thermal properties of the building envelope (e.g. its thermal mass, internal door opening) as well as to the building geographic location (e.g. different climatic zones in Norway). The main conclusions are summarized here below but the reader is invited to consult the two reference papers for an exhaustive presentation:

- State-of-the-art pellets stoves have a large power modulation capability that enables stoves of 6-8 kW to operate up to 90 min without generating overheating. They can indeed operate down to $\sim 30\%$ of their nominal power (P_n).
- State-of-the-art wood log stoves have a smaller modulation range (typically down to 50% of P_n) and are characterized by longer combustion cycles, especially at part load. A 6-8 kW stove can operate without overheating if some measures are taken in the building itself (i.e. having internal doors open along with a large building thermal mass). Wood log stoves should be further improved to properly be integrated in passive houses regardless of the building thermal properties, for example having lower P_n and higher stove thermal inertia.
- Except for cold regions with subarctic climate (as in northern Scandinavia), a stove used as a single point heating source for the overall envelope can cover a large part of the SH needs without unacceptable low temperatures in bedrooms if the internal doors are open. Nevertheless, temperatures will be too low during the coldest days in winter (here tested using the SH design outdoor temperature).

These conclusions are given for stoves without large heat storage capacity so that they should be considered as conservative scenarios. Furthermore, conclusions correspond well with another existing reference from Germany (Blumrich et al., 2007). Finally, the modeling procedure is also currently used to perform quick-prototyping of the next generation of stoves designed for houses with low SH demand (Skreiberg, 2011-2014).

In this aforementioned context, a simplified wood stove model has been developed in order to perform all-year simulations at an acceptable computational cost (Georges & Novakovic, 2012). The present work reports on this model and on a measurement campaign performed in a PH in Trondheim in order to validate this modeling and conclusions from simulations. Experiments are based on an electric stove developed at NTNU which enables to mimic the

thermal comfort generated by different stove technologies. Practically, it enables testing (or emulating) different stoves and operating conditions in the same building. A parametric analysis on the influence of stove properties can then be performed: stove thermal mass, nominal power, power modulation capabilities and combustion cycle length.

3. SIMULATION MODEL

In order to investigate the integration of wood stoves in PH, it is important to look at the thermal comfort throughout the entire heating season. By definition, internal and solar heat gains play a major role in PH so that it is difficult to determine a priori the critical operating conditions during the heating season. On the contrary, it is wise to perform all-year simulations to determine these critical conditions. Once known, more advanced simulation techniques, as Computational Fluid Dynamics (CFD), can be applied to get a refined solution. There is thus a need for a simple stove model for detailed dynamic simulations (here using TRNSYS) to quickly screen the thermal comfort during all-year simulations at an acceptable computational cost. Furthermore, this model can be used to support and complement measurement campaigns as they are most often limited in time (e.g. from a couple of days to some weeks).

The overall modelling procedure is illustrated in Figure 1. Starting with the instantaneous room temperature (T_s) at a given time from the multi-zone building simulation, this quantity is used to control the combustion power of the stove (P_c) along with the room set-point temperature (T_{set}). A model is then applied for the wood combustion dynamics that ultimately gives the power delivered to the stove envelope as a function of time (P_d). A specific module then computes the heat transfer within the stove envelope. The instantaneous stove surface temperature (T_{stove}) or the power emitted to the room (P_e) is then obtained. Finally this last quantity is introduced as an internal gain inside the multi-zone building model. It is a *loosely-coupled* approach as all the models and equations are not solved simultaneously. For instance, the stove geometry and heat transfer in its envelope is not accounted for in the building model: the building model only “views” the stove as an internal gain. At each time step, several sub-iterations are performed between the model components until the overall system convergence. It is a rather natural way to formulate and solve multi-domain and multi-physical problems in TRNSYS.

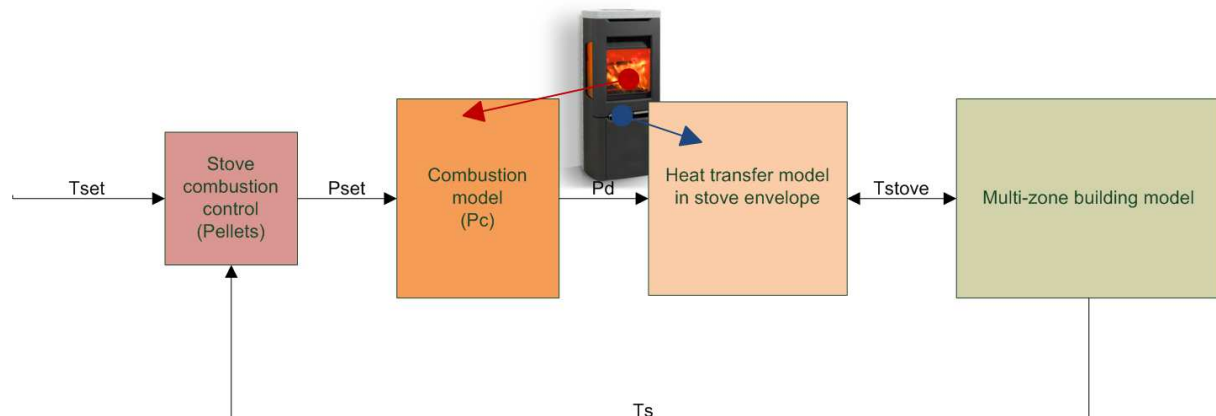


Figure 1: Modelling chain for the wood stove integration.

Each model component can then be developed in more details:

- The stove combustion control essentially applies for wood pellet stoves, here using a proportional-integral (PI) action. Up to now, it was assumed that wood log stoves do not have an active power modulation: the modulation is selected by the user a priori by adjusting the combustion air vents and is not changed during the batch combustion cycle.

- In terms of combustion, there is a fundamental difference between pellets and log stoves. Compared to the physical timescale of the stove (i.e. the heat transfer in its envelope), the pellets combustion can be considered as instantaneous so that P_c is assumed immediately adapted to the set-point combustion power (P_{set}). It is an approach already followed in other modelling works (Haller et al., 2011; Persson, Fiedler, Nordlander, Bales, & Paavilainen, 2009). The wood log combustion is fundamentally different and has timescales comparable with the stove and building envelopes. It should therefore be essentially considered as a batch process (Saastamoinen, Tuomaala, Paloposki, & K., 2005). In that respect, SINTEF Energy Research has developed a semi-empirical combustion model that provides profiles of P_c and P_d as function of time (Skreiberg, 2002). This model can account for the batch load (i.e. initial amount of wood in the combustion chamber in kWh), the stove efficiency, nominal power and modulation. Examples of computed profiles are given in Figure 2.
- The unsteady heat transfer through the stove envelope is assumed one-dimensional. Currently the heat transfer through the combustion chamber window is not accounted for. This last contribution may reduce the delay between the heat release P_c and the resulting power emitted to the room (P_e).
- By default, the power emitted by the stove surface by convection (P_{ec}) is obtained using the well-known Churchill and Chu correlation for laminar and turbulent flows over an isothermal plate (Churchill & Chu, 1975). Given the range of T_s and usual characteristic lengths considered for stoves, the correlation is further simplified into:

$$P_{ec} = 1.22A(T_{stove} - T_s)^{4/3} \quad \text{Eq.(1)},$$

where A is the stove external area. If the exact stove geometry is known, better correlations can be established.

- The power emitted by the stove surface by radiation (P_{er}) is here evaluated by assuming that the stove is very small compared to the room. Then,

$$P_{er} = \sigma A \epsilon (T_{stove}^4 - T_s^4) \quad \text{Eq.(2)},$$

where σ is the Stefan-Boltzmann constant and ϵ the emissivity of the stove surface (Incropera, Dewitt, Bergman, & Lavine, 2007).

- Once the convective and radiative powers of the stove are evaluated, equivalent internal gains are injected into the building model. The P_{ec} is applied to the zone air-node while P_{er} is distributed among the walls of the rooms as a function of the view factors (from the stove to the different walls of the room). In general, the room geometry is not convex so that view factors cannot be easily evaluated analytically. Therefore, many simulation tools fail to evaluate these factors properly (e.g. TRNSYS or IDA-ICE). In that case, they should be pre-computed externally with dedicated tools.
- As many stoves developed for super-insulated envelopes, the stove is here assumed airtight, extracting its combustion air directly from the outside using a proper air-intake duct. Then, the stove does not use air from the building envelope and does not interact with the balanced mechanical ventilation.
- In PH, the opening of internal doors is proved to be an efficient process to exchange heat between rooms (Feist, et al., 2005). In order to investigate the natural convection inside the envelope, the airflow rates between rooms are computed using a ventilation network model, here using TRNFLOW (TRANSSOLAR, 2009) based on the COMIS library. The bi-directional flow through doors is then modelled using a large opening approximation introducing a discharge coefficient (C_d) to tune the model to a specific flow physics. It may typically range from 0.4 to 0.8 (Etheridge & Sandberg, 1996; Heiselberg, 2006).
- The thermal dynamics of the building is computed using the TRNSYS model component termed *Type56b* (TRANSSOLAR, 2011).

The thermal comfort is evaluated globally using the operative temperature (T_{op}) assuming that the user is far from the stove: a distance where the effect of radiation asymmetry and the direct radiation from the combustion chamber can be neglected. In this case, a recent study (Ghali, Ghaddar, & Salloum, 2008) has shown that the thermal comfort can be evaluated globally using a method based on the Fanger's approach, here using the ISO 7730 (CEN, 2005).

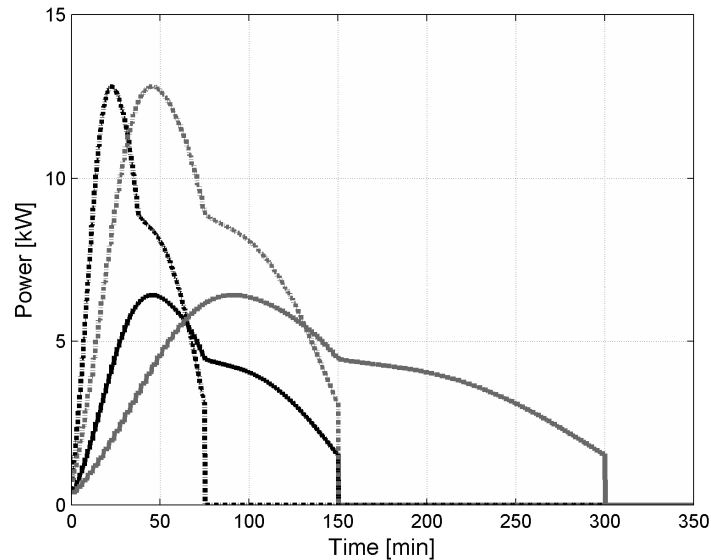


Figure 2: Instantaneous combustion power as a function of time for a 8 kW log stove: the stove operated at 50% of P_n is shown in solid line while dash-dotted lines are representative of an on-off stove; two batches of 10 and 20 kWh are in black and gray colour, respectively.

To limit the computational time and the number of parameter inputs, the model is kept deliberately simple. This was done by adopting a set of reasonable assumptions. The present work especially focuses on the simplifications done on the physical interaction between the stove surface and the building, as well as the resulting thermal comfort. For instance, building simulation models most often assume a single room air temperature (i.e. well-stirred tank approximation) while one may suspect large vertical or horizontal temperature differences to occur within a thermal zone. Furthermore, it is worth investigating whether the ventilation network approach and the large opening approximation are compatible with the natural convection between rooms driven by a wood stove (Wang & Chen, 2008). Using this modeling approach, the mass flow generated by the bi-directional flow through a door is computed in the following way (TRANSSOLAR, 2009):

$$m_{12} = C_d \int_0^H \sqrt{2 \cdot \rho_1(z) \cdot f_{12}(z) \cdot w(z)} \cdot dz \quad \text{Eq.(3),}$$

$$m_{21} = C_d \int_0^H \sqrt{2 \cdot \rho_2(z) \cdot f_{21}(z) \cdot w(z)} \cdot dz \quad \text{Eq.(4),}$$

where

- z is the vertical direction and H , the height of the doorway,
- the subscript 1 refer to the warm zone (here the living room),
- the subscript 2 refer to the cold zone (here the staircase),
- m_{12} refers to the mass flow from zone 1 to zone 2,
- m_{21} refers to the mass flow from zone 2 to zone 1,
- $f_{12}(z)$ is equal to $p_1(z) - p_2(z)$ if positive, or is equal to zero,
- $f_{21}(z)$ is equal to $p_2(z) - p_1(z)$ if positive, or is equal to zero,
- $w(z)$ is the width of the door.

The pressure $p_i(z)$, with subscript i equaling 1 or 2, is evaluated based on the reservoir conditions on both sides of the doorway:

$$p_i(z) = p_i(0) - \int_0^z \rho_i(\tau) \cdot g \cdot d\tau \quad \text{Eq.(5),}$$

where g is the gravity acceleration and $p_i(0)$ the reference pressure of zone i . This last value is computed to get the conservation of mass throughout the ventilation network. For instance, in the measured PH, the reference pressures of zone 1 and 2 are adjusted to get $m_{21} = m_{12} + \rho_2 \cdot 33$, where $33 \text{ m}^3/\text{h}$ is the net mass flow from zone 2 to zone 1 induced by the mechanical ventilation (see Section 4). As the air temperature field is assumed uniform in building simulation models, $T_i(z)$ and $p_i(z)$ are then not dependent on z .

MOVABLE ELECTRIC STOVE

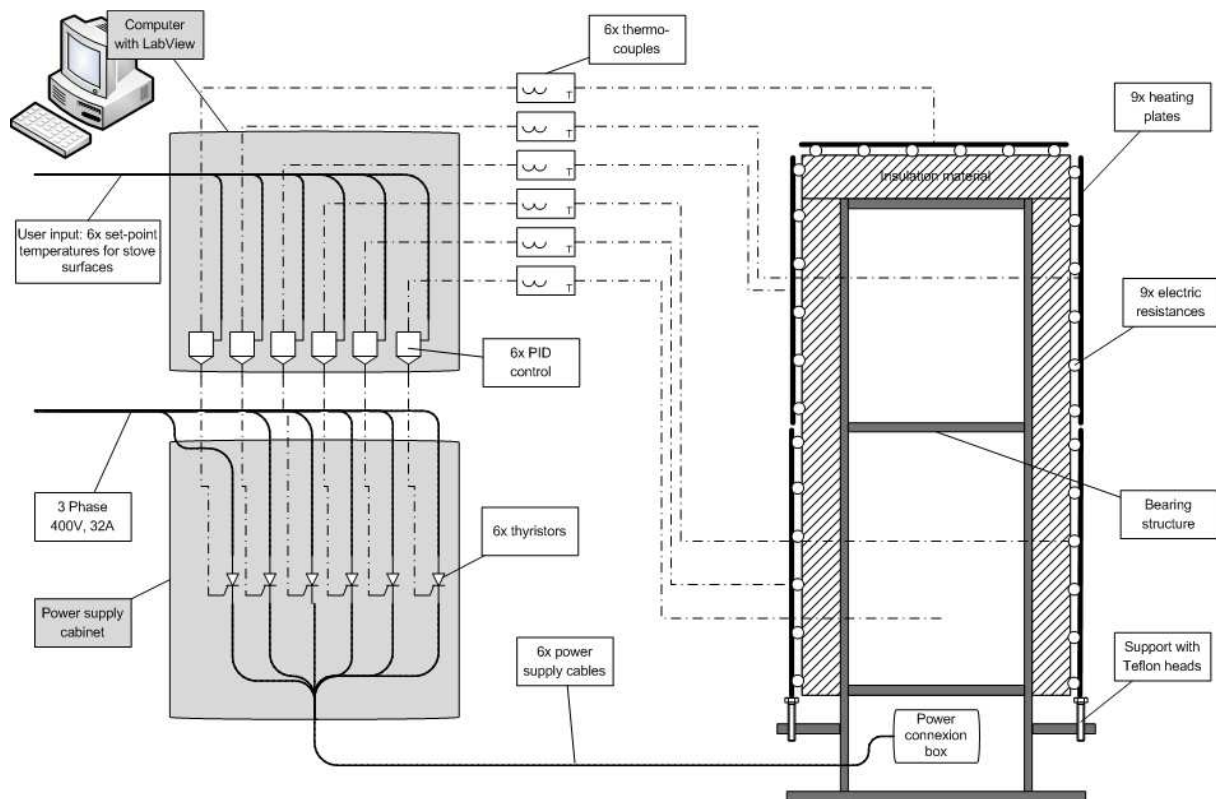


Figure 3: Layout of the movable electric stove experimental setup.

In order to validate the model and conclusions, an experimental campaign was needed. The main issue was to find PH in Norway already equipped with wood stoves. To our knowledge, most Norwegian passive houses are equipped with hydro-stoves that deliver a significant part of the P_c to a water jacket (and subsequently to a storage tank and a hydronic system). It was not really relevant for our investigations as the heat directly emitted to the room is then limited to 1-3 kW. Furthermore, it is rather difficult to evaluate accurately the power delivered to the stove envelope during real stove operation. It would be difficult to make a direct relation between the heat release of the stove and the resulting comfort. For these reasons, it was decided to build an electric stove that mimics the thermal environment generated by a real one. In addition, it enables to install the system in any PH disregarding the presence of a chimney and avoiding problems with the IAQ (e.g. pollution by small particles).

The layout the experimental setup is shown in Figure 3. The 15.5 kW_e movable electric stove is a box of 0.60 m x 0.60 m x 1.20 m. It is constituted of 9 heating plates where a flexible electric resistance has been fastened on their back side, see Figure 4. The back side of the

heating plates is then further insulated with 10 cm mineral wool that can withstand high temperatures. In this way, the stove structure is not storing heat: all the electric power is delivered to the plate and subsequently emitted to the room. The plates are made in aluminium to ensure a uniform temperature distribution on the surface. Their thickness has been limited to 3 mm to get a quick response time of the stove surface temperatures. Finally, the plates have been covered by a layer of special stove paint in order to get the correct emissivity, ϵ . The black paint emissivity was calibrated at 0.9 using an infrared (IR) camera. In practice, 3 surface temperatures are controlled independently while the 6 remaining surface temperatures are controlled in pairs of 2 surfaces. In total, 6 different set-point temperatures can be imposed to the movable stove surfaces. This has been done to be able to mimic stoves that have complex internal constitutions (e.g. internal heat storage, water jacket) that result in different surface temperatures. It also enables to approximate the influence of the power directly emitted by the combustion chamber through a stove window. The 6 currents of the 9 resistances are modulated using thyristors which are controlled to enforce the 6 set-point surface temperatures given as an input. The instantaneous surface temperatures are measured using thermocouples and transferred to a computer equipped with LabView. A PID control is implemented in this program to evaluate the thyristors control signal. Profiles of the set-point surface temperatures are given as an input. These time profiles can be provided by the batch combustion model of SINTEF Energy Research or from measurements. This strategy enables to mimic the thermal environment generated by different stove technologies in a same building, for instance having different P_n , batch load, power modulation and heat storage capabilities. Only the shape of the stove cannot be changed: this parameter mainly influences the ratio between convected and radiated power emitted to the room (i.e. P_{ec}/P_{er}).

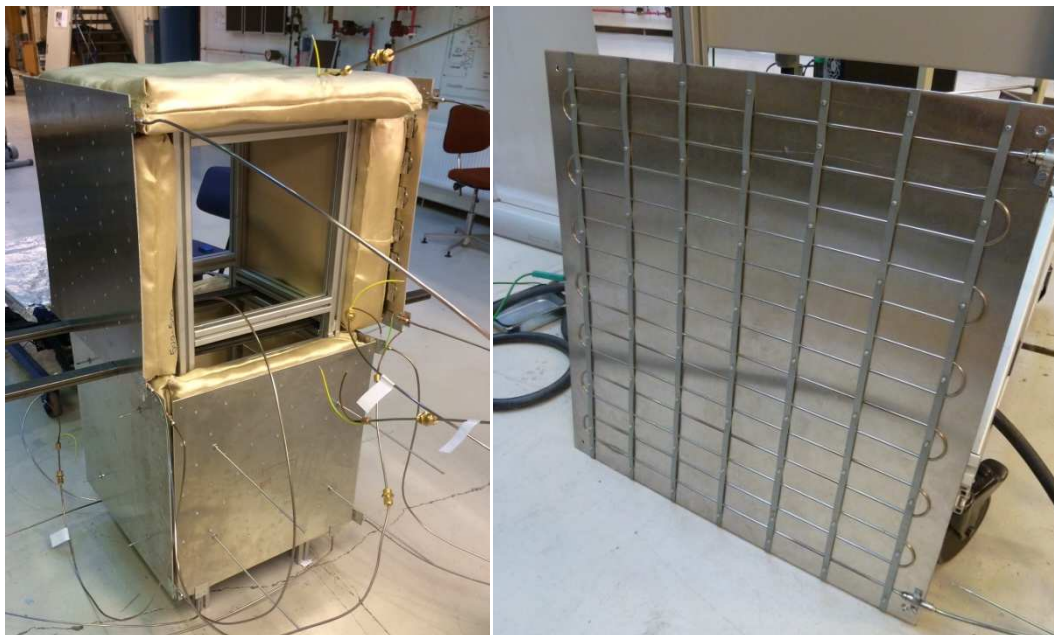


Figure 4: Movable electric stove under construction.

At first, laboratory measurements were done on the stove to prove that it operates correctly and safely. They clearly demonstrated that the heat release of the electric resistance is well distributed along the plate and gives rather uniform surface temperatures (i.e. $< 10^{\circ}\text{C}$ difference). It has been verified using an IR camera giving pictures such as Figure 5. The stove has almost no thermal bridges so that all the heat emitted to the room originates from the stove plates. Furthermore, the heat exchange between the stove heating plates and the feet is negligible, which enables to operate it safely in a building.

The relationship between the emitted heat power (i.e. $P_e = P_{ec} + P_{er}$) and the stove surface temperature has also been tested in the lab. It has been compared to the modelling approximations, Eqs. (1) and (2). Results are reported in Figure 6 where the heat released to the room has been obtained experimentally by measuring the delivered electricity to the stove at steady-state conditions. Two methodologies have been employed to measure the delivered electrical power: using a current measurement (#1) and using the output signal of the thyristors (#2). In both cases, the model proved to give accurate results. In practice, the surface temperature is imposed by the stove control, so this relationship is important to exactly know the actual emitted power (P_e) to the room for a given stove temperature (T_{stove}).

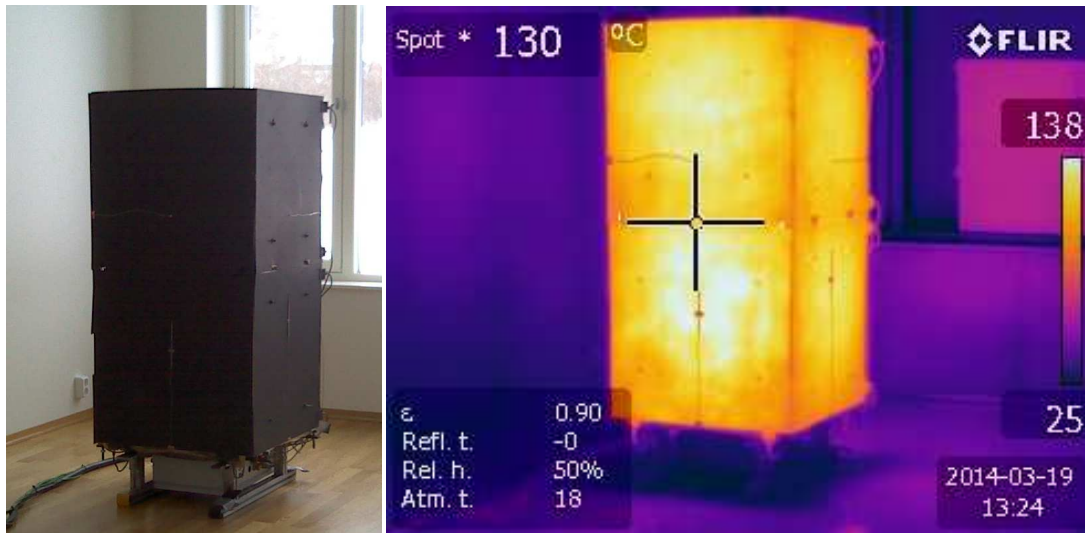


Figure 5: IR picture of the movable stove during operation.

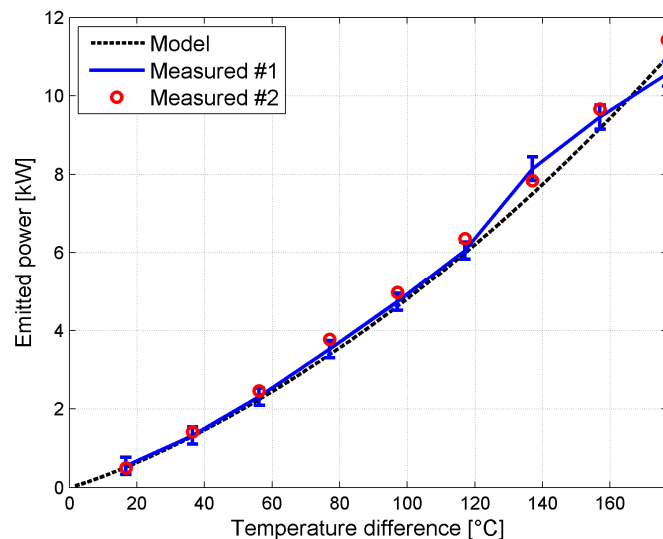


Figure 6: Heating power emitted to the room as a function of the temperature difference between the stove surface (T_{stove}) and the room temperature (T_s).

4. EXPERIMENTAL SETUP IN THE PASSIVE HOUSE

The stove has then been placed in a PH in Trondheim during the months of March and April 2014. This a terraced house of the MiljøGranåsen project, which is the largest PH construction project in the Nordic countries. It will consist of 430 dwelling units with a total heated area of 34000 m². MiljøGranåsen is developed by Heimdal Bolig and is also part of the EBLE,

Concerto and Eco-city research projects. During the measurement campaign, the PH was unoccupied and not furnished. It consists of three storeys as shown in Figure 7.

The building is constructed in wood except for the basement that is in concrete. In that respect, the building thermal mass may be characterized as *very-light* or *light* (CEN, 2008). The heated area is 142.5 m² which is rather similar to the 173.5 m² detached house of previous investigations using simulations (Georges, Skreiberg, et al., 2014). The U-value of the external walls is 0.15 W/m².K while the triple-glazed windows have an overall value between 0.7 and 0.85 W/m².K. The roof has a thermal transmittance of 0.06 W/m².K and the equivalent U-value of the basement floor is 0.1 W/m².K while the basement walls have an equivalent U-value of 0.19 W/m².K. The movable stove is placed in the living room at the ground floor. The hygienic ventilation has an air change rate (ach) of 0.52 while the heat recovery (HR) unit of the balanced mechanical ventilation has a rated temperature efficiency (EN 308) of 88%. A net mass flow of 33 m³/h is moving from the first to the ground floor. The SH needs are evaluated at 17.1 kWh/m².year according to Norwegian standards (Standard Norge, 2007, 2010).



Figure 7: Picture of the building block and sketches of the basement, ground and first floors.

The house has then been instrumented to monitor the thermal environment during the stove operation, see Table 1:

- As regards the local temperature distribution at the ground floor, the thermal stratification has been measured by five PT-100 sensors distributed on a vertical rod from the floor to the ceiling level. This bar is located in the middle of the room. A second bar equipped with ten thermocouples of type T measures the stratification in the living room area, and is located 2.7 m from the stove. In the kitchen and the living room areas, probes are placed to measure

the sensible air (T_s) and operative (T_{op}) temperatures 0.8 m above the ground. Given the ground floor layout, these probes are located opposite in the room. The horizontal temperature distribution can then be checked. Five PT-100 temperature sensors are taped to different walls to have an approximation of the temperature difference between the walls. For half of the test cases, the airflow in the doorway between the ground and second floor has been measured using a vertical pole located in the middle of the door mounted with ten omni-directional air velocity transducers (TSI 8475). In that case, the ten aforementioned thermocouples are used to measure the vertical temperature distribution in the doorway. Basically, the building has an open staircase which would have made the measurement of velocities difficult (i.e. very low speed < 0.1 m/s). It was decided to screen the staircase with thermally insulated plates to leave only a single opening of 0.9 m x 2.35 m that should represent a door. For each of these probes, data was registered every minutes.

- As regards the temperature distribution between rooms, eleven temperature sensors were placed in the building. Three sensors measured the temperature of the ventilation inlet air before and after the heat recovery unit, as well as after the pre-heating battery. Finally, the outdoor temperature was also registered in a sheltered place. These sensors are registering the temperature every fifteen minutes.

Table 1: List of measurement probes.

Type	Number	Location	Precision	Measure
PT-100	5	Ground floor	$\pm 0.1^\circ\text{C}$	T_s , stratification
	5	Staircase	$\pm 0.1^\circ\text{C}$	T_s , stratification
	1	Living-room	$\pm 0.1^\circ\text{C}$	T_s , 0.8 m height
	1	Kitchen	$\pm 0.1^\circ\text{C}$	T_s , 0.8 m height
	1	Kitchen	$\pm 0.1^\circ\text{C}$	T_{op} , 0.8 m height
	7	Walls	$\pm 1^\circ\text{C}$	T_{wall}
Radiant temperature transducer INNOVA MM0036	1	Living-room	$\pm 0.5^\circ\text{C}$	T_{mrt} , 0.8 m height
Thermocouples Type T	10	Doorway or living-room	$\pm 1\%$ $\pm 0.5^\circ\text{C}$	T_s , profile or stratification
Anemometer TSI 8475	10	Doorway	$\pm 3\%$ ± 0.005 m/s	Air velocity profile
Temperature logger iButton Maxim Integrated DS1922L	11	Each room	$\pm 0.06^\circ\text{C}$	T_s , one by room
	1	Outdoor	$\pm 0.06^\circ\text{C}$	T_s , sheltered
	3	Air Handling Unit	$\pm 0.06^\circ\text{C}$	T_s fresh air

In total, twelve different stove cycles have been tested. They were taken representative of the performance of state-of-the-art stoves already available in the market. For the pellet stove, P_n of 6 and 8 kW have been tested during combustion cycles of 90 min along with stove thermal masses (I_{th}) of 50 and 150 kJ/K and with a constant power modulation of 30% as well as without modulation. Only the four most critical cases were tested. For the log stove, P_n of 4 and 8 kW were tested for batch loads of 5 and 10 kWh along with stove thermal masses of 50 and 150 kJ/K and with a constant power modulation of 50% as well as without modulation. The measurement matrix is reported in Tables 2 and 3.

Table 2: Matrix of test cases that emulate pellet stoves.

Case	P_n	Modulation	I_{th}	Cycle length
N°	[kW]	[% of P_n]	[kJ/K]	[min]
1p	6	100	50	90
2p	6	100	150	90
3p	8	30	50	90
4p	8	100	150	90

Table 3: Matrix of test cases that emulate wood log stoves.

Case	P_n	Modulation	I_{th}	Batch load
N°	[kW]	[% of P_n]	[kJ/K]	[kWh]
1w	4	50	50	5
2w	4	100	50	5
3w	4	50	50	10
4w	4	100	50	10
5w	8	50	50	10
6w	8	100	50	10
7w	8	50	150	10
8w	8	100	150	10

The measurement campaign was performed between the 19th of March and the 10th of April 2014. During this period of time, the weather was unusually mild in Norway including in the Trondheim area. It results in outdoor temperatures (T_{ext}) oscillating between -1°C and 8°C, giving a low space-heating demand.

5. DISCUSSION AND RESULT ANALYSIS

5.1 Modelling approximation

For the building model (e.g. Type56) or the ventilation network model to be valid (e.g. TRNFLOW), a set of assumptions must be fulfilled. The main assumption is that the air temperature field in each room can be simplified into a single air temperature (Chen, 2009; Wang & Chen, 2008), sometimes called air-node (i.e. a well-stirred tank approximation). For the twelve test cases, the following indicators are monitored: the maximal operative temperature increase during a cycle ($\Delta T_{op,max}$) in the kitchen at 0.8 m height, the maximal air temperature difference in an horizontal plane at 0.8 m height at the ground floor ($\Delta T_{s,hor,max}$), the maximal air temperature difference from floor to ceiling at the ground floor ($\Delta T_{s,vert,z1,max}$) and the maximal air temperature difference from the ground floor to the first floor ceiling measured in the staircase ($\Delta T_{s,vert,z2,max}$). Measurements are reported in Table 4 where a distinction has been made between cases with a large direct sun irradiation and cases with overcast sky. With a large sun irradiation from the south façade, the temperature of the living room increases locally. This gives a large horizontal temperature difference at the ground floor. On the contrary, without large solar gains, the air temperature is relatively uniform in the horizontal direction (i.e. lower than 1°C). On the contrary, the vertical temperature stratification in the living room is significant. The higher the power and energy delivered to the room, the higher the stratification. Thermal stratification is in fact the largest source of discrepancy between the detailed dynamic simulations and reality. In the worst cases, the stratification is so large that it should also be accounted for in the evaluation of the thermal comfort. According to ISO 7730, it should be done by comparing the air temperature difference between head and ankle height. Except for the test case 6w, this temperature difference for a person sitting (between 0.1 and 1.1 m height) is lower than 3°C which leads to a thermal environment of category B according to ISO 7730.

If the person is assumed standing (between 0.1 and 1.7 m height), many test cases lead to a temperature difference between head and ankle larger than 3°C.

Table 4: Maximal temperature differences during each stove cycle.

Case	Sun	T _{ext}	$\Delta T_{\text{op,max}}$	$\Delta T_{\text{s,hor,max}}$	$\Delta T_{\text{s,vert,z1,max}}$	$\Delta T_{\text{s,vert,z2,max}}$
	Living room	Outside	Kitchen	Ground floor	Ground floor	Staircase
N°	[Yes-No]	[°C]	[°C]	[°C]	[°C]	[°C]
1p	No	-1	4.5	0.2	11	4.1
2p	No	+8	3.3	0.5	8.1	2.0
4p	No	+5	5.5	1.4	11	5.3
2w	No	+6	4.2	1.5	8.4	6.5
4w	No	+5	6.4	0.6	3.1	5.0
5w	No	+5	4.7	0.3	9.3	5.1
7w	No	+5	4.0	0.4	7.6	4.2
8w	No	+7	5.3	0.8	8.9	3.6
3p	Yes	+4	3.9	2.8	5.5	3.6
1w	Yes	+4	3.8	3.5	4.3	3.7
3w	Yes	+4	6.8	4.6	6.7	7.1
6w	Yes	+4	6.0	4.5	13	7.8

Table 5: Radiation asymmetry at the end of each stove cycle, only reported for test cases during overcast sky ($T_{\text{mrt,front}}$ and $T_{\text{mrt,back}}$ are the radiant temperatures facing and opposite to the stove, respectively).

Case	Sun	T _{mrt,front}	T _{mrt,back}	T _{mrt,front}	T _{mrt,back}
	Living room	Living room	Living room	Kitchen	Kitchen
N°	[Yes-No]	[°C]	[°C]	[°C]	[°C]
1p	No	35.4	26.6	-	-
2p	No	32.3	25.2	-	-
4p	No	36.2	27.5	-	-
2w	No	33.2	28.4	28.9	26.2
4w	No	32.0	27.3	28.8	27.1
5w	No	31.6	26.7	28.0	26.1
7w	No	31.1	25.2	27.2	24.9
8w	No	36.1	27.9	29.1	25.0

While the horizontal air temperature difference is small (in absence of sun), the wall temperature is significantly influenced by the distance from the stove. Four wall sensors were placed at the ground floor with three attached to walls close to the stove and one to an external wall of the kitchen. It is difficult to measure the space-averaged wall temperatures but, based on punctual values, a difference of ~5°C may be found. This is also confirmed using the radiant temperature transducer, showing a significant mean radiant temperature (T_{mrt}) difference between the kitchen and the living room, see Table 5. It clearly demonstrates the importance of using accurate view factors when distributing the stove internal gains into the room model, as well as when evaluating the resulting thermal comfort of a user. To our knowledge, this step can be critical for many usual building simulation tools as they can only compute the accurate view factors for convex room geometries (where view factors can be evaluated analytically). When rooms are concave, softwares as TRNSYS distribute by default the gains between the walls in an area-weighted manner. This is obviously not convenient for the present application. The software user should rather pre-evaluate these view factors in dedicated software (e.g. ANSYS Fluent). The room geometry should then be reintroduced an additional time and the identity number of surfaces strictly respected. This procedure is cumbersome and is currently

the main technical barrier for a widespread application of the present modeling approach. Complementary quantitative comparisons between the detailed and the area-weighted view factors approaches can be found in (Georges & Novakovic, 2012). As regards the room geometry, an additional constraint for simulations is that each wall should be subdivided in sections of maximum $\sim 3\text{m}$ wide to enable the wall temperature to vary within the room.

Finally, it is worth investigating whether the ventilation network approach along with the large opening approximation is able to correctly reproduce the airflow through the doorway. The agreement appears to be fairly good as shown in Figure 8. The measured time-averaged velocity is close to the theoretical velocity profile obtained by the large opening approximation. In this case, the discharge coefficient C_{dv} has been evaluated to minimize the error with the measured velocities using a least-squares approach. This coefficient is reported in Table 6 for all the test cases where the velocity was measured properly in the doorway. For all cases, this coefficient ranges between 0.36 and 0.41 and thus appears rather constant as well as fits within the typical range of $[0.4;0.8]$ reported in the literature.

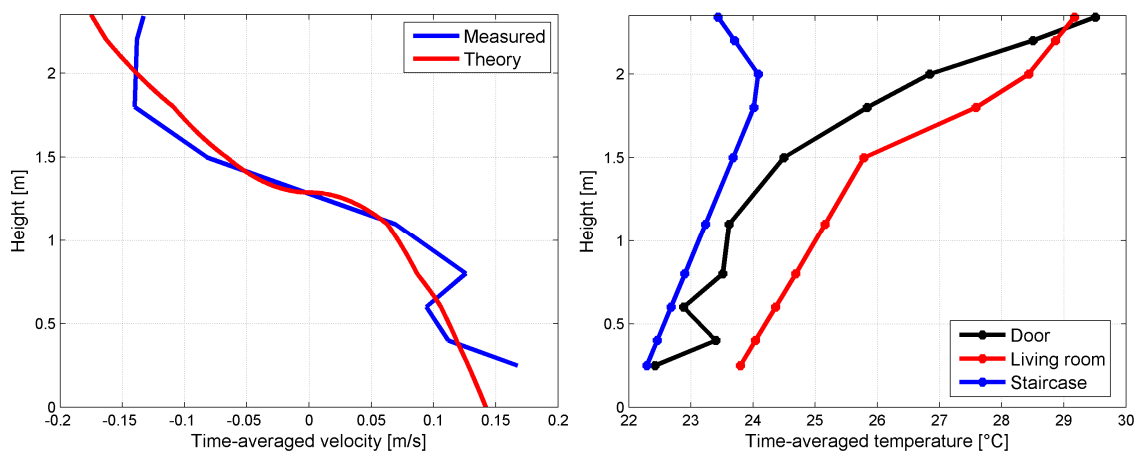


Figure 8: Time-averaged profiles along the door height for test case $n^{\circ}1p$.

As regards building simulation, it is more relevant to calibrate the discharge coefficient using the mass flow rate. One can distinguish between the coefficients obtained if the thermal stratification is known on both sides of the door (C_{dm}) and the coefficient assuming that both rooms are isothermal (C_{dms}). Their magnitudes are rather similar, meaning that the isothermal approximation does not lead to a large error in the mass flow. This is a known conclusion already reported in IEA EBC Annex 20 (Allard et al., 1992).

Table 6: Discharge coefficients for the bidirectional flow through the doorway.

Case	C_{dv}	C_{dm}	C_{dms}	C_{des}	C_{desm}
N°	[-]	[-]	[-]	[-]	[-]
1p	0.36	0.35	0.32	0.58	0.40
3p	0.40	0.38	0.36	0.61	0.35
1w	0.39	0.37	0.35	0.54	0.33
2w	0.39	0.38	0.33	0.62	0.41
3w	0.41	0.40	0.39	0.62	0.43
5w	0.38	0.36	0.35	0.53	0.33

Nevertheless, it is also known that the error using this isothermal hypothesis is significant when considering the convective heat exchange between the rooms (Allard, et al., 1992). In our application, the convective heat exchange is more relevant than the mass flow. In that case, one could tune the discharge coefficient to make the large opening model coupling two isothermal rooms fit the measurement (C_{des}). In that case, one should increase the coefficient to 0.53-0.62.

In reality, the temperature of the two opposite flows is not equal to the space-averaged temperature of their respective originating room, as depicted in Figure 8. A significant temperature mixing takes place near the doorway. The real convective heat exchange between rooms should be computed using this temperature profile rather than the two space-averaged room temperatures. In this case, the discharge coefficient can be adapted to make the large opening approximation based on isothermal rooms fit to the measurement (C_{desm}). The temperature mixing decreases the discharge coefficient to values between 0.33 and 0.41. This range is rather similar to discharge coefficients that fit the velocity and the mass flow. In other words, neglecting the vertical stratification leads to a large error when considering the convective heat transfer between rooms. Nevertheless, this effect is counterbalanced by the temperature mixing near the doorway which reduces the amount of heat exchanged. In the present measurement campaign, these two effects almost cancel each other out. As a conclusion, the large opening approximation connecting two isothermal rooms is a fair approximation for detailed dynamic simulations. Nevertheless, as proposed in the modeling procedure, a range of discharge coefficients should be analyzed, typically [0.4;0.8], rather than using a single specific value.

5.2 Stove performance

In the previous section, assumptions done using detailed dynamic simulations were compared to field measurements (i.e. stratification, need for detailed view factors and airflows through doors). As the PH building typology is similar to the one investigated using simulations in previous communications, see e.g. (Georges, Skreiberg, et al., 2014), it is possible to *qualitatively* compare their conclusions in terms of overheating in the living room: the thermal environment using wood stoves has not yet been simulated for the specific case of the PH in MiljøGranåsen. In fact, a direct *quantitative* comparison between simulations and measurements is difficult to perform as the real PH building is always in unsteady thermal state with its environment making the establishment of consistent initial conditions for the dynamic simulations complex. Considering previous simulation works for qualitative comparison, their set-point air temperature was taken to be 21°C while the highest acceptable T_{op} is assumed as ~24.5°C (i.e. the limit of category B comfort in ISO 7730 using a *clo* and *met* of 1.0).

Previous simulations gave the following conclusions for a light building construction mode located in a similar climatic zone (i.e. Bergen) along with open internal doors:

- The 8 kW pellets stove with 30% power modulation is able to avoid overheating after 90 min operation. It corresponds to case 3p of the present measurement campaign which gave the same conclusion (see Table 4), even though this test case was performed during a period of large solar gains.
- The 6 and 8 kW pellet on-off stoves gave an unacceptable overheating after 90 min operation, as confirmed experimentally by the test cases 1p and 4p in Table 4.
- The 4 kW log stove with 50% power modulation do not generate unacceptable overheating as confirmed by the test case 1w during experiments. Nevertheless, the case 3w gave overheating essentially due to the concomitant large solar gains.
- The 8 kW log stove with 50 kJ/K thermal inertia does not manage to limit the overheating sufficiently, as confirmed by cases 5w and 6w. Nevertheless, the models shows that a 8 kW log stove with 50% power modulation and 150 kJ/K thermal inertia would be able to limit the overheating which is confirmed by test case 7w.

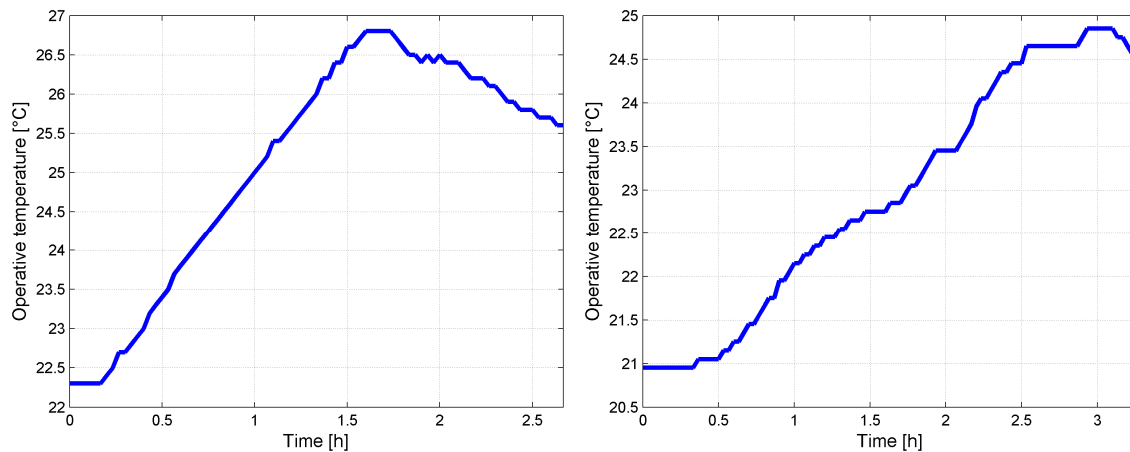


Figure 9: Example time profiles of the operative temperature in the kitchen during stove cycles (test case 1p on the left and 1w on the right).

In conclusion, there is a rather good correspondence between the qualitative conclusions obtained using detailed dynamic simulations and experimental data. Nevertheless, one may argue that the weather conditions during the experiments were way too mild and are thus not representative. In fact, given the mild outdoor temperatures, the building did not need any space-heating in periods with high solar gains. Nonetheless, considering the present PH architectonic properties and location, previous simulations showed that the overheating magnitude is almost constant throughout the heating season. Therefore, conclusions from experiments are not narrowed down by the limited timeframe of the measurement campaign nor the mild weather conditions..

6. CONCLUSIONS

Wood stoves are popular space-heating solutions in many European countries. Nevertheless, nominal powers of the state-of-the-art products on the market are oversized compared to the needs of highly-insulated building envelopes. In this respect, a simplified wood stove model has been developed in order to investigate the thermal comfort at an acceptable computational cost. A specific experimental setup has been developed to validate this modelling approach, especially as regards the interaction between the stove and the building. The largest source of error appears to be the thermal stratification in the room where the stove is placed. This can simultaneously affect the conductive heat transfer between rooms, the thermal comfort sensation in the room as well as the convective heat exchange by flows through doorways. Nonetheless, this last effect can be limited in simulations by performing a sensitivity analysis on the discharge coefficient of the door (C_d). Finally, thermal comfort measurements during the experimental campaign support the conclusions of previous simulation results, verifying the proposed guidelines for the integration of wood stoves in passive houses. As a future work, the simplified wood stove model will be further validated. For instance, a calibration procedure will be established in order to be able to directly compare the T_{op} from measurements and simulations, e.g. both considering the MiljøGranåsen case. The thermal comfort using the movable electric stove will be also tested in other passive houses, presenting other typologies (e.g. detached houses, apartments) as well as during colder periods of the heating season. The model and measurement will also be compared with Computational Fluid Dynamics (CFD) which has the capacity to properly capture the thermal stratification. Furthermore, most of the CFD packages compute view factors accurately in a quasi-automatic manner.

REFERENCES

- Allard, F., Bienfait, D., Haghghat, F., Liébecq, G., et al. (1992). Air flow through Large Opening in Buildings. In J. van der Maas (Ed.), *Annex 20: Air flow patterns within Buildings*: International Energy Agency.
- Blumrich, F., Feist, W., Hasper, W., Krause, H., et al. (2007). Protokollband nr. 36: heizung mit biobrennstoffen für passivhäuser. In P. Institut (Ed.). Darmstadt: Passivhaus Institut.
- CEN. (2005). EN ISO 7730 : Ergonomics of the thermal environment: analytical determination and interpretation of thermal comfort using calculation of the PMV and PPD indices and local comfort criteria.
- CEN. (2008). EN ISO 13790-2008 : Energy performance of buildings, calculation of energy use for space-heating and cooling.
- Chen, Q. (2009). Ventilation performance prediction for buildings: a method overview and recent applications. *Building and Environment*, 44, 848-858.
- Churchill, S., & Chu, H. (1975). Correlating equations for laminar and turbulent free convection from a vectlal plate. *International Journal of Heat and Mass Transfer*, 18, 1323-1329.
- Etheridge, D., & Sandberg, M. (1996). *Building ventilation: theory and measurements*. New Jersey: John Wiley and Sons.
- European Parliament. (2010). Directive 2010/31/EU of the European Parliament and the Council of 19th May 2010 on the energy performance of buildings (recast). *Official Journal of European Union*.
- Feist, W., Schnieders, J., Dorer, V., & Haas, A. (2005). Re-inventing air heating: convenient and comfortable within the frame of the Passive house concept. *Energy and Buildings*, 37, 1186-1203.
- Georges, L., Berner, M., & Mathisen, H. M. (2014). Air heating of passive houses in cold climate: investigation using detailed dynamic simulations. *Building and Environment*, 74, 1-12.
- Georges, L., & Novakovic, V. (2012). *On the integration of wood stoves for the space-heating of passive houses: assessment using dynamic thermal simulations*. Paper presented at the BSO 2012 conference, Lhouborough.
- Georges, L., Skreiberg, Ø., & Novakovic, V. (2013). On the proper integration of wood stoves in passive houses: investigation using detailed dynamic simulations. *Energy and Buildings*, 59, 203-213. doi: 10.1016/j.enbuild.2012.12.034
- Georges, L., Skreiberg, Ø., & Novakovic, V. (2014). On the proper integration of wood stoves in passve houses under cold climates. *Energy and Buildings*, 72, 87-95.
- Ghali, K., Ghaddar, N., & Salloum, M. (2008). Effect of stove asymmetric radiation field on thermal comfort using a multisegmented bioheat model. *Building and Environment*, 43, 1241-1249.
- Haller, M. Y., Paavilainen, J., Konersmann, L., Haberl, R., et al. (2011). A unified model for the simulation of oil, gas and biomass space heating biolers for energy estimating purposes: part I & II. *Journal of Building Performance Simulation*, 4(1), 1-36.
- Heiselberg, P. (2006). Modelling of natural and hybrid ventilation *Lecture notes No.004*: Aalborg University.

- Incropera, F., Dewitt, D., Bergman, T., & Lavine, A. (2007). *Fundamental of heat and mass transfer* (6th ed.). New Jersey: John Wiley and Sons.
- Norwegian Ministry of Petroleum and Energy. (2008). Strategi for økt utbygging av bioenergi: Norwegian Ministry of Petroleum and Energy.
- Pérez-Lombard, L., Ortiz, J., & Pout, C. (2008). A review on buildings energy consumption information. *Energy and Buildings*, 40, 394-398.
- Persson, T., Fiedler, F., Nordlander, S., Bales, C., et al. (2009). Validation of a dynamic model for wood pellet boilers and stoves. *Applied Energy*, 86, 645-656.
- Saastamoinen, J., Tuomaala, P., Paloposki, T., & K., K. K. (2005). Simplified dynamic model for heat input and output of heat storing stoves. *Applied Thermal Engineering*, 25, 2878-2890.
- Skreiberg, Ø. (2002). Fuelsim-Transient: a mass, volume and energy balance spreadsheet for batch combustion applications *Post-doc report* (Vol. Part 3). Trondheim: NTNU.
- Skreiberg, Ø. (2011-2014). StableWood: new solutions and technologies for heating of buildings with low heating demand, from <http://www.sintef.no/Projectweb/StableWood/>
- Standard Norge. (2007). NS 3031 : Calculation of energy performance of buildings, methods and data.
- Standard Norge. (2010). NS 3700 : Criteria for passive houses and low energy houses (residential buildings).
- TRANSSOLAR. (2009). TRNFLOW: a module of an air flow network for coupled simulation with TYPE 56 (multi-zone building of TRNSYS).
- TRANSSOLAR. (2011). TRNSYS 17: Volume 5, Multizone Building modeling with Type56 and TRNBuild.
- Wang, L., & Chen, Q. (2008). Evaluation of some assumptions used in multizone airflow network models. *Building and Environment*, 43(10), 1671-1677.

ACKNOWLEDGEMENTS

The authors acknowledge Kristian Stensrud and Heimdal Bolig for their support and giving access to the passive house of the Miljø Granåsen project located in Trondheim. They also want to thank the Research Council of Norway for their support as this work was performed within the framework of the Research Centre for Zero Emissions Buildings (ZEB) and the StableWood project.

NOMENCLATURE

- C_d = discharge coefficient for the bidirectional flow in a doorway
- $C_{d,v}$ = C_d tuned to match the velocity profile
- $C_{d,m}$ = C_d tuned to match the mass flow
- $C_{d,ms}$ = $C_{d,m}$ but assuming two isothermal rooms on both sides of the door
- $C_{d,es}$ = C_d tuned to match the convective heat exchange between rooms without mixing
- $C_{d,em}$ = C_d matching the real heat exchange between rooms including temperature mixing
- ε = stove surface emissivity
- σ = Stefan-Boltzmann constant

I_{th}	= thermal mass of the stove envelope in [kJ/K]
m_{12}	= mass flow from the warm to the cold room
m_{21}	= mass flow from the cold room to the warm room
P_n	= nominal combustion power of the stove
P_c	= instantaneous combustion power of the stove
P_d	= power delivered to the stove envelope
P_e	= power emitted to the room
P_{ec}	= power emitted to the room by convection
P_{er}	= power emitted to the room by radiation
T_s	= air sensible temperature
T_{op}	= operative temperature
T_{set}	= set-point air sensible temperature for the room
T_{ext}	= outdoor air sensible temperature
T_{mrt}	= mean radiant temperature
T_{stove}	= instantaneous stove surface temperature
$\Delta T_{op,max}$	= maximal T_{op} increase in kitchen during a stove cycle
$\Delta T_{s,hor,max}$	= maximal horizontal T_s difference in ground floor during a stove cycle
$\Delta T_{s,vert,z1,max}$	= maximal vertical T_s difference in living room during a stove cycle
$\Delta T_{s,vert,z2,max}$	= maximal vertical T_s difference in staircase during a stove cycle

A TRNSYS-LabVIEW bi-directional connection for HVAC equipment testing using hardware-in-the-loop simulation

Francesca Macdonald¹, Katherine D'Avignon¹, Michaël Kummert¹, and Ahmed Daoud²

¹ *Polytechnique Montréal*, Mechanical Engineering, Montréal, Canada

² Institut de Recherche d'Hydro-Québec, Shawinigan, Canada

1. ABSTRACT

A methodology for using hardware-in-the-loop load emulation as a practical alternative to HVAC equipment testing in its actual environment is presented. Diverse and realistic operating conditions are mathematically represented through building performance simulation and imposed on an HVAC system component under test using Data Acquisition and Control software. The paper presents the implementation methodology in TRNSYS and LabVIEW, and the choices that were made to implement real-time data exchange between the two software environments. The "Semi-Virtual Laboratory" environment for testing hydronic heating and cooling is presented together with a discussion of the initial results.

Keywords: Hardware-in-the-loop, HVAC testing, TRNSYS

2. INTRODUCTION

Heating, Ventilation and Air-Conditioning (HVAC) system components are both influenced by and have an effect on their surroundings. As these effects are complex and vary with building construction and climate, accurate performance simulation for design, online control or diagnostics requires obtaining data encompassing the whole operating range of each component. Unfortunately, standardized data provided by manufacturers or performance rating organizations often only includes data for a limited number of operating points. Most ratings represent full-load performance and part-load data are often aggregated into seasonal indices.

Heat pumps are a good example of HVAC components that present a highly variable performance for different operating conditions. The ability to accurately assess a variety of applications is critical for maximizing energy savings and ensuring technology uptake (Bourke and Bansal, 2010). Novel components, such as storage tanks with Phase-Change Materials, are another example of components for which the nominal capacity data (storage capacity in kWh) is not enough for designers to assess their correct operation – the rate at which heat can be stored or extracted is a critical parameter, which varies significantly with operating conditions (Liu et al., 2011).

A number of modeling and simulation techniques may be used to predict HVAC equipment performance (Byrne et al., 2012). However, experimental validation is almost always required to determine the actual performance of the system. As actual operating conditions for HVAC equipment are so varied, characterizing performance by field testing is both impractical and unrealistic on account of the variations in application. To mitigate this issue, hardware-in-the-loop load emulation can be used to perform a task similar to that of an environmental test chamber. Hardware-in-the-loop (HIL) simulation is frequently used in the development and testing of complex real-time embedded systems to reduce testing cost and provide a more flexible and controlled testing environment. An HIL testing configuration is typically used as

an intermediate or alternate step for testing a system in its actual environment (Otten et al., 2010).

This paper describes a novel method for testing HVAC equipment in a laboratory using building performance simulation to mathematically represent diverse and realistic operating conditions. The methodology used to exchange information between the simulation environment (TRNSYS) and the laboratory Data Acquisition and Control software (LabVIEW) is generic and can be used for any air-based or water-based HVAC system component. The semi-virtual laboratory at Polytechnique Montréal is, however, dedicated to water-loop components, so this paper focuses on using this configuration in heat pump testing.

Diverse building constructions and varied climatic conditions can be represented through simulation, and electrical emulation of sensors and actuators is used to interface between the simulation and the heat pump under test. There are several examples of component testing using building simulation and hardware-in-the-loop emulation (Lahrech et al. 2002), (Lahrech et al. 2007), (Nouidui et al., 2011), (Rhee et al., 2011), (Wetter, 2011) including examples where TRNSYS is used to calculate building performance (Leconte et al, 2012), (Pan et al., 2011), (peitsman et al. 1994). TRNSYS has also been used in conjunction with HIL testing of ground source heat pumps where results obtained are more representative of actual performance than standard COP and EER figures (Riederer et al., 2009).

3. METHODOLOGY

TRNSYS simulations predict system performance, calculating the flowrates and temperatures of the fluid streams entering HVAC equipment under test, which are used as actuator control signals in the Laboratory. The equipment’s response to these operating conditions is sensed in the laboratory and imposed back on the building simulation. Figure 1 describes the HIL testing configuration used to characterize the performance of a heat pump.

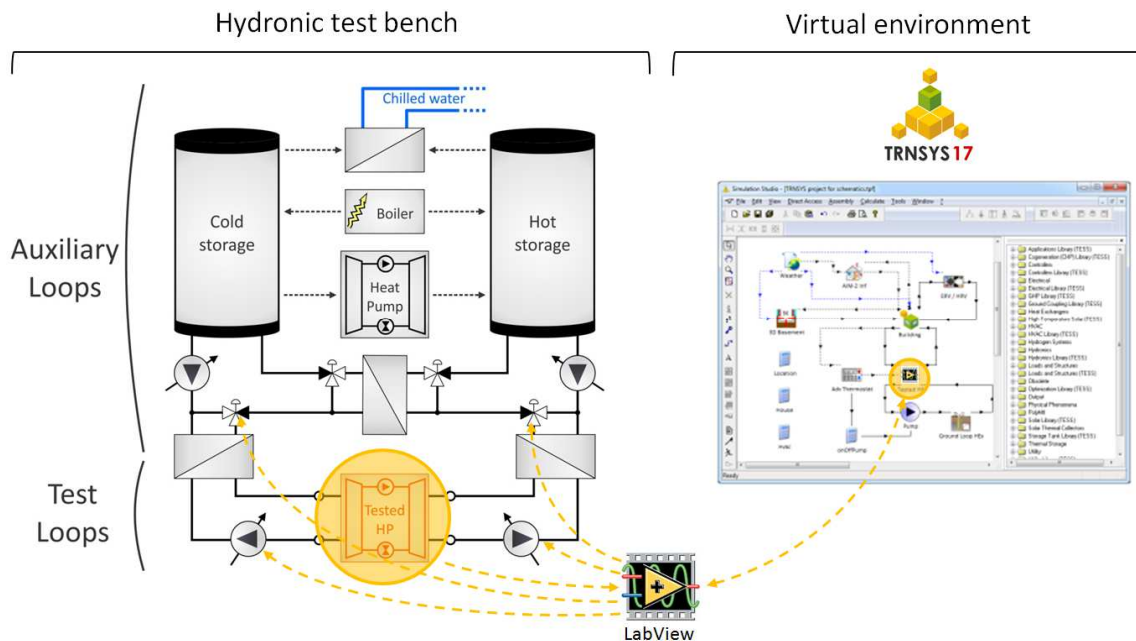


Figure 1: Hardware-in-the-loop setup for heat pump testing

3.1 TRNSYS

TRNSYS (Klein, 1979) is based on a modular, component-based architecture where all physical (and non-physical) components in a system are modelled within separate routines. These routines are then called by the TRNSYS kernel (utility routines and solver) to simulate the performance of the whole system. The components, known as “Types”, compute outputs from their inputs and parameters. The default TRNSYS solver uses successive substitution and makes no assumption about the nature of the equations inside components. The TRNSYS kernel is responsible for mapping the inputs, equations and outputs of the different types in a simulation and for managing convergence. During iterations the kernel calls the types whose inputs have changed until convergence is achieved. The TRNSYS kernel is programmed in Fortran and is compiled into a Windows Dynamic Link Library (DLL) called TRNDll.dll. A DLL is a shared library under the Windows operating system. Shared libraries are libraries of functions that are loaded into memory by executables at run time. TRNSYS components can be either compiled into the same DLL or programmed in different languages and compiled into their own DLLs. The main DLL is normally loaded by the TRNSYS executable program (TRNExe.exe) which in turn loads other DLL's with additional components.

3.2 LabVIEW

LabVIEW (Laboratory Virtual Instrument Engineering Workbench) (Santori, 1990) is a development environment from National Instruments. It is commonly used for data acquisition, instrument control, and industrial automation. LabVIEW provides extensive support for accessing instrumentation hardware. Drivers and abstraction layers for many different types of instruments and buses are available as graphical nodes. The abstraction layers offer standard software interfaces to communicate with hardware devices, which saves program development time. A reconfigurable embedded control and acquisition system, the CompactRIO, provides high-speed signal acquisition and generation which has been used to interface with the heat pump under test. The CompactRIO's hardware architecture includes I/O modules, a reconfigurable FPGA chassis, and embedded real-time processor.

LabVIEW programs/subroutines are called virtual instruments (VIs). Each VI has three components: a front panel, a block diagram, and a connector panel.

- The **front panel** is built using controls and indicators. Controls are used for inputs and indicators display outputs.
- The **block diagram** contains the graphical source code. All of the objects placed on the front panel appear on the block diagram as terminals, together with structures and functions which perform operations on controls and supply data to indicators. Collectively controls, indicators, structures and functions are referred to as nodes. Nodes are connected to one another using wires. These wires propagate variables, and any node can execute as soon as all its input data become available. Since this might be the case for multiple nodes simultaneously, LabVIEW programs are inherently capable of parallel execution.
- The **connector panel** is used to represent the VI in the block diagrams of other, calling VIs. A VI can be run as a program, with the front panel serving as a user interface, or as a function represented by a node on another block diagram, where the front panel defines the inputs and outputs for the given node through the connector panel.

LabVIEW provides the Call Library Function Node to facilitate calling functions in DLLs. As TRNSYS is compiled as a DLL, it can be run from LabVIEW using the Call Library Function Node.

4. TRNSYS-LABVIEW COOPERATION

The LabVIEW program written to enable this HIL load emulation comprises a number of VIs responsible for different aspects of the program. As such, the design enables the substitution of VIs without affecting program flow. This could facilitate using different building performance simulation tools or different laboratory configurations. Global variables are used to synchronise the data exchange with TRNSYS and to share key measured variables and set point variables between the VIs. The global variables have been employed with careful consideration to preventing race conditions. A race condition is the name given to a type of software problem in which two or more pieces of code execute in parallel and have access to a shared piece of memory (global variables), and the order of events do not happen as the programmer intended, resulting in unpredictable behavior.

The main LabVIEW program, SemiVirtualLab.vi, consists of a stacked sequence structure comprised of three frames, which execute sequentially. In the first frame, global variables are initialized and a file dialog is used to prompt the user for a root filename (used in all the data files created throughout the programs run time). The main data acquisition file is opened and the column headers are written. In the second frame the lab.vi reference is opened and inserted into SemiVirtualLab.vi's front panel. The use of a subpanel permits the display of a front panel from another VI on the VIs own front panel. This allows the use of different laboratory VIs (used for different experimental setups) to be inserted into the project and used in conjunction with TRNSYS. To use SemiVirtualLab.vi for a different laboratory set up, the Lab VI (and it's path), together with appropriate column headers for the DAQ file need to be changed to reference the new lab.vi. The third frame contains three parallel while loops: one to enable the user to terminate running the VI, one to allow the user to switch between manual mode and synchronous mode in which key set points for the lab are either controlled manually or by a TRNSYS simulation, and one which continually runs the lab.vi, responsible for data acquisition and control.

Figure 2 presents a flow diagram describing the semi-virtual lab application. The SemiVirtualLab.vi is the framework VI in which Lab.vi and TrnsysMain.vi are dynamically loaded and unloaded. Loading TrnsysMain.vi dynamically into memory enables cleaning up the memory allocation from loading TRNDll.dll. SemiVirtualLab.vi is also responsible for creating, writing and closing files, and for data averaging in synchronous mode.

Lab.vi runs inside a while loop in SemiVirtualLab.vi to ensure continuous data acquisition. In manual mode, Lab.vi executes only once before returning to SemiVirtualLab.vi, ensuring the software is responsive to user interaction and facilitating synchronization. In synchronous mode, Lab.vi is executed a number of times equal to $\text{TrnsysTimestep}/\text{DAQTimestep}$ (see the Synchronization section below) before returning to SemiVirtualLab.vi where relevant data is averaged and written to file.

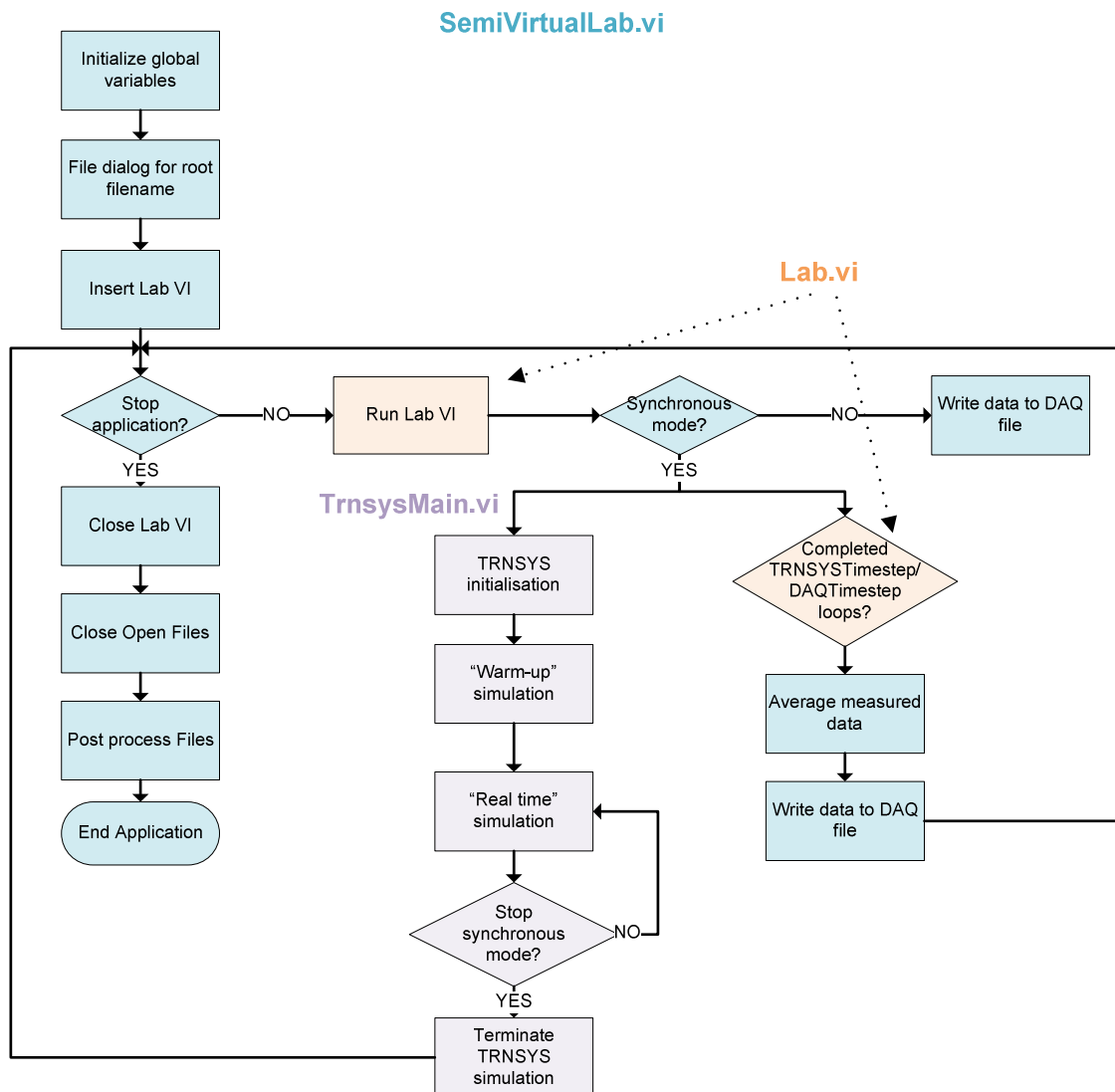


Figure 2: Flow diagram of semi-virtual lab application

4.1 Lab.vi

As described in the LabView Section, a VI can be run as a function represented by a node on another block diagram. Any Lab.vi can be substituted in the SemiVirtualLab.vi, with its front panel defining the inputs and outputs for the given node through the connector panel.

The prerequisites for a Lab VI are that it has the DAQ timestep as an input, and outputs for hydronic and air based components (comprising flowrates, inlet and outlet temperatures and, in the case of air based components, outlet relative humidities). In laboratory set ups used only to examine either air based or hydronic components, the redundant 'outputs' do not need to be connected. Any additional data required for recording purposes can be exported into the SemiVirtualLab.vi as outputs in the form of a string array and a real matrix. As the application's primary requirement is synchronisation between the DAQ and TRNSYS, data processing needs to be kept to a minimum within the timed loops used to run the lab and TRNSYS. For this reason file opening and closing is done out with the loops and any extra data processing is done after the simulation is complete, in the PostProcessFile.vi and not inside the Lab.vi.

Figure 3 illustrates Lab.vi configured as a node in SemiVirtualLab.vi with the outputs 'wired' through the connector panel for subsequent data exchange with TRNSYS.

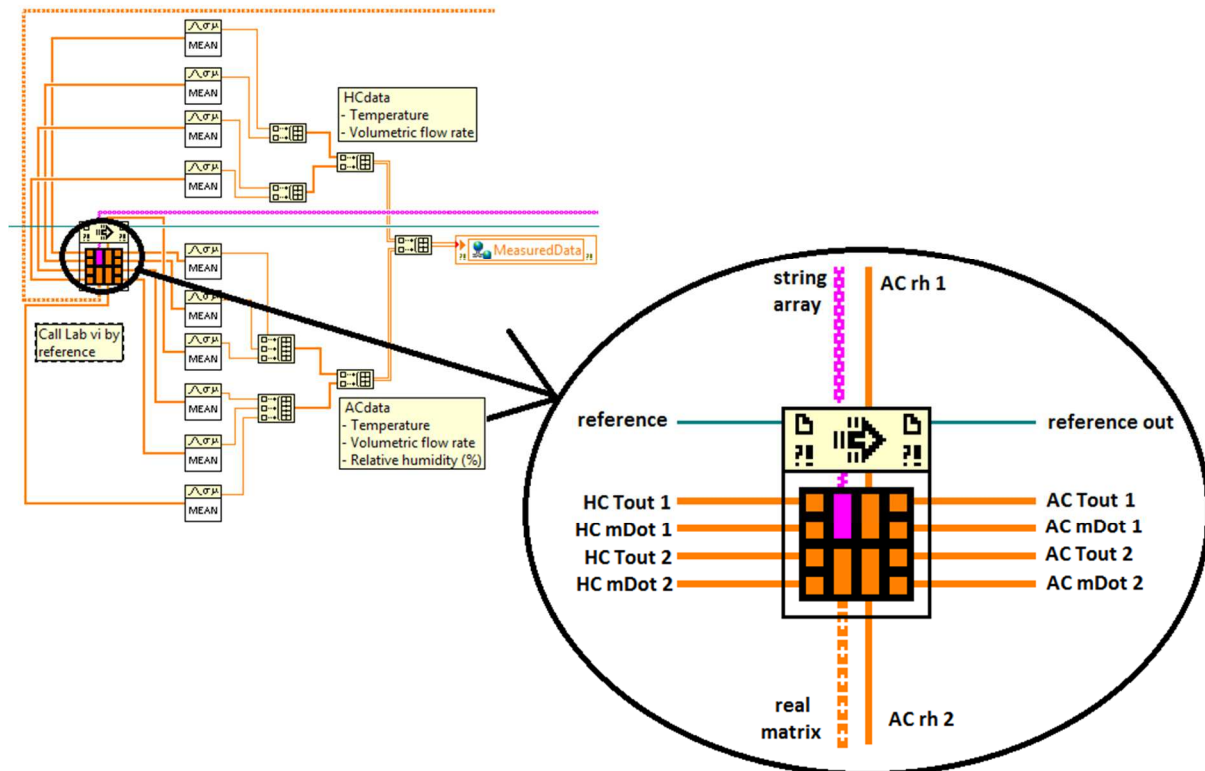


Figure 3: Connections required between Lab.vi and SemiVirtual.vi

4.2 TrnsysMain.vi

TrnsysMain.vi assumes the role of the TRNSYS executable (TRNExe) in regular TRNSYS operation and is responsible for loading and initializing TRNDll.dll (including parsing the TRNSYS input file) and for acting as the simulation clock, controlling the marching forward through time. Once TRNSYS is initialized, TrnsysMain.vi runs the desired “warm-up” simulation to establish the initial conditions and then the “real time” simulation until the user manually ends synchronous mode. Real time simulation maintains synchronous mode executing the DAQ loop TrnsysTimestep/DAQtimestep number of times, and sending the average of these values to TRNSYS to calculate the next setpoints.

Similar to the approach used in the co-simulation between Esp-r and TRNSYS, where the middleware controls the TRNDll.dll (Beausoleil-Morrison et al. 2010), TrnsysMain.vi controls the TRNSYS program flow (using a sequence frame) as described by Figure 4.

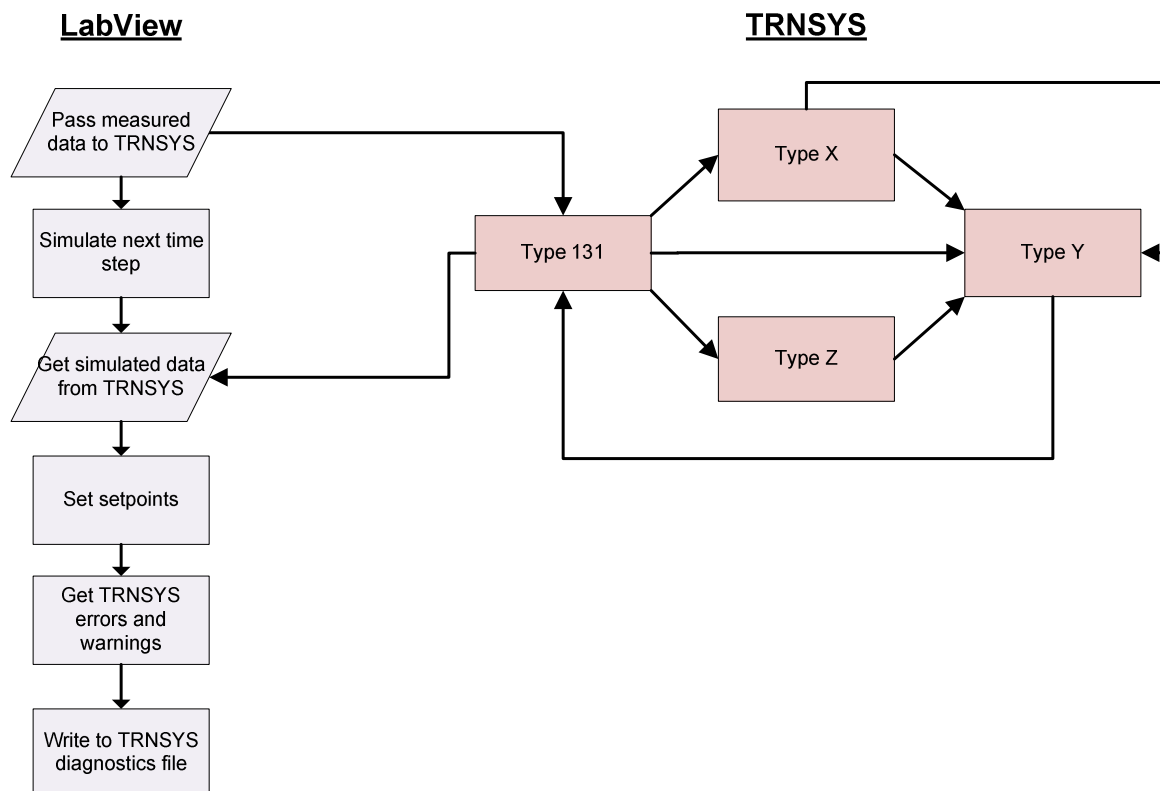


Figure 4: LabVIEW interaction with TRNSYS

The order of calls made to TRNSYS are as follows:

1. PassMeasuredDataToTrnsys passes averaged measured values to Type 131.
2. TRNSYS is instructed to proceed with the next simulation time step.
3. GetSimulatedDataFromTrnsys retrieves relevant simulation data from Type 131, which are used to adjust setpoints in Lab.vi.
4. GetNumberOfWarnings and GetNumberOfErrors retrieve any warnings or errors.

The time taken to complete a TRNSYS timestep calculation (i.e. an iteration in which the TRNSYS kernel calls the types whose inputs have changed until convergence is achieved) is monitored to ensure it does not exceed the data exchange period. If the data exchange period is exceeded, the measured data sent to TRNSYS is no longer synchronized with the TRNSYS timestep and the user is alerted to this erroneous condition.

4.3 TRNSYS Code Changes

Source code additions to TRNSYS consist of a Fortran module (data structures and subroutines) and a TRNSYS component (Type 131).

The LabviewTrnsysLink module declares data types to contain the information exchanged back and forth between the programs for each hydronic or air-based port (see the Derived Data Structure section below). In addition, the Fortran module also declares the two subroutines (PassMeasuredDataToTrnsys and GetSimulatedDataFromTrnsys) that are called by LabVIEW (respectively before and after performing the timestep simulation in TRNSYS).

The new TRNSYS component, known as Type 131, was created to encapsulate all the communication between other TRNSYS components and LabVIEW. Type 131 is used to specify the mapping of laboratory measured data to the simulated system and the calculated outputs back to the laboratory. The standard TRNSYS procedure for connecting components

facilitates this mapping, where measured laboratory temperatures and flowrates comprise the inputs to Type 131, and Type 131 outputs are connected to the inputs of the other TRNSYS types. Likewise, the outputs of other TRNSYS types in the system model are mapped to Type 131 inputs which are mapped back to the laboratory. Figure 4 illustrates the interaction between LabVIEW and TRNSYS at every timestep of the simulation.

The code for Type 131 is relatively simple. During normal iterative calls, the Type sets its outputs to the data that was received from LabVIEW at the beginning of the current time step (these data represent the behaviour of the tested equipment over the previous measuring period, i.e. time step). At the last call of a time step, after convergence between all TRNSYS components has been reached, Type 131 sets the data, ready to be exchanged with LabVIEW to its inputs (received from other TRNSYS components). These inputs represent the converged values for the current time step and will be imposed as setpoints for the inlet conditions in the real lab. Note that the `PassMeasuredDataToTrnsys` and `GetSimulatedDataFromTrnsys` routines are not called by Type 131 itself, they are called by LabVIEW.

4.4 Derived Data Structure

A derived data structure (DDS) comprising the flowrates and temperatures required in the LabVIEW-TRNSYS communication is passed between LabVIEW and TRNSYS subroutines in the same way as intrinsic data types. Build array functions are used in LabVIEW create the derived data structure. The derived data structure comprises the variables exchanged for hydronic and air couplings. Hydronic couplings require the temperatures and volumetric flowrates for each inlet/outlet connection. Air based couplings have an additional requirement for the relative humidity. This additional variable requires that an empty placeholder variable is incorporated into the hydronic data structure to ensure compatibility with LabVIEW data structures whose inputs are padded to accommodate the longest inputs (i.e. those of air based connections).

4.5 Synchronisation

The simulation and the “real world” cannot be fully synchronized, because TRNSYS components exchanges values averaged over the time step. This poses a problem as to calculating the inlet conditions to the tested equipment, TRNSYS would need to know the outlet conditions until the end of the current time step. It is therefore assumed that the thermal mass in the simulated system (which probably includes a building) is more significant than the thermal mass in the tested equipment, and the simulated values over a time step are applied during the next time step, to the tested equipment.

The TRNSYS simulation requires a warm-up period to establish some initial conditions, e.g. one week (168 h). Once synchronized mode is started, LabVIEW collects X data points (where $X = \text{TRNSYS time step/data acquisition time step}$) without changing the lab’s operating conditions. TRNSYS is then called to run the simulation as fast as it can over the warm-up period. During that time, TRNSYS uses constant inputs which are the average values of the data points collected. If this method is not suitable, the TRNSYS simulation must include another component modeling the tested equipment and a mechanism to switch between the model and the LabVIEW data exchange when the synchronous mode starts.

The last time step calculated in this sequence is for time = 168 h, which in TRNSYS represents average values between 167.99 and 168 (assuming a time step of 0.01 h). TRNSYS then passes the inlet conditions to the tested equipment, to LabVIEW. For the sake of the discussion, we will assume that the real-time is 0 h at that time. So the test start time (real-time = 0) corresponds to when TRNSYS returns after simulating the warm-up period.

The following discussion assumes a 1-sec DAQ time step (the lab data acquisition and control loop used to measure all sensors, calculate control values and set outputs) and a TRNSYS time step of 36 sec (0.01 h). LabVIEW imposes the TRNSYS ‘warm-up’ conditions to the tested equipment for the whole averaging period (36 sec) – these are the setpoints for inlet flowrate and inlet temperatures 1 and 2. So between real-time = 0 h and real-time = 0.01 h, LabVIEW then performs 36 DAQ and control loops and uses constant setpoints from TRNSYS (the ones calculated for timestep 168 in TRNSYS, i.e. average values between 167.99 and 168.00).

After running the DAQ and control loop with a 1-sec time step 36 times, LabVIEW passes the average outlet conditions over 36 sec to TRNSYS and initiates the next TRNSYS time step. At that time TRNSYS calculates its “168.01” time step (meaning average values between 168.00 and 168.01 h) using the average outlet conditions from the equipment between real-time 0.00 and real-time 0.01 h.

During the TRNSYS calculations, the setpoints to the tested equipment remain constant. The assumption is that TRNSYS will take at the most a few seconds to complete.

When TRNSYS returns from the time step (assuming there are no errors), the setpoints for the DAQ and control loop are updated. If we assume that TRNSYS took 3.6 seconds (0.001 h) to simulate the time step, this means that for the first 3 “1-sec” DAQ and control loops LabVIEW has used previous setpoints. For the 4th DAQ and control step, LabVIEW is now using the setpoints calculated by TRNSYS for TRNSYS timestep “168.01”, meaning average values between 168.00 and 168.01. At that moment, real-time is 0.011 and the 1-sec DAQ and control loop will keep running using these setpoints until real-time reaches 0.02 h. This example is rather extreme and used as an example to indicate how the developed communication mechanism handles synchronization issues. In practice, running a single TRNSYS simulation time step usually takes much less than 1 sec, so that the outdated setpoints are only used during one data acquisition and control cycle.

At real-time = 0.02 h, LabVIEW calculates the average values over the last 36 “1-sec” loops (or if the TRNSYS calculation for one timestep took longer than 1s, calculates the average values since TRNSYS returned) – these represent the average measured outlet conditions from the tested equipment between real-time = 0.01 and 0.02 h.

LabVIEW then calls TRNSYS to calculate the “168.02” time step, meaning average values between 168.01 and 168.02 using the average measured values between real-time = 0.01 and 0.02 h.

- Synchronisation is achieved through the use of global variables which communicate the following conditions between TRNSYSMain.vi and Lab.vi:
- When the user initiates synchronous mode.
- When the warm-up data has been collected (i.e. the average values over the most recent TRNSYS time step).
- When the warm-up simulation is complete.
- When TrnsysTimestep/DAQtimestep number of data points have been collected.

5. LABORATORY SETUP

The test bench is designed to reproduce the wide variety of operating conditions under which small commercial-size hydronic equipment usually function. The hydronic system shown in Figure 5 contains two test loops which supply the load-side and source-side operating conditions to the tested equipment (also see Figure 1, bottom left). Each test loop has a pump equipped with a variable-frequency-drive (VFD) allowing for changing flow rates up to 7.6 L/s

(120 US GPM). A balancing valve to partially by-pass the tested equipment can be used to reduce the flow rate imposed below 35 US GPM (30% of the pump's nominal flow rate). Each test loop has a turbine flow meter with magnetic pick-up on the inlet to the tested equipment and a PT-100 platinum resistance sensor on both inlet and outlet in order to precisely measure the operating conditions imposed on the equipment and the equipment's response.

Different heating and/or cooling units can be alternatively connected to either of the auxiliary loops according to the operating conditions required. A non-reversing water-to-water heat pump with scroll-type tandem compressors is connected to both auxiliary loops. The "hot" auxiliary loop serves as its load-side and the "cold" auxiliary loop as its source-side, though the heat pump's temperature set point can be either on the "cold" or "hot" loop. The heat pump has a nominal capacity of 100 kW of cooling with flow rates from 3.6 to 6 L/s (48 to 80 US GPM) and can heat the load-side auxiliary loop to 60 °C with source-side temperatures as low as -3.8 °C. Alternatively, an electric boiler with a capacity of 54 kW can be used by either of the auxiliary loops to reach a water temperature of 90 °C. Additionally, a heat exchanger connected to the building's chilled water loop (7 °C nominal) can be used to cool either auxiliary loop. Another heat exchanger is connected to both auxiliary loops, allowing them to directly transfer heat between themselves. A series of 3-way valves allows each of the units to be used individually or in series with either of the others. For example, if the heat pump is used to cool the source-side auxiliary loop, the heat exchanger linked to the chilled water loop could be used to evacuate excess heat generated by the heat pump on the load-side auxiliary loop.

Similarly, 3-way valves are also used to control the flow rate sent to the heat exchanger linking each auxiliary loop to its respective test loop, allowing a precise control of the operating conditions imposed upon the HVAC unit tested, on both the source and load sides. Each auxiliary loop has a pump equipped with a variable-frequency-drive (VFD) allowing for changing mass flow rates up to 7.6 L/s. Each auxiliary loop is also equipped with an insulated 974 L tank which adds some thermal mass to the system to help stabilise the test-bench's control algorithm. Several PT-100 platinum resistance sensors installed throughout the auxiliary loops, downstream from each heating/cooling unit, allow for accurate monitoring of the evolution of loop temperature. These sensors provide feedback to the system controlling the test bench through the choice of unit set points, control valve opening and pump flow rates.

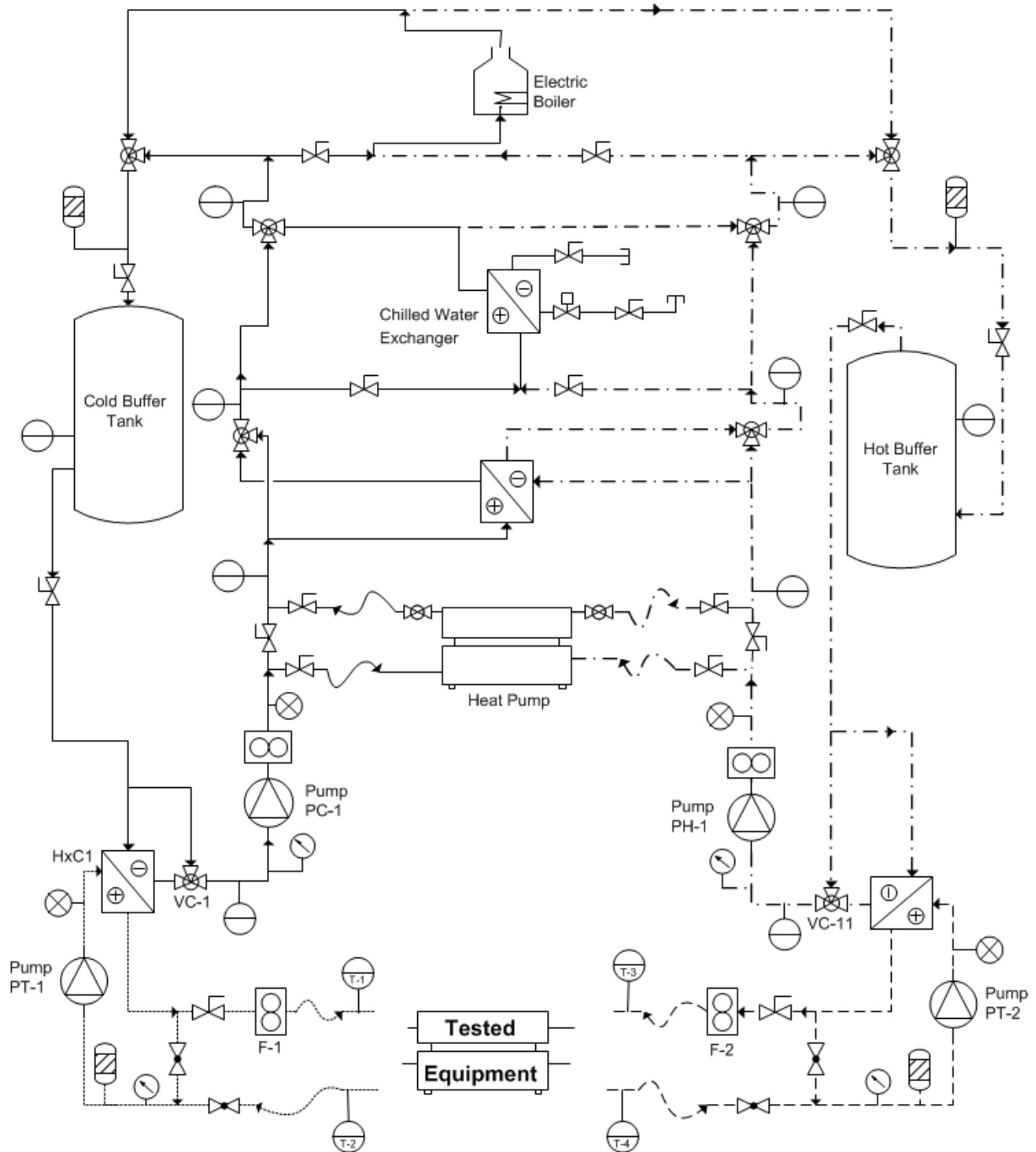


Figure 5: Hydronic test bench

6. RESULTS

Simple tests were performed to confirm the applicability of the proposed method and the correct operation of the code developed in LabVIEW and TRNSYS.

This section will present some results obtained in a configuration where the tested equipment is simply the lab itself. In Figure 5 above, the two test loops are connected to form an “8”, with T-1 connected to T-4 and T-2 connected to T-3. The two test loop pumps (PT-1 and PT-2) are in series and controlled to impose the same flowrate in F-1 and F-2, according to the setpoint coming from the simulation. The “warm” auxiliary loop of the lab (on the right in Figure 5) plays the role of the tested equipment, and represents a heating plant. The control valve VC-11 is left at a fixed position and not actively controlled. The lab’s “cold” auxiliary loop (on the left

in Figure 5) is used to provide a controlled cooling rate through HxC1, and the VC-1 control valve is actively controlled to impose T-1 at values coming from the TRNSYS simulation. The boiler is used on the “warm” side. It has a constant setpoint of 65 °C but the VC-11 control valve is only half-open which provides a limited heating capacity (and fluctuating temperature) to the test loop. The “cold” side is connected to the building chilled water loop which has a very large capacity and is approximately maintained at 7 °C. This test setup is capable of providing more cooling than heating power to the test loops – it is used here to model a limited-capacity heating plant serving a heating load.

Figure 6 shows a schematic view of the TRNSYS simulation. A simple building is heated by a radiator connected to a main heating loop. The weather conditions and internal gains are kept constant for this simple test, and lead to an average heating demand of 20 kW (16 kW to the radiator, with large fluctuations over time, and 4 kW in standby losses, almost constant). The 3-way valve supplying the radiator is controlled by an ON/OFF thermostat maintaining the room temperature at 21 °C with a 2 °C deadband. The radiator has a rated capacity of 50 kW at a supply temperature of 65°C and a room temperature of 20 °C. The heating loop is simply modeled by supply and return pipes and a buffer tank (100 L) modeling additional thermal mass and standby losses in the system. The circulating pump is always ON and imposes a flowrate of 0.5 kg/s, which is the rated flowrate of the radiator.

Two options are illustrated in Figure 6: in TRNSYS-only mode, a simple (perfect) heater is modeling the heating plant. It is controlled to maintain a constant supply temperature of 65 °C to the heating loop, and its heating power is unlimited. In the LabVIEW mode, the heating plant is replaced with data coming from the real equipment in the laboratory. The inputs to the LabVIEW component are the return temperature and flowrate from the heating loop, which are imposed as setpoints to the test loop (respectively T-1 and F-1). The outputs from the LabVIEW component come from LabVIEW: T-3 and F-2, which represent the outlet conditions from the heating plant.

The data acquisition and control time step is set to 1 sec and the TRNSYS simulation time step is varied between 10 sec and 1 min.

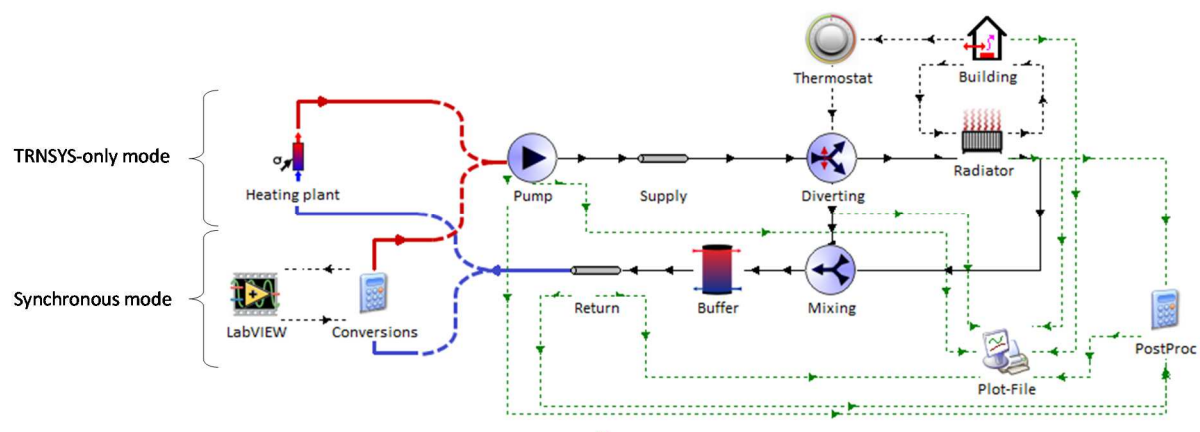


Figure 6: TRNSYS simulation (stand-alone and synchronous modes)

Figure 7 shows the results obtained from a TRNSYS-only simulation. The heating plant has an unlimited capacity, and maintains a constant supply temperature of 65 °C. The initial conditions set the building at a temperature of 22 °C, so for almost one hour the thermostat is OFF, no water flows to the radiator and the heating plant only has to compensate for the standby losses. After approximately one hour, the building temperature reaches 20 °C and the thermostat switches the diverting valve to send the full flow to the radiator. The heat emitted by the radiator

goes up to 50 kW and then gradually decreases as the room temperature increases (note that the simple radiator model does not account for thermal mass in the radiator itself). The total heating power compensated by the heating plant rises to its maximum value more slowly due to the thermal mass in the system. After approximately 30 min, the building reaches 22 °C and the thermostat switches the control valve OFF, stopping the flow towards the radiator. The total heating power then gradually goes back down to 4 kW (standby losses). This cycle is then reproduced with approximately one hour OFF, 30 min ON.

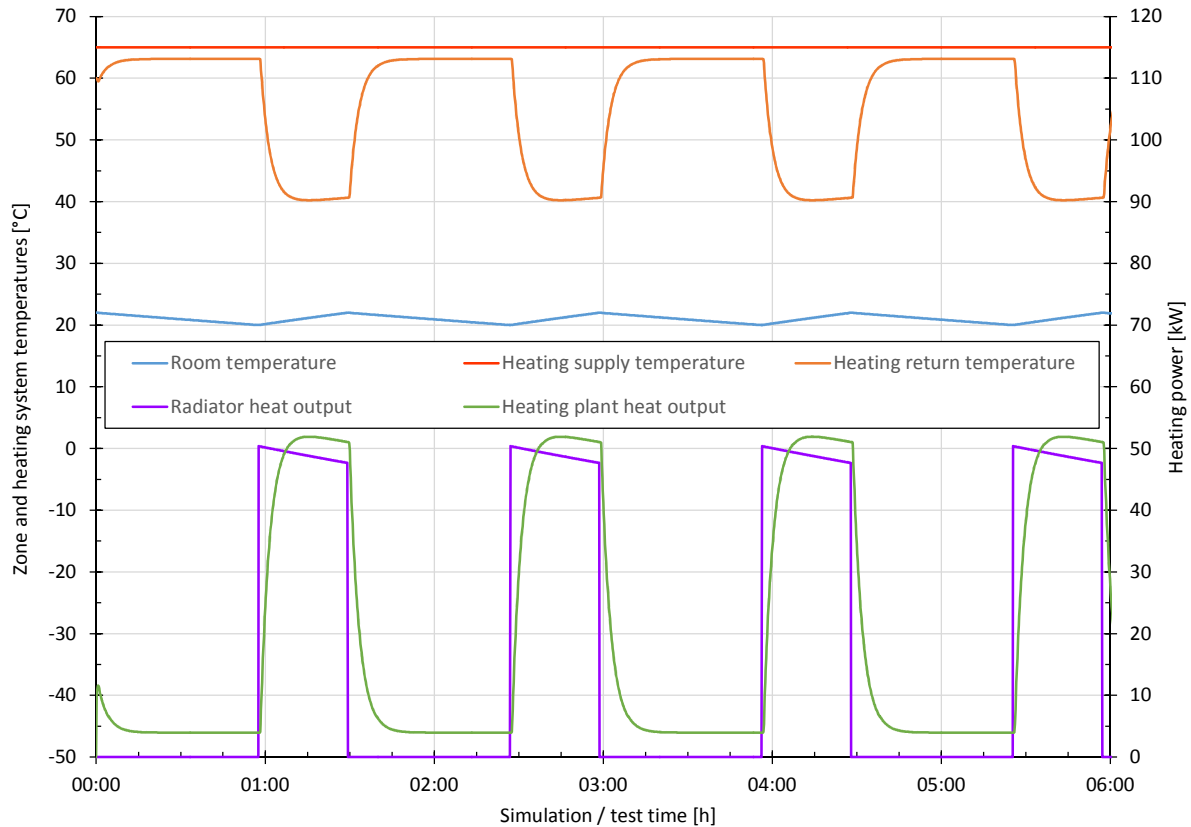


Figure 7: Simulation results (TRNSYS-only)

Figure 8 shows the results of the same test in synchronous (HIL) mode. The heating demand is successfully imposed on the HIL equipment. The most obvious effect is the drop in the heating supply temperature (in the laboratory setup, the available heating power is limited by the VC-11 control valve setting). When the thermostat switches ON, the water supply temperature drops from about 65 °C to temperatures around 53 °C. The results also show that information is successfully sent back from the real lab to the simulation: the drop in water supply temperature leads to a different heat output from the radiator, a different return temperature, and the building takes longer to heat up from the lowest point of the dead-band (20 °C) to the highest point (22 °C). So the ON/OFF cycles are markedly longer (for the heating up part), and fewer cycles are completed per hour.

As explained above, the TRNSYS simulation receives the measured heating supply temperature and calculates the behaviour of the building with the heating system and controller. This results in a water return temperature that is sent to the lab and used as a setpoint for the control valve VC-1. The achieved control is not perfect in the current lab setup, which explains the difference between the plain orange line (water return temperature effectively imposed during the interval between two TRNSYS calls) and the dotted black line (setpoint).

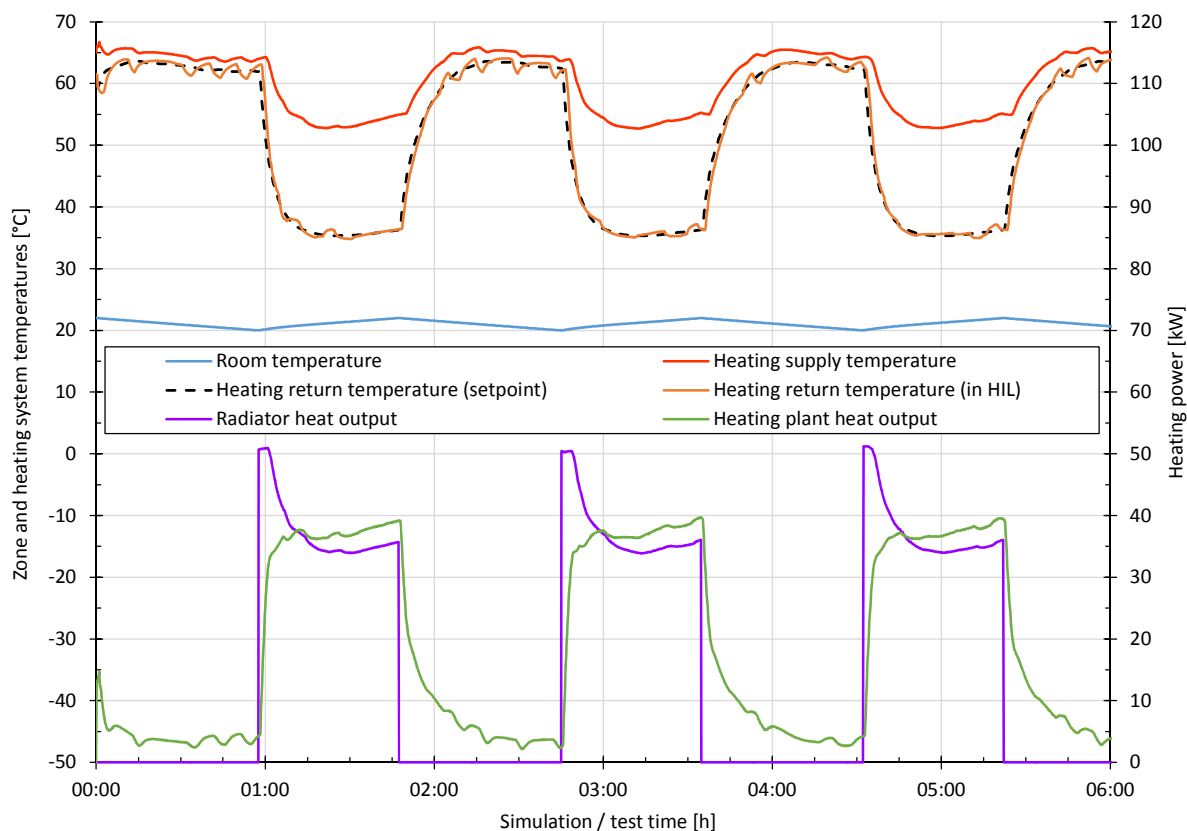


Figure 8: HIL test (LabVIEW and TRNSYS in Synchronous mode)

7. CONCLUSIONS

A new method is proposed to perform Hardware-in-the-Loop (HIL) testing with TRNSYS and LabVIEW. A bidirectional data exchange is implemented between the two programs in a flexible way. The LabVIEW VI's developed for this application essentially consist of a shell for handling the data exchange and a "lab" VI that can be tailored to different hardware setups. The TRNSYS implementation encapsulates all communication within a new TRNSYS component (Type 131) and performs efficient data exchange by loading the TRNSYS DLL from the LabVIEW application. The method is demonstrated using a hydronic heating loop in the SemiVirtual Lab at Polytechnique Montréal. Bidirectional data exchange is achieved with the simulation imposing setpoints to the lab and real equipment performance affecting simulation results in real-time.

Future work will aim at testing the software in a different laboratory with the ability to include air-based components (and therefore data exchange of humidity in addition to temperature and flowrate). Experimental testing using the software will continue on compact storage tanks (using one inlet and one outlet) and heat pumps (using 2 inlets and 2 outlets).

REFERENCES

- Beausoleil-Morrison, I., Macdonald, F., Kummert, M., McDowell, T. & Jost, R., 2013. *Cosimulation between ESP-r and TRNSYS*, Journal of Building Performance Simulation, volume 1-19, 2013.
- Bourke, G. & Bansal, P., 2010. *Energy consumption modelling of air source electric heat pumpwater heaters*, Applied Thermal Engineering 30, 1769-1774.

- Byrne, P., Miriel, J. & Lénat, Y., 2012. *Modelling and simulation of a heat pump for simultaneous heating and cooling*, Building Simulation, September 2012, Volume 5, Issue 3, pp 219-232.
- Klein, S. A., 1979. *TRNSYS: A transient simulation program*, Solar Energy Laboratory, University of Wisconsin-Madison, 1979.
- Lahrech R., Gruber P., Riederer P., Tessiera P., Visier J. C., 2002. *Development of a testing method for control HVAC systems by emulation*, Energy and Buildings, Vol3, Issue 9, pp 909-916.
- Lahrech, R., Gruber, P., Riederer, P., Tessier, P. & Visier, J. C., 2007. *Simulation Models for Testing Control Systems for HVAC Applications*, Seventh International IBPSA Conference, Rio de Janeiro, Brazil, 2001.
- Leconte, A., Achard, G. & Papillon P., 2012. *Solar Combisystem Characterization with a Global Approach Test and a Neural Network Based Model Identification*, SOLAR ENERGY, VOLUME 86, ISSUE 7, JULY 2012, PAGES 2001–2016.
- Liu, M., Bruno, F., & Saman, W., 2011. *Thermal performance analysis of a flat slab phase change thermal storage unit with liquid-based heat transfer fluid for cooling applications*. Solar Energy, Vol. 85, pp 3017-3027, 2011.
- Nouidui, T. S., Wetter, M., Li, Z., Pang, X., Bhattacharya P. & Haves, P., 2011. *Bacnet and Analog/Digital Interfaces of the Building Controls Virtual Testbed*, 12th Conference of International Building Performance Simulation Association, Sydney, Australia, 2011.
- Otten, R., Li, B. & Alleyne, A., 2010. *Hardware-in-the-Loop Load Emulation for Air Conditioning and Refrigeration Systems*, International Refrigeration and Air Conditioning Conference at Purdue, 2010.
- Pan, Y., Lin, X., Huang, Z., Sun, J. & Ahmed, O., 2011. *A Verification Test Bed for Building Control Strategy Coupling TRNSYS with a Real Controller*, 12th Conference of International Building Performance Simulation Association, Sydney, Australia, 2011.
- Peitsman, H.C., Wang, S., Karki, S.H., Park, C., Haves, P., 1994. *The reproducibility of tests on energy management and control systems using building emulators*, Ashrae Transaction, Vol. 100, pp.1455-1464
- Riederer P., Partenay, V. & Raguideau, O., 2009. *Dynamic Test Method for the Determination of the Global Seasonal Performance Factor of Heat Pumps Used for Heating, Cooling and Domestic Hot Water Preparation*, Eleventh International IBPSA Conference, Glasgow, Scotland, 2009.
- Rheea K. N., Yeo M. S., Kimb K. W., 2011. *Evaluation of the control performance of hydronic radiant heating systems based on the emulation using hardware-in-the-loop* Santori, M., 1990. *An Instrument that Isn't really* (Laboratory Virtual Instrument Engineering Workbench), Spectrum, IEEE27, no.8, 1990, 36-39.
- Wetter, M., 2011. *Co-simulation of building energy and control systems with the BuildingControls Virtual Test Bed*, Journal of Building Performance Simulation, Journal of Building Performance Simulation, Vol. 4, Issue 3, pp. 185-203

Experimental study on a new energy-efficient VRF system

Xiaochen Mao*, Jianjun Xia¹

⁽¹⁾ Building Energy Research Centre, Tsinghua University, Beijing, China.

1. ABSTRACT

A new energy-efficient variable refrigerant flow (VRF) system was presented. The system consists of one outdoor unit and five indoor units, same as the normal, with improved control strategy: by controlling expansion valves (EXV), indoor fans and compressors co-ordinately, the VRF system keeps indoor thermo temperature near the set value and gets high energy efficiency ratio (EER) at partial loads. To control the indoor temperature more stable, EXVs and indoor fans act continually, instead of on-off switch. To get higher partial load EER, this study presented a method to calculate optimal evaporating temperature, which is lower at larger cooling load and higher at less load. So that the outdoor unit consumed less energy at partial loads. To test the new efficient control strategy, a series of experiments were carried out besides simulation in this study. The results indicated that the control error of indoor temperature is less than 1°C while the normal systems can just keep it to more than 2°C. And partial loads EER is increased obviously compared to main companies' VRF products in real using conditions.

Keywords: VRF, control method, partial load

2. INTRODUCTION

VRF system have been promoted as an alternative to typical centralized HVAC systems. In VRF systems, each unit can be controlled and adjusted individually, satisfying the occupants' comfort levels. As it has these advantages, VRF system has been widely used in various kinds of buildings. In offices and school buildings, people want to control the indoor units individually. Well, for hospitals and wards, HVAC system should avoid the air of different rooms being combined to prevent disease spread. In addition, the historical buildings have benefited from the minimum alterations needed for the addition of a multi-split VRF system. Retrofit situations can also be good applications for the ductless systems since additional ductwork can be minimized with the multi-split VRF systems compared to ducted systems.

HVAC systems are reported to consume as much as 40% of the energy consumption of the building. Many efforts have been spent to design new efficient types of air conditioning systems. VRF system changes refrigerant flow to adapt to cooling load change, so it has high energy efficiency at partial loads. Moreover, the control strategy affect the operating a lot. As shown by Xia et al. (2002), on-off control method, which means EXV swifts off and on to control the indoor temperature, is a normal control strategy, but the temperature changes in relatively big wave. Besides, the system tends to go unstable with small numbers of working indoor units. In the other control method, EXV changes the opening continually to keep indoor thermo comfort, and the compressor changes speed referring to certain low pressure region. The temperature is controlled more precisely, but it causes the problem of high superheat sometimes. Wang carried out several experiments to study how unevenness index affect system's energy efficiency, and results showed unevenness index hardly affected COP with the control method of keeping certain low pressure rage (Wang, et al, 2010). Zhao showed a model written with C++ to simulate VRF systems working in different conditions. He concluded that refrigerant pipe length affected COP at high cooling load, and suggested that when designing VRF system as a HVAC plan, indoor units should better be put to rooms with almost the same cooling load (Zhao, 2009).

Based on previous studies, this paper presented a control method to improve VRF's energy efficiency. The compressor constitutes the maximum part of the whole system's energy use. So we have to decrease compressor's energy consumption to raise energy efficiency. And on the premise of guaranteeing the indoor units refrigeration effect, higher evaporating temperature benefits the systems' EER because of less compressor's output capacity. Therefore the question goes to how to get the optimal evaporation temperature in every different conditions. In this study, indoor fans adjust speed according to the change of return air temperature to make it close to set value. EXVs keep the super heat around 2°C . Meanwhile the compressors collect of indoor units' operating data to decide output capacity. The control method will be well described in the next part. In this study, the control program was written to the chip of GMV5S VRF product, and experiments were carried out at the enthalpy laboratory of GREE Electric Appliance Co. LTD (China Company). Although these tests are in the lab, we design conditions to simulate real office rooms.

3. CONCLUSION

3.1 Laboratory

The outdoor unit was set in an outside-box, with the size of $4.5\text{m} \times 4.5\text{m} \times 4\text{m}$. The walls have good heat preservation performance, so that there is little heat transfer from outside ambient. Furthermore, the room is equipped with a cooling/heating system to make a certain thermo environment with the sensors of dry bulb and wet bulb temperature. And the five indoor units were set dividedly in three inside-boxes, the differences are the inside-box rooms are equipped with air flow box and temperature sensors to test cooling capacity (Figure 1).

3.2 VRF system

The parameters of VRF system are shown in Figure 2. The system charged with R410a had two frequency conversion compressors, and the whole cooling capacity is about 40kW . Five indoor units (14kW , 11.2kW , 6.3kW , 5kW , 3.6kW) were connected to the VRF system.

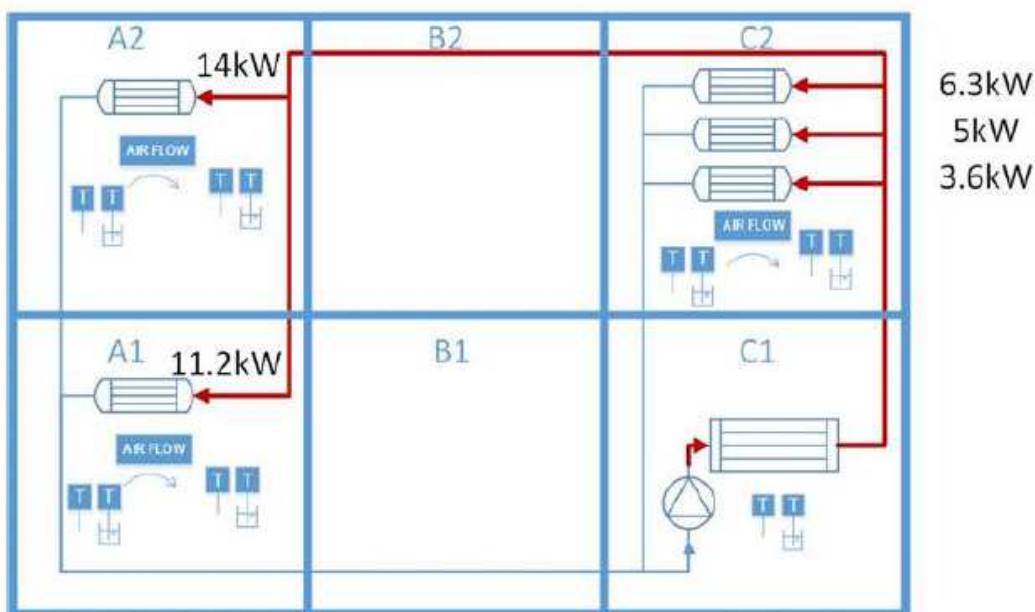


Figure 1: The installation on the VRF system

Table 1: Equipment nameplate

	Items		Quantity
Outdoor	Compressor	No.1	70Hz (frequency convertible scroll compressor, type number: E656DHD-65D2YG)
		No.2	90Hz (frequency conversion)
	Fan	No.1	70Hz (frequency conversion)
		No.2	70Hz (frequency conversion)
Indoor	Cooling capacity (Fan max speed)	No.1	14.0kW (1300rad/min)
		No.2	11.2kW (1300rad/min)
		No.3	6.3kW (1300rad/min)
		No.4	5.0kW (1300rad/min)
		No.5	3.6kW (1300rad/min)
		Sum	40kW

The testing bench included temperature and pressure of the refrigerant side. The VRF system can also record compressor speed, fan speed and expansion valve steps timely (Figure 2).

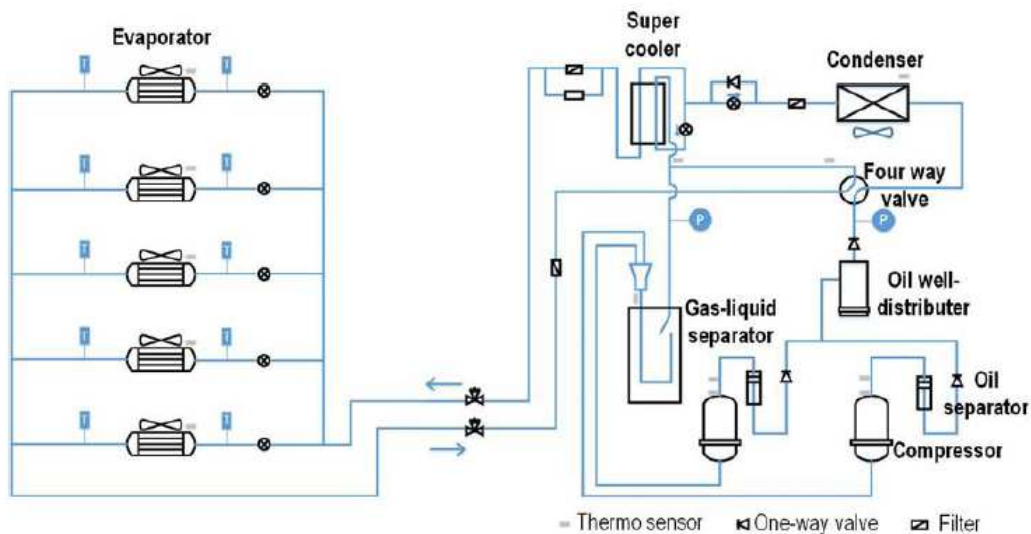


Figure 2: Schematic diagram of the VRF system

4. CONTROL STRATEGY

The common control method used in VRF system was using expansion valves to control indoor temperature, and a certain pressure value was taken as basic parameter target to regulate the compressor's output capacity.

Differing from other control methods, this one aims to improving the operation efficiency by increasing low pressure while assuring the indoor comfort. Namely, air flow of indoor is not controlled by users, but is used as one of the control variable. Fan frequency changes according to indoor temperature (using PI algorithm), while the expansion valve changes the opening to keep the super heat around 2°C. Compressors of outdoor adjust output according to the indoor cooling load. If the cooling load is at low partial ratio, the compressors decrease output capacity.

- 1) Indoor fan uses PI algorithm, the control parameters of which have been already adjusted to appropriate value through

$$S_{PI} = \beta/100 \cdot S_{max} \quad (1)$$

Where:

S_{PI} is the target fan speed §calculated every 40s),

β is the speed coefficient operated by PI control method,

S_{max} is the maximum fan speed.

- 2) Expansion valve can change the opening steps from 80 to 480PLS steps to keep the super heat around 2°C.
- 3) The compressors adjust output capacity (every 7 circles, 280s) according to the information from indoor units. Indoor units sent three items back, one is indoor ambient temperature, and one is integral item and another is fan speed. Specially, if one indoor unit satisfies three conditions as follows, it sends “1” to outdoor unit. Or it sends “0”.

$$|T_{set} - T_{amb}| \leq 0.6 \quad (2)$$

$$Max(Output_I) - Min(Output_I) \leq 2 \quad (3)$$

$$\beta_{avg} \leq 90 \quad (4)$$

Where:

T_{set} is the set value of indoor temperature,

T_{amb} is the average indoor ambient temperature in 280s,

$Max(Output_I)$ is the maximum of integral item among 7 samplings,

$Min(Output_I)$ is the minimum of integral item among 7 samplings,

β_{avg} is the average of β s in 280s.

The compressors regular output capacity with these “0”s and “1”s sent from indoor units. The control process is shown in Figure 3. When 80%-100% indoor units sent 1 to outdoor unit, it means most indoor units have got the set value while indoor fans are not at high speed, so there is space to raise evaporation temperature. In that condition, the compressor should reduce some output. The compressor work automatically following the control strategy at other conditions (Figure 3).

5. VALIDATION OF THE CONTROL STRATEGY

5.1 Test results of a certain condition

- 1) Temperature. At the first period (about 30 minutes), return temperature of each indoor unit decreased sharply, and then went to the target to the target control region ($27 \pm 1^\circ\text{C}$). Which means the indoor unit can cool room quickly and control the temperature precisely during the stable period (Figure 4).
- 2) Fan speed. Figure 5 shows the timely change of fan speed of indoor units. At the quick-cooling part, the fans were all operating at highest speed. As the fan speed were controlled by PI method, with temperature getting close to the set value, fan temperature getting close to the set value, fan speed also declined. But remind that, compressors regulated output capacity according to partial load ratio. If the compressor cut down the output, the indoor temperature will raise as result, and the fan, will change speed as well. When it went to

stable period, the fans are all at a high speed, and the evaporate temperature of indoor unit cannot raise anymore.

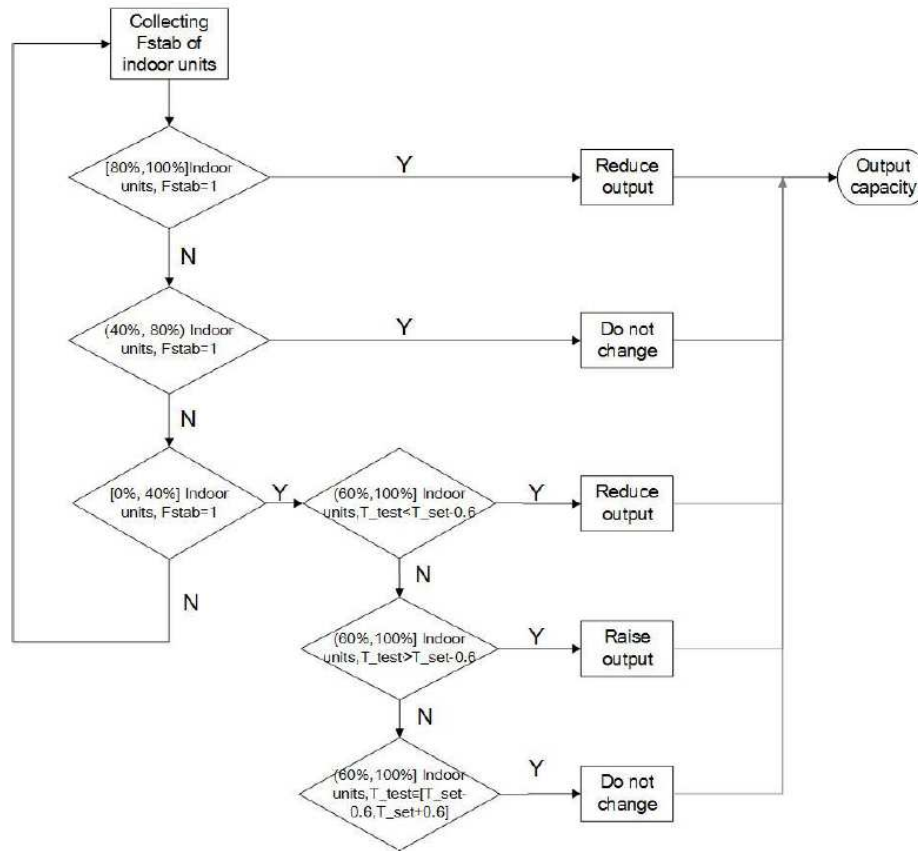


Figure 3: Control logic diagram of compressors

- 3) EXV. Take indoor unit 4 as an example to see how the expansion valve control the superheat. It's shown in Figure 6 that the superheat was controlled within the scope around 2°C though the expansion valve adjusting the opening steps continually. Overall, the indoor units could make the superheat fluctuate around 2°C.
- 4) Compressors. The compressors adjusted output capacity following the control method. At first, the compressors had work hard to cool the room, and then decline the output to raise up evaporate to an appropriate value (Figure 8). During the stable period, the average evaporating temperature is 14°C (much higher than a conventional VRF system), and the average condensing temperature is 41°C (Figure 9).
- 5) Efficiency. By collecting the power consumption of the whole system and cooling capacities of indoor units, EER was calculated as follows. Energy consumption of each part was shown in Table 2.

$$EER = \sum \frac{Q_I}{W} = \frac{15.73kW}{3.9kW} = 4.04.$$

Table 2: Details of energy consumption.

	Outdoor Consumption			Indoor Consumption /W
	Compressors /W	Fans /W	Total /W	
Average	3079	433.5	3512.5	376
Proportion	87.7%	12.3%	90.3%	9.7%

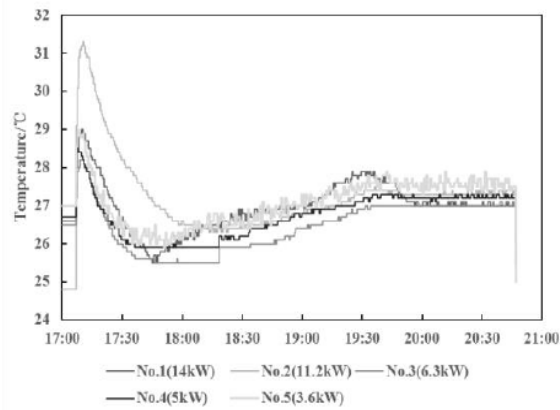


Figure 4: Temperature change of the rooms

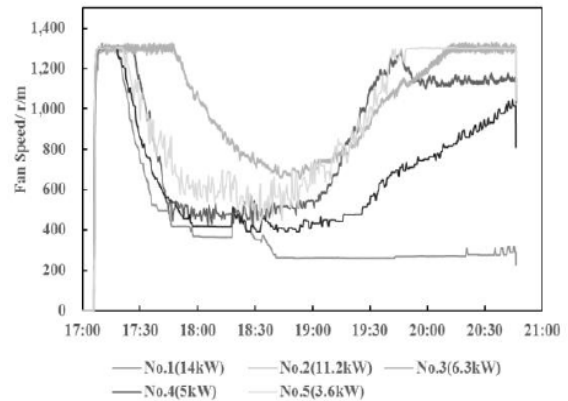


Figure 5: Fans speed change of IDUs

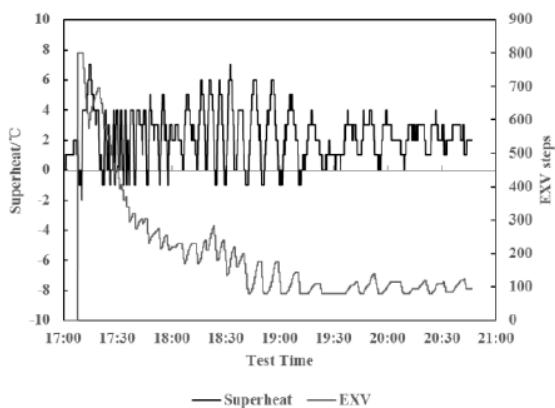


Figure 6: Superheat change with EXV (IDU4)

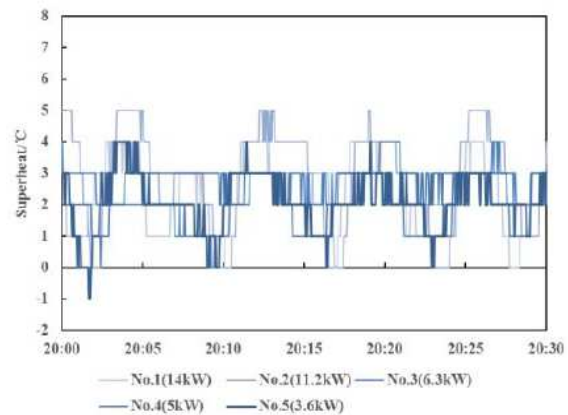


Figure 7: Superheat change IDUs

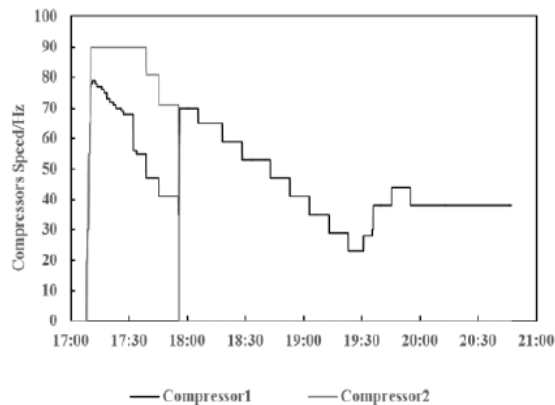


Figure 8: Output of compressors

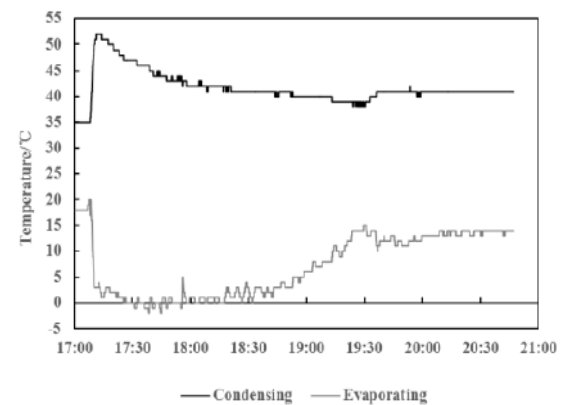


Figure 9: Evaporating and condensing T

5.2 Comparison of various testing results

In order to look into how the control measure work in variable conditions, a couple experiments were carried out.

- 1) Under the condition of $T_{set} = 25^{\circ}\text{C}$, we changed the partial load ratio to see the change of system EER. The Figure 10 shows that the EER increased with the increase of PLR, and then reduce with the increase of PLR. The reason of that is presented in Figure 11 and Figure 12 when the PLR was too small, the power consumption of compressor changed a little with

the decrease of PLR. The indoor unit had to keep the evaporating temperature lower than the supplying air, so even if the PLR is smaller the evaporating temperature couldn't rise anymore (Figure 10).

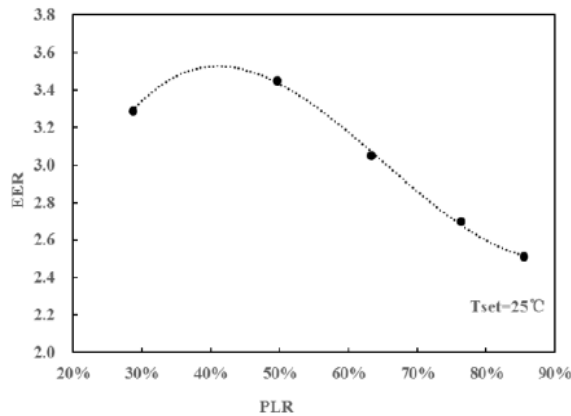


Figure 10: Temperature change of the rooms

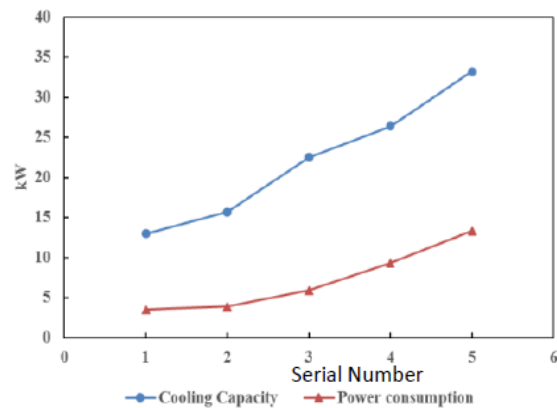


Figure 11: Fans speed change of IDUs

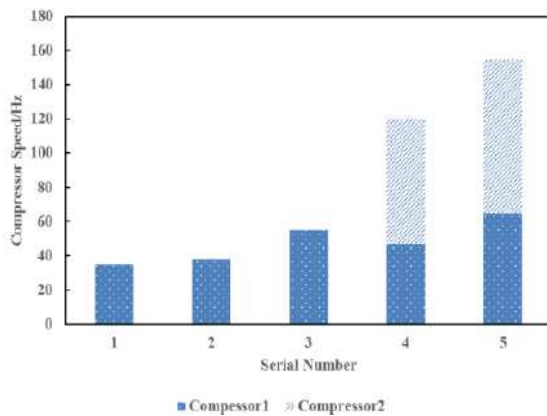


Figure 12: Superheat change with EXV (IDU4)

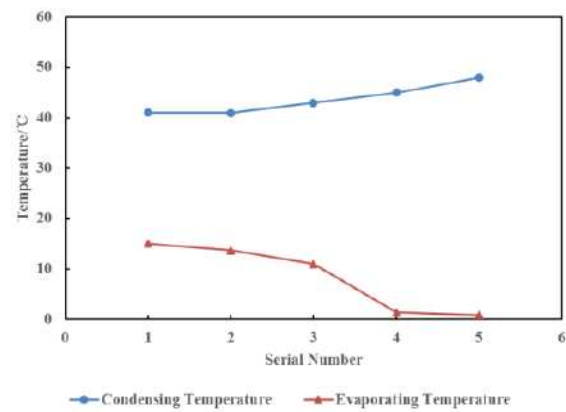


Figure 13: Superheat change IDUs

Table 3: Details of test results.

	PLR	Cooling Capacity kW	Power Consumption kW	EER	T _{set} °C	T _{outdoor_amb} °C
1	29%	11.47	3.49	3.29	25	35
2	50%	19.86	5.75	3.45	25	35
3	63%	25.33	8.29	3.05	25	35
4	76%	30.54	11.31	2.70	25	35
5	86%	34.21	13.65	2.51	25	35

2) As to conditions of T_{set} = 27°C and T_{set} = 20°C, EERs calculated were shown in the Figure 14. We can see the trend that the EER is higher T_{set} with higher value, because if the T_{set} is higher, the evaporating temperature can be higher, which do help to improve compressors' operation. When T_{set} was set low, the cooling system had to keep the evaporating temperature at a low range, so there is little space for compressors to reduce output capacity in partial load conditions. (Figure 14)

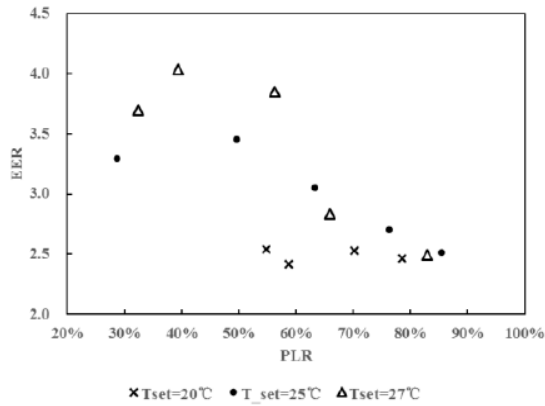


Figure 14: EER with different T_{set}

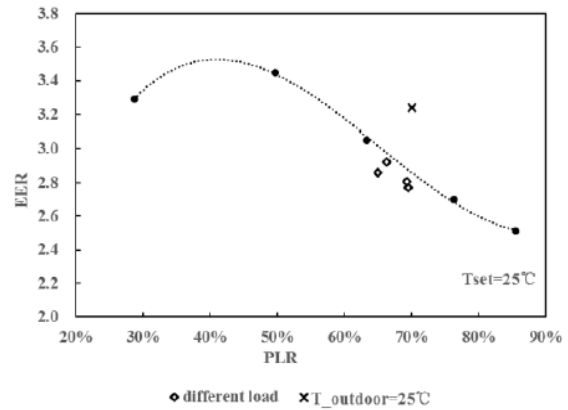


Figure 15: EER of uneven load & different $T_{outdoor}$

3) In practical, PLRs of indoor units are different from each other. Here are some testing results of different partial load conditions. Although indoor ambient temperature were all controlled precisely, the comprehensive energy efficiencies all went down comparing to even cooling load conditions (Figure 15).

Table 4: Test results of uneven load conditions.

	PLR				Cooling Capacity kW	Power Consumption kW	EER
	Total	A1	A2	C2			
1	65.1%	70.5%	75.2%	51.0%	26.0	9.1	2.858
2	66.2%	63.7%	79.8%	54.7%	26.5	9.0	2.925
3	69.2%	72.1%	67.9%	67.9%	27.7	9.9	2.806
4	69.5%	73.4%	76.9%	59.2%	27.8	10.0	2.770

4) In real conditions, outdoor ambient temperature changes a lot. To see the influence on the system by outdoor thermo environment, we took series of experiments, the results of which are shown in Table 5. Lower outdoor temperature is helpful to improve the efficiency.

Table 5: Test results of different $T_{outdoor}$

	PLR	Cooling Capacity kW	Power Consumption kW	EER	T_{set} °C	$T_{outdoor_amb}$ °C
Experimental	56%	22.3	7.00	3.17	25	30
Reference	58%	23.1	7.60	3.04	25	35
Experimental	70%	28.0	8.60	3.24	25	25
Reference	74%	29.4	9.86	2.98	25	35

5) In some conditions, users may set different temperature for indoor units. To make sure if the VRF system can control the temperatures well, a couple of experiments were carried out. Description of the conditions are shown in table. And the average temperature of each indoor units during stable period are shown in table. In the first condition, two of the indoor units were set to 24°C, while the others were 27°C. And the result shows that the real average temperature of indoor ambient is close to the set value, the errors are limited to 0.5°C. In the second condition, temperature set value of those two indoor units decrease to 20°C, while the others were still 27°C. Now that those two indoor ambient temperature went out of control, though the fans had already reached the max speed. The same thing happened in condition 3 and condition 4. The reason is that the compressor had a low

pressure limitation, which regulated the low temperature lower than 0°C to avoid the indoor units frosting. As we can see in Table 9, the compressors are not at the max speed, if we improve the control strategy, we can control the temperature in condition 2, condition 3 and condition 4. In the fifth condition, one of four indoor units set 20°C was out control, due to the control strategy allow 20 percent indoor units be out of the scope. If the four indoor units raise temperature set value to 25°C, all of them were well controlled.

Table 6: Test results of uneven T_{set}

	PLR	Cooling Capacity kW	Power kW	EER	T_{set} °C					$T_{outdoor}$ °C
					14.0 kW	11.2 kW	6.3 kW	5.0 kW	3.6 kW	
1	57%	22.6	7.9	2.872	24	24	27	27	27	35
2	60%	23.7	9.5	2.500	20	20	27	27	27	35
3	60%	23.7	8.4	2.824	20	27	27	27	27	35
4	53%	21.2	6.4	3.341	16	27	27	27	27	35
5	62%	24.7	9.3	2.652	30	20	20	20	20	35
6	40%	15.8	3.8	4.193	30	25	25	25	25	35

Table 7: Temperature of indoor units

	14kW	11.2kW	6.3kW	5kW	3.6kW
1	24.0	24.1	27.0	27.0	27.5
2	22.3	23.8	27.0	27.0	27.5
3	22.1	27.0	27.0	27.0	27.5
4	20.7	27.0	27.0	27.1	27.4
5	30.1	23.1	20.1	20.2	20.4
6	30.1	25.2	24.9	25.0	25.2

Table 8: Speed of indoor fans

	14kW	11.2kW	6.3kW	5kW	3.6kW
1	1082	1299	411	414	1300
2	1301	1301	343	505	1300
3	1300	747	427	371	1300
4	1300	1217	588	1233	1301
5	663	1300	1300	1300	1300
6	699	1301	395	701	1301

Table 9: Test results uneven T_{set}

	Condensing Temperature/°C	Evaporating Temperature/°C	Compressor1 /Hz	Compressor2 /Hz
1	43.8	3.1	38	66
2	44.5	0.7	45	78
3	44	1	41	71
4	44	9	60	0
5	45	2	44	76
6	41	12	37	0

6. CONCLUSION

The proposed method is an optimal one based on previous controlling strategy. It is verified that the system could control indoor temperature more precisely and work more efficiently at partial load. Test results indicated that the system could reduce energy consumption significantly by raise evaporation temperature at small partial load. However, if the indoor units had uneven loads, the system EER couldn't get high value, which told the HVAC engineering designers to not set VRF's indoor units to those rooms having extremely different cooling loads from each other.

In this study, experiment tests were described in details in spite of programming process or correction which actually took more time working on. Further study will focus on strategy optimal to make it more suitable for real buildings. Optimal work will also involve improving robustness and reliability, maybe some simulation will help accomplish the study.

REFERENCES

- Goetzle, W., 2007. Variable refrigerant flow systems. *ASHRAE journal*.49, 24-31. Yonghua Zhu, Xinqiao Jin, Xing Fang, Zhimin Du, 2014. Optimal control of combined air conditioning system with variable refrigerant flow and various air volume for energy saving. *International Journal of refrigeration* 42, 14-25.
- Chua, K.J., Chou, S.K., Yang, W.M., Yan, J., 2013. Achieving better energy-efficient air conditioning- a review of technologies and strategies. *Appl. Energ.* 104, 87-104.
- Jianjun Xia, Eric Winandy, Bernard Georges and Jean Lebrun, 2002. Testing Methodology for VRF Systems, Proceedings of the International Refrigeration and Air Conditioning Conference at Purdue July, USA.
- Choi J M, Kim Y C, 2003. Capacity modulation of an inverter-driven multi-air conditioner using electronic expansion valves. *Energy*, 28: 141-155.
- Wei Zhao, 2009. Study on part load performance of variable refrigerant flow system. Beijing, Tsinghua University.
- Matsuok H. Development of VRV System for Renewal .*Refrigeration*, 2004, 79(5): 58-60.
- Japan Air Conditioning, Heating & Refrigeration News. JARN. 2004, 430.
- Ichikawa T, Yoshida S, Nobe T. Running Performance of Split-type Air Conditioning Systems installed in School and Office Buildings in Tokyo. *International Refrigeration and Air Conditioning Conference at Purdue* 2008.
- Winkler J, Aute V, Radermacher R. Comprehensive investigation of numerical methods in simulating a steady-state vapor compression system. *International Journal of Refrigeration*, 31 (5): 930-942.
- Park Y C, Kim Y C, Min M K. Performance analysis on a multi-type inverter air Conditioner. *Energy Conversion & Management*, 2001, 42: 1607-1621.
- Shao S Q, Shi W X, Li X T, et al. Simulation model for complex refrigeration systems based on two-phase fluid network - part I: model development. *International Journal of Refrigeration*. 2008, 31 (3): 500-509.
- Xuhui Wang, Jianjun Xia, Chen Peng, Da Yan, Yi Jiang, 2010. Experimental tests on VRF system at part load conditions. *Building Science* 26, 151-156.

SIXTH SESSION
**BUILDING MODEL
VALIDATION**

Calibrating whole house thermal models against a coheating test standard: solid wall case studies

James Parker^{1*}, David Farmer¹, Martin Fletcher¹

⁽¹⁾Leeds Beckett University, Leeds, UK

1. ABSTRACT

Accurately predicting building energy performance is becoming increasingly important due to rising fuel costs, fuel shortages and anthropogenic carbon dioxide emissions. Despite the significance of these predictions there is often a substantial gap between the predicted and the actual in-use energy consumption; this can mean that the energy use and utility costs in-use are much higher than originally expected. This paper describes a methodology for calibrating the predicted fabric performance of a dwelling with as-built measured results by combining Dynamic Thermal Simulation (DTS) techniques and the recorded data from *in-situ* fabric performance testing. Using such a method it is possible to recreate the environment of a coheating test using DTS software, enabling the predicted heat loss coefficient of the whole building fabric to be calibrated against measured test results. This eliminates the need for actual year weather files, occupancy data and operating profiles which are required to calibrate a model when following more established methodologies. A refined baseline model can then be used to predict the performance of a dwelling under different occupancy and operating patterns and to more accurately predict the impact of retrofit measures and fabric upgrades in particular; this could have important implications for policy instruments and incentives for low-energy retrofit.

Keywords: Calibration, Domestic, Energy Performance, Thermal Modeling

2. INTRODUCTION

In the United Kingdom (UK), there are approximately twenty-eight million dwellings (HM Government, 2014) and the housing stock increases by an estimated 0.8% per year, although this will need to rapidly increase if projected increases in population are to be accommodated by 2050 (Ravetz, 2008). Domestic buildings account for just under 30% of the UK's total CO₂ emissions (DECC, 2013a), It is expected that the vast majority of existing housing will still be in use by 2050 (Boardman, 2007; Kelly, 2009 & Killip, 2008) and it is therefore through retrofit that the greatest carbon emission savings are likely to be realised in this sector. Both new build and existing dwellings that are being either sold or rented are required under national law to produce a prediction of their energy consumption in accordance with the European Directive 2002/91/EC (Department for Communities and Local Government, 2008). In the UK, this takes the form of an Energy Performance Certificate (EPC) which benchmarks a specific dwelling against a national standard. These EPCs are produced using the Standard Assessment Procedure (SAP), which is a calculation methodology approved by the UK Government to meet the Part L: Conservation of Fuel and Power section of the Building Regulations (HM Government, 2010a; HM Government, 2010b).

There are limitations to the effectiveness of existing methodologies that estimate building energy consumption for compliance purposes and these are described further in the literature review that follows this introduction. A growing body of research has identified a significant performance gap between the energy consumption predicted by regulatory compliance design

calculations and actual performance (Bordass *et al.*, 2001; Carbon Trust, 2011; Austin, 2013). In the domestic sector this is particularly evident for the whole building fabric thermal performance (Zero Carbon Hub, 2010; Carbon Trust, 2011 & Stafford *et al.*, 2012).

The purpose of this paper is to define a methodology that can be used to calibrate the outputs obtained from a domestic dynamic thermal simulation (DTS) model against the *in situ* measured fabric performance of the same dwelling. The results presented here will demonstrate that a much greater degree of accuracy for fabric performance can be achieved using such a modelling approach and that the resultant predictions of energy performance are therefore likely to be more reliable. The calibration methodology has the advantage of being independent of actual weather files and occupancy data, which are a pre-requisite for other calibration approaches. Such a modelling approach will be particularly useful for existing buildings that are the subject of low-energy refurbishment.

3. LITERATURE REVIEW

3.1 Domestic Energy Modeling and the Performance Gap

The Department of Energy and Climate Change (DECC) mandate that the Standard Assessment Procedure (SAP) is used to predict the energy performance for new build dwellings in the UK (DECC, 2014; DECC, 2013b) and that reduced data SAP (RdSAP) must be used for existing dwellings. At present, SAP extensively underpins domestic building energy performance policy in the UK. As well as being central to Part L compliance, it is also used in the calculation of domestic EPCs and is linked to a raft of policies including Stamp Duty Exemption for Zero Carbon Homes, the Code for Sustainable Homes, the Feed in Tariff, the Renewable Heat Incentive and most recently, the Green Deal (Kelly *et al.*, 2012). The success of the Green Deal relies on predictions from RdSAP as it is the magnitude of utility cost savings that will dictate whether the 'Golden Rule' of payback is achieved. Despite this crucial role in UK policy, completed research has questioned the effectiveness of SAP and its fit for purpose (Carke and Reason, 2008; Kelly *et al.*, 2012).

Conventions included within the SAP methodology also restrict the accuracy of energy consumption and CO₂ emission estimates for specific buildings. In order to allow comparison across the UK, the same weather data, occupancy profiles and heating/cooling set points are used in the calculation (Kelly *et al.*, 2012). It is therefore inevitable that there will be a gap between the predicted and the actual performance for any given dwelling. In practice, this gap can be widened further in existing dwellings, due to the addition of a number of assumptions made in RdSAP that are designed to reduce the complexity of the calculation. Some of the default selections in RdSAP are the most cost efficient options which will lead to a higher rating and inaccurate estimates (Kelly *et al.*, 2012).

The energy required for space heating, domestic hot water (DHW), lighting and ventilation are all estimated in SAP (DECC, 2014). As with non-domestic buildings, the exclusion of non-regulated plug loads (equipment) from the regulatory calculations also results in a performance gap. The SAP 2012 outputs do provide an estimate of appliance energy consumption. However, this is based upon the total floor area of the dwellings and the number of occupants. Inevitably, due to the stochastic comparative behavior and variation in activities from one home to the next, this results in a difference between estimated and actual energy consumption. It is also likely that there is a greater surface area to internal volume ratio in domestic properties which at a fundamental level equates to a greater potential for fabric heat losses (Nicholls, 2009). This places more emphasis on the fabric performance of domestic properties, as it has a greater influence on total energy consumption and CO₂ emissions.

In the past, differences between predicted and monitored energy performance of housing had been attributed to variance between occupant behaviors, but it has since been shown that the building fabric performance of a dwelling can have a significant impact on energy consumption and associated CO₂ emissions (Wingfield *et al.*, 2009a; Zero Carbon Hub, 2010). A number of techniques and tools have been developed that allow the as-built performance of whole building and elemental fabric to be measured.

Established methods for evaluating whole fabric performance include the Primary and Secondary Terms Analysis and Renormalization (PSTAR) method and the Coheating test methodology. The PSTAR method allows comparison of designed and actual performance based upon field test data (Subbarao, 1988 and Subbarao *et al.*, 1988). It is essentially a modeling approach in which short term energy monitoring (STEM) tests are used to refine model input parameters which are then extrapolated to produce annual simulations. Heat flows are first calculated based upon an audit description of a building, but because measured values from the actual building differ from the audit description, the measured values will not satisfy the heat balance equation. Specific parameters are then renormalized to produce a test protocol. Site STEM tests including heat flux measurements and air pressure tests are then used to refine model inputs in an iterative process.

Neither the PSTAR nor Coheating approaches are new. The PSTAR approach was developed in the 1980s and the Coheating methodology was first developed in the 1970s (Subbarao, 1988; Sonderegger *et al.*, 1979a; Sonderegger *et al.*, 1979b and Ortega *et al.*, 1981). Recent work has focused on refining the Coheating approach as a tool that can help to identify discrepancies between predicted and actual fabric performance (Johnston *et al.*, 2013).

The Coheating test is described as “...a quasi-steady state method that can be used to measure the whole dwelling heat loss (both fabric and background ventilation) attributable to an unoccupied dwelling.” (Johnston *et al.*, 2012, p.4). As mentioned above, this is not a new concept but, despite refinement of the methodology, it is in its infancy in the UK. Unoccupied dwellings are heated to a mean elevated internal temperature for between one and three weeks dependent upon dwelling characteristics and external environmental conditions (Johnston *et al.*, 2013). Measured parameters include: electrical energy input; internal temperatures and relative humidity; and weather conditions. Monitored daily electrical energy input (heat input to the dwelling) can then be plotted against the difference between internal and external temperatures to ascertain an uncorrected Heat Loss Coefficient (HLC) in Watts per Kelvin (W/K) for the entire fabric (Johnston *et al.*, 2013).

The measured HLC can be used to compare designed with as-built performance. However, if differences between these values are identified, the Coheating test alone does not indicate the reasons for any discrepancy. However, the internal conditions present during the test are conducive to carrying out detailed forensic investigation using other measurement techniques which can collectively help to identify flaws in as-built fabric performance (Johnston *et al.*, 2013). The Coheating methodology has been successfully employed in a number of academic studies and funded research (Miles-Shenton *et al.*, 2009; Miles-Shenton, 2011; Wingfield, 2009b; Wingfield, 2011). It is also one of the techniques being used to evaluate domestic properties that form part of the Technology Strategy Board's Building Performance Evaluation Programme (Technology Strategy Board, 2012). The application of these techniques to the case study buildings is described in the methodology section.

3.2 Building Simulation Calibration Techniques

A research project commissioned by the American Society of Heating, Refrigerating and Air-Conditioning Engineers (ASHRAE) in 2003 aimed to develop a ‘coherent and systematic

calibration methodology.’ This study produced an extensive literature review of established techniques (Reddy, 2006). Replicating this exercise is not necessary, but it is beneficial to provide a synopsis of the findings. Simulation calibration is defined as a “...*process of using an existing building simulation computer program and ‘tuning’ or calibrating the various inputs to the program so that observed energy use matches closely with that predicted by the simulation program.*” (Reddy, 2006, p.227).

Informing ‘investment grade’ decisions relating to low-energy retrofits is a broadly acknowledged application of calibrated simulation (Reddy, 2006; Raftery *et al.*, 2011a; and Heo *et al.*, 2011). It is also particularly important when retrofits are multiple and interactive. In this instance, creating more accurate models of existing dwellings will allow building owners to evaluate major retrofit upgrades. Calibration techniques are divided in to four categories in the review: (a) manual, iterative and pragmatic interventions; (b) informative graphical comparative displays; (c) special tests/analytical procedures; and (d) analytical and mathematical methods.

Approach (b) utilizes different types of informative graphics but is reliant on access to extended periods of utility consumption data (Haberl and Bou-Saada, 1998), (McCray *et al.*, 1995); it is also therefore reliant on occupant activity being known and accessing actual weather data for simulation to be most effective. Analytical/mathematical optimization approaches (d) can lead to inaccuracies due to the heterogeneous nature of dwellings and the limited number of parameters used in the process (Reddy *et al.* 2006 and Raftery *et al.* 2011a). A robust mathematical technique based upon Bayesian regression for normative models has been shown to be as accurate as a calibrated transient simulation (Heo *et al.*, 2012). This type of calibration technique can have a high computational expense and parameters are screened to identify those with the highest relative effect on results. The basic model used to demonstrate the Bayesian technique requires approximately eight hours computational time using an Energy Plus model that took only three minutes to estimate annual heating consumption (Heo *et al.*, 2012).

Limitations restrict the accuracy of iterative approaches (a) although the process can be refined (Yoon *et al.*, 2003). It often relies upon an analyst’s own knowledge and understanding which is sometimes applied in an unstructured way (Reddy *et al.* 2006). It is possible to structure iterative approaches; one example uses the concept of ‘calibration signatures’ and ‘characteristic signatures’ (Claridge, 2011). Calibration signatures can be identified from consumption data and plotted against an external variable, for example, external dry-bulb temperature, and then used to compare with model outputs. Characteristic signatures provide a baseline profile from a similar reference building type to compare with model outputs. This approach is best suited to the calibration of heating and cooling system energy consumption. Signature values are plotted against a temperature range to allow errors to be visualized. Actual weather and performance data are required for this technique.

Standard systematic methodologies for calibrated simulation based upon the iterative approach have been developed. They have incorporated elements of the four types previously defined and a higher resolution and range of real data from the subject building, most accurately hourly end-use records (Reddy *et al.*, 2007a; Reddy *et al.*, 2007b; Raftery *et al.* 2011a; and Raftery *et al.* 2011b). These do however rely upon actual weather data and detailed information recorded within existing buildings. The approach described in the next section utilizes a combination of the iterative approach (a) and approach (c). Invasive ‘blink-tests’ where different end-use loads are activated and deactivated can be used to quantify consumption and improve model inputs (Shonder *et al.*, 1997 and Soebarto, 1997). Another approach in this category, short-term energy monitoring (or STEM tests), rely on access to an operational and occupied building (Subbarao, 1988 and Manke & Hittle, 1996). The methodology employed for this research uses iterative

improvement of models (a) based upon fabric performance measurements which would be deemed to be part of group (c) in the categories of calibration techniques.

Although the accuracy of DTS software has been questioned in the past, inaccuracies are most often associated with a misunderstanding between using DTS for regulatory compliance purposes and using it as a low-energy design tool. When used for compliance purposes, it is reliant upon default data inputs that are defined within the National Calculation Method (NCM) which underpins regulatory compliance calculations (Department for Communities and Local Governance, 2011). When used in this way, input estimates included in the NCM and the omission of various energy consuming end-uses can contribute to gaps in performance (Cohen, 2011). However, it has been demonstrated that using refined data inputs reduces this element of the performance gap significantly (Burman *et al.*, 2012; Parker *et al.*, 2012). There has been criticism of the accuracy achievable by simulation software (Raslan and Davies, 2010) but results from the case studies noted above (Burman *et al.*, 2012; Parker *et al.*, 2012) demonstrated that DTS models can be calibrated to closely simulate actual performance. It has further been proposed that “...*the impact of modeling tools on the overall discrepancy between predicted and actual performance is constantly being diminished.*” (Menezes *et al.*, 2012, p.356). It is mainly assumptions made in regulatory compliance calculations that account for the modeling related gap in performance (Austin, 2013; Burman *et al.*, 2012; Cohen, 2012).

4. METHODOLOGY

4.1 Coheating and *in situ* fabric performance measurement

An estimate of the HLC for each test dwelling was obtained from coheating tests undertaken in accordance with the protocol developed by Leeds Beckett University (Johnston *et al.*, 2013). The test dwellings were heated using electric resistance point heaters to a mean elevated internal temperature (in this case 23°C and 22°C) over nineteen days (6th – 24th February 2014). A number of parameters were measured, namely total electrical energy input to the dwelling, internal temperatures and relative humidity, and various external weather conditions. By measuring the total amount of electrical energy required to maintain the mean elevated internal temperatures each day in response to the external environmental conditions, the mean daily heat input (in Watts) to the dwellings was determined. The HLC for the dwellings was then calculated by plotting the mean daily heat input (in Watts) against the mean daily difference in temperature between the inside and outside of the dwellings (ΔT). The resulting slopes of the plots provided the raw uncorrected heat loss coefficient in W/K. The data is then corrected against measured solar gains and wind speed.

In situ U-value measurements were undertaken during the coheating tests in accordance with ISO 9869 (ISO, 1994). *In situ* measurements of heat flux density, from which *in situ* U-values are derived, were obtained using Hukseflux HFP01 heat flux plates (HFPs). An illustration of a HFP is provided in Figure 1. The voltage induced by the HFPs was recorded at one minute intervals by either a Thermo Fisher Scientific DataTaker DT80 data logger, or at two minute intervals using an Eltek SQ851 logger. Numerous HFPs were positioned in locations considered to be representative of the whole element, as well as other locations of interest to the research team. The HFP positioning was informed by the use of a thermographic survey using a Flir T620bx thermal imaging camera. The HFPs were affixed to the surface of each element using thermal compound and adhesive tape.

The elevated and stable mean internal temperatures experienced during the coheating test are conducive to obtaining accurate measurements of *in situ* U-values. Air circulation fans were used during the coheating test to ensure even distribution of temperatures throughout the test

dwellings. However, care was taken to ensure that HFPs were not unduly influenced by excessive air movement by positioning fans in such a way that air was not blown directly on to the HFPs.

To compensate for thermal inertia and storage effects in heavier elements, U-values were calculated using the Average Method contained within ISO 9869; which is a cumulative moving average of measured heat flux and ΔT . It must be noted that the *in situ* U-value measurements presented may not be representative of each thermal element as a whole, as measurement of heat flux was obtained from only a small proportion of the total thermal element surface area, and that conditions present during the measurement period may not be representative of conditions under which the building is routinely subject to. Unless otherwise stated, the uncertainty associated with the *in situ* U-values presented in this paper is 9%.

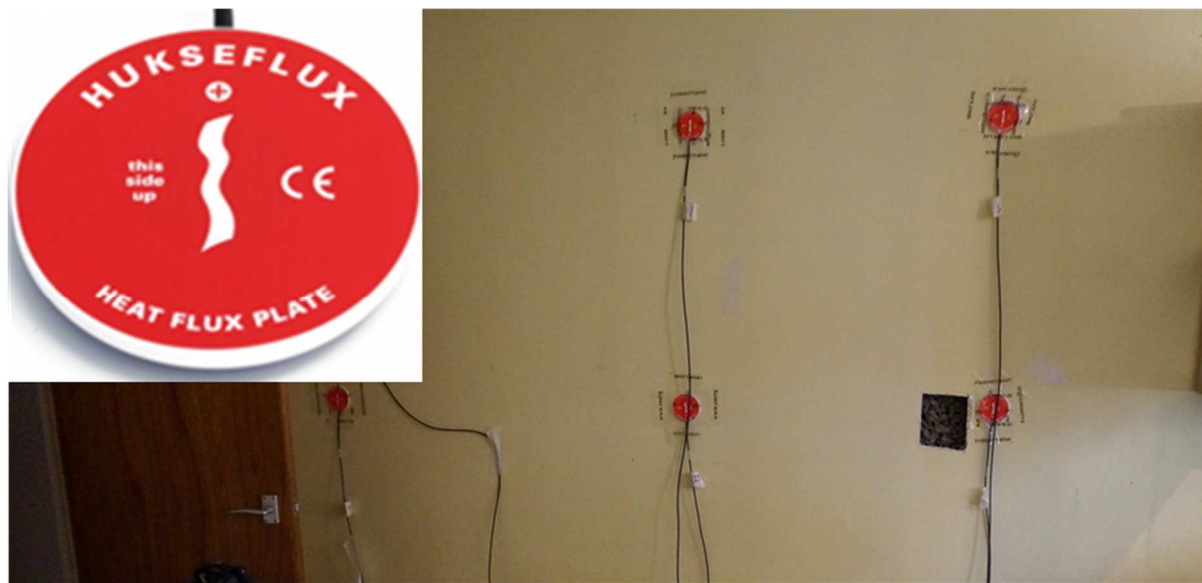


Figure 1: HFP (inset) and HFPs in situ on the kitchen wall in a case study dwelling

The air permeability of the test dwellings was measured by building pressurisation tests using a blower door in accordance with ATTMA Technical Standard L1 (ATTMA, 2010). The uncertainty associated with this method is highly dependent upon the environmental conditions present during the test. The background ventilation rate of each test dwelling was estimated using two methods. It was first derived from the building pressurisation test air leakage rate at 50 pascals (n_{50}) using the $n_{50}/20$ rule (Sherman, 1987). The derivation includes the correction factor for dwelling shelter factor which is contained within the SAP 2012 methodology (DECC, 2014). In the second method, CO_2 was released into the test dwellings. Background ventilation rates were determined based upon the period of time taken for the CO_2 concentration to decay to the background level. These were calculated in accordance with the decay method described within Roulet and Foradini (2002).

External air temperature, relative humidity, wind speed and wind direction was measured using a Vaisala WXT520 weather transmitter located on the gable end of one of the case study dwellings at ridge level. Solar insolation was measured using a south facing vertically orientated Kipp and Zonen CMP 11 pyranometer. Surface temperature measurements on the external elevations and below the ground were obtained using Type U thermistors. Internal air temperatures were obtained using a TMS PT100 RTD connected to an Eltek GD52 transmitter. Internal surface and cavity temperatures were obtained using Type K thermocouples. All

environmental and temperature measurements were logged at five minute intervals using an Eltek Squirrel RX250AL data logger. Missing data was corrected using linear interpolation.

4.2 Case Study Dwellings

The two case study examples used in this work are part of a larger project designed to investigate the low-energy refurbishment of hard-to-treat solid wall houses (www.simpler.com). Built in the 1960s, the houses were constructed using no-fines concrete, a type of concrete using only large aggregate. Due to the relatively quick construction time required, this archetype was used throughout the UK to meet rapidly rising housing demand. They are located in Antrim, Northern Ireland and are owned by the Northern Ireland Housing Executive. As these dwellings are part of an on-going research project and will potentially be occupied at time of publication, address details have been kept anonymous. The buildings are referred to as dwelling A and dwelling B within this paper. Case study dwellings form part of a small terrace as can be seen from the model visualisations presented in Figures 2 and 3.

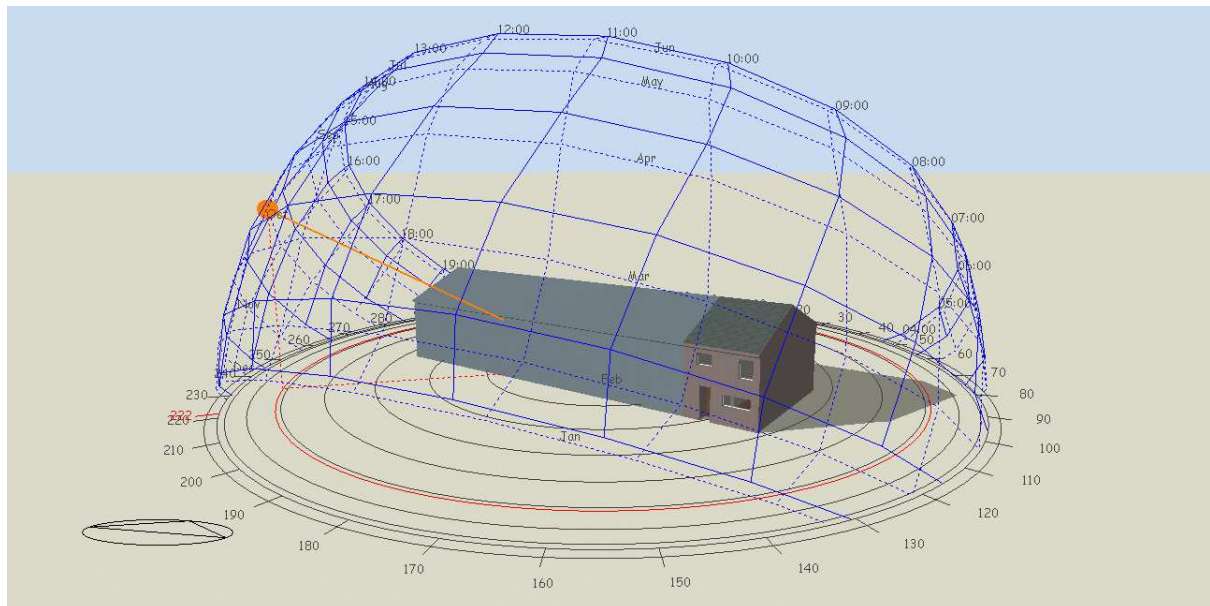


Figure 2: Visualisation of dwelling A at 15.00 hours on April 15th

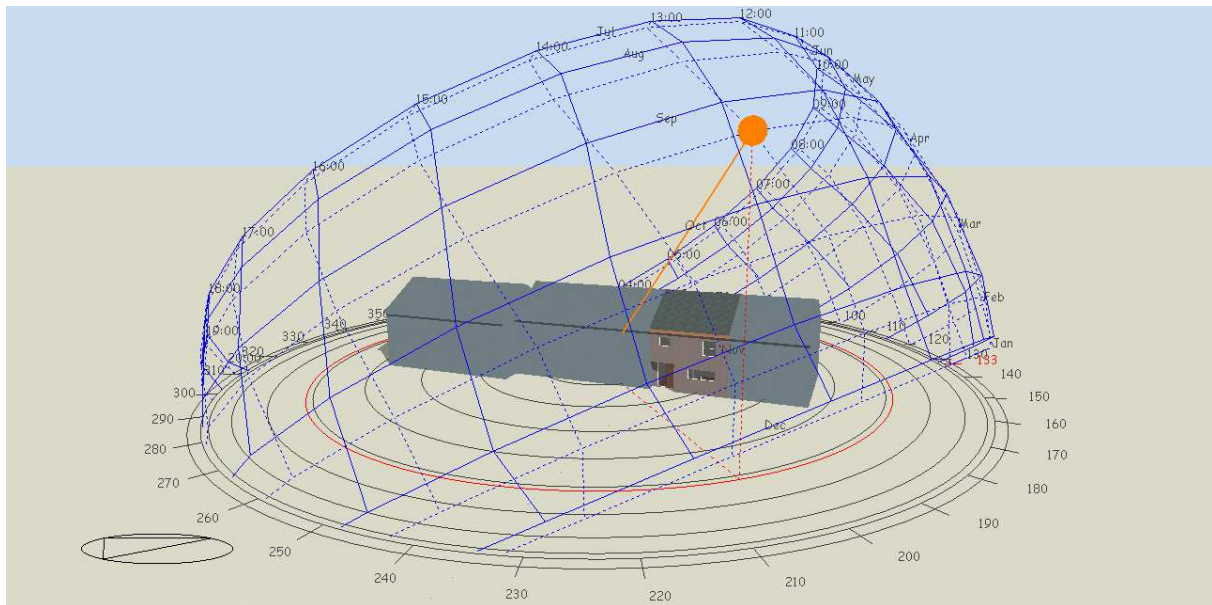


Figure 3: Visualisation of dwelling B at 15.00 hours on April 15th

4.3 Calibration methodology

Results from the *in situ* fabric performance measurements for the two no-fines concrete dwellings have been used as a basis for the calibration of the DTS models. Model outputs for both dwellings have then been compared with the *in situ* test results, using the predicted and measured HLC as the comparative metric. The calibration methodology follows a simple iterative process to refine model inputs. There are four stages to this process: an initial model based upon surveyed information (Surveyed); an update that includes the influence of linear thermal bridging (+bridging); an update that includes measured air changes per hour (+ac/h); and an update that includes measured U-values (+U-values). The order of these updates is arbitrary to some extent but they were introduced chronologically in terms of when the data was available (a scenario that is likely to be repeated in other projects). The abbreviated names stated in parentheses are used to reference each stage of calibration throughout this paper.

DesignBuilder software version 3.3 (DesignBuilder, 2013) was used to create the models; this software uses EnergyPlus as its building physics engine. The initial model (Surveyed) is based upon a measured survey of the dwelling to determine the dimensions for the fabric elements. Plan drawings were imported into DesignBuilder and used as a template to create the geometry; ceiling and ridge heights were taken from elevation and section survey drawings. The orientation of the building was measured using site plans and the nearest ASHRAE/IWEC weather file for the site location (Belfast/Aldergrove) was used from the software database. Neighbouring dwellings have been included in the models as local shading and adiabatic spaces as indicated in Figures 2 and 3.

Dimensions and U-values for the main thermal elements in the 'Surveyed' iteration of the model are shown in Table 1. The U-values for each element are calculated within the simulation software and are calculated according to BS EN ISO 6946 (BSI, 2008). Although the effects of repeat thermal bridging (from timber battens used to mount plasterboard for example) are not calculated in this version of EnergyPlus, they have been included in the model; DesignBuilder includes a function that allows the adjusted U-value to be calculated including repeat bridging, the elemental U-value can then be altered to reflect the revised U-value. This is done by adjusting the thickness of the most insulating material in a fabric element; this may have some impact on the thermal capacitance of the structure in the model and affects will be explored in

further work. Air permeability rates were set at a default value for a leaky two storey house of $17 \text{ m}^3/(\text{h}\cdot\text{m}^2)$ @ 50Pa, equivalent to 0.85 ac/h which is also based on the $n_{50}/20$ rule (CIBSE, 2006).

Table 1: Main fabric elements in ‘Surveyed’ iteration of models

Element:	Construction (outside – inside):	U-value (W/m².K)
External wall	External render 20mm; No-fines concrete 215mm; Air void 25mm (bridged by softwood battens); Plasterboard 12.5mm	1.418
Roof	Concrete roof tiles 12mm; Air void (various depth due to pitched roof); Mineral wool insulation (dwelling A 100mm; dwelling B 250mm); Plasterboard 12.5mm	A = 0.446 B = 0.162
Ground floor	Lightweight concrete 200mm; Floor screed 10mm; Linoleum floor tiles 5mm.	1.286
Windows	Softwood frame, single glazing 6mm	5.778

Under normal conditions, coheating tests are completed over at least two weeks but would be conducted over even longer periods if feasible. As there are no real-world limitations in the virtual environment, a full winter period (1st December – 28th February) can be simulated. In this instance, both a full winter period and actual dates were simulated for comparative purposes. Physical testing ran over nineteen days in dwelling A and seventeen days in dwelling B. To mimic the conditions of the coheating tests, no internal heat gains from people, lighting and equipment were input, electrical heating was specified from a heat source with a coefficient of performance of 1.0 and blinds were added on the inside of all windows and controlled as always shut. Blinds were closed in the actual test properties to minimise the effects of any excessive solar gains. The heating set points were specified as constantly at 23°C and 22°C in dwellings A and B respectively. The set points were selected to minimise heat transfer between adjoining dwellings.

Full SAP calculations were available for the two test dwellings as they were prepared as part of the wider research project that these buildings are included within. The Heat Loss Parameters included in the SAP calculations have been used as the baseline comparison in the results section, and these have been compared to the HLCs estimated in the DTS models and measured *in situ*. Extensive thermal bridging calculations were completed by a third party as part of the S-IMPLER project and the resultant ψ -values were used to calculate a Y-value to include in the SAP estimates. These Y-values were then used to adjust the elemental U-values for the second iteration of the models (+bridging). The Y-values for dwellings A and B were calculated to be 0.116 and 0.127 respectively. The third iteration of the models introduces the measured air permeability (+ac/h) and the fourth iteration includes the measured U-values (+U-values); the measured values for both of these inputs are presented in Table 2 in the next section. The U-values in the final iteration of the model were adjusted in the software using the same technique described previously. Measured U-values were input for specific elements and these were then adjusted by the software to meet that value by changing the thickness of the most insulating material.

5. RESULTS

Table 2 notes the main findings from the fabric testing following extensive analysis of the final data set recorded on site. It can be seen from these results that the measured U-values for the external walls are significantly different despite being of the same construction type. Further

research is required to establish the exact reason for this although wide variation in the thermal resistance of no-fines concrete has been noted in previous work (see Sommerville *et al.*, 2011). As the test dwellings form part of two separate terraces, it is possible that the consistency of no-fines concrete mix is different and that the terraced dwellings were constructed using completely different batches of concrete and/or by different site operatives. Visual inspection suggested that the concrete in dwelling B was denser than that found in dwelling A; the increased proportion of air voids in dwelling A's concrete could account for the lower U-value.

Table 2: Summary of measured fabric performance test results

Thermal characteristic	Parameter	Dwelling A (end-terrace)	Dwelling B (mid-terrace)
Ventilation	Air permeability [Q_{50}] ($m^3/(h.m^2)$ @ 50Pa)	16.3	17.2
	Background ventilation rate (ACH)	0.74	0.69
	Ventilation heat loss factor of HLC (W/K)	54.5	52.9
Whole house heat loss	HLC (W/K)	249.7 ± 3	217 ± 2.6
	Wind corrected HLC (W/K)	226.6 ± 8.8	201.3 ± 9.7
<i>In situ</i> thermal transmission of individual elements	No-fines external wall U-value (W/m^2K)	0.84 ± 0.10	1.25 ± 0.05
	Roof U-value (W/m^2K)	0.40 ± 0.04	0.13 ± 0.01
	Ground floor U-value (W/m^2K)	0.79 ± 0.07	0.67 ± 0.07

Data used to calculate the coheating HLC are normalised to account for a number of factors that affect fabric heat loss. In properties that include party walls, due to the elevated temperatures during test conditions, the measured heat flow through these walls has been subtracted from the heat load. This an area of on-going research; it has been found that heat transfer can occur through party walls that cannot be explained solely by the temperature difference between the two adjacent dwellings (see Miles-Shenton *et al.*, 2009). However, in this instance, the walls are theoretically solid, so no associated heat losses should be evident; thermography studies indicated otherwise and this is discussed further in section 6. Data are also normalised to account for the wind speeds experienced during the coheating test that can affect fabric thermal performance; a multiple linear regression analysis is performed with power as the dependant variable and ΔT , solar irradiation and wind speed as independent variables. Both of these normalisations are in keeping with the DTS model as adjoining properties are treated as adiabatic spaces and the effects of wind-washing are not included in the calculations; the impact of wind-washing on fabric heat losses is not fully understood in the current literature. Data are often also normalised for solar gains, but were not in this instance as the measured solar irradiation data had no significant statistical impact; this could have been the results of inaccurate pyranometer data and requires further investigation. Statistical uncertainty relating to measured ach rates is nominal and below 0.1 ACH in all cases.

Ground floor U-values were similar in both properties. The large difference in roof U-values was primarily attributable to dwelling B having had an additional 150mm layer of mineral wool insulation in the loft space. Air permeability and background ventilation rates were also similar across the two test properties.

Figures 4 – 7 illustrate the HLCs calculated by the DTS models at each stage of calibration. These charts include the measured HLCs as a comparison to the modelled output. The x axis represents the ΔT and the heat input in Watts is plotted against this on the y axis. Text annotating the trendline shows the resultant HLC value. The values in italics in the bottom left corner are for the measured results and the value in bold on the right is the HLC for the calibrated model (final iteration '+ U-values').

As can be seen from these charts, the final calibrated models achieve a relatively good level of agreement compared with the measured results in both the full winter and actual test period scenarios. Although these represent positive outcomes for the work, results should also be treated with caution. More detailed analysis of the model output data is required to understand the impact of solar gains through the glazing and on the opaque elements of the building fabric. Previous work has shown that the cumulative effects of solar gain on building fabric in the field and in models designed to mimic coheating test environments can have an impact on results (Stamp *et al.*, 2013). It should also be noted that the measured results were normalised to account for the difference in ground temperature when compared with external air temperature which results in the ground floor having a different ΔT than other elements. This has not been accounted for in the simulation results at this stage. The software allows the monthly mean ground temperature to be adjusted and this is set at a default value of 14°C. Measured site data was not available for a full winter period (1st December – 28th February) at the time the modelling work was completed. Site ground temperature has been monitored since February 2014 and future analysis will include adjusted values. The measured mean ground temperature during the test periods was 7.8°C. It should be noted that this was measured at a depth of 0.1 m and was therefore likely to have been partially influenced by external air temperature and weather conditions.

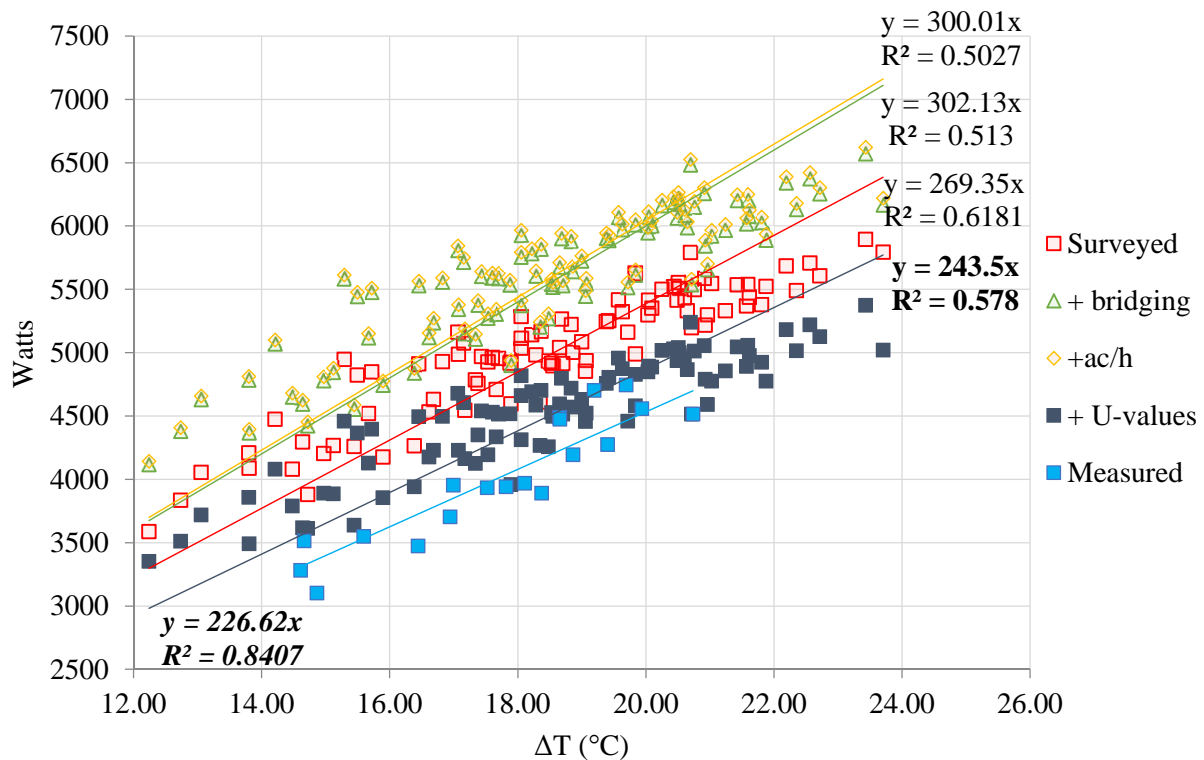


Figure 4: Modelled and measured HLCs for dwelling A over the winter period

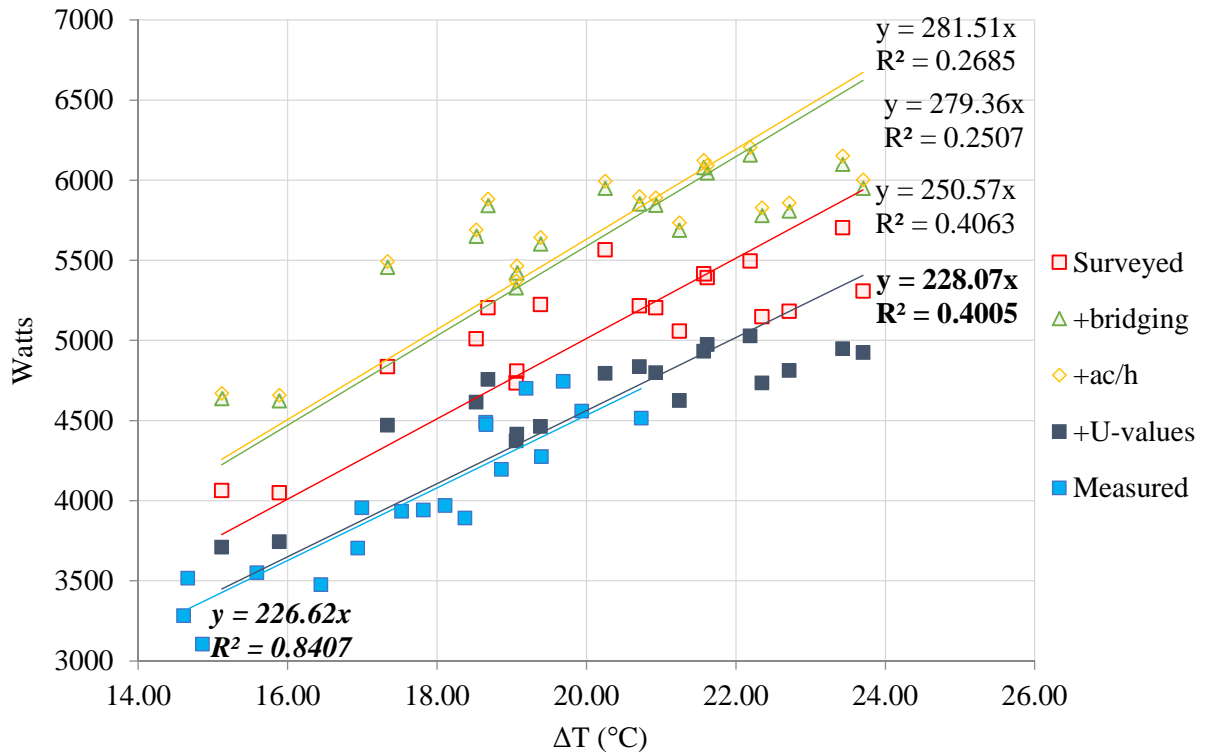


Figure 5: Modelled and measured HLCs for dwelling A 6th – 24th February

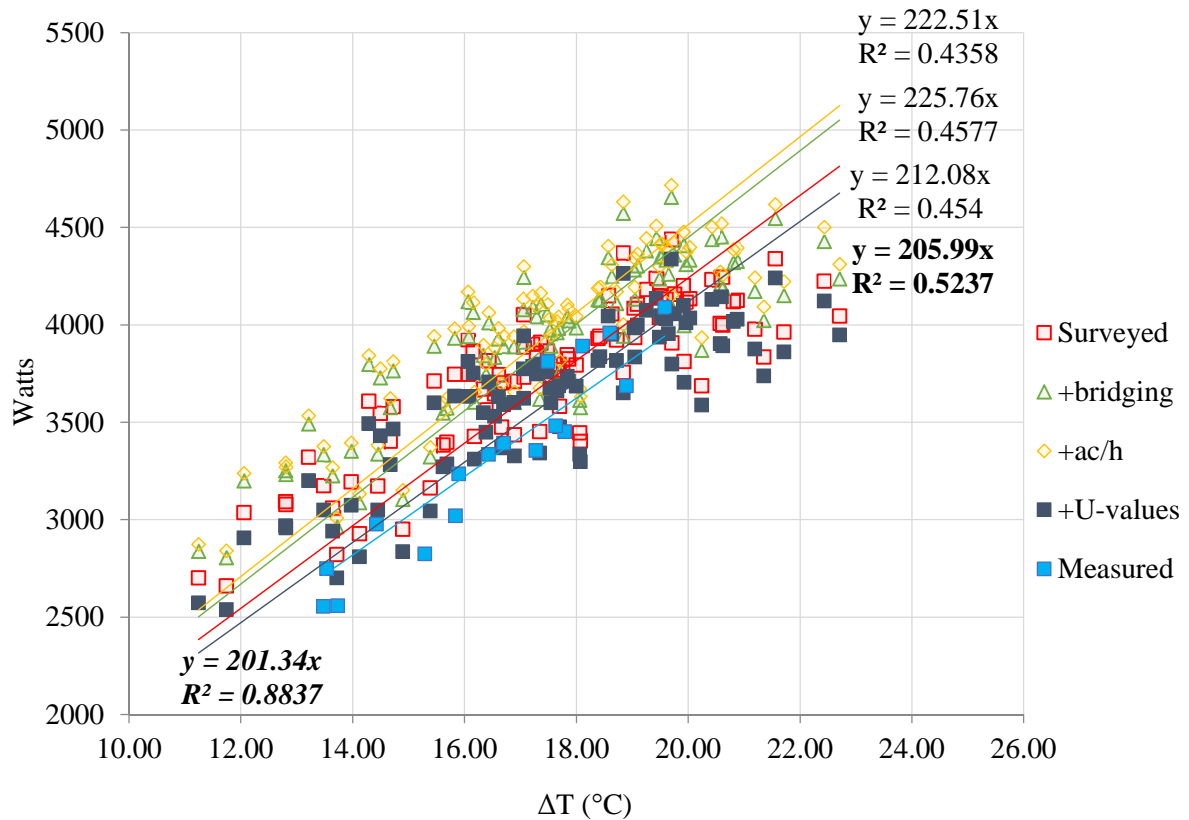


Figure 6: Modelled and measured HLCs for dwelling B over the winter period

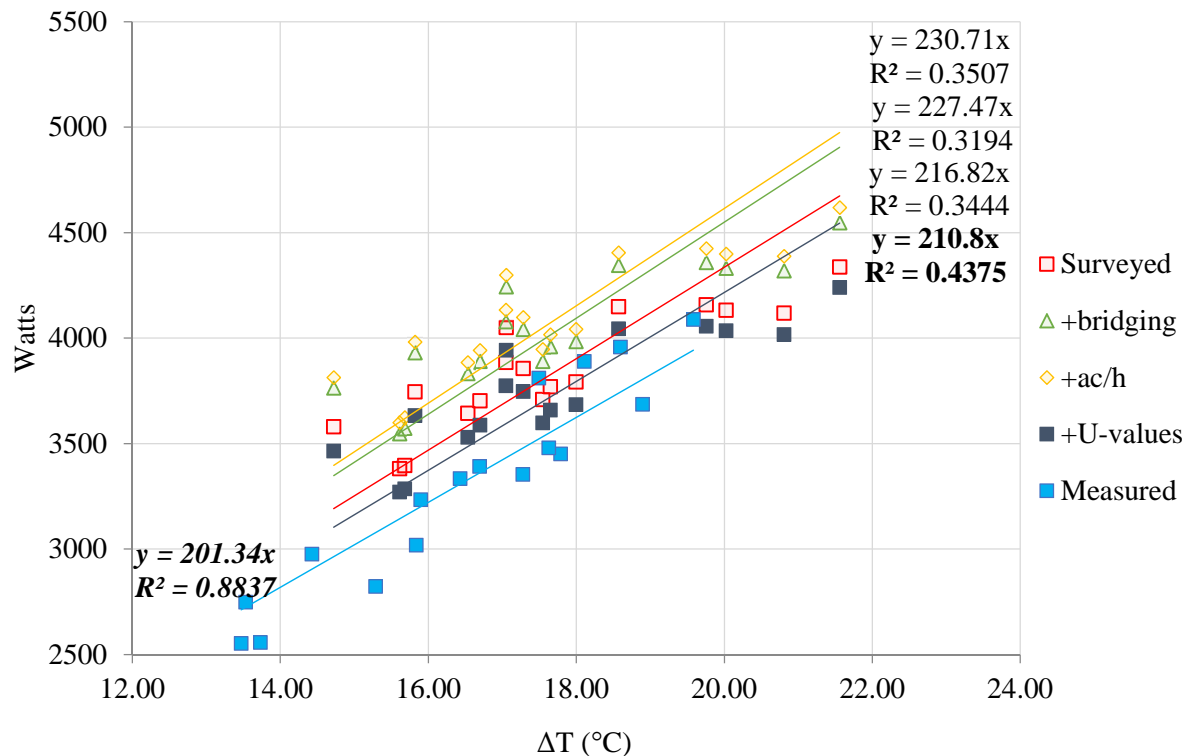


Figure 7: Modelled and measured HLCs for dwelling B 8th – 24th February

Although a reasonable estimation of the HLC is achieved in the initial models that are based upon simple surveyed data, the error actually increases as measured data is input to account for the linear thermal bridging and measured air exchange rate. It is not until the measured U-values are added that the predicted HLC provides a close match to the measured value, which would be expected as the HLC in the case study dwellings is dominated by heat losses through the plane elements. This also emphasises the significance of including accurate U-value inputs in the DTS models. These results suggest that the assumed thermal resistance of no-fines concrete in the modelling software database is lower than found *in situ*. However, as previously stated, a variance in the thermal resistance of no-fines concrete has been noted in the past.

A comparison has also been undertaken between the outputs of each DTS model and the SAP Heat Loss Parameter (see Figure 8); the percentage difference shown is in comparison with the measured HLC. The model for dwelling A is within 1% (0.64%) of measured HLC and the model for dwelling B is within 5% (4.49%) of the measured. These results are also indicative of the inaccuracies that come from the assumptions included in the SAP calculations. The standard weather file will have a significant impact on results as will the assumed U-value for no-fines concrete included in the SAP calculations (1.23 W/m²/K) which is higher than found in dwelling B (0.85 W/m²/K) and slightly lower than measured in dwelling B (1.25 W/m²/K). The SAP U-values do account for the timber-stud mounted plasterboard on the internal leaf of the building. Total floor areas, total plane element area and total volume differed slightly between the SAP and DTS models which will also have some effect on results and requires further investigation. For example, the total floor area in the SAP calculations for property A was 97.66m² as opposed to 95.34m² in the DTS model; there is a similar difference for property B with the total floor areas being 99.99m² and 97.91m² for the SAP calculations and DTS models respectively. This is most likely due to discrepancies between the surveys of the dwellings.

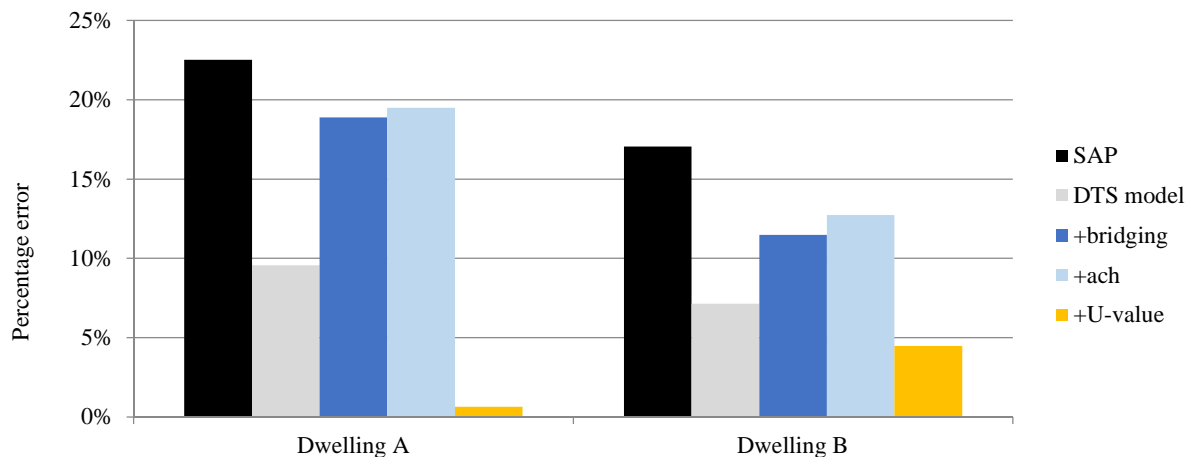


Figure 8: Agreement of predicted HLC compared to the measured value

6. CONCLUSIONS AND FURTHER WORK

Results presented in this paper demonstrate that the fabric performance predicted by DTS models can be closely calibrated to measured performance by refining model inputs using *in situ* fabric performance test results. This can be done independently of actual weather files by using the HLC and ΔT as the comparative metrics. Traditional measures of accuracy such as Mean Biased Error (MBE) and the Cumulative Variation of the Root Mean Square Error (CVRMSE) require the use of site-specific actual weather data in the DTS models to provide meaningful results.

Using the methodology in this paper means that greater confidence can be placed on models to more accurately predict energy consumption when occupants and space conditioning systems are added to the calculation. This approach produces a significantly more accurate estimate of fabric performance than that predicted by SAP. However, this work represents a very small sample and more research is required to provide proof of concept. This will need to include a range of dwelling types and constructions to fully validate this methodology. Additional analysis of results is also required to better understand the impact of solar irradiation on opaque fabric elements in particular. Thermography studies also suggested that heat transfer was occurring within the no-fines structure. Although treated in calculations as solid walls, the construction actually includes a network of small voids. These voids collectively act as a form of cavity so could actually improve the elemental U-value. However, they may also aid the transfer and loss of heat from the dwelling as a whole. Measuring this type of heat transfer within the structure itself and the impact it has on elemental U-values would be complex. Although this represents an unknown factor it may not be economically viable to investigate this as it is highly specific to this type of construction.

This approach needs to be rationalised for it to become more practicable. Air pressure testing data should be available in many cases although there is currently no quick and reliable way of measuring U-values *in situ*. There is however some progress being made in testing procedures that can calculate HLCs relatively quickly and the latest version of DesignBuilder allows linear bridges to be modelled. Ideally the amount of measured data required to calibrate models will be reduced as it is neither practical nor economically viable to complete the extent of fabric testing described here on every new or retrofitted dwelling. Current work is exploring the development of coheating tests that utilise installed heating, ventilation and air conditioning (HVAC) systems as well as combinations or short-term testing.

The internal heat gains associated with occupancy, human operation of HVAC plant performance and natural ventilation represent much more variable parameters than the fabric elements. The models could also be calibrated to accurately represent the impact of these variables but this would require a much more detailed set of monitored data. The value of this type of exercise is questionable in practice; if fabric elements and HVAC system performance can be reliably modelled and calibrated this would provide a reliable baseline. The remaining variables will change from occupant to occupant and year to year depending on the demographic of the people living in the home and changeable weather conditions, which are not always reliably forecast.

Inevitably, there are some limitations to this work at this stage. Although results are normalised to eliminate the impact of wind and solar, differences between the actual weather recorded on site and that used in the simulation need to be evaluated further. Further case studies will also be completed, particularly in relation to highly insulated, air-tight buildings as margins of error become more pronounced at this scale. Some additional work is also required to test the sensitivity of results to variable model parameters and also to quantify and understand the uncertainty associated with this approach.

There would be some value in fully calibrating a model against all of the parameters provided above if data is available. This would help to provide evidence that would further validate this fabric performance calibration approach. If a model calibrated using this methodology could then be accurately calibrated against an extended period of operation (ideally a full year) it would demonstrate that the initial model could be used to more accurately predict dwelling performance in virtually any occupied scenario, including low-energy retrofit applications. There is scope for this type of validation exercise to be completed, as these case study properties will be subject to extensive in-use monitoring as part of the wider research project that they are connected to. However, this will be dependent on suitable resources being available when the full data set has been collected.

This work also demonstrates the importance of including accurate U-values in energy performance calculations but also that assumed values can be significantly different than those measured *in situ*. As with the methodology as a whole, more work is required to try and quantify the extent of this variance and its frequency within the existing stock. As noted at the beginning of this paper, the existing stock represents the vast majority of dwellings in the UK and this will continue to be the case well past the Government's deadlines for major CO₂ reductions. Future work will therefore use these calibrated models to predict the performance of retrofitted properties and compare predictions with those generated by SAP and RdSAP as these remain important policy instruments in the current climate.

ACKNOWLEDGEMENTS

The fabric testing element of this work was funded by the Technology Strategy Board as part of the S-IMPLER (www.s-impler.com) project. The Author's would also like to thank Jack Francis of the Northern Ireland Housing Executive for his invaluable help on site and Professor David Johnston of Leeds Beckett University for reviewing the paper prior to submission. Professor Christopher Gorse is the Principle Investigator for the S-IMPLER project and Dominic Miles-Shenton has provided on-going advice during this research.

REFERENCES

ATTMA, 2010. ATTMA Technical Standard L1. Measuring the Air Permeability of Building envelopes (Dwellings). October 2010 Issue. Air Tightness Testing and Measurement Association, Northampton, UK.

- Austin, B., 2013. The performance gap: causes and solutions. Arup: London, UK.
- Boardman, B., 2007. Home Truths: A Low Carbon Strategy to Reduce UK Housing Emissions by 80% by 2050. ECI Research Report 34. Oxford, University of Oxford Environmental Change Institute.
- Bordass, B., Cohen, R., Standeven, M. and Leaman, A., 2001. Assessing building performance in use 3: energy performance of probe buildings. *Building Res Inform*, 29(2), pp. 114-28.
- BSI, 2008. Building components and building elements. Thermal resistance and thermal transmittance. Calculation method. BSI, London, UK.
- Burman, E., Rigamonti, D., Kimpain, J. and Mumovic, D., 2012. Performance gap and thermal modelling: a comparison of simulation results and actual energy performance for an academy in North West England. In: IBPSA England First Building Simulation and Optimization Conference, Loughborough, 10th-11th September 2012, pp. 35-42.
- Carbon Trust, 2011. Closing the gap: lessons learned on realising the potential of low carbon building design. London: HMSO. Available from: <http://www.carbontrust.co.uk/Publications> [Accessed 12th June 2013].
- CIBSE, 2006. Guide A: Environmental Design. CIBSE, London, UK.
- Clarke, A. and Reason, L., 2008. Projecting energy use and CO₂ emissions from low energy buildings: a comparison of the Passivhaus Planning Package (PHPP) and SAP. Available at: http://www.aecb.net/PDFs/Combined_PHPP_SAP_FINAL.pdf [Accessed 2nd June 2009].
- Claridge, D.E., 2011. Building simulation for practical operational optimization. In: Hensen, J. and Lamberts, R. eds. Building performance simulation for design and operation. Spon Press: Abingdon, UK.
- Cohen, R., 2013. The performance gap in non-domestic buildings: evidence collected from the Technology Strategy Board's Building Performance Evaluation Programme. Verco Ltd: London, UK. Available from: http://www.greenconstructionboard.org/images/stories/pdfs/performance-gap/CPG%20Evidence%20Base%20from%20BPE%20Final%20Report%2005Mar13_.pdf [Accessed 5th May 2013].
- Department for Communities and Local Governance, 2011. National Calculation Method modelling guide (for buildings other than dwellings in England and Wales). Communities and Local Government Publications: Wetherby, UK.
- Department for Communities and Local Governance, 2008. Improving the energy efficiency of our buildings: A guide to Energy Performance Certificates for the construction, sale and let of dwellings. Communities and Local Government Publications: Wetherby, UK.
- DECC, 2014. The Government's Standard Assessment Procedure for Energy Rating of Dwellings, 2012 Edition. [Internet] Watford, UK, Published on behalf of DECC by Building Research Establishment, Available at: < http://www.bre.co.uk/filelibrary/SAP/2012/SAP-2012_9-92.pdf > [Accessed: 14th July, 2014].
- DECC, 2013a. 2012 UK Greenhouse Gas Emissions, Provisional Figures and 2011 UK Greenhouse Gas Emissions, Final Figures by Fuel Type and End-user [Internet]. London, Department of Energy & Climate Change. Available from: <<https://www.gov.uk/government/publications/provisional-uk-emissions-estimates> [Accessed January 14th, 2014].

DECC, 2013b. Standard Assessment Procedure: Guidance on how buildings will be SAP energy assessed under the Green Deal and on recent changes to incentivise low carbon developments. [Internet] Available at: <https://www.gov.uk/standard-assessment-procedure> [Accessed 25th June 2013].

DesignBuilder, 2013. DesignBuilder Version 3.3.0.043 BETA. DesignBuilder Software Ltd, Stroud, UK.

HM Government, 2014. Table 101: by tenure, United Kingdom. Available from: <https://www.gov.uk/government/statistical-data-sets/live-tables-on-dwelling-stock-including-vacants>. [Accessed 12th June 2014].

HM Government, 2010a. The Building Regulations 2000, Approved Document L1A: Conservation of fuel and power (new dwellings), 2010 edition. NBS, London.

HM Government, 2010b. The Building Regulations 2000, Approved Document L1B: Conservation of fuel and power (existing dwellings), 2010 edition. NBS, London.

IPCC, 2014. Climate change 2014: Mitigation of Climate Change. Available from: <http://www.ipcc.ch/> [Accessed 12th June 2014].

ISO, 1994. ISO 9869: Thermal insulation – Building elements - In situ measurement of thermal resistance and thermal transmittance. International Organization for Standardisation, Geneva, Switzerland.

Johnston, D., Miles-Shenton, D., Wingfield, J., Farmer, D. and Bell, M., 2012. Whole house heat loss test method (Coheating). Part of: International Energy Agency Annex 58: Reliable building energy performance characterization based on full scale dynamic measurements.

Leeds Metropolitan University: Leeds. Available at: <http://www.leedsmet.ac.uk/as/cebe/projects.htm> [Accessed 28th June 2013].

Johnston, D., Miles-Shenton, D., Farmer, D., and Wingfield, J., 2013. Whole House Heat Loss Test Method (Coheating). June 2013. Leeds, UK, Centre for the Built Environment, Leeds Metropolitan University

Kelly, S., Crawford-Brown, D. and Pollitt, M.G., 2012. Building performance evaluation and certification in the UK: is SAP fit for purpose? *Renewable and Sustainable Energy Reviews*, 16, pp. 6861 – 6878.

Kelly, J.M., 2009. Retrofitting the existing UK building stock. *Building Research and Information*, 37, 196-200.

Killip, G. 2008. Building A Greener Britain: Transforming the UK's Existing Housing Stock. A report for the Federation of Master Builders by the University of Oxford Environmental Change Institute. Federation of Master Builders, London, UK.

Manke, J. and Hittle, D., 1996. Calibrating building energy analysis models using short term test data. Proceedings of the 1996 ASME International Solar Engineering Conference, ASME Solar Energy Division, 369-378.

McCray, J.A., Bailey, P.L. and Parker, J.L. 1995. Using data visualization tools for the calibration of hourly DOE-2.1 simulations. IBPSA Conference, Madison, WI, Aug. 14-16, 461-466.

Menezes, A.C., Cripps, A., Bouchlaghem, D. and Buswell, R., 2012. Predicted vs. actual energy performance of non-domestic buildings: using post-occupancy evaluation data to reduce the performance gap. *Applied Energy*, 97, pp. 355-364.

- Miles-Shenton, D., Bootland, J., Fong Chiu, L., Corbey, S., Lowe, R., Wingfield, J. and Bell, M., 2009. *LowCarb4Real: Developing low carbon housing, lessons from the field*. Final Report. Leeds Metropolitan University: Leeds. Available at: <http://www.leedsmet.ac.uk/as/cebe/projects.htm> [Accessed 28th June 2013].
- Miles-Shenton, D., Wingfield, J., Sutton, R. and Bell, M., 2011. *Temple Avenue Project: Report to Joseph Rowntree Housing Trust*. Leeds Metropolitan University: Leeds. Available at: <http://www.leedsmet.ac.uk/as/cebe/projects.htm> [Accessed 28th June 2013].
- Nicholls, R., 2008. *The green building bible volume 2: Fourth Edition*. Llandysul: The Green Building Press, UK.
- Ortega, J. K. E., Anderson, J. V., Connolly, J. M. and Bingham, C. E., 1981. Electric coheating experiment to determine the heat loss coefficient of a double-envelope house. In *Proceedings of the Sixth National Passive Solar Conference*, Portland, OR, USA (1981), pp. 74–78.
- Parker, J., Cropper, P. and Shao, L., 2012. A calibrated whole building simulation approach to assessing retrofit options for Birmingham Airport. In: *IBPSA England First Building Simulation and Optimization Conference*, Loughborough, 10th-11th September 2012, pp. 49-56.
- Raftery, P., Keane, M. and O'Donnell., 2011a. Calibrating whole building energy models: An evidence-based methodology. *Energy and Buildings*, 43, 2356-2364.
- Raftery, P., Keane, M. and O'Donnell., 2011b. Calibrating whole building energy models: Detailed case study using hourly measured data. *Energy and Buildings*, 43, 3666-3679.
- Raslan, R. and Davies, M., 2010. Results viability in accredited building energy performance compliance demonstration software in the UK: an inter-model comparative study. *Journal of Building Performance Simulation*, 3(1), pp. 63-85.
- Ravetz, J., 2008. State of the stock: What do we know about existing buildings and their future prospects? *Energy Policy*. Volume 36 (2008) pp. 4462-4470.
- Reddy, T., Maor, I. and Panjapornpon, C., 2007a. Calibrating detailed building energy simulation programs with measured data – Part I: General methodology. *HVAC&R Research*, 13, 2, 221-241.
- Reddy, T., Maor, I. and Panjapornpon, C., 2007b. Calibrating detailed building energy simulation programs with measured data – Part II: Application to three case study office buildings. *HVAC&R Research*, 13, 2, 243-265.
- Reddy, T., 2006. Literature review on calibration of building energy simulation programs: uses, problems, procedures, uncertainty and tools. *ASHRAE Transactions*, 211, 226-240.
- Roulet, C-A. and Foradini, F. (2002) Simple and Cheap Air Change Rate Measurements Using CO₂ Concentration Decay, *International Journal of Ventilation*, Volume 1, No.2, pp 39-44.
- Sherman, M., 1987. Estimation of Infiltration for Leakage and Climate Indicators. *Energy and Buildings* 10(81).
- Shonder, J.A., Hughes, P.J. and Thornton, J.W., 1998. Using calibrated engineering models to predict energy savings in large-scale geothermal heat pump projects. *ASHRAE Transactions* 104(1).
- Soebarto, V.I., 1997. Calibration of hourly energy simulations using hourly monitored data and monthly utility records for two case study buildings. *IBPSA Conference Proceedings*, Prague, Czech Republic, Sept. 13-15.

- Sommerville, J., Craig, N. and Charles, N., 2011. No-fines concrete in the UK social housing stock: 50 years on, *Structural Survey*, Vol. 29: 4, pp.294 – 302
- Sonderegger, R. C. Condon, P. E. and Modera, M. P., 1979a. In-situ measurements of residential energy performance using electric co-heating. *ASHRAE Transactions*, 86 (I), 1980. LBL-10117.
- Sonderegger, R. C. and Modera, M. P., 1979b. Electric co-heating: A method for evaluating seasonal heating efficiencies and heat loss rates in dwellings. In: *Proceedings of the Second International CIB Symposium, Energy Conservation in the Built Environment*, Copenhagen: 1979. LBL-8949.
- Stafford, A., Bell, M. and Gorse, C., 2012. *Building Confidence – A Working Paper*. The Centre for Low Carbon Futures: York, UK.
- Stamp, S., Lowe, R. and Altamirano-Medina, H., 2013. An investigation into the role of thermal mass on the accuracy of coheating tests through simulations & field results. *Proceedings of BS2013: 13th Conference of International Building Performance Simulation Association*, Chambéry, France, August 26-28.
- Subbarao, K., 1988 *PSTAR - Primary and Secondary Terms-Analysis and Renormalization: A Unified Approach to Building and Energy Simulations and Short-Term Testing – A Summary*. September 1988. SERI/TR-254-3347. Colorado, USA, Solar Energy Research Institute.
- Subbarao, K. Burch, J. D. Hancock, C. E. Lekov, A. and Balcomb, J. D., 1988. *Short-Term Energy Monitoring (STEM): Application of the PSTAR Method to a Residence in Fredericksburg, Virginia*. TR-3356. Solar Energy Research Institute: Colorado, USA.
- Technology Strategy Board (2012) *Building Performance Evaluation*. London, Technology Strategy Board. Available from:
<<http://webarchive.nationalarchives.gov.uk/20130221185318/www.innovateuk.org/content/competition/building-performance-evaluation-.ashx>> [Accessed February 2014].
- Wingfield, J., Bell, M., Miles-Shenton, D., South, T. and Lowe, R.J., 2009a. *Evaluating the Impact of an Enhanced Energy Performance Standard on Load-Bearing Masonry Construction – Final Report: Lessons From Stamford Brook - Understanding the Gap between Designed and Real Performance*. PII Project CI39/3/663. Leeds Metropolitan University: Leeds. Available at: <http://www.leedsmet.ac.uk/as/cebe/projects.htm> [Accessed 28th June 2013].
- Wingfield, J., Miles-Shenton, D. and Bell, M., 2009b. *Evaluation of the party wall thermal bypass in masonry dwellings*. Leeds Metropolitan University: Leeds. Available at: <http://www.leedsmet.ac.uk/as/cebe/projects.htm> [Accessed 28th June 2013].
- Wingfield, J., Bell, M., Miles-Shenton, D. and Seavers, J., 2011. *Elm Tree Mews field trial: evaluation and monitoring of dwellings performance*. Final technical report. Leeds Metropolitan University: Leeds. Available at: <http://www.leedsmet.ac.uk/as/cebe/projects.htm> [Accessed 28th June 2013].
- Zero Carbon Hub, 2010. *Closing the performance gap: Building low carbon housing for real*. Report of Topic Work Group 4, Carbon Compliance Tool Policy Assumptions Task Group. July 2010, Zero Carbon Hub: Milton Keynes.

An adapted co-heating test and experimental infrastructure for thermal dynamic response and performance identification of residential buildings

Guillaume Lethé*, Paul Steskens, Gilles Flamant, Brieuc Meurisse

*Belgian Building Research Institute, Brussels, Belgium (gl@bbri.be)

1. ABSTRACT

Co-heating tests have been used by many researchers and building professionals [1] for the characterization of a building's thermal characteristics, mainly focusing on the building's heat loss coefficient. Dependent of the mathematical model applied, the reliable determination of a building's thermal dynamics often requires accurate identification of its various time constants, response to temperature changes, solar radiation, ventilation rate and its effective thermal capacity.

On-site measurement campaigns and data analysis for building energy performance evaluation require in-depth and balanced skills setting up a good test environment, designing and executing a well-suited experimental procedure and appropriately managing the building dynamic model structure choice and the data analysis. Failing at one level implies increased uncertainty and reduced reliability of the results [4].

The uses of such on-site measurement include the validation of laboratory measurements and measurement of complex products difficult to assess in a laboratory (for product manufacturers and certification bodies), a warranty of thermal performance and labelling of as-built performances (for building makers and authorities), the validation of building dynamic simulation software's (for editors and users of simulation tools) and finally a contribution towards the emergence of smart grids and smart building management. The many uses call for various measurement protocols that need to be adapted to the specific purpose and constraints. Measurements can be applied on building components or building envelopes, and may be analysed through static, transient or dynamic approaches.

This paper focuses on the dynamic measurement of building envelopes by the application of optimized short heating sequences, an adequate modular experimental infrastructure and grey-box model identification. Air change rate measurements have also been performed which better allows comparing results of the many possible experimental designs and analysis methods.

Keywords: on-site measurement, co-heating test, intelligent control, dynamic sequence, grey-box model, thermal performance

2. INTRODUCTION

On-site measurement campaigns and data analysis require in-depth and balanced skills regarding the test environment, the experimental procedure and the data analysis. While the in-situ measurement and identification of static performance indicators of building components are already covered by a standard [13], global building envelopes are still under investigation. The Heat Loss Coefficient (HLC in W/K) expresses the heating power that is lost by transmission and ventilation through a building envelope under a temperature gradient of 1K. Steady-state thermal conditions and energy balance are required to derive this "static" parameter. Such conditions are nevertheless merely approached during on-site experiments. Using the steady-state conditions assumption requires at least daily-averaging of multiple

weeks measured data. Faster methods to determine a building's thermal dynamics go along with an accurate identification of its various time constants, response to temperature changes, solar radiation, ventilation rate and its effective thermal capacity [2, 3, 9]. The application of several thermal solicitation sequences and subsequent data analysis has been investigated.

The measurement may happen quickly if time constants of the system under investigation are small enough, like in lightweight and moderately insulated buildings. A 'transient' approach has been investigated [12]. This method usually can be applied during just one night. Nevertheless, only one time constant is evaluated.

Typical co-heating measurements (thermostatically controlled temperature) on the contrary last for about 2 weeks at least. Daily-averages resampling enables applying linear regressions from which the physical parameters are extracted. Details and variants of these methods can be found in [10]. Nevertheless, the infrastructure is intrusive and the building should remain unoccupied during the test.

Another approach is emerging thanks to less intrusive energy monitoring systems making long-term monitoring possible. Nevertheless, corrections for specific occupants' behaviour have to be dealt with. With the integrated test (also called "in-use" test) the distribution and emission characteristics are evaluated jointly with the building envelope ones, giving a more representative image of the building behaviour than when experimental heaters and fans are used. This approach was recently studied [11] and requires additional investigations, even for empty buildings.

Intermediately, shorter dynamic measurements have recently been investigated in the context of the Annex 58 of the International Energy Agency (IEA) under the EBC research program. Typically, PRBS (Pseudo-Random Binary Sequences) heating power solicitations are used covering about 10 days. Other dynamic sequences such as multi-sine sequences have been studied and optimized [5].

Finally, an even shorter (5 days) hybrid dynamic sequence for thermal solicitation of the building has been developed and investigated. This hybrid sequence enforces optimal decorrelation of the acquired data used for the model identification, as well as a good signal-to-noise ratio, smooth time series and homogeneous temperatures.

The air change rate (ventilation rate) and the solar aperture (solar gains) are important parameters that require careful attention, since they might significantly bias the identified heat transmission losses of the building envelope (H_D according to ISO 13789, sometimes noted UA in this paper), especially for heavily insulated buildings, and forcedly the total heat loss coefficient too, which would also make experimental inter-comparison more difficult.

The various methods present advantages and drawbacks in terms of monitoring and data analysis skills, measurement length, accuracy and cost.

3. OBJECTIVES AND STRUCTURE OF THIS STUDY

We firstly (section 4) recall the basic static energy balance of a building envelope, according the notations of the EN ISO 13789 standard. We then (section 5) summarize previous work on dynamic heating sequences optimization using simulation and grey-box modelling. We go on (section 6) with the description of the developed experimental infrastructure. We next (section 7) detail the test environment and review the performed experiments and acquired data. We continue (section 8) with the data analysis according to static, transient and dynamic analysis methods as described above. Finally (section 9) we draw some conclusions towards better on-site measurements and dynamic thermal modelling and performance identification of buildings.

4. ENERGY BALANCE OF A BUILDING ENVELOPE

The Heat Loss Coefficient (HLC) of a building can be expressed in terms of its various components, after multiplication by the temperature gradient between the inside and outside environments. The following set of equations is a steady-state representation of the system's energy balance.

$$\text{HLC} (T_i - T_a) = Q_h + A_w q_s \text{ [W]} \quad \text{with} \quad (1)$$

$$Q_h + A_w q_s = Q_V + Q_T = (0.33nV + \sum_i U_i A_i + \sum_k l_k \psi_k) \Delta T \text{ [W]} \quad (2)$$

where Q_h is the electric heating power, T_i and T_a are the inside and outside environmental temperatures, and $A_w q_s$ is the solar gains term. The HLC parameter only can be obtained when $A_w q_s$ is correctly identified. The heat losses are twofold: transmission losses (Q_T) and ventilation losses (Q_V). If Q_T is correctly identified (in statics by $\text{HLC} \cdot \Delta T - Q_V$) it then could be further decomposed into components' UA-values (and thermal bridges' $l\psi$ -values) but carries a huge uncertainty. Therefore, if the U-value of a specific homogeneous component of the building envelope is required, direct heatflowmeter measurements are recommended. The ventilation losses are proportional to the temperature gradient and to the air change rate estimated either by direct measurement (n_{ue}) or by infiltrometry (n_{50}), according to the following relationship:

$$Q_V = 0.33 V n_{ue} \Delta T \cong 0.33 V \frac{n_{50}}{15} \Delta T \text{ [W]} \quad (3)$$

Which includes the volume V of the building (m^3), by the volumetric heat capacity of the air ($0.33 \text{ Wh/m}^3\text{K}$).

Usually the identification of the building envelope HLC parameter is the main parameter of interest. In this study Q_V has been obtained by direct measurement, which theoretically allows deducing Q_T and hence performing more consistent comparisons between various experimental protocols performed under various weather conditions.

An example of the corresponding dynamic equations of a building envelope system is given in section 8. Rich dynamic data collection and analysis is useful in order to identify the main time constant of the building (or its effective thermal capacity) as well as the individual influence of solar radiation, and heating power on the thermal response of the building. As explained in the next sections, smooth evolution of the heating power is preferable while the temperature homogeneity inside the building has to be guaranteed as much as possible [6, 7]. For these reasons, a dedicated infrastructure is required and has been developed.

5. DYNAMIC SEQUENCES FOR ADAPTED CO-HEATING TESTS

Dynamic heating sequences have been investigated in order to develop an adapted co-heating test⁵ that more accurately and more robustly identifies the dynamic characteristics of a building envelope model. Additionally, dynamic sequences may show several advantages such as:

- exciting the system with a broad dynamic content in order to emphasize the various time constants of the system, which contributes to reducing the measurement time
- avoiding high peaks in the residuals of the system's model output, in order to make easier an unbiased statistical analysis and validation, thanks to their smooth characteristics

⁵The term « co-heating » is used here in the broadest sense and is not limited to measurements under constant indoor temperature.

The steps of the study presented in [5] included the modelling of two variants (lightweight and heavyweight) of a unique monozone building envelope geometry and its thermal simulation during 2 different periods of the year and under various dynamic heating sequences. The identification is done using various sample time data, with ARMAX statistical models using the inside temperature as output.

Multi-sine and PRBS sequences yielded good results for the investigated combinations of building envelope thermal mass and outdoor environmental conditions. Though, the study also showed that PRBS sequences are more susceptible to redundancy and reluctance compared to multi-sine sequences and more susceptible to the sampling time of the data. However, multi-sine signals require a pre-selection of suitable frequencies. Figure shows the two best dynamic sequences that were investigated in that study.

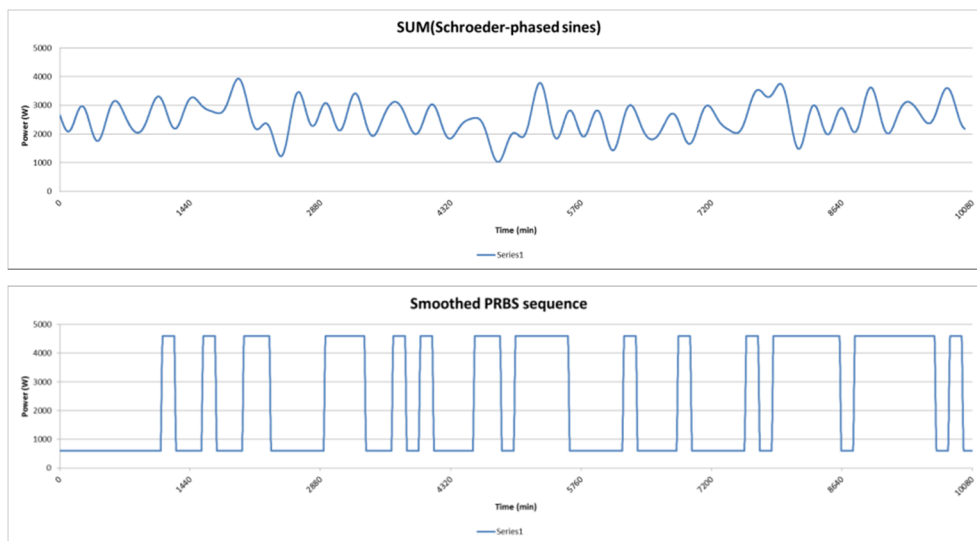


Figure 1: Representation of typical multi-sine and PRBS sequences used as thermal solicitation of the simulated building

The illustration on Figure 2 extracted from [8] shows why the use of a non-smooth dynamic excitation actually leads to a more difficult analysis of the results. Under such excitation, the heating signal (upper time-series, black line) is harsh and generates peaks in the residuals of the output predictors (bottom time-series, black lines). These peaks involve a higher stochastic error term and hence biased auto-correlation functions (ACF) and cumulated periodogram bounds, which eventually lead to weak interpretation of the model validity (top-right graphs). A workaround has been to identify two different stochastic error terms switching at a predefined and arbitrary pace to follow the shape of the solicitation sequence, which yields different ACF and periodogram (bottom-right graphs). This workaround is questionable and difficult to apply by inexperienced practitioners.

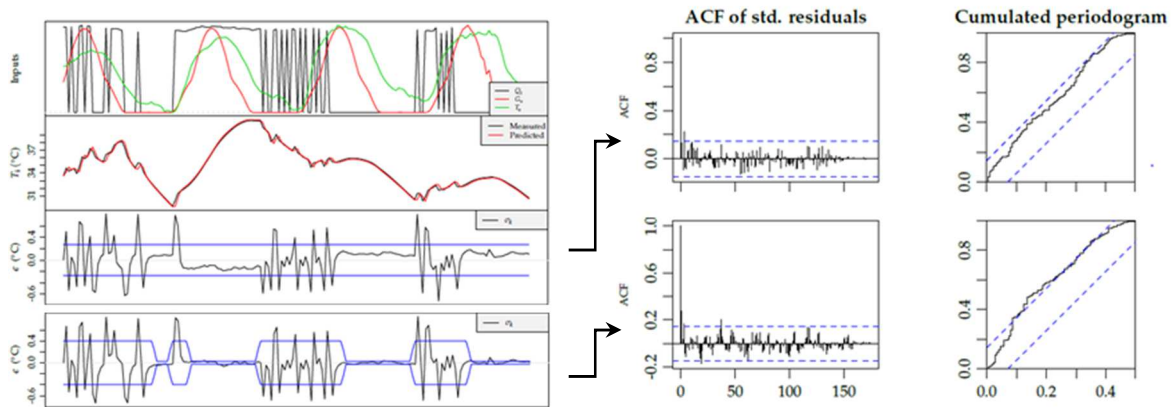


Figure 2: Example of residuals between measured and predicted indoor temperature and its harsh nature under rough PRBS heating power solicitation [8].

Peaks in the inputs and hence in residuals may be consistently avoided by smoothing the power input signal itself right from the experiment when PRBS sequences are used. The pre-filtering of this type of signal is useful only if the smooth transition occurs in a sufficiently long time compared to data sampling while not influencing the overall dynamic pattern of the PRBS signal. Transitions of 20 minutes with a sampling time of 5 minutes represent a possible trade-off.

Another possibility is to use intrinsically smooth multi-sine signals (here after X-sines) instead.

6. DEVELOPMENT OF THE EXPERIMENTAL INFRASTRUCTURE

6.1 Functional and technical requirements

As mentioned in section 5, appropriate dynamic sequences are required to solicitate all time constants of the system such a smoothed PRBS signals. Continuous time-varying sequences such as X-sines are also of particular interest. Therefore, a scalable power management system is required to conduct the experiments. In addition, a homogeneous temperature inside the complete building is an important prerequisite of such measurements [7] that cannot be met at the building scale by only using air-mixing fans.

Technically, this requires in each zone at least one temperature sensor, an energy meter, a relay that controls the heater, one electric heater and one fan. Several heaters and/or fans can be used if the zone is larger. The measurement of other temperatures (outside, adjacent spaces, etc.) and solar radiation is compulsory. Additionally, solar radiation must be measured at a higher frequency than other variables because of its unstable nature.

Outdoor environmental conditions (longwave radiation balance with the sky, wind speed and direction, rain, relative humidity, etc.) could be of interest depending on the depth of the analysis.

In order to obtain the ventilation losses (Q_V), multi-channel tracer gas air change rate measurements following a constant concentration scheme have been used.

6.2 Description of the experimental infrastructure

6.2.1 Multi-zone and continuous communication setup

The test infrastructure of the co-heating experiments consists of “kits” installed in each zone and connected to the central control & acquisition unit. The communication between the main

unit and the kits happens via a serial port (see Figure 3) with instructions updated every 100 seconds.

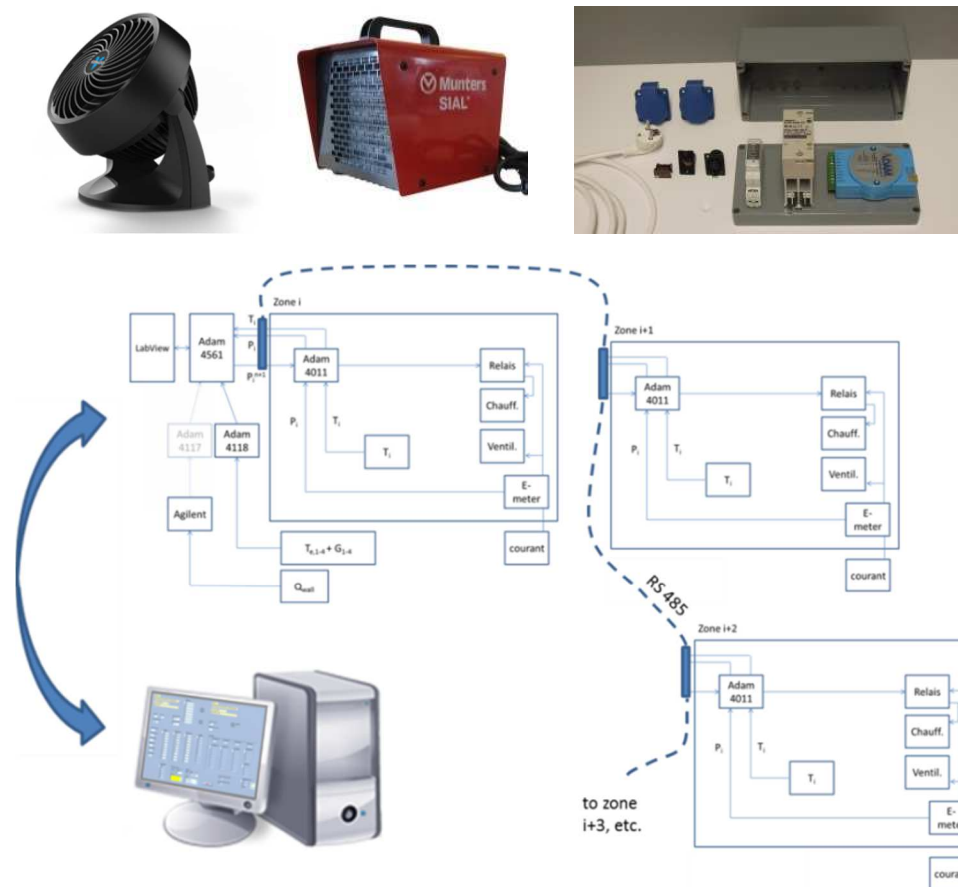


Figure 3: Electric fan, heater, temperature sensor plugged to the local module, all connected to the PC control & acquisition program through a serial port

Several adaptations are required to account for the fans, non-linearities of the heaters, potential drift in time of their nominal power, etc. A robust system is implemented through a hybrid closed-loop/open-loop control system.

Other boxes are used to monitor the outdoor environmental conditions, heat flow meters, etc.

A software user interface is also developed such that the type of experiment can be selected and adjusted, and current variables can be monitored. The control and acquisition program currently incorporates a broad range of utilizations and can be further extended. The user can specify a target temperature or total heating power in the building. This target can be defined as a time function from the LabView libraries or read from an external file. At every moment and without interrupting the measurement, it is possible to switch from one to another setup, which enables to generate more complex dynamic sequences.

6.2.2 Adaptive power distribution

The distribution of the total power towards the individual building zones is continuously adapted in order to ensure more homogeneous temperatures within the building. This is especially useful when performing a power driven test since for these types of test, simple (decentralized) thermostatic control is not possible. The power is spread among the zones using the following expression:

$$P_i^{n+1} = \frac{P_{tot}^{n+1} P_i^n / T_i^n}{\sum_i P_i^n / T_i^n} \quad (4)$$

where the P_i and T_i terms are the zonal powers and temperatures of the previous cycle and P_{tot} is the total power required during the new cycle.

6.3 Justification of the developed infrastructure

6.3.1 Smooth heating power and homogeneous temperature

The developed infrastructure merely allowed for dynamic and smooth heating sequences such as X-sines signals but it also significantly improved the temperature homogeneity within the building.

In the example illustrated in Figure 4, the total targeted heating power is spread among the 7 zones of the measured building. The graph shows a complete (clear sky and sunny) day from midnight to midnight, where the daytime has a white background and night-time a light blue background.

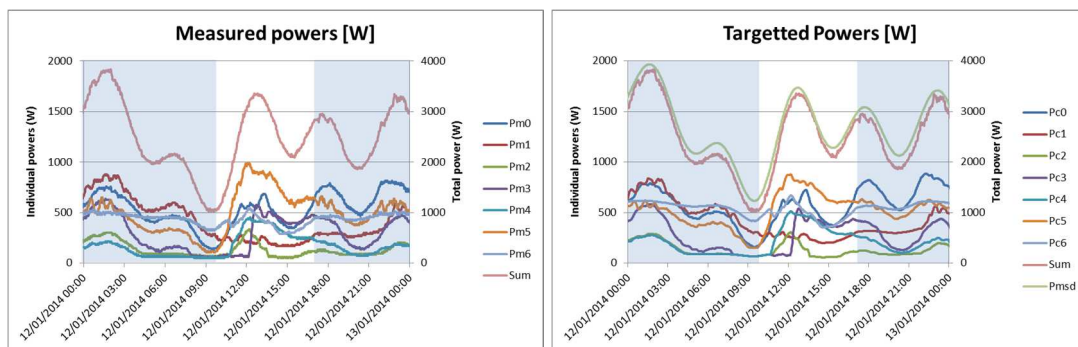


Figure 4: Heating power adaptive spread under dynamic measurement and correspondence between target (on the right) and measured (on the left) individual and global power

The total actual power (measured, in pink) follows the target quite well (in light green, on the right graph) and varies between 1000W and 4000W (right vertical axes of the graphs). Individual powers (left vertical axes) are distributed adaptively in order to maintain a homogeneous temperature in the building. The zone n°1 (Pm1, in red) is the largest of the house and logically requires a relatively high heating power during the night. Nevertheless, this zone also has a very large glazed surface oriented to the South. Hence almost no power is required in that zone during a sunny day because of large solar gains. Inversely a major part of the remaining heating power is directed to zone 5 (Pm5, in orange), a mid-size room oriented to the North-West which does not receive solar gains.

In Figure 5, one can see the evolution of the individual room's temperature during two days. At the very beginning, the temperatures are homogeneous due to the absence of solar radiation, and the adaptive heating power distribution. When the adaptive power distribution is turned off the temperatures quickly get inhomogeneous. Temperature inhomogeneity of 4K is observed inside the building while the temperature gradient between the indoor and the outdoor environment was only about 16K during these days (Figure 5).

A ratio between the degree-hour difference between the hottest and coldest rooms and the degree-hour difference between the average indoor temperature and outdoor temperature is proposed as:

$$\int_{t1}^{t2} \frac{T_{i,max}(t) - T_{i,min}(t)}{T_{i,mean}(t) - T_e(t)} dt \quad (5)$$

Applying this expression to the time window between noon and 4PM of the second day, the indicator reaches a significant value of 33%, which means a high uncertainty in defining the “mean” indoor temperature, hence in the Heat Loss Coefficient that is expressed as function of the denominator of the ratio. For the entire 2-days period the indicator value is lower but still reaches 11%.

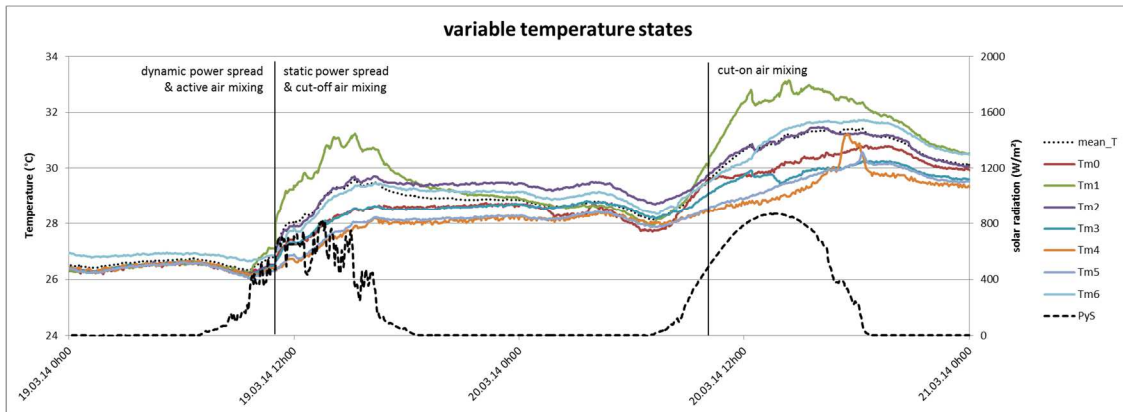


Figure 5: Temperature spread in the building under static distribution of heating power when doorframe fans are cut-off (centre) and after their reactivation (right)

In Figure 6, the adaptive power distribution is always turned on. The degree-hour ratio indicator between noon and 4PM yields 7% for the second day and only 3% for the entire 2-days period, which is much more acceptable.

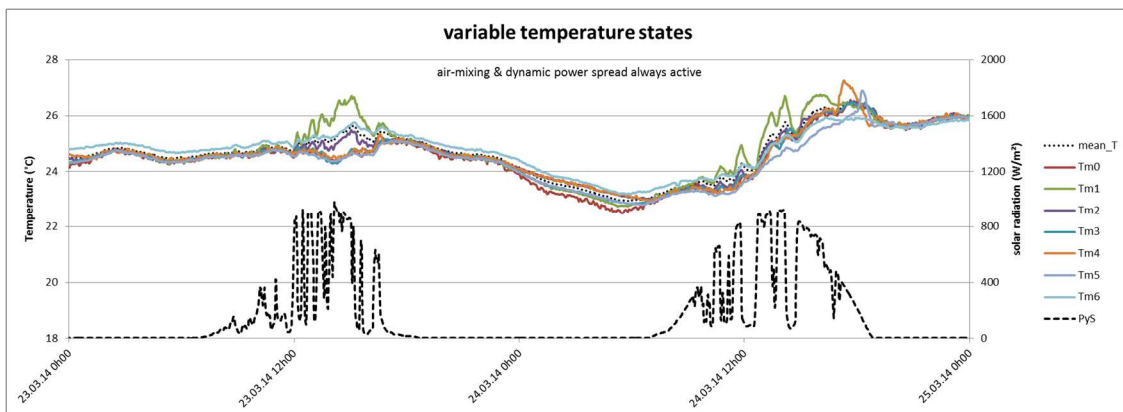


Figure 6: Temperature spread in the building under dynamic distribution of heating power with doorframe fans always activated

From the nearly-homogeneous individual temperatures, the building average temperature can confidently be obtained using a weighting function based on the volumes of the various zones (if they are sufficiently well defined), or by making a principal component analysis of all acquired temperatures. The first option is explicit and was used for the real-time control scheme, while the second one is only applicable after large enough statistics become available.

6.3.2 A short-term hybrid dynamic sequence

The developed infrastructure sets the basis for the design of a hybrid dynamic heating sequence, designed on the following observations. The static transmission term is emphasized with a stable temperature during the night, when there is no solar radiation and stable outside temperatures. The thermal capacity and time constants are emphasized with dynamic conditions at night for example using a sine-like signal. To identify the solar aperture, free-floating conditions during a clear day is ideal. Finally a temperature ramp makes the indoor and building

envelope smoothly recover their initial temperatures to exclude thermal accumulation in the building envelope during the test. These portions can be assembled to form a single dynamic data set, as illustrated in Figure 7.

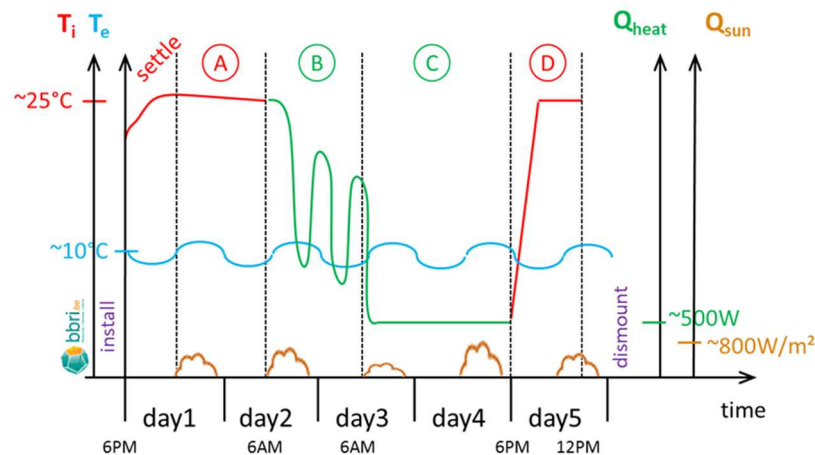


Figure 7 : Illustration of the hybrid 4-segments heating sequence

This 4-segments “hybrid” sequence is programmatically designed such that the inputs are the least correlated possible, such that the segments are smoothly connected and such that the total length is kept short, here 5 days. This is implemented and showed later in Figure 10 (bottom-left graph).

7. TEST ENVIRONMENT AND PERFORMED EXPERIMENTS

7.1 Test environment

A whole set of experiments has been executed onto an experimental building located on a small hill (see Figure 8). It is a detached house exposed to the winds with a ventilated attic and cellar. The effective internal surface area is 86m² and the ceiling height is 2.55m, the internal volume being 220m³. The external dimensions are 8.2m by 13.1m. The building is located at the BBRI facilities in Limelette, Belgium. The exterior walls are cavity walls insulated with 10cm of mineral wool. The ceiling is a light and mineral wool insulated wall. The floor is heavy and weakly insulated. The living room is oriented southwards and is heavily glazed. The windows are composed of double glazing and wooden frames.

The overall designed UA-value (H_D according to ISO 13789) is about 110W/K for the surface components of the envelope and about 40W/K for thermal bridges, such that the transmission loss coefficient reaches 150W/K. The ventilation system is not active and is sealed during the measurements. The air tightness of the building is 4.3 h⁻¹. The standardized ventilation losses are then about 21 W/K, which is about 14% of the reference transmission loss coefficient, leading to an overall heat loss coefficient of around 170W/K. This value is only a rough estimation since several design parameters are unknown and the building is not recent.



Figure 8: Localization and plans (upper), general outside view and inside view of a zone (lower) of the BBRI X2 experimental building

The plans and the instrumentation of the experimental building are shown in Figure 9.

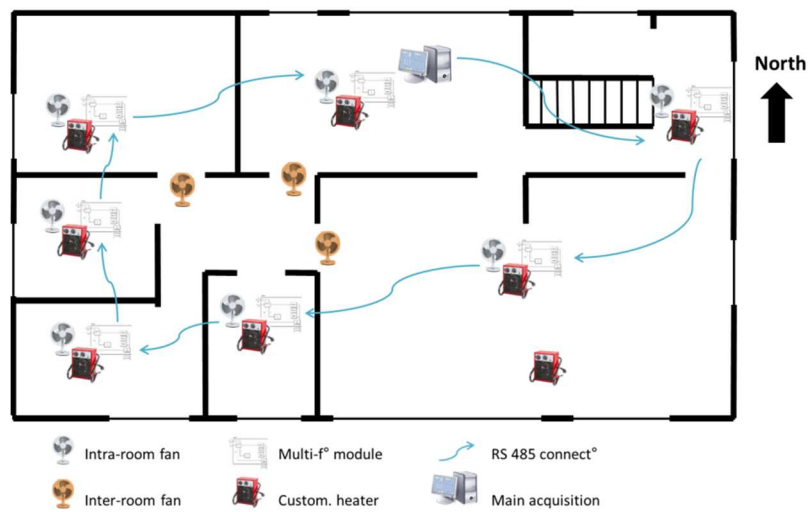
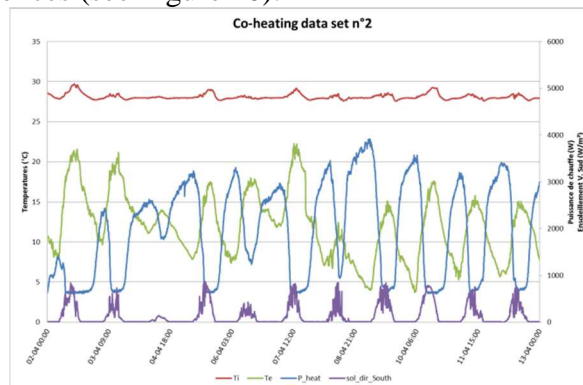


Figure 9: Co-heating infrastructure components and positioning in the house

7.2 Performed experiments

As explained in Section 5.2 the developed infrastructure allows obtaining all kinds of dynamic data. Various sequences have been applied such as temperature set-point, (smoothed) PRBS, X-sines sequence, hybrid (labelled SMART here below) and QUB (stands for quick-U-building, see [12]) sequences (see Figure 10).



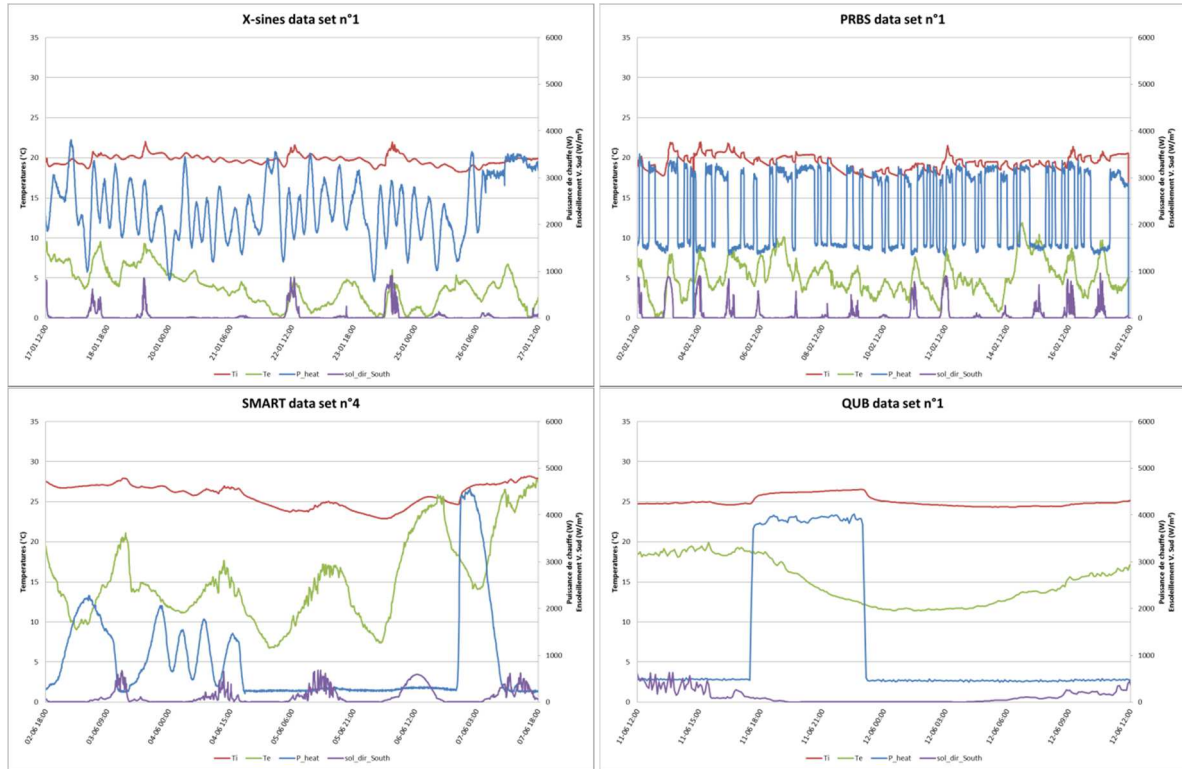


Figure 10: Various measurement data sets. Temperature set-point co-heating (top), smoothed PRBS and X-sines (center), SMART and QUB (bottom)

For all sets, 5min sample time data files are available, Multi-zone data is aggregated at building level. Outdoor climate sensors installed near the building include air temperature and relative humidity, vertical global solar radiation on the East, South and West façades, wind speed and direction, as well as horizontal global and diffuse solar radiation a.o.

8. STATIC, TRANSIENT AND DYNAMIC DATA ANALYSIS METHODS

8.1 Possible data analysis procedures

Various procedures from the very simple towards much more complex are already developed [1, 7, 12]. We briefly expose these procedures before applying them on the acquired data sets.

8.1.1 Dynamic analysis

The most promising analysis methods are parameter identification methods applied on dynamic data sets, such as the PRBS, X-sines and the hybrid (SMART) ones. In this paper, a grey-box stochastic model is used to represent the entire building. It is rather simple and often appears suitable:

$$dT_i = \frac{(T_e - T_i)}{R_{ie}C_i} dt + \frac{Q_h}{C_i} dt + \frac{A_w q_s}{C_i} dt - \frac{Q_v}{C_i} dt + \sigma_i d\omega_i \quad (6)$$

$$dT_e = \frac{(T_i - T_e)}{R_{ie}C_e} dt + \frac{(T_a - T_e)}{R_{ea}C_e} dt + \sigma_e d\omega_e \quad (7)$$

$$\frac{1}{R_{ie} + R_{ea}} \cong HLC - \frac{Q_v}{T_i - T_a} = HLC - 0.33n_{ue}V \quad (8)$$

The corresponding one-dimensional whole-building RC-network is represented in Figure 11 :

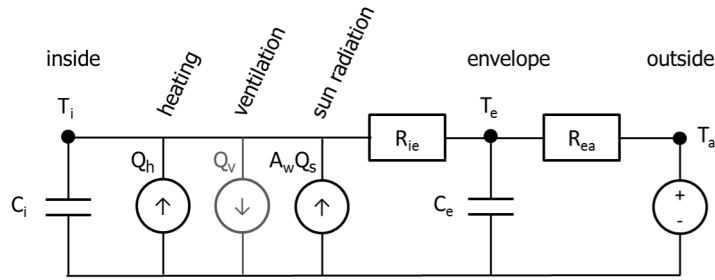


Figure 11: Equivalent RC-network of the whole building envelope thermal model

The interior temperature is the output state of the model and is associated with a thermal capacity (air & furniture). The outdoor temperature is chosen as input. The (unobservable) building fabric envelope temperature is assumed to be aggregated in one single node and is obviously associated with a thermal capacity. The overall thermal resistance offered by the envelope against the heat losses is represented by two thermal resistances in series. Finally, the system is subjected to three other inputs: the electric heating power, the ventilation losses and the solar radiation, all predominantly acting on the inside air node temperature. The solar radiation is given in W/m² and is associated to an aperture coefficient that gives an equivalent surface through which the radiation is fully transmitted. The ventilation loss is applicable if an instantaneous air change rate can be measured or estimated.

Removing the envelope state and neglecting ventilation losses would combine equations (6) and (7) into equation (9) only:

$$dT_i = \frac{(T_a - T_i)}{R_{ia} C_i} dt + \frac{Q_h}{C_i} dt + \frac{A_w q_s}{C_i} dt + \sigma_i d\omega_i \quad (9)$$

Additional states and input variables could reversely be added to refine the model, yet avoiding over-fitting or modelling of the noise terms (Wiener process $\sigma d\omega$) instead of the actual physical phenomena. This is especially the case with in-situ measurements that can be noisier than laboratory measurements, or if the inputs are cross-correlated, which is frequent when extending the number of inputs.

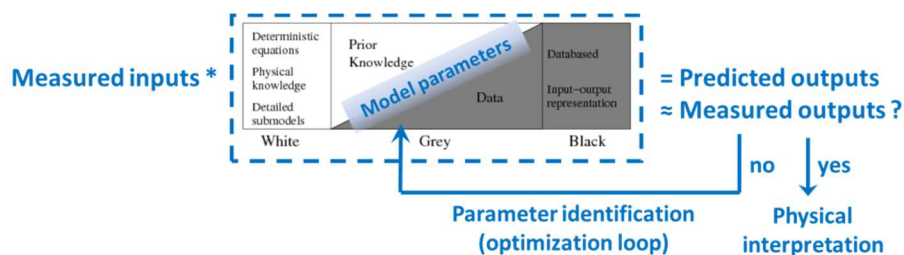


Figure 12: Optimization scheme to identify the parameters of the dynamic model or transfer function between inputs and outputs

The solving and identification of the model parameters (R's, C's, and A_w in this case) is executed by a dedicated mathematical/statistical solver which minimizes the residuals between the predicted and the measured outputs in an optimization scheme, as shown in Figure 12. The post-processing of the identified model parameters then enables a physical interpretation of the overall HLC, C and A_w characteristics of the building.

8.1.2 Transient analysis

Another analysis method has been promoted by an insulating material manufacturer [12] and is typically applied on nightly transient data sets. The proposed method has been shown to give reasonably accurate values of the HLC under certain conditions. If the measurement is

performed at night when there is no solar radiation, and if T_a and Q_h are sufficiently stable then eqn. (9) can be reduced to:

$$\alpha \triangleq \frac{dT_i}{dt} \cong \frac{d\Delta T}{dt} = \frac{-\Delta T}{RC} + \frac{Q}{C} \quad (10)$$

This relation can be rewritten twice with the h (heating) and c (cooling) indexes for two periods with significantly different values of Q :

$$\alpha_h = \frac{-\Delta T_h}{RC} + \frac{Q_h}{C} \quad \text{and} \quad \alpha_c = \frac{-\Delta T_c}{RC} + \frac{Q_c}{C} \quad (11) \text{ and } (12)$$

By isolating R from (10) and inserting it into (9) we obtain:

$$C = \frac{Q_h \Delta T_c - Q_c \Delta T_h}{\alpha_h \Delta T_c - \alpha_c \Delta T_h} \quad (13)$$

By making (11) * Q_c – (12) * Q_h and then substituting C by (13) we finally get:

$$HLC = \frac{1}{R} = \frac{\alpha_h Q_c - \alpha_c Q_h}{\alpha_h \Delta T_c - \alpha_c \Delta T_h} \quad (14)$$

The expressions for HLC and C are the two unknowns resolved from of a simple set of two equations. The two measurements can happen in one single night if the conditions are propitious and if the main time constant of the building is small enough (limited thermal resistance and mass). Otherwise, two (consecutive) nights are required. This approach could also be applied onto building envelope components, provided the heat flux density across the component can be maintained with an adequate control system.

8.1.3 Static analysis

The most basic analysis is associated to the historical co-heating experiment assuming quasi-steady state conditions and is obtained by further simplification of equation (9) for which T_i is supposed invariable. When then can rewrite:

$$C_i \frac{dT_i}{dt} = 0 = \frac{(T_a - T_i)}{R_{ia}} + Q_h + A_w q_s \quad [\text{W}] \quad (15)$$

$$\text{or} \quad HLC - \frac{A_w q_s}{\Delta T} = \frac{Q_h}{\Delta T} \quad [\text{W/K}] \quad (16)$$

$$\text{where} \quad HLC = \frac{1}{R_{ia}} \quad \text{and} \quad \Delta T = T_i - T_a$$

In equation (19), both the HLC and $A_w q_s$ terms are found implicitly from a bi-linear regression.

It is then also possible to correct the used energy term by the ventilation losses if one requires estimating the building UA-value (H_D according to ISO 13789) instead of the overall heat loss coefficient HLC. Equation (16) can then be modified as:

$$H_D - \frac{A_w q_s}{\Delta T} = \frac{Q_h - Q_V}{\Delta T} \quad [\text{W/K}] \quad (17)$$

This correction is used in order to better compare the experimental designs and analysis methods since the actual air change rate could strongly vary in time and hence impact the HLC. Further in this paper we will refer as to building HLC and building UA-value depending if the correction is applied or not.

If both solar radiation and ventilation heat loss are (supposed to be) negligible, the HLC value can be obtained from the simple ratio between the cumulated electric power that is injected into the building and temperature gradient between the inside and outside during a long enough measurement. The most widespread method is to use the regression line for daily averages of these two terms:

$$HLC = \frac{\int Q_h}{\int \Delta T} \Leftrightarrow HLC = \frac{Q_h}{\Delta T} \text{ [W/K]} \quad (18)$$

Since the solar gains are neglected, the heat loss coefficient will be underestimated.

Another small variant of the co-heating test is to split the measurement into several periods during which the temperature set-point is different, for example 18°C-23°C-28°C. This enables obtaining a larger range of temperature gradients and a better correlation coefficient of the regression line.

8.2 Static analysis

Applying both linear and bilinear regressions at both the complete HLC then the sole UA-value, the graphs of Figure 13 and results of Table are obtained.

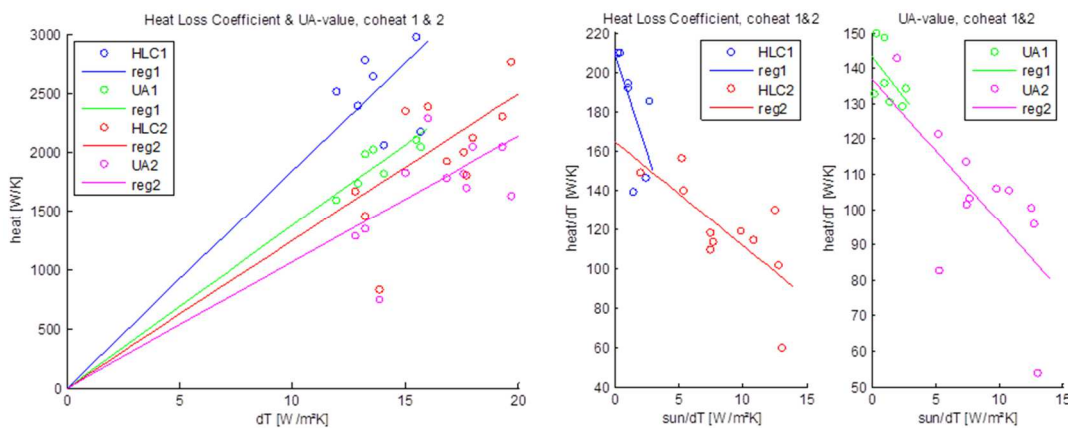


Figure 13: Linear and bi-linear regression from two co-heating tests, at HLC and UA levels

Table 1: Results of static analysis on transient data sets

	Parameter	coheat 1		coheat 2	
		Linear	Bi-linear	Linear	Bi-linear
HLC	Aw (m ²)	-	-13.3	-	-5.4
	Losses (W/K)	183	198.9	124	161.7
UA	Aw (m ²)	-	-3.7	-	-4.4
	Losses (W/K)	137	141.9	106	137.1

The linear regression shows smaller UA results than HLC ones and a high discrepancy from one test to the other, especially at the HLC level (60 W/K). The bilinear regression still shows scattered HLC results and much more reproducible UA results (intercepts of the regression). Moreover, this is also true for the solar aperture coefficients (slopes). This proves that both the air change rate and the solar radiation must be taken into account if accurate and reproducible results are wished.

UA results based on bi-linear regressions are very close to the design value.

8.3 Transient analysis

The transient analysis method only can be applied to the QUB data sets. Both results from the specific analysis method and from the more general dynamic analysis method are shown in Table 2, directly at the UA level. The solar gains are neglected since the measurement is executed overnight.

Table 2: Results of transient analysis on transient data sets

		qub1	qub2	qub3	qub4
UA	trans. (W/K)	185.2	104.2	158.7	192.3
	dyn. (W/K)	181.4	150.0	144.3	144.2

A relatively good agreement is shown between the last three tests when a dynamic analysis of the data is performed. This is less the case when the simplified analysis method developed in 8.1.2 is applied. Moreover the first test result seems to be an outlier. It is not known if this is caused by a wrong measurement or by specific measurement conditions.

The last three UA results are very close to the design value, when based on dynamic analysis of the data.

8.4 Dynamic analysis

In this section, the results obtained on four fundamentally different data sets are analyzed: the co-heating set is typically longer but less rich, the PRBS and X-sines are shorter and richer but are either harsh or have lower signal-to-noise ratio, while the hybrid (smart) set is very short, rich and well-conditioned.

Analysis has been done on 15min sample time data. The solar aperture, the heat losses and thermal capacity of the envelope are given for each set, both with the ‘HLC’ and the ‘UA’ approaches. Heat losses and thermal capacity at the component level is also estimated.

At the building level, the UA-values are lying in a narrow band of 143 to 152 W/K. It should be noted that the data sets are acquired during the winter (PRBS and X-sines), the mid-season (co-heating) and the nearly-summer (smart) and that this has necessarily an impact on the solar aperture. The impact on the UA-values nevertheless remains small. The difference between identified HLC and UA-values renders well the amount of losses by ventilation which cannot be simply overlooked. This is for example the case for the prbs1 dataset.

Discrepancies are to be noted on the thermal capacities: clearly, the most dynamic data sets (PRBS and X-sines) also show the smaller “effective” capacities since the thermal mass is not best activated with fast dynamic solicitations.

Areal effective thermal capacities of the building envelope components (Wh/m²K) are shown in

Table 3. The ceiling generally appears less massive than the floor and walls. Better knowledge of the wall composition would be required to extract reference dynamic thermal capacities, for example using the ISO 13786 standard and a solicitation cycle of one day.

Table 3: Results of dynamic analysis on selected dynamic data sets

		Static/Dynamic/Transient						
15 min sampling		coheat2	prbs1	xsines1	smart4	avg	st dev	
mean(Ach_avg) (1/h)		0.14	0.88	0.26	0.25	0.38	0.34	
mean(Sol_5) (W/m ²)		139	80	54	121	98.25	38.52	
HLC	Aw (m ²)	4.23	4.32	5.98	2.96	4.36	1.22	
	HLC (W/K)	159.98	183.62	157.87	143.34	161.20	16.67	
	Ctot (Wh/K)	11052.90	6438.10	9715.50	13579.60	10196.53	2974.09	
UA	Aw (m ²)	5.15	7.41	7.94	11.79	8.07	2.76	
	UA (W/K)	152.12	132.99	150.96	143.63	144.93	8.80	
	Ctot (Wh/K)	16035.00	12121.17	12668.87	13234.50	13514.89	1740.48	
HLC-UA		7.86	50.63	6.91	-0.29	16.28	23.19	
comp.	Λ_{fl} (W/m ² K)	0.46	0.42	0.49	0.42	0.45	0.03	
	C _{fl} (Wh/m ² K)	64.49	37.56	44.30	55.02	50.34	11.86	
	Λ_{wal} (W/m ² K)	0.58	0.43	0.52	0.50	0.51	0.07	
	C _{wal} (Wh/m ² K)	100.15	113.00	82.88	62.89	89.73	21.74	
	Λ_{cell} (W/m ² K)	0.19	0.30	0.28	0.22	0.25	0.05	
	C _{cell} (Wh/m ² K)	8.66	46.44	43.23	7.58	26.48	21.24	

The thermal properties of the three measured components (floor on cellar, external walls and ceiling under attic) are given in accordance to the WD/ISO 9869-1 standard. Measured thermal conductances (Λ -values) are compared in Table 4 to the assumed design values:

Table 4: Results of dynamic analysis of building components

Λ -values (W/m ² K)	Floor	Wall	Ceiling
Identified value	0.45	0.53	0.31
Design value	0.45	0.41	0.22

Identified and design values are comparable but are not fully consistent and need more investigations; among others, better reference values are required. Note nevertheless that standard deviation of results for Λ -values from various experiments are very small.

We finally show below an example of the dynamic analysis procedure, executed with the CTSM-R tool and using the model structure illustrated by the set of equations (6) and (7), applied on the hybrid (smart4) data set for the whole building envelope.

After statistical optimization, the estimates, standard errors, and significance tests obtained for each one of the model parameter are given in Table 5.

Table 5: Results of dynamic analysis of building components

	Estimate	Std. Error	t value	Pr(> t)
T _i (0)	2.8E+01	4.3E-02	6.4E+02	0.0E+00
T _e (0)	2.4E+01	2.6E+00	9.2E+00	0.0E+00
A _w	1.2E+01	2.0E+00	6.0E+00	4.2E-09
C _e	1.4E+03	8.2E+02	1.8E+00	7.8E-02
C _i	1.2E+04	1.8E+03	6.4E+00	4.3E-10
e ₁₁	-2.2E+01	1.3E+02	-1.7E-01	8.6E-01
p ₁₁	-2.5E+00	9.3E-02	-2.7E+01	0.0E+00

p_{22}	1.3E+00	3.9E-01	3.4E+00	8.3E-04
R_{ea}	6.0E-03	2.3E-04	2.6E+01	0.0E+00
R_{ie}	1.0E-03	2.9E-05	3.5E+01	0.0E+00

The last two lines of the table (relating to the two thermal resistances R_{ea} and R_{ie}) enable computing the final transmission loss coefficient (UA-value) and its 95% confidence interval which gives a value of 143.6 +/- 9.5 W/K, or 143.6 +/- 6.6 %. The other physical parameters are the solar aperture (A_w) and the two thermal capacities (C_e and C_i).

The dynamic model is optimized such that the one-step ahead prediction of the inside temperature is the closest to the measured inside temperature with time steps of 15 minutes in this example. The validation of the model relies on the analysis of the difference between the measured and predicted inside temperature, or residuals. These residuals are shown at the top of Figure 14a. It is seen in Figure 14b that these are nearly white-noise but that the model could be further refined. In Figure 14a, it is clearly seen that the residuals are correlated with solar radiation.

Since the residuals happen at a relatively high frequency it can be concluded that they relate to faster dynamics of the system. Hence, refining the model should not significantly improve the transmission loss coefficient estimation (static parameter), based on the available data.

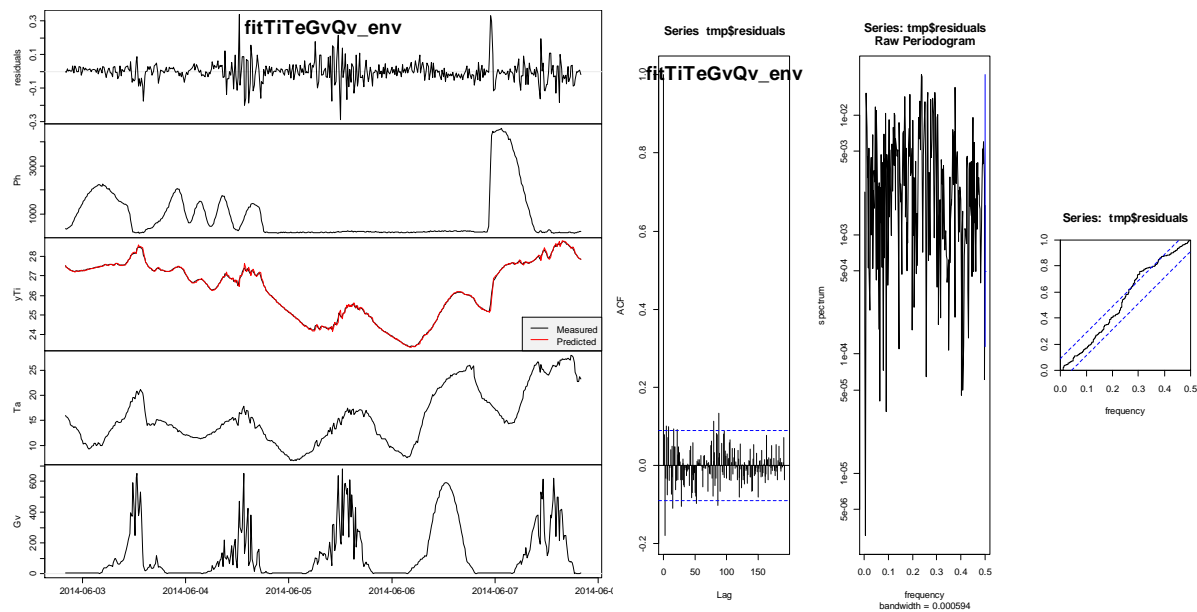


Figure 14: a) residuals between the measured and predicted output of the model, heating power, inside temperature (measured and predicted), outside temperature and vertical south solar radiation. b) autocorrelation of the residuals, raw and cumulated periodograms.

8.5 Conclusions

Reliably determine the main parameters of a building model or building component requires care in the test environment, experimental procedure and data analysis. If prerequisites are met, the heat loss coefficient and more specifically the transmission losses can be estimated using various methods.

The usage of the results will depend on the used methodology. At the building level, static analysis only gives the UA-value and some indication on the solar aperture. Transient analysis gives some insights about the thermal capacity but no indication on the solar aperture. Dynamic analysis enables the most correct identification of thermal capacity, solar aperture, and

transmission loss. Additionally it could serve to predict energy use. This is a first step towards smart grids supply-side management, especially in case of electricity-driven buildings.

More research is required to improve dynamic models, among others concerning the representation and identification of solar gains which have a predominant effect for heavily insulated and glazed buildings.

9. DISCUSSION AND PERSPECTIVES

The newly developed infrastructure enables performing all kinds of dynamic experiments with more homogeneous temperatures and gradual control of the system. A hybrid dynamic sequence, short in time yet rich in content has been developed on that basis and proved to be adequate to identify dynamic building parameters. Air change rate measurements with a constant concentration tracer gas method showed that ventilation losses may have a significant impact in the total heat loss coefficient while they also vary with the weather conditions.

Similarly to other infrastructure, the developed equipment and procedure remains intrusive (even for only 5 days) and is not applicable to occupied building, nor large or uninsulated buildings that require higher installed electric capacities.

A balance between accuracy and applicability of the methods might be located towards less intrusive methods, such as the “in-use” testing where the central heating system is used to conduct the thermal solicitation. This test is more representative of the envelope thermal performance under real usage, including distribution and emission efficiency of the heating system. However, when the building is occupied, specific user behaviour has to be monitored, and thermal solicitation should be respectful of occupants’ comfort. Nevertheless, the measurement is less limited in time and may bring complementary information.

Static, transient and dynamic measurement and analysis methods have been presented in section 8.1. When data analysis and experimental design methods are adequately paired, most of them are able to deliver consistent results, both at building and component levels. The identified dynamic models and structure could be further optimized and confidence interval of the identified parameters reviewed. The analysis of the acquired data nevertheless showed that shorter (<1 week) and rich dynamic measurements are a reasonable alternative to longer (>2 weeks) co-heating test under constant indoor air temperature.

10. OVERALL CONCLUSIONS

A new type of (hybrid) dynamic sequence for the thermal solicitation of a residential building, short in time, rich in content and ensuring a homogeneous temperature throughout the building has successfully been applied in an experimental building and the analysis of the acquired data showed that the proposed protocol is a reasonable alternative to longer quasi-static or adapted co-heating tests. The developed infrastructure remains intrusive and is less suited for measurements in occupied or high energy buildings. Integrated or “in-use” tests using the building’s heating system and smart meters and the best balance between accuracy and applicability should be further studied in function of the application.

ACKNOWLEDGMENT

This paper is published in the context of the pre-normative research project 'PERFECT' with the financial support of the Belgian Bureau for Standardization (NBN).

Were hereby thank all the people involved in the measurements for their support and more specifically Didier L’Heureux and Philippe Voordecker.

We also thank the whole group of Annex58 members for the interesting discussions and shared ideas during the expert meetings (among others P. Bacher, G. Bauwens and G. Pandraud).

REFERENCES

- [1] Bacher, P. et al. 2011, Informatics and Mathematical Modelling, Technical University of Denmark. *Identifying suitable models for the heat dynamics of buildings*. Energy and buildings 3121.
- [2] Steskens, P. et al. 2013, Belgian Building Research Institute. *The inverse modelling of a testbox's heat dynamics*. IEA Annex 58 - Subtask 3 – Common Exercise 4.
- [3] Lethé, G. et al. 2013, Belgian Building Research Institute. *Dynamic analysis replication of a testbox in various climates*. IEA Annex 58 - Subtask 3 – Common Exercise 4.
- [4] Roels, S. et al. 2013, Building Physics Section KU Leuven. *Characterising the actual thermal performance of buildings: round robin experiment within IEA EBC Annex 58*.
- [5] Steskens, P., Lethé, G., Flamant, G., 2014, Belgian Building Research Institute. *The application of a modified co-heating test and grey-box modelling for predicting building thermal dynamics*. 10th Nordic Symposium on Building Physics.
- [6] Bacher, P., Thavlov, A., Madsen, H., 2010, Informatics and Mathematical Modelling, Technical University of Denmark. *Models for Energy Performance Analysis*.
- [7] Johnston, D., Miles-Shenton, D., Framer, D., Wingfield, J. 2013, N0191 Whole House Heat Loss Test Method (Co-heating). CEN/TC 89/WG 13 - *In-situ thermal performance of construction products, building elements and structures*.
- [8] Bacher, P., Delff, Ph. 2013, Technical University of Denmark. *Grey-box models for thermal performance characterization of a testbox*. IEA Annex 58 - Subtask 3 – Common Exercise 4.
- [9] Subbarao, K. et al. 1988, Solar Energy Research Institute, US Department of Energy. *Short-Term Energy Monitoring (STEM): Application of the PSTAR Method to a Residence in Fredericksburg, Virginia*. Task No. SB811241.
- [10] Bauwens, G., Roels, S., 2014, KU Leuven – Building Physics Section, *Co-heating test: a state-of-the-art*.
- [11] Gorse, C., et al. 2014, Leeds Sunstainability Institute, CeBE, *The gap between calculated and real performance: experiences from the field and the measures required o address the difference*.
- [12] Pandraud G, Mangematin E, Roux D and Quentin E, 2013, *QUB: a new rapid building energy diagnosis method*. 11th REHVA World Congress and 8th International Conference on IAQVEC.
- [13] ISO 9869-1, 2014, 1st edition, Thermal insulation - Building elements - *In-situ* measurement of thermal resistance and thermal transmittance - Part 1: Heat flow meter method

FULL SCALE EMPIRICAL VALIDATION FOR BUILDING ENERGY SIMULATION PROGRAMS

M. C. Kersken¹, I. Heusler¹ and P. Strachan²

⁽¹⁾ Fraunhofer Institute for Building Physics IBP, Holzkirchen, Germany

⁽²⁾ University of Strathclyde, ESRU, Dept. of Mechanical and Aerospace Eng., Glasgow, Scotland

1. ABSTRACT

This document describes the development of a full-scale empirical validation dataset for building energy simulation tools. This development is part of the IEA ECB ANNEX 58 "Reliable building energy performance characterization based on full scale dynamic measurement" (ANNEX 58 Homepage). The validation method consists of a set of high quality measurement data and a precise documentation of all boundary conditions. This enables a user to create a very complete model of the different validation scenarios. The results of this model can be compared to the real measurement data. Because of the detailed modelling the remaining deviations should indicate the limitations of the tool under investigation. The definition of the scenarios consists of extensive weather data and a detailed description of the building geometry, components compositions, thermal bridges, air tightness, ventilation, etc.

The UK author acknowledges support from the Engineering and Physical Sciences Research Council Ref: EP/K01532X/1.

The effort of the German authors is supported from the German Federal Ministry for Economic Affairs and Energy under the reference 03ET1144A.

Keywords: Simulation, validation, measurement data, in situ, BESTEST

2. INTRODUCTION

In the planning of complex modern buildings, dynamic building simulation is commonly used for predicting design performance. A prerequisite for the use of these software tools is the assumption that they are able to accurately reflect the diverse physical processes of the building service equipment and within a building. The established qualification systems for simulation tools are BESTEST (Building Energy Simulation Tests) (Judkoff et al., 1995), other tests within ASHRAE Standard 140 (ASHRAE 140) and CEN (ISO 13791, 15255 and 15265). These tests are all comparative tests: The "real" comparison values are based on a certain range, determined by calculated reference values from existing simulation tools or prescribed calculation methods. They have been shown to be useful for diagnostic purposes and for showing that programs produce consistent results for checking compliance with building energy standards.

The aim of the study reported in this paper is to generate a dataset of high quality measurement data for the purposes of empirical validation. By providing a very detailed documentation of the boundary conditions of this data set, the validation of the most important physical models of a simulation program is possible. The work carried out can be broken down into four separate work packages: The development of the experiment to obtain the measurement data, its implementation and quality assurance, the construction of models by the modelling teams using the known boundary conditions (blind validation), and the review of the individual model results after release of the measured heating energy and air temperatures. This paper shows what sub-models of a Building Energy Simulation (BES) program can be re-viewed and how this is made possible by the experimental setup and the validation procedures. The measurement

of the validation data is performed on the Twin Houses of the Fraunhofer Institute for Building Physics IBP on the outdoor test site at Holzkirchen, south of Munich in Germany. The IBP's Twin Houses are two completely identical, typical German single family houses. These homes are instrumented in such a way that a complete collection of all relevant boundary conditions is possible. Thus, a sufficiently accurate simulation model should be able to reproduce the measured indoor air temperatures and heating energy consumption. In order to check the different sub models of a BES software, different scenarios are included in the experimental program. In parallel with various ventilation scenarios in different rooms, scenarios with respect to set temperatures, heating powers and shading devices are provided. For space reasons this document does not contain a complete documentation validation procedures itself. The results of the validations will be published in a separate document.

3. MOTIVATION AND RELEVANCE

Simulation programs are in common use for evaluating building energy and environmental performance. As more low-energy technologies for supply and storage get embedded within designs, the complexity of the interactions of heat and mass transfer processes increases: Fabric and ventilation losses decrease, the options for power, heating and cooling supply and storage increase, and the buildings become more dynamic, with potential control and overheating problems. It is essential that the simulation programs are fit for purpose, and that they are seen to be so. An overall validation methodology is well established and comprises elements of analytical, inter-program comparison and empirical test (Judkoff et al 1983, Jensen 1993). Inter-program comparative tests have the advantages that they are relatively easy to apply and that many parameters can be tested. They have been successful, particularly in their diagnostic role in detecting program errors (e.g. BESTEST, resulting from an International Energy Agency (IEA) project; Judkoff and Neymark 1995). The European Standards for heating/cooling energy and summer overheating calculations (ISO 13790, ISO 13791, EN 15255, EN 15265) allow detailed thermal simulation for the calculations. However, all the tests involve only inter-program comparisons and a few simple analytical tests with tolerance bands for predictions.

There is criticism that there is no truth standard in such comparative tests. Empirical tests can provide this, but gathering high quality experimental data is expensive and time consuming. There have been some high quality datasets collected within large-scale international (IEA) projects for empirical validation purposes, but these have been at component level, e.g. for testing micro-cogeneration models in IEA Annex 42 (IEA EBC Annex 42), or on outdoor test cells, e.g. IEA Annex 43/Task 34 (IEA ECB Annex 43).

It is recognized that there is a need for high quality datasets at the full building scale to provide confidence in the use of detailed simulation programs. Although previous attempts to undertake such studies have not been wholly successful, a combination of factors should now improve chances of success: Namely widespread availability of comprehensive sensor and instrumentation equipment, the availability of sophisticated test buildings, knowledge regarding errors in previous experimental programs and improvements in simulation programs to model low energy technologies to assist in the experimental design.

The difficulty with conducting empirical validation on full-scale buildings is the level of detail required of the building construction and operation, plus detailed knowledge of the time-varying boundary conditions during the experiment. If any heat flow path is not monitored or if any building details are unknown, then there will be doubt about whether any mismatches between measurements and model predictions are caused by deficiencies in the program or measurement uncertainties. The challenge for those conducting such experiments are to minimize uncertainties in the building and its boundary conditions, as well as providing enough

detail on the spatial and temporal variation in temperatures and heat fluxes to help narrow down the cause of discrepancies between measurements and predictions. It is also necessary to design the experiments to test the modelling of as many heat flow paths as possible (e.g. modelling of ventilation, fabric heat loss, solar transmission).

This implies that all building details, such as building geometry, construction materials, thermal bridges, optical glazing properties, etc. are available with a high degree of reliability. Also, all boundary conditions that may affect the internal temperatures and fluxes should be measured - external temperature, solar radiation, wind conditions, ground temperature etc.

A significant advantage (and difficulty) for empirical validation is that thermal processes that are usually ignored in comparative validation need to be considered. When validating with real measurement data, all physical phenomena occurring in a real building will necessarily be included in this data because they originate from a real building. For example, thermal stratification in a room may not be included in the comparative tests mentioned earlier in this section, but it might occur in reality. In that case the air and surface temperatures at the ceiling will be higher in reality than in the validation data. This could result in higher heat losses through the ceiling and so in a changed energy balance for the whole room.

There are also disadvantages with empirical validation. Even a quite simple building like the one used in this study is quite complex to model. Many thermal bridges have to be calculated with a high degree of detail. Internal walls and doors that acting as thermal bridges between the single rooms have to be considered when the trends of all room temperatures and heating powers need to be compared. Care must also be taken to ensure the building information is accurate. For example, the thickness of a construction layer may be different than indicated in the available specifications or may vary locally. Also the thermal properties of building fabric can be different from the manufacturer's specification. So the exterior plaster might have some little cracks resulting in some moisture penetrating into an external insulation reducing its effectiveness. The thermal conductivity specified in a product data sheet usually is lower than the conductivity of the real product. This is necessary to ensure that no significant amount of delivered fabric is missing its specifications (DIN 4108 4).

4. EXPERIMENTAL VALIDATION PROCEDURE

Within IEA ECB Annex 58, the empirical validation procedure followed a structured approach. Firstly, simulations were conducted as part of the experimental design using known building details and typical weather data for the site. This allowed a detailed experimental specification to be developed with information on the building, the test schedule, the magnitude of heat injections and the necessary measurements. The test buildings were then prepared and the experiment conducted. This paper focuses mostly on the work carried out in preparing the experiment. One important feature of the designed experiment was to use two essentially identical buildings in a side-by-side configuration with slightly different experimental set-ups, so that not only absolute comparisons of measured temperatures and heat fluxes could be made with the predictions but also measured and predicted differences between the two buildings could be compared.

After the experiment was completed, the measured data was processed and boundary conditions distributed to modelling teams as part of a "blind" validation (i.e. they were not told the internal conditions). Modelling teams were provided with the detailed specification, containing information on all relevant aspects of the building:

- Location
- Geometry

- Glazing and frame areas
- Constructions
- Glazing optical and thermal properties
- Roller blind properties
- Thermal bridges
- Ventilation
- Heating
- Air leakage measurement data
- Ground reflectivity
- Images, both internal and external views
- Weather data

Modellers were then asked to submit hourly averaged predictions of heat inputs or temperatures (as appropriate for the particular phase of the experiment) plus a modelling report with details of the simulation program used, the main technical features of the program and any assumptions made. The validation organizers responded to any questions posed by the modelling team, distributing the questions and responses to all teams. This process was used to further identify the level of detail the validation specification requires.

The results from this phase of the procedure will therefore include both limitations and errors in the programs, user input errors and some uncertainties in the experiment.

Because different tools use different mathematical approaches and physical models, different input parameters are required depending on the tool under investigation. As an example, flow coefficients may be necessary to calculate infiltration air flows as well as airflow and backdraft through the open doors between the ventilated rooms. These parameters are chosen by the modelling team based on experience. Other programs may use a simpler method (e.g. fixed air flow rates) to represent infiltration.

Within the IEA project, 21 datasets from 13 organizations using 11 different simulation programs were submitted.

Following this phase, all measured data were distributed, together with some updates on the building specification developed from the questions of the modelling teams. Modelling teams have been investigating differences between measurements and predictions. Modelling teams have re-submitted their predictions. To avoid modelling teams fitting their predictions to the measured data by a generic adjustment of the parameters, any changes they have made to their initial models have to be documented and justified by a physical meaning.

The remaining deviations of temperature and heating power can then be attributed to the limits of the algorithms and model assumptions behind the BES tool under investigation. The final results from the analysis should give an indication of the reliability of a simulation program to model real full scale buildings.

5. EXPERIMENTAL DESIGN

5.1 Location and Geometry

The IBP's identical Twin Houses (Figure 1) are two typical German single family detached houses equipped with extensive measurement and control equipment. They provide a cellar, ground floor and an attic space. For the validation only the ground floor is considered. The floor plan can be taken from Figure 2. The external walls are insulated according to the German energy code (EnEV 2009). The windows consist of 2 pane thermal insulation glass ($U=1.2 \text{ W}/(\text{m}^2\text{K})$) and are equipped with electric roller blinds. During the measurement all roller blinds

in the ground floor are up except for the southern windows that are explained later in this document.

As discussed previously in this paper, even though these are quite simple buildings, they are not trivial to model with BES software. To limit the model's complexity the two attic spaces and the cellar are not included in the validation experiment. Their measured air temperatures are provided to the experiment as simple boundary conditions for the floor and the ceiling. Keeping the cellar out of the validation exercise avoids the necessity to model the heat transfer of the cellars' walls and floor to the ground. Heat conductivity of the ground can vary considerably with the prevailing type of material and the groundwater situation. The heat losses of attic spaces are often dominated by the heat losses through roof construction. Many roofs, as is the case with the Twin Houses, consist of a rafter construction with insulated compartment areas. This kind of construction results in a quite complex 2 and 3 dimensional problem. Even if this is a very interesting and relevant problem it was decided that the evaluation on just the ground floor provided enough insight into BES tools by keeping the required modelling effort feasible. Also the roller blinds in the attics were closed to avoid solar absorption on the ground floor's ceiling. For these reasons the free floating attic and cellar temperatures were recorded and used as boundaries. As can be seen in Figure 3 the temperatures in the attic and cellar are relatively stable and the difference is smaller than from the ground floor to the outside air. This way the ground floor's boundary is much simpler since just the temperature differences and the constructions and thermal bridges of floor and ceiling are required.



Figure 1: Twin Houses from east.

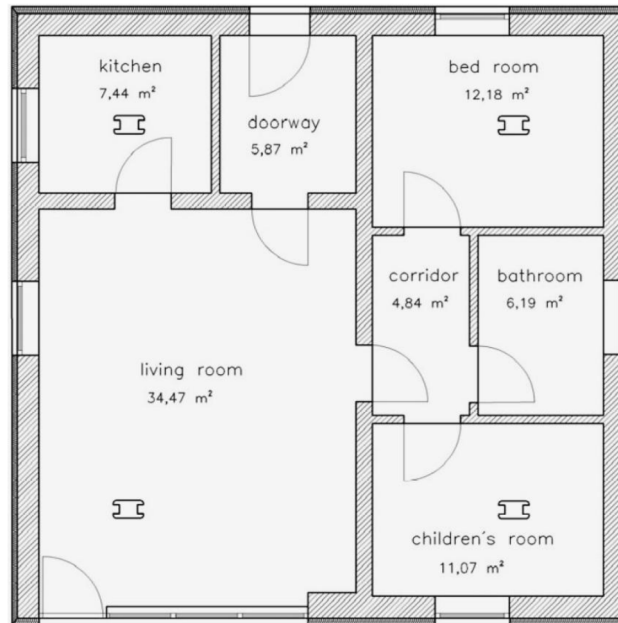


Figure 2: Floor plan of the Twin Houses.

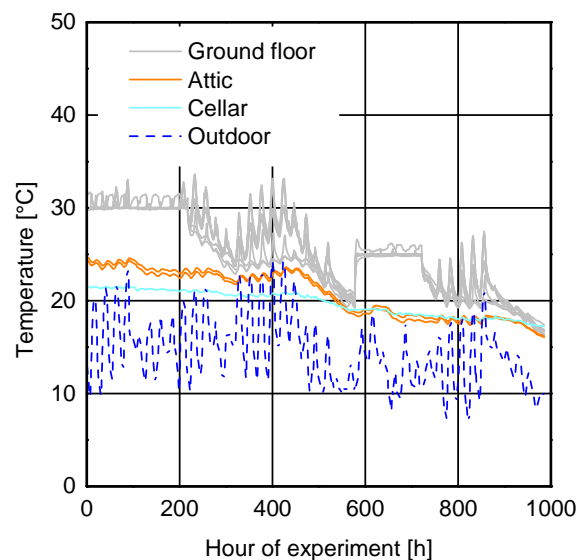


Figure 3: Ground floor, cellar and attic temperatures of one Twin House.

5.2 Quality control

To obtain high quality measurement data the condition of the equipment and facilities used in an experiment has to be known. The first step in quality control was the calibration of all instrumentation installed. The specified uncertainty of all sensors is provided later in this document.

A further step was the conduction of pressurization tests to gain knowledge about the buildings' air tightness. Two separate tests were performed on each building. The first one examined the complete area of the validation scenario, the ground floor. With n_{50} values of 1.62 h⁻¹ and 1.54 h⁻¹ both buildings were quite similar. These air exchange rates can be converted to average air change rates of 0.113 h⁻¹ and 0.108 h⁻¹ resulting in a difference of 5 % between the buildings. Since the accuracy of the pressurization test is 14 % according to EN 13829 no actual difference

in air tightness could be determined. Also since 1.5 h^{-1} is a typical value for a new building with mechanical ventilation this part of the validation scenario can be considered realistic. A second pressurization test was performed for the four southern, ventilated rooms. The doors to the bedroom, doorway and the kitchen were already sealed and the blower door fan was installed in the patio door. n_{50} values of 2.2 h^{-1} and 2.3 h^{-1} were obtained.

The third step was to compare the real in situ performance of the heating energy consumption of both buildings while ensuring the same temperature set points and shading configuration. In case both buildings behave identically it can be assumed that no undetected hidden flaws are remaining. In Figure 4 the performance of the Twin Houses during this baseline measurement can be seen. The black line, indicating the deviation between the cumulative heating energy consumptions of both buildings, stayed at about 0.5 % at the end of the baseline measurements and never exceeded 2 % deviation.

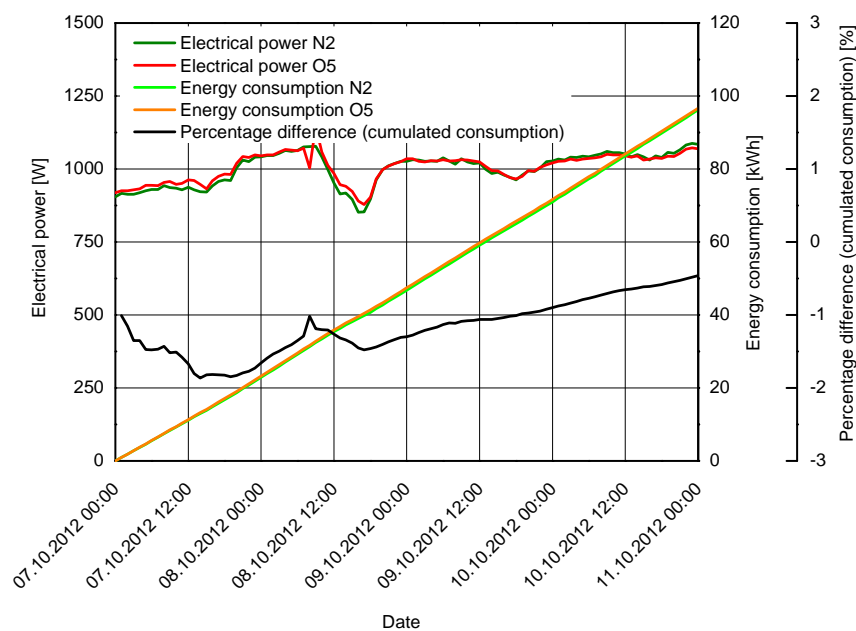


Figure 4: Preceding baseline measurement of both Twin Houses.

5.3 Test schedules

The sub models of the BES tools that are being checked by this validation relate to thermal storage, heat transmission through the building fabric, zone interaction, ventilation and infiltration, solar gains and shading, basic heating and climate calculations like solar distribution on tilted surfaces and sky temperature. The validation is divided into four different periods, preceded by an initialization phase (Figure 5 and Table). In this initialization phase both buildings were heated to a constant temperature of $30 \text{ }^{\circ}\text{C}$ to obtain identical and well defined start conditions. These slightly elevated temperatures were used because the experiments were undertaken in summer 2013, due to availability of the test buildings at this time.

In the first period the room air temperatures were kept constant at $30 \text{ }^{\circ}\text{C}$ with a required heating power controlled by the building management system. These measured temperatures are provided as inputs for the BES tools to be validated while the heating power to achieve these measured temperatures is predicted. In this period the correct control between building temperature and heat input is particularly relevant. This is a very typical setup as keeping a certain temperature is required in nearly all simulation projects.

In the second period, a Randomly Ordered Logarithmic Binary Sequence (ROLBS) for heat inputs into the living room was enacted, with heat injections of 0 and 500 W. The use of a pseudo-random sequence of heat injections ensures that the solar and heat inputs are uncorrelated, which helps to disaggregate the fabric heat transfer and solar gains in the analysis. This test sequence lasted for 2 weeks – the sequence has heat pulses ranging from 1 hour to 90 hours in duration to cover the expected range of time constants in the building, known from the previous simulations. These sequences were developed in the EC COMPASS project (van Dijk and Tellez 1995) and customized in this case to cover the expected time constants of the Twin Houses – large in this case as the houses contain a significant amount of thermal mass. All other rooms are without heating power in this period. The ROLBS sequence of heat inputs is provided to the BES tool and in this case, the resulting temperatures should be predicted. Here the model responses to additional heat inputs are tested separately from the controlled heating. This is important because most real usages have some internal heat sources like electric appliances. The fact that heat is only injected to the living room increases the interaction between the ventilated and the unventilated rooms.

The third period is a constant temperature scenario again in order to re-initialize the two houses to the same state. The controlled temperature level was set at 25 °C (lower temperatures as the external temperatures were expected to decrease in late summer). Again the measured indoor air temperatures are provided to the BES tool and the resulting heating power is to be calculated.

In the fourth period, the indoor temperatures are floating free without any artificial heat sources. The resulting indoor air temperatures are required from the BES tool. Free float usages without any heat input are usually more variable than calculations with heat inputs. Free float scenarios are very relevant in reality, for example in determining the overheating behaviour of buildings in summer.

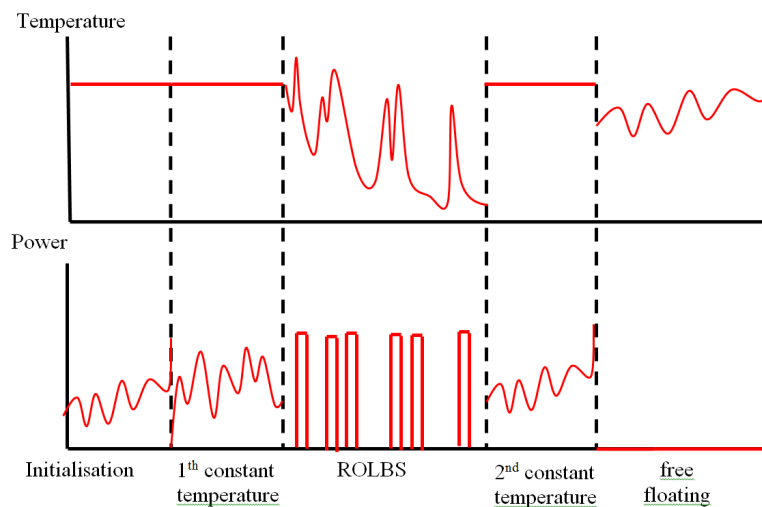


Figure 5: Schematic validation schedule.

Table 1: Experimental schedule.

Days		Blinds (south facade)	
		House O5	House N2
1-22	Initialisation - Constant temperature - 30°C in all spaces	down	down
23-29	Constant temperature – 30°C in all spaces	up	down
30-44	ROLBS sequence in living room. No heat inputs elsewhere.	up	down
45-50	Constant temperature 25°C in all spaces.	down	down
51-61	Free-float	up	down

5.4 Building equipment

Both Twin Houses are equipped with a sophisticated building management system (PLC), also capable of acquiring the instrumentation with the required scientific precision. All sensors are sampled once per second. These measurement data are resampled and stored with a 1 minute frequency. For the BES model validation these data are provided at 10 and 60 minutes frequency. The heating power is provided to the rooms through fast responding 2 kW electric convectors driven by a phase controlled modulator. All windows of the building are equipped with automated external roller blinds. Except for the south windows all blinds are up all the time. The southern blinds are closed on one house permanently and are closed only for the initialisation and the constant temperature scenarios on the other house. The southern rooms of the ground floor, the living and children's room, corridor and bath are ventilated as can be seen in Figure 6. The supply air enters the living room with a volume flow of 120 m³/h and is extracted through the bath and the children's room with a flow of 60 m³/h. These flow rates are controlled by phase modulated fans, so they are quasi constant. The supply air temperatures to the ground floor are provided as inputs to the BES tools. The doors to the remaining three rooms are sealed air tight to minimize their thermal interaction. The hatch to the attic space is an insulated double door and it is closed all the time.

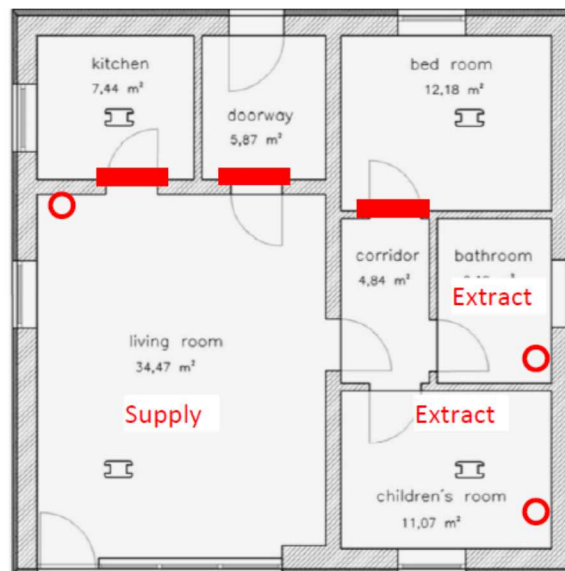


Figure 6: Floor plan including ventilation concept of the IBP's Twin Houses during the measurement of the validation scenarios. The sealed doors are marked with a red rectangle.

5.5 Sensors

These measurements were conducted during August and September 2013. Inside both Twin Houses the following sensors, listed in Table 2 were used to record the buildings performance. These sensors are calibrated before the experiment. Some of these sensors can be seen in the internal views of the Twin Houses in Figure 7. The climate data from the IBP's weather station were provided as boundary conditions. These sensors are calibrated regularly as recommended by the manufacturer.

Table 2: Instrumentation of the Twin Houses.

Each Twin House		Meteorological	
Sensor	Accuracy	Sensor	Accuracy
Air temperature in all 7 rooms at a height of 125 cm (radiation shielded)	± 0.12 K	Ambient air temperature (ventilated)	± 0.10 K
Additional air temperatures in the living room at a height of 67 cm and 187 cm (radiation shielded)	± 0.14 K	Ambient relative humidity	± 2.0 %
Air temperatures in the cellar and attic spaces	± 0.14 K	Ground temperatures, depth of 0, 50, 100 and 200 cm	
Relative humidity living room	± 2.3 %	Wind speed (@ 10 m height)	± 0.1 m/s
Fresh, supply and exhaust air temperatures measured in the cellar	± 0.04 K	Wind direction (@ 10 m height)	± 1.0 °
Heating power of the 6 heated rooms	± 1.5 %	Solar radiations: global, diffuse and vertical (north, east, south, west)	± 2.0 %
Supply and exhaust fan power	± 1.5 %	Long wave radiation (horizontal, west)	< 34 W/m ²
Ventilation flow rates	± 3.5 m ³ /h		
Heat flux at the west facade	± 0.65 W/m ²		
West wall temperatures: Internal, external and between layers	± 0.14 K		



Figure 7: Internal views of the Twin Houses.

5.6 Configuration of the ventilation system

As explained in section 5.4 the three northern rooms (kitchen, doorway and bed room) are set up without any mechanical or natural ventilation. The windows were closed and the internal doors were sealed. Just the small amount of air infiltration influences the performance of these rooms. The four southern rooms (corridor, bath-, children's- and living room) are equipped with mechanical ventilation while the windows and the terrace door are kept closed all the time. Mechanical ventilation was chosen because air temperatures and volumes flow rates can be measured and controlled very well. To gain the same quality of information using natural ventilation requires much extensive instrumentation. Also free ventilation air flows are driven by the same factors as infiltration, so these models can already be validated through the northern rooms. A second issue is the importance of mechanical ventilation systems for building service equipment and the capability to model them accurately. The energetic impact of the ventilation system is approximately of the same significance as the transmission heat losses and 15-times as high as the heat losses by infiltration. So it is obvious that high accuracy is required when controlling and recording the ventilation air temperatures and air volumes during the measurements. For this validation scenario a balanced ventilation system was chosen to avoid unknown air flow (and therefore heat flow) through the building's air tightness leaks. A balanced ventilation system runs both the supply and the extract fan with the same amount of air volume to prevent under- or overpressure within the building's envelope. To guarantee identical volume flows in this experiment both the supply and the extract air ducts are equipped with thermo anemometers for measuring the air velocities in the ducts. Using profile factors these velocities can be converted to mass flows (not volume flows). Since the ventilation system is mass balanced a volume difference can occur depending on the temperature difference between supply and exhaust air. By phase modulation the fan's powers are controlled to keep the desired flow rates of 120 m³/h as displayed in Figure 8. This is achieved with a standard deviation of only ± 0.2 m³/h, below the resulting uncertainties of the anemometers. The exhaust air fan draws its air from two different outlets, one in the bathroom and one in the children's room. To ensure that the exhaust air amount is symmetrical from these two rooms, during the experimental setup the disc valves in both rooms were adjusted using a second, temporary flow meter. After this procedure the valves are not changed anymore. All duct joints are sealed carefully using tape to minimize pressure losses throughout the ducts' length. The supply air temperature is measured after the fan, so the fan's waste heat is included in this temperature. The exhaust air temperature is measured before the fan so its heat is not included, as required. Both supply and exhaust air temperatures are measured in the basement, where the air handling is located. A part of the supply air duct to the living room is running through the kitchen as an uninsulated folded spiral-seam duct. The heat transfer from the kitchen to the living room has to be included into the calculations. In case a BES tool is not capable of simulating detailed ventilation systems including their heat losses an estimation of the changed supply air temperatures and heat transfers is supplied with the input data, already for the blind validation. This estimation is conducted with the free "PHLuft" software from the Passivhaus-Institute (PHI 2014). In a subsequent measurement period an additional supply air temperature sensor was installed directly in the living room to validate the quality of the PHLuft estimation. The results of this validation of the estimated living room supply air temperature and kitchen heat losses can be seen in Figure 9.

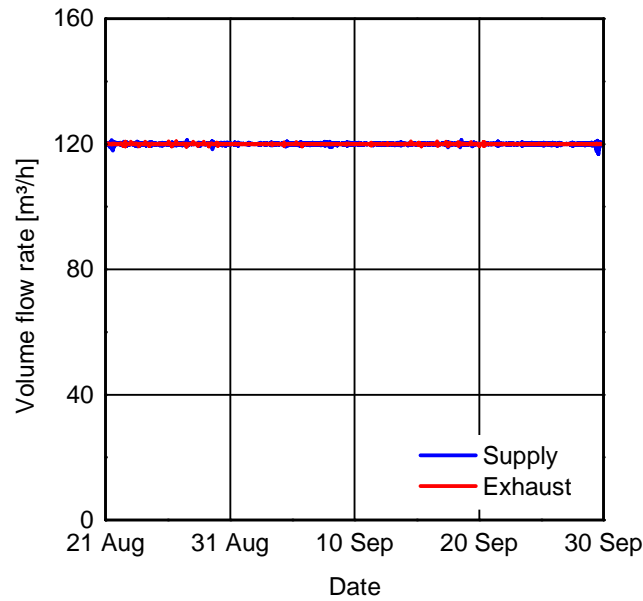


Figure 8: Supply and exhaust air flow rates during the experiment. 10-minute values.

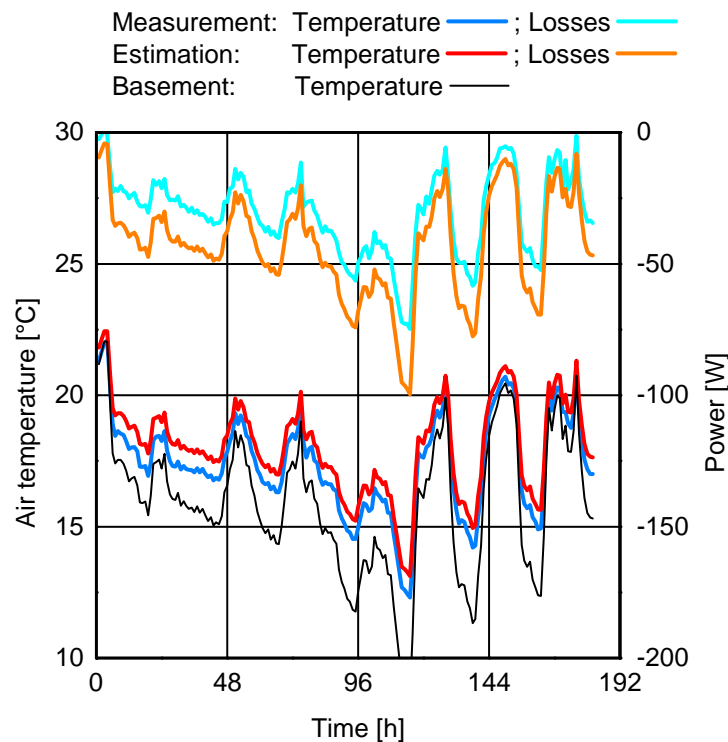


Figure 9: Estimated and measured living room inlet temperatures and kitchen heat losses through the supply air duct.

5.7 Measurement data

During the experiment, measurement data are recorded every second, compressed and stored as 1-minute means and are subsequently distributed to the modelling teams as 10- and 60 minutes values. Since the Twin Houses have a very high thermal mass and no fast oscillating controls are present, these sampling rates should suffice for the thermal-energetic building simulation. The measurement data of one house's living room are shown in Figure 10. It can be seen that in the constant temperature phases a small amount of overheating occurs

occasionally and that stratification occurs only during the constant temperature phases but never during the ROLBS phase. This underlines the importance of BES tool validation on real in situ measurement data as complex and sometime unexpected effects appear in reality, as explained in section 3 of this document. Figure 11 shows the climatic conditions prevailing during the measurement for the validation scenario.

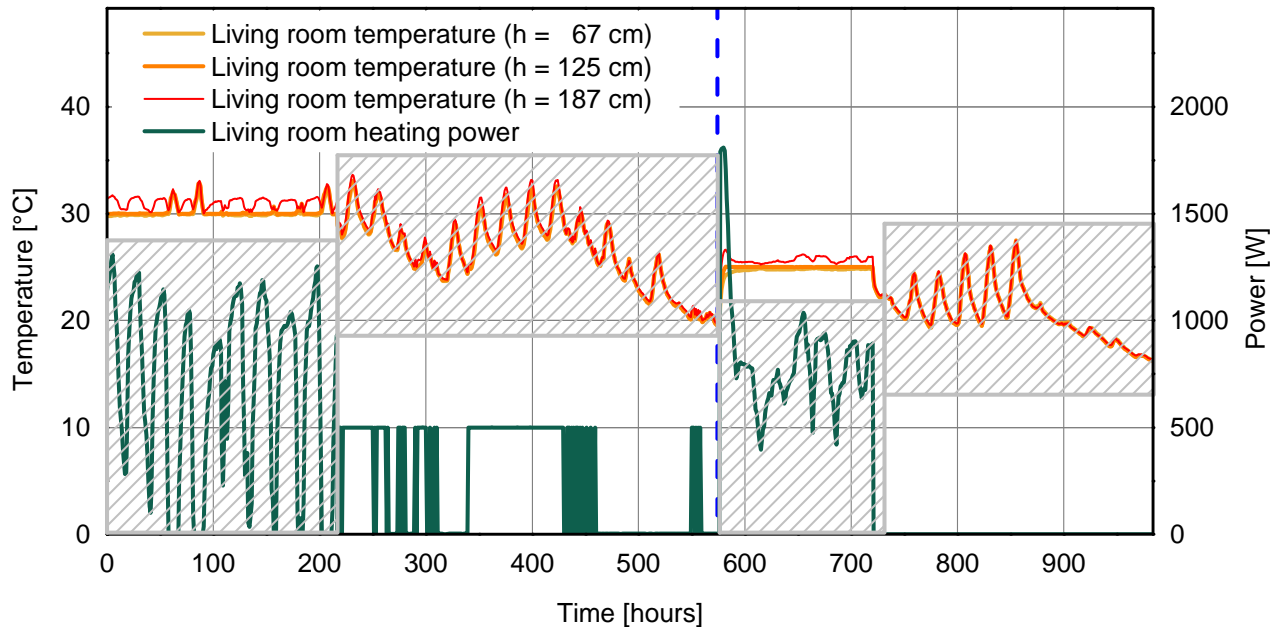


Figure 10: Trend lines of the heating power and the air temperature at all three measurement heights of the living room of one of the houses. The grey shaded data are the validation targets that are not provided for the blind validation.

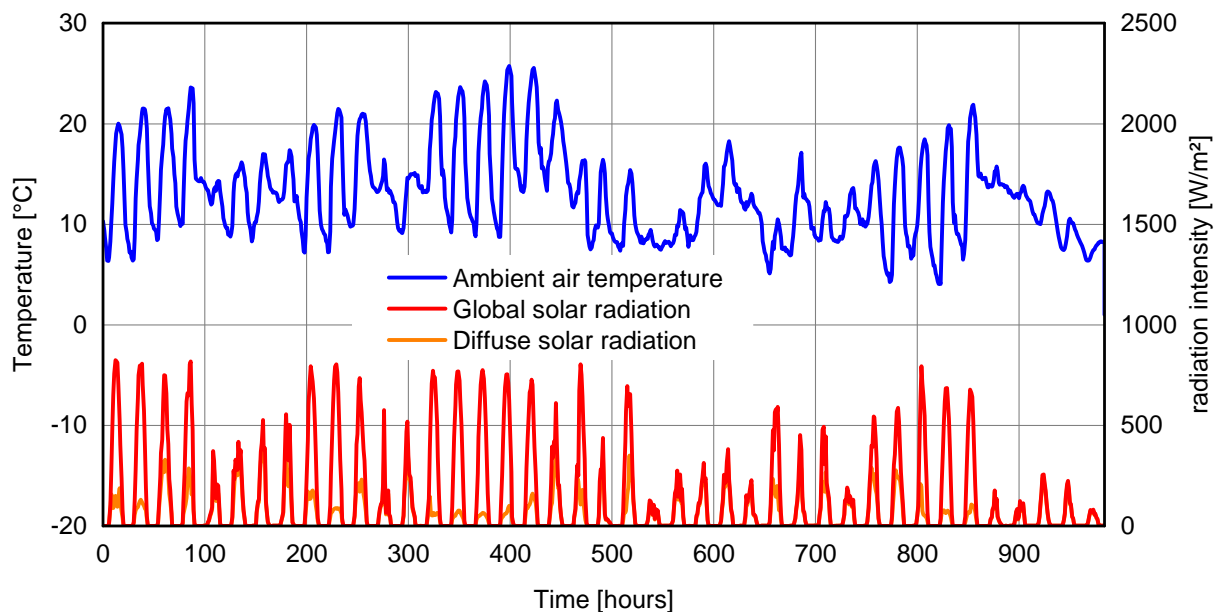


Figure 11: Prevailing weather condition during the measurement of the validation scenario.

6. CONCLUSION

Within the IEA ECB ANNEX 58 "Reliable building energy performance characterisation based on full scale dynamic measurement" a new measurement data based method for validating the accuracy of Building Energy Simulation Tools has been developed. The method uses high

quality measurement data and detailed documentation of the Twin Houses of the Fraunhofer Institute for Building Physics IBP at Holzkirchen, Germany. The validation consists of four different periods providing different configurations of heating inputs and temperature control. The first phase of the validation procedure adopted was a blind validation which tests both the user and the modelling program. The second phase, after all measured data has been released to the modelling teams, should help to eliminate user error. The resulting comparison of measurements and predictions should then give an estimate of the reliability of simulation programs to model realistic scale buildings, albeit this experiment is mostly focused on the building fabric, ventilation and solar processes, excluding plant systems and occupant effects.

The measurement dataset and associated building specification documentation should provide a valuable resource for program development teams. There are too few high quality empirical validation datasets available.

In the upcoming months the full validation specification will be published within the Annex 58 final report. Also several modelling teams and several available software tools are already performing this validation. Additional publications will show the performance of the different tools with the remaining differences between the modelling teams validating the same software anonymously. Additionally several participating modelling teams have already indicated that they will be publishing their experiences with their individual validation processes including their results and the corrections they have been required to implement.

REFERENCES

- ASHRAE 140-2001 (2001). Standard Method of Test for the Evaluation of Building Energy Analysis Computer Programs.
- DIN 4108-4:2013-02 (2013). Wärmeschutz und Energie-Einsparung in Gebäuden - Teil 4: Wärme- und feuchteschutztechnische Bemessungswerte.
- EN 13829:2000 (2000). Thermal performance of buildings. Determination of air permeability of buildings. Fan pressurization method.
- EN 15255:2007 (2007). Energy performance of buildings - Sensible room cooling load calculation - General criteria and validation procedures.
- EN 15265:2007 (2007). Energy performance of buildings - Calculation of energy needs for space heating and cooling using dynamic methods - General criteria and validation procedures.
- EnEV 2009 (2009). Energieeinsparverordnung 29. April 2009.
- IEA EBC ANNEX 58, Reliable Building Energy Performance Characterisation Based on Full Scale Dynamic Measurements URL: <http://www.ecbcs.org/annexes/annex58.htm>.
- IEA EBC Annex 42, The Simulation of Building-Integrated Fuel Cell and Other Cogeneration Systems (COGEN-SIM) URL: <http://www.ecbcs.org/annexes/annex42.htm>.
- IEA EBC Annex 43/ SHC Task 34, Testing and Validation of Building Energy Simulation Tools, URL: <http://www.ecbcs.org/annexes/annex43.htm>.
- ISO 13791:2012: Thermal performance of buildings - Calculation of internal temperatures of a room in summer without mechanical cooling - General criteria and validation procedures.
- ISO 13790:2008: Energy performance of buildings - Calculation of energy use for space heating and cooling.

Jensen S O (ed) (1993). Validation of Building Energy Simulation Programs, Part I and II, Research Report PASSYS Subgroup Model Validation and Development, CEC, Brussels, EUR 15115 EN.

Judkoff, R., Neymark, J. (1995). International Energy Agency Building Energy Simulation Test (BESTEST) and Diagnostic Method, NREL, Colorado USA.

Judkoff R, Wortman D, O'Doherty R and Burch J, A (1983). Methodology for Validating Building Energy Analysis Simulations, SERI/TR-254-1508, Golden, Colorado, USA: SERI (now NREL).

PHI Passiv Haus Institut, (2014). PHLuft software,

URL:http://www.passiv.de/de/05_service/02_tools/03_phluft/03_phluft.htm.

van Dijk, H.A.L. and Tellez, F.M (1995). Measurement and Data Analysis Procedures, Final Report of the JOULE II COMPASS Project (JOU2-CT92-0216).

Back from Holzkirchen full scale dynamic testing experiment

G. Masy¹, F. Delarbre¹, J. Lebrun², E. Georges³, F. Randaxhe³, V. Lemort³,

I. Rehab⁴, P. André⁴,

⁽¹⁾Master School of Province de Liège, Belgium

⁽²⁾JCJ Energetics, Liège, Belgium

⁽³⁾Labothap, University of Liège, Belgium

⁽⁴⁾BEMS, University of Liège, Belgium

1. ABSTRACT

Holzkirchen full scale dynamic experiment was conducted in the framework of AIE Annex 58 research program with the aim to obtain and apply a high quality experimental dataset for model validation of the energy and environmental performance of full scale buildings. Two identical houses were submitted to a side by side experiment, one with blinds up, one with blinds down. The experience included an initialization period, a ROLBS heat input sequence, a re-initialization followed by a free-float period. Path of explanations for discrepancies are first found through a deeper analysis of thermal bridges, a better assessment of solar heat gains, and the introduction of convective coupling effect occurring between the interconnected zones of the houses. An energy balance analysis is proposed in order to calibrate the simulation model according to measured data.

Keywords: Building thermal dynamics, co-heating test, dynamic sequence.

2. INTRODUCTION

The need to promote best practice in building design requires a better characterization of real building thermal performances through in-situ test procedures. Those performances involve aspects related to air tightness, envelope insulation, response to temperature changes and solar radiation. Characterizing the actual performance and dynamic behavior of building is essential to obtain – not only on paper, but in reality – high performance buildings.

The ability to predict reliable building energy demand and indoor temperature profiles depends on the quality of the models. These models should be able to accurately simulate the instantaneous heat demand and indoor temperatures of buildings with a low computation cost. Available buildings dynamic models range from very detailed models to more simplified ones (Bacher and al. (2010), Reynders and al. (2014)).

Since 2011, international experts are working within the research project IEA EBC Annex 58 on the topic of ‘Reliable building energy performance characterization based on full scale dynamic measurements’. This project takes place in the framework of the ‘Energy in Buildings and Communities Programme’ of the International Energy Agency. Major aim of the project is to develop the necessary knowledge, tools and networks to achieve reliable in situ dynamic testing and data analysis methods that can be used to characterize the actual thermal performance of building components and whole buildings.

3. EXPERIMENT

An empirical model validation study was conducted within the scope of IEA Annex 58 subtask 4 (Strachan and al. (2014)). The experiment was undertaken during 42 days in August and

September 2013 on identical Twin Houses in Holzkirchen, Germany (see layout and section on fig. 1).

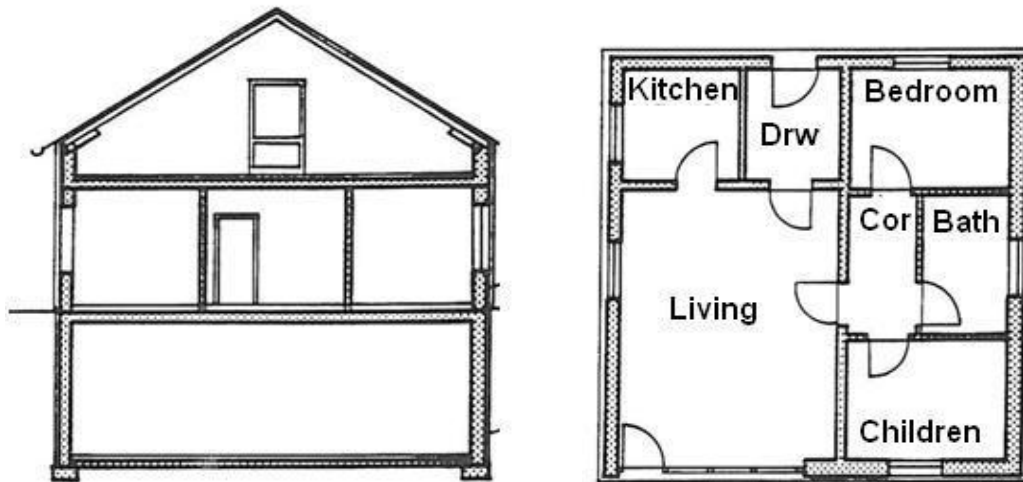


Figure 1: Holzkirchen experimental houses: section and layout.

The houses are not occupied during the whole co-heating experiment. The internal doors between kitchen and living room, doorway and living room, bedroom and corridor are sealed with tape (Fig. 2). A ventilation system was used to reduce the amount of overheating. The un-insulated mechanical ventilation ductwork leading from the cellar to the living room via the kitchen, supplies continuously a 120 m³/h air flow in the living room. Air is exhausted from the bathroom and children bedroom, with equal air volumes (about 60 m³/h at each exhaust duct), so that the ventilation air flows are balanced.

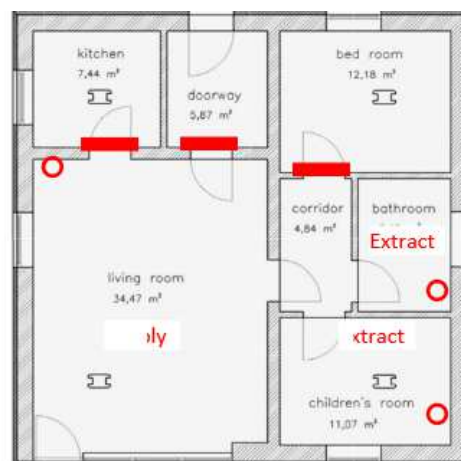


Figure 2: Holzkirchen houses: sealed internal doors and ventilation air vents.

Electric heaters were used for the heat injections. The co-heating is simultaneously conducted in both houses, with external roller blinds down on the south facing windows of the living room and children bedroom for one house (house N2), and fully up for the other house (house O5). Other windows are sun exposed for both houses.

A ROLBS sequence (Randomly Ordered Logarithmic Binary Sequence) is included in the co-heating process, as a sequence of heat pulses ranging from 1 hour to 90 hours in duration in order to cover the expected range of time constants in the building. Heat pulses of 500 W magnitude are used in the experiment (fig. 3).

The co-heating process includes an initialisation period of 9 days with a heating set point of 30°C in all rooms, followed by a ROLBS sequence of 15 days where a 500 W heat power is supplied in the living room and no heat inputs elsewhere (fig. 3). A re-initialisation period is then scheduled during 6 days with heating set point of 25°C in all rooms, followed by 11 days free floating period.

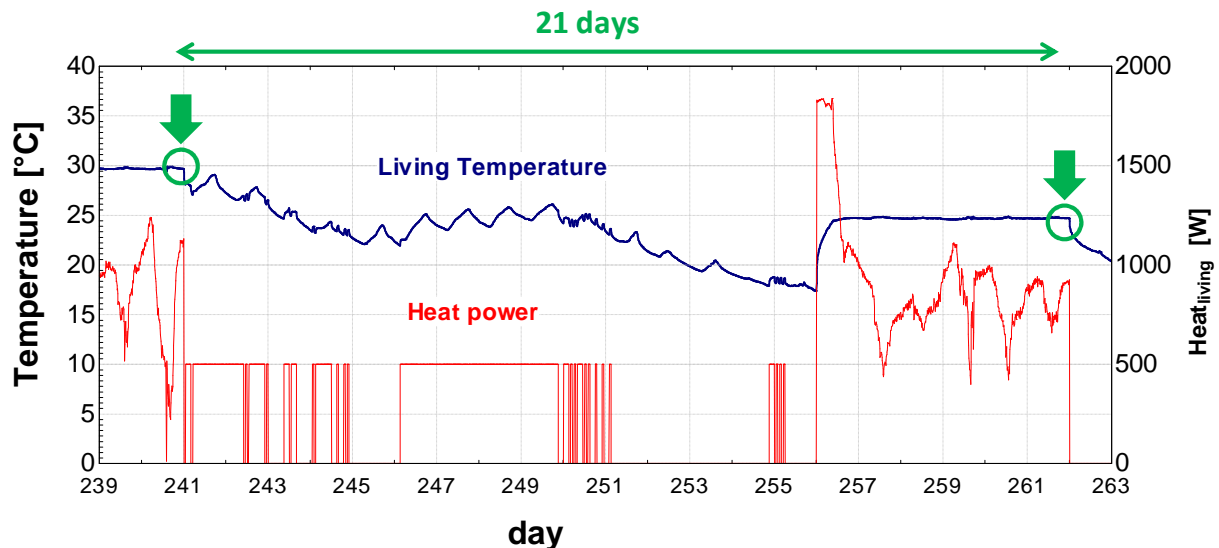


Figure 3: Schedule of the ROLBS sequence in the living room.

Weather data were collected with a time step of 10 min. A first blind simulation exercise was proposed in January 2014 in order to reproduce the measured data. All the measured data were sent in March 2014 so that all the teams should be able to calibrate their models. A calibration process is described here on the basis of the following methodology:

The temperature profiles resulting from the first blind simulation exercise showed discrepancies. In order to orient the calibration process, a study of the energy balance of the building was performed on a 21 days period starting from the end of the first initialisation period, until the end of the reinitialisation period, *using the measured indoor temperature as input for the simulation* (fig. 3). Integral calculations of the heat losses through transmission and ventilation were performed over that period of time, including infiltration and convective coupling, both computed *on the basis of measured indoor temperatures*. The amount of heat released from the thermal mass of external and internal walls was included in the heat balance, as equal to the thermal mass times 5K. Heat inputs due to solar gains were computed independently. Measured heat inputs from electric heaters were also considered. The balance (resulting imbalance) was then computed in order to orient the calibration process.

Energy balances of both houses are presented on Figure 8. Heat gains exceed heat losses in almost all zones. Transmission and ventilation heat losses don't even reach the amount of heat provided by the electric heating in four zones of house N2. They must be higher. As ventilation losses are dominated by mechanical ventilation losses (Table 2) for which air flows and air temperatures are resulting from measurements, transmission losses have to be increased.

Deeper analysis were made in April 2014 in the framework of AIE Annex 58 research program in order to better assess the heat loss coefficients related to wall thermal bridges and heat losses due to the un-insulated ventilation ductwork leading from the cellar to the living room via the kitchen (Strachan and al. (2014)). Considering the updated heat loss coefficients, thermal bridges heat losses are multiplied by factor of 1.77 for external walls and by a factor of 6.65 for internal walls (fig. 4).

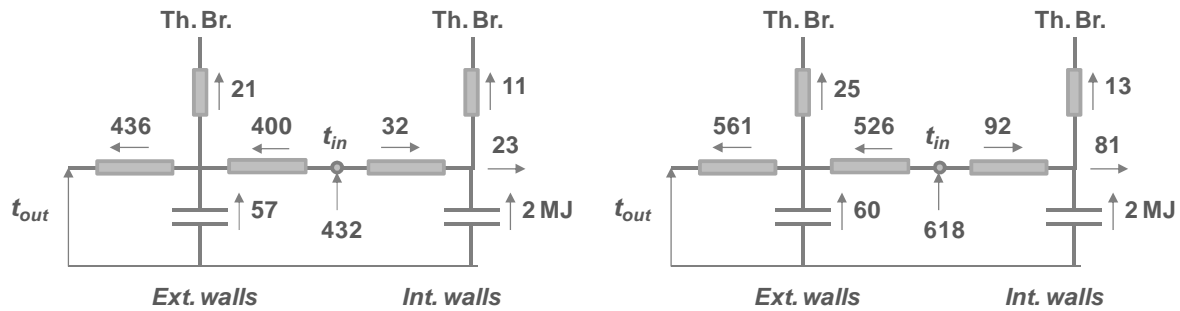


Figure 4: Living zone heat losses through external and internal walls after calibration in house N2 (left) and house O5 (right), for the 21 days time period.

Energy balances of Figure 8 show exceeding solar heat gains. The calculated solar intensities received by the facades are in accordance with measurements (fig. 7). The first simulation used a global solar heat gain factor equal to 0.62 (given by the glazing supplier). The calibrated model uses an angle dependent solar factor obtained from the International Glazing Database for AN410 spectra (Strachan and al. (2014)). The shading due to the set back of the window is computed as well. Solar heat gains to the windows are reduced by 26 % for house N2 and by 29 % for house O5.

Convective coupling effect between interconnected zones is introduced. Dynamic simulation is required to compute convective coupling air flows, as they are strongly dependant from indoor air temperatures (fig. 6). Here again, air flows are computed *on the basis of measured indoor temperatures*. Simulation performed on the calibrated model showed significantly improved indoor temperature profiles.

4. SIMULATION

Simulations were performed using EES solver (Engineering Equation Solver). The building walls are modelled through 2R1C networks (table 1).

The wall thermal capacity is the total capacity of the inside portion of the wall, defined as the sum of wall layers located on the indoor side of the insulation layer. The wall thermal capacity is located in the middle of the thermal resistance of that inside portion of the wall.

Fixed surface heat transfer coefficients are considered: External 23 W/m²-K, Internal 8 W/m²-K.

Boundary conditions in the cellar and attic are treated using time varying measured temperatures.

Table 1: Building walls dynamic parameters ($U=1/R$).

	U [W/m ² .K]	C [kJ/m ² .K]	θ
Ceiling	0.24	6	0.01
Floor	0.28	130	0.01
External Wall South	0.20	288	0.14
External Wall West – South portion	0.27	288	0.19
External Wall West – North portion	0.27	288	0.19
External Wall North	0.20	288	0.14
External Wall East	0.19	288	0.13
Internal wall Heavy	0.94	224	0.50
Internal wall Light	1.49	120	0.50

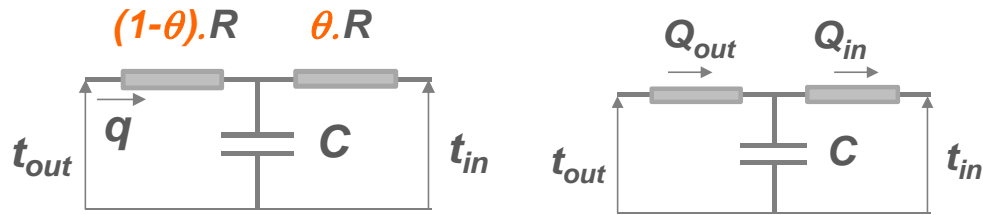


Figure 5: 2RIC wall model.

A global U-value 1.2 W/m²-K is considered for the windows. Glazing and frame are not modelled separately. A blind thermal resistance of 0.17 m²-K/W is added to the window thermal resistance when blind is closed.

Infiltration air flows are low as the building envelope air tightness level is rather high: n₅₀=1.58h⁻¹. Infiltration and exfiltration air flows are estimated using a simplified model through windows and external doors frames (Masy, (2008)). The model is based on the following generic equation that allows mass air flows to be positive or negative, depending on the air flow direction:

$$\Delta p = K \cdot |\dot{M}|^n \cdot \dot{M}$$

Δp : Pressure drop through ventilation aperture Pa

\dot{M} : Mass air flow rate through ventilation aperture kg/s

n : Exponent ranging from 0 when the flow is laminar to 1 for a turbulent flow

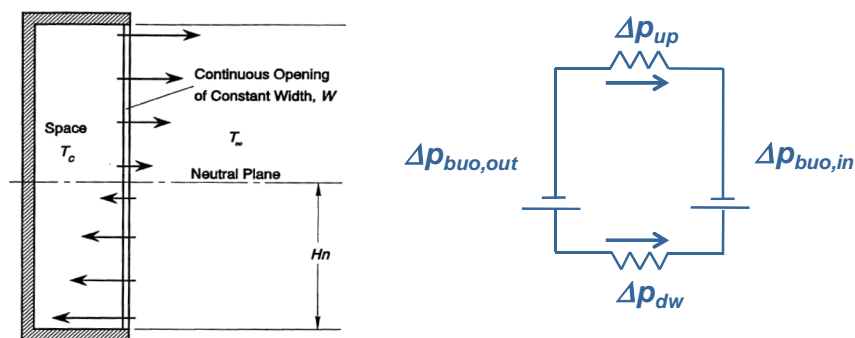
K : Constant Pa.(s/kg)¹⁺ⁿ

The driving forces are due to wind pressure and to buoyancy effects over 2/3 of the windows height:

$$\Delta p_{wind} = p_c \cdot \frac{u^2}{2 \cdot v_a} \qquad \Delta p_{buo} = g \cdot \frac{(z_2 - z_1)}{v_a}$$

The building site is considered as exposed to wind.

Air flows due to convective coupling between interconnected zones are estimated through circulating two ways models defined over 2/3 of the height of internal door openings, with driving forces due to buoyancy effects (fig. 6). Internal doors are considered as opened at 50% of their whole area. A discharge factor equal to 0.61 is considered, corresponding to zeta pressure drop factor equal to 2.7.



$$\Delta p_{up} - \Delta p_{buo,in} - \Delta p_{dw} + \Delta p_{buo,out} = 0$$

Figure 6: Model of the convective coupling between interconnected zones.

Calculation of energy gains and losses are performed through the following equations where $t_{a,in}$ is the measured indoor air temperature. In the living room, the indoor air temperature is measured at 67 cm height.

For the internal air node:

$$U_{c,a} = t_{a,in} \cdot C_{a,in} \qquad C_{a,in} = 5 \cdot V \cdot \frac{c_{p,a}}{v_a}$$

For the wall capacity nodes (fig. 4):

$$U_{c,init} = A_{wall} \cdot C_{wall} \cdot t_{wall,init} \qquad t_{wall,init} = 30^\circ C$$

$$\dot{Q}_{out} = \frac{A_{wall} \cdot (t_{out} - t_{wall})}{R_{wall} \cdot (1 - \theta_{wall})} \qquad \dot{Q}_{in} = \frac{A_{wall} \cdot (t_{wall} - t_{a,in})}{R_{wall} \cdot \theta_{wall}}$$

$$U_c = U_{c,init} + \int_{\tau_{initial}}^{\tau_{final}} \frac{dU_{c,wall}}{d\tau} \cdot d\tau \qquad \frac{dU_{c,wall}}{d\tau} = \dot{Q}_{out} - \dot{Q}_{in}$$

$$t_{wall} = \frac{U_c}{A_{wall} \cdot C_{wall}}$$

Transmission and ventilation energy losses computed *on the basis of measured indoor temperatures* are presented in table 2: transmission losses are dominated by external wall transmissions, while ventilation losses are dominated by mechanical ventilation losses (or gains). The effect of convective coupling between interconnected zones (living, corridor, bathroom and children room) differs for both houses. It brings heat from the living zone to the others in house O5, whilst it brings heat from the bathroom to the other zones in house N2.

Table 2: Energy losses computed from the measured indoor temperatures.

House N2	Transmission losses [MJ]		Ventilation losses [MJ]		
	External walls	Internal walls	Mechanical	Infiltration	Coupling
<i>Living</i>	400	32	448	43	-16 (gains)
<i>Kitchen</i>	119	8	0	3	0
<i>Doorway</i>	101	-4 (gains)	0	4	0
<i>Bedroom</i>	133	0	0	3	0
<i>Corridor</i>	19	15	15	0	4
<i>Bath</i>	93	30	9	8	35
<i>Children</i>	139	3	-5 (gains)	2	-23 (gains)

House O5	Transmission losses [MJ]		Ventilation losses [MJ]		
	External walls	Internal walls	Mechanical	Infiltration	Coupling
<i>Living</i>	526	92	557	53	25
<i>Kitchen</i>	126	-19 (gains)	0	3	0
<i>Doorway</i>	108	-28 (gains)	0	5	0
<i>Bedroom</i>	144	-25 (gains)	0	4	0
<i>Corridor</i>	23	34	-7 (gains)	0	-12 (gains)
<i>Bath</i>	106	29	-3 (gains)	8	-3 (gains)
<i>Children</i>	169	7	-5 (gains)	3	-10 (gains)

Direct indoor solar radiations through windows are computed from the window solar factor g and from the direct solar intensity reaching each window I_b , which in turn can be expressed as function of the direct solar intensity reaching a horizontal plane I_{bh} (weather data) :

$$q_{b,w} = g \cdot I_b \cdot A_w \quad g = (1 - f_{fr}) g_{gl} \quad I_b = I_{bh} \cdot \frac{\cos \theta}{\cos \theta_z}$$

Index b: direct

Index h: horizontal

g : window solar factor

g_{gl} : glazing solar factor

A_w : window area (m²)

f_{fr} : frame fraction 0.32 for standard windows, 0.23 for living zone South window

θ : angle between sun beams and the window normal direction

θ_z : angle between sun beams and the vertical direction.

The values of the ratio $\cos \theta / \cos \theta_z$ are tabulated for vertical windows as function of the vertical window azimuth, for Holzkirchen location (latitude and longitude).

Diffuse and reflected indoor solar radiations through vertical windows are computed from the diffuse and reflected solar intensities reaching the window I_{dr} , which in turn can be expressed as function of the direct and diffuse solar intensities reaching a horizontal plane I_{bh} and I_{dh} (weather data):

$$q_{dr,gl} = g \cdot I_{dr} \cdot A_w \quad I_{dr} = \frac{1}{2} (I_{dh} + \rho \cdot I_{th}) \quad I_{th} = I_{dh} + I_{bh}$$

Index b: direct

Index d: diffuse

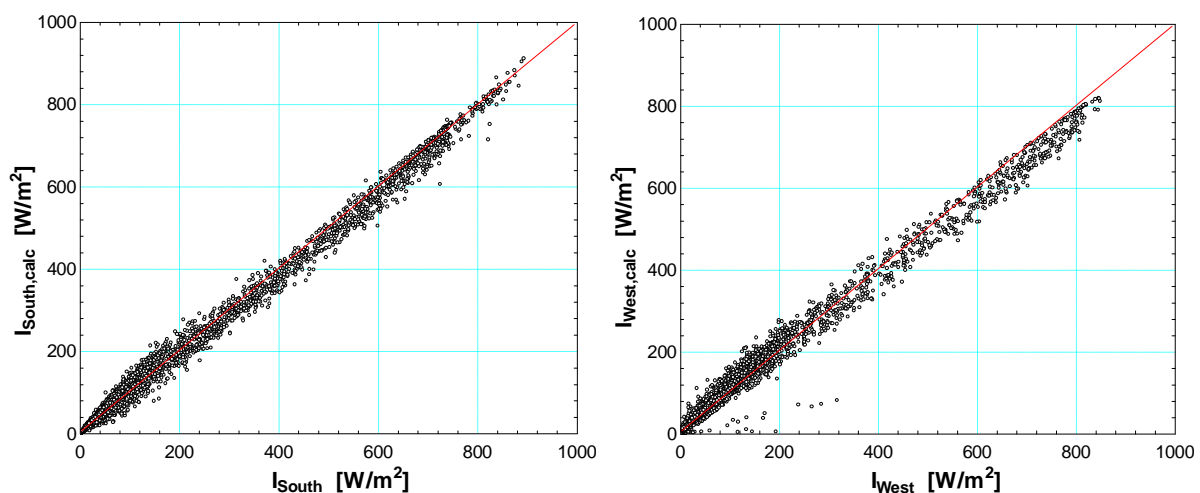
Index r: reflected

Index t: total

Index h: horizontal

The glazing solar factor is angle dependent for the calibrated model. There is no view factor calculation. Internal solar radiation is totally input on the indoor temperature node (operative temperature). Solar heat gains absorbed on the external surface of opaque walls are not considered. Infrared radiation heat losses are not considered neither on the windows, nor on the opaque walls.

Electric heating powers are measured. Emission of electric heaters is considered as 100% convective.



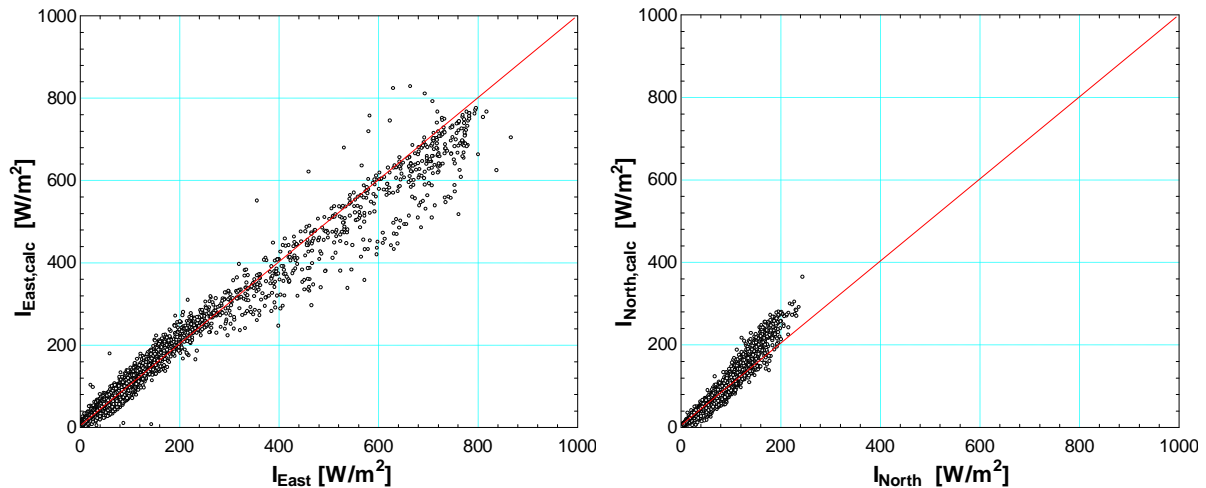


Figure 7: Calculated and measured solar intensities received by the facades.

Computed solar heat gains as well as recorded electric heating energy are presented in table 3. The heat losses due to the un-insulated ventilation ductwork leading from the cellar to the living room via the kitchen have been estimated and subtracted from the heat power provided to the kitchen; that's the reason why a negative value is obtained for the heating power provided to that zone.

Table 3: Solar heat and electric heating energy gains.

House O5	Solar heat gains [MJ]	Electric heating [MJ]	House N2	Solar heat gains [MJ]	Electric heating [MJ]
<i>Living</i>	574	1043	<i>Living</i>	98	1090
<i>Kitchen</i>	98	-4 (losses)	<i>Kitchen</i>	98	19
<i>Doorway</i>	14	70	<i>Doorway</i>	14	83
<i>Bedroom</i>	58	97	<i>Bedroom</i>	58	127
<i>Corridor</i>	0	0	<i>Corridor</i>	0	0
<i>Bath</i>	97	74	<i>Bath</i>	97	74
<i>Children</i>	94	149	<i>Children</i>	0	183

5. RESULTS

The resulting balances of the energy losses and gains before and after calibration are presented on table 4 and illustrated on figure 8 and 9.

Table 4: Balance of heat energy gains and losses (positive when gains exceed losses).

Before calibration			After calibration		
Balance [MJ]	House N2	House O5	Balance [MJ]	House N2	House O5
<i>Living</i>	347	683	<i>Living</i>	281	365
<i>Kitchen</i>	163	160	<i>Kitchen</i>	-13	-17
<i>Doorway</i>	8	10	<i>Doorway</i>	-3	-1
<i>Bedroom</i>	85	71	<i>Bedroom</i>	48	32
<i>Corridor</i>	-35	-33	<i>Corridor</i>	-53	-38
<i>Bath</i>	81	81	<i>Bath</i>	-4	33
<i>Children</i>	65	147	<i>Children</i>	65	79

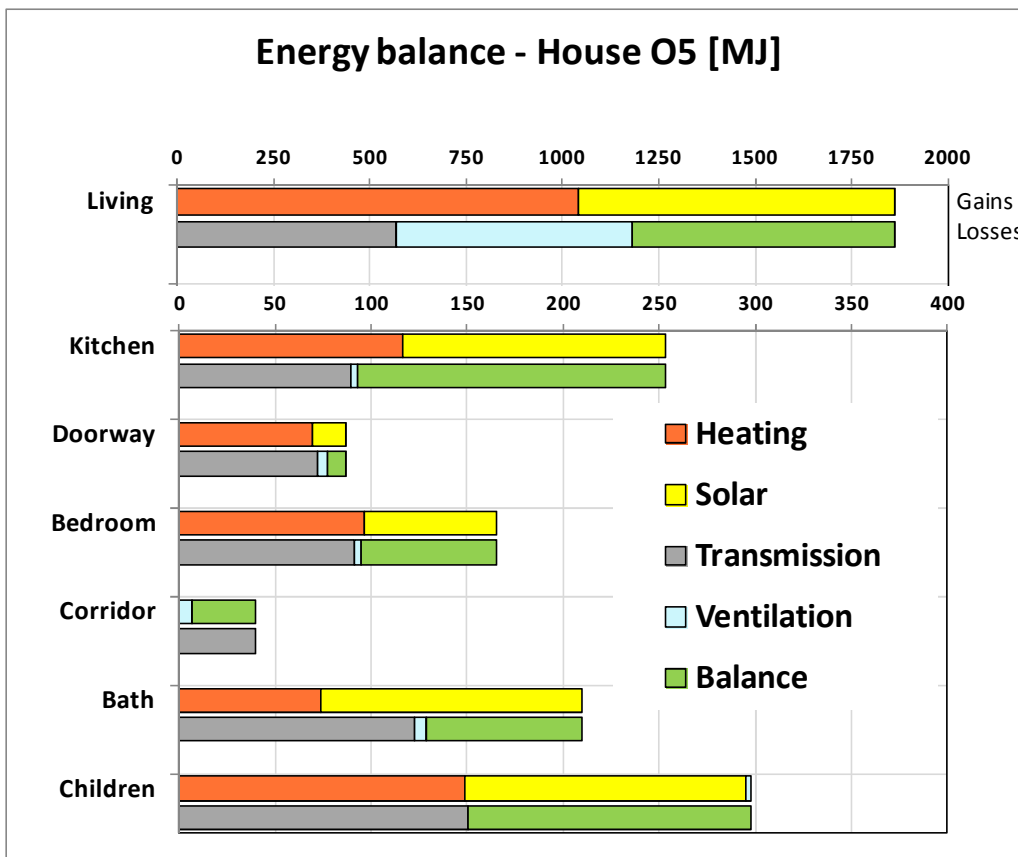
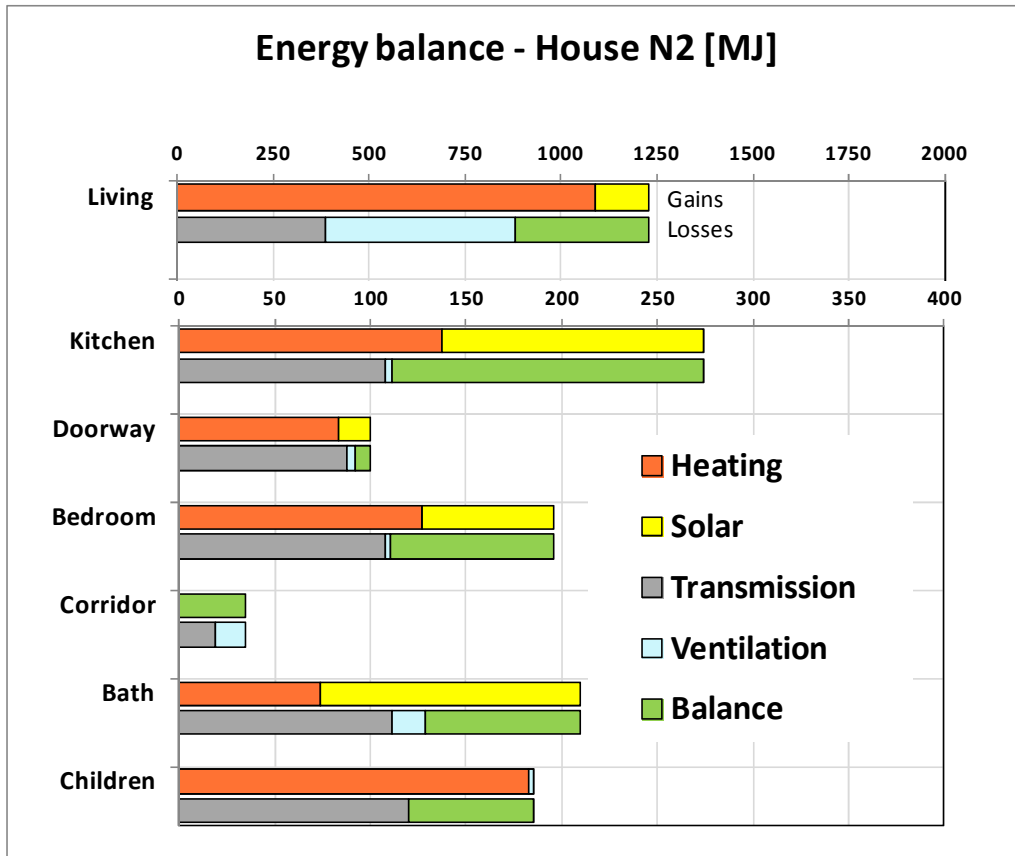


Figure 8: Energy balance of houses N2 and O5 before calibration process. N2: Sun protected (O5: Sun exposed) South windows.

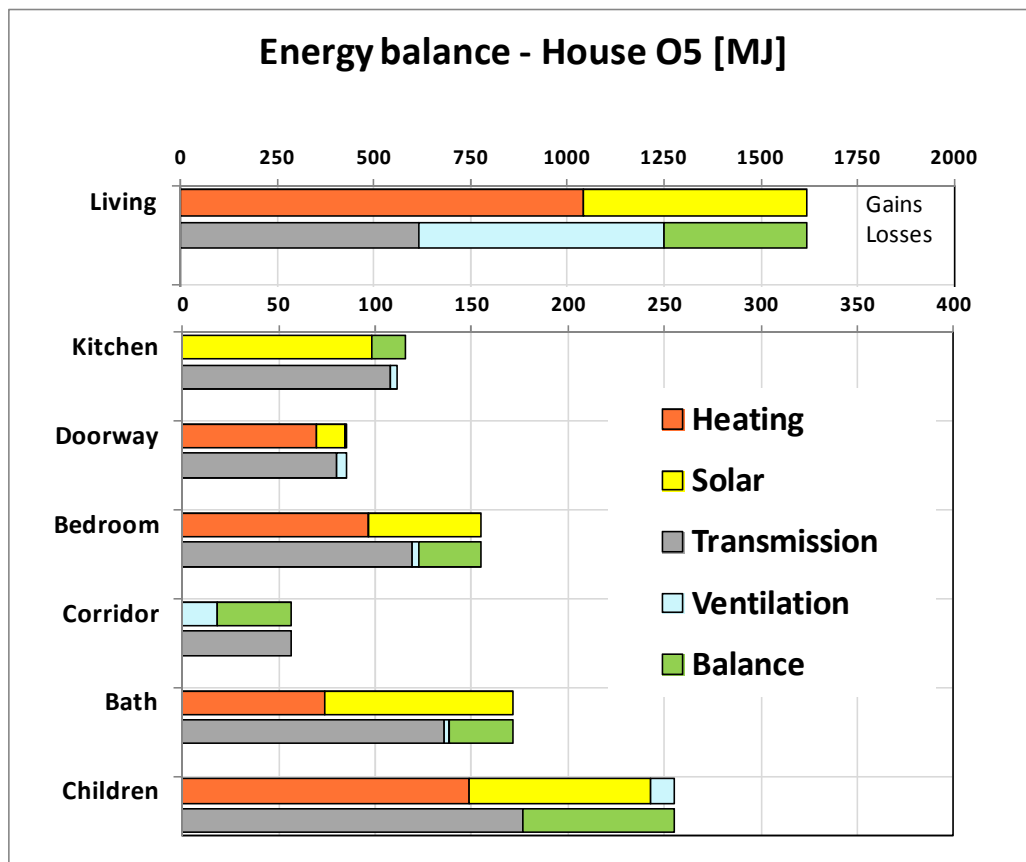
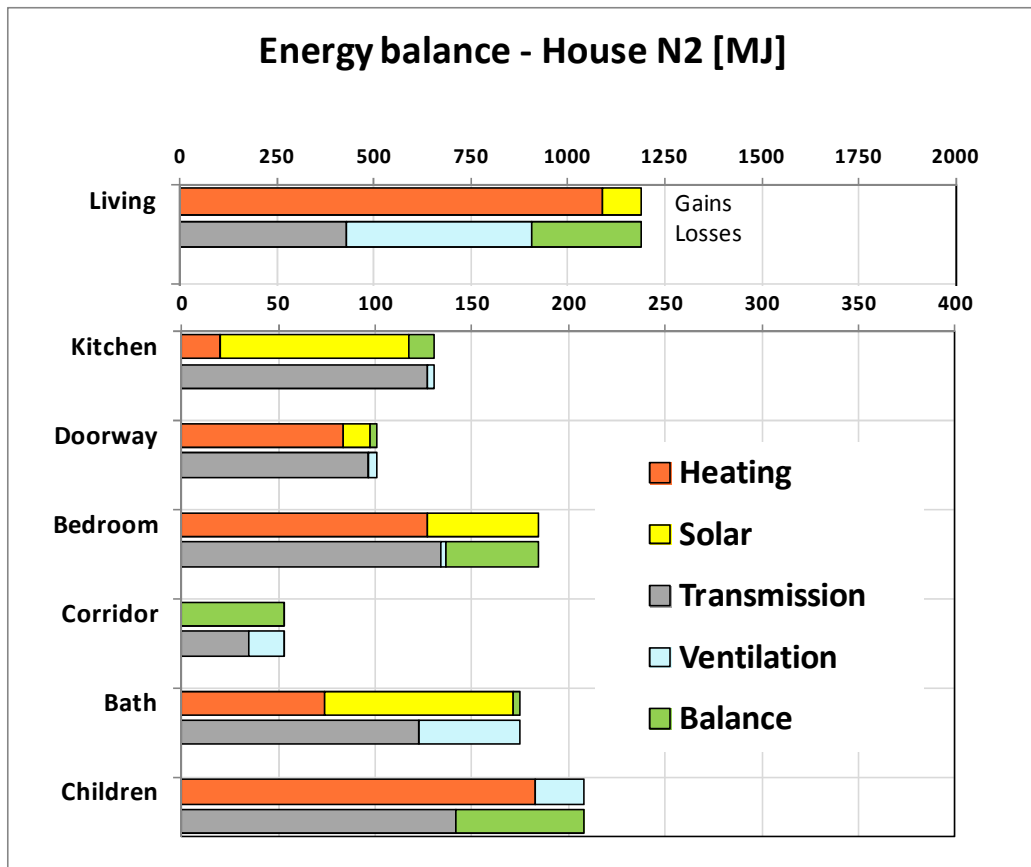


Figure 9: Energy balance of houses N2 and O5 after calibration process.
 N2: Sun protected (O5: Sun exposed) South windows.

The houses energy balance is dominated by the energy balance of the living zone. Most of the zones present an excess of heat gains.

Transmission and ventilation are calculated as function of measured indoor temperatures. Ventilation heat losses are dominated by mechanical ventilation, whose air flows are recorded. Thermal bridges heat loss coefficients have been deeply analyzed. For all those reasons, transmission and ventilation heat losses are not suspected of high uncertainty. However, the addition of infrared heat losses could help to solve the heat balance problem. Heating energy gains are measured values.

Solar heat gains are calculated from the solar intensities recorded on a horizontal plane. An uncertainty remains regarding why solar heat gains are overestimated for South oriented windows. Path of explanations are still to be found.

The indoor temperature profiles calculated by simulation on the calibrated model are presented in annex of the paper for the whole duration of the experiment. Convective coupling between interconnected zones (living, corridor, bathroom and children bedroom) seems to have a positive impact on the indoor temperature profiles obtained for the corridor and bathroom of house O5, but not in house N2. The overestimation of calculated solar heat gains in the living room affects the doorway and the North bedroom by transmission heat exchange through internal sealed doors.

6. CONCLUSION

Holzkirchen experiment is a challenging tool for benchmarking building simulation models. It offers the opportunity to check the validity of models, and to debug implemented simulation codes.

A simplified simulation tool written with EES solver has been calibrated through a better assessment of wall thermal bridges heat loss coefficients, angle dependant solar factor for glazing and introduction of convective coupling effect between interconnected zones. Effect of heat losses due to un-insulated air ducts were added as well.

The analysis of the balance between energy heat losses and gains, on the basis of the measured indoor temperatures, makes appear an underestimation of heat losses and an overestimation of solar heat gains. The overestimation of solar heat gains in the living room is responsible for discrepancies regarding indoor temperature profiles that affect not only the living zone, but the doorway and North bedroom by transmission heat exchange through internal sealed doors. Convective coupling effect impact positively the indoor temperature profiles in house O5, while it doesn't in house N2.

Path of explanations are still to be found. A deeper analysis of infrared heat losses could help to solve the heat balance problem. Whatever the explanation will be, it would be useful to quantify how its contribution affects the whole building energy balance.

ACKNOWLEDGMENTS

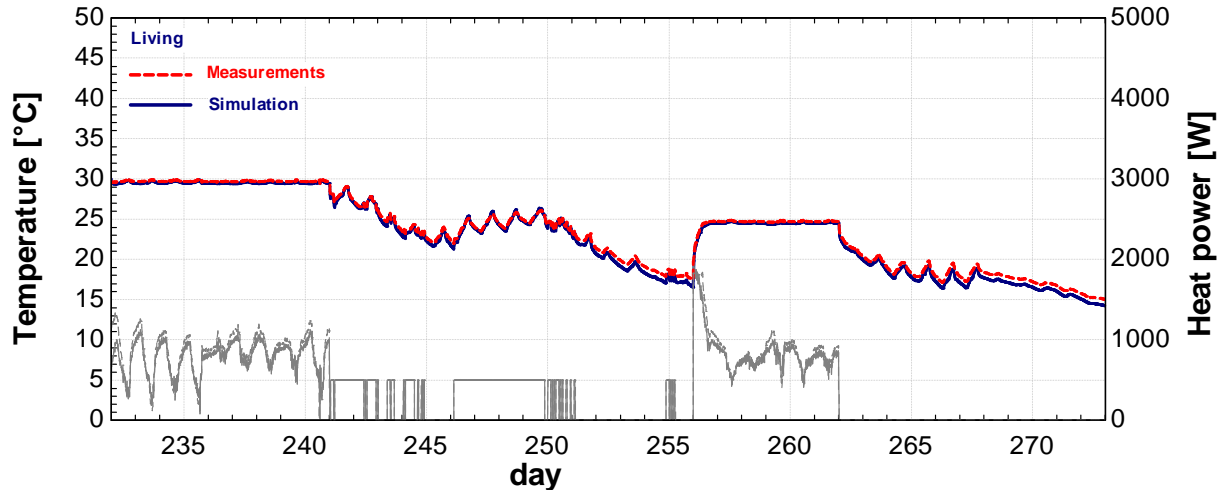
The financial support of the Walloon Region of Belgium to this project is gratefully acknowledged.

REFERENCES

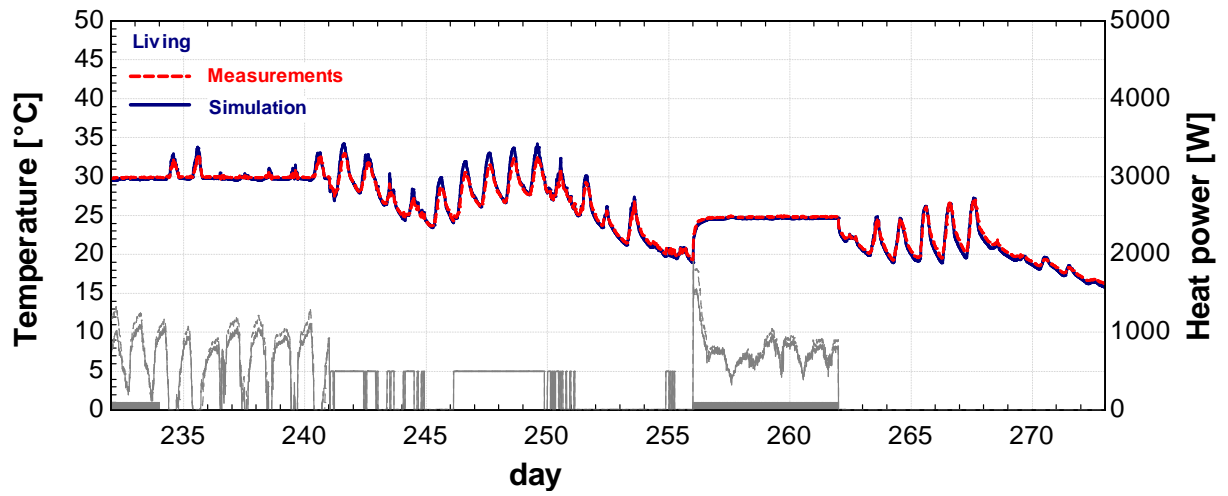
- Bacher P. And Madsen H., *Procedure for identifying models for the heat dynamics of buildings*, 2010, Technical University of Denmark.
- Reynders G., Saelens D., *Dynamic bottom-up modelling of a building stock: different shades of grey*, 6th meeting AIE 58, Ghent, April 2014, KU Leuven, Belgium.
- Roels S., *Reliable building energy performance characterization based on full scale dynamic measurements*, 6th meeting AIE 58, Ghent, April 2014, KU Leuven, Belgium.
- Strachan P., I. Heusler, *Empirical whole Model Validation Modelling Specification: Test case Twin_House_1*, IEA ECB Annex 58 Validation of Building Energy Simulation Tools, Subtask 4, May 2014.
- Masy G. and André P., *Total energy use in air conditioned buildings; analysis of main influencing factors*, 2012, *ASHRAE HVAC&R Research Journal*, Vol. 18, issue 1-2, pp. 21-36.
- Masy G., 2008, *Definition and validation of a simplified multi-zone dynamic building model connected to heating system and HVAC unit*, Ph.D. thesis, University of Liège, Belgium.

ANNEX: INDOOR TEMPERATURE PROFILES

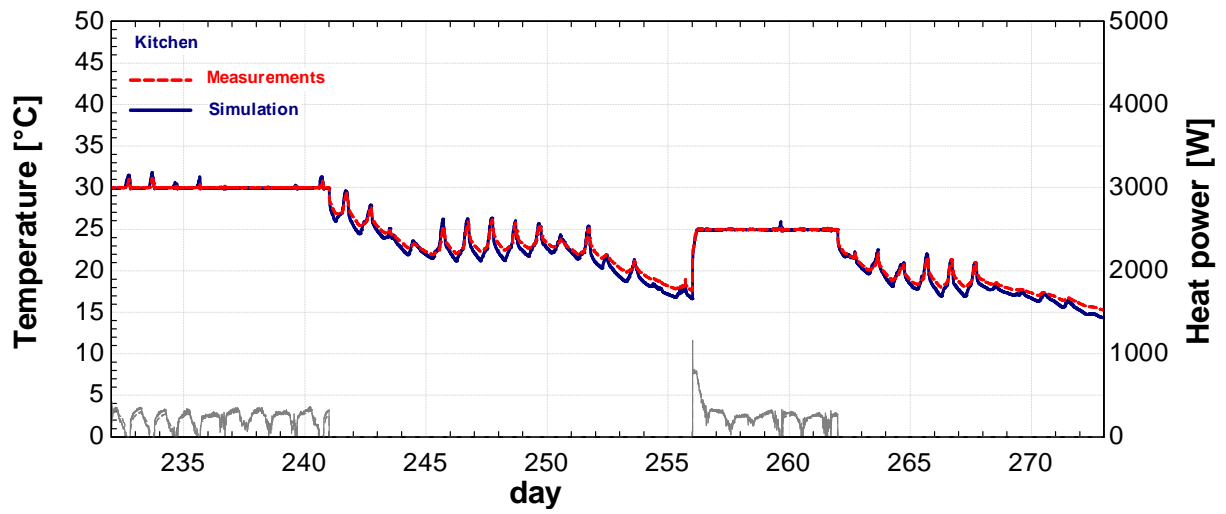
LIVING ZONE – N2



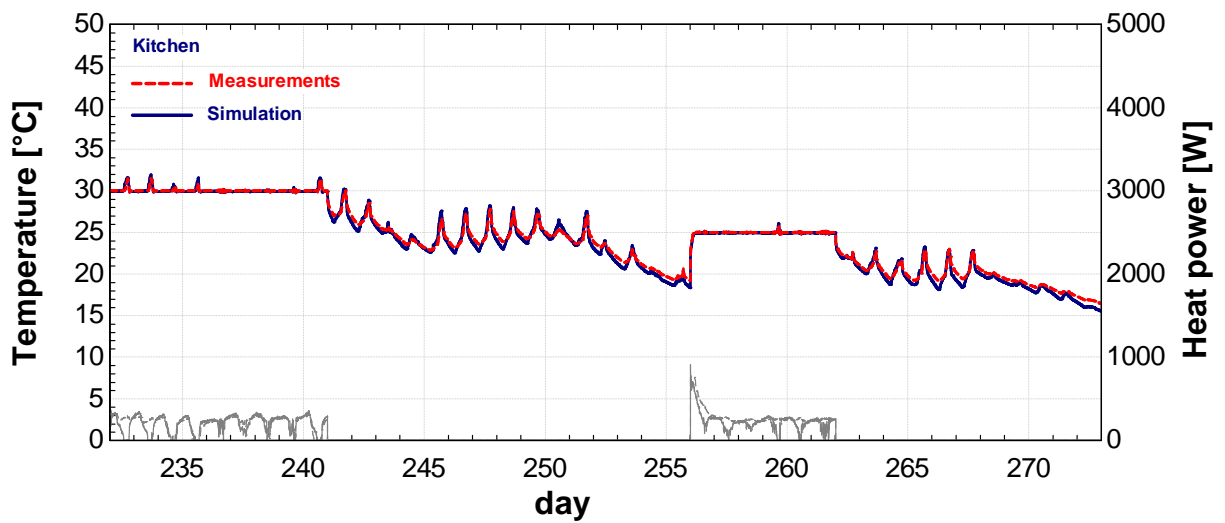
LIVING ZONE – O5



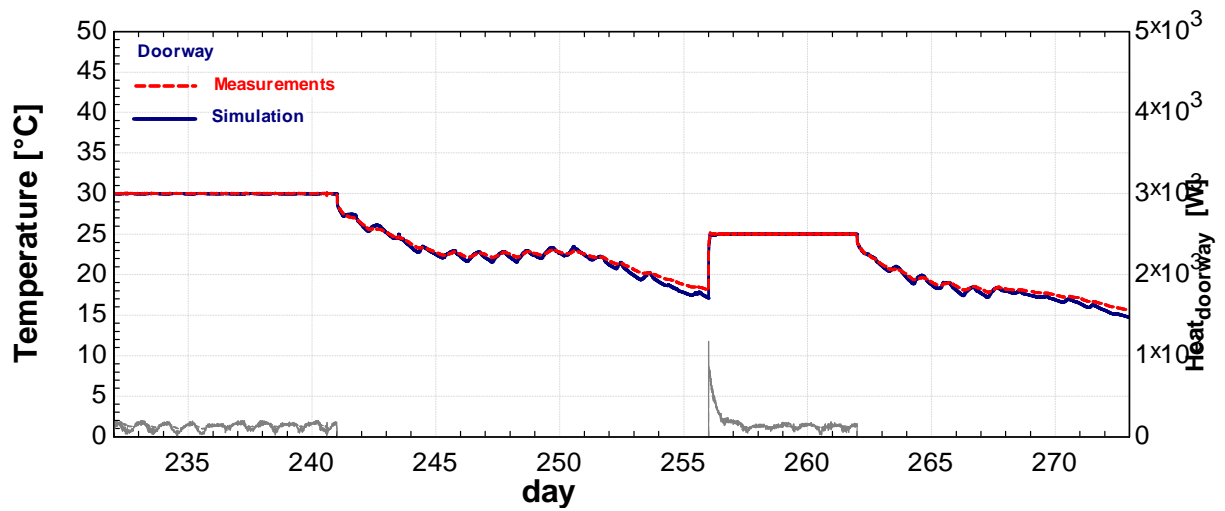
KITCHEN ZONE – N2



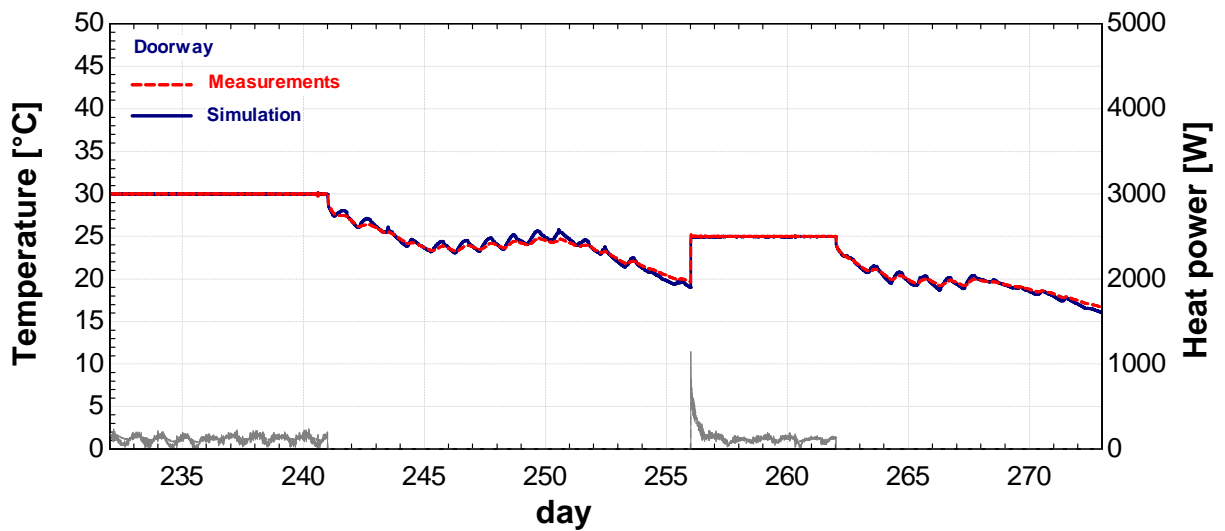
KITCHEN ZONE – O5



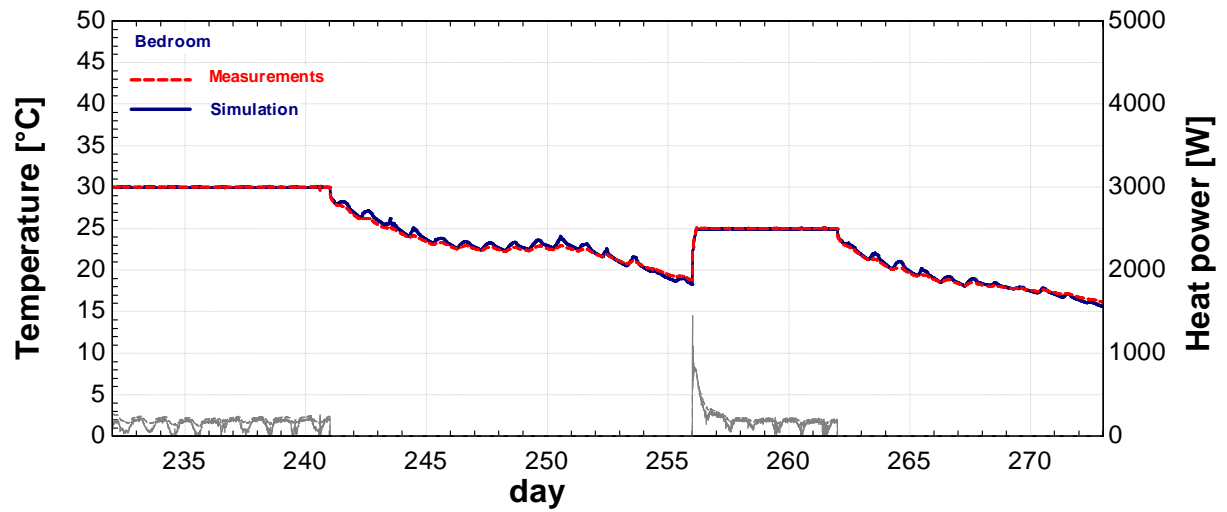
DOORWAY ZONE – N2



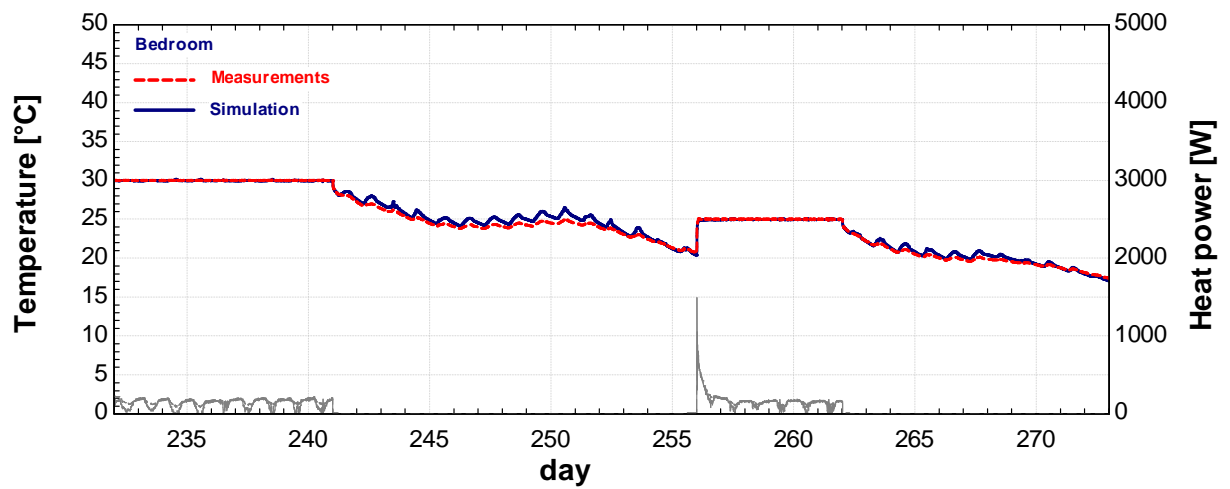
DOORWAY ZONE – O5



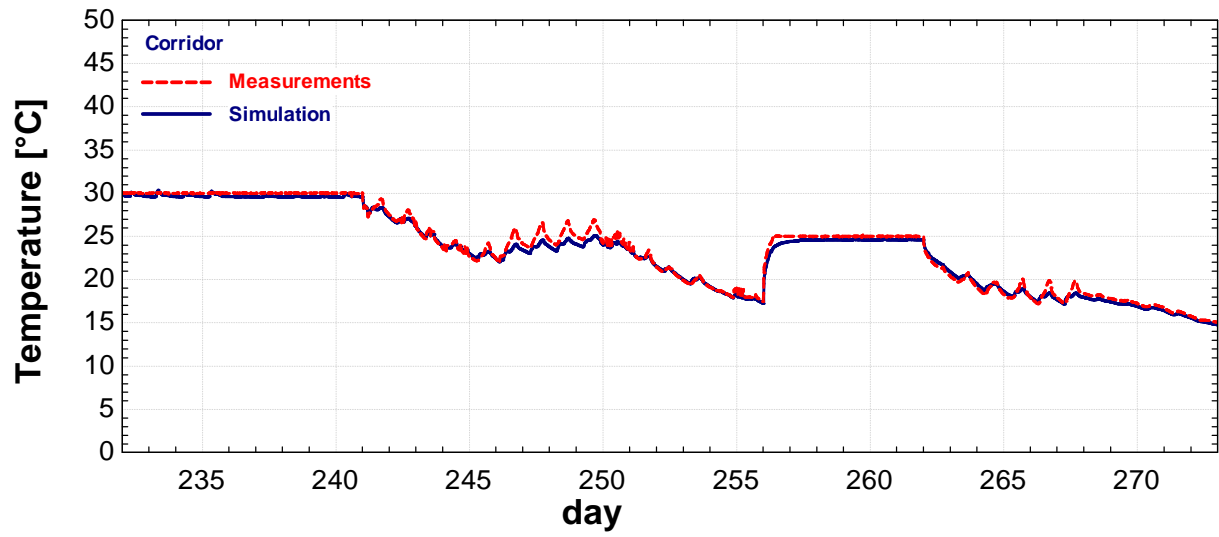
BEDROOM ZONE – N2



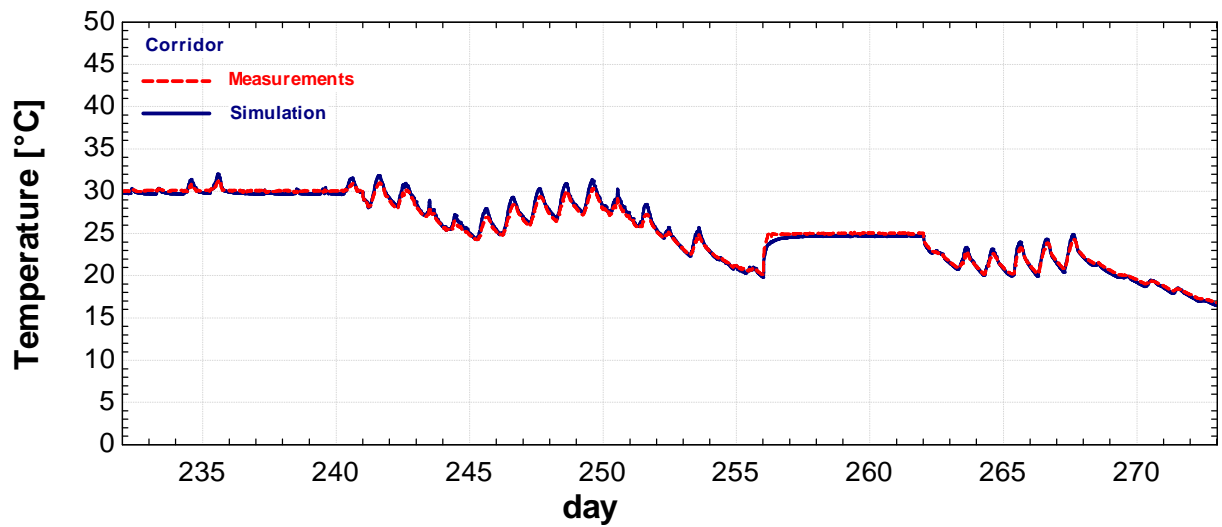
BEDROOM ZONE – O5



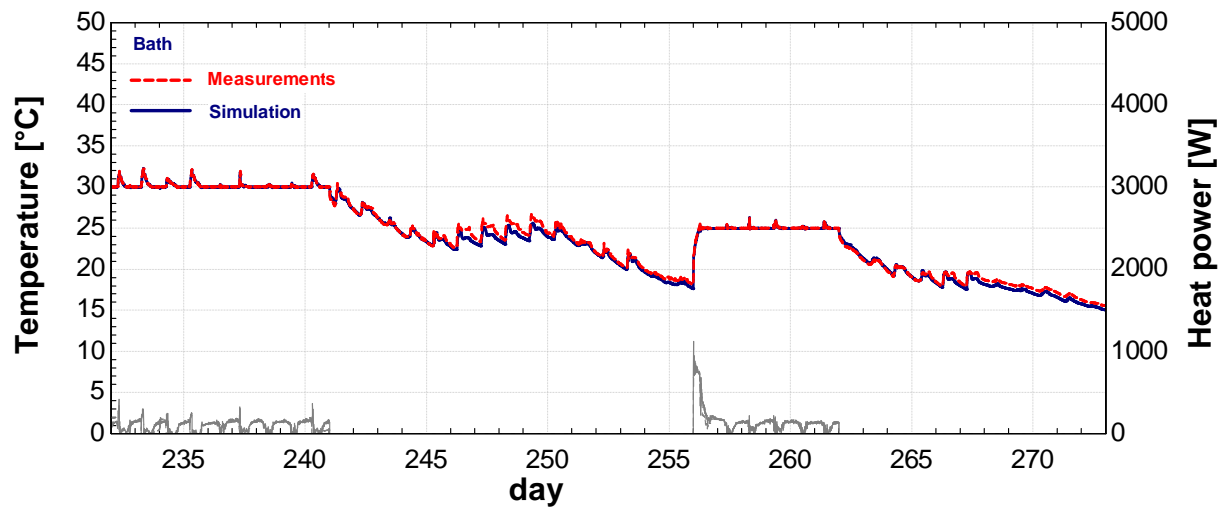
CORRIDOR ZONE – N2



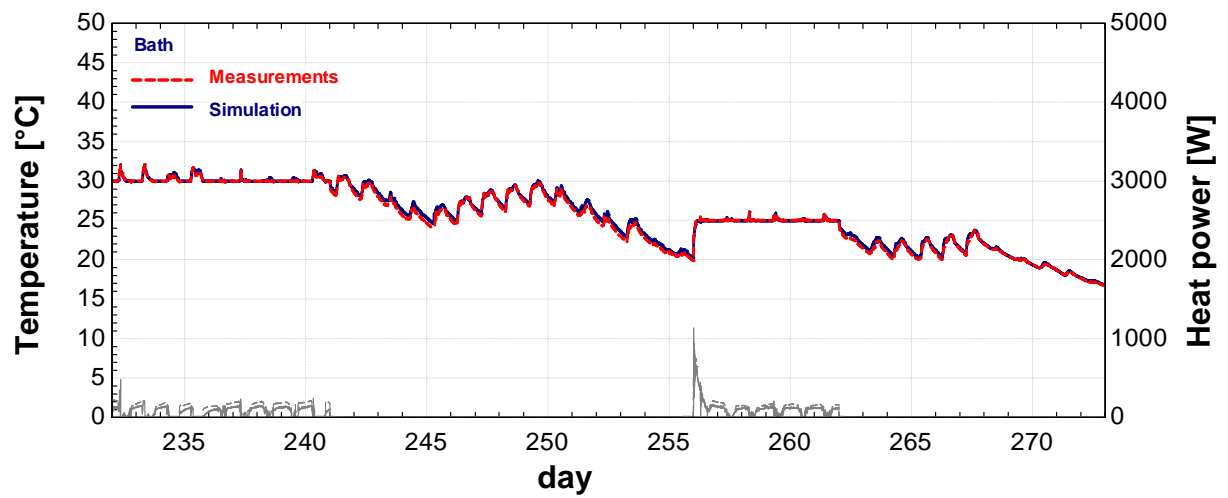
CORRIDOR ZONE – O5



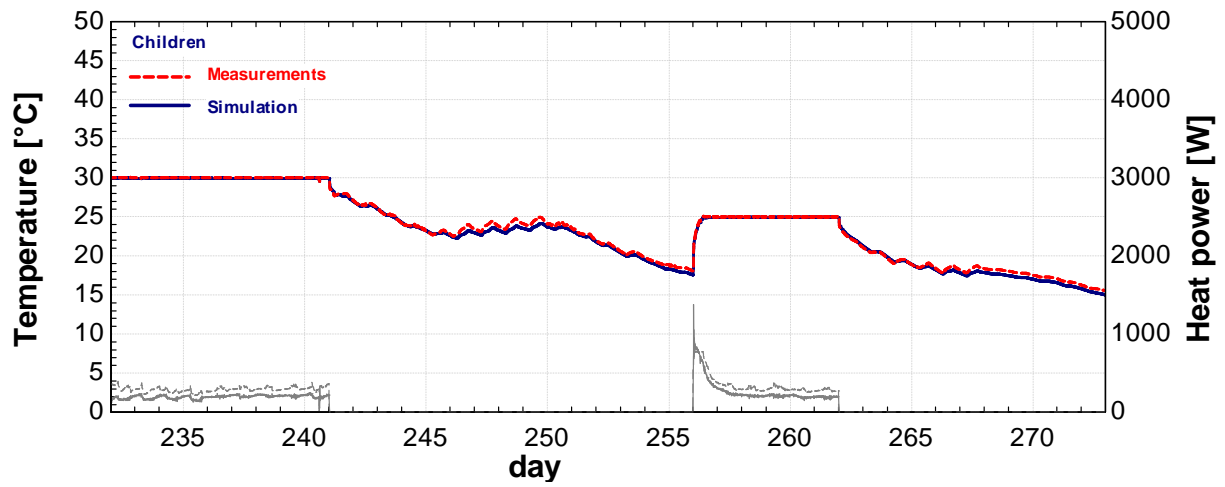
BATH ZONE – N2



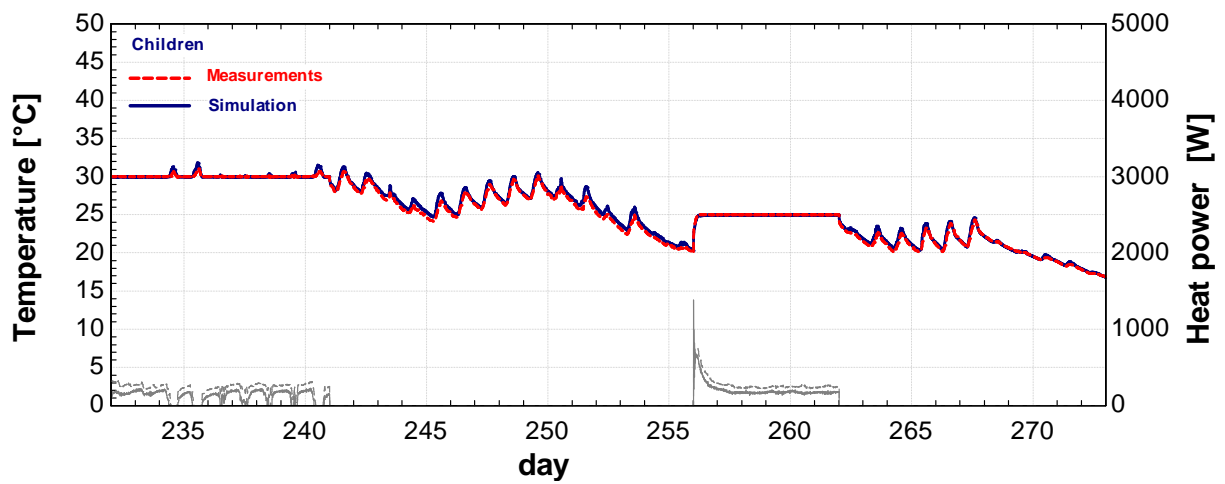
BATH ZONE – O5



CHILDREN ZONE – N2



CHILDREN ZONE – O5



SEVENTH SESSION
**INTEGRATION OF BUILDINGS
IN SMART ENERGY GRIDS**

Impact of net metering programs on optimal load management in US residential housing – a case study

E. Georges^{1*}, J. E. Braun², E. Groll², W. T. Horton², V. Lemort¹

⁽¹⁾ Thermodynamics Laboratory, University of Liège, Liège, Belgium

⁽²⁾ Ray W. Herrick Laboratories, Purdue University, West-Lafayette, Indiana, USA

1. ABSTRACT

In the US, buildings represent around 40% of the primary energy consumption and 74% of the electrical energy consumption (U.S. DOE, 2012). Incentives to promote the installation of on-site renewable energy sources have emerged in different states, including net metering programs. The fast spread of such distributed power generation represents additional challenges for the management of the electricity grid hence the interest in smart control of building loads and demand response programs.

This paper presents a study of a typical American house built in the 1990s in the Midwest and equipped with a single-speed air-to-air heat pump, an electric water heater and PV collectors. The study investigates the impact of different net metering tariffs on the optimal building electrical load management. The potential of load matching is characterized in terms of percentage of the electricity production consumed on-site and the proportion of the demand covered. Simulations are performed assuming perfect prediction of the electrical load profiles.

Results show a potential increase of load matching greater than 7% through control optimization with a suitable net-metering tariff. The associated cost saving for the consumer is about 10% greater compared to no optimization. Depending on the PV panel area, pay-back time increase due to lower buy-back tariffs can be reduced by 3 to 55% through optimal load matching.

Keywords: net metering, load matching, heat pump, electric water heater

2. INTRODUCTION

Since the late 1990s, many states in the US have started incentive programs to promote the installation of on-site renewable energy sources, such as tax incentives, low-interest loans and net energy metering. Net metering allows customers to supply their excess local electricity production to the electricity grid. These customers are often referred to as “prosumers”. The introduction of such distributed electricity generation and fluctuating renewable energy complicate the planning and operation of the power system and may affect its reliability. At the distribution level, the main negative impacts are the overload of feeders and transformers, the risk of overvoltage and power quality disturbance (Bollen & Hassan, 2011). For example, Baetens et al. (2012) identified electrical challenges associated to the evolution of a neighborhood in Belgium composed of 33 detached residential houses towards net zero energy buildings (NZEBs) using heat pumps and building-integrated photovoltaic (PV) systems. Fraction of local PV supply wasted by inverter curtailment and peak transformer loads were quantified for different existing feeder strengths.

On-site generation can also help reduce the need for expansion and strengthening of transmission lines. In the residential sector, space heating and cooling and domestic hot water represent 72% of the energy consumption of a building (U.S. DOE, 2012). In the frame of this

work, heating and cooling needs are met through the use of a reversible heat pump and domestic hot water (DHW) is produced by an electric water heater. From an electricity grid system operator standpoint, such loads are identified as thermostatically controlled loads and represent a large potential for improvement of grid reliability through demand side management strategies (Kamgarpour et al., 2013). There are two ways for these buildings to interact with the electricity grid. On the one hand, they can offer flexibility (load shifting, peak shaving, etc.) in response to signals from the grid. On the other hand, if equipped with on-site generation, such as PV collectors, they can be used to diminish the impact of distributed energy production by promoting better load matching through load shifting. In both cases, these systems work in synergy to reduce the additional burden on the grid created by renewable energy generation (Sartori et al., 2012). Several studies have been performed both at the building and district levels. Arteconi et al. (2013) presented a study focusing on the influence of switching off a heat pump coupled to thermal energy storage during peak hours on the occupants' thermal comfort and on the electricity load curve in the UK context. D. Vanhoudt (2012) presented the results from lab tests of smart management strategies of a heat pump (with thermal storage for DHW and for space heating separately) in order to promote load matching with PV collectors. R. Shleicher-Tappeser (2012) considered different storage strategies between the production of electricity and the end-users in order to increase flexibility for power consumption. Main challenges associated to the consumer's behavior as well as to the development of incentives to develop new tariff structures were pointed out. De Coninck et al. (2013) investigated rule-based control strategies to shift heat pump operation for domestic hot water production to reduce curtailing losses in NZEBs neighborhood. Load shifting was initiated by different triggers: a given time frame, the power exchange with the grid or the voltage.

Another possibility to promote load shifting is through price signals from the electricity grid. In the US, net metering policies vary according to the states: so far, the excess power generation supplied to the grid is either "bought" at retail or at wholesale price tariffs (U.S. EIA, 2012). With the increase in the number of prosumers, electricity grid congestion and PV curtailment become more frequent, which restricts the amount of distributed power supplied to the grid. Such tariffs could become a direct reflexion of the level of saturation of the electricity grid. The purpose of this study is to evaluate the impact of different net metering tariffs as an incentive to increase load matching of on-site PV generation through optimal control of the domestic electrical load in the frame of demand-side management programs. The potential for load matching is characterized in terms of percentage of the electricity production consumed on-site and the proportion of the demand covered by decentralized electricity generation (Baetens et al., 2012 and Van Roy et al., 2013). Simulations are performed assuming perfect prediction of the electricity consumption profiles of the house. The newness of the study resides the assessment of the influence of such tariffs on the consumer's economic benefit through optimal load management.

In future work, stochastically generated load profiles will be introduced to take into account the uncertainty associated with occupants' behavior.

3. METHODOLOGY

3.1 Case studies

A typical 4-bedroom single-story ranch-type American house built in the 1990's is investigated (Figure). Building characteristics have been detailed by Holloway (2013). The building structure consists of a wood frame on a concrete ground floor. The 2-by-6 wood framing has been replaced by 2-by-4 construction, which is more common. The envelope insulation levels meet standard efficiency code (IECC, 2003) for the climate zone associated to the city of

Indianapolis in the Midwest (zone number 5, IECC 2009). Overall air-to-air heat transfer coefficients (U values) for walls, roof and windows are given in Table . Breakdown of the annual energy consumption is given in Figure .

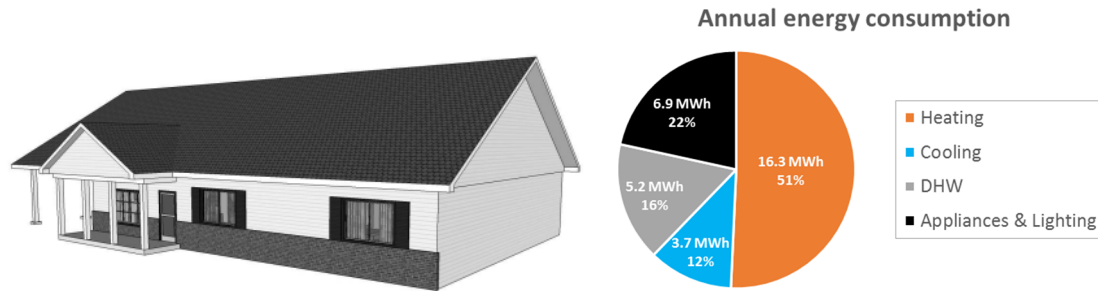


Figure 1: Left: Case study - Ranch house (Holloway, 2013) – Right: Breakdown of annual energy consumption

Table 1: Building envelope characteristics

U values [W/m²K]	
External walls	0.41
Roof	0.17
Windows	1.96

A detailed dynamic model of the house is available in TRNSYS (Holloway, 2013). Yearly simulation results were used to train a grey-box model that was implemented in the optimizer (see section 3.2.2). The grey-box model structure is illustrated in Figure 2. The model provides an accurate representation of the thermal response of the house at significantly reduced computational requirements. Root mean square error in free-floating zone temperature prediction was 0.18°C over a year for training data, and 0.19°C for the one-year validation data set.

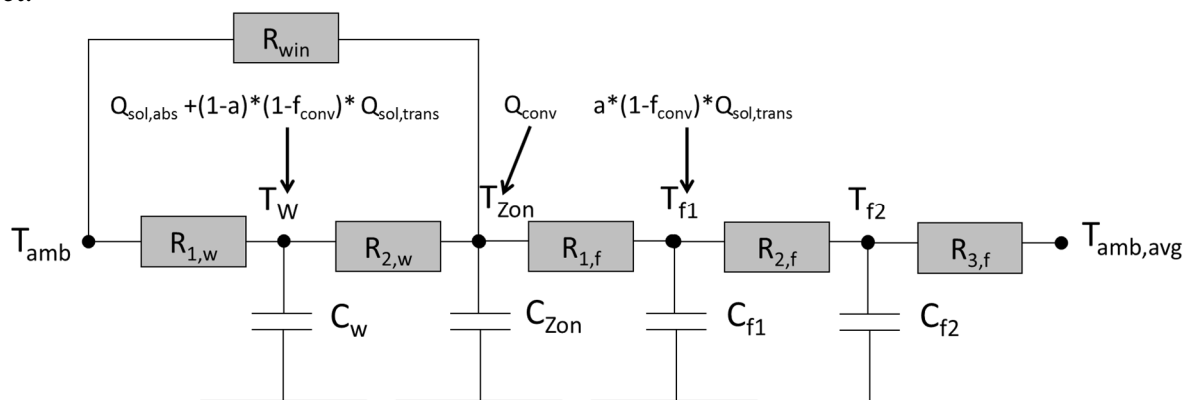


Figure 2: Grey-box model structure

The building is equipped with a reversible single speed air-to-air heat pump for space conditioning. It is modelled according to the ASHRAE toolkit model (Brandemuehl et al., 1993) in which capacity and coefficient of performance (COP) are defined as functions of their values at rated conditions (AHRI, 2008) and correction coefficients taking into account the dependency on the indoor and outdoor air temperatures and mass flow rates.

$$X = X_{rat} * f_{X_T} * f_{X_m}$$

$$f_{X_T} = a_0 + a_1 * T_{amb} + a_2 * T_{amb}^2 + a_3 * T_{Zon} + a_4 * T_{Zon}^2 + a_5 * T_{Zon} * T_{amb}$$

$$f_{X_m} = b1 + b2 * \dot{m}/\dot{m}_{rat}$$

All the coefficients for both COP and capacity were derived from performance maps for commercially available heat pumps (Holloway, 2013).

Domestic hot water production is ensured by an electric water heater equipped with two thermostats and two heating elements located in the upper third and in the lower two-thirds of the tank. Both heating elements can't be switched on simultaneously, and priority is given to the upper element. Hot water is drawn from the top of the tank and cold water is supplied at the bottom. The water in each part of the tank is assumed to be homogeneously mixed.

High efficiency photovoltaic panels are installed on the roof of the house. Two orientations are considered: south and west.

Table 2 summarizes the characteristics of each system.

Table 2: Systems characteristics summary for ranch-type house

<i>Systems characteristics – Ranch house</i>		
<i>Heat pump</i>	Heating rated capacity / Rated COP (47°F/70°F)	8.33 kW / 3.85
	Cooling rated capacity / Rated COP (95°F/70°F)	8.03 kW / 3.41
	Back up electric heater	5 kW
<i>Water heater</i>	Volume	0.189 m ³
	Lower / upper element heating power	4.5 kW / 4.5 kW
<i>PV panel</i>	Total area	20m ² – 35m ² – 50m ²
	Rated power	4.3 kW _p – 7.5 kW _p – 10.75 kW _p
	Efficiency (PV manufacturer, 2014)	21.5%

3.2 Problem formulation

3.2.1 Net metering tariffs and cover factors

As already stated, net metering allows consumers to deliver surplus electricity generated on-site to the local distribution grid. Currently, in most states of the US, the tariff applied to this excess power generation is the retail tariff. From a customer's standpoint, this implies the same economic benefit whether the electricity produced by the PV system is consumed on-site or delivered to the grid. There is therefore no incentive to shift the electricity consumption in time to match the local production. With the increase in participation in electricity net-metering programs, this excess electricity released to the grid complicates the management of the electricity grid and can threaten its stability. Different net-metering tariffs are investigated here below.

To promote better load matching between production and consumption, four additional ratios of buy-back tariff (p_{PV}) to the retail tariff (p_{elec}) were considered:

- the excess power tariff is 75% of the retail tariff : $p_{PV}/p_{elec} = 0.75$
- the excess power tariff is 25% of the retail tariff : $p_{PV}/p_{elec} = 0.25$

- the excess power tariff follows a predetermined daily profile:
 - o $p_{PV}/p_{elec} = 1$ during peak hours (7 to 9 am and 6 to 8 pm)
 - o $p_{PV}/p_{elec} = 0.1$ during off-peak hours.
- the excess power buy-back tariff tends to zero : $p_{PV}/p_{elec} = 0.01$

The buy-back ratio is defined as p_{PV}/p_{elec} . It should be noted that the retail tariff p_{elec} chosen as reference is a flat tariff.

Load matching potential is determined by the following cover factors (Baetens et al., 2012):

- supply cover factor: represents the percentage of local electricity production consumed on-site:

$$\gamma_S = \frac{\sum \min(W_{cons.}, W_{PV})}{\sum W_{PV}}$$

(1)

- demand cover factor: represents the percentage of electricity consumption covered by on-site generation:

$$\gamma_D = \frac{\sum \min(W_{cons.}, W_{PV})}{\sum W_{cons.}}$$

(2)

3.2.2 Optimal response

Both water heater and grey-box building models can be represented by discrete state space formulations, and the overall system can be described by

$$\mathbf{x}(k+1) = \mathbf{A}\mathbf{x}(k) + \mathbf{B}\mathbf{u}(k) + \mathbf{E}\mathbf{w}(k) \quad (3)$$

where \mathbf{x} is the state space variable vector composed of the zone, wall, first and second floor temperature nodes, and top and bottom water tank temperature nodes:

$$\mathbf{x}^T = [T_{Zon}, T_W, T_{f1}, T_{f2}, T_{tank_{tp}}, T_{tank_{bt}}]$$

(4)

\mathbf{u} is the vector of decision variables, namely the heat provided by the heat pump (or air-conditioning unit) to the house and the electric power supplied to the water heater:

$$\mathbf{u}^T = [Q_{house}, W_{WH,tp}, W_{WH,bt}]$$

(5)

and \mathbf{w} is the vector of disturbances, i.e., the outdoor air temperature, the solar gains and the mains water temperature.

The methodology followed in this work consists in determining the optimal electrical consumption profile of the building in response to different net metering tariffs for a given prediction horizon. The cost function for this problem aims at minimizing the cost of electricity for the consumer, which is expressed by

$$Cost = \sum_{i=1}^p \left(\max(W_{cons.}(i) - W_{PV}(i), 0) - \max(W_{PV}(i) - W_{cons.}(i), 0) * \frac{p_{PV}}{p_{elec}} \right) \quad (6)$$

where p is the prediction horizon and the total electrical consumption $W_{cons.}$ is the sum of the power consumed by the heat pump (or air-conditioning unit), the auxiliary heater, the water heater and the appliances and lighting:

$$W_{cons.} = W_{HP/AC} + W_{WH,tp} + W_{WH,bt} + W_{aux. heater} + W_{appliances \& lighting} \quad (7)$$

Perfect predictions of the PV generation and of the use profiles for DHW, appliances and lighting are assumed (section 3.3). As for model predictive control methods, an optimal control response is obtained over the prediction horizon p and is applied to a defined control horizon m (with $m \leq p$). The prediction horizon is then shifted forward in time to the end of the control horizon, following a so-called “receding horizon” control scheme.

The following constraints should be satisfied:

- the building zone temperature should remain within a predefined dead band
- $$T_{sp,low} \leq T_{Zon} \leq T_{sp,high} \quad (8)$$

with $T_{sp,low}$ and $T_{sp,high}$ set respectively to 20°C and 22°C in this case study.

- similarly, the water tank temperature in the upper and lower parts should remain within an imposed dead band:

$$T_{sp,low,DHW} \leq T_{tank,bt}, T_{tank,tp} \leq T_{sp,high,DHW} \quad (9)$$

with $T_{sp,low,DHW}$ and $T_{sp,high,DHW}$ set respectively to 35°C and 50°C in the bottom part and 50°C and 60°C in the top part of the tank.

- the heat delivered to/retrieved from the house should not exceed the full load capacity of the heat pump and auxiliary heater combined in heating mode or of the air-conditioning unit in cooling mode.
- similarly, the power supplied to the water tank should remain below the maximum value for each heating element, and both heating resistances can't work simultaneously.

The control of the HVAC systems is carried out following an “energy rate approach”, which considers that the system is allowed to cycle freely to meet the energy requirement for a given simulation time step. Performance degradation due to cycling will be taken into account in future work.

The resulting minimization problem is a convex mixed linear integer programming problem and is solved with the open-source MATLAB compatible toolbox YALMIP (Löfberg, 2004) coupled to CPLEX solver (IBM, 2013).

3.3 Load profiles

The total building energy demand includes the building space heating (SH) and cooling (AC) loads, the domestic hot water needs and the electricity consumption of appliances and lighting. Water draw-off events as well as appliances and lighting use are modelled by predefined load profiles.

Realistically, it is not likely for the controller to have an exact prediction of the DHW, appliances and lighting events, since they directly relate to the unpredictable occupants' behavior. However, typical average load profiles are available and can be used for the prediction of the optimal response.

In the “Building America House Simulation Protocols”, Wilson et al. (2014) provide a set of data including consumption and typical daily use profiles for an average American dwelling. Profiles for a four-bedroom/two-bathroom dwelling are illustrated in Figure 3. The DHW consumption includes hot water for baths, showers and sinks as well as a dishwasher and a clothes washer. The hot water daily consumption is 265 liters for weekdays and 290 liters on weekends at a supply temperature of 125°F (51.6°C). For lighting, a seasonal effect is taken into account. The annual electricity consumption for appliances and lighting is 6936 kWh.

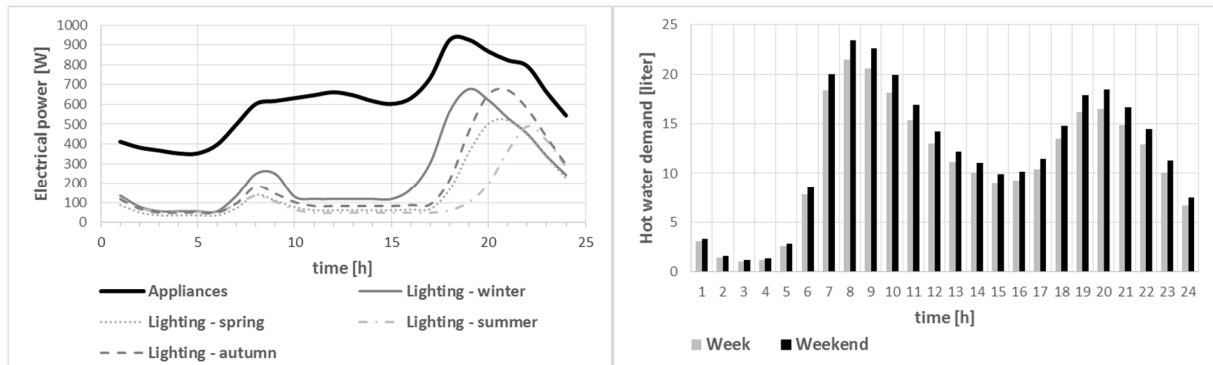


Figure 3: Average daily load profiles: Appliances and lighting (left) – DHW (right)

4. RESULTS AND DISCUSSION

The results presented in this section are obtained with optimal control, for a one-hour simulation time step, a prediction horizon of 24 hours and a control horizon of 12 hours for a year of simulation.

4.1 Influence of the net metering tariff

For the following results, a total surface of PV panels of 35m² was installed on the west slope of the roof, corresponding to a 30° tilt angle. The choice of orientation can be justified by the interest of a mid-afternoon peak PV production in the case of high peak electricity consumption in the evening. Five net-metering tariffs are investigated.

Results are presented in terms of demand and supply cover factors (section 3.2.1), total annual electricity consumption and cost saving for the consumer compared to the cost without PV collectors. They are summarized in Table 3. It should be noted that these results constitute an upper limit of the load matching potential, and that in practice, restrictions in the buy-back tariff may only apply during time-periods of grid congestion.

On a yearly basis, both demand and supply cover factors increase with lower surplus PV production tariff. When the electricity surplus sale price is reduced from 100% to 75% of the retail price, demand and supply cover factors increase by about 5% and 7% respectively. A less significant improvement (1% and 3%) is observed when reducing the tariff from 75% to 25%. The total cost saving for the consumer diminishes by 8% and 22% when the PV production buy-back price is reduced respectively from 100% to 75% and from 100% to 25%.

The results in terms of cover factors obtained with the variable tariff for peak and off-peak periods (predefined daily profile) are very similar to those obtained for a flat buy-back price of 25% of the retail price. For the present case study, with limited storage capacity, the values for the demand and supply cover factors tend to 0.37 and 0.57 respectively for a buy-back tariff approaching zero. A monthly analysis of the cover factors is illustrated in Figure 4. As expected, the demand cover factors are higher in the summer, whereas the supply cover factors are higher in the winter.

Despite the increase in on-site consumption of local electricity production with lower net-metering tariffs, the total electricity consumption cost for the consumer seems to increase. However, the cost saving should not be compared between the different tariffs. For the same tariff enforced by the electricity supplier, optimizing the consumer's load profile to match PV production brings about up to 10% additional cost saving compared to the cost without optimization.

Table 3: Supply/demand cover factors, total electricity demand and total cost for three net metering tariffs

p_{PV}/p_{elec}	Optimal control				No optimization			Comparison
	γ_D []	γ_S []	$W_{consumption}$ [MWh/year]	Cost saving [%]	γ_D []	γ_S []	Cost saving [%]	Cost saving increase
1	0.30	0.46	15.9	66.1	0.27	0.46	59.7%	6.4%
0.75	0.35	0.53	16.0	58.0	0.27	0.46	51.6%	6.4%
0.25	0.36	0.56	16.1	43.7	0.27	0.46	35.4%	8.3%
profile	0.36	0.54	16.1	43.1	0.27	0.46	34.4%	8.7%
0.01	0.37	0.57	16.2	37.4	0.27	0.46	27.6%	9.8%

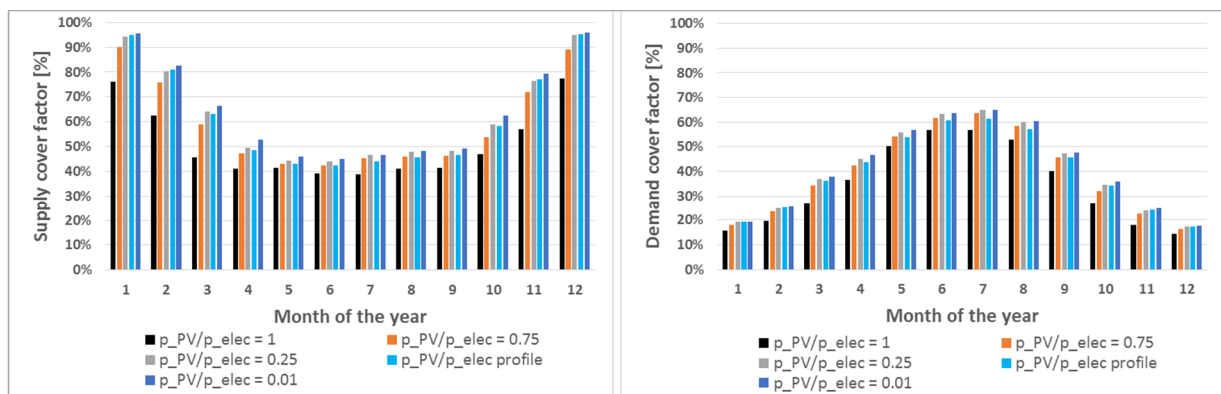


Figure 4: Demand and supply cover factors per month of the year.

Figure 5 and Figure 6 compare example optimal responses obtained for two buy-back tariffs: 100% and 25% of the retail price. As can be observed in Figure 5, for lower net-metering tariffs, the optimal control tends to shift the heat pump electrical demand to periods of time with simultaneous PV production. The building zone is preheated in order to lower the electricity consumption during periods of time with absence of sun. For the example highlighted in Figure 5, preheating the indoor air allows the heat pump to remain off for the next hour, and to work for shorter time periods the following two hours. An analogous trend is observed in Figure 6 for the electric water heater. Preheating the water typically allows for up to five-hour slowdown of the system.

The heating and cooling loads for space conditioning and the DHW heat load shifted towards sun production periods compared to the non-optimized heat load is illustrated in Figure 7 for two pay-back tariffs. The building structure provides a larger storage capacity in the winter. It should be noted that the values obtained are strongly dependent on temperature dead bands set as constraints, and would differ for a building with higher thermal inertia.

However, load shifting to increase load matching can lead to an increase in the total annual electricity consumption (Table 4). The slightly higher set points achieved increase the ambient heat losses and can slightly deteriorate the COP of the heat pump. Overconsumption of up to 2% were observed. One could argue that overconsumption could counter-balance the benefits retrieved from using on-site renewable electricity production in terms of CO₂ emissions. In Indiana, in 2011, the electricity production mix was composed of 89% coal, 7% natural gas, 1% petroleum and 3% renewables (eia, 2011). Hourly CO₂ emissions per MWh of electricity generated are illustrated in Figure 8 (OpenEI, 2011). Results in Table 4 show that despite overconsumption, increasing load matching allows to reduce CO₂ emissions by up to 8.4%.

Finally, the optimal total electricity demand profile obtained with the time-varying net-metering pricing is illustrated in Figure 9. Load matching is enforced during off-peak hours, typically in the afternoon when the PV production is maximum. This also tends to shift part of the morning and night consumption peaks to off-peak periods, but not as significantly as for constant tariffs. Indeed, since surplus electricity production can be sold at a higher price during these periods, it remains interesting for the consumer to deliver electricity back to the grid. Therefore, flat tariffs seem more suitable as incentive for load matching.

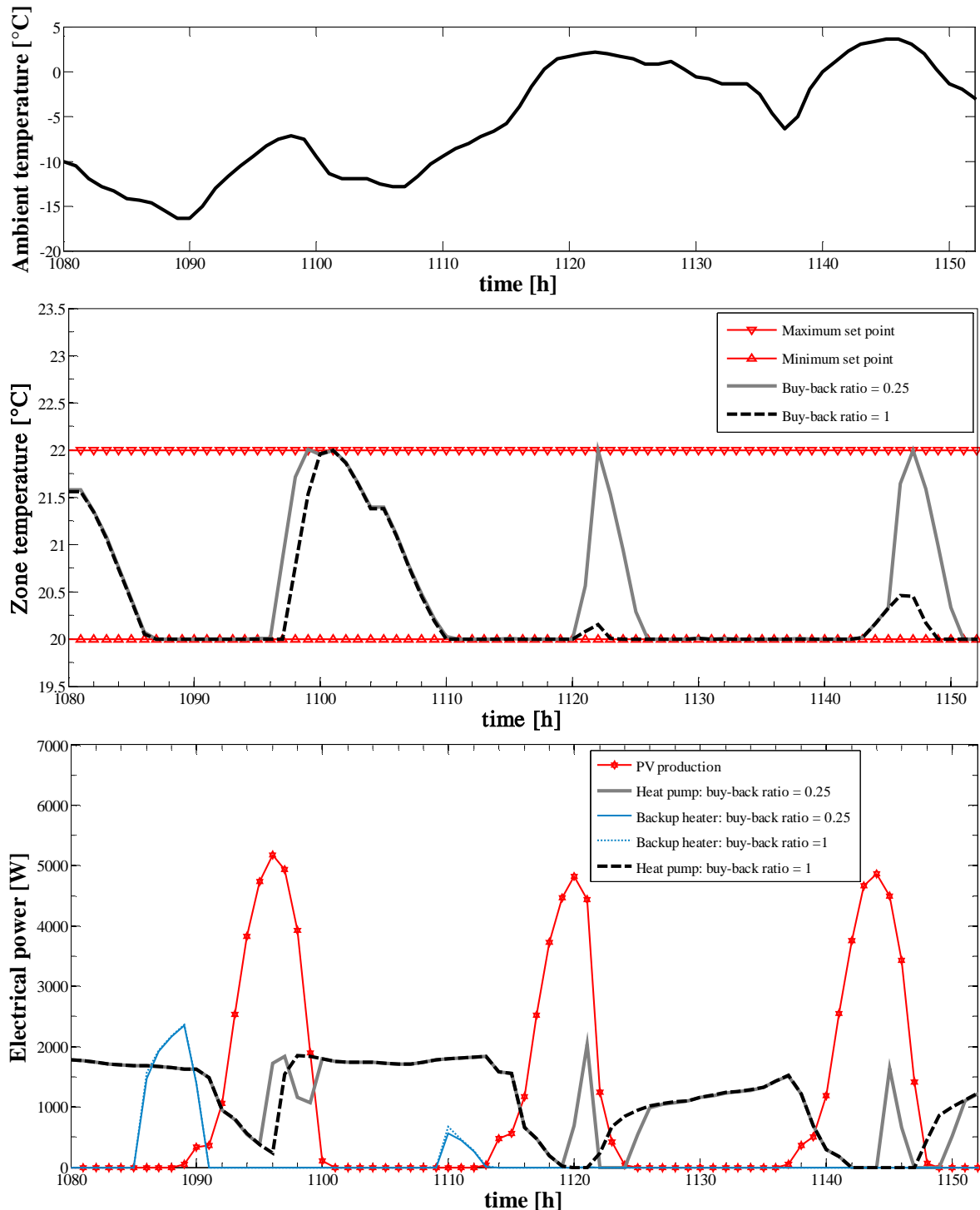


Figure 5: Bottom - Electrical power consumption for space heating for $p_{PV}/p_{elec}=1$ and $p_{PV}/p_{elec}=0.25$ and PV production for hours number 1080 to 1152 (February 14th to February 17th). Top – Corresponding zone and ambient temperatures.

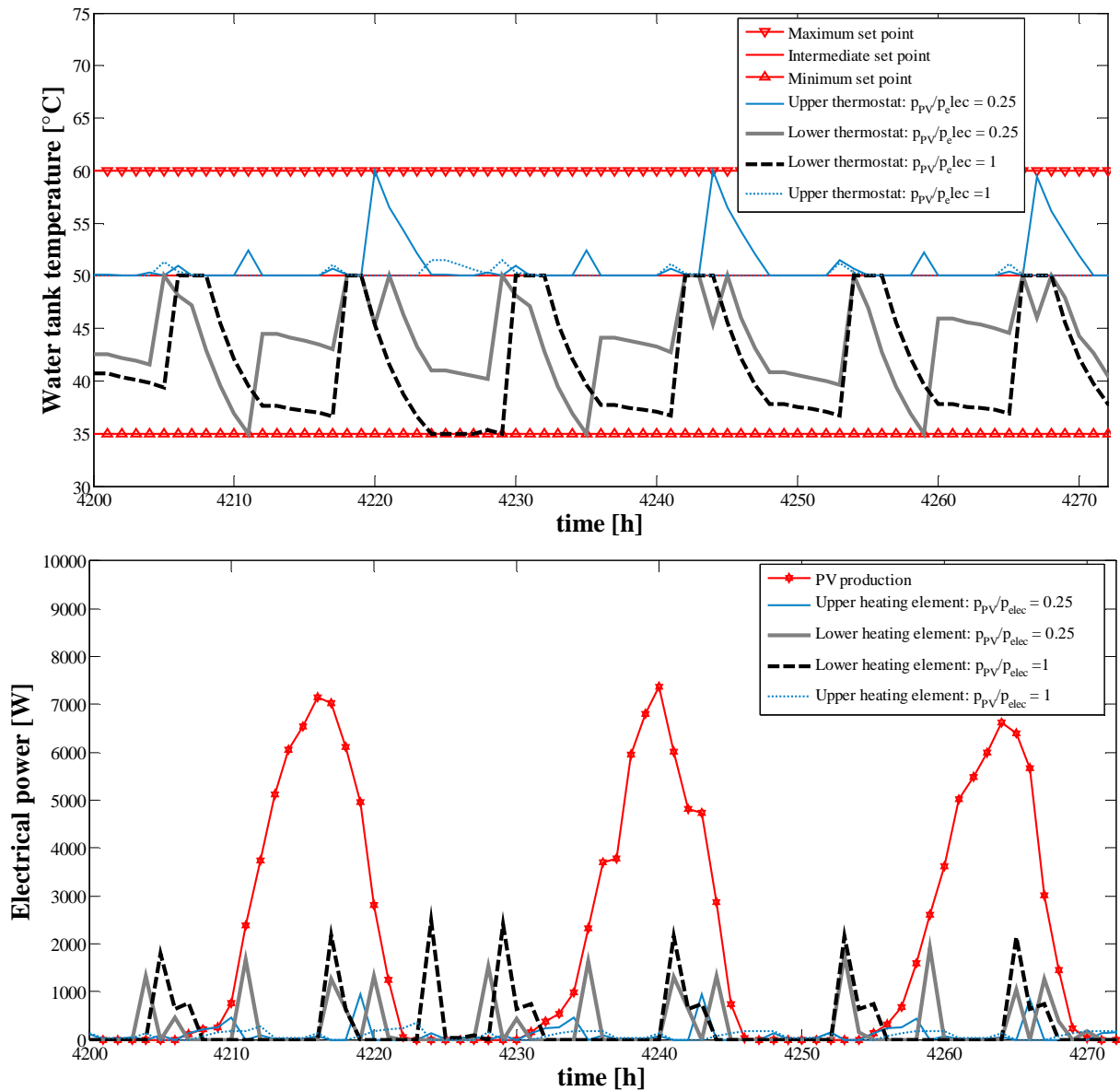


Figure 6: Bottom - Electrical power consumption for DHW for $p_{PV}/p_{elec}=1$ and $p_{PV}/p_{elec}=0.25$ and PV production for hours number 4200 to 4272 (June 24th to June 27th). Top – Corresponding water tank lower and upper thermostat temperatures.

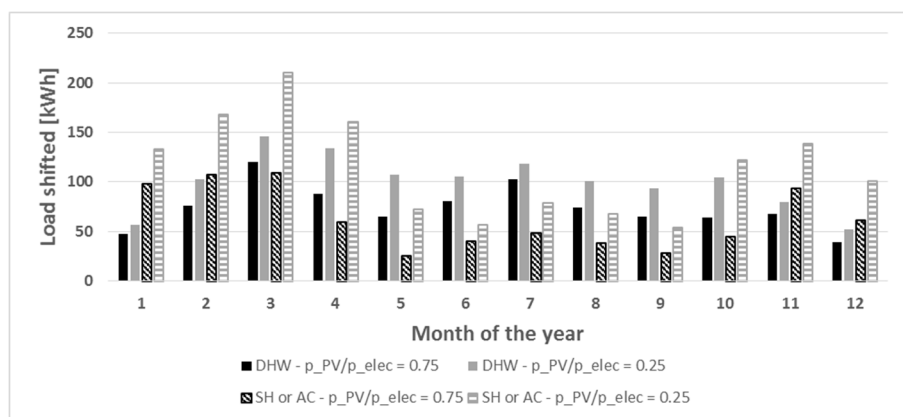


Figure 7: Thermal load shifted to match PV production per month for DHW and space heating or air-conditioning (SH or AC)

Table 4: Over-consumption and CO2 emissions with optimal control

p_{PV}/p_{elec}	$W_{cons.}$ [MWh/year]	Over-consumption [%]	CO2 emissions [t]	Reduction in CO2 emissions
1	15.9	/	8.33	/
0.75	16.0	0.6	7.83	6.0%
0.25	16.1	1.1	7.65	8.2%
profile	16.1	1.1	7.77	6.7%
0.01	16.2	1.9	7.63	8.4%

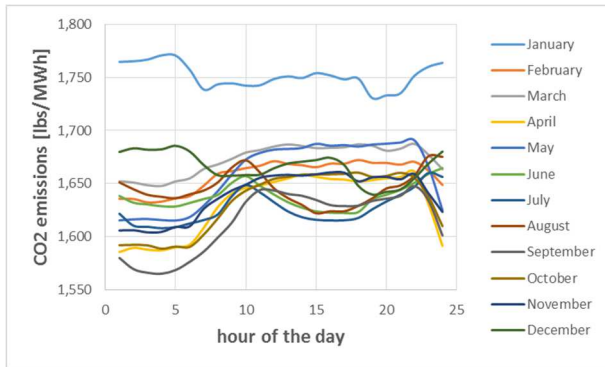


Figure 8: Average CO2 emissions per month in Indiana

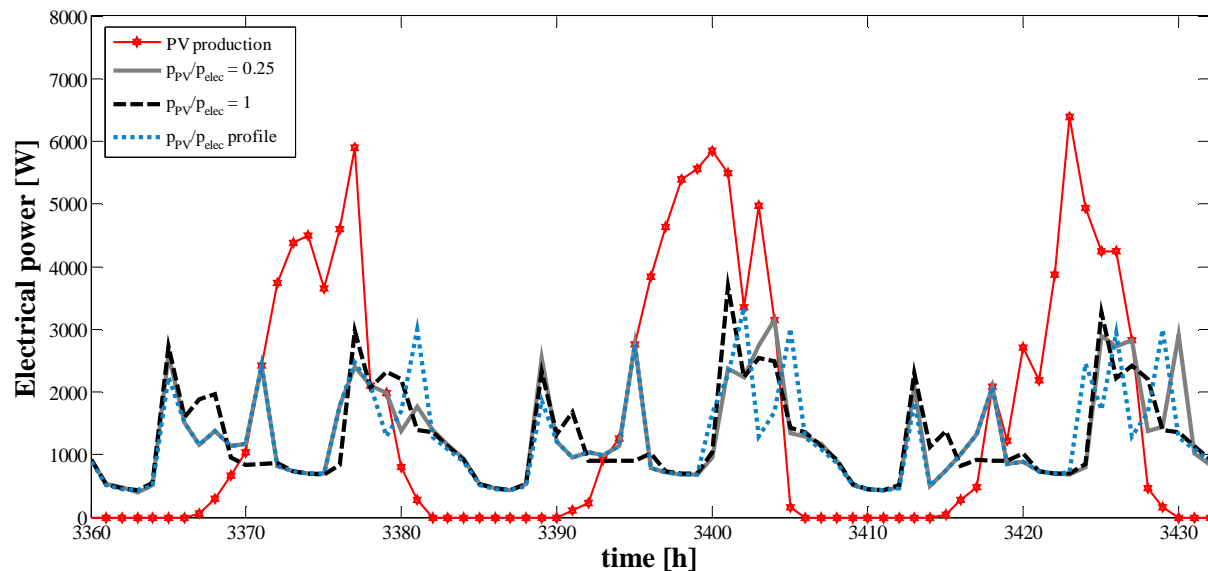
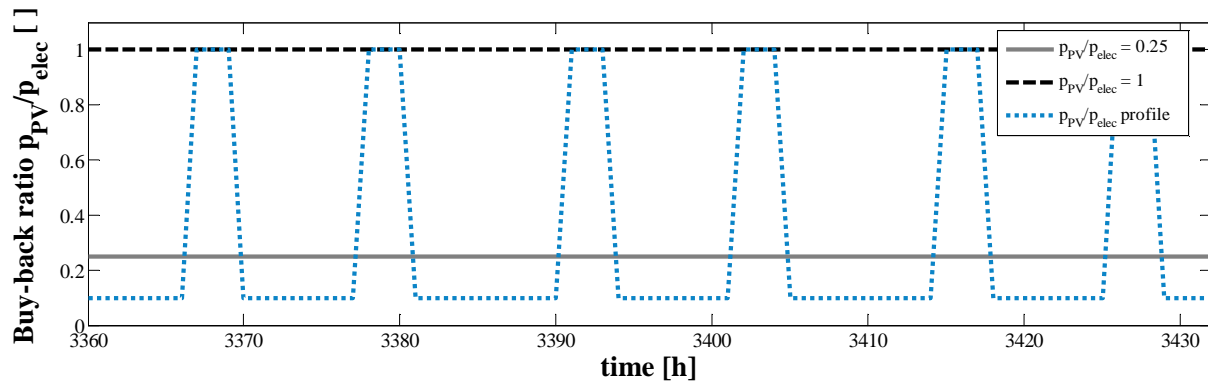


Figure 9: Comparison of total electricity consumption and PV production for p_{PV}/p_{elec} following a daily profile (1 during peak hours and 0.1 during off-peak hours), $p_{PV}/p_{elec} = 0.25$ and $p_{PV}/p_{elec} = 1$.

4.2 Influence of the PV panels orientation

In the previous section, the results were presented for 35m² of PV panels facing west. In this section, a comparison is presented with 35m² of south-oriented PV panels. The results given in Table 5 show an overall electricity demand coverage by on-site generation slightly larger (1%) with south-facing PV panels. Contrariwise, the proportion of electricity produced by the PV panels and consumed on-site is up to 7% greater for west orientation. This can be explained by the limited storage capacity of the building presented in this study and the existence of peak in electricity demand in the evening. Therefore, despite the lower total annual electricity production compared to south-oriented PV collectors, west facing PV panels seem more suitable to increase load matching in the case of low inertia buildings with peak electricity demand in the evening.

Table 5: Influence of PV panels orientation: west-facing and south-facing

	<i>West-oriented PV</i>		<i>South-oriented PV</i>	
	γ_D []	γ_S []	γ_D []	γ_S []
p_{PV}/p_{elec}				
<i>1</i>	0.30	0.46	0.31	0.40
<i>0.75</i>	0.35	0.53	0.36	0.46
<i>0.25</i>	0.36	0.56	0.38	0.49
<i>profile</i>	0.36	0.54	0.38	0.49
<i>0.01</i>	0.37	0.57	0.40	0.51

4.3 Influence of PV panel area

This section studies how the cover factors and consumer's pay-back time change with PV panels installed power for the different buy-back ratios. The total surface of PV panels was set respectively to 20m², 35m² and 50m². These areas correspond 38%, 66% and 94% coverage of the annual electrical consumption of the house.

The results obtained after optimization are summarized in Table 6. As expected, for approximately the same total electricity consumption, the demand cover factor increases with the surface area of PV panels. The same tariff incentive promotes load shifting to different extents depending on the PV area. For a buy-back ratio of 0.25, the supply cover factor reaches 0.80 for 20m² PV area, 0.57 for 35m² PV area and 0.45 for 50m² PV area. The proportion of electricity delivered to the distribution grid thus increases significantly with the PV area. This effect may seem negligible for a single house, but may affect the grid reliability at a neighbourhood scale.

Table 6: Comparison of supply/demand cover factors for different PV area and different buy-back ratios.

	<i>PV Area = 20 m²</i>		<i>PV Area = 35 m²</i>		<i>PV Area = 50 m²</i>	
	γ_D []	γ_S []	γ_D []	γ_S []	γ_D []	γ_S []
p_{PV}/p_{elec}						
<i>1</i>	0.24	0.64	0.30	0.46	0.34	0.36
<i>0.75</i>	0.28	0.74	0.35	0.53	0.38	0.41
<i>0.25</i>	0.29	0.78	0.36	0.56	0.40	0.43
<i>0.01</i>	0.30	0.80	0.37	0.57	0.41	0.45

In the US, the average installation cost of PV panels was 4.7\$ per watt peak in 2013 (NREL, 2013). No significant scale benefits can be observed for an installed power in the range of 5kW_p to 10 kW_p. A federal tax credit incentive provides 30% reduction of the cost for residential PV systems (IREC, 2012). Therefore, the installation costs are respectively 14150, 24675 and 35370 dollars for 20m², 35m² and 50m² PV areas. The electricity retail tariff for residential consumers in Indiana is 0.0945 \$/kWh. The pay-back time for the consumer can be defined by the total installation cost divided by the annual cost saving.

Figure 10 (left) compares the consumer's pay-back time for optimized and non-optimized consumption profiles as a function of the buy-back ratio for different PV areas. The pay-back time increases significantly with decreasing buy-back ratios, and especially for larger PV areas. For buy-back ratios decreasing from 1 to 0.25, the pay-back time for non-optimized response increases by 36%, 69% and 93% respectively for 20m², 25m² and 50m² PV areas. Optimizing load profiles to match on-site PV production allows to reduce this increase by 16% to 19%. These results are in accordance with the evolution of the supply cover factors in Table 6.

Thus, for net-metering programs with buy-back tariffs lower than retail price and no other economic incentives, installing larger PV areas without increasing on-site storage capacity to promote load matching may become unprofitable. Given a life expectancy of about 30 years for PV panels, optimum sizing of PV panels, expressed in terms of percentage of the annual electricity consumption covered, can be derived for each buy-back ratio. Results are illustrated in Figure 10 (right). For a buy-back ratio of 1, there is no theoretical limit, and a maximum of PV panels should be installed. For buy-back ratios inferior to 1, the maximum coverage can be as low as 20% for non-optimized load profiles and 34% for optimized ones.

These conclusions are closely linked to net metering programs implemented in this study. The electricity supplier could promote other incentives in parallel, such as payoffs to prosumers who optimize on-site electricity consumption.

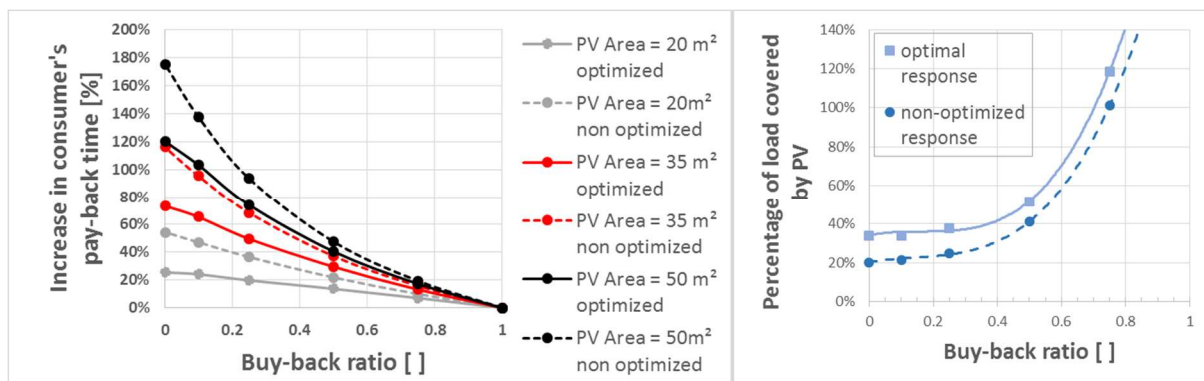


Figure 10: Left: Buy-back ratio as a function of p_{PV}/p_{elec} for three different total PV areas (20m², 35m² and 50m²) – Right: Optimal PV area expressed as a percentage of the annual load coverage vs buy-back ratio.

5. CONCLUSIONS

In this study, optimal management of the electricity demand of a typical US house equipped with a reversible heat pump, an electric water heater and PV panels has been investigated. The objective was to minimize the excess electricity production delivered to the grid by promoting on-site consumption through the use of different net metering tariffs.

Imposing a tariff lower than the retail tariff for the excess electricity generated proved to be a good incentive to promote load matching. Indeed, with 35 m² of PV panels on the west slope of the roof and for a price set to 25% of the retail price, the yearly percentage of demand directly covered by on-site generation and the percentage of PV production consumed directly in the house increased by 6% and 9%. It was also shown that the increase in load matching is not proportional to the diminution in the tariff for a given installed PV power. Despite the increase in cover factors, the overall electricity cost for the consumer increases with a lower buy-back tariff. However, for the same tariff enforced by the electricity supplier, optimizing the consumer's load profile to match PV production brings about up to 10% additional cost saving compared to the cost without optimization, hence the interest in load-matching for both the consumer and the supplier. In terms of potential improvement in load matching, the choice of a flat tariff seems more suitable than a time-varying tariff.

With regard to PV panel orientation, it was shown that despite a lower total annual electricity production, west facing PV panels present supply cover factors up to 11% higher than south-facing ones and seem more suitable to promote load matching in the case of low inertia buildings with peak electricity demand in the evening.

Finally, for larger PV areas, reducing buy-back tariffs has a less significant impact on load matching improvement, and increases dramatically the consumer's pay-back time. For 50m² PV areas and non-optimized electricity load profiles, the pay-back time increases by up to 93% for pay-back ratios ranging from 1 to 0.25. Optimizing the load profile allows to reduce this increase by 19%. For 20m² PV area, the reduction in pay-back time reached up to 36%. Optimal percentage of installed load coverage were derived as a function of the buy-back ratio imposed.

In future work, the buy-back tariff could be adjusted to reflect the level of grid congestion. Other financial incentives from the electricity supplier could be investigated, such as complimentary payoffs for prosumers optimizing their load profiles to reduce their impact on the grid. Different heating and cooling schedules, such as night set-back strategies as well as different on-site storage capacities (higher thermal inertia buildings, complimentary hot water storage for space heating, etc.) will be studied. Finally the impact of the occupant's behavior will be introduced through stochastic load profiles for DHW draw-off events and appliances and lighting use.

REFERENCES

- AHRI, 2008, *Performance Rating of Unitary Air-Conditioning & Air-Source Heat Pump Equipment*, No. 210/240-2008, 211 Wilson Boulevard, Suite 500, Arlington, VA 22201, USA.
- Arteconi A., Hewitt N.J. and Polonara F., 2013, *Domestic demand-side management (DSM): Role of heat pumps and thermal energy storage (TES) systems*, Applied Thermal Engineering, vol. 51, 2013, pp. 155-165.
- Baetens, R., De Coninck, R., Van Roy, J., Verbruggen, B., Driesen, J., Helsen, L., Saelens, D., 2012, *Assessing electrical bottlenecks at feeder level for residential net zero-energy buildings by integrated system simulation*, Applied Energy, vol. 96, pp. 74-83.
- Bollen M., Hassan F., 2011, *Integration of Distributed Generation in the Power System*, 1st ed., John Wiley & Sons, IEEE press, Piscataway, NJ, USA.

Brandemuehl, M. J., Gabel, S., & Andresen, I., 1993. *HVAC 2 Toolkit: A Toolkit for Secondary HVAC System Energy Calculations*, Atlanta, Ga.: American Society of Heating, Refrigerating and Air-Conditioning Engineers.

De Coninck, R., Baetens R., Saelens, D., Woyte A. and Helsens L., 2013, *Rule-based demand side management of domestic hot water production with heat pumps in zero energy neighbourhoods*, accepted in Journal of Building Performance simulation.

EIA Independent Statistics & Analysis - US. Energy Information Administration, 2011, *State Profiles and Energy Estimates*, <http://www.eia.gov/state/seds/>

Holloway, S., 2013, *An annual performance comparison of various heat pumps in residential applications*, PhD dissertation, Purdue University, IN, USA.

IBM ILOG, 2013, CPLEX Optimization Studio.

International Code Council. 2003, 2009, *International Energy Conservation Code (IECC)*.

Interstate Renewable Energy Council (IREC), 2012, *Database of State Incentives for Renewables and Efficiency (DSIRE) - Residential Renewable Energy Tax Credit*.

Kamgarpour M., Ellen C., Soudjani S. E. Z., Gerwinn S., Mathieu J. L., Müllner N., Abate A., Callaway D. S. Fränze M., Lygeros J., 2013, *Modeling Options for Demand Side Participation of Thermostatically Controlled Loads*, IREP Symposium-Bulk Power System Dynamics and Control - IX, August 25-30, 2013, Rethymnon, Greece.

Löfberg J., 2004, *YALMIP: A Toolbox for Modeling and Optimization in MATLAB*, In Proceedings of the CACSD Conference, Taipei, Taiwan.

National Renewable Energy Laboratory (NREL), 2013, *The Open PV Project*, <https://openpv.nrel.gov/>

OpenEI, 2011, *Hourly Energy Emission Factors for Electricity Generation in the United States*, <http://en.openei.org/datasets/dataset/hourly-energy-emission-factors-for-electricity-generation-in-the-united-states>

Sartori I., Napolitano A., Voss K., 2012, *Net zero energy buildings: a consistent definition framework*, Energy and Buildings, vol. 48, pp. 220-232.

Shleicher-Tappeser R., 2012, *The building as system level for management and storage - electricity and heat storage in apartment and office buildings*, 7th International renewable Energy Storage Conference and Exhibition (IRES 2012), Berlin, November 12-14, 2012.

U.S. Department of Energy (DOE), 2012, *2011 Buildings energy data book*, Energy Efficiency & Renewable Energy.

U.S Energy Information Administration (EIA), 2012, *Policies for compensating behind-the-meter generation vary by State*, Today in Energy, May 9th, 2012.

Vanhoudt D. (VITO), 2012, *Lab test results of an active controlled heat pump with thermal energy storage for optimal integration of renewable energy*, 7th International renewable Energy Storage Conference and Exhibition (IRES 2012), Berlin, November 12-14, 2012.

Van Roy J., Salenbien R., Vanhoudt D., Desmedt J. and Driesen J., 2013, *Thermal and Electrical Cover Factors: Definition and Application for Net-Zero Energy Buildings*, in Proceedings of CLIMA 2013 Conference, Prague, Czech Republic, 16-19 June 2013.

Wilson E., Engebrecht Metzger, C., Horowitz S., Hendron R., 2014, *2014 Building America House Simulation Protocols*, National Renewable Energy Laboratory, Technical Report NREL/TP-5500-60988.

9th International Conference on System Simulation in Buildings, Liege, December 10-12, 2014

ACKNOWLEDGEMENTS

FNRS (Fond de la Recherche Scientifique) in Belgium is gratefully thanked for the funding of Emeline Georges as PhD research fellow.

NOMENCLATURE

Symbols		Subscripts	
C	thermal capacity	abs	absorbed
f	fraction	AC	air-conditioning
m	control horizon	amb	ambient
p	prediction horizon or price	avg	average
Q	heat transfer capacity	bt	bottom
R	thermal resistance	cons.	consumption
T	temperature	conv	convective
W	electrical power	D	demand (consumption)
X	capacity or COP	elec	electricity
		f	floor
		HP	heat pump
		m	mass flow rate
		p	peak
		rat	rated
		S	supply
		sol	solar
		sp	set point
		T	temperature
		tp	top
		trans	transmitted
		w	wall
		WH	water heater
		win	window
		Zon	zone

GIS supported city district energy system modeling

J. Schiefelbein¹, A. Javadi¹, M. Diekerhof², R. Streblov¹, D. Müller¹, A. Monti²

RWTH Aachen University, E.ON Energy Research Center

⁽¹⁾Institute for Energy Efficient Buildings and Indoor Climate

⁽²⁾Institute for Automation of Complex Power Systems

Mathieustr. 10, 52074, Aachen, Germany

E-mail: [jschiefelbein], [ajavadi], [mdiekerhof], [rstreblov], [dmueller], [amonti]@eonerc.rwth-aachen.de

1. ABSTRACT

The energetic optimization of city districts offers great potential for primary energy saving and CO₂-emission reduction. Until now the optimization has primarily focused on individual buildings or homogeneous building groups and therefore, neglects possible synergy effects within heterogeneous city zones. This paper presents a holistic approach for a city district modeling solution method. A city district database is designed and linked to a geographical information system (GIS). A database interface enables automated building model and user profile generation for a simulation environment, based on Modelica (for thermal energy systems) and NEPLAN (for electrical energy systems). The planning tool is verified with datasets from the Welheimer Mark, a mixed area within the city of Bottrop, Germany. The tool can support urban planning and energetic optimization of complex city districts.

Keywords: City district, GIS, energy system modeling, Modelica, NEPLAN

2. INTRODUCTION

Around 40% of German final energy consumption is caused by the building sector (Amecke, 2012). Additionally, more than 70% of the German population lives in cities (Bundesministerium für Wirtschaft und Energie, 2014). Therefore, the energetic optimization of city districts plays an important role for the German Energiewende. It offers great potential for primary energy saving and CO₂-emission reduction.

Until now the optimization has primarily focused on individual buildings or homogeneous building groups. Focusing on a single building simplifies the optimization process, due to the smaller analysis area and common technical and legislative constraints. One disadvantage of this approach is the neglect of positive synergy effects between heterogeneous building groups and mixed areas. Thus, it is important to tap energy saving potentials by shifting the focus to urban districts.

City quarter optimization is challenging due to its complexity. It can consist of residential, commercial, and industrial buildings, and includes various types of thermal and electrical energy systems. First, there is a large data acquisition and management effort. Second, it complicates the generation of standardized schemata for the analysis and optimization of heterogeneous city structures. Even if suitable data and models are available, the simulation on city district scale can cause impracticable calculation time. Therefore, a trade-off between level of detail and simulation run time has to be found.

The following paper describes a holistic approach for city district energy system modeling. An integrated planning tool is designed. It takes the interaction between buildings, energy systems, as well as thermal and electrical networks into account. A city district database builds the tool core. The database structure contains entities for residential, commercial, and industrial

buildings as well as centralized and decentralized energy systems. It is linked to a geographic information system (GIS) to combine location and data of buildings and energy systems.

In addition, an interface between the GIS database and tools for the automated generation of physical building models and user profiles is designed. It provides a multi-physics simulation environment with required data. The environment consists of the object oriented programming language Modelica and the tool NEPLAN. Modelica enables building and thermal energy system simulation, while NEPLAN is used to investigate the electric grid behavior via static electrical load flow calculations. A co-simulation approach for the analysis of interaction between thermal and electrical components on urban scale is chosen (Molitor et al., 2012).

The method for residential electrical load profile generation is verified with datasets of the reference city district Welheimer Mark, a mixed area within the city of Bottrop, Germany. First, generated 24 hour profiles are compared with the German standardized load profile (SLP). Second, the calculated annual energy demand is compared with measurement data. A sufficient fit between calculated and measured electrical load profiles and annual demands is shown. Finally, options for further development of the planning tool are discussed.

3. TOOL SURVEY

There is a huge variation of tools for the analysis of city district energy systems, often linked to GIS software. According to the Environmental System Research Institute, GIS is "an organized collection of computer hardware, software, geographic data, and personnel designed to efficiently capture, store, update, manipulate, analyze, and display all forms of geographically referenced information." (Environmental System Research Institute, 1990). In combination with city district tools, additional information, such as construction or energy demand data, is often added to the spatial information of GIS. The combination enables energy system analysis within GIS. Mohammadi et al. distinguishes energy system tools into the classes supply, demand, and integrated models as well as top-down and bottom-up tools (Mohammadi, Vries, & Schaefer, 2013). The same classification is used for the tool survey in this paper.

On the energy supply side, Tiba et al. developed a GIS-integrated planning tool for renewable energy, especially solar systems (Tiba et al., 2010). It supports planners with the identification of optimal photovoltaic placement and dimensioning in rural areas. Vettorato et al. used a spatial approach to analyze the fit between renewable energy supply potentials and energy demand of cities (Vettorato, Geneletti, & Zambelli, 2011). They considered solar irradiation, ground-source heat, biomass and hydropower as renewable energy systems. The primary aim is the support of low carbon urban design. Kurka et al. worked on a GIS supported planning approach for bioenergy CHP systems (Kurka, Jefferies, & Blackwood, 2012). Their approach allows the identification of biomass supply areas and the estimation of transportation cost, as well as CO₂ emissions. Strzalka et al. discussed the usage of GIS and CityGML systems for the integration of large scale photovoltaic systems within city districts (Strzalka, Alam, Duminil, Coors, & Eicker, 2012). Photovoltaic potentials are analyzed based on 3D building models with shadow effects especially taken into account.

On the energy demand side, Mavrogianni et al. discussed a GIS-based bottom-up approach for identification of space heating demand in London (A. Mavrogianni, M. Davies, M. Kolokotroni, & I. Hamilton, 2009). The focus is put on the building architecture and heat island effect. Finney et al. (Finney et al., 2012) developed a concept for the estimation of thermal energy demand within cities, which allows heat map generation and supports the planning of district heating systems. Ascione et al. worked on a similar approach (Ascione, Canelli, De Masi, Rosa Francesca, Sasso, & Vanoli, 2013). Their software tool enables the calculation of

thermal, electrical, and cooling demands of urban areas within Italy. The outputs are urban energy maps. Nouvel et al. developed a 3D city model for urban planning, based on the CityGML standard (Nouvel, Schulte, Eicker, Pietruschka, & Coors, 2013). The model is used to estimate heating demands within two residential areas in Germany.

Girardin et al. have chosen a holistic approach for their urban planning tool (Girardin, Marechal, Dubuis, Calame-Darbellay, & Favrat, 2010). They consider energy demand as well as smart usage of energy conversion systems. Robinson et al. developed a planning tool, which takes energy supply, demand, as well as user behavior under uncertainty into account (Robinson et al., 2007). An approach of Robinson et al. is the development of the software CitySim, a planning tool for urban settlements (Darren Robinson et al., 2009), which supports the analysis of building energy, water, and waste flows within city districts.

Besides GIS tools, there are diverse developments in the field of Modelica libraries for building and city district simulation. Wetter developed a Modelica library for building energy and control systems, which supports design and analysis of innovative building structures and energy supply systems (Wetter, 2009). Schwan et al. presented a Modelica library, which enables the modeling of complex systems, including building structures, renewable energy as well as storage systems (Schwan, Unger, Lerche, & Kehrer, 2014). Low-order thermal building models can be found within the Modelica AixLib Library (RWTH-Aachen University, E.ON Energy Research Center, Institute for Energy Efficient Buildings and Indoor Climate, 2014). They support run time reduction for the simulation of multiple houses or whole city quarters.

Recent developments are the SimStadt software (Hochschule für Technik Stuttgart, 2014) or the planning and optimization approach from Lauster et al. for university areas and district heating systems (Lauster, Fuchs, Teichmann, Streblow, & Mueller, 2013). SimStadt simulation software should enable the energetic analysis of whole regions and cities, while the approach of Lauster et al. aims at energetic optimization of complex energy systems via dynamic simulation.

Most holistic approaches for city districts still focus on the thermal or electrical side of residential building types only. Especially non-residential buildings are often neglected, despite their potentials for primary energy saving. Therefore, the approach chosen by this paper aims at a thorough modeling concept for city districts, including residential and non-residential, as well as thermal and electrical systems. This concept should enable thermo-electrical, dynamic simulations and therefore, support analyses and developments in the field of energy and load management.

4. INTEGRATED PLANNING TOOL

4.1 Requirements

The development of a city district planning tool is challenging due to the city district complexity. A city quarter can consist of diverse types of buildings, such as residential, commercial, and industrial structures, as well as all kinds of energy supply systems. Furthermore, the number of existing buildings and units within the district can be high. Therefore, the planning tool should consider all kind of building types and energy systems. To deal with a large number of buildings it should simplify the city district parameterization and modeling. For the analysis of future energy supply scenarios, dynamic simulations of thermal and electrical systems should be possible. Results can be used to identify optimized energy supply strategies. Finally, data management should be simplified.

Therefore, the tool requirements are:

- Support of data management and analysis
- Account for the majority of possible building types and energy systems.
- Simplify city district modeling
- Enable complex city district simulation and optimization

To enable an easy data management and to consider diverse building types and energy supply systems, a city information model (CIM) is designed and implemented on a GIS database. An interface is programmed to automate the city district modeling based on the CIM structure. The models enable city district simulations within a simulation environment. Results can be saved back to the database. Furthermore, they can be analyzed within GIS. Figure shows the tool workflow.

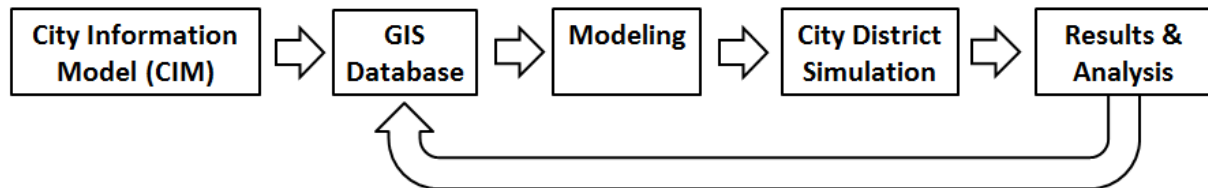


Figure 1: Tool workflow

4.2 City information model

To generate a sufficient city information model for energetic purposes the complete energy flow, from generation and distribution to consumption, has to be taken into account. Therefore the models are divided into classes:

- Energy generation / supply units
- Distribution
- Demand

Considered energy supply systems are thermal units, such as boilers, heat pumps or solar thermal systems, electrical power units, such as photovoltaic systems, and thermo-electrical units, such as combined heating and power (CHP) or combined heating, cooling, and power (CCHP) systems. Energy distribution is realized via thermal networks, electrical grids, as well as thermal and electrical storage systems.

The following classification is chosen for demand side:

- Residential buildings
- Industrial buildings
- Small and medium sized enterprises (SME) / other non-residential buildings

Residential buildings are chosen as one class because of their homogeneity. The division into industrial and (other) non-residential buildings is primarily based on the question of process energy usage.

As an important factor on energy consumption, user behavior has to be taken into account. Therefore, the CIM scheme includes parameters for status quo of occupants and attendees, such as number of occupants per apartment, number of apartments per building or number of employees per office. In combination with user behavior profiles and statistics, for instance data of SIA norms (Schweizerischer Ingenieur- und Architektenverein) or occupancy profiles (Richardson, Thomson, Infield, & Clifford, 2010), user influence on energy demand can be estimated.

To implement the CIM structure into a database two steps have to be taken: First, the CIM scheme has to be transformed into an entity-relationship (ER) structure. Second, necessary (or

preferable) datasets for city district modeling have to be defined. These datasets determine the entity parameters for the database.

Every building or zone can either be residential, industrial, commercial, (other) non-residential, or an energy system, such as a central power plant or a decentralized CHP system. Building and zones can be connected to a thermal or electrical grid. Moreover, they can include thermal and electrical power generation units and storage systems. Figure 2 shows a simplified ER database concept for a city district.

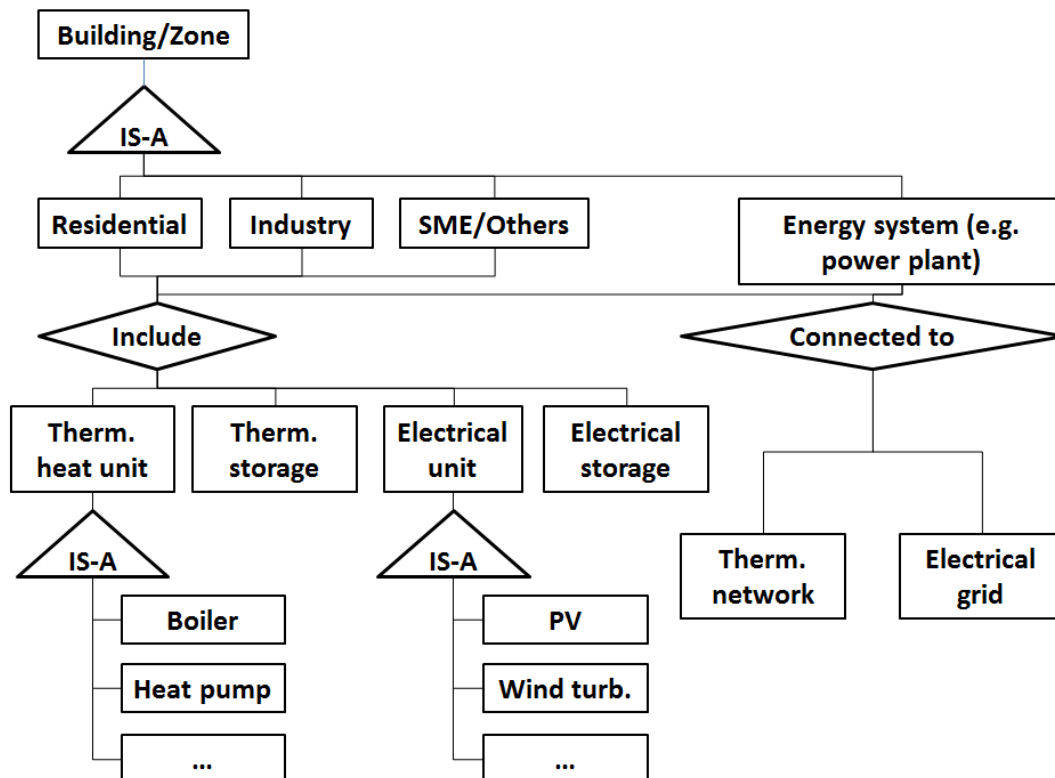


Figure 2: Simplified entity-relationship structure of city district

Subsequently, the entity parameters have to be defined depending on required (and available) data for the city district modeling. Therefore, the next step is the development of a sufficient modeling approach.

4.3 Modeling approach

The city district classes for energy generation, distribution and demand have to be modeled for the simulation environment. A Modelica library for building and energy system simulation is used to model the thermal city district energy systems (Mueller & Hosseini Badakhshani, 2010). Moreover, NEPLAN is chosen for electrical grid modeling (BCP Busarello Cott Partner Erlenbach, 2014).

4.3.1 Residential buildings

A simplified housing model, according to the VDI 6007 (Verein deutscher Ingenieure (VDI), 2007), is used to generate the residential building models. As shown by Lauster et al. (Lauster, Teichmann, Fuchs, Streblow, & Mueller, 2014) these low order models are suitable for simulations on urban scale. The simplified models consist of thermal resistances and capacities (R-C parameters), which depend on building physics and geometry parameters. Figure 3 shows the low order building model of the Modelica AixLib (RWTH-Aachen University, E.ON

Energy Research Center, Institute for Energy Efficient Buildings and Indoor Climate, 2014). It includes thermal capacity and resistance for inner and outer building wall. Furthermore, models for air capacity, air exchange and solar radiation are implemented. Thermal output of active occupants, lighting and machine usage is lead into the model via heat ports. Moreover, thermal energy systems, such as boilers or CHP units, can be connected to the building model to ensure thermal energy supply.

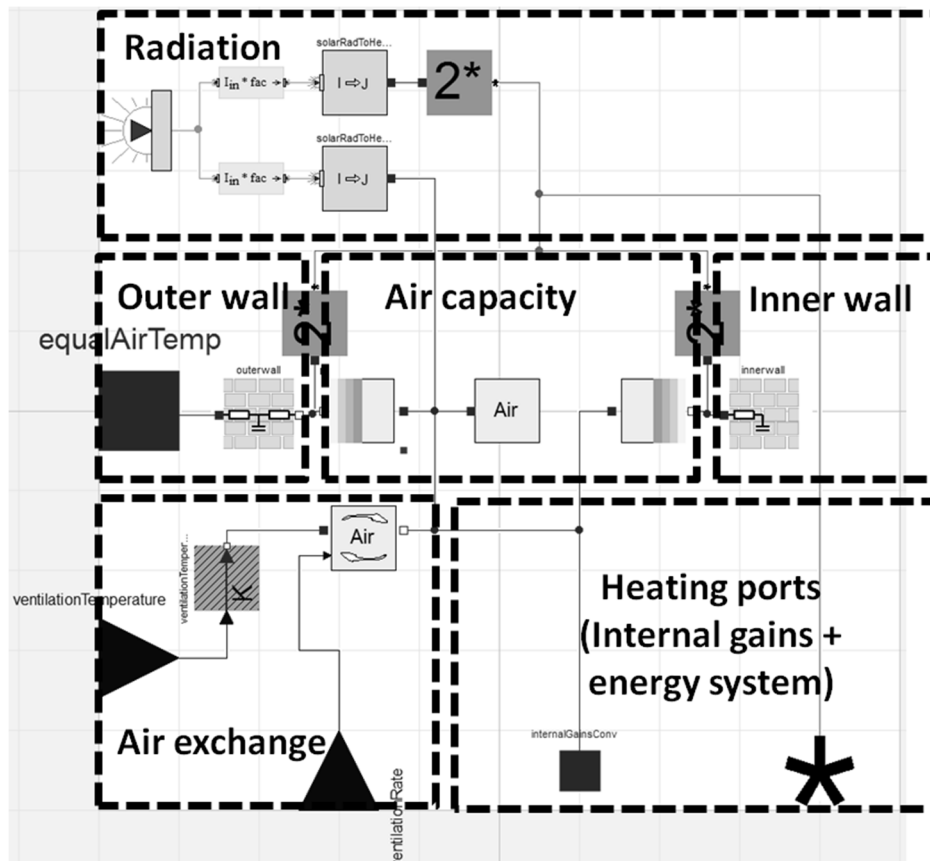


Figure 3: Low order building envelope model of Modelica AixLib

Due to the fact that precise data about building physics and geometry is hardly available for the majority of residential buildings, a method based on IWU datasets for representative residential buildings is chosen (Institut für Wohnen und Umwelt - IWU, 2005). Material parameters are derived from the building year, or the year of modernization. Similarly, geometry parameters, such as outer wall or window areas, can be converged with information about the building ground size, number of floors, and floor height. This method enables the modeling of physical, residential housing models.

To consider thermal and electrical energy demands of residential buildings, user behavior and internal gains have to be taken into account. Therefore the number of apartments per buildings as well as the number of occupants per apartment has to be considered. Based on statistic values of DESTATIS, apartments and residents can be distributed over the number of residential buildings (Statistisches Bundesamt, 2011). Therefore, the total number of residential buildings and occupants has to be known or estimated. Local urban administrations can serve as sources for residential data.

The Richardson tool is chosen for user profile generation (Richardson, Thomson, & Infield, 2008). It is based on a survey of domestic user behavior and distribution of appliances, such as personal computers or refrigerators, within the UK. Transition probability matrices, which define the probability of attendance of an active person related to the prior time step, define the

basis for stochastic occupancy profile calculation. The number of occupants and appliances per apartment as well as the month of the reference year are input parameters. Occupancy profiles and electrical load profiles build the output. The combination of residential building models, appliance, lighting, and occupancy profiles enables thermal demand simulation.

4.3.2 Non-residential buildings

Because of their heterogeneity, the modeling process of non-residential buildings is complex and uncertain. Depending on the non-residential building type there is a huge variation of internal gains, appliances, user profiles, and building conditions. Furthermore, detailed data collections of industrial and commercial buildings require a lot of time and resources. Therefore, a simplified modeling approach is chosen for non-residential buildings. It distinguishes between buildings with process energy demand and those with exclusively heating demand.

Based on statistics about specific energy demands of non-residential buildings (Fraunhofer Institut für System- und Innovationsforschung ISI, 2013) (Bundesministerium für Verkehr, Bau und Stadtentwicklung, 2009) thermal and electrical energy demand of non-residential buildings can be estimated depending on building type and net floor area. If energy consumption per street side or building block is available, the statistics can be used to distribute thermal and electrical energy consumption to single buildings on the street side. This leads to annual thermal and electrical energy demand per non-residential building.

To account for energy demand dynamics, German standardized load profiles (SLP) are generated for every non-residential building. Thermal SLP are based on analyses of Hellwig (Hellwig, 2003). Input parameters are:

- Thermal SLP type
- Final energy demand (e.g. monthly or annually)
- Weather data of building location
- Process type (process oriented or heating oriented)

Electric SLP are generated based on BDEW data (BDEW, 2014). Input parameters are:

- Electrical SLP type
- Final energy demand (e.g. monthly or annually)

The modeling approach via energy distribution and SLP generation is not valid for buildings with a high share of process energy demand, such as industrial complexes. To account for industrial buildings, measured load profiles are a minimum requirement.

4.3.3 Energy systems

Thermal energy systems data within residential buildings are rarely available. Therefore, the design heat load of every residential building is calculated based on the DIN EN 12831 (Deutsches Institut für Normung e.V., 2008). The design heat loads support the selection of thermal energy supply systems for residential buildings. In combination with local statistics of combustible usage, often available at chimney sweeper organizations, the type of thermal energy system per building can be chosen.

For non-residential buildings with exclusive heating demand, the SLP is used to define the design heat load of the thermal energy supply unit. For industrial areas knowledge about the share of process energy, space heating, and hot water demand is required. In this context, waste heat potentials can be of interest for energetic optimization. The final energy demand for processes provides orientation for possible waste heat, which could be used as a heat source.

Energy system capacities for industrial space heating and hot water demand are planned with non-process standardized load profiles.

The Modelica building library provides models for thermal energy systems, such as boilers or CHP units, which can be parameterized for every city district building. Furthermore, external gains, like outdoor temperature or radiation, are taken into account via weather models. Simplified thermo-hydraulic elements of the Modelica library can be used to model district heating networks.

The electrical grid is modeled within NEPLAN. Therefore, grid data of energy supply companies are required. If these datasets are not available, mapping and GIS programs can be used to estimate low and medium voltage grid connections and elements. Node positions and cable dimensions can be identified via GIS distance measurement tools. Moreover, mapping and GIS tools support the identification of photovoltaic or solar thermal systems within the city district. While solar thermal systems are provided by the Modelica library, photovoltaic profiles are generated based on an approach by Zhou et al. (Zhou, Yang, & Fang, 2007).

4.4 GIS database

The necessary parameters for the modeling approach are added to the city district entity-relationship diagram. The resulting entity-relationship scheme is implemented on a PostgreSQL database server (PostgreSQL Global Development Group, 2014).

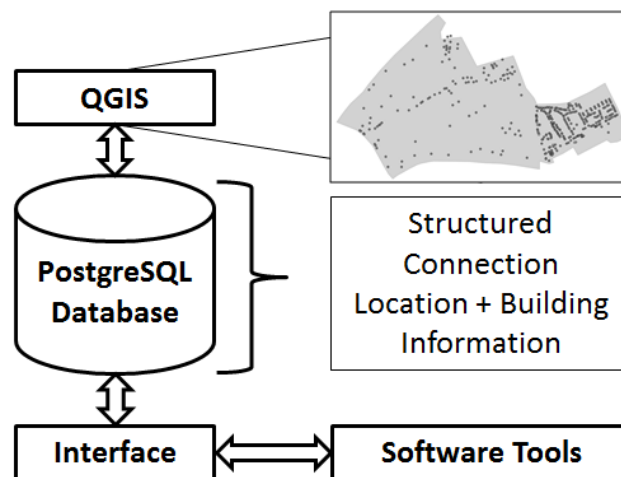


Figure 4: GIS-database connection

To simplify data management and analysis, the city district database is linked to a GIS tool. The non-commercial software QGIS is chosen for database connection (QGIS, 2014). Figure 4 shows the connection concept.

Within the database, general building information, such as year of construction or net floor area, is linked to the building location (longitude and latitude). This connection enables graphical output within the QGIS software. Furthermore, graphical database queries are possible. Moreover, an interface for data import and export is designed. Figure 5 shows a QGIS screenshot of a city district.

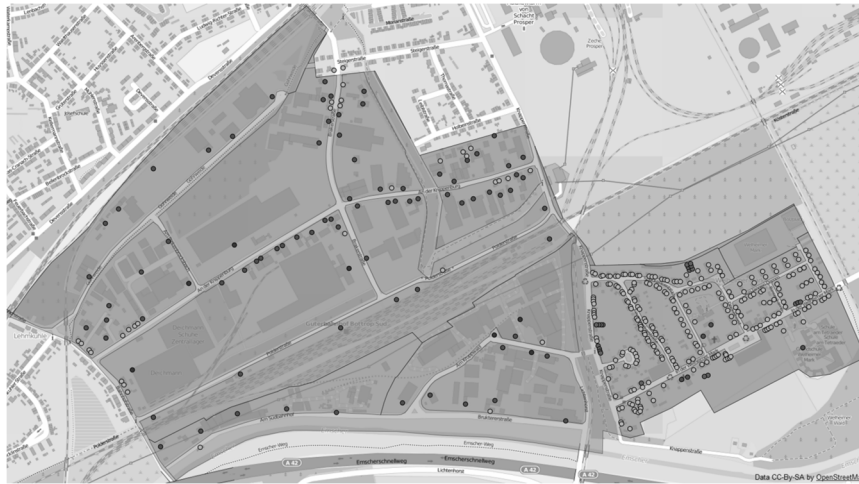


Figure 5: Screenshot of city district model within QGIS interface

[Uses map of OpenStreetMap - Deutschland (Licence: CC-BY-SA 2.0)]

4.5 Database interface

A database interface is developed to support the user with the city district modeling process. Figure 6 demonstrates the tool chain. The GIS database forms the tool core. Data import is done with an import tool. It scans the entity-relationship-structure and compares entity-names and parameters with dataset parameters. Successive entities are filled with corresponding datasets.

A residential building tool, based on the Richardson software, is supplied with residential data, such as number of residential building, apartments per building, and occupants per apartment. The appliance configuration per apartment is set based on appliance proportion numbers of the Richardson tool. It automatically generates occupancy and electrical load profiles for every residential building for a chosen reference year.

A Python tool for building parameterization by Hillebrand et al. (Hillebrand, Arends, Streblow, Madlener, & Mueller, 2014) is implemented into the tool chain. It imports XML files with necessary data for residential building modeling, such as year of construction and net floor area. If no information about wall and window areas is given, the tool will generate typical building setups based on IWU statistics (Institut für Wohnen und Umwelt - IWU, 2005). The residential buildings are saved as thermal resistance and capacity models according to the VDI 6007.

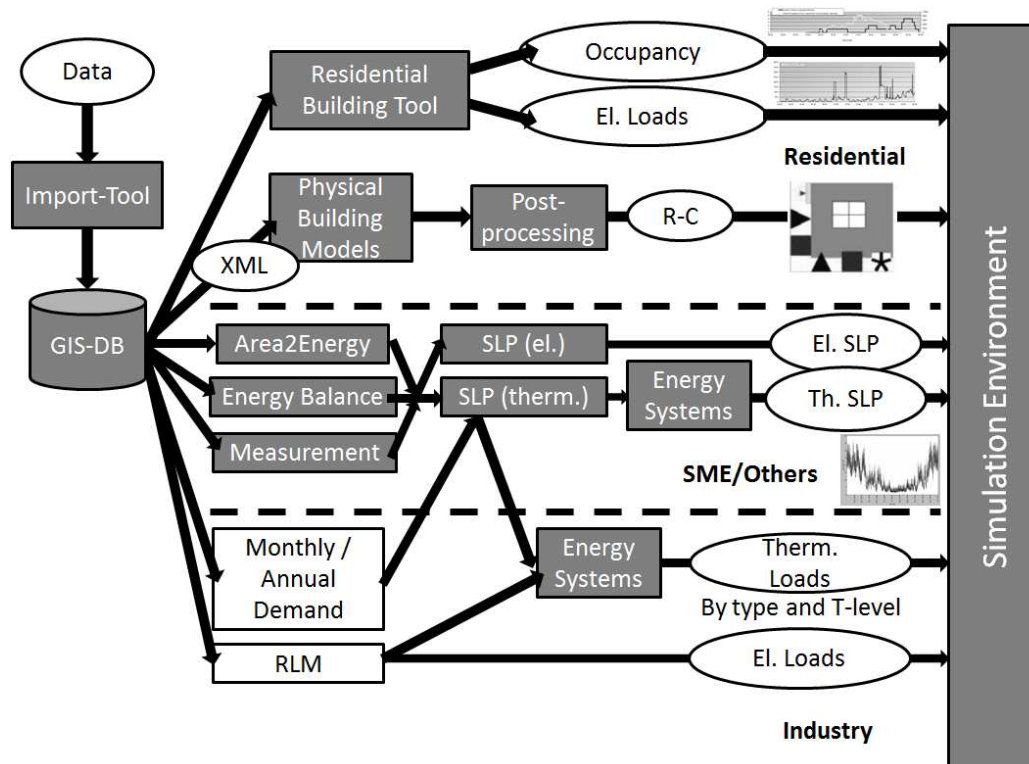


Figure 6: Planning tool chain

Depending on the data situation, small and medium sized enterprises and other non-residential, non-industrial buildings can be modeled via top-down or bottom-up approach. On one hand, if no energy consumption data are given, the energy demand per building structure can be estimated with information about building type and net floor area. On the other hand, if an energy balance for the building block is given, the energy consumption can be distributed on the existing buildings. Measurement values of single non-residential buildings can be added to both methods. The resulting annual thermal and electrical demands per building serve as input for the SLP generation. Depending on the thermal energy systems, the thermal net energy load is calculated.

Industrial buildings are taken into account via registered load measurements (RLM). If no RLM profile is available, annual energy consumption data can serve as input for the SLP tools. Due to unconsidered process energy loads within the SLP tools this calculation is uncertain. Therefore industrial building analysis is recommended.

4.6 Simulation environment

Dymola is used as the modeling and simulation software for thermal energy system and building simulation (Dassault Systems, 2014) and operates with the Modelica language. A Modelica building library of the Institute for Energy Efficient Buildings and Indoor Climate (Mueller & Hosseini Badakhshani, 2010) is chosen for modeling and simulation of thermal energy systems and buildings. Additionally, electrical load flow calculations are performed with NEPLAN. To take the interaction between thermal and electrical systems into account, a co-simulation approach of Molitor et al. has been chosen (Molitor et al., 2012). It connects the thermal building models of Modelica, electrical utilities and grid infrastructure of NEPLAN with a control system, based on MATLAB (Mathworks, 2014) or the Java Agent Development Framework (JADE) (Jade, 2007) for instance. Figure 7 shows the co-simulation concept.

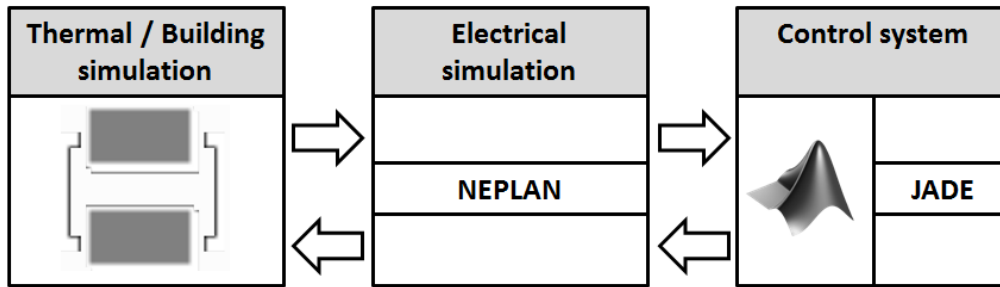


Figure 7: Co-Simulation environment

4.7 Method verification

For first verification, electrical load profiles are generated and compared with energy consumption statistics from the city district Welheimer Mark as well as the German standardized load profiles (SLP). These comparisons demonstrate the modeling approach as sufficient for electrical loads within residential buildings.

4.7.1 Reference city district

Figure 8 shows an aerial view of Welheimer Mark.

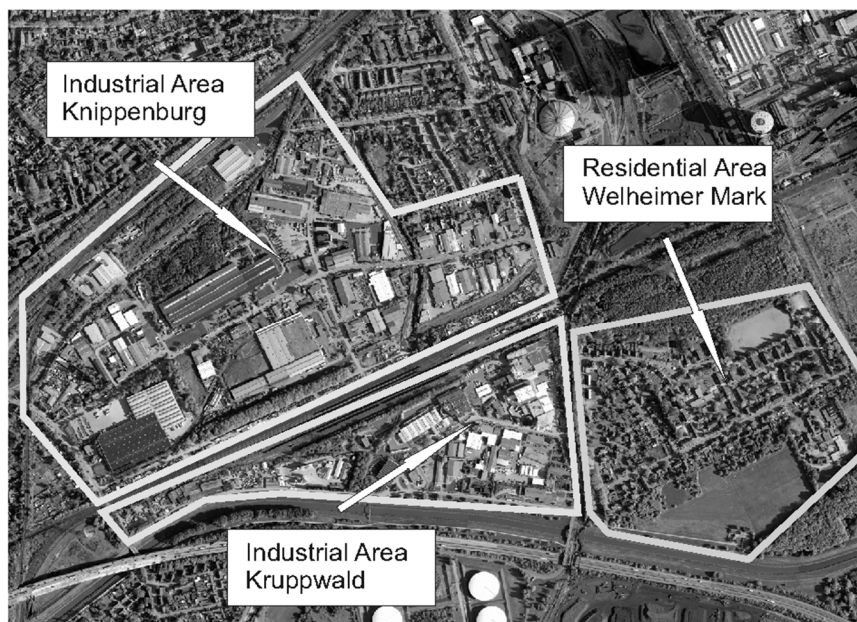


Figure 8: Aerial view of city district Welheimer Mark, Bottrop, Germany

The Welheimer Mark is a city district within the city of Bottrop, Germany. It is a mixed area, consisting of residential, commercial and industrial buildings. Therefore Welheimer Mark is suitable for test and verification of the city district GIS database and modeling approach.

In the context of the project “EnEff:Stadt – Bottrop, Welheimer Mark” energy consumption statistics of the city district are available for comparison. First, the toolbox is used to generate multiple 24 hour electrical demand profiles for comparison with German SLP. Second, annual demand profiles of all residential buildings within the residential area of Welheimer Mark are generated and compared with energy consumption statistics.

4.7.2 Comparison with German standardized load profiles

A Python Script is used to randomly generate 30000 apartments as input for electric load profile generation. The number of residents per apartment (between 1 and 5 persons) is set based on a normal distribution. In comparison to the original Richardson configuration all electrical heating devices, such as electrical showers or electrical space heating systems, are neglected. This has two major reasons: First of all, thermal devices are going to be modeled within Modelica, and secondly, the share of electrical heating devices or electrical showers is estimated to be low within Welheimer Mark. Furthermore, the lighting setup is kept constant for every apartment. The first lighting configuration of the Richardson tool is chosen as reference. The maximum lighting power per light bulb is limited to 50 Watt. The German SLP profile for a winter day is chosen as reference (Stadtwerke Unna, 2014).

The toolbox is used to generate 24 hour profiles for every apartment. All 30.000 load curves are aggregated to one load profile and normalized to a daily electrical energy demand of 100 kWh. Figure 9 shows the comparison between the aggregated Richardson profile and the German SLP for a winter day.

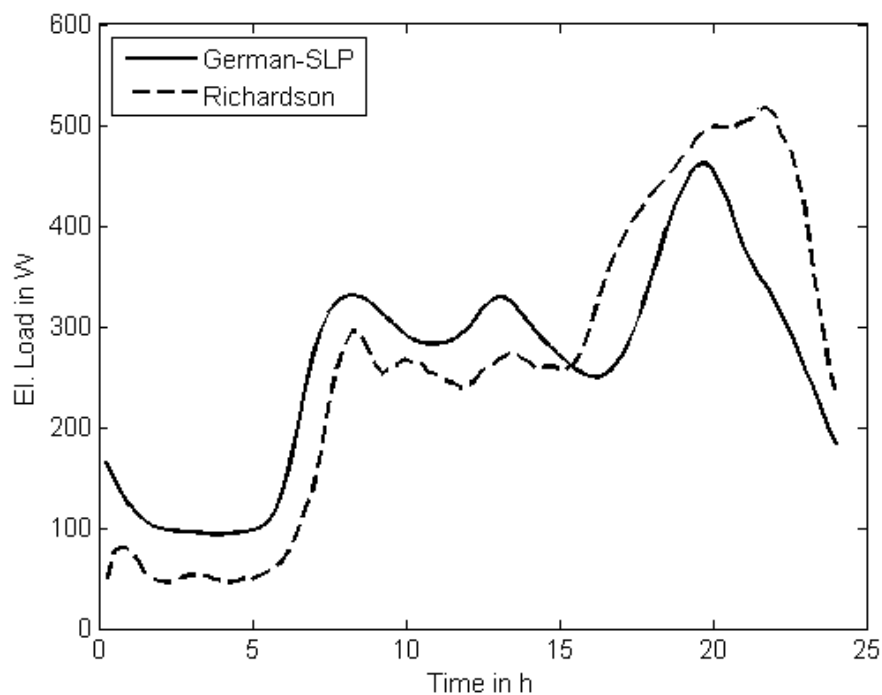


Figure 9: Comparison between sum of Richardson profiles and German SLP

On one hand, the aggregated Richardson curve shape is similar to the German SLP, while on the other hand, there are differences in the energy consumption distribution in the times before and after 3pm. In comparison to the German SLP, the modified profile generator emphasizes the energy demand in the evening hours as opposed to the morning hours. Different user behavior and working hours of the UK in comparison to Germany might lead to this discrepancy. However, the profile tool meets the requirements to generate realistic electrical loads for domestic buildings on city district scale, while the aggregate profile might not be representative for single buildings.

4.7.3 Comparison with electrical consumption data

In the next step annual electrical load profiles are generated for every residential building within the Welheimer Mark residential zone. The parameters are:

- 248 residential buildings
- 459 apartments
- 1143 residents

The number of apartments per residential building is known. First, the planning tool is used to distribute the residents to every apartment within the city district. The number of occupants per apartment serves as input for the electrical load generation. Second, annual electric load profiles for every apartment are generated and summed up for every building. The constraints are identical with those set for the 24 hour profile generation in chapter 4.7.2. The resulting total annual energy demand is compared with energy consumption data of the residential zone. Due to confidentiality, the electric consumption is normalized to 1000 MWh.

Table 1: Comparison between measured and calculated energy consumption

	Measurement	Calculation
Electrical energy demand / MWh	1000	936 (-6,4%)

The calculated energy demand is 6,4% smaller than the measured energy consumption. Uncertainties in user behavior and distribution of appliances can cause such differences. However, the results show that the approach for electrical load profile calculation leads to realistic energy consumption.

5. DISCUSSION AND FUTURE WORK

The presented planning tool enables a simplified modeling of complex city districts, especially for energetic systems. The GIS interface speeds up the modeling process for a high number of buildings within mixed areas. The GIS interface and linkage with the database supports the data management and analysis via graphic representation of the city district. Therefore, GIS usage can be advantageous for city district planning of diverse actors, such as local governments or energy consulting companies.

The development of the integrated planning tool is going to be continued. There is potential for further development in the fields of:

- Retrofit options (for physical building modeling)
- Set up of typical German lighting and appliances configurations
- Hot water profile generator (based on occupancy profiles)
- Stochastic functions for SLP generation
- Automated electrical and thermal grids modeling, based on city district database
- Optimization on the levels of
 - o Energy supply system distribution and dimensioning
 - o Energy supply unit scheduling
- Co-Simulation environment

The analysis of the interaction between thermal and electrical energy systems is of notable interest. Thermal-electrical simulation can support the analysis of load and energy management strategies. Moreover, further verification and validation with Welheimer Mark data is going to be performed, especially for thermal simulation. This process will support the development and optimization of the planning tool. Furthermore, the tool chain is going to be used for energetic optimization of city districts, such as Welheimer Mark.

6. CONCLUSION

This paper deals with a holistic approach for city district modeling. An integrated planning tool is explained, based on a city information model (CIM) for city district energy systems. It takes residential, commercial, and industrial buildings as well as thermal and electrical energy systems into account. The CIM is implemented on a PostgreSQL database and linked to a geographical information system (GIS). The combination of GIS and the city district database enables simplified data management and analysis. Visualization of the city district structure is especially helpful for city district planners.

A database interface for automated profile generation and physical building modeling is designed. First, it takes residential buildings into account. Occupancy and electrical load profiles are generated with a Python code, based on the Richardson tool. Furthermore simplified physical housing models are generated as thermal resistance and capacity units, according to the VDI 6007. Second, industrial buildings are considered via registered load profiles and information about process energy demand. Third, commercial and other non-residential buildings are taken into account via standardized load profiles (SLP). Thermal energy system models are provided by a Modelica building library (Mueller & Hosseini Badakhshani, 2010). Electrical grid infrastructure is modeled with NEPLAN. A simulation platform of Molitor et al. is chosen for co-simulation (Molitor et al., 2012), which should enable thermal-electric simulation of city district energy systems.

For method verification, generated electrical load profiles are compared with German SLP and measurement data of a reference city district, Welheimer Mark, within the city of Bottrop, Germany. Although the share between evening and morning energy consumption is higher for the generated profiles than for German SLP, there is a good match between the curve shapes of the generated profiles and SLP. Furthermore, the calculated annual energy demand lies at the same level as the measured annual energy consumption. Therefore, the electrical modeling approach for residential buildings on city district scale seems to be suitable.

ACKNOWLEDGEMENTS

We gratefully acknowledge the financial support for this project by BMWi (German Federal Ministry of Economics and Energy) under promotional reference 03ET1138D. Furthermore, we would like to thank our project partners City of Bottrop, Innovation City Management GmbH, Imtech Deutschland, infas enermetric, Pro:21 GmbH and ELE Verteilnetz GmbH for the productive cooperation.

REFERENCES

- A. Mavrogianni, M. Davies, M. Kolokotroni, & I. Hamilton. (2009). A GIS-BASED BOTTOM-UP SPACE HEATING DEMAND MODEL OF THE LONDON DOMESTIC STOCK. In International Building Performance Simulation Association (IBPSA) (Ed.), *Proceedings of Building Simulation 2009: 11th International IBPSA Conference*. Glasgow.
- Amecke, H. (2012). The impact of energy performance certificates: A survey of German home owners. *Energy Policy*, 46, 4–14. doi:10.1016/j.enpol.2012.01.064
- Ascione, F., Canelli, M., De Masi, Rosa Francesca, Sasso, M., & Vanoli, G. P. (2013). Combined cooling, heating and power for small urban districts: An Italian case-study. *Applied Thermal Engineering*. doi:10.1016/j.applthermaleng.2013.10.058
- BCP Busarello Cott Partner Erlenbach. (2014). *NEPLAN*. Retrieved June 10, 2014, from http://www.neplan.ch/html/e/e_home.htm.

- BDEW. (2014). *Lastprofilverfahren Strom*. Retrieved June 10, 2014, from <http://www.vsg-netz.de/vsgnetz/Stromnetz/Lastprofilverfahren.php>.
- Bundesministerium für Verkehr, Bau und Stadtentwicklung (BMVBS). (2009). *Bekanntmachung der Regeln für Energieverbrauchskennwerte und der Vergleichswerte im Nichtwohngebäudebestand: Vom 30. Juli 2009*.
- Bundesministerium für Wirtschaft und Energie (BMWi). (2014). *Energieeffiziente Stadt und dezentrale Energiesysteme*. Retrieved April 10, 2014, from <http://www.bmwi.de/DE/Themen/Energie/Energieforschung-und-Innovationen/foerderschwerpunkte,did=455374.html>.
- Darren Robinson, F. Haldi, J. Kämpf, P. Leroux, D. Perez, A. Rasheed, & U. Wilke. (2009). CITYSIM: COMPREHENSIVE MICRO-SIMULATION OF RESOURCE FLOWS FOR SUSTAINABLE URBAN PLANNING. In International Building Performance Simulation Association (IBPSA) (Ed.), *Proceedings of Building Simulation 2009: 11th International IBPSA Conference* (pp. 1083–1090). Glasgow.
- Dassault Systems. (2014). *Dymola*. Retrieved June 11, 2014, from <http://www.3ds.com/products-services/catia/capabilities/systems-engineering/modelica-systems-simulation/dymola>.
- Deutsches Institut für Normung e.V. (2008). *DIN EN 12831 - Heizsysteme in Gebäuden - Verfahren zur Berechnung der Norm-Heizlast*. Berlin.
- Environmental System Research Institute. (1990). *Understanding GIS: The ARC/INFO Method*. Redlands.
- Finney, K. N., Sharifi, V. N., Swithenbank, J., Nolan, A., White, S., & Ogden, S. (2012). Developments to an existing city-wide district energy network – Part I: Identification of potential expansions using heat mapping. *Energy Conversion and Management*, 62, 165–175. doi:10.1016/j.enconman.2012.03.006
- Fraunhofer Institut für System- und Innovationsforschung ISI. (2013). *Energieverbrauch des Sektors Gewerbe, Handel, Dienstleistungen (GHD) in Deutschland für die Jahre 2007 bis 2010: Endbericht an das Bundesministerium für Wirtschaft und Technologie (BMWi)*.
- Girardin, L., Marechal, F., Dubuis, M., Calame-Darbellay, N., & Favrat, D. (2010). EnerGis: A geographical information based system for the evaluation of integrated energy conversion systems in urban areas. *Energy*, 35(2), 830–840. doi:10.1016/j.energy.2009.08.018
- Hellwig, M. (2003). *Entwicklung und Anwendung parametrisierter Standard-Lastprofile*. TU München, München. Retrieved from <http://tumb1.biblio.tu-muenchen.de/publ/diss/ei/2003/hellwig.pdf>
- Hillebrand, G., Arends, G., Streblow, R., Madlener, R., & Mueller, D. (2014). Development and design of a retrofit matrix for office buildings. *Energy and Buildings*, 70, 516–522. doi:10.1016/j.enbuild.2013.10.029
- Hochschule für Technik Stuttgart. (2014). *SimStadt*, from <http://www.simstadt.eu/de/index.html>.
- Institut für Wohnen und Umwelt - IWU. (2005). *Deutsche Gebäudetypologie: Systematik und Datensätze*. Darmstadt.
- International Building Performance Simulation Association (IBPSA) (Ed.). (2010). *Proceedings BauSIM 2010*. Wien.

- Jade. (2007). *Java Agent DEvelopment Framework*. Retrieved May 07, 2014, from <http://jade.tilab.com/>.
- Kurka, T., Jefferies, C., & Blackwood, D. (2012). GIS-based location suitability of decentralized, medium scale bioenergy developments to estimate transport CO2 emissions and costs. *Biomass and Bioenergy*, 46, 366–379. doi:10.1016/j.biombioe.2012.08.004
- Lauster, M., Fuchs, M., Teichmann, J., Streblow, R., & Mueller, D. (2013). Energy Simulation of a Research Campus with Typical Building Setups. In International Building Performance Simulation Association (IBPSA) (Ed.), *Proceedings of BS2013: 13th Conference of International Building Performance Simulation Association, Chambéry, France* (pp. 769–775).
- Lauster, M., Teichmann, J., Fuchs, M., Streblow, R., & Mueller, D. (2014). Low order thermal network models for dynamic simulations of buildings on city district scale. *Building and Environment*, 73, 223–231. doi:10.1016/j.buildenv.2013.12.016
- Mathworks. (2014). *MATLAB*. Retrieved June 11, 2014, from <http://www.mathworks.de/products/matlab/>.
- Mohammadi, S., Vries, B., & Schaefer, W. (2013). A Comprehensive Review of Existing Urban Energy Models in the Built Environment. In S. Geertman, F. Toppen, & J. Stillwell (Eds.), *Lecture Notes in Geoinformation and Cartography. Planning Support Systems for Sustainable Urban Development* (pp. 249–265). Berlin, Heidelberg: Springer Berlin Heidelberg.
- Molitor, C., Cali, D., Streblow, R., Ponci, F., Mueller, D., & Monti, A. (Eds.) 2012. *New energy concepts and related information technologies: Dual Demand Side Management*. Innovative Smart Grid Technologies (ISGT), 2012 IEEE PES.
- Mueller, D., & Hosseini Badakhshani, A. (2010). GEKOPPELTE GEBÄUDE- UND ANLAGENSIMULATION MIT MODELICA. In International Building Performance Simulation Association (IBPSA) (Ed.), *Proceedings BauSIM 2010*. Wien.
- Nouvel, R., Schulte, C., Eicker, U., Pietruschka, D., & Coors, V. (2013). CITYGML-BASED 3D CITY MODEL FOR ENERGY DIAGNOSTICS AND URBAN ENERGY POLICY SUPPORT. In International Building Performance Simulation Association (IBPSA) (Ed.), *Proceedings of BS2013: 13th Conference of International Building Performance Simulation Association, Chambéry, France* (pp. 218–225).
- OpenStreetMap - Deutschland. *OpenStreetMap: (Licence: CC-BY-SA 2.0)*. Retrieved July 04, 2014, from <http://www.openstreetmap.de/>.
- PostgreSQL Global Development Group. (2014). *PostgreSQL*, from <http://www.postgresql.org/>.
- QGIS. (2014). *QGIS Software*. Retrieved June 10, 2014, from <http://www.qgis.org/de/site/>.
- Richardson, I., Thomson, M., & Infield, D. (2008). A high-resolution domestic building occupancy model for energy demand simulations. *Energy and Buildings*, 40(8), 1560–1566. doi:10.1016/j.enbuild.2008.02.006
- Richardson, I., Thomson, M., Infield, D., & Clifford, C. (2010). Domestic electricity use: A high-resolution energy demand model. *Energy and Buildings*, 42(10), 1878–1887. doi:10.1016/j.enbuild.2010.05.023
- Robinson, D., Campbell, N., Gaiser, W., Kabel, K., Le-Mouel, A., Morel, N., . . . Stone, A. (2007). SUNtool – A new modelling paradigm for simulating and optimising urban sustainability. *Solar Energy*, 81(9), 1196–1211. doi:10.1016/j.solener.2007.06.002

RWTH-Aachen University, E.ON Energy Research Center, Institute for Energy Efficient Buildings and Indoor Climate. (2014). *Modelica AixLib*, from <https://github.com/RWTH-EBC/AixLib>.

Schwan, T., Unger, R., Lerche, C., & Kehrer, C. (2014). Model-Based Design of Integrative Energy Concepts for Building Quarters using Modelica. In : *Linköping Electronic Conference Proceedings, the 10th International Modelica Conference, March 10-12, 2014, Lund, Sweden* (pp. 97–106). Linköping University Electronic Press.

Schweizerischer Ingenieur- und Architektenverein. SIA Merkblatt 2024 Standard-Nutzungsbedingungen für die Energie- und Gebäudetechnik.

Stadtwerke Unna. (2014). *VDEW-Lastprofile*. Retrieved June 10, 2014, from http://www.gipsprojekt.de/featureGips/Gips;jsessionid=36DBE8EAF15E68329A3F6493121749DB?SessionMandant=sw_unna&Anwendung=EnWGKnotenAnzeigen&PrimaryId=133029&Mandantkuerzel=sw_unna&Navigation=J.

Statistisches Bundesamt (Destatis). (2011). *Bevölkerung und Erwerbstätigkeit: Entwicklung der Privathaushalte bis 2030*. Ergebnisse der Haushaltsvorausberechnung. Wiesbaden.

Strzalka, A., Alam, N., Duminil, E., Coors, V., & Eicker, U. (2012). Large scale integration of photovoltaics in cities. *Applied Energy*, 93, 413–421.

Tiba, C., Candeias, A., Fraidenraich, N., Barbosa, E.M. de S., de Carvalho Neto, P.B., & de Melo Filho, J.B. (2010). A GIS-based decision support tool for renewable energy management and planning in semi-arid rural environments of northeast of Brazil. *Renewable Energy*, 35(12), 2921–2932. doi:10.1016/j.renene.2010.05.009

Verein deutscher Ingenieure (VDI). (2007). *VDI-Richtlinie 6007 - Berechnung des instationären thermischen Verhaltens von Räumen und Gebäuden*.

Vettorato, D., Geneletti, D., & Zambelli, P. (2011). Spatial comparison of renewable energy supply and energy demand for low-carbon settlements. *Cities*, 28(6), 557–566. doi:10.1016/j.cities.2011.07.004

Wetter, M. (2009). A MODELICA-BASED MODEL LIBRARY FOR BUILDING ENERGY AND CONTROL SYSTEMS. In International Building Performance Simulation Association (IBPSA) (Ed.), *Proceedings of Building Simulation 2009: 11th International IBPSA Conference* (pp. 652–659). Glasgow.

Zhou, W., Yang, H., & Fang, Z. (2007). A novel model for photovoltaic array performance prediction. *Applied Energy*, 84(12), 1187–1198. doi:10.1016/j.apenergy.2007.04.006

Strategies for an Optimal Chiller Operation (in a Smart Grid)

Julian Buderus, Arno Dentel, Wolfram Stephan

Technische Hochschule Nürnberg Georg Simon, Institute for Energy and Building,
Nuremberg, Germany

1. ABSTRACT

Modern Chillers are equipped with variable speed compressors, variable speed pumps and fans. Integrated in a smart grid, chillers are flexible components and in combination with storage tanks or the storage capacity of the building, there is a large opportunity for power management.

For an energy efficient operation of the whole chiller system, the control system has to identify the optimal speed of compressor, pumps and fans. As compressor and condenser fans are the most important electrical consumer, an optimization strategy has to focus on them.

Simplified physical models of the compressor (volumetric and isentropic efficiency as inputs), the evaporator and the condenser have been developed in the EES (Engineering Equation Solver) environment and integrated into a chiller model. All model parameters can easily be derived from manufacturers and design data.

The optimization capabilities of EES are used to find the optimal curves of high energy efficiency ($P_{el,total,min} = f(Q_{evap,rel}, t_c)$). This optimization is done for different chiller configuration (air/air; water/air; water/water) as well as for different compressor types (screw, piston), using the Golden Section search.

The results can be generalized and the optimal curves will be implemented in the control and management system of chillers. An energy saving potential of up to 10 % is promised.

In addition the optimized control can be used in a smart grid to minimize the energy demand in a certain time period, for e.g. when electrical power is rare and expensive.

Keywords: Chiller, EES, Modeling; Optimal Control, Smart Grid

2. INTRODUCTION

The generation of cooling energy is one of the large-scale consumers of electricity in Germany, representing 14 % of the whole electricity demand (Deutscher Kälte- und Klimatechnischer Verein, 2002). The food industry is the biggest consumer, with an utilization of 67 % of this energy, followed by air conditioning systems for buildings (21,7 %) and the cooling energy used for industrial processes (9,1 %). Several studies predict rising energy consumption for air conditioning systems, in the next years, as a result of the increasing percentage of glazing in building facades (Schmidt-Pleschka et.al., 2006).

Taking this development into account, manufacturers and plant operators aim to minimize the energy consumption of cooling units.

Modern chillers are already highly efficient through the use of variable speed compressors, variable speed pumps and fans. However, the implementation of an optimal control strategy for the chiller system can increase the energy efficiency even further.

Predicting the power demand of energy systems would enable a Demand-Side-Management (DSM) in a smart grid. Cooling units are, especially in combination with cold storage tanks, a flexible consumer and could be used to switch loads during the day. Rising percentage of

fluctuating power generation from solar and wind power makes DSM even more important to balance the relation between power generation and consumption.

In this paper, we show, how simulating the energy consumption of chillers leads to optimal control strategies and opens possibilities to use chillers more effectively in a DSM strategy.

Background and scope

The Energy Efficiency Ratio (EER_c) describes the efficiency of cooling units regarding the generated cooling energy and the electrical power used by the compressor. The EER_c is negatively correlated to the condensation temperature (t_c). Therefore, a standard control strategy of a cooling unit always aims to keep t_c at a defined low value ($t_{c,min}$). In order to ensure a correct operation of the expansion valve, $t_{c,min}$ is often set between 35 to 40 °C.

However, for an energetic evaluation of a cooling unit all energy consumers have to be considered, not only the compressor (Verband Deutscher Maschinen- und Anlagenbau, 2011). The standard situation changes when the power consumption of the condenser fans is taken into account. Especially in part load operation and at high ambient temperatures, the standard control strategy can lead to high fan speeds, even when not needed. In some cases, the power consumption of the condenser fans might even exceed the power consumption of the compressor (Roth, P., 2012). In this case, a reduction of the fan speed would improve the total EER-value (EER_{total}) despite the higher t_c .

To test this hypothesis, a physical model of a cooling unit is modeled, using the EES (F-Chart Software, Madison, USA) capabilities. All components of a standard cooling unit are modeled by simplified physical equations. The models for the compressor, evaporator, condenser and the pumps are based on manufacturer data. This strategy enables us to model custom-built cooling units under various environmental and technical conditions.

We performed two parametric studies to examine the behavior of a specific cooling unit in different operating conditions.

The results of these simulations are used to derive polynomial functions describing the EER_{total} and the electrical power consumption of the cooling unit under various cooling demands and ambient temperatures. These functions allow for the prediction of the operation status and will be used for load management in a smart grid.

3. SIMULATION

3.1 Technical Data of the simulated Chiller System

The chiller configuration used in this research is based on a system, which is currently being planned by a company participating in the research project FOREnergy. The air-cooled water chiller (R134a) has a cooling capacity of 530 kW and a supply temperature of 18°C. The whole system is constructed with modern components and shows high values for the EER.

Compressor

A semi-hermetic screw compressor with integrated frequency inverter is used for the compression in the refrigeration cycle. It is optimized for water chiller systems and a highly flexible component due to the variable speed operation. A selection of the performance data at the design point of this chiller configuration is shown in Table 1.

Table 1: Performance data of the screw compressor (CSVH26-200Y-40A)

cooling capacity	547 kW
Range	30% -100%
electrical power consumption	133,9 kW
EER _c	3,96
subcooling	5 K
overheating	10 K

Condenser

For the condensation process a condenser with a rib tube heat exchanger is used. The condenser is equipped with nine fans powered by electronically commutated (EC) motors. The variable-speed motors are highly efficient in full load as well as in part load operation. Selected performance data, taken from the data sheet provided by the manufacturer, is listed in Table 2.

Table 2: Performance data of the condenser (GVD 090.1D/2x9-SL.E)

condensation output	666 kW
condensation temperature	50,8 °C
air volume flow	173 070 m ³ /h
ambient temperature	38 °C
electrical power consumption	7,2 kW
energy ratio at design point	92,5

Evaporator

A plate heat exchanger serves as an evaporator. It is optimized for the use of the refrigerant R134a. The evaporator is highly efficient in full and in part load operation.

Table 3: Performance data of the evaporator (DS500x294)

evaporation output	530 kW
evaporation temperature	14 °C
water mass flow	21,12 kg/s
water supply temperature	18 °C
water return temperature	24 °C

3.2 Modeling

The model of the chiller system is designed with the software environment EES. The following chapter gives a general overview of the model. Next, the data acquisition for the compressor, evaporator und condenser is described in detail.

In the EES environment the user is enabled to design a graphical interface to use his code more easily. Figure 10 shows the graphical interface of the chiller model. This interface allows to enter data and to check the results after a simulation process. Moreover EES supports different calculation options for the model. Therefore, it is possible to calculate a defined operating point of the system with designated compressor and fan speed as well as an optimization of selected variables. This allows, for example, to minimize the total power consumption of a cooling unit with $P_{total,min}$ as a function of the compressor and fan speed.

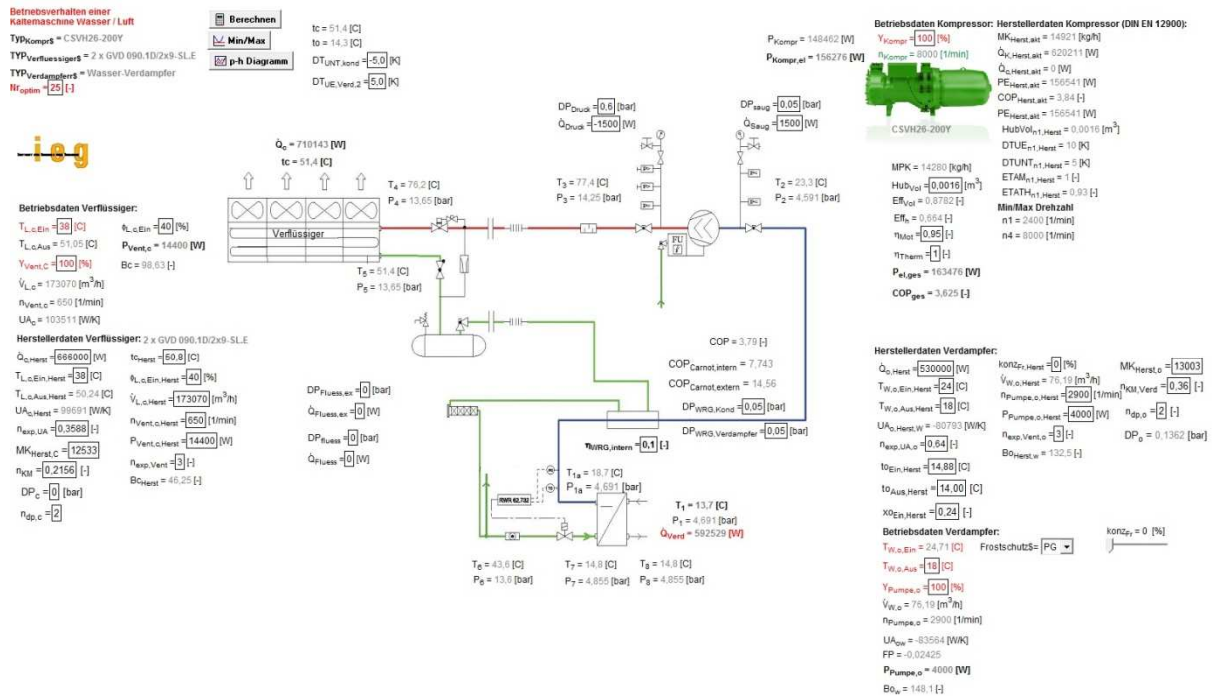


Figure 10: Overview of the graphical interface in EES

Screw Compressor

To model the compressor, polynomial equations for volumetric and isentropic efficiency are used. Those equations are based on DIN EN 12900, which regulates, the way manufacturers have to provide the performance characteristics of their products (Deutsches Institut für Normung e.V., 2013). DIN EN 12900 enforces the use of the evaporation and condensation temperature as inputs (Equation 1). The results of the functions are solely dependent on the used coefficients. Therefore a calculation of the power consumption, the refrigerant mass flow or the EER of the cooling unit is possible, by changing the coefficients provided by the manufacturer (see Appendix A2). The polynomial function is shown in Equation 1.

$$y = c_1 + c_2 \cdot t_o + c_3 \cdot t_c + c_4 \cdot t_o^2 + c_5 \cdot t_o \cdot t_c + c_6 \cdot t_c^2 + c_7 \cdot t_o^3 + c_8 \cdot t_o \cdot t_c^2 + c_9 \cdot t_o \cdot t_c^2 + c_{10} \cdot t_c^3 \quad (1)$$

with

- y - result, depending on the used coefficients [-]
- t_o - evaporation temperature [°C]
- t_c - condensation temperature [°C]
- c_i - coefficients [-]

In order to model the compressor, Equation 1 is converted to a pressure-dependent form, shown in Equation 2. On the basis of the manufacturer's data for cooling power (\dot{Q}_o), electrical power consumption ($P_{el,comp}$) and refrigerant mass flow rate (\dot{m}_{refr}), the volumetric and the isentropic efficiency are calculated and expressed in this pressure dependent functions. These efficiencies do not depend on the size of the compressor and can be generally used.

$$y = c_1 + c_2 \cdot p_o + c_3 \cdot p_c + c_4 \cdot p_o^2 + c_5 \cdot p_o \cdot p_c + c_6 \cdot p_c^2 + c_7 \cdot p_o^3 + c_8 \cdot p_c \cdot p_o^2 + c_9 \cdot p_o \cdot p_c^2 + c_{10} \cdot p_c^3 \quad (2)$$

with

y	-	<i>volumetric / isentropic efficiency, depending on the used coefficients [-]</i>
p_o	-	<i>evaporation pressure [bar]</i>
p_c	-	<i>condensation pressure [bar]</i>
c_i	-	<i>coefficients for volumetric / isentropic efficiency [-]</i>

The coefficients of the polynomial functions are calculated for various motor speeds (n). Unknown values for the volumetric or the isentropic efficiency are extrapolated. Additional inputs for the compressor model are the displaced volume (V_h), the thermal efficiency of the compressor (η_{therm}) and the thermal efficiency of the motor (η_{mot}). The thermal efficiencies describe the heat losses of the compressor and the motor to the ambient. The volumetric efficiency (η_{vol}) describes the ratio between the effective volume flow to a theoretical volume flow based on the displaced volume and the compressor speed. The isentropic efficiency is the ratio between ideal and a non-ideal compression.

Volumetric efficiency:

$$\dot{V}_{\text{eff}} = \dot{V}_h \cdot \eta_{\text{vol}} \quad (3)$$

$$\dot{V}_h = V_h \cdot n_{\text{comr}} \cdot 60 \quad (4)$$

with

\dot{V}_{eff}	-	<i>effective refrigerant volume flow [m³/s]</i>
\dot{V}_h	-	<i>theoretical displaced volume flow [m³/s]</i>
V_h	-	<i>displaced volume [m³]</i>
n_{compr}	-	<i>compressor speed [1/min]</i>
η_{vol}	-	<i>volumetric efficiency [-]</i>

Isentropic efficiency:

$$\eta_{\text{isentr}} = \frac{h_{3,\text{isentr}} - h_2}{h_{3,\text{polytr}} - h_2} \quad (5)$$

with

η_{isentr}	-	<i>isentropic efficiency [-]</i>
$h_{3,\text{isentr}}$	-	<i>isentropic enthalpy after compression [J/kg]</i>
$h_{3,\text{polytr}}$	-	<i>polytropic enthalpy after compression [J/kg]</i>
h_2	-	<i>enthalpy at compressor input [J/kg]</i>

Power consumption:

$$P_{\text{el,compr}} = \frac{(h_{3,\text{isentr}} - h_2)}{\eta_{\text{isentr}} \cdot \eta_{\text{therm}} \cdot \eta_{\text{mot}}} \quad (6)$$

with

$P_{\text{el,compr}}$	-	<i>power consumption of the compressor [W]</i>
η_{isentr}	-	<i>isentropic efficiency [-]</i>
η_{therm}	-	<i>thermal efficiency compressor [-]</i>
η_{mot}	-	<i>thermal efficiency motor [-]</i>

Condenser

The condenser model is built by the use of design data, which is provided in the data sheet. The heat transfer is calculated using the LMTD- method and counter flow operation. The heat transfer coefficient (UA) of a heat exchanger is strongly influenced by the flow rates of the fluids passing the device. The decrease or the increase of the heat transfer depends on the flow characteristics (laminar or turbulent) in the design point. To implement the influence of the flow rates on the heat transfer, a simplified exponential function is used (Equation 7).

$$UA_{c,operate} = UA_{c,design} \cdot Y_{c,Vent}^{n_{exp,UA,c,air}} \cdot Y_{c,refr}^{n_{exp,UA,c,refr}} \quad (7)$$

with

$UA_{c,operate}$	-	heat transfer coefficient at operating point [W/K]
$UA_{c,design}$	-	heat transfer coefficient at design point [W/K]
$Y_{c,Vent}$	-	rel. air flow through the condenser [-]
$Y_{c,refr}$	-	rel. refrigerant mass flow [-]
$n_{exp,UA,c,air}$	-	exponent for influence of air flow [-]
$n_{exp,UA,c,refr}$	-	exponent for influence of refrigerant mass flow [-]

In this function the influence of the flow rates is described by the exponents $n_{exp,UA,c,air}$ and $n_{exp,UA,c,refr}$ and the variable Y, which describes the relative flow rate compared to the design conditions. To evaluate these exponents, data from the manufacturer has been examined. The exact determination is shown in chapter 3.3.

The electrical power consumption of the condenser fans is calculated with Equation 8. To take an operation under partial load into account, the exponent $n_{exp,Vent}$ describes the relation between fan speed and electrical power consumption.

$$P_{el,Vent} = P_{el,Vent,o,design} \cdot Y_{Vent}^{n_{exp,Vent}} \quad (8)$$

with

$P_{el,Vent}$	-	power consumption at operation point [W]
$P_{el,Vent,o,design}$	-	power consumption at design point [W]
Y_{Vent}	-	rel. fan speed [-]
$n_{exp,Vent}$	-	exponent for power consumption [-]

Evaporator

The modeling of the evaporator is very similar to the one of the condenser. Data provided by the manufacturer is used for the parameterization of the design point. As mentioned before, the flow rates of the passing fluids have a strong influence on the heat transfer rate of the heat exchanger. Therefore, an exponential equation is implemented in the evaporator model to address the influence of the mass flow on the UA-value.

$$UA_{o,operate} = UA_{o,design} \cdot Y_{o,pump}^{n_{exp,UA,o,water}} \cdot Y_{o,refr}^{n_{exp,UA,o,refr}} \quad (9)$$

with

UA_o	-	heat transfer coefficient at operating point [W/K]
$UA_{o,design}$	-	heat transfer coefficient at design point [W/K]

$Y_{o,pump}$	-	<i>rel. cold water mass flow [-]</i>
$Y_{o,refr}$	-	<i>rel. refrigerant mass flow [-]</i>
$n_{exp,UA,o,water}$	-	<i>exponent for influence of pump speed [-]</i>
$n_{exp,UA,o,refr}$	-	<i>exponent for influence of refrigerant mass flow [-]</i>

To determine the values for the exponents $n_{exp,UA,o,water}$ and $n_{exp,UA,o,refr}$ the evaporation output at different flow rates has been examined by the use of software provided by the manufacturer. This examination is shown in chapter 3.3.

The cold water is transported from the chiller to the energy consumers via water network and water pump. The electrical power consumption of the pump is calculated with Equation 10.

$$P_{el,pump,o} = P_{el,pump,o,design} \cdot Y_{o,pump}^{n_{exp,o,pump}} \quad (10)$$

with

$P_{el,pump,o}$	-	<i>power consumption pump (operation point) [W]</i>
$P_{el,pump,o,design}$	-	<i>power consumption pump (design point) [W]</i>
$Y_{o,pump}$	-	<i>rel. cold water pump speed [-]</i>
$n_{exp,o,pump}$	-	<i>exponent for power consumption [-]</i>

Using a speed variable pump requires the modeling of the partial load behavior of the pump. Therefore, the exponent $n_{exp,o,pump}$, which describes the connection between pump speed and power consumption, is used.

3.3 Data acquisition

The parameterization of the model has to be done for the compressor, the condenser and the evaporator in a detailed way, based on manufacturer data. Other machine specific input parameters, like pressure or thermal losses of the pipe network are estimated.

This chapter shows which data for the main components (compressor, condenser and evaporator) are necessary and how they have to be implemented in the simulation model.

Screw Compressor

DIN EN 12900 regulates how manufactures have to provide the performance data of their compressors. The performance data has to include at least cooling power and power consumption of the compressor at different t_c and t_o . For speed-controlled compressors, the data has to be available for maximum, minimum and at least one additional compressor speed.

In this example, a speed controlled screw compressor is used. Table 4 shows an abstract of the performance data as provided by the manufacturer. The data provided in Table 4 only show performance data under maximum compressor speed.

Table 4: Performance data for Bitzer CSVH26-200Y at $n = 8000$ 1/min (selected values)

t_c [°C]	t_o [°C]	10	5	0	-5	-10
30	Q [W]	631469	523089	429502	349284	281086
	P[kW]	101,3	97,8	94,2	90,2	85,9
	EER [-]	6,24	5,35	4,56	3,87	3,27
	\dot{m}_{refr} [kg/s]	13251	11180	9356	7759	6372
40	Q [W]	571334	470972	384732	311193	249026
	P[kW]	121,9	116,5	111	105,6	100,4
	EER [-]	4,69	4,04	3,46	2,95	2,48
	\dot{m}_{refr} [kg/s]	13125	11039	9208	7611	6228
50	Q [W]	508333	416836	338641	272361	216691
	P[kW]	146	138,3	131	124,3	118,6
	EER [-]	3,48	3,01	2,59	2,19	1,83
	\dot{m}_{refr} [kg/s]	12943	10854	9025	7435	6065

The data of Table 4 is used for determining the volumetric and the isentropic efficiencies. The coefficients (c_1 to c_{10}) of Equation 2 are determined by the use of multiple linear regressions. With a coefficient of determination around 0,99 the polynomial equations correspond well with the original data. The results for the coefficients are also listed in the Appendix. With the help of those two functions, it is possible to describe the performance of the compressor for the simulation model.

Figure 11 and Figure 12 show the volumetric and the isentropic efficiency dependent on the evaporation and the condensation pressures at full rational speed of the compressor.

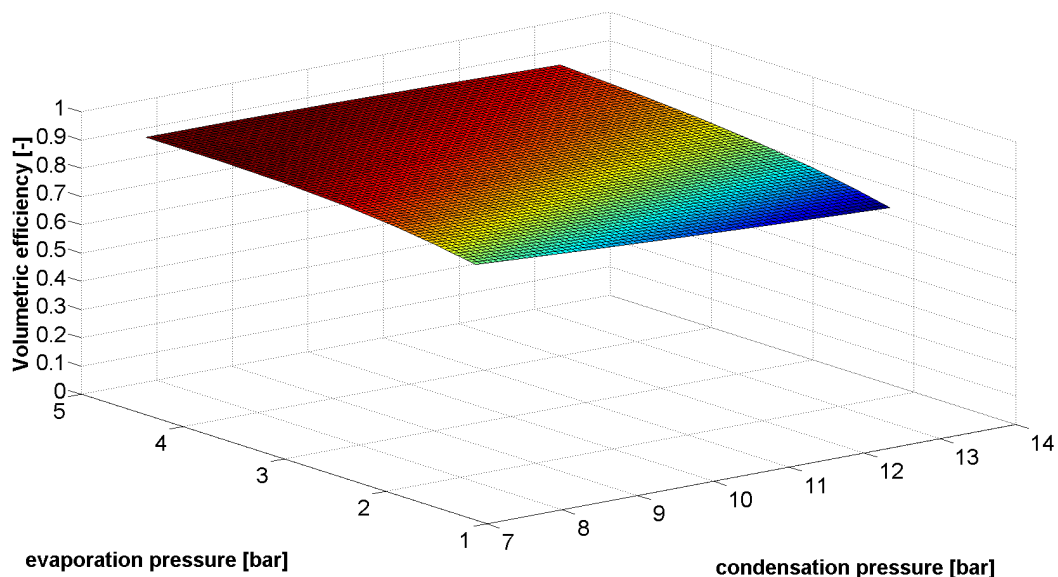


Figure 11: Volumetric efficiency of a screw compressor

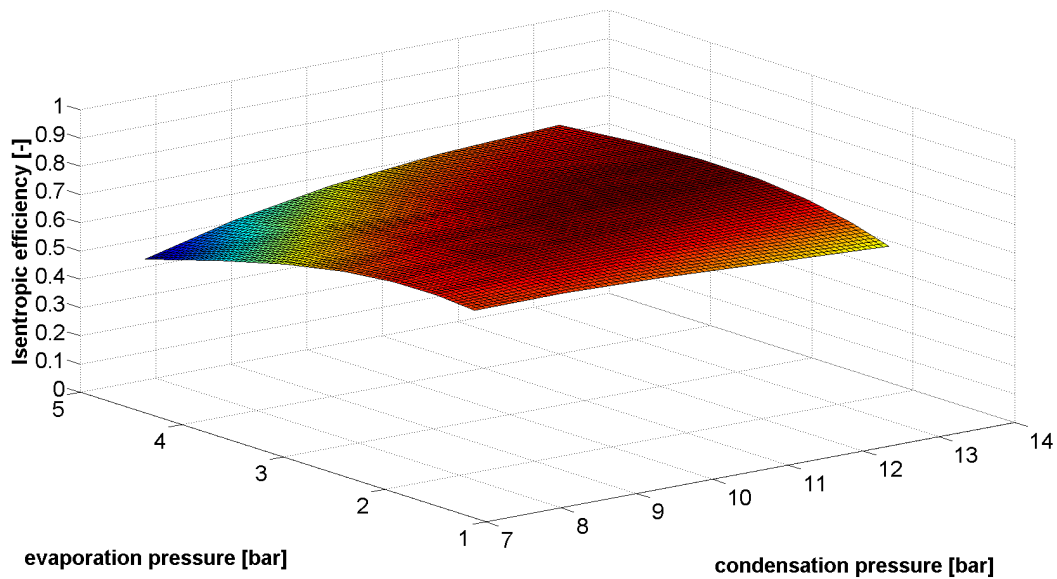


Figure 12: Isentropic efficiency of a screw compressor

Condenser

For the modeling of the condenser, condenser data, taken from the manufacturer, is implemented into the simulation model. Mainly data of the design point of the device is necessary, which could be taken from the manufacturer data sheet. For describing the part load behavior, Equation 7 is used. For determining the two exponents describing the influence on the heat transfer, further information is necessary. Table 5 shows the inputs for specifying the condenser in the simulation model.

Table 5: Inputs for condenser model

Input	Variable	Unit
condensation output	$\dot{Q}_{c,design}$	W
air temperature	$t_{a,c,in,design}$	°C
evaporation temperature	$t_{c,design}$	°C
air flow	$\dot{V}_{a,c,in,design}$	m ³ /h
el. power consumption fan	$P_{el,vent,c,design}$	W
exponent for power consumption	$n_{exp,P,vent}$	-
fan speed	$n_{Vent,c,design}$	1/min
refrigerant mass flow	$\dot{m}_{c,refr,design}$	kg/h
relative humidity of air	$\phi_{a,c,in,design}$	-
exponent for influence of fan speed	$n_{exp,UA_c,air}$	-
exponent for influence of refr. mass flow	$n_{exp,UA_c,refr}$	-

As mentioned before, the determination of the exponents $n_{exp,UA_c,air}$ and $n_{exp,UA_c,refr}$ requires further information. In cooperation with the condenser manufacturer, performance data at different fluid mass flows through the condenser was examined. By using this data, the following values for the exponents are determined: $n_{exp,UA_c,air} = 0,36$; $n_{exp,UA_c,refr} = 0,22$

For an evaluation of the simplified equation, the resulting values are compared to the values given by the manufacturer. Table 6 shows the heat transfer rate (manufacturer data and results from Equation 7) at different operation conditions.

Table 6: Comparison of heat transfer coefficient (UA) at part load operation of the condenser

ambient temperature	condensation temperature	air flow	mass flow refrigerant	heat transfer coefficient (manufacturer)	heat transfer coefficient Equation 7
t_{amb} [°C]	t_c [°C]	$\dot{V}_{a,c}$ [m ³ /h]	$\dot{m}_{c,refr}$ [kg/h]	$UA_{c,manuf}$ [W/K]	$UA_{c,operate}$ [W/K]
38	50,8	173070	12553	87224	87224
38	50	173070	11665	85976	85885
38	50	129803	9304	74773	73776
38	50	86535	6636	61425	56305
38	50	51921	4227	47501	44798
38	40	173070	1926	50446	58246
38	40	129803	1525	42860	49955
30	50	173070	19161	94651	95584
30	50	129803	15260	81367	82081
30	50	86535	10843	65522	65927
30	40	173070	9350	84408	81885
30	40	129803	7480	73781	70385
30	40	86535	5335	60497	56579
20	50	173070	28024	99324	103749
20	50	129803	22446	84984	89202
20	50	86535	15995	68051	71691
20	50	51921	10193	51310	54160
20	40	173070	18208	94587	94538
20	40	129803	14589	81431	81289
20	40	86535	10436	66035	65386
20	30	173070	9011	85784	81235
20	30	129803	7235	74997	69882

Table 6 shows that the data derived from the simplified equation differs by 4,2% in average to the actual values of the manufacturer. This deviation is probably resulting from additional temperature influences at the condenser that are not considered by Equation 7.

Figure 4 shows a comparison of the heat transfer rates of the manufacturer and of data from the approximation polynomial.

The figure shows the heat transfer coefficient as a function of the refrigerant mass flow rate at different fan rates. As expected the heat transfer rate deteriorates with decreasing flow rates on both sides.

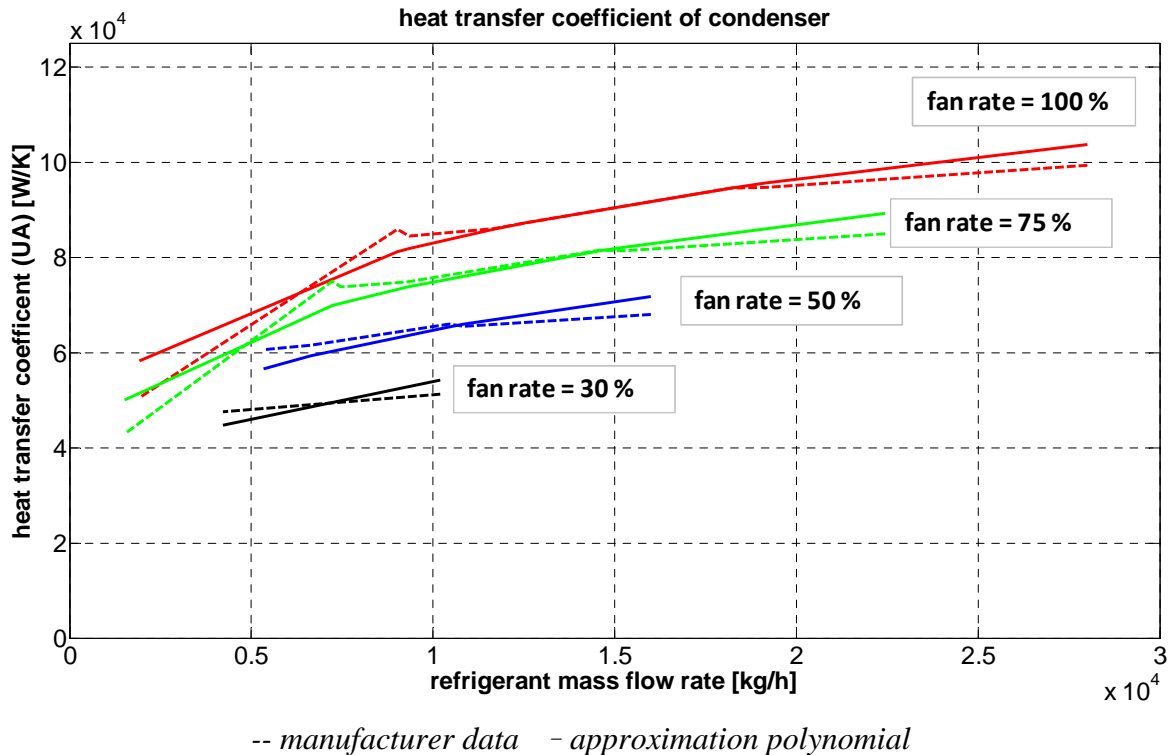


Figure 13: Heat transfer coefficient of the condenser as a function of air and refrigerant flow rate (comparison of data from the manufacturer with the approximation polynomial)

Evaporator

For modeling the evaporator, design data, taken from the data sheet, has to be implemented in the simulation model. Like the condenser model, the evaporator model requires incorporation of further information about the partial load behavior of the device. In Table 7, the inputs to specify the evaporator model are shown.

Table 7: Inputs for evaporator model

Input	Variable	Unit
evaporation output	$\dot{Q}_{o,design}$	W
water inlet temperature	$t_{w,o,in,design}$	°C
water outlet temperature	$t_{w,o,out,design}$	°C
evaporation temperature	$t_{o,design}$	°C
concentration of brine	$conc_{brine,design}$	m ³ /h
el. power consumption pump	$P_{el,pump,o,design}$	W
exponent for power consumption	$n_{exp,pump}$	-
pump speed	$n_{Pump,o,design}$	1/min
refrigerant mass flow	$\dot{m}_{o,refr,design}$	kg/h
exponent for influence of pump speed	$n_{exp,UA_o,water}$	-
exponent for influence of refr. mass flow	$n_{exp,UA_o,refr}$	-

By using the design software of the manufacturer, data is collected for the determination of the exponents of Equation 9. The collected data leads to the following values for the exponents: $n_{\text{exp,UA,o,water}} = 0,36$; $n_{\text{exp,UA,o,refr}} = 0,64$. Table 8 shows the results of the data evaluation and compares the simplified heat transfer rates to the manufacturer data.

Table 8: Comparison of heat transfer coefficient at part load operation of the evaporator

eva- poration output	cold water temperature	evaporation temperature	mass flow cold water	mass flow refrigerant	heat transfer coefficient (manufacturer)	heat transfer coefficient (simplified)
\dot{Q}_o [kW]	$t_{w,o,\text{out}}$ [°C]	t_o [°C]	$\dot{m}_{o,\text{water}}$ [kg/h]	$\dot{m}_{o,\text{refr}}$ [kg/h]	$UA_{o,\text{manuf}}$ [W/K]	$UA_{o,\text{operate}}$ [W/K]
530	18	14	76032	13003	75714	75714
500	18	14	71748	12262	71429	71430
450	18	14	64548	11038	64286	64275
400	18	14	57384	9814	57143	57143
350	18	14	50220	8582	50000	49994
300	18	14	43056	7358	42857	42862
250	18	14	35870	6132	35714	35712
200	18	14	28696	4906	28571	28570
150	18	14	21521	3679	21429	21425
100	18	14	14350	2453	14286	14285

The mean deviation for the observed operation points shown in Table 8 there is less than 1 %.

4. DISCUSSION AND RESULT ANALYSIS

With the simulation model obtained in chapter 3, the initially described hypotheses should now be proved. Hence, two parametric studies are performed using the temperature-controlled and the energy-optimized control strategy. The results of those studies are shown in the following chapter.

4.1 Comparison of temperature-controlled and energy-optimized strategy

Temperature-controlled strategy

To control the heat dissipation at the condenser, the temperature-controlled strategy is a commonly used method. This strategy aims to keep the condensation temperature at $t_{c,\text{min}}$, depending on the range of performance of the expansion valve.

In this control strategy, a condensation temperature above $t_{c,\text{min}}$ represents high fan speeds. The speed is not reduced until the temperature reaches the fixed value at which the operation of the expansion valve is endangered. The disadvantage of this control strategy is that high fan speeds and a high power consumption of the fans also occur in part load operation. Sometimes, the power consumption of the fans even exceeds the power consumption of the compressor. This leads to a lower EER_{total} of the chiller system and is increased by using condenser fans with low energy efficiencies.

Energy-optimized strategy

The energy-optimized strategy does not have a fixed temperature value as a set point. The target of this strategy is to minimize the energy consumption of the chiller system by reducing the speed of the condenser fans. The effect of higher t_c is also an higher p_c in the condenser. This leads to a decreasing EER_c and a higher compressor power to guarantee the same cooling capacity. However, it is possible that the reduction of the fan speed saves more energy than the

rising compressor power costs, which leads to a higher EER_{total} . This effect is most pronounced in part load conditions. Initial calculations show, that an energy saving potential of up to 10% is possible.

Comparison of the control strategies

To compare the two control strategies, various inputs of the simulation model have been tested. For the ambient temperature, values between -15°C and 38°C have been chosen. The cooling demand has been varied in a range from 30% to 100%.

The minimal condensation temperature was set to 35°C to ensure a correct operation of the expansion valve. Table 9 shows the results of the two parametric studies for an ambient temperature of 38°C .

Table 9: Differences between temperature-controlled and energy-optimized strategy at 38°C

$\dot{Q}_{o,rel}$ [%]	$Y_{Vent,opt}$ [%]	$Y_{Vent,temp}$ [%]	$Y_{compr,opt}$ [%]	$Y_{compr,temp}$ [%]	$EER_{total,opt}$ [-]	$EER_{total,temp}$ [-]	$t_{c,opt}$ [$^{\circ}\text{C}$]	$t_{c,temp}$ [$^{\circ}\text{C}$]
100	100	100	98,1	98,1	3,67	3,67	51,2	51,2
90	100	100	86,6	86,6	3,91	3,91	49,9	49,9
80	100	100	75,4	75,4	4,16	4,16	48,6	48,6
70	95	100	64,9	64,7	4,41	4,41	47,6	47,3
60	87	100	54,7	54,3	4,71	4,67	46,8	46,0
50	78	100	45,0	44,5	4,99	4,87	46,0	44,8
40	69	100	35,7	35,1	5,29	4,99	45,1	43,5
30	59	100	26,1	25,6	5,69	5,05	44	42,2

Table 9 shows, that the energy-optimized strategy leads to lower fan speeds ($Y_{Vent,opt}$) and to a higher t_c . This results in higher condensation pressure and higher compressor power. A comparison the EER_{total} of the cooling unit ($EER_{total,opt}$, $EER_{total,temp}$) demonstrates, that in some operation modes, the energy-optimized strategy leads to higher efficiencies of the cooling process. This is also obvious in Figure 14.

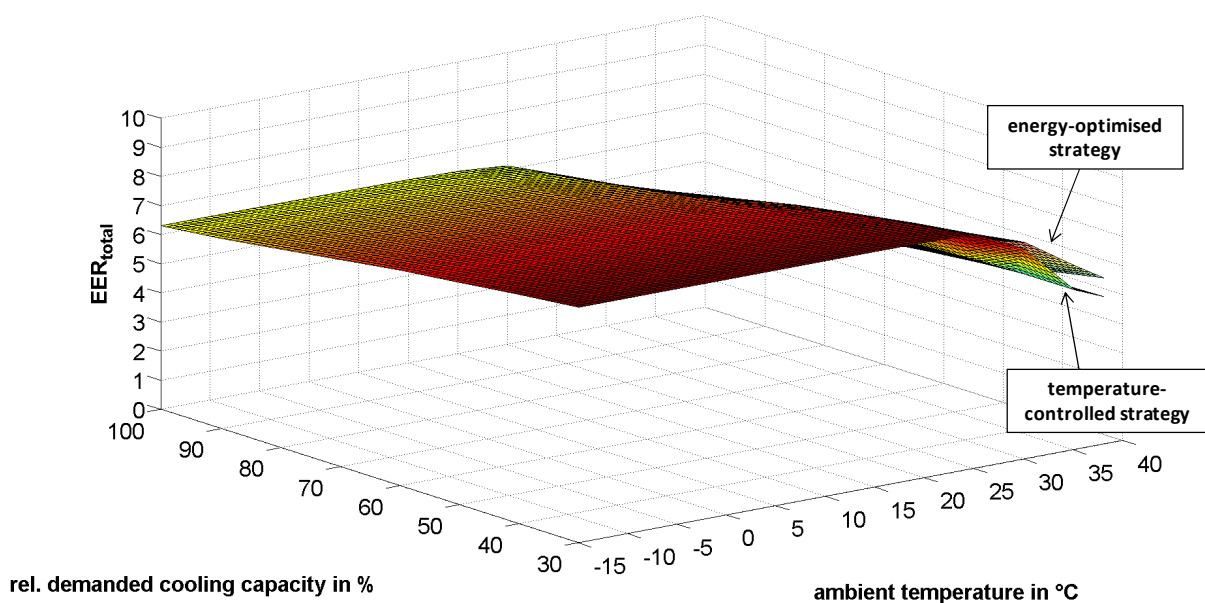


Figure 14: Energy Efficiency Ratio (EER) of cooling unit at different control strategies

Figure 14 shows the EER_{total} as a function of the cooling demand and the ambient temperature. In full load operation, there is no difference between the control strategies. In part load

operation and especially at high temperatures, the energy-optimized strategy leads to a higher EER_{total} . The reason is that, at full load operation, the influence of the condenser fans on the total energy consumption is getting lower. Moreover, it is important to raise the efficiency of the compression as high as possible in this operation status.

This effect can also be seen in Figure 15, which shows the power consumption of the chiller system as a function of cooling demand and ambient temperature.

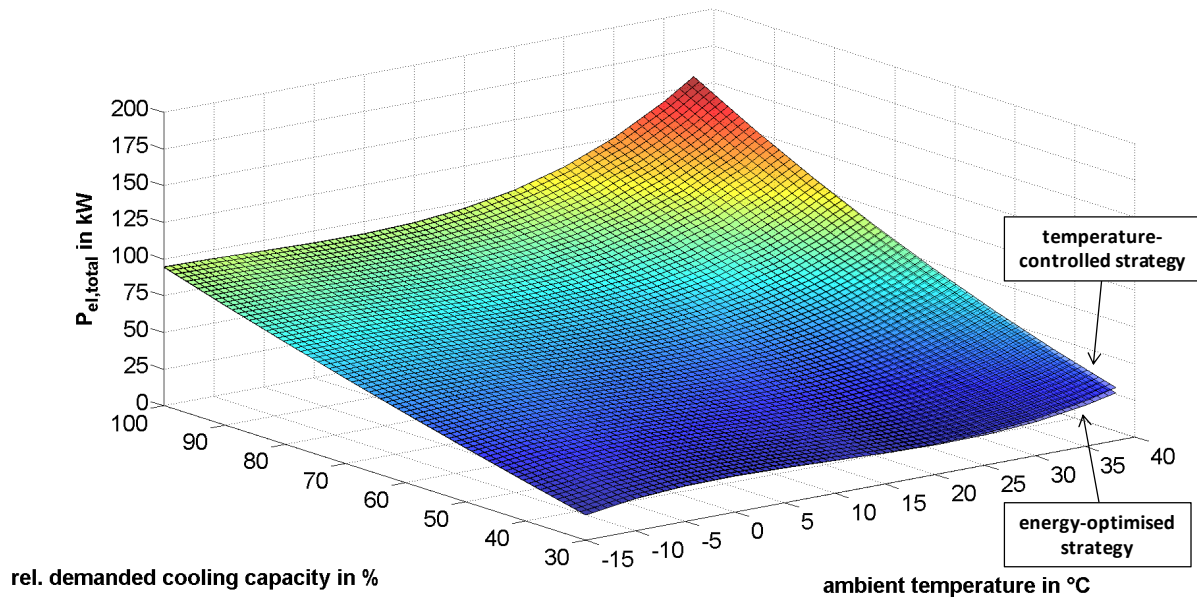


Figure 15: Power consumption of cooling unit at different control strategies

At a cooling demand of 30% and an ambient temperature of 38°C an energy saving of 4 kW is attainable. In this operation status, that represents an energy saving of 10%, compared to the temperature-controlled strategy. As mentioned before, the saving potential of this strategy is increasing with a decrease in the efficiency of the condenser fans. The relative differences in the power consumption of the two control strategies are compared in Figure 16.

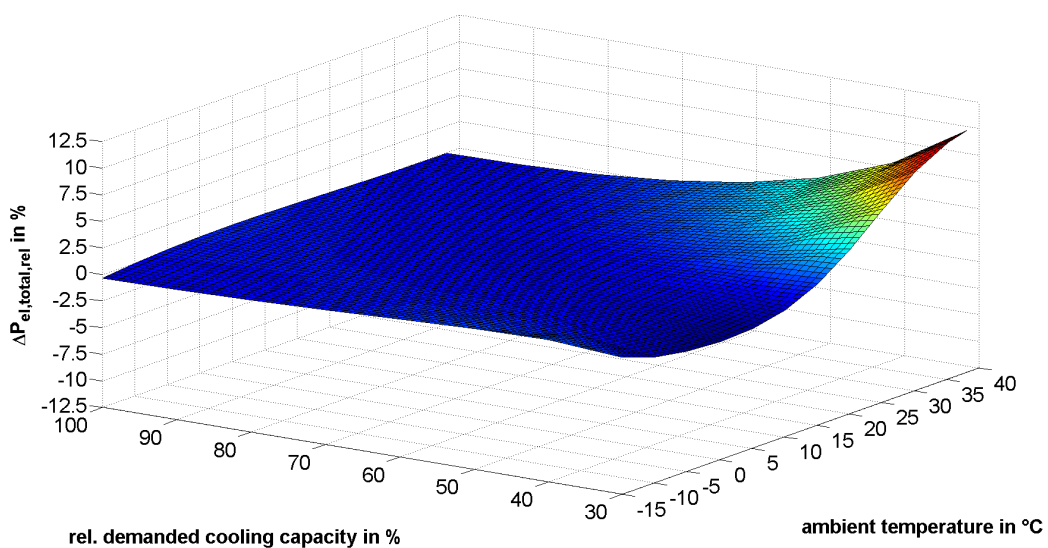


Figure 16: Relative differences in power consumption between the control strategies

To further understand where the differences concerning the power consumption originate from, the operation of the compressor and the condenser fans is detailed in the following figures.

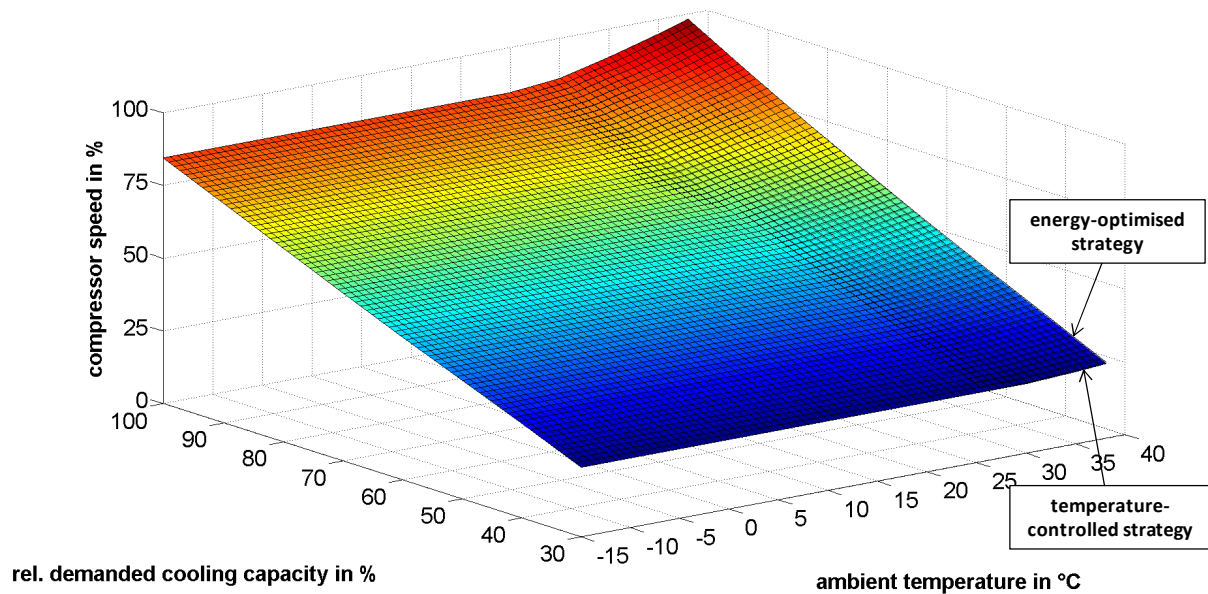


Figure 17: Compressor speed at different control strategies

Figure 17 shows the compressor speed for the two control strategies as a function of the cooling demand and the ambient temperature. It becomes obvious, that the difference between the two strategies is slim. The values from the calculation in Table 9 show that the energy-optimization leads to an increase in the compressor speed, but the difference is under 1%.

A more distinct comparison between the strategies is shown by the fan speed in Figure 18.

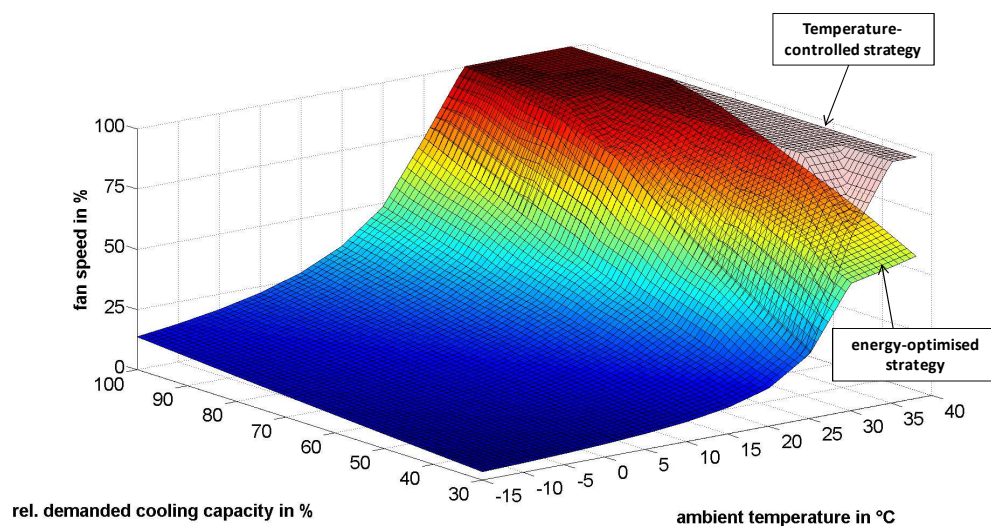


Figure 18: Fan speed at different control strategies

In this figure the difference between the two strategies is apparent. Instead of keeping the fan speed at high values to reach a low condensation temperature, the energy-optimized strategy reduces the fan speed at high temperatures and in part load operation. The low power consumption of the fans leads to the higher EER_{total} .

4.2 Implementation of the energy-optimized strategy in a chiller control

To implement the energy-optimized control strategy in a chiller system, different options are available. One possibility is that the data collected in the parametric study are implemented into the chiller control system by a tabular form. A further approach is to produce a polynomial function based on the collected data, which is used by the chiller control to find the optimal compressor and condenser speed. The second method will be addressed in this chapter.

Compressor

In order to implement the results of this study in a real chiller control system, they must be described in a simplified way. An approach is to build polynomial equations delivering the aimed result. Based on the data obtained in the parametric study, two equations are derived, one for the compressor and one for the fan speed. Therefore also the method of the multiple linear regressions is used. The equations in accordance with DIN EN 12900, thereby uses two parameters, the ambient temperature and the cooling capacity.

$$y = c_1 + c_2 \cdot \dot{Q}_{rel} + c_3 \cdot t_{a,c,in} + c_4 \cdot \dot{Q}_{rel}^2 + c_5 \cdot \dot{Q}_{rel} \cdot t_{a,c,in} + c_6 \cdot t_{a,c,in}^2 + c_7 \cdot \dot{Q}_{rel}^3 + c_8 \cdot t_{a,c,in} \cdot \dot{Q}_{rel}^2 + c_9 \cdot \dot{Q}_{rel} \cdot t_{a,c,in}^2 + c_{10} \cdot t_{a,c,in}^3 \quad (11)$$

with

- y - compressor speed, fan speed [%]
- \dot{Q}_{rel} - rel. cooling capacity [%]
- $t_{a,c,in}$ - ambient temperature [$^{\circ}C$]
- c_i - coefficients for compressor or fan speed[-]

In the later application \dot{Q}_{rel} and $t_{a,c,in}$ are inputs that are depended on the load and the environment of the chiller. The relative cooling capacity can be determined from the cold water mass flow and the temperature difference between supply and return temperature. The ambient temperature is measured by a temperature sensor at the position of the condenser.

For the compressor speed, the corresponding coefficients are shown in Table 10.

Table 10: Coefficients of the polynomial function for calculating the compressor speed ($R^2 = 0,99$)

coefficient	value
c_1	-0,702225
c_2	0,871027
c_3	0,071444
c_4	-0,001121
c_5	-0,003607
c_6	-0,010256
c_7	0,000009
c_8	0,000024
c_9	0,000126
c_{10}	0,000214

This function correlates well with the results of the parametric study. Thus, it is possible to use the polynomial function for the control system of the chiller.

The same procedure was tested for the fan speed, but because of the sharp kink it is not possible to describe the behavior of the fan speed with a single polynomial function. The kink is evident in Figure 18. The result of the polynomial function shows big deviations from the values of the parametric study and would not implement the control strategy in a satisfying way.

A possible alternative would be to produce two polynomial functions and implement a differentiation across the input range.

4.3 Implementation of the chiller system into a smart grid

Another possibility for using the data from the parametric studies is to produce polynomial functions that describe the behavior of the chiller system in different operation status. This polynomial function could be used for load prediction and can be integrated into a power management system. By predicting the power consumption of the cooling unit there is a potential for an optimized storage tank strategy, which aims to reduce load peaks by using load shifting.

For the regarded chiller system, the coefficients of Equation 11 have been determined for the power consumption and the EER_{total} as shown in Table 11.

Table 11: Coefficients of the polynomial function of the power consumption and the EER

coefficient	power consumption ($R^2 = 0,99$)	EER ($R^2 = 0,99$)
c ₁	7,388093	8,441823
c ₂	0,490889	- 0,002472
c ₃	0,288911	0,0334458
c ₄	0,002757	- 0,000357
c ₅	- 0,014897	- 0,000536
c ₆	- 0,043809	- 0,000214
c ₇	0,000007	0,000002
c ₈	0,000104	0,000003
c ₉	0,000601	- 0,000001
c ₁₀	0,000861	- 0,000062

5. CONCLUSION

In conclusion, the model described here enables the simulation of different chiller designs by using data provided by the manufacturer for the main components of the chiller system (compressor, condenser, evaporator). With this model it becomes possible to change single components of the system and perform an energetic evaluation for distinct chiller designs with only a few inputs.

Moreover, this simulation model provides opportunities for testing new control strategies for chiller systems and to evaluate the strategies under certain aspects. These studies allow for derivation of polynomial functions that can be used for an optimal chiller strategy of a load prediction in a Demand-Side-Management.

The examined energy-optimized strategy offers a potential for an energy saving of up to 10%, compared to a temperature-controlled strategy. The saving potential depends on the efficiency of the single components and increases by using inefficient condenser fans. A requirement for the control strategy is that the compressor and the condenser fans are equipped with speed-controlled drives.

The next step in this research is the implementation of the proposed control strategy in a real chiller in order to test the hypotheses of this paper, as well as to optimize the model and the polynomial functions in an iterative process.

REFERENCES

Deutscher Kälte- und Klimatechnischer Verein, 2002. *Energiebedarf für die technische Erzeugung von Kälte. Statusbericht des Deutschen Kälte- und Klimatechnischen Vereins Nr. 22.* ILK, FKW Uni Essen, Stuttgart.

Schmidt-Pleschka, R. & Milles, U., 2006. *Energie sparen bei der Kälteerzeugung.* BINE Informationsdienst, Bonn.

Verband Deutscher Maschinen- und Anlagenbau, 2011. *Energieeffizienz von Kälteanlagen – Teil 2: Anforderungen an das Anlagenkonzept und die Komponenten.* Beuth Verlag GmbH, Berlin.

Roth, P., 2012. *Energetische Systembetrachtung zur Regelung von Verlässigern in Teillast.* Güntner AG & Co. KG, Fürstenfeldbruck.

Deutsches Institut für Normung e.V., 2013. *DIN EN 12900:2013: Kältemittel-Verdichter – Nennbedingungen, Toleranzen und Darstellung von Leistungsdaten des Herstellers.* Beuth Verlag GmbH, Berlin.

Bitzer Kühlmaschinenbau GmbH, 2014. *BITZER Software v6.4.1 rev1210.* <http://www.bitzer.de/eng/Products-Service/BITZER-Software2>

Güntner AG & Co. KG, 2014. *GPC.EU Customer Version 2013.45.* <http://www.guentner.de/know-how/product-calculator-gpc/gpc-software/>

SWEP International AB, 2014. *SSP G7 Version 7.0.3.31.* <http://www.swep.net>

ACKNOWLEDGEMENTS

This work was realized during the research project “FOREnergy – Energy flexibility in production” funded by the Bayerische Forschungsstiftung (Bavarian Research Foundation). Further information is available at www.FOREnergy.de.

Special thanks to *Combitherm GmbH* and *Güntner GmbH & Co. KG* for the support in the research project.

Residential buildings with heat pumps, a verified bottom-up model for demand side management studies

Dieter Patteeuw¹, Lieve Helsen^{1*}

⁽¹⁾Applied Mechanics and Energy Conversion, Department of Mechanical Engineering, KU Leuven, Belgium

1. ABSTRACT

The increasing use of intermittent renewable energy sources has reawakened the interest for demand side management, among which thermostatically controlled loads are a much mentioned option. One of these load types are residential buildings equipped with heat pumps, which can shift electricity consumption in time without compromising indoor thermal comfort. A pre-requisite for the widespread application of this technology is a thorough understanding of its potential for demand side management. This type of studies needs models which on the one hand are computationally efficient enough to be scaled up to a country's building stock but on the other hand are still a correct system representation. These issues are tackled by considering multiple levels of detail in reduced order models and verifying these models to a detailed simulation model. A second step is the aggregation of buildings with different occupant behavior. The aggregation's performance is assessed by comparing the response to various electricity price profiles. Results show that the proposed aggregated model is sufficiently accurate in representing the considered buildings. The methodology presented in this paper can also be applied to other building types, resulting in an aggregated and verified model of a country's building stock for demand side management studies.

Keywords: residential building, heat pump, demand side management, linear model, reduced order model, aggregated model

2. INTRODUCTION

Demand side management (DSM) is the altering of consumer's electricity demand in order to obtain a more desirable load shape for utilities (Gellings, 1985). Strbac (2008) states that such shifting of electricity demand can have numerous benefits such as reducing the need for back-up power plants, grid investments and so on. He identified two main drivers for an increasing potential of DSM, being the increase in renewable energy sources and the improvement of information and communication technologies. Heat pumps are often regarded as a promising technology for DSM, for example to increase voltage security (Wang et al., 2012) or to increase the usage of wind energy (Hedegaard, Mathiesen, Lund, & Heiselberg, 2012). One of the factors hampering its widespread application is a lack of understanding of the potential benefits (Strbac, 2008) which requires appropriate models to enable estimating the potential. This paper aims at presenting a model which can be used to study the flexibility potential of residential buildings equipped with heat pumps. This can be done by means of co-optimization of the presented model and state of the art electricity generation park models. Bruninx, Patteeuw, Delarue, Helsen, and D'haeseleer (2013) showed the added value of this co-optimization, as it can be used to assess the potential of applying DSM. The electricity generation park model is a mixed integer linear optimization problem, which sets requirements for the building and heating system model structure (see section 3.2.1 and section 3.2.2).

Studies on the DSM potential of buildings equipped with heat pumps tend to focus on either the buildings energy demand or on the electricity generation park. The former studies focus on one building or a limited cluster of buildings, using existing building performance simulation

tools (e.g. Kelly, Tuohy, and Hawkes (2013); Henze, Felsmann, and Knabe (2004)) or experiments (e.g. Kok et al. (2012)). The disadvantage of these studies is that the electricity generation system is simplified to a fixed electricity price profile, sometimes leading to spectacular cost savings, going up to 57% (Henze et al., 2004). This potential benefit might diminish when the market penetration of these flexible systems increases (Bruninx et al., 2013).

An increasing number of DSM potential studies models both electricity generation park and buildings simultaneously. Typically, these studies start from an electricity generation park model (Eq. (1)-(3)) in which the operational cost $cost_{op}$ of generating electricity gen_j is minimized over a certain time period, with j being the time step. The flexibility in electricity demand offered by the buildings with heat pumps, is modelled as follows. The heat pumps cause an additional electricity demand $P_j^{hp,tot}$ which is limited by a linear state space model (Eq. (4)) of building and hot water tank temperatures T_j , comfort constraints (Eq. (5)) and power constraints (Eq. (6)). The overall model is hence the following optimization problem:

$$\begin{aligned} & \underset{gen_j, P_j^{hp,tot}, T_j}{\text{minimize}} && \sum_j cost_{op}(gen_j) && (1) \\ & \text{subjected to} && \forall j: con_{op}(gen_j) = 0 && (2) \\ & && \forall j: gen_j = demand_j + P_j^{hp,tot} && (3) \\ & && \forall j: P_j^{hp,tot} = ss(T_j) && (4) \\ & && \forall j: comfort(T_j) \geq 0 && (5) \\ & && \forall j: power(P_j^{hp,tot}) \geq 0 && (6) \end{aligned}$$

in which equation (3) makes sure that at each time step, the total electricity generation gen_j covers the traditional electricity demand $demand_j$ and the additional electricity demand $P_j^{hp,tot}$. These studies tend to oversimplify the building: a heat pump is often considered to have a constant coefficient of performance (COP) while solar heat gains and thermal energy storage in the building structure are often neglected. Regarding the COP, only two studies could be found that have a more complicated representation of the COP, namely by considering the COP either linearly (Good, Navarro-espinoza, Mancarella, & Karangelos, 2013) or non-linearly (Wang et al., 2012) dependent on ambient air temperature. Solar heat gains are sometimes indirectly included by considering these as part of the model's white noise (Callaway, 2009; Kamgarpour et al., 2013). In order to shift a heat pump's electricity demand in time without compromising the users' comfort, some thermal energy storage must be present in the system. This can be either in storage tanks (active thermal storage) or in the building structure itself (passive thermal storage). Some authors focussing on active thermal energy storage in domestic hot water tanks (Barton et al., 2013; Kondoh, Lu, Member, & Hammerstrom, 2011) or high capacity space heating systems (Long, Xu, & He, 2011; Meibom et al., 2007) consider buildings as providers of a fixed thermal energy demand profile, hereby neglecting the energy storage potential of the building structure.

In order to determine the DSM potential of passive energy storage, the building structure is in some cases represented by two (Pedersen, Andersen, Nielsen, Stærmose, & Pedersen, 2011; Wang et al., 2012) or three thermal capacities (Hedegaard & Balyk, 2013). In general though, only one thermal capacity is considered (Good et al., 2013; Hedegaard et al., 2012; Muratori, Roberts, Sioshansi, Marano, & Rizzoni, 2013). Modelling the building structure as one thermal capacity allows statistical aggregation techniques in order to study the DSM potential of large

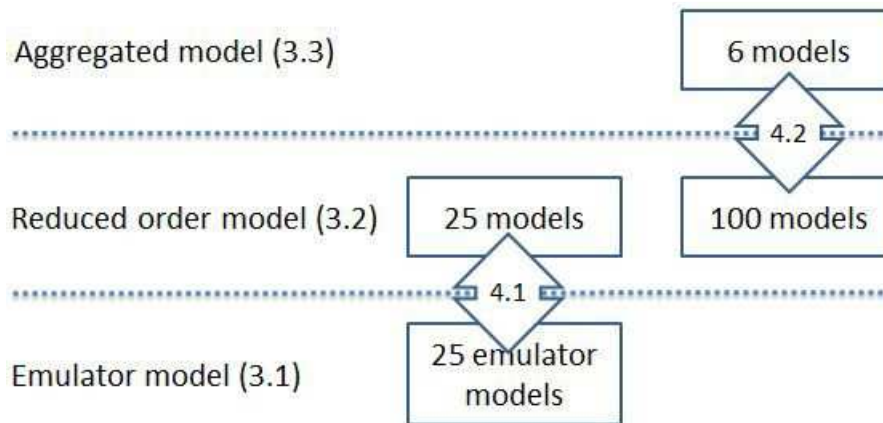


Figure 1: The aim of the paper is to develop an aggregated model which is derived from a detailed building simulation (emulator) model. Section 4.1 compares multiple reduced order models to this emulator model. In section 4.2 the aggregated model is compared to a large set of these reduced order models.

sets of buildings (Malhame, 1985; Kamgarpour et al., 2013; Callaway, 2009). Another advantage is that the model becomes similar to that of other thermostatically controlled loads, such as fridges and freezers, allowing similar modelling techniques (Lu & Vanouni, 2013; Mathieu, Dyson, & Callaway, 2012). One could argue which level of detail is needed to describe the transient behaviour of a building. This is discussed in section 3.2.1.

The aim of this paper is to present a set of equations in the form of Eq. (4)-(6) that accurately represents the DSM potential of thousands of buildings equipped with heat pumps. In order to achieve feasible computation times, an aggregated, reduced order model of these buildings is required. This paper presents three levels of modelling detail and a procedure to verify the top-level aggregated, reduced order model (see figure 1). The highest level of detail can be found in the building performance simulation model, which acts as the emulator model. From this, a reduced order model (ROM) is deduced. A second level of simplification aggregates multiple of these ROMs, based on their occupants behaviour. The results section shows the comparison between the different levels of details, linking the performance of the most detailed model to the top-level aggregated ROM model. The discussion section elaborates on this comparison, to support the conclusions in the conclusion section.

3. METHODOLOGY

This section describes three levels of modelling detail (Figure 1). The first model (section 3.1) is a fully physical model which acts as an emulator model. From this, multiple reduced order models are deduced (section 3.2). The final level of simplification is the aggregation of multiple buildings by a mathematical operation on the comfort bounds (section 3.3).

3.1 Emulator model

A detailed emulator model of the building is developed using the IDEAS library in Modelica, described by Baetens et al. (2012). This modelling environment has been verified and validated using the BESTEST methodology (Judkoff & Neymark, 1995). The parameters for the single zone building are taken from Reynders, Diriken, and Saelens (2014), who interpreted the parameters of a typical post 2005 built Belgian dwelling as described in the TABULA project (Cyx, Renders, Van Holm, & Verbeke, 2011). The building has a floor surface of 270 m² and

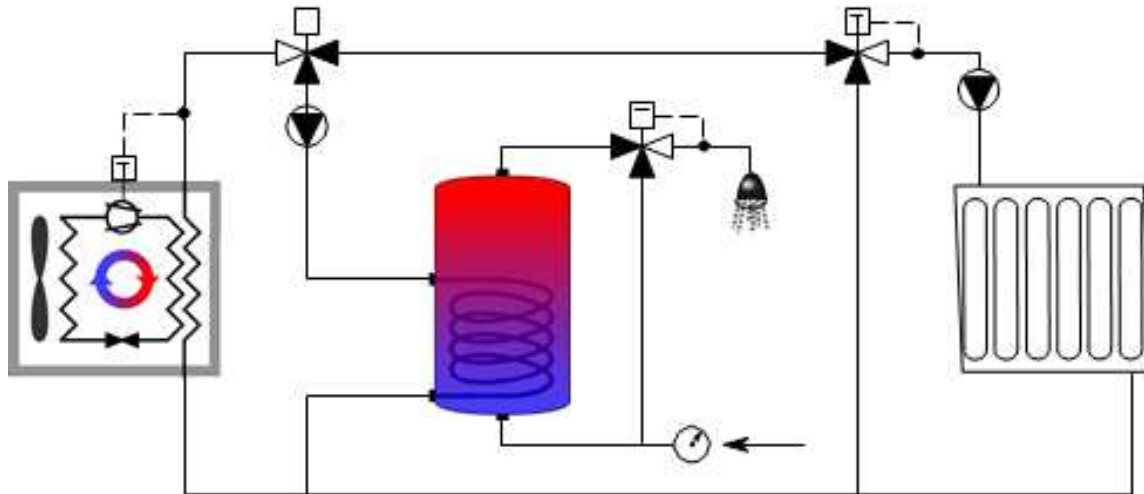


Figure 2: Hydraulic scheme of the heating system, based on De Coninck et al. (2014). A modulating air coupled heat pump supplies heat for domestic hot water (DHW) via a storage tank and space heating (SH) via a radiator.

a protected volume of 741 m³. The combination of infiltration and ventilation cause 1.5 air changes per hour. The exterior walls, roof and windows have a U-value of 0.4 $\frac{W}{m^2K}$, 0.5 $\frac{W}{m^2K}$ and 1.4 $\frac{W}{m^2K}$ respectively. In each cardinal direction, the building has an average of about 10 m² window surface, resulting in a percentage glazing of 22%. The Belgian climate is considered, based on the measurements in Uccle and distributed by Meteonorm (*METEONORM Version 6.1 Edition 2009, 2009*).

The heating system is also modelled using the IDEAS library. It consists of a modulating air coupled heat pump supplying both warm water to a radiator for space heating (SH) and a domestic hot water (DHW) tank (Figure 2). All components are based on physical equations, while the parameters for these components are determined from either manufacturer data or empirical correlations. A full description of the heat pump model, along with a validation of the domestic hot water tank model is described by De Coninck, Baetens, Saelens, Woyte, and Helsen (2014). The model for the radiator is described by Baetens et al. (2012). The heat pump and radiator are sized to meet 80% of the design heat demand of 8900W, in accordance with the code of good practice in Belgium (“Code van goede praktijk voor de toepassing van warmtepompsystemen in de woningbouw”, 2004).

Table 1: Multiple buildings are considered having a different number of occupants with each their own DHW tank for supplying domestic hot water.

Household size [Persons]	1	2	3	4	5	6
Number of households (25 case)	8	8	4	3	1	1
Number of households (100 case)	32	32	16	12	4	4
Daily DHW demand at 50°C [liter]	62.5	125	162	200	237	300
DHW tank size [liter]	120	160	160	200	300	300
DHW tank UA [W/K]	0.117	0.098	0.098	0.085	0.085	0.077

Since the model is aimed to be scaled up in order to represent thousands of buildings, also various numbers of occupants per house are considered. To this aim, 25 buildings are considered, each having the same building structure, but with different number of occupants and different occupant behaviour (Table 1). For the aggregation method, the aggregated model was compared to 100 ROMs, each having again the same building model but different occupant

behaviour. The household size determines the daily DHW demand, which is based on Peuser, Remmers, and Schnauss (2010). This daily demand determines the size of the DHW tank. The parameters of the tanks are based on the Vitocell 100-W gamma of Viessmann.

3.2 Reduced order model

The reduced order model describes the dynamic behaviour of both building and heating system with fewer equations and detail than the emulator model. This ROM is the set of linear equations (4)-(6) that still describes the flexibility in electricity use provided by the presented system. In order to obtain profiles of how the ROM performs with respect to the emulator model (figure 5), the optimization problem (Eq. (1)-(6)) is reduced to

$$\underset{gen_j, P_j^{hp,tot}, T_j}{\text{minimize}} \quad \sum_j cost_{op}(P_j^{hp,tot}) \quad (7)$$

$$\text{subjected to} \quad \forall j: P_j^{hp,tot} = ss(T_j) \quad (8)$$

$$\forall j: comfort(T_j) \geq 0 \quad (9)$$

$$\forall j: power(P_j^{hp,tot}) \geq 0 \quad (10)$$

in which $cost_j$ is the electricity cost at time step j (Figure 8(a)). Thus given a specific electricity price profile, the optimization gives a resulting electricity consumption and temperatures, which can be compared to the emulator model.

A linear model of the building was already developed by Reynders et al. (2014) and is described shortly in section 3.2.1. This paper mainly focuses on the reduced order model of the heating system. Table 2 summarizes various aspects of the heating systems that can be modelled in different ways. Section 3.2.2 describes in detail the multiple representations for the heat pump. Section 3.2.3 focuses on the DHW tank and finally section 3.2.4 describes the radiator model.

Table 2: Component model description for the emulator model. Per component two options for the reduced order model (ROM) are considered. T_{amb} is the ambient air temperature. P^{hp} is the electrical power used by the heat pump.

Component	Emulator model	ROM option 1	ROM option 2
Heat pump COP	Interpolation of manufacturer data	Constant COP, average from correlation	COP from correlation, function of T_{amb}
Heat pump modulation	Interpolation of manufacturer data	mixed integer formulation (Eq.12-15)	linear in P^{hp} (Eq.16-19) + post processing
DHW storage tank	multiple layers with energy balance equation	fully mixed with mixed integer constraint (Eq.22-23)	fully mixed with linear constraint (Eq.24-29)
Radiator	radiator formula and one thermal capacity	no radiator model	linearised heat transfer and one thermal capacity (Eq.30)

3.2.1 Building model

Reynders et al. (2014) deducted a linear model with five states (Figure 3(a)) by performing system identification on the emulator model described in section 3.1. These five states are the indoor operative temperature T_{air} and the temperature of inner walls T_{wi} , roof T_{roof} , floor T_f and

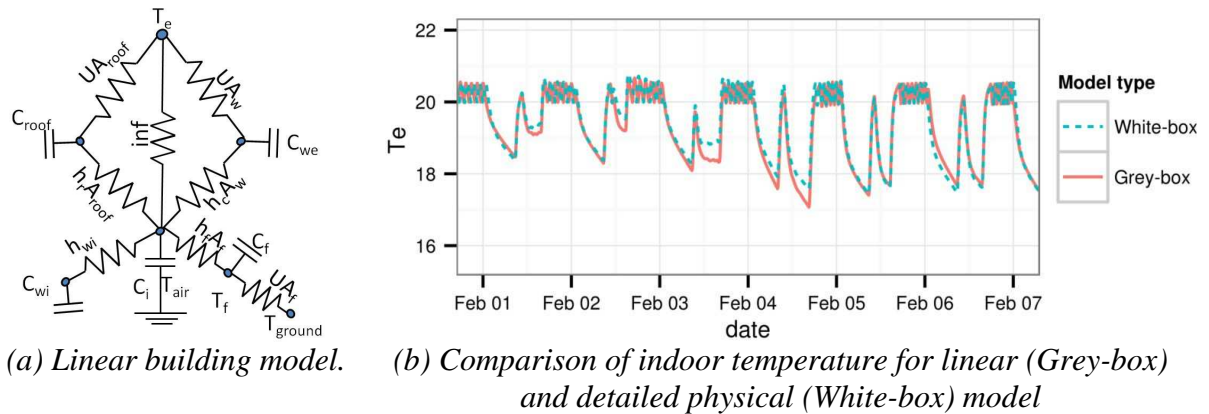


Figure 3: The linear model (left) comprises of five thermal capacities and hence five states. It is a model able to approximate the behaviour of the detailed physical model (right). Source: Reynders et al. (2014).

exterior walls T_{we} . The thermal capacities and heat transfer coefficients associated with these states have the same indices. Inputs to the model are the ambient air temperature T_e , ground temperature T_{ground} and the heat gains due to solar irradiation, internal gains and radiators. Multiple linear models were considered, from which the five states model clearly outperforms the rest. This model shows an RMSE error of only 0.3°C on a two day ahead prediction of the indoor operative temperature of the detailed physical model. Figure 3(b) shows the comparison between both models. The linear model can be written in the following state space structure for a certain time step j :

$$\dot{T}_j = A \cdot T_j + B \cdot U_j \quad (11)$$

in which T_j and U_j are vectors with the above mentioned states and inputs respectively. The parameters in the matrices A and B were determined from system identification. This five states model is used as part of the ROM in this paper.

3.2.2 Heat pump model

This paper focuses on modulating heat pumps for which the performance strongly depend on the supply and source temperature, and on the modulation. Verhelst, Logist, Van Impe, and Helsen (2012) studied multiple representations of the heat pump COP based on these variables, among which non-linear representations. Since the ROMs discussed in this paper are intended to be combined with electricity generation park models (Bruninx et al., 2013), a non-linear representation is out of the question, hence only linear and mixed integer representations of heat pump performance are allowed. The two remaining options for this framework are thus a constant COP or a COP that is a function of the ambient air temperature only. The heat pump integrated in the emulator model can supply warm water to both space heating (SH) and domestic hot water (DHW), hence the decision variables are the electric power of the heat pump to supply space heating $P_j^{hp,sh}$ or domestic hot water $P_j^{hp,dhw}$ at time step j . The most detailed mixed integer representation of the heat pumps performance is the set of equations (12)-(15).

The equations for the domestic hot water supply are analogous to (12)-(14).

$$\forall j: P_j^{hp,sh} = P_j^{min,hp,sh} \cdot z_j^{hp,sh} + P_j^{int,hp,sh} \quad (12)$$

$$\forall j: 0 \leq P_j^{int,hp,sh} \leq (P_j^{max,hp,sh} - P_j^{min,hp,sh}) \cdot z_j^{hp,sh} \quad (13)$$

$$\forall j: \dot{Q}_j^{hp,sh} = COP_j^{i,sh} \cdot P_j^{min,hp,sh} \cdot z_j^{hp,sh} + P_j^{int,hp,sh} \cdot (COP_j^{a,sh} - COP_j^{i,sh}) \quad (14)$$

$$\forall j: z_j^{hp,sh} + z_j^{hp,dhw} \leq 1 \quad (15)$$

This representation has the advantage of being directly convertible to control signals for the heat pump and the pumps connecting the heat pump to the DHW tank and space heating by means of the integer variables $z_j^{hp,sh}$ and $z_j^{hp,dhw}$ that can only be zero or one. It is also possible to take into account a different COP at full load $COP_j^{a,sh}$ and at minimal modulation $COP_j^{i,sh}$. The power that the heat pump consumes does not violate the working constraints, it is either off or between the maximal $P_j^{max,hp,sh}$ and minimal $P_j^{min,hp,sh}$ modulating power. The integer power level $P_j^{int,hp,sh}$ is a dummy variable to cope with these constraints. The disadvantage is the number of integers used, since these are known to cause the calculation time to explode. Solvers for mixed integer linear problems can typically handle problems with up to 105 integers, however when exceeding this order of magnitude, this becomes a lot harder (Koch et al., 2011). Considering a time horizon of 48 hours with two integers each hour per house, this would limit the number of buildings in one optimization problem to 104 buildings.

Another option to represent the heat pump is a linear model (16)-(19), in which the electric power of the heat pump towards space heating or domestic hot water can vary between 0 and $P_j^{max,hp,sh}$, as long as the sum of the two remains below $P_j^{max,hp,sh}$. Linear optimization models are computationally very efficient to solve, the optimization takes only some seconds on a regular laptop while the mixed integer representation (12)-(15) can easily take minutes to hours to solve. This linear model consists of the following equations:

$$\forall j: P_j^{hp,sh} + P_j^{hp,dhw} \leq P_j^{max,hp} \quad (16)$$

$$\forall j: P_j^{hp,sh}, P_j^{hp,dhw} \geq 0 \quad (17)$$

$$\forall j: \dot{Q}_j^{hp,sh} = COP_j^{sh} \cdot P_j^{hp,sh} \quad (18)$$

$$\forall j: \dot{Q}_j^{hp,dhw} = COP_j^{dhw} \cdot P_j^{hp,dhw} \quad (19)$$

The disadvantage of the linear optimization model is the extra effort needed to derive control signals for the individual heat pump and circulation pumps, respecting the lower modulation level of the heat pump. To this aim, a post processing is applied in order to obtain feasible profiles for 'scheduled operation' as explained by Kosek, Costanzo, Bindner, and Gehrke (2013). Since multiple buildings are controlled at once, the electricity demand per building can be redivided among the buildings, as long as the sum of these electricity demands remains the same. In this way, some buildings that require less than the minimal modulation of the heat pump, are switched off and this difference is made up for in other buildings. The buildings from which the heat pumps were switched off, are compensated for this fact in a later time step.

3.2.3 Domestic hot water tank

The central component in the DHW model is the DHW tank. This tank can either be modelled as perfectly stirred or perfectly stratified. The latter storage tank model was not considered in this study, since it was noticed in the simulations of the emulator model, that the heat exchanger usually destroys the thermal stratification. The tank is thus assumed to be a perfectly stirred

water tank, meaning that all water in the tank is at the same temperature T_j^{tank} at time step j . The water in the DHW tank can either be heated up by the heat pump, $\dot{Q}_j^{hp,dhw}$ or by a back up electrical heater $\dot{Q}_j^{aux1,dhw}$. Heat is extracted from the DHW tank through demand for hot water \dot{Q}_j^{dem} and heat loss to the surroundings. The discretized version of the energy balance for the DHW tank leads to the following equation:

$$\forall j: \rho c_p V_{tank} \frac{T_{j+1}^{tank} - T_j^{tank}}{\Delta t} = \dot{Q}_j^{hp,dhw} + \dot{Q}_j^{aux1,dhw} - UA \cdot (T_j^{tank} - T_j^{surr}) \quad (20)$$

with ρ [kg/m³] and c_p [J/kgK] the density and heat capacity of water and V_{tank} [m³] the volume of the tank. With Δt the time step of the optimization, the time derivative of T_j^{tank} is approximated as $\frac{T_{j+1}^{tank} - T_j^{tank}}{\Delta t}$. The term $UA \cdot (T_j^{tank} - T_j^{surr})$ determines the heat loss to the surroundings, which is at temperature T_j^{surr} . The thermal conductance UA [W/K] is that of the insulation around the DHW tank, which is the dominant resistance to heat transfer.

The temperature of the cold tap water T^{cold} and the temperature of the supplied DHW T^{dem} are both assumed to be constant. A lower boundary for the temperature of the water in the DHW tank stems from the demand for a comfortable temperature of DHW. Since the tank is perfectly stirred, the whole tank must be heated up to at least T^{dem} when the occupants desire hot water. In the meantime, the water in the tank can get as low as T^{cold} :

$$\forall j: T_j^{tank} \geq T^{dem} \cdot hdw_j + T^{cold} \cdot (1 - hdw_j) \quad (21)$$

with hdw_j a binary parameter which is 1 when hot water is demanded in time step j and 0 when this is not the case. The water in the DHW tank can be at a higher temperature than what is demanded, in which case a three way valve is used to mix it with the cold water to the desired temperature. Given the constant T^{cold} and T^{dem} and the fact that the whole tank is above T^{dem} in case of DHW demand, \dot{Q}_j^{dem} is independent of the tank temperature (Patteeuw, Bruninx, Delarue, D'haeseleer, & Helsen, 2013).

The heat pump can deliver heat up to a maximum temperature T_{max}^{hp} , typically 60°C, which is lower than the maximum allowed temperature of the DHW tank T_{max}^{tank} , typically 90°C. This difference introduces the need for a boolean variable $z_j^{hp,dhw}$ and the following constraints

$$\forall j: T_j^{tank} + \frac{\Delta t}{\rho \cdot V_{tank} \cdot c_p} \cdot \dot{Q}_j^{hp,dhw} \leq (1 - z_j^{hwd}) \cdot T_{max}^{hp} + z_j^{hwd} \cdot T_{max}^{tank} \quad (22)$$

$$\forall j: \frac{\dot{Q}_j^{hp,dhw}}{COP_j^{hp,dhw}} \leq (1 - z_j^{hwd}) \cdot P_{max}^{hp} \quad (23)$$

When z_j^{hwd} is zero, the temperature of the DHW tank is lower than T_{max}^{hp} and the heat pump's j max output is limited by either the temperature up to which it can heat, Eq. (22), or by its maximal electrical power, Eq. (23). In case z_j^{hwd} is one, the temperature of the DHW tank is higher than T_{max}^{hp} and the heat pump's output is zero through Eq. (23). In that case, Eq. (22) becomes an upper constraint on the temperature of the DHW tank.

The boolean z_j^{hwd} makes the problem a mixed integer linear problem, with the above mentioned problems. A linear alternative for the model is defining the tank temperature T_j^{tank} as the sum of a temperature which is influenced by the heat pump T_j^{hp} and a temperature difference influenced by the auxiliary heater dT_j^{aux} (the latter for the temperature range above 60°C). The

model hence becomes:

$$\forall j: \rho c_p V_{tank} \frac{T_{j+1}^{hp} - T_j^{hp}}{\Delta t} = \dot{Q}_j^{hp,dhw} + \dot{Q}_j^{aux1,dhw} - \dot{Q}_j^{hp,dem} - UA \cdot (T_j^{hp} - T_j^{surr}) \quad (24)$$

$$\forall j: \rho c_p V_{tank} \frac{dT_{j+1}^{aux} - dT_j^{aux}}{\Delta t} = \dot{Q}_j^{aux2,dhw} - \dot{Q}_j^{aux,dem} - UA \cdot dT_j^{aux} \quad (25)$$

$$\forall j: \dot{Q}_j^{hp,dem} + \dot{Q}_j^{aux,dem} = \dot{Q}_j^{dem} \quad (26)$$

$$\forall j: \dot{Q}_j^{aux1,dhw} + \dot{Q}_j^{aux2,dhw} = \dot{Q}_j^{aux,dhw} \quad (27)$$

$$\forall j: T_{max}^{hp} \geq T_j^{hp} \geq T^{dem} \cdot hwd_j + T^{cold} \cdot (1 - hwd_j) \quad (28)$$

$$\forall j: (T_{max}^{tank} - T_{max}^{hp}) \geq dT_j^{aux} \geq 0 \quad (29)$$

The heat demand \dot{Q}_j^{dem} for supplying DHW has to be extracted either from the heat pump influenced temperature $\dot{Q}_j^{hp,dem}$ or from the auxiliary influenced temperature $\dot{Q}_j^{aux,dem}$. The heat pump can hence only heat up T_j^{hp} to T_{max}^{hp} . The auxiliary heater can supply heat to both the j max heat pump influenced temperature ($\dot{Q}_j^{aux1,dhw}$) and the auxiliary heater influenced temperature ($\dot{Q}_j^{aux2,dhw}$).

3.2.4 Heat emission system

The heat emission system is a radiator, that is modelled as a thermal capacity C_{rad} at a temperature T_j^{rad} :

$$\forall j: C_{rad} \frac{T_{j+1}^{rad} - T_j^{rad}}{\Delta t} = \dot{Q}_j^{hp,sh} + \dot{Q}_j^{aux,sh} - (UA)_{rad} \cdot (T_j^{rad} - T_j^{zone}) \quad (30)$$

The thermal capacity of the radiator $C_{p,rad}$ is the sum of the thermal capacities of the radiator's dry mass and water content. The constant overall heat transfer coefficient $(UA)_{rad}$ is attained by linearising the radiator formula around the design supply temperature.

3.3 Aggregated model

In order for a building model to represent thousands of buildings, the same building model is considered multiple times, each time with a different user behaviour. The motivation to model multiple buildings with different user behaviour, is to attain a reasonable load diversity in order to avoid an unrealistically high peak load. In the field of electricity distribution systems, Kersting (2012) concluded that considering the electricity demand of 70 buildings is enough to represent the load diversity of a much larger cluster of buildings. In this paper, some margin was taken and 100 buildings were considered. The number of inhabitants in each building was chosen in such a way that it represents the population structure in Belgium (FOD economy Belgium, 2008), see Table 1.

The methodology presented in this section can be applied for any occupancy schedule. For this study in particular, time profiles of how many occupants are present and awake in the building were extracted from the model of Richardson, Thomson, and Infield (2008). This data is processed in order to get the thermal comfort limits for the building: if at least one occupant is present and awake during at least half an hour, the lower temperature set-point becomes 20°C instead of 16°C. Based on Peeters, Dear, Hensen, and D'haeseleer (2009), an upper bound for the indoor operative temperature is on average 24°C. The hot water demand at 60°C is inspired by Peuser et al. (2010), namely 50 litre per person for the first two inhabitants and

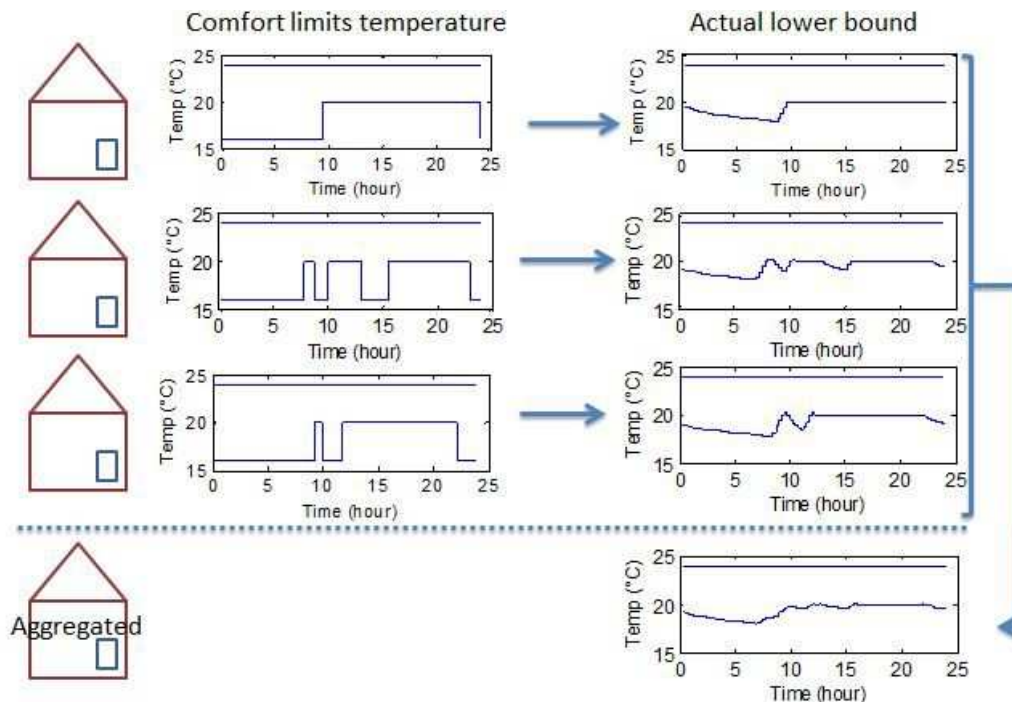


Figure 4: Concept of the aggregation. For multiple buildings with identical building structure but different user behaviour, the actual lower temperature limits are determined from the occupant's temperature set-points. The aggregated model then has the same building structure, but a lower bound for the indoor operative temperature which is the mean of the actual lower temperature limits of the larger cluster of buildings.

30 litre per person for the following number of inhabitants. For each number of inhabitants, one or two tap moments are generated during the periods the occupants are present. These tap moments are distributed in such a way that the sum of the hot water demand for all 100 buildings corresponds to the profile denoted by Peuser et al. (2010). This aggregated hot water tapping profile was measured from a very large apartment building in Germany.

A cluster of hundred building models, even if all these models are linear, is still a large problem to solve. A method is thus needed to reduce the number of buildings, namely by aggregation. In this paper, a new methodology is presented to aggregate building models which have the same physical parameters but different user behaviour. This methodology is illustrated in figure 4. Assume that the 32 households consisting of one person from Table 1 have the same building structure and the same hot water storage tank. Most of the models for these 32 households will be similar, except for the fact that these will have different temperature set-points for the indoor air temperature and domestic hot water, along with different internal heat gains in the building and different heat demand for domestic hot water.

The principle of the aggregation is explained for the case of space heating in figure 4. For each of the 32 buildings with one occupant, the actual lower bound for the indoor air temperature is determined. Thus not the set-point is taken as a lower bound, but the lowest temperature possible if thermal comfort is to be attained. This actual lower bound is determined by taking into account the warm-up and cool-down curve of the building. This bound is thus dependent occupant behaviour, ambient air temperature, building parameters and heating system parameters. The aggregated model then consists of one building model for which the lower temperature bound is the average of the 32 actual lower temperature bounds. The internal heat gains are averaged over the 32 internal heat gain profiles. A similar procedure is followed for

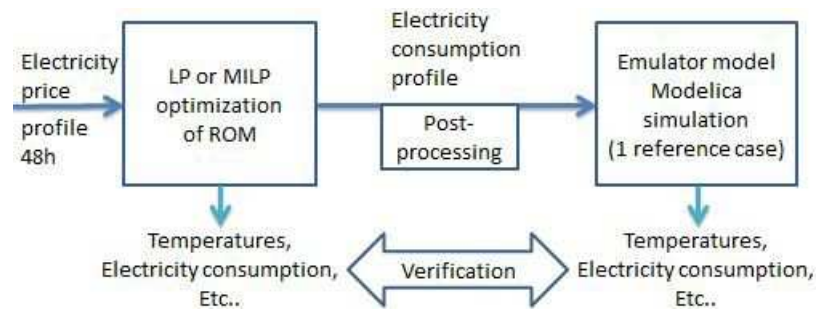


Figure 5: The verification is performed as follows: the outcome of multiple ROMs are compared to a reference emulator model. The reference emulator model tries to track the electricity consumption profile from the ROM as closely as possible.

domestic hot water: the actual lower bounds for the storage tank temperatures is determined along with the average hot water demand. As there are 6 cases of number of inhabitants, and hence 6 different hot water storage tanks, the aggregated model consists of 6 building models that represent the 100 building models. But these 6 building models could easily represent a thousand or more buildings, since the procedure is the same. The similarity between the two levels of detail is illustrated in section 4.2.

3.4 Summary

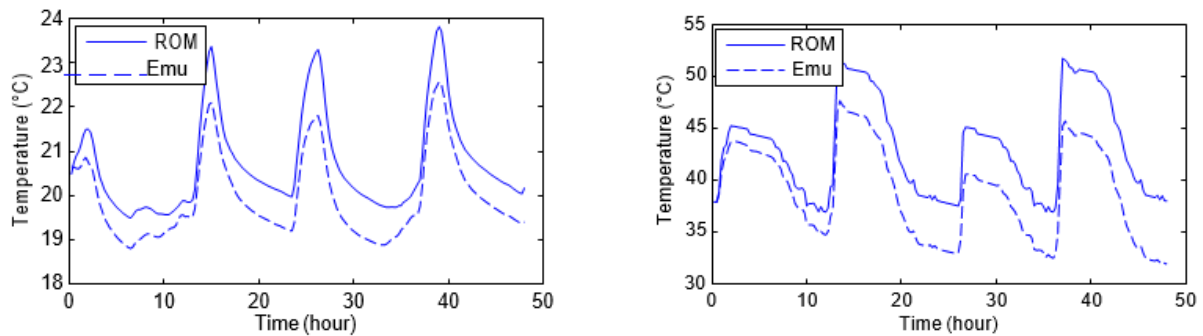
The methodology section gives an overview of all modelling levels needed to come up with an aggregated, reduced order model of buildings equipped with heat pumps. The aim of these models is a co-optimization with electricity generation park models in order to investigate the potential for demand side management. Hence, simplifications are needed with respect to the detailed physical model. Whether the simplifications presented in the methodology section can be justified, is discussed in the following section.

4. RESULTS AND DISCUSSION

The results and discussion section is split up into two parts. The first section compares the reduced order model to the emulator model, which is done for multiple user behaviours and multiple hot water storage tank sizes. The second section shows the performance of the aggregation.

4.1 Verification w.r.t. emulator model

The reduced order model is verified with respect to the emulator model as shown in figure 5. For multiple electricity price profiles, the ROM is used in the optimization (Eq. (7)-(10)) determining optimal system operation for a time period of 48 hours. From this optimization, profiles for the electricity consumption, indoor air temperature, COP, etc can be obtained. The verification is done by letting the emulator model track this electricity consumption profile with an intermediate post-processing in some cases. The resulting profiles for indoor air temperature and hot water storage tanks are then compared, as shown in figure 6. In the ROM, the thermal comfort constraints are always met, since these are a constraint in the optimization. Thermal comfort is not always met for the emulator model. As shown in table 2, there are multiple ROM options for all the components. All these model options were compared for three electricity price profiles, namely in the shape of a sine wave with a mean value of $0.10 \frac{EUR}{kWh}$ and an amplitude of 1.1, 0.02 and $0.05 \frac{EUR}{kWh}$. The results for the three electricity price profiles did not



(a) Average indoor operative temperature.

(b) Average DHW tank temperature.

Figure 6: Comparison of some average temperatures over all 25 buildings in case of the ROM and the emulator (Emu) model. The reduced order model approximates the detailed simulation model well, but there is still a (steady-state) deviation between both models.

show much difference though, therefore the results of this section are only discussed for the electricity price profile with an amplitude of $0.02 \frac{EUR}{kWh}$, as shown in Figure 8(a).

Results reference case. As reference case, all model options 2 of table 2 are chosen. So the reference ROM consists of a heat pump with a COP that is a function of the ambient air temperature and has no modulation constraints. The lack of modulation constraints is corrected by performing a post-processing on the electricity demand profile as explained in section 3.2.2. In the reference model, the radiator is also included with a constant UA value and a thermal capacity. Finally, this reference ROM also has the linear, fully mixed model for the domestic hot water tank. Figure 6 shows the indoor operative temperature and DHW tank averaged over the 25 buildings. As can be seen from the figure, these buildings react upon the price profile (Figure 8(a)), preheating the zone and DHW tank when the price is low.

The indoor operative temperature of the ROM shows an almost constant deviation from the emulator model. This is due to two factors, namely a deviation in tracking of the electricity consumption profile and losses in the distribution pipes. Firstly, the emulator model consumes 5% less electricity than the ROM, as shown in figure 8(b). Secondly, the lack of a distribution pipe model in the ROM causes an additional 5% difference in thermal energy supplied. Regarding the thermal comfort in the reference ROM, only the temperatures in periods when thermal comfort is demanded, are important. The distribution of indoor operative temperature when occupants are present is shown in figure 7. The indoor operative temperature drops regularly below the demanded temperature of $20^{\circ}C$ but rarely below $19^{\circ}C$. This deviation is clearly noticeable in figure 6: the indoor operative temperature in the emulator model is between $0.5^{\circ}C$ and $1^{\circ}C$ lower than in the ROM. This causes a substantial thermal discomfort of 3.96Kh per building per day with respect to $20^{\circ}C$. When taking a reference temperature of $19.5^{\circ}C$ for the thermal discomfort, this value is 1.04Kh.

For the DHW tank model, the error of the ROM tends to become larger in time. This is mainly due to a small underestimation of the heat pump's COP, which tends to build up as the simulation time is longer. Figure 7 shows the distribution of temperatures when the occupants tap DHW from the tank. As can be seen from the figure, the temperature at which the DHW is tapped is never below $45^{\circ}C$. The total discomfort for DHW with regard to the reference of $50^{\circ}C$ is 0.87Kh per building per day.

Another important aspect of the comparison between ROM and emulator model is how good the emulator model is able to track the electricity consumption profile as determined by the

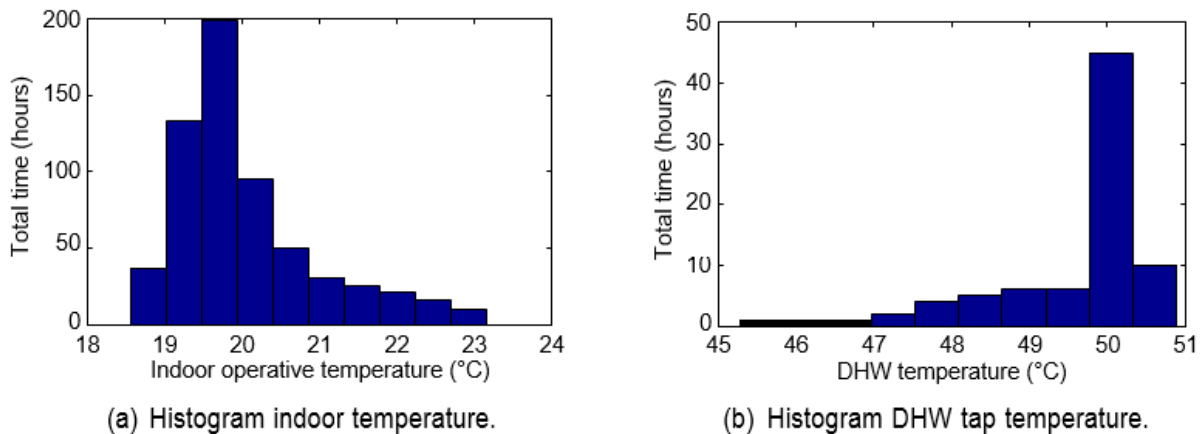


Figure 7: Histogram of temperature during comfort periods for the 25 buildings. The indoor air temperature that should be above 20°C (left). The temperature of the domestic hot water when this is tapped from the tank, should be above 50°C (right).

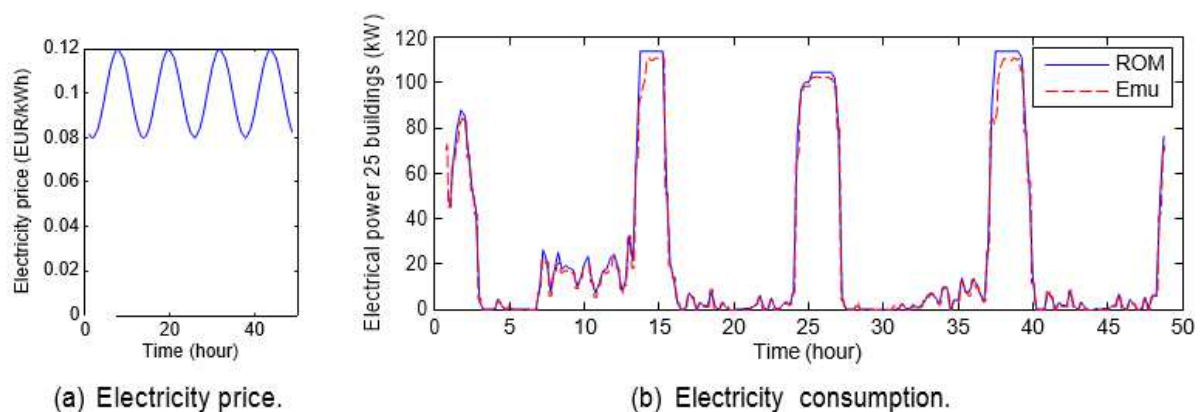


Figure 8: The variation in electricity price (left) induces a reaction of the reduced order model (right). The emulator model (Emu) is not always able to attain the electricity consumption that the reduced order model (ROM) determined.

ROM. This tracking performs well (Figure 8(b)), except when the electricity demand peaks significantly. The emulator model is not able to attain this electric power, especially when starting up. This causes the total electricity consumption of the emulator model to be 4.8% lower than that of the ROM.

Discussion reference case. Table 3 shows the deviation of various ROMs compared to the emulator model. The RMSE on the electric power is about 200W per building, which is acceptable given the average power usage of 3500W per building when a heat pump is switched on. In the reference case, the deviation of the indoor operative temperature is about 0.8°C. Do note that the deviation of the building linear model with respect to the emulator model is already 0.3°C (Reynders et al., 2014) (Figure 3). The addition of a ROM for the heating system seems to increase the error on the indoor operative temperature. The DHW tank temperature in the emulator model was usually about 2.7°C lower than in the ROM, but this did not have a large effect on DWH comfort.

Results and discussion of comparison with other ROM options. Table 3 shows the deviation of various ROM options compared to the emulator model. The cases presented are variations of some aspects of the ROM. There are two other linear models, namely the 'No radiator' case, which leaves out the radiator model, and the 'Constant COP' case, which takes a constant COP

Table 3: Four results of the verification, the first three being the root mean square errors (RMSE) on electric power[W/building]-indoor operative temperature[°C]-DHW tank temperature[°C] and the last being the calculation time of the ROM optimization [sec]. These quantities are shown for two chosen time steps (15 and 60 minutes).

Time step	15 min	60 min
Reference	208-0.80-2.75-8	375-0.71-3.50-1
Noradiator	170-0.90-2.70-5	320-1.05-3.36-1
Constant COP	195-0.73-2.54-6	380-0.60-2.55-1
DHW tank integer	217-0.81-2.62-7200	425-0.70-3.16-7200
Switch SH/DHW	185-0.77-3.01-7200	290-0.70-1.96-7200
Modulation	210-0.71-2.80-7200	(150-0.74-1.35-20)

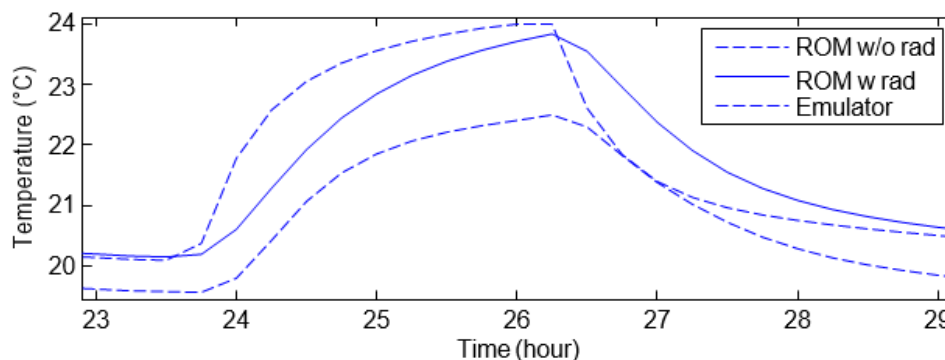


Figure 9: The indoor operative temperature in the case of the reduced order model with (w) and without (w/o) a radiator model included. The ROM without radiator overestimates the rate at which the indoor temperature can rise and drop.

instead of a COP as a function of the ambient air temperature. The other cases include integer variables. In the 'DHW tank integer' case, the higher limit for the DHW tank temperature is given by equations (22)-(23). The 'Switch SH/DHW' case introduces one integer variable to force the heat pump to supply either SH or DHW during a time step. In the final 'Modulation' model, the heat pump model includes boundaries for minimal modulation as given by equations (12)-(15). Table 3 shows that using a smaller time-step lowers the root mean square error (RMSE) on the electric power, but does not always lower the RMSE on the temperatures.

As radiators have a relatively small time constant compared to that of the building structure, one could suggest to neglect its thermal capacity. Leaving out the radiator lowers the error on the electric power but increases the error on the indoor temperature significantly. As figure 9 shows, this increase is mainly due to different dynamical behaviour, which can be explained by the absence of the thermal capacitance associated to the emission system. Hence the radiator model is not negligible for the dynamic aspects of the model.

Figure 10 shows the COP of the emulator model as compared to that of the ROM with variable COP. Note the large peaks in COP of the former model when the heat pump is switched on. This is because the distribution pipes are still cold at this point in time, allowing a high thermal power at condenser side. A part of this gain in COP is thus directly lost due to intermittent heating of these distribution pipes. As can be seen in Table 3, using a constant COP (3.8 for space heating and 2.4 for DHW) has an overall positive impact on the performance of the ROM, albeit limited in some cases. This is because the constant COP model approximates the COP of the emulator heat pump model 4% better than the reference case. Note that this constant COP

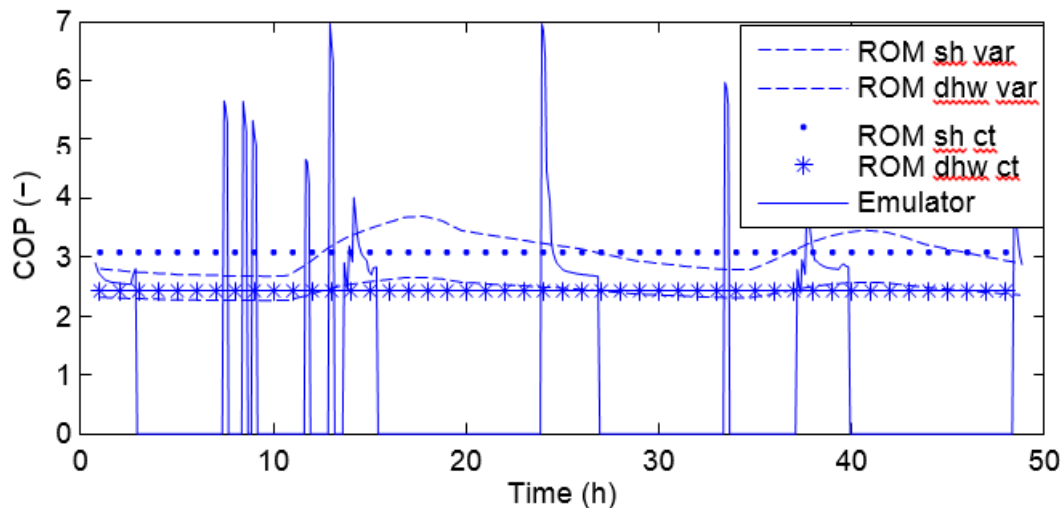


Figure 10: The COP in the reference ROM is either a function of the ambient temperature (var) or constant (ct). As the optimization sometimes chooses to operate the heat pump for only fifteen minutes, the COP in the emulator model can become very high. However, a part of this extra produced heat is lost when the heat distribution system cools down again.

is the average of the COP in the reference case, which changes as a function of the ambient air temperature. The results of the COP are in line with Verhelst et al. (2012), who studied multiple COP formulations, from which there were two linear representations: a constant COP and a COP that is function of the ambient air temperature only. When no electricity price profile was considered, a constant COP formulation performed better, since this formulation did not cause peaks in the electric power of the heat pump. When an optimization towards minimal cost was considered, both COP formulations performed equally.

The cases with integer variables 'DHW tank integer', 'Switch SH/DHW' and 'Modulation' do not show a significant improvement to the performance of the reference model (Table 3). The far longer calculation time (in most cases the maximum calculation time of 7200 seconds) is not worth the minor extra detail these integer variables add. Another possible advantage of the 'Modulation' case, namely the abolishment of a post-processing phase as the electricity usage is conform with the real heat pump constraints, is questionable. The linear reference model (8 seconds) with post processing as discussed in section 3.2.2 (5 seconds) takes up 13 seconds in total, which is a lot faster than the 'Modulation' model.

The results for the case 'Modulation' with a time-step of 60 minutes are put between brackets because it is a special case. When the heat pump would operate at its lower modulation limit (30% of maximal power) for an hour to supply hot water to the DHW tank, the temperature would exceed the upper limit. So the solution attained is one in which the back-up electrical resistance heater covers all DHW demand. As one can note from the table, the model for this alternative heating performs well for the DHW tank temperature.

4.2 Performance of aggregation

As explained in section 3.3, the aim of the aggregation is reducing the number of building ROMs needed. 100 building models with a different number of inhabitants and different user behaviour are aggregated to 6 building models. The way to determine the accuracy of this aggregated model, is to examine whether it attains the same total electricity cost with respect to an identical electricity price profile. Figure 11(a) shows how the total electricity cost per dwelling changes with respect to a higher amplitude of a sine wave electricity price profile

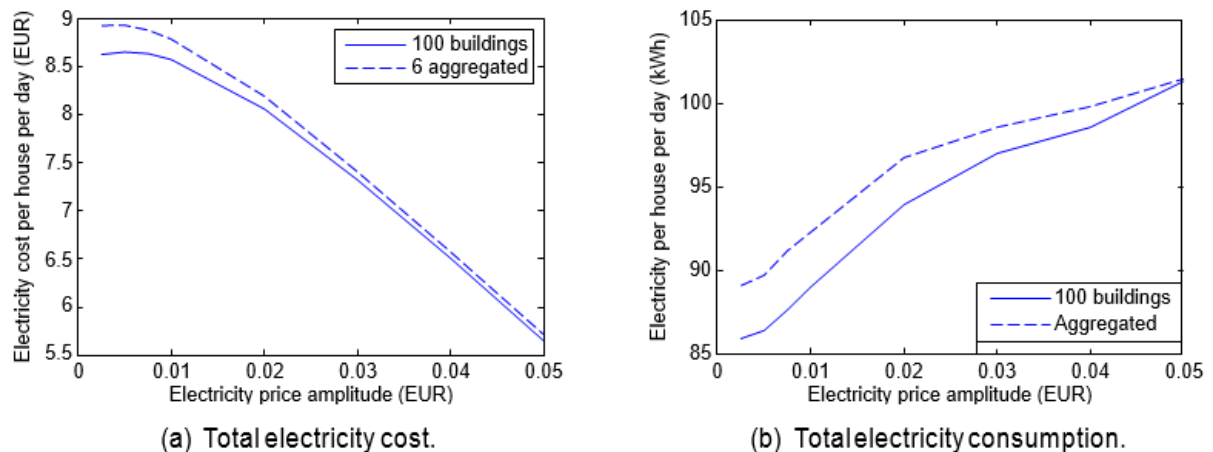


Figure 11: The total electricity cost per dwelling in case of the original model consisting of 100 buildings and the aggregated model consisting of 6 buildings. In the aggregated case, the total cost is about 1% to 3.5% higher than is possible to attain with the larger cluster of buildings.

around a mean price of $0.10 \frac{\text{EUR}}{\text{kWh}}$. As this amplitude increases, the building structure and DHW tank are increasingly used as energy storage, lowering total electricity cost. The aggregated building model shows the same trend, and predicts this cost with an error between 1% and 3.5%. This decrease in total electricity cost has the downside of increasing the energy consumption, as figure 11(b) shows. The electricity consumption of the aggregated model also shows the same trend, being between 0.5% and 4% higher than in the original model.

The comparison between the 100 buildings model and the aggregated 6 buildings model was also performed for random and wholesale market profiles on top of the sine wave electricity price profiles. Figure 12 plots the relative difference in total electricity cost and mean indoor operative and DHW tank temperature between the aggregated and the original model. The aggregated model overestimates the total electricity cost with about 1% to 3.5%, the indoor temperature with -2% to 2% and the DHW tank temperature with 4% to 8%.

A check was also performed, whether the 100 buildings model would be able to track the electricity usage of the aggregated model. This was performed for all price profiles, by minimizing the deviation given the constraints of the 100 buildings model. This check proved to be successful: the deviation on the profile is lower than 0.1%.

Discussion The model with 100 buildings has a slightly higher potential for DSM than the aggregated model: it can lower the electricity cost per building and attain lower energy losses in doing so. This is because the model with 100 buildings has more options to shift some energy demand, as there will always be more opportunities to make a small change in very specific cases. Nevertheless the aggregated model comes very close to the larger model. Since the aggregated model always overestimates electricity cost and consumption, one could say that the aggregated model can act as a lower boundary for the performance of the larger model. In other words, the aggregated model is always a small underestimation of the flexibility potential.

5. CONCLUSION

The aim of this paper is to present a verified, aggregated building stock model, useful for studying the potential of DSM programmes for residences equipped with heat pumps. The mathematical form of the model is chosen such that it can be combined with electricity generation park models (Bruninx et al., 2013). Multiple reduced order models were studied, where the fully linear model with radiator model, constant COP and linear formulation of heat

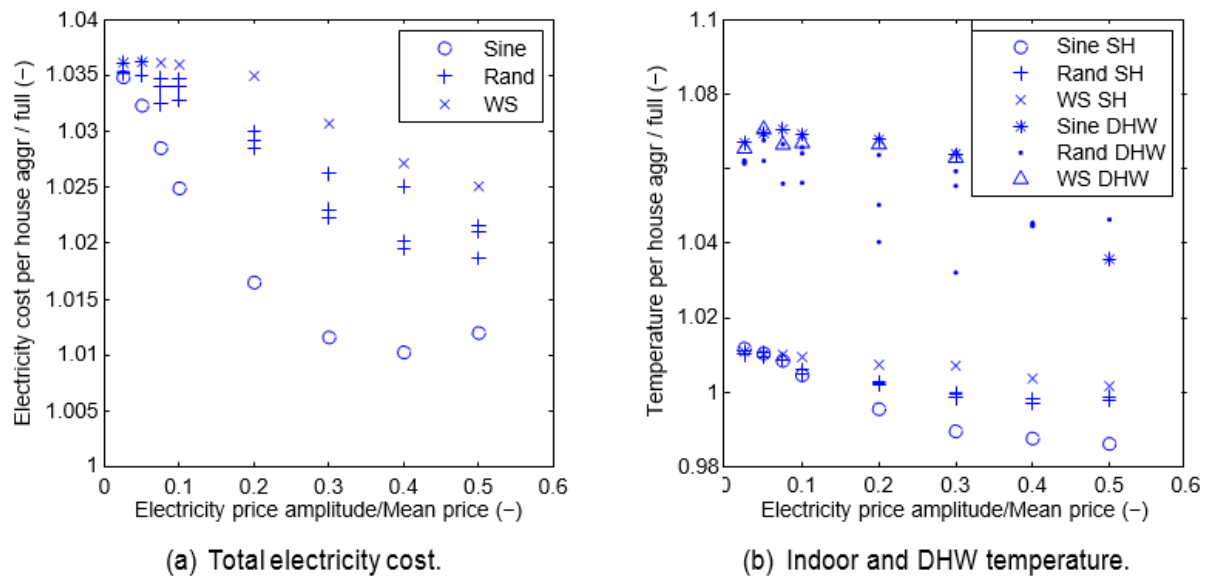


Figure 12: Difference in total cost, indoor operative temperature (SH) and DHW tank temperature (DHW) in the aggregated case of 6 buildings compared to that of the original model with a 100 buildings. This comparison was done for multiple price profiles with a certain amplitude and a shape based on a sine wave (sine), random (rand) or wholesale market prices (WS).

pump modulation and DHW tank constraint performed the best. This is because of its favourable computation time and smallest deviation with respect to the detailed physical emulator model: 0.8°C on the indoor operative temperature and 2.7°C on the DHW tank temperature. The output of this fully linear model is convertible to control signals to be applied to the physical emulator model or a real-life implementation by a post-processing method discussed in this paper. Additionally, an aggregation method was presented, which is able to reduce the number of buildings needed in order to represent multiple user behaviours. This aggregated model can act as a worst case for the performance of a large cluster of buildings, as it overestimates the costs with 1% to 4%.

ACKNOWLEDGEMENTS

The author, Dieter Patteeuw, gratefully acknowledges the KU Leuven for funding his work in the framework of a PhD within the GOA project on a 'Fundamental study of a greenhouse gas emission-free energy system'.

REFERENCES

- Baetens, R., De Coninck, R., Van Roy, J., Verbruggen, B., Driesen, J., Helsen, L., & Saelens, D. (2012, August). Assessing electrical bottlenecks at feeder level for residential net zero-energy buildings by integrated system simulation. *Applied Energy*, 96, 74–83.
- Barton, J., Huang, S., Infield, D., Leach, M., Ogunkunle, D., Torriti, J., & Thomson, M. (2013, January). The evolution of electricity demand and the role for demand side participation, in buildings and transport. *Energy Policy*, 52, 85–102.
- Bruninx, K., Patteeuw, D., Delarue, E., Helsen, L., & D'haeseleer, W. (2013). Short-term demand response of flexible electric heating systems: the need for integrated simulations. In *European Energy Market (EEM), 2013 10th international conference on the* (pp. 1– 10).

Callaway, D. S. (2009, May). Tapping the energy storage potential in electric loads to deliver load following and regulation, with application to wind energy. *Energy Conversion and Management*, 50(5), 1389–1400.

Code van goede praktijk voor de toepassing van warmtepompsystemen in de woningbouw [Computer software manual]. (2004).

Cyx, W., Renders, N., Van Holm, M., & Verbeke, S. (2011). IEE TABULA - typology approach for building stock energy assessment. (Tech. Rep.). VITO, Belgium (BE).

De Coninck, R., Baetens, R., Saelens, D., Woyte, A., & Helsen, L. (2014, July). Rule-based demand-side management of domestic hot water production with heat pumps in zero energy neighbourhoods. *Journal of Building Performance Simulation*, 7(4), 271–288.

FOD economy Belgium. (2008). Structuur van de bevolking volgens huishoudens: per jaar, gewest en aantal kinderen. Online: <http://statbel.fgov.be/nl/statistieken/cijfers/bevolking/>.

Gellings, C. W. (1985). The concept of demand-side management for electric utilities. *Proceedings of the IEEE*, 73(10), 1468–1470.

Good, N., Navarro-espinosa, A., Mancarella, P., & Karangelos, E. (2013, May). Participation of electric heat pump resources in electricity markets under uncertainty. In 10th international conference on the European Energy Market (EEM).

Hedegaard, K., & Balyk, O. (2013, October). Energy system investment model incorporating heat pumps with thermal storage in buildings and buffer tanks. *Energy*, 63, 356–365.

Hedegaard, K., Mathiesen, B. V., Lund, H., & Heiselberg, P. (2012, November). Wind power integration using individual heat pumps - analysis of different heat storage options. *Energy*, 47(1), 284–293.

Henze, G. P., Felsmann, C., & Knabe, G. (2004). Evaluation of optimal control for active and passive building thermal storage. *International Journal of Thermal Sciences*, 43(2), 173–183.

Judkoff, R., & Neymark, J. (1995). International energy agency building energy simulation test (BESTEST) and diagnostic method (Tech. Rep.). National Renewable Energy Lab., Golden, CO (US).

Kamgarpour, M., Ellen, C., Esmaeil, S., Soudjani, Z., Gerwinn, S., Mathieu, J. L., Fr, M. (2013, August). Modeling options for demand side participation of thermostatically controlled loads. In Symposium-bulk power system dynamics and control -ix (IREP).

Kelly, N. J., Tuohy, P. G., & Hawkes, A. D. (2013). Performance assessment of tariff-based air source heat pump load shifting in a UK detached dwelling featuring phase change-enhanced buffering. *Applied Thermal Engineering*.

Kersting, W. H. (2012). *Distribution system modeling and analysis*. CRC press.

Koch, T., Achterberg, T., Andersen, E., Bastert, O., Berthold, T., Bixby, R. E., Wolter, K. (2011). Miplib 2010. *Mathematical Programming Computation*, 3(2), 103–163.

Kok, K., Roossien, B., Macdougall, P., van Pruissen, O., Venekamp, G., Kamphuis, R., . . .

Warmer, C. (2012, July). Dynamic pricing by scalable energy management systems-field experiences and simulation results using powermatcher. In Power and energy society general meeting.

Kondoh, J., Lu, N., Member, S., & Hammerstrom, D. J. (2011, July). An evaluation of the water heater load potential for providing regulation service. In Power and energy society general meeting.

9th International Conference on System Simulation in Buildings, Liege, December 10-12, 2014

- Kosek, A. M., Costanzo, G. T., Bindner, H. W., & Gehrke, O. (2013). An overview of demand side management control schemes for buildings in smart grids. In *Smart energy grid engineering (SEGE)*, 2013 IEEE international conference on (pp. 1–9).
- Long, H., Xu, R., & He, J. (2011, October). Incorporating the Variability of Wind Power with Electric Heat Pumps. *Energies*, 4(10), 1748–1762.
- Lu, N., & Vanouni, M. (2013, November). Passive energy storage using distributed electric loads with thermal storage. *Journal of Modern Power Systems and Clean Energy*.
- Malhame, R. (1985, September). Electric load model synthesis by diffusion approximation of a high-order hybrid-state stochastic system. *IEEE Transactions on Automatic Control*, 30(9), 854–860.
- Mathieu, J., Dyson, M., & Callaway, D. (2012, August). Using residential electric loads for fast demand response: The potential resource and revenues, the costs, and policy recommendations. In *ACEEE summer study on energy efficiency in buildings*.
- Meibom, P., Kiviluoma, J., Barth, R., Brand, H., Weber, C., & Larsen, H. V. (2007, July). Value of electric heat boilers and heat pumps for wind power integration. *Wind Energy*, 10(4), 321–337. doi: 10.1002/we.22
- Meteonorm version 6.1 edition 2009 (Tech. Rep.). (2009). Meteotest.
- Muratori, M., Roberts, M. C., Sioshansi, R., Marano, V., & Rizzoni, G. (2013, July). A highly resolved modeling technique to simulate residential power demand. *Applied Energy*, 107, 465–473.
- Patteeuw, D., Bruninx, K., Delarue, E., D’haeseleer, W., & Helsen, L. (2013). Working paper: Short-term demand response of flexible electric heating systems: an integrated model.
- Pedersen, T. S., Andersen, P., Nielsen, K. M., Stær mose, H. L., & Pedersen, P. D. (2011, September). Using heat pump energy storages in the power grid. In *IEEE international conference on control applications (CCA)* (pp. 1106–1111).
- Peeters, L., Dear, R. d., Hensen, J., & D’haeseleer, W. (2009). Thermal comfort in residential buildings: comfort values and scales for building energy simulation. *Applied Energy*, 86(5), 772–780.
- Peuser, F., Remmers, K.-H., & Schnauss, M. (2010). *Solar thermal systems, succesful planning and construction*. Berlin, Germany: Beuth Verlag GmbH.
- Reynders, G., Diriken, J., & Saelens, D. (2014). Quality of grey-box models and identified parameters as function of the accuracy of input and observation signals. *Energy and Buildings*, 82, 263–274.
- Richardson, I., Thomson, M., & Infield, D. (2008). A high-resolution domestic building occupancy model for energy demand simulations. *Energy and Buildings*, 40(8), 1560–1566.
- Strbac, G. (2008). Demand side management: Benefits and challenges. *Energy Policy*, 36(12), 4419–4426.
- Verhelst, C., Logist, F., Van Impe, J., & Helsen, L. (2012). Study of the optimal control problem formulation for modulating air-to-water heat pumps connected to a residential floor heating system. *Energy and Buildings*, 45, 43–53.
- Wang, D., Parkinson, S., Miao, W., Jia, H., Crawford, C., & Djilali, N. (2012, January). Online voltage security assessment considering comfort-constrained demand response control of distributed heat pump systems. *Applied Energy*, 96, 104–114.

EIGHTH SESSION
**ADVANCES IN COMPONENT
MODELING**

Finite cylinder-source model for pile/borehole heat exchangers: effects of temperature response to time varying thermal load

Tatyana V. Bandos^{1,3}, Álvaro Campos-Celador², Luis M. López González³,
José M. Sala Lizárraga^{1,2}

⁽¹⁾Dpto. de Máquinas y Motores Térmicos, University of the Basque Country UPV/EHU, Bilbao, Spain.

⁽²⁾Grupo de Investigación ENEDI, Dpto. de Máquinas y Motores Térmicos, University of the Basque Country UPV/EHU, Spain.

⁽³⁾Grupo de Investigación GI-TENECO, Universidad de La Rioja, Spain.

1. ABSTRACT

Analytical and simulation models of ground heat exchangers (GHE) are necessary for proper sizing piles with smaller depth to radius ratio than boreholes. Most existing methods of design ignore the transient thermal processes within the piles or boreholes: some software programs are based on the classical “hollow” cylindrical surface source or line-source models. In order to take into account thermal capacity of large diameter piles, an integral mean temperature approach is applied to the response induced by “solid” cylinder-source of heat (Man et.al, 2011). The average temperature response to a constant heat rate is reduced to a single integral only by integrating the exact solution over the depth of a finite cylindrical source of heat embedded in ground on a distance D from its surface. The effect of buried depth is examined using the mean solution at the center of a single GHE and a multiple configuration of line-sources. Simple form of the obtained solution is suitable for implementation into a design code. In addition, exact mean temperature response to time-varying heat rate is also provided in the closed form.

Keywords: Ground Heat Exchangers, Energy Piles, Borehole Heat Exchangers, Ground Coupled Heat Pumps

2. INTRODUCTION

A ground coupled heat pumps (GCHP) is one of the sustainable energy technologies for heating and cooling buildings. A ground heat exchanger consists of U-tube positioned in the center of borehole and is connected to a heat pump through which a heat-carrier fluid is circulated. Long-term financial reward and space requirements retard wide spread of the GCHP systems. Heat exchangers in foundations or energy piles are an alternative to more expensive ground heat exchangers used in ground-source heat pump systems for nearby buildings.

Further development of simulation models of energy piles is desirable for proper sizing piles with smaller depth to radius ratio than boreholes (Xing et al., 2011). Most existing methods of design ignore the transient thermal processes within the piles or boreholes: some commercial software is based on the traditional “hollow” cylindrical surface source (Carslaw and Jaeger, 1959; Kavanaugh and Rafferty, 1997) or line-source (Eskilson, 1987) models. However, the thermal capacity of large diameter piles that can be used as a temporal storage of thermal energy needs to be taken into account (Claesson and Javed, 2011; Cimmino et al., 2013; Loveridge and Powrie, 2013). To overcome this drawback, one can use so-called “solid” cylinder-source of heat (Man et al., 2010) that models a foundation pile covered by tubes with heat-carrier fluid as either infinite or finite cylindrical surface of heat; in the later case, pile wall temperature is evaluated at middle point of its depth.

For the design purpose the best solution is to use an average temperature (Zeng et al, 2002) and it was developed on the base of analytical solution for finite line-source (Lamarche and Beauchamp, 2007; Bandos et. al, 2009a; Claesson and Javed, 2011) and finite cylinder-source (FCS), starting from the ground surface (Bandos et al., 2014). However, currently an average temperature field can only be determined by means of further numerical integration of the solution to finite “solid” cylinder-source model of buried ground heat exchanger (GHE) over its thermo-active length.

This study develops the mean integral approach to analyze pile modeled as finite cylindrical surface source of heat, which is located on a finite distance D from the ground surface. The effect of buried depth was examined by the mean line-source method (Cimmino et al, 2013), though analysis by the mean FCS method is highly desirable to account for inside thermal capacity of energy piles. Furthermore, there are approaches of combining solution to a number of different short-term models and mean solution for temperature response to FLS model for long times (Claesson and Javed, 2011; Loveridge and Powrie, 2013; Kim et al, 2014). The short-term response can be described accurately from the infinite or finite “solid” cylinder-source models, while the long-term temperature response converges to one from the finite line-source (FLS) of constant heat rate. At larger time scales our proposal is to use mean solution to the FCS, instead of one based on the FLS, in particular, when coupling to a model of the interior of a buried pile/borehole for early times.

Ground heat transfer from a time-varying line-source has solution in the form of the double integral and the CPU cost of its evaluation is prohibitively high. To mitigate this problem the transient z -dependent FLS solution was approximated to a single integral for sinusoidal variations of the heat rate (Duan and Naterer, 2008). However, it is still desirable to have the mean temperature response to a variable heat rate from the cylinder-source. One of the aims of this paper is to modify cylinder-source solution for time-varying rate from the triple to a single integral form.

This paper presents: (i) analytical expression for the mean temperature response to buried FCS of constant heat flow; and (ii) exact analytical solution for the mean thermal response function (G -function) to buried FCS that allows arbitrary heat flow variations, and formula for quasi-steady behavior of temperature response to periodic cylinder-source of heat. The limitations of the mean temperature approach to design of buried GHE are discussed in terms of different geometries from borehole to pile heat exchangers since the algorithm is highly configurable by user who can select radius of cylindrical source of heat.

3. FINITE CYLINDRICAL SURFACE SOURCE OF HEAT: MEAN TRANSIENT TEMPERATURE

3.1 Temperature response from finite cylinder-source at a constant heat rate buried under the ground surface

For the analysis of thermal response to the heat source, the ground is assumed to be a homogeneous semi-infinite medium characterized by its thermal conductivity λ , thermal diffusivity α , which are assumed to be the same for the external and internal heat conduction problem, i.e. for $r_0 < r$, and $r_0 > r$, respectively.

Man et al., 2010 presented the formulation for the finite cylinder-source (FCS) of heat starting at the ground surface, i.e. at $D=0$, and its solution approximating energy pile or borehole. This paper considers heat flow along the vertical cylindrical surface with z axis in the semi-infinite

region; ground surface is kept at zero temperature at the $z=0$. The heat is released at a constant rate q_z from $z=D$ to $z=D+H$ along the borehole or pile, and is transferred by thermal conduction to surroundings with undisturbed temperature T_0 . A vertical cylindrical surface source of heat of radius r_0 starting from the surface at $z=D$ to $z=H+D$ is shown in Fig. 1.

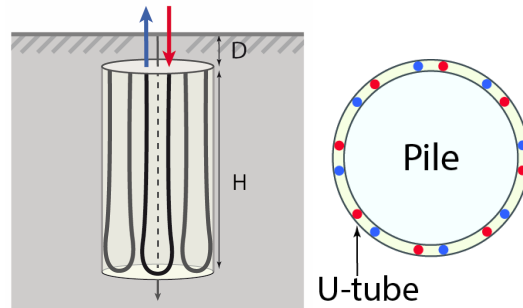


Figure 1: Scheme of thermo-active foundations with vertical U-tubes.

A drawback for applications of the FCS is that the temperature field induced by the heat flow from the cylindrical surface will vary along the thermo-active depth of GHE. The magnitude of this variation increases with approaching the ground surface, and the borehole bottom, attaining minimum value around the mid-point. However, selection of a point for estimation may result in a significant error. The mean temperature approach allows to solve this problem also for this cylindrical model of the heat source.

Typically one applies a so-called g -function introduced by Eskilson (1987), which represents the temperature response of line-source at GHE wall to a heat pulse at the mid-depth. Using the same scale, we define G -function as follows

$$\langle T(r, r_0, t) - T_0 \rangle = \frac{1}{H} \int_D^{H+D} (T(z, r, t) - T_0) dz = \frac{q_z}{2\pi\lambda} G_{FCS}(r, r_0, t), \quad (1)$$

where G_{FCS} is the dimensionless mean temperature response at radial distance r from the axis of the FCS top distant D from the ground surface. In the FCS model the solution of heat diffusion is invariant under spatial rotation about the z -axis of the vertical borehole or pile. The new exact solution for the mean temperature response is derived in the following closed form of one-dimensional integral.

$$G_{FCS}(r, r_0, t) = \frac{1}{2} \int_{1/\sqrt{4\alpha t}}^{\infty} S_D(Hu, Du) I_0(2u^2 r r_0) e^{-u^2(r^2+r_0^2)} \frac{du}{u} \quad (2)$$

where I_0 denotes the modified Bessel function of the zero-th order, and

$$S_D(h, d) = \frac{2}{h\sqrt{\pi}} \int_d^{h+d} \int_d^{h+d} \left[e^{-(z-z')^2} - e^{-(z+z')^2} \right] dz dz' \quad (3)$$

Then integrating the first term results in the following D -independent function

$$L(h) = \frac{2}{h\sqrt{\pi}} \int_d^{h+d} \int_d^{h+d} e^{-(z-z')^2} dz dz' = 2 \cdot \text{erf}(h) - 2 \frac{1 - e^{-h^2}}{h\sqrt{\pi}} \quad (4)$$

and the above double integral can be expressed in the following form

$$S_D(h, d) = L(h) - L(2d)D/H - L(2d + 2h)(D/H + 1) + L(2d + h)(2D/H + 1), \quad (5)$$

where the function $L(h)$ is related to the integral from the error function $\text{ierf}(h)$ as: $2hL(h) = \text{ierf}(h)$. The latter function was introduced for the mean finite line-source (FLS) solution by Claesson and Javed (2011), which is recovered by our solution to the buried FCS if $r_0 = 0$ because of the $I_0(0) = 0$ in Eq.(2). In the long-term limit the FCS solution approaches the FLS one as expected. This integral mean FLS solution has proved to be especially useful as a base for the overall solution including a short-term radial solution for vertical GHEs developed by Claesson and Javed (2011) for numerical simulations. However, a problem occurs when approximating solution of the short-term model by solution of the FLS: they don't intercept. That is due to the fact that the line-source model underestimates the temperature response and then requires adding a positive constant to find a breaking time in the range between short- and long-term scales (Claesson and Javed, 2011). As a by-product, this drawback might be overcome by the usage of the mean FCS solution properly accounting thermal capacity of the GHE itself, as it was shown for $D=0$ by the authors. This paper proposes to use the mean FCS solution instead of the FLS for GHE buried at any depth.

It is worth noting that the proposed mean solution in the form of a single integral is not more complex than one for the z -dependent temperature (Cui et al., 2011), but includes properly the effects of the ground surface and the deep earth. Furthermore, the solution from the FCS at $r=0$ is equivalent to that from the FLS located at the radius $r=r_0$. Indeed, the modified Bessel function $I_0(x)$ is characterized by the property: $I_0(0) = 0$, so that the exact value of G_{FCS} function at the center $r=0$ coincides with that G_{FLS} obtained from the FLS model at $r=r_0$

$$G_{FCS}(r=0, r_0, t) = G_{FLS}(r=r_0, t) \quad (6)$$

Fig. 2(a) gives a comparison between the time-dependence of the temperature responses calculated at $r=0$ from the finite cylinder-source models for a deep GHE in the semi-infinite medium. Inspection of the temperature response curves for a single pile center, shown in Fig.2 (a) allows to conclude that the time of attaining steady-state at a single pile center depends on the buried depth: the G -functions converge with increasing the D . The mean temperature response from the GHE at large distance from the ground surface, $D/H=10$, attains its steady-state slower than one at $D/H=0$: the process of reaching steady-state limit (SSL) starts to slow over time with buried depth D increase and then stops changing at $D \gg H$. Therefore, the lower and upper bound solutions correspond to $D=0$ and $D=\infty$, respectively, whereas the solution for FCS at any D lies between these limits. It also follows from Eq.(2) and (3), that the difference between the temperature response from GHE buried at arbitrary depth and $D=0$ is within the range that may be expressed as

$$G_{FCS}(D \rightarrow \infty) - G_{FCS}(D=0) = \frac{1}{2} \int_{1/\sqrt{4\alpha t}}^{\infty} (L(2Hu) - L(Hu)) I_0(2u^2 r r_0) e^{-u^2(r^2+r_0^2)} \frac{du}{u}. \quad (7)$$

The thermal effect of buried depth varies with the pile aspect ratio H/r_0 as well at different radial positions.

Fig. 2 (b) and (c) show how the FCS mid-point temperature attains steady-state limit (SSL) at $r=0$ in a semi-infinite medium with Dirichlet boundary condition imposed on the ground surface ($z=0$) and in an infinite- medium with Neuman boundary condition at the middle $z=0$, respectively.

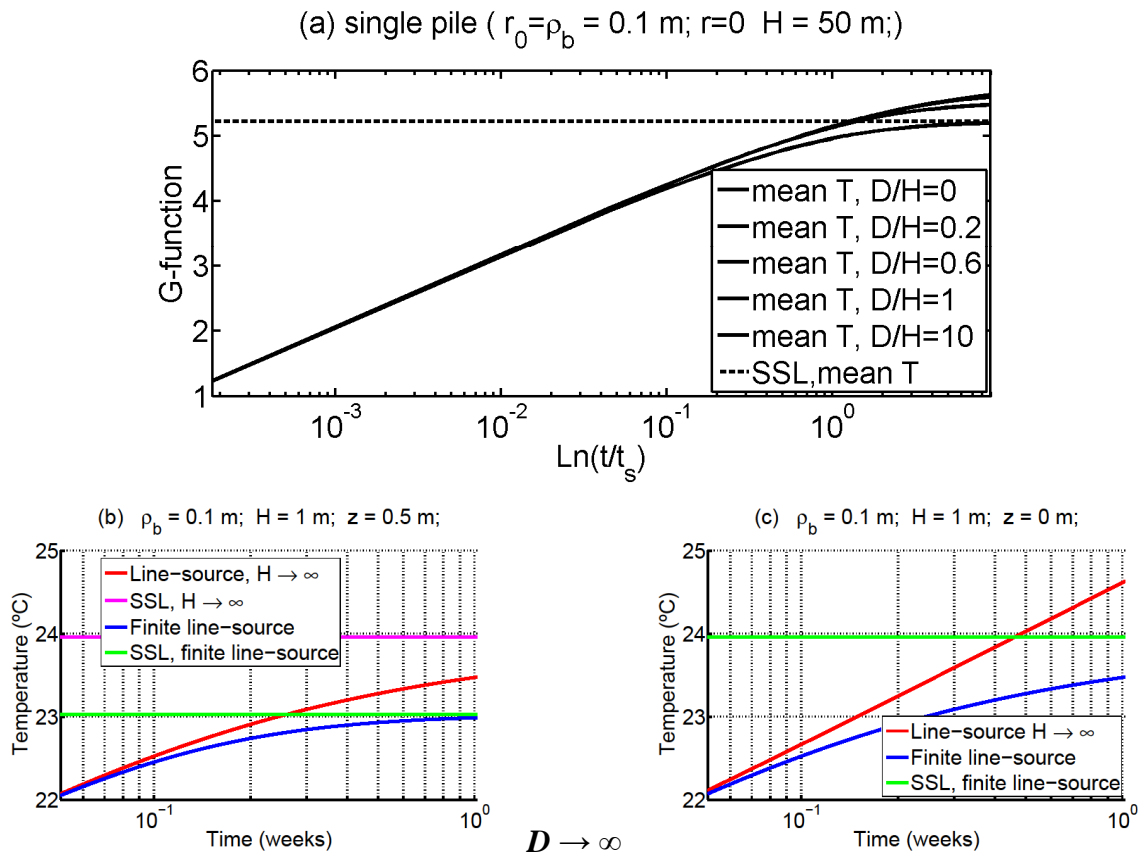


Figure 2: Temperature response ($^{\circ}\text{C}$) for a deep (a) and a shallow (b, c) ground heat exchanger (GHE) at $r=0$ versus the time in semi-log scale from four models: mean temperature from the finite cylinder-source (FCS) model in the semi-infinite medium for $D=0, \dots, \infty$ (a) and for $D=0$ temperature at $z=H/2$ (red line) and its steady-state limit (SSL) (magenta line) from the semi-infinite cylinder-source model, mid-point temperature (blue line) and its SSL (green line) from the FCS model in the semi-infinite medium (b); for $D=\infty$ z -independent temperature (red line) from the infinite cylinder-source (ICS) model, mid-point temperature at $z=0$ (blue line) and its SSL (green line) from the FCS model in an infinite medium (c).

Here the (semi-)infinite cylinder-source model in the (semi-)infinite medium is only provided for comparison with the finite cylinder-source model at $r=0$; in the following it will not be considered. Fig. 2(b) shows that the ground temperature values from the FCS are smaller than those from the semi-infinite cylinder-source model when approaching steady-state. Moreover, the FCS model predicts a different time-asymptotic approach to the SSL because of the influence of the heat flow from the bottom of the borehole. The solution at the mid-point of the GHE based on the FCS with $D=0$, shown in Fig.2 (b), attains its steady state faster than one might expect using the one based on the FCS buried at $D=\infty$, plotted in Fig.2(c). Figs.2 (b) and 2(c) show comparison between the FCS solution obeying the Dirichlet boundary condition on the ground surface and the one obeying the zero heat flow condition on the middle of the FCS, when D tends to infinity. In the latter case the heat is released from $z=-H/2$ to $z=H/2$ along the vertical cylindrical surface. The solutions calculated at $r=0$ by the finite and infinite cylinder-source model in the infinite medium are compared in Fig.2(c). The following parameters were set in the numerical calculations for Figs.2 (b) and 2(c): $\alpha = 1.62 \cdot 10^{-6} \text{m}^2/\text{s}$, $\lambda = 4.3 \text{ W}/(\text{m K})$, $q_z = 46.32 \text{ W}/\text{m}$, $T_0 = 20^{\circ}\text{C}$. Comparison between two mid-point FCS models at the same parameters demonstrates that the SSL of 23°C is already reached by the shallow GHE system starting at $z=0$, i.e. $D=0$, see Fig. 2(b), while this GHE system at $D=\infty$ is still far from the SSL of 24°C as shown in Fig. 2(c). Selected values of parameters, in particular

thermal diffusivity, influence the onset of the long-term behavior for temperature inside the pile and its surroundings, absolute values of the temperatures, but the results of the comparison between GHE starting at the ground surface and infinitely buried GHE remain the same.

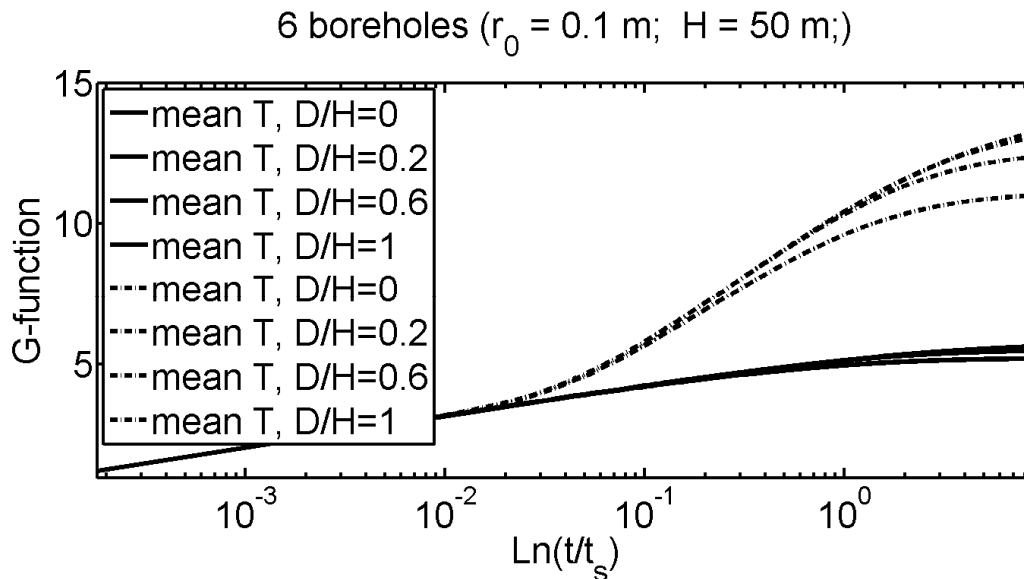


Figure 3: G -functions for a single GHE center compared to thermal response curves for a central borehole from the 2×3 configuration (with an inter-borehole distance B of 3 meters) for different buried depths. Comparison between (1) the mean temperature at the center for the single GHE (solid line) and (2) the mean temperature for the central borehole in the 2×3 configuration (dashed line) at different D values.

The proposed G -function in Eq. (2) can easily be applied to estimate the transient temperature field of an arbitrary borehole configuration using the superposition principle (Carslaw and Jaeger, 1959). The buried depth becomes even more an important factor than for a single GHE when there is heat source interference, since in this case the effect of increasing the temperature response with D accumulates. Fig. 3 compares the differences between the axial temperature of a single borehole for different buried depths from the FCS model and that of a six-borehole pattern for the mean temperatures from the FLS, which can be used for long-time values. The figure shows that the rate of accumulating the effect in time changes noticeably when the heat pulse from the neighboring boreholes reaches a given GHE. The time scale of this heat diffusion is about B^2/α (B is the distance between the nearest boreholes) is significantly less than the steady-state time $t_s = H^2/\alpha$. Fig. 3 illustrates the temperature field calculated as the superposition of the temperature of each borehole with relative depth $r_0/H = 0.002$ for the 2×3 GHE pattern by using Eq.(2). The overall temperature response function remains nearly the same when the buried depth to length ratio is sufficiently large, and therefore, the finite heat source can be considered as embedded in the infinite medium. Accordingly, the thermal interaction between boreholes changes.

3.2 Temperature response from FCS of varying heat rate buried under the ground surface and periodic infinite cylindrical surface source.

In this section a single energy pile or borehole is approximated as a cylinder-source of heat. The new response G -functions for any D can be applied to a varying heat transfer rate by using the superposition principle in time (Carslaw and Jaeger, 1959). This technique is widely used for discrete time intervals in which the heat rate is considered constant (Cimmino et. al, 2013).

In addition, this paper proposes the exact mean solution for the heat conduction problem with the prescribed continuously varying heat rate, $q(t)$, on the surface of the finite cylindrical source buried in the semi-infinite medium, we reduce it to the single integral

$$\langle \Delta T(r, r_0, t) \rangle = \frac{1}{4\pi\lambda} \int_{1/\sqrt{4\alpha t}}^{\infty} q\left(t - \frac{1}{4\alpha u^2}\right) S_D(Hu, Du) I_0(2u^2 r r_0) e^{-u^2(r^2 + r_0^2)} \frac{du}{u}, \quad (8)$$

where the line-sources are distributed round the circle of radius r_0 . For $r_0=0$, this solution recovers the mean thermal response function to the finite line-source with variable heat rate (Bandos et. al, 2009b). If heat rate $q(t)$ is constant and equal to q_z the mean solution is provided in Eq. (2). The lumped approach in the form of convolution integral (8) is alternative to the sum in time steps, which is applied to the products of thermal load and temperature response functions in numerical simulations (Cimmino et. al, 2013). Though the latter approach is common for design of multiple configurations, the proposed analytical solution might be useful in analysis. In general, the overall temperature response developed for semi-infinite medium with a vertical finite cylinder-source of variable heat rate consists of a new temperature response function in Eq.(8) and the solution for time-varying ground surface temperature (Bandos et al., 2009b).

To demonstrate the application of the new solution, a periodic thermal load has been used to calculate a simultaneous temperature response inside and outside the cylindrical surface source. In order to take into account the heat flow oscillations, the varying heat rate function is taken in the form: $q_s \exp(i\omega t)$. In this functional form the time scale $1/\omega$ is related to the frequency ω of the heat-carrier fluid temperature change.

Since $S_D \rightarrow 2$, as $H \rightarrow \infty$ in Eq.(3), the FCS solution in Eq.(2) recovers the solution for the infinite cylinder source (ICS) model (Man et. al, 2010). Separating the influence of the constant heat rate allows to present the solution for varying heat rate $q_s \exp(i\omega t)$ as follows

$$2 \frac{q_s}{4\pi\lambda} \int_{1/\sqrt{4\alpha t}}^{\infty} \exp\left(i\omega\left(t - \frac{1}{4\alpha u^2}\right)\right) I_0(2u^2 r r_0) e^{-u^2(r^2 + r_0^2)} \frac{du}{u}. \quad (9)$$

By making use of the following integral representation $I_0(x) = \frac{1}{\pi} \int_0^\pi d\varphi \exp(-x \cos \varphi)$ the above ICS solution can be approximated in the long-term limit as

$$\frac{q_s}{2\pi\lambda} e^{i\omega t} \frac{1}{\pi} \int_0^\pi K_0\left(\sqrt{2i} \frac{R(\varphi)}{d_p}\right) d\varphi, \quad (10)$$

where $R = \sqrt{r^2 - 2rr_0 \cos \varphi + r_0^2}$ is the distance from the cylindrical surface, K_0 is the modified Bessel function of the second kind of order zero, and $d_p = \delta = \sqrt{2\alpha/\omega}$ is the depth of thermal penetration from the source surface, which naturally appears in the frame of the cylinder-source model. The time-oscillations of temperature response to the ICS provided in Eq.(10) decay outside the pile. Therefore, a significant temperature response is predicted only up to a certain radial distance from the surface of heat source. It is worth noting that for the special case of $r_0 = 0$ the solution (10) reduces to the well-known periodic line-source

(Carslaw and Jaeger, 1959), therefore, it is validated. Effectiveness of heating/cooling in radial direction depends on the heat penetration depth and the radius of the pile or borehole.

4. CONCLUSIONS

New solutions for mean temperature responses from ground coupled heat exchanger (GHE) modeled as a finite cylinder-source (FCS) of constant heat flow have been presented in a single integral form. Buried GHE has been analyzed using upper and lower bound solutions obtained for different distances of GHE top from the ground surface. Temperature response functions for FCS buried at any depth are limited by these solutions corresponding to infinite and zero distances from the ground surface, respectively.

A method of accounting the influence of variable heat rate has been developed for the mean temperature response inside and outside the cylindrical surface of heat source and can be applied in the estimation process of the thermal response test for energy pile. We have provided new approximate expression for the temperature response function to periodic infinite cylinder-source (ICS) at arbitrary radius under quasi-steady conditions. The classical result of the periodic line-source model is recovered as well as the known result for mean temperature response to the buried finite line-source of heat.

Simple form of the obtained FCS and ICS solutions might make it attractive to implement for the design. The thermal effect of daily and annual heat rate fluctuations varies with time and radial position around the energy pile.

This effect of frequency of the heat flow variations is the subject of on-going research by the proposed method.

ACKNOWLEDGEMENTS

This paper has been supported by the Spanish Ministry of Science and Innovation (ENE2012-38633-C03-03).

REFERENCES

- Bandos, T.V., Á. Montero, E. Fernández, J.L.G. Santander, J.M. Isidro, J. Pérez, P.J. Fernández de Córdoba, Urchueguía J.F., 2009a. *Finite line-source model for borehole heat exchangers: effect of vertical temperature variations*, *Geothermics* **38**: 263-270.
- Bandos, T.V., Montero Á., Fernández E., Reig A., Urchueguía J.F., 2009b. *Improvement in the estimating of ground thermal properties from geothermal response tests* In: Proceedings of the 11th International Conference on Thermal Energy Storage, June 14-17, Stockholm, Sweden, Effstock: P **22**: 1-7.
- Bandos, T.V., Á. Campos-Celador, L.M. López-González, J. M. Sala-Lizárraga. 2014. *Finite cylinder-source model for energy pile heat exchangers: effects of thermal storage and vertical temperature variations*, *Energy* **78**: 649-658.
- Bernier, M. A., 2001. *Ground-coupled heat pump system simulation*. ASHRAE Transactions **107**: 605-16.
- Carslaw, H. S., and Jaeger J. C., 1959. *Conduction of Heat in Solids*, Marcel Dekker. Inc, New York.
- Claesson, J., Javed, S., 2011. *An analytical method to calculate borehole fluid temperatures for time scales from minutes to decades*. ASHRAE Transactions, Vol. **117**: 279-288.

- Cimmino, M., Bernier, M., Adams, F., 2013. *A contribution towards the determination of g-functions using the finite line source*. Applied Thermal Engineering, Vol. **51**: 401-412.
- Cui, P., Li, X., Man, Yu., Fang, Z.H., 2011. *Heat transfer analysis of pile geothermal heat exchangers with spiral coils*, Applied Energy **88**: 4113–4119.
- Eskilson P., 1987. *Conductive heat extraction by a deep borehole; analytical studies. Thermal Analysis of Heat Extraction Boreholes*, Dept. of Mathematical Physics University of Lund, (Sweden), pp. 1-26.
- Duan, X., Naterer, G.F., 2008. *Ground thermal response to heat conduction in a power transmission tower foundation*, Heat and Mass Transfer **44**: 547-558.
- Kavanaugh, S. P., Rafferty, K., 1997. *Ground-source heat pumps, design of geothermal systems of commercial and institutional buildings*, Atlanta: ASHRAE.
- Kim, E., Bernier, M., Cauret O., Roux J. 2014. *A hybrid reduced model for borehole heat exchangers over different time-scales and regions*, Energy (in press), <http://dx.doi.org/10.1016/j.energy.2014.08.091>.
- Lamarche L. and Beauchamp B., 2007. *A new contribution to the finite line-source model for geothermal boreholes*. Energy and Buildings, Vol. **39**: 188-198.
- Loveridge, F., Powrie, W. 2013. *Temperature response functions (G-functions) for single pile heat exchangers*. Energy **57**: 554-64.
- Man, Yu., H. Yang, N. Diao, Fang, Z.H. 2010. *A new model and analytical solutions for borehole and pile ground heat exchangers*, International Journal of Heat and Mass Transfer **53**: 2593–2601.
- Xing L., Spitler J.D., Cullin J.R., 2010. *Modeling of foundation heat exchangers*. In: Proceedings of the 8th International Conference on System Simulation in Buildings, Liege, Belgium: P128, 1-9.
- Xing, L., Cullin, J. R., Spitler, J.D., Im ,P., Fisher D.F., 2011. *Modeling of foundation heat exchangers for residential ground source heat pump systems*, HVAC&R Research **17**: 1069-1074.
- Zeng H., Diao N. and Fang Z., 2002. *A finite line-source model for boreholes in geothermal heat exchangers*. Heat Transfer Asian Research, **31**: 558-567.

Table 1: Nomenclature.

D	Distance from the ground surface to the thermo-active part of the borehole [m]
G_{FCS}	Cylindrical thermal response function, Eq.(2)
H	Depth of the GHE [m]
r	Radial coordinate [m]
r_0	Radius of the ground heat exchanger [m]
q_z	Heat flow per length unit [W/m]
$R(=\sqrt{r^2 - 2rr_0 \cos \varphi + r_0^2})$	Distance between the r and point on the cylinder surface in a perpendicular cross section [m]
t	Time [s]
$t_r = r_0^2 / \alpha$	Short time scale for the borehole heat exchanger [s]
$t_s = H^2 / 9\alpha$	Eskilson (1987) steady-state time scale [s]
$t_z = H^2 / \alpha$	Large time scale for the borehole heat exchanger [s]
T	Temperature [K or °C]
T_0	Undisturbed ground temperature [K or °C]
z	Vertical axial coordinate [m]
Greek Letters	
$\alpha = \lambda / C$	Ground thermal diffusivity [m ² /s]
γ	Euler's constant
λ	Ground thermal conductivity [W/(Km)]
Superscripts	
$\langle \dots \rangle (= \frac{1}{H} \int_0^H \dots dz)$	Integral mean

Thermodynamic Modeling of a Membrane Dehumidification System

J. D. Bynum^{1*} and D. E. Claridge²

⁽¹⁾ Eindhoven University of Technology, Eindhoven, The Netherlands

⁽²⁾ Texas A&M University & Energy Systems Laboratory, College Station, TX, USA

1. ABSTRACT

In warm and humid climates, dehumidification is a primary source of building energy use. The proposed membrane dehumidification system utilizes a selective zeolite membrane to remove water vapour from ambient air instead of a vapour compression cycle or a desiccant. A theoretical analysis is used to analyze the impact of different operating parameters and determine performance potential through model simulation. The project sponsor's target dehumidification system COP is 3.34 for 32.2°C (90°F) and 90% relative humidity feed air with outlet conditions of 12.8°C (55°F) and 50% relative humidity. The model simulations show one version of this system can meet this goal with a maximum COP of 3.36.

Keywords: dehumidification, membrane, system modeling

2. INTRODUCTION

In warm and humid climates, a primary source of building energy use is related to dehumidification which is traditionally accomplished by reducing the temperature of the air below the dew point temperature until the desired absolute humidity level is achieved. Commonly, this level is near the 12.8°C (55°F) and 90% relative humidity condition. This approach requires significant sensible as well as latent cooling to remove moisture from the air as shown by the upper process line in the psychrometric chart in Figure 1.

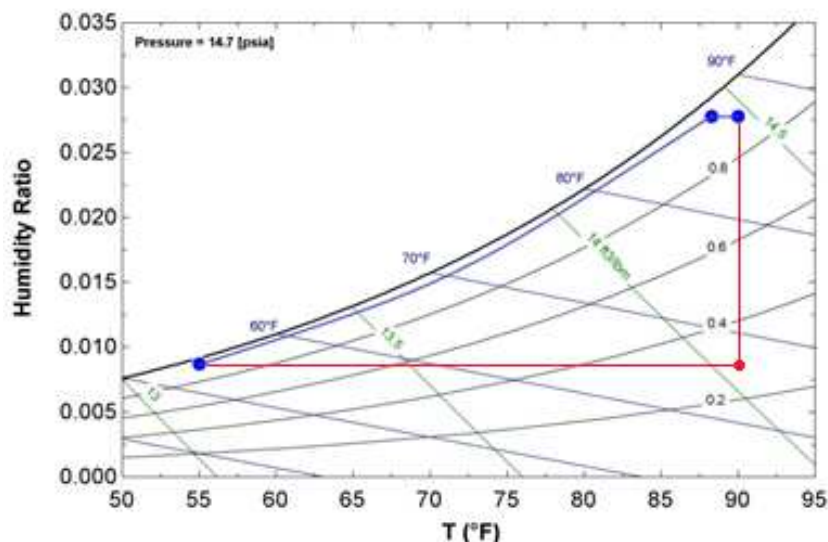


Figure 1: Psychrometric chart showing two dehumidification process paths.

The proposed system utilizes a selective membrane to separate water vapour from the other components in an air stream. Water vapour is continuously removed from an air stream on one side of the membrane and subsequently discharged to atmosphere on the other side. The gas

separation is accomplished via a pressure gradient across the membrane and is a constant temperature process that does not require a heat source for regeneration. By using a selective membrane to dehumidify the air, the sensible and latent cooling of the air stream are decoupled (as shown by the lower process line in Figure 1) so the cooling of the air is not driven by the need for dehumidification.

The components of the proposed system are shown in Figure 2. The dehumidification unit is made up of numerous membrane sections arranged so that a channel is produced where the humid air at point 1_i passes on the outside of the channel until reaching a lower humidity level at state 1_o . The permeated gas at point 2 on the low pressure side of the membrane would be pure water vapour for an ideal membrane, but with real membranes the permeate at point 2 is a mixture of water vapour and air. This mixture is passed to a “compressor” which raises the pressure of the air and water vapour to state 3. The air and water vapour then enter a condenser where a portion of the water vapour is condensed. The air and remaining water vapour simply pass through in gaseous form to state 4. The liquid water is captured in a liquid reservoir and then discharged to the atmosphere (state 5) via a liquid pump. The non-condensable gases (air and some water vapour) are rejected to the atmosphere (state 5) via a vacuum pump.

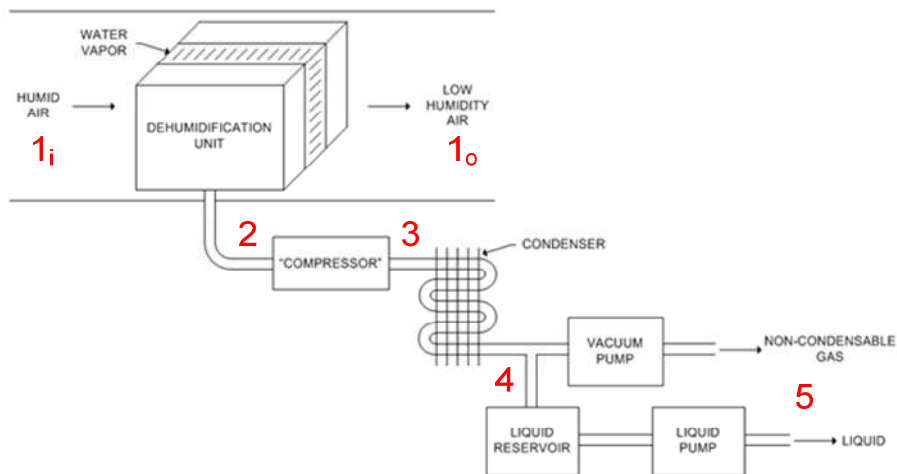


Figure 2: Basic diagram of proposed membrane dehumidification system

This paper identifies the optimum operating parameters of the system such as the pressure on the permeate side of the membrane, the pressure in the condenser, and the optimum cooling method for the condenser for practical levels of membrane selectivity via simulation. All of the simulations discussed in this paper were conducted using the Engineering Equation Solver (EES) software (2013).

3. BACKGROUND

The background is organized into four separate focus areas: membrane gas separation, the condensation of a vapour in the presence of a non-condensable gas, existing building system dehumidification technologies and system performance goals.

3.1 Membrane Separation Processes

Membrane gas separation is accomplished by passing a feed stream of gas mixture across one side of a selective membrane at a pressure which is elevated relative to the pressure on the opposite side of the membrane. The selective membrane is most permeable to one component of the gas mixture in the feed stream which results in a permeate stream that is enriched in that

component of the original mixture. For gas separation, this can be accomplished using both porous and dense membranes (Baker, 2004). Porous membranes are separated into types based on the pore size and the separation mechanism. If the membrane pores are very small (5 to 20 Å), the gases are separated by molecular sieving which is the diffusion of gas molecules through openings that are similar in size to the molecule (Williams and Koros, 2008). For dense membranes, the solution-diffusion model is employed to describe the transport of gases through the membrane. Most current commercial gas separation utilizes dense polymer membranes based on this solution-diffusion model (Williams and Baker, 1995). When the solution-diffusion model is applied to zeolite and ceramic membranes it is sometimes referred to as the adsorption-diffusion model (Sekulic et al., 2005).

Gavalas (2008) describes three methods of quantifying multi-component diffusion: Fick's law, Onsager irreversible thermodynamics and the Maxwell-Stefan method. For binary diffusion, all three of these methods are analogous and have been shown to be equivalent (Wang and LeVan, 2008). The most basic quantitative treatment of binary gas diffusion is given by Fick's law which describes the movement of one species through another species due to a driving force gradient in the particular species of interest (Bird et al, 2002; Incropera and DeWitt, 2002). Fick's law is similar in form to Newton's law of cooling, but instead of the convection coefficient Fick's law utilizes the diffusivity to describe the rate of diffusion. In the simplest version of the Fickian model the driving force for membrane gas separation is the partial pressure difference between the feed and permeate sides (Baker, 2004).

The generalized Maxwell-Stefan theory is most often applied to processes involving gas permeation in recent literature and is based on a microscopic model of the physical effects governing diffusion. The application of the Maxwell-Stefan theory to zeolite membranes in particular has been investigated and found to be superior to the much simpler Fick's law (Krishna and van den Broeke, 1995). Specifically, the Fick's law approach fails to model the flux maximum which has been observed experimentally (van den Broeke and Krishna, 1995). The Maxwell-Stefan method can model this behaviour because it accounts for the variation in the diffusion coefficient that is not included in the Fick's law approach.

3.2 Condensation of a Vapour in the Presence of a Non-Condensable Gas

In the building industry, most vapour condensation processes (other than condensing water vapour from ambient air) occur as part of a conventional vapour compression refrigeration cycle. In these cycles, the refrigerant vapour passes through a heat exchanger where it condenses from a gas to a liquid. The systems are evacuated prior to the refrigerant being added to ensure that the refrigerant is the only component in the system. The analytical study of condensation of pure vapours was first undertaken by Nusselt (1916) who investigated the film condensation of a stationary pure vapour on a vertical flat plate; however, the problem at hand involves a forced convection internal flow condition which has been given much attention with many different correlations available (Carey, 2008). One of the most widely applicable correlations for single component condensation available is that of Shah (1979).

The presence of a non-condensable gas changes the rate of vapour condensation so that it is no longer dependent entirely on Nusselt's condensing mechanism. Under steady state conditions, once a condensate film has formed condensation occurs at the interface of the condensate film and the gas vapour mixture. When the vapour condenses only the non-condensable gas is left at the interface resulting in an increased concentration of non-condensable gas near the interface. Conversely, the concentration of the vapour near the interface is decreased. In order for condensation to occur, the vapour must transfer through the gas film near the interface via diffusion. The reduced partial pressure of the vapour at the interface causes the saturation

temperature of the vapour near the interface to decrease. The result is for the effective thermal driving force, and thereby the net heat transfer, to be reduced due to the reduction in the effective temperature difference.

The earliest design procedure for multi-component condensers was presented by Colburn & Hougen (1934). This is a film method which equates the heat transferred through the condensate, the tube wall, and the cooling-water film to the sum of the sensible heat transferred by cooling the uncondensed gas and the latent heat from the condensed vapour. This method was modified by Bras (1953a; 1953b) to allow for the analysis of superheated mixtures entering the condenser. The Bras method was presented in greater detail and compared to measured results by Stern (1966) and Stern and Votta (1968).

The Colburn & Hougen method is commonly regarded as the most physically accurate of the common design methods but is more difficult to implement than the commonly used Silver, or Silver-Bell, equilibrium method. A recent study (Sacramento-Rivero and Hegggs, 2009) found that the film method used in the Colburn & Hougen methodology is superior to the equilibrium method which underestimates the overall heat transfer coefficient. These results are similar to a previous comparison of the two methods (Webb et al., 1996). Even earlier comparisons by Webb (1990) and McNaught (1981) also found the film method to be more accurate.

3.3 Existing Building System Dehumidification Technologies

There are three conventional methods of removing moisture from air: sorbent dehumidification, refrigerant dehumidification and air-cycle dehumidification (Brundrett, 1987; Rowland and Wendel, 2005). Sorbent dehumidification involves putting the moist air in contact with a solid or liquid which absorbs water due to a change in the physical or chemical structure of the substance. For these systems, no sensible cooling is required to remove the moisture. Refrigerant dehumidification is accomplished by reducing the temperature of the air below the dew point temperature by passing the air through a heat exchanger which is cooled either directly or indirectly via a vapour compression refrigeration cycle. With this system, significant sensible cooling of the moist air must be done before condensation, or latent cooling, occurs. Air-cycle dehumidification is not utilized in the building industry.

In addition to these conventional methods, several researchers have sought to use different types of membranes for dehumidification in buildings. El-Dessouky et al. (2000) proposed a device using tubular ceramic membranes. A similar device for air dehumidification comprised of tubular membrane modules was developed by a separate team from Korea (Song et al., 2008). Supported liquid membranes have been studied in detail by Ito and colleagues (Akira, 2000; Li and Ito, 2008). A detailed description and analysis of the membrane system proposed in this work (as described above) can be found in Bynum (2012).

3.4 System Performance Goals

The goal of this project is to determine the performance capabilities of the proposed membrane dehumidification system. An overall target COP was established by the funding agency (U.S. Department of Energy's Advanced Research Projects Agency – Energy, or ARPA-E) and was given as a thermal COP (COP_{th}) of 1.12 which is the source energy efficiency of the system. The thermal COP value can be converted to a site total performance (COP_{total}) using a simple factor of 3.2 (provided by ARPA-E) resulting in a required total site COP of 3.58 for ambient conditions of 32.2°C (90°F) and 90% relative humidity and system outlet conditions of 12.8°C (55°F) and 50% relative humidity.

To find the sensible and latent cooling, the enthalpies of air at the stated inlet and outlet conditions are used with the required total cooling load of 3.52 kW (1 ton) to find the inlet air flow rate of 40 L/s (85 ft³/min) for the system. Next, the sensible (Q_{sensible}) and latent (Q_{latent}) cooling loads are found using the dry bulb temperature difference and the humidity ratio difference, respectively. The total COP is found from a combination of the latent cooling, sensible cooling, the latent COP ($\text{COP}_{\text{latent}}$) and the sensible COP ($\text{COP}_{\text{sensible}}$) using Equation 1 below.

$$\text{COP}_{\text{total}} = \frac{Q_{\text{sensible}} + Q_{\text{latent}}}{Q_{\text{sensible}}/\text{COP}_{\text{sensible}} + Q_{\text{latent}}/\text{COP}_{\text{latent}}} \quad (1)$$

Using an assumed $\text{COP}_{\text{sensible}}$ of 4.6 the required latent cooling system COP is found to be 3.34. This value will be useful in assessing the size of the membrane required during system design and in assessing the calculated performance of the system.

4. SIMULATION METHODOLOGY, RESULTS AND DISCUSSION

Initially, to assess the performance limits of the proposed system as well as estimate the performance of the real device, several different system models were developed. All of the simulations presented below utilize a simple model of the membrane separation process based on Fick's law. Specifically, three different models were developed: an ideal condenser simulation assuming full water condensation in the condenser, a single-component condenser model assuming only water vapour is present in the condenser and a multi-component condenser model which simulates the real device. In addition to assuming full water condensation in the condenser, the ideal case assumes fully isothermal compression devices and ideal cooling tower performance. The single component condensation model where the air and water vapour are separated prior to entering the condenser was developed to explore the limits of a real condenser. A multi-component condensation model was also developed to provide a basic assessment of the real system performance.

The COP values discussed below represent only the performance of the dehumidification portion of the system with no sensible cooling of the moist air on the unpermeated (i.e. ambient) side of the membrane. As a result, the stated outlet conditions describe only the humidity level of the outlet air while the dry bulb temperature is constant and equal to the inlet temperature as shown with the red vertical line at 32.2°C (90°F) in Figure 1 above.

4.1 Fick's Law Modeling

The model of the mass transfer utilizes a numerical approach which recommends analyzing the membrane as 100 discrete elements (Stern and Wallawender, 1969). Based on this recommendation and the limits of the EES software used for the simulation, the membrane is broken into 100 segments. For each segment, a set of six equations (Equations 2 through 7) is solved to determine the permeate side gas composition.

$$X_{a,2,i} * N_{\text{total},m,i} = A_{m,i} * \tau_a * (P_{oa} * X_{a,h,i} - P_2 * X_{a,2,i}) \quad (2)$$

$$X_{w,2,i} * N_{\text{total},m,i} = A_{m,i} * \tau_w * (P_{oa} * X_{w,h,i} - P_2 * X_{w,2,i}) \quad (3)$$

$$X_{a,h,i-1} * N_{\text{total},h,i-1} = X_{a,h,i} * N_{\text{total},h,i} + X_{a,2,i} * N_{\text{total},m,i} \quad (4)$$

$$X_{w,h,i-1} * N_{\text{total},h,i-1} = X_{w,h,i} * N_{\text{total},h,i} + X_{w,2,i} * N_{\text{total},m,i} \quad (5)$$

$$X_{w,2,i} = 1 - X_{a,2,i} \quad (6)$$

$$X_{w,h,i} = 1 - X_{a,h,i} \quad (7)$$

A diagram of one membrane segment with the related inputs and outputs is shown in Figure 3. Once the analysis has been performed for all 100 segments, the outlet unpermeated stream conditions are calculated as shown below in Equations 8 and 9 where $N_{w,m,total}$ (or $N_{w,2}$) is the water molar flow rate through the entire membrane and $N_{a,m,total}$ (or $N_{a,2}$) is the air molar flow rate through the entire membrane.

$$N_{w,m,total} = \sum_{i=1}^{100} (X_{w,2,i} * N_{total,m,i}) = N_{w,2} \quad (8)$$

$$N_{a,m,total} = \sum_{i=1}^{100} (X_{a,2,i} * N_{total,m,i}) = N_{a,2} \quad (9)$$

For a given set of operating conditions and membrane characteristics, the system of equations outlined above is all that is necessary to determine the low pressure permeate stream and high pressure unpermeated stream compositions. The simulation repeatedly solves the system of equations above for all 100 segments in order to determine the permeate side total pressure that is required in order to obtain the desired unpermeated stream outlet humidity condition.

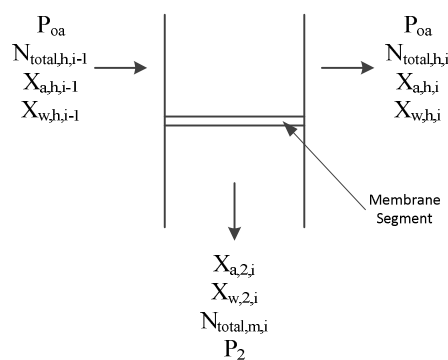


Figure 3: Diagram of membrane mass transfer analysis for one segment

4.2 Membrane Performance Characteristics and Metrics

Using the simple pressure gradient driven form of Fick's law outlined above requires the use of a specific set of units for the membrane characteristics. These units differ from those which are sometimes used for more general descriptions of membrane mass transfer characteristics when the simple pressure gradient driven form of the Fick's law analysis is not appropriate.

The characteristics commonly used to describe membranes in gas separation applications are the permeability, the permeance and the selectivity (Baker et al., 2010). The permeability (P) is the flux of a component through a membrane of unit thickness. When the membrane thickness is not known, the membrane is described using the permeance (τ) which is equal to the permeability divided by the membrane thickness. The permeance is the flux of a species through the membrane normalized by the driving force. The membrane selectivity (α) is simply the ratio of the permeabilities, or permeances, of two components for the given membrane.

For this application, the permeance will be used to describe the membrane mass transfer performance. Using the permeance has a number of advantages including ease of measurement in laboratory testing and the fact that detailed knowledge regarding the membrane thickness is unnecessary. The permeance in this work is reported in units of $\text{mol/m}^2\text{-s-Pa}$.

4.3 Ideal Condenser Simulation

The simplest model of the processing of the permeate stream assumes that all of the water vapour is condensed to liquid form. Condensing the water is advantageous because compressing a liquid to a given pressure (i.e. ambient pressure in this case) requires much less energy than compressing a gas. By condensing the water vapour to liquid first, the mass of gas that must be compressed is minimized and includes only the air that passes through the membrane. The inputs for the ideal condenser analysis are labelled as simulation group A in Table 3.

4.4 Single Component Condenser Simulation

To test the upper limit of the real condenser performance, a model was developed which is not the ideal case and is also not the real case where a water vapour and air mixture enter the condenser. In this case the air simply bypasses the condenser and is mixed with the water vapour again before entering the vacuum pump. This allows for the condenser to deal with a single component (i.e. water vapour) which will presumably increase the amount of water vapour condensed as compared to the real condenser. A general correlation by Shah (1979) was selected for use in modelling the single component condenser. The general form of this correlation is shown in Equation 10 (with the reduced pressure (p_r) defined in Equation 11) where h_{TP} is the two phase region heat transfer coefficient, h_L is the Dittus-Boelter equation heat transfer coefficient, x_{in} is the inlet molar fraction of vapour, p_c is the critical pressure and p is the pressure of the fluid in the inner tube. This condenser consists of 40 sets of concentric tubes 45.7 cm (1.5 ft) long with the cooling water flowing upward in the annulus and the water vapour downward inside the inner tube. The inputs for the single component condenser analysis are labelled as simulation group B in Table 3.

$$h_{TP} = h_L \left[(1 - x_{in})^{0.8} + \frac{3.8 \cdot x_{in}^{0.76} \cdot (1 - x_{in})^{0.04}}{p_r^{0.38}} \right] \quad (10)$$

$$p_r = \frac{p}{p_c} \quad (11)$$

One of the main limitations of the effectiveness of the condenser is the entering cooling water temperature. If an ideal cooling tower is assumed, the entering cooling water temperature will be equal to the ambient wet bulb temperature; however, for a real cooling tower, the minimum entering cooling water temperature will likely be between 2.78°C (5°F) and 5.56°C (10°F) greater than ambient wet bulb temperature (this difference is the cooling tower approach temperature).

Four combinations of water permeance, air permeance and membrane area were chosen for operational analysis using Houston, TX, USA, bin weather data for the inlet conditions with a feed side flowrate of 47 L/s (100 ft³/min) and an outlet condition at the 12.8 °C (55°F) and 90% RH humidity ratio at the bin dry bulb temperature with a single component condenser. The flowrate was changed for this particular analysis simply to make scalability of the results to higher flowrates (i.e. for full scale systems) simpler when considering average annual performance. The single component condenser is modelled with approach temperatures of 0°C, 2.8°C and 5.6°C. The results below are for a water permeance of 8.00·10⁻⁶ mol/m²-s-Pa and an air permeance of 5.33·10⁻⁸ mol/m²-s-Pa with a membrane area of 2.0 m². In this case, the permeate side pressure changes for each bin depending on the amount of water vapour that must be removed to meet the outlet condition. For these membrane characteristics, the annual average COP for the case with an approach temperature of 0°C is 21.4% less than the COP for the ideal condenser. The results for the two cases with approach temperatures of 2.8°C and

5.6°C (see Table 1) show the COP decreases even further when real approach temperatures are considered.

Table 1: Single component condenser results

Ideal	Approach=0°C		Approach=2.8°C		Approach=5.6°C	
COP	COP	%Diff	COP	%Diff	COP	%Diff
2.2	1.73	21.4%	1.43	35.1%	1.35	38.5%

4.5 Multi-Component Condenser Simulation

The Colburn & Hougen design model in its original form is a trial and error procedure which calculates the total heat transfer area required to obtain a given output condition. For operational performance analysis, the full Colburn & Hougen procedure is carried out in an iterative procedure that guesses the output conditions of the non-condensed gas and checks the total area required to obtain those conditions until the results match the area of the actual device. Similarly, the cooling water flow rate is assumed in the Colburn & Hougen device and the change in temperature is calculated. Given the small difference between the temperature of the gas entering the condenser and the temperature of the cooling water entering the condenser, the temperature change of the cooling water is a limiting factor in this analysis. As a result, the model procedure utilizes a set temperature difference for the cooling water and a variable cooling water flow rate which must be checked as well. The inputs for the multi-component condenser analysis are labelled as simulation group C in Table 3.

4.6 Comparison of Multi-component and Single Component Condenser Results

All of the Colburn & Hougen method based simulations assume a cooling tower approach temperature of 0°C. The results in Figure 4 are calculated using Houston, TX, USA, bin data (i.e. ambient dry bulb temperature) for a membrane with a water permeance of $8.00 \cdot 10^{-6}$ mol/m²-s-Pa, an air permeance of $5.33 \cdot 10^{-8}$ mol/m²-s-Pa and an area of 2.0 m².

The graphical results presented below clearly show the degradation in COP when a multi-component condenser is compared to the single component condenser and the ideal condenser. The COP results are most similar when there is either not much water in the permeate stream (low ambient dry bulb temperatures) or when the difference between the ambient dry bulb and wet bulb temperatures is large (high ambient dry bulb temperatures).

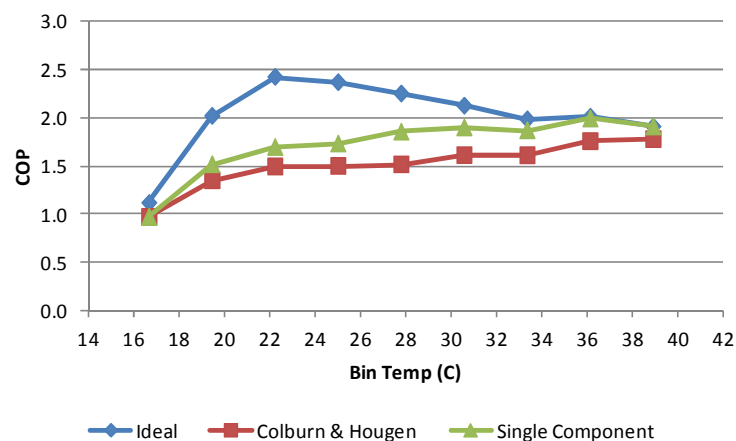


Figure 4: Comparison of results for three simulation types with Approach=0°C

4.7 System Optimization Analysis

Two initial system optimizations were investigated to increase system performance. These include the use of multiple condenser stages to condense more of the water vapour and the optimization of the pressure entering the condenser. Adding multiple condenser stages was found to have too small of an effect on the performance of the system to justify the added system complexity; therefore, this optimization is not utilized. For instance, for a membrane with a water permeance of $8.00 \cdot 10^{-6}$ mol/m²-s-Pa, an air permeance of $5.33 \cdot 10^{-8}$ mol/m²-s-Pa, an area of 2.0 m² and a flowrate of 47 L/s (100 ft³/min) outside air at Houston, TX, USA, bin conditions exiting at the 12.8°C (55°F) and 90% RH humidity ratio and bin dry bulb temperature, the annual average COP increases by 7.56% when a second stage is added and by 12.14% when a third stage is added. This analysis is based on the multi-component condenser model. While a 12.14% increase is not insignificant the system complexity would greatly increase to realize this gain. The inputs for the multiple condenser stages optimization analysis are labelled as simulation group D in Table 3.

In the previous simulations, the condenser water vapour partial pressure was set based on the saturation pressure of the permeate side gases. Increasing the partial pressure of the water vapour increases the saturation temperature of the water vapour which increases the temperature difference driving the condensation process. In order to increase the amount of water vapour condensed, the entering condenser pressure was increased in even increments until a maximum COP_{latent} was found. All of the following analysis was conducted using the single component condenser analysis to explore the limit of the performance of the system under real operating conditions. All of the simulations include a 65% simple efficiency for the isothermal compressors and an outside air feed stream flowrate of 40 L/s (85 ft³/min). The inlet and outlet unpermeated stream conditions are the specified design conditions. The inputs for the condenser pressure optimization analysis are labelled as simulation group E in Table 3.

This analysis was conducted using only a small number of membrane characteristic combinations to demonstrate the presence and behaviour of the maximum performance conditions. The first test case uses a water permeance of $8.00 \cdot 10^{-6}$ mol/m²-s-Pa and an air permeance of $2.00 \cdot 10^{-8}$ mol/m²-s-Pa with a membrane area of 10.0 m². The membrane area has increased since the pressure differential across the membrane has been decreased requiring more surface area of membrane to remove enough moisture to meet the outlet condition. The results show that the COP reaches a maximum value when 85-90% of the water has been condensed. The simulation was also conducted for three different approach temperatures. The results show that the COP is decreased by approximately 24-30% for an approach temperature of 5.6°C and 21-27% for an approach temperature of 2.8°C when compared to the ideal case. Additionally, only one realistic case with an approach of 2.8°C exceeds the COP target of 3.34 as shown in Table 2.

Table 2: Condenser pressure optimization results

Sim. Type	COP	% Diff	T ₃ (°C)	T ₃ Increase (°C)	P _{w3} (kPa)	P _{w3} Increase (kPa)	P ₃ Percent Increase
Ideal	4.57	--	32.2	--	4.82	--	--
A=0°C	3.53	-22.8%	43.1	19.5	8.67	3.85	80%
A=2.8°C	3.36	-26.5%	46.0	24.9	10.1	5.30	110%
A=5.6°C	3.21	-29.8%	48.7	29.7	11.6	6.75	140%

Table 3: Summary of simulation inputs (CT: concentric tube and S&T: shell and tube)

Sim. Group	Condenser		Approach	State 1 _i			State 1 _o	Membrane Properties	
	Type	Shape	T (°C)	T _{ab} (°C)	RH (%)	L/s	T (°C)	Air Perm. (mol/m ² -s-Pa)	A _m (m ²)
A	Ideal	--	--	Houston, TX Bins		47	Inlet DB	5.33E-08	2.0
B	Single	CT	Table 1	Houston, TX Bins		47	Inlet DB	5.33E-08	2.0
C	Multi	S&T	0	Houston, TX Bins		47	Inlet DB	5.33E-08	2.0
D	Single	CT	0	Houston, TX Bins		47	Inlet DB	5.33E-08	2.0
E	Single	CT	0, 2.8, 5.6	32.2	90	40	32.2	2.00E-08	10.0

5. CONCLUSION

Multiple simulations of a membrane dehumidification system were developed. The model presented here was used to develop the system, analyze operating parameters and simulate performance. The results indicate that the system requires optimization to meet the target COP of 3.34 with a maximum system COP of 3.36 at the ARPA-E specified conditions. The modifications considered include multiple condenser stages and increased condenser inlet pressure. Further improvement of the models presented above will be presented elsewhere. Improvements include a more detailed mass transfer model, a more detailed heat transfer model, a non-isothermal compression model and a new condenser design as well as uncertainty analysis using the improved model. The systems analyzed in this paper are covered by United States patent Nos. 8,496,732, 8,500,848 and six pending U.S. and international patents.

ACKNOWLEDGEMENTS

The authors gratefully acknowledge financial support of this work by the United States Department of Energy ARPA-E Program under the BEETIT Program.

NOMENCLATURE

A or A _m	membrane area (m ²)
c	specific heat (J/kg-K)
CFM	volumetric airflow rate (ft ³ /min or L/s)
COP	coefficient of performance (-)
CT	concentric tube
d _o	outside diameter of inner tube (m)
DB	dry bulb temperature (°C)
g	gravitational acceleration (m/s ²)
h	heat transfer coefficient (W/m ² -K)
h _s	sensible only heat transfer coefficient (W/m ² -K)
k	thermal conductivity (W/m-K)
K	gas film mass transfer coefficient (kmol/s-m ² -Pa)

M_{cond}	mass flow rate of condensate (kg/s)
M_m	average molecular weight (kg/kmol)
N	molar flow rate (kmol/s)
P	permeability (mol/m-s-Pa)
P	pressure (kPa)
Q	cooling load (kW)
R	gas constant (kJ/kmol-K)
S&T	shell and tube
X	molar fraction (-)
α	selectivity (-)
γ	ratio of specific heats (-)
ε	heat transfer ratio (-)
η_{poly}	polytropic efficiency (-)
μ	kinematic viscosity (kg/m-s)
ρ	density (kg/m ³)
τ	permeance (mol/m ² -s-Pa)

Subscripts

a	air
c	condensate
c	critical
g	gas
h	high pressure side of membrane
i	ith membrane segment
in	inlet
L	liquid
m	low pressure side of membrane
oa	outside air
r	reduced
T	total
TP	two phase
v	vapour
w	water

REFERENCES

Akira, I. 2000. Dehumidification of air by a hygroscopic liquid membrane supported on surface of a hydrophobic microporous membrane, *Journal of Membrane Science*, 175 (1), pp. 35-42.

9th International Conference on System Simulation in Buildings, Liege, December 10-12, 2014

- Baker, R.W. 2004. *Membrane technology and applications*, 2nd ed., J. Wiley: Chichester, New York.
- Baker, R.W., Wijmans, J.G., Huang, Y. 2010. Permeability, permeance and selectivity: A preferred way of reporting pervaporation performance data, *Journal of Membrane Science*, 348 (1–2), pp. 346-352.
- Bird, R.B., Stewart, W.E., Lightfoot, E.N. 2002. *Transport phenomena*, 2nd ed., J. Wiley: New York.
- Bras, G.H. 1953a. Design of Cooler Condenser for Vapour-Gas Mixtures - I, *Chemical Engineering*, 60 (4-5), pp. 223-226.
- Bras, G.H. 1953b. Design of Cooler Condensers for Vapour-Gas Mixtures - II, *Chemical Engineering*, 60 (4-5), pp. 238-240.
- Brundrett, G.W. 1987. *Handbook of dehumidification technology*, Butterworths: Boston, MA, USA.
- Bynum, J.D. 2012. Thermodynamic Modelling of a Membrane Dehumidification System, PhD Dissertation, Texas A&M University, College Station, TX, USA.
- Carey, V.P. 2008. Liquid-vapour phase-change phenomena : an introduction to the thermophysics of vapourization and condensation processes in heat transfer equipment, 2nd ed., Taylor and Francis: New York.
- Colburn, A.P. , Hougen, O.A. 1934. Design of Cooler Condensers for Mixtures of Vapours with Noncondensing Gases, *Industrial & Engineering Chemistry*, 26 (11), pp. 1178-1182.
- EES. 2013. Engineering Equation Solver for Microsoft Windows Operating Systems. F-Chart Software, Madison, WI, USA.
- El-Dessouky, H.T., Ettouney, H.M., Bouhamra, W. 2000. A Novel Air Conditioning System: Membrane Air Drying and Evaporative Cooling, *Chemical Engineering Research and Design*, 78 (7), pp. 999-1009.
- Gavalas, G.R. 2008. Diffusion in Microporous Membranes: Measurements and Modeling, *Industrial & Engineering Chemistry Research*, 47 (16), pp. 5797-5811.
- Incropera, F.P., DeWitt, D.P. 2002. *Fundamentals of heat and mass transfer*, 5th ed., J. Wiley: New York.
- Krishna, R., van den Broeke, L.J.P. 1995. The Maxwell-Stefan description of mass transport across zeolite membranes, *The Chemical Engineering Journal and the Biochemical Engineering Journal*, 57 (2), pp. 155-162.
- Li, J. Ito, A. 2008. Dehumidification and humidification of air by surface-soaked liquid membrane module with triethylene glycol, *Journal of Membrane Science*, 325 (2), pp. 1007-1012.
- McNaught, J.M. 1981. An Assessment of Design Methods for Condensation of Vapours from a Noncondensing Gas, in: J. Taborek, G.F. Hewitt, N. Afgan (Eds.) *ICHMT Seminar on Advances in Heat Exchangers*, Hemisphere Pub. Corp./McGraw-Hill, Dubrovnik, Yugoslavia.
- Nusselt, W. 1916. Des oberflächenkondensation des wasserdampfes, *Zeitschrift des Vereines Deutscher Ingenieure*, 60, pp. 541-564.
- Rowland, C.A., Wendel, Jr., M.J. 2005. Dehumidification Technologies, *Heating/Piping/Air Conditioning Engineering : HPAC*, 77 (3), pp. 48-50.

- Sacramento-Rivero, J.C., Heggs, P.J. 2009. The Evaluation of a Vent Condenser by the Film and Equilibrium Methods for Steam/Air Mixtures, *Heat Transfer Engineering*, 30 (7), pp. 590-597.
- Sekulić, J., Elshof, J.E.t., Blank, D.H.A. 2005. Separation mechanism in dehydration of water/organic binary liquids by pervaporation through microporous silica, *Journal of Membrane Science*, 254 (1-2), pp. 267-274.
- Shah, M.M. 1979. A general correlation for heat transfer during film condensation inside pipes, *International Journal of Heat and Mass Transfer*, 22 (4), pp. 547-556.
- Song, K.-H., Cho, S.-H., Lee, K.-R. 2008. Dehumidification of Air by the Composite Membrane Coated with Hydrophilic Polymer on Inorganic Substrate, *Materials Science Forum*, 569, pp. 337-340.
- Stern, F. 1966. *Condensation from Superheated Gas-Vapour Mixtures*, Chemical Engineering, University of Rhode Island.
- Stern, F., Votta, F. 1968. Condensation from Superheated Gas-Vapour Mixtures, *AIChE Journal*, 14 (6), pp. 928-933.
- Stern, S.A., Wallawender, W.P. 1969. Analysis of Membrane Separation Parameters, *Separation Science*, 4 (2), pp. 129-159.
- Van Den Broeke, L.J.P., Krishna, R. 1995. Experimental verification of the Maxwell-Stefan theory for micropore diffusion, *Chemical Engineering Science*, 50 (16), pp. 2507-2522.
- Wang, Y., LeVan, M.D. 2008. Mixture Diffusion in Nanoporous Adsorbents: Equivalence of Fickian and Maxwell–Stefan Approaches, *The Journal of Physical Chemistry B*, 112 (29), pp. 8600-8604.
- Webb, D.R. 1990. Multicomponent Condensation, in: 9th International Heat Transfer Conference, Jerusalem, Israel.
- Webb, D.R., Fahrner, M., Schwaab, R. 1996. The relationship between the colburn and silver methods of condenser design, *International Journal of Heat and Mass Transfer*, 39 (15), pp. 3147-3156.
- Wijmans, J.G., Baker, R.W. 1995. The solution-diffusion model: a review, *Journal of Membrane Science*, 107 (1-2), pp. 1-21.
- Williams, P.J., Koros, W.J. 2008. Gas Separation by Carbon Membranes, in: N. Li, N., A.G. Fane, W.S.W. Ho, T. Matsuura (Eds.) *Advanced Membrane Technology and Applications*, Wiley & Sons., Inc.: Hoboken, NJ.

Numerical analysis on the performance of two-stage desiccant wheel system

Yuwei Zheng^{1*}, Xiaohua Liu^{1*}, Rang Tu²

⁽¹⁾Department of Building Science, Tsinghua University, Beijing 100084, China

⁽²⁾School of mechanical engineering, University of Science and Technology Beijing, Beijing 100083, China

1. ABSTRACT

Nowadays the desiccant wheel is applied widely in air-conditioning system. One-stage desiccant wheel system is compared with two-stage system in present study, with hot/chilled water as heating and cooling source. Many studies show that the regeneration temperature of the two-stage desiccant wheel system is apparently low compared with one-stage system. In this paper, required hot water inlet temperature is also taken as a comparison index. It is found that, required hot water inlet temperature depends on water and air flow rate ratio. With small water flow rate, one-stage system is recommended. And with high water flow rate, two-stage system is recommended. For the condition that the air of 18g/kg is dehumidified to 9g/kg, with the airflow rate of 1 kg/s and water flow rate of 0.24kg/s, the required hot water inlet temperature is 76.4°C and it increases to 80.9 °C for two-stage. But when the water flow is 1.2kg/s, the temperature is 66.0 °C and it decreases to 58.9°C for two-stage.

Keywords: desiccant wheel, regeneration, heating source temperature, multi-stage

2. INTRODUCTION

Air-conditioning systems applying the rotary desiccant wheel draw more and more attention as an effective dehumidification method. The substrate of desiccant wheel is honeycomb construction coated with solid desiccant material, forming many air channels, and heat and mass transfer between air and solid desiccant occurs on the walls of channels. Much absorbing heat is released into air while dehumidification and much heat is absorbed while regeneration, which is isenthalpic process. To regenerate the solid desiccant material with high moisture content, high-temperature regeneration air is needed. Many studies try to reduce the required regeneration air inlet temperature (regeneration Temp.) of desiccant wheels and improve system performance by many methods, such as developing advanced desiccant materials with high moisture capacity (Eicker et al., 2012), applying alternative wheel design (Yadava et al., 2013) or improving air conditioning process with evaporative cooling (Goldsworthy, 2011). Thus, low-grade heating sources can be utilized to desiccant regeneration, such as solar energy, waste heat from cogeneration system (La et al., 2010).

Two-stage desiccant wheel systems have gained considerable attention from researchers in recent years because of the possibility of low regeneration temperature. Cooling source and heating source is utilized between two stages to cool the processed air and reheat regeneration air. Thus, the processed air can maintain in relatively low temperature level, and so as the desiccant material. Tu et al. (2014) investigated the performance of a heat pump-driven two-stage desiccant wheel system, and the required regeneration temperature is about 44°C, lower than 80°C required by one-stage system driven by heat pump. Jeong et al. (2011) proposed a system that combines a heat pump system with two desiccant wheels or one four-part desiccant wheel. For the same dehumidification target, the regeneration temperature of conventional desiccant dehumidification systems, the system with the pre-cooler and the double-stage-type

systems (including above mentioned two types) are approximately 62.2°C, 49.9°C, 43.2°C, respectively. La et al. (2011) studied a two-stage desiccant wheel system driven by hot water from solar thermal collector. The regeneration air with 1000m³/h flow rate is heated in heat exchanger by hot water (0.5~2m³/h) from solar collector and then simultaneously comes into two desiccant wheels, and the hot water temperature is 50-90°C.

To achieve the similar dehumidification capacity, the regeneration temperature of the two-stage system is apparently low compared with one-stage system no matter what kind of heating or cooling source is. For the desiccant system driven by hot and chilled water, although the required regeneration temperature of two-stage system is lower than one-stage, how does the required hot water inlet temperature? The present study will focus on this question. The heat and mass transfer model in the desiccant wheel and model of heat exchanger are first provided. Based on the validated theoretical model, the performance of one-stage and two-stage systems with the same entire heat transfer area is compared, which is driven by hot/chilled water. With different water flow rate, the required regeneration air inlet temperatures and hot water inlet temperatures are evaluated and contrasted.

3. MODEL INTRODUCTION

The typical desiccant wheel air-conditioning system composes of desiccant wheel, heater, and cooling coils, as depicted in Figure 1. The regeneration air is heated by external heating source (R1 → R2) before coming into desiccant wheel, aimed at supporting regeneration heat, and processed air is cooled before and after desiccant wheel (P1 → P2, P3 → P4) to maintain low air temperature and improve dehumidification ability of desiccant wheel. The heating and cooling source can be hot/chilled water or refrigerant in heat pump cycle, and the systems driven by hot and chilled water are investigated in this article. In the following analysis, the regeneration sector takes up the half of the wheel, and the processed air flow rate and regeneration air flow rate are equal.

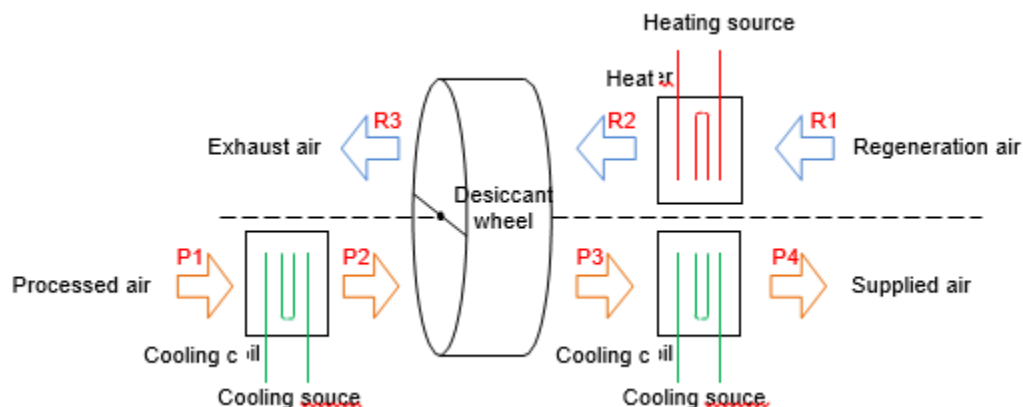


Figure 1: Operating principle of one-stage desiccant wheel air-conditioning system.

3.1 Heat and mass transfer model of desiccant wheel

Desiccant wheel is the key part in the desiccant wheel air-conditioning system, and the heat and mass transfer model in the previous paper (Tu et al., 2013) is adopted. The desiccant wheels mentioned in present study are with sinusoidal air channels. The schematic of desiccant wheel is shown in Figure 2. Every single air channel is taken as an individual control unit in the two-dimensional model.

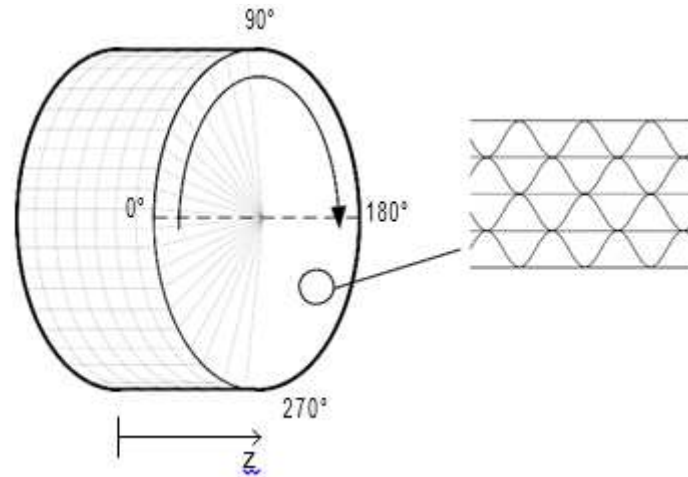


Figure 2: Schematic of desiccant wheel.

Both gas diffusion (DA) and surface diffusion (DS) are considered in this model. The main assumptions for the model are (Zhang et al, 2002): 1) the heat conduction and mass transfer along the desiccant wall direction are neglected due to its thin thickness of about 0.1 mm; 2) the axial heat conduction and mass diffusion in the air flow are neglected; 3) the air channels are equal and uniformly distributed throughout the whole wheel; 4) the thermodynamic properties in the solid are constant and uniform; 5) air leakage between two air flows is neglected at low revs. Energy conservation and mass conservation of air and desiccant are calculated as follows (Tu et al., 2013):

$$\frac{1}{u_a} \frac{\partial T_a}{\partial \tau} + \frac{\partial T_a}{\partial z} = \frac{4h}{\rho_a c_{pa} u_a d_h} (T_d - T_a) \quad (1)$$

$$\frac{1}{u_a} \frac{\partial Y_a}{\partial \tau} + \frac{\partial Y_a}{\partial z} = \frac{4h_m}{\rho_a u_a d_h} (Y_d - Y_a) \quad (2)$$

$$\rho_d \left(c_{pd} + \frac{\rho_{ad} x}{\rho_d} c_{pw} W \right) \frac{\partial T_d}{\partial \tau} + x \rho_{ad} c_{pw} T_d \frac{\partial W}{\partial \tau} = k_d \frac{\partial^2 T_d}{\partial z^2} + r_s \rho_{ad} x \frac{\partial W}{\partial \tau} + \frac{4h}{d_h f} (T_a - T_d) \quad (3)$$

$$\kappa \rho_a \frac{\partial Y_d}{\partial \tau} + \rho_{ad} \frac{\partial W}{\partial \tau} = \rho_a \kappa D_A \frac{\partial^2 Y_d}{\partial z^2} + \rho_{ad} D_S \frac{\partial^2 W}{\partial z^2} + \frac{4h_m}{x d_h f} (Y_a - Y_d) \quad (4)$$

where T_a and T_d are the temperatures of the air and the desiccant material, respectively; Y_a and Y_d are the humidity ratio of the air and the equilibrium humidity ratio of the desiccant, respectively; d_h is the hydraulic diameter of the air channel; u_a is the face velocity of the air; and h and h_m are the convective heat transfer coefficient and the convective mass transfer coefficient, respectively; ρ_d and c_{pd} are the equivalent density and heat capacity of the solid, respectively, which are weighted values of substrate and desiccant material (subscript ad); x is the volume ratio of the desiccant material in the solid, which is combined with substrate and desiccant material; f is the frontal area ratio of the solid and air in the control unit; k_d is heat conductivity coefficient; r_s is adsorption heat; κ is porosity of desiccant material.

As indicated in the four conservation equations, the air states vary with wheel angle (τ direction) and wheel thickness direction (z direction). $(T_d - T_a)$ and $(Y_d - Y_a)$ are heat and mass transfer driving force, respectively. The equivalent humidity ratio of desiccant means the humidity ratio of the air on surface of desiccant, at equivalent state with the desiccant material. Figure 3 shows the relationship of equivalent humidity ratio and water content of RD silica gel in psychrometric

chart. Empirical formula about equilibrium isotherm of solid desiccant can be integrated in to complete the mathematic model. To calculate the two-dimensional model, the wheel is divided into many grids in thickness and angle (time) directions, as shown in Figure 2. Solving the above equations with two air flows inlet parameters can give the distributions of the air and desiccant parameters inside the wheel and the parameters at the outlets of the desiccant wheel. Comparison results of the predicted values by the theoretical model with the corresponding experimental findings are given by Tu et al. (2013), and show good agreement. Therefore, the theoretical model is adopted for following research on dehumidification wheels.

Desiccant wheel rotates between processed air and regeneration air. Absorbing heat is released along with dehumidification process, while heat is absorbed along with regeneration process of solid desiccant material. Figure 4 gives two air flow inlet and outlet parameters during processes. The air handling process is isenthalpic due to interaction of the air and solid desiccant material along air flow direction and angle direction. The air flow rate of two flows are usually the same, and the temperature changes and humidity ratio changes of the processed air are equal to those of the regeneration air, as shown in psychrometric chart. The outlet parameters are not uniform along the angle direction, so the outlet points in Figure 4 mean average value.

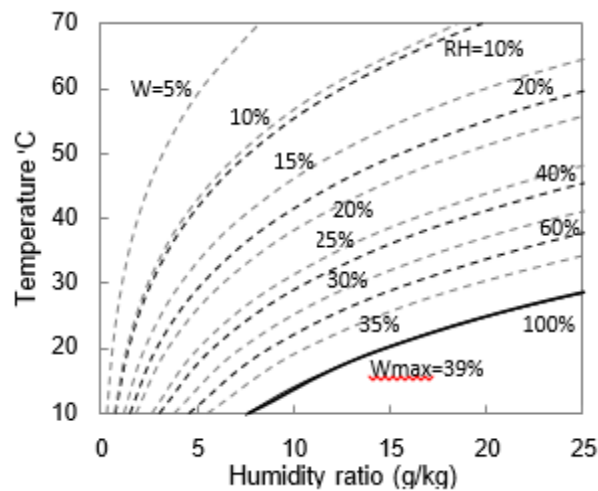


Figure 3: Usual solid desiccant states shown in air psychrometric chart (RD silica gel).

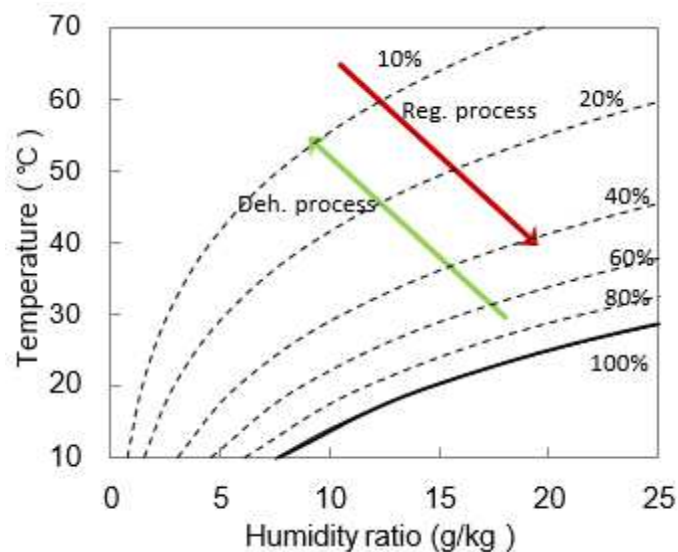


Figure 4: Air handling process of dehumidification and regeneration in psychrometric chart.

The radius and thickness of the wheel are 500 mm and 200 mm, respectively, and the wheel moves at 25 r/h rotation speed. The wheel is meshed into 40 (thickness) \times 144 (angle) grids in calculation model, according to 5 mm and 1s step size respectively. The air states and solid desiccant states at every node of the grids are calculated through an iterative model. The temperature field and humidity ratio field is depicted in Figure 5. The states of the air and solid desiccant are compared along the angles at three different thickness positions of the wheel ($Z=0$, $L/2$ and L). It indicates that, in dehumidification sector, the temperature of the air is lower than solid desiccant, and heat transfer direction is from solid desiccant to the air. The temperature of the air increases with increasing Z , and decreases with increasing angle. Different with temperature, the humidity ratio of air is higher than equivalent humidity ratio of the solid desiccant, so mass transfer direction is from the air to solid desiccant, i.e., dehumidifying the air. The humidity ratio of the air and solid desiccant decreases with increasing Z , and decreases first and then increases with increasing angle. The condition is absolutely opposite in regeneration sector.

The temperature and humidity ratio states of the air and solid desiccant along with the thickness at 90° and 270° are represented in Figure 6. As shown by the middle two lines in Figure 5 and Figure 6, the driving force is relatively uniform throughout the desiccant wheel.

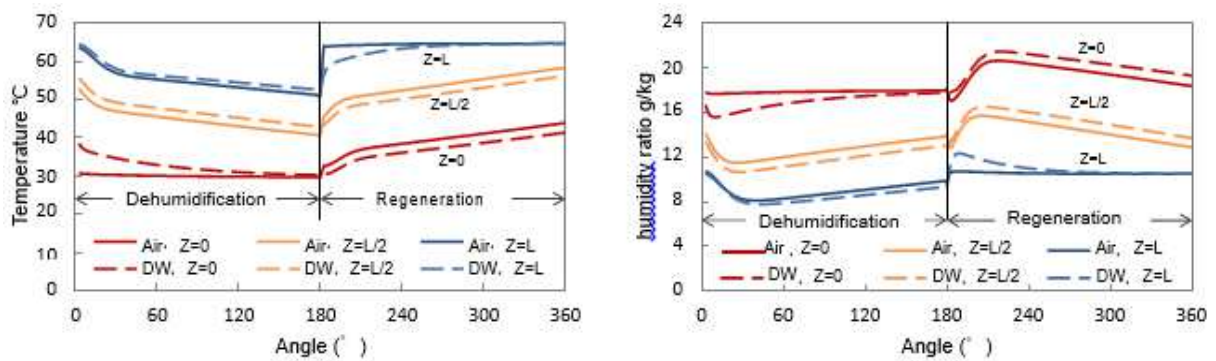


Figure 5: The states of the air and solid desiccant along with angles at three thickness positions.

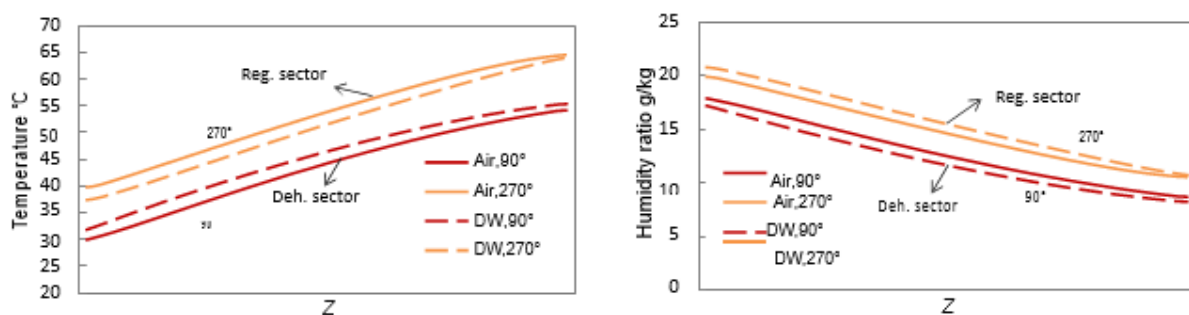


Figure 6: The states of the air and solid desiccant along with thickness at different angles.

3.2 Model of heat exchanger

Water-air heat exchanger is another key component of desiccant wheel air-conditioning system. And $\epsilon - NTU$ model is utilized to calculate outlet temperatures at counter-flow configuration. For the given heat transfer ability ($K \cdot A$), NTU is determined by heat capacity flow rate, and then ϵ can be obtained, as Eqs. (5) - (6), where ϵ means air side heat exchange effectiveness. Heat capacity flow rate ratio Cr is defined as Eq. (7), and it has much effect on heat exchange effectiveness. Air side heat exchange effectiveness are shown in Figure 7, at different water flow rates and $K \cdot A$.

$$NTU = \frac{KA}{\dot{m}_a c_{p,a}} \quad (5)$$

$$\varepsilon = \frac{T_{a,in} - T_{a,out}}{T_{a,in} - T_{w,in}} = \frac{1 - e^{-NTU(1-1/C_r)}}{1 - \frac{1}{C_r} e^{-NTU(1-1/C_r)}} \quad (6)$$

$$C_r = \frac{\dot{m}_w c_{p,w}}{\dot{m}_a c_{p,a}} \quad (7)$$

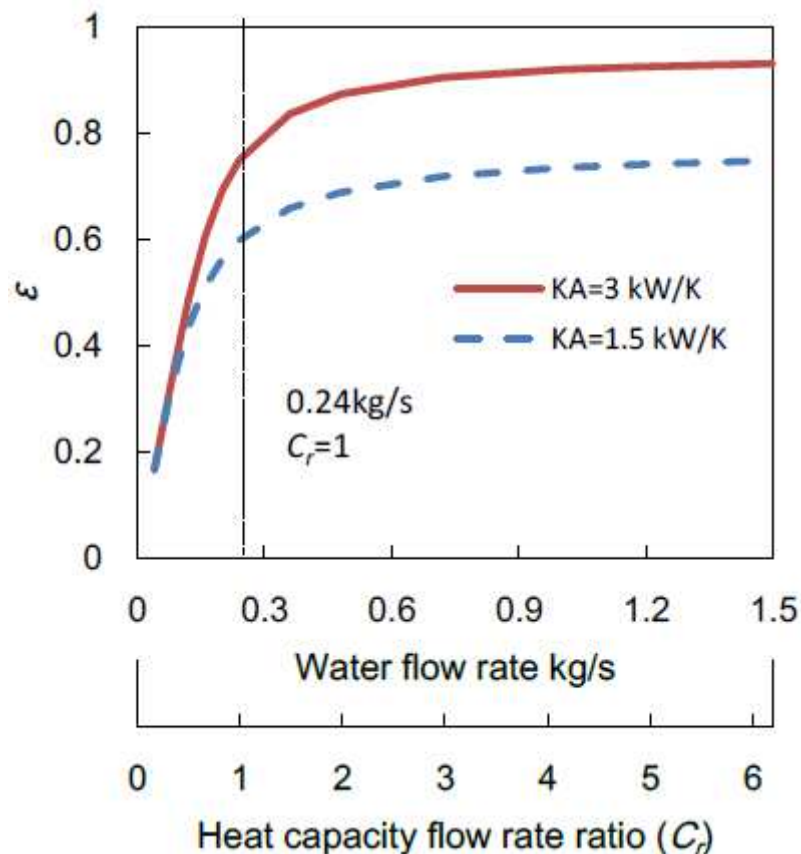


Figure 7: Air side heat exchange effectiveness at different water flow rates (air flow rate: 1kg/s)

4. SYSTEMS COMPARISON

The one-stage desiccant wheel system is described in Figure 1, and the operating conditions and component information are listed in Table 1. When the system is divided into two stages, the thickness of wheel, the heat transfer area of all heat exchangers and the water flow divide equally, and two air streams flow through the components in turn, as shown in Figure 8. The inlet parameters of two air flows, dehumidification target and chilled water temperature (28°C) are set invariant. For all systems, every desiccant wheel is operating at the optimum rotation speed. The optimum can be obtained by repeated trial calculation. In this way, the required regeneration air inlet temperature and required hot water inlet temperature of one-stage mode and two-stage mode can be evaluated and compared.

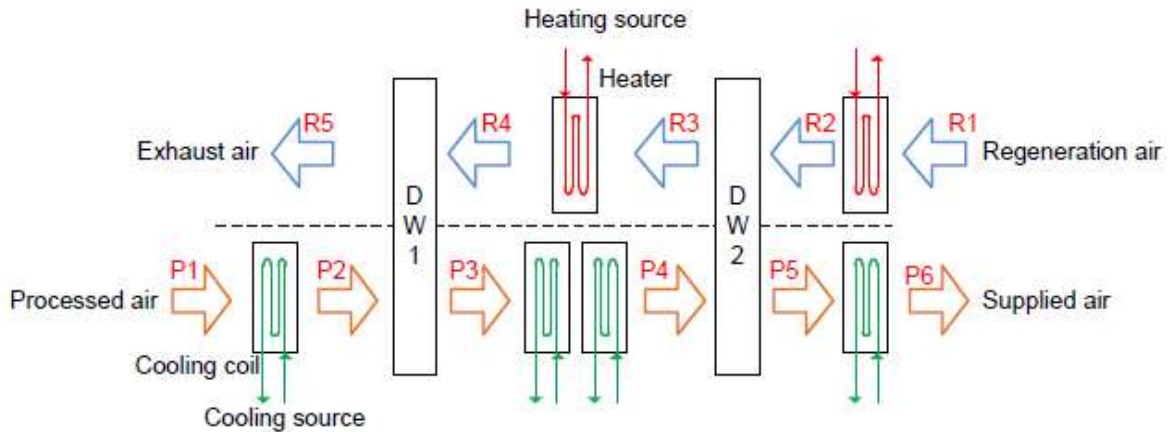


Figure 8: Operating principle of two-stage desiccant wheel air-conditioning system.

Table 1: Operating conditions and component information.

Operating conditions	Desiccant wheel	Heat exchangers
Processed air: 35°C, 18 g/kg, 3000 m ³ /h Regeneration air: 26°C, 10.5g/kg, 3000 m ³ /h	Radius: 0.5m. Thickness: 0.2m Material: silica gel <i>Nu</i> of air channel: 2.463 Divide thickness equally for two-stage	For each heat exchanger of one-stage Heat transfer ability: 3 kW/k. Efficiency: 75% The water flow is inconstant Divide heat transfer ability and water flow equally for two-stage

The comparison results of one-stage and two-stage desiccant wheel system are shown in Figure 9 and Table 2. Figure 9(a) shows the air handling processes of one-stage mode, with the water flow rate of 0.24kg/s for each heat exchanger. The required regeneration temperature is 64.7°C. Equivalent humidity ratio and water content of desiccant material throughout the wheel are 7.8~21.5g/kg and 7.4%~33.7%, respectively, of wide ranges. High air inlet regeneration temperature is essential for regeneration process. Figure 9(b) shows the air handling processes of the two-stage system. Keep the total water flow the same as one-stage system, i.e., water flow rate of each heat exchanger is 0.12kg/s. The required regeneration air inlet temperatures are 59.1°C and 50.9°C respectively for two stages. The two stages desiccant material states are separately in high humidity and low humidity regions in psychrometric chart. Equivalent humidity ratio and water content of the 1st-stage desiccant material are ranging in 11.3~20.8g/kg and 12.7%~30.0%, respectively. Meanwhile that of 2nd-stage is ranging in 8.5~14.5g/kg and 13.9~24.6% respectively. Also Figure 10 shows desiccant states throughout the wheel while rotating in psychrometric chart. The desiccant water content of two-stage system maintains higher than 12%, while the desiccant water content of one-stage should be regenerated to 7.4%. Maintaining desiccant material in high humidity region is the key cause of decreasing regeneration air inlet temperature, i.e., regeneration temperature. However, the hot water temperature of two-stage system is higher than that of one-stage system, as shown in Table 2. When the water flow rate is small, water flow rate is halved with invariant air flow rate for each heat exchanger, so heat capacity flow rate of water is much smaller than that of air. Heat transfer ability becomes much poorer. Though the regeneration temperatures of two-stage are lower than one-stage, the required hot water inlet temperature is higher. When the water flow rate is high, the regeneration temperature and required hot water inlet temperature of two-stage are both lower than those of one-stage, as shown in Table 2. The dehumidification performance of desiccant wheel and the heat transfer effect of heat exchangers are both

improved. Furthermore, dehumidification amount of each stage desiccant wheel is more uniform when high water flow rate.

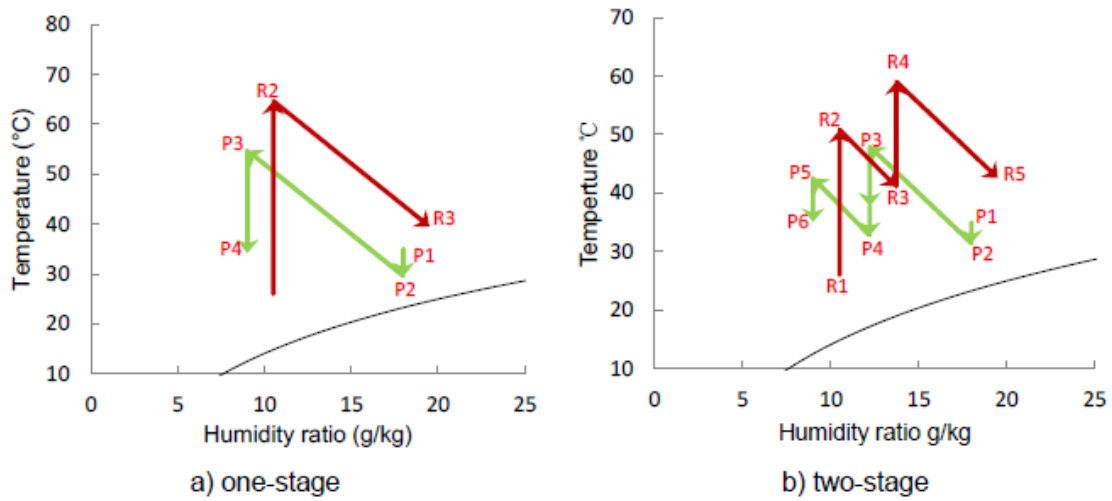


Figure 9: Air handling processes of two systems with small water flow: a) one-stage; b) two-stage.

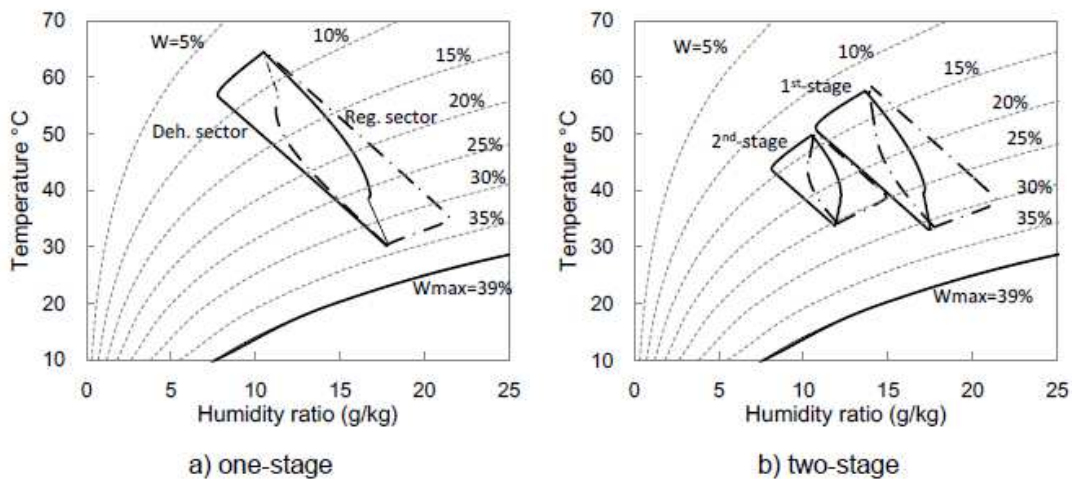


Figure 10: Desiccant states of two systems with small water flow: a) one-stage; b) two-stage

Table 2: Simulation results comparison of two systems modes at different water flow.

System	One-stage	Two-stage	One-stage	Two-stage
Water flow rate of each heat exchanger, kg/s	0.24	0.12	1.2	0.6
C_r	1	0.5	5	2.5
Regeneration Temp., °C	64.7	59.1 / 50.9	63.6	53.5 / 50.3
Hot water Temp., °C	76.4	80.9	66	58.9
Dehumidification amount, g/s	9	5.7 / 3.2	9	5.0 / 4.0
Supply air Temp., °C	34.2	35.1	29.6	30.7
Exhaust air Temp., °C	39.6	42.6	38.3	39.1

It is found that the increasing or decreasing of required hot water temperature after dividing the desiccant wheel system depends on the water flow rate, according to the previous simulation results. Figure 11 shows the required hot water temperature of one-stage and two-stage systems with various water flows. The abscissa total hot water flow rate means the sum of hot water flow rates for two-stage modes.

When the total hot water flow rate increases from 0.12 kg/s to 1.5 kg/s (chilled water flow rate of each cooling coil is equal to hot water flow rate of each heater), the required hot water inlet temperature of two system modes both decreases. Due to different changing slopes, the critical water flow exists. For the given input parameters, 0.33 kg/s water flow rate is determined as the critical value. Therefore, when water flow rate is small (<0.33 kg/s in this case), the performance of one-stage system is better. When water flow rate is high (>0.33 kg/s in this case), two-stage desiccant wheel system shows better performance.

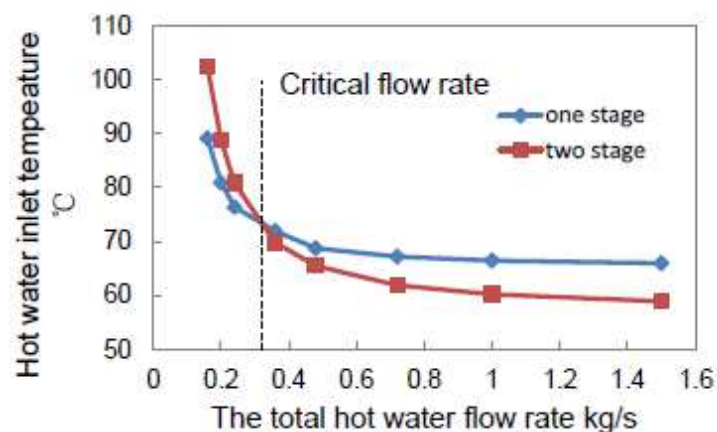


Figure 11: The required hot water temperature with various water flows.

Decreasing of required regeneration air inlet temperature is the original aim of two-stage desiccant wheel air-conditioning system. And simulative analysis proves that two-stage can effectively reduce required regeneration air inlet temperature by adding middle heat and cooling source between two stage desiccant wheels. As explained in Section 4 and Figure 9, intermediate input cold and heat can realize regeneration at high water content region. However, the required hot water inlet temperature of two-stage is not always lower than one-stage. And it depends on the hot water flow rate, i.e., heat capacity flow rate ratio Cr .

5. CONCLUSION

One-stage and two-stage desiccant wheel system driven by hot and chilled water are simulative examined in this paper. The regeneration temperature and required heat source temperature are compared by adopting theoretical models of desiccant wheel and heat exchangers. The main conclusions are summarized as follows:

- To gain the same dehumidification capacity, the required regeneration air inlet temperature of two-stage is certain to be lower than that of one-stage, with the same heat exchange area, so two-stage mode is a possible way to use low-grade heat source.
- For hot and chilled water driven desiccant wheel system, the required hot water inlet temperature of two-stage is not always lower than that of one-stage, and it depends on the hot water flow rate.
- With high hot water flow rate, the required hot water inlet temperature of two-stage is lower than one-stage, and two-stage system is recommended. With small hot water flow rate, the required hot water inlet temperature of one-stage is lower, and one-stage desiccant wheel system is recommended.

ACKNOWLEDGEMENTS

The authors appreciate the support from the National Natural Science Foundation of China (No. 51138005) and Tsinghua University Initiative Scientific Research Program.

REFERENCES

- Eicker U., Schürger U., Köhler M., et al., 2012. Experimental investigations on desiccant wheels . Applied Thermal Engineering.
- Yadava A., Bajpai V.K., 2013. Analysis of various designs of a desiccant wheel for improving the performance using a mathematical model. Journal of Renewable and Sustainable Energy.
- Goldsworthy M., White S., 2011. Optimization of a desiccant cooling system design with indirect evaporative cooler. International Journal of Refrigeration.
- La D., Dai Y.J., Li Y., et al., 2010. Technical development of rotary desiccant dehumidification and air conditioning: a review. Renewable and Sustainable Energy Reviews. Tu R., Liu X.H., Jiang Y., 2014. Performance analysis of a two-stage desiccant cooling system. Applied Energy.
- Jeong J., Yamaguchi S., Saito K., et al., 2011. Performance analysis of desiccant dehumidification systems driven by low-grade heat source. International Journal of Refrigeration.
- La D., Dai Y., Li Y., et al., 2011. Case study and theoretical analysis of a solar driven two-stage rotary desiccant cooling system assisted by vapor compression air-conditioning. Solar energy.
- Zhang L.Z., Niu J.L., 2002. Performance comparisons of desiccant wheels for air dehumidification and enthalpy recovery. Appl Therm Eng.
- Tu R., Liu X.H., Jiang Y., 2013. Performance comparison between enthalpy recovery wheels and dehumidification wheels. International Journal of Refrigeration.

NOMENCLATURE

cp	specific heat capacity, J/kg
D0	surface diffusion constant, m ² /s
DA	gas diffusion coefficient, m ² /s
DAK	Knudsen diffusion coefficient, m ² /s
DAO	ordinary diffusion coefficient, m ² /s
dh	hydraulic diameter, m
DS	surface diffusion coefficient, m ² /s
f	area ratio, dimensionless
F	area, m ²
h	convective heat transfer coefficient, W/(K•m ²)
hm	convective mass transfer coefficient, kg/(kg•m ²)
kd	heat conductivity, W/(m ² • K)
NTU	number of heat transfer unit
P	pressure, kPa
rs	adsorption heat, J/kg

T	temperature, °C
u	velocity, m/s
W	water content, kg water/kg dry desiccant
x	volume ratio of desiccant material in the desiccant plate, dimensionless
Y	humidity ratio, g/kg
Z	wheel thickness direction, m

Greek symbols

δ	tortuosity factor, dimensionless
ε	heat exchange effectiveness
κ	porosity, dimensionless
ρ	density, kg/m ³
τ	time

Subscripts

a	air
ad	adsorption material
d	solid
w	water

Model development and experimental parameter identification for biomass pellet boilers in buildings

Jens Petzold, Daniel Büchner, Andreas Ortwein

Deutsches Biomasseforschungszentrum gemeinnützige GmbH, Torgauer Str. 116, 04347 Leipzig, Germany

1. ABSTRACT

Biomass is currently the most important renewable energy source for heating in Germany (FNR e.V., 2013). It helps to reduce carbon dioxide footprint and dependency on fossil fuels. However, solid biomass boilers operate generally less dynamic than conventional boilers fired with gaseous or liquid fuels. Clean combustion of solid biomass requires a certain minimum of fuel and combustion air flow rate to maintain a stable and hot fire bed. Both of these constraints have major influence on performance ratio and emissions. As a result, biomass heating systems in low energy buildings, possibly combined with other heat sources are prone to unfavorable operational conditions. Therefore, advanced design and control strategies are required.

Within the presented study, a biomass boiler model for the simulation software TRNSYS (Klein et al., 2012) has been developed on the basis of an existing model for a pellet stove (Type 210), developed by Nordlander (Nordlander, 2003). This was necessary since that stove model is not suitable for simulation of boilers with high water masses (Persson et al., 2009). The parameters of the adapted model were identified and validated.

The basis for the parameter identification is measured data of a dynamic reference load cycle. The parameter identification itself was done using GenOpt© with the combined Particle Swarm and Hooke Jeeves optimization method (Wetter, 2011). The validation of the parameterized model was done with a one days' load cycle. The heat output of a wood pellet boiler in a single family home was measured and like the reference cycle reconstructed with the wood pellet boiler test stand at the DBFZ.

The simulation results of both cycles agree well with the measurements. The adaptation of the pellet stove model and parameter identification with a measured dynamic load and optimization algorithm were successful.

2. INTRODUCTION

Biomass boilers show a lower dynamic combustion behavior than oil and gas boilers and require a certain minimum of fuel and combustion air flow rate for clean combustion. It can be expected that the heat demand of new built and also refurbished single family houses will further decrease in the future. This trend might lead to heat loads significantly lower than the operating range causing the boiler to start and stop more frequently. The result of that would be a poor performance ratio due to higher standby losses, higher electricity consumption for the ignition and higher emissions (Heckmann et al., 2010). If other heat sources are combined with a biomass boiler in described environment, further problems regarding performance and emissions could arise due to mismatch of all involved controllers. A development of an intelligent controller which controls the boiler, other possible heat sources, pumps etc. could solve these problems. It could take weather forecast, self-trained user behavior and fixed parameters such as size of the thermal storage and thermal properties of the building into account.

Another field of interest is the planning of biomass heating systems in buildings with a relative high heat load per biomass boiler unit such as apartment, office and industrial buildings. The mentioned problem of too small heat loads, i.e. the heat load being in the range of the minimum possible combustion power, is unlikely to occur. However, performance ratios and emissions still would be interesting for the planner.

Another interesting aspect is the determination of annual performance ratios and emissions for biomass boilers in existing installations. In practice, this would take a lot of effort to accomplish.

By using suitable simulation software and a biomass boiler model, adequate results in all of these fields can be generated. In order to select the right simulation software, it is necessary to identify the main factors that have an effect on the operation of the biomass boiler.

These are basically the fluctuating heat demand, the components used in the hydraulic system, the hydraulic system's circuitry as well as the control strategy of the components. The heat demand depends on user behaviour and the heat requirement of the building, which again is affected by the insulation value of the thermal envelope, the thermal mass and the climate conditions at the site. User behaviour must be considered with a load profile and the heat requirement of the building with an appropriate building model. Furthermore, there are a number of hydraulic components with different properties which need to be modelled.

With the simulation software TRNSYS these factors can be taken into account. The program has a variety of standard models, as well as an extensive set of meteorological data to account for different climate conditions. As for the pellet boiler, a total of five models of different qualities were identified (Glembin & Rockendorf, 2012). The model developed by Nordlander was originally designed for the simulation of pellet stoves. Nevertheless, it was chosen because it describes the operational behaviour and the processes occurring in pellet stoves in great detail. The available source code made it possible to adapt the model in order to simulate pellet boilers and biomass boilers in general. If necessary, additional features regarding combustion control, chemical and physical features can be realized in the future.

3. BIOMASS BOILER MODEL

As mentioned before, the biomass boiler model has been developed on basis of an existing pellet stove model (Nordlander, 2003). The adaptation was necessary since the model does not consider the thermal mass of the boiler water. Further adaptations were made to improve the model:

- Fixed heat transfer value to ambient air
- Instantaneous combustion replaced by a pseudo-first order kinetics (Atkins, 1990)
- Integrated combustion power control in automatic mode
- Chemical composition of fuel as parameters
- Calculation of heat capacities of hot gas
- Calculation of stoichiometric combustion air to fuel ratio
- Temperature correction factor for liquid outlet temperature (T_{out}) and boiler liquid temperature (T_{m3}) respectively

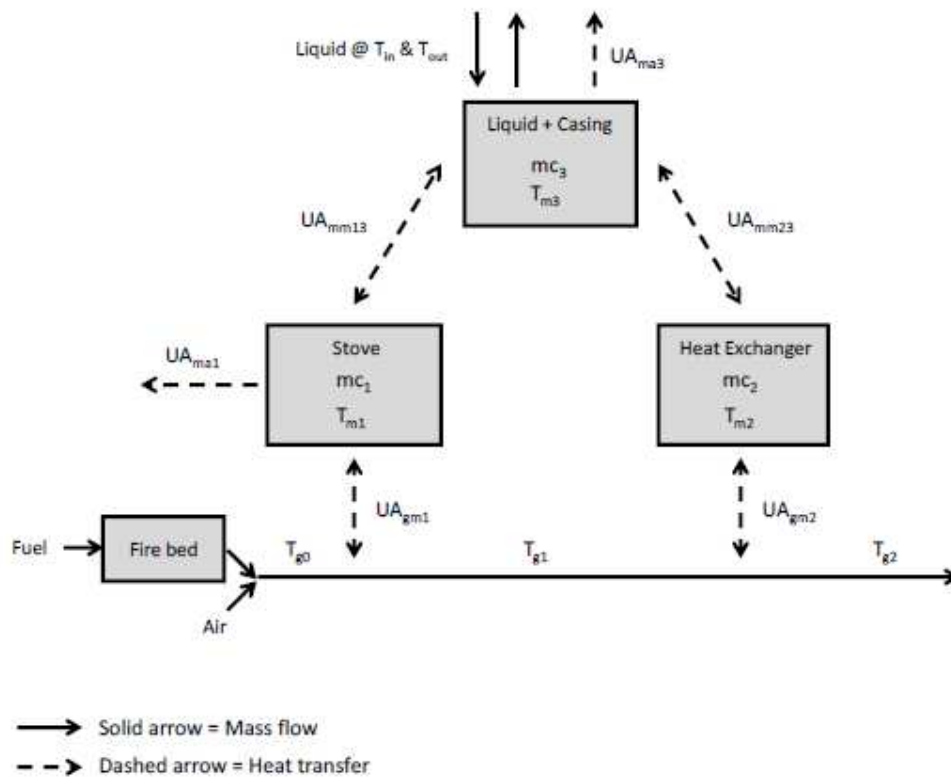


Figure 1: Schematic of the biomass boiler model

The basic structure of the adjusted model is shown in Figure 1. The thermal mass m_{c1} represents the combustion chamber, m_{c1} the relatively large gas/liquid heat exchanger and m_{c3} the water jacket including the liquid. From the supplied fuel and the combustion air, the mass flow and temperature T_{g0} is calculated adiabatically. Part of the energy of the hot gas is transferred to the combustion chamber and to the heat exchanger before it leaves at temperature T_{g2} .

The model uses a linear relationship between heat transfer and combustion power rate. Accordingly, two heat transfer values that describe this function are provided as parameters. The heat transfer from m_{c1} and m_{c3} to ambient air require only one parameter each since the heat transfer coefficient theoretically does not vary too much. It is therefore assumed to be independent from the combustion power rate. This approximation reduces the amount of parameters which again reduces the number of possible solutions for the optimization algorithms. All heat transfer parameters are considered independent from the dimensions and geometries of the heat transfer areas.

The instantaneous combustion was replaced by pseudo-first order kinetics, see Equation 1 and 2. This way it is possible to introduce a life time of the fuel during combustion and a fire bed. The life time k , which is the inverse of the rate constant, is the duration after which the fuel has e^{-1} of its original mass. This enables the model to handle solid biofuels with different sizes.

$$m_{fb} = m_{fb-1} + \left(\dot{m}_{Fin} - \frac{m_{fb-1}}{k} \right) \Delta t \quad (1)$$

$$\dot{m}_{FCmb} = \frac{m_{fb}}{k} \quad (2)$$

As for the combustion power control in automatic mode, the objective was to emulate the boiler's combustion power control. In real life, controllers are programmed to maintain the set point of the boiler water temperature. For the time being, the approach used to emulate this

behavior is to look at surplus or deficit energy of the boiler water. Combustion power reduces or increases by taking a time constant c into account. In automatic mode only the heat request (on/off) is an input. The combustion air mass flow rate and fuel mass flow rate, which are inputs in manual mode, are calculated using the stoichiometric air to fuel ratio, combustion air ratio and combustion power factor γ , which again is calculated according to Equation 3.

$$\gamma = \gamma_{-1} + \frac{mc_3c(T_{Set} - T_{m3-1})}{P_{max}} \quad (3)$$

The chemical composition of the fuel (carbon, hydrogen and nitrogen fractions), ash content, fuel moisture and relative humidity of the combustion air is considered by the model. It is used to calculate the heat capacities of the hot gas at temperatures T_{g0} , T_{g1} and T_{g2} as well as the stoichiometric air to fuel ratio. The lower heating value, related to mass of dry fuel, is a separate parameter. Together with the composition, this value is determined in the laboratory and usually provides more accurate values than calculation from the fuel's composition. The lower heating value related to the mass of wet fuel is then calculated internally, using Equation 4. If either of the composition, ash or fuel moisture parameters (model parameters 2 to 6) is zero, standard values are used (Table 1). If composition, ash and fuel moisture is provided without a heating value, it is calculated according to Boie. In any case, LHV_{wet} is provided as output.

$$LHV_{wet} = LHV_{dry}(1 - u_{fuel}) - \Delta H_{water}u_{fuel} \quad (4)$$

Table 1: Standard fuel properties.

Carbon	0.5100	kg/kg _{dry}
Nitrogen	0.0020	kg/kg _{dry}
Hydrogen	0.0629	kg/kg _{dry}
Ash	0.0022	kg/kg _{dry}
Moisture	0.0618	kg/kg _{wet}
LHV_{dry}	19163	kJ/kg _{dry}
LHV_{wet}	19002	kJ/kg _{wet}

The boiler liquid is treated as fully mixed, i.e. stratification is not considered. Instead a temperature correction factor for the liquid outlet temperature has been introduced. In reality, boiler water temperature in the water jacket and water outlet temperature differ, depending on where the temperature gauge sits inside the water jacket. By adjusting T_{out} , the boiler water temperature changes according to the amount of heat taken from the water jacket. The factor can be taken from the measurements directly.

$$tkf = \frac{T_{out}}{T_{m3}} \quad (5)$$

The model with its governing equations is described in detail in (Nordlander, 2003). A list of all model parameters, inputs and outputs with brief description is provided in the Appendix.

4. TEST STAND AND WOOD PELLET FUEL

The test stand, illustrated in Figure 2, primarily consists of a pellet boiler, a housing around the boiler, an electric heater, a hydraulic load circuit with computer controlled pump, mixing valves and various measurement instruments.

The pellet boiler has an integrated pellet storage tank which holds sufficient fuel for experiments lasting up to one day.

The housing around the boiler allows to measure heat losses to the ambient air. It is equipped with a fan and temperature sensor inside a duct on top of the housing. By providing a constant volume flow, the heat losses are a simple function of the increase of the air temperature inside the housing.

The electric heater is used to heat up the entire system, including the thermal mass of the boiler up to a defined temperature.

The computer controlled pump and mixing valves allow running any desired load profile. The response of the pellet boiler can then be measured using the following instruments.

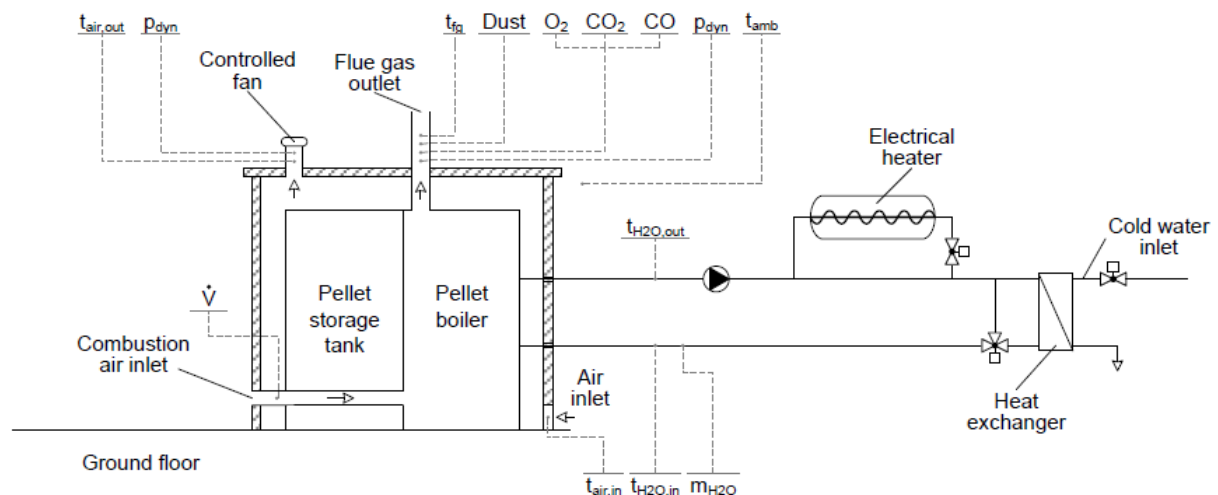


Figure 2: Schematic of the pellet boiler test stand.

Flue gas:

- Dynamic pressure with Pitot tube (of the Prandtl-type) and pressure gauges
- Temperature with temperature gauge
- Chemical composition with gas analyser
- Particulate Matter Emissions (Dust)

Combustion air:

- Volume flow rate with gas meter
- Temperature with temperature sensor

Fuel consumption:

- Mass with scales
- Mass flow rate through feeding screw with boiler internal encoder

Hydraulic circuit:

- Water mass flow rate with flow meter
- Several temperatures with temperature gauges

Heat losses to ambient air:

- Dynamic pressure inside duct with Prandtl tube and pressure gauges
- Ambient air and duct temperature with temperature gauges

The pellet boiler has a rated combustion power of 17.5 kW and a rated heat output of 15 kW. Its general structure is illustrated in Figure 3.

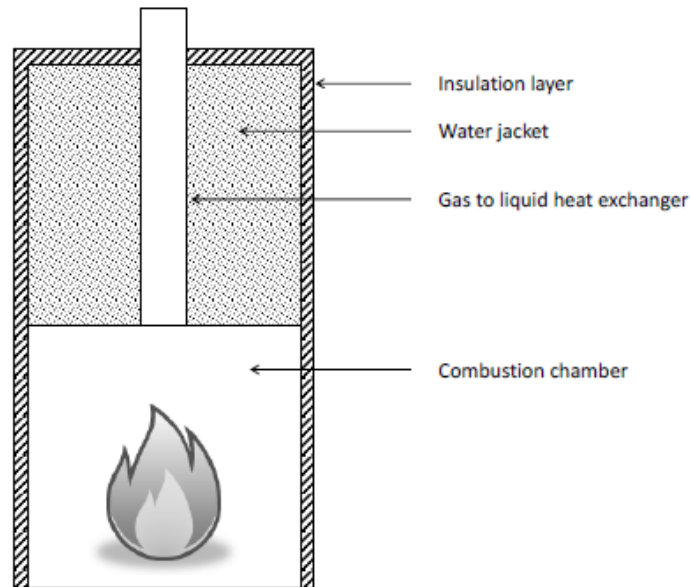


Figure 3: Schematic structure of the boiler.

For both of the cycles, wood pellets of the same lot were used. The relevant properties were determined according to the standards, listed in Table 2.

Table 2: Properties of the wood pellets used for the tests.

Carbon	0.4990	kg/kgdr	DIN EN 15104
Nitrogen	0.0039	y	
Hydrogen	0.0673	kg/kgdry	
Ash	0.0036	kg/kgdry	
Moisture	0.0818	kg/kgwet	
LHV _{dry}	18370	kJ/kgdry	DIN EN 14774-1 DIN EN 14346
LHV _{wet}	16667	kJ/kgwet	DIN EN 14918

5. PARAMETER IDENTIFICATION

For model parameter identification, measured data of an annual reference load cycle is used at the test stand. The cycle, described in (Heckmann et al., 2010), is derived from an average annual load and compressed to an eight hour cycle.

The measured data are inputs to the model, running in manual mode:

- Mass flow rate fuel, combustion air and liquid
- Boiler inlet temperature
- Ambient air temperature

The resulting model outputs used for the parameter identification are boiler outlet temperature and flue gas temperature.

The aim of the parameterization is to find the correct heat transfer values. All other parameters can be taken from the measurements directly. Thermal masses can be derived from the total weight of the boiler and the heat capacities of the materials.

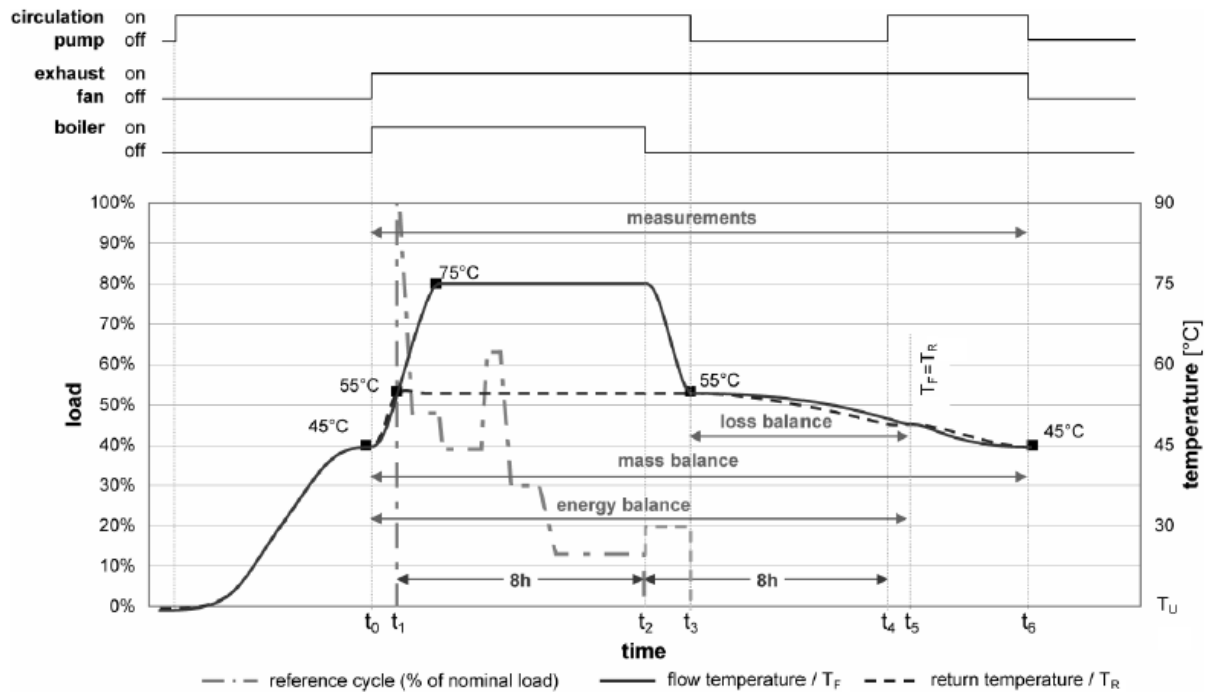


Figure 4: Annual reference load cycle.

For a start, the fixed heat transfer values which describe losses to the ambient (UA_{ma1} , UA_{ma3}) can be estimated by assuming a total heat loss of around five to ten percent of the supplied energy. That leaves eight heat transfer parameters to be identified with the optimization program GenOpt©.

Table 3: Heat transfer parameters.

Heat transfer	Gas to mc_1	Gas to mc_2	mc_1 to mc_3	mc_2 to mc_3
$\gamma = 0\%$	UA_{gm10}	UA_{gm20}	UA_{mm130}	UA_{mm230}
$\gamma = 100\%$	UA_{gm11}	UA_{gm21}	UA_{mm131}	UA_{mm231}

For the optimization, the Particle Swarm and Hooke Jeeves optimization method (GPSPOCCHJ, described in (Wetter, 2011)) are applied. The optimization algorithm tries to find the global minima of the cost function (Equation 6) by varying the parameters, listed in Table 3, for each simulation. The range for variation of each parameter should be relatively large. The cost function considers the boiler water outlet temperature as well as the flue gas temperature with a weighting factor. The inclusion of flue gas temperature excludes solutions where the boiler water temperature would fit but the flue gas temperature would not.

$$cf = \sum_{i=0}^N \left(0.9(T_{Os,i} - T_{OM,i})^2 + (T_{FS,i} - T_{FM,i})^2 \right) \quad (6)$$

After the first optimization is finished, the thermal masses and the heat transfer parameters which describe losses to the ambient air can be tuned. This is done in the same way as the first

parameter identification. The only difference is that GenOpt© is given the identified parameters as a starting point and that the range for variation of all parameters to be tuned is relatively small. This way all heat transfer parameters and thermal masses are readjusted and the best fit for boiler outlet temperature and flue gas temperature is achieved.

6. VALIDATION

The heat output of a wood pellet boiler in a single family home was measured and reconstructed with our test stand to validate the model with realistic values. The load profile, shown in Figure 5, consists of twelve boiler starts and the load ranges from 20% to 90% of the boiler's rated power.

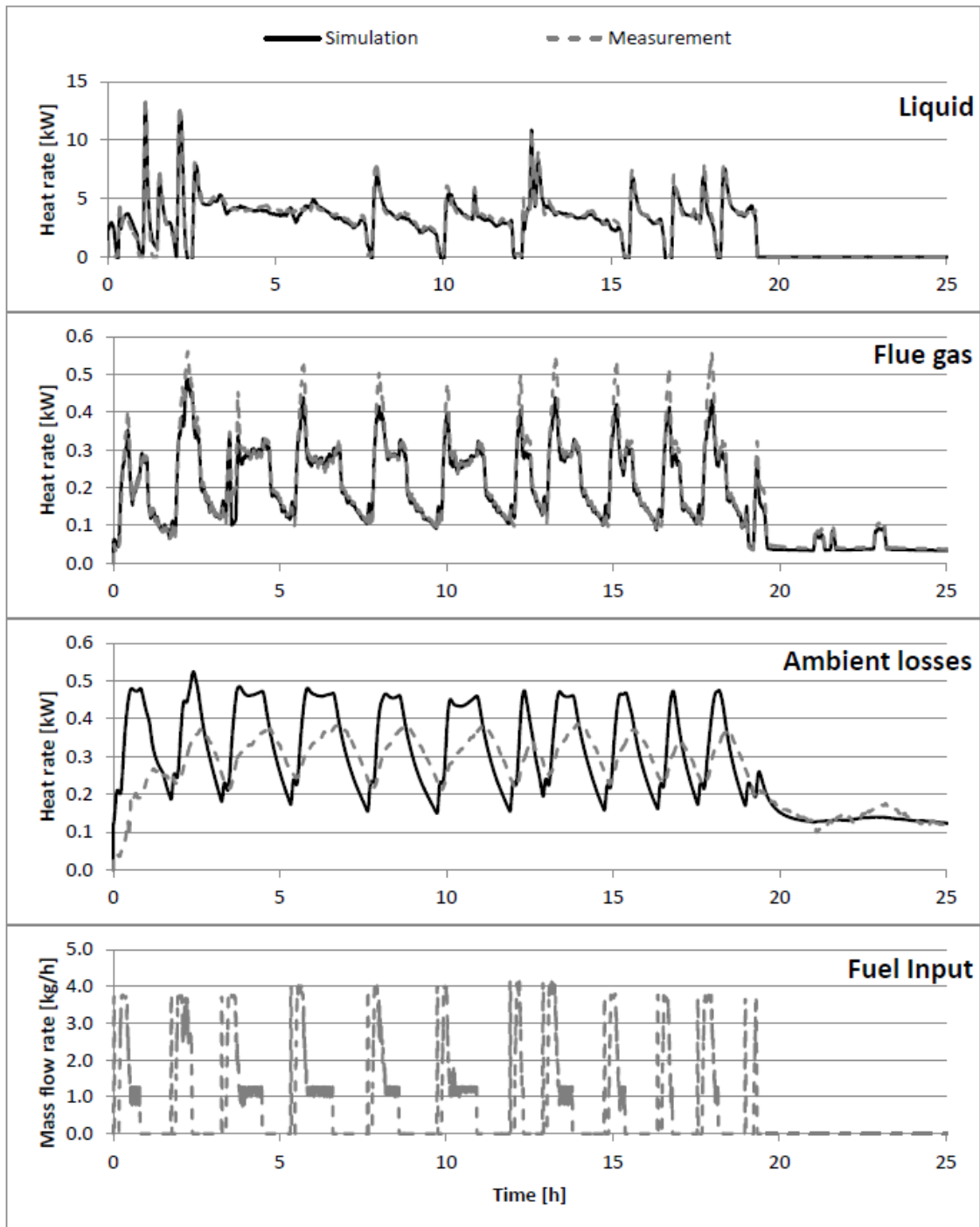


Figure 5: Results of the validation.

The parameters, identified with the reference cycle, remain unchanged and the model is used with the measured data of the validation cycle. The model outputs and the measured data are shown in Figure 5.

Most noticeable is the time shift between simulation and measurement for the ambient losses. It is possible that the above described measurement method with the housing is not suitable if accurate time resolved results are required. The housing itself consists of a metal frame cladded with a drywall on the outside, Styrofoam (EPS) and aluminium foil on the inside. This could act as a (small) thermal mass and therefore cause a delay in heating up and cooling down phases.

Unfortunately, carbon monoxide data for the validation cycle is not available due to technical problems. The CO values for the model parameters 36 to 39 and the combustion air ratios (see Appendix) were taken from the reference cycle.

An evaluation of the results is given in the following chapter.

7. COMPARISON OF REFERENCE AND VALIDATION CYCLE

To see how well the simulations of the validation cycle and reference cycle fit the measurements, a histogram of temperature differences between measured and simulated values can be used. This was done for the boiler outlet temperature (Figure 6) and the flue gas temperature (Figure 7). For a more meaningful evaluation, average and standard deviation is given in Table 4.

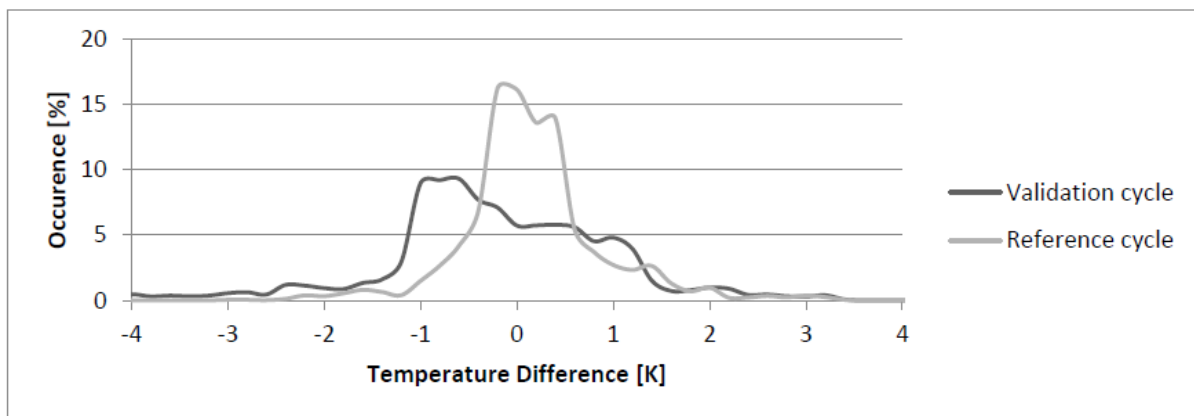


Figure 6: Histogram of measured and simulated boiler water temperature differences.

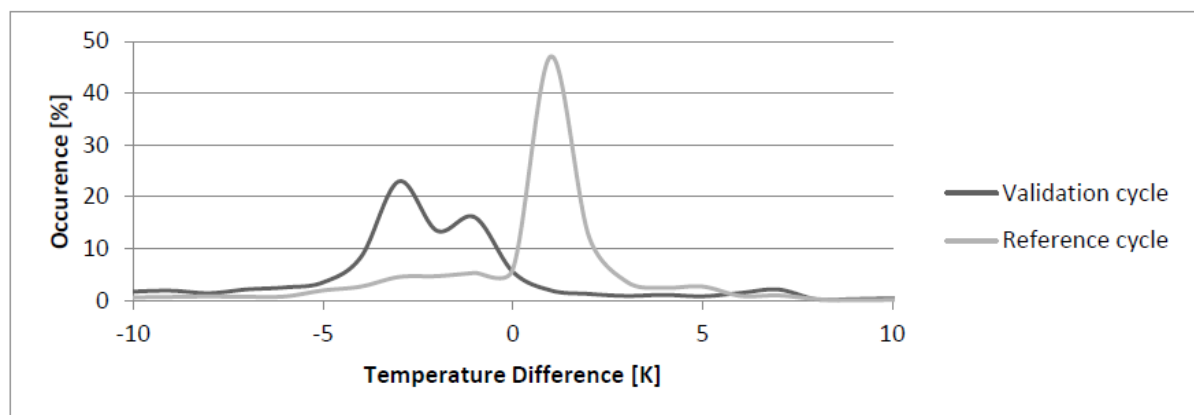


Figure 7: Histogram of measured and simulated flue gas temperature differences.

Table 4: Evaluation of simulated reference cycle and validation cycle.

	Reference cycle	Validation cycle
Boiler outlet		
Standard deviation [K]	1.57	1.44
Average [K]	0.08	-0.36
Flue gas		
Standard deviation [K]	3.26	5.59
Average [K]	0.16	-4.04

Another indication is the energy balance for the two cycles and the comparison between them (Table 5). The energy balances for the two simulations are not completely closed. This is because of uncertainties of the measurements (fuel input rate, boiler inlet temperature, water mass flow rate, combustion air mass flow rate) which are passed on to the inputs of the model.

Table 5: Measured and simulated energy balances for the reference and validation cycle with estimated measurement uncertainties.

	Reference cycle		Validation cycle		Measurement uncertainties [%]
	Measured [%]	Simulated [%]	Measured [%]	Simulated [%]	
Fuel & Electricity	100.0	100.0	100.0	100.0	± 0.5
Hot water	82.3	83.8	86.6	83.7	± 1.3
Flue gas	6.3	5.1	6.1	5.7	± 3.0
Losses to ambient	8.6	8.4	8.5	9.3	± 3.5
Balance	2.8	2.8	-1.2	1.3	

The relative errors of the transferred heat energies are calculated with Equation 7.

$$\varepsilon = \frac{Q_S - Q_M}{Q_M} * 100 \quad (7)$$

	Reference cycle [%]	Validation cycle [%]
$\varepsilon_{Q_{Water}}$	1.8	-3.4
$\varepsilon_{Q_{Flue}}$	6.4	-6.4
$\varepsilon_{Q_{Ambient}}$	-3.0	9.9

The effect of the introduced fire bed is shown in Figure 8. The boiler water temperature slightly overshoots the measured and simulated w/o fire bed temperature values. In return, the model is more accurate in its time dependent behaviour.

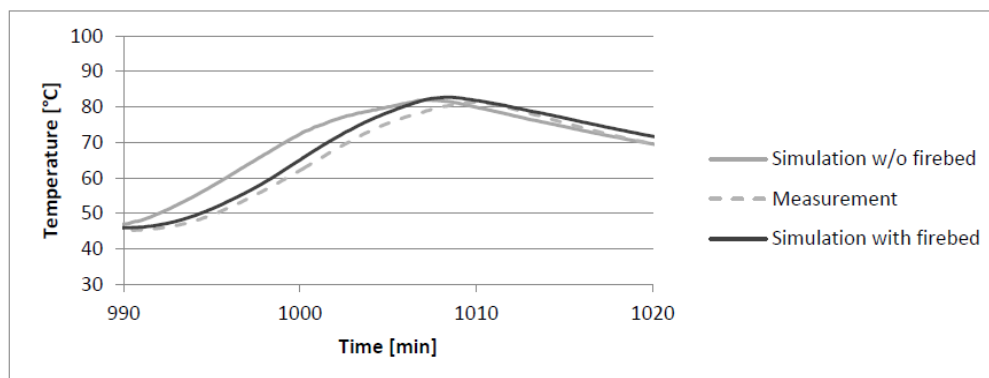


Figure 8: Comparison of boiler water temperature with and without fire bed.

8. SUMMARY AND CONCLUSIONS

The pellet stove model Type 210 for the simulation software TRNSYS has been adapted in order to simulate biomass boilers. Further changes, such as including a fire bed and consideration of the chemical composition of the fuel, improve the performance of the model. The model was parameterized with measured data of a dynamic reference load cycle and a hybrid global optimization algorithm. The validation of the model with the identified parameters was done with measured data of a one day's load cycle. This load profile was measured in a single family home and reconstructed with our boiler test stand. The model was running in "manual mode" for both of the simulations, meaning that mass flow rates of combustion air and fuel were inputs to the model. The resulting outputs of interest were the time dependent values of liquid outlet temperature and flue gas temperature. Next to the energy balances they have been used for evaluation of the simulations. Altogether, it can be stated that the simulation results show good agreement with the measurements and that parameter identification using the described method delivers good results. If different controller strategies and variations of the thermal masses as part of a design process are to be tested, relative errors as calculated with Equation 7 are in an acceptable range, providing a good basis for comparison.

A validation in "automatic mode", where only heat request (on/off) is given as input to the model, needs to be carried out. In fact, it would be a validation which additionally takes the combustion power control, stoichiometric air to fuel calculation, electricity consumption and the combustion air ratio into account. Since TRNSYS is widely used by planners, it would also make sense to provide some help for the parameter identification. Parameter identification for two or three more units of the same type but with different nominal combustion power could be carried out. If obvious mathematical relations between the same heat transfer parameters exist, each heat transfer parameter could be calculated using a given factor and the rated power of the boiler. The other remaining parameters such as electricity consumption, durations of operation phases, combustion air ratio and air mass flow rates during burn-off and standby phases could be derived from these three or four units, too.

ACKNOWLEDGEMENT

This study has been performed in the frame of the BioMaxEff project. The research leading to these results has received funding from the European Union Seventh Framework Programme (FP7/2007-2013) under Grant Agreement n° 268217.

REFERENCES

- Atkins, P. W. (1990). *Physical Chemistry* (4th ed.). Oxford: Oxford University Press. FNR e.V. (2013). *Basisdaten Bioenergie Deutschland 2013*. Fachagentur Nachwachsende Rohstoffe e.V. Retrieved from <http://www.vrd-stiftung.org/wp-content/uploads/Basisdaten-Bioenergie-2013-FNR.pdf>
- Glembin, J., & Rockendorf, G. (2012, ca). *Integration von Heizkesseln in Wärmeverbundsysteme mit großen Solaranlagen*. Retrieved from http://www.delta-q.de/export/sites/default/de/downloads/Endbericht_T2_Kesselmodell.pdf
- Heckmann, M., Friedl, G., Schwarz, M., Rossmann, P., Hartmann, H., Baumgartner, H., ... Themessl, A. (2010). *Bestimmung von Jahresnutzungsgrad und Emissionsfaktoren von Biomasse-Kleinfeuerungen am Prüfstand*. Bioenergy 2020+ GmbH. Retrieved from http://www.bioenergy2020.eu/files/publications/pdf/815650_Jahresnutzungsgrad_Endbericht.pdf
- Klein, S. A., Beckmann, W. A., Mitchell, J. W., Duffie, J. A., Duffie, N. A., & Freemann, T.

L. (2012). TRNSYS, a transient system simulation program (Version 17). Solar Energy Laboratory, University of Wisconsin, Madison USA.

Nordlander, S. (2003). TRNSYS model for Type 210 - Pellet stove with liquid heat exchanger. Högskolan Dalarna. Retrieved from <http://du.diva-portal.org/smash/get/diva2:522636/FULLTEXT01.pdf>

Persson, T., Fiedler, F., Nordlander, S., Bales, C., & Paavilainen, J. (2009). Validation of a dynamic model for wood pellet boilers and stoves. *Applied Energy*, 86(5), 645–656. doi:10.1016/j.apenergy.2008.07.004

Wetter, M. (2011, December). GenOpt© Generic Optimization Program. Lawrence Berkeley National Laboratory. Retrieved from <http://simulationresearch.lbl.gov/GO/download/manual-3-1-0.pdf>

NOMENCLATURE

Symbols

ε_{QWater}	[%]	Relative simulation error of hot water generation
ε_{QFlue}	[%]	Relative simulation error of flue gas
$\varepsilon_{QAmbient}$	[%]	Relative simulation error of losses to ambient air
γ	[-]	Combustion power factor
T_{OS}	[°C]	Boiler water outlet temperature, simulated
T_{OM}	[°C]	Boiler water outlet temperature, measured
T_{FM}	[°C]	Boiler water temperature, measured
T_{FS}	[°C]	Flue gas temperature, simulated
T_{FM}	[°C]	Flue gas temperature, measured
T_{Set}	[°C]	Boiler water set temperature
T_{m3}	[°C]	Temperature of thermal mass Nb. 3
T_{out}	[°C]	Liquid outlet temperature of the model
m_{fb}	[kg]	Mass of fire bed
m_{fb-1}	[kg]	Mass of fire bed at previous time step
\dot{m}_{Fin}	[kg/h]	Fuel mass flow rate, input
\dot{m}_{FCmb}	[kg/h]	Fuel mass flow rate, releasing energy at current time step
m_{c3}	[kg]	Thermal mass of boiler water and water jacket
P_{max}	[kJ/h]	Rated combustion power
Q_S	[kJ]	Simulated heat energy
Q_M	[kJ]	Measured heat energy
ct	[K ²]	Cost function
k	[h]	Life time of the fuel during combustion
t	[h]	Time

c	[1/h]	Time constant of thermal mass m_{c3} for combustion power control
tkf	[-]	Temperature correction factor
ΔH_{water}	[kJ/kg]	Specific evaporation enthalpy of water (2450 kJ/kg)
u_{fuel}	[kg/kg]	Moisture content of the fuel
LHV_{dry}	[kJ/kg]	Lower heating value related to mass of dry fuel
LHV_{wet}	[kJ/kg]	Lower heating value related to mass of wet fuel

APPENDIX – MODEL PARAMETER, INPUT AND OUTPUT LIST

Parameter	Mode	Description	Value	Unit
1		Operation Mode (1-Automatic; 2-Manual)	2	-
2	1;2	Carbon fraction kg/kg dry fuel	0.4990	kg/kg
3	1;2	Hydrogen fraction kg/kg dry fuel	0.0673	kg/kg
4	1;2	Nitrogen fraction kg/kg dry fuel	0.0039	kg/kg
5	1;2	Ash fraction kg/kg dry fuel	0.0036	kg/kg
6	1;2	Fuel moisture ratio kg/kg moist fuel	0.0818	kg/kg
7	1;2	Lower heating value dry fuel	18370	kJ/kg
8	1;2	Life time of the fuel during combustion	0.033	h
9	1;2	Specific heat of liquid	4.19	kJ/kg.K
10	1;2	Thermal mass of mass 1	30	kJ/K
11	1;2	Thermal mass of mass 2	35	kJ/K
12	1;2	Thermal mass of mass 3	270	kJ/K
13	1	Maximum combustion power	63000	kJ/h
14	1	Minimum combustion power	18900	kJ/h
15	1	Average combustion power during ignition and flame stabilisation phases	18900	kJ/h
16	1	Electrical power during ignition phase	3290	kJ/h
17	1	Electrical power during modulation phase, at $\gamma=0$	139	kJ/h
18	1	Electrical power during modulation phase, at $\gamma=1$	232	kJ/h
19	1	Duration of ignition phase	0.153	h
20	1	Duration of flame stabilisation phase	0.053	h
21	1	Duration of burn-off phase with fan on	0.214	h
22	1	Mass flow of flue gas during burn-off phase with fan	12.5	kg/h
23	1	Flue gas leak flow @ 50°C in standby and after-glow phases	Not tested	kg/h
24	1;2	UA between gas and m1, at $\gamma=0$	60	kJ/(h.K)
25	1;2	UA between gas and m1, at $\gamma=1$	280	kJ/(h.K)
26	1;2	UA between gas and m2, at $\gamma=0$	625	kJ/(h.K)
27	1;2	UA between gas and m2, at $\gamma=1$	550	kJ/(h.K)
28	1;2	UA between m1 and ambient	10	kJ/(h.K)
29	1;2	UA between m3 and ambient	10	kJ/(h.K)
30	1;2	UA between m1 and m3, at $\gamma=0$	75	kJ/(h.K)
31	1;2	UA between m1 and m3, at $\gamma=1$	700	kJ/(h.K)
32	1;2	UA between m2 and m3, at $\gamma=0$	175	kJ/(h.K)
33	1;2	UA between m2 and m3, at $\gamma=1$	200	kJ/(h.K)
34	1;2	Outlet Temperature correction factor	1.03	-
35	1	Time constant for combustion power control	8	1/h
36	1;2	CO emission factor, at $\gamma=0$	0.329	g/MJ

37	1;2	CO emission factor, at $\gamma=1$	0.065	g/MJ
38	1;2	Lumped CO emission during start phase	3.2	g
39	1;2	Lumped CO emission during stop phase	1.3	g
Input	Mode	Description	Value	Unit
1	1	Boiler control (on/off)		-
	2	Fuel mass flow rate		kg/h
2	1	Combustion air ratio, at $\gamma=0$	4.47	-
	2	Combustion air mass flow rate		kg/h
3	1	Combustion air ratio, at $\gamma=1$	2.51	-
	2	Electrical power supplied to boiler		kJ/h
4	1;2	Temperature of liquid entering water jacket		°C
5	1;2	Mass flow of liquid entering water jacket		kg/h
6	1;2	Relative humidity of combustion air		%
7	1;2	Ambient temperature around boiler		°C
8	1	Outdoor temperature		°C
9	1;2	Temperature of combustion air		°C
10	1	Boiler temperature for combustion start	45	°C
11	1	Boiler temperature for combustion stop	85	°C
12	1	Boiler set temperature	75	°C
Output	Mode	Description	Unit	
1	1;2	Temperature of mass 1 (stove)	°C	
2	1;2	Temperature of mass 2 (heat exchanger)	°C	
3	1;2	Temperature of mass 3 (water jacket)	°C	
4	1;2	Temperature of hot gas Tg0	°C	
5	1;2	Temperature of hot gas Tg1	°C	
6	1;2	Temperature of flue gas Tg2	°C	
7	1;2	Liquid outlet temperature	°C	
8	1;2	Liquid mass flow rate	kg/h	
9	1;2	Fuel mass flow rate	kg/h	
10	1;2	Combustion air mass flow rate	kg/h	
11	1;2	Flue gas mass flow rate	kg/h	
12	1;2	Mass flow rate of CO in flue gas	kg/h	
13	1;2	Cumulative number of starts	-	
14	1;2	Cumulative mass of fuel used	kg	
15	1;2	Cumulative mass of emitted CO	kg	
16	1;2	Combustion Power	kJ/h	
17	1;2	Electrical Power	kJ/h	
18	1;2	Sum of Power to ambient air in room	kJ/h	
19	1;2	Power to liquid	kJ/h	
20	1;2	Power of flue gas	kJ/h	
21	1;2	Power mass 1 to mass 3	kJ/h	
22	1;2	Power mass 2 to mass 3	kJ/h	
23	1;2	Power hot gas to mass 1	kJ/h	
24	1;2	Power hot gas to mass 2	kJ/h	
25	1;2	Power mass 1 to ambient air in room	kJ/h	
26	1;2	Power mass 3 to ambient air in room	kJ/h	
27	1;2	Air factor	-	

28	1	Operation phase during time step: 0 – Standby 1 – Flushing & Ignition 2 – Flame stabilisation 3 – Modulation 4 – Burn-off with fan 5 – After-glow without fan	-
29	1;2	Power rate	% base 1
30	1	Liquid mass flow rate control (equals parameter 29 for now)	% base 1
31	1;2	Mass of fire bed	kg
32	1;2	Lower heating value of fuel, related to mass of wet fuel	kJ/kg

NINTH SESSION
MODEL REDUCTION

Bottom-up modeling of the Belgian residential building stock: influence of model complexity

Glenn Reynders^{1,2,3*}, Jan Diriken^{1,3}, Dirk Saelens^{1,2}

⁽¹⁾ Energyville, Dennenstraat 7, BE-3600 Genk, Belgium

⁽²⁾ Building Physics Section, Civil Engineering Department, KU Leuven, Kasteelpark Arenberg 40, box 2447, BE-3001 Heverlee, Belgium

⁽³⁾ Unit Energy Technology, VITO, Boeretang 200, BE-2400 Mol, Belgium

1. ABSTRACT

Demand-side management using the thermal storage capacity of buildings is often suggested as an efficient and economically feasible technology to enable a wide-spread integration of intermittent renewable energy sources. Nevertheless, to quantify the potential benefits of activating the structural storage capacity on a national level, a dynamic bottom-up building stock model is needed. Thereby the aim is not only on the calculation of the annual heat demand, but mostly on an accurate dynamic simulation of the instantaneous heat demand and the indoor temperature, since these are directly linked to active demand response measures. In this paper the suitability of reduced-order models for the application in a dynamic bottom-up building stock model for Belgium is evaluated. Thereby a detailed building energy simulation is compared to reduced-order models of increasing complexity. For the latter both a theoretical approach and a parameter estimation method are analyzed. The building stock description is based on the typical housing approach of the TABULA-project. The reduced-order models show an acceptable prediction of the dynamic temperature profile and heat demand during the heating season, whilst reducing the calculation time significantly. Nevertheless, the reduced-order models are, due to the strong simplifications, less accurate when applied on boundary conditions which significantly differ from the identification data. Especially the coupling between two adjacent rooms is found to reduce the identifiability of the model parameters, resulting in unreliable estimates of inter-zonal heat flows.

Keywords: reduced-order models, system-identification, building stock modeling

2. INTRODUCTION

In order to allow a more sustainable integration of renewable energy sources in the electricity network and avoid possible stability problems and efficiency losses (Baetens et al., 2012; Lund, Marszal, & Heiselberg, 2011) resulting from the mismatch between intermittent renewable production and demand, development of intelligent networks or Smart Grids is suggested. Smart Grids integrate real-time communication between actuators on both demand and supply side, to enable demand-side management and the use of storage technologies (Zahedi, 2011; Battaglini, Lilliestam, Haas, & Patt, 2009). In this context of Smart Grids, buildings can be of significant importance, since the thermal mass of the building may be actively used as a thermal storage capacity to enable demand-side management of the energy demand for heating (Kummert, Andre', & Nicolas, 2001; Henze, Felsmann, & Knabe, 2004; Braun, 2003). Thereby intelligent control strategies e.g. model predictive control (MPC) are used to optimize the energy use and thermal storage capacity of buildings by adequate control of the indoor air temperature.

Whereas such control strategies show their potential to optimize the use of storage in order to match demand and load profiles, avoid peak loads and take into account time of use pricing,

research shows that, as a down-side, activating the structural storage capacity may lead to increased transmission and ventilation losses (Reynders, Nuytten, & Saelens, 2013; De Coninck, Baetens, Saelens, Woyte, & Helsen, 2014). These increased thermal losses need to be compensated by an increase of energy efficiency of heat and electricity production systems or by an increased penetration of renewable energy sources. To evaluate this balance, a thorough analysis of the use of structural storage for demand-side management needs to be carried out on district and even national level, taking into account the impact of demand-side management on both the demand and production side (Bruninx, Patteeuw, Delarue, Helsen, & D'haeseleer, 2013). Even though many studies include or even focus on demand-side management (Arteconi, Hewitt, & Polonara, 2013; Pina, Silva, & Ferrão, 2012; Ellerbrok, 2014; Gottwalt, Ketter, Block, Collins, & Weinhardt, 2011; Muratori, Schuelke-Leech, & Rizzoni, 2014), often the supply- or the demand-side is oversimplified. For example, when the focus is on electric power generation, the demand is commonly represented by a price elastic demand or by virtual generator models (De Jonghe, 2011). In this paper, a reduced-order bottom-up dynamic building stock model is developed to quantify the demand-side management potential of the structural storage capacity of the Belgian building stock. This dynamic model aims at providing a computational efficient and accurate simulation of the dynamic behavior of the dwellings that allows for the evaluation of active demand response using the structural thermal mass of dwellings on an aggregate (e.g. district or national) level.

For Belgium a number of studies have been published on the inventory and modeling of the Belgian housing stock (Cyx, Renders, Van Holm, & Verbeke, 2011; Allacker, 2010; Verbeeck, 2007; KULeuven, VITO, & BBRI, 2001). Nevertheless, modeling approaches typically consist of monthly averaged heat balance and degree-day calculations instead of dynamic building energy simulations. A dynamic analysis is however a prerequisite to quantify the demand-side management potential of the structural thermal storage capacity of buildings. Moreover, the available data is mostly focused on geometry, insulation thickness, ventilation type and glazing properties and does not provide the detailed information needed for the dynamic modeling of building e.g. material properties, properties of internal walls and floors, etc.

Therefore in this paper, the framework and building descriptions obtained from the TABULA-project are elaborated using engineering assumptions and knowledge about traditional construction methods to develop suitable dynamic reduced-order models. These models should be able to accurately simulate the instantaneous heat demand and indoor temperatures of buildings with a low computation cost. In the context of demand-side management an accurate simulation of the instantaneous heat demand as well as the indoor temperature are a prerequisite, since optimal control strategies will optimize the heat demand to e.g. reduce the peak demand and increase the match with renewable electricity production, by adapting the temperature setpoint for heating. As such these control strategies have a direct impact on the thermal comfort of the occupants. Inadequate prediction of the indoor temperature and the dynamic thermal behavior of the building may thus not only influence the efficiency of smart buildings and districts, it may also jeopardize thermal comfort.

The main research question in this work is therefore formulated as: 'Are reduced-order models suitable for simulation of the dynamic behavior and instantaneous heat demand of buildings with the high temporal resolution needed for the quantification of the demand-side management potential?' Therefore, the influence of the method used to establish the reduced-order models is evaluated. In this paper, two approaches to calculate the model parameters are analyzed: (1) a theoretical calculation of the building parameters based on the building stock data completed by assumptions and rules-of-thumb, and (2) parameter identification using grey-box modeling. The performance of the obtained reduced-order models is evaluated by a quantitative and qualitative comparison of the instantaneous heat demand and indoor temperature profiles






























Main matrix of the Belgian housing typology							
Region	Construction Year Class	Single Family House - Detached	Single Family House - Semi detached	Single Family House - Terraced	Multi-Family House - Small	Multi-Family House - Medium	Multi-Family House - Large
1	national (Belgium) ... 1945	 BE.N.SFH.01.det	 BE.N.TH.01.sem	 BE.N.TH.01.terr	 BE.N.MFH.01.small	 BE.N.MFH.01.medium	
6	national (Belgium) 1946 - 1970	 BE.N.SFH.02.det	 BE.N.TH.02.sem	 BE.N.TH.02.terr	 BE.N.MFH.02.small	 BE.N.MFH.02.medium	 BE.N.MFH.02.large
12	national (Belgium) 1971 - 1990	 BE.N.SFH.03.det	 BE.N.TH.03.sem	 BE.N.TH.03.terr	 BE.N.MFH.03.small	 BE.N.MFH.03.medium	 BE.N.MFH.03.large
18	national (Belgium) 1991 - 2005	 BE.N.SFH.04.det	 BE.N.TH.04.sem	 BE.N.TH.04.terr	 BE.N.MFH.04.small	 BE.N.MFH.04.medium	 BE.N.MFH.04.large
24	national (Belgium) 2006 ...	 BE.N.SFH.05.det	 BE.N.TH.05.sem	 BE.N.TH.05.terr	 BE.N.MFH.05.small	 BE.N.MFH.05.medium	 BE.N.MFH.05.large

Figure 1: Main matrix of the Belgian housing typology following the harmonized TABULA approach.

of the reduced-order models against detailed building energy simulations. The latter are, in the absence of qualitative time-series data on the heat demand for the different building typologies, used as a reference case.

In section 3.1 the data and assumptions regarding the Belgian building stock are discussed. As a basis the TABULA-project is used. Section 3.2 and 3.3 describe the detailed and reduced-order models respectively. In section 4, the verification and validation of the building models is presented. For these models quantitative and qualitative comparison of the annual and instantaneous heat demand and the indoor temperature profiles is carried out between the different models. The impact of the modeling approach on the aggregated national level is shown in section 4.3. The main findings and suggestions for future work are discussed in section 5.

3. METHODOLOGY

In this section the methodology used to develop a reduced-order dynamic model for the Belgian residential building stock is presented. The building stock data is obtained from the European TABULA-project and is discussed in paragraph 3.1. Additional assumptions that were needed for the development of the dynamic models are postulated.

Different reduced-order modeling approaches are evaluated for their ability to accurately simulate the dynamic behavior of the buildings typologies. An accurate and computational efficient simulation of the transient response of buildings to the outdoor climate, internal gains and heating is a prerequisite to evaluate the demand-side management potential of the structural storage capacity on an aggregate level. The performance of the reduced-order models is, in the absence of measurement data of the heat demand, analyzed by a quantitative and qualitative comparison with detailed building energy simulations in Modelica. The detailed model, used as reference scenario, is described in paragraph 3.2. The reduced-order models are described in paragraph 3.3.

3.1 Building stock description

The development of the dynamic building stock models is based on the typology data presented in the TABULA-project (Loga, Balaras, Dascalaki, & Zavri, 2010). The TABULA-project is a European project that focuses on the evolution of energy-related properties of buildings,

regarding the energy performance of the particular building elements as well as the possibilities of improvement. The 13 partners and 2 associated partners involved in the European TABULA project have committed themselves to develop a housing typology for their respective countries. The Belgian residential building stock is represented by 30 typical dwellings grouped in 6 typologies and 5 age classes as shown in figure 1. In this paper only the single family houses are addressed. Multi-family houses are not considered since their dynamic behavior as well as the modeling approach significantly differ from single-family dwellings.

In the TABULA-project, the geometry and U-values of the envelope components are specified for each typical dwelling together with a typical infiltration and ventilation rate. Although the exact material properties used to calculate the U-values of the envelope components are not specified, a typical composition of the components is provided for the envelope components. Based on these proposed compositions, the material properties and thicknesses, used in the detailed model, have been designed to match the U-values given in the TABULA specification. Note that both geometry and material properties of the interior walls and floors have not been specified.

The main assumptions are summarized in table 1. Since the TABULA project uses a single zone heat balance calculation, most assumptions are related to convert the geometry description for a two-zone model.

3.2 Detailed building simulation model in IDEAS

The detailed simulations are carried out using the IDEAS library developed at KU Leuven. The IDEAS library is implemented in Modelica and expresses transient thermal processes in detail, based the control volume method (CVM) as described in (Baetens et al., 2012). The detailed, or white-box (WB) model is simulated for the heating dominated climate of Uccle (Belgium) as a 2-zone building: the day-zone (ground floor) and night-zone (first floor). Thereby 1-minute climate data obtained from Meteororm 6.1 are used for the boundary conditions (Meteotest, 2008). The output is generated with a sample time of 5 minutes.

Since in this study only the heat demand of the building and not the energy use of the heating system is considered, an ideal heating system is implemented. The heating system consists of an ideal production unit with a limited power output equal to the nominal design power according to EN12831 (CEN, 2003). The emission system consists of low temperature radiators, modeled to take into account their thermal mass and dynamic effects as described in (Reynders, Baetens, & Saelens, 2012). Ventilation and infiltration are implemented with a constant airflow model. Hygienic ventilation is only implemented after 2005 with a constant ventilation rate of 0.4 ACH, in accordance with the TABULA report. The use of the thermostat is implemented by a deterministic pattern based on Aerts et al. (2014), as shown in table 2.

Due to the absence of adequate disaggregated measurement data on the energy demand of the building stock, the obtained detailed model is used as a base model. The simulations obtained by these white-box models will be used as virtual experiments on which the reduced-order models are identified. Thereby it is assumed that, although simplifications are made in the detailed models, these simulations correctly represents the thermodynamics of the different buildings in the Belgian building stock. The most important simplifications and assumptions for the base model that might influence the parameter estimation of reduced-order building models are:

- uniform surface temperatures, resulting in 1D-heat transfer through building components.
- uniform air temperature for complete zone.

- solar gains and radiant components of internal gains and heating are distributed using area and emissivity weighted distribution factors. Time dependent effects corresponding to e.g. the incident angle of solar radiation can thus not be taken into account.
- the internal mass of furniture is taken into account by increasing thermal capacity of zone air by factor 5 (Sourbron, 2012).
- the infiltration rate is constant and not depending on wind conditions.

Table 1: Additional assumptions to complete 2 zone building models based on TABULA building stock description.

Aspect	Detached	Semi-detached	Terraced
Unheated spaces	All components except floors and common walls are assumed to be in contact with the outdoor environment. The whole ground floor is in contact with the ground.		
Floor area day-zone ($A_{fl,D}$)	The entire ground floor is considered as day-zone		
Floor area night-zone ($A_{fl,N}$)	Calculated as: $A_{fl,use} - A_{fl,D}$		
Volume day-zone (V_D)	Calculated as: $A_{fl,D} h_{fl}$		
Volume night-zone (V_N)	Calculated as: $V_{prot} - V_D$ (with V_{prot} the protected volume)		
Floor height (h_{fl})	Calculated as: $V_{prot} / A_{fl,use}$		
Number of floors (n_{fl})	2	3	3
Area facades	55% of the total wall area is oriented front-back; 45% is oriented left-right	The depth of the building is assumed to be 2 times the width. The dimensions are calculated assuming a rectangular ground floor.	The width of the front and back facade is $w = A_{ext} / (2h_{fl}n_{fl})$ calculated as: The depth of the building is calculated as: $d = A_{fl,D} / w$
Allocation of facades to day-zone	Front/back = 100% Left/right = 70%	For all facades: $f_{day} = A_{fl,D} / A_{fl,use}$	
Orientation front	North		
Orientation windows	Window area is specified for each direction in TABULA specification		
Orientation roof	Pitched roof oriented front and back		
Area of internal walls	Equal to outer wall area		Sum of outer area and half of the common wall area
Area floor between day- and night-zone	Equal to ground floor area		
Area internal floor	Calculated as: $A_{fl,N} - A_{fl,D}$		

3.3 Reduced-order building models

In order to reduce the computation time, reduced-order models in the form of lumped-capacity models have been developed for the each typology defined for the Belgian residential building stock. Lumped capacity models have been used widely to simulate the thermal dynamics in a comprehensive and computational efficient manner. For these models the heat balance equations are simplified by lumping the distributed thermal mass of the building structure, indoor air and furniture to a discrete set of thermal capacities interlinked by a network of thermal resistances. Note that for this paper only the building model is adapted. The models for the heating system are the same as for the detailed simulations and the calculated heat emitted by the radiators is used as an input for the building model.

Table 2: Thermostat schedule

Zone	Setpoint high	Setpoint low	High setpoint period
Day-zone	22°C	16°C	07:00–22:00
Night-zone	18°C	16C	21:00–09:00

The reduced-order model structure is shown in figure 2. To obtain the adequate model structure system identification has carried out in this work following a forward selection procedure. Thereby the model order is systematically increased until the identified model captures all dynamics that are available in the dataset. This process has been demonstrated in previous studies (Bacher & Madsen, 2011; Reynders, Diriken, & Saelens, 2014) and will not be elaborated in this paper. For this study, the system identification process showed that for the all typologies the thermal dynamics can be described by 4 thermal capacities for the day-zone, 3 thermal capacities for the night-zone and 2 thermal capacities for the floor between day- and night-zone. The resulting model structure is shown in figure 2. The model validation is discussed in paragraph 4.1.

The day-zone is modeled with a thermal capacity for the exterior walls (C_w), the ground floor (C_f), the internal walls (C_{wi}) and the indoor air (C_i). The thermal mass of the night-zone is lumped to a capacity for the envelope (roof + walls) (C_w), the internal walls (C_{wi}) and the indoor air (C_i). Both zones are linked by the internal floor which is modeled by 2 thermal capacities (C_{fi1}) and (C_{fi2}). The outdoor temperature (T_e) and the ground temperature (T_g) are used as boundary conditions. The solar gains, internal gains and heating are distributed to the different capacities using distribution coefficients.

Two approaches are used to calculate the model parameters. Firstly, the parameters are calculated directly from the building stock specification. Secondly, system identification is used to estimate the model parameters based on virtual measurements generated with the detailed building energy simulations models described in section 3.2. Both approaches are presented in the following paragraphs.

3.3.1 Theoretical RC model

For the theoretical RC model, the lumped parameters are calculated directly from the building stock specification, taking into account the assumptions presented in section 3.1.

Previous studies on the identification of the active thermal mass in buildings showed that as a rule of thumb the active thermal mass of the envelope corresponds to the thermal mass of the material layers within the insulation barrier (Reynders et al., 2014). This rule of thumb is applied to quantify the thermal capacities of the envelope and the ground floor. The thermal resistance for the envelope (R_w) [W/K] is calculated using the wall compositions defined for the detailed model. In line with the rule of thumb for the thermal capacity of the wall, the internal resistance (R_{w1}) is defined as the thermal resistance between the indoor environment

and the middle of the material layers within the insulation layer, taking into account standard heat transfer coefficients at the surface. R_{w2} is then defined as the thermal resistance between the middle of the layers within the insulation barrier and the outdoor environment. For the

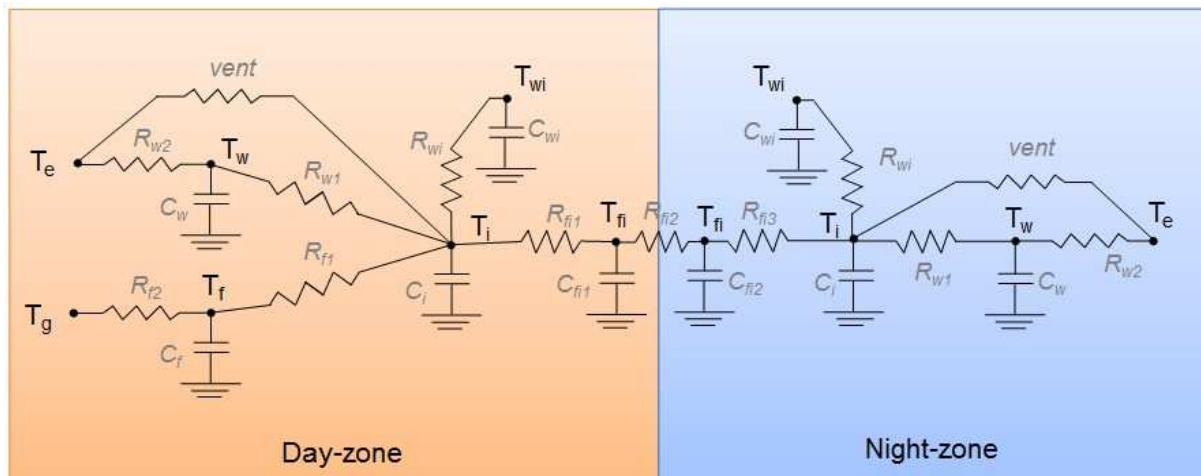


Figure 2: Structure of the 2-zone reduced order models. The day-zone is modeled as a 5-state model with states for the indoor air (T_i), the exterior walls (T_w), the interior walls (T_{wi}), the ground floor (T_f) and the floor between day- and night-zone (T_{fi}). A 4-state model is used for the night zone with states for the indoor air (T_i), the exterior walls (T_w), the interior walls (T_{wi}) and the floor between day- and night-zone (T_{fi}). Note that the gain inputs and the related parameters are not shown

internal walls and floor the entire thermal mass has been taken into account, since the components are entirely within the insulation barrier. The thermal resistance R_{wi} is taken equal to 50% of the total resistance of the wall, since the thermal mass is assumed to be in the center of the wall and is accessible from both sides.

In accordance with the findings of previous studies (Reynders et al., 2014), the UA-values of the windows have been combined with the ventilation and infiltration losses. This is done since the thermal mass of the windows is negligible compared to the massive building structure.

The convective and radiative heat flow from the low temperature radiators are combined with the internal gains as 1 input signal for the model. Since the radiators have a radiative heat fraction of 0.3, 70% of the heat input is distributed to the air capacity. The remaining 30% is distributed to the capacities of the different components using area weighted distribution factors, hence assuming that all emissivity factors are equal. Solar gains are entirely allocated to the components using area weighted distribution coefficients. The fraction going to the windows is allocated to the air capacity.

3.3.2 Grey-box modeling

Grey-box models consist of a set of continuous stochastic differential equations derived from the physical laws which define the dynamics of the building. The unknown parameters in these equations are derived using parameter estimation techniques. Due to the physics-based model structure, this approach is interesting from a research perspective since the parameters may be directly interpreted as physical properties (Madsen, 2008). The model structure is formulated in a state space form, given by equation 1.

$$dX(t) = A(\theta)X(t) + B(\theta)U(t) + \sigma(\theta)d\omega \quad (1)$$

In this equation $X(t)$ is the state vector of the dynamic system. In the case of thermal models for buildings these states mostly correspond to the temperatures of different building components. $U(t)$ is a vector containing the measured inputs of the system. These inputs can be controllable, such as the heat delivered by the heating system or the air flow rate of the ventilation system, or uncontrollable, such as the outdoor temperature, solar gains, internal gains... The second term in this equation represents the system noise, with ω a Wiener process. The measured output of the system $Y(t)$ is given in equation 2 as a function of the states $X(t)$ and the inputs $U(t)$. E is the measurement error.

$$Y(t) = C(\theta)X(t) + D(\theta)U(t) + E \quad (2)$$

The parameters θ are estimated using the Continuous Time Stochastic Modeling (CTSM) toolbox implemented in R (Kristensen & Madsen, 2003). CTSM uses maximum likelihood estimation (MLE) to find the unknown parameters for a given model structure.

In this paper the state space form is derived from the RC representation shown in figure 2. The data for the identification process has been generated using the detailed simulation model described in section 3.2. Two types of virtual experiments have been carried out. In the first experiment the dataset is generated by simulating a PRBS experiment. Thereby a pseudo-random binary sequence (PRBS) is implemented on the heating system. Two uncorrelated signals have been used for the day- and night-zone. In the second experiment in-use behavior with the deterministic thermostatic control of table 2 is simulated. In both cases measurements of the indoor air temperature and the heat fluxes to the different components are used as observation variables.

It is important to note that for the identification process, convergence issues occurred when the 2-zone model is fitted as a whole (see section 4.1). These issues are caused by the correlation between day- and night-zone. Even though different PRBS signals are used in both zones, the thermal coupling of the zones as well as the correlation with the climate data have an impact on the identifiability of the parameters. To overcome this problem, the identification process was repeated on the decoupled models. More precise the parameters of the day-zone are identified using the air temperature of the night-zone as a boundary condition and vice versa. The parameters for the floor between day- and night-zone are estimated in a third identification step.

4. RESULTS

In this section the accuracy of the reduced-order models is analyzed. Since for Belgium disaggregated transient measurement data, for example obtained by smart meter readings, are not available to validate the models, the results of the detailed simulation using the white-box model (WB) is used as a reference scenario. For the total annual heat demand, an average difference of 13% is found between the detailed simulation model and the results specified in the TABULA-report (Protopapadaki, Reynders, & Saelens, 2014). The latter were obtained by the monthly-averaged calculation method implemented in the EPB software (Cyx et al., 2011). Given the differences that were found by Protopapadaki et. al. (2014) for different descriptions of the Belgian building stock, the accuracy of these detailed simulations is found acceptable. Moreover, since this paper aims at demonstrating the capabilities of reduced-order models the precise value of the heat demand of the Belgian building stock is not of significant importance. Section 4.1 shows the results of the validation process for the grey-box models identified on the detailed simulation data. Section 4.2 gives an overview of the qualitative and quantitative comparison of the instantaneous energy demand as well as the temperature profiles obtained for the different models.

4.1 Validation of grey-box models

Three steps have been considered to validate the identified grey-box models. First an analysis of the residuals has been carried out, taking into account the RMSE values for 1-step predictions and simulation, the auto-correlation function and the correlation of the residuals of to the inputs. In a second validation step, cross-validation is carried out to evaluate the accuracy of the model on a new dataset. Finally, the estimated parameters are compared against the corresponding thermal properties of the building.

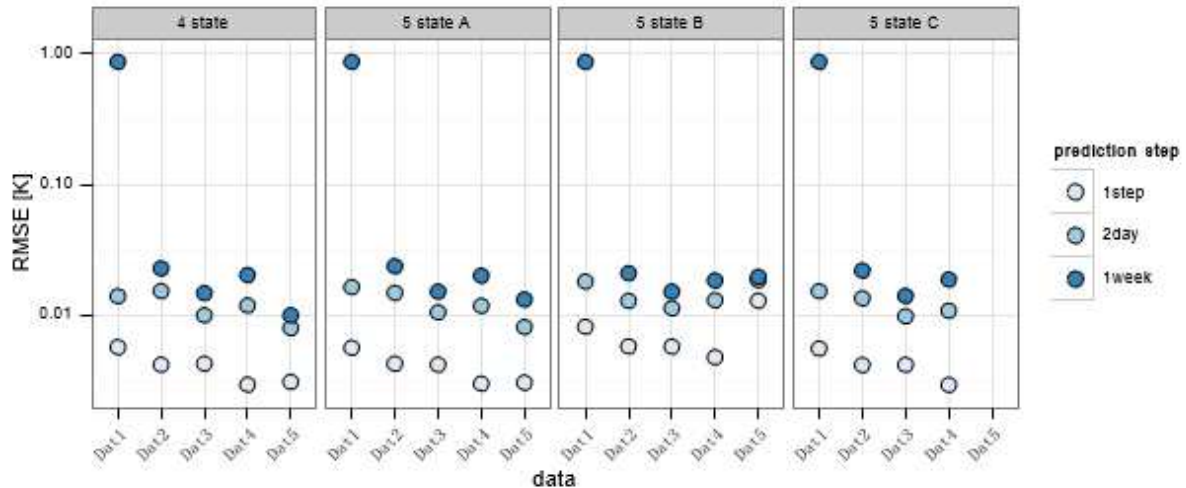
Whereas no white-noise residuals were obtained, indicating that the model does not explain all the dynamic information contained in the data, the RMSE values showed acceptable results and no significant correlation of the residuals to the inputs.

Figure 3 gives an overview of the RMSE-values of the residuals of the indoor air temperature for the different scenarios evaluated in the model validation process. It is evident that the model quality is significantly higher when the day- and night-zones are identified separately. For the coupled models the RMSE value of the indoor air temperature increased with an order of magnitude.

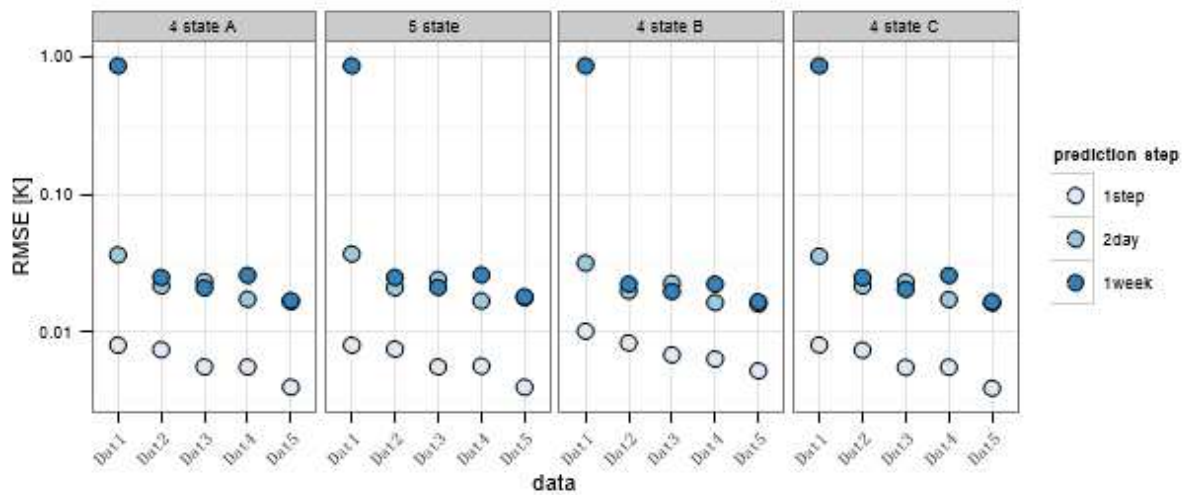
In line with Reynders et al. (2014), a comparison is made between models of different order, the type of data used as observation measurements and the data period. For both the day and night-zone a 4 and 5 state models have been identified. Thereby the 5 and 4 state model resulted in the best results for respectively the day and night-zone. These models correspond to the structure shown in figure 2. In addition to a variation of the order of the model also the impact of the type of input and observation measurements was considered. The variations A, B and C of each model correspond to respectively an identification with idealized inputs, a dataset where no information of internal gains was available and solar gains are measured by the global horizontal irradiance and finally a dataset that uses the solar irradiance on the vertical planes and the domestic electricity demand as an input for the internal gains. Similar to Reynders et al. (2014), the results show that dataset C results in a similar model quality compared to using idealized inputs, which are often not available in practice.

Finally, the impact of the data period is analyzed. Thereby 'Dat1' corresponds to 1 week of measurement data in April. Thereby it is evident that the dataset contains insufficient information given the high level of residuals in long term prediction. 'Dat2' and 'Dat3' are 2 week observation data in respectively February and April. While 'Dat4' and 'Dat5' are 1 month data sets for these periods. Thereby it is shown that the level of residuals does not drastically change as function of the training data. Nevertheless, for well insulated buildings convergence problems sometimes occurred for the mid-season data. This was explained by the low input of the heating system during this time of the year. Therefore, the dataset of 1 month in February (Dat4) is used with a sample time of 15 minutes.

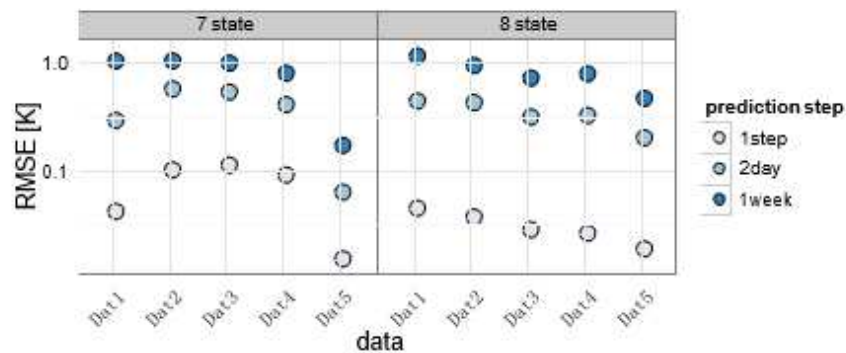
In a next validation step, the identified parameters are compared against the physical parameters used for the detailed simulation model. Figure 4(a) show the estimated thermal capacities of the indoor air, the outer walls, the inner walls and the floor for respectively the day-zone of the DE building. As discussed earlier, the theoretic value for the capacity of the envelope components only takes into account the thermal mass of the layers within the thermal mass. For both the identification on the PRBS and the in-use data, the estimated thermal capacities of the walls are smaller than the theoretical values. These results are in line with previous studies (Reynders et al., 2014). In case of a PRBS experiment the estimated value for the interior walls is close to the theoretic value, indicating that the thermal mass of the interior walls is fully excited. In contrast, the estimated value for the outer walls is closer to the theoretical value when in-use data are used.



(a) Day-zones



(b) Night-zones



(c) Coupled

Figure 3: RMSE-values for the indoor air temperature obtained for 1-step, 2-day and 1-week predictions (DE dwelling)

Whereas differences in the estimated thermal capacities are limited, a significant impact of the dataset on the estimated heat transfer coefficients is shown (Figure 4(b)). Note that the

theoretical heat transfer coefficients are obtained by the thermal resistance between the middle of the layers within the insulation barrier and the inner air, taking into account standard heat transfer coefficients. Nevertheless, temperature dependent convective heat transfer coefficients are implemented in the detailed simulation model. Figure 5 shows the convective heat transfer coefficients for the vertical components as function of the difference between the air temperature and the indoor surface temperature. For the data period used in the identification with in-use data, the average difference between the surface temperature and the indoor air is 2 – 5°C. As such, the simulated heat transfer coefficient is about 50% lower than the one assumed in the theoretical RC-model. As such, less heat is absorbed by the building fabric as the resistance between the indoor air and the fabric increases. For the PRBS dataset, the temperature difference becomes higher resulting in an estimated heat transfer coefficients of the inner walls and the envelope in the same order of magnitude as the theoretical values.

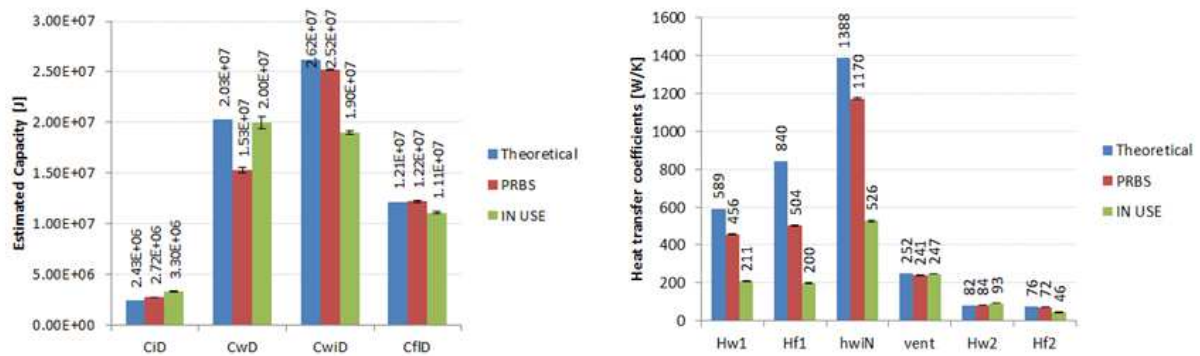


Figure 4: (a) Estimated thermal capacities of the indoor air (CiD), the exterior walls (CwD), the interior walls (CwiD) and the ground floor (CfID) of the day-zone of the DE dwelling. (b) Estimated heat transfer coefficients between the indoor air and respectively the exterior walls (Hw1), the ground floor (Hf1) and the interior walls (Hwi), the infiltration and ventilation rate (vent) and the heat transfer coefficients between the thermal capacity of the exterior walls (Hw2) and the ground floor (Hf2) to respectively the outdoor environment and the ground for the day-zone of the DE dwelling.

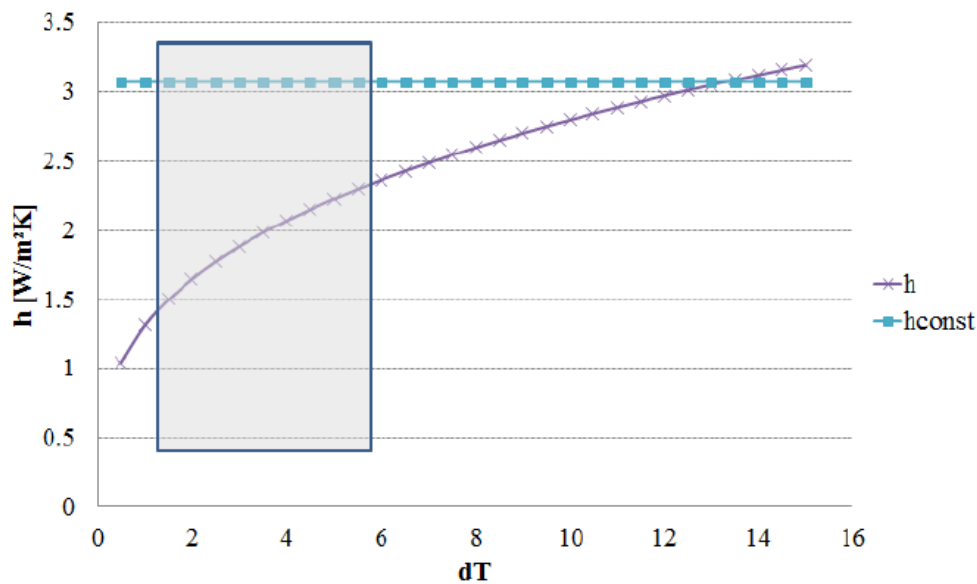


Figure 5: Comparison of temperature dependent heat transfer coefficient, as implemented in IDEAS, and the theoretic value used in the RC models

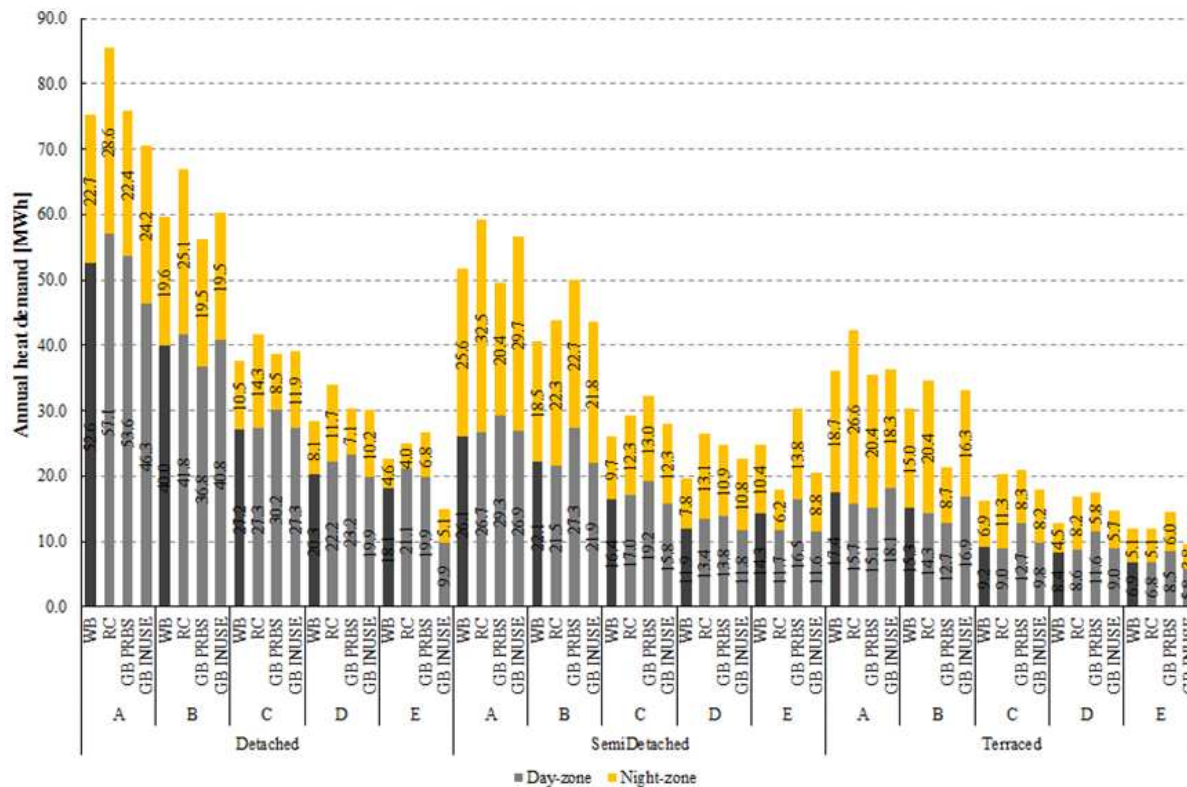


Figure 6: Calculated annual energy demand [MWh/a] for the single family detached houses as function of the age class and model types. 'WB' and 'RC' correspond to the detailed simulation model and the theoretical RC-model respectively. The grey-box models estimated on the PRBS data and the in-use data are referred to as 'GB PRBS' and 'GB INUSE' respectively.

4.2 Comparison of reduced order models

4.2.1 Annual heat demand

Figure 6 gives an overview of the annual energy demand for the different model and building types. Comparison of the theoretical RC-model (RC) with the reference case (WB) shows an overestimation of the energy demand for the RC-models of on average 20%. The overestimation is more pronounced for the night-zones and can be explained by overestimation of the heat loss coefficient of the opaque parts. Due to the big difference in thermal mass of the light-weight roof and the massive walls, it is found that the calculation of the aggregated heat transfer coefficients between the air and the thermal mass and between the thermal mass and the outer environment by adding the corresponding heat transfer coefficients of the individual components is no longer valid.

For the reduced-order models obtained by system identification, the difference between the detailed simulation is less pronounced. For the buildings before '05 (periods A to D), the average difference is reduced to 7% and 10% for respectively the models identified on in-use and PRBS data. The estimated models for the buildings after '05 (period E) show higher deviations. Additional research is there for needed in order to improve the accuracy of the identified models for the well-insulated dwellings.

In general an overestimation of the heat demand is shown for the identified models. The overestimation is more pronounced for the semi-detached and terraced buildings and is mainly due to and overestimation of the heat demand in the night-zone. This is explained by the unreliable

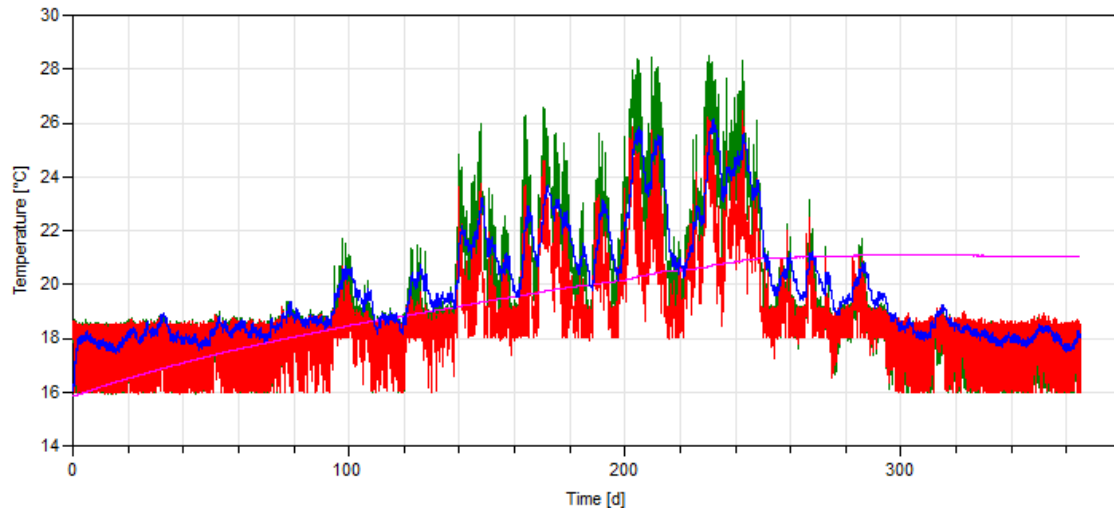


Figure 7: Simulated air temperature of the night zone of the SDC building (green = detailed, red = GB in-use) and the temperature corresponding the state of the internal floor (blue = detailed, violet = GB in-use)

estimates of the internal floor between the day- and night-zone. The identification significantly overestimates the thermal resistance and thermal capacity of the internal floor. As a result, no heat transfer is shown between day- and night-zone for the grey-box models, resulting in lower indoor temperatures and a higher heat demand for the night zones. These unreliable estimates result from the fact that the temperature within the center of the floor is almost constant during the identification process, as shown in figure 7. As a consequence the model is able to accurately simulate the heat demand during the heating season for which the model is trained (Fig. 8). Nevertheless, in summer the mean temperature in the building rises. This temperature rise is not handled properly by the reduced-order model due to the severe overestimation of the thermal capacity (Fig. 7). As a consequence, the temperature rise in the grey-box model is less sharp and the heat demand is higher. A dedicated identification experiment, activating the thermal mass of the internal floor is therefore necessary.

Regardless of the large deviations in summer, the reduced order models show acceptable correspondence to the detailed simulations during the winter period, especially for the day-zone (Fig. 7).

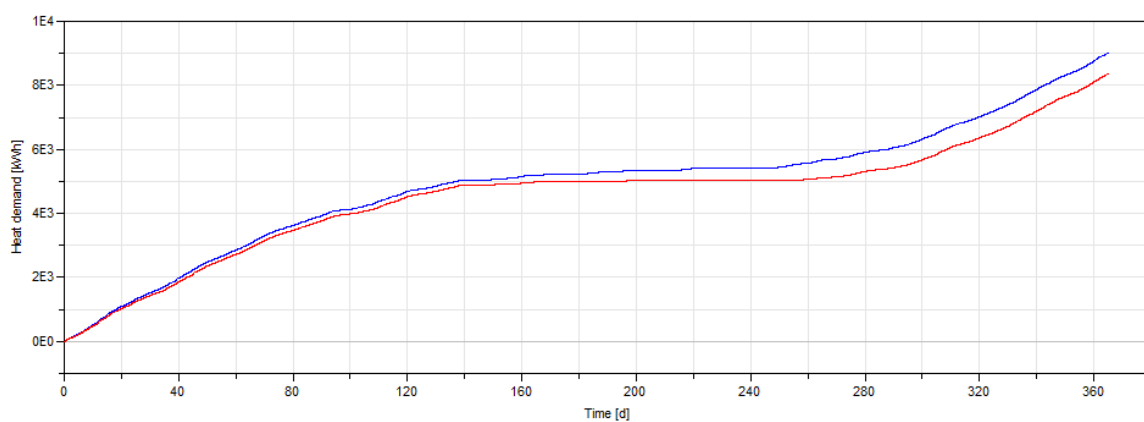


Figure 8: Simulated cumulative heat demand of the TD building (red = detailed, blue = GB in-use)

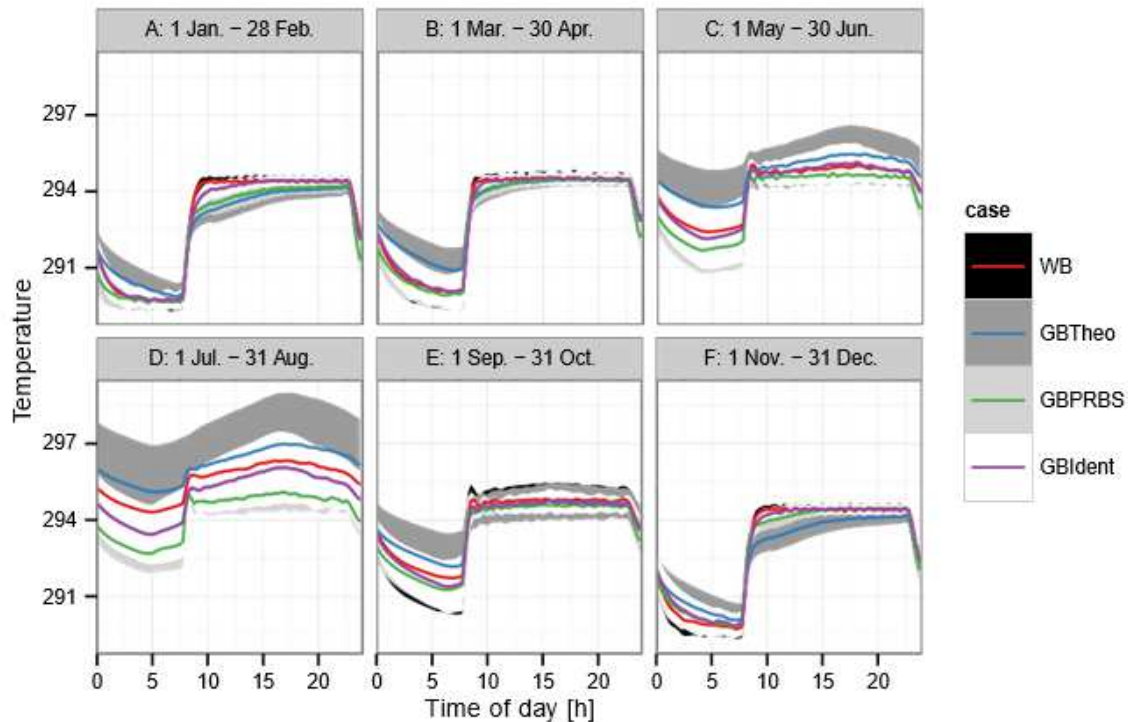


Figure 9: Averaged air temperature day zones. (Building type SDC)

4.2.2 Dynamic behavior of the dwellings

Figure 9 shows a less sharp response of the air temperature for the RC-model compared to the reference case (WB), which is used as the control signal for the heating system, to the heat input. Consequently the heating system is operated for longer times at high power to provide thermal comfort (Figure 10). As was shown in Fig 5, the slow response of the theoretical RC model is explained by the overestimation of the convective heat transfer coefficient. Whereas the identification on the PRBS data, results in a better correlation with the temperature profile of the detailed simulation, it is evident from the strong low temperatures in summer that the heat loss coefficients are slightly overestimated. The grey-box model fitted on the in-use dataset is able to capture the strong temperature swings in the indoor air temperature. As shown in figure 4(b), smaller values of the heat transfer coefficient between the indoor air and the building components are obtained for the grey-box models identified on the in-use data, indicating that the thermal mass of the components is less available for storage and on a short timescale most heat is stored in the thermal capacity of the indoor air. Figure 10 shows that consequently the temperature profile of the reduced-order model accurately matches the detailed simulation, especially during winter and mid-season when the potential for demand-side management using the heating system is highest.

Finally, it is noted that the level of uncertainty on the night zone (Figure 11) is much higher than for the day zone. This can be explained on the one hand by the fact that the overall heat demand of the night-zone is small compared to the day zone. On the other hand, the identified thermal properties for the internal floor between both zones show a high level of uncertainty. Consequently, the heat transfer between the warmer day-zone and the night-zone, which has a significant impact on the heat demand of the night-zone, is not well captured.

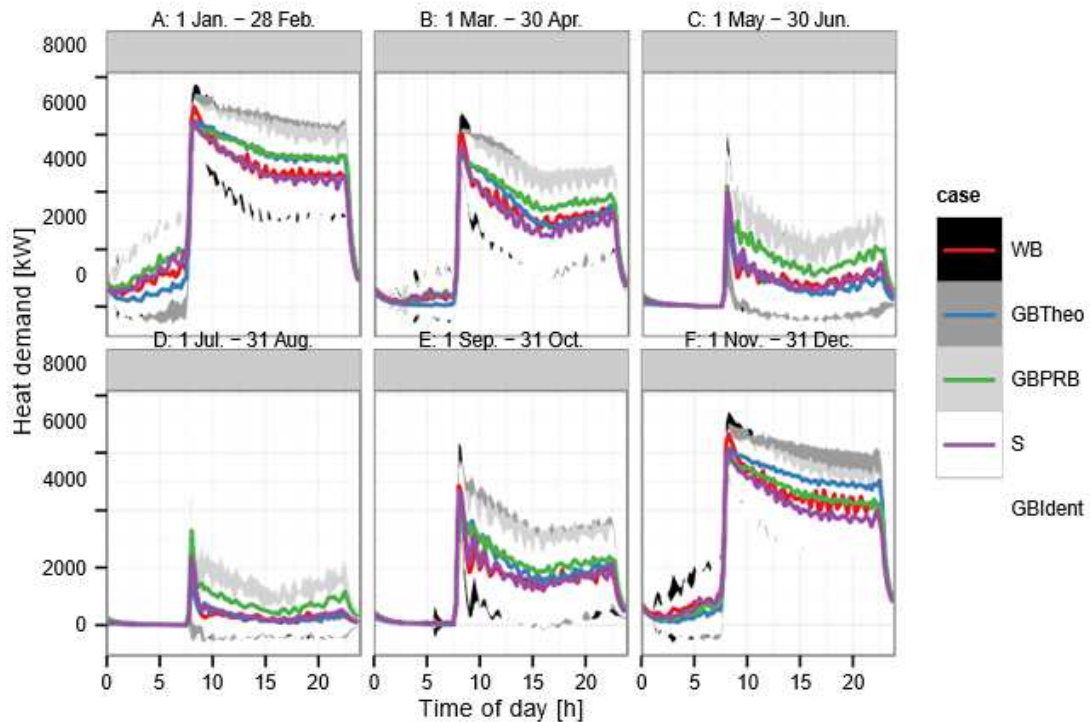


Figure 10: Averaged heat demand day zones. (Building type SDC)

4.3 Impact at aggregate level

In this final section the impact of the modeling approach on the aggregated heat demand for the Belgium residential building stock is evaluated. To aggregate the heat demand of the different typologies to the heat demand of the total stock the approach described in Protopapadaki et al. (2014) is used.

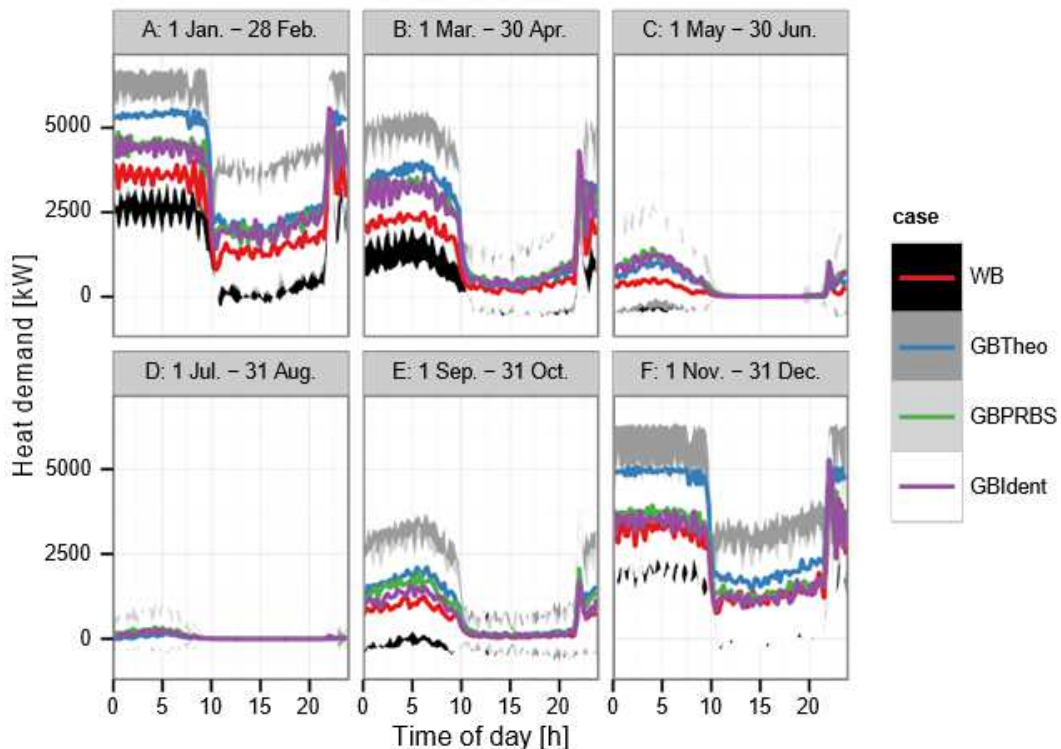


Figure 11: Averaged heat demand night zones. (Building type SDC)

The aggregation of the heat demand of each building type to the demand of the entire stock is not explicitly carried out in the TABULA project for the typical housing approach. As stated in the introduction the typical housing approach merely presents a set of typical dwellings for each building type and age class. In order to get an estimate of the heat demand of the whole stock the heat demand of each dwelling is multiplied by the number of dwellings of each building case. The number of dwellings is obtained from the SuFiQuaD project (Cyx et al., 2011), which is also mentioned as a data source in the TABULA project and is in line with the Belgian land registry, though more detailed. However, there exist some discrepancies between the numbers shown in SuFiQuaD and our implementation for the TABULA building stock. The fourth period in the SuFiQuaD data ends in 2007 instead of 2005 in the Tabula project and there is no data for period E (2005-2012). The number of buildings as used for the ULg typology (see section 3.2.3) is therefore used for the period 2007-2012 and a linear interpolation is used to attribute the 2005-2007 buildings to period E instead of D. The results are summarized in Table 3.

Table 3: Number of buildings used for aggregation of TABULA building stock

Age class	D: Detached	SD: Semi-detached	T: Terraced
A: Pre 1945	269771	375000	766884
B: 1946-1970	309263	275838	242952
C: 1971-1990	446481	158123	87706
C: 1991-2005	266050	81677	54519
D: Post 2005	74135	29046	19388

Figure 12 shows the resulting load duration curve for the aggregated Belgian residential stock. Although small differences are shown, an acceptable prediction of the load-duration curve is obtained using the reduced order models. Where the theoretic reduced-order models show a more accurate prediction of the peak demand, the grey-box models identified on the in-use data show good correspondence for medium and lower loads.

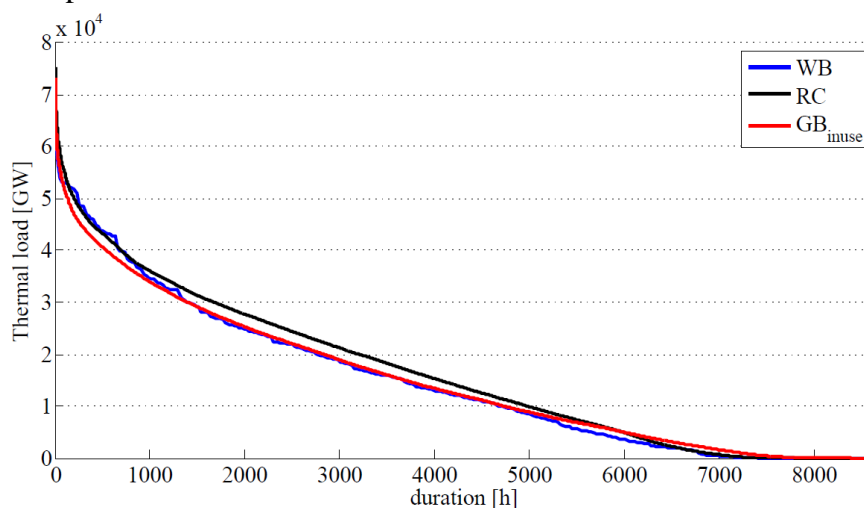


Figure 12: Load duration curve for the aggregated heat demand

Taking into account the uncertainty on the building stock description that was found by Protopapadaki et al. (2014), the use of both the theoretic and the identified reduced-order model for building stock simulations is considered as acceptable.

5. CONCLUSIONS AND FUTURE WORK

Reduced-order building models have been evaluated for their application in a dynamic bottom-up models have for the Belgian building stock. In this paper the case of single family detached

houses is handled and the models are used to simulate the heat demand and indoor temperature for the Belgian climate with a time-step of 15 min.

In a first phase, detailed building models are implemented in the IDEAS-library in Modelica. Thereby the lack of qualitative statistical data of the building stock, required a significant amount of assumptions ranging from material properties, wall compositions to the allocation of the useful area to day- and night-zones. Verification of the models against the heat demand calculation provided by TABULA showed an overestimation of less than 10% of the annual heat demand of the dwellings. Verification of the heat demand profile could not be carried out, since no dynamic data are available on national level. As such, the dynamic profiles obtained by the detailed simulations have been used as a reference scenario to compare the accuracy of reduced-order building models.

For the analysis of the demand-side management potential of buildings on a district or even national level, reduced-order models should be able to accurately model the dynamic thermal response of buildings to the outdoor environment as well as the heating and internal gains. A correct simulation of this response at a high temporal resolution is needed to correctly assess the peak demand of the building but also quantify structural storage properties such as the state of charge. Therefore two reduced-order modeling approaches have been considered to develop reduced-order models for the Belgian building stock. Firstly, reduced-order lumped capacity models, analogue to electric networks, have been implemented using theoretic parameter values for the thermal capacities and resistances. These values were directly calculated from the TABULA data, taking into account similar assumptions as for the detailed simulations. Secondly, grey-box models have been identified using data from virtual experiments carried out with the detailed simulations. Two types of virtual experiments were defined: (1) a PRBS-signal for the heat input and (2) an in-use experiment using a day-night schedule for heating and stochastic occupant behavior.

Comparison of the reduced order models showed that for all cases the simulation of the annual heat demand is acceptable. The main differences are found in the night-zone, where the unreliable estimate of parameters of the floor between day- and night-zone results an over-prediction of the heat demand. This is especially the case during the summer period. During winter season, when the heat demand is high, good agreement is found between the reduced order models identified on in-use data and the detailed simulations.

As for the short term dynamic effects, the theoretical RC-models overestimated the contribution of the thermal mass of the building, underestimating the temperature fluctuations and overestimating the heat demand. In contrast, simulations using the grey-box models identified on the in-use data, show good agreement of the temperature and heat demand profiles of the day-zone to those obtained with the detailed models for the winter and mid-season period. The major differences between the models were found in the estimated thermal capacity of the interior walls and especially the thermal properties of the internal floor between the two zones shows unreliable estimates.

Further development is needed on the identification of the walls between two zones. The thermal coupling between the zones obtained by the virtual experiments that were carried out, resulted in a significant correlation between the temperatures in both zones. As a result, identifiability problems occur for the walls between the zones as well as for the integrated models for which both zones are identified at the same time. Moreover, the influence of the thermal resistance between the air node and the capacities of the walls will be further examined, in order to fully understand the contribution of the building fabric to the active thermal mass of the building.

REFERENCES

- Aerts, D., Minnen, J., Glorieux, I., Wouters, I., & Descamps, F. (2014, February). A method for the identification and modelling of realistic domestic occupancy sequences for building energy demand simulations and peer comparison. *Building and Environment*. doi: 10.1016/j.buildenv.2014.01.021
- Allacker, K. (2010). *Sustainable building: the development of an evaluation method* (PhD thesis). KU Leuven.
- Arteconi, a., Hewitt, N., & Polonara, F. (2013, March). Domestic demand-side management (DSM): Role of heat pumps and thermal energy storage (TES) systems. *Applied Thermal Engineering*, 51(1-2), 155–165. doi: 10.1016/j.applthermaleng.2012.09.023
- Bacher, P., & Madsen, H. (2011, July). Identifying suitable models for the heat dynamics of buildings. *Energy and Buildings*, 43(7), 1511–1522. doi: 10.1016/j.enbuild.2011.02.005
- Baetens, R., De Coninck, R., Van Roy, J., Verbruggen, B., Driesen, J., Helsens, L., & Saelens, D. (2012, August). Assessing electrical bottlenecks at feeder level for residential net zero-energy buildings by integrated system simulation. *Applied Energy*, 96, 74–83. doi: 10.1016/j.apenergy.2011.12.098
- Battaglini, A., Lilliestam, J., Haas, A., & Patt, A. (2009, July). Development of SuperSmart Grids for a more efficient utilisation of electricity from renewable sources. *Journal of Cleaner Production*, 17(10), 911–918. doi: 10.1016/j.jclepro.2009.02.006
- Braun, J. E. (2003). Load Control Using Building Thermal Mass. *Journal of Solar Energy Engineering*, 125(3), 292. doi: 10.1115/1.1592184
- Bruninx, K., Patteeuw, D., Delarue, E., Helsens, L., & D'haeseleer, W. (2013, May). Short-term demand response of flexible electric heating systems: The need for integrated simulations. In *2013 10th international conference on the european energy market (eem)* (pp. 1–10). IEEE. doi: 10.1109/EEM.2013.6607333
- CEN. (2003). EN 12831 Heating systems in buildings - Method for calculation of the design heat load. Brussels.
- Cyx, W., Renders, N., Van Holm, M., & Verbeke, S. (2011). IEE TABULA - Typology Approach for Building Stock Energy Assessment (Tech. Rep. No. August).
- De Coninck, R., Baetens, R., Saelens, D., Woyte, A., & Helsens, L. (2014, July). Rule-based demand-side management of domestic hot water production with heat pumps in zero energy neighbourhoods. *Journal of Building Performance Simulation*, 7(4), 271–288. doi: 10.1080/19401493.2013.801518
- De Jonghe, C. (2011). *Short-term demand response in electricity generation planning and scheduling* (PhD thesis). KU Leuven.
- Ellerbrok, C. (2014). Potentials of Demand Side Management Using Heat Pumps with Building Mass as a Thermal Storage. *Energy Procedia*, 46(0), 214–219. doi: 10.1016/j.egypro.2014.01.175
- Gottwalt, S., Ketter, W., Block, C., Collins, J., & Weinhardt, C. (2011, December). Demand side management - A simulation of household behavior under variable prices. *Energy Policy*, 39(12), 8163–8174. doi: 10.1016/j.enpol.2011.10.016

- Henze, G. P., Felsmann, C., & Knabe, G. (2004, February). Evaluation of optimal control for active and passive building thermal storage. *International Journal of Thermal Sciences*, 43(2), 173–183. doi: 10.1016/j.ijthermalsci.2003.06.001
- Kristensen, N. R., & Madsen, H. (2003). CTSM: Continuous Time Stochastic Modelling. Retrieved from <http://www.ctsm.info/pdfs/mathguide.pdf>
- KULeuven, VITO, & BBRI. (2001). SuFiQuad - Sustainability, Financial and Quality evaluation of Dwelling Types, BELSPO (Tech. Rep.).
- Kummert, M., Andre´, P., & Nicolas, J. (2001, July). Optimal heating control in a passive solar commercial building. *Solar Energy*, 69, 103–116. doi: 10.1016/S0038-092X(01)00038-X
- Loga, T., Balaras, C., Dascalaki, E., & Zavrl, M. (2010). Use of Building Typologies for Energy Performance Assessment of National Building Stocks: Existent Experiences in European Countries and Common (No. June 2009). Institut Wohnen und Umwelt GmbH.
- Lund, H., Marszal, a., & Heiselberg, P. (2011, July). Zero energy buildings and mismatch compensation factors. *Energy and Buildings*, 43(7), 1646–1654. doi: 10.1016/j.enbuild.2011.03.006
- Madsen, H. (2008). *Time Series Analysis*. Chapman & Hall/CRC. Meteotest. (2008). METEONORM Version 6.1 - Edition 2009. Bern.
- Muratori, M., Schuelke-Leech, B.-A., & Rizzoni, G. (2014, May). Role of residential demand response in modern electricity markets. *Renewable and Sustainable Energy Reviews*, 33, 546–553. doi: 10.1016/j.rser.2014.02.027
- Pina, A., Silva, C., & Ferraõ, P. (2012, May). The impact of demand side management strategies in the penetration of renewable electricity. *Energy*, 41(1), 128–137. doi: 10.1016/j.energy.2011.06.013
- Protopapadaki, C., Reynders, G., & Saelens, D. (2014). Bottom-up modelling of the Belgian residential building stock: impact of building stock descriptions. In *Submitted to SSB 2014 (Liège)*.
- Reynders, G., Baetens, R., & Saelens, D. (2012). Using thermal mass to counter decreasing overall heating system efficiencies in low-energy dwellings. In 5th international building physics conference. Kyoto.
- Reynders, G., Diriken, J., & Saelens, D. (2014, October). Quality of grey-box models and identified parameters as function of the accuracy of input and observation signals. *Energy and Buildings*, 82, 263–274. doi: 10.1016/j.enbuild.2014.07.025
- Reynders, G., Nuytten, T., & Saelens, D. (2013, March). Potential of structural thermal mass for demand-side management in dwellings. *Building and Environment*, 64, 187–199. doi: 10.1016/j.buildenv.2013.03.010
- Sourbron, M. (2012). *Dynamic thermal behaviour of buildings with concrete core activation* (PhD. Thesis) (Unpublished doctoral dissertation). KU Leuven.
- Verbeeck, G. (2007). *Optimisation of extremely low energy residential buildings* (phd-thesis). K.U.Leuven.
- Zahedi, A. (2011, January). Maximizing solar PV energy penetration using energy storage technology. *Renewable and Sustainable Energy Reviews*, 15(1), 866–870. doi: 10.1016/j.rser.2010.09.011

ISABELE: a Method for Performance Assessment at Acceptance Stage using Bayesian Calibration

P. Schetelat¹, R. Bouchie¹

⁽¹⁾ CSTB Champs sur Marnes, France

1. ABSTRACT

The rise of environmental issue awareness resulted in a significant pressure to reduce energy consumption. As the energy performance requirements of buildings have become more demanding, several studies showed significant deviations between predictions at the design phase and actual performances, putting into light the need for better performance assessment at the acceptance stage.

In this paper we present a new building performance assessment method at the acceptance stage called ISABELE (In Situ Assessment of Building Envelope performancEs). Performances and uncertainties are obtained by calibrating a lumped thermal model derived from the international ISO standard 13790:2008. Calibration is performed using Bayesian inversion of the model using in situ dynamic temperature and power measurement.

Metrological quality of the inverse measurement is evaluated by using detailed building thermal simulation as a virtual standard sample. The method is then demonstrated on actual in situ measurements.

Keywords: Bayesian calibration, Performance assessment, Uncertainty statement, Acceptance stage

2. INTRODUCTION

This paper concerns itself with model calibration as a way to perform inverse measurement of intrinsic thermal performance of buildings, namely heat loss coefficient by transmission through the envelope H_{tr} .

As a new technique, we aim to provide an assessment of the measurement accuracy of the ISABELE procedure. Measurement accuracy encompass two different notions (Joint Committee for Guides in Metrology (JCGM), 2012):

- Measurement trueness, which is related to the notion of biased measurement
- Measurement precision, which is related to the uncertainty of the measurement

Measurement trueness is traditionally assessed using a measurement standard as a reference, which in the case of building thermal performances is technically hard to achieve. Measurement trueness of the ISABELE procedure has been carried out in (Boisson & Bouchié, 2014) using thermal simulation as a virtual measurement standard and benchmarked with other techniques on an actual building in (Rémi Bouchié, Alzetto, Brun, Boisson, & Thebault, 2014).

Measurement precision assessment is either estimated through repeatability tests (type A error) or through composition of estimated uncertainty (type B error) (Joint Committee for Guides in Metrology (JCGM), 2008). Once again, type A uncertainty estimation is technically unfeasible for inverse measurement of building performances due to time and economic constraints. While classical composition of uncertainty and uncertainty propagation are suited for measurements that are based on forward model evaluation, they are no longer suited for inverse measurement.

As pointed out in a recent review of building energy simulation calibration techniques (Coakley, Raftery, & Keane, 2014): “There are currently few studies which account for uncertainty in model inputs and predictions, thus leading to a lack of confidence in [their] outputs.”

One notable attempt is the work of (Heo, Choudhary, & Augenbroe, 2012) in the context of retrofit analysis. Uncertainty is estimated by performing Bayesian calibration of building static energy model using monthly bill as observed data. Bayesian inverse measurement is indeed suited as it estimates the likelihood of a model given a set of observed data and their uncertainty.

This paper proceeds to evaluate the measurement precision of the ISABELE procedure using Bayesian calibration of an hourly energy model. It takes into account observed data and boundary condition uncertainty to assess the inverse measurement confidence interval.

The measurement is carried out on a small building (wood structure chalet) and compared to design stage value of heat loss coefficient with their uncertainties.

3. PROPOSED METHOD: BAYESIAN CALIBRATION

3.1 Problem formulation

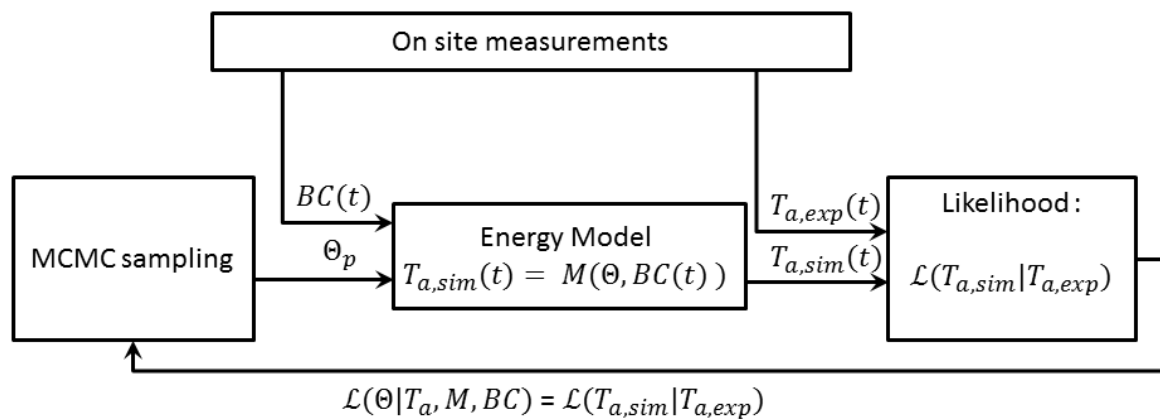


Figure 1 : Bayesian calibration principle

Let us consider an energy model M such that:

$$T_{a,sim}(t) = M(\theta, BC(t)) \quad (1)$$

Where $T_{a,sim}(t)$ is the air temperature inside the envelope, θ the set of physical parameter of M and $BC(t)$ denotes the set of time dependent boundary conditions applied to the envelope, such as the external temperature $T_{ext}(t)$, heating power $P(t)$, solar fluxes and air infiltration flow rate $Q_v(t)$.

Calibrating an energy model M given a measurement of $T_{a,exp}(t)$ and $BC(t)$ is equivalent to finding a parameter set $\hat{\theta}$ minimizing the error between model prediction and measurement :

$$\hat{\theta} = \underset{\theta}{\operatorname{argmin}} \left\| T_{a,exp}(t) - M(\theta, BC(t)) \right\|_D \quad (2)$$

Where $\| \cdot \|_D$ is a measure of distance. A classical approach is for instance least square error minimization using gradient descent. While most practical usages of calibration only require the best estimate for $\hat{\theta}$, it is of paramount importance to estimate the uncertainty over the calibrated $\hat{\theta}$ when the risk over the prediction of the calibrated model $M(\hat{\theta}, BC(t))$ is to be assessed.

Bayesian calibration (a.k.a Bayesian inversion or Bayesian inference) is an efficient framework to evaluate the uncertainty of inverse measurement (Forbes & Sousa, 2011). In this paradigm, the calibration of a model is equivalent to finding $P(\Theta | M, BC, T_a)$, the posterior probability of having Θ given the model M and the measurements $T_{a,exp}$ and BC .

Using the Bayes theorem, we have:

$$P(\Theta | M, BC, T_a) = \frac{P(T_a | \Theta, M, BC)P(\Theta)}{P(T_a)} \quad (3)$$

$P(T_a | \Theta, M, BC)$ is the likelihood of measuring T_a given the boundary conditions BC , the energy model M and the parameter Θ . This likelihood allows us to take into account the measurement of uncertainty over $T_{a,exp}$ and BC .

$P(\Theta)$ is called a prior. It is the *a priori* belief we hold over the probable value of parameter Θ . Prior selection based on expert knowledge is covered in length in the guide to the expression of uncertainty in measurement first supplement ((JCGM), 2008). If the only available information regarding a non-negative quantity X is a best estimate x (e.g. design stage values), the principle of maximum entropy dictates to choose an exponential law $Ex(1/x)$.

$P(T_a)$ is a constant for a given measurement. It is treated as a normalization constant. We will see later on that its estimation is not required for the analysis.

Assuming we have a measurement of $T_{a,exp}$ and BC , a model M and an *a priori* belief $P(\Theta)$ of Θ , we can readily estimate the posterior probability up to a multiplicative constant of proportionality:

$$P(\Theta | M, BC, T_a) \propto P(T_a | \Theta, M, BC)P(\Theta) \quad (4)$$

Considering that evaluating the posterior for every possible value of Θ is not practically feasible, Bayesian calibration relies on Monte Carlo Markov Chain (MCMC) sampling to directly sample from the posterior distribution $P(\Theta | M, BC, T_a)$ by using equation (4). Such algorithm yields an n-sample $\{\Theta_1, \dots, \Theta_n\}$ of the random variable Θ which is used to estimate the empirical probability density function of the posterior. The most probable value for Θ in the n-sample is called Θ_{MAP} , the *maximum a posteriori*.

It should be noted that least squares minimization and Bayesian calibration yield the same optimum value for Θ ($\hat{\Theta} = \Theta_{MAP}$) when assuming flat prior distribution and time independent Gaussian error in the Bayesian approach.

3.2 MCMC sampling:

MCMC sampling is a class of algorithm used to draw a random variable from an arbitrary distribution. Its main advantage is to be able to sample from any distribution as long as its probability density function can be evaluated up to a multiplicative constant. In this work we use the Metropolis Hasting (MH) algorithm, an MCMC sampling technique using acceptance / rejection of a candidate sample. This algorithm is detailed in Figure 2.

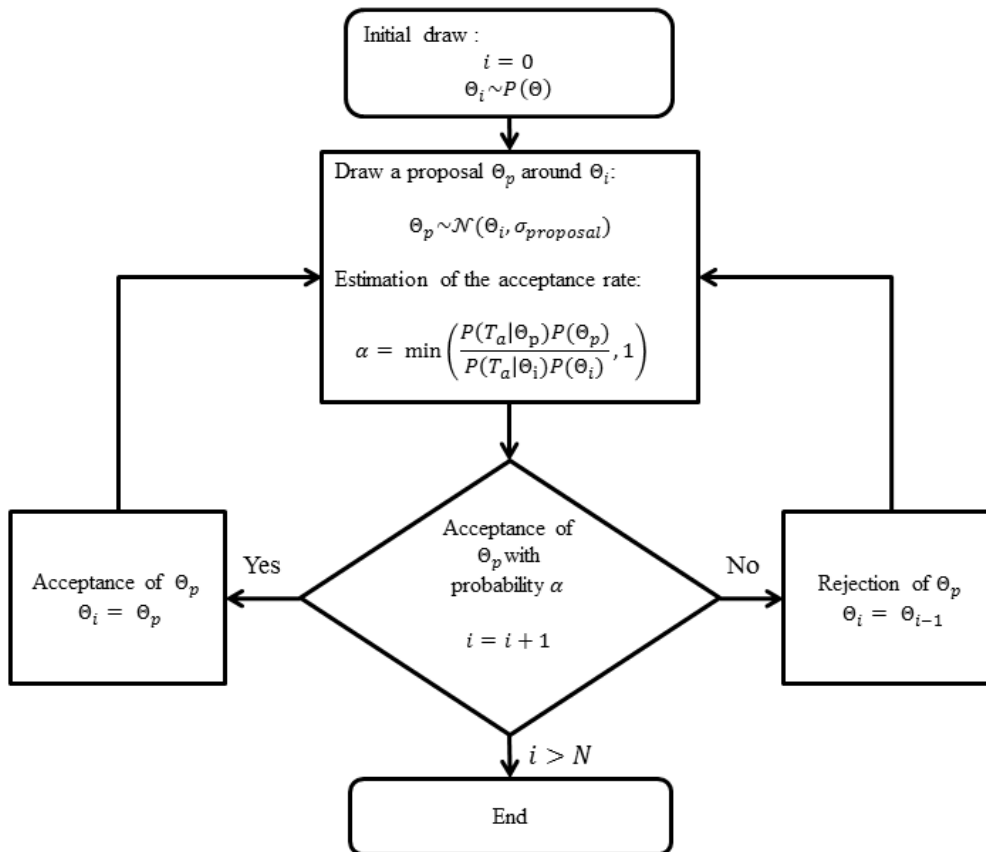


Figure 2 : Metropolis-Hasting Algorithm

3.3 Likelihood function:

The most important part of the Bayesian calibration is the choice of the likelihood function. The likelihood tells how likely a prediction is compared to observed data. Classically, the likelihood is assumed to be solely dependent on metrological error. In such case, and assuming the measurement error over $T_{a,exp}$ is a normal independent and identically distributed (i.i.d) random variable of standard error $\sigma_{a,exp}$, we have:

$$\mathcal{L}(\theta | T_{a,exp}, M, BC) = P(T_{a,exp} | \theta, M, BC) = \mathcal{N}(T_{a,exp} - M(\theta, BC), \sigma_{a,exp}) \quad (5)$$

Although equation (5) accounts for the measurement uncertainty of $T_{a,exp}$, it does not account for the measurement uncertainty of the boundary condition BC . In order to take this extra source of uncertainty into account, we proceed to estimate the prediction uncertainty $\sigma_{a,sim}$ by propagating the boundary condition uncertainty in $M(\theta, BC)$. Since uncertainty propagation using Monte Carlo integration can in itself be computationally intensive, it is only performed once θ_{MAP} , the *maximum a posteriori* value of θ , is found. Prediction uncertainty $\sigma_{a,sim}$ is then combined with measurement uncertainty $\sigma_{a,exp}$ and used to estimate the likelihood of the prediction being equal to the measurement.

If we assume both uncertainties to be normally distributed, then:

$$\mathcal{L}(\theta | T_a, M, BC) = P(T_a | \theta, M, BC) = \mathcal{N}\left(T_{a,exp} - M(\theta, BC), \sqrt{\sigma_{a,sim}^2 + \sigma_{a,exp}^2}\right) \quad (6)$$

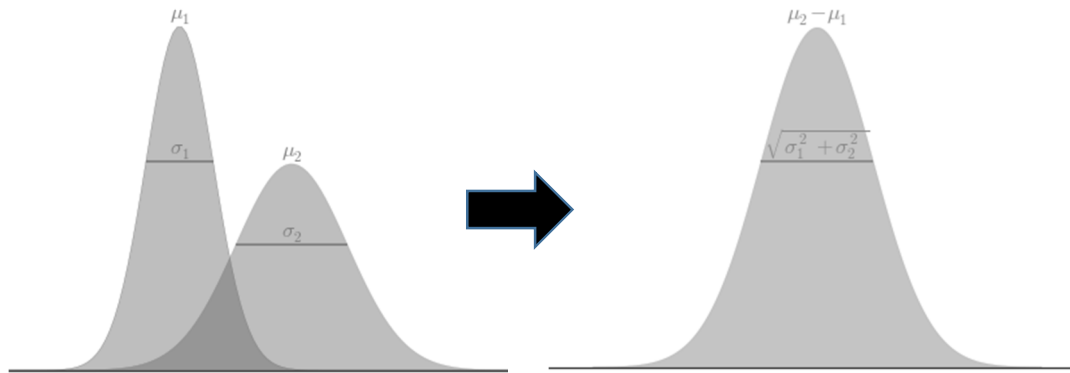


Figure 3 : Two distributions likelihood

Should the normality assumption fail, the combined uncertainty could still be estimated by bootstrap.

The global procedure goes according to the following steps:

- 1- Estimation of Θ_{MAP}
- 2- Propagation of the boundary conditions uncertainties in the energy model $M(\Theta_{MAP}, BC(t))$
- 3- Estimation of the likelihood function that combines uncertainty over $T_{a,exp}$ and $T_{a,sim}$
- 4- Sampling from the posterior distribution $P(T_a | \Theta, M, BC)$

3.4 Deterministic model of the envelope

The identification procedure is based on a thermal model of the building envelope used in French Thermal Regulation RT 2012 (Th-BCE, 2012), which is itself derived from the international standard ISO 13790:2008. The model includes five thermal resistances and one thermal capacity:

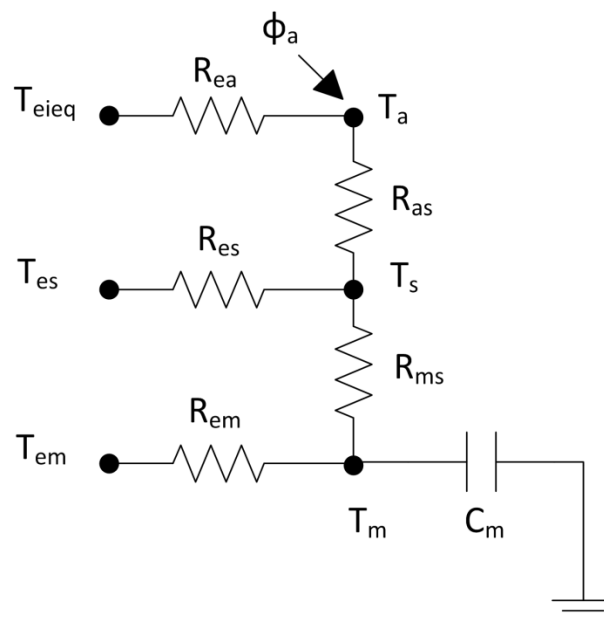


Figure 4 : 5RIC thermal model used for the identification procedure (Th-BCE, 2012)

T_a , T_s and T_m are the air, star and mass equivalent temperature that arise when arranging a triangle thermal network into a star thermal network through the so called Y- Δ transform (Kennelly, 1899).

T_{eieq} , T_{es} and T_{em} are equivalent external temperatures that arise when transforming Neumann boundary condition (e.g. incoming solar heat flux) at each node into an equivalent Dirichlet boundary condition (imposed temperature). They correspond respectively to the air incoming in the building by ventilation and infiltration, glazing components (windows, curtain walls...) and opaque walls. A single thermal capacity representing the walls interior thermal inertia is connected to the mass equivalent temperature T_m . Full description of the model and its numerical scheme can be found in (Th-BCE, 2012).

The model leads to an ordinary differential equation of the first order in T_m numerically solved using the semi-implicit Crank-Nicolson scheme.

Experimental conditions lead to another set of simplifications:

- All glazing component are covered, meaning that incoming solar flux inside the building are null.
- Ventilation is blocked and infiltration is supposed small or known.
- Heating inside the building is purely convective, meaning that all the heat is directed on T_a .
- R_{as} and R_{ms} are fixed and estimated using conventional values for convection and radiation transfer coefficient inside the building and a global surface parameter A_m .
- R_{es}/R_{em} ratio is assumed to be known through the building geometric parameters

The model ends up being a function of a vector of two free parameters, $\Theta = [H_{tr}, C_m]$, with $H_{tr} = 1/R_{em} + 1/R_{es}$.

Boundary conditions $BC(t)$ are as follow:

- $\Phi_a(t)$ the convective heating power.
- $T_{em}(t)$ and $T_{es}(t)$ the equivalent external temperature taking into account solar fluxes and cold sky radiation.
- $Q_v(t)$ the volume air flow caused by infiltrations.

3.5 Stochastic model of the measuring chain

As seen in section 3.3, Bayesian calibration requires the estimation of both measurements and prediction uncertainties. To that end, we combine calibration data from the sensors to evaluate the uncertainty over all the data used in the inversion $T_{a,exp}(t)$ and $BC(t)$. In the following we assume that temperature and heating power sensors were calibrated such that there is no systematic measurement error.

3.5.1 Indoor air temperatures measurement

Air temperature inside the envelope is estimated using a set of k sensors assumed to be evenly distributed in the heated air volume. Each i indoor temperature is measured at time step $\Delta t = 1min$ with calibrated PT100 platinum resistance thermometers following:

$$\mathcal{L}(\Theta | T_{a,exp}, M, BC) = P(T_{a,exp} | \Theta, M, BC) = \mathcal{N}(T_{a,exp} - M(\Theta, BC), \sigma_{a,exp}) \quad (7)$$

$$T^i \sim \mathcal{N}(T_{PT100}^i, \sigma_{PT100})$$

Leading to the estimation of the uncertainty of the hourly average of the i^{th} sensor:

$$\mathcal{L}(\Theta|T_{a,exp}, M, BC) = P(T_{a,exp} | \Theta, M, BC) = \mathcal{N}(T_{a,exp} - M(\Theta, BC), \sigma_{a,exp}) \quad (8)$$

$$\langle T^i \rangle_H \sim \mathcal{N} \left(\langle T_{PT100}^i \rangle_H, \frac{\sigma_{PT100}}{\sqrt{60}} \right)$$

Since forced convection is assumed inside the envelope, temperature stratification is supposed to be small and fluctuations are assumed to be homogeneous in the volume. In this case each sensor reading is a realization of the mean temperature in the heated air volume in a one hour time step:

$$\mathcal{L}(\Theta|T_{a,exp}, M, BC) = P(T_{a,exp} | \Theta, M, BC) = \mathcal{N}(T_{a,exp} - M(\Theta, BC), \sigma_{a,exp}) \quad (9)$$

$$T_a \sim \mathcal{N}(\langle T^i \rangle_H, \sigma_V)$$

Where T_a is the average temperature of the heated volume in an hour of time and σ_V the standard error of the temperature due to the volume inhomogeneity.

σ_V^2 is estimated with the unbiased variance $s_V'^2$:

$$s_V'^2 = \frac{1}{k-1} \sum_{i=1}^k [\langle T^i \rangle_H - T_a]^2 \quad (10)$$

This allows us to estimate the uncertainty over T_a :

$$T_a \sim \mathcal{N} \left(\frac{1}{k} \sum_{i=1}^k \langle T^i \rangle_H, \frac{s_V'}{\sqrt{k}} \right) \quad (11)$$

$$T_a \sim \mathcal{N} \left(\frac{1}{k} \sum_{i=1}^k \langle T_{PT100}^i \rangle_H, \sqrt{\frac{s_V'^2}{k} + \frac{\sigma_{PT100}^2}{60}} \right)$$

3.5.2 Equivalent external mass temperatures measurement

Outer wall boundary condition in the energy model is approximated by a single equivalent temperature T_{em} taking into account external temperature as well as solar radiations. Two cases are considered: Dirichelt boundary temperatures T_{em} and T_{es} are either directly measured with the CSTB developed SENS sensor (Remi Bouchié, Abele, Derouineau, & Millet, 2014) or estimated using solar flux estimation based on an onsite weather station.

3.5.2.1 SENS sensor

A specific sensor has been developed at CSTB to directly measure this equivalent temperature and consequently dispensing us to evaluate direct and diffuse solar radiation (Remi Bouchié et al., 2014). It consists in measuring the temperatures of two surfaces, one black $T_{esb,j}$, one white $T_{esw,j}$, disposed at the center of the j^{th} external wall.

Let us consider the j^{th} equivalent external temperature $T_{em,j}$:

$$T_{em,j}(t) = T_{esb,j}(t) \frac{(\alpha_{ep,j} - \alpha_{esw})}{\alpha_{esb} - \alpha_{esw}} + T_{esw,j}(t) \frac{(\alpha_{esb} - \alpha_{ep,j})}{\alpha_{esb} - \alpha_{esw}} \quad (12)$$

Where α_{esb} and α_{esw} are respectively the absorbance of the black and of the white surface and $\alpha_{ep,j}$ the absorbance of the j^{th} wall.

Let us now use $T_{em,j}$ to estimate $T_{em}(t)$ and $T_{es}(t)$:

$$T_{em}(t) = \frac{\sum_j A_{p,j} U_{p,th,j} T_{em,j}(t)}{\sum_j A_{p,j} U_{p,th,j}} \quad (13)$$

$$T_{es}(t) = \frac{\sum_j A_{ws}(j) U_{ws,th}(j) T_{em}(j, t)}{\sum_j A_{ws}(j) U_{ws,th}(j)} \quad (14)$$

Uncertainty over T_{em} and T_{es} is numerically estimated with the following assumption:

- $T_{esb,j} \sim \mathcal{N}(T_{esb,j,PT100}, \sigma_{es})$
- $\alpha_{es} \sim \mathcal{N}(\alpha_{es,input}, 0.03)$
- $\alpha_{ep} \sim \mathcal{N}(\alpha_{ep,input}, 0.2)$

3.5.2.2 Radiation heat flux estimation

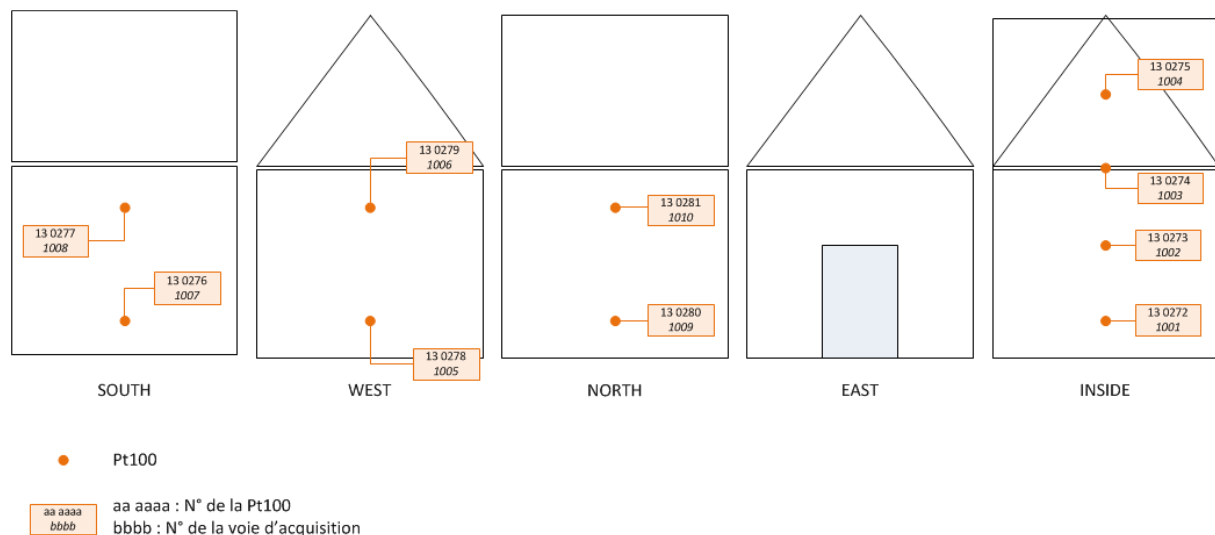
Weather station data, global and diffuse horizontal radiation, relative humidity and outdoor temperature are used to estimate T_{em} according to (Th-BCE, 2012). Sky temperature is estimated using (Aubinet, 1994).

3.5.3 Air infiltration

Air infiltration is estimated according to (Th-BCE, 2012) using wind speed measured at the weather station. Uncertainty is estimated to be about 10%.

4. EXPERIMENTAL SET UP

4.1 Building description



The two wooden structures have a square ground surface (about 13 m² from internal side). They are built with wood structural components on a concrete floor on the ground.

The Faraday wood-structure, on which the validation test has been conducted, is insulated by a multi-foiled thin reflective product, installed between two unventilated air spaces.

Thermal loss through the ground is limited by an important thickness of polyurethane foam. Structural thermal bridges are also limited. The access door is composed by two doors with a mineral wool layer between them.

Airtightness has been measured using a blow-door test according to the standard EN 13829: 2001 (CEN, 2001). Airtightness of the tested structure for a 4 Pa pressure difference can be estimated to be: $Q_{4Pa_{surf}} = 0.43 \pm 0.14 \text{ m}^3/(\text{h.m}^2)$

Heating power is provided by electrical radiant panels plugged on a PID thermal controller in order to maintain internal environment to a constant mean temperature. Maximum heat power available is about 2 kW.

Fans have been installed inside the tested structure to mix the air and make the internal temperature more homogeneous.

4.2 Instrumentation

Energy injected inside the tested structure is measured by a pulse energy meter, indoor air temperature is measured by nine platinum RTDs. Comparative tests have shown that there is no significant difference between air indoor temperature and operative temperature measured according to EN ISO 7726 standard (ISO, 2002).

External solicitations are measured using a weather station recording outdoor air temperature, global horizontal solar radiation, diffuse horizontal solar radiation, wind direction and velocity.

Beside, a specific sensor has been developed in order to directly measure the global effect of all external solicitations (Remi Bouchié et al., 2014). The principle is to group all thermal flows coming from the outside environment into an equivalent external temperature T_{em} .

4.3 Theoretical H_{tr} value

H_{tr} value has been calculated according to French national calculation rules (CSTB, 2012) based on international standards. These calculation rules take into account some in-situ effects such as averaged temperatures in insulation products or air layers (ISO-2, 2008), (ISO-5, 2008), thermal bridges (ISO-1, 2008), thermal transfer via the ground (ISO-3, 2008).

The uncertainty analysis has been preceded by assuming that simplified thermal transfer models included in calculation rules are always correct, that means that no systematic error is present. The global principle is to desegregate the H_{tr} value into the last input needed for its calculation. Indeed, the H_{tr} coefficient depends on heat loss coefficient by both surfaces and structural thermal bridges (ISO-4, 2013) :

$$H_{tr} = \sum_i A_i \cdot U_i + \sum_j L_j \cdot \Psi_j$$

But each component depends on several data such as:

- Geometrical data (thickness, area...)
- Thermal properties of materials that can be measured in laboratory under standardized conditions for insulation products, or estimated according standardized values for other materials (wood, concrete, soil...)
- Design thermal properties for insulation products, which can include a correction due to difference between standardized conditions and real conditions during the test (temperature, moisture...)
- Convective and radiation transfer in air layers and on internal and external sides, linked with experimental boundary conditions (external and internal averaged temperatures, wind velocity...)

For all these inputs for calculation, assumptions are needed to assess their uncertainties. Geometrical data is supposed to be correct (no uncertainty). The core thermal resistance and

surface emissivity of the multifoiled reflective product used in this test has been measured, so uncertainty on this set of data has been estimated using measurement standards. In-situ test solicitations uncertainties (temperatures, wind velocity...) have been calculated and then propagated to correct design values of insulation products and surface exchange coefficients. Uncertainty on standardized thermal properties of other materials is estimated to be 20% of the standardized value if enough information is available (for instance density of the product) or the overall scale available in standardized value. For example, thermal conductivity of the soil can vary from 1.5 to 3.5 W/(m.K) depending on the soil composition (CSTB, 2012), as this composition is unknown, we have considered the value to be 2.5 ± 1 W/(m.K). The uncertainty on Ψ -value due to thermal bridges has been estimated using 3D-modelings based on (ISO-1, 2008) by a sensibility study on uncertain input. As an example the thermal bridge of the vertical outside corner is linked with wood thermal conductivity estimated as 0.145 ± 0.035 W/(m.K), that leads to $\Psi = 0.040 \pm 0.007$ W/(m.K).

These uncertainties have then been propagated using explicit propagation described in the GUM (Joint Committee for Guides in Metrology (JCGM), 2008), assuming that the last input uncertainties follow an uniform rule ($\sigma_i^2 \approx \Delta_i^2 / 3$ where Δ_i is the estimated uncertainty on the last input i). Assuming that geometrical data are certain, the variance on H_{tr} is obtained by:

$$\sigma^2_{H_{tr}} = \sum_i A^2_{i.} \cdot \sigma^2_{U_i} + \sum_j L^2_{j.} \cdot \sigma^2_{\Psi_j}$$

The following tables give U and Ψ -value at the 95% confidence level using the general methodology described above :

Component	Ap [m ²]	Up [W/(m ² .K)]	σ^2 Up [W ² /(m ⁴ .K ²)]	Δ Up [W/(m ² .K)]
Walls	34.19	0.44	0.00031	0.04
Roof	14.63	0.55	0.00048	0.04
Door	1.85	0.19	0.00054	0.05
Ground	12.96	0.11	0.00116	0.07

Junction	Lp [m]	Ψ [W/(m.K)]	σ^2 Ψ [W ² /(m ² .K ²)]	$\Delta\Psi$ [W/(m ² .K)]
Wall / ground	14.40	0.019	1.73E-06	0.002
Wall / roof (north/south)	9.00	0.058	8.01E-07	0.002
Wall / roof (east/west)	7.20	0.043	1.84E-06	0.002
roof / roof (edge)	8.13	0.041	2.70E-07	0.001
Wall / door	3.60	0.031	8.42E-06	0.005

We can deduce then the global result on H_{tr} to be:

$$H_{tr} = 26.5 \pm 1.6 \text{ W/K}$$

4.4 Results

4.4.1 Experimental data

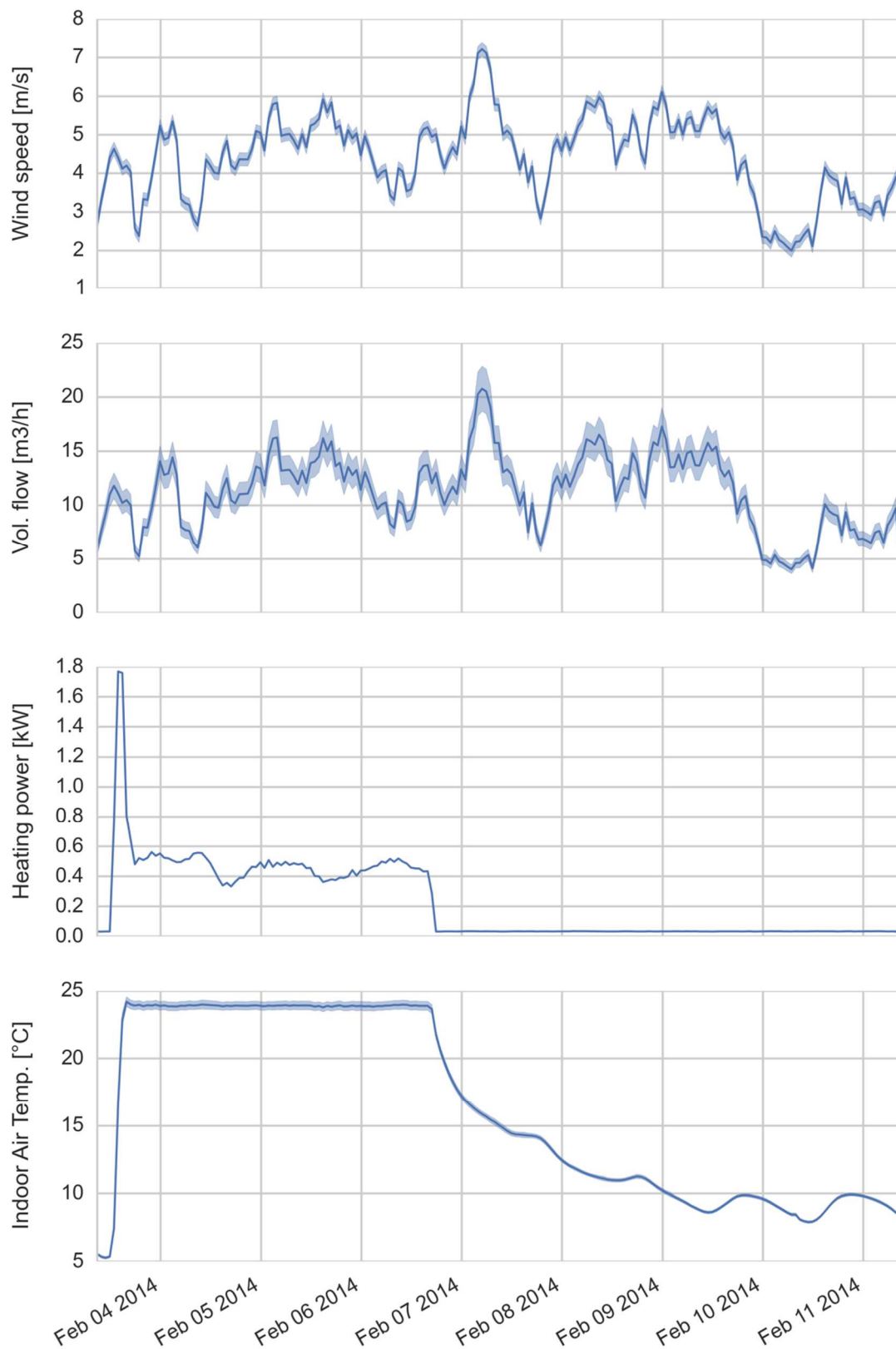


Figure 5 : Experimental data at the 95% confidence level

4.4.2 Equivalent external mass temperature

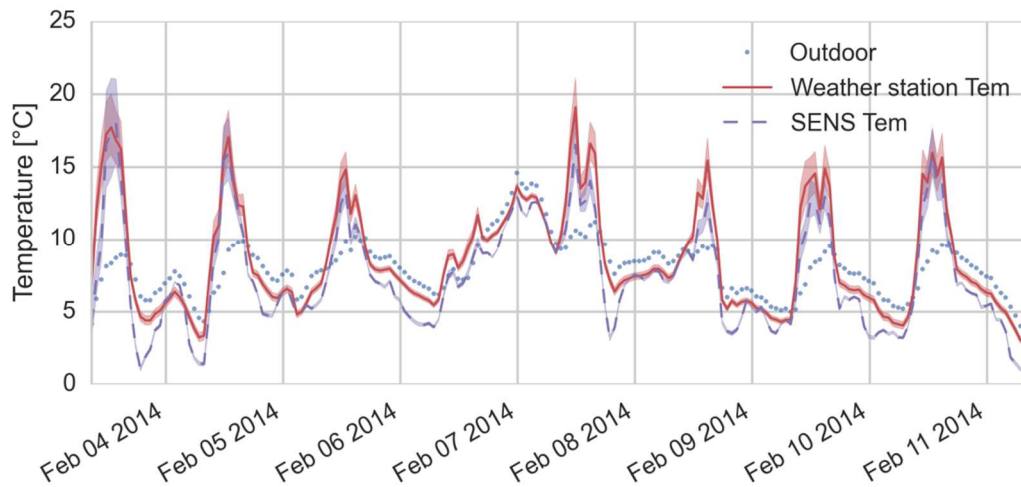


Figure 6 : Estimated Tem at the 95% confidence level

The different method to estimate the equivalent mass temperature shows discrepancy during night time. Such deviation is probably caused by a difference in accounting cold sky heat transfer.

4.4.3 Variance contribution in the likelihood

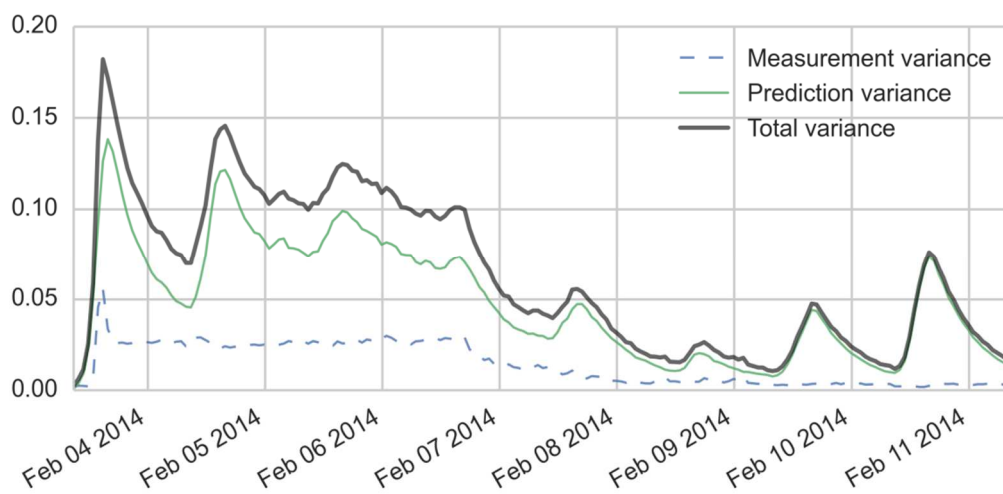


Figure 7 : Variance contributions

The total variance used in the likelihood estimation is made of two contributions, the measurement variance of indoor temperature and the prediction variance, which is obtained by propagating the boundary conditions uncertainty in the model. As shown in Figure 7, the prediction variance is nearly always greater than the measurement variance. This underlines the need to take into account this source of uncertainty in the Bayesian inversion.

4.4.4 MCMC fit

The MCMC sampling has been implemented using the PyMC framework in Python (Patil, Huard, & Fonnesbeck, 2010). Maximum a posteriori and 95% confidence intervals are

presented in Figure 8 for both weather station and SENS sensors T_{em} estimation. Inverse measurement of H_{tr} as well as C_m are show in Table 1.

Both fit present a relatively high root mean square error (RMSE of 0.76 and 0.98 respectively), especially considering that the building has a small thermal inertia (about 16 hours). This result appears to be consistent with previous results on virtual experiment (Boisson & Bouchié, 2014), especially considering the relative high value of lag between measured and predicted temperature in the free float regime. This lag shows that the thermal model is too quick to propagate external temperature variation inside the building compared to the actual measurement. This could be explained by the use of a single thermal capacity inside the building.

The results discrepancy when choosing between the different methods of estimating T_{em} tends to imply a bias in the boundary conditions estimation. As seen in Figure 1, the equivalent external mass temperature calculated by the two different methods (weather station data and SENS sensor) shows discrepancies at night, which implies that cold sky radiation is causing the deviation. This deviation could be caused by an error in taking into account the long wave emissivity of the materials (building walls and SENS sensors black and white surfaces). Further investigation is required.

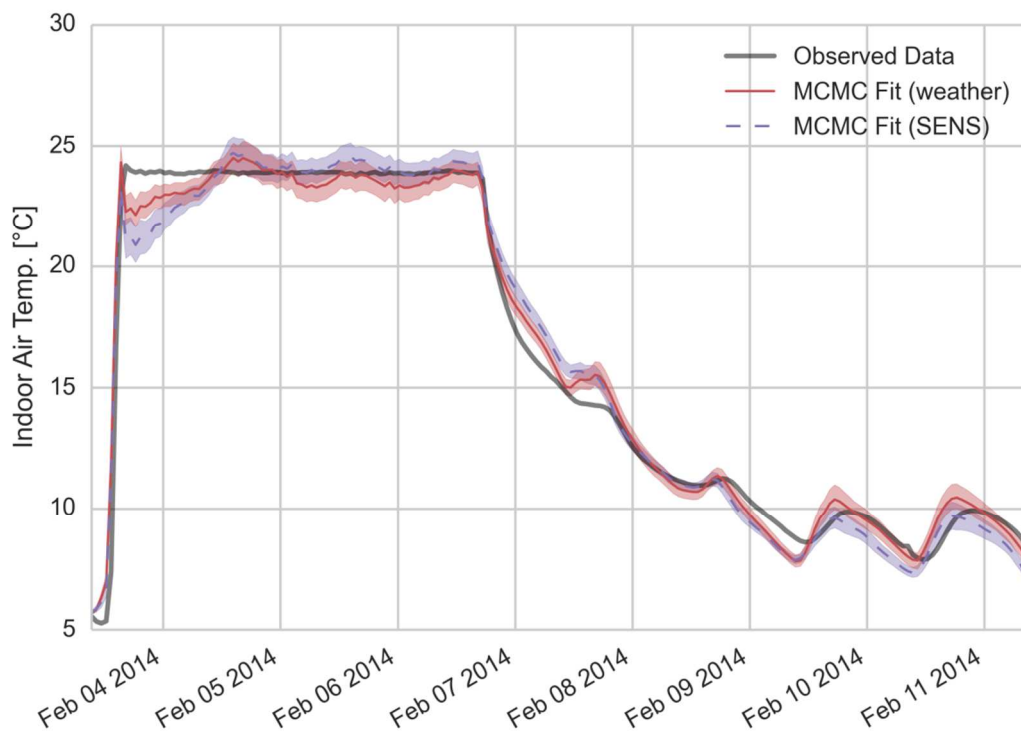


Figure 8 : Fitted and measured indoor temperature at 95% confidence level.

Table 1 : inverse measurement

	H_{tr}	C_m	Fit RMSE
Theoretical value	26.5 ± 1.5 W/K	1017	-
SENS sensors	24.11 ± 0.13 W/K	1675 ± 17 kJ/K	0.98
Weather station	26.77 ± 0.14 W/K	1527 ± 15 kJ/K	0.79

Measured values of H_{tr} using the weather station data is in agreement with the theoretical value, whereas the one using SENS sensor data fall outside the 95% confidence interval. Its higher RMSE suggests a greater bias in using SENS sensor data.

5. DISCUSSION

Inverse measurement is an over specified and under determined problem. As the formula $P(\Theta | M, BC(t))$ implies, it also has the singular property of being highly dependent on the choice of the model we inverse.

In this work we choose a well-known model used in the French Thermal Regulation RT-2012 mostly to insure that the measured heat loss coefficient would be consistent between design stage and acceptance stage. This also has some shortcomings. Such model becomes rapidly over parameterized and it can become tricky to draw the line between setting a parameter at a conventional values or setting it as a free parameter to optimize.

In this context, it appears difficult to assign a clear cause for measurement bias. Even though boundary condition seems at fault for the high level of RMSE, the phase shift and amplitude bias in the free floating regime is most probably linked to the thermal model used in the inversion.

6. CONCLUSION

A new performance assessment protocol has been described. It allows the measurement of the heat loss coefficient of a building and estimates its uncertainty by taking into account input and output uncertainty. The method has been demonstrated on a small building. The inverse measurement of the heat loss coefficient is in agreement with its theoretical value.

ACKNOWLEDGEMENTS

This work was supported by the Centre Scientifique et Technique du Bâtiment (CSTB). The authors gratefully extend their thanks to Marion Delahaie (CSTB) for the experimental set-up and the sensors calibration.

REFERENCES

- (JCGM), J. C. for G. in M. (2008). *Evaluation of measurement data - Guide to the expression of uncertainty in measurement (GUM) - Supplement 1: Numerical methods for the propagation of distributions* (1ère ed.). International Organization for Standardization.
- Aubinet, M. (1994). Longwave sky radiation parametrizations. *Solar Energy*, 53(2), 147–154. Retrieved from <http://cat.inist.fr/?aModele=afficheN&cpsid=4219314>
- Boisson, P., & Bouchié, R. (2014). ISABELE method: In-Situ Assessment of the Building Envelope performances. In *System Simulation in Buildings*.
- Bouchié, R., Abele, C., Derouineau, S., & Millet, J.-R. (2014). ABELE, Charlotte; MILLET, Jean-Robert Conception et validation d'un capteur de mesure de la température extérieure équivalente d'une paroi opaque d'un bâtiment. In *IBPSA France*. Arras.
- Bouchié, R., Alzetto, F., Brun, A., Boisson, P., & Thebault, S. (2014). SHORT METHODOLOGIES FOR IN-SITU ASSESSMENT OF THE INTRINSIC THERMAL PERFORMANCE OF THE BUILDING ENVELOPE. In *Sustainable places*.
- Coakley, D., Raftery, P., & Keane, M. (2014). A review of methods to match building energy simulation models to measured data. *Renewable and Sustainable Energy Reviews*, 37, 123–141. doi:10.1016/j.rser.2014.05.007

- Forbes, A. B., & Sousa, J. A. (2011). The GUM , Bayesian inference and the observation and measurement equations. *Measurement*, 44(8), 1422–1435. doi:10.1016/j.measurement.2011.05.007
- Heo, Y., Choudhary, R., & Augenbroe, G. A. (2012). Calibration of building energy models for retrofit analysis under uncertainty. *Energy and Buildings*, 47, 550–560. doi:10.1016/j.enbuild.2011.12.029
- Joint Committee for Guides in Metrology (JCGM). (2008). *Evaluation of measurement data - Guide to the expression of uncertainty in measurement (GUM)* (1ère ed.). International Organization for Standardization.
- Joint Committee for Guides in Metrology (JCGM). (2012). *Vocabulaire international de métrologie (VIM)– Concepts fondamentaux et généraux et termes associés*. (JCGM, Ed.) (3ème ed.). International Organization for Standardization.
- Kennelly, A. E. (1899). The equivalence of triangles and three-pointed stars in conducting networks. *Electrical World and Engineer*, 34(12), 413–414.
- Patil, A., Huard, D., & Fonnesbeck, C. J. (2010). PyMC: Bayesian Stochastic Modelling in Python. *Journal of Statistical Software*, 35(4), 1–81. Retrieved from <http://www.pubmedcentral.nih.gov/articlerender.fcgi?artid=3097064&tool=pmcentrez&rendertype=abstract>
- Th-BCE. (2012). Arrêté du 30 avril 2013 portant approbation de la méthode de calcul Th-BCE 2012 prévue aux articles 4, 5 et 6 de l'arrêté du 26 octobre 2010 relatif aux caractéristiques thermiques et aux exigences de performance énergétique des bâtiments nouveaux et des . *Journal Officiel*, n°0106: 77.
- ISO-1. «ISO 10211:2008 - Thermal bridges in building construction - Heat flows and surface temperatures - Detailed calculations.» 2008.
- ISO-2. «ISO 10456: 2008 - Building materials and products - Hygrothermal properties - Tabulated design values and procedures for determining declared and design thermal values.» June 2008.
- ISO-3. «ISO 13370: 2008 - Thermal performance of buildings - Heat transfer via the ground - Calculation methods.» April 2008.
- ISO-4. «ISO 13790: 2013 - Energy performance of buildings - Calculation of energy use for space heating and cooling.» *Energy performance of buildings - Calculation of energy use for space heating and cooling*. 2013.
- ISO-5. «ISO 6946:2008 - Building components and building elements - Thermal resistance and thermal transmittance - Calculation method.» 2008.

A practical and scalable inverse modeling approach for multi-zone buildings

J. Cai and J. E. Braun

⁽¹⁾ Ray W. Herrick Laboratory, Purdue University, US

1. ABSTRACT

To study the dynamic behavior of an existing building, data-driven models are preferred and these types of models can be established via system identification techniques. However, most of the time the identification problem is difficult to solve for multi-zone buildings due to high dimensionality of the model and poor excitations in the training data. This paper adopts a physically based modeling structure for multi-zone buildings and develops a practical and scalable approach to identify the parameters in the proposed structure. The approach decouples the zones with weak interactions and groups together the ones with strong couplings so that each group can be estimated individually. To reduce the number of estimated parameters and improve identifiability, a two-step algorithm was developed to determine the significant parameters and fix the non-significant ones to some nominal values in the estimation process. As a case study, the proposed approach was applied to model a medium-size commercial building with nine thermal zones from measured data and the estimated model was validated with different periods of data in the cooling season.

Keywords: building envelope model, gray-box model, system identification, multi-zone building dynamic model, sensitivity analysis

2. INTRODUCTION

To perform control analysis of an existing building, it is critical to have a model that provides a good approximation of the actual system dynamics. To achieve this, data-driven modeling approaches, which use measured data to identify the system behavior via some system identification techniques, are typically applied. The identified model can then be used for optimal control, fault detection or some types of retrofit analysis.

A variety of different methods can be found in the open literature that focus on data-driven modeling of buildings, but most of them are dedicated to single-zone buildings or multi-zone buildings with a small number of thermal zones. Practical approaches for data-driven modeling of multi-zone buildings are still needed. Identification of a single-zone building is already challenging due to the high complexity and large uncertainties associated with environmental and operational inputs. Identifying a multi-zone building adds more difficulties since interactions exist between different zones and simultaneous identification of all the zones could quickly become impossible as the number of zones increases.

Some previous researchers have investigated different approaches for multi-zone building inverse modeling. Subspace identification seems to be a good candidate for modeling a multi-zone building and several previous studies have adopted this approach (e.g., Cigler and Privara 2010; Cai and Braun, 2013). However, it is a black-box modeling approach so extrapolating performance is not guaranteed, which is especially important when a model is trained with limited data. To improve extrapolating performance of the subspace model, Cigler and Privara (2010) carried out an experiment where test signals were injected continuously in the building control system over a two-month period. This would be an expensive solution to apply in general.

Gray-box modeling approaches are more robust and can provide better extrapolating performance although they require more effort to setup and estimate a model. Choosing an appropriate model structure and developing a good estimation algorithm is still an ongoing effort. Privara et al. (2011) proposed an approach that first establishes a detailed forward model with EnergyPlus and then trains a simplified resistance-and-capacitance (RC) model with some specially designed excitation signals for a large multi-zone building. But it is literally a model order reduction technique and does not fall into the category of data-driven models in a strict sense. Goyal et al. (2011) proposed an identification method for the inter-zonal thermal interactions in multi-zone buildings from measured data. A 3R2C branch was used to represent thermal coupling between the zones and resistances and capacitances were estimated from measured data. But all other construction elements (except the external wall) were ignored and it did not consider the gains from solar radiation, occupants or equipment. Bacher and Madsen (2011) proposed a set of candidate models with increasing complexity and applied likelihood ratio tests to identify the suitable model structure. However, even the most complex model in the candidate set is still simplified and no validation results were presented. Although the method was applied to a multi-zone case study, the model adopted a single-zone structure and did not consider any internal heat gains.

This study adopts a simplified RC network structure for a multi-zone building that is similar to previous work. The main contribution is the development of a three-step estimation methodology: 1) identify and eliminate weak couplings and group strongly coupled zones; 2) identify and eliminate non-influential parameters in the identification process; 3) de-correlate the parameters by fixing those highly correlated parameters to some nominal values. These steps reduce the estimate parameter set and can improve identifiability of the problem significantly. A case study was performed on a medium sized commercial building with nine thermal zones. The model was estimated using a set of measurements obtained from the site and then validated with two separate testing data sets.

3. MULTI-ZONE BUILDING MODEL

3.1 Model structure

Figure shows a general thermal network for a multi-zone building that is employed in this study where the coupling branches are depicted in the dash box. The coupling elements are either a wall with a 3R2C representation or some low or no-capacitance interaction, such as a window or simply an opening, with a pure resistance representation. In general, each individual thermal zone has a thermal network as shown in Figure as described by Cai and Braun (2012). In this representation, a 3R2C external wall is used to capture the slow coupling dynamics and a pure resistance is used for the fast coupling dynamics to the outdoor environment. There is an internal wall that is being used to capture the thermal storage inside a room including furniture and walls that are not interacting with other zones. Again, the coupling element is contained in a dash box in Figure and it could be either a pure resistance or a 3R2C branch depending on the zone configurations. Transmitted solar radiation is absorbed by the floor while the radiative internal heat gains are applied to all walls with a uniform heat flux. However, to simplify the model setup process, the radiative internal heat gains could be configured to only enter the walls with significant thermal masses. Ventilation heat exchanges and convective internal heat gains interact with zone air directly.

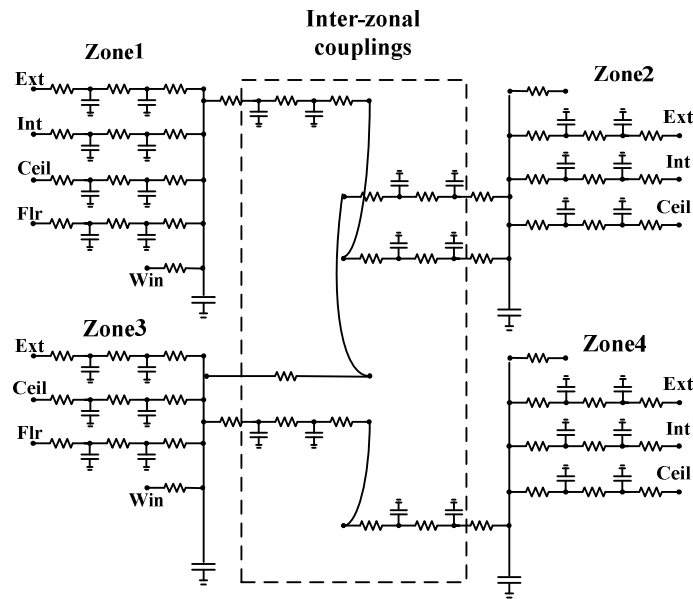


Figure 1: Multi-zone thermal network

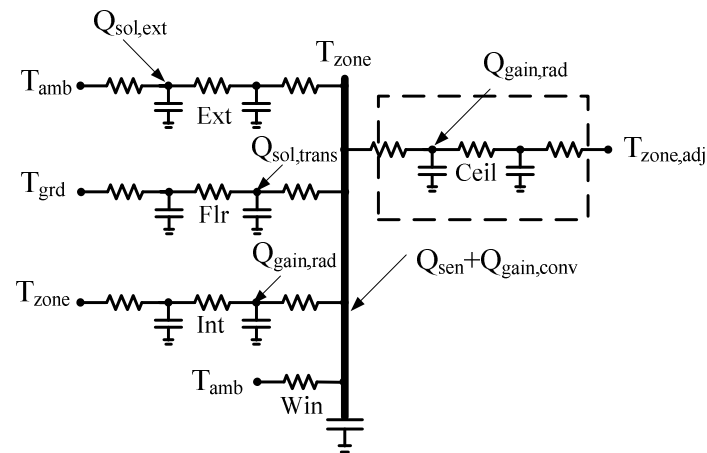


Figure 2: Single zone thermal network

3.2 Mathematical formulation

Applying an energy balance to each temperature node a state-space representation is formulated as:

$$\begin{aligned} \dot{\mathbf{x}} &= \mathbf{A}\mathbf{x} + \mathbf{B}_w\mathbf{w} + \mathbf{B}_u\mathbf{u} \\ \mathbf{y} &= \mathbf{C}\mathbf{x} + \mathbf{D}_w\mathbf{w} + \mathbf{D}_u\mathbf{u} \end{aligned} \quad (1)$$

where \mathbf{w} is a vector of uncontrollable inputs or disturbances including outdoor conditions and internal heat gains due to occupants and equipment, \mathbf{u} is the controllable input which is chosen to be heating or cooling that the HVAC system is providing to each of the zones and \mathbf{x} is the state vector containing all temperatures in the thermal network. Output vector \mathbf{y} contains all zone air temperatures. For n zones, the state and input vectors could be partitioned in the following manner:

$$\begin{aligned}\mathbf{x}^T &= [\mathbf{x}_1^T \mid \mathbf{x}_2^T \mid \dots \mid \mathbf{x}_n^T] \\ \mathbf{w}^T &= [\mathbf{w}_1^T \mid \mathbf{w}_2^T \mid \dots \mid \mathbf{w}_n^T] \\ \mathbf{u}^T &= [u_1 \ u_2 \ \dots \ u_n] \\ \mathbf{y}^T &= [y_1 \ y_2 \ \dots \ y_n]\end{aligned}$$

where \mathbf{x}_i and \mathbf{w}_i correspond to the states and disturbance inputs that are associated with zone i . For a coupling wall that is shared by two zones, each of the two temperature nodes is assigned to the zone that it is closer to it. Also, the inputs that are shared by multiple zones (e.g., ambient temperature is taken as a disturbance input for all the perimeter zones) are replicated in each of the input vectors owned by the corresponding zones. Using these special arrangements, the state-space representation in Equation (1) can be reformulated in Equation (2).

$$\begin{aligned}\begin{bmatrix} \mathbf{x}_1 \\ \mathbf{x}_2 \\ \vdots \\ \mathbf{x}_n \end{bmatrix} &= \begin{bmatrix} \mathbf{A}_{11} & \mathbf{A}_{12} & \dots & \mathbf{A}_{1n} \\ \mathbf{A}_{21} & \mathbf{A}_{22} & & \vdots \\ \vdots & \vdots & \ddots & \vdots \\ \mathbf{A}_{n1} & \dots & & \mathbf{A}_{nn} \end{bmatrix} \begin{bmatrix} \mathbf{x}_1 \\ \mathbf{x}_2 \\ \vdots \\ \mathbf{x}_n \end{bmatrix} + \begin{bmatrix} \mathbf{B}_{1w} & \mathbf{0} & \dots & \mathbf{0} \\ \mathbf{0} & \mathbf{B}_{2w} & & \vdots \\ \vdots & \vdots & \ddots & \vdots \\ \mathbf{0} & \dots & & \mathbf{B}_{nw} \end{bmatrix} \begin{bmatrix} \mathbf{w}_1 \\ \mathbf{w}_2 \\ \vdots \\ \mathbf{w}_n \end{bmatrix} + \begin{bmatrix} \mathbf{B}_{1u} & \mathbf{0} & \dots & \mathbf{0} \\ \mathbf{0} & \mathbf{B}_{2u} & & \vdots \\ \vdots & \vdots & \ddots & \vdots \\ \mathbf{0} & \dots & & \mathbf{B}_{nu} \end{bmatrix} \begin{bmatrix} u_1 \\ u_2 \\ \vdots \\ u_n \end{bmatrix} \\ \begin{bmatrix} y_1 \\ y_2 \\ \vdots \\ y_n \end{bmatrix} &= \begin{bmatrix} \mathbf{C}_1 & \mathbf{0} & \dots & \mathbf{0} \\ \mathbf{0} & \mathbf{C}_2 & & \vdots \\ \vdots & \vdots & \ddots & \vdots \\ \mathbf{0} & \dots & & \mathbf{C}_n \end{bmatrix} \begin{bmatrix} \mathbf{x}_1 \\ \mathbf{x}_2 \\ \vdots \\ \mathbf{x}_n \end{bmatrix}\end{aligned}\quad (2)$$

This special formulation is particularly useful for decentralized estimation, which will be considered in later sections, as well as decentralized controller design (Rawlings and Mayne, 2007) since all matrices are block diagonal (\mathbf{B}_w , \mathbf{B}_u and \mathbf{C}) except for matrix \mathbf{A} . Although matrix \mathbf{A} is not block diagonal, it is extremely sparse in the sense that any coupling sub-matrix \mathbf{A}_{ij} has only k nonzero entries if there are k coupling branches between room i and room j . Most often only one coupling branch, either a 3R2C or a pure resistance depending on which has dominant dynamics, is considered, so \mathbf{A}_{ij} usually has all entries zero except for the coupling one. If two zones, say, zone i and zone j , are weakly coupled, the coupling matrix \mathbf{A}_{ij} can be approximated with a zero matrix and the two zones can be totally decoupled. If groups of zones have weak interaction with each other, then the zones can be divided into several decoupled subgroups and each subgroup can be estimated individually. In this case, matrix \mathbf{A} can be approximated with a block diagonal matrix where each block corresponds to each of the subgroups. This is a critical step in identification of multi-zone buildings and the details will be discussed in section 4.2.

4. ESTIMATION ALGORITHM

Even for a single zone, the estimation problem is difficult to solve since there is a large set of parameters that need to be estimated with only one output. For a typical room with four walls and one window like the one shown in Figure , there are 21 RC parameters to estimate along with window transmittance, heat gain scaling factors, and other parameters. All of these parameters need to be identified simultaneously to minimize predictions between measured and predicted zone temperature, which is a difficult problem because of local minimums and computational requirements. The situation is much worse for a multi-zone building where the problem can become unsolvable as the number of zones increases. To overcome these difficulties, most previous approaches have resorted to using lower order model structures (e.g., Goyal, 2011; Lin, 2012). However, the simplifications limit the applicability of the model because (1) a lower order model may not distinguish between some different heat flow paths so some critical information may be missing; (2) the model may have difficulty extrapolating beyond the training data leading to long training requirements; (3) radiant effects are usually hard to capture. The current study tries to attack the problem from a different perspective: keep

the complexity of the model structure but improve the identifiability using a multi-step scheme that is discussed in the following sub-sections.

It needs to be emphasized that the three steps presented in the following three subsections are carried out for each zone separately using adjacent zone temperatures as boundary conditions. Although performing the steps on all the zones simultaneously could lead to a more accurate model, zone-wise analysis can reduce the computation burden significantly since computation complexity increases with the size of the system at least quadratically.

4.1 Parameter initial guess

An important advantage of the gray-box modeling approach for buildings is that it does not require detailed geometry or construction information in the model setup phase, as a forward model does. So the effort that is required to set up a model is lower and only rough information is needed to provide some initial guesses for the parameters. The obtained initial guesses are used as the starting point for nonlinear regression. More importantly, they provide some information on the feasible region for the parameters in the identification process to make sure the estimated parameter values lie within reasonable ranges. For uncertain parameters, a relatively large feasible region can be used to allow the regression to explore within a large range. However, if more accurate information is available then a small feasible region can be assigned in the estimation process. In the case study within this paper, the feasible range for all parameters was assumed to be within 1/3 and 3 times of the initial guesses.

The building information can be acquired by collecting surveys that are filled out by someone who has access to the building and/or blueprints. The survey should include information about the key construction elements, e.g., walls and windows, for each zone. Table shows a sample survey. All internal surfaces are assumed to have an initial value for convective heat transfer coefficient of 11 kJ/hr-m²-K and the corresponding value for an external surface is assumed to be 64 kJ/hr-m²-K. With this assumption and all the information provided in the survey, initial guesses for parameter values can be calculated easily.

Table 1: Sample inquiry survey for building information

<i>Zone information</i>					
Zone	Zone volume				
Z1	1000 m ³				

<i>Wall information</i>					
Zone	Wall area	Wall thickness	Orientation	Wall construction	Adjacent air node
Z1	50 m ²	0.2 m	East	Concrete: 0.1m; plasterboard: 0.01m.	Ambient
	10 m ²	0.1 m	-	Plasterboard: 0.06m.	Z2

<i>Window information</i>				
Zone	Window area	Window U-value	Window transmittance	Orientation
Z1	25 m ²	0.2 Btu/ft ² -hr-F	0.45	East

It needs to be emphasized that different levels of accuracy are required for different types of information in the survey. To estimate some parameters, visual inspection is enough, such as the wall areas. But construction properties are more important and building blueprints might be

needed to obtain some reasonable estimates. For example, the wall resistance would be significantly different for walls with and without insulation. For the parameters with very limited information, a large feasible region needs to be assigned in the estimation process. As long as the actual parameter values fall within the specified feasible region, the decoupling and parameter-reduction analysis in the following subsections are able to tolerate significant deviations between initial guesses and actual values.

4.2 Decoupling and merging zones

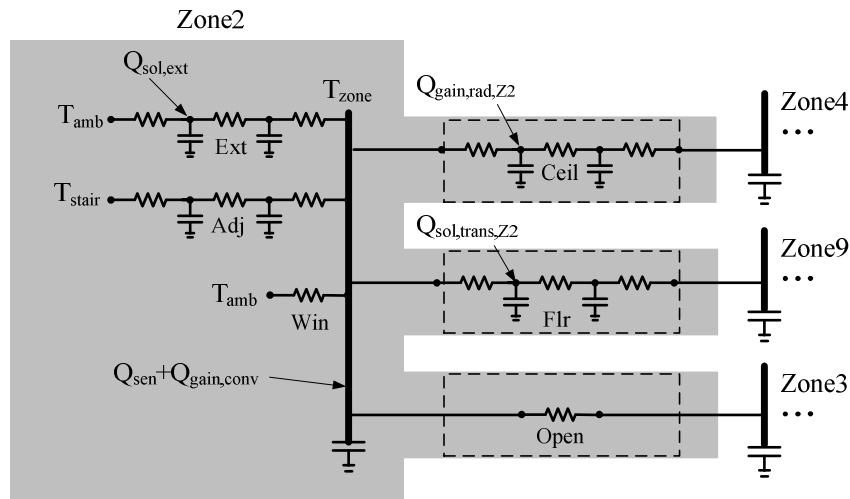


Figure 3: Inter-zonal coupling for Zone 2.

Decoupling the zones that have weak interactions can break down a large estimation problem into several small sub-problems that can be estimated individually. This procedure is critical for identification of multi-zone buildings since the original problem could be infeasible to solve due to the dimensionality issue. In addition, multi-zone models have poor identifiability and the parameter estimates could be highly correlated if the training data is not informative enough. Thus, eliminating the weak inter-zonal thermal interactions and grouping the strongly coupled zones can improve both the solvability of the identification problem and the accuracy of the parameter estimates.

As a first step in the estimation process, a simple data-dependent method is adopted to decouple the thermal zones. To illustrate the process, Zone2 in the case study is considered and the associated thermal network is depicted in Figure 3. This zone is coupled with Zone4 via the ceiling and with Zone9 via the floor. The two coupling walls adopt a 3R2C structure due to their high thermal masses. Zone2 is also connected with Zone3 by an internal wall with significant openings. The thermal interactions due to air exchange through the openings are dominant so a pure resistance branch is used to represent the coupling effect between these two zones. The coupling strength between Zone2 and Zone4 is calculated as

$$CS(2,4) = \left\| g(\mathbf{U}_{Z2}, \boldsymbol{\theta}_{Z2}) - g(\mathbf{U}_{Z2}, \boldsymbol{\theta}_{Z2,decoupl}) \right\|_2 / \sqrt{\text{length}(\mathbf{U}_{Z2})} \quad (3)$$

where \mathbf{U}_{Z2} is the excitation data in the training data set of Zone2, $\boldsymbol{\theta}_{Z2}$ is the nominal parameters (initial guesses) restricted to Zone2, $\boldsymbol{\theta}_{Z2,decoupl}$ is the same as $\boldsymbol{\theta}_{Z2}$ but with infinite coupling resistance, $g(\mathbf{U}, \boldsymbol{\theta})$ is the output of the model for Zone2 shown in Equation (1) and $\text{length}(\mathbf{U}_{Z2})$ is the number of samples in the training data. The coupling resistance corresponds to the middle resistance in a 3R2C branch and corresponds to the sole resistance in a 1R branch. The calculated coupling strength is simply the root mean square (RMS) deviation between the model outputs with the nominal coupling resistance and with infinite coupling resistance when the

model is fed with the training data. When the calculated RMS deviation is large, the coupling wall transfers significant heat to the zone and it cannot be eliminated. For a small RMS deviation, it would be safe to ignore the corresponding coupling effect.

Performing the calculation in Equation (3) for each of the zones, an $n \times n$ matrix \mathbf{CS} , where n is the number of zones, can be obtained, the element of which indicates the pair-wise coupling strengths. The matrix \mathbf{CS} is not necessarily symmetric so the following operation needs to be carried out to average the two directional effects between two zones:

$$\mathbf{CS} = (\mathbf{CS} + \mathbf{CS}') / 2$$

where \mathbf{CS}' is the transpose of matrix \mathbf{CS} and the equal sign essentially overwrites the left-hand side of the equation with the right-hand side. The obtained matrix \mathbf{CS} is the final coupling matrix and its element indicates the bi-directional coupling strength between those two zones corresponding to the specific row and column.

4.3 Reducing estimate parameter set

After discretizing Equation (1), the model output can be written in the form shown in Equation (4) which indicates that model prediction is a time series dependent on parameter $\boldsymbol{\theta}$ and excitation data \mathbf{U} . Since this paper is mainly concerned with passive identification, which means there is no active control during the data collection period, the dependence on input data is not important and only the parameter dependence is considered. So the excitation data \mathbf{U} is omitted in the argument list of the following equations.

$$\hat{y}(t, \boldsymbol{\theta}) = g(t, \mathbf{U}(1), \mathbf{U}(2), \dots, \mathbf{U}(t-1), \boldsymbol{\theta}) \quad (4)$$

Define

$$\bar{\mathbf{Y}}(\boldsymbol{\theta}) = [\hat{y}(1, \boldsymbol{\theta}), \dots, \hat{y}(t, \boldsymbol{\theta})]^T$$

and let

$$\begin{aligned} \mathbf{J}(\boldsymbol{\theta}) &= \frac{\partial}{\partial \boldsymbol{\theta}} [\bar{\mathbf{Y}}(\boldsymbol{\theta})] \in \mathcal{R}^{t \times np} \\ \mathbf{M}(\boldsymbol{\theta}) &= \mathbf{J}^T(\boldsymbol{\theta}) \mathbf{J}(\boldsymbol{\theta}) \in \mathcal{R}^{np \times np} \end{aligned} \quad (5)$$

where $np = \dim(\boldsymbol{\theta})$. $\mathbf{J}(\boldsymbol{\theta})$ is the sensitivity matrix and $\mathbf{M}(\boldsymbol{\theta})$ is the information matrix, both evaluated at parameter $\boldsymbol{\theta}$. Define the significance vector as

$$\mathbf{S}(\boldsymbol{\theta}) = \{\sqrt{\mathbf{M}_{ii}(\boldsymbol{\theta})} \mid i = 1, 2, \dots, np\},$$

which consists of the square roots of the diagonal elements of $\mathbf{M}(\boldsymbol{\theta})$. The i -th element, $\mathbf{S}_i(\boldsymbol{\theta})$, is an index of the significance level for the i -th parameter in the model output. In linear regression theory (Kutner et al., 2005), the square of this value is inversely proportional to the size of the confidence region for the corresponding parameter. For nonlinear regression, which is the case in our study, the square of the elements in $\mathbf{S}(\boldsymbol{\theta})$ can also be used to approximate the inverse of the confidence interval locally (Donaldson et al., 1987). So a higher value of $\mathbf{S}_i(\boldsymbol{\theta})$ leads to a smaller confidence interval, which also indicates a higher significance for the i -th parameter.

Parameters have different scales so normalization is needed for the information matrix to account for the scaling effects and the normalized version of the information matrix is shown in Equation (6), where $\mathbf{Diag}(\boldsymbol{\theta})$ represents the diagonal matrix constructed from the vector $\boldsymbol{\theta}$.

$$\mathbf{M}_{norm}(\boldsymbol{\theta}) = \mathbf{Diag}(\boldsymbol{\theta}) (\mathbf{J}^T(\boldsymbol{\theta}) \mathbf{J}(\boldsymbol{\theta})) \mathbf{Diag}(\boldsymbol{\theta}) \quad (6)$$

This can be implemented in the numerical sensitivity matrix calculation as shown in Equation (7),

$$\begin{aligned}\mathbf{J}_{cal,i}(\boldsymbol{\theta}) &= \bar{\mathbf{Y}}(\boldsymbol{\theta}) - \bar{\mathbf{Y}}(\boldsymbol{\theta}_{\delta,i}) = \delta \boldsymbol{\theta}(i) \frac{\bar{\mathbf{Y}}(\boldsymbol{\theta}) - \bar{\mathbf{Y}}(\boldsymbol{\theta}_{\delta,i})}{\delta \boldsymbol{\theta}(i)} \\ &= \delta \boldsymbol{\theta}(i) \mathbf{J}_i(\boldsymbol{\theta}) \in \mathfrak{R}^{r \times 1}\end{aligned}\quad (7)$$

where

$$\boldsymbol{\theta}_{\delta,i}(j) = \begin{cases} \boldsymbol{\theta}(j) & , i \neq j \\ (1-\delta)\boldsymbol{\theta}(j) & , i = j \end{cases}$$

and $\mathbf{J}_{cal,i}(\boldsymbol{\theta})$ is the j -th column of the calculated sensitivity matrix and it corresponds to deviation in the output caused by a perturbation in the j -th parameter and $\boldsymbol{\theta}$ corresponds to the perturbation level. Plugging the calculated sensitivity matrix into Equation (5) provides the estimated information matrix shown in Equation (8). So the information matrix calculated is equal to the normalized information matrix up to a constant scalar depending on the perturbation level.

$$\begin{aligned}\mathbf{M}_{cal}(\boldsymbol{\theta}) &= \mathbf{J}_{cal}^T(\boldsymbol{\theta}) \mathbf{J}_{cal}(\boldsymbol{\theta}) \\ &= \delta^2 \text{Diag}(\boldsymbol{\theta}) \left(\mathbf{J}^T(\boldsymbol{\theta}) \mathbf{J}(\boldsymbol{\theta}) \right) \text{Diag}(\boldsymbol{\theta}) \\ &= \delta^2 \mathbf{M}_{norm}(\boldsymbol{\theta})\end{aligned}\quad (8)$$

$$\mathbf{S}_{cal}(\boldsymbol{\theta}) = \left\{ \sqrt{\mathbf{M}_{cal,ii}(\boldsymbol{\theta})} \mid i = 1, 2, \dots, np \right\}$$

One advantage of this numerical routine is that the elements of the calculated significance vector, $\mathbf{S}_{cal}(\boldsymbol{\theta})$, have physical meaning: the root mean square of deviations in the output caused by the corresponding parameter perturbation. Then it is straightforward to impose a threshold for determining influential/non-influential parameters.

4.4 Parameter de-correlation

The elements of the calculated significance vector, $\mathbf{S}_{cal}(\boldsymbol{\theta})$, are good indicators of the significance of the corresponding parameters. A small value implies that the associated parameter is not significant, i.e., perturbation in the corresponding parameter value does not affect the model output much. However, a large element does not necessarily mean the corresponding parameter is significant if the parameter is correlated with other parameters. De-correlating the remaining parameters can lead to a further-reduced parameter set by fixing the most correlated parameters to their initial guesses.

This paper adopts a method based on principal component analysis and it consists of the following steps:

1. Calculate information matrix, \mathbf{M}_{cal} , for the remaining parameters using Equation (8)
2. Find the minimum eigenvalue λ_j

$$i = \arg \min_j \lambda_j \in \text{EigValue}(\mathbf{M}_{cal})$$

3. Find the maximum entry of the eigenvector, \mathbf{v}_j , associated with the minimum eigenvalue that is identified in step 2

$$k = \arg \max_i |u_i| \text{ with } \mathbf{v}_j = (u_1, \dots, u_p)$$

4. The k -th parameter is the most correlated parameter; remove the k -th row and k -th column from \mathbf{M}_{cal}

5. Check termination condition; if not satisfied, repeat from step 2 to the reduced information matrix.

The steps can be carried out iteratively to find the most correlated parameters one by one. The termination condition used in the case study involved evaluating whether the condition number of the remaining information matrix \mathbf{M}_{cal} was below some threshold.

4.5 Global analysis

In the preceding sections, the coupling strength matrix (\mathbf{CS}) and information matrix (\mathbf{M}_{cal}) are evaluated at some nominal parameter values. However, the parameters are unknown *a priori*, and local analysis could be misleading if the nominal parameter values deviate significantly from the actual values. In this regard, global analysis is more appropriate and it is able to provide more comprehensive information over a pre-defined parameter region.

The idea of a global analysis is to randomly generate a set of parameter points in a pre-defined region and then perform local analysis for each of the generated points. The concerned variables/matrices can be averaged over the local points. In the case study, the Sobol sequence generator (Burhenne et al., 2011) was used to construct a set of random points in the feasible parameter region:

$$\boldsymbol{\theta}_{GA} = \{\boldsymbol{\theta}_{GA,i} \mid i = 1, \dots, N_{GA}\}.$$

Then the concerned matrix was calculated at each of the generated points and the matrices were averaged in the following way

$$\mathbf{MAT}_{GA,avgd} = \frac{\sum_{i=1}^{N_{GA}} \mathbf{MAT}(\boldsymbol{\theta}_{GA,i}) \cdot f(\boldsymbol{\theta}_{GA,i})}{\sum_{i=1}^{N_{GA}} f(\boldsymbol{\theta}_{GA,i})}$$

where $\mathbf{MAT}(\boldsymbol{\theta})$ can be either the coupling strength matrix or the information matrix, and $f(\boldsymbol{\theta})$ is a weighting factor evaluated at parameter $\boldsymbol{\theta}$. This study used a weighting factor of the form:

$$f(\boldsymbol{\theta}) = \exp\left(-\frac{\|\bar{\mathbf{Y}}(\boldsymbol{\theta}) - \mathbf{Y}\|_2^2}{2\sigma^2}\right)$$

where \mathbf{Y} is the measured output extracted from the training data set. When the estimation error is independent and identically distributed and Gaussian with variance σ^2 , the weighting factor function is essentially the likelihood function for parameter $\boldsymbol{\theta}$ up to a constant (Ljung, 1999). A typical successful identification of a building should have the RMSE within 1°C. So in the weighting factor calculation, σ^2 was set to 1.

Once the averaged matrices are obtained, the analysis illustrated in the preceding subsections can be carried out with the averaged matrices to decouple the zones and reduce the parameter set.

5. CASE STUDY

As a case study, a medium-sized commercial building was modeled with the techniques elaborated above. It is a 4-story building located in Philadelphia, PA. There are three wings in the building and only the north wing with a total area of 7,000 square feet was considered. One air handler unit (AHU) serves this portion of the building with 9 VAV boxes. The 9 thermal zones associated with these VAV boxes were considered for the inverse model in this case study. The floor plan of the building showing the 9 zones is shown in Figure 4.

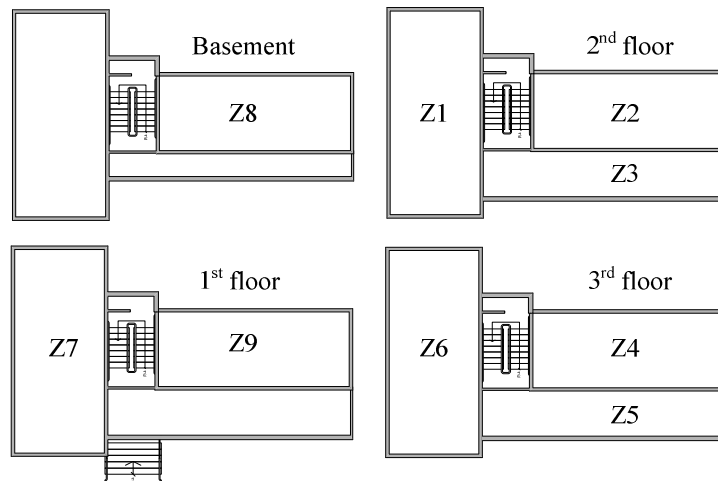


Figure 4: Floor layout of case study building

5.1 Available measurements

Table 2 summarizes a list of measurements that were used within this case study. Data was collected from the sensors every minute, but averaged values within 30-minute time windows were used to train or validate the model. So the continuous model in Equation (1) was discretized with a 30-minute time step assuming zero-order hold for all the inputs.

Table 2: Measurement points in case study

	Measurement point	Measurement location
Zone	Supply air temperature	VAV box
	Supply air flow	VAV box
	Zone air temperature	Thermostat
Weather	Ambient temperature	Weather station at PHL airport
	Global horizontal irradiance (GHI)	
Power Meter	Whole building power	Electrical panel
	HVAC power	

5.2 Data pre-process

The measurements were pre-processed to obtain some readable training data for the model. Details of generating each input data set from the raw measurements are covered in the following subsections.

5.2.1 Sensible heat extraction/injection

This is the sole controllable input to the model and it can be modulated by varying the flow rate and temperature of the air entering a room. Assuming supply and return air flow rates are identical and that the return air temperature is the same as the space temperature, the sensible heat extraction/injection rate can be calculated by

$$Q_{sen} = m_{sup} c_{p,air} (T_{sup} - T_{zone})$$

5.2.2 Convective/radiative internal heat gains

Power meters are installed in the building which measure both the HVAC system power (P_{HVAC}) and the whole building power ($P_{whole,bui}$). The difference between the two measurements is the power that is consumed by all of the electrical equipment in the building. Most of the electrical power consumption is eventually converted to internal heat gains to the space so the convective/radiative internal heat gains can be calculated as

$$Q_{gain,conv(rad)} = \theta_{conv(rad)}(P_{whole,bui} - P_{HVAC})$$

where $\theta_{conv(rad)}$ is ratio of convective (or radiative) heat gains for a specific room to the total electrical power consumption and this parameter is estimated together with the structural (RC) parameters in the identification process. In the case study, convective and radiative heat gains were assumed to be equal in order to reduce the number of parameters. However, in general, separate parameters could be learned for the convective and radiative parts. This calculation assumes implicitly that the ratios of the internal heat gains between different zones are time invariant. The estimated gains can also include gains coming from occupants assuming that the occupancy profile follows the same profile as the building electrical power curve. The scaling parameter for convective and radiative heat gains that is learned from the data, $\theta_{conv(rad)}$, can account for the combined effects.

5.2.3 Energy input from solar

The global horizontal irradiance (GHI) measurement was available but irradiance on other surfaces was lacking. This study used Reindl's method (1990) to decompose the GHI to beam and diffuse radiation on a horizontal surface and then calculated the irradiance on different surfaces via trigonometric relationships (TRNSYS, 2010). Radiation absorbed on outer surfaces of external walls was calculated based on an solar absorptance of 0.6. Window transmittance is an individual parameter that needs to be estimated in the identification procedure. Dependence of transmittance on solar incidence angle could be captured with additional estimate parameters as well as extra inputs (Cai and Braun, 2012), but this variation was not considered in this case study.

5.3 Zone decoupling

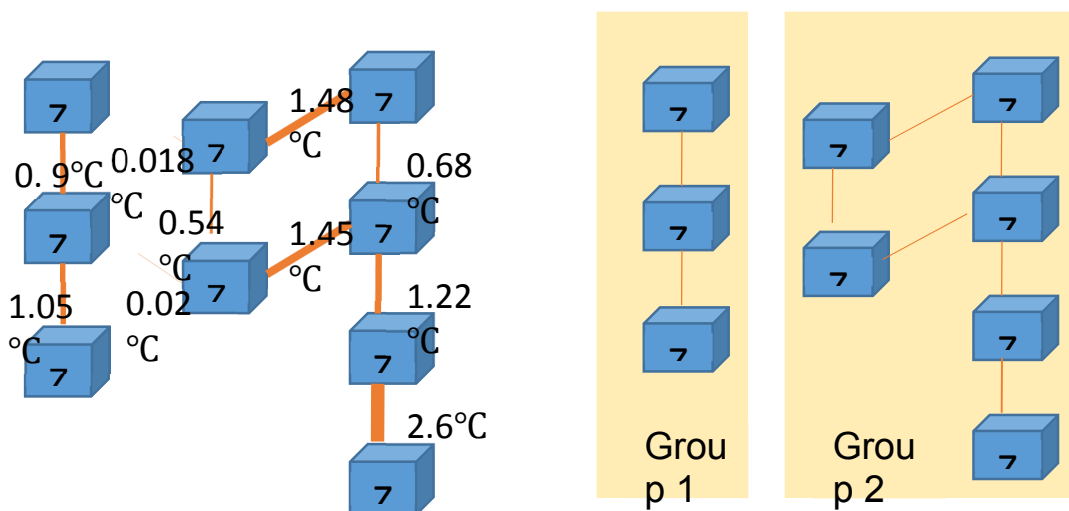


Figure 5: Left: coupling strength between the zones. Right: grouping of the zones based on coupling analysis.

Applying the decoupling techniques illustrated in section 4.2, a coupling strength matrix was obtained which is represented by the width of the connecting lines shown in Figure 5 on the left hand side. It can be seen that the couplings are negligible for the pairs of Zone5-Zone6 and Zone1-Zone3. Eliminating these two couplings leads to a grouping of the zones shown on the right-hand side of Figure 5. In the estimation process, these two groups were estimated separately. The threshold for distinguishing strong and weak couplings can be adjusted per case study. Higher threshold values can further break down the problem into more sub-problems with lower estimate dimensions, but it might compromise the model accuracy by over-eliminating the couplings. In this case study, the two eliminated couplings have significantly lower strength than other couplings and can be easily identified. If the threshold value were increased to 0.7°C, Group 2 would further break down to 2 smaller groups with the pairs of Zone5-Zone3 and Zone4-Zone2 decoupled. However, the estimation algorithm was able to identify Group 2 with 6 zones and the model error increased with the elimination of Zone5-Zone3 and Zone4-Zone2 couplings, so these two couplings remained in this case study.

5.4 Reducing parameter set with sensitivity analysis

Sensitivity analysis was performed as a first step to identify non-influential parameters. As discussed in section 4.3, the elements of the significance vector $\mathbf{S}(\mathbf{p})$ indicate the significance of the corresponding parameters. Figure 6 and Figure 7 plot the un-weighted and weighted significance, respectively, of different parameters with $\delta=0.05$ for Zone1. The x-axis shows indices for different parameters and Table 3 lists the correspondence between the parameters and their indices.

Table 3: Parameter correspondence in Figure 6 and Figure 7

Group	Parameter index	Parameter description
External wall	1,2,3	Wall resistance
	4,5	Wall capacitance
Ceiling	6,7,8	Wall resistance
	9,10	Wall capacitance
Floor	11,12,13	Wall resistance
	14,15	Wall capacitance
Adjacent wall to Zone3	16,17,18	Wall resistance
	19,20	Wall capacitance
Adjacent wall to the stairwell	21,22,23	Wall resistance
	24,25	Wall capacitance
Augmented parameters	26	Window resistance
	27	Zone air capacitance
	28	Ratio of internal heat gains to total electrical power
	29	Window transmittance

There are 5 walls and each wall has 5 structural (RC) parameters so there are 25 wall parameters and they are indexed from 1 to 25. The 26th and 27th parameters are window resistance and zone air capacitance respectively, and the last two parameters are scaling ratios for internal heat gain and window transmittance. The result shows that the external wall (1st to 5th) is important and this is because the external wall of Zone1 has significant area and it is not insulated which allows significant heat exchange from the ambient. Walls adjacent to Zone3 and the stairwell (16th to 25th) have almost negligible impact on the model output due to the small coupling area. This result also matches the finding from the decoupling analysis that Zone3 and Zone1 are weakly coupled. The ceiling and floor (6th to 15th) have several critical parameters but most of them are non-influential. Window resistance and transmittance (26th and 28th) are both significant because there is a significant area of window. The internal heat gain scaling factor is also important since the convective gains interact with zone air directly.

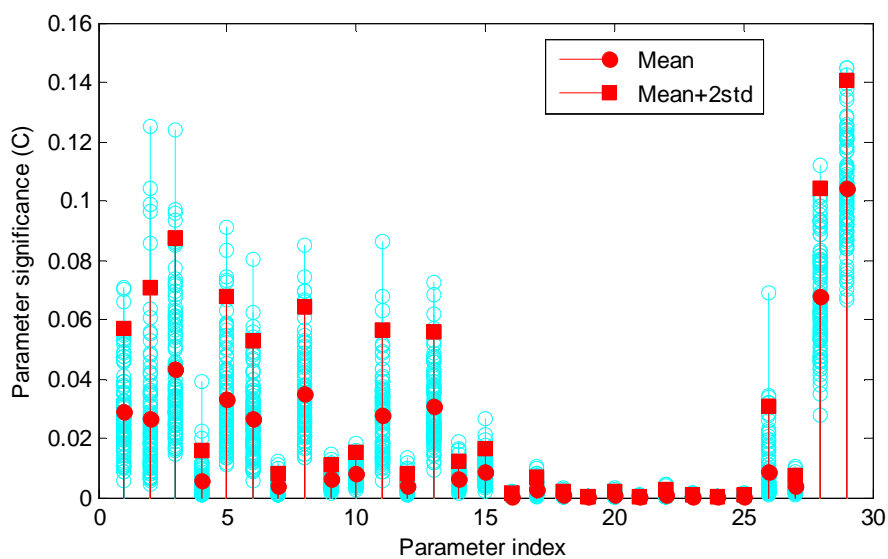


Figure 6: Un-weighted parameter significance for Zone1

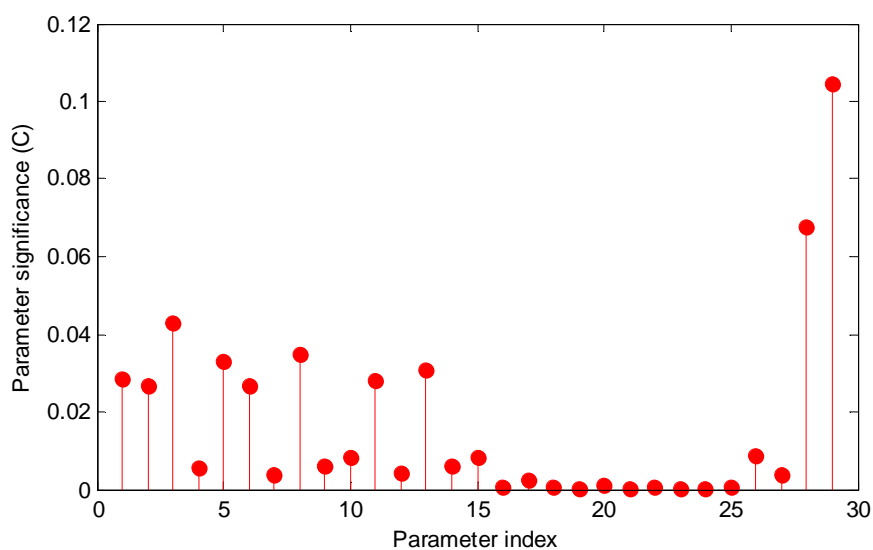


Figure 7: Weighted parameter significance for Zone1

The calculated significance values for the cases with and without weighting are slightly different and it makes more sense to use the weighted significance values. A threshold of 0.01 ($^{\circ}\text{C}$) was used, and any parameter with significance lower than this value was considered non-influential. Among the 29 parameters in this zone, only 10 of them were identified as candidates for influential parameters. Again, the remaining 10 parameters are not necessarily influential due to the potential existence of correlations.

By de-correlation analysis, the remaining parameters were ordered in regard to their significance. The non-influential parameters were eliminated one by one by fixing them to some nominal values (i.e., initial guesses) and Figure 8 plots the 10-base log of the condition number of the information matrix in the elimination process. It can be seen that the 11th and 13th parameters have strong correlations to other remaining parameters, and fixing their values leads to a reduction of the condition number from 2520 to 319. The termination criteria that was used in this elimination process is when the condition number is lower than 1000. This threshold is a parameter that can be adjusted before performing identification. A higher value leads to more estimated parameters and higher parameter correlation. A lower value could compromise the accuracy of the estimated model by over-eliminating the parameters. A value of 1000 is a good candidate for this threshold based on the author's experience.

For Zone1, the 1st step (sensitivity analysis) reduced the size of the parameter set from 29 to 10. The 2nd step (de-correlation) identified two highly correlated parameters and further reduced the parameter set by 2. After applying this parameter-reduction technique to all of the 9 zones, the number of estimated parameters was reduced from 86 to 27 for group 1 and from 143 to 45 for group2.

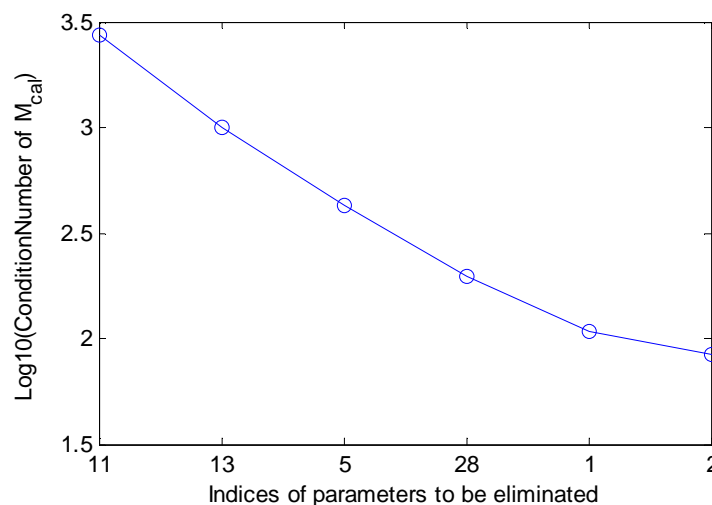


Figure 8: De-correlation of parameters

5.5 Validation of the estimated model

The model was trained with data collected from July 4 to 10, 2013. Two data sets were used to validate the model, one of which was collected from July 12 to 28, 2013 and the other from August 2 to 28, 2013. The validation results are plotted in Figure 9 and Figure 10 for zone groups 1 and 2, respectively. The validation root mean square errors (RMSE) are listed in Table 4.

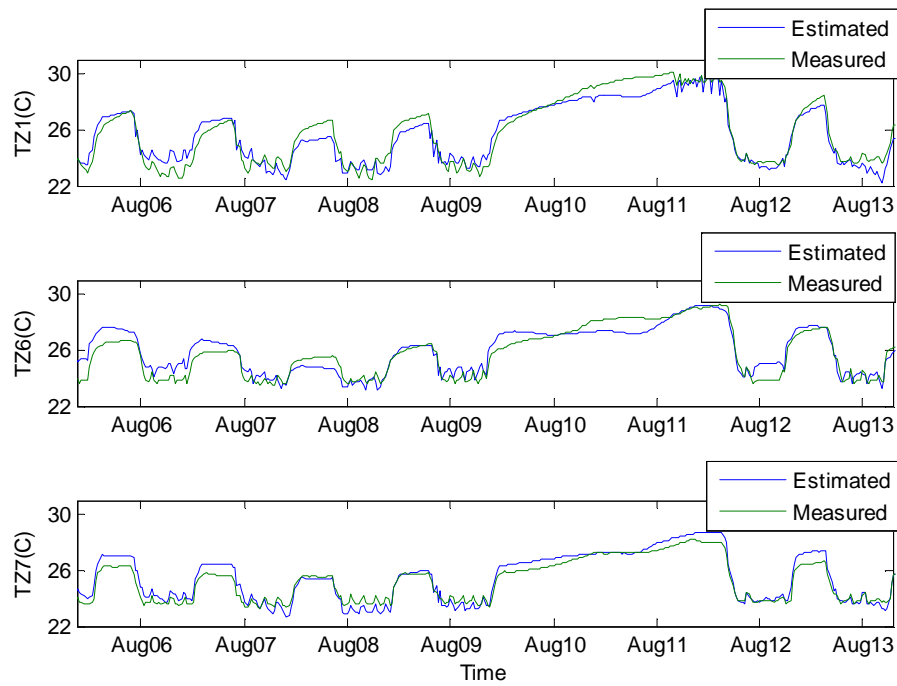


Figure 9: Model validation results for group 1 with August data set

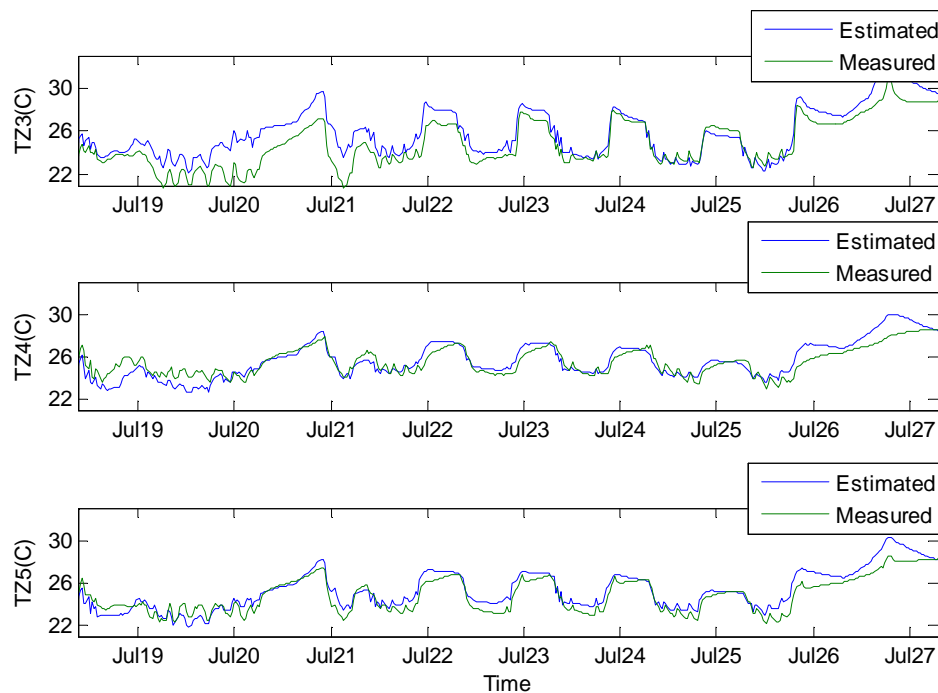


Figure 10: Representative model validation results for group 2 with July data set

The zones in group 1 all have good agreement between the model outputs and measurements in the two validation periods. For most of the zones in group 2, the estimated models also have good accuracy. However, the testing errors are relatively large for Zone2 and Zone3, which can be observed from the Zone3 temperature plot in Figure 10. The poor performance of the estimated models for these two zones is caused by significant uncertainties associated with the occupants' activities. Those two zones have highly irregular meetings and conferences which cannot be quantitatively measured or captured. So there are highly uncertain heat gains associated with occupants, computers, and projection equipment. However, the model is still

able to predict the temperature trend in general. To overcome this problem and obtain a more accurate model, occupancy counters could be installed to capture the occupancy profile for the zones with significant occupancy variations.

Table 4: Model testing RMSEs (°C)

	Validation periods	
	Jul. 12~ Jul. 28	Aug. 02~ Aug. 28
Z1	0.63	0.68
Z2	1.11	1.5
Z3	1.31	1.14
Z4	0.78	0.85
Z5	0.74	0.84
Z6	0.68	0.85
Z7	0.61	0.63
Z8	0.92	0.88
Z9	0.62	1.01

To evaluate the load prediction capability of the estimated models, sensible loads were estimated with Equation (12)

$$\mathbf{Q}_{sen}[k] = (\mathbf{C}_d \mathbf{B}_{u,d})^{-1} (\mathbf{T}_{z,sp}[k+1] - \mathbf{C}_d \mathbf{A}_d \mathbf{x}[k] - \mathbf{C}_d \mathbf{B}_{w,d} \mathbf{w}[k]), \quad (12)$$

where $\mathbf{T}_{z,sp}$ are the zone temperature setpoints for the next step, k in the brackets indicates the time step and the state-space matrices with subscript d are discrete versions of the matrices in Equation **Erreur ! Source du renvoi introuvable.**. The estimated loads were compared with the measured loads for the two validation periods and Figure 11 plots the comparison of the loads for group 1 with the estimated model. The results show that the testing relative RMSE's are close to 9% for most of the zones and Zone2 and Zone3 have relatively large errors, approximately 17%, due to the uncertain occupant activities.

6. SUMMARY

This paper demonstrates a robust and scalable inverse modeling methodology for multi-zone buildings that is implementable at low cost. The training data is typically available from the BMS with input weather conditions accessible from the internet. The approach adopts a gray-box model structure and only requires an approximate building description with only a moderate effort for the model setup phase.

The scalability of the proposed procedure comes from three steps that reduce the dimension of the estimation problem. The first step decouples the weakly coupled zones and groups the ones with strong thermal interactions. Estimation can be applied to each group independently. The second step identifies the non-influential parameters based on sensitivity analysis and by fixing those non-influential parameters to some nominal values, the parameter set that needs to be estimated can be significantly reduced. As a final step, correlation analysis is carried out on the

remaining parameters and the parameter set is further reduced by de-correlating the highly correlated parameters.

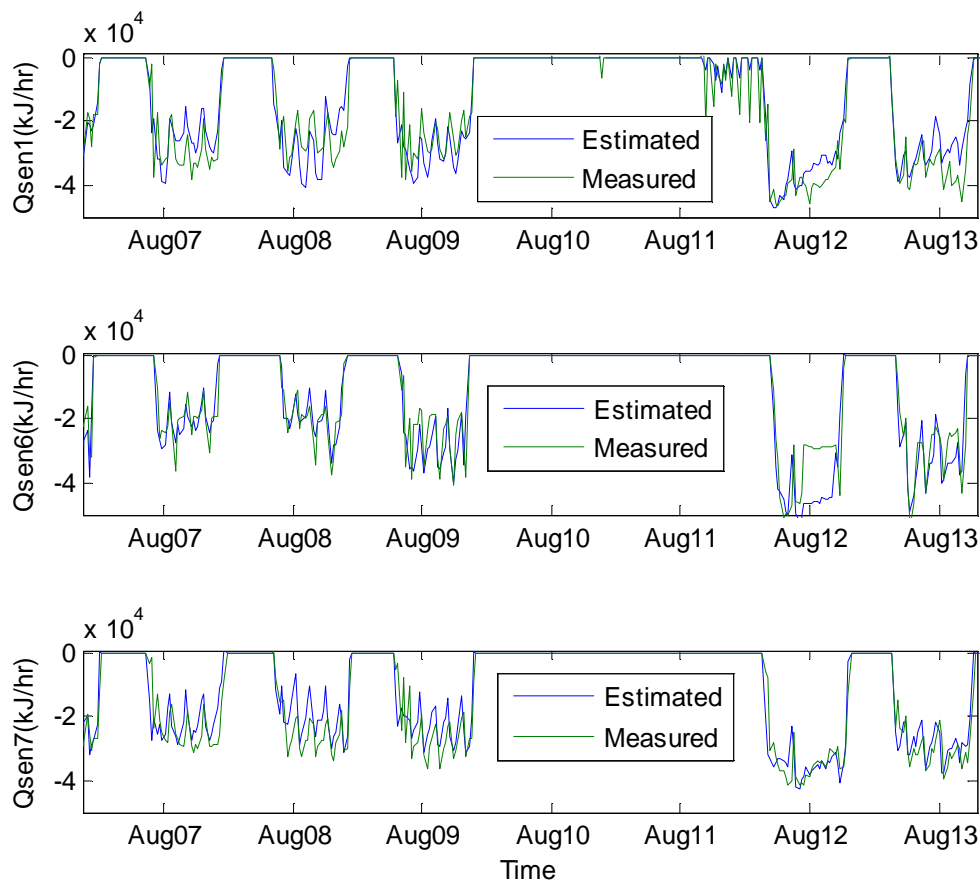


Figure 11: Model sensible load predictions for group 1 with August data set

To test the proposed estimation methodology, a multi-zone building was modeled with on-site measurements. The target building has 9 thermal zones and the decoupling algorithm divided those 9 zones into 2 groups, one with 3 zones and the other with 6. Then the sensitivity analysis and correlation analysis revealed that two thirds of the parameters were non-significant and were eliminated in the estimation process. With these three steps, the estimation problem was significantly simplified. The estimated model was validated with two test data sets and the model outputs agree well with the measurements for both periods.

Models that are developed with the proposed approach can be used for different purposes. Since a gray-box model structure is adopted, the developed model has physical meaning and is suitable for energy performance or retrofit analysis. In addition, a simplified model structure is utilized so the model is computationally efficient which makes it suitable for online controller design. One application of the developed model can be found in Cai and Braun (2014), where a simulation platform was constructed with the developed model and the platform was used to test the performance of a heuristic control for DX units. In Cai et al. (2015), a portion of the model (corresponding to the three zones on the 2nd floor) was used as a testbed for analyzing multi-agent control.

REFERENCES

Bacher, P. and Madsen, H., 2011, "Identifying suitable models for the heat dynamics of buildings", *Energy and Buildings*

- Burhenne S., Jacob, D. and Henze, G. P., 2011, "Sampling based on Sobol sequences for monte carlo techniques applied to building simulations", *12th Conference of International Building Performance Simulation Association*
- Cai, J. and Braun, J. E., 2012, "Efficient and robust training methodology for inverse building modeling and its application to a multi-zone case study", *International High Performance Buildings Conference at Purdue*
- Cigler, J. and Privara, S., 2010, "Subspace Identification and Model Predictive Control for Buildings", *11th International Conference on Control, Automation, Robotics and Vision*
- Donaldson, J.R. and Schnabel, R.B., 1987, "Computational Experience With Confidence Regions and Confidence Intervals for Nonlinear Least Squares", *Technometrics*
- Goyal, S., Liao, C. and Barooah, P., 2011, "Identification of multi-zone building thermal interaction model from data", *50th IEEE Conference on Decision and Control and European Control Conference*
- Kutner, M.H., Nachtsheim, C.J., Neter, J. and Li, W., 2005, *Applied Linear Statistical Models*, McGraw-Hill/Irwin
- Lin, Y., Middelkoop, T. and Barooah, P., 2012, "Issues in identification of control-oriented thermal models of zones in multi-zone buildings", *IEEE Conference on Decision and Control*
- Ljung, L., 1999, *System Identification: Theory for the User*, Prentice Hall.
- Privara, S., Vana, Z., etc., 2011, "Modeling and Identification of a Large Multi-Zone Office Building", *IEEE International Conference on Control Applications*
- Rawlings, J. B. and Mayne, D. Q., 2009, *Model Predictive Design: Theory and Design*, Nob Hill Pub
- Reindl, D. T., Beckman, W. A. and Duffie, J. A., 1990, "Diffuse Fraction Correlations", *Solar Energy*
- TRNSYS 17, 2010, Solar Energy Laboratory, University of Wisconsin-Madison.
- Cai, J. and Braun, J. E., 2014, "Generalized heuristic control for direction-expansion (DX) cooling systems with capacity modulation and variable air flow", *International High Performance Buildings Conference at Purdue*
- Cai, J., Kim, D., Putta, V., Braun, J. E. and Hu, J., 2015, "Multi-agent control for centralized air conditioning systems serving multi-zone buildings", *American Control Conference, submitted*

ACKNOWLEDGEMENT

This work was supported by the Department of Energy through the Consortium for Building Energy Innovation.

NOMENCLATURE

m_{sup}	= supply air mass flow rate
$P_{\text{whole,bui}}$	= whole building power
P_{HVAC}	= HVAC system power
$Q_{\text{sol,ext}}$	= solar radiation absorbed on the external walls

$Q_{\text{sol,trans}}$	= solar radiation transmitted through the windows
$Q_{\text{gain,rad}}$	= radiative internal heat gains
$Q_{\text{gain,conv}}$	= convective internal heat gains
Q_{sen}	= sensible cooling/heating to the space
T_{amb}	= ambient temperature
T_{grd}	= ground temperature
T_{sup}	= supply air temperature
T_{zone}	= zone air temperature
$T_{\text{zone,adj}}$	= air temperature of the adjacent zone
δ	= parameter perturbation level
σ	= model error standard deviation
\mathbf{x}	= state vector
\mathbf{y}	= output vector
\mathbf{w}	= disturbance vector
\mathbf{u}	= input vector
\mathbf{U}	= excitation data
$\boldsymbol{\theta}$	= estimate parameters
\mathbf{CS}	= coupling matrix for the zones
\mathbf{J}	= sensitivity matrix
\mathbf{M}	= information matrix

Subscripts

cal	= calculated/estimated matrix
$norm$	= normalized matrix
GA	= generated points in global analysis
$avgd$	= averaged value

Comparative analysis of model reduction methods applied to building simulation benchmarks

Jordan Gauvrit, Guillaume Ansanay-Alex

⁽¹⁾Centre Scientifique et Technique du Bâtiment, 84 avenue Jean Jaurès, Champs sur Marne, 77447 Marne la Vallée Cedex 2

1. ABSTRACT

Many research and development studies use virtual buildings represented by building thermal models at a detailed level. Such models need relatively long computation times for one-year simulations: the use of these tools is then often too time-consuming when it comes to compare technical solutions during the design stage. Model reduction methods allow models with shorter computation times to be synthesized. In this paper, the linear state-space representation of a whole model is extracted and a balanced truncation method is applied to it. The detailed models are built from the SIMBAD library, a Simulink library of building modeling components developed at CSTB. Both linear state-space and reduced order models ensure shorter computation times than the full detailed model. However, the choice of the order of the reduced model has an impact on the final results. The main strengths and weaknesses of using the linear state-space and reduced models built from the same detailed model are investigated. To this end, the physical descriptions of idealized test buildings provided by ASHRAE standard 140 for building simulation tools assessment are used, and the results obtained through the different approaches for computation time reduction are compared.

Keywords: thermal model, model order reduction, computation time, spectral analysis

2. INTRODUCTION

In 2012, commercial and residential buildings accounted for 44% of the final energy consumption in France and were responsible for 21% of Greenhouse Gas Emissions (Ademe, 2013). Among this consumption, heating and cooling systems stand for a large share (59%, (Ademe, 2013)). Therefore, reducing energy consumption requires the improvement of HVAC (Heating, Ventilation, and Air Conditioning) systems efficiency. There are two ways to reach this goal. First, replacing old systems with high efficiency systems increases energy performance (Visier, 2008). Secondly, control methods allow to adapt the system operation to match occupants' needs or renewable energy production ((Visier, 2008), ("Energy future, Think Efficiency," 2010)) and reduce energy waste.

Modelling innovative systems, complex distribution networks or control strategies for design and optimization purposes require detailed models and often short time steps. This can lead to long computations, hardly affordable during the design stage or for embedded control models.

The SIMBAD (SIMulator of Building And Devices) library, developed at CSTB (Husaunndee, Lahrech, Vaezi-Nejad, & Visier, 1997), is composed of a set of Matlab/Simulink components enabling user to build dynamic models of buildings, their systems and especially their control strategies. The components of this library will be used in this paper.

Simulating buildings with this level of detail leads to much longer computation times than static hourly models. In SIMBAD's case, an annual simulation of a mono-zone building takes approximately 130s with a fixed time step $\Delta t = 20s$. Consequently, and considering even longer simulations when all production, distribution and emission systems are modelled, using

such detailed models during the design stage may be difficult. It could then be useful to implement methods which reduce computation time while keeping sufficiently accurate results. The building envelope model considered in this paper will not take into account air transfer or non-linearized radiative transfers, but still shows a nonlinear behaviour regarding long wave radiations through windows.

The concern in this paper is to evaluate the performances of reduced models. On the one hand, the computation time saved with a reduced order model, and on the other hand, the accuracy difference between the results of detailed, linearized and reduced order models. Section 5 is dedicated to the problem of evaluating how well linearized or reduced order models perform with respect to the original detailed model.

In order to evaluate the detailed and reduced order building models on reference cases, the reference buildings used are those described by ASHRAE Standard 140-2001 (“ANSI/ASHRAE Standard 140-2001, Standard method of test for the evaluation of building energy analysis computer programs,” 2001). It defines test procedures for evaluating capabilities of building energy programs. In fact, it gives a physical description of different buildings and the predictions from well-known programs (such as TRNSYS, DOE-2 or S3PAS) applied to them. Some of these test cases were implemented to compare synthesized models with the SIMBAD detailed model.

Section 3 will introduce the SIMBAD models used as the detailed modelling level. In section 4, the linearization and common model order reduction methods will be presented. Section 5 clarifies the mobilized benchmarks indicators. Benchmark results will be presented and discussed in section 6. Finally, a variant of the order reduction method will be tested to improve its performance in section 7.

3. DETAILED SIMBAD MODEL

The SIMBAD multi-zone building model is a white box model where each component (zones, walls, windows ...) is described by a set of physical parameters. It includes a dynamic model of each wall surface and zone air temperature.

SIMBAD models are built using Simulink. Each component has inputs and outputs that are connected to create the whole model. Two cases are set up. The first one is the free floating case (indoor building temperature is not controlled, Figure 1). The second one is the regulated case (indoor building temperature is regulated using a PID controller, Figure 2).

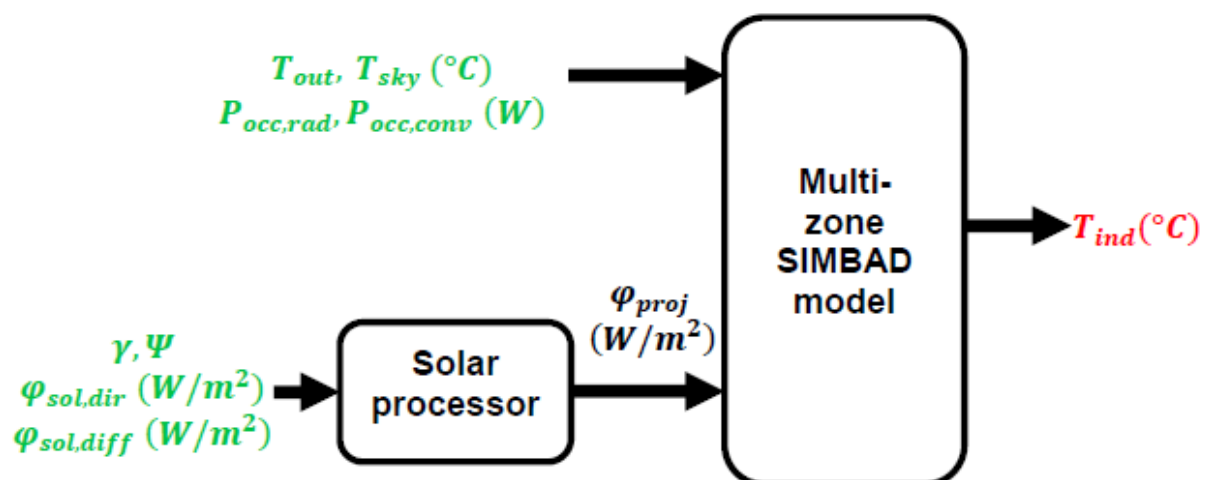


Figure 1: Detailed SIMBAD model - Free floating case

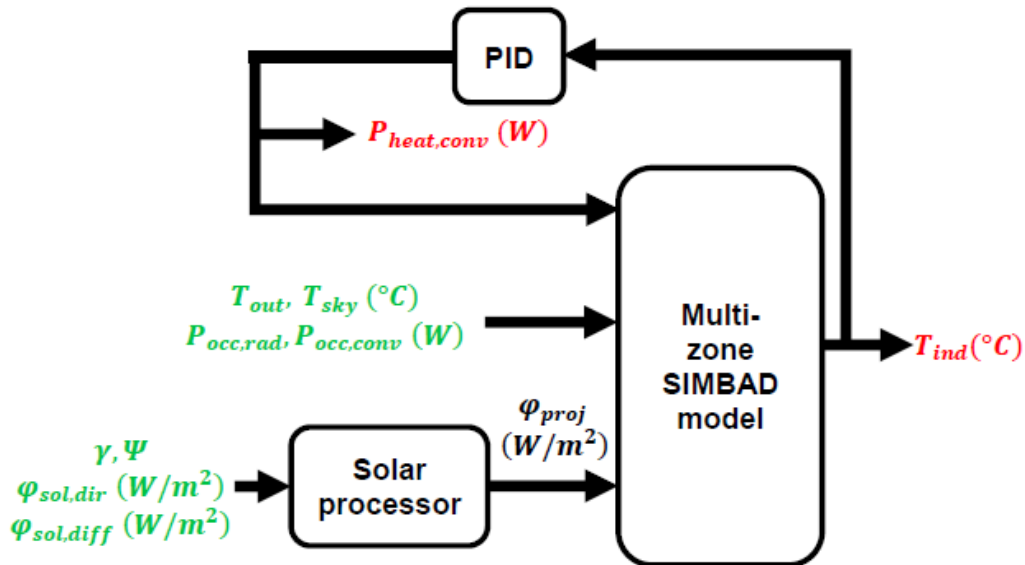


Figure 2: Detailed SIMBAD model - Regulated case

With:

T_{out} : Outdoor temperature ($^{\circ}\text{C}$)

T_{sky} : Sky temperature ($^{\circ}\text{C}$)

$P_{occ,rad}, P_{occ,conv}$: Occupation convective power and occupation radiative power (W).

γ, Ψ : Solar height and azimuth ($^{\circ}$)

$\varphi_{sol,dir}, \varphi_{sol,diff}$: Direct solar radiation and diffuse solar radiation (W/m^2)

φ_{proj} : Solar radiation projected on building surfaces (W/m^2)

T_{ind} : Indoor temperature ($^{\circ}\text{C}$)

$P_{heat,conv}$: Heating convective power (W). Positive for heating, negative for cooling.

The solar processor block projects solar flows on surfaces of the building envelope. This block uses many trigonometric functions and is as such strongly nonlinear.

The multi-zone block calculates indoor temperature by evaluating surface temperatures taking radiative, convective and conductive heat exchanges into account.

The PID controller computes the heating convective power in order to reach the setpoint value. It is strongly nonlinear and won't be subject to model order reduction.

In the rest of this paper, the detailed model will be represented by the letter D.

4. COMPUTATION TIME AND MODEL ORDER REDUCTION TECHNIQUES

4.1 Linearization

Linearization replaces any block or set of blocks with a State Space Model (SSM) block. Matlab function *linmod* extracts the SSM from a component by a numerical perturbation and gives four matrices: A, B, C, D . They allow writing the state space representation (1) of the model called in the following the linearized model (L).

$$\begin{aligned} \dot{T}(t) &= AT(t) + BU(t) \\ Y'(t) &= CT(t) + DU(t) \end{aligned} \quad (1)$$

With:

$T(t)$: State vector	A : State matrix
$Y'(t)$: Output vector	B : Input matrix
$U(t)$: Input vector	C : Output matrix
	D : Feedforward matrix. In this case it is always null

This technique works by nature without any loss of precision when blocks are linear. There are two ways to apply this technique to the detailed building model:

- The first one is the linearization of the multi-zone building block only. This block is then replaced with a SSM block but the solar processor is maintained. The resulting SSM block has 23 inputs.
- The second one is the linearization of the assembly between the solar processor and the multi-zone block. As the solar processor is not linear, a simplification is made to make it linear: the sun position is set to a constant and becomes a model parameter. Then, the assembly is replaced with a SSM block. Solar radiations are adjusted to fit the initial solar radiation projected on the window. This SSM block requires 8 inputs

4.2 Model order reduction

After projecting (1) on a particular basis, the system is truncated (2).

$$\begin{aligned}\dot{\tilde{T}}(t) &= \tilde{A}\tilde{T}(t) + \tilde{B}U(t) \\ \tilde{Y}'(t) &= \tilde{C}\tilde{T}(t)\end{aligned}\quad (2)$$

In the following parts, the notation will stand for the outputs of linearized models as well as the outputs of the reduced order model.

The order of (2) has decreased from (1). Several methods performing this reduction are available. One of the first method was the balanced truncation and appeared in the early 80's. It was described by B.C. Moore in (Moore, 1981). Other methods followed in the same decade as the Hankel-norm reduction of Glover (Curtain & Glover, 1985) or whether the proper orthogonal decomposition described by Sirovich (Sirovich, 1987). Finally, in the 90's, two other methods came out. The first one was explained by P. Feldmann in (Feldmann & Freund, 1995) and was related to Krylov subspaces and Padé approximation. The second one is called PRIMA and was the subject to the paper (Odabasioglu, Celik, & Pileggi, 1997). In this study, the balanced truncation is used. It has been applied in thermal building modelling since the mid-1990s. Dautin's works (Dautin, 1997) or Déqué's works (Déqué, Delille, & Dautin, 1997) can be quoted. More recently, other studies like (Kim & Braun, 2012) used this technique.

The main idea is to delete states that have a small sensitivity to inputs (controllability) and a small impact on outputs (observability). The controllability gramian (resp. observability gramian) characterizes the state's controllability (resp. observability). It is shown (Bruq & Folliot, 1988) that they can be calculated by Lyapunov equations (3):

$$\begin{aligned}AW_c + W_cA^T + BB^T &= 0 \\ A^TW_o + W_oA + C^TC &= 0\end{aligned}\quad (3)$$

W_c and W_o depend on the basis where (1) is represented. It should be noted that a state can be sensitive to inputs and have a small impact on outputs at the same time. States thus cannot be deleted by considering the gramians only. Using a balanced representation overcomes this obstacle.

It consists in applying a transform $T(t) = PX(t)$ to (1) such that the gramians of system (4) are equal.

$$\begin{aligned}\dot{X}(t) &= P^{-1}APX(t) + P^{-1}BU(t) \\ Y'(t) &= CPX(t)\end{aligned}\quad (4)$$

Palomo (Palomo, 2011) gives steps to establish P :

- 1st step: Computation of W_c and W_o with (3)
- 2nd step: Calculation of with R Cholesky decomposition:

$$W_c = RR^T \quad (5)$$

where R is a lower triangular matrix

- 3rd step: Diagonalization of R^TW_oR (symmetric, positive definite) obtained by solving the following symmetric eigenvalues/eigenvectors problem:

$$R^TW_oR = U\Sigma^2U^T \quad (6)$$

Where Σ is a diagonal matrix and U is such that $UU^T = I$.

- 4th step: Calculation of P :

$$P = RU\Sigma^{-1/2} \quad (7)$$

Then, (4) can be reduced by deleting the less influential states, leading to (2). The reduction order is the number of remaining states.

This model will be called (R) for Reduced order model. A reduced order model of order 5 will be denoted R5.

5. BENCHMARKING

5.1 Computation time notation

The reference time is obtained by the simulation time of D. As regards L and Rx models, the time spent to reduce the detailed model is taken into account.

5.2 An a priori evaluation

The “quality” of R can be evaluated by analyzing its state space representation without the aid of a simulation. Palomo ((Palomo, 2011), (Palomo, Bonnefous, & Déqué, 1997)) defines an index of the spectral quality called $\eta_i(\omega)$. For each output i , it gives the relative error (between L and R) according to input frequency ω .

To achieve this target, transfer function matrix of the linearized (resp. reduced order) model $G(\omega)$ (resp $\tilde{G}(\omega)$) is calculated by:

$$\begin{aligned}G(\omega) &= C(j\omega I - A)^{-1}Bj\omega \\ \tilde{G}(\omega) &= \tilde{C}(j\omega I - \tilde{A})^{-1}\tilde{B}j\omega\end{aligned}\quad (8)$$

Then $\eta_i(\omega)$ is determined by:

$$\eta_i(\omega) = \frac{\sum_{j=1}^{j=p} |G_{ij}(\omega) - \tilde{G}_{ij}(\omega)|^2}{\sum_{j=1}^{j=p} |G_{ij}(\omega)|^2} \quad (9)$$

With:

p : Number of inputs

$G_{ij}(\omega)$ (resp $\tilde{G}_{ij}(\omega)$): Transfer function of the i^{th} output from the j^{th} input. It belongs to the matrix $G(\omega)$ (resp. $\tilde{G}(\omega)$).

Thus, the reduction order can be chosen by setting a risk tolerance threshold on the index.

5.3 An evaluation by simulation

Also, L and Rs have to be compared with the detailed model. A one year simulation is performed for each model and the results are studied. The gap between detailed model outputs and reduced model outputs, written $e(t)$, is called the reduction error.

Statistical analysis

A first statistical analysis of $e(t)$ by calculating the mean and the standard deviation will be made. Moreover, heating power and cooling power results will be integrated:

- over one hour time steps to compare maximum peaks (ASHRAE standard indicator)
- over a year to compare annual consumptions

Spectral analysis

Secondly, a spectral analysis of $e(t)$ will be performed. It is especially described for building thermal modeling in (Dautin, 1997) or (Ramdani et al., 1997). It aims at evaluating the dynamic behavior of reduced models in comparison with the detailed model.

The power spectral density (PSD) of $e(t)$, noted $S_{ee}(f)$ and calculated by (10), shows how the energy of the signal is distributed over the different frequencies. It must not be confused with the energy of the physical quantity.

$$S_{ee}(f) = |\hat{e}(f)|^2 \quad (10)$$

where $\hat{e}(f)$ is the Fourier transform of $e(t)$.

The links between reduction error and model inputs are also investigated. Spectral coherence of $e(t)$ and an input signal $x(t)$ gives information about these. It is noted $K_{ex}^2(f)$ and calculated by (11). It expresses the linear correlation between both signals according to the frequency.

$$K_{ex}^2(f) = \frac{|S_{ex}(f)|^2}{S_{ee}(f)S_{xx}(f)} \quad (11)$$

Where $S_{ex}(f)$ is the cross spectral density (CSD) of both signals and is determined by :

$$S_{ex}(f) = \hat{e}(f)\hat{x}(f)^* \quad (12)$$

Coherence allows comparing the influence of each input on reduction error of one reduced model. However, it is not a sufficient tool for comparing the influence of one input over two models. The partial coherence method (PCM) is an answer to this problem.

PCM offers a decomposition of $S_{ee}(f)$ such as:

$$S_{ee}(f) = \sum_{j=1}^p \Lambda_j(f) + Z(f) \quad (13)$$

With:

$\Lambda_j(f)$: Linear contribution of the j^{th} input to $S_{ee}(f)$

$Z(f)$: Unexplained part of $S_{ee}(f)$

(Ramdani et al., 1997) provides equation (14). Knowing the contribution of the j^{th} input requires to know the contribution of the $(j - 1)^{th}$ input. The whole contribution computation is then an iterative process. The computation scheme, drawn on the Figure 3, is established in the case of a model with 3 inputs.

$$\Lambda_j(f) = K_{je/1..j-1}^2(f)S_{ee/1..j-1}(f) \quad (14)$$

With:

$K_{je/1..j-1}^2(f)$: Coherence between the j^{th} input and $e(t)$ after removing the linear contributions of the 1st input to the $(j - 1)^{th}$ input. It is called partial coherence.

$S_{ee/1..j-1}(f)$: PSD of $e(t)$ after removing the linear contributions of the 1st input to the $(j - 1)^{th}$ input.

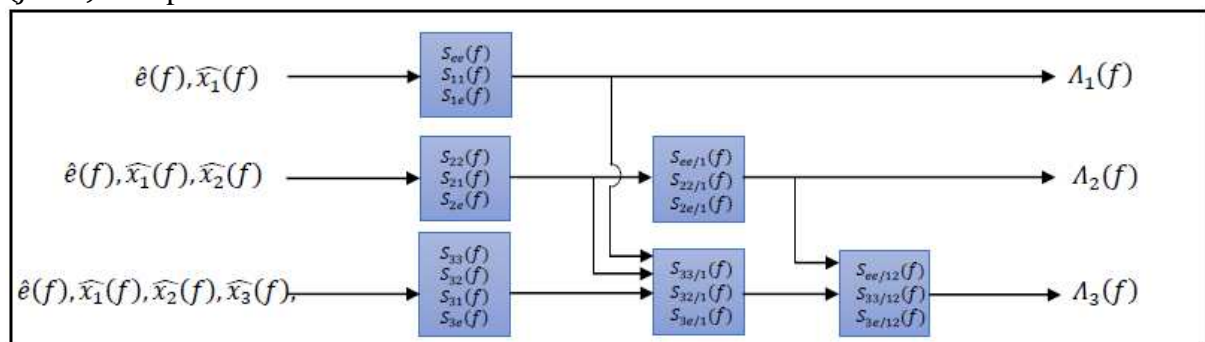


Figure 3: Computation scheme of input's contribution to $S_{ee}(f)$ by PCM method in case of a 3 inputs model.

In Figure 3, terms like $S_{XY/1..j}(f)$ and partial coherence $K_{je/1..j-1}^2(f)$ are calculated by:

$$S_{XY/1..j}(f) = \frac{S_{jj/1..j-1}(f)S_{XY/1..j-1}(f) - S_{Xj/1..j-1}(f)S_{jY/1..j-1}(f)}{S_{jj/1..j-1}(f)} \quad (15)$$

$$K_{je/1..j-1}^2(f) = \frac{|S_{je/1..j-1}(f)|}{S_{jj/1..j-1}(f)S_{ee/1..j-1}(f)}$$

This pattern is generally applicable with any number of inputs. In addition, it should be noticed that the order in which inputs are sorted affects the computed values of contributions.

For instance, considering two inputs which are severely correlated with $e(t)$ ($K_{e1}^2(f) \sim 1$ and $(K_{e2}^2(f) \sim 1)$). If the contribution of input 1 is calculated at first, then $\Lambda_1(f) = K_{e1}^2(f) \sim 1$ and $\Lambda_2(f) \sim 0$. Now, if the contribution of input 2 is calculated at first, then $\Lambda_2(f) = K_{e2}^2(f) \sim 1$ and $\Lambda_1(f) \sim 0$. However, the unexplained portion stays the same regardless of the order of inputs. For the following parts, the order of inputs will be fixed for the comparison of models.

Finally, results of the spectral analysis will be summed up by frequency bands. They are defined by the observation of the PSD of a signal. Here, (Figure 4), the signal is the error on the indoor temperature prediction of L. Four frequency bands are chosen:

- VLF band: Very low frequency band (between 0 to $(48h)^{-1}$). It describes quasi-static behavior.
- LF band: low frequency band (between $(48h)^{-1}$ to $(16h)^{-1}$). It describes slow dynamic behaviour.
- HF band: high frequency band (between $(16h)^{-1}$ to $(9h)^{-1}$). It describes medium dynamic behaviour.
- VHF band: very high frequency band (superior to $(9h)^{-1}$). It describes fast dynamic behavior.

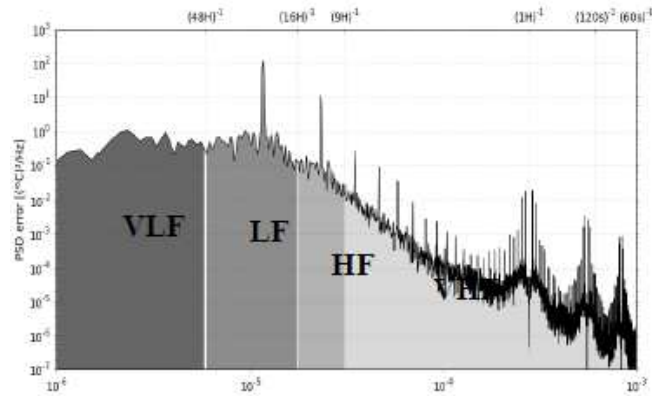


Figure 4: PSD signal example and frequency bands

The portion of the energy of the signal $e(t)$ contained in the frequency band B_i is noted s_{ee,B_i} and is calculated by:

$$s_{ee,B_i} = \frac{\int_{B_i} S_{ee}(f) df}{\sum_{i=1}^4 \int_{B_i} S_{ee}(f) df} \quad (16)$$

The part of the energy of the signal $e(t)$ explained by input j , contained in the frequency band B_i , is noted λ_{j,B_i} and is calculated by:

$$\lambda_{j,B_i} = \frac{\int_{B_i} \Lambda_j(f) df}{\int_{B_i} S_{ee}(f) df} \quad (17)$$

The portion which cannot be explained by the inputs is called the unexplained part. A graphic representation of these quantities is available in section 6.2.3.

6. RESULTS

6.1 Hypotheses

6.1.1 Test cases

In this paper, ASHRAE test cases used are case600FF, case900FF, case600 and case900. They reflect a mono-zone building with two south-oriented windows (Figure 5). Simulations are conducted over a one year period with a fixed time step $\Delta t = 20s$.

The weather data come from the ASHRAE standard and match the weather in Denver, Colorado, USA.

According to the case, envelope inertia and indoor temperature control change (Table 1). In particular:

- Free floating case: indoor temperature is not controlled
- Regulation case: indoor temperature is regulated. The heating set-point is 20°C and the cooling set-point is 28°C .

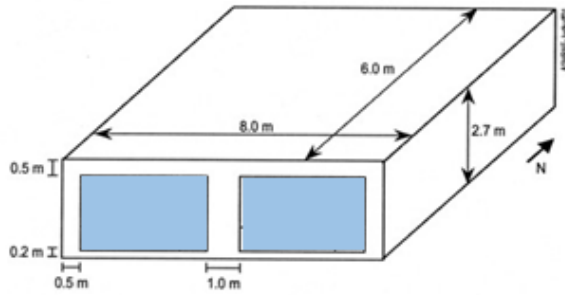


Figure 5: Building geometry of cases

Table 5: Cases' names

	Low mass	High inertia
Free floating	case600FF	case900FF
Regulation	case600	case900

6.1.2 Choice of reduced model orders

The spectral index, defined in subsection 5.2, is a useful tool to anticipate the quality of the results of R_s according to reduction order. It should be reminded that the spectral index is calculated by comparing L and R_s . Figure 6 and Figure 7 show indices estimated for case600 and case900 with SSM block including 23inputs or 8inputs. On each chart, a gap of the index may be observed between order5 and order6. Then, R_6 and L make very close predictions. In the following parts, the results of R_2 , R_4 and R_6 will be exposed

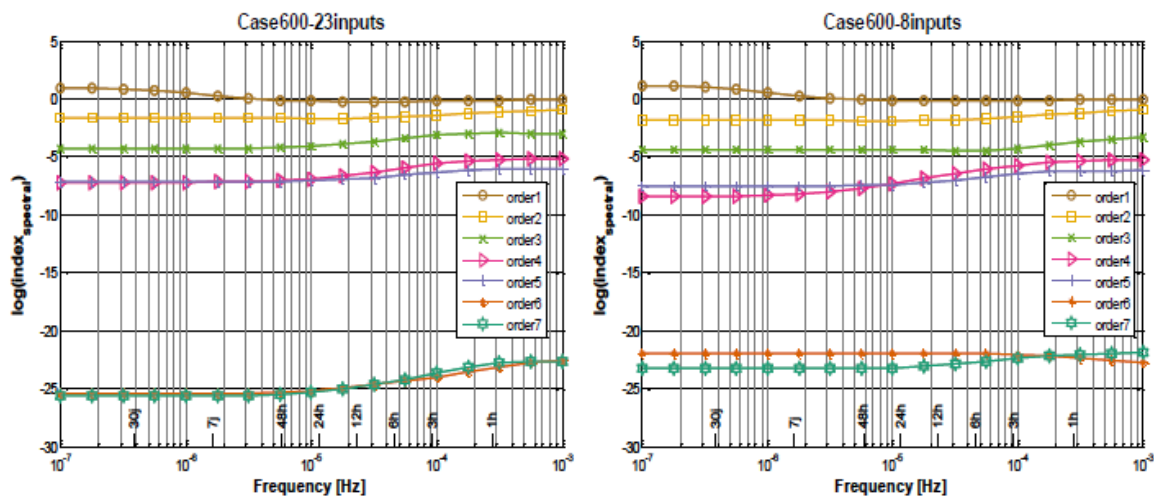


Figure 6: Spectral indices according to model input numbers - Case600

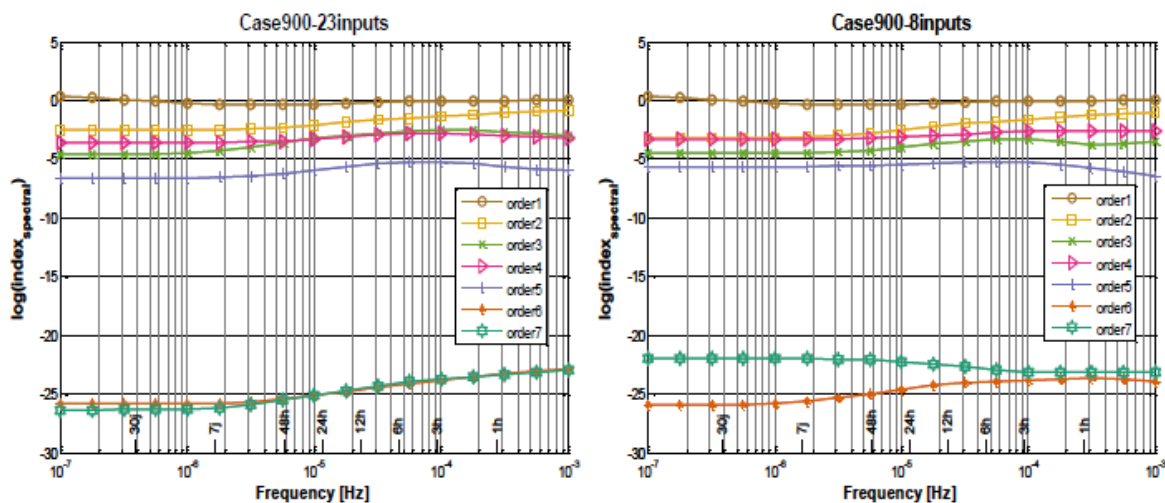


Figure 7: Spectral indices according to model input numbers – Case900

6.2 Free floating cases

6.2.1 Computation times

Computation times are shown in Table 2. L with 23 inputs (resp. 8 inputs) roughly divides by two (resp. by three) the simulation time. In fact, for D, Matlab computes the outputs of each subcomponent at each time step: it considers the detailed model as a time variant system. In L's case, time invariance property is ensured through the linearization stage. That's why this computation is simplified and faster.

Secondly, it can be noticed that 8-input models have shorter computation times than 23-input models. Indeed, the solar processor block has been linearized and has been "included" in the SSM block. Moreover, a SSM with 8 inputs is smaller than a SSM with 23 inputs.

Table 1

Case	D	L	R2	R4	R6
Case600FF/8inputs	110,45s	29,71s	28,29s	28,61s	30,45s
Case600FF/23inputs		55,97s	53,90s	55,63s	60,33s
Case900FF/8inputs	108,41s	28,65s	26,26s	27,06s	27,70s
Case900FF/23inputs		55,59s	53,62s	55,03s	57,05s

Finally, Rs have results very close to L. It seems to be a paradox because matrices of Rs are smaller than L's ones. In fact, matrices of L are sparse (Figure 8) and Matlab optimizes the solving of SSM according to the number of null coefficient inside matrices. Then, even if sizes of L matrices are bigger, their sparsity must be taken into account to understand computation times.

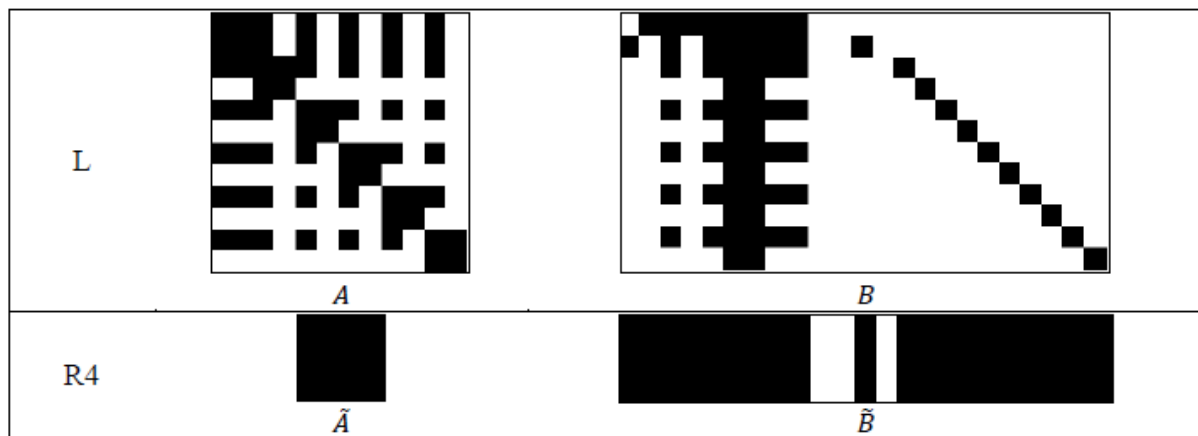


Figure 8: Sparsity of matrices for L and R4

6.2.2 Statistical analysis

Differences between indoor temperature prediction of D with L and Rs have been calculated. Means and standard deviation of the reduction errors are shown in Table 3 and Table 4.

As could be expected, L and R6 give very similar results. The mean of the difference between their results is close to 10-11°C.

Table 2: Mean of reduction error (°C) - Free floating cases

Case	L	R2	R4	R6
Case600FF/8inputs	-3.17e-02	-2.77e+00	-2.66e-02	-3.17e-02
Case600FF/23inputs	-8.00e-06	-3.82e+00	-2.27e-03	-8.00e-06
Case900FF/8inputs	-2.90e-02	-9.91e-01	-7.51e-01	-2.90e-02
Case900FF/23inputs	-5.12e-06	1.31e+00	-4.24e-01	-5.12e-06

Results of L with 8 and 23 inputs are close to D. However, R2s give results far from D. Models with 23 inputs give generally better results than model with 8 inputs. This probably stems from an exaggerated simplification of projected solar radiations made in the 8-input model.

Table 3: Standard deviation of reduction error (°C) - Free floating cases

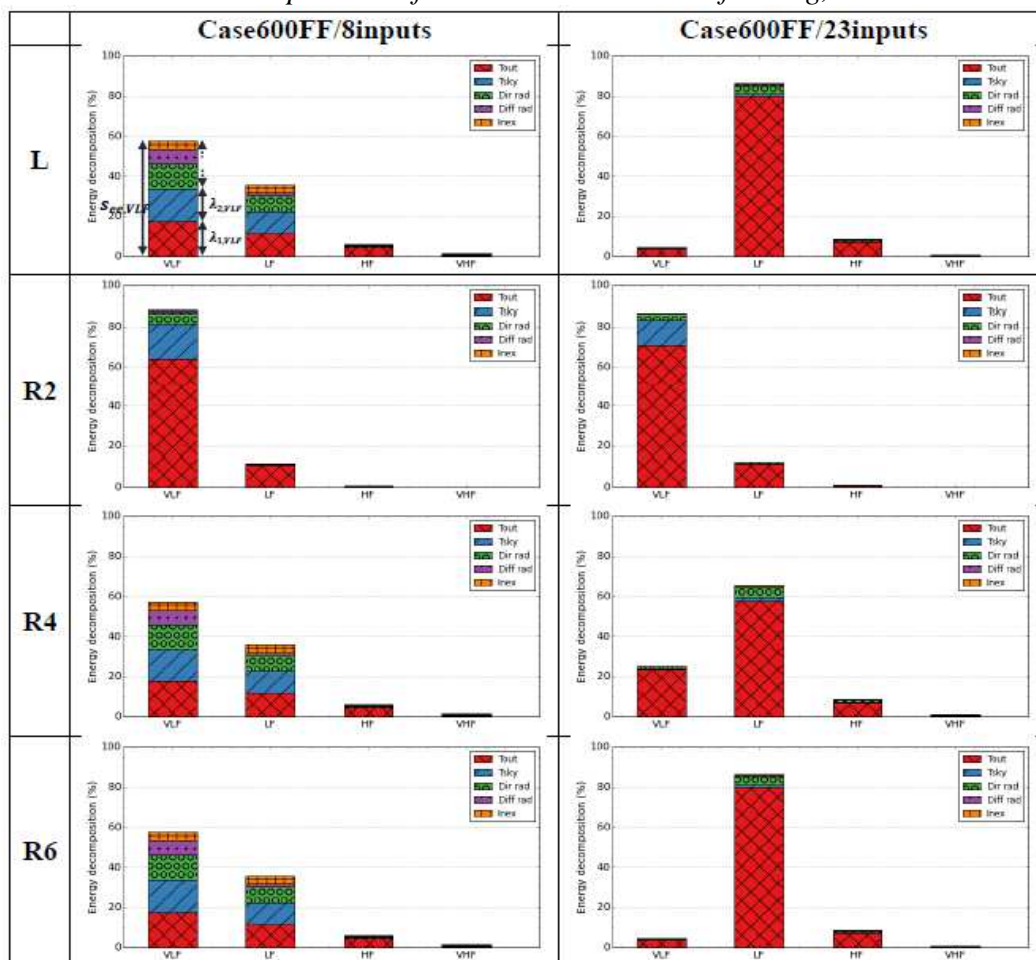
Case	L	R2	R4	R6
Case600FF/8inputs	5.09e-01	1.49e+00	5.09e-01	5.09-01
Case600FF/23inputs	7.27e-03	2.22e+00	7.24e-03	7.27-03
Case900FF/8inputs	3.60e-01	3.89e-01	3.34e-01	3.60-01
Case900FF/23inputs	6.03e-04	5.33e-01	1.45e-01	6.03-04

6.2.3 Spectral analysis

For each model, the decomposition of the reduction error was calculated thanks to (16) (energy of the residual in a frequency band) and (17) (energy explained by each specific input in a frequency band). The inputs are meteorological variables (outdoor temperature, sky temperature, diffuse and direct solar radiations). Table 5 (resp. Table 6) shows results for case600FF (resp. case 900FF). In these graphs “Inex” denotes the energy unexplained by inputs.

Less than 10% of the reduction error is not explained by the chosen inputs. Moreover, the reduction error is mainly connected with static and slow dynamic behaviors (more than 80% of the signal’s energy, i.e. the error). Then, climatic data are relevant to explain the error.

Table 4: Decomposition of reduction error - Free floating, case600FF



Concerning case600FF, the decomposition of reduction error of L with 8 inputs shows an important effect of meteorological inputs linked to radiative transfers (with regard to decomposition of the model with 23 inputs). The same observation can be made for R4 and R6. Here shows up the effect of the simplification of the solar processor for the 8 inputs model.

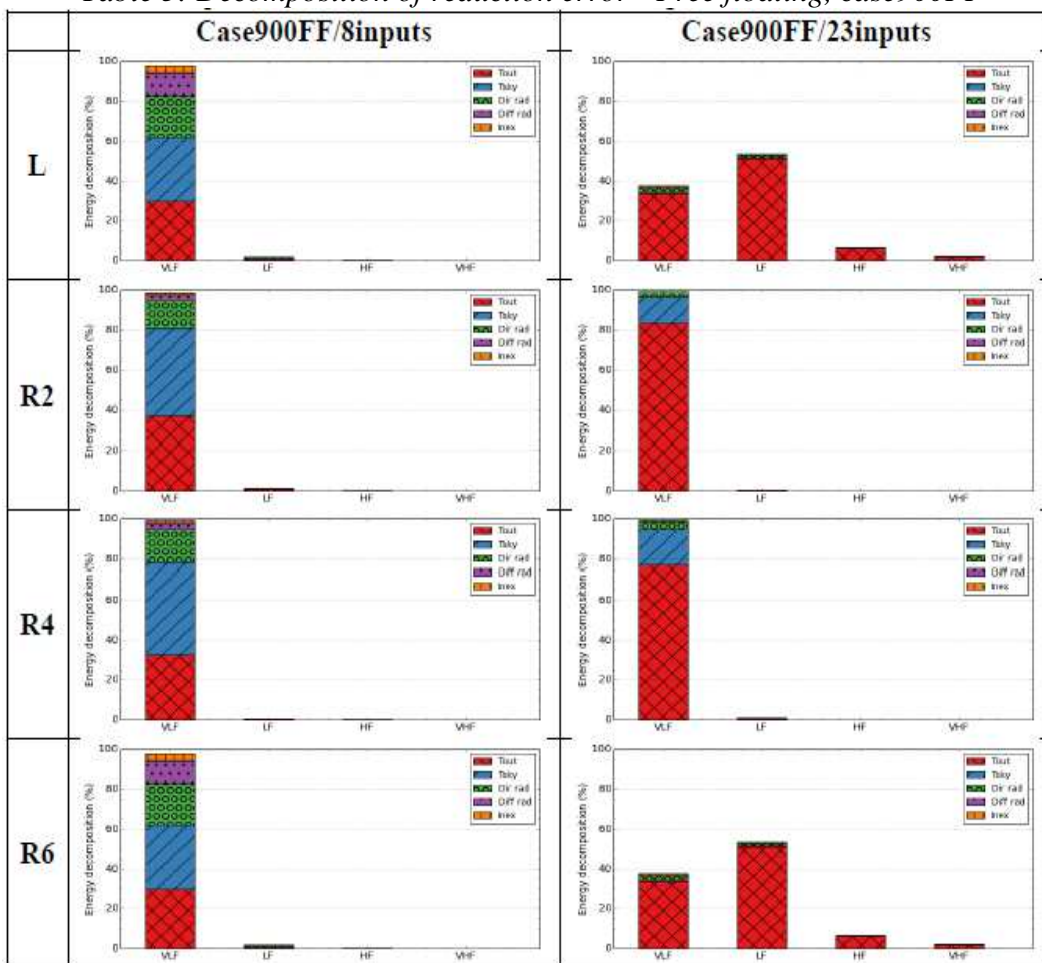
The decomposition of R2 looks similar for both models. The effect of radiative transfer modeling is then pretty close and they produce equivalent dynamic behaviors.

It can be noticed that the VLF part of the reduction error decreases with the reduction order being higher.

Concerning case900FF, reduction error is more connected with static behavior than in case600FF. That shows the effect of building inertia on the reduction error.

Also, an important effect of inputs linked to radiative transfer on models with 8 inputs can be observed, which points towards the simplification made to the solar processing part.

Table 5: Decomposition of reduction error - Free floating, case900FF



6.3 Regulation cases

6.3.1 Computation times

Computation times of regulation cases are shown in Table 7. The same observations as the previous case can be made about time savings and reduction methods.

Table 6: Computation times - Regulation cases

Case	D	L	R2	R4	R6
Case600/8inputs	138,67s	55,85s	52,83s	53,88s	57,22s
Case600/23inputs		83,78s	84,67s	85,37s	87,53s
Case900/8inputs	147,94s	55,59s	53,62s	55,03s	57,12s
Case900/23inputs		86,46s	83,83s	86,59s	88,06s

6.3.2 Statistical analysis

Differences between output predictions of D and L and Rs have been calculated. Mean and standard deviation of the reduction error on indoor temperature are shown in Table 8 and Table 9.

Two behaviors can be distinguished in the regulation case. The first one is the period when indoor temperature is controlled (heating or cooling period). The temperature is quasi constant. The second one is a free floating period. When the indoor temperature is between 20°C and 28°C (the two set-points), indoor temperature is not controlled. In fact, periods when indoor temperature has a static behavior limit the value of reduction error. Then, the mean is often lower than free floating case. Mean reduction errors higher than in the free floating case are underlined in the following tables.

Table 7: Mean of reduction error on indoor temperature (°C) – Regulation cases

Case	L	R2	R4	R6
Case600/8inputs	2.00e-02	-3.06e-01	2.07e-02	2.00e-02
Case600/23inputs	2.75e-04	-4.58e-01	-2.04e-05	2.75e-04
Case900/8inputs	-1.80e-02	-2.62e-01	-1.78e-01	-1.80e-02
Case900/23inputs	<u>4.89e-05</u>	2.60e-01	-7.04e-02	4.89e-05

About the standard deviation, the same observations can be made about models with 8 inputs. However, in this case, the reduction error of models with 23 inputs is more scattered than free floating case.

Table 8: Standard deviation of reduction error on indoor temperature (°C) - Regulation cases

Case	L	R2	R4	R6
Case600/8inputs	1.51e-01	5.76e-01	1.56e-01	1.51e-01
Case600/23inputs	4.38e-02	8.14e-01	6.20e-02	4.38e-02
Case900/8inputs	1.42e-01	4.00e-01	2.45e-01	1.42e-01
Case900/23inputs	2.69e-02	3.39e-01	1.13e-01	2.69e-02

Finally, these statistical indicators show predictions of L and Rs are pretty close to those of D.

For confirming this trend, annual consumptions and hourly peaks of heating and cooling system have calculated. Results are presented in Table 10 and Table 11.

In the background of each chart, the banner represents the score interval of the set of tools presented in the ASHRAE standard. The dotted line is the mean result of the standard.

R2, with 23 or 8 inputs, gives results outside the banner. It can be noticed for the cooling and the heating consumptions in Case600. However, all other models make coherent predictions with the standard.

Finally, R4 seems to be a sufficient model to predict consumptions and hourly peaks close to those of D. In fact, a maximum deviation of 3.2% can be found between R4 and D results. It concerns cooling peak of a model with 8 inputs.

Table 9: Consumptions and hourly peaks - Case600

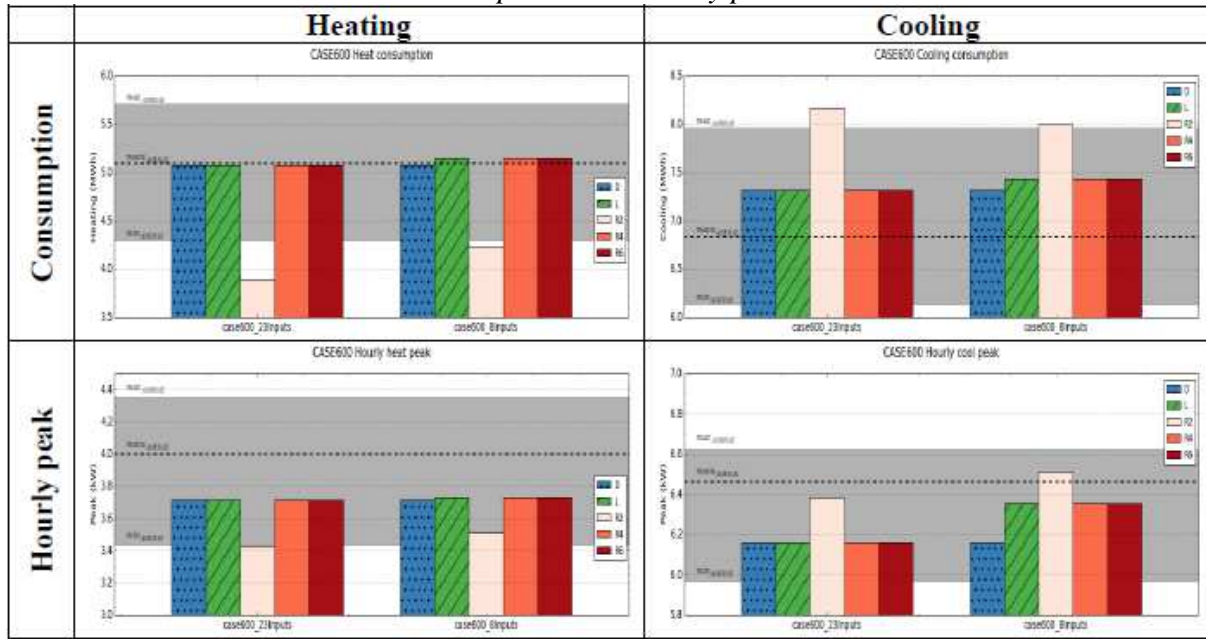
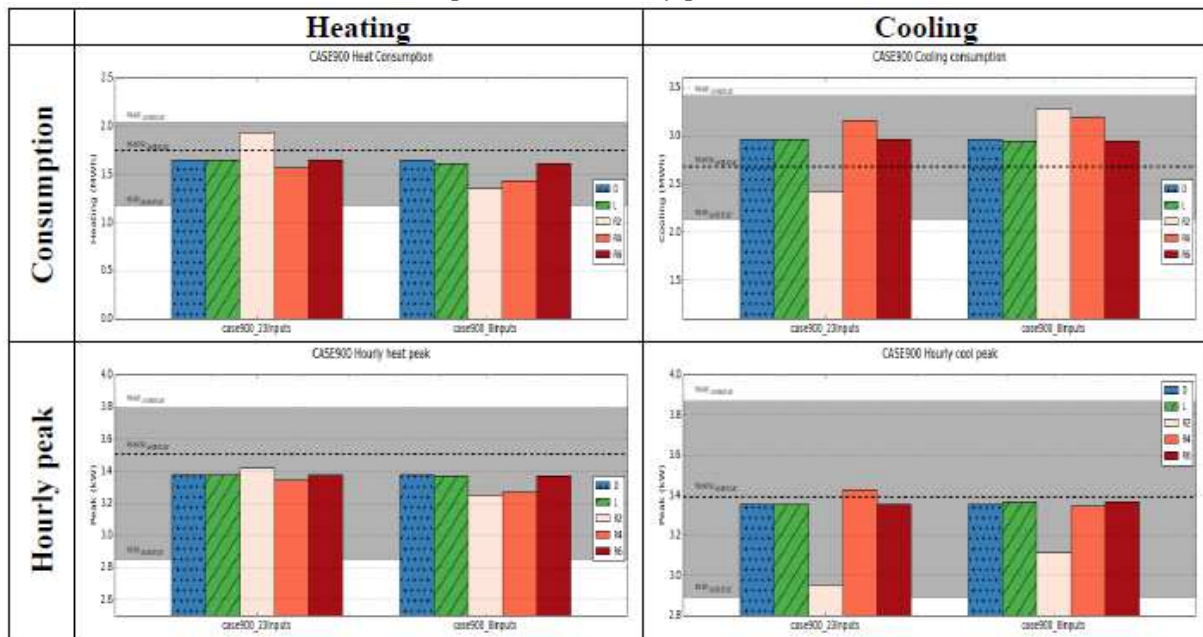


Table 10: Consumptions and hourly peaks results – Case900



6.3.3 Spectral analysis

The decomposition of indoor temperature reduction error has been calculated for each model. It is shown in Table 12 for case600 and in Table 13 for case900. The effect of heating convective power has been added to the analysis.

In case600, reduction error of L, R4 and R6 is mainly in the very high frequency band: this could be expected considering that the VHF band spans frequencies higher than (9h). Decompositions are close between the model with 8 inputs and the model with 23 inputs but the simplification on the solar processor in the 8-input model creates low frequency error. The unexplained part is quite important (more than 10% here). It can be noticed all the inputs have the same contribution on the reduction error (around 16%).

In case900, a higher order model (R6) is necessary to get rid of the reduction errors showing up in the VLF, LF and HF frequency bands. The errors on solar heat gain implied by the simplification of the solar processor have much more impact than in the lighter case600.

In the following graphs, Pcl denotes the convective power input.

Table 11: Decomposition of indoor temperature reduction error - Regulation, case600

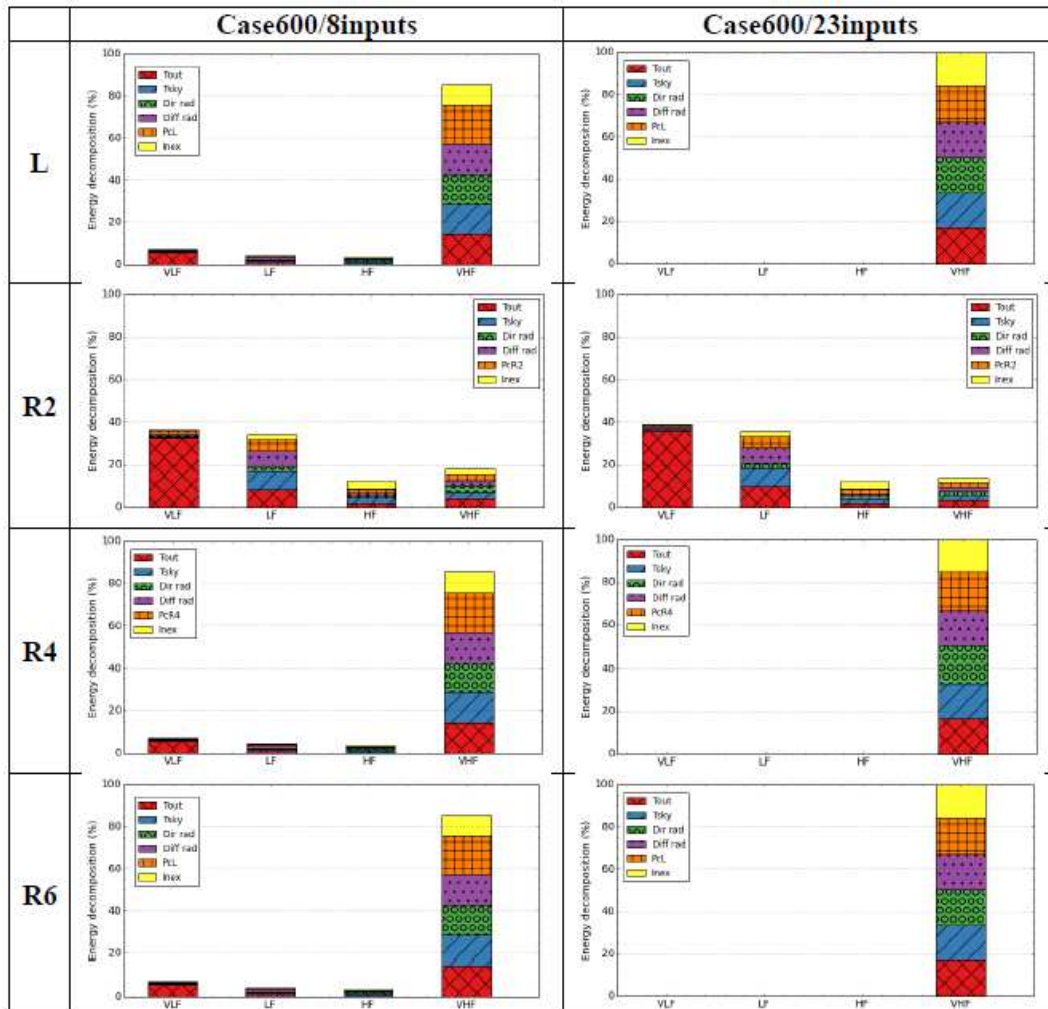
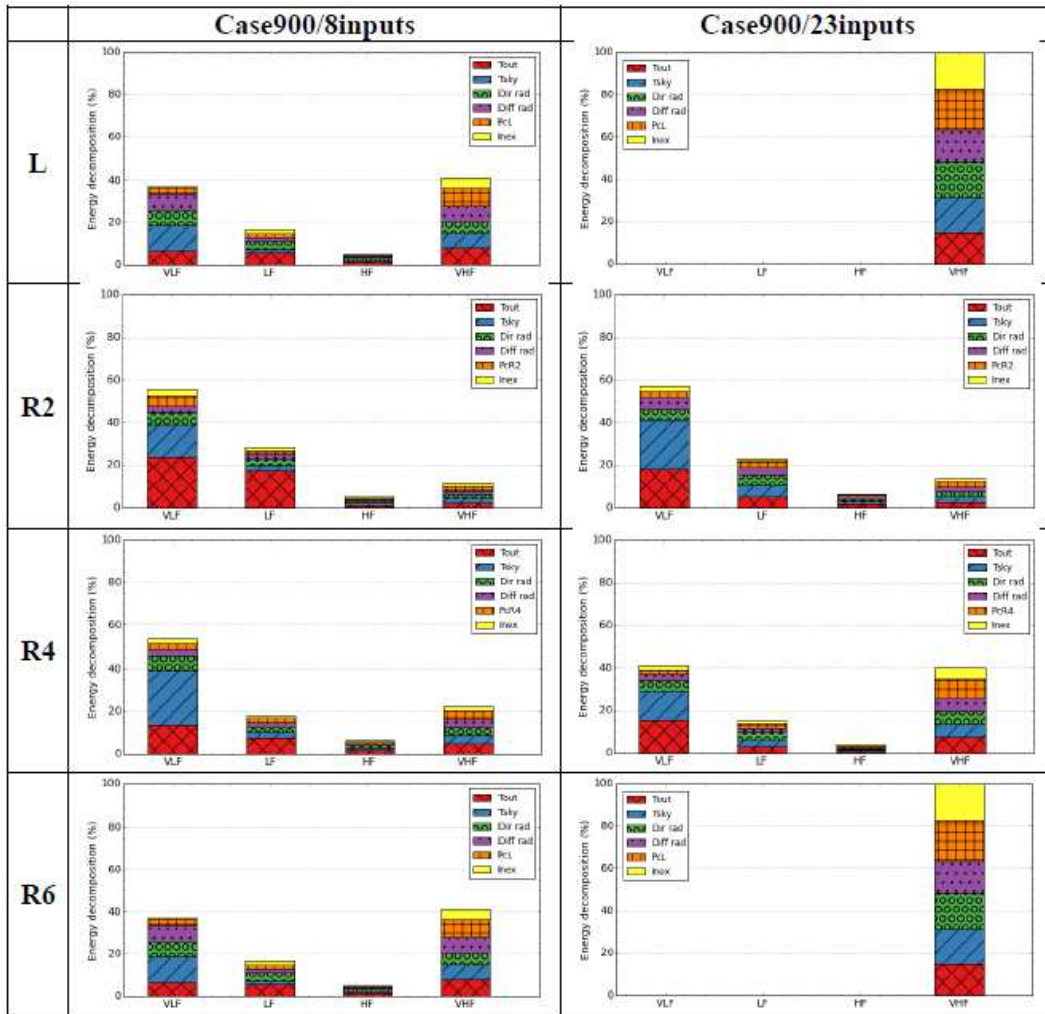


Table 12: Decomposition of indoor temperature reduction error - Regulation, case900



7. A VARIANT OF BALANCED TRUNCATION

7.1 Description

With a sufficient order, balanced truncation gave results close to L. However, computation time does not decrease because, contrary to L, matrices of reduced order models are not sparse and the number of inputs is large. Recent methods such as SVD MOR and RecMOR (Feldmann & Liu, 2004) or TermMerg (Liu, Tan, & McGaughy, 2007) are able to reduce model with a large number of inputs. In this paper, the ESVD MOR method will be used, a generalised version of SVD MOR, which was introduced by Liu & Tan (Liu, Tan, Yan, & McGaughy, 2008).

There are two steps to perform this method. First, the number of terminals is reduced by finding some correlations between the terminals thanks to Singular Value Decomposition (SVD). Secondly, the order of the SSM is reduced with a common method of Model Order Reduction. In this paper, the balanced truncation will be used. Table 14 summarizes these steps. Plain black rectangles symbolise dense matrices and hatched rectangles denote sparse matrices.

Table 13: ESVD MOR process

ESVD MOR with balanced truncation	
Initial state space representation	$\dot{X} = \mathbf{A} X + \mathbf{B} U$ $Y = \mathbf{C} X$
Step1: Decomposition of controllability and observability matrices with a SVD of output moment responses matrices. It leads to the identification of a state space model with a lower number of terminal.	$\dot{X} = \mathbf{A} X + \mathbf{B} \underbrace{\begin{bmatrix} \leq \\ \dots \\ \leq \end{bmatrix} U}_{U'}$ $Y = \mathbf{V}_o \underbrace{\mathbf{C} X}_{Y'}$
Step2: Reduction of the order of the identified state space with balanced truncation method.	$\dot{X} = \mathbf{A} X + \mathbf{B} U'$ $Y' = \mathbf{C} X$

In the current case study, there is only one output. ESVD MOR will then just reduce the number of inputs. It will be performed on the SSM with 23 inputs.

7.2 Choice of the number of inputs

Liu & Tan suggest choosing the number of inputs in order to preserve significant singular value computed in step 1. However, this method was not adapted to the problem at hand. Indeed, with this criterion, only one input was preserved and the predictions of the reduced model were imprecise. So, in order to determine the number of inputs, the spectral index previously defined (Figure 9) will be used. In this figure, the balanced truncation is performed at the order 6. When the 23 inputs are preserved, the spectral index is the same as Figure 6 (case600) and Figure 7 (case900). Spectral index is quickly downgraded when the number of inputs decreases. However, it is still satisfying. To confirm that, in the following part, the results of ESVD MOR will be compared to those of simple balanced truncation.

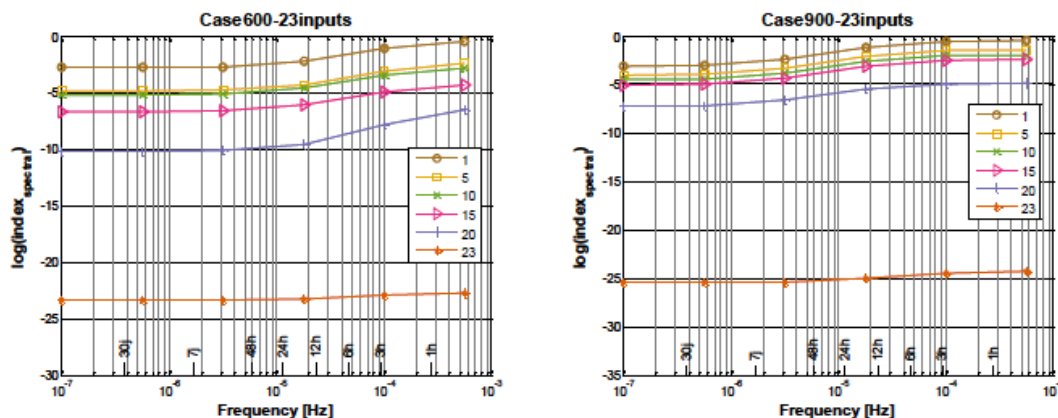


Figure 9: Spectral indices according to the number of inputs – ESVD MOR

7.3 Results

The main results of simulation with ESVD MOR are shown in Table 15. The model with 5 inputs gives results with the best compromise between computation time and results quality.

However, the saving is not significant (less than 0,2s on around 50s). In fact, the step which allows computing U' from U and Y from Y' is added in this method. So, the gain obtained thanks to the reduced number of inputs is compensated by this additional step.

Table 14: Results of ESVDMOR - Free floating cases

Method	Computation time	Case600FF () mean/st. dev. (°C)	Case900FF () mean/st. dev. (°C)
Moore	54,33s	-8.00e-06/7.27e-03	-5.12e-06/6.03e-04
ESVDMOR (1input)	51,53s	1.43e-01/8.04e-01	1.67e-01/7.80e-01
ESVDMOR (5inputs)	54,13s	-1.57e-01/4.97e-02	3.18e-01/3.30e-01
ESVDMOR (10inputs)	55,15s	-1.18e-01/3.21e-02	4.23e-01/3.37e-01
ESVDMOR (15inputs)	56,45s	7.33e-02/9.49e-02	4.36e-01/5.78e-01

8. CONCLUSION

In this study, two methods to reduce the order of a detailed building model were used. The first was the balanced truncation. If the order is sufficient, the reduced order model will make predictions close to the detailed model. Two indicators were used to qualify the models. The spectral index gives an a priori evaluation of the adequate reduction order. The spectral analysis of the residual between the results of detailed and reduced models gives a good qualitative insight of the contribution of inputs on the residual and is as such an indication of the submodels responsible for the gaps between model results. It should, though, be used with caution when it comes to quantitative evaluations, since the order in which inputs are considered matters. The time saving of model order reduction is not significant on the test cases used, compared to the time saving obtained by the extraction of a time-invariant state- space model. The sparsity of the matrix corresponding to the linearized detailed model, and the large number of inputs of the linearized system, explain this low time saving.

Then, a second method called ESVDMOR was tested. It permits to create a state space model with a lower number of inputs and perform balanced truncation on it. However, an additional step is required. It has to be taken into account because it is computed at each time step. The results are quickly downgraded according to the number of inputs but still acceptable. Nevertheless, this method does not allow saving much time.

ACKNOWLEDGEMENT

This research was supported by an Agence Nationale de la Recherche grant (Project MAEVIA # ANR-12-VBDU-0005).

REFERENCES

- Ademe. (2013). Climat, air et énergie. Chiffres-clés.
- ANSI/ASHRAE Standard 140-2001, Standard method of test for the evaluation of building energy analysis computer programs. (2001).
- Bruq, D., & Folliot, G. (1988). Théorie du signal: modélisation statistique, automatique et traitement.
- Curtain, R. F., & Glover, K. (1985). Balanced realizations for infinite dimensional systems.
- Dautin, S. (1997). Réduction de modèles thermiques de bâtiments: amélioration des techniques par modélisation des sollicitations météorologiques. Université de Poitiers.

Déqué, F., Delille, S., & Dautin, S. (1997). Réduction d'un système linéaire et invariant par la technique de Moore. Application à la thermique du bâtiment. *Revue Générale de Thermique*, 36(3), 170–179.

Energy future, Think Efficiency (2010). The American Physical Society.

Feldmann, P., & Freund, R. (1995). Efficient linear circuit analysis by Padé approximation via the Lanczos process. *IEEE Transactions on Computer-Aided Design of Integrated Circuits and Systems*, 14(5), 639–649.

Feldmann, P., & Liu, T. (2004). Sparse and efficient reduced order modeling of linear subcircuits with large number of terminals. *IEEE/ACM International Conference on Computer Aided Design*, 2004. ICCAD-2004, 88–92.

Husaunndee, A., Lahrech, R., Vaezi-Nejad, H., & Visier, J.-C. (1997). SIMBAD: A simulation toolbox for the design and test of HVAC control systems. In *Proceedings of the 5th IBPSA Conference* (pp. 269–276).

Kim, D., & Braun, J. (2012). Reduced-order building modeling for application to model-based predictive control. *SimBuild 2012*, 554–561.

Liu, P., Tan, S., & McGaughy, B. (2007). Termmerg: an efficient terminal-reduction method for interconnect circuits. *IEEE Transactions on Computer-Aided Design of Integrated Circuits and Systems*, 26(8), 1382–1392.

Liu, P., Tan, S. X.-D., Yan, B., & McGaughy, B. (2008). An efficient terminal and model order reduction algorithm. *Integration, the VLSI Journal*, 41(2), 210–218.

Moore, B. (1981). Principal component analysis in linear systems: Controllability, observability, and model reduction. *IEEE Transactions on Automatic Control*, 26(1), 17–32.

Odabasioglu, A., Celik, M., & Pileggi, L. (1997). PRIMA: passive reduced-order interconnect macromodeling algorithm. *IEEE/ACM International Conference on Computer Aided Design*, 1997. ICCAD-1997, 58–65.

Palomo, E. (2011). Résolution de problèmes thermiques de grande dimension.

Palomo, E., Bonnefous, Y., & Déqué, F. (1997). Guidance for the selection of a reduction technique for thermal models. *Proceedings of Building Simulation'97*.

Ramdani, N., Candau, Y., Dautin, S., Delille, S., Rahni, N., & Dalicieux, P. (1997). How to improve building thermal simulation programs by use of spectral analysis. *Energy and Buildings*, 25(3), 223–242.

Sirovich, L. (1987). Turbulence and the dynamics of coherent structures.

Visier, J.-C. (2008). Vers des bâtiments à énergie positive. *Annales Des Mines - Réalités Industrielles*.

TENTH SESSION
SIMULATION ASSISTED
ANALYSIS AND EVALUATION
OF BUILDING ENERGY USE

Bottom-up modelling of the Belgian residential building stock: impact of building stock descriptions

C. Protopapadaki^{1,2*}, G. Reynders^{1,2,3}, D. Saelens^{1,2}

⁽¹⁾ Building Physics section, KU Leuven, Kasteelpark Arenberg 40 – box 2447, BE-3001 Heverlee, Belgium

⁽²⁾ Energyville, Dennenstraat 7, BE-3600 Genk, Belgium

⁽³⁾ VITO, Unit Energy Technology, Boeretang 200, BE-2400 Mol, Belgium

1. ABSTRACT

Building stock modelling is a key element for the analysis of energy policy scenarios at an aggregate level, such as the integration of buildings in smart grids. To analyse the impact of new technologies and evaluate the dynamic behaviour at an aggregate level, bottom-up dynamic models are a prerequisite. Nevertheless, data on the building stock characteristics is scarce and assumptions need to be made.

A comparison of two residential building stock typologies for Belgium is performed in this work with the aim of identifying their differences and investigating how variations in the representation of a building stock can influence the outcome of the model. For this purpose detailed models of the two typologies are implemented and simulated in Modelica using the IDEAS library. Qualitative and quantitative analysis of the heat demand and dynamic behaviour of the stock implementations showed that the inherent differences in the descriptions lead to strong differences in the results, especially when conclusions must be made for specific building cases. This study highlights the need for more reliable and comprehensive data for the building stock, which is a prerequisite for qualitative bottom-up modelling.

Keywords: bottom-up modelling, building stock description, residential, building simulation, Modelica

2. INTRODUCTION

Facing major energy challenges like the climate change, the depletion of natural resources and the energy dependence, the European regulations on energy consumption and energy efficiency become nowadays more and more stringent (European Parliament, 2012). Important focus is put on the building sector, which has a big share in the consumption but also great potential for improvement. More renewable energy and new technologies as well as application of demand side management (DSM) techniques and the integration in smart grids are some solutions towards reducing the energy consumption and increasing the efficiency of the sector (Xing, Hewitt, & Griffiths, 2011).

In order to evaluate the potential of a proposed measure, an accurate bottom-up model of the building stock is needed. Thereby these building stock models not only need to provide reliable results for the total energy demand on an aggregated level, but also have to capture the dynamic behaviour of buildings at high temporal resolutions. When the flexibility of the stock is studied for the implementation of DSM, then this dynamic behaviour of the buildings is also an important output of the model. Bottom-up engineering residential stock models are reviewed by Kavgić et al. (2010). Those models however don't provide high resolution results that could be used for DSM. Further research has to be done on improving building stock models, making them suitable for such purposes. Regardless of the model, the focus should also be put on the input data, as it influences significantly the accuracy of the model.

In Belgium, several studies of the residential building stock have been published (Karen Allacker, 2010; Cyx, Renders, Van Holm, & Verbeke, 2011; Gendebien, Georges, Bertagnolio, & Lemort, 2014; Hens, Verbeeck, & Verdonck, 2001; Kints, 2008; Singh, Mahapatra, & Teller, 2013). Their scope and purpose may vary, but they all use building typologies to characterise the stock, which vary for the different studies. In this paper we compare two of the latest typologies, namely the TABULA typology (Cyx et al., 2011) and the ULg typology (Gendebien et al., 2014). As these two have the same structure and spatial and temporal resolution, they allow for good comparison. The purpose of the comparison is to analyse the differences in terms of geometry and thermal properties of the described buildings. Further, to assess the impact of these differences on the output of a building stock model that uses those typologies. In order to do so, both typologies are implemented as detailed building models in the same modelling environment with the same occupancy schedules (see paragraph 4). The resulting heating demand and dynamic behaviour of each building case as well as of the total stock are then examined and compared for the two typologies. The energy use is not evaluated since only the thermal behaviour of the buildings is studied and not of the installations.

For the purpose of this study the stock of 2012 is examined for both typologies. Only the single family buildings are considered, since the heating system and control in multi-family buildings often significantly differs from single-family dwellings and needs to be handled differently in studies on DSM. Furthermore, there is a debate on whether the multi-family buildings should be treated as whole buildings or as individual apartments. The typologies include three building types: detached (D), semi-detached (SD) and terraced (T) houses. Each type is further split into five construction periods: pre 1945 (A), 1945-1970 (B), 1971-1990 (C), 1991-2005 (1991-2007 for ULg) (D) and 2005-2012 (2007-2012 for ULg) (E). In the following each building case will have a name indicating the building type and the construction period (e.g. DA is the detached house constructed before 1945, SDC is the semi-detached house constructed between 1971 and 1990, etc.).

A verification of the resulting heat demand for either stock against real data is not possible. Only energy consumption data for the residential sector as a whole can be found in statistics, e.g. Eurostat (European Commission, 2014). Disaggregated data per building case and for specific end-uses is not available for validation of the models. In order to compare with overall residential energy consumption statistics, modelling of the multi-family buildings would be required. Furthermore the HVAC systems of all types of buildings (perhaps several HVAC cases per building) should be modelled as well. More heating schedules should be introduced to represent realistic users and the same would be needed for the internal gains. Domestic hot water (DHW) use should be also included in the model.

In the next paragraph the two typologies are introduced. First, in sections 3.1 and 3.2, the background of each typology is presented explaining the work done in the reference projects, followed by a description of the stocks as implemented in this paper. In section 3.3 a comparison of the main differences in geometry and thermal properties of the two implementations is performed. Paragraph 4 consists of a brief description of the model used for our implementation of the two typologies. In paragraph 5 the simulation results for each building case and for the total stock are presented and commented. The annual heating demand and the heat load and average daily temperature profiles are analysed in the respective sections. Overall conclusions and findings are discussed in the last paragraph.

3. BUILDING STOCK DESCRIPTION

3.1 TABULA

3.1.1 Background

The TABULA-project is a European project that focuses on the evolution of energy-related properties of buildings, regarding the energy performance of the particular building elements as well as the possibilities for improvement.

On the Belgian level two approaches have been implemented in the TABULA-project, referred to as (i) the Belgian housing typology or typical housing approach and (ii) the representative building stock approach. The representative building stock approach is a statistical bottom-up model used for scenario analysis on Belgian level. In this approach the characteristics of the building geometry, construction components and installations, cannot be directly mapped with a physical representation of a dwelling, but result from regression analysis. Moreover, the details are not available in the TABULA-report. In contrast, the typical housing approach implemented in TABULA provides a set of 29 typical dwellings grouped in 6 building types and 5 age classes as shown in Figure 1. This typical housing approach has been used to implement the dynamic bottom-up building stock model in this paper and will be further referred to as the TABULA building stock. The characteristics of the buildings are compiled from national building statistics. As such, they should be considered as average dwellings representing the building types of the typology and are closely linked to real dwellings.

Main matrix of the Belgian housing typology							
Region	Construction Year Class	Single Family House - Detached	Single Family House - Semi-detached	Single Family House - Terraced	Multi-Family House - Small	Multi-Family House - Medium	Multi-Family House - Large
1 national (Belgium)	... 1945						
6 national (Belgium)	1946 - 1970						
12 national (Belgium)	1971 - 1990						
18 national (Belgium)	1991 - 2005						
24 national (Belgium)	2006 - ...						

Figure 1: Main matrix of the Belgian housing typology following the harmonized TABULA approach (Cyx et al., 2011).

In the TABULA-project, the geometry and U-values of the envelope components are specified for each typical dwelling together with a typical infiltration and ventilation rate. For the single-family dwelling cases, the geometry is derived from the Energy Advice Procedure (EAP) database (see Cyx et al., 2011) for Flanders and Wallonia. This database consists of dwellings that have voluntarily applied for an energy performance audit. Analysis of the data from approximately 11 000 EAP audits resulted in some 9 600 suitable datasets, which allowed deriving average geometrical characteristics for the 15 single-family dwelling cases in the typology (3 building types – detached, semi- detached, terraced – combined with 5 age classes). It has to be noted that the EAP audits are conducted on a voluntary basis. As such, the database might be biased due to a larger share of larger and less performant buildings, since building owners with a high energy bill are more likely to subscribe for an energy audit.

3.1.2 Assumptions for implementation of dynamic model

To implement the dwellings of the TABULA building stock description as dynamic building models, assumptions have been made to extend the data provided by the TABULA report. These assumptions can be categorized in two groups. The first group completes the geometry specification needed for the dynamic building models. The implementation is based on a two-zone building model, taking into account the significant differences between day and night zones. Since this subdivision is not made in the TABULA project, most assumptions are related

to subdividing the building in these two zones. In addition, assumptions were needed for the internal walls and floors, as they are not considered in the TABULA project. All assumptions used to complete the geometry specification are summarized in Table 1.

Table 1: Summary of the assumptions made to complete the geometry description of the TABULA building stock.

Aspect	Detached	Semi-detached	Terraced
Unheated spaces	All components except floors are assumed to be in contact with the outdoor environment. The whole ground floor is in contact with the ground.		
Floor area day-zone ($A_{fL,D}$)	The entire area of the ground floor is considered as day-zone		
Floor area night-zone ($A_{fL,N}$)	Calculated as: $A_{fL,use} - A_{fL,grd}$ (with $A_{fL,use}$ the usable floor area and $A_{fL,grd}$ the ground floor area)		
Volume day-zone (V_D)	Calculated as: $A_{fL,grd}h_{fl}$		
Volume night-zone (V_N)	Calculated as: $V_{prot} - V_D$ (with V_{prot} the protected volume)		
Floor height (h_{fl})	Calculated as: $V_{prot}/A_{fL,use}$		
Number of floors (n_{fl})	2	2	3
Area façades	55% of total wall area is oriented front-back; 45% is oriented left-right	The depth of the building is assumed 2 times the width. The dimensions are calculated assuming a rectangular ground floor.	The width (w) of the front and back façade is calculated as: $w = A_{ext}/(2h_{fl}n_{fl})$ (with A_{ext} the surface area of the external walls) The depth of the building (d_{gf}) is calculated as: $d_{gf} = A_{fL,D}/w$
Allocation of façade to day-zone	Front/back façade= 100% Left/right façade= 70%	For all façades factor is: $f_{day} = A_{fL,D}/A_{fL,use}$	
Allocation of windows to day-zone	70%	50%	50%
Orientation front façade	North		
Orientation windows	Window area is specified for each direction in TABULA specification		
Orientation roof	Pitched roof oriented to front and back		
Area of internal walls	Equal to outer wall area	Sum of outer wall area and half of the common wall area	
Area of floor between day- and night-zone	Equal to area of ground floor ($A_{fL,D}$)		
Area of internal floor night-zone	Calculated as: $A_{fL,N} - A_{fL,D}$		

The second set of assumptions concerns the thermal characteristics of the building (component characteristics, air tightness, ventilation rate...). For each envelope component (floor, walls, windows, roof) the composition and corresponding U- and g-values are specified within the TABULA project. Although the exact material properties and dimensions related to the U-values are not specified. Instead only a typical composition is provided. Based on these proposed compositions, the material properties used in this paper have been designed to match the U-values given in the TABULA specification. The thermal conductivity, specific heat capacity and density of the materials are based on the ISO 10456:2007 standard (ISO 10456, 2007). Note that an exception has been made for the U-values of the floor of period A (pre '45) and B ('46-'70) as the value specified by TABULA was considered unrealistic for an

uninsulated floor. The U-value is increased from 0.85 W/(m²K) as specified by TABULA to 2.82 W/(m²K).

The air tightness for each building type is specified in the TABULA project by the v_{50} -value. This value is translated to the n_{50} -value, used in the model, by taking into account the protected volume and total envelope area specified in the TABULA descriptions. Note that in the TABULA it is not specified if the volume is based on internal or external dimensions. Therefore, in this paper the same value is used to calculate the compactness as for the calculation of the ventilation rates. As specified in the TABULA report, the ventilation rate is zero for all cases before 2005. For the E (post '05) buildings, a mechanical ventilation system with a ventilation rate of 0.4 ACH and a heat recovery unit with an efficiency of 80% is considered.

Some of the main resulting properties of the stock (protected volume, heated floor area, overall UA- and gA-values, infiltration and ventilation rates, nominal heating power) for all buildings can be found in Table 5, together with those of the ULg typology.

3.1.3 Aggregation to national level

The aggregation of the heat demand of each building type to the demand of the entire stock is not explicitly carried out in the TABULA project for the typical housing approach. As stated in the introduction the typical housing approach merely presents a set of typical dwellings for each building type and age class. In order to get an estimate of the heat demand of the whole stock the heat demand of each dwelling is multiplied by the number of dwellings of each building case. The number of dwellings is obtained from the SuFiQuaD project (Allacker et al., 2011), which is also mentioned as a data source in the TABULA project and is in line with the Belgian land registry, though more detailed. However, there exist some discrepancies between the numbers shown in SuFiQuaD and our implementation for the TABULA building stock. The fourth period in the SuFiQuaD data ends in 2007 instead of 2005 in the Tabula project and there is no data for period E (2005-2012). The number of buildings as used for the ULg typology (see section 3.2.3) is therefore used for the period 2007-2012 and a linear interpolation is used to attribute the 2005-2007 buildings to period E instead of D. The results are summarized in Table 2.

Table 2 also shows the correction factors that have been suggested by the TABULA report. As stated in the TABULA report, the correction factors were introduced as the calculated energy use showed an overestimation compared to the energy use for heating specified in the EAP-database that was used to

Table 2: Number of buildings and correction factor used for the TABULA implementation.

	D: Detached		SD: Semi-Detached		T: Terraced	
	Number of dwellings	Correction factor	Number of dwellings	Correction factor	Number of dwellings	Correction factor
A:Pre-'45	269771	0.34	375000	0.41	766884	0.42
B:1946-1970	309263	0.38	275838	0.45	242952	0.45
C:1971-1990	446481	0.45	158123	0.50	87706	0.52
D:1991-2005	266050	0.60	81677	0.64	54519	0.67
E:Post '05	74135	1.00	29046	1.00	19388	1.00

define the typology. According to the TABULA report the correction factors account mostly for the poor incorporation of the actual occupant behaviour especially in old buildings where an average indoor temperature of 18°C is seldom applicable. Although we have included an occupancy schedule and taken into account the differences in temperature between day- and night-zones, an analysis with and without correction factor is carried out in this paper. Thereby

we assumed that the same correction factor can be used to correct the heat demand that we calculate from our TABULA implementation.

3.2 ULG

3.2.1 Background

Within the framework of a bottom-up approach to simulate the domestic energy use in Belgium, Georges, Gendebien, Bertagnolio and Lemort (2013) (University of Liège [ULg]) have developed a tree structure to characterise the Belgian residential stock. They have used it in combination with a dynamic simulation tool (described in Georges et al., 2013) to assess the impact of different penetration scenarios of HVAC technologies on gas and electrical load profiles and on the annual consumption of the stock (Georges, Gendebien, Dechesne, Bertagnolio, & Lemort, 2013). Gendebien et al. (2014) presents the methodology used to create the tree structure and illustrates its potential by assessing different energy policy scenarios using a Heating Degree Day (HDD) calculation method.

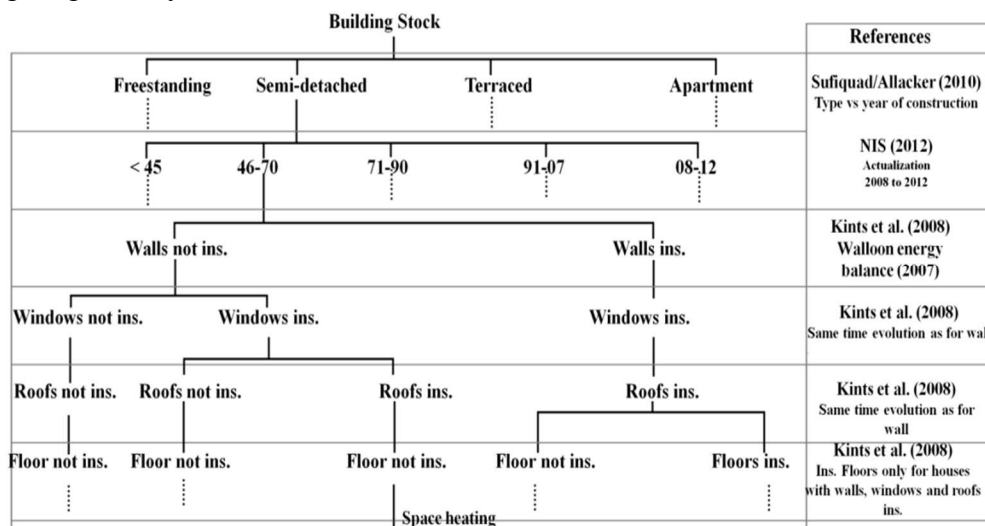


Figure 2: Belgian residential building stock tree structure developed by Gendebien et al. (2014).

In the tree structure representative buildings are identified for 4 building types (detached, semi-detached, terraced and apartment) and 5 construction periods, similar to TABULA. For each of these building cases a number of variations are applied concerning the insulation levels and the heating and DHW production systems, thus resulting in 992 cases in total, see Figure 2. Every end of the tree structure is accompanied by the percentage of occurrence in the total stock, in order to perform the aggregation of the results to the national level. Note that for the purpose of this paper, we do not take the discretization into different energy vectors and heating systems into account, as we only calculate the heat demand.

Various data sources were used for the development of the tree structure. The buildings were taken from the work of Karen Allacker (2010), where a set of existing buildings are chosen to represent the different building types and age classes. As a result, the geometry of the buildings is derived from the available plans. The share of each building type in the total stock is based on the SuFiQuaD project (Allacker et al., 2011), but is brought up to date using data from the Belgian National Institute of Statistics (NIS, 2011). The ratio of insulated to uninsulated building components (walls, windows, roofs and floors) is taken from Kints (2008). For the reconstruction of the envelope components the typical compositions proposed by the TABULA project (Cyx et al., 2011) were used combined with own assumptions for the conductivity,

thicknesses, etc. A detailed description of the procedure and the assumptions used to create the tree structure can be found in the article of Gendebien et al. (2014).

3.2.2 Assumptions for implementation of dynamic model

In total 63 cases are realized for this paper, accounting for 3 building types, 5 construction periods and 5 insulation cases (only one case for each building of period E). It must be clarified that the typology used by Gendebien et al. (2014) differs from the reference typology (Allacker, 2010) with regard to the terraced houses built in the first two periods. Allacker specifies two types of terraced houses for period A and none for the next period, while Gendebien et al. considers the second type to be representative of period B. Here we follow the assumption of Gendebien et al. as well, although this leads to an abnormally large building representing the second period and a rather small one for the first period, see Table 5. The consequence of this is commented in the results section as well. Our implementation of the typology of Gendebien et al. will be further referred to as ULg typology or ULg stock.

Each building is modelled as a 3-zone model, except for the buildings DC and SDC which don't have unheated spaces and therefore only have two zones:

- Day zone (includes living room, kitchen and “study” spaces, as well as adjacent corridors or small storage rooms; usually comprises the whole ground floor)
- Night zone (includes bedrooms and “dressing” rooms, but also the bathroom and corridors of the same floor; usually comprises the whole upper floor)
- Unheated spaces
 - Attic (in this case other unheated spaces are incorporated in the other zones)
 - Big storage rooms and the garage, if there is no attic

The surface areas of all the components are derived from the plans available from Allacker (2010). As those are given in rough detail, subjective judgment could have influenced the outcome. To make it more clear, all assumptions regarding the geometry are listed below.

- The height of the storeys is not specified in Allacker's work. The heights chosen by S. Gendebien and E. Georges (personal communication, December 2013) are thus used, except for the one of the 2nd floor of the SDB building which was corrected to 4.2m instead of 6m.
- Allacker gives only the total area of windows for each façade of the buildings. Respecting the totals, each zone was allocated an area of windows per orientation based on interpretation of the plans.
- The orientation of the buildings is not provided with the plans either. In this paper a base case orientation is chosen but different cases are then investigated. As a start, the general rule is that the façades of the buildings point towards the cardinal directions and the living room is facing south.
- For buildings of period E (2007-2012) no building type is given by Allacker. The same geometry is used as for the buildings of the previous period, but with different construction elements. This is the same approach as that of Gendebien et al. (2014).

Regarding the thermal properties of the buildings, each building type is assumed to appear in the 2012 stock with 5 different insulation cases, as suggested by Gendebien et al. The frequency of each insulation case per type of building was provided by Gendebien (personal communication, March 2014) and results in the number of buildings shown in Table 3. The 5 cases are listed below:

- Insulation Case 1: original state when built
- Insulation Case 2: replacement of windows (also changes the infiltration rate)
- Insulation Case 3: new windows and insulation of roof
- Insulation Case 4: new windows, insulation of roof and walls
- Insulation Case 5: new windows, insulation of roof, walls and ground floor

To form these 5 cases, two states of each construction element are taken into account: original state and renovated state. Thus, in Insulation Case 1 all elements are in their original state whereas in Insulation Case 5 all elements are renovated. The exact composition of the construction elements – original state as well as renovated state – is the one described by Gendebien (personal communication, March 2014) with only few exceptions. In the following the differences and additions are discussed:

- The improvement of the air tightness was here attributed to the replacement of the windows rather than to the insulation of the walls (assumed by Gendebien et al.). In the opinion of the authors, infiltration losses are primarily linked to leaky windows and roofs. Instead of implementing the improvement in steps, which would reflect more the reality, the reduced infiltration rate was used as from Case 2 for simplicity.
- The composition of the floors has been corrected to resemble more the common practice in Belgium. Thus, instead of 3 cm reinforced concrete above 13 cm of light-weight concrete we implemented 3 cm of light-weight concrete on top of 13 cm of reinforced concrete (resulting in approx. 10% higher U-value).
- For our implementation, the composition of the flat roof was derived from the TABULA descriptions. For the renovation scenario the same average insulation thickness was used as for the pitched roofs, see (Gendebien et al., 2014).
- The composition of the internal walls and floors, since not described in the ULg model, are assumed to be the same as those created in this paper for the TABULA implementation.
- Windows: The U-values specified by Gendebien et al. are maintained choosing appropriate glazing and frame properties. The frame to window area fraction was assumed to be 0.25 for all windows.

Regarding the infiltration rates, the same v_{50} -values specified by the TABULA project were used for the air tightness (as used by Gendebien et al.), but here the conversion to air change rates is different. The v_{50} -values are converted to n_{50} -values, used in our models, by taking into account the protected volume and total envelope areas. The building plans provided by Allacker (2010) are not detailed enough to differentiate between internal and external dimensions, so the same dimensions are used to calculate volumes and areas for all cases. In this way the same approach is used in both our implementations (ULg and TABULA). The ventilation rate is zero for all cases except for the E buildings where a mechanical ventilation system with ventilation rate of 0.6 ACH and a heat recovery unit with an efficiency of 80% is considered, as done by Gendebien et al. (2014). The resulting properties for this model are summarized in Table 5 **Erreur ! Source du renvoi introuvable.**, where a comparison is made with the TABULA model.

3.2.3 Aggregation to national level

As mentioned above, 63 different combinations of building type, age and thermal quality are modelled to represent the whole stock of single-family houses in Belgium for the ULg typology.

In order to obtain results for the national level the results of the simulations of each case are aggregated in a simple way. Within the work of Gendebien (personal communication, March 2014) the occurrence of each of these combinations in the total stock of 2012 is specified, see Table 3. The total number of single family buildings results in 3 456 833 for that year (same as for the TABULA stock). Thus, the heating demand of the stock is derived by multiplying the demand of each studied case by the number of buildings it represents. When comparing building types, all insulation cases are included for the ULg buildings, unless it is differently specified.

Different orientations of the buildings are also taken into account for the ULg stock. As stated earlier, a base-orientation was chosen for each building, representing orientation 0° (either south or north). Then the buildings were rotated by 90°, 180° and 270°, resulting into 4 simulations for each building case. Figure 3 shows the deviation of the annual heat demand from the average value. The average results are derived from simply

Table 3. Number of buildings per building type, construction period and insulation case used for the ULg stock (Gendebien, personal communication, March 2014).

		InsCase1	InsCase2	InsCase3	InsCase4	InsCase5
D: Detached	A:Pre 1945	86824	106576	38564	18892	18869
	B:1946-1970	86953	106652	38393	38690	38643
	C:1971-1990	65258	79933	28923	136248	136085
	D:1991-2007	14812	18168	6540	132321	132163
	E:2008-2012	36191				
SD: Semi-Detached	A:Pre 1945	92127	112887	117447	13701	38793
	B:1946-1970	59100	72417	75343	17997	50956
	C:1971-1990	17615	21585	22457	25170	71267
	D:1991-2007	3467	4248	4420	21197	60016
	E:2008-2012	17474				
T: Terraced	A:Pre 1945	165264	202478	291732	1192	106165
	B:1946-1970	45664	55947	80608	674	60065
	C:1971-1990	8575	10506	15138	594	52928
	D:1991-2007	2030	2487	3584	602	53618
	E:2008-2012	11597				

averaging the results from the four simulations, as no data was found to support a different distribution of the buildings to the various orientations. This figure shows the case with the highest deviation (for most buildings) which occurs for the insulation case 5 because the solar gains influence more the energy demand when the building is better insulated. The SDC and SDD buildings show a slightly different behaviour because they have the majority of their windows concentrated in two adjacent façades, whereas the other buildings have them in opposite façades. The difference is maintained within ±4% for most buildings, while SDC and SDD reach above 6% for two of the orientations. For the peak loads the difference is much smaller (no more than 0.33%) and therefore is not displayed here. This is explained by the fact that the peak load mainly depends on the nominal power of the heating system, which remains the same for all orientations.

Note that the aggregation of many rooms into one thermal zone (like was done in our model) makes the influence of the orientation fade away as all rooms can

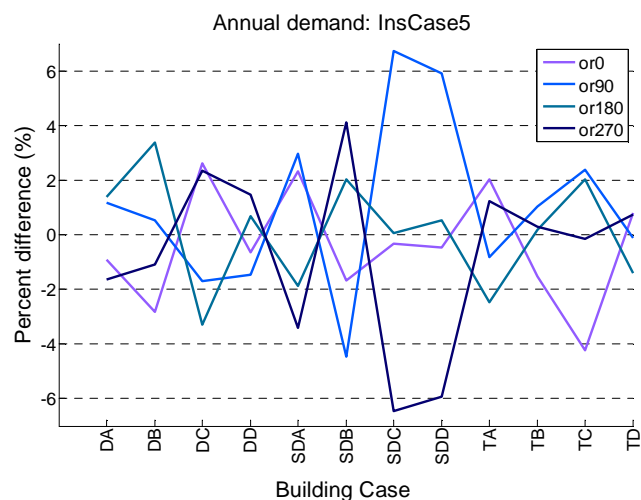


Figure 3: Percent difference of the 4 orientations compared to the average in total annual demand for the insulation case 5 for all building cases.

share the solar gains reducing the heating (or cooling in other cases) demand. Therefore, although the differences appear to be small enough for this particular model, all orientations are taken into account and the average results of all four are further used in this paper.

3.3 Comparison of building stock descriptions

Both abovementioned typologies mean to represent the Belgian residential building stock and as such can be used in building stock modelling. The outcome of a building stock model depends on the modelling technique used but also on the typology itself. For this paper the same model is used for both implementations in order to compare the typologies. Significant dissimilarities can be identified regarding the stock descriptions, as presented in this paragraph.

3.3.1 Geometry

The main difference regarding the geometry of the buildings is that TABULA uses “average” buildings, derived from analysis of energy audit databases, while ULg uses existing buildings, chosen for their characteristics that are assumed to be representative. In the TABULA report it is stated that “considering that these audits were commissioned by owners or residents, we are aware of the fact that the EAP-databases do not contain a representative sample of the actual housing stock” (Cyx et al., 2011, p. 19). Recognising this fact, the thermal properties of these buildings were not used in the report. However the database was used for the calculation of the geometrical properties of the buildings. This must be taken into account for this comparison. On the other hand, the selection of the houses in the ULg typology is not clearly explained in the relevant reference (Allacker et al., 2011) and can be debated as well.

In Table 5 the main differences in size of the buildings can be observed. In general, TABULA buildings tend to be significantly larger. The heated volume for the total single family stock of Belgium is $2.2 \cdot 10^9 \text{ m}^3$ according to the TABULA stock whereas for ULg it is only $1.2 \cdot 10^9 \text{ m}^3$. It must be noted that TABULA does not specify which spaces are included in that volume, which can create a lot of confusion. For the ULg stock the unheated spaces (attics, big storage, garage) are not taken into account in the above calculation. Some unheated spaces indeed might have changed use over the years becoming heated spaces (e.g. attics become bedrooms) but these effects are not modelled. The inclusion of all unheated spaces in the total volume for ULg results in $1.45 \cdot 10^9 \text{ m}^3$, which doesn't explain the large difference between both stock descriptions.

A comparison can be made between the heated surface areas of the two typologies and the average values given by Kints (2008, p. 15). The latter refer to Wallonia and are based on the General Socio-economic survey of 2001 (Vanneste, Decker, & Laureyssen, 2007), however they can be used to evaluate the order of magnitude of the buildings' size. In Table 4 the average areas of TABULA and ULg are calculated based on the contribution of the different age classes to the total number of buildings within one building category (see Table 2 and Table 3). It can be thereby deduced that the ULg areas appear to be much closer to the results of the General Socio-economic survey.

Table 4: Comparison of average heated surface area (m^2) per building type.

	Detached	Semi-detached	Terraced
Kints (2008)	146.6	128	116.1
TABULA	251.4	213.8	213.9
ULg	127.4	110.6	144.8

This large difference is expected to affect the outcome at the individual dwelling comparison but even more at the aggregate level.

Table 5: Summary of the properties of TABULA and ULg stock implementations.

	Detached					Semi-Detached					Terraced					
	A	B	C	D	E	A	B	C	D	E	A	B	C	D	E	
Protected volume [m ³]	TABULA	766	648.5	655.7	710.5	714.4	651.8	531.7	509.6	615.9	642.7	621.3	546.6	462.8	526.9	549.8
	ULg	335.5	250.5	423.2	293.2	293.2	192.2	331.1	442.5	382.2	382.2	215	970.5	686	402.2	402.2
Heated floor area [m ²]	TABULA	279	235.8	238.4	258.4	269.6	237	193.4	185.3	224	233.7	225.9	198.8	168.3	191.6	199.9
	ULg	104.8	104.5	148.5	138.4	138.4	68.6	118.3	185.6	126.3	126.3	76.8	323.5	245	143.7	143.7
UA-value [W/K]	TABULA	1268	1031	628	462	313	945	741	466	458	262	713	599	324	247	190
	ULg InsCase1	961	716	571	252	186	409	585	355	244	177	345	1039	471	264	199
	ULg InsCase5	302	192	316	181	-	145	215	190	175	-	131	441	297	204	-
gA-value [m ²]	TABULA	35.8	36.2	31	26.8	20.7	25.9	26.6	24.9	20.1	21.7	27.4	25.9	18.8	20.6	21.6
	ULg InsCase1	12.2	15.7	39.3	18.5	11.3	6.1	10.9	19.3	13.9	8.5	6.1	53.9	32.3	13.9	8.5
	ULg InsCase5	6.6	8.5	24	11.3	-	3.3	5.9	11.8	8.5	-	3.3	29.1	19.7	8.5	-
Infiltration rate [L/h]	TABULA	0.7	0.75	0.715	0.47	0.23	0.6	0.6	0.6	0.4	0.2	0.4	0.405	0.39	0.25	0.145
	ULg InsCase1	0.8	0.8	0.9	0.5	0.3	0.7	0.6	0.6	0.4	0.2	0.4	0.27	0.265	0.26	0.155
	ULg InsCase5	0.3	0.27	0.315	0.26	-	0.2	0.2	0.2	0.2	-	0.2	0.11	0.11	0.155	-
Ventilation rate [L/h]	TABULA	0	0	0	0	0.4	0	0	0	0	0.4	0	0	0	0	0.4
	ULg InsCase1	0	0	0	0	0.6	0	0	0	0	0.6	0	0	0	0	0.6
	ULg InsCase5	0	0	0	0	-	0	0	0	0	-	0	0	0	0	-
Nominal heating power [kW] (sum of day and night zones)	TABULA	40.3	33.8	22.6	19.2	13.7	30.3	24.8	17	14.6	11.3	22.1	19.2	12.2	10.6	10.7
	ULg InsCase1	21.6	19	17.9	9.7	8.3	10.5	13.8	12.9	9.8	8.4	8.2	28.4	19.9	10.2	9
	ULg InsCase5	10.4	7.5	11.7	8.2	-	5.6	8.4	9.5	8.3	-	5.3	20.3	15.3	9.2	-

3.3.2 Thermal properties

The U-values used for the envelope components of both stocks are summarized in Table 6. The windows have the same U-values for the original state, see Table 7, while the internal walls and floors are the same for both stocks. As can be seen here, a major mismatch exists in the thermal properties used for the roofs of the first two periods. This difference results from the discrepancy between the component description and the corresponding U-value that is presented in the TABULA project. In the ULg implementation the U-value is calculated based on the component description, as done by Gendebien et al. (2014), whereas for the TABULA implementation the value presented in the TABULA project is used.

Table 6: Comparison of U-values [$W/(m^2K)$] of the envelope components used in both stocks.

Component:	Exterior walls					Pitched Roof					Floor on Ground				
Period:	A	B	C	D	E	A	B	C	D	E	A	B	C	D	E
TABULA	2.2	1.7	0.99	0.6	0.4	1.71	1.66	0.85	0.6	0.3	2.82	2.82	0.84	0.67	0.53
ULg Org.	2.28	1.57	0.92	0.48	0.41	4.74	3.7	0.79	0.44	0.31	3.73	3.73	1.19	0.74	0.4
ULg Renov.	0.59	0.53	0.43	0.41	-	0.46	0.45	0.31	0.31	-	0.79	0.79	0.54	0.41	-

Table 7: Comparison of window properties

Property:	U-value of window [$W/(m^2K)$]					g-value of glazing [-]				
Period:	A	B	C	D	E	A	B	C	D	E
TABULA	5	5	3.5	3.5	2	0.87	0.87	0.77	0.77	0.47
ULg Org.	5	5	3.5	3.5	2	0.87	0.87	0.77	0.77	0.47
ULg Renov.	2.75	2.75	2.75	2	-	0.47	0.47	0.47	0.47	-

The infiltration rates were based for both stocks on the TABULA specifications for the v_{50} -values leading to similar results, as shown in Table 5. No ventilation is taken into account for the majority of the dwellings. However, different ventilation rates were assumed for the buildings of the last period: 0.4 ACH for TABULA and 0.6 ACH for ULg.

Taking into account the transmission and ventilation losses, as well as the intermittency of the heating, the nominal power needed for heating the dwellings was calculated in this paper based on the EN12831:2003 standard (EN 12831, 2003). Table 5 clearly demonstrates the higher needs of the TABULA buildings, mostly due to their bigger size.

4. MODEL

In order to compare the two building stock typologies the same model is used for the two implementations. A tool that can simulate dynamic physical phenomena is needed in order to be able to simulate demand profiles and peak loads for DSM and integration in smart grids. All parameters of the models that are not specific to one stock description are kept the same for the two implementations.

The detailed simulations of both stocks for this paper are carried out using the IDEAS library developed at the KU Leuven. The IDEAS library is implemented in Modelica (2014) and expresses transient thermal processes in detail based the control volume method (CVM) as described by Baetens et al. (2012). The buildings are modelled as 2- and 3-zone models, taking into account the different requirements of different rooms of a dwelling (day-zone, night-zone, unheated zone). Since the paper only aims at calculating the heat demand, ideal heating systems with maximum power input equal to the nominal power of each zone (day and night zones) obtained by the EN12831:2003 (EN 12831, 2003) standard were implemented.

Regarding the temperature requirements for the heating, a fixed schedule is used in order to make in inter-building comparison. The set-point for the operative room temperature is set to 21°C and 18°C for respectively the day and night zones in accordance to EN15251:2007 (EN 15251, 2007). A set-back temperature of 16°C is implemented. The day-zone is assumed to be heated between 07:00-22:00; the night-zone between 21:00-09:00 (Aerts, Minnen, Glorieux, Wouters, & Descamps, 2014). For the internal gains a model based on Markov-chains that is largely consistent with the model of Richardson, Thomson, Infield and Clifford (2010) but adapted to the Belgian case was used (Baetens et al., 2012). The outputs of the model are presence and activity of the occupants and the usage of electric appliances and lighting resulting in internal heat gains for the building. A random profile was chosen and used for all buildings of both stocks. It must be noted that although the deterministic approach used in this paper is acceptable for the inter-building and inter-model comparison, a stochastic representation of the occupant behaviour should be implemented for a bottom-up analysis of the energy use of the Belgian building stock.

For modelling purposes, the walls adjacent to neighbouring houses were considered to be adiabatic. Also the thermal capacity of the zone's air was estimated to be 5 times that of the air (Sourbron, 2012, p. 229). The air change rates were calculated using rule of thumb by dividing the n_{50} values by 20. Last, the simulations were performed for the moderate climate of Uccle (Belgium), for which climatic data is obtained by Meteororm v6.1 (2009).

5. RESULTS

A comparison of the calculated heat demand is performed in order to evaluate the differences between the two stocks introduced in the previous paragraph. The annual demand as well as the dynamic heating load and temperature profiles are examined, since the latter are also important when DSM is to be studied.

5.1 Annual heat demand

Simulation of the heat demand for both building stock descriptions results in an annual use of 63 020 GWh and 51 275 GWh (or 79.7 kWh/m² and 115.5 kWh/m²) for the corrected TABULA and ULG cases respectively. The aggregation of the results of individual building cases is done as explained in sections 3.1.3 and 3.2.3. The uncorrected TABULA demand was much higher (145 768 GWh), demonstrating the need for correction factors of the buildings in the TABULA project. These results cannot be compared to real data (as explained in the introduction), which doesn't allow for a conclusion on which typology gives more accurate results. However, the obtained difference (65% for uncorrected and 18.6% for the corrected TABULA results) indicates that none of the typologies can be accepted as reliable without validation. Nonetheless, verification of the simulation model based on a comparison of the results obtained by our simulations with those obtained in the reference studies is possible.

In the TABULA project the total annual demand for each building type was calculated using a monthly averaged method implemented in the EPB-software (EPB Besluit Bijlage V, 2013), the Flemish implementation of the EPBD. Multiplied by the number of dwellings for each case and taking into account the correction factors, this results in a reference value for the total annual demand of 86 154 GWh. As such the heating demand obtained by our dynamic model is 26.9 % lower than the value obtained by the static calculations in the TABULA project. This difference is mainly due to the fact that the EPB calculation, used in the TABULA project, assumes a default value for the ventilation loss, whereas in our dynamic model the ventilation rate is set to 0 ACH for all buildings before 1990, as described in the TABULA project. Moreover, the EPB software used in the TABULA project accounts for thermal bridges by

increasing the average U-value of the components by $\Delta U_b = 0.1 * (C + 2)/3$, with C the compactness of the building. Implementing the ventilation according to the EPB-calculation into the dynamic model, resulted in an air change rate of approximately 0.4 ACH for each dwelling and an increased heat demand of 72 020 GWh, reducing the discrepancy with the TABULA project to 16.4 %. Since the current version of IDEAS does not support a detailed calculation of thermal bridging effects, an estimation of the impact is made by increasing the UA-value of the envelope by 10%. As such, the annual heat demand is further increased to 75 200 GWh, reducing the difference with the TABULA report to 12.7%. Note that both modifications are not maintained in the paper, as both aspects are not included in the specifications reported by the TABULA project.

For the ULg stock a clear comparison cannot be made between our calculation and results from Gendebien et al. (2014). In their work the annual demand for heating per average dwelling is calculated (18.8 MWh/y/av. dwell), which however results from the inclusion of apartments in the stock and from different calculation method, heating schedules and climatic data. The calculated 14.8 MWh from our implementation is then 21.3% lower. This difference can additionally be attributed to the few different assumptions made regarding the stock, e.g. the infiltration rates of the insulation cases (see section 3.2.2). Indeed, the same dynamic simulation but following the assumption of Gendebien et al. for the improvement of the air tightness leads to a heating demand of 16.0 MWh per average dwelling, limiting the difference to 14.9%. This is an indication that such assumptions made out of lack of data can have a noticeable effect on the outcome. These results are nonetheless of the same order of magnitude, showing that the difference in the building characteristics, as found between the TABULA and ULg descriptions, is of greater importance.

A more elaborate examination of the results and inter-comparison between the two stocks will help revealing the causes of the differences. In Figure 4 the annual heat demand is presented for each building case. The results from the TABULA implementation without and with the use of the correction factor are compared to the results from the ULg implementation for the buildings at their original state (Insulation Case 1) and for the all-ins.-cases state. The latter is calculated as the weighted average of all insulation cases for each building (based on the number of buildings in each insulation case). Additionally the annual heat demand per “average dwelling” is shown for the two TABULA cases, for the ULg all-insulations case and for the reference projects (Cyx et al., 2011; Gendebien et al., 2014). Values for the “average dwelling” are obtained when dividing the stock’s demand by the total number of buildings. This figure demonstrates the impact of the correction factor in the TABULA approach, as well as the inherent differences of the two stocks. If one compares the original states for both stocks without taking into account correction factors it becomes obvious that the larger TABULA dwellings result in much higher needs (around 86% higher in average, but with values ranging from -5% up to 260% for the TB and TA buildings respectively), although the U-values are similar or even larger for ULg in a few cases.

The corrected TABULA demand is substantially lower and much closer to the ULg-all-ins.-cases outcome, especially for the older buildings. It appears then that the correction factor could account not only for the occupant behaviour and rebound effects as stated by Cyx et al. (2011), but also for the possible renovations that have occurred to the buildings and are not modelled explicitly. This interpretation cannot be verified for the TABULA buildings, however a closer look to the ULg stock reveals that the inclusion of 5 insulation levels for each building type reduced the annual demand of a building by 34% in average (range: 17-46% for the DA and SDC buildings respectively) compared to the original state alone.

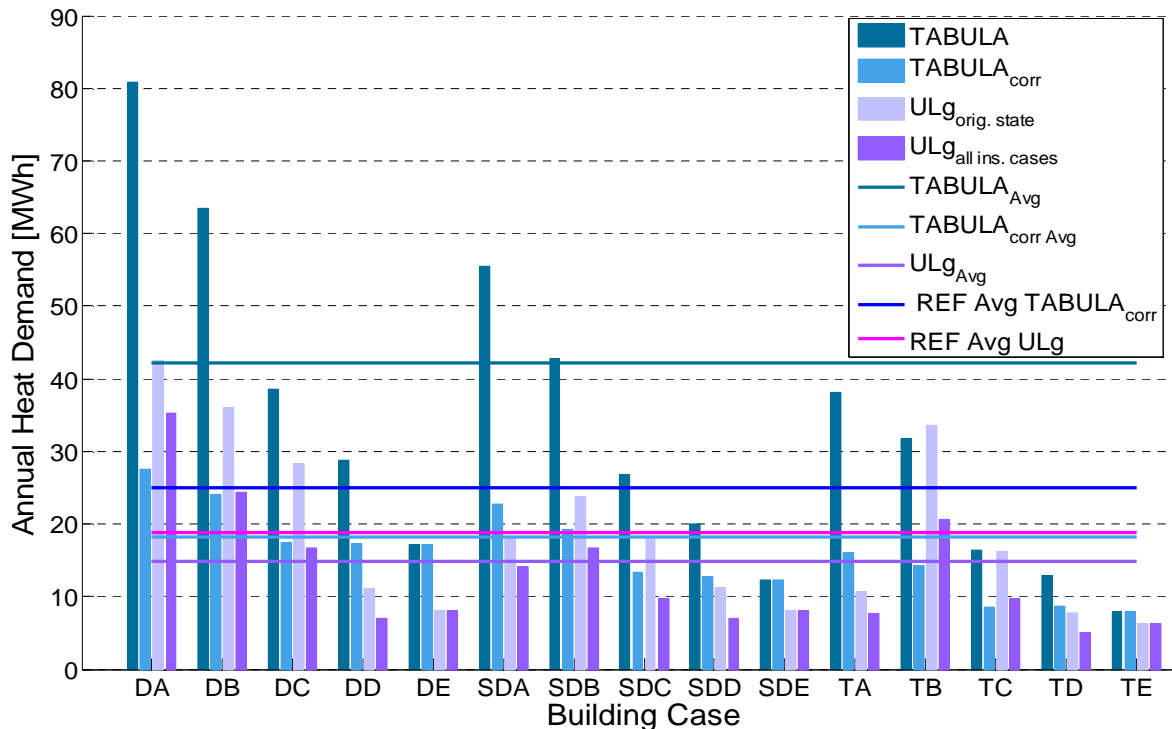


Figure 4: Annual heat demand [MWh] of all building cases for the two stocks. For TABULA: with and without correction. For ULg: original building state and with all insulation cases considered. Average dwelling annual demand for the above and additionally for the reference studies (Cyx et al., 2011; Gendebien et al., 2014).

For certain buildings, i.e. the DD, DE and SDA the larger dimensions of the TABULA buildings cannot be compensated by larger U-values or the correction factor, which explains the still smaller needs of the ULg dwellings. The strange behaviour of the TA and TB buildings is further commented for Figure 6.

Figure 5 shows the annual heat demand per m^2 of heated area for each building type, for the same cases as mentioned for Figure 4. When the difference in size is filtered out by analysing the heat demand per m^2 of heated floor area, a strong similarity is shown between the stock implementations without application of the correction factors. For both implementations the heat demand clearly decreases for newer buildings. In line with the expectations, terraced houses have a lower heat demand compared to semi-detached and detached houses. This figure demonstrates that the difference in heat demand between the TABULA and ULg buildings is mainly due to size effects. The application of the reduction factors for the TABULA dwellings results in a significant underestimation of the heat demand per m^2 compared to the ULg dwellings. This suggests that the correction factors possibly also account for the fact that the heated surface area of the TABULA dwellings is much higher than that of ULg and might therefore be overestimated. Nevertheless, the absence of reliable validation data does not permit to prove this hypothesis.

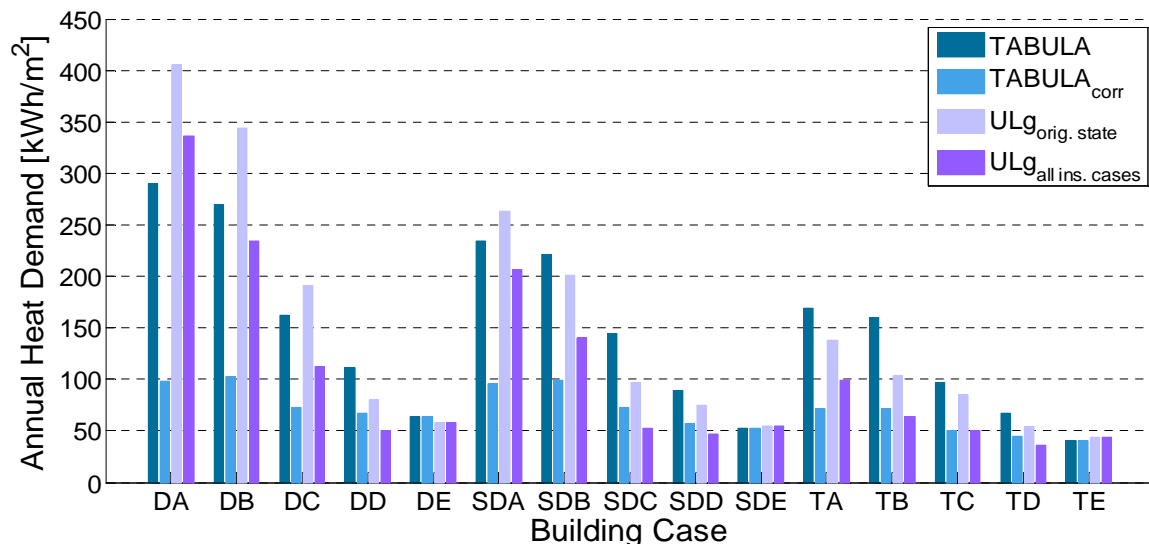


Figure 5: Annual heat demand per heated area [kWh/m^2] of all building cases for the two stocks. For TABULA: with and without correction. For ULg: original building state and with all insulation cases considered.

Figure 6 shows the demand aggregated for the total number of buildings for each building case. The importance of the age of the Belgian stock can be noticed. The new dwellings built after 1990 represent only 15.2 % of the single family houses and account for 12.6% of the total heating demand for the TABULA stock (only 7% for ULg). This fact indicates that energy efficiency policies targeting old buildings would have a higher impact on the stock's efficiency.

The evident trend of the heat demand decreasing from detached to terraced houses observed in Figure 5 is no longer obvious in the demand of the total stock. The relative contribution of each building case in the overall heat demand of the Belgian housing stock differs between the two typologies, although the same total number of buildings is used for the two descriptions. For the TABULA and ULg typologies, the dominant building types are respectively the terraced (TA) and detached (DA) buildings from before 1945.

This figure demonstrates the problematic behaviour of the TA and TB buildings for the ULg typology, where the small size of the TA building results in a much smaller share of those buildings in the total stock heat demand compared to the TABULA typology. The important contribution of the TA buildings in the Belgian stock was already noticed by Allacker (2010) who specified two types of terraced buildings for that period (but unjustifiably none for the next period). These two types were, in the opinion of the authors, mistakenly assigned by Gendebien et al. (2014) to the two periods (A and B) respectively. To test this, a simulation of the ULg stock was performed using the so far TB building as a TA-type2 building (keeping TA as TA-type1), as suggests Allacker. The number of buildings for the new TA-type1 and TA-type2 were adjusted and are both equal to the average of the previous TA and TB buildings. This was done for each insulation case separately. There was no TB building in this simulation. The result is an annual demand of the new TA (type1+type2) building of 16.7 (3.8+12.9) GWh, much closer to the corrected TABULA 16.0 GWh. Furthermore, the stock's demand is increased to 57 115 GWh, 11.4% higher than before. This reduces also the difference of the two stocks from 18.6% to 9.4% (for the corrected TABULA). It is therefore the authors' suggestion that for future use of the ULg typology both types of buildings should be used for the terraced houses of the period A, but also a building type (other than the oversized TA-type2 one) should be implemented for period B. For the remaining part in this paper the original approach is still used.

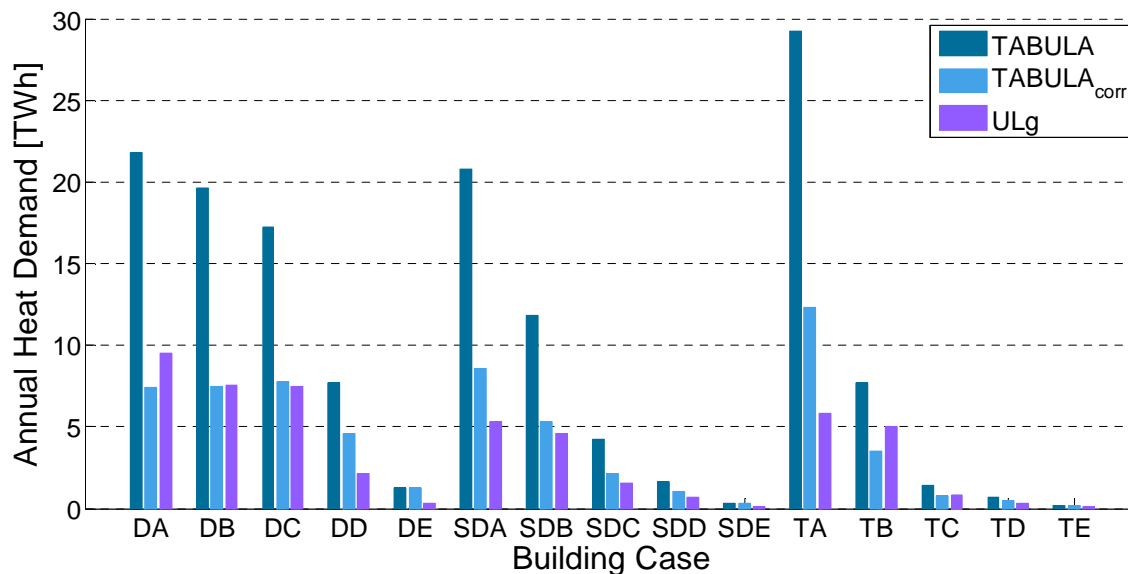


Figure 6: Annual heat demand aggregated for the total stock [TWh] of all building cases for the two stocks. For TABULA: with and without correction. For ULg: all insulation cases considered.

The analysis of the heat demand calculated by modelling the two stock typologies helped in identifying the main causes for the observed discrepancies. The high overestimation of the size of the TABULA buildings compared to the ULg ones appears to be the main influencing factor. A misuse of the TA-TB ULg building types was revealed to be of significant importance. Furthermore, possible interpretations of the purpose of the correction factor of the TABULA stock have been suggested. However, due to lack of validation data it is not possible to draw conclusions on the correctness of either typology. Moreover, it is the authors' opinion that the use of correction factors is not desired in a bottom-up model, since this would reduce the usability towards the assessment of new technologies.

5.2 Dynamic temperature and load profiles

In this section an analysis of the dynamic behaviour of the buildings is performed. Knowledge of the temperature profiles and peak loads is important for the implementation of DSM, where loads have to be shifted while maintaining the comfort levels.

Figure 8a and b shows the operative temperature profiles of an average day in January (average of 31 days). The day and night zone profiles are shown for the three building types of construction periods A (a) and D (b). In those graphs one can notice the fixed heating schedules of the day and night zones. For both stocks it can be observed that the older buildings cool down much faster, which is expected, due to higher infiltration rates and U-values. The TABULA buildings tend to have shorter cool-down and longer heat-up periods and reach lower temperatures than the ULg ones. In order to explain the observed divergence in behaviour a study of the heat balance of both stocks must be done.

The TABULA buildings have much bigger size as pointed out in the previous paragraph. This leads to larger transmission losses (U-values are comparable) and to larger infiltration losses, since infiltration rates are similar for both stocks (see Table 5). The proportionally larger solar gains of the TABULA buildings (average gA-value of dwellings for original state: TABULA=25.6m², ULg=18m²) compensate for the higher losses at a certain extent, but this effect is limited in January, due to less solar radiation. In addition, because of the assumption of same occupancy and thus same amount of internal gains in both stocks, the gains per heated area are much smaller for the TABULA buildings, as shown in Figure 7. The thermal mass of

the buildings in both stocks is of the same order, as the same element compositions were used and the area of internal walls was found comparable. Taking the above into account the dissimilarities on the temperature profiles can be better understood.

Figure 8c and d shows the corresponding average daily heating demand in January for the buildings of periods A and D respectively. Immediately one can see that in order to achieve the same thermal comfort the older buildings need much more energy. Also it is clear once again that the TABULA buildings have higher heating demand. Further, the peak demand period is slightly longer for the TABULA buildings, which corresponds to the slower temperature rise in Figure 8a and b. The trend that was observed in Figure 4, with the highest heat demand for the oldest detached dwellings is also clearly demonstrated in these graphs. Two peaks can be observed corresponding to the times when the day and night zones start to be heated. Of course this is only the result of the selected heating schedule (see paragraph 4). In reality the schedules (and temperature set-points) highly depend on the occupant's presence and preferences. The stochastic nature of these factors must be taken into account not only for the calculation of the total demand but more importantly for the study of DSM. For this purpose more reliable data is needed describing user behaviour.

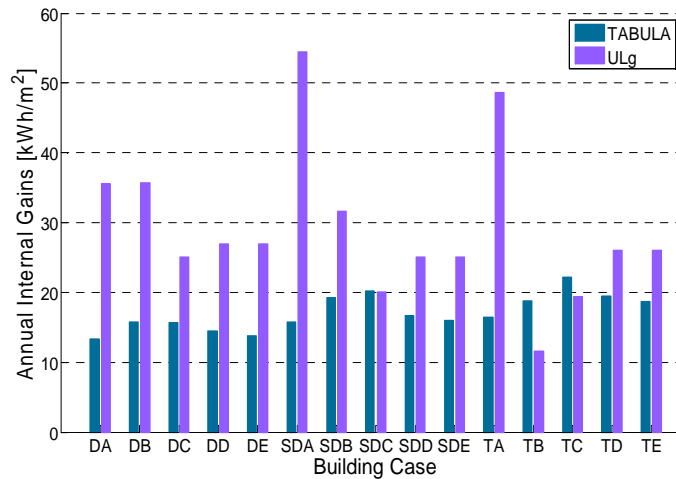


Figure 7: Annual internal gains per m² of heated area for all building cases and both stocks.

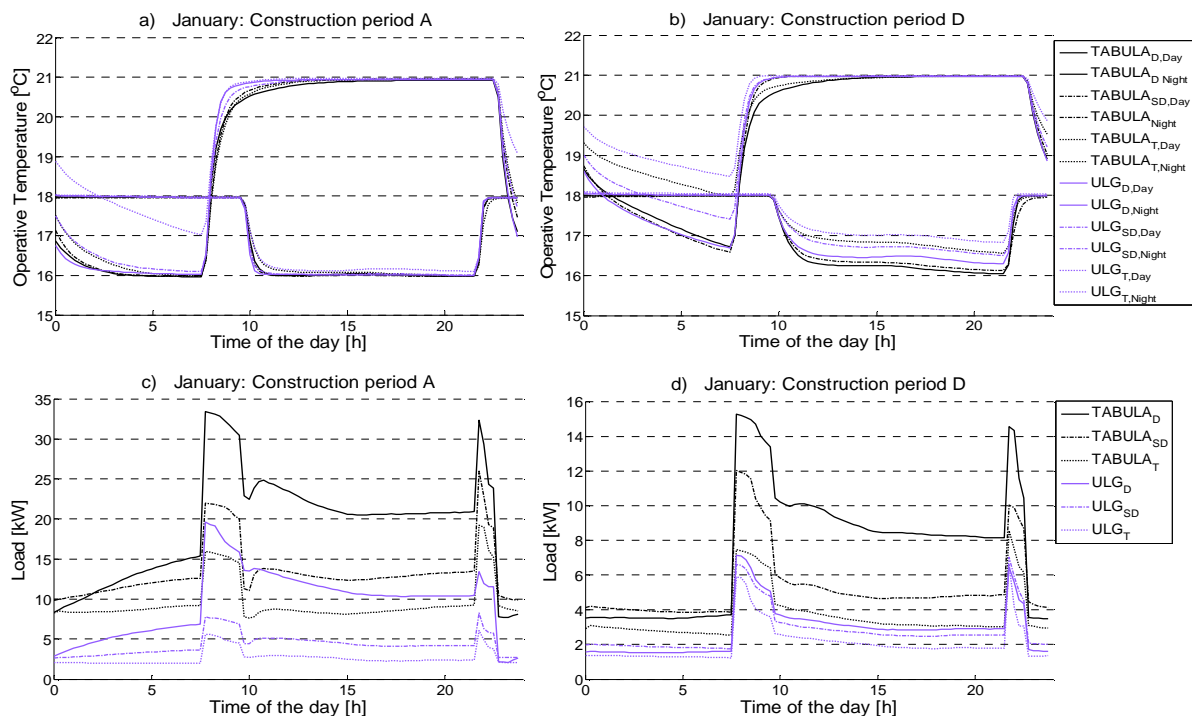


Figure 8: Average daily temperature profiles for January of the day and night zones of the three building types of the age classes A (a) and D (b). For both stocks the original insulation state is presented. Corresponding average daily heat demand (c and d respectively). No correction factor is used for TABULA.

On building stock level, the peak load demand (translated to electricity load) is a useful metric to define the generation, transmission and distribution capacity of an electricity system. This aspect can be evaluated by examining the load-duration curve of the stock, shown in Figure 9 for the TABULA and ULg implementations. Each curve is the result of aggregation of the instantaneous heating demand of all the buildings of the stock, for one implementation. One can conclude that the TABULA and ULg stocks have similar behaviour and comparable peak loads (TABULA: 35GW, ULg: 44GW) only when the correction factor is used. However, the correction factor is meant to be used for the annual demand and its use cannot be justified for correcting the dynamic behaviour of the buildings.

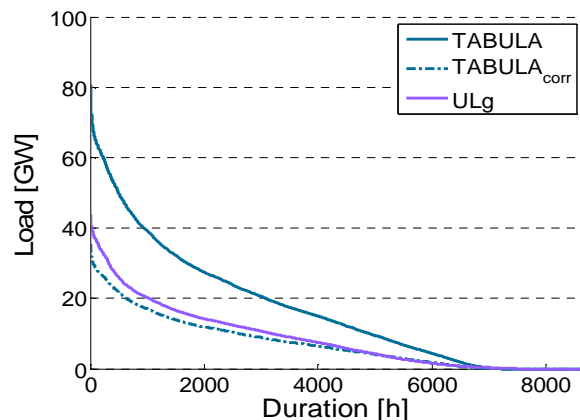


Figure 9: Load duration curves aggregated for the stock for the two implementations.

The comparison of the dynamic behaviour of individual buildings and of the entire stock indicated that the two typologies give much different results and would lead to different conclusions if used to evaluate energy saving measures. The need for validation data at a disaggregated level is again highlighted by these results.

6. CONCLUSION

In this paper two different single-family residential building stock typologies for Belgium were compared, namely the TABULA and ULg typologies. For this purpose detailed simulations of both stocks were performed using the IDEAS library implemented in Modelica. For the sake of the comparison the buildings were equipped with ideal heating systems where deterministic schedules were applied. Furthermore, the same occupant profile (defining the internal gains) was used for all buildings. The results were evaluated in terms of annual heating demand and dynamic heating load and temperature profiles.

The examination of the descriptions and the analysis of the results showed that the two typologies differ significantly, resulting in large disagreement when comparing individual dwellings and the stocks. The TABULA buildings had an average annual heating demand 86% higher than the ULg dwellings. At an aggregate level the difference in annual demand was found to be 65%. Such large discrepancies indicate that at least one of the typologies is far from representing accurately the Belgian single-family residential stock. However, due to lack of validation data, it is not possible to conclude on which of the two performs better. The large discrepancies were primarily attributed to the differences in the size of the buildings and to the fact that the ULg typology considers five quality levels for each building case. The latter approach is thought as more appropriate in the sense that more cases represent better the heterogeneity of the stock, provided that there is enough data to support the additional discretization.

The use of correction factors to account for occupant behaviour and rebound effects, as proposed by the TABULA project for the Belgian stock, reduced the difference in annual demand between the two stocks to 18.6%. However, the use of correction factors is no valid part of a bottom-up approach as their value cannot be explained based on known parameters. As was shown by the analysis of the results, the correction probably accounts for more effects than just the ones specified by the TABULA project. Additionally, the scope of these factors is

only limited to the purpose for which they were introduced. This reveals the weakness of the TABULA typology, which relies on correction factors to model the energy demand.

The comparison performed in this paper also emphasized the lack of reliable and comprehensive data for the building stock of Belgium. The existing typologies differ in such an extent that a question rises whether any of them is reliable enough. As the need for better and more detailed models increases to cover the requirements of the new technologies, the quality of the input data should follow. Therefore, a more systematic effort should be put on collecting and processing building related data. Further, relevant information on the energy use, e.g. obtained by smart meter readings, could support the validation of these building stock models, which is currently not possible. As soon as this data becomes available, future work could focus on setting up a validated residential stock typology that can be used for bottom-up modelling and analysis of the energy efficiency of the national stock.

ACKNOWLEDGEMENT

The authors would like to express their gratitude to Samuel Gendebien and Emeline Georges (University of Liège) for their valuable contribution to this paper.

REFERENCES

- Aerts, D., Minnen, J., Glorieux, I., Wouters, I., & Descamps, F. (2014). A method for the identification and modelling of realistic domestic occupancy sequences for building energy demand simulations and peer comparison. *Building and Environment*, 75, 67–78.
- Allacker, K. (2010). *Sustainable Building - The development of an evaluation method*. KU Leuven.
- Allacker, K., De Troyer, F., Trigaux, D., Geerken, T., Debacker, W., Sprinckx, C., Van Dessel, J., et al. (2011). *SuFiQuaD-Sustainability, financial and quality evaluation of dwelling types*. Brussels, Belgium: BELSPO.
- Baetens, R., De Coninck, R., Van Roy, J., Verbruggen, B., Driesen, J., Helsen, L., & Saelens, D. (2012). Assessing electrical bottlenecks at feeder level for residential net zero-energy buildings by integrated system simulation. *Applied Energy*, 96, 74–83.
- Cyx, W., Renders, N., Van Holm, M., & Verbeke, S. (2011). *IEE TABULA - Typology Approach for Building Stock Energy Assessment*.
- EN 12831. (2003). Heating systems in buildings - Method for calculation of the design heat load.
- EN 15251. (2007). Indoor environmental input parameters for design and assessment of energy performance of buildings addressing indoor air quality, thermal environment, lighting and acoustics.
- EPB Besluit Bijlage V. (2013). Bijlage V Bepalingsmethode van het peil van primair energieverbruik van woongebouwen.
- European Commission. (2014). Eurostat. Retrieved from <http://epp.eurostat.ec.europa.eu/>
- European Parliament. (2012). Directive 2012/27/EU of the European Parliament and of the Council of 25 October 2012 on energy efficiency, amending Directives 2009/125/EC and 2010/30/EU and repealing Directives 2004/8/EC and 2006/32/EC.
- Gendebien, S., Georges, E., Bertagnolio, S., & Lemort, V. (2014). Methodology to characterize a residential building in the frame of a bottom-up approach - a case study applied to Belgium. *Submitted to Building Simulation in September 2014*.
- 9th International Conference on System Simulation in Buildings, Liege, December 10-12, 2014

- Georges, E., Gendebien, S., Bertagnolio, S., & Lemort, V. (2013). Modeling and simulation of the domestic energy use in Belgium following a bottom-up approach. *CLIMA 2013 11th REHVA World Congress & 8th International Conference on IAQVEC*. 16-19 June 2013, Prague, Czech Republic.
- Georges, E., Gendebien, S., Dechesne, B., Bertagnolio, S., & Lemort, V. (2013). Impact of the integration of various heating technologies on the energy load profiles of the Belgian residential building stock. *8th International Renewable Energy Storage Conference and Exhibition (IRES 2013)* (pp. 1–11). 18-20 November 2013, Berlin, Germany.
- Hens, H., Verbeeck, G., & Verdonck, B. (2001). Impact of energy efficiency measures on the CO₂ emissions in the residential sector , a large scale analysis. *Energy and Buildings*, *33*, 275–281.
- ISO 10456. (2007). Building materials and products - Hygrothermal properties - Tabulated design values and procedures for determining declared and designed thermal values.
- Kavgic, M., Mavrogianni, A., Mumovic, D., Summerfield, A., Stevanovic, Z., & Djurovic-Petrovic, M. (2010). A review of bottom-up building stock models for energy consumption in the residential sector. *Building and Environment*, *45*(7), 1683–1697.
- Kints, C. (2008). *La rénovation énergétique et durable des logements Wallons. Analyse du bâti existant et mise en évidence de typologies de logements prioritaires*.
- Meteotest. (2009). METEONORM Version 6.1 - Edition 2009.
- Modelica Association et al. (2014). Modelica. Retrieved from <https://www.modelica.org/>
- NIS. (2011). Statistics Belgium. Retrieved from <http://statbel.fgov.be/>
- Richardson, I., Thomson, M., Infield, D., & Clifford, C. (2010). Domestic electricity use: A high-resolution energy demand model. *Energy and Buildings*, *42*(10), 1878–1887.
- Singh, M. K., Mahapatra, S., & Teller, J. (2013). An analysis on energy efficiency initiatives in the building stock of Liege, Belgium. *Energy Policy*, *62*, 729–741.
- Sourbron, M. (2012). *Dynamic thermal behaviour of buildings with concrete core activation*. KU Leuven.
- Vanneste, D., Decker, P. De, & Laureyssen, I. (2007). *Enquête socio-économique 2001 - Monographie "Le logement en Belgique."* Brussels.
- Xing, Y., Hewitt, N., & Griffiths, P. (2011). Zero carbon buildings refurbishment—A Hierarchical pathway. *Renewable and Sustainable Energy Reviews*, *15*(6), 3229–3236.

Dynamic exergy simulation coupled with thermoeconomic analysis to support retrofit decisions in non-domestic buildings

I. Garcia Kerdan^{1*}, R. Raslan², P. Ruyssevelt¹

⁽¹⁾Energy Institute, University College London, U.K.

⁽²⁾Institute for Environmental Design and Engineering, University College London, U.K.

1. ABSTRACT

Building energy retrofits should be encouraged to reduce energy use and carbon emissions at a national level. Research indicates that buildings' space conditioning needs can be met by low-grade (low-quality) sources and it is here where the biggest potential to improve the sector thermodynamic efficiency can be found. In this paper the application of a thermoeconomic-based framework oriented to assess the impact of a diverse range of retrofit measures applied to typical non-domestic buildings is presented. The modelling framework is based on a widely-used dynamic energy simulation software (EnergyPlus) coupled with an exergy and thermoeconomics post-processing analysis tool developed for the purpose of this research. Two non-domestic archetype buildings (a typical office and a primary school) are simulated to test the model. Different scenarios based in retrofitting the insulation levels of the envelope as well as the energy systems (a ground-source heat pump and a district heating/cooling) are assessed. For the school case, the district network retrofits represent the greatest thermodynamic efficiencies and lower total exergetic cost. For the office case, the installation of a district system has the greatest exergy efficiency; meanwhile a combination of GSHP with high insulation levels has the lowest exergetic cost. It is concluded that the framework can assist the selection of retrofit projects based on energy use, exergy consumption, and exergy destructions rates as well as considering the exergetic cost of the system, adding value and minimizing uncertainty in the retrofit decision-making process.

Keywords: exergy, simulation, thermoeconomics, retrofits, non-domestic

2. INTRODUCTION

One of the main challenges in today's societies is to develop strategies for the smart deployment and utilisation of fossil fuels as these are scarce and regionally limited. Particularly in the UK, the non-domestic sector, which is comprised of approximately 1.8 million of buildings, is responsible of 17% of the national energy use; where 60% is used only to cover the space conditioning demand. At present, the sector still relies heavily on fossil fuels to cover this demand, where 60% and 10% is delivered in forms of gas and oil respectively; meanwhile 25% is delivered in form of electricity (DECC, 2013), which is largely generated by this same fossil fuels. The expansion of HVAC systems in new and existing buildings represent higher energy usage rates every year, mainly driven by the constant increasing of cooling demands. For heating, gas boilers are the predominant technology in the non-domestic sector. On the other hand, some non-domestic buildings such as offices and IT buildings have high cooling demands to remove excessive heat gains; this is normally carried out by electric cooling equipment such as chillers, packaged systems and VAV units. It is estimated that by 2050 the majority of the existing buildings will still be in operation, where actions are required to achieve the 80% reduction target set by the government (UK-Government, 2008). Improving energy utilisation in the existing non-domestic sector is one of the most important actions to reach a low-carbon society in the future. One of the major barriers lays in the current limitations and uncertainties

that current retrofit analysis methods have for the identification of the optimal conservation measures (Ma et al., 2012), where the economic aspect is still the most important objective function.

Currently in the UK there is a wide range of building energy codes and programmes that stimulate the implementation of energy refurbishment projects on existing buildings by setting minimum values for energy efficiency. For example, Part L2B (DCLG, 2010) sets minimal envelope insulation levels when retrofits actions are implemented in existing non-domestic buildings. Moreover, financial mechanism strategies exist with the goal to drive down demand and improve efficiency in buildings (e.g. Climate Change Levy, CRC Energy Efficiency Scheme, ECO and Fuel Poverty, Green Deal). Also, policies to support the implementation of low carbon HVAC systems have been developed (Energy Labelling Directive, Renewable Heat Incentive). Systems such as biomass boilers, geothermal heat pumps, and solar thermal equipment are technologies that are widely supported. Other example at a European level is the recast of the Energy Performance of Buildings Regulations (DCLG, 2012), officially known as “Directive 2010/31/EU of the European Parliament and of the Council”. The directive took effect in 2013 and among the articles it sets minimum energy performance requirements on all renovated buildings (Article 7) as well as minimum energy performance on energy systems retrofits (Article 8).

Recent research have shown that the majority of the current buildings are still very inefficient in thermodynamic terms, which means there is potential for improvements (Hammond and Stapleton, 2001; Shukuya, 2009). Gasparatos et al. (2009) performed a UK thermodynamic sectoral analysis where the commercial sector efficiency was calculated to be at 12.3% (only 6.5% for space heating). This efficiency values are not based on the typical energy analysis but instead on the exergy concept, linked to the 2nd law of thermodynamics that states that unlike energy, exergy actually is destroyed in any real process. In any thermal system, to obtain a product (e.g. heating or cooling in buildings) the exergy content would be less than the exergy contained in the fuel entering the system. The high inefficiency of the UK commercial sector is due to the poor match between the qualities of the supply fuels with the quality of the demands. Building technologies are made such that high grade fuels (gas, electricity) are required for the proper functioning of the equipment to give the necessary thermal and non-thermal comfort conditions required by the users. These inefficiencies or the amount of destructions give us a clear signal on the thermodynamic improvement potential that any thermal system has. A major limitation for efficiency improvement is that current retrofit decisions are not taking into consideration these losses because the typical analysis based only on the 1st law does not have the potential to give this type of information. Also, 2nd law analysis could be seen as complex or cumbersome by some practitioners (Rosen, 2002). Research also suggests that current retrofit methods typically lead to big discrepancies between the modelling results and actual results post-retrofit; this could be due to the lack of information that 1st law analysis give in comparison with 2nd law analysis, where building energy systems are very sensitive to subsystems or components with high exergy destructions or irreversibilities (Jansen et al., 2012). Exergy analysis applied to buildings and its systems has become more popular over the last years, especially with the development of the International Energy Agency’s Energy in Buildings and Communities Programme (IEA – ECB) Annex 37 (ECB-Annex37, 2007) and Annex 49 (ECB-Annex49, 2011); however researches have focused more on residential buildings having limited studies on the complicated and diverse non-domestic sector.

2.1 Exergy and Retrofit

Consequently, it can be suggested that exergy analysis can become essential in locating the aforementioned inefficiencies and seeking opportunities for improvement in the non-domestic

sector. Widely used in chemical and industrial processes as well as in large energy generation plants, exergy is a concept that helps to design more efficient systems as finds exact locations and magnitudes of inefficiencies throughout the process. Efficient energy use can be achieved if actions are made to reduce these inefficiencies. Because knowing the energy interactions between the different subsystems localized in the building is a big uncertainty when applying energy renovations (Ma et al., 2012), the exergetic approach could overcome or reduce this problem by applying the method of separating the supply chain into different subsystems. Few studies have shown the potential that exergy analyses has over using solely the energy concept for retrofit decisions (Jansen et al., 2012; Terés-Zubiaga et al., 2013), where exergy theory could provide a more detailed analysis of the true losses and a deeper insight on potential improvements. Unfortunately exergy analysis is not a common practice between building practitioners or in the decision making process. A particular case is the one found in the Canton of Geneva, Switzerland, where since early 2000s local authorities requires to practitioners who want to develop any new design or refurbishment projects for buildings, the calculation and delivery of exergy indicators. To vulgarize a method that could facilitate the comprehension of the exergy analysis approach, Favrat et al. (2008) developed a simplified calculation methodology for this purpose.

2.1.1 Exergy-based simulation tools for buildings

The use of simulation tools for retrofit projects represents a quick and cost-effective method to estimate pre and post retrofit energy use of a building. Although building simulation tools lack direct orientation to retrofit analysis, the outputs of these tools can be used in life cycle cost analysis (LCC) tools to calculate energy and money savings and make decisions on these results. Regularly, building retrofit practitioners use simulation and optimization software to help them to perform calculations that result in design parameters; although considering the whole energy supply chain in the analyses is not a common practice. Some tools have been developed with the intention to calculate exergy consumption throughout building energy systems. Sakulpipatsin and Schmidt (2005) presented an outline of an exergy analysis tool for building and building services including a GUI for engineers and architects based on the IEA ECB Annex 37 Pre-Design method. Later, Schlueter and Thesseling (2009) developed a tool that calculates the buildings exergy performance at an early design stage. The aim was focused on the integration of energy and exergy analysis into the architectural design process. To achieve this, the same Annex 37 exergy steady-state method was incorporated into BIM software. As is noted in the final report of the ECB Annex 49, a steady state assessment can only be used to get a first comparison between systems but contains high uncertainty on the results. To overcome the limitation of using a steady-state exergy method on retrofit projects a dynamic exergy-based retrofit-oriented modelling framework was recently developed by the author (Garcia Kerdan et al., 2014).

2.2 Exergy and economics for retrofit investments in buildings

Apart from the ability to calculate the true inefficiencies of any system, the concept of exergy has a great potential to be used to cost accounting and economic analysis (Gaggioli Richard, 1983). Regularly the selection of retrofit projects in buildings are commonly based on technical characteristics, environmental impact and availability of a resource or a technology; however, the money savings that can be achieved compared to the investment made on a project are still the main focus on any final decision. Combining thermal simulation and economic analysis is one of the most popular methods applied in the retrofit industry to determine the life-cycle cost of each design. This method can be seen in several retrofit-oriented research (Kumbaroğlu and Madlener, 2012; Rysanek and Choudhary, 2013). Conventionally, the investments decision for

energy retrofits in the building industry follows the typical methods of Net Present Value (NPV) and Internal Rate of Return (IRR). Research on the limitations of typical economic methods for retrofit decisions can be found in Menassa (2011).

A clear relationship exists between economics and thermodynamics analyses where thermo-economics, developed in the mid-20th century, is the discipline that connects these two concepts. Entrop and Brouwers (2008) explained the financial benefits of exergetic optimization in the built environment and introduced how the exergy concept could improve the typical LCC analysis. Recently, other combinations of exergy analysis with economic models have been developed. Methods such as exergoeconomics, EXCEM analysis (exergy, cost, energy and mass), exergy pricing and cost allocation, and loss-cost ratio analysis are a few examples (Rosen, 2008). The physical magnitude that connects thermodynamics with economics is entropy generation or irreversibilities. The more irreversible the process more natural resources are consumed (Valero and Torres, 2009). The objective of thermoeconomics is to minimise the objective function, which is usually a cost equation dependant on capital, maintenance, and running cost (Tozer et al., 1996). Irreversibilities or exergy destructions increase the life cycle cost of the system so this can represent investments opportunities to reduce cost and find the true system efficiency. Since prices reflect value, cost allocation should be put on availability or quality (exergy), so assigning cost to energy can be misleading. Thus, thermoeconomics can determine the internal cost of each process at every component of the building energy supply chain. This could help to optimize individual components or the whole system. A large potential lies in the application of thermoeconomics to retrofit designs that could be the link that supports a better understanding of the usefulness of the exergy concept applied to buildings and its systems.

2.2.1 Exergy-based economic methods studies applied to buildings

Since exergy studies focused on buildings are still relatively a new field of study, little research on the application of thermoeconomics exist in the built environment. Few researches have shown the potential of thermoeconomics to improve and optimize several design parameters in non-domestic buildings construction characteristics and energy systems. Tozer et al. (1996) applied a thermoeconomic method to a theoretical HVAC system (an absorption chiller driven by a CHP plant). With the method it was possible to locate the most appropriate location for optimization, consisting in the substitution of the dry coolers with a cooling tower, achieving a reduction of 35% in energy cost. Ozgener et al. (2005) analysed exergoeconomically a geothermal heat pump system installed in a University building located in Turkey. With the method it was possible to determine the optimal design of the system by finding that the major losses take place in the condenser and the compressor. Ucar (2010) applied thermoeconomics to optimize the insulation thickness depending on indoor and outdoor temperatures based on four different regions in Turkey. Balta (2012) used energy, exergy and cost analysis to assess and compare three different heating systems (conventional boiler, condensing boiler and air heat pump) for a sports hall. For this particular case and based on exergetic cost, it was found that the condensing boiler was the best option.

In an indirect manner these studies have shown the potential to use exergy-based economic theory on retrofit projects by analysing the thermodynamic loss rate of different systems, as well as the exergetic costs of energy streams and the exergetic costs of equipment. These outputs could help a designer to decide which component or subsystem of the building should be retrofitted first. Also, this can help to improve the cost-benefit of retrofit projects in current buildings and the quality in the design of the components. The aim of the current paper is to incorporate exergy and thermoeconomic analysis into the typical analysis applied to retrofit projects. In this study, the energy, exergy and thermoeconomic performance of two archetypal

non-domestic buildings (a primary school and an office located in London, UK) are presented. The typical HVAC systems are analysed and compared with other low-exergy systems such as a ground source heat pump (GSHP) and a hypothetical connection to a district heating/cooling (DHC) network. Also, the authors are interested in knowing the impact of envelope refurbishment as we consider it also has a high impact on exergy utilisation/destruction at every level of the building energy supply chain.

3. MODELLING METHODOLOGY AND SIMULATION

3.1 The modelling framework

To analyse the feasibility of different refurbishment options, a model-based simulation approach is used. The modelling framework (a dynamical exergoeconomic simulation tool) is based on the EnergyPlus software (EnergyPlus, 2012a) for first law analysis, an exergy method applied to buildings for second law analysis, and a thermoeconomic analysis module that in the future will be combined with cost-benefit analysis to improve design parameters. The selection of EnergyPlus was made because of the capabilities of the software to deliver all the detailed inputs needed for a dynamic exergy analysis (i.e. loads per zone, inside temperature per zone, auxiliary energy use, HVAC gas/electricity/district energy rates, total energy use, etc.). On the other hand, the selected exergy method, which has the potential to analyse the whole building energy supply chain is based on the model developed by Schmidt (2004) that was further improved in the ECB IEA Annex 49. This method follows an input-output approach based on seven different subsystems that are very strong related to each other, meaning that the performance of one subsystem highly depends on the other subsystems (Figure 1).

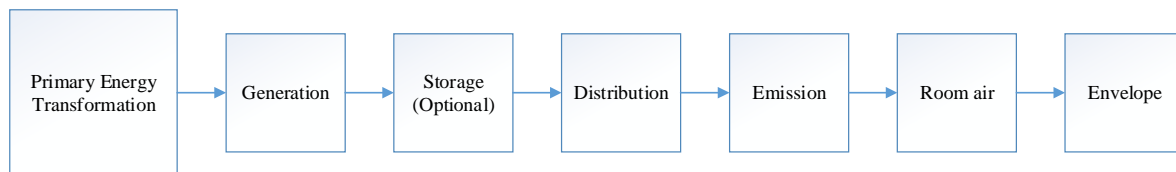


Figure 1: Energy supply chain for space conditioning of buildings (Schmidt, 2004)

Each subsystem has one or more exergy inputs streams, and will have one or more outputs or product streams. In the first subsystem, only an input stream is located, but later the products of a previous subsystem become the input of the next. At each stage, exergy destructions take place due to irreversibilities. The outputs (energy and exergy flows) are determined throughout the supply chain, from the energy transformation subsystem to the boundaries of the building envelope, where exergy leaves the building at its lowest value after the decreasing of quality due to all energy transfers occurring in the system, thus closing the thermodynamic cycle and making room for more exergy to enter the supply chain. Because exergy analyses are not common in the majority of building energy simulation tools, a python code add-on was developed that functions as a post-processing tool that requires the aforementioned specific values obtained by EnergyPlus. This modelling framework allows the comparison between different retrofit options and assesses the exergy efficiency of different energy systems as well as locates where the exergy is consumed along the energy supply chain. The dynamic equations inserted in the model have the clear intention to consider the temporal effects of a dynamic reference environment and the energy/exergy storage phenomenon. Finally, a thermoeconomic/exergoeconomic module currently under development is inserted with the intention to optimize designs and support retrofit decisions (Figure 2).

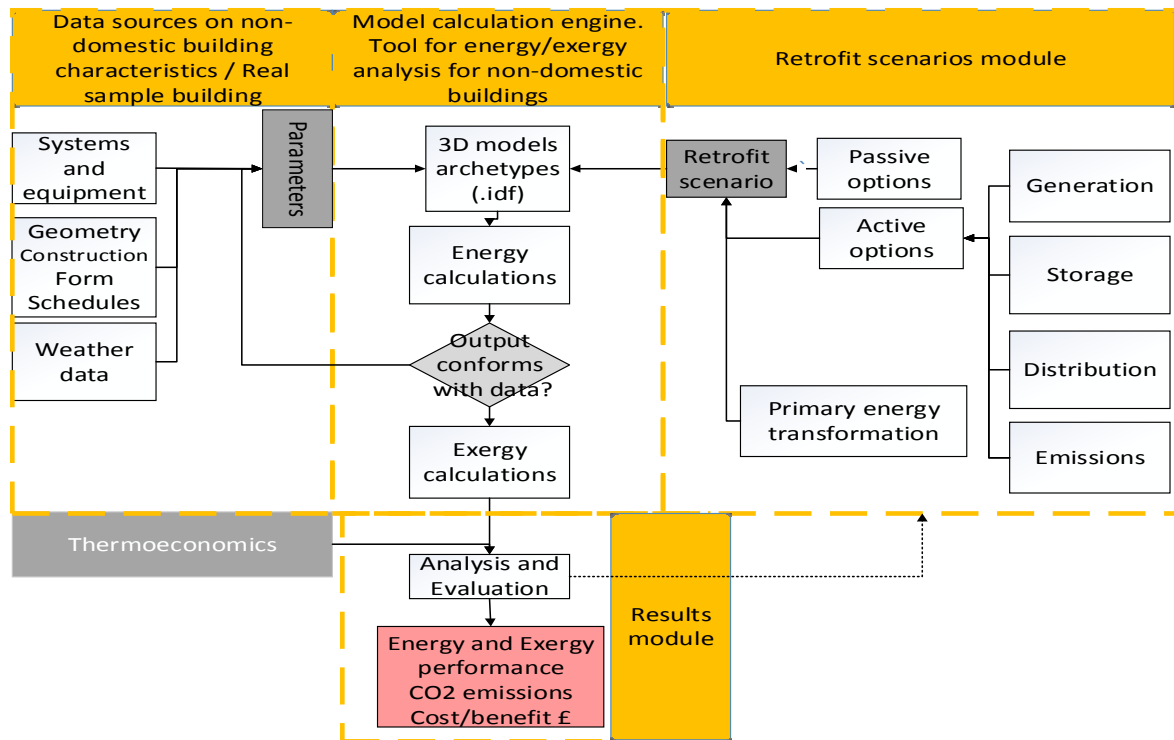


Figure 2: Exergy-based modelling framework to assess refurbishment options in buildings

3.1.1 The reference environment

Exergy calculations highly depend on the choice of the reference environment that is determined with a preliminary analysis locating which environment could act as entropy-disposal sink. An essential characteristic of the reference environment is that has to be irreversibilities-free, where all the major exergy destructions should occur on the system or process to analyse. The majority of research performs steady state calculations using monthly or seasonal average temperatures. In this research, by using the TMY2 weather files, hourly simulations are performed to account for all the heat transfer effects inside the buildings and the systems. Because this research only considers thermal exergy, mechanical and chemical exergy are neglected.

3.2 Case Study

The described model was applied to two archetypal UK non-domestic buildings (a primary school and an office building), with the purpose to understand the difference in performance and the impact of similar retrofit scenarios on the exergy use and destruction on the buildings energy systems. The method for the development of archetypes is based on an extensive review of literature combined with simple statistical analysis from data sources (Famuyibo et al., 2012). For the development of the archetypes used in this study, research in the UK context is taken into consideration (Bruhns et al., 2000; Korolija et al., 2013; Steadman et al., 2000). The main data can be seen in Table 1. Only in the UK, both the school and the office subsectors demand more than 200 PJ every year (Pout et al., 2002). The types of buildings analysed were chosen for two reasons: a) for comparative purposes and b) to perform analysis for both heating and cooling cases (as in the case of the office building).

Table 1: Characteristics of the UK primary school and office sector

Characteristics	Primary School	A/C Office	Unit
Mean area	1512	2653	m ²
Most common form	Daylit cellular	Daylit cellular/Open-plan	-
Most common structure	Frame	Frame	-
Walls/Floor Ratio	0.6	0.6	-
Glazing/Wall Ratio	0.28	0.30	-
Number of floors (mean)	2.44	3	floors

As a comprehensive case study, the city of London is considered for this analysis. Thus, the London TMY2 weather file is used as a reference temperature for the dynamic simulations.

3.2.1 Archetype models

The primary school form and geometry is based on the baseline designs for primary schools developed by the UK Education Funding Agency (EFA, 2014). These designs demonstrate good practice and are based on the department's guidelines for area planning. The model simulation consists of 14 thermal zones building spread over two stories. The largest proportion of the surface is occupied by classrooms, staff's offices, laboratories, and the main hall. Other minor zones are comprised by corridors, bathrooms, and other common rooms. The considered HVAC system is based on a conventional gas boiler with an efficiency of 80% with no heat recovery; also, no cooling mode is considered. High-temperature radiators with 90/70 inlet/outlet temperatures are considered as the emission system. On the other hand, and following the UK offices archetypes developed by Korolija et al. (2013), in this research an open-plan office model based on 6 thermal zones spread over three stories is used. A previous analysis of the model showed high homogeneity between areas, for this reason fewer thermal zones are analyzed compared with the primary school. This archetype consists only in office areas and common areas (including bathrooms and kitchen) at each of the three floors. The HVAC system is encompassed by a gas boiler for heating purposes and a chiller to cover the cooling demands. Fan-coil units are considered as the emission systems. For both models a poor insulation on the buildings' envelope is considered as the baseline scenario. Finally, storage technologies are not considered in this study. Both virtual models can be seen in Figure 3. All the variables to populate the model such as envelope characteristics, occupancy patterns, thermostat temperatures, infiltration, and interior equipment are based on CIBSE guides and can be seen in Table 2.

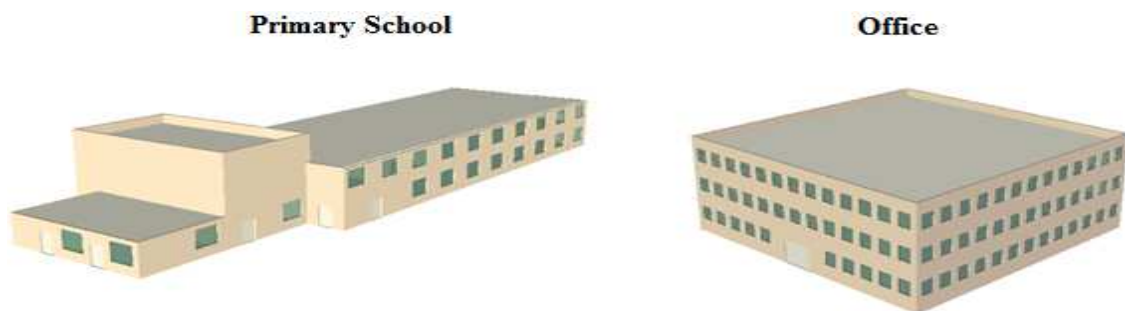


Figure 3: Archetype models buildings of a UK primary school and an office building

Finally, the calibration process of the models is supported with a recently CIBSE report from Hong and Steadman (2013) based on a robust statistical analysis made on 73,160 Display

Energy Certificates of non-domestic buildings located in England and Wales. A great part of these certificates are from primary schools and air-conditioned offices (6,631 and 234 respectively) which give us confidence to calibrate the archetypes with the EUI (energy usage indicators – kWh/m²-year) obtained in the study.

3.3 Carbon reduction/Retrofit Scenarios

A “retrofit module” was developed that encompasses a variety of common retrofit measures applied to the case study buildings. The paper puts special attention on analysing the impact of systems such as gas boilers, ground-source heat pumps and district cooling/heating systems with their respective emission systems. Both archetypes are retrofitted with the same scenarios. *Case A* represents the same building model but with high thermal insulation levels as requested by the local current regulations. The purpose of *Case A* is to explore how effective are this current regulations (Part L2B) on the overall exergy efficiency of the system. This comes from the premise that these codes are developed under the first law only, and the impact on the exergy destructions is fairly unknown. The purpose of the rest of the cases is to analyze those programs that incentive low carbon technologies, especially those focused on the non-domestic sector. *Case B* and *Case C* consider same thermal properties as the *baseline* scenario but with a refurbishment at the generation and heating emission subsystems. For *Case B*, a ground source heat pump is analysed considering that the typical 90/70 radiators are retrofitted by AHU with heating/cooling coils. On the other hand, *Case C* studies the impact of connecting the premises to a hypothetical district heat network (heating and cooling modes for the office), where a CHP tri-generation plant generates heating and cooling energy. To maximize the potential of district heating, the heat emission system is retrofitted to slab and floor emission systems to handle low temperature heating and high temperature cooling. Finally, *Case D* and *Case E* are similar to *B* and *C* but with the difference that the building envelope is retrofitted to the latest regulations requirements, as simulated in *case A*. For each case, the HVAC system inlet and outlet temperatures required to achieve thermal comfort, are taken from the energy simulation outputs. For example, outputs for *Case E* (slab and floor heating connected to a district network) showed average inlet and outlet temperatures of 30 °C and 27 °C for heating mode and 15 °C and 20 °C for cooling mode. In all cases DHW system generation is not retrofitted and it is considered that the *baseline* gas boiler supplies the demanded hot water. Important values for the analysis such as Primary Energy Factors are taken from the Standard Assessment Procedure (Pout, 2011). Technical values of efficiency of HVAC equipment such as generation, distribution and emission systems had been taken from the EnergyPlus Engineering Reference document (EnergyPlus, 2012b) supported with values from Annex 49 pre-design tool manual (ECB-Annex49, 2011). A summary of the scenarios and assumptions is shown in Table 2.

3.4 Thermo-economic analysis

The exergetic cost of a product in a process is the exergy containing the fuel passing through the component plus the sum of irreversibilities or exergy destructions along the whole process. In the case of building energy systems, each subsystem has consumed some resource to produce a particular product. Typically the final products (P) are cooling, heating, heated water and electricity. But these products come from several resources (R), typically fuels with high exergy content like natural gas, electricity, or steam. To define this cost is necessary to define the limits of the system. In this research these boundaries were already defined as shown in section 2.1. First, an unitary exergy cost needs to be calculated for each part of the energy supply chain, and the cost of the inputs and outputs can be used to gain an understanding on the economics inside the whole chain process. The exergy cost of an energy

Table 2: Baseline building characteristics and refurbishment scenarios for the primary school and A/C office archetypes

Building and system Characteristics	Baseline	Case A	Case B	Case C	Case D	Case E
External wall (W/m ² K)	1.7	0.17	1.7	1.7	0.17	0.17
Roof (W/m ² K)	1.42	0.19	1.42	1.42	0.19	0.19
Ground floor (W/m ² K)	1.42	0.25	1.42	1.42	0.25	0.25
Glazing (W/m ² K)	5.7	1.3	5.7	5.7	1.3	1.3
Infiltration (ach)	1.05	0.35	1.05	1.05	0.35	0.35
Glazing (%)	30%	30%	30%	30%	30%	30%
Lighting load (W/m ²)	12	12	12	12	12	12
Misc. Load avg.(W/m ²)	5 / 15 ^a	5 / 15 ^a	5 / 15 ^a	5 / 15 ^a	5 / 15 ^a	5 / 15 ^a
HVAC System*	<i>Gas Boiler and Chiller</i>	<i>Gas Boiler and Chiller</i>	<i>Ground heat pump W/W</i>	<i>LT District Heating/ Cooling</i>	<i>Ground heat pump W/W</i>	<i>LT District Heating/ Cooling</i>
Main energy sources for space conditioning	Natural Gas and Electricity	Natural Gas and Electricity	Electricity	Heated/ Cooled Water	Electricity	Heated/ Cooled Water
Thermal efficiency	0.8	0.8	4.61	0.89	4.61	0.89
Cooling efficiency/ COP	2.5	2.5	3.0	0.89	3.0	0.89
Primary energy factor fossil $F_{P, \text{fossil}}$	1.112	1.112	2.58	0	2.58	0
Heating/Cooling supply temperatures (°C)	90/5 ^a	90/5 ^a	60/12 ^a	50/15 ^a	60/12 ^a	30/15 ^a
Emission System	<i>Office: Fan coil School: Radiator HT 90/70</i>	<i>Office: Fan coil School: Radiator HT 90/70</i>	<i>AHU (heating / cooling coils)</i>	<i>Hydronic Slab and floor heating</i>	<i>AHU (heating / cooling coils)</i>	<i>Hydronic Slab and floor heating</i>
Heating/Cooling return Temp (°C)	70/13 ^a	70/13 ^a	30/19 ^a	38/20 ^a	30/19 ^a	27/20 ^a
Heat loss / efficiency	0.95	0.95	0.95	0.99	0.95	0.99

*Cooling equipment is only considered for the A/C Office archetype,

^a Values only for the office archetype

stream is the amount of exergy required to produce it. According to Valero and Torres (2009) the average exergy cost can be written as:

$$k_i^* = \frac{E_i^*}{E_i} \quad (1)$$

Where E_i^* represents the exergy cost and E_i is exergy of the product stream. A complete exergoeconomic analysis takes into consideration the economic cost of the consumed fuel c_F (market price in £/kWh) plus as the capital investment and the cost of the installation and operation of the system (\dot{Z} [£/h]); this defines the amount of total money needed to generate an energy flow. Therefore the economic cost balance is written as:

$$C_{p,tot} = C_{F,total} + Z_{tot}^{CI} + Z_{tot}^{OM} \quad (2)$$

In buildings the determination or estimation of products cost can be essential to analyse retrofit options. The cost of each final product can be traced through the whole energy supply chain. If each cost of the internal streams between the subsystems is assessed, this can be used to compare them with standard or reference cost values with the objective to avoid excessive resource consumption. The determination of all cost of the streams is useful to make trade-off analysis of the economics of the subsystem components to help the retrofit decision making. For this research only a first insight into the exergy cost of the fuels used at the generation subsystem in the different scenarios is presented. According to Balta (2012), the exergy cost is calculated using the next equation:

$$C_{F,total} = \dot{E}x_{dest} * (t * k * z) \quad (3)$$

Therefore, unitary cost (£/kWh) is given by

$$\dot{C}_{F,total} = \frac{C_{F,total}}{Ex_{in}} \quad (4)$$

4. RESULTS ANALYSIS AND DISCUSSION

4.1 Pre-retrofit analysis (Baseline Scenarios)

4.1.1 Energy analysis (electricity and gas use)

With the intention to understand the typical performance, a comparison is made between the primary school and the office energy outputs. The results show different usage patterns, especially in summer months where a cooling demand can be appreciated in office buildings. In both buildings, the largest resource demand is gas, which represents 80.3% and 58.3% of the annual demand for the primary school and the office respectively. The normalized energy use obtained from the primary school model was at 264.82 kWh/m²-year, where nearly 68% is represented by heating, 11% by DHW, 8% by lighting and 5% by internal equipment. Meanwhile for the office baseline scenario the EUI obtained was at 254.46 kWh/m²-year, where 52% is used for heating, and only 6% to cooling. Both interior equipment and lights represent 32% of the total usage. Detailed information of monthly energy usage by type of building, end-use and type of fuel can be seen in Figure 4.

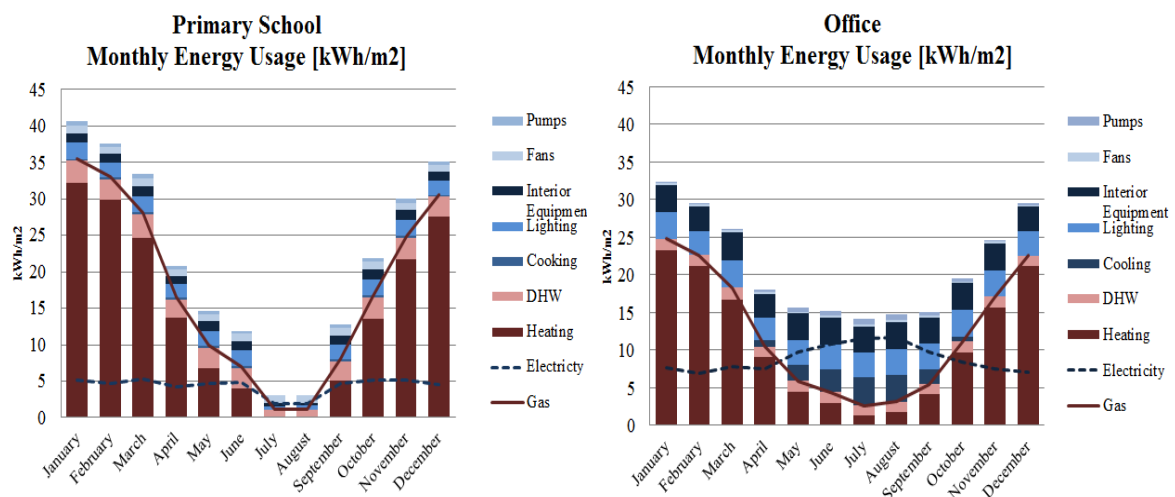


Figure 4: Monthly energy usage for both case studies baseline scenarios

4.1.2 Exergy analysis at baseline scenarios (irreversibilities)

So far no studies on exergy utilisation, irreversibilities and/or exergy efficiency improvement potential have been applied to the UK non-domestic sector. The result obtained expresses the

actual thermodynamic efficiency of the typical analysed buildings and gives us more insight on how exergy is diminishing inside the energy supply chain. To show the advantages of a dynamical exergy modelling, Figure 5 shows the hourly exergy destructions at each stage of the supply chain. This gives us a direct comparison on the magnitudes of exergy irreversibilities in typical subsystems of non-domestic buildings located in London, UK.

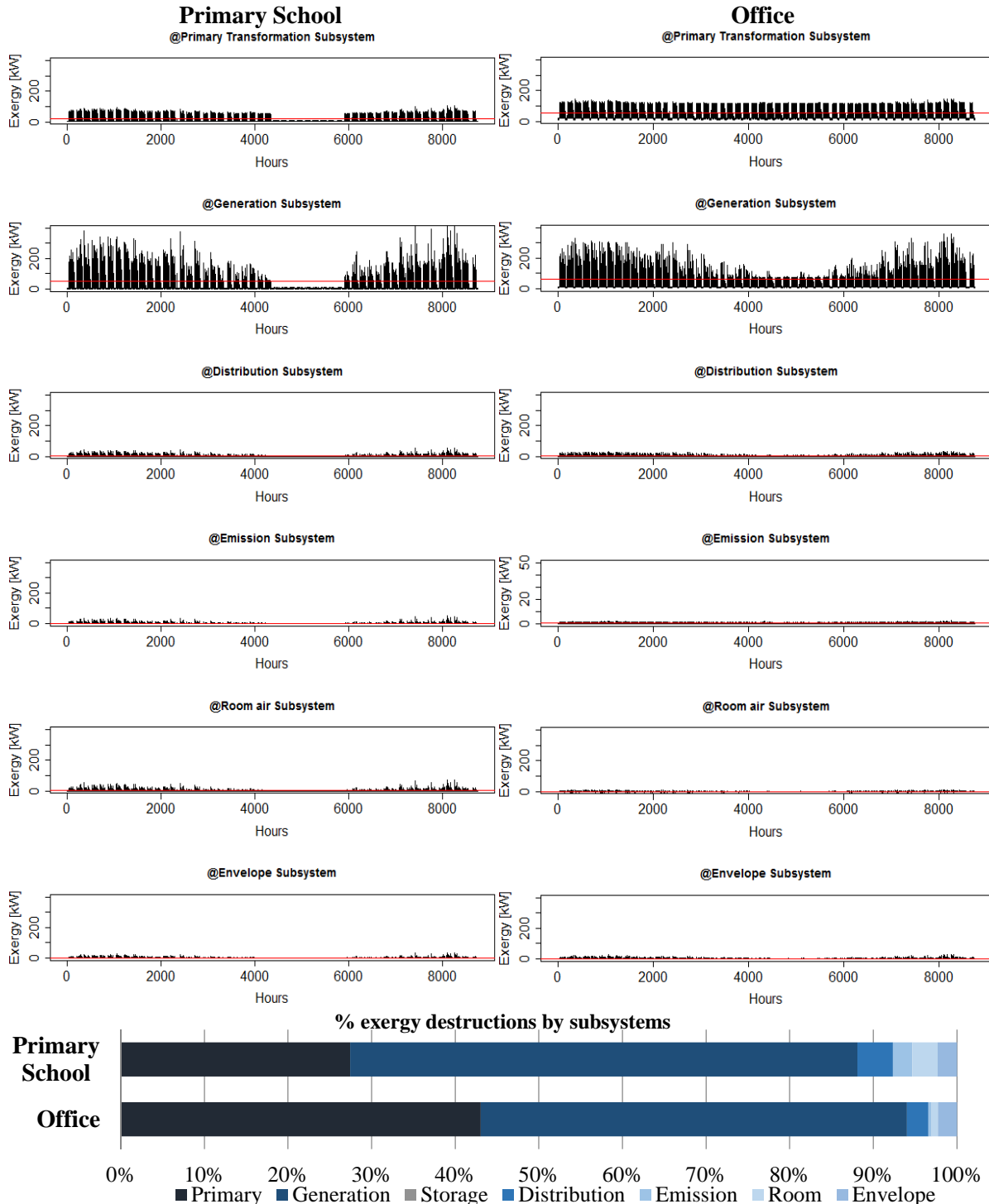


Figure 5: Hourly exergy destructions and percentage of exergy by subsystems of a typical primary school and an A/C office building

In both types of buildings the largest exergy destructions occur at the primary transformation and at the generation stage, representing 88% and 94% of the total exergy destructions for

schools and offices respectively. Also, special attention should be put on the distribution subsystem, where the range of destructions is between 3% and 5% of the total.

4.2 Retrofit scenarios analysis

In this section, outputs from the five different retrofit scenarios are assessed by analyzing the annual energy use and exergy destruction savings through the building energy supply chain.

4.2.1 Energy Analysis

By considering only the typical energy calculations that is applied to the majority of retrofit projects, the 1st law analysis shows that for the primary school the largest energy demand reductions come from implementing *Case E*, which means retrofitting the school with the latest minimum requirements for insulation plus connecting the premise to a district heating network supported by low temperature hydronic emission system (floor and slab heating). The model shows a maximum improvement of 70.1% (From 264.8 to 79.2 [kWh/m²-year]). For the office building the outputs are different, the model shows that the largest reductions will come by implementing *Case D*, which is the installation of a GSHP with high insulation levels on the building envelope. This will result in an improvement of 49.8% of the annual demand (From 254.7 to 127.9 [kWh/m²-year]). The outputs confirms, only from a 1st law perspective, that full advantage is taken when both cooling and heating modes are met by the heat pump. Also, unlike in the school case, the model shows that by having higher insulation levels, the cooling demand increased; for this reason, the same scenarios have a lower impact that those found on the primary school. Figure 6 summarises the outputs of all retrofit scenarios.

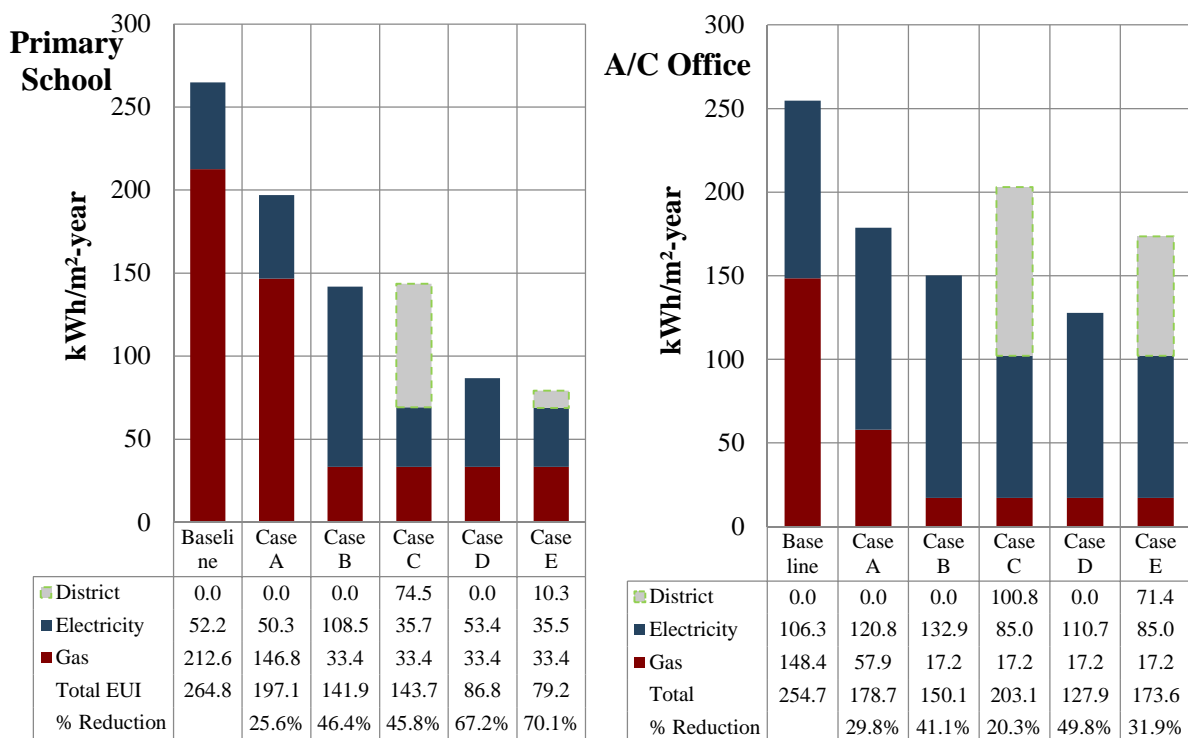


Figure 6: Energy analysis of the different refurbishment measures applied to a typical primary school and an A/C office building.

For both buildings it can be concluded that typical insulation improvements have a reduction impact of almost 30% on the total energy demand. Holistic retrofits (at envelope and HVAC system level) have a high impact on the primary school; while for the office building, only the use of the GSHP combined with insulation improvements has a significant variation (almost 50%).

4.2.2 Exergy analysis

Before analysing all the cases, it is of interest of this research to know the impact that insulation improvement have on the exergy demand of the analysed non-domestic buildings. The simplified exergy demand at the room and a comparison between the exergy demands for the *baseline* scenario against the *Case A* is made. Unlike the energy analysis, the exergy demand is not calculated using “exergy balance” equations, instead is calculated by using the energy balance values (in this case given by EnergyPlus) multiplied by the Carnot factor (Eq. 6).

$$Ex_{dem}(t_k) = \left(1 - \frac{T_o(t_k)}{T_r(t_k)}\right) * Q(t_k) \quad (5)$$

Figure 7 shows the impact that the insulation levels have on the hourly exergy demand. It is noted a big reduction in both cases. For the office, the values below zero on the vertical axis do not represent a negative demand; instead it represents the demand for cooling exergy. Because the primary school lacks cooling demand all the values are on zero or above zero.

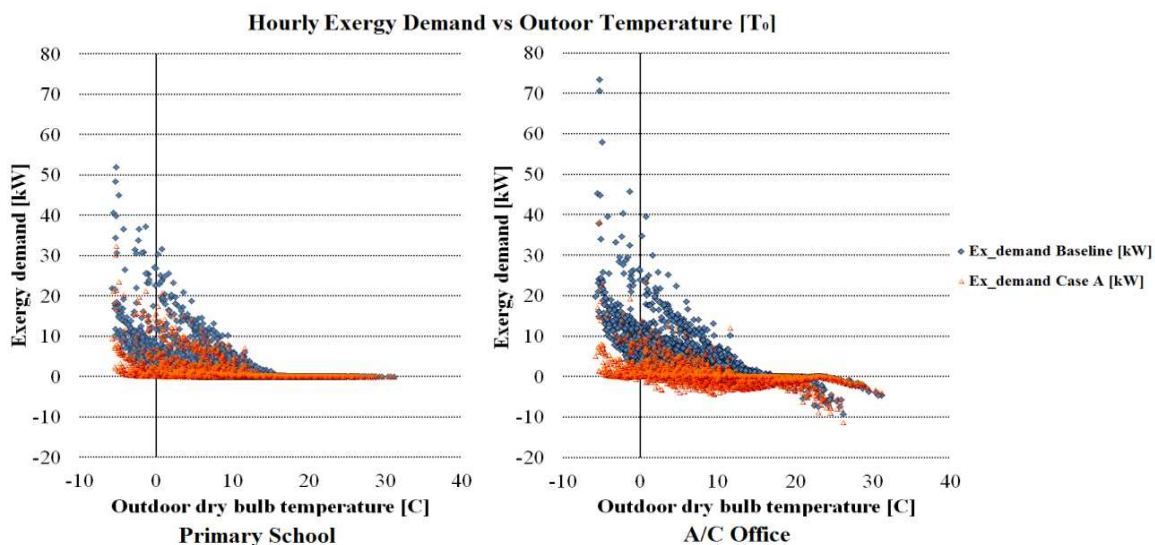


Figure 7: Exergy demand vs Outdoor Temperature of low insulated and high insulated non-domestic building archetypes

Unlike energy, when more exergy is supplied than demanded, this will not lead to overheating or overcooling, instead it leads to more thermodynamic destructions or irreversibilities (ECB-Annex49, 2011).

4.2.3 Exergy flows

In Figure 8 and Figure 9 the flow of exergy through the supply chain is showed for the primary school and the office respectively. Because the retrofits were oriented to the thermal and space conditioning systems improvement, the graphs only show exergy destruction inside the HVAC systems (including destructions by auxiliary energy); therefore, in this case we are not showing the exergy flows of other end uses (lighting, equipment, DHW). For the school, the *baseline* and *Case A* scenarios present the largest destructions at the “generation subsystem” (where high grade fuel is burned by the boiler). For the rest of the cases the largest destructions take place at the “primary energy transformation subsystem” where electricity is generated in power plants. Also, the “distribution subsystem” present losses equivalent to 10% of the total losses. Overall, the largest exergy destruction minimization is given by *Case E*, with a total exergy destruction reduction of 70.7%. The minimum improvement is given by *Case B*, with an improvement of only 5.6%. *Case C*, the district heating scenario with poor insulation values, also gives significant reductions (41.5%).

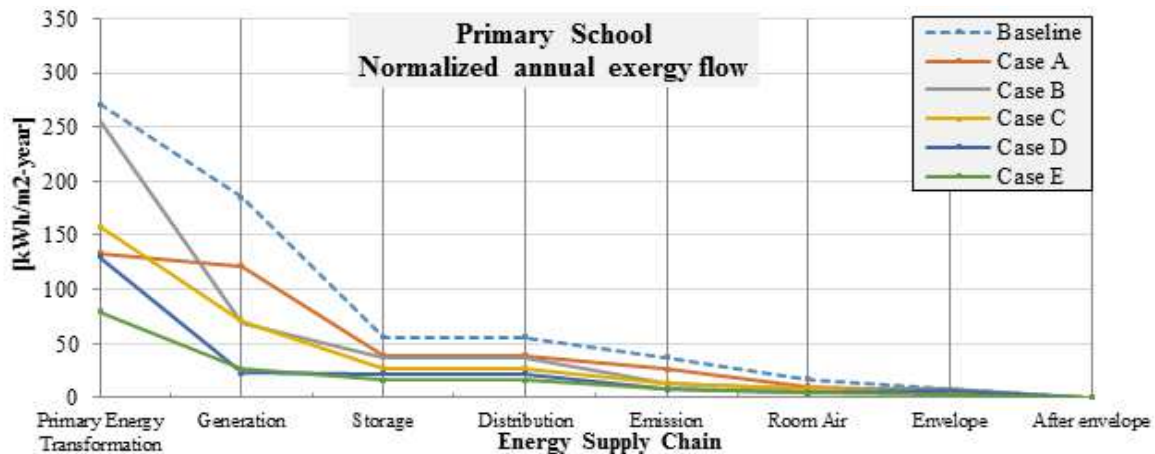


Figure 8: Normalized exergy flows for a typical primary school in the UK.

For all the scenarios in the office case, the major irreversibilities take place at the “primary transformation” level, due to the high demand of electricity from the chillers or heat pumps to cover the cooling demand and the constant daily use of high grade fuel at the district plant to generate the heating and cooling energy. As it can be seen in the graph, the exergy improvement is not as large as in the school case. In fact, *Case A* present the best exergy improvement with a 30.4% reduction. The lowest impact is given by *Case B* with a reduction of only 6.7%. The improvement of only the HVAC equipment (*Case B* and *Case C*) doesn't lead to significant reductions compared to the installation of a GSHP combined with an improvement of insulation at the envelope, leading to a reduction of 25.8%. If we consider the analysis from the Generation stage (only at a building level), similar to a typical energy retrofit analysis, the largest reductions are given by *Case D* (blue line). This shows the importance of how different thermodynamic boundaries can affect the analysis.

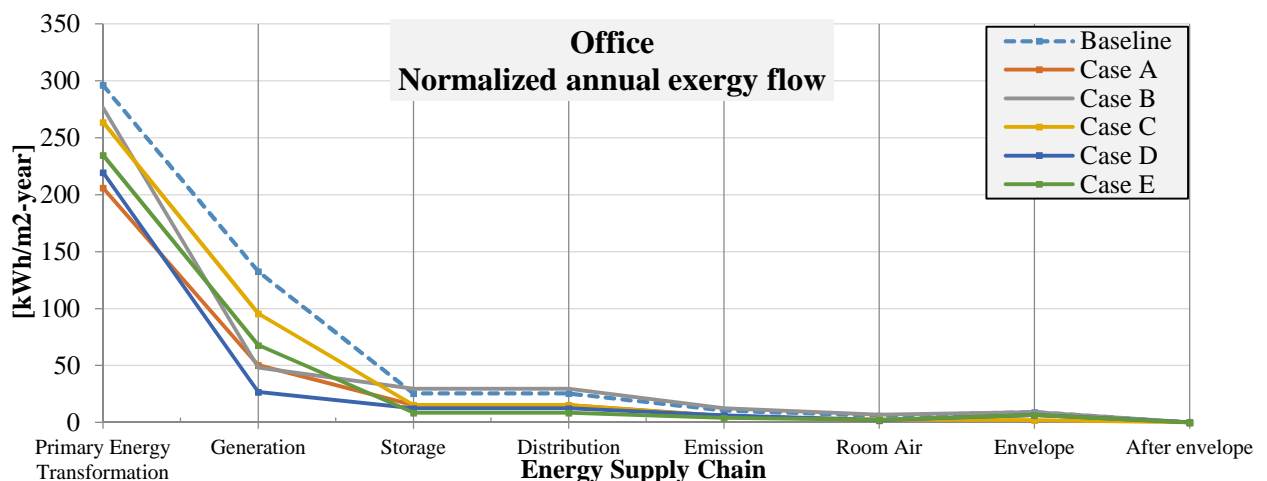


Figure 9: Normalized exergy flows for a typical A/C office building in the UK.

In both buildings, the installation of heat pumps without improving any levels on the insulation (as in *Case B*), leads to the lowest exergy improvements. On the other hand, the solely improvement of insulation levels (as *case A*) leads to a much larger exergy destruction reductions (50.7% and 30.4% for the school and office respectively). A holistic approach will lead to the largest reductions, but in a real situation the economic factor will probably limit these scenarios. Analysing the district systems cases (*C* and *E*) we have to consider that the Primary Transformation, Generation, and part of the Distribution subsystems usually are located outside the building physical boundary. Also, it appears that a district system functions

better when only heating mode is considered as shown in the school case. When both heating and cooling are required, a heat pump system appears to be a better option.

4.2.4 Exergy efficiency

Exergy efficiency is based on the relationship between the exergy demand by the building and the exergy supplied by the system. The annual exergy efficiency of each case is calculated by using the hourly efficiencies obtained by the model and the related internal zone temperatures and outdoor temperatures. These are given by the next equation:

$$\psi_{avg} = \frac{1}{N} \sum_{k=1}^{k=N} \eta(t_k) \left(1 - \frac{T_o(t_k)}{T_r(t_k)}\right) \quad (6)$$

If the “whole-system exergy efficiency” were the main decision factor in a retrofit project, the chosen scenario for the primary school will be the connection to a district heating system and the improvement of the insulation levels of the building. For the office, it will be also the connection to a district heating/cooling network but leaving the same insulation levels of the building envelope as found on the *baseline* case. But these efficiencies have a larger impact at a national level, because it considers the whole chain, meaning that the irreversibilities at power plants are also considered.

Table 3: Whole supply chain exergy efficiency (Ψ) for every retrofit scenario

(Ψ) system	Baseline	Case A	Case B	Case C	Case D	Case E
Primary School	2.18%	2.28%	2.10%	2.30%	2.28%	2.41%
Office	2.47%	2.71%	2.90%	4.46%	3.12%	4.00%

If we only consider the efficiency at the building level, which is the efficiency that most building practitioners care about, the best value for both the primary school and the office is found at *Case D*. This case represents the installation of the GSHP and the improvement of the envelope insulation, with efficiencies close to 10%.

Table 4: HVAC exergy efficiency (Ψ) for every retrofit scenario

(Ψ) HVAC	Baseline	Case A	Case B	Case C	Case D	Case E
Primary School	2.43%	2.54%	6.05%	3.00%	11.74%	3.13%
Office	3.40%	4.75%	8.07%	4.96%	8.54%	4.45%

These results show how important are for the analysis the selection of boundaries. While some cases are more beneficial at the national energy system level, others will be more beneficial at the building level. Here lies the importance of creating policies and incentives that are beneficial for all the stakeholders involved in this type of projects.

4.3 Thermo-economic analysis

4.3.1 Annual cost by exergy destructions at the generation stage

To give a larger picture, a simplified thermo-economic analysis is applied after the latest exergy analysis. An exergy cost of the fuels and a unitary cost per kWh are assessed for all cases by using equations 3 and 4. An important variable that is needed is the price of the fuels (Z). Natural gas, electricity, and district heating/cooling are the main fuels used in this analysis. The cost (£/kWh) of natural gas and electricity are taken from the latest national average quarterly prices (DECC, 2014). The cost of the fuel varies depending on the size of the consumer. According to the annual MWh usage of the models, the primary school *baseline* and *case A* scenario can be considered as a small non-domestic gas consumers (between 278 and 2777 MWh annually) that has an average price of 3.68 p/kWh. All other cases are considered as “very small” consumers

(<278 MWh), with an average price of 4.20 p/kWh. For electricity, all the cases lie into the “small” consumer category (between 20-499 MWh annually), with an average price of 11.84 p/kWh. These same tariffs are considered for the office building with a few differences between scenarios. In the case of the office, only the *baseline* scenario is considered as a “small” gas consumer with an annual usage above 278 MWh (400.7 MWh). All others scenarios are on the “very small” usage category. For electricity, all 6 cases are on the “small” category. On the other hand, district network prices (6.50 p/kWh) were taken from Shetland Heat and Energy Power tariffs (<http://www.sheap-ltd.co.uk/commercial-tariffs>), one of the few district networks that work in the UK market. The exergoeconomic values of the fuels and the unitary exergy cost are summarized in Table 5 and Table 6 for the school and the office respectively.

In the case of the school, *Case B* has the largest annual exergy cost due to the large usage of electricity by the heat pump system. *Case E* represents the lowest, where exergy from the district network is the predominant fuel. If we compare this value with the baseline scenario, a reduction of 91.92% is achieved. Also this scenario has the greatest exergy efficiency (as seen in section 3.2.3), which gives us the confidence that this is most effective scenario for the primary school.

Table 5: Exergy cost analysis at a generation subsystem in a Primary School

<u>Primary School</u>	Total Exergy Input (kWh)			ψ (%)	k (1/ ψ)	t (h/year)	$C_{F,total}$ (£/year)	$\dot{C}_{F,total}$ (£/kWh-year)
	Natural Gas	Electricity	District Energy					
Baseline	366,277	37,312	0	2.18	0.46	3,007	7,353	55
Case A	231,736	33,144	0	2.28	0.44	2,774	4,928	52
Case B	0	150,023	0	2.10	0.48	3,007	8,281	166
Case C	0	1,299	152,719	2.30	0.43	3,007	4,282	84
Case D	0	50,999	0	2.28	0.44	2,774	2,588	141
Case E	0	819	21,073	2.41	0.41	2,774	594	75

For the office, the exergoeconomic values show that the baseline scenario has the largest exergy cost for fuels. On the other hand, the most cost-effective scenario is represented by *Case D*, where the GSHP turned out to have a reduction of 48.51% compared to the baseline. Unlike in the school case, the lower exergetic expenditure is not followed by the most exergy efficient case (*Case C*). So a decision has to be made to which factor is more important from a retrofit point of view, exergy efficiency or total exergy cost.

Table 6: Exergy cost analysis at a generation subsystem in an A/C Office

<u>A/C Office</u>	Total Exergy Input (kWh)			ψ (%)	k (1/ ψ)	t (h/year)	C_{total} (£/year)	$\dot{C}_{F,total}$ (£/kWh-year)
	Natural Gas	Electricity	District Energy					
Baseline	332,166	26,073	0	2.47	0.40	4,669	5,505	72
Case A	103,098	32,833	0	2.71	0.37	4,663	2,950	101
Case B	0	129,956	0	2.90	0.34	4,669	5,152	185
Case C	0	2,310	255,904	4.46	0.22	4,669	3,622	65
Case D	0	72,638	0	3.12	0.32	4,663	2,671	171
Case E	0	2,055	181,203	4.00	0.25	4,663	2,885	73

For comparison purposes, the total exergetic cost (C_{total}) for both cases are summarized in Figure 10. It is notable the different impacts that each measure has on the total exergetic expenditure every year. For the primary school, *case E* improves 92% on the total exergetic cost, but *Case B* represents an increment of 13% on the annual exergy costs. For the office, *Case D* has an exergetic cost improvement of 51%, meanwhile *case B* only 6%.

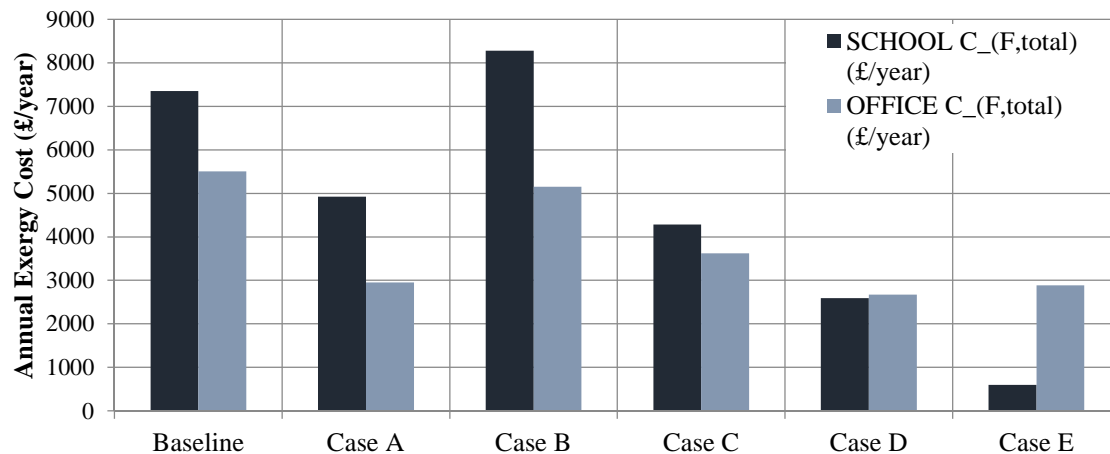


Figure 10: Comparison of the total annual exergy cost for the generation subsystem at a Primary School and a A/C Office building

Although this result only gives a first insight on the potential of using thermoeconomics by showing the total exergetic cost of the fuels at each scenario, still a complete thermoeconomic analysis is needed that considers capital cost investments and operation & maintenance costs, with the intention to have a more robust economic perspective. Also, the exergetic cost analysis needs to be implemented at each subsystem of the energy supply chain to discover where are located the largest economic expenditures throughout the whole system. This will give us enough information to locate the most energy/exergy efficient and cost-effective scenario.

5. CONCLUSIONS

The focus of this paper was to present how 2nd law theory (exergy and thermoeconomics) can be added to energy simulation tools to strengthen the typical analysis applied for the comparison and selection of the most optimal retrofit project. EnergyPlus was successfully used as a tool to perform 1st law analysis, which combined with an exergy and thermoeconomic module, it could become a powerful tool for a complete thermodynamic analysis. In this work this was done with the development of a post processing exergoeconomic add-on model.

The typical energy analysis, where building retrofit decisions are commonly based on, has shown the impact of different refurbishment projects on two typical non-domestic buildings. When we considered only “energy quantity”, the best retrofit scenario for the school was a combination of a district heating connection with high envelope insulation levels (*Case E*), obtaining a reduction of 70.1% of the annual energy used compared to the baseline scenario. For the office, the best scenario was represented by the installation of a GSHP combined with a high insulated building envelope (*Case D*); this scenario had a reduction of 49.8% compared to the baseline. When exergy analysis is added with the purpose to identify improvements that energy analysis is not adequate to do, the primary school showed that the largest minimization of irreversibilities were given by the same *Case E* scenario, with a reduction of 70.7%. But the results are different for the office, where *Case A*, that represents only the refurbishing on the building insulation levels, bring the largest minimization of exergy destructions with a decreasing of 30.4%. Last, a first insight of using exergy cost theory gave us a straight comparison on the different economic impact of the studied cases. When the exergetic cost is considered, the school still shows that *Case E* is the most cost-efficient scenario, with an exergetic expenditure of 593.93 £/year, representing a saving of 91.92% of the baseline exergy cost. But for the office, *case A, D* and *E* are very similar and all represent good exergy cost options. Of these scenarios, *Case E* has the largest economic reduction with a saving of 49.51% compared to the baseline scenario.

In the future, both heat pumps systems and district networks are technologies that could become the largest actors in the supply of energy to cover the UK space condition demand. Nowadays only 2% of the UK heating demand is covered by district networks. Technically, benefits apart for a reliable constant supply is the reduction of electricity peak demand, the reduction of power generation, and the reduction on infrastructure electricity distribution cost, including operational cost over the years. All this benefits indirectly were shown by the simple exergoeconomic study developed in this paper. Economics applied to retrofit projects should be more than a technique for energy saving, but should help in the diagnostic and optimization of system designs options. More robust economic models can assist and improve the accuracy of retrofit design options for non-domestic buildings. We believe that thermoeconomics could help to achieve important savings in life cycle cost and capital investments, making thermoeconomics an ideal tool for investment decisions by giving NPV and IRR analysis more information to work with. Also, exergy-oriented policies and taxation could help to deliver exergoeconomic methods applied to buildings more rapidly. Although at this moment, a big drawback of using thermoeconomics for retrofit decisions is that the second law is not a familiar concept between practitioners and others stakeholders in the building industry.

In the future it is intended to improve the thermoeconomic module by adding information on capital investment and operating cost of technologies. Data on cost of labour, equipment cost, operation & maintenance cost, and energy process are needed to perform a complete thermoeconomic analysis. Also, since the selected model archetypes are fairly representatives of the UK non-domestic sector, it is intended to develop a bottom-up exergy-based stock model that could serve as a basis for a large-scale stock analysis with the objective of minimizing irreversibilities and improve efficiency along the non-domestic sector. This could also help for the formulation of new policies based on exergy indicators.

REFERENCES

- Balta, M.T., 2012. *Exergetic cost analysis and sustainability assessment of various low exergy heating systems*. Energy and Buildings 55, 721-727.
- Bruhns, H., Steadman, P., Herring, H., 2000. *A database for modeling energy use in the non-domestic building stock of England and Wales*. Applied Energy 66, 277-297.
- DCLG, 2010. *L2B Conservation of fuel and power in existing buildings other than dwellings*. NBS, UK.
- DCLG, 2012. *Recast of the Energy Performance of Buildings Regulations*. Department for Communities and Local Government DCLG 1051.
- DECC, 2013. *The Future of Heating: Meeting the challenge*, United Kingdom.
- DECC, 2014. *Quarterly Energy Prices June 2014*, A.N.S. (Ed.), UK.
- ECB-Annex37, 2007. *Technical Synthesis Report: Low Exergy Systems for Heating and Cooling of Buildings*, IEA ECBCS, Jagpal, R. (Ed.), UK.
- ECB-Annex49, 2011. *Detailed Exergy Assessment Guidebook for the Built Environment*, IEA ECBCS, Torio, H., Schmidt, D. (Eds.). Fraunhofer IBP.
- EFA, 2014. *Baseline designs for schools: guidance*. Education Funding Agency, UK.
- EnergyPlus, 2012a. *Getting Started with EnergyPlus. Basic Concepts Manual*, University of Illinois and the University of California.
- EnergyPlus, 2012b. *EnergyPlus Engineering Reference*, p.p. 1278.

- Entrop, A.G., Brouwers, H.J.H., 2008. *Profit of exergy in the built environment*, World Sustainable Building Conference, Melbourne, Australia, pp. 3367-3374.
- Famuyibo, A.A., Duffy, A., Strachan, P., 2012. *Developing archetypes for domestic dwellings—An Irish case study*. *Energy and Buildings* 50, 150-157.
- Favrat, D., Marechal, F., Epelly, O., 2008. *The challenge of introducing an exergy indicator in a local law on energy*. *Energy* 33, 130-136.
- Gaggioli Richard, A., 1983. *Second Law Analysis for Process and Energy Engineering, Efficiency and Costing*. American Chemical Society, pp. 3-50.
- Garcia Kerdan, I., Raslan, R., Ruyssevelt, P., 2014. *An exergy - based simulation tool for retrofit analysis in UK school buildings*, Building Simulation & Optimization Conference 2014, London, UK.
- Gasparatos, A., El-Haram, M., Horner, M., 2009. *Assessing the sustainability of the UK society using thermodynamic concepts: Part 2*. *Renewable and Sustainable Energy Reviews* 13, 956-970.
- Hammond, G.P., Stapleton, A.J., 2001. *Exergy analysis of the United Kingdom energy system*. *Proceedings of the Institution of Mechanical Engineers, Part A: Journal of Power and Energy* 215, 141-162.
- Hong, S., Steadman, P., 2013. *An analysis of Dispal Energy Certificates for Public Buildings, 2008 to 2012*, in: CIBSE (Ed.). UCL Energy Institute.
- Jansen, S.C., Terés-Zubiaga, J., Luscuere, P.G., 2012. *The exergy approach for evaluating and developing an energy system for a social dwelling*. *Energy and Buildings* 55, 693-703.
- Korolija, I., Marjanovic-Halburd, L., Zhang, Y., Hanby, V.I., 2013. *UK office buildings archetypal model as methodological approach in development of regression models for predicting building energy consumption from heating and cooling demands*. *Energy and Buildings* 60, 152-162.
- Kumbaroğlu, G., Madlener, R., 2012. *Evaluation of economically optimal retrofit investment options for energy savings in buildings*. *Energy and Buildings* 49, 327-334.
- Ma, Z., Cooper, P., Daly, D., Ledo, L., 2012. *Existing building retrofits: Methodology and state-of-the-art*. *Energy and Buildings* 55, 889-902.
- Menassa, C.C., 2011. *Evaluating sustainable retrofits in existing buildings under uncertainty*. *Energy and Buildings* 43, 3576-3583.
- Ozgener, O., Hepbasli, A., Dincer, I., Rosen, M.A., 2005. *Modelling and assessment of ground-source heat pump systems using exergoeconomic analysis for building applications*. Ninth International IBPSA Conference. Montréal, Canada, 15–18.
- Pout, C.H., 2011. *Proposed Carbon Emission Factors and Primary Energy Factors for SAP 2012*, in: BRE (Ed.), Technical papers supporting SAP 2012, UK.
- Pout, C.H., Mackenzie, F., Bettle, R., 2002. *Carbon Emissions from Non-Domestic Buildings: 2000 and beyond*. Report 442 for DEFRA, BRE Ltd.
- Rosen, M.A., 2008. *A concise review of exergy-based economic methods*, Proceedings of the 3rd IASME/WSEAS international conference on Energy & environment. World Scientific and Engineering Academy and Society (WSEAS), Cambridge, UK, pp. 136-144.
- Rosen, M.A., 2002. *Does industry embrace exergy?* *Exergy, An International Journal* 2, 221.

- Rysanek, A.M., Choudhary, R., 2013. *Optimum building energy retrofits under technical and economic uncertainty*. Energy and Buildings 57, 324-337.
- Sakulpipatsin, P., Schmidt, D., 2005. *Exergy analysis applied to building design*, pp. 1-8.
- Schlueter, A., Thesseling, F., 2009. *Building information model based energy/exergy performance assessment in early design stages*. Automation in Construction, 18(2), 153-163.
- Schmidt, D., 2004. *Methodology for the Modelling of Thermally Activated Building Components in Low Exergy Design*, Civil and Architectural Engineering. Kungliga Tekniska Högskolan, Sweden.
- Shukuya, M., 2009. *Exergy concept and its application to the built environment*. Building and Environment 44, 1545-1550.
- Steadman, P., Bruhns, H., Gakovic, B., 2000. *Inferences about built form, construction, and fabric in the nondomestic building stock of England and Wales*. Environment and Planning B: Planning and Design 27, 733-758.
- Terés-Zubiaga, J., Jansen, S.C., Luscuere, P., Sala, J.M., 2013. *Dynamic exergy analysis of energy systems for a social dwelling and exergy based system improvement*. Energy and Buildings 64, 359-371.
- Tozer, R., Lozano Serrano, M.A., Valero Capilla, A., James, R., 1996. *Thermoeconomics applied to an air conditioning system with cogeneration*. Building Services Engineering Research and Technology 17, 37-42.
- Ucar, A., 2010. *Thermoeconomic analysis method for optimization of insulation thickness for the four different climatic regions of Turkey*. Energy 35, 1854-1864.
- UK-Government, 2008. *Climate Change Act 2008*. UK Government.
- Valero, A., Torres, C., 2009. *Thermoeconomic Analysis*, Frangopoulos, C.A. (Ed.), Exergy, energy system analysis, and optimization. EOLSS, p. 454.

ACKNOWLEDGEMENTS

The first author acknowledges support from The Mexican National Council for Science and Technology (CONACyT) through a scholarship to pursue graduate studies.

NOMENCLATURE

$C_{F,total}$	total exergetic cost of the fuel (£)	Q	energy demand (kW)
$\dot{c}_{F,total}$	unitary exergetic cost of the fuel (£/kWh)	t	operation hours per year (h/year)
$C_{p,tot}$	total exergoeconomic cost of the product (£)	T_0	reference temperature (k)
E_i	exergy cost (£)	T_r	room temperature (k)
E_i^*	exergy cost of the product (£)	z	exergetic cost of the fuel (£/kWh)
$\dot{E}x_{dest}$	exergy destructions (kW)	Z_{tot}^{CI}	capital investment cost (£)
Ex_{dem}	hourly exergy demand (kW)	Z_{tot}^{OM}	operation & maintenance cost (£)
$\dot{E}x_{in}$	average exergy input (kW)	η	energy efficiency (-)
k	inverse of the exergy efficiency (-)	ψ_{avg}	exergy efficiency (-)
k_i^*	average exergy cost (£)		

The Potential of Air-Water Heat Pumps in a Belgian Residential Retrofit Context in relation to Future Electricity Prices

Evelyn Heylen^{1*}, Romain Jordens¹, Dieter Patteeuw², Lieve Helsen²

⁽¹⁾Master Energy KU Leuven, Leuven, Belgium

⁽²⁾Department of Mechanical Engineering, Division of Applied Mechanics and Energy Conversion (TME),
Leuven, Belgium

1. ABSTRACT

Retrofitting plays an important role in reducing space heating energy demand in the Belgian residential building stock. Moreover, retrofitted buildings allow the application of low temperature heat emission systems combined with heat pumps. In this context, the potential of air-water heat pumps is assessed from an energetic and economic point of view, by considering multiple combinations of building retrofit options, heating system components and energy prices, resulting in different scenarios. Each scenario leads to a different space heating demand while domestic hot water demand is equal in all cases. Results of dynamic simulations in Modelica show that retrofitting the building envelope is always beneficial from an energetic point of view, but the economic viability strongly depends on the age of the dwelling and energy prices. Regarding the heating system, a single stage heat pump combined with a low temperature heat emission system, amongst which the recuperated original radiators are also taken into account, leads to the lowest energy use. A gas condensing boiler is still the most cost effective solution with current prices in Belgium, but the ratio between mean electricity price and gas price appears to be one of the most important drivers for the competitiveness of heat pumps.

Keywords: Air water heat pump, hybrid heat pump, fan supported radiator, retrofit, residential, electricity price profiles

NOMENCLATURE

CAPEX Capital expenditures

DHW Domestic hot water

DPP Dynamic pay back period

FH Floor heating

FSR Fan supported radiators

GCB Gas condensing boiler

HDD Heating degree days

HTHP High temperature heat pump

LTHP Low temperature heat pump

NZEB Nearly zero energy building

OPEX Operational expenditures

PPD Predicted percentage of dissatisfied

TCO Total cost of ownership

2. INTRODUCTION

Climate change, large energy expenses and energy security have made the European Union set strict regulations within energy policy, amongst which regulations considering the electricity sector and residential buildings. The former regulations are expected to lower the CO₂-intensity of electricity generation in the future (Delarue et al., 2011; Keay, Rhys, & Robinson, 2012). The latter regulation is the European Energy Performance of Buildings Directive (EPBD) and regulates the energy performance of new dwellings (The European parliament & the Council of the European Union, 2010). However, presently the existing residential building stock accounts for 25% of total energy use in Europe (Poel, van Cruchten, & Balaras, 2007), of which 82% for domestic hot water (DHW) production and space conditioning (Pérez-Lombard, Ortiz, & Pout, 2008). Therefore, the existing building stock presents a large potential for reducing energy demand, since in Europe more than 50% of today's buildings is built before 1970 and about 33% of the dwellings between 1970 and 1990 (Poel et al., 2007; Norris & Shielsn, 2004). Retrofitting older buildings can significantly lower energy demand, because it reduces the need for space conditioning (Verbeeck & Hens, 2005) and makes these buildings suitable for low temperature emission systems (Schmidt, 2009). The possibility of applying these emission systems, combined with the expected lower CO₂-intensity of electricity, can make heat pumps a competitive heating system as opposed to conventional heating solutions using fossil fuels. Especially air-source heat pumps are seen as an attractive option for residences, due to their lower investment cost compared to ground-coupled heat pumps (Cabrol & Rowley, 2012). The latter have benefits when the building has both heating and cooling loads, typically in the tertiary sector.

This paper investigates two approaches for decreasing the energy demand of old buildings. On the one hand, an improvement of the building envelope by insulating roofs, floor and walls and placing windows with high performance glazing is considered. Three generations of building stock, from the periods 1946 - 1970, 1971 - 1990 and 1991 - 2005, are retrofitted to the newest standards (Flemish Energy Agency (VEA), 2013). On the other hand, the reference gas condensing boiler (GCB) is compared to more energy efficient heating systems, being low and high temperature heat pumps (resp. LTHP and HTHP) and hybrid heat pumps (HHP). These heat production systems are combined with three heat emission systems, namely the recuperated radiators, fan supported radiators (FSR) and floor heating (FH). Well-chosen system configurations that combine the two energy demand reduction approaches, are compared by performing dynamic simulations. The advantage of this methodology is that the energy use can be determined more precisely, since effects such as lower part load efficiencies and losses due to intermittent heating are included in the simulation models. These dynamic simulations are based on a global system approach using IDEAS component models (De Coninck, Baetens, Saelens, Woyte, & Helsen, 2014; Baetens et al., 2012) in the modelling language Modelica using Dymola as interface.

Various studies investigate the performance of heat pumps, but these studies generally lack to consider retrofitting the building envelope or other emission systems (Cabrol & Rowley, 2012; Huchtemann & Müller, 2012; Kelly & Cockroft, 2011; Van der Veken, Hens, Peeters, Helsen, & D'haeseleer, 2006). Results of these studies strongly depend on the boundary conditions considered, such as the CO₂-intensity of the electricity generation park and the primary energy factors. However, they indicate that lower CO₂-emissions are already possible if air water heat pumps are applied, even with current fuel mixes for electricity production (Huchtemann & Müller, 2012).

Verbeeck et al. (Verbeeck & Hens, 2005) proposed a logical hierarchy of energy-saving measures, preferring insulation improvement of building components above more energy

efficient heating systems and renewable energy systems. These conclusions were based on a static calculation procedure as stated in the Flemish Energy Performance Regulation (EPR) (Department of the Flemish community, 2006; Flemish government, 2006). This EPR calculation method will be used in the current work to verify results of dynamic simulations even though it does not contain the newest technologies such as hybrid heat pumps or fan supported radiators.

The aim of this work is to assess how various combinations of retrofit measures impact the energetic and economic potential of air-water heat pumps in a residential retrofit context. First, the assessment methodology is described in section 3, followed by an overview of data and models in section 4. The results of the energetic and economic analysis are summarized in section 5 and a discussion of the results is given in section 6. Finally, section 7 summarizes the main conclusions of the paper.

3. METHODOLOGY

The quantitative indicator in the energy analysis is primary energy use for heating cumulated over one year. The energy use considered in this study includes the gas use of the GCB ($P_{gas}(t)$ [W]), electricity needed for the electronics and the fan of the GCB ($P_{GCB,elec}(t)$ [W]) and the electricity use of the heat pump ($P_{HP}(t)$ [W]), circulation pumps ($P_{pumps}(t)$ [W]) and fan supported radiators ($P_{FSR}(t)$ [W]) if present. Mechanical ventilation and other electrical appliances are not taken into account. The conversion factor between electricity and primary energy is taken equal to 2.5 and 1 for natural gas to primary energy (Verbeeck & Hens, 2005). Equation (1) is used to calculate the primary energy use.

$$E_{prim} = \int_{1year} P_{elec}(t) dt \cdot 2.5 + \int_{1year} P_{gas}(t) dt \cdot 1 \quad (1)$$

with $P_{elec}(t) = P_{HP}(t) + P_{pumps}(t) + P_{FSR}(t) + P_{GCB,elec}(t)$

In order to make an honest energetic comparison, the indoor operative temperature needs to be within similar comfort bounds in every case (Peeters, de Dear, Hensen, & D'haeseleer, 2009; Van der Linden, Boerstra, Raue, Kurvers, & De Dear, 2006).

The economic viability of the retrofit options for the building envelope and the heating system is evaluated based on two indicators, namely the total cost of ownership (TCO) [€] and the dynamic pay back period (DPP) [years]. The total cost of ownership (Verbeeck & Hens, 2005; Kaynakli, 2012) is a financial indicator which is used to assess the viability of a certain investment by actualizing all associated costs over a period:

$$TCO = I_0 + \sum_{x,y,z} \frac{I_j}{(1+a_g)^j} + \sum_{i=1}^n \left[\frac{K_{elec}(1+r_{elec})^i}{(1+a_g)^i} + \frac{K_{gas}(1+r_{gas})^i}{(1+a_g)^i} + \frac{K_M(1+r_M)^i}{(1+a_g)^i} + \frac{K_{CO_2}(1+r_{CO_2})^i}{(1+a_g)^i} \right] \quad (2)$$

In this study, the costs of initial investment I_0 and reinvestment I_j in the years x, y and z, and the annual costs of maintenance K_M , electricity K_{elec} , gas K_{gas} and CO₂-emissions K_{CO_2} are considered to determine the TCO. Investment costs consist of material costs of different elements of the heating system and the improvement of the building envelope, labour cost and 6% VAT (Federal State Service for Finances, 2012). Prices of the installations used are a combination of prices and information of manufacturers complemented with prices of research centers as shown in table 1. Prices of retrofit measures of the building envelope are given in the lower part of table 1 (based on updated information from (De Coninck & Verbeeck, 2012)).

The heating system and the windows need reinvestments every 20 and 25 years respectively. Local subsidies are not taken into account.

Table 1: Investment costs of installations and prices of retrofit measures of the building envelope based on updated information from (De Coninck & Verbeeck, 2012) and manufacturers' data.

Installation	Price I_0 [€] ¹	Maintenance [€/year]	Life time [years]
GCB	2605	$0.02I_0$	20
HHP	6000	$0.04I_0$	20
LTHP ²	$424.73 \cdot \dot{Q}_{nom,2/35} + 2996.8$	$0.04I_0$	20
HTHP ²	$322.32 \cdot \dot{Q}_{nom,2/35} + 5645.7$	$0.04I_0$	20
FSR ³	$1379 \cdot \#pieces$	///	>35
FH ^{3,4}	$740 \cdot \dot{Q}_{nom} + 109$	///	>35

¹ Excl. VAT

² $\dot{Q}_{nom,2/35}$ = Nominal power of the heat pump at 2°C/35°C [kW]

³ Labour cost included

⁴ \dot{Q}_{nom} = Heat power demand of the building by prEN 12831 [kW]

Retrofit measure	Price I_0 [€] ¹
Roof insulation	$132 \cdot \text{Volume insulating material [m}^3\text{]}$
Floor insulation	$221 \cdot \text{Volume insulating material [m}^3\text{]} + 4 \cdot \text{Floor area [m}^2\text{]}$
Facade insulation ²	$265 \cdot \text{Volume insulating material [m}^3\text{]} + 93 \cdot \text{Facade area [m}^2\text{]}$
Facade insulation ³	$22 \cdot \text{Facade area [m}^2\text{]}$
Windows	$328.5 \cdot \text{Window area [m}^2\text{]}$
Air tightness	$8.5 \cdot \text{Surface area to the outside [m}^2\text{]}$

¹ Excl. VAT and labor cost included

² Outside insulation of the facade

³ Cavity filling

Next to the capital expenditures (CAPEX), operational expenditures (OPEX) consist of maintenance costs, energy costs and CO₂-costs. Annual maintenance cost is expressed as a percentage of the investment cost (Parys, 2013), as indicated in table 1, and prices of gas and electricity are summarized in table 2. Only CO₂-emissions associated with energy use for heating in the dwelling are taken into account, thus embedded CO₂ is out of the scope of this research. As shown in the third and fourth column of the upper part of table 2, CO₂-cost is only a fraction of the total cost. As long as CO₂-costs do not rise significantly, these will not have a significant influence on the conclusions of the economic analysis.

Due to the variability of several cost parameters in the future, different scenarios are proposed. CO₂-prices and maintenance costs are kept constant in this study (r_M and r_{CO_2} equal 0). r_{gas} and r_{elec} represent the yearly percentage increase on top of the inflation of respectively the gas and electricity price, as shown in table 3. The exponent i in equation 2 corresponds to the considered year, while n is the period under consideration, which equals 50 years in this study. The actualisation rate a_g equals 2.5%.

The second evaluation method, the dynamic payback period, is defined as the period after which benefits outweigh costs. Contrary to the static payback period, the dynamic payback period takes into account derating of cash flows.

Table 2: The upper part summarizes energy prices (Flemish regulator of the electricity & gas markets (VREG), 20/05/2013; Eurostat European Commission, 2013) and CO₂-emissions (Verbeeck & Hens, 2005; Van der Veken et al., 2006) in the Belgian context. The last two columns show the total resource cost, CO₂-emissions included for two different CO₂-costs. The lower part gives the average, maximum and minimum value, and standard deviation of the variable electricity price profiles for France, Belgium and Germany.

Resource	Price	CO ₂ -emissions	Price + CO ₂ -cost	Price + CO ₂ -cost
	[€/kWh]	[kg/kWh]	€4.5/ton [€/kWh]	€40/ton [€/kWh]
Gas	0.07	0.2	0.0709	0.0780
Electricity (night)	0.15	0.31	0.1514	0.1624
Electricity (day)	0.25	0.31	0.2514	0.2624
Variable	Average	Maximum	Minimum	σ
Electricity price	[€/kWh]	[€/kWh]	[€/kWh]	[€/kWh]
France	0.14	0.27	-0.11	0.020
Belgium	0.22	0.35	-0.03	0.019
Germany	0.28	0.38	0.15	0.016

Table 3: Evolution of energy prices in Europe over the past 13 years. Yearly increases in terms of percentage are on top of the inflation (European commission, 2012; Flemish regulator of the electricity & gas markets (VREG), 20/05/2013)

Region or country	Yearly increase r_{gas} [%]	Yearly increase r_{elec} [%]
EU15	3.5	1.2
Germany	4.4	4.0
Belgium	4.0	1.6
Used yearly increase	4.0	2.1

4. CASE STUDY AND MODELLING

For this study, three representative dwellings constructed in different time periods are considered, each having construction components with an insulating quality that is typical for the respective building period in Belgium. As a reference case, all original dwellings are considered to be equipped with a gas condensing boiler and radiators designed for a supply temperature of 75°C and a temperature difference of 10°C.

4.1 Dwellings

The national brochure about the Belgian dwelling typology (Holm, Verbeke, & Stoppie, 2011) identifies different generations in Belgian building standards of which three generations are considered in this study, namely 1946-1970, 1971-1990 and 1991-2005. Table 4 summarizes typical parameters of the building envelope for each generation and values of these parameters after retrofitting the building in order to meet the requirements of EPB2014 energy regulations for buildings in Flanders (Flemish Energy Agency (VEA), 2013). The additional insulation of the facades is assumed to be added at the outside wall of the building. This technique requires higher investment costs than other insulation techniques, but the narrowness or absence of a cavity in walls of older building generations implies this insulation technique.

Table 4: Overview of building envelope parameters for considered building generations and after retrofitting (Retr) (Holm et al., 2011; Hens, 2010)

U-Value [W/m ² K]	'46-'70	'71-'90	'91-'05	Retr
Facade	1.7	1	0.6	0.24
Roof	1.9	0.85	0.6	0.24
Floor	0.85	0.85	0.7	0.3
Windows	5	3.5	3.5	1.8
Door	4	4	3.5	2
n_{50} -value [h^{-1}]	10	7	7	4
Heat power demand [kW]	29.3	18.2	14.5	8.7

In order to make reasonable comparisons for different generations, all dwellings are considered to be detached houses with the geometrical characteristics of the average Belgian detached dwelling as determined in the EL2EP study (Verbeeck & Hens, 2002) based on statistical data. The geometry of the dwellings is given in appendix A. The protected volume is 565 m³, the floor surface area 93 m² and the total external surface area 421 m². Table 5 summarizes percentage of glazing compared to the overall area of facades in different orientations.

Table 5: Areas of construction components complemented with the share of glazing in a particular building component

Building component	Area [m ²]	Percentage glazing [%]
Northern facade	47	1
Southern facade	58	19
Eastern facade	48	16
Western facade	48	14
Floor	93	-
Southern roof	54	-
Northern roof	73	-

The building is considered to be a single zone with convective and radiative heat transfer towards high order lumped capacitance building components (Baetens & Saelens, 2011). Building components such as facades, roofs and floors consist of typical Belgian construction layers. Facades as from generation 1971 - 1990 have typically an inner and outer wall with a cavity, eventually filled with insulation. The heat demand of every dwelling is calculated based on the EN12831- standard (European committee for standardization, 2003) using a design outside temperature of -10°C and an inside design temperature of 20°C for the single zone building.

4.2 Heating systems

Four heat production systems and three heat emission systems are considered. The considered heat production systems are: a gas condensing boiler (GCB), a low temperature heat pump (LTHP), a high temperature heat pump (HTHP) and a hybrid heat pump (HHP). The low temperature heat pump uses a single compression stage and can deliver heat up to a supply temperature of 60°C, while the high temperature heat pump employs two compression stages in order to reach supply temperatures of 80°C. These supply temperatures determine whether the system is considered in a certain scenario or not.

The models of the LTHP and gas condensing boiler are based on manufacturers' data and component models taken from the IDEAS library³ (De Coninck et al., 2014; Baetens et al., 2012). In case of the heat pump, manufacturers' data give the thermal and electrical power as a

function of the ambient air temperature, the supply temperature to the emission system and the frequency modulation of the heat pump compressor. For the GCB, the efficiency of the boiler is given as a function of mass flow rate and supply temperature to the emission system. The model of the HTHP is similar to the one of the LTHP, but based on other manufacturers' data. The LTHP and the HTHP, having a COP of 3.31 and 3.28 at 2°C/35°C respectively, are sized based on their heat power delivered at -10°C outside temperature and the required supply temperature of the emission system ($-10^{\circ}\text{C}/T_{supply}$) at 100% modulation in order to deliver the heat power demand as shown in the last row of table 4.

The hybrid heat pump is a combination of a LTHP and a GCB and is able to switch between the two devices depending on which of the two is the most cost effective at a specific moment in time. The model of the hybrid heat pump combines the model of the GCB and the LTHP complemented with an algorithm that controls the switching between the two devices based on cost effectiveness (Heylen & Jordens, 2013).

The three heat emission systems considered in this study are radiators (Rad), floor heating (FH) and fan supported radiators (FSR). In all buildings before retrofit (denoted with 'O' in table 6) radiators are installed with a nominal supply and return temperature of 75°C and 65°C, respectively. After a retrofit (denoted with 'R' in table 6), it is possible to recuperate these radiators. This results in a lower required supply temperature, because the nominal power of the radiators is higher than the heat demand of the dwelling, which makes the installation of a heat pump more attractive (Radson, 2012).

Floor heating is only considered in the retrofitted building, since the floor needs to be sufficiently insulated in order to use this emission system and the supply temperature should be kept below an upper limit, which limits the available heating power. Floor heating is modelled as a thermal resistance and capacitance circuit that transfer heat of water in embedded pipes through the floor to the room.

Fan supported radiators have a higher heat transfer coefficient than conventional radiators due to the combination of forced (fan assisted) convection and radiation, which lowers the needed supply temperature. They can be used in four different fan states. The model of the fan supported radiator is an extension of the model of the conventional radiator (similar to equation 3) with a heat transfer coefficient depending on different states of the fan as given by equation 4. As the nominal power of the four states Q_{nom} differ, the model will change the heat transfer coefficient of the FSR depending on the state of the fan. For a conventional radiator, the heat transfer coefficient in equation 4 remains constant and is calculated using nominal values. The equations of the conventional radiator model are the same as equations 3 and 4, with all values replaced by the respective values of the conventional radiator and a fixed nominal power \dot{Q}_{nom} .

³<https://github.com/open-ideas/IDEAS>

$$\dot{m}\Delta h + \dot{Q}_{total} = (m_{water}c_{p,water} + m_{drymass}c_{p,drymass}) \frac{dT_{avg,FSR}}{dt} \quad (3)$$

$$\text{with } \dot{Q}_{total} = UA(0.5(T_{sup} + T_{ret}) - T_{zone})^m$$

$$\text{and } UA = \frac{\dot{Q}_{nom}}{(0.5(T_{sup,Nom} + T_{ret,Nom}) - T_{zoneNom})^m} \quad (4)$$

\dot{m}	Mass flow rate of water through the FSR [kg/s]
Δh	Enthalpy difference between inlet and outlet of the FSR [J/kg]
m_{water}	Mass of the water in the FSR [kg]
$m_{drymass}$	Dry mass of the FSR [kg]
$c_{p,water}$	Specific heat constant of water [J/kgK]
$c_{p,drymass}$	Specific heat constant of the material of the FSR [J/kgK]
$T_{avg,FSR}$	Average temperature of the FSR [K]
\dot{Q}_{total}	Emitted heat power of the FSR [W]
T_{sup}	Supply temperature [K]
T_{ret}	Return temperature [K]
T_{zone}	Temperature of the zone [K]
m	Exponent of emission (i.e. 1.1 for FSR and 1.3 for radiators based on manufacturers' data)
\dot{Q}_{nom}	Nominal power of the respective state of the FSR, constant value for conventional radiator

$T_{i,nom}$ is indicating the nominal values of the respective temperatures. The algorithm to control switching between the four states of the fan can be found in (Heylen & Jordens, 2013).

Sizing of the FSR is based on data from manufacturers that give the nominal power in the four fan states as a function of the temperature difference between room and mean temperature of the FSR. On the one hand, it is advisable to keep the supply temperature as low as possible to increase the efficiency of the heat production device. On the other hand, this increases the investment cost because more radiator units are needed due to lower heat emission per unit. The used FSRs have a nominal power emission of respectively 204 W, 796 W, 1084 W and 1452 W in the four fan states at a mean temperature difference of 20°C between radiator and zone. The needed number of units to supply sufficient heat is determined based on the maximal power emission of 1452 W and the heat demand of table 4.

Table 6 summarizes combinations of heat production systems and heat emission systems that are considered. Combinations are selected based upon the required supply temperature of the emission system, as given between brackets. After a retrofit of the building envelope of the older dwellings, the recuperated radiators can be supplied with water at a lower temperature, as they were originally sized for a larger heat demand. Domestic hot water (DHW) profiles are the same in all dwellings and they are supplied by the heat production system that generates the space heating demand.

4.3 Heating curve control

The set point temperature of the heat production system is controlled using a heating curve approach (De Coninck et al., 2010), which determines the supply temperature to the emission system as a function of the ambient temperature as given by equation 5.

Table 6: Overview of considered combinations of heat production systems and heat emission systems. (Rad = radiators with nominal power expressed at 75/65/20 °C)

	GCB	HHP	HHP	LTHP
Rad 1946-1970	O(75) R(45)	R(45)	O(75)	R(45)
Rad 1971-1990	O(75) R(55)	R(55)	O(75) R(55)	R(55)
Rad 1991-2005	O(75) R(60)	R(60)	O(75) R(60)	
FSR		R(45)		O(45)R(45)
FH		R(35)		R(35)

O(x): Original state (without retrofit of building envelope)

R(x): Retrofitted state (with retrofit of building envelope)

x: Supply temperature [°C]

$$T_{sup} = T_{zone} + \left(\frac{T_{sup,Nom} + T_{ret,Nom}}{2} - T_{ret} \right) [z_{rel}^m]^{-1} + \left(\frac{T_{sup,Nom} - T_{ret,Nom}}{2} - T_{ret} \right) z_{rel} \quad (5)$$

with $z_{rel} = \frac{T_{zone} - T_{amb}}{T_{zone} - T_{design}}$ [], T_{zone} the actual room temperature [°C], T_{sup} the supply temperature [°C], $T_{sup,Nom}$ the nominal supply temperature [°C], T_{ret} the return temperature of the emission system, $T_{ret,Nom}$ the nominal return temperature, T_{amb} the ambient temperature [°C] and T_{design} the minimal ambient temperature used in the nominal heat demand calculation [°C]. The exponent m depends on the characteristics of the heat emission system and equals 1.3, 1.1 and 1 for radiators, FSR and FH respectively. (Hens, 2010; CEN, 2006)

4.4 Boundary conditions

Inhabitants are assumed to be present between 7 am and 10 pm, during which the set point of the room temperature is 20°C. Outside this period, the set point is taken to be 16°C. This study is carried out using Belgian climate data measured in Uccle (Brussels) (2002). In order to assess the influence of different electricity price profiles as given in table 2, the simulations are repeated for the climate data of 2013, a year for which whole sale market prices are available. The characteristics of both climates, i.e. average temperature T_{avg} , maximal temperature T_{max} , minimal temperature T_{min} and heating degree days (HDD) with respect to 16°C (Hens, 2010) are summarized in table 7.

Table 7: Overview of the climate characteristics of 2002 and 2013 of Uccle (Brussels).

Year	T_{avg} [°C]	T_{max} [°C]	T_{min} [°C]	HDD
2002	10.9	29.3	-7.5	2210
2013	10.2	35.2	-9.1	2364

5. RESULTS

Figure 1 compares the total cost of ownership (TCO) before and after retrofitting the building envelope for various generations of dwellings. The bar graph differentiates the types of costs

that are involved in a retrofit. Part of the CAPEX of the building envelope, namely €29420, is equal in the three cases, due to the costs of new windows, air tightness improvement and the large share of labour cost that are equal for all generations irrespective of the level of improvements. Next to that, the variable part of the CAPEX of the building envelope and investment costs of installations have to be added and finally operational costs, namely energy costs, CO₂-costs and maintenance costs.

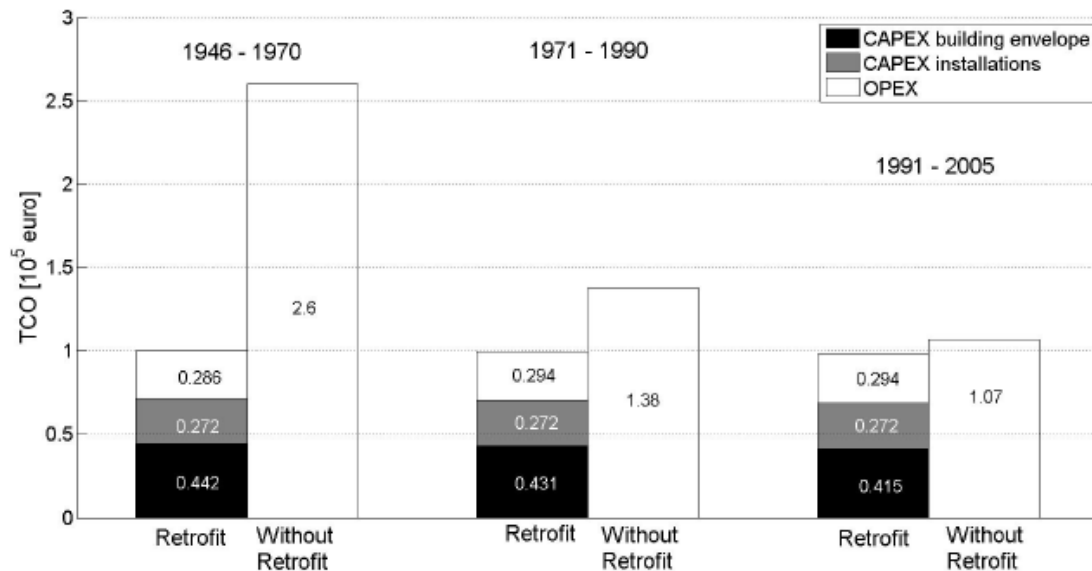


Figure 1: Average total cost of ownership for a period of 50 years of the three considered building generations for relevant combinations of the heat emission and production system as stated in table 6, with and without a retrofit of the building envelope. Energy prices rise according to scenario 1 ($r_{gas} = 4\%$ and $r_{elec} = 2.1\%$).

Benefits of a building envelope retrofit in the oldest generation are clear as shown by the large difference in TCO with and without retrofit in figure 1, but in more recent generations, profits strongly depend on the evolution of energy prices. Also table 8 clarifies this, as the DPP is much higher when energy prices remain constant.

Table 8: Summary of average dynamic pay back periods (DPP) for retrofitting the building envelope of dwellings of different generations for relevant combinations of the heat emission and production system as stated in table 6. Comparison between outside insulation of the facade and filling of the cavity wall. Standard deviation for different combinations of heat emission and production system is given between brackets

Outside insulation DPP [years]	1946 - 1970	1971 - 1990	1991 - 2005
Rising energy prices	14.3 (0.9)	31.3 (1.9)	47.5 (3.1)
Constant energy prices	24.2 (5.2)	> 50	> 50
Filling cavity wall DPP [years]	1946 - 1970	1971 - 1990	1991 - 2005
Rising energy prices	-	19.9 (3.6)	41.1 (3.3)
Constant energy prices	-	32.3 (7.6)	> 50

Expensive outside insulation of the facade leads to these limited benefits in more recent dwellings. From a pure economical point of view, outside insulation can even not be cost effective in recent dwellings. However, this insulation technique incorporates an aesthetic advantage by completely renewing the facade of dwellings. When cavity filling is used in the

two most recent generations, the DPP reduces considerably, as shown in table 8. If it is possible to apply the latter insulation technique, it is preferred over outside insulation of the facade.

Table 9 compares the different emission systems for the retrofitted dwelling. This table shows the average relative TCO of appropriate combinations of heat production and emission systems as indicated in table 6 for a retrofit of the three original dwellings of different ages. The TCO of different solutions is expressed relatively to the TCO of the solution with maximal TCO, in this case fan supported radiators. Radiators or a new floor heating system have nearly the same TCO after retrofitting the building envelope and are nearly 10% cheaper over a 50 year period than FSR. From the energetic point of view, however, the FSR has the highest potential of reducing the primary energy demand of the dwelling, as shown in the last column of table 9, which shows the relative primary energy demand. Radiators have the advantage that no extra labour is needed, but the floor heating system and FSR require a lower supply temperature, which leads to a higher efficiency of the heat production system counteracted by the higher investment cost. The relative cost effectiveness of the emission systems is nearly independent of the evolution of the energy (natural gas and electricity) prices.

Table 9: Comparison between different emission systems after retrofitting the building envelope. The second column presents TCO expressed relatively to the TCO of the device with maximum TCO. The third column shows the standard deviation for combinations with various production systems as stated in table 6, while the fourth and fifth column indicate the relative average primary energy use with respect to the FSR and the standard deviation, respectively.

Emission System	Relative TCO [%]	σ_{TCO} [%]	E_{prim} [%]	$\sigma_{E_{prim}}$ [%]
Recuperated Radiator	90.1	6.5	107.4	11.7
FH	92.3	6.8	101.9	11.9
FSR	100	4	100	10.5

Without a retrofit of the building envelope, heat emission systems' performance strongly depends on the efficiency of the heat production device. In the oldest dwelling, a lot of energy can be saved by using fan supported radiators in combination with a low temperature heat pump. This results in a lower total cost of ownership than using radiators. However, the energy saved by retrofitting the building envelope is much higher, so ignoring a retrofit of the building envelope is not advisable. In newer generations of dwellings, the absolute reduction of energy is more limited and radiators are a more economically favorable solution.

Using the recuperated radiators is not the best option from an energetic point of view, however the results are not far behind FH and FSR. Thus, from an economical point of view, using the existing radiators can be profitable. Therefore, figure 2 shows the comparison of the different heat production systems with (recuperated) radiators as emission system for the retrofitted building envelope. Thermal discomfort is expressed using hot degree hours and cold degree hours, which are defined as the temperature difference respectively above and below the temperature limit of a predicted percentage of 10 % of dissatisfied (PPD) multiplied by the duration of the limit violation. The level of discomfort is of the same order of magnitude for different heating system configurations, which allows a correct comparison of different system configurations based on annual primary energy use.

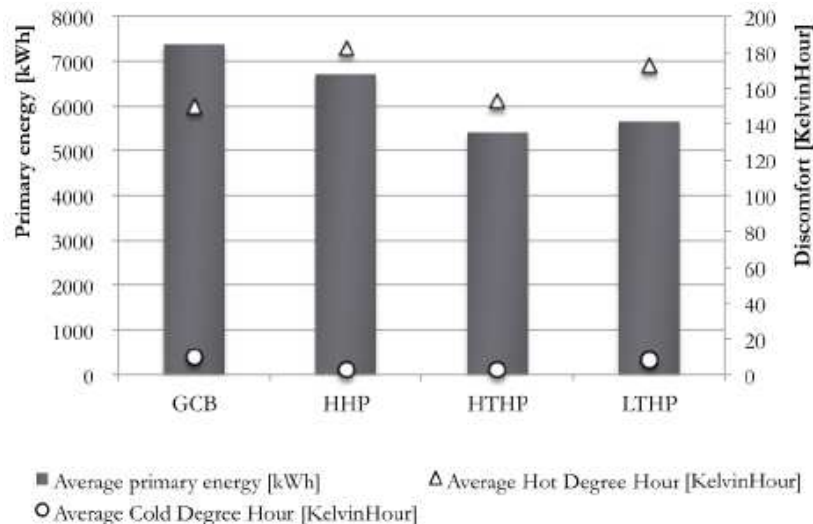


Figure 2: Annual primary energy use of heat production systems combined with radiators in a retrofitted building envelope with the current (2013) Belgian energy prices used for all production systems.

The lowest primary energy demand with radiators as emission system is obtained with a HTHP. The results of the LTHP are almost similar, although if an emission system is used that requires a lower supply temperature, the primary energy use of a LTHP reduces significantly. Therefore, a HTHP especially makes sense when relatively high supply temperatures are required, e.g. radiators in older buildings. Since the HHP combines a GCB and a LTHP, one expects its energy use to be between this of a GCB and a LTHP. The simulations show that the HHP behaves mainly as a LTHP when the gas price is relatively high compared to the electricity price and vice versa. The economic viability of the hybrid heat pump strongly depends on the energy cost savings that can be made with respect to the GCB by choosing for the most cost effective device, i.e. LTHP or GCB. Therefore, the ranking of heat production devices in combination with radiators based on TCO is influenced by the age of the dwelling. The age of the dwelling determines the supply temperature when the original radiators are recovered after retrofitting the building envelope and thus the efficiency of the heat production system, which determines possible energy savings. Table 10 compares the TCO of different heat production systems that supply heat to radiators with a retrofitted building envelope. If energy prices are constant (scenario 2), the gas condensing boiler outperforms the others, but an increase of energy prices (scenario 1) nearly levels out the differences. In the oldest generation, TCO of the hybrid heat pump is even smaller than TCO of the GCB for two reasons. First, the low temperature heat pump in the hybrid heat pump is used more in this case, because it can use a working point with a higher efficiency due to the lower supply temperature of recovered radiators. Secondly, the rapid increase of the gas price favors the use of electricity. However, in more recent dwellings higher investment costs of the hybrid heat pump with respect to the gas condensing boiler cannot be recovered, because the nominal power of the recovered radiators is lower than in the older buildings, so required supply temperatures are higher. Therefore, the hybrid heat pump uses working points with lower efficiencies, thus its gas condensing boiler will be preferred over its low temperature heat pump. As a consequence, there will be no net benefit compared to the gas condensing boiler. The high temperature heat pump is the most expensive solution.

The lower part of table 10 shows results with decreasing investment costs due to learning aspects in development and manufacturing of systems. A decrease of 1.6% per year is considered for all devices (Weiss, Junginger, & Patel, 2008; Weiss, Dittmar, Junginger, Patel,

& Blok, 2009; Bettgenhäuser et al., 2013). This also lowers maintenance costs which are expressed as a percentage of investment costs. Due to these learning aspects, the cost effectiveness of the heat pumps improves. However, the GCB is still the most profitable solution, except for the oldest generation of dwellings with rising energy prices. Without learning aspects, the LTHP was approximately 5% more expensive in the generation 1971 - 1990 with rising energy prices than the GCB. With learning aspects included, the cost effectiveness of the LTHP comes close to that of the GCB. The relative cost difference between the GCB and the heat pumps reduces, because the GCB already walked through a large part of the learning curve. Therefore, reductions in investment cost are lower. Values for the HHP with learning aspects included are not given in table 10, because the learning curve is difficult to estimate for this novel device, which is the combination of two devices that walked through different parts of their learning curves.

Table 10: Comparison between TCO of heat production systems combined with radiators in buildings of three different ages after retrofitting the building envelope. The TCO is relatively scaled to the TCO of the gas condensing boiler. Scen 1 represents the first scenario with increasing energy prices. Energy prices are constant in scen 2. The upper part of the table does not take into account learning effects in investment and maintenance costs in contrast to the lower part.

Generation	LTHP		HTHP		GCB		HHP	
W/O Learning	Scen 1	Scen 2	Scen 1	Scen 2	Scen 1	Scen 2	Scen 1	Scen 2
1946 - 1970	104	125	110	133	100	100	97	113
1971 - 1990	106	127	110	133	100	100	102	115
1991 - 2005	110	131	116	140	100	100	106	119
W Learning	Scen 1	Scen 2	Scen 1	Scen 2	Scen 1	Scen 2	Scen 1	Scen 2
1946 - 1970	99	119	105	128	100	100	-	-
1971 - 1990	101	121	105	127	100	100	-	-
1991 - 2005	105	125	111	134	100	100	-	-

As the high temperature heat pump seems less economically interesting based on table 10, the focus will be on the LTHP, HHP and GCB. In order to assess the impact of the source of electricity generation in different countries on the potential of heat pumps, variable customer electricity prices can be considered as smart metering systems might become more wide-spread in the future. In this study, these prices are based on whole sale price profiles of 2013 (Epexspot, 2013) supplemented with grid tariffs, taxes etc. These supplements can be calculated by assuming the average of the variable price profile equal to the average price of the fixed price contracts in the different countries. The main characteristics of the variable electricity prices are summarized in the lower part of table 2. The simulations of dwellings with retrofitted building envelope and a heating system using radiators as emission system are repeated for different ratios of the average electricity price to average gas price, which results in figure 3. The climate data of 2013, as given in table 7, are used for these simulations. Figure 3 allows assessing the potential of a heat pump, if the ratio between the average electricity price and average gas price and the yearly energy cost for a system with GCB are known. It gives the yearly energy cost of a LTHP or HHP solution expressed relatively to the yearly energy cost with a GCB for different electricity price profiles. The maximum investment cost that can be paid back by the energy cost savings within the lifetime of the devices can be determined based on figure 3, if a certain evolution of the electricity prices and gas prices is assumed. The obtained investment cost can be compared with the current investment cost of the different types of heat pumps. The hybrid heat pump, which could effectively handle the price variations,

is an effective investment in France, even if the current electricity and gas prices remain constant over the years. This is the case due to the much lower electricity costs as clearly shown in figure 3. In Germany, the electricity prices are much higher, which causes the gas condensing boiler to outperform the heat pump solutions. The results are mainly influenced by the average electricity price rather than by the price profile.

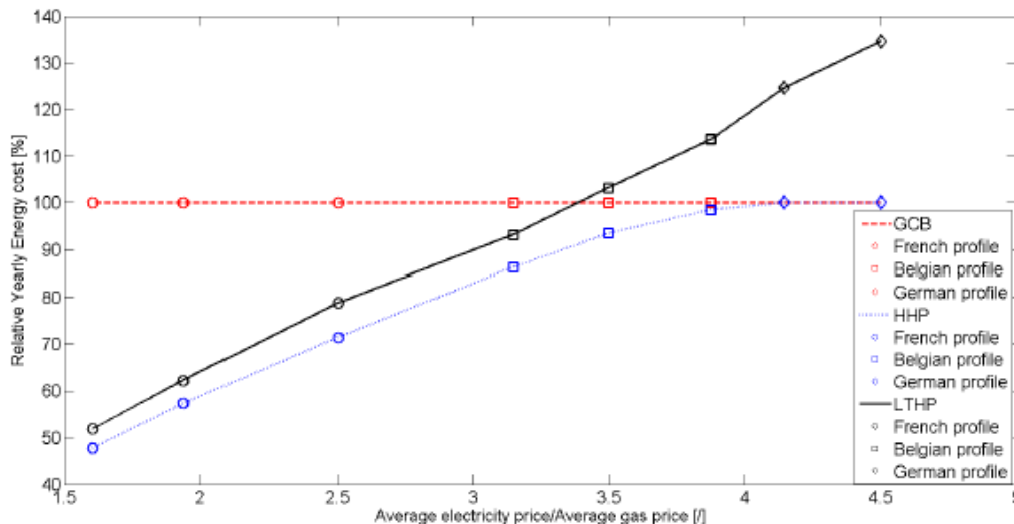


Figure 3: Yearly energy cost of the HHP and LTHP as a percentage of yearly energy cost of the GCB, as a function of the ratio of the average electricity price to the average gas price using electricity price profiles of France, Belgium and Germany after retrofitting the building envelope using radiators as heat emission system. The seasonal performance factor (SPF) of the LTHP equals 3.42. Results for the HTHP are very similar to the LTHP, and hence not shown.

6. DISCUSSION OF THE RESULTS

The results show a large potential to cut costs and energy usage by retrofitting the oldest buildings. In order to lower primary energy use, a LTHP combined with FSR leads to the best result for both the retrofitted and non-retrofitted dwellings considered in this study. When the building envelope has been retrofitted, FH supplied by a LTHP is a very good alternative to FSR from an energetic point of view. Also using the existing radiators with the correct heat production system is possible, i.e. a LTHP with low supply temperature emissions systems and a HTHP when a higher supply temperature is required.

A comparison of the results with other studies is difficult due to the assumptions made. Nevertheless, table 11 compares the primary energy demand with the values of the Tabula project (Holm et al., 2011) for a Belgian single family house. The lower primary energy use averaged over the different heating systems for each generation compared to the Tabula study is amongst others the result of the retrofitting applied in this study. The heat production systems used in the Tabula project are a local stove with fuel oil ($\eta = 75\%$) in generation 1946 - 1970, central heating with a fuel oil boiler ($\eta = 70\%$) in generation 1971 - 1990 and central heating with a gas boiler ($\eta = 76\%$) in generation 1991 - 2005, while this study also uses more efficient heat production systems such as heat pumps in the original dwellings. Therefore, the average primary energy use is lower. Next to that, the global heat insulation quality is worse in Tabula than in this study for generation 1946 - 1970 and 1971 - 1990 due to differences in the geometry and air tightness of the building. Another important aspect is the large amount of solar gains due to the large percentage of glazing in the southern facade of the considered dwelling. Finally,

the static calculation method for the energy use applied in Tabula results in an overestimation of energy demand.

Table 11: Comparison of the primary energy use (E_{prim}) in the original dwellings averaged over various heating system in this study with values in the Tabula brochure (Holm et al., 2011).

Generation	Floor Area Tabula [m^2]	E_{prim} Tabula [kWh/m^2]	E_{prim} [kWh/m^2]
1946-1970	200	275.1	242.0
1971-1990	203	188.4	123.3
1991-2005	219.6	155.7	79.6

From an economic point of view, the literature confirms that the outside insulation of the facade is not an economically optimal measure. Therefore, investment costs are higher and primary energy use is lower in this study compared to the results of Verbeeck et al. (Verbeeck & Hens, 2005). Verbeeck et al. also consider insulation measures, especially roof and floor insulation, and better performing glazing, before more efficient heating systems, even though the total net present value might be similar or even lower. On the one hand, insulation has a longer life span than the heating system and on the other hand, the building's thermal quality determines the design and dimensions of the heating system with a risk of not being adapted if insulation is placed after replacing the installation. However, the aim of this paper is not to find the optimal solution but to compare different heating systems.

An important factor in the cost effectiveness of air source heat pumps is the evolution of the energy prices. It seems that current Belgian electricity prices are too high compared to gas prices, thus the energetic benefits cannot favor heat pumps from the economic point of view. This conclusion can also be drawn with learning aspects included, but the economic viability of heat pumps is already better in this latter case. However, even with decreasing installation costs the cost effectiveness of the heat pumps strongly depends on the evolution of energy prices. So, commercializing heat pump systems is one point, but, more importantly, policy makers have to focus on the large difference between gas and electricity prices. Possible measures could be to introduce a separate and cheaper electricity tariff for owners of a heat pump, e.g. only night tariff, or research in thermal energy storage could be stimulated which can lead to using heat pumps when electricity is cheaper. With the current evolution to nearly zero energy buildings (NZEB) the integration of renewable energy sources is a hot topic. PV systems often feed heat pumps, which is an extra incentive for heat pump systems. Mismatch in time between supply and demand asks for thermal energy storage. However this applies mainly to new buildings. For building owners, a gas condensing boiler is still an economically safe investment today.

7. CONCLUSION

Retrofits of building envelope and heating systems in the residential sector have a very large potential for the reduction of primary energy consumption. From the energetic viewpoint, it is always advised to retrofit the building envelope. The heating system has to be upgraded by choosing a heat production device that delivers the appropriate supply temperature for the emission system, where a heating system with low supply temperature gives better results than a high temperature system. Overall, the air source heat pump has a large energetic saving potential.

In contrast, the economic potential of air water heat pumps strongly depends on the evolution of the energy prices and investment costs. This discrepancy between the energetic and economic results can be diminished by using a more favorable electricity tariff for owners of a heat pump.

Nevertheless, today the gas condensing boiler still seems to be a cost effective choice for building owners in Belgium and Germany due to the low gas price with respect to the electricity price. In France, however, especially hybrid heat pumps are a more cost effective investment due to the relatively low average electricity price with respect to the average gas price.

ACKNOWLEDGEMENT

The work of Evelyn Heylen is funded by the Research Foundation - Flanders (FWO) KU Leuven is founding member of EnergyVille.

REFERENCES

- Baetens, R., De Coninck, R., Van Roy, J., Verbruggen, B., Driesen, J., Helsen, L., & Saelens, D. (2012). Assessing electrical bottlenecks at feeder level for residential net zero-energy buildings by integrated system simulation. *Applied Energy*, 96, pp 74–83.
- Baetens, R., & Saelens, D. (2011). Integrating occupant behaviour in the simulation of coupled electric and thermal systems in buildings. In 8th int. modelica conf., march (pp. 20–22).
- Bettgenhäuser, K., Offermann, M., Boermans, T., Bosquet, M., Grözinger, J., von Manteuffel, B., & Surmel, N. (2013). Heat pump implementation scenarios until 2030: an analysis of the technology's potential in the building sector of Austria, Belgium, Germany, Spain, France, Italy, Sweden and the United Kingdom. http://www.ehpa.org/about/media-library/studies-and-reports/?eID=dam_frontend_push&docID=12040.
- Cabrol, L., & Rowley, P. (2012). Towards low carbon homes—a simulation analysis of building-integrated air-source heat pump systems. *Energy and Buildings*, 48, pp 127–136.
- CEN. (2006). Heating systems in buildings: Method for calculation of system energy requirements and system efficiencies (part 4-2: Space heating generation systems, heat pump systems) prEN 15316-4-2:2006 (E). http://www.cres.gr/greenbuilding/PDF/prend/set2/set2/WI_09_TC-approval_version_prEN_15316-4-2_Space_heating_generation_systems-Heat_pump_systems.pdf.
- De Coninck, R., Baetens, R., Saelens, D., Woyte, A., & Helsen, L. (2014). Rule-based demand-side management of domestic hot water production with heat pumps in zero energy neighbourhoods. *Journal of Building Performance Simulation*, 7(4), pp 271–288.
- De Coninck, R., Baetens, R., Verbruggen, B., Saelens, D., Driesen, J., & Helsen, L. (2010). Modelling and simulation of a grid connected photovoltaic heat pump system with thermal energy storage using modelica. In 8th international conference on system simulation (pp.1–21).
- De Coninck, R., & Verbeeck, G. (2012). Techno-economic analysis of the cost effectiveness of investments for energy savings. (in Dutch).
- Delarue, E., Meeus, L., Azevedo, I., Belmans, R., D'haeseleer, W., & Glachant, J.-M. (2011). Decarbonizing the European electric power sector by 2050: A tale guided by different studies. KU Leuven TME working paper - Energy and Environment. Retrieved from http://www.mech.kuleuven.be/en/tme/research/energy_environment/Pdf/WPEN2010-11
- Department of the Flemish community. (2006). Energy performance regulation: module 1: General legislative framework (in Dutch).
- Epexspot. (2013). Market data auction. <http://www.epexspot.com/en/market-data>.
- European commission. (2012). Price developments on the EU retail markets for electricity and gas 1998-2011. http://ec.europa.eu/energy/observatory/electricity/doc/analysis_retail.pdf.

European committee for standardization. (2003). Heating systems in buildings - method for calculation of the design heat load (norm prEN 12831:2003(E)).

Eurostat European Commission. (2013). Electricity and natural gas price statistics. http://epp.eurostat.ec.europa.eu/statistics_explained/index.php/Electricity_and_natural_gas_price_statistics#Electricity_prices_for_household_consumers.

Federal State Service for Finances. (2012). 6% VAT for the retrofit measures for private dwellings older than 5 years (in Dutch). <http://koba.minfin.fgov.be/commande/pdf/brochure-verbouwen-btw-6-2012.pdf>.

Flemish Energy Agency (VEA). (2013). Requirements for the energy performance of new dwellings in Flanders in 2014 (in Dutch). <http://www2.vlaanderen.be/economie/energiesparen/epb/doc/epbeisentabel2014voormb.pdf>.

Flemish government. (2006). Conclusions of the Flemish government on behalf of the energy performance and climate conditions of buildings (in Dutch).

Flemish regulator of the electricity, & gas markets (VREG). (20/05/2013). Evolution of the electricity and natural gas prices (incl. VAT) for domestic users (in Dutch). <http://www.vreg.be/hoe-evolueren-de-prijzen-op-dit-moment>.

Hens, H. (2010). Applied building physics and installations: inside environment, energy, heating and ventilation (in Dutch). Acco.

Heylen, E., & Jordens, R. (2013). The potential of air water heat pumps in a retrofit context: high temperature heat pump vs. low temperature emission system (in Dutch), master thesis KU Leuven, Belgium.

Holm, M. V., Verbeke, S., & Stoppie, J. (2011). National brochure about the tabula building typology, Belgian building typology (in Dutch). Flemish institute for technological research (VITO).

Huchtemann, K., & Müller, D. (2012). Evaluation of a field test with retrofit heat pumps. *Building and Environment*, 53, pp 100–106.

Kaynakli, O. (2012). A review of the economical and optimum thermal insulation thickness for building applications. *Renewable and Sustainable Energy Reviews*, 16(1), pp 415–425.

Keay, M., Rhys, J., & Robinson, D. (2012). Decarbonization of the electricity industry: is there still a place for markets. Report Oxford institute for Energy studies. Retrieved from <http://www.oxfordenergy.org/wpcms/wp-content/uploads/2012/11/EL-9.pdf>

Kelly, N., & Cockroft, J. (2011). Analysis of retrofit air source heat pump performance: Results from detailed simulations and comparison to field trial data. *Energy and Buildings*, 43(1), pp 239–245.

Norris, M., & Shielsn, P. (2004). Regular national report on housing developments in European countries, synthesis report. The Housing Unit, Dublin, Ireland.

Parys, W. (2013). Cost optimization of cellular office buildings based on building energy simulation (Unpublished doctoral dissertation). KU Leuven, Belgium.

Peeters, L., de Dear, R., Hensen, J., & D'haeseleer, W. (2009). Thermal comfort in residential buildings: Comfort values and scales for building energy simulation. *Applied Energy*, 86(5), pp 772–780.

Pérez-Lombard, L., Ortiz, J., & Pout, C. (2008). A review on buildings energy consumption information. *Energy and Buildings*, 40(3), pp 394-398. Retrieved from

<http://www.sciencedirect.com/science/article/pii/S0378778807001016>

doi:<http://dx.doi.org/10.1016/j.enbuild.2007.03.007>

Poel, B., van Cruchten, G., & Balaras, C. A. (2007). Energy performance assessment of existing dwellings. *Energy and Buildings*, 39(4), pp 393-403. Retrieved from <http://www.sciencedirect.com/science/article/pii/S037877880600212X>
doi:<http://dx.doi.org/10.1016/j.enbuild.2006.08.008>

Radson. (2012). Guide for low temperature radiators (in Dutch). http://www.radson.com/docs/HeatingGuide_NL_LR.pdf.

Schmidt, D. (2009). Low exergy systems for high-performance buildings and communities. *Energy and Buildings*, 41(3), pp 331–336.

The European parliament, & the Council of the European Union. (2010). Directive 2010/31/EU of the European parliament and the council of May 19th, 2010 regarding the energy performance of buildings (in Dutch). Publication board of the European Union.

Van der Linden, A., Boerstra, A. C., Raue, A. K., Kurvers, S. R., & De Dear, R. (2006). Adaptive temperature limits: A new guideline in The Netherlands: A new approach for the assessment of building performance with respect to thermal indoor climate. *Energy and Buildings*, 38(1), pp 8–17.

Van der Veken, J., Hens, H., Peeters, L., Helsen, L., & D'haeseleer, W. (2006). Economy, energy and ecology based comparison of heating systems in dwellings. In *Proceedings of the third international building physics conference* (pp. 661–668).

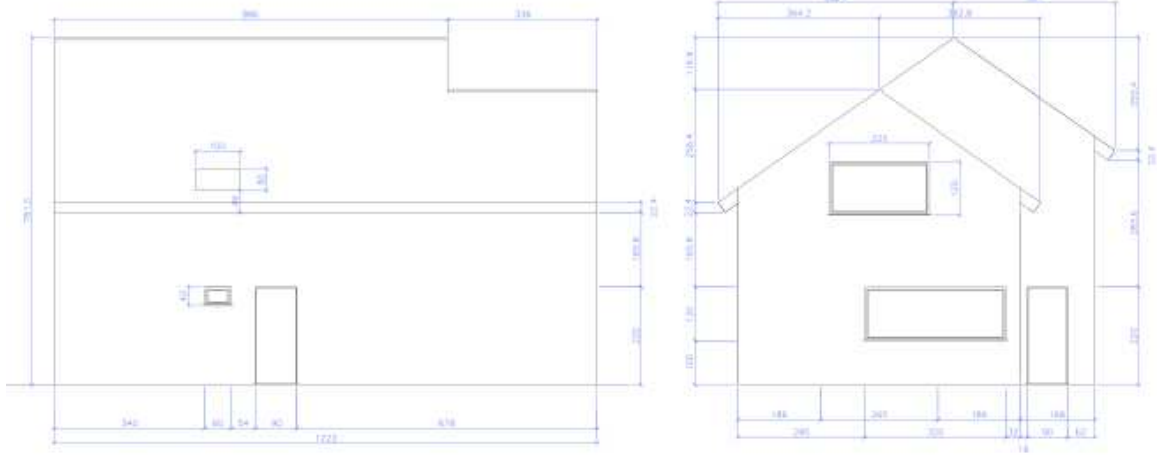
Verbeeck, G., & Hens, H. (2002). Energy efficient retrofitting: economic optimum, cost effectiveness, report project knowledge of the CO₂-emissions, phase 4, Electrabel and SPE (in Dutch).

Verbeeck, G., & Hens, H. (2005). Energy savings in retrofitted dwellings: economically viable? *Energy and Buildings*, 37(7), pp 747-754. Retrieved from <http://www.sciencedirect.com/science/article/pii/S0378778804003366> doi: <http://dx.doi.org/10.1016/j.enbuild.2004.10.003>

Weiss, M., Dittmar, L., Junginger, M., Patel, M. K., & Blok, K. (2009). Market diffusion, technological learning, and cost-benefit dynamics of condensing gas boilers in the netherlands. *Energy Policy*, 37(8), 2962–2976.

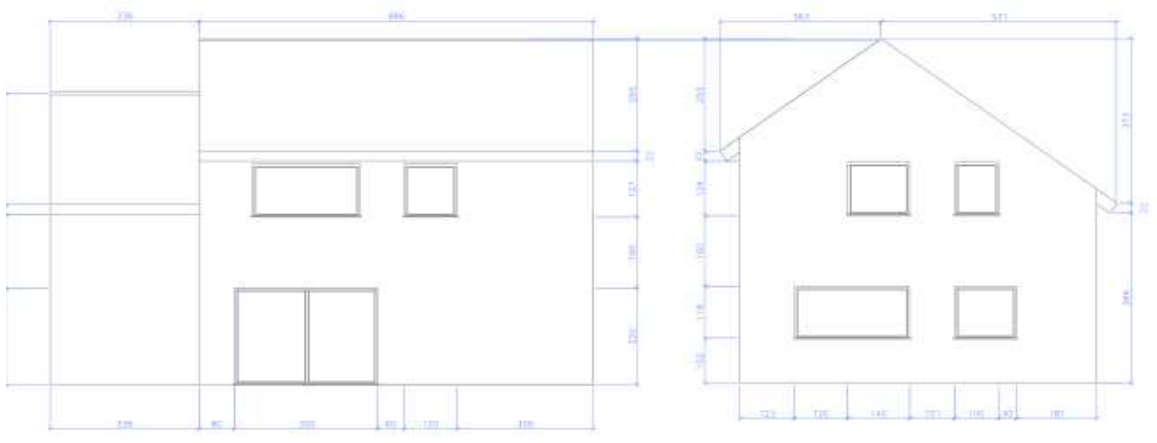
Weiss, M., Junginger, H., & Patel, M. K. (2008). Learning energy efficiency: experience curves for household appliances and space heating, cooling, and lighting technologies. Copernicus Institute, Utrecht University.

A. GEOMETRY OF THE BUILDING



Northern facade

Western facade



Southern facade

Eastern facade

Figure 4: Geometry of the building

Short conclusions by Vincent Lemort

One of the major topics covered by the conference was simulation of advanced control of HVAC systems in buildings. Advanced control is a mean of improving the energy performance of buildings, of allowing for their efficient integration into energy grids and more generally of reducing their operating cost.

- Among others, Model Predictive Control has been largely covered by the conference.
- A technique to cope with the non-convexity of the optimal control of HVAC systems was proposed.
- The coordination of the control of roof top units in buildings, based on appropriate algorithms, can yield significant energy savings.
- A new methodology, using Generalized Linear Models, was proposed to extract decision models from the dynamic programming results.

The integration of renewable energy sources into buildings was illustrated during the conference.

- It was investigated how to increase the SPF of a ground source heat pump coupled to solar collectors and to a buffer tank.
- A new concept of reversible heat pump/organic Rankine cycle system was proposed.
- Various energy efficiency measures to achieve net zero energy in a mid-rise apartment in Canada were investigated using Trnsys. Different heating systems were investigated: conventional heat pumps, solar assisted GSHPs, cold climate HPs. Optimizing the solar assisted heat pump showed promising results.
- A computational model of a district heating network (DHN) has been built in Modelica. It includes the heating plant (gasifier), the DHN, the buildings and a thermal energy storage. Thanks to the latter, the utilization of the gasifier was improved.

Simulation, with different degrees of complexity, is often necessary to analyse and assess the building energy use.

- The impact of refined HVAC systems efficiency determination on monthly calculation was investigated.
- Not only more efficient and better-controlled HVAC systems can contribute to the improvement of energy performance. There is an urgent need for realistic models of lighting and appliances load profiles
- Occupant behavior plays a large role on building energy consumption. It can explain (at least partially) the gap between prediction by Energy Performance Certificate and actual performance of buildings.

Buildings can play an important role in the management of energy grids. The topic of Demand Side Management has been largely covered during the conference.

- Electrification of domestic heating and vehicle is a mean of achieving greenhouse gases emissions reduction. Through simulation, the impact of moving heat pumps and electric vehicle consumption to off-peak periods was investigated.
- The investigation of the upper limit of potential of net-metering programs to promote load matching through load shifting was shown. This work emphasized the consumer's cost benefit.
- An integrated city planning tools combining GIS with electricity grid and building simulation programs was presented.
- The optimal chiller operation for integration into smart grids was studied. Optimal curves of high-energy efficiency to be implemented into control and management

system of chillers have been derived based on semi-empirical models calibrated using manufacturer data.

Advanced control often relies on reduced order models of systems and buildings.

- Optimization of heating start-up was conducted using algorithms based on low order models.
- A methodology to aggregate set of buildings to model country's building stock for demand side management studies with heat pumps was shown. The work answered the question of how to reduce the number of buildings needed in order to represent multiple user behaviors. It investigated the influence of model complexity (COP formulation, emission systems modeling, etc.) on the aggregated results.
- A computational efficient and accurate building stock model, based on a typology of buildings was proposed. The work addressed the impact of the modeling approach on the accuracy of the building stock model.
- A practical and scalable multi-zone building inverse modeling methodology was presented. It is useful for control and analysis of existing buildings. It decouples the weakly coupled zones and groups the ones with strong thermal interactions + eliminate non-significant parameters.

Building and HVAC systems models have to be validated with experimental data

- A new systematic and experimental methodology has been proposed in order to determine parameters of simple R-C building models.
- An adapted co-heating test and experimental infrastructure for characterising the dynamics of residential buildings was presented.
- Results of "blind validation" of building energy simulation tools, conducted in the frame of the EBC Annex 58, were analysed.

Besides control of HVAC systems, a way of improving the energy performance of buildings is to design innovative and efficient components. Such developments require advances in modeling techniques. Examples of innovative components and advanced modeling techniques were presented during the conference.

- An optimized hydraulic layout can increase the seasonal COP and decrease the primary energy demand of geothermal heat pumps associated with TABS.
- A new simple wood stove model has been proposed.
- A design tool for piles heat exchangers (smaller depth to radius ratio than boreholes) was developed.
- A new system of dehumidification based on a zeolite membrane was shown and investigated based on modeling. It is an alternative to refrigerant dehumidification or desiccant dehumidification.
- A comparison between one-stage and two-stage desiccant wheels was presented

Control strategies of HVAC components can be tested on simulated duty cycles by means of Hardware-in-the-loop (HiL) methods. A new building emulator has been presented. It can replace field tests by imposing real conditions to HVAC systems.

